A GLOBAL STUDY ON PHASE VELOCITY, GROUP VELOCITY AND ATTENUATION OF RAYLEIGH WAVES IN THE PERIOD RANGE 20 TO 100 SECONDS

Vol 1

by

JOÃO WILLY CORRÊA ROSA

B.S. Universidade de Brasília
(December, 1981)

Submitted to the Department of Earth,
Atmospheric, and Planetary Sciences
in Partial Fulfillment of the
Requirements of the
Degree of

DOCTOR OF PHILOSOPHY

at the

MASSACHUSETTS INSTITUTE OF TECHNOLOGY

October 1986

Signature of Author: _____
Department of Earth, Atmospheric and Planetary Sciences
October 17, 1986

Certified by _____
Keiiti Aki, Thesis Supervisor

Accepted by _____
Chairman, Department Committee on Graduate Students

A GLOBAL STUDY ON PHASE VELOCITY, GROUP VELOCITY AND ATTENUATION OF RAYLEIGH WAVES IN THE PERIOD RANGE 20 TO 100 SECONDS

by

JOÃO WILLY CORRÊA ROSA

Submitted to the Department of Earth,
Atmospheric, and Planetary Sciences
in partial fulfillment of the requirements
for the degree of Doctor of Philosophy
at the Massachusetts Institute of Technology

ABSTRACT

Global studies on the propagation parameters of fundamental mode Rayleigh waves namely, their phase velocity, group velocity, and attenuation coefficient, have been restricted to periods longer than 100 sec. Advances on the determination of the moment tensor of earthquakes from the observed spectra of these waves, together with the classical role played by the phase velocity of such waves on the study of the crustal and upper mantle structure, are just some of the possible applications of a global study on fundamental mode Rayleigh waves with period shorter than 100 sec.

A first step on our goal of global coverage consisted of the collection from the geophysical literature of all previously measured phase velocity data in the period range 20 to 100 sec. These prior measurements were made using either one, two, or up to three seismographic stations. The measurement error differs greately among these data. Measurements involving just one station require the knowledge of the initial phase at the source, in contrast with the other types of measurement. On the other hand, observations by the one-station method are more reliable when it is possible to accuratelly determine the initial source phase, since we do not need to be concerned with the contamination of the signal by inhomogeneities outside the region of study.

Three regionalized Earth models have been widely used in the study of surface waves with longer periods. They were

introduced by Okal (1977), Lévêque (1980), and Jordan (1981), and we used our collected data set to determine the average phase velocity values as well as the standard deviation of these for each of the above models. The models were statistically tested and the result showed that these were equally efficient while separating the data set.

The addition of new information to our collected data set was made by the application of the one-station measurement method to observations by the Worldwide Standardized Seismograph Network. These correspond to recorded Rayleigh waves generated by a set of 45 worldwide distributed earthquakes. The determination of the initial source phase at these sources was possible due to the availability of the source mechanism and focal depth of these events, which were recently determined by other workers using the body waveform data. The regionalized Earth model of Jordan (1981) was used for unwrapping the observed phase in each case. At the end of this part of our work, we had a phase velocity data set which was more than twice as large as our data set collected from the literature.

In the next step, we used the increased data set to obtain the global distribution of phase velocity at nine reference periods, using the stochastic inversion of Franklin (1970). This method has been widely used in Seismology since Aki *et al.* (1977) applied it to the study of the three-dimensional velocity distribution from body-wave residual travel time data. Its application to surface waves has been still limited to smaller areas (*e.g.* Yomogida, 1985). The initial model used to study the residual travel time data in the inversion process is a variation of the model of Jordan (1981), with the blocks measuring $10^{\circ} \times 10^{\circ}$. The result of our analysis is summarized in a set of corrected velocity maps, followed by the corresponding error and resolution levels achieved by the inversion process. The velocity anomalies correlate well with large-scale tectonic features (such as mid-ocean ridges, trenches, mountain ranges, and shield areas). The velocity is also correlated with the sea-floor age and with the presence of hot-spots. These solutions also showed to be consistent with results obtained by other authors, and the variance improvement achieved at the longer period was better than that associated with the result obtained by Tanimoto and Anderson (1985) for waves with 100 sec. Furthermore, the errors associated with these results at long periods showed that these maps are within the acceptable

error levels for application in the recovery of the moment tensor of other events by linear inversion. The application of the results of shorter periods in a similar fashion requires a larger phase velocity data set.

The group velocity data set gathered while determining new phase velocity values were separated in the same way used to treat the phase velocity data set collected from the literature. In this case, the model of Lévêque (1980) proved to be more effective in the separation of the data. An approach similar to that used in the phase velocity study was attempted in order to obtain the global distribution of group velocity at the same reference period values. This task proved to be unsuccessful due to the larger errors involved in the measurement of group velocity. This reveals that the solution obtained in Eurasia by Feng and Teng (1983b) using a similar approach, may be associated with large errors.

Finally, the amplitude data was used to measure the attenuation coefficient at periods between 20 and 100 sec for the region-types of the model of Jordan (1981). This part still requires further improvements, which we expect to be achieved by application of newly developed techniques to account for the focusing, defocusing, and multipath interference effects, which are more significant in the study of amplitude.

Thesis Supervisor: Keiiti Aki

Title: W. M. Keck Professor of Geological Sciences,
University of Southern California
(Formerly, R. R. Shrock Professor of Earth and
Planetary Sciences, M.I.T.)

ACKNOWLEDGMENTS

I would like to thank Keiiti Aki for all the lessons and the support that he provided me during my stay at M.I.T.. I will never forget his incredible ability of being simultaneously creative and simple in his reasoning. He also showed to have confidence in my work, allowing me to go over large stages of this thesis by myself.

Gene Simmons and Sean Solomon were very friendly with me ever since I arrived in the U.S.. They also encouraged me in my research projects.

This work could not have been done without the support of the administration staff of our department. Sharon Feldstein managed all funds needed to finish this task. This included many magic steps which I still have not figured out. I would like to name a few other great M.I.T. people which helped me along the way: Jan Barbaro, Sara Brydges, Dorothy Frank, Lyle Hodgson, Donna Martel, Linda Meinke, Ann Page, Doug Pfeiffer, Janet Sallstrom, and Al Taylor. Jimmy Byrne would provide me with all late-evening news about the Red Sox. Jean Eaglesfield, leading the Lindgren Library staff, was very kind to me during my long literature search. I also acknowledge Kei's people at U.S.C., whom I did not meet yet but, some way contributed to this work.

The collection of seismograms, which was done partially at the Lamont-Doherty Geological Observatory, could not have been successful without the help of Maggie Yamasaki. At this point, Roger Buck also played an important role since he would let me stay in his house whenever I was too tired to view the records. He and his wife Sharon Quale were also very nice and made the evening work shifts on the 5th floor enjoyable.

Many colleagues and friends whom I met during these years also played an important role in my formation. I would like to name a few of them here: Rafael Benites, Eric Bergman (his wife Susie Saarinen, and little Katie), Greg Beroza, Carol Blackway, George Blumberg, Tianquing Cao, Lou Caruso (along with the Boston Celtics), Ted Charrette, Bob Cicerone, Rob Comer, Jim Davis, Mavis Driscoll, Karl Ellefsen, Danny Fain, Emilio Farco (and his wife Jean), Paul Filmer, Adam Friedman, Lind Gee, Carl Godkin, John Goff, Bob Grimm, Lynn Hall, Tom and Laura Herring, Stephen Hickman, Paul Huang and Theresa Wang, Craig Jones, George Keough, Jeff Mann (and his wife Mary), Mark Murray, John Nabelek, Mike Nelson, Paul Okubo, Federico Pardo-Casas, Scott Phillips, Justin Revenaugh, Peter Roberts; Steven, Debbie, and Geoff Roecker; Jeanne Sauber, Anne Sheehan, Barbara Sheffels, EAP Soccer, Stuart Stephens,

Joann Stock, Gerardo Suarez; Tom and Sim Wissler; and Kiyoshi Yomogida. I also would like to thank all the support I got from my colleagues from Brazil studying at M.I.T..

I came to continue my studies in the United States by encouragement of my former teachers at the Seismological Station, University of Brasília: Jorge A. Mendiguren and José Alberto V. Veloso. Two of my former geology professors, João Hirson and Othon Leonardos Jr., also supported the idea.

This project was made possible by a NSF grant (EAR-8408714), and was partially supported by DARPA contract F19628-85-K-0018. My studies at M.I.T. were supported by the National Research Council, CNPq, process 201.022/81, República Federativa do Brasil.

to my parents,

Wilson and Maria de Lourdes

my sisters,

Solange and Simone

and my brother,

José Wilson.

Table of Contents

CHAPTER 1:

Introduction:

The main purpose of this thesis is to determine the global distribution of phase velocity of fundamental mode Rayleigh waves with period ranging between 20 and 100 sec.

Global studies on surface waves have, until now, been restricted to longer periods, which can be done using data from existing digital seismograph stations: I.D.A. and G.D.S.N. which includes S.R.O., A.S.R.O., and D.W.W.S.S.N.. This task has been pursued by two research groups, one at the California Institute of Technology (Nakanishi and Anderson, 1982, 1983, 1984a,b; Tanimoto and Anderson, 1984, 1985; and Tanimoto, 1985), and the other at Harvard University (Woodhouse and Dziewonski, 1984). The period range covered by such studies, as well as the source and amount of data used, are summarized in Table 1.1, and compared with those of our studies. Notice that our data set is much larger than others.

The phase velocity information on shorter period surface waves is essential for the application of the moment tensor inversion technique to surface waves from smaller earthquakes

which do not generate sufficient long-period energy. It is also useful for more detailed studies of the structure of lithosphere and asthenosphere.

It is important to stress here the fact that the work summarized in this thesis is the first attempt to invert globally a phase velocity data set consisting entirely of R_1, which do not suffer from polar passages which tend to complicate the waveform by multipath interferences. Furthermore, the R_1 data set does not suffer from the non-uniqueness of the great circle phase velocity data (*e.g.* Nakanishi and Anderson, 1983), which cannot fully describe the Earth's lateral heterogeneity.

Measuring phase velocity of these waves at the period range shorter than 100 sec is by no means a simple task involving extensive digitizing of W.W.S.S.N. records, because of the lack of coverage of the period band by some of the existing digitally recording seismographic stations. To pursue our objective of global coverage, we started this project by collecting the phase velocity data already measured by other authors. We used published phase velocity dispersion curves measured using either the one-, two-, or, in some cases, three-station method. The results of a systematic

search throughout the geophysical literature are summarized in Chapter 2. We then formed a complete collection of R_1 data obtained previously.

We constructed initial models of phase velocity distribution using the phase velocity data collected from the literature by grouping the data according to the tectonic types of their paths. This procedure has been used in the past by a number of authors. We adopted three different Earth models due to Okal (1977), Leveque (1980) and Jordan (1981) in this process as described in Chapter 3. These models have been used in the study of waves with greater period: Silver and Jordan (1981) used the model of Jordan (1981), Dziewonski and Steim (1982) used a four-region model very similar to that introduced by Leveque (1980), while Nataf *et al.* (1986) considered the model of Okal (1977). We also used a statistical test to verify the effectiveness of these models for separating the data set.

In order to increase the amount of our data, we measured the phase velocity between the epicenter and W.W.S.S.N. stations for 45 earthquakes, for which focal mechanisms have recently been determined by other authors using body waveform data. The details on the measurement method used, as well as

discussion on possible error sources, are given in Chapter 4. This work more than doubled the number of paths for which the phase velocities are measured for our period range.

This increased phase velocity data set was then used in the determination of the global distribution of phase velocity of fundamental mode Rayleigh waves for the 20 to 100 sec period range. We used the stochastic inverse of Franklin (1970), which has been widely used in Seismology to study the three-dimensional velocity distribution since Aki *et al.* (1977). The application of this method to surface waves, as well as a discussion on the determination of the damping parameter, are given in Chapter 5.

The resulting phase velocity anomalies are then compared with results obtained by other authors in the Pacific, and with those obtained by Tanimoto and Anderson (1985) for the whole Earth. The latter work considered R_2 and R_3 data for periods longer than 100 sec. The possible usage of our results to moment tensor inversion to other globally distributed events is also considered in Chapter 5.

The group velocity measurements made during the processing for the phase velocity measurements in Chapter 4, were used in Chapter 6 to establish group velocity values for

the same regionalized Earth models as used in the phase velocity study. We also tried to obtain the global distribution of group velocity by applying the method of Chapter 5.

Finally, we describe in Chapter 7 the attenuation coefficient measurements made using the amplitude spectrum data for the paths considered in Chapter 4.

TABLE 1.1 - SOME RECENT STUDIES ON GLOBAL DISTRIBUTION OF PHASE AND GROUP VELOCITY OF SURFACE WAVES

reference	period range (sec)	type of study	number of paths	recording network
Nakanishi and Anderson (1982)	152-252	Rayleigh wave --------- group velocity	215	I.D.A.
Nakanishi and Anderson (1983)	100-330	Love wave ---------- Rayleigh wave --------- phase velocity	200 250	I.D.A. G.D.S.N.
Nakanishi and Anderson (1984a,b) also: Tanimoto and Anderson (1984,1985) and Tanimoto (1985)	100-330	Love wave ---------- Rayleigh wave --------- group velocity	408 399	I.D.A. G.D.S.N.
		Love wave ---------- Rayleigh wave --------- phase velocity	289 414	
Woodhouse and Dziewonski (1984)	greater than 135 sec	Love and Rayleigh ----- as well as body waveform data	870	I.D.A. G.D.S.N.
this work	20-100	Rayleigh wave -------- phase velocity	2147	W.W.S.S.N.

CHAPTER 2

Previous studies on the phase velocity of fundamental mode Rayleigh waves for the period range 20 to 100 sec.

2.1 - Introduction:

The purpose of this chapter is to review the literatures containing the phase velocity data for Rayleigh waves in the 20-100 sec period range. These data are then used to form a computer database that contain most of the information gathered by previous workers and can then be used as the starting point for our studies of the lateral variation of phase velocity of these waves on the surface of the Earth. In this review, we shall focus our attention on the methods of phase velocity determination and the errors in determination for the data to be used in the present thesis.

The first phase velocity measurements of Rayleigh waves were made by Press (1956b) using a three-station array. This method is widely known as the three-station (or tripartite) method. He first presented this method at the thirty-seventh annual meeting of the American Geophysical Union (Press, 1956a). In his work, he established a sequence of phase

velocity data interpretation that is still followed in recent papers: measurement of phase velocity, calculation of theoretical phase velocity curves for a given structure, comparison of observed and theoretical curves, and interpretation of the structure which theoretical dispersion curve had the best fit under the light of additional geological and geophysical information available for the area.

Measurement of phase velocity for Rayleigh waves between a source and a receiver was first used by Brune *et al.* (1960). They applied the method to seismic records of nuclear explosions and of an earthquake located in the Hudson Bay area. The main difficulty in this method was the correction of the observed phases for the source initial phase. They avoided the complexities involved in this correction by assuming frequency-independent source phase.

Aki (1961) determined the phase velocity of Rayleigh waves for seven different regions of Japan by analysing simultaneously the records from the Japanese network of an event that occurred in the Samoa Islands. He used a least-squares method to obtain the solution that best explained the observed arrival time of a certain peak recorded at each station.

Determination of phase velocity for Rayleigh waves between two stations was first performed by Brune and Dorman (1963). Their method consists in choosing an event that lies on the same great-circle joining the two stations. This way, the source phase correction required for the one-station method can be avoided.

In the following sections we will discuss the details of each of these measurement methods, describe the procedure we followed to extract results from the literature, and discuss the accuracy of these measurements.

2.2 - The three-station method:

2.2.1 - The method:

As we mentioned earlier, the first phase velocity measurement of Rayleigh waves was done by Press (1956a, 1956b). He identified the crests and troughs of Rayleigh waves generated by an event at three stations located in southern California, and measured the difference in travel time observed at the stations. From these differential travel times, the velocity and the angle of incidence of the wave are calculated assuming that incident wave is a plane wave. This

assumption is one of the limitations of the application of the method to large arrays. As Press (1956b) points out, the array dimensions have to be comparable to the smallest wavelength so that unambiguous identification of peaks and troughs can be done. He also cautions applications of the method to areas where the effect of lateral heterogeneities outside the array may violate the assumption of plane wave composed of a single mode.

We present a simple sketch of the three-station method of Press (1956a, 1956b) in Figure 2.1, where a surface wave with period T, and phase velocity c(T) approaches an array composed of stations 1, 2 and 3. The phase velocity measured by the observation of the wave front arrival at each station can be obtained from

$$c(T) = \frac{\Delta_{12} \sin A(T)}{\Delta t_{12}(T)} = \frac{\Delta_{13} \sin [A(T) + \alpha]}{\Delta t_{13}(T)} \qquad (2.1)$$

where

Δ_{12} and Δ_{13}, $\Delta t_{12}(T)$ and $\Delta t_{13}(T)$ are the distance between station pairs 1-2 and 1-3, and the arrival time differences of the phase with period T at these stations pairs, respectively.

α is the angle between the triangle legs containing the station pairs 1-2 and 1-3.

A(T) is the incident angle of the wave front. It can be measured using Snell's law,

$$A(T) = \tan^{-1} \left[\frac{\sin \alpha}{\frac{\Delta t_{12}(T)\ \Delta_{13}}{\Delta t_{13}(T)\ \Delta_{12}} - \cos \alpha} \right] \qquad (2.2)$$

The refraction of Rayleigh waves in a continental margin had been studied previously by Evernden (1953, 1954). He found that both deviations of observed direction of incidence of Rayleigh waves from the greatcircle paths, and anomalous particle motion of observed Rayleigh waves were due to refraction of these waves. He used a three-station array located near San Francisco, California, to determine the angle of incidence of waves generated by thirty-nine earthquakes distributed at several azimuthal directions from the center of the array. The observed differential travel time were then used (for all the earthquakes) to determine an average phase velocity curve for the array region. He tentativelly interpreted the results by calculating several theoretical phase velocity dispersion curves considering different crustal thicknesses for the region. Press (1956b) suggested that a more appropriate procedure would be the comparison of the

observed values with a set of phase velocity dispersion curves he obtained integrating a group velocity dispersion curve measured for a path in Africa (Press *et al.*, 1956). Press (1957) then re-interpreted the phase velocity dispersion curve obtained by Evernden (1953, 1954) in terms of crustal thickness using his standard phase velocity curves.

Ewing and Press (1959) chose an event that occurred in the Samoa Islands as the source for a study of the distribution of Rayleigh waves phase velocity in the whole United States. They chose this source because its location permitted the generation of waves that were not signifficantly contaminated due to lateral heterogeneities, because they travelled through a path in the Pacific, which they knew would not affect the waves considerably. Another advantage for using the waves generated by that event was the fact that the direction of propagation of its wavefront was roughly perpendicular to the western coast line (*i.e.* they expected little lateral refraction of these waves at the ocean-continent transition region) so that larger array dimensions could be used. They used the same graphic technique from Press's earlier works (Press 1956a, 1956b, 1957) to identify the peaks and troughs and then measure the

period and phase velocity for each phase. They assumed (as in other earlier studies) that the crustal thickness at each region was the only factor controlling the form of the phase velocity dispersion curves, and compared the observed curves for each of the twenty-four tripartite arrays they studied with the reference curves of the earlier studies (Press, 1956b, 1957). These arrays were grouped into several tectonic provinces, and a mean crustal thickness was determined from the average of the measurements made for each province. An important correlation was found between phase velocity and the topographic and Bouguer gravity anomaly. This correlation was used to check the assumption made on the main dependence of phase velocity curves with the local crustal thickness for the period range they studied (15 to 35 sec), and to conclude that, in addition to crustal thickness variations, there were density changes of crustal material between the different regions in the United States.

The use of phase velocity data together with gravity and refraction data to study the Earth's crust, was emphasized by Press (1960). He presents some modifications for the standard curves used in his previous work (Press, 1956b, 1957) so that it would incorporate information on new crustal structure

available from refraction profiles. So, an interpretation based solely on changes in crustal thickness for the region was considered inappropriate due to the non-uniqueness of the interpretation of phase velocity data only. In the mean time, seismologists began to use multiple layered model to compute the theoretical dispersion curves. This was possible due to the matrix method introduced by Haskell (1953) and applied by Dorman *et al.* (1960) to compute dispersion curves for several crust and upper mantle velocity models, such as the still used (*e.g.* Yomogida, 1985) model 8099 for oceanic structure.

2.2.2 - Published measurements using the three-station method:

In the preceding section, we reviewed the early studies of fundamental mode Rayleigh wave in which tripartite station arrays were used to determine the phase velocity. Here, we review the measurements made by several workers using the same method in several other regions of the world. We use a combined chronological and regional order to describe these works in order to follow the steps of improvement made on the measuring technique, as well as to correlate the measurements made in the same region.

Oliver *et al.* (1961) measured the phase velocity of Rayleigh waves with period between 15 to 45 sec for an area covered by three stations in the northeastern U.S.. They used waves generated by four events located in the Pacific. The resultant dispersion curves are compared with Press' reference curves (Press, 1956b) and they also calculated several dispersion curves for theoretical Earth models derived using seismic refraction information for that region. The same data set is interpreted by Dorman and Ewing (1962) using the method of Haskell (1953) applied in a form that a shear velocity profile is found by an iterative least-square fit between observed and calculated dispersion curves for the area.

Another study in the U.S. using the three-station method was performed by Alexander (1963) in the Basin and Range Province using waves generated by nuclear explosions at Novaya Zemlya, U.S.S.R.. He also measured the phase velocity for several three-station arrays in southern California using waves from several events in the south Pacific. A typical standard error for the phase velocity found 64 these measurements is about 0.5 percent for periods below 22 sec, and about 1 percent for longer periods. He reviewed all the phase velocity measurement techniques existing at that time,

comparing their advantages and discussing the main sources of error for each method. We shall refer to his work again when we discuss the errors related with the phase velocity measurement methods. Another topic discussed in his work is the lateral refraction of Rayleigh waves at the continental margin in California. A determination of the direction of the continental margin in this region was made using the direction of approach of Rayleigh waves observed in southern California. The resultant direction was approximately parallel to the coast line.

Tryggvason (1961) measured the phase velocity for several three-station arrays located in Fennoscandia. He used records of two earthquakes, one occurred in Mexico, and the other in the Kuril Islands region. A simple correction was applied to the data to account for the effect of irregularities in the wave front observed at stations composing the network. These irregularities were attributed to the effect of inhomogeneities along the paths outside the region covered by the network. The resultant dispersion curves were interpreted to determine the crustal thickness for the region covered by each tripartite array.

The reference curves obtained by Tryggvason (1961) were used by Luosto (1965) to determine the crustal thickness in southern Fennoscandia. He measured the phase velocity for a region covered by a triangle formed by three W.W.S.S.N. stations in that area (COP, KON, and NUR). Records from three nuclear explosions in the Novaya Zemlya region were used to obtain phase velocity dispersion curves in the 20-50 sec period range. Because of the proximity of these stations to the source region, a correction was applied to the original method of Press (1956a, 1956b) so that the deviation of the wavefront from plane could be accounted for. The period and phase velocity of the observed waves were then determined using the graphic method.

Tseng and Sung (1963) measured phase velocity for some regions in China using waves generated by two earthquakes that occurred in the New Britain Islands. They applied the three-station method to several arrays (a total of twelve stations involved) and the resultant phase velocity dispersion curves were used to estimate the crustal thickness in each region.

Payo (1965) used two W.W.S.S.N. stations located in Spain together with a station in Portugal to determine the phase velocity in the 15-50 sec period range for the Iberian Peninsula using the three-station method. He used the records of four earthquakes and found a set of dispersion curves that differed considerably from an average of phase velocity for the path between the two spanish stations (MAL and TOL). This average value was obtained using the two-station method for records of seven earthquakes. The observed differences between this average and the values obtained using the three-station method were larger than the standard error of the average. The explanation for this difference was attributed to some multipath effect by heterogeneities outside the array region. The events used had different azimuthal directions from the array, and the differences between the propagation paths outside the array region would cause scatter in the measurements, specially because he could not explain how local structure changes could cause the discrepancy.

Pilant and Knopoff (1964) studied the beating observed for long-period records of Rayleigh waves. They concluded that this phenomenon is caused by either the interference of two or more different signals generated by the same source and

recorded approximately at the same time or, by multipathing transmission of a single signal. In their work, they also calculate the three-station phase velocity using an array in Europe (one station in France, another in Germany, and the third one in Italy). In this measurement, they used records of an event that occurred in the Mid-Atlantic Ridge. The calculated phase velocities (between 15 and 75 sec) showed considerable scatter due to multipathing evidenced by beating of the record. They tried several smoothing techniques of the observed phases, but failed to reduce the scatter. They point out that measurements using records showing multipathing effect cannot be reliable.

Knopoff *et al.* (1966) used a network composed of five seismographic stations in Europe to determine the phase velocity using a modified version of the three-station method. In this case, events located near a great-circle connecting two of the stations of the array were selected. The criterion used in this work is that useful events lie within 10 degrees of the greatcircle. The period range was 10-80 sec. Along with this modification of the method, they also introduced Fourier analysis techniques together with some filtering procedures for minimizing the beating effects discussed by Pilant and Knopoff (1964).

Their discovery that the third station, from a tripartite array with the other two stations aligned in the same greatcircle with the source, has little influence on the calculated three-station phase velocity, enabled us to assign this measured velocity value to the path between the two stations. We included the results obtained by this technique in Table 2.1, where we collected all the phase velocity data associated with particular paths.

Knopoff *et al.* (1967) also contributed to the modification of the three-station method. They used seismic networks located in Europe and one in northern California to determine the phase velocity. Paths were paralel to the legs of triangular arrays, or along the sides of networks formed by four stations. The effect of lateral heterogeneity in the region studied can be checked by using two different triangular configurations to calculate the phase velocity along one side that is coincident to both triangular arrays. This effect can also be studied using an event that has its direction of propagation along two parallel legs of a four-station network. They concluded that, in a region where there is a known source of lateral heterogeneity, the use of the three-station method for waves incident from directions

which differ from the directions of any of the triangle's leg is not appropriate. This was shown using several observations and proved that the three-station method applied to the cases mentioned above may have large errors.

We have included the dispersion data for the paths along the triangle legs and those along the four-station array sides from their work in our database (Table 2.1).

Berry and Knopoff (1967) measured the phase velocity along several paths in the Mediterranean sea using tripartite stations with the sides paralel to the direction of propagation of waves generated by several earthquakes. In the interpretation, they used an estimated error of about 0.03 km/sec in the phase velocity data over the whole period range they studied (20 to 90 sec). The dispersion data set corrected for the ellipticity of the Earth (Bolt and Dorman, 1961) was divided into two groups for which flat-Earth shear velocity profiles were obtained using a least-squares technique to determine the best fit between observed and calculated dispersion curves. The difference between the propagation direction of the waves and the direction of the legs of the triangular arrays was less than 13 degrees for all the paths studied and, in most cases, less than 7 degrees.

In another paper on the phase velocity of Rayleigh waves in the Iberian Peninsula, Payo (1970) studied the records of Rayleigh waves corresponding to 7 earthquakes from the same set of W.W.S.S.N. stations (MAL, PTO, and TOL) that he used in his first study (Payo, 1965). As we have seen earlier, the three-station measurement reported in that paper was not successful due to the large variability among the measured dispersion curves. This time, he reported the results of measurements made along the legs of the triangle formed by those three stations using the idea developed by Knopoff *et al.* (1966, 1967) that we just reviewed. He obtained 7 phase velocity dispersion curves corresponding to each one of the events studied. All the legs of the triangular array were studied by at least one profile from each direction (*i.e.* the phase velocity was determined using waves approaching from the two opposite directions using two different earthquakes). The estimated error in phase velocity reported for this work is: 0.009 km/sec for 30 sec, 0.019 km/sec for 60 sec, and 0.032 km/sec for 90 sec waves (approximately 0.3 percent for 30 sec, 0.5 percent for 60 sec, and 0.8 percent for 90 sec). He made these estimates assuming that the most significant source of error in this case was the uncertainty in phase differences

between the two stations at each measurement. The angle of incidence of the waves at the array was also calculated for each case. Deviations up to 20 degrees from the greatcircle path were observed. He explains the deviations in the short period cases by refraction of these wave fronts at the continental border for waves approaching the Peninsula from the ocean, but not for long periods, which show larger variations in some cases.

2.3 - The multiple-station method:

2.3.1 - The method and the determination of phase velocity of Rayleigh waves in Japan:

The method we discuss here was first used by Aki (1961), who studied the records of 35 stations of the japanese seismological network from the same Samoa event used by Ewing and Press (1959). Aki (1961) used the peak and trough method to measure the period and the arrival time of the observed phases. He then divided the region studied into seven sub-regions, each containing a group of stations, and corresponding to different geological settings. One station in each region was selected as a reference and the least

squares method was applied to determine the phase velocity c_i, the direction of propagation of the wave front θ_i, and the arrival time t_i at the reference station for the i-th peak, using the observation equation;

$$t_{ji} = \frac{\cos \theta_i}{c_i} \Delta\theta_j + \frac{\sin \theta_i}{c_i} \Delta\varphi_j + t_i \qquad (2.3)$$

where t_{ji} is the observed arrival time of the i-th peak at the j-th station, θ_i is the azimuth of propagation direction of the i-th peak (measured from the north), c_i is the phase velocity for the observed peak, and $\Delta\theta_j = \theta_j - \theta_0$, $\Delta\varphi_j = \varphi_j - \varphi_0$ (θ_j, φ_j and θ_0, φ_0 are respectively the latitude and longitude of the j-th station and of the reference point at each region all measured in km).

He determined the errors in the estimation of c and θ for each region from the regression analysis. The results show that the errors in c range between 1 and 1.5 percent.

The phase velocity values obtained were then compared with the standard dispersion curves of Press (1960) to obtain the crustal thickness for each region. Discrepancies between crustal thickness obtained by this method and results from

refraction studies for some of the regions showed that the use of the standard curves constructed by Press (1960) was not applicable to Japan. Aki (1961) calculated then a new set of dispersion curves which are consistent with the results from refraction studies. The crustal thickness of each region was then obtained using these new standard curves. He also correlated the phase velocity result with Bouguer anomaly and topographic changes. The resultant correlation is approximately the same obtained by Ewing and Press (1959) in the U.S..

Further developments on the phase velocity distribution in Japan were made by the use of a new event (this time an event located in the Aleutian Islands) by Kaminuma and Aki (1963). Since the path from this earthquake is approximately parallel to the trend of the Japanese Islands and they could study more regions than his earlier work. They used a total of 45 seismological stations divided into 10 regions. The arrival time and period of seven different phases were calculated for each station using the peak and trough method. These measurements were then used in the least squares method to determine the phase velocity at each of those 10 areas in the 20-40 sec period range. The calculated errors for these

phase velocity values range from 1 percent for periods about 40 sec to up to 9 percent for 20 sec periods. The resultant dispersion curves were used to determine the crustal thickness at each of the 10 regions. These were obtained by comparison of the dispersion curves with the standard curves of Press (1960) and Aki (1961). Again the curves of Aki (1961) generate results that are more consistent with crustal thickness values obtained from refraction studies. For areas studied by Aki (1961), they obtained thickness values that agree with the earlier results. Since in the second work they covered most of Japan, a crustal thickness map was constructed using the results. Again a strong correlation was found between Bouguer anomaly values, elevation, and phase velocity-determined crustal thickness for each region.

Kaminuma (1964) further studied the phase velocity in Japan using an earthquake of Mindanao, Phillipines. The direction of approach of the waves generated by this event was the opposite of that of the Aleutian event studied by Kaminuma and Aki (1963). He found phase velocity values and crustal thickness that agreed with the ones obtained in those previous studies for most regions. For the central part of Japan, however, the path along the trend of Japanese island showed

phase velocity 4 percent greater than those in a perpendicular direction (the ones generated by the Samoa earthquake studied by Aki, 1961). A new map of crustal thickness in Japan was presented as the result of analysis of all the phase velocity measurements to that date.

Kaminuma (1966a) compares the phase velocity values obtained by previous works in Japan with values obtained in other parts of the world. He measured an additional set of 6 Rayleigh waves dispersion curves between two stations located in central Japan. In these measurements, the two-station method was used (Brune and Dorman, 1963). He used records of 6 different events analyzed by the peak and trough method to identify the periods associated with the different observed phases. The requirement used for the choice of the events was that the angle between the greatcircle joining the two stations, and the one joining the first station with the source, was less than 20 degrees. The data were corrected for the angle of deviation between the greatcircle path and observed path directions measured in the previous works in Japan. This procedure could not avoid a final estimated error of about 5 percent for the phase velocity values. An additional dispersion curve, obtained for the path as an

average of the previous observations for the area was added to the 6 measured curves. We have included this data set in our database (Table 2.1). The comparison of the phase velocity values obtained in Japan with others obtained in other parts of the world led him to conclude that the phase velocity of surface waves is dependent on the age of the studied region.

Additional interpretation of the regional crust and upper mantle structure based on phase velocity data obtained for Japan are given by Kaminuma (1966b,c).

2.3.2 - Other phase velocity measurements using multiple-station array data:

Glover and Alexander (1969) studied the records of stations of the LASA array in Montana for two earthquakes. One of these events was located in the Greenland Sea and the other in the North Atlantic. The objective of their studies was to verify the existence of lateral variations in the structure within the array location. They considered the observed differences between phase and group velocity dispersion curves measured using all the stations combined, and measured with these stations divided into groups, as evidence for the existence of such inhomogeneities within the

array. The measurements were made in the 15-60 period range and the observed dispersion curves were compared with curves calculated using different crustal structures based on the information from refraction profiles in the region. They used a variation of the method introduced by Aki (1961). The procedure they followed is summarized in an earlier work (Alexander, 1963). It is done in the frequency domain and allows a precision in the determination of phase velocity of about 2 percent for 60 sec, and of about 1 percent for 15 sec in their analysis (this error estimate was made from the observed variations of the measurements).

Calcagnile *et al.* (1979) used five stations located in north and central Italy to determine the average phase velocity curve for that region using records of two earthquakes. One of these events was located in Japan, the other in the Kuril Islands. The records were processed using the same steps summarized by Pilant and Knopoff (1964) and Knopoff *et al.* (1966). Using the peak and trough method, they obtained the phase velocity values in the 25-250 sec period range. The errors corresponding to these values range from about 4 percent for 25 sec to about 2 percent for 250 sec (it is approximately 1 percent for 100 sec waves and it

consistently decreases with increasing period for the interval 25-100 sec). These phase velocity values were used (after correction for the sphericity according to Bolt and Dorman, 1961) to obtain the crust-upper mantle structure of the region.

Calcagnile and Panza (1979) applied the same method used by Calcagnile *et al.* (1979) to study the central and southern portions of the Italian Peninsula. This time, they applied the method to records of four stations located within that region, that recorded an earthquake for which the wave path is in the direction of the peninsula. The resultant phase velocity dispersion curve in the 12-83 sec period range for the whole array region was used to determine the local crustal and upper mantle structure. The estimated errors of phase velocity range from about 2.5 percent for 12 sec period, to about 1.7 percent for 83 sec. This error estimate was made from the observed variations in the phase arrival time with distance along the array.

2.4 - The two-station method:

2.4.1 - The method:

The first measurements of Rayleigh waves phase velocity using the two-station method were performed by Brune and Dorman (1963) for paths within the Canadian Shield. They studied waves with period ranging from 3 to 90 sec, generated by 8 earthquakes that were selected so that the greatcircle path going through each station pair would pass as close to the epicenter as possible. The fundamental idea behind this is the assumption that most of the energy propagated as Rayleigh waves will approximately follow this path.

The routine followed to determine the phase velocity curve for each path begins with the identification of several phases from records of both stations for each event considered. These phases were plotted in a diagram relating phase number and arrival time at the station. The period of each phase can then be determined using this peak and trough method. If we consider the arrival time of a given peak and trough with period T at each station, t_1 and t_2, we can calculate c(T) the phase velocity for the Rayleigh wave with

period T from the relation:

$$c(T) = \frac{\Delta}{\Delta t - \frac{T}{2\pi}\,[\Delta\varphi(T) + 2\pi\, N(T)]} \qquad (2.4)$$

where $\Delta t = t_2 - t_1$ if the wave propagates from station 1 to station 2 (Figure 2.2); Δ is the distance between these two stations, $\Delta\varphi(T) = \varphi_2(T) - \varphi_1(T)$ (the difference in phase observed between the two stations), and N(T) is an unknown integer which must be correctly determined. It is usually determined by calculating c(T) for several trial values of N(T) and comparing the results so that a realistic value for c(T) is found.

It is generally difficult to find an event whose epicenter will be on the great-circle path connecting the two stations. We, then, choose events that will be as close as possible to such an alignement. Brune and Dorman (1963) compare the intersect angle between the greatcircle direction of the epicenter to the first station, with the greatcircle path connecting the two stations (angle θ in Figure 2.2). In their case, all the eight events selected all had this intersect angle less than four degrees, because they found

that measuring phase velocity using events with this angle greater than four degrees induced large error in the measurement. They associate this error to either the azimuthal variation of initial phase of these waves or the effect of lateral heterogeneity on the paths before reaching one of the stations. The practice of measuring the intersect angle became a routine by other authors that applied the method. Most reports of two-station measurements made to date include information on the limit chosen for the intersect angle. We think that this information may be useful to judge the accuracy of each measurement, and to study lateral heterogeneity effects in the areas covered by the paths. We then include this value, whenever it is available, for each reference we discuss where the two-station method was used. For this reason, we list the earthquakes used for each reference in Table 2.1 that contained measurements of phase velocity of Rayleigh waves using the two-station method.

Brune and Dorman (1963) made nine measurements using the two-station method in the period range 20 to 90 sec. They estimate a precision of 0.03 km/sec for their measurements (this corresponds to a precision better than 0.8 percent for 90 sec period, and better than 0.9 percent for 20 sec period,

if we consider typical values obtained for c(T)). They attribute these uncertainties to several possible effects, including measurement errors on the phase correlation in the peak and trough method, on the instrument correction applied to the phase, on 'interference', and on refraction. It is not clear in their work what the interferences are or what causes these. On the other hand, they describe the refraction effects (mostly due to lateral inhomogeneities, and considered more significant for paths crossing ocean-continent boundaries). They consider the refraction effects the most important source of error in their observations.

Brune and Dorman (1963) also used the one-station method, to determine the phase velocity for periods ranging from 3 to 40 sec. They used the records of 2 events in the northern part of North America, and one in the Arctic for this second part of their study on the Canadian shield. They used the procedure introduced by Brune *et al.* (1960) with the initial phase chosen by trial and error, in order that the phase velocity values at periods larger than 20 seconds be in agreement with the values determined by the two-station method. An assumption made was that the initial phase was frequency independent (*i.e.* they used the same values of N to

determine c(T) for periods less than 20 sec). For these measurements, they believe the main sources of errors are the uncertainties on the initial phase estimate, and on the location of the epicenters. An accuracy of 0.03 km/sec was estimated considering these two sources of error (this corresponds to a 1 percent error for 2 sec waves, and 0.8 percent error for 40 sec).

The average phase velocity dispersion curves for the Canadian Shield were then compared with the dispersion curves obtained by several workers in other regions: Press (1957, 1960), Ewing and Press (1959), and Oliver *et al.* (1961). The crustal thickness for the Canadian shield is then obtained by means of this comparison.

The average data for the Canadian shield was also used (after the sphericity correction introduced by Bolt and Dorman, 1961 was applied) to obtain a layered structure that best explained the observed data. The method used was introduced by Dorman and Ewing (1962) and is based on the least squares fit between observed and theoretical dispersion curves.

2.4.2 - Published measurements using the two-station method:

In this section, we refer to the publications we found in the literature where the phase velocity of Rayleigh waves was measured using the two-station method. Some of the references also include phase velocity measurements using other methods. The phase velocity dispersion curves in these papers were all included in our database (unless stated otherwise when we refer to the paper in here).

Thomson and Evison (1962) studied the phase and group velocity dispersion curves obtained from the study of earthquakes recorded by a local seismic network in New Zealand. The purpose of the study was to measure the thickness of the crust in that region, in order to determine if it is either continental or oceanic. They applied the three-station method to determine the phase velocity for two small arrays and the two-station method to measure the phase velocity for a path along the main island. Waves generated by two earthquakes were used in the phase velocity measurements: one with epicenter in the Samoa Islands region, and the other with epicenter in Wyoming, U.S. The latter was the one used in the two-station measurement. The crustal thickness,

determined by the comparison between observed and calculated phase and group velocity dispersion curves, made them conclude that the crust in the region is of continental kind.

The study of phase velocity of Rayleigh waves in Australia was pioneered by Bolt and Niazi (1964). They measured the phase velocity for periods ranging from 13 to 42 sec for two paths in Australia, using the two-station method and records from two earthquakes, one located in the Loyalty Islands, the other one in the Solomon Islands. The deviation angle between the greatcircle path joining the events to the first station, and the greatcircle joining the two stations, was 4 degrees for one path and 18 degrees for the other. The resulting phase velocity curves were compared with calculated values and with values obtained by Brune and Dorman (1963) for the Canadian Shield. The crustal thickness in the area covered by the paths was then obtained from this analysis, aided by the information gathered by a similar comparison of the observed and calculated group velocity dispersion curves.

In another study of Rayleigh waves propagating in Australia, Thomas (1969) measured the phase velocity for 39 paths, between four W.W.S.S.N. stations located within that continent (ADE, CTA, MUN, and TAU). The period range covered

was between 15 and 58 sec, and the dispersion curves were used in an inversion process in order to find a shear velocity profile for each of the regions covered. This inversion was carried out using the average dispersion curve obtained for each of the six interstation paths for those stations. These curves were compared to calculated curves from assumed crustal models, and to the curves obtained by Brune and Dorman (1963) for the Canadian Shield, and by Bolt and Niazi (1964) in Australia.

Landisman *et al.* (1969) measured the phase velocity of Rayleigh waves travelling in a path between W.W.S.S.N. stations CTA and ADE. The period range studied was 15 to 180 sec, and three earthquakes were used in the determination of dispersion curves. The standard deviation reported for these measurements is 0.016 km/sec, but the period corresponding to this estimate was not specified. In the data processing of the digitized seismograms, time variable filtering was used, together with Fourier analysis, after the group velocity used to design the filter was calculated by application of moving window analysis to the seismograms. These techniques were described earlier in the same paper, and are important since several of the authors whose work we reviewed here made use of this sequence in the data treatment.

Gupta and Negi (1970) considered the Rayleigh wave phase velocity data obtained by Bolt and Niazi (1964), and by Thomas (1969), that we just referred above. They determined the group velocity dispersion curves for the several paths studied by those previous workers through differentiation of the phase velocity curves. These group velocity curves were then compared to the reference group velocity curves of Santo (1965b). The conclusion is that the Australian data are best represented by the shield region dispersion curves. The phase velocity data set included in the work of Gupta and Negi (1970) was collected from those previous works in Australia that we have just reviewed, and was then not included in our database.

Goncz et al. (1975) investigated the phase velocity dispersion in Australia for periods up to 200 sec, from the records of 44 earthquakes of the same five W.W.S.S.N. stations used by Thomas (1969). In this study, signal processing was performed using Fourier analysis, in contrast with the peak and trough method used by Thomas (1969). The authors believed that the use of the techniques described by Dziewonski *et al.* (1969), and summarized by Dziewonski and Hales (1972) allowed them to obtain better signal for long periods. We will

discuss these techniques later in this section. The measured phase velocity dispersion curves were used together with group velocity data for both Rayleigh and Love waves to study the structure of Australia. The deviation angle between the path joining the two stations and the greatcircle to the events ranged from zero to about 13 degrees.

The phase velocity dispersion curves for two paths in Finland were measured by Noponen (1966), from the records of five earthquakes located in Greece. In this work, Fourier analysis, after band-pass filtering, and phase smoothing of the seismograms, was used to determine the phase differences for the two-station method calculation of phase velocity. The three stations used in the measurement were all aligned in the same greatcircle path from the earthquakes. The deviation angle between paths joining two stations and the greatcircle paths to the events, was less than four degrees for all cases. Dispersion curves for each station pair were averaged, and the mean standard deviation was found to be less than 0.02 km/sec (less than 1 percent error for the period range covered: 9 to 40 sec). The phase velocities for the two station pairs used (that cover different regions of Finland) were found to be the same. The observed errors in the measurements were related to

possible problems with timing, instrument response, deviation angle between greatcircle path and the two-station line, or with data processing errors. It was found that none of these sources could explain the observed error and the author suggested that further measurements could clarify this point. A comparison wth the results of Brune and Dorman (1963) for the Canadian Shield, indicated that the phase velocity curves for these two areas are different.

We have already referred to the work of Payo (1965) in the section on measurements using the three-station method. We will now describe on the measurements he made on the 16 to 60 sec period range using the two-station method. These were made for the path between W.W.S.S.N. stations MAL and TOL, using records of six different earthquakes, and one Russian nuclear explosion. The peak and trough method was used to calculate the period of the phases. The standard deviation for the calculated average using the seven measurements reported in this paper is 0.05 km/sec (about 1.5 percent of the typical value for 16 sec period, and 1 percent for 60 sec period). The crustal thickness in the region was evaluated using the average phase velocity dispersion curve, together with other geophysical data.

The eastern portion of the Mediterranean region was studied by Papazachos (1969), who made a total of five phase velocity measurements for the 15 to 60 sec period range, using the two-station method. The measurements were made for paths between stations AQU, ATU, HLW, IST, AND TRI, that belong to the W.W.S.S.N., using records of 14 earthquakes. Three of the paths studied had the phase velocity determined by measurements that used waves approaching from both directions of the profile. All measurements were made using the peak and trough technique to determine the period and the phase difference of the waves. The resultant phase velocity dispersion curves were used to determine the crustal structure for each path, by comparing the observed dispersion curves with curves calculated considering crustal models based on the body-wave information available for each case.

Payo (1969) studied the crust and upper mantle structure of the Mediterranean Sea. In this study, he measured the phase velocity of Rayleigh waves for the 20 to 60 sec period range by the two-station method for six paths using waves from six different earthquakes. The seismograph stations on this part of his study all belong to the W.W.S.S.N. The paths for the two-station method analysis were all between stations AQU

and TOL, or between AQU and MAL. The deviation angle of these paths from the greatcircle of the events was less than 0.7 degrees for measurements between AQU and TOL, and less than 2.5 degrees for measurements between AQU and MAL. These measurements were compared with the observations made by Berry and Knopoff (1967), which we have already reviewed. One-station method measurements were also made using earthquakes within the studied area. These measurements will be reviewed in a later section, where we will refer to this paper again on the summary of measurements made using the one-station method. We should just add here the fact that Payo (1969) used all the information he obtained from the dispersion curves he measured, together with information from gravity and travel time studies in the Mediterranean Sea, to compare the eastern and western portions of this area. The main conclusion is that the two portions have signifficantly different crustal and upper mantle structures.

The Iberian Peninsula and the Mediterranean Sea were further studied by Payo and Ruiz de la Parte (1974). This time, Fourier analysis was used to study the crust and upper mantle structure of these areas and of part of the North Atlantic. Phase smoothing was applied to the obtained phase

spectra. The inversion of the observed dispersion curves was performed in order to study the shear-wave velocity structure of these regions. Errors related to the measurements were not discussed in their work, neither the deviation angle of the paths from the greatcircle to the events.

Gabriel and Kuo (1966) reported the results of four phase velocity measurements for the path between W.W.S.S.N. stations LAH (located in Pakistan), and NDI (located in India). They used the records of four events located in southeastern Asia, to obtain the phase velocity for the 15 to 40 sec period range in that area. Reverse profiles, using events located in North and South America, were reportedly used in the study, although the results of these measurements are not shown in the paper. They just mention that, for some period band, these later measurements agree with the former. The measurements using waves generated by the events in southeastern Asia are used to determine, by trial and error fitting of the observed and calculated dispersion curves, a model for the crustal and upper mantle structure in the area. The theoretical dispersion curve calculated for this model was then compared with the Canadian Shield structure determined by Brune and Dorman (1963), and to the continental dispersion curve shown in the work of Oliver (1962).

Another phase velocity calculation in India was reported by Gupta *et al.* (1977) between the W.W.S.S.N. stations CHG (located in Thailand) and NDI (located in India). The phase velocity values were reported in the 70 to 200 sec period range, and were calculated using the records of an earthquake with epicenter located in the New Hebrides Islands. They used Fourier analysis in the phase velocity determination. The maximum measurement error reported is 0.1 km/sec (about 2.5 percent in that period range, if we consider typical phase velocity values obtained).

Further surface wave studies in Asia include those by Levshin *et al.* (1966), that determined the phase velocity of Rayleigh waves in the 12 to 36 sec period range using two stations and events located in the Kuril Islands and in the Kamchatka regions. The reported standard deviation of the phase velocity dispersion curve obtained is about 0.05 km/sec (about 1.6 percent for 12 sec period, and 1.3 percent for 36 sec). These results were used, together with travel time of P and S waves observed for local events, to determine the crustal structure of that area.

Savarensky *et al.* (1969) used both the peak and trough method and Fourier analysis to determine the phase velocity in

some regions of Asia using the two-station method. They studied waves in the 10 to 50 sec period range and reportedly measured the phase velocity in the reverse direction in one of the profiles, in order to check the results. They also compared the results obtained by the analysis using the peak and trough method with those obtained using Fourier analysis for determination of the phase spectra. The resultant phase velocity curves for the three station pairs studied, were analyzed using calculated dispersion curves for some crustal models, in order to determine the local crustal model in each case. They also reported phase velocity curves obtained using the three-station method.

Another Asian study including phase velocity dispersion curves of Rayleigh waves is that of Proskuryakova *et al.* (1970) in the Black Sea region. They measured the phase velocity of these waves in the 20 to 90 sec period range using three station pairs and waves generated by eight earthquakes. As in the paper we have just reviewed (Savarensky *et al.*, 1969), both the peak and trough method and Fourier spectral analysis were used to determine the period and phase. They also reported the resultant crustal structure obtained from the comparison of the observed dispersion curves with those calculated from theoretical crustal models.

Brooks (1969) reviewed both the two- and the one-station phase velocity measurement methods, and the results obtained by several workers to that date. The inversion techniques used to obtain the crustal and upper mantle structure for a region from the observed phase velocity dispersion curves were also reviewed. Two-station phase velocity measurements were performed using records of three events by three station pairs located in New Guinea. The period range from 10 to 50 sec was studied by this method. One-station measurements were also made in the region, this time in the 8 to 70 sec period range. We shall refer to Brook's (1969) work again in the section on the one-station method. The RMS deviation of the measured phase velocity data was estimated by fitting a polynomial to the observations. The reported value was about 0.02 km/sec for the whole period band studied. This value was compared with error estimates done by other workers for previous measurements in other areas. The interpretation of the observed phase velocity dispersion curves was made through the analysis of the result obtained by the inversion of those curves. These results are compared with the models obtained by Brune and Dorman (1963) for the Canadian Shield and other models.

In southern Africa, the phase velocity of Rayleigh waves in the 20 to 110 sec period range was also determined by Bloch and Hales (1968). They used Fourier analysis of digitized seismograms of three W.W.S.S.N. stations: BUL, PRE, and WIN thatrecorded eight earthquakes. The reported deviation angle between the station paths and the greatcircle path from the event was less than 5.5 degrees for all cases. The records were processed first using the moving window analysis to determine the group velocity of fundamental mode Rayleigh waves. The next step of data processing was the application of the time variable filter to the signal and then the phase velocity calculation was performed. Some smoothing was also applied to the phase velocity values. The details on how each step was performed are summarized by Landisman *et al.* (1969). The measurements made by Bloch and Hales (1968) were later used by Bloch *et al.* (1969), together with other geophysical data, to study the structure of southern Africa.

Further studies on the phase velocity of Rayleigh waves in Africa were performed by Gumper and Pomeroy (1970), who made measurements in the 30 to 63 sec period range. They were interested in studying the structure of the shield regions in that continent. The measurements were performed using three

earthquakes located in Eurasia and in South Africa, and recorded by eight station pairs. The period and the phase differences were obtained using the peak and trough method. The deviation angle between the paths used for the measurements, and the greatcircle paths to the events was less than five degrees in all cases. The measured phase velocity values were corrected for the sphericity of the Earth using the empirical relation obtained by Bolt and Dorman (1961). These corrected values were then used in a trial and error search for a model that would lead to theoretical dispersion curves consistent with these observations.

The model determined by Gumper and Pomeroy (1970) for Africa was used by Long *et al.* (1972) to study the crustal and upper mantle structure of an area along the East African Rift. In their work, they compared the phase velocity dispersion curves obtained for paths between W.W.S.S.N. stations AAE and LWI, AAE and NAI, and BUL and NAI. For the last two paths, measurements were taken in both directions of the profile. The phase velocity curves were reportedly obtained using Fourier analysis in the data processing.

Gregersen (1970) measured the phase velocity of Rayleigh waves in the 17 to 54 sec period range for two W.W.S.S.N.

station pairs (KTG to GDH, and NOR to GDH). The resultant dispersion curves are the same for these two paths. The peak and trough method was used in the determination of the period and phase differences for the recorded waves. The deviation angle between the paths containing the station pairs and the greatcircle paths to the 21 events used was reported for each case. The waves generated by these events approached the profiles from both directions, and the deviation angle was less than 20 degrees in all cases. Only the calculated mean for all the measurements was reported. The standard error calculated for this curve is 0.061 km/sec for all periods (less than 2 percent error for 17 sec, and less than 1.5 percent error for 54 sec, if we consider the mean value obtained at these periods). This uncertainty was associated by Gregersen (1970) to measurement errors, and to contamination of the waves by the effect of inhomogeneities prior to the arrival of the wave fronts to the first station in the path. The deviation angle up to 20 degrees was found to have no signifficant effect on the observed standard error for the average. This was tested by considering the standard errors and the calculated averages using only data for deviation angle within certain limits. Effects due to

refraction of waves within the profiles were also tested and no significant influence was detected. The calculated mean for all the measurements was then corrected for the Earth's sphericity and used to determine a shear velocity profile for the crust and upper mantle of that region. The resultant profile was compared with the one obtained by Brune and Dorman (1963) for the Canadian Shield.

In South America, the phase velocity of Rayleigh waves was first studied by James (1971) and by Sherburne and Alexander (1971). James (1971) used the two-station method to determine the phase velocity for waves with period ranging from 15 to 160 sec approximately. He used eight earthquakes in these calculations, and none of these were used in reverse profiles. The deviation angle between each station pair path and the greatcircle path to the earthquake was less than 3.5 degrees for all cases. Ellipticity correction was used to calculate the interstation distances for the measurements. All the profiles studied lie within the east Andean region. The data processing techniques used are based on the work of Dziewonski *et al.* (1969) and similar to those described above in reference to the work of Bloch and Hales (1968). Group velocity for Rayleigh waves was determined in this data

processing, and Love waves phase and group velocities were also determined. All these data were used to obtain the crust and upper mantle structure for the area. In the phase velocity data set, the trial and error fit to calculated dispersion curves using the Haskell (1953) technique was applied. The observed values were corrected for the sphericity of the Earth prior to this trial and error fit. The uncertainty in the phase velocity measurements were estimated to vary from about 0.01 km/sec to about 0.05 km/sec. These estimates were based on the scatter of the measured values and were related to effects due to inhomogeneities within the regions studied. If we consider the largest error estimation, 0.05 km/sec for the typical phase velocity values measured for 15 sec and 100 sec periods, we obtain errors of about 2 percent and about 1 percent, respectively. The main result of this work is a contour map of crustal thickness for the area studied.

The study reported by Sherburne and Alexander (1971) refers to measurements of phase velocity for Rayleigh waves propagating in the eastern portions of South America. We could not include these observations in our database because we did not find these dispersion curves in any publication.

They report in their work that a crustal and upper mantle structure for that area was found, and that it is similar to the results for other tectonically stable areas obtained by other workers.

McEvilly (1964) measured the phase velocity dispersion curves using the two-station method applied to 13 station pairs located in the central U.S. region, using records of 13 different earthquakes. A three-station method measurement was also made in the same area using records of another event. We could not include these data in our database because the resultant dispersion curves were all plotted in the same figure without identification of the measurements. Both the peak and trough method and Fourier analysis were used in the phase velocity determination. The reported accuracy of the measurements is about 0.02 km/sec for the whole period range studied (10 to 60 sec). For typical values, this corresponds to a 1.5 percent accuracy for 10 sec, and 0.5 percent accuracy for 60 sec period. The observed dispersion curves were used to get the crustal and upper mantle structure for the area. Love wave dispersion data measured in the same work, together with refraction data for the area were used as constraints in this determination.

Biswas (1971) studied the phase velocity of Rayleigh waves in the 20 to 250 sec period range in the U.S.. He measured the phase velocity for 18 interstation paths using the records of the W.W.S.S.N. for 11 different shallow earthquakes. The deviation angle between the interstation paths and corresponding greatcircle to the epicenter of these events was less than 7 degrees for all cases. A time variable filter similar to that described by Pilant and Knopoff (1964) and Knopoff *et al.* (1966), was applied to the records prior to the phase velocity determination, which was made using Fourier analysis. For 100 sec period, an estimate of the uncertainty on the determination of the phase difference showed that the phase velocity uncertainty in this study is about 1 percent. The phase velocity data were divided according to the tectonic setting of the region of each measurement, and significantly different crustal and upper mantle structure was obtained for each region from the inversion of these curves after the sphericity correction (Bolt and Dorman, 1961) was applied. This work was also reported in another publication by Biswas and Knopoff (1974).

A previous study of the phase velocity of Rayleigh waves in the 20 to 51 sec period range propagating in North America

was done by Pilant (1966a,b and 1967). In his first report, Pilant (1966a) presented a set of five maps for this region showing contour lines corresponding to the phase time delay for a set of five periods (20, 25, 33.3, 40, and 51 sec). These delays were measured between seismographic stations using records of one event with epicenter in the Mid Atlantic ridge. The second report (1966b) contains the results of the phase velocity measurements using the two-station method using records of five earthquakes from those seismographic stations. These data were used to construct a contour map of phase velocity distribution for North America for each of the reference period values above. These maps were modified using the results of the analysis of additional events, totalling 12 earthquakes, in the work reported by Pilant (1967). We did not include these measurements in our database since it was not clear which limit was used for the deviation angle in all these measurements, since this is an important reference as shown in the similarity between the analysis used in the work above, and the analysis we describe in Chapter 5, concerning the determination of the phase velocity for each portion of the path from the path-averaged value obtained in the phase velocity measurement.

Mitchel (1977) reports two measurements of phase velocity in the 20 to 100 sec period range between two station pairs in North America (between W.W.S.S.N. stations TUC and UNM, and BKS and UNM). He does not indicate which events were used in the measurements, nor gives any information on the errors involved in the data.

Phase velocity two-station measurements in Africa have been reported by Knopoff and Schlue (1972). They measured the phase velocity in the 20 to 125 sec period range for 3 paths between W.W.S.S.N. stations located in northeastern Africa and in the Middle East. Records from 3 different earthquakes were used. Band-pass filtering, after group velocity determination, was applied to the seismograms. The phase velocity was obtained using Fourier analysis. The phase velocity values were then corrected for the Earth's sphericity using the empirical relation determined by Bolt and Dorman (1961), and used in an inversion process to determine the regional crust and upper mantle structure. The reported standard deviation for the measurements was 0.03 km/sec (less than 1 percent for all typical values obtained on the 20 to 100 sec period range).

In an earlier work on the phase velocity of Rayleigh waves in the Middle East region, Niazi (1968) measured the phase velocity for the 20 to 48 sec period range between W.W.S.S.N. stations AAE and SHI. He used the records of a shallow earthquake that occurred in the South Sandwich Islands region. The deviation angle between the two stations line and the greatcircle from AAE to the epicenter was 0.4 degrees. He used the peak and trough method in the phase velocity determination. The resultant phase velocity dispersion curve was corrected for the sphericity of the Earth following Bolt and Dorman (1961), and then used to determine the crustal structure of the region. The crustal thickness he got was comparable to the one Brune and Dorman (1963) obtained for the Canadian Shield.

Fouda (1973) measured the phase velocity using the two-station method in the 20 to 100 sec period range for seven paths in India, southern Africa, and in the Middle East. He used stations from the W.W.S.S.N. and records of five earthquakes. Some of the measurements are referred in another publication (Knopoff and Fouda, 1975). The data processing techniques are the same as described by Knopoff *et.al.* (1966) (in this case, moving window analysis to calculate the group

velocity, and Fourier analysis were used). The resultant phase velocity values were interpreted for each separate region where the measurements were taken. After correction for sphericity using the relationship introduced by Bolt and Dorman (1961), the crustal and upper mantle structure of each region was obtained through inversion of the phase velocity data. The standard deviation of the phase velocity measurements was assumed to be the same as that estimated by Biswas (1971) (*i.e.*, 0.03 km/sec) for the whole period range, and for all measurements. We would like to add that the standard deviation value reported by Biswas (1971) was 1 percent. We will take this as the same for the work of Fouda (1973) because in this later work, the same data processing procedure as Biswas (1971) was reportedly used.

Moazami-Goudarzi (1974) determined the phase velocity of Rayleigh waves within the 25 to 53 sec period range between two W.W.S.S.N. stations located in Iran (MSH and SHI) using records of nine earthquakes.

Further studies in Iran and in the Arabian Peninsula area are reported by Tubman (1980), who used two-station method to measure the phase velocity between the W.W.S.S.N. stations MSH and SHI for the 15 to 50 sec period range. He determined four

phase velocity dispersion curves, for waves from four earthquakes located in the Red Sea, and in Central Asia. The deviation angle between the two-station path and the greatcircle to the events was roughly 5 degrees for two measurements, and about 11 degrees for the other two. The method described by Dziewonski *et al.* (1969) involving Fourier analysis of the records, was used in the phase velocity determinations. The dispersion curves, and those obtained using the one-station method were inverted, together with the group velocity curves for the area, using a maximum likelihood scheme. The shear velocity profile for the crust and upper mantle were then obtained. The estimated error for the phase velocity measurements was 0.09 km/sec for all periods (this corresponds to about 3 percent error at 15 sec, and 2 percent at 50 sec).

In Europe, Panza *et al.* (1978), determined the phase velocity of Rayleigh waves in the 10 to 60 sec period range for a path between two stations located in East Germany. They used two earthquakes for the measurements in the two opposite directions and averaged the two measurements, that showed consistency. For the data processing, time variable filtering was used following Landisman *et al.* (1969). In another data

processing sequence they used, this step was replaced by applying a different bandpass filter, this time one of the Butterworth type. The largest assumed error for the period range studied was 0.05 km/sec (about 1.6 percent at 10 sec, and 1.3 percent at 60 sec).

Stuart (1978) measured the phase velocity for 15 paths, corresponding to waves generated by 15 different earthquakes for three interstation profiles, between W.W.S.S.N. stations COP, ESK, and KON, all in northern Europe. Each interstation profile was studied using waves generated by at least one event in each direction. Consistent dispersion curves were found for all measurements in the 13 to 100 sec period range. The maximum deviation angle between the path joining two stations and the greatcircle path to the epicenter was less than 4.2 degrees for all cases. Statistical analysis showed that the calculated mean for each inter-station path is not significantly different from the other two. An average dispersion curve for the North Sea was then calculated using all three means for those paths. The calculated standard deviation for the average reported in his work is about 0.04 km/sec for 100 sec, and about 0.02 km/sec for 13 sec (approximately 1 percent at 100 sec, and 0.6 percent at 13

sec). This average phase velocity dispersion curve was corrected for the Earth's sphericity using the empirical relation of Bolt and Dorman (1961), and then used in an inversion process to determine the shear wave velocity distribution for a typical profile in the area.

The phase velocity of Rayleigh waves in the 15 to 100 sec period range was studied by Calcagnile and Panza (1978) for three inter-station paths through the Barents Sea and Fennoscandia. They used the same data processing techniques described in the work of Biswas (1971) or Biswas and Knopoff (1974), which we reviewed previously. For each of the three interstation profiles studied, they calculated the average phase velocity using six measurements, including some measurements done by other authors in the area. The maximum standard deviation for these averages reported in their work is 0.05 km/sec (almost 1.5 percent at 15 sec and 1.2 percent at 100 sec).

A synthesis of the published phase velocity data for the Fennoscandia region, measured using the two-station method for waves in the period range considered in our work, was done by Calcagnile (1982). The data set used consists of 12 phase velocity measurements, some of them by works we have reviewed

above (Noponen, 1966, Stuart, 1978, and Calcagnile and Panza, 1978). The main result is a set of four maps of Fennoscandia showing the contour line distribution of phase velocity for 25, 40, 50, and 80 sec. These regionalized models were then used, through inversion, to obtain the crust and upper mantle shear wave structure for that region.

Soriau-Thevenard (1976a) measured the phase velocity of Rayleigh waves in the 15 to 50 sec period range for five paths between two stations in France. The same measurements are presented in another paper, Soriau-Thevenard (1976b). These measurements were made using records from five earthquakes. The maximum deviation angle between the two-station path and the greatcircle to the epicenter was 11 degrees. She used both the peak-and-trough method, and the cross-correlation of seismograms after time variable filtering, for the phase velocity determination. The measurements include paths in both directions of the profile. A graphic representation was presented, showing estimates of the errors obtained for the phase velocity dispersion curves. These estimates vary with period from about 0.05 km/sec at 15 sec, and decreases to about 0.02 km/sec at 30 sec. It then increases to about 0.07 km/sec at 50 sec (approximately 0.6 to 0.5 and then to 0.2

percent errors, respectively). The average value for the path was corrected for the effect of a sedimentary layer, and for the Earth's sphericity (Bolt and Dorman, 1961). It was then used to determine the shear wave velocity profile through the crust and the upper mantle.

In another study on the phase velocity of Rayleigh waves in France and in northern Europe, Soriau (1979) reported 27 additional measurements. These were made using W.W.S.S.N. stations COP, ESK, STU, and VAL, and three stations from the french network. She studied the period band from 25 to 150 sec. The measurements were made between five station pairs using records of 27 earthquakes. The maximum deviation angle between the station paths and the greatcircle to the epicenter was 19.7 degrees. The data processing sequence used includes time variable filtering applied to the records, and the determination of the phase velocity was made using cross-correlation between the records. The phase velocity values were corrected for the effect of sediments in the region. These values were then used to obtain, through inversion, the shear velocity profile for the crust and upper mantle for each profile.

Soriau and Vadell (1980) determined the phase velocity of Rayleigh waves with period ranging from 20 up to 170 sec for eight paths between stations located in the Pyrenees region. They used records of nine earthquakes. The maximum deviation angle for this study was 13.8 degrees. They used time variable filtering on the records, and determined the phase velocity using cross-correlation of the records from each station pair. The dispersion curves were again used to determine the shear wave velocity structure of the area.

The phase velocity of Rayleigh waves with period ranging from 20 to 100 sec in Italy was measured by Caputo *et al.* (1976) between stations AQU and TNO, both with W.W.S.S.N. equipament. The data processing techniques used are those described by Biswas (1971), which include band-pass filtering of the data, and Fourier analysis for the phase velocity calculation. The deviation angle between the two-station paths, and the greatcircle to the epicenter of each of the two earthquakes located in the North Atlantic used in the measurements, was less than 3 degrees. The maximum difference in phase velocity values obtained for these two measurements was 0.04 km/sec (this corresponds to an uncertainty of about 1.2 percent at 20 sec, and 1 percent for 100 sec, considering

the phase velocity values measured at these periods). The average value obtained from the two measurements was then corrected for the sphericity of the Earth using the relation of Bolt and Dorman (1961), and used to obtain the crust and upper mantle shear wave velocity profile for the area. The phase velocity in the 20 to 80 sec period range for this same region was determined in another work by Mueller and Sprecher (1978). They studied the Apennines region of Italy using the results of application of the two-station method in the area. These were also used in an inversion process for the determination of the shear wave velocity profile.

Baldi *et al.* (1979) studied the phase velocity of Rayleigh waves with period ranging from 20 to 130 sec measured for eight paths in Italy using the two-station method. Three of these paths had already been studied by Baldi *et al.* (1978). For the latter, the maximum reported deviation angle from the two-station path to the greatcircle to the epicenters, was 7 degrees. Considering both references above, a total of nine earthquakes were used in this study. The data processing techniques were the same as used by Biswas (1971). These include filtering of the data, and Fourier analysis. For the determination of the shear velocity profile through

the crust and upper mantle, the phase velocity values were transformed to account for the Earth's sphericity following Bolt and Niazi (1961). The maximum standard deviation associated with the measurements was about 0.05 km/sec for all periods (1.4 percent for 20 sec and 1.2 percent for 100 sec, considering typical phase velocity values obtained for these periods).

Calcagnile and Panza (1980) used the two-station method to determine the Rayleigh wave phase velocity for two pahts between two pairs of stations in Italy in the 20 to 190 sec period range. They used records of two earthquakes, one located in the South Atlantic and the other in the Queen Charlotte Islands. The maximum deviation between the measurement path and the greatcircle path to the epicenter was 6 degrees. The method of measurement used was the same as Biswas (1971). The standard deviation reported at 20 sec was 0.07 km/sec, at 96 sec it was 0.05 km/sec (2 percent at 20 sec and about 1.2 percent at 96 sec, considering the average value at these periods). An inversion for the crust and upper mantle velocity structure was performed using the average dispersion curve obtained from the measurements.

An area in southeastern Europe was studied by Calcagnile *et al.* (1984) using the two-station method to obtain phase velocity values for Rayleigh waves with period ranging from 30 up to 250 sec for four different paths. They used records of W.W.S.S.N. stations AQU, ATU, and IST for four earthquakes in their work. The measurement process used was the same as the preceding references. The deviation of the interstation paths from the greatcircle to the epicenter was less than 7 degrees for all cases. The standard deviation for the period band from 30 to 100 sec was 0.06 km/sec for all cases (this corresponds to about 1.6 percent at 30 sec and 1.4 percent at 100 sec). The inversion process used by Biswas (1971) was used to obtain the shear wave velocity profile for the crust and upper mantle of the three paths for which the measurements were made (since two of the measurements were between stations ATU and IST).

A path between a station in the Madeira Islands and a station in southern Protugal, and another path between that station in Portugal, and one in Switzerland, were studied using the records of 12 earthquakes to measure the phase velocity for periods between 15 and 260 sec. For both paths, seven measurements were made, totalling 14 measurements in

Mitrovas' (1977) work. The seismograms were processed using time variable filtering after moving window analysis was used to determine the group velocity dispersion curve (as proposed by Landisman *et al.*, 1969). Mitrovas (1977) reportedly determined the phase velocity in the area using the three-station method, with the objective of checking the deviation of the wave path from the greatcircle to the epicenter. No significant deviation was found and this test served to assure that the approaching waves were not been affected by lateral heterogeneities in their propagation. For one of the station pairs, measurements were made using waves approaching from both directions. The angle between the two-station path and the greatcircle path to the epicenter was less than 10 degrees for all 14 measurements. From all these, the average phase velocity dispersion curve was obtained for each of the two profiles using the seven measurements reported for each one. The calculated standard deviation of the average ranges from 0.028 km/sec for 20 sec, to 0.009 km/sec for 100 sec perios (it ranges from 0.7 percent for 20 sec to about 0.2 percent for 100 sec, considering the average values in each case).

For Antarctic, Knopoff and Vane (1978) measured the phase velocity of Rayleigh waves in the 22 to 74 sec range using the two-station method for three paths and using two W.W.S.S.N. stations in that continent (SBA and SPA), and a third station with equipament similar to W.W.S.S.N. installed in a soviet station. Records of two Tonga earthquakes were used, with the deviation angle between the greatcircle and the station pair path being less than 7.3 degrees for all measurements. The data processing was done following the sequence described by Biswas (1971). Caution should be taken on the values reported for the path from SPA to the Russian station, because they reportedly used records for two different events, one recorded by each station. A correction was used in this measurement so that the travel time difference due to the different location of the two events would be accounted for. The initial phase of the two events were assumed to be the same from the similar fault plane solutions obtained from the first motion of P waves. The main coclusion from their work is that the structure of Antarctic is similar to the structure of other shield regions.

In the Pacific region, Kaminuma (1966a), whose work we have already reviewed, measured the phase velocity in Japan

for six interstation paths travelled by waves of six different earthquakes, using the same station pair for all these, and included the phase velocity values for the same path measured using the records of another event, which was previously studied by Kaminuma and Aki (1963). The errors involved in those measurements, together with other data processing information, were mentioned earlier.

Okal and Talandier (1980) measured the phase velocity of Rayleigh waves with period varying from 17 to 100 sec for four paths between stations located in the French Polynesia. In their study, ten earthquakes were used, with the deviation angle between the station paths and the greatcircle less than 2 degrees for all cases. The standard deviation for the measurements was about 0.02 km/sec for all periods, which was estimated from the variability of measurements taken along the same path and assumed as due to the digitizing of the records. For one of the measurements, the dispersion curve values were calculated for an interstation path with the event located in between the two stations. For this case, it was assumed that the initial phase for the event was the same for the two stations because of the particular source mechanism. This latter measurement served to estimate the effect that a nearby

structure, located outside the array, had on the waves approaching from teleseismic events. They correlated the presence of this structure with multipathing effects observed at the stations in records of teleseismic events. Comparison was made with results from previous works in the Pacific (Kausel *et al.*, 1974, Leeds, 1975, Forsyth, 1975, and Yu and Mitchell, 1979), where longer paths were used to determine the age-dependence and anisotropy of phase velocity.

Some recent works that have been reported recently include those of Sinno and Keller (1986), and Schlue *et al.* (1986) in the Rio Grande rift. Hadiouche *et al.* (1986) measured the phase velocity between two recently installed stations from the global GEOSCOPE in Africa.

2.5 - The one-station method:

2.5.1 - The method:

Brune *et al.* (1960) introduced the one-station method for measurement of Rayleigh wave phase velocity. In contrast with the other phase velocity measurement methods we reviewed sofar, this requires the knowledge of the initial phase of the waves at the source. This is due to the fact that we have to separate the phase change that is caused solely by the effect

of the propagation path. This separation of source and path effects was done in the other methods by using one or more additional stations assumed to share the common source effect.

The one-station method was first applied to Rayleigh waves recorded at Wyoming from a nuclear explosion in Nevada to determine the phase velocity for the period range from about 15 sec to about 35 sec. For the source function, they arbitrarily assumed an initial impulse form, and chose the unknown integer multiples of 2π by comparing with the reference curves of Press (1956b) at long periods. Brune *et al.* (1960), also studied Rayleigh waves from Russian nuclear explosion obtained at Uppsala, Sweden. They had an additional source of uncertainty, because the location of the source was determined based on data of only three swedish seismographic stations. We did not include this measurement in our data set. A third phase velocity measurement reported in their work is for a Canadian seismographic station of a Russian nuclear explosion at the Novaya Zemlya region. No remarks were made on the location uncertainties for this event, and we added the resultant phase velocity dispersion curve (in the 12 to 48 sec period range) to our database (Table 2.1). In this measurement, the cycle uncertainty was also solved by choosing

the dispersion curve with the most 'reasonable' values expected for these waves in this period range. A study of the possible initial phase of an earthquake with epicenter in the Hudson Bay region was made using the records of this event in a seismographic station located in Palisades, N.Y.. In this study, several dispersion curves, calculated for different initial phase values, were compared with the theoretical dispersion curves of Press (1956b). The curve which best fitted the dispersion curve expected for the region was chosen as the one representing the phase velocity curve for that path. Under the assumption that the initial phase was independent of the period, the selected dispersion curve yields the initial phase for that event-station pair. The authors admitted that this assumption was not always correct, and recommend further study of the source mechanism dependence of initial phase. We did not include the dispersion curve determined for this last path in our database.

The phase response curve for seismographs computed by Hagiwara (1958) was not correctly used by Brune *et al.* (1960), and an error of π was identified and corrected in a later paper by Brune (1962a).

The correct formula for the phase velocity c(T) of Rayleigh waves with period T measured using the one-station method is given by the following equation,

$$c(T) = \frac{\Delta}{t + \frac{T}{2\pi}\left[\phi^{s}(T) - \phi^{o}(T) + \frac{\pi}{4} + 2\pi N(T)\right]} \qquad (2.5)$$

where Δ is the epicentral distance of the observing station (Figure 2.3), t is the travel time of the Rayleigh wave package arriving at the station, $\phi^{o}(T)$ is the observed phase corrected for the instrument response, $\phi^{s}(T)$ is the source phase (dependent on the focal mechanism, depth of the event and the crustal structure), and N(T) is the integer used in the unwrapping of the observed phase. This latter variable is determined using the ***a priori*** knowledge of 'reasonable' phase velocity values at the longest of the period range with significant signal power.

The $\pi/4$ factor corresponds to the phase shift due to the dispersion, which should be eliminated if the Fourier method is used instead of the peak-trough method for measuring ϕ.

2.5.2 - Published measurements using the one-station method:

We proceed now to the review of the surface wave studies that included the measurement of phase velocity of Rayleigh waves with period less than 100 sec using the one-station method. As in the section where we described the measurements using the two-station method, all paths were included in our database, but in a few cases, which we specify in the text.

In the Pacific region, Kuo *et al.* (1962) determined the phase velocity of Rayleigh waves with period in the 20 to 140 sec range propagating from earthquakes that occurred in the Pacific to stations in the Fiji Islands, Hawaii, and in Japan. In their work, they assumed that the initial phase correction for phase velocity calculation using the one-station method was independent of the period. The initial phase was determined by choosing a value that will make the calculated phase velocity for long periods consistent with previously determined values for these periods. The period of the observed waves was measured using the peak and trough method. For the phase velocity dispersion curves obtained using the one-station method, they estimated that there was an error of

less than 0.03 km/sec for waves with period around 80 sec, and associated this error to uncertainties in the instrument correction, and to errors in the epicentral location of the events used.

They compared the results of the one-station method with those of the two-station method applied to the same region. Although the dispersion curves obtained using the two different measurement methods agree well, they believe that the ones measured using the one-station method are more reliable.

Papazachos (1964) used the one-station method to measure the phase velocity of Rayleigh waves with period between 15 and 60 sec for 31 paths between 21 earthquake epicenters located in Central America and in the Carabbean Sea, and four seismograph stations in the southeastern United States. In the calculation of the initial phase of these waves, it was assumed that it was independent of the period. The value of initial phase was selected so that the phase velocity at the longest period agrees with the theoretical value for a reference structure. He believes that the obtained initial phase values have an uncertainty of about one-eighth of a cycle. In the data processing for this work, Fourier analysis

was used to calculate the phase velocity. The resultant phase velocity dispersion curves were compared with the continental and oceanic standard curves compiled by Oliver (1962).

He also determined five phase velocity dispersion curves of Rayleigh waves in the 20 to 50 sec period range for five paths between station NDI of the W.W.S.S.N., and earthquakes with intermediate depth located in east India by the same procedure, except that the peak-trough method was used instead of the Fourier method.

We have reviewed the work of Payo (1969) in the section on the two-station method. In his work, he also used the one-station method to measure the phase velocity for nine paths for waves with period between 8 and 40 sec. These paths are from earthquakes with epicenter in the Mediterranean Sea to W.W.S.S.N. stations located in Italy and Spain. The initial phase for the Rayleigh waves generated by the events was obtained by the same method as used by Papazachos (1964). The author was aware that the initial phase value is not necessarily constant with period but he believed that the errors associated with the assumption were not signifficant.

Another work we reviewed in the section on the two-station method is that of Brooks (1969), who determined

the phase velocity of Rayleigh waves for six paths in the New Guinea region. In this work, paths between epicenters of four earthquakes located in western New Guinea and three stations in southern New Guinea were studied using the one-station method to measure the phase velocity of Rayleigh waves in the 8 to 70 sec period range. The initial phase was again assumed to be independent of period, and determined in the same way as Papazachos (1964). Fourier analysis was used to determine the phase.

Knopoff *et al.* (1969) used the one-station method for measuring the phase velocity of Rayleigh waves in the 10-65 sec period range from the records of earthquakes in the Rivera Fracture Zone region obtained in Gulf of California. The precision of these measurements was reported as better than 0.05 km/sec for all periods studied. The initial phase for these events was determined assuming the same strike-slip mechanism as found for larger events with epicenter in the same region. The determination of the initial phase followed the result of Knopoff and Schwab (1968). Fourier analysis was applied to band-pass filtered records. The resultant phase velocity dispersion curves were then used in an inversion process to determine the shear wave velocity structure of the crust and upper mantle for the region.

Weidner (1972) was the first to determine the phase velocity of Rayleigh waves in the 20 to 100 sec period range for 72 paths in the Atlantic Ocean, using the one-station method without assuming the focal depth and source mechanism. These paths were from two pairs of earthquakes with epicenter in the Mid Atlantic ridge, to stations of the W.W.S.S.N. and of the canadian network. His work was divided into two parts. In the first part, he describes a method for determination of the depth and focal mechanism of each earthquake, so that the source and path effects can be separated from observed Rayleigh wave amplitude and phase spectra. Both phase and amplitude spectra of the records were used in the determination of the depth and focal mechanism of the earthquakes. This is a major improvement over the amplitude spectra method, ***e.g.***, used by Mendiguren (1971) to study an earthquake located in the Nazca plate. He used records of two pairs of earthquakes located close to each other. At each pair of events, one has almost pure strike-slip mechanism and the other, almost pure dip-slip. The mechanism was determined using P-wave first motion observations for all four events. The initial focal mechanism was assumed to be about the same of the body-wave study, and the focal depth was allowed to

vary in the calculation of the differences between calculated and observed amplitude and phase spectra for each event pair. The focal depth and improved mechanism were then determined so that these differences would be as small as possible. In the calculations of theoretical spectra for a laterally homogeneous, vertically heterogeneous Earth model, he used the method of Saito (1967), initially used by Tsai (1969) to study amplitude and phase spectra of Rayleigh and Love waves. In both cases, the oceanic model of Harkrider and Anderson (1966) was used. The final depths and focal mechanisms determined by the above method were then used to calculate the initial phase of the Rayleigh waves for use in the phase velocity determination by the one-station method. A very important conclusion from the first part of his work was the strong dependence of the initial phase on the source mechanism and focal depth.

In the phase velocity determination, Weidner (1972) used time variable filters following Landisman *et al.* (1969), after determination of the group velocity dispersion curves by the moving window analysis technique. Fourier analysis was used in the phase velocity calculation. This second part of his work was reported in a later paper, Weidner (1974), where the

phase velocity data set are shown in figures, as well as in tables. He reports an extensive error analysis for the phase velocity measurements, of which the main conclusion is that the major sources of error are the mislocation of the earthquakes and uncertainties in the origin time. According to this analysis, the error in these phase velocity measurements is about 0.02 km/sec for paths about 4000 km long, and about 0.04 km/sec for paths about 2000 km long.

In addition to the phase velocity measurements using the one-station method, Weidner (1972) reports the results of two measurements using the two-station method. These measurements were made between W.W.S.S.N. stations MAL and TRN using records of an earthquake located in Greece, and between W.W.S.S.N. stations MAL and SJG, using records of an earthquake located in Central America. These phase velocity dispersion curves were compared with curves obtained by the one-station method for paths approximately aligned with the inter-station paths. The differences found in the comparison were very small (maximum of 0.02 km/sec at about 100 sec period), and associated with possible noise in the two-station method measurements (*i.e.*, with effects due to possible inhomogeneities outside the portion of the paths between

stations). The results of the measurements using the two-station method were also reported in the paper by Weidner and Aki (1973).

Forsyth (1973) measured the phase velocity of Rayleigh waves in the 17-167 sec period range for 76 paths in the East Pacific using the one-station method. These paths are from a set of 16 earthquakes with epicenter in the East Pacific to W.W.S.S.N. stations located in North, Central, and South America. Forsyth's (1973) objective was to study the dependence of the phase velocity of Rayleigh waves on the age of the sea floor. He also determined the relation between the phase velocity of these waves and their direction of propagation within an oceanic plate (Forsyth, 1975).

The focal mechanisms needed to measure the phase velocity by the one-station method were determined using both P-wave first motion, and Rayleigh wave amplitude radiation pattern for 14 of the earthquakes studied. For two other events focal mechanisms were determined from the observed P-wave first motion alone. For the calculation of the theoretical amplitude radiation pattern and the initial phase, the method of Saito (1967) was used, together with the oceanic Earth model of Harkrider and Anderson (1966) with a 3 km water

layer. Most of the events were of strike-slip type, and Forsyth (1973) assumed that their focal depths are all 5 km, instead of determining them as Weidner (1972) did using a pair of events with different source mechanisms. In the only case of the thrust earthquake located within the Nazca plate, Forsyth (1973) used the focal depth determined by Mendiguren (1971) to be about 9 km deep. For this event, the application of the amplitude radiation pattern yielded a very reliable focal depth.

Forsyth (1973) found that the phase velocity increases with the age of sea floor and that the phase velocity shows azimuthal anisotropy, *i.e.* the Rayleigh waves travel faster in the direction perpendicular to the ridge.

In the selection of the paths for which phase velocity was measured, the data obtained at stations lying within 10 degrees of a nodal direction were eliminated. Each record was processed using a moving window analysis to check if interference exists from refracted or reflected modes, or higher modes. If any of these interference sources were present, a time variable filter designed on the basis of the group velocity was used to separate the signal. The phase velocity was then calculated from the Fourier phase spectrum of the signal.

Two additional phase velocity measurements were reported by Forsyth (1973) using the two-station method. The same data processing described above was used to treat the records, and the phase velocity was calculated by the cross-correlation of the two seismograms at a station pair. The resultant dispersion curves from the measurements using the two-station method served as a check for the phase velocity determinations using the one-station method.

The error in all these phase velocity measurements was estimated to be at most 0.06 km/sec. Forsyth (1973) believes that this estimate is independent of the period. The largest part of the error was believed due to errors in the epicentral location.

Another set of Rayleigh waves phase velocity dispersion curves for the Pacific region was reported by Forsyth (1977) and included in our data base. This set corresponds to 23 paths in northwest Pacific where the phase velocity of Rayleigh waves was measured in the 20 to 200 sec period range by the one-station method using records of six W.W.S.S.N. stations from 4 earthquakes. The result confirmed the conclusions of his early work (Forsyth, 1973, 1975) on the relation between age of the sea floor and phase velocity of

Rayleigh waves. We believe that Forsyth (personal communication, 1985) used the same data processing sequence as in his earlier work, Forsyth (1973, 1975), but this information was not provided by Forsyth (1977).

The Pacific region was also studied by Leeds (1973), who measured the phase velocity of Rayleigh waves with period varying from 20 to 200 sec for 35 paths using the one-station method. He found an increase in phase velocity with the distance from the mid-ocean ridge, as in the work of Forsyth (1973). For his measurements, the initial phases of 11 earthquakes used in the measurements were calculated using a multilayered Earth model with a water layer and the focal mechanism and depth given by other authors from body wave observations. Most of the events had strike-slip focal mechanism. The records were processed following the steps described by Biswas (1971), which we reviewed earlier. The estimated error in the phase velocity measurements is 0.02 km/sec at 100 sec period. He found that the accuracy of the data decreases with increasing period, and the errors are mainly due to errors in source phase, origin time, and epicenter. The largest contribution is due to epicenter mislocation.

The phase velocity measurements made by Leeds (1973) were published by Kausel *et al.* (1974), and the results of the regionalization and inversion were published by Leeds *et al.* (1974). Leeds (1975) reported the measurement of seven additional phase velocity dispersion curves in the 30 to 160 sec period range for the Pacific area using the one-station method. The initial phases were calculated using the focal mechanism and depth given by other authors from body wave observations. The errors in the measured phase velocities were due to uncertainties on the focal mechanism, depth and epicenter, together with noise at the longer periods.

Schlue (1975), Schlue and Knopoff (1976, 1977) also used the same data set measured by Leeds (1973), together with Love wave phase velocity measurements, to study the shear wave structure of the crust and upper mantle, and the anisotropy effects on surface wave propagation in the Pacific region. Then, the data set formed by the phase velocity measurements of Rayleigh waves by Leeds (1973, 1975), and of Love waves by Schlue (1975), was used by Burkhard (1977) together with a free-air gravity anomaly data set for the Pacific in the determination of the crust and upper mantle structure under the sea-floor. He found the error bounds on the phase

velocity measurements of Leeds (1973) to be underestimated by a factor of two. In the inversion process, he considered the density at different depths as unknowns. This was based on the work of Burkhard and Jackson (1976), who show that the density effect on the surface wave phase velocities is larger than previously expected.

Other phase velocity studies in the Pacific were made by Yu and Mitchell (1979) and Mitchell and Yu (1980). Yu and Mitchell (1979) reported the result of the regionalization of phase and group velocities for Rayleigh and Love waves in the Pacific region located west of the East Pacific Rise. They measured the phase velocity of Rayleigh waves in the period range 16 to 110 sec for 33 paths using the one-station method. Records from W.W.S.S.N. stations of 12 earthquakes located around the Pacific region were used in the study. The focal mechanism of the earthquakes studied were taken from the published literature, and used in the calculation of the initial source phase. Paths within 15 degrees of nodal directions were not considered. In the data processing, group velocity was determined using the multiple-filter method of Dziewonski *et al.* (1969). The maximum error reported for the phase velocity measurements was 0.02 km/sec. In the analysis

of the measured data set, they detected the presence of anisotropy and of the increase of group and phase velocities with age. The shear velocity structure of each region was also determined. Yu and Mitchell (1979) reported only five of the phase velocity dispersion curves they obtained. We did not include these data in our database. In their second paper, Mitchell and Yu (1980) reported the regionalized phase and group velocities of Rayleigh and Love waves with some correction to the result reported in the first paper, which had incorrect epicentral location in that study. This time, the results of the regionalization are compared with those made by other workers in the Pacific region.

In the Indian Ocean, Patton (1973) measured the phase velocity for 19 paths from six shallow earthquakes, for which he calculated initial phases using the focal mechanism obtained from P and S-wave radiation pattern by other workers. The data processing steps follow the ones used by Forsyth (1973).

Panza and Calcagnile (1974) measured the phase velocity using the one-station method for Rayleigh waves in the 12 to 30 sec period range for a path in California, between the epicenter of the 1971 San Fernando earthquake and the station

BKS. Band-pass filtering of the records was used, after the determination of the group velocity values, and Fourier analysis applied to calculate the phase velocity dispersion curve. The mechanism of the earthquake and focal depth were known by other workers, using both body wave and surface wave radiation patterns. The initial phase at the source was calculated using this focal mechanism and depth.

Chang (1979) measured the phase velocity of Rayleigh waves in the 30 to 250 sec period range for 40 paths in Eurasia. The measurements used records from eight earthquakes and one nuclear explosion. The source mechanisms of these earthquakes were studied using the first motion of P waves except for one case, in which the observed radiation pattern of Rayleigh waves was compared with the theoretical pattern. The focal mechanism of eight events were taken from the Preliminary Determination of Epicenters issued by the U.S.G.S., and determined from the amplitude radiation pattern study of the last earthquake. The data processing and inversion procedure is the same as described by Biswas (1971).

We have reviewed the work of Tubman (1980) in a previous section on the two-station method determining the phase velocity for four paths in Iran and in the Arabian Peninsula.

We will discuss now the phase velocity measurements that he made using the one-station method. The sources used were two earthquakes with epicenter in the Red Sea, recorded at station JER. One of the earthquakes had the fault plane solution obtained in a previous work using P wave first motions. The focal mechanism of the second event was assumed to be the same as the first one. Errors in the measurements were estimated to be similar to the two-station method measurement (*i.e.*, about 0.09 km/sec for all periods). The major sources of error were both the timing errors in the seismograms, and the errors in the focal mechanism used for the calculation of source phase.

Liao (1981) studied the anisotropy effect in Eurasia. In her work, she used the Rayleigh wave phase velocity dispersion curves in the 30 to 250 sec, that were determined by Chang (1979). An addititonal set composed of four dispersion curves measured using the one-station method, and one measured using the two-station method, was also used. She combined the Rayleigh wave phase velocity data with Love wave phase velocity measurements she made, and used inverse theory to obtain the shear velocity structure of the upper mantle of several parts of Eurasia, in order to study the anisotropy

effect in the upper mantle of these regions. The phase velocity dispersion curve measured by Liao (1981) using the two-station method corresponds to a path in the Atlantic Ocean, between stations BEC and PTO. This dispersion curve was used together with the one obtained by Weidner (1972) in an attempt to determine the shear velocity structure of the upper mantle in the Atlantic. The records of an earthquake located in Central America were used in the two-station measurement. The four additional phase velocity measurements made with the one-station method used records of Eurasian W.W.S.S.N. stations of an earthquake with epicenter in Japan. The data processing of the records of the phase velocity measurements included band-pass filtering and moving window analysis, and the Fourier transform was used to obtain the observed phase.

The moment tensor representation of the free oscillations was introduced by Gilbert (1970). Equations for Love and Rayleigh waves in terms of moment tensor components were derived by McCowan (1976) and Mendiguren (1977). Mendiguren (1977) also proposed that the Rayleigh and Love wave observations could be used to obtain the moment tensor of earthquakes. Aki and Patton (1978) pointed out the need for

correction of the observed Rayleigh wave spectrum for the propagation effect prior to inversion for the moment tensor components. In order to make this correction, Aki and Patton (1978) estimate that the phase velocity dispersion curve for each path must be known with an accuracy of 0.5 percent. To achieve this accuracy, they recommended the Weidner (1972) method based on the use of two earthquakes with different focal mechanism that occurred at locations close to each other in a given region. The focal mechanism and the focal depth of other earthquakes in the same region can then be determined using observations at the stations for which we have obtained the phase velocity dispersion curves. These dispersion curves are then referred to the 'reference point', which is chosen to be close to the two initial earthquakes.

The technique described above was used by Patton (1978), who studied a set of nine earthquakes with epicenter in the Pamir region, in Asia. In his study, he determined phase velocity for 44 paths from the reference point in the epicentral region, to W.W.S.S.N. stations located at various azimuths from the point. The period of the waves studied ranges from 30 to 90 sec. These phase velocity measurements were used to regionalize the Eurasian continent into five

regions. He used the phase velocity values to correct the observations of Rayleigh waves by those W.W.S.S.N. stations which had reference dispersion curves. Patton (1978) was the first who actually applied the linear inversion formula of Mendiguren (1977) to actual data.

Patton (1978) was also the first to determine the focal depth by plotting residuals of the moment-tensor inversion as a function of trial depth.

Errors in the phase velocity measurements were considered by Patton (1978) as due to a series of possible effects, the most important sources of errors seem to be possible epicentral mislocation and multipathing effects in the wave propagation. An average error estimate of the phase velocity values was made for the following periods: 0.5 percent for 50 sec, 0.6 percent for 34 sec, and 0.8 percent for 26 sec. In addition to phase velocity, attenuation coefficient measurements were also reported by Patton (1978). We will refer to these in a later part of this thesis. The thesis work of Patton (1978) was published in a series of papers. Patton and Aki (1979) discuss the effects of errors of different sources on the moment tensor inversion procedure. Patton (1980a) describes the reference point method for

determination of the moment tensor of a series of earthquakes, and the application of the method to earthquakes in the Pamir region of Asia. Patton (1980b) reviews the results of the regionalization of the phase velocity dispersion curves, and Q for Rayleigh waves.

Further application of the moment tensor inversion technique of Patton (1978) to earthquakes in Eurasia was made by Romanowicz (1981) for events located in Tibet. She tried to use the phase velocity curves for the reference point of Patton (1978) to correct for the path effect of earthquakes located in the Pamir region in order to apply the linear moment tensor inversion. The procedure worked well for earthquakes located near the reference point, but not for those further away. She then measured the phase velocity reference curves for a new reference point, this time located in Tibet, using earthquakes in this region for which the focal mechanism and depth were constrained by the P-wave first motion data, as well as the P-wave-form modelling developed by Langston and Helmberger (1975) and others. In the present thesis we will use basically the same idea to measure phase velocity dispersion curves for many, many paths. Romanowicz (1981) was the first to apply the body wave-form modelling

technique to constrain the focal mechanism and depth of earthquakes in order to determine phase velocity of Rayleigh waves. The initial phase was calculated using the Pamir model of Patton (1978). The unwrapping of the phase spectra was made by using the phase velocity curves of Patton (1978) as reference. For most measurements, the error was reported to be less than 0.5 percent for the 30 to 90 sec period range. The use of the phase velocity values measured by Romanowicz (1981) for the Tibet area than the values based on the regionalization of Patton (1978) gave more satisfactory results on linear moment tensor inversion and focal depth determination for earthquakes in the Tibet region.

Romanowicz (1982b) also determined the phase velocity for a path between two events in essentially the same way as the two station method was used to determine the phase velocity for a path between two stations. The two event method uses the observations at one station of two different events, that are roughly aligned with the station in a greatcircle. For the events Romanowicz (1982b) studied, this alignement was perfect within one degree, and the error estimate by the comparison of all the dispersion curves reported for all measurements was about 0.02 km/sec, or 0.5 percent, for the whole 30 to 90 sec period range considered.

Additional phase velocity measurements for Rayleigh waves in Tibet in the 30 to 90 sec period range using both the one-station method and the two-event method were made by Brandon and Romanowicz (1984, 1986). The paths were located in Tibet and the alignement of the event pairs with the observation stations was within 1.5 degrees for all cases. The focal mechanism and depth of the earthquakes considered were determined by body wave modelling, P-wave first motions, S-wave data, and by the study of the Rayleigh wave radiation pattern. We could not include their dispersion data in our data base because they were only recently published.

Lyon-Caen (1980) measured the phase velocity of Rayleigh waves with period from 30 to 90 sec using the one-station method for 25 paths. She used records of Rayleigh waves generated by an earthquake in northern Italy and two aftershocks recorded at W.W.S.S.N. stations in Africa and in Europe. The source mechanisms of these events were determined using the P-wave first motion, and the S-wave polarization. The depth was found to be shallow for all of them from the study of P-wave form modeling study. The measurements on records of each earthquake resulted in a set of three dispersion curves for each path, since the earthquake

epicenters are in the same area. The variation of phase velocity among these curves is 0.5 percent in the worst cases, considering the whole period range studied. Lyon-Caen (1980) suggests that the phase velocity values obtained in this study could be used to determine the moment tensor and focal depth of other earthquakes in the area, using the method of Patton (1978).

Pujol (1982) applied the moment tensor inversion procedure developed by Patton (1978) to determine the focal mechanism and depth of an earthquake located in the Seward Peninsula, in Alaska. He calculated the phase velocity dispersion curves for 12 paths to a reference event, for which previous workers had determined the focal mechanism using body wave observations.

Romanowicz (1982a) proposed a modification of the moment tensor inversion used by Patton (1978). She noticed that the complex spectra of Rayleigh waves generated by an earthquake can be separated into two parts, for each period. One of these components is sensitive to the depth of the source, while the other component is not. After separation of the insensitive component, the focal depth and focal mechanism can be determined, using linear inversion, more accurately than in

the procedure used by Patton (1978). The application of this modification of the original moment tensor inversion method has the advantage that less accurate phase velocity are required, compared with the 0.5 percent accuracy estimated by Aki and Patton (1978) as necessary in the original method. Romanowicz (1982a) does not give any error bounds to the phase velocity values required for the propagation correction, but states that, for a given station the propagation path effect for earthquake with the epicenter within 500 to 1000 km from the reference point can be eliminated by the use of phase velocity curves for the path to the reference point.

Suarez (1982) used the method of moment tensor inversion using only amplitude data described by Romanowicz and Suarez (1983) to obtain the focal mechanism and depth of an earthquake in Central Andes. This information was then used to calculate the phase velocity dispersion curves in the 20 to 100 sec period range for 46 paths between this reference event and W.W.S.S.N. stations at different azimuthal directions. These phase velocity curves were then used in the separation of the propagation effects on Rayleigh waves recorded at these stations that were generated by other earthquakes with epicenter near the reference point. The focal mechanism and

depth for these earthquakes was then determined by moment tensor inversion of the Rayleigh wave spectra corrected for the path effect. The phase velocity values for the reference point were then adjusted according to information from both earthquakes, and the whole process was repeated using a third event. The final phase velocity dispersion curves were then used to correct the observed phase spectra generated by other events in the region, in order to check how far away from the reference point this method still gives reliable results. This can be determined because the focal mechanism and depth of the events considered have been studied using P-wave first motion and waveform modeling. The result showed that the reference phase velocity curves could be used to determine the focal mechanism and focal depth for events located as far as 800 km away from the reference point.

Shudofsky (1984) studied a set of earthquakes with epicenter in East Africa using the method of Romanowicz and Suarez (1983). He used the procedure of Suarez (1982), checking the resultant focal mechanism and depth with those obtained by body wave modelling for seven of the events studied. P-wave first motion observations were available for all events. He reported the phase velocity values in the 20

to 92 sec period range for 64 paths with most of their portion inside the African continent. These paths were between W.W.S.S.N. stations and seven reference points used in the study. The use of the dispersion curves determined for a reference point can be used efficiently for eliminating the path effect for events with epicenters up to 600 km away from the reference point.

Among the phase velocity data we found in the literature that we did not include in our database are those reported by Cisternas (1961), that determined the phase velocity for Rayleigh waves with period between 20 and 45 sec generated by five earthquakes with epicenter in western South America, and recorded by a seismographic station located in Peru. We did not include this data because Cisternas (1961) did not know the initial phase correction for these events, and suggested that the measurements should be reconsidered whenever the calculation of this correction could be made properly.

Pomeroy (1963) measured the phase velocity of Rayleigh waves with period from 15 to 40 sec for paths between the site of two american nuclear explosions in the Pacific, and four stations located on the Pacific rim. We did not include these measurements in our data set because they used a

frequency-independent initial source correction in all measurements.

Patton (1982) obtained the phase velocity of Rayleigh waves in the 6 to 20 sec period range for paths between the Nevada Test Site and four stations in the U.S.. Several measurements were made using the records of nuclear explosions at each of these stations, by the one-station method. In the calculations, the initial source correction was made appropriate for an explosive source. The phase velocity dispersion curve for each station was used to correct the phase of the observed phase spectra of one earthquake with epicenter near the Nevada Test Site. The corrected phase spectra, together with the amplitude at each station were used to obtain the focal mechanism and depth by the moment tensor inversion technique. The resultant focal mechanism checked well with the one that resulted from the P-wave first motion studies for that event, but the focal depth was a little shallower than the depth obtained by previous workers from the P-wave analysis. Patton (1982) did not include the coordinate of the stations used in his work so, we could not include these data in our database.

Patton (1982) compared the phase velocity dispersion curves obtained by the one-station method with those obtained by Priestley and Brune (1978) for similar paths. We did not include them in our data base due to difficulties in separating different curves overlapping each other in the diagram.

2.6 - Source of errors:

We shall discuss now the reliability of the phase velocity measurements we have selected from the literature which are summarized in Table 2.1 and plotted in Figure 2.4. We have already described in the text the error estimates made by the authors in each reference where this information was available. These estimates were based on different assumptions regarding the major sources of error and different ways of estimation. These phase velocity measurements were made using epicentral data and origin time information of varied quality, which has improved considerably with time. Improvements on data processing techniques have also played an important role on the accuracy of phase velocity value (and

also on the capability of analyzing longer periods, as was possible with the use of Fourier analysis in substitution of the earlier peak and trough analysis), together with the development of methods used to obtain the focal mechanism and depth of earthquakes from body wave data. These latter developments were helpful to the calculation of the initial source phase for the application of the one-station method. We have described most of these developments in the previous sections.

All these progresses enable the use of the one-station method more extensively, covering large areas of the Earth. Aki and Richards (1980) pointed out that, whenever the accurate determination of the initial source phase is possible, the one-station method can provide a more accurate measurement than two and three station method. This is mainly because the effect of inhomogeneities outside the region covered by the array can contaminate the signal. They also discussed the advantages of the two-station method over the three-station method, because of the difference in signal coherence between the directions parallel and perpendicular to the wave front for waves propagating in a heterogeneous medium. A review of the phase velocity measurement methods

and their evolution was also presented earlier by Kovach (1978).

We could then argue that our data set should be classified according to the method used on the phase velocity measurement. Unfortunately, there are complications due to the different data processing treatment, unmatched seismographic instruments, and other complications that cannot be accounted for by such a simple analysis. The errors reported by the authors we referred in this chapter, were evaluated using various techniques. We have specified these whenever the information was available.

McGarr (1969a) studied the effects of the ocean-continent boundary on the amplitude of observed Rayleigh waves. In his study, an ocean bottom seismometer and a seismological station on near-by land, were used to compare the transmission from the ocean and from the continent. The main conclusion is that the ocean-continental boundary plays a significant role on the refraction of these waves, specially on the shorter periods portion of the surface wave spectrum. Further studies on this effect are reported by McGarr (1969b), who showed that structures such as island chains could also cause amplitude variations on Rayleigh waves observed at W.W.S.S.N. stations located in the U.S., from earthquakes in the Pacific.

The multipathing effect on Rayleigh waves was demonstrated by Capon (1970), who studied records of the LASA array in Montana, U.S.A., and by Bungum and Capon (1974) who studied records of the NORSAR array located in Norway. Their conclusion was that the multipathing effect is caused mostly by the refraction and reflection of surface waves at the ocean-continent boundaries, mountain ranges or mid-ocean ridges. The effects of these structures on the phase velocity measurements of surface waves was further studied by Sobel and von Seggern (1978), who made a selection of previously measured phase velocity data from the literature (similar to the one in this chapter), used these data to regionalize the phase velocity values for the Earth, presenting the regionalized model in a similar fashion that we present in Chapter 3, and performed surface wave ray tracing to study the importance of the refraction and reflection effects. They found that, for Rayleigh waves with 20 sec period, significant effects on phase velocity and attenuation coefficient measurements can be caused by the refraction and/or reflection. Patton (1978) considered the focusing and multipathing of the Rayleigh waves by inhomogeneities as one of the major sources of errors in the phase velocity

measurements reported in his work. He made a study of surface wave ray tracing (Patton, 1980b) that showed results similar to those of the work of Sobel and von Seggern (1978).

Thus care should be taken when analyzing the Rayleigh wave data that might be affected by lateral heterogeneities. A careful selection of paths is the best way to avoid such complications, as emphasized by Aki *et al.* (1972) in their reply to the comments by McGarr (1972) on the effect of lateral heterogeneity on the Rayleigh wave spectra.

TABLE 2.1

REFERENCE	SOURCE OF INFORMATION	EVENTS STUDIED	MEASUREMENT METHOD	NUMBER OF PATHS
Bache et al.. 1978	Figure 2	Apr 14, 1966 14:13:43 Jun 02, 1966 15:30:00 Jun 06, 1966 14:00:00	1 SM	6
Baldi et al, 1979 (some paths are also in Baldi et al, 1978)	Figure 1	Mar 25, 1972 22:59:40.3 Mar 31, 1972 15:36:53.5 Feb 19, 1973 08:42:52.1 Mar 12, 1973 19:39:21.0 Nov 11, 1973 02:43:06.2 Jan 08, 1974 21:47:21.6 Jan 22, 1974 13:28:20.0 Jun 24, 1974 20:34:35.4 May 25, 1975 19:04:34.4 Jan 23, 1976 15:14:16.0	2 SM	8
Berry and Knopoff, 1967	Figure 3	Jun 11, 1961 05:10:26.3 Jul 28, 1961 01:05:30.0 Aug 08, 1961 12:18:23.1 Aug 17, 1961 21:16:30.1 Aug 27, 1961 01:50:51.8 Aug 30, 1961 03:35:02.7	3 SM†	7
Biswas, 1971	Tables V and VI	Sep 16, 1964 22:23:36.3 Sep 17, 1964 15:02:00.9 Sep 19, 1964 05:08:15.1 Oct 12, 1964 21:55:33.2 Nov 30, 1964 12:27:38.6 Jun 02, 1965 23:40:23.5 Jul 05, 1965 08:31:58.3 Aug 20, 1965 21:21:51.5 Nov 15, 1965 11:18:50.3 Nov 16, 1965 15:24:43.0 Sep 02, 1966 07:59:05.2	2 SM	18
Bloch and Hales, 1968	Figure 7	Mar 01, 1963 19:14:11.1 Mar 24, 1963 02:07:09.4 Mar 25, 1963 22:46:16.7 Nov 24, 1964 12:40:51.4 Nov 30, 1964 12:27:38.6 May 29, 1965 15:36:31.9 Sep 19, 1965 13:55:39.9 Dec 19, 1965 22:06:32.7	2 SM	8

(TO BE CONTINUED)

TABLE 2.1 (CONTINUED)

REFERENCE	SOURCE OF INFORMATION	EVENTS STUDIED	MEASUREMENT METHOD	NUMBER OF PATHS
Bolt and Niazi, 1964	Table 3	Feb 01, 1956 01:32:56.9 Jun 29, 1959 07:16:06.0	2 SM	2
Brooks, 1969	Figure 4 Table 5	Jan 23, 1965 16:09:01.9 Feb 13, 1966 06:35:55.7 Mar 02, 1966 07:32:42.6 May 25, 1966 08:28:58.6 Aug 10, 1966 12:33:42.2 Sep 07, 1966 05:53:45.7	2 SM 1 SM	3 6
Brune et al., 1960	Figures 6 and 11	Oct 18, 1958 15:00:00 Oct 22, 1958 08:21:11	1 SM	2
Brune and Dorman, 1963	Tables 3 and 4	Jan 07, 1956 16:41:04 Jun 03, 1956 05:19:23 Sep 14, 1958 14:21:37 Nov 12, 1958 06:09:10 Jan 30, 1959 05:17:32 Jun 14, 1959 00:11:57 Jul 09, 1959 16:05:18 Nov 03, 1959 09:40:05	2 SM 1 SM	9 5
Burkhard, 1977	Table 1	Mar 07, 1963 05:21:56.6 Mar 29, 1965 10:47:37.6 Jul 29, 1965 08:29:21.2 Aug 20, 1965 21:21:49.7 Oct 01, 1965 08:52:04.4 Nov 12, 1965 17:52:27.6 Dec 06, 1965 11:34:48.9 Feb 10, 1966 14:21:11.2 Jun 28, 1966 04:26:13.4 Jul 04, 1966 18:33:37.1 Aug 07, 1966 02:13:04.7 Aug 07, 1966 17:36:27.3 Sep 09, 1966 10:02:25.1 Jan 19, 1967 12:40:09.5 Apr 09, 1968 02:28:59.1	1 SM	37
Calcagnile and Panza, 1978	Table II	Dec 28, 1967 06:26:15.8 Aug 05, 1968 16:17:04.8 Sep 17, 1969 18:40:45.8	2 SM	3

(TO BE CONTINUED)

TABLE 2.1 (CONTINUED)

REFERENCE	SOURCE OF INFORMATION	EVENTS STUDIED	MEASUREMENT METHOD	NUMBER OF PATHS
Calcagnile and Panza, 1979	Table 2	Apr 04, 1975 05:16:16.2	N SM	1
Calcagnile and Panza, 1980	Table 1	Mar 11, 1965 17:07:05.5 Feb 23, 1976 15:14:16.0	2 SM	2
Calcagnile et al., 1984	Table 2	May 19, 1963 01:03:06.2 Jul 14, 1963 05:41:43.0 Jan 27, 1964 01:12:23.5 Mar 19, 1964 09:42:34.9	2 SM	4
Caputo et al., 1976	Table I	Apr 03, 1972 18:52:59.3 Apr 03, 1972 20:36:22.2	2 SM	2
Chang, 1979	Table 4	Aug 25, 1964 13:47:20.6 Dec 26, 1964 14:30:29.1 Feb 13, 1966 10:44:41.3 Mar 07, 1966 21:29:17.4 Apr 25, 1966 23:22:49.3 Jun 06, 1966 07:46:16.1 Mar 31, 1969 07:15:54.4 Oct 14, 1970 07:29:58.6 Dec 28, 1974 12:11:43.7	1 SM	40
Chandhury, 1966	Figure 6	Jun 19, 1963 10:47:24.7 Jun 21, 1963 15:26:31.0 Jan 22, 1964 15:58:46.5 Feb 27, 1964 15:10:48.8 Feb 28, 1964 17:47:05.9	1 SM	5
Forsyth, 1973	Table 4	Mar 07, 1963 05:21:59.6 Apr 19, 1964 05:13:00.5 Oct 06, 1964 07:17:56.7 Oct 12, 1964 21:55:34.0 Nov 03, 1965 18:21:08.6 Nov 06, 1965 09:21:48.6 Nov 25, 1965 10:50:40.2 Jul 20, 1966 13:22:53.6 Dec 29, 1966 11:56:23.1 Jan 21, 1967 02:54:00.4 to be continued	1 SM 2 SM	76 2

(TO BE CONTINUED)

TABLE 2.1 (CONTINUED)

REFERENCE	SOURCE OF INFORMATION	EVENTS STUDIED	MEASUREMENT METHOD	NUMBER OF PATHS
Forsyth, 1973 (continued)		continued Apr 01, 1967 10:41:00.2 Jun 26, 1969 02:30:58.4 Sep 09, 1969 15:23:10.8 Sep 20, 1969 15:26:41.5 Nov 18, 1970 20:10:58.2 May 09, 1971 08:25:01.7		
Forsyth, 1985	Table	Feb 07, 1965 Oct 01, 1965 May 15, 1966 Mar 19, 1967	1 SM	23
Fouda, 1973	Tables 5 thru 9	Oct 11, 1964 21:15:03.9 Nov 30, 1964 12:27:38.6 Apr 29, 1965 15:28:43.4 Aug 18, 1966 10:33:16.5 Feb 02, 1967 06:25:49.5	2 SM	7
Gabriel and Kuo, 1966	Figures 3 and 4	Nov 03, 1963 03:10:12.7 Nov 23, 1963 07:50:46.3 Dec 16, 1963 01:51:30.6 Feb 10, 1964 17:27:58.0 Feb 29, 1964 23:49:40.8 Jul 05, 1964 19:07:57.8 Jul 08, 1964 11:55:39.0	2 SM	1
Goncz et al., 1975	Figure 5	Dec 25, 1962 12:09:45.6 Mar 28, 1963 11:12:31.3 Mar 28, 1963 23:29:14.6 Mar 31, 1963 19:22:53.3 Apr 02, 1963 04:43:30.9 May 13, 1963 22:48:10.3 May 18, 1963 12:20:31.9 Jun 02, 1963 10:00:00.1 Jun 15, 1963 15:30:37.7 Jun 17, 1963 18:30:54.3 Jun 24, 1963 16:17:15.4 Jul 14, 1963 00:02:22.8 Aug 13, 1963 21:52:37.4 Aug 14, 1963 02:46:44.1 Oct 02, 1963 03:31:27.0 Oct 04, 1963 02:47:32.1 to be continued	2 SM	9

(TO BE CONTINUED)

TABLE 2.1 (CONTINUED)

REFERENCE	SOURCE OF INFORMATION	EVENTS STUDIED	MEASUREMENT METHOD	NUMBER OF PATHS
Goncz et al., 1975 (continued)		continued Oct 27, 1963 10:38:49.0 Oct 31, 1963 03:17:42.0 Nov 24, 1963 16:30:16.0 Aug 20, 1964 12:48:47.7 Dec 30, 1964 13:19:47.4 Mar 02, 1965 09:19:41.6 Jun 27, 1965 09:45:48.7 Jul 17, 1965 07:20:30.7 Jul 21, 1965 02:51:39.0 Oct 23, 1965 08:33:47.4 Dec 09, 1965 06:07:47.7 Feb 17, 1966 11:47:56.8 Oct 12, 1966 00:06:38.8 Dec 27, 1967 16:22:48.5 May 26, 1968 14:41:52.0 Jul 10, 1968 11:16:44.6 Jul 22, 1968 05:09:15.7 Nov 26, 1968 00:03:14.3 Apr 05, 1969 02:18:29.9 Apr 21, 1969 07:19:27.5 Jun 29, 1969 17:09:13.9 Oct 22, 1969 22:51:33.5 Oct 31, 1969 11:33:04.8 Feb 04, 1970 05:08:48.0 Jun 25, 1970 05:13:58.6 Aug 13, 1970 04:22:38.5 Aug 24, 1970 12:30:19.5 Oct 25, 1970 12:00:35.2		
Gregersen, 1970	Figure 3	Apr 02, 1964 01:11:43.5 Apr 03, 1964 04:12:39.4 Jun 14, 1964 12:15:31.3 Jun 30, 1964 13:46:18.5 Jul 05, 1964 19:07:57.8 Jul 25, 1964 19:31:07.0 Jul 28, 1964 21:38:43.5 Oct 21, 1964 07:38:31.0 Jan 12, 1965 13:32:24.0 Feb 26, 1965 08:55:42.2 Mar 09, 1965 17:57:53.7 Mar 13, 1965 04:08:40.5 Mar 22, 1965 22:56:26.5 Mar 28, 1965 16:33:14.6 Apr 05, 1965 03:12:54.2 Apr 09, 1965 23:57:03.2 to be continued	2 SM	2

(TO BE CONTINUED)

TABLE 2.1 (CONTINUED)

REFERENCE	SOURCE OF INFORMATION	EVENTS STUDIED	MEASUREMENT METHOD	NUMBER OF PATHS
Gregersen, 1970 (continued)		continued Apr 29, 1965 15:28:43.3 May 19, 1965 06:03:58.9 Jun 21, 1965 00:21:14.5 Sep 09, 1965 10:02:25.4 Nov 13, 1965 04:33:53.0 Dec 06, 1965 11:34:53.7 Dec 15, 1965 23:05:20.7 Jan 23, 1966 01:56:38.0 Mar 07, 1966 01:16:05.8 Mar 27, 1966 18:53:41.3 May 09, 1966 00:42:55.6 Jul 12, 1966 18:53:08.5 Jul 27, 1966 04:48:59.4 Aug 19, 1966 12:22:09.6 Jan 20, 1967 01:57:23.1		
Gumper and Pomeroy, 1970	Figures 3 thru 7	Jan 05, 1964 23:46:10.7 Aug 25, 1964 13:47:20.6 Jul 12, 1966 18:53:10.4	2 SM	8
Gupta et al., 1977	Figure 4	Jul 09, 1964 16:39:49	2 SM	1
James, 1971	Figures 6, 8,9,10,11, 12,13,17	Feb 21, 1966 00:22:29.5 Mar 20, 1966 01:42:49.9 Sep 14, 1966 23:18:40.8 Sep 15, 1966 11:51:56.4 Oct 11, 1966 16:25:55.1 Apr 19, 1968 09:04:27.3 Dec 05, 1968 09:44:11.0 Sep 29, 1969 20:03:32.8	2 SM	9
Kaminuma, 1966	Table 3b	Mar 09, 1957 14:22:27 Mar 01, 1964 08:18:56.4 Nov 11, 1964 13:17:37.5 Nov 11, 1964 19:06:57.1 Dec 17, 1964 05:18:34.0 Mar 03, 1965 19:29:16.1 Mar 05, 1965 13:42:44.1	2 SM	7

(TO BE CONTINUED)

TABLE 2.1 (CONTINUED)

REFERENCE	SOURCE OF INFORMATION	EVENTS STUDIED	MEASUREMENT METHOD	NUMBER OF PATHS
Knopoff et al., 1966	Figures A1 thru A16	Oct 16, 1960 19:55:42.2 Oct 27, 1960 05:25:03.6 Oct 28, 1960 04:18:41.9 Oct 28, 1960 13:18:14.3 Oct 29, 1960 13:26:10.0 Nov 06, 1960 04:38:16.7 Jan 19, 1961 17:22:16.9 Mar 07, 1961 06:43:10.6 Mar 09, 1961 03:59:08.7 Mar 28, 1961 21:01:56.2 Apr 04, 1961 09:46:36.6 Apr 06, 1961 01:33:46.9 May 06, 1961 16:04:33.1 May 07, 1961 15:40:52.5 May 14, 1961 15:08:04.2 May 14, 1961 15:38:07.5	3 SM†	16
Knopoff et al., 1967	Figures 1 thru 6	Oct 29, 1960 13:26:10.0 Jun 11, 1961 05:10:26.3 Aug 30, 1961 03:35:02.7 Nov 29, 1962 19:06:37.6 Feb 22, 1963 07:10:28.0 Mar 08, 1963 02:44:31.5	3 SM†	8
Knopoff et al., 1970	Figure 2	Feb 22, 1965 20:46:36.0 Feb 22, 1965 21:22:34.3 Apr 11, 1965 04:59:39.3	1 SM	5
Knopoff and Schlue, 1972	Figure 3	Nov 12, 1965 Mar 07, 1966 Apr 20, 1966	2 SM	1
Knopoff and Vane, 1978	Table 2	Aug 07, 1972 09:24:15 Sep 09, 1972 02:44:03	2 SM	3
Kuo et al., 1962	Figures 10 thru 23, and 26	Jan 15, 1958 19:14:29 Feb 22, 1958 10:50:23 Mar 20, 1958 01:38:04 Apr 12, 1958 11:46:58 Sep 04, 1958 21:51:08 May 24, 1959 19:17:40 to be continued	1 SM 2 SM	14 2

(TO BE CONTINUED)

TABLE 2.1 (CONTINUED)

REFERENCE	SOURCE OF INFORMATION	EVENTS STUDIED	MEASUREMENT METHOD	NUMBER OF PATHS
Kuo et al., 1962 (continued)		continued Oct 27, 1959 06:52:50 Dec 27, 1959 15:52:55 Feb 08, 1960 12:45:34 Mar 22, 1960 02:31:17 Mar 23, 1960 00:23:22 Apr 15, 1960 03:25:36 Jun 20, 1960 02:01:08 Aug 09, 1960 07:39:22.6 Oct 07, 1960 15:18:30.8 Nov 09, 1960 10:43:43.1		
Landisman et al., 1969	Figure 13	Apr 29, 1963 21:44:17.2 Jun 24, 1963 04:26:37.9 Apr 04, 1964 04:54:01.7	2 SM	3
Leeds, 1975	Table II	Mar 29, 1965 10:47:37.6 Jul 29, 1965 08:29:21.2 Oct 01, 1965 08:52:04.4 Nov 12, 1965 17:52:27.6 Feb 10, 1966 14:21:11.1 Jul 04, 1966 18:33:37.1	1 SM	7
Levshin et al., 1966	Table 2	'Kamchatka and Kuril Islands shocks'	2 SM	1
Liao, 1981	Tables 15 and 23	Sep 19, 1967 10:56:08.8 Sep 25, 1968 10:38:38	1 SM 2 SM	4 1
Lyon-Caen, 1980	Figures 6 thru 15	May 06, 1976 20:00:12.5 Sep 15, 1976 03:15:18.7 Sep 15, 1976 09:21:18.6	1 SM	25
Mitchel, 1977	Figure 10	information not available	2 SM	2
Mitrovas, 1977	Tables 2A and 2B	Jan 02, 1974 10:42:29.9 May 09, 1974 23:23:25.2 Oct 23, 1974 06:14:54.8 Nov 09, 1974 12:59:49.8 to be continued	2 SM	14

(TO BE CONTINUED)

TABLE 2.1 (CONTINUED)

REFERENCE	SOURCE OF INFORMATION	EVENTS STUDIED	MEASUREMENT METHOD	NUMBER OF PATHS
Mitrovas, 1977 (continued)		continued Jan 19, 1975 08:00:24.3 Feb 07, 1975 04:51:44.0 Mar 13, 1975 15:26:42.5 Mar 27, 1975 05:15:06.2 May 10, 1975 14:27:40.5 Jun 16, 1975 22:35:23.2 Jul 10, 1975 18:29:16.0 Oct 28, 1975 06:54:22.4		
Moazami-Goudarzi, 1974	Table 4	9 earthquakes (origin time information not available)	2 SM	1
Mueller and Sprecher, 1978	Figure 2	Jul 03, 1973 16:59:35.1	2 SM	1
Noponen, 1966	Figure 5	Feb 23, 1964 22:41:06.3 Apr 11, 1964 16:00:42.8 Apr 29, 1964 04:21:06.7 Apr 29, 1964 17:00:02.9 Apr 05, 1965 03:12:54.2	2 SM	2
Okal and Talandier, 1980	Tables 3 and 4	Dec 29, 1975 03:39:43.0 Jul 27, 1976 19:42:54.6 Jul 28, 1976 10:45:35.2 Mar 19, 1977 23:00:58.3 Jul 29, 1977 11:15:45.3 Nov 23, 1977 09:26:24.7 Feb 22, 1978 06:07:37.0 Jun 12, 1978 08:14:26.4 Nov 29, 1978 19:52:47.6 Feb 16, 1979 10:08:54.4	2 SM	4
Panza and Calcagnile, 1974	Figure 2	Feb 10, 1971 05:18:07.0	1 SM	1
Panza et al., 1978	Figure 3a	Dec 17, 1971 19:06:07.1 Oct 06, 1973 15:07:37.3	2 SM	1

(TO BE CONTINUED)

TABLE 2.1 (CONTINUED)

REFERENCE	SOURCE OF INFORMATION	EVENTS STUDIED	MEASUREMENT METHOD	NUMBER OF PATHS
Papazachos, 1964	Figures 2, 3,4,6,7,8, 9,11,12	Nov 14, 1961 04:42:26.5 Dec 03, 1961 01:00:35.2 Jan 08, 1962 01:00:24.2 Jan 30, 1962 08:34:26.8 Feb 10, 1962 19:31:56.2 Mar 05, 1962 01:50:50.6 Mar 11, 1962 02:26:05.7 Mar 12, 1962 11:40:12.8 Mar 27, 1962 21:19:29.4 Apr 04, 1962 14:02:32.2 Apr 20, 1962 05:47:55.3 May 19, 1962 14:58:13.3 May 20, 1962 15:01:20.7 Jul 24, 1962 21:08:22.6 Jul 25, 1962 04:37:50.7 Jul 30, 1962 20:18:49.3 Sep 16, 1962 03:05:33.0 Sep 18, 1962 00:29:05.2 Feb 22, 1963 21:14:06.1 Feb 24, 1963 13:34:15.7 Nov 19, 1964 09:46:17.7	1 SM	31
Papazachos, 1969	Figures 1 thru 5	Jan 11, 1963 12:12:16 Mar 07, 1963 12:16:28 May 19, 1963 01:03:04 May 23, 1963 07:43:58 May 30, 1963 06:56:09 Jul 14, 1963 05:41:44 Dec 16, 1963 01:51:31 Jan 15, 1964 21:36:05 Jan 27, 1964 01:12:24 Mar 19, 1964 09:42:35 Mar 26, 1964 13:29:56 Aug 20, 1964 03:56:29 Dec 03, 1964 03:50:01 Mar 01, 1965 21:32:12	2 SM	5
Patton, 1973	Tables III thru VII	Oct 18, 1964 09:06:26.0 Dec 03, 1964 03:50:01.2 Sep 12, 1965 22:02:34.3 Dec 19, 1965 22:06:32.7 Feb 17, 1966 11:48:00.8 Apr 06, 1966 02:59:01.7	1 SM	19

(TO BE CONTINUED)

TABLE 2.1 (CONTINUED)

REFERENCE	SOURCE OF INFORMATION	EVENTS STUDIED	MEASUREMENT METHOD	NUMBER OF PATHS
Patton, 1978	Figures C1 thru C8	May 11, 1967 14:50:57 Aug 28, 1969 03:58:36.7 Sep 14, 1969 16:15:25.6 Jul 24, 1971 11:43:39.3 Oct 28, 1971 13:30:56.4 Nov 12, 1972 17:56:52.9 Aug 11, 1974 20:05:30.9 Aug 11, 1974 21:21:37.1 Aug 27, 1974 12:56:01.0	1 SM	44
Payo, 1969	Figures 1, 4a, and 4b	Jun 03, 1962 15:02:26.4 Jul 16, 1962 04:49:21.5 Aug 21, 1962 18:09:06 Aug 21, 1962 18:19:33.3 Aug 25, 1962 19:58:47.9 Aug 26, 1962 16:30:47 Sep 12, 1962 20:57:00.4 Mar 24, 1963 02:07:12.8 Apr 30, 1963 18:43:14 Jun 20, 1963 19:47:41.3 Jun 26, 1963 10:27:03.1 Jul 16, 1963 18:27:18.4 Jul 15, 1968 02:01:03	1 SM 2 SM	9 6
Payo, 1970	Figures 4a 4b, and 4c	Jun 07, 1963 19:30:35.6 Jul 04, 1963 22:56:15.7 Sep 07, 1964 11:27:16.0 Apr 08, 1966 05:52:40.0 Aug 12, 1966 15:36:17.0 Sep 01, 1966 01:38:29.9 Sep 01, 1966 21:27:39.0	3 SM†	7
Payo and Ruiz de la Parte, 1974	Figures 1 and 2	events with epicenter in Alboran Sea Algeria Atlantic Ocean Morocco	2 SM	4
Proskuryakova et al., 1970	Figures 6, 7, and 8	Jun 27, 1966 10:59 Jun 28, 1966 04:26 Aug 01, 1966 21:03 Aug 07, 1966 17:36 to be continued	2 SM	3

(TO BE CONTINUED)

TABLE 2.1 (CONTINUED)

REFERENCE	SOURCE OF INFORMATION	EVENTS STUDIED	MEASUREMENT METHOD	NUMBER OF PATHS
Proskuryakova et al., 1970 (continued)		continued Aug 16, 1966 19:45 Aug 18, 1966 10:33 Sep 01, 1966 11:29 Sep 15, 1966 11:51		
Pujol, 1982	Figures 9a thru 9e	Apr 16, 1965 23:22:19	1 SM	12
Romanowicz, 1981b	Figure 16	Jul 14, 1973 13:39:29.4 Sep 08, 1973 07:25:41 May 05, 1975 05:18:46.3	1 SM	32
Romanowicz, 1982	Table 3 Figures 10 and 17	Jun 24, 1972 15:29:22.3 Jul 14, 1973 13:39:29.4 Aug 11, 1973 07:15:38.2 Sep 08, 1973 07:25:41 Dec 28, 1974 12:11:46.6 Apr 28, 1975 11:06:43.7 Jun 04, 1975 02:24:32.9 Agu 21, 1976 21:49:52	1 SM from one event to another	9 7
Savarensky et al., 1969	Figures 3, 5, and 6	Nov 05, 1952 00:20:02 Nov 05, 1952 19:08:26 Nov 07, 1952 14:08:35 Nov 13, 1952 07:58:47 Apr 14, 1957 19:17:57 Aug 18, 1959 06:37:18 Aug 18, 1959 15:26:10 Sep 08, 1961 11:26:33 May 11, 1962 14:11:54 May 19, 1962 14:58:13 Mar 28, 1963 00:15:50 Aug 03, 1963 10:21:37 Oct 15, 1963 09:59:26 Feb 12, 1964 20:31:53 Feb 14, 1964 16:29:45	2 SM	3
Shudofsky, 1984	Table (Appendix II)	May 07, 1964 05:45:31.9 Mar 20, 1966 01:42:51.8 Mar 20, 1966 02:39:41.0 Mar 20, 1966 03:22:43.6 to be continued	1 SM	64

(TO BE CONTINUED)

TABLE 2.1 (CONTINUED)

REFERENCE	SOURCE OF INFORMATION	EVENTS STUDIED	MEASUREMENT METHOD	NUMBER OF PATHS
Shudofsky, 1984 (continued)		continued Mar 20, 1966 08:55:34 Mar 21, 1966 01:30:38.0 Mar 21, 1966 09:23:49.9 May 06, 1966 02:36:53.8 May 17, 1966 07:03:29.7 Oct 05, 1966 08:34:40.1 Oct 14, 1967 23:29:31.6 May 15, 1968 07:51:16.5 Dec 02, 1968 02:33:42.4 Sep 29, 1969 20:03:32.1 Apr 14, 1970 19:08:21.8 Nov 13, 1971 15:47:44 Feb 13, 1972 10:02:42.4 Dec 18, 1972 01:18:53.4 Apr 25, 1974 00:03:47 Feb 15, 1975 06:16:25.7 Mar 26, 1975 03:40:48.4 Apr 04, 1975 17:41:16.1 Jul 01, 1976 11:24:04.7 Sep 19, 1976 14:59:43.4 Jul 06, 1977 08:48:37.4 Jul 08, 1977 06:23:03.1 Dec 15, 1977 23:20:49		
Soriau-Thevenard, 1976a	Figure 2a	Sep 16, 1973 21:26:53.5 Nov 24, 1973 15:22:09.8 Jun 12, 1974 17:55:08.7 Jul 13, 1974 15:57:25.2 Apr 16, 1975 01:27:18.7	2 SM	5
Soriau, 1979	Figures 7 thru 11	Feb 09, 1971 14:00:41.6 Mar 13, 1971 23:51:35.5 Dec 05, 1971 05:50:05.8 Jan 22, 1972 13:08:49.4 Apr 03, 1972 18:52:59.8 Apr 03, 1972 20:36:20.0 Jul 05, 1972 10:16:38.4 Sep 16, 1972 09:14:32.9 Oct 20, 1972 08:17:49.2 Nov 13, 1972 04:43:47.6 Jan 01, 1973 11:42:36.1 Jun 07, 1973 18:34:43.0 Jun 17, 1973 20:37:52.0 Jul 22, 1973 02:36:52.0 to be continued	2 SM	27

(TO BE CONTINUED)

TABLE 2.1 (CONTINUED)

REFERENCE	SOURCE OF INFORMATION	EVENTS STUDIED	MEASUREMENT METHOD	NUMBER OF PATHS
Soriau, 1979 (continued)		continued Sep 15, 1973 01:45:57.7 Sep 16, 1973 21:26:53.5 Nov 04, 1973 15:52:11.7 Nov 08, 1973 08:59:12.9 Jan 25, 1976 12:23:55.5 Mar 04, 1976 02:50:00.5 Aug 23, 1976 03:30:07.6 Sep 22, 1976 00:16:08.2 Feb 19, 1977 22:34:04.1 Apr 20, 1977 23:42:50.5 Jun 28, 1977 16:18:15.2 Jun 28, 1977 19:35:01.9 Jul 29, 1977 11:15:45.0		
Soriau and Vadell, 1980	Figures 2 thru 5	Oct 05, 1977 05:34:46.8 Dec 28, 1977 02:45:36.7 Apr 15, 1978 23:33:47.2 May 23, 1978 23:34:11.4 Nov 05, 1978 22:02:08.3 Feb 20, 1979 06:32:38.0 May 21, 1979 22:22:24.0 Jun 10, 1979 06:49:57.0 Aug 25, 1979 08:44:05.6	2 SM	8
Stuart, 1978	Figure 1	Aug 19, 1971 08:28:53.1 Oct 30, 1971 20:48:48.0 Sep 16, 1972 03:53:26.5 Sep 19, 1972 01:36:52.4 Sep 22, 1972 19:57:27.4 Sep 23, 1972 02:14:26.8 Nov 14, 1972 04:31:42.8 Nov 21, 1972 10:06:29.6 Dec 09, 1972 06:44:40.4 Dec 27, 1972 22:59:29.7 Dec 28, 1972 14:36:07.3 Mar 18, 1973 11:06:14.7 Apr 07, 1973 03:00:58.8 Sep 27, 1973 12:29:04.3 Nov 04, 1973 15:52:11.7	2 SM	15
Suarez, 1982	Table (Appendix 2)	Jul 24, 1969 02:59:20.9 Oct 01, 1969 05:05:50.0 May 15, 1976 21:55:55.0	1 SM	46

(TO BE CONTINUED)

TABLE 2.1 (CONTINUED)

REFERENCE	SOURCE OF INFORMATION	EVENTS STUDIED	MEASUREMENT METHOD	NUMBER OF PATHS
Thomas, 1969	Tables 6 thru 14	Dec 25, 1962 12:09:45.6 Dec 29, 1962 10:41:04.1 Mar 28, 1963 11:12:31.3 Mar 28, 1963 23:29:14.6 Mar 31, 1963 19:22:53.3 Apr 02, 1963 04:43:30.9 May 13, 1963 22:48:10.3 May 18, 1963 12:20:31.9 Jun 02, 1963 10:00:00.1 Jun 05, 1963 22:54:28.7 Jun 15, 1963 15:30:37.7 Jun 24, 1963 16:17:15.4 Jul 14, 1963 00:02:22.8 Jul 14, 1963 14:28:22.1 Aug 13, 1963 21:52:37.4 Aug 14, 1963 02:46:44.1 Sep 14, 1963 03:52:16.9 Sep 24, 1963 16:30:16.0 Oct 02, 1963 03:31:27.0 Oct 04, 1963 02:47:32.1 Oct 26, 1963 22:41:29.8 Oct 27, 1963 10:38:49.0 Oct 27, 1963 18:24:42.9 Oct 31, 1963 03:17:42.0 Nov 18, 1963 21:11:10.2 Nov 20, 1963 11:59:58.5 Jul 25, 1964 21:29:33.2 Aug 20, 1964 12:48:47.7 Oct 11, 1964 11:10:33.6 Oct 12, 1964 15:42:54.7 Oct 17, 1964 01:38:36.0 Nov 19, 1964 15:45:31.2 Dec 30, 1964 13:19:47.4 Mar 16, 1965 16:46:15.5 Mar 29, 1965 10:47:37.6	2 SM	39
Thomson and Evison, 1962	Figure 11	Aug 18, 1959 06:37:13	2 SM	1
Tubman, 1980	Figures 5 and 10	Mar 13, 1967 19:22:19.5 Mar 16, 1967 03:11:59.3 Mar 29, 1970 03:48:47.3 Jul 29, 1970 05:50:56.4	2 SM 1 SM	4 2

(TO BE CONTINUED)

TABLE 2.1 (CONTINUED)

REFERENCE	SOURCE OF INFORMATION	EVENTS STUDIED	MEASUREMENT METHOD	NUMBER OF PATHS
Weidner, 1972	Figures 2.31, 3.9 thru 3.18	May 17, 1964 19:26:16.4 Jun 02, 1965 23:40:22.5 Nov 16, 1965 15:24:40.8 May 01, 1967 07:09:03.0 Jun 19, 1970 14:25:18.4	2 SM 1 SM	2 72

Chapter 2 - Figure Captions

Figure 2.1 - Schematic representation of plane wave incident on a tripartite array, where observed arrival times are used to determine the phase velocity c(T) for the region covered by the triangle, and the incident angle A(T).

Figure 2.2 - A station pair with spacing Δ is used to measure the phase velocity c(T) for the path between the two stations.

Figure 2.3 - The one-station method gives the phase velocity for the total path between the epicenter of the event and the observing station.

Figure 2.4 - Plot of all the phase velocity data previously determined and included in our database.

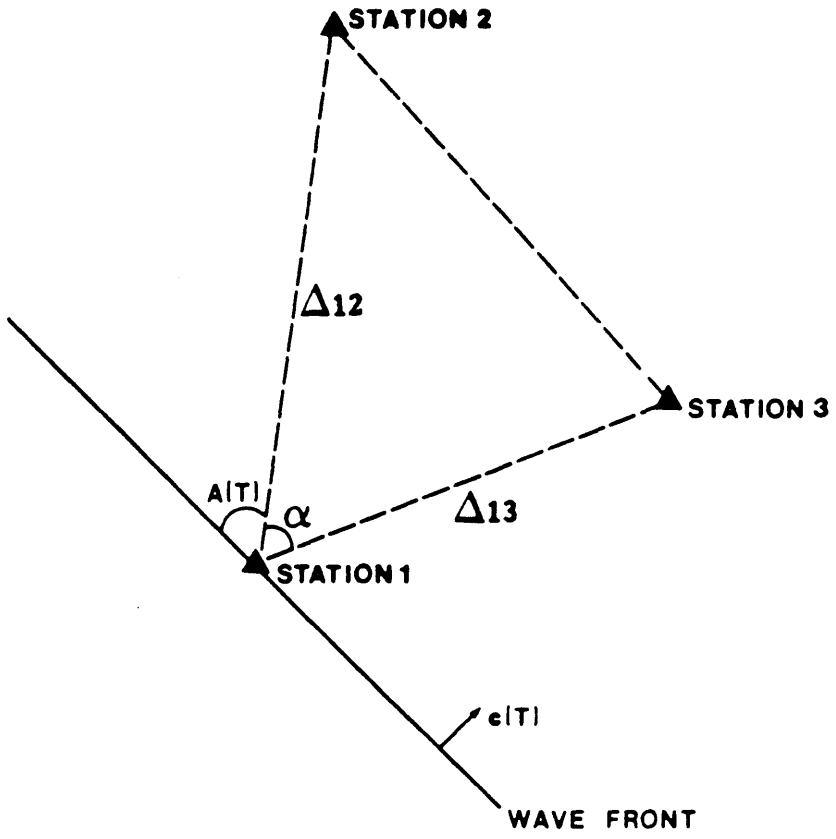

FIGURE 2.1

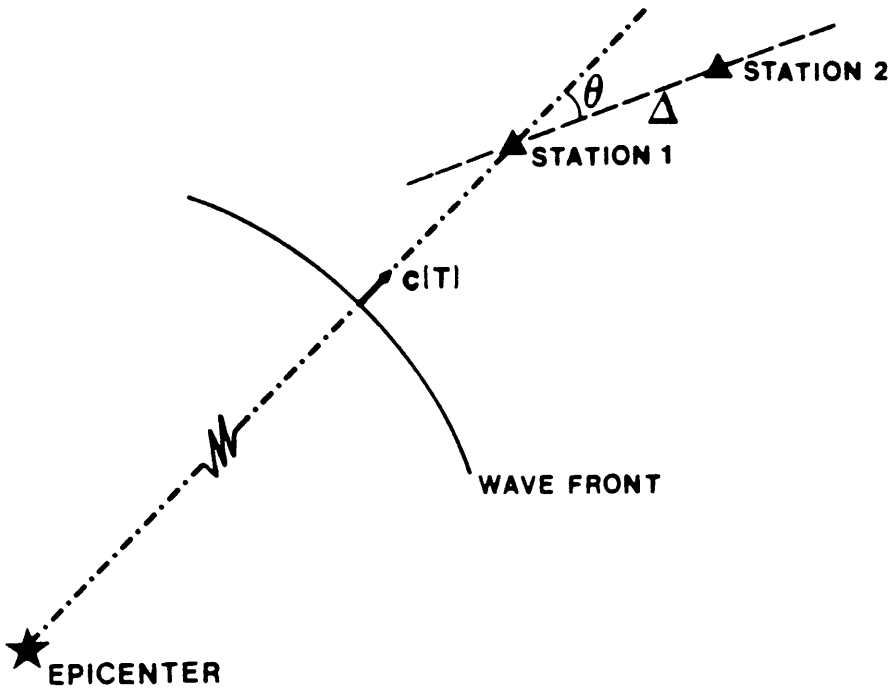

FIGURE 2.2

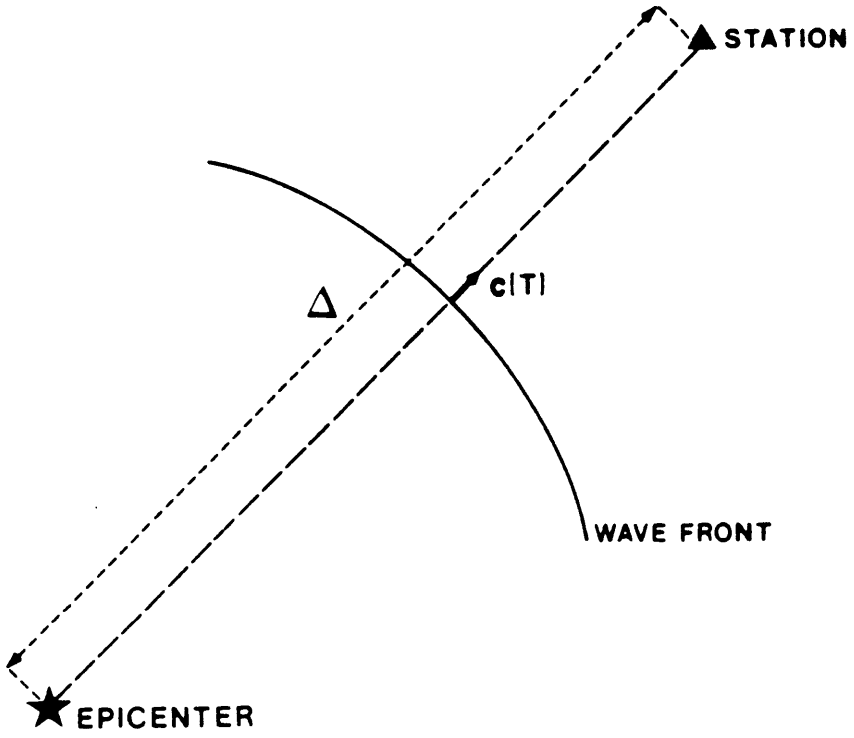

FIGURE 2.3

FIGURE 2.4 WORLDWIDE PHASE VELOCITY

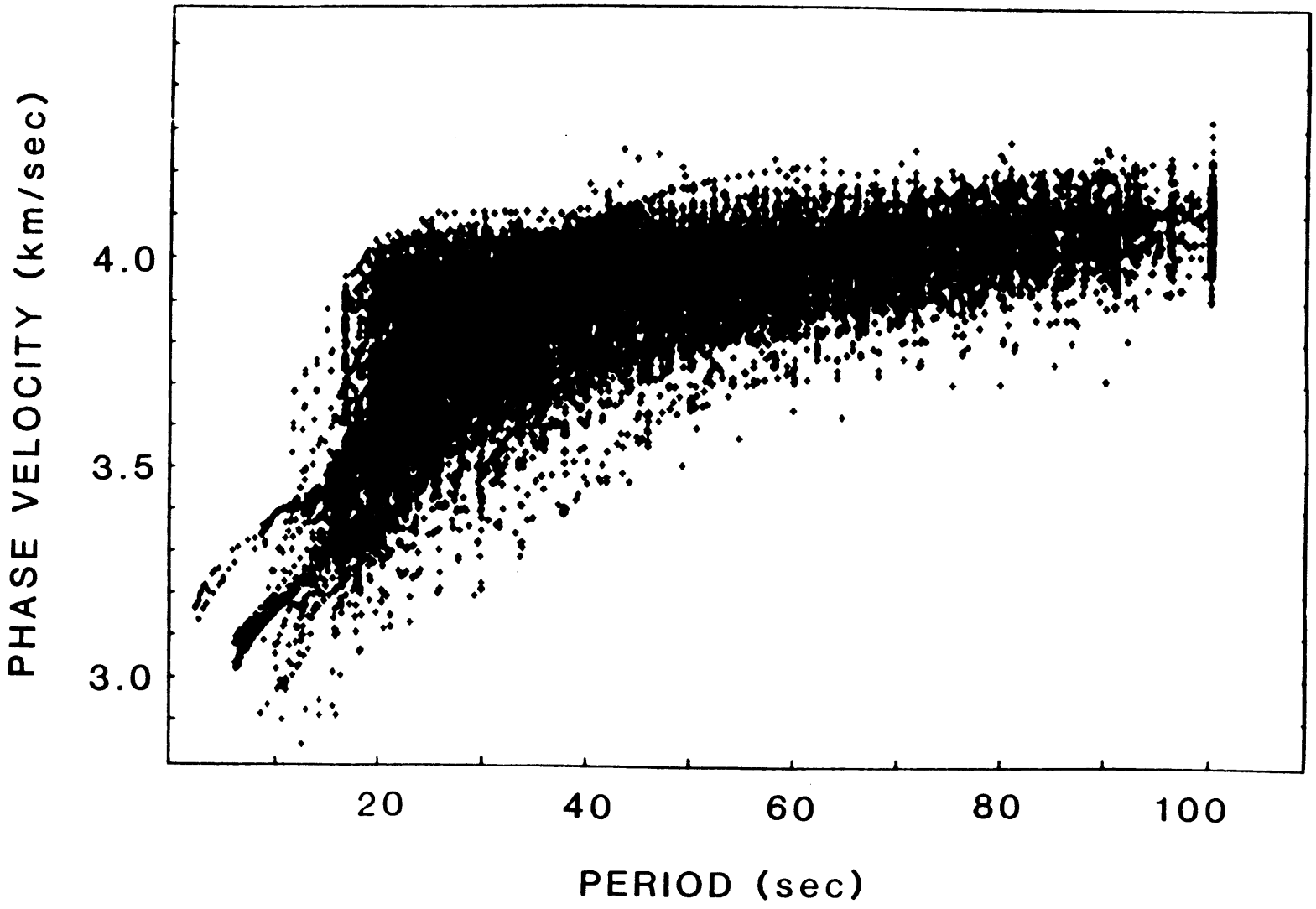

CHAPTER 3

Global regionalization of phase velocity of fundamental mode Rayleigh waves for the period range 20 to 100 sec.

3.1 - Introduction:

The objective of this chapter is the investigation of the phase velocity data collected from the literature which we discussed in chapter 2. The importance of this work is twofold: to determine the regions of the Earth where better coverage of paths are needed, and for grouping of the existing phase velocity data according to the tectonic types of their paths in order to have an initial model of global distribution of phase velocity.

Similar studies on a global scale have been done previously by a number of authors including Oliver (1962), Brune (1969), Dorman (1969), Knopoff (1972, 1983), and Sobel and von Seggern (1978).

The regionalization of phase velocity values for Rayleigh waves with period less than 100 sec on a global scale can have a number of applications: it can be used to detect major differences in the crustal and upper mantle structure of

different areas, to obtain the focal mechanism and depth of earthquakes from the inversion of the observations of such waves generated by these events, and to calculate synthetic seismograms of surface waves. In the references above, Oliver (1962), Brune (1969), Dorman (1969), and Knopoff (1972, 1983) all studied the correlation of the different regionalized phase velocity curves with the different crustal and upper mantle structure associated with several tectonic types. Sobel and von Seggern (1978) investigated the effects of lateral refraction of Rayleigh waves with 20 sec period propagating in a regionalized Earth model. The importance of regionalized phase velocity models in the study of the focal mechanism of earthquakes was demonstrated in the work of Tréhu *et al.* (1981), who studied the focal mechanism and depth of two earthquakes located in the North Atlantic using a regionalized phase velocity model of that region for the propagation correction applied to the observed Rayleigh wave phase spectra prior to the application of the moment tensor inversion method. The success of the work of Tréhu *et al.* (1981) was cited by Aki (1982a), who emphasized the importance of the determination of a worldwide phase velocity regionalized model for routine determination of moment tensor

and focal depth. The first attempt for calculation of synthetic seismograms of Rayleigh waves using regionalized phase velocity values was made by Aki and Nordquist (1961) who considered only the effect of dispersion. The latest attempt by Yomogida (1985) includes the effect of lateral variation in phase velocity on the wave form and amplitude.

The importance of the knowledge of the distribution of phase velocity around the world has been emphasized by Brune *et al.* (1960), Press (1960), Oliver *et al.* (1961), and Alexander (1963). Brune *et al.* (1960) proposed the use of the phase velocity data obtained from a global seismograph network (nonexistent then) to determine the source mechanism of global events, and to study the structure of the Earth. Press (1960) pointed out the importance of the knowledge on phase velocity to achieve the seismologist's goal of interpreting the whole seismograms. Oliver *et al.* (1961) proposed to accumulate and tabulate phase and group velocity information for all periods and all regions of the Earth, and emphasized its importance as comparable to the existing travel-time tables for body waves. Alexander (1963) proposed 'the construction of a world wide map' of surface wave dispersion data so that observations can be corrected for the propagation effects in source studies using surface wave data.

3.2 - Phase velocity data for reference periods:

In this section, we discuss the procedure used to regionalize the phase velocity data from the database described in Chapter 2 and plotted in Figure 2.4. As we can see in that graph, we have values of phase velocity for the period range up to 100 sec. We selected the period from 20 to 90 sec, with an increment of 10 sec, and the period 98 sec. The phase velocity at each of these nine period points was determined for each phase velocity dispersion curve through the interpolation of the values entered in our database from either tables or figures presented in each of the original reference work of Table 2.1. The interpolation scheme used involved the application of a cubic spline to the original phase velocity dispersion curve, so that if we have values $c_1(T_1)$ and $c_2(T_2)$ corresponding to period values T_1 and T_2, respectively, we can obtain the phase velocity value c(T) at

the reference period T (Hildebrand, 1974), for $T_1 < T < T_2$,

$$c(T) = c_1'(T_1)\frac{(T_2 - T)^2 (T - T_1)}{(T_2 - T_1)^2} - c_2'(T_2)\frac{(T - T_1)^2 (T_2 - T)}{(T_2 - T_1)^2} +$$

$$+ c_1(T_1)\frac{(T_2 - T)^2 [2(T - T_1) + (T_2 - T_1)]}{(T_2 - T_1)^3} +$$

$$+ c_2(T_2)\frac{(T - T_1)^2 [2(T_2 - T) + (T_2 - T_1)]}{(T_2 - T_1)^3} \qquad (3.1)$$

In this case, we chose the derivative values $c_1'(T_1)$ and $c_2'(T_2)$ to be estimated by the relation,

$$c_i'(T_i) = \frac{(\omega_i m_i + \omega_{i+1} m_{i+1})}{(\omega_i + \omega_{i+1})} \qquad (3.2)$$

with

$$\omega_i = \frac{1}{\max\{|m_i|, \varepsilon\}}$$

and

$$m_i = \frac{(c_i(T_i) - c_{i-1}(T_{i-1}))}{(T_i - T_{i-1})}$$

where m_i represents the slope of the curve between period values T_i and T_{i-1}, and ε is a small number chosen to avoid a singularity when calculating $c_i'(T_i)$. The above calculation of the spline weights $c_i'(T_i)$, i=1,2 was suggested by Wiggins (1976) for the interpolation of points in a digitized seismogram. We found it appropriate in the interpolation of the phase velocity dispersion curves of our database. Each curve was plotted for a visual check, and no problem was found in the interpolation routine. We show one of these curves, with the interpolated values, in Figure 3.1.

The histogram of the phase velocity for each of the reference periods 20 to 98 sec are shown in Figures 3.2 thru 3.10. We notice a trend from somewhat skewed distribution at 20 sec period, to a nearly symmetrical distribution at 98 sec reflecting the increasingly homogeneous region of the Earth sampled by longer period waves.

3.3 - Regionalized Earth models:

To regionalize the phase velocity data shown in Figures 3.2 thru 3.10, it is necessary to define a regionalized Earth model. Several models have been proposed as reviewed by Soriau and Soriau (1983). They selected three models and

compared how well these models behave in the regionalization of a data set composed of 296 phase velocity measurements in the 125 to 350 sec period range. The data were taken from the literature, and they concluded that all the three regionalized Earth models used showed approximately the same performance. Let us describe these three models in some detail.

One of these models was introduced by Okal (1977) in a study of phase velocity of Rayleigh waves in the 185 to 290 sec period range. The data set was composed of measurements collected by previous workers and new measurements made by Okal (1977). The objective of his work was to verify the existence of differences in phase velocity between oceanic and continental regions at long periods. His model was composed of seven regions: four oceanic, two continental, and one formed by areas of 'trenches and marginal seas'. The oceanic regions were bounded as follows: areas older than 135 m.y., with age between 135 and 80 m.y., with age between 80 and 30 m.y., and younger than 30 m.y.. The continents were divided into shield and 'phanerozoic mountainous' regions.

Lévêque (1980) used published and new observations of phase velocity of Rayleigh waves with period ranging from 150 to about 300 sec. The objective of this study was to

determine the shear velocity models for each region by an inversion process. The regionalized Earth model used in this work consists of four regions: young ocean (for portions of the sea floor younger than 30 m.y.), old ocean (oceanic areas older than 30 m.y.), 'shield and platform' region (consisting of tectonically stable continental areas), and a 'tectonic' region (formed by portions of continents and oceans which are more tectonically active today).

The third regionalized Earth model is due to Jordan (1981). This model was first published in Jordan (1979a, 1979b), and was used later by Silver and Jordan (1981) to account for regional differences determined by the study of free-oscillations. The discretized representation of this model used in this work was taken from Jordan (1981). His model consists of three oceanic and three continental regions. The oceans were divided into young, intermediate-age, and old ocean. The age boundary between young and intermediate is 25 m.y., and that between intermediate and old is 100 m.y.. The continental areas were divided into 'Precambrian shields and platforms'; 'Phanerozoic platforms'; and 'Phanerozoic orogenic zones and magmatic belts'.

Jordan (1981) suggested that such a regionalized Earth model should be used as a 'starting point for the development of laterally heterogeneous models of the upper mantle'. We shall follow this suggestion in the determination of regionalized phase velocity models for the Earth.

In Figure 3.11, we show the discretized version of Jordan's regionalization, using the same block size of $5^{\circ} \times 5^{\circ}$. Figure 3.11a represents the model used for waves with period less than or equal to 50 sec, while Figure 3.11b was used for waves with period greater than 50 sec. We adjusted the block size at high latitudes as shown in these figures, in order to make the size of these blocks comparable to wave length. Figures 3.12 and 3.13 shows regionalized Earth models of Lévêque (1980) and Okal (1977), respectively. We have taken these figures from the paper by Soriau and Soriau (1983), since the original papers by those two authors did not include the discretized version. The Earth model to be used for waves with period less than 50 sec has a total of 2412 blocks, and that to be used for waves with period longer than 50 sec 2286 blocks.

3.4 - Tracing greatcircle ray path:

We shall now describe our procedure for characterizing a given ray path in terms of a given regionalized Earth model. For simplicity, we assume a spherical Earth model and a great circle path.

Consider a system of cartesian coordinates (x, y, z) defined so that the z-axis intersects the Earth's surface at the North Pole, and the x-axis intersects it at the point with zero longitude lying on the Earth's equator. So, the cartesian coordinates of the two end points (1 and 2) of a ray path, are given by:

$$\begin{cases} x_i = R\cos\theta_i\cos\lambda_i \\ y_i = R\cos\theta_i\sin\lambda_i \\ z_i = R\sin\theta_i \end{cases} \quad ,i = 1, 2 \qquad (3.3)$$

where R is the Earth's equatorial radius.

We also define a system of cartesian coordinates (x', y', z') in a way that the x' and y' axes are in a plane that contains the greatcircle path between the two points as shown in Figure 3.14. The x' axis is defined to intersect the surface of the Earth at the point 1.

Using the new system of coordinates (x', y', z'), we define equally spaced points at an interval d along the ray path by the following equation.

$$\begin{cases} x_i' = R\cos\lambda_i' \\ y_i' = R\sin\lambda_i' \\ z_i' = 0 \end{cases} \qquad (3.4)$$

with $\lambda_i' = i \cdot d \quad (i = 1, 2, \ldots, N)$

To calculate the corresponding coordinates (x_i, y_i, z_i), of these N points, we use the rotation operator

$$\begin{bmatrix} x_i \\ y_i \\ z_i \end{bmatrix} = \begin{bmatrix} a_{11} & a_{12} & a_{13} \\ a_{21} & a_{22} & a_{23} \\ a_{31} & a_{32} & a_{33} \end{bmatrix} \begin{bmatrix} x_i' \\ y_i' \\ z_i' \end{bmatrix} \qquad (3.5)$$

The matrix elements a_{ij} were determined by the following correspondence: (1, 0, 0) to (x_1, y_1, z_1); (0, 0, 1) to $(x_1, y_1, z_1) \times (x_2, y_2, z_2)$; and (0, 1, 0) to $[(x_1, y_1, z_1) \times (x_2, y_2, z_2)] \times (x_1, y_1, z_1)$, where the symbol $\times$ means cross product.

The next step consists of the determination of the spherical coordinates (θ_i, λ_i) of each point (x_i, y_i, z_i),

$$\begin{cases} \theta_i = \tan^{-1}\left[\dfrac{y_i}{x_i}\right] \\ \lambda_i = \tan^{-1}\left[\dfrac{z_i}{\sqrt{x_i^2 + y_i^2}}\right] \end{cases} \qquad (3.6)$$

We finally calculate the Mercator projection coordinates (X_i, Y_i) using the following relation,

$$\begin{cases} X_i = \ln\left[\tan\left[45^\circ + \dfrac{\theta_i}{2}\right]\right] \\ Y_i = \lambda_i \end{cases} \qquad (3.7)$$

With the use of the above formulas, we can find which region a point on a given ray path belongs to.

3.5 - Regionalization of phase velocity data:

Taking advantage of the large amount of data in our database, we shall use a simple and robust method for constructing an initial model of regionalized phase velocity.

We shall use the formulas described in the preceding section to find what fraction of a given ray path in one of the regions specified by each of the three regionalized Earth models described earlier. We shall select ray paths for which more than 70% of the total path length lies in one of the specified regions, and assign the phase velocity for the path to the region as a sample. We repeat this selection process for all periods, and all ray paths for each of the three regionalized Earth models. The resulting histogram of phase velocity for each region is shown in Appendix A. The increment used in phase velocity while plotting the histograms in Appendix A was 0.01 km/sec for all cases. We calculated the sample mean $\bar{c}(T)$ and the square root of the sample variance $s^2(T)$ for each region, from the distribution shown in Appendix A by the following formulas.

$$\bar{c}(T) = \frac{1}{n} \sum_{i=1}^{n} c_i(T) \qquad (3.8)$$

$$s(T) = \sqrt{\frac{\sum_{i=1}^{n} (c_i(T) - \bar{c}(T))^2}{n - 1}} \qquad (3.9)$$

where n is the number of samples assigned to the region, $c_i(T)$ is the i-th sample of phase velocity value for a given region. The values of $\bar{c}(T)$, n, and s(T) are given in Table 3.1 for the regionalized Earth model of Jordan (1981), in Table 3.2, for the model of Leveque (1980), and in Table 3.3 for the model of Okal (1977). The sample average and standard deviation for the whole data set, for which histograms were presented in Figures 3.2 thru 3.10 for each reference period, are also shown in Table 3.1. The sample average for each case of Tables 3.1 thru 3.3 were plotted in Figures 3.15 thru 3.17. The histogram for regionalized phase velocity data show much narrower symmetric shape as compared to the skewed and broad histograms of global data shown in Figures 3.2 thru 3.10.

3.6 - Statistical analysis of the results of regionalization:

Let us now compare the models of Jordan (1981), Lévêque (1980), and Okal (1977) in order to see which model is the most effective in performing regionalization. This comparison can be made by the use of hypothesis testing (*e.g.*, DeGroot, 1975, Lass and Gottlieb, 1971; and Huang, 1985 for a recent geophysical publication).

For a given regionalization model, we shall test the hypothesis that any two regions may have the same mean and variance. If the hypothesis is accepted, we must conclude that the regionalization model is not effective because there is no reason to distinguish the two regions. Let us compare region 1 with ($\bar{c}_i(T)$, n_i and $s_i(T)$) and region 2 with ($\bar{c}_{ii}(T)$, n_{ii} and $s_{ii}(T)$).

Step 1: The first step is to determine a value $F'_{1-\alpha/2}(T)$ for the degrees of freedom pair, ($n_i(T)-1$, $n_{ii}(T)-1$) and another value $F''_{1-\alpha/2}(T)$ for the second pair, ($n_{ii}(T)-1$, $n_i(T)-1$), both values are taken from a table that contains the percentile of the F distribution for such pairs. If specified values for the degree of freedom values were not available, linear interpolation was used. The value for α was chosen to be 2 percent in all cases.

We then computed the values of F(T),

$$F(T) = \frac{s_i^2(T)}{s_{ii}^2(T)} \qquad (3.10)$$

and tested if $F(T) > F'_{1-\alpha/2}$ or $F(T) < 1/(F'_{1-\alpha/2})$. If any of these was true, the null hypothesis stating that σ_i^2 is the

same as σ_{ii}^2 was rejected. Otherwise, there is no reason to believe that σ_i^2 and σ_{ii}^2 differ on the 98 percent confidence interval.

Step 2: If we had concluded from the first step that $\sigma_i^2(T)$ and $\sigma_{ii}^2(T)$ are different, we used the following test to check if the phase velocity means $m_i(T)$ and $m_{ii}(T)$ are different:

We first calculate the estimated variance for both regions i and ii,

$$\begin{cases} V_i(T) = \dfrac{s_i^2(T)}{n_i(T)} \\ V_{ii}(T) = \dfrac{s_{ii}^2(T)}{n_{ii}(T)} \end{cases} \qquad (3.11)$$

we then find f(T), the effective number of degrees of freedom,

$$f(T) = \frac{(V_i(T) + V_{ii}(T))^2}{\left[\dfrac{V_i^2(T)}{n_i(T) + 1}\right] + \left[\dfrac{V_{ii}^2(T)}{n_{ii}(T) + 1}\right]} - 2 \qquad (3.12)$$

A search for the value of $t_{1-\alpha/2}(T)$ was made using a table containing the percentiles of the t-distribution that corresponds to f(T) (linear interpolation was again used in the process, whenever it was needed). We finally computed the value of u(T), using

$$u(T) = t_{1-\alpha/2}(T) \sqrt{V_i(T) + V_{ii}(T)} \qquad (3.13)$$

Step 3: If the result of step 1 did not reject the hypothesis that $\sigma_i^2(T)$ and $\sigma_{ii}^2(T)$ are the same, we proceeded to determine if $m_i(T)$ and $m_{ii}(T)$ differ:

Given the number of degrees of freedom,

$$V(T) = n_i(T) + n_{ii}(T) - 2 \qquad (3.14)$$

We then search for the corresponding value of $t_{1-\alpha/2}(T)$ in the same table containing the percentiles of the t distribution of step 2. The computation of the value of u(T) can then be made

using:

$$s_p(T) = \sqrt{\frac{(n_i(T) - 1)\, s_i^2(T) + (n_{ii}(T) - 1)\, s_{ii}^2(T)}{n_i(T) + n_{ii}(T) - 2}} \qquad (3.15)$$

so that,

$$u(T) = t_{1-\alpha/2}\; s_p(T) \sqrt{\frac{n_i(T) + n_{ii}(T)}{n_i(T)\, n_{ii}(T)}} \qquad (3.16)$$

The value of u(T) for each region, obtained using either steps 2 (Equation 3.13) or 3 (Equation 3.16), is then compared with the absolute value of the difference between the measured phase velocity averages $\bar{c}_i(T)$ and $\bar{c}_{ii}(T)$. If $u(T) > |\bar{c}_i(T) - \bar{c}_{ii}(T)|$, we decide that $\bar{c}_i(T)$ and $\bar{c}_{ii}(T)$ are different. Otherwise, we state that 'there is no reason to believe that regions i and ii differ with regard to their average'.

The results of the above tests are summarized in Tables 3.4 thru 3.6. From these, we can see that the above analysis determined which of the values for both m(T) and $\sigma^2(T)$ of each case, to be significantly different.

We have repeated the above analysis for the three regionalization models using the significance level α of 20 percent, and the results show only small differences among Tables 3.4 thru 3.6. Comparing these results, we see that the performance of the models is about the same: approximately 73 percent of the comparisons made using the model of Jordan (1981) showed the regions to have significantly different mean, compared with 72 percent of the comparisons using the four-region model of Lévêque (1980), and with 80 percent of the comparisons between the seven region types of Okal (1977). We then decided to use Jordan's (1981) model in our analysis of new phase velocity data in Chapters 4 and 5.

TABLE 3.1 - JORDAN'S MODEL - PHASE VELOCITY (includes also all data)

REGION / T (sec)	a	b	c	p	q	s	ALL DATA
20	3.805 38 0.053	3.882 19 0.089	3.937 23 0.045	3.580 7 0.044	3.496 103 0.141	3.631 12 0.046	3.709 426 0.199
30	3.819 41 0.044	3.959 19 0.082	4.028 37 0.037	3.828 16 0.058	3.702 197 0.173	3.876 32 0.057	3.821 736 0.155
40	3.821 40 0.040	3.965 23 0.078	4.039 46 0.033	3.968 15 0.067	3.811 190 0.143	3.996 33 0.056	3.908 786 0.122
50	3.834 39 0.042	3.960 24 0.079	4.042 45 0.034	4.034 14 0.069	3.869 177 0.105	4.033 28 0.072	3.945 745 0.101
60	3.862 36 0.027	3.975 22 0.076	4.047 45 0.035	4.068 14 0.071	3.922 155 0.090	4.064 24 0.075	3.977 676 0.088
70	3.890 34 0.028	3.994 21 0.068	4.054 45 0.039	4.102 12 0.061	3.965 132 0.080	4.097 21 0.066	4.004 633 0.079
80	3.922 31 0.028	4.015 17 0.062	4.068 45 0.042	4.119 12 0.069	4.003 114 0.067	4.121 19 0.066	4.031 581 0.073
90	3.958 31 0.027	4.044 16 0.065	4.092 43 0.045	4.146 10 0.089	4.036 84 0.057	4.146 18 † 0.069	4.058 435 0.068
98	3.985 28 0.027	4.082 12 0.066	4.120 41 0.034	4.165 9 0.103	4.076 40 0.052	4.193 5 † 0.103	4.084 261 0.064

† paths containing more than 40% of their portion inside the region were used in the indicated cases

TABLE 3.2 - LÉVÊQUE'S MODEL - PHASE VELOCITY

REGION / T (sec)	N	=	0	
20	3.766 54 0.136	3.933 57 0.075	3.610 61 0.117	3.495 57 0.163
30	3.800 72 0.081	4.008 78 0.065	3.846 123 0.073	3.656 149 0.169
40	3.832 70 0.073	4.020 97 0.052	3.968 126 0.084	3.778 162 0.133
50	3.859 68 0.080	4.023 95 0.051	4.007 104 0.084	3.856 163 0.091
60	3.888 62 0.083	4.030 94 0.050	4.035 89 0.087	3.910 139 0.069
70	3.918 57 0.083	4.038 93 0.051	4.062 79 0.081	3.950 119 0.054
80	3.958 52 0.081	4.058 88 0.044	4.088 67 0.073	3.988 110 0.048
90	3.969 39 0.052	4.083 81 0.043	4.122 45 0.073	4.020 72 0.046
98	3.994 33 0.036	4.111 61 0.040	4.131 24 0.086	4.062 28 0.047

TABLE 3.3 - OKAL'S MODEL - PHASE VELOCITY

REGION / T (sec)	N	#	=	- †	0	.	✗
20	3.841 32 0.078	3.795 37 0.212	3.987 8 0.022	3.914 8 0.038	3.585 60 0.081	3.534 39 0.170	3.555 35 0.218
30	3.855 36 0.065	3.927 41 0.114	4.042 15 0.028	4.032 14 0.035	3.834 153 0.073	3.621 110 0.162	3.733 74 0.160
40	3.858 37 0.063	3.955 40 0.090	4.038 20 0.029	4.045 17 0.033	3.962 156 0.071	3.738 113 0.120	3.853 68 0.118
50	3.872 38 0.062	3.965 36 0.072	4.033 19 0.034	4.051 17 0.035	4.017 139 0.072	3.828 116 0.091	3.897 65 0.095
60	3.890 35 0.057	3.977 35 0.069	4.035 19 0.036	4.054 17 0.036	4.048 117 0.075	3.894 103 0.080	3.943 56 0.073
70	3.916 31 0.054	3.996 33 0.064	4.039 19 0.038	4.060 17 0.039	4.076 103 0.068	3.939 93 0.070	3.973 51 0.062
80	3.946 27 0.055	4.026 31 0.058	4.052 19 0.042	4.074 17 0.039	4.104 87 0.057	3.985 87 0.061	3.998 46 0.060
90	3.981 27 0.054	4.054 28 0.043	4.082 17 0.031	4.103 14 0.046	4.141 56 0.062	4.026 56 0.044	4.027 36 0.060
98	4.002 24 0.047	4.089 13 0.039	4.105 16 0.032	4.135 13 0.031	4.150 32 0.076	4.057 23 0.054	4.086 21 0.041

† paths with more than 40% of their length inside this region were used

TABLE 3.4 - JORDAN'S MODEL

T (sec)	REGIONS axb	axc	axp	axq	axs	bxc	bxp	bxq	bxs	cxp	cxq	cxs	pxq	pxs	qxs
20	Y Y	N Y	N Y	Y Y	N Y	Y N	N Y	N Y	N Y	N Y	Y Y	N Y	Y Y	N N	Y Y
30	Y Y	N Y	N N	Y Y	N Y	Y Y	N Y	Y Y	N Y	N Y	Y Y	Y Y	Y Y	N N	Y Y
40	Y Y	N Y	Y Y	Y N	N Y	Y Y	N N	Y Y	N N	Y Y	Y Y	Y Y	Y Y	N N	Y Y
50	Y Y	N Y	Y Y	Y Y	Y Y	Y Y	N Y	N Y	N Y	Y N	Y Y	Y N	N Y	N N	N Y
60	Y Y	N Y	Y Y	Y Y	Y Y	Y Y	N Y	N Y	N Y	Y N	Y Y	Y N	N Y	N N	N Y
70	Y Y	N Y	Y Y	Y Y	Y Y	Y Y	N Y	N N	N Y	N Y	Y Y	Y Y	N Y	N N	N Y
80	Y Y	N Y	Y Y	Y Y	Y Y	N Y	N Y	N N	N Y	Y N	Y Y	Y Y	N Y	N N	N Y
90	Y Y	Y Y	Y Y	Y Y	Y Y	N Y	N Y	N N	N Y	Y N	N Y	N Y	N Y	N N	N Y
98	Y Y	N Y	Y Y	Y Y	Y Y	Y N	N N	N N	N Y	Y N	Y Y	Y N	Y N	N N	Y N

Example: null hypotheses when comparing regions i and ii:

Y<--- σ^2_i and σ^2_{ii} are different? Yes
N<--- m_i and m_{ii} are different? No

TABLE 3.5 - LÉVÊQUE'S MODEL

T (sec)	REGIONS Nx=	NxO	Nx$\not\beta$	=xO	=x$\not\beta$	Ox$\not\beta$
20	Y Y	N Y	N Y	Y Y	Y Y	Y Y
30	N Y	N Y	Y Y	N Y	Y Y	Y Y
40	Y Y	N Y	Y Y	Y Y	Y Y	Y Y
50	Y Y	N Y	N N	Y N	Y Y	N Y
60	Y Y	N Y	N N	Y N	Y Y	N Y
70	Y Y	N Y	Y Y	Y N	N Y	Y Y
80	Y Y	N Y	Y Y	Y Y	N Y	Y Y
90	N Y	N Y	N Y	Y Y	N Y	Y Y
98	N Y	Y Y	N Y	Y N	N Y	Y Y

Example: null hypotheses when comparing regions i and ii:

Y<--- σ^2_i and σ^2_{ii} are different? Yes
N<--- m_i and m_{ii} are different? No

TABLE 3.6 - OKAL'S MODEL

T (sec)	REGIONS														
	Nx#	Nx=	Nx-	Nx0	Nx.	Nx/	#x=	#x-	#x0	#x.	#x/	=x-	=x0	=x.	=x/
20	Y N	Y Y	N Y	N Y	Y Y	Y Y	Y Y	Y Y	Y Y	N Y	N Y	N Y	Y Y	Y Y	Y Y
30	Y Y	Y Y	N Y	N N	Y Y	Y Y	Y Y	Y Y	Y Y	Y Y	N Y	N N	Y Y	Y Y	Y Y
40	N Y	Y Y	Y Y	N Y	Y Y	Y N	Y Y	Y Y	N N	N Y	N Y	N N	Y Y	Y Y	Y Y
50	N Y	Y Y	Y Y	N Y	Y Y	Y N	Y Y	Y Y	N Y	N Y	N Y	N N	Y N	Y Y	Y Y
60	N Y	N Y	N Y	N Y	N N	N Y	Y Y	Y Y	N Y	N Y	N N	N N	Y N	Y Y	Y Y
70	N Y	N Y	N Y	N Y	N N	N Y	N Y	N Y	N Y	N Y	N N	N N	Y Y	Y Y	N Y
80	N Y	N Y	N Y	N Y	N Y	N Y	N N	N Y	N Y	N Y	N N	N N	N Y	N Y	N Y
90	N Y	N Y	N Y	N Y	N Y	N Y	N N	N Y	N Y	N Y	N N	N N	Y Y	N Y	Y Y
98	N Y	N Y	N Y	Y Y	N Y	N Y	N N	N Y	Y Y	N N	N N	N Y	Y Y	N Y	N N

TO BE CONTINUED

Example: null hypotheses when comparing regions i and ii:

Y<--- σ^2_i and σ^2_{ii} are different? Yes
N<--- m_i and m_{ii} are different? No

TABLE 3.6 - OKAL'S MODEL
(CONTINUED)

T (sec)	REGIONS -x0	-x.	-xϕ	0x.	0xϕ	.xϕ
20	N Y	Y Y	Y Y	Y N	Y N	N N
30	Y Y	Y Y	Y Y	Y Y	Y Y	N Y
40	Y Y	Y Y	Y Y	Y Y	Y Y	N Y
50	Y Y	Y Y	Y Y	Y Y	Y Y	N Y
60	Y N	Y Y	Y Y	N Y	N Y	N Y
70	Y N	Y Y	N Y	N Y	N Y	N Y
80	N N	N Y	N Y	N Y	N Y	N N
90	N N	N Y	N Y	Y Y	N Y	N N
98	Y N	N Y	N Y	N Y	Y Y	N N

Example: null hypotheses when comparing regions i and ii:

Y<--- σ^2_i and σ^2_{ii} are different? Yes
N<--- m_i and m_{ii} are different? No

Figure 3.1 - Plot of the phase velocity data (crosses) given in Figure 13 of the work by Kuo *et al.* (1962), and the interpolated values (circles).

Figures 3.2 thru 3.10 - Histogram of the phase velocity at reference periods from 20 thru 98 sec. A velocity increment of 0.01 km/sec was used to construct these histograms.

Figures 3.11a, 3.12a, and 3.13a - Discretized representation of the regionalized Earth models of Jordan (1981), Lévêque (1980), and Okal (1977) respectively, to be used for waves with period less than or equal 50 sec. Note that, for latitudes larger than 80 degrees, some adjustment was made on the block size.

In the model by Jordan (1981), symbol 'a' represents young oceanic regions (0 to 25 m.y.), 'b' is used for intermediate-age ocean (25 to 100 m.y.), 'c' corresponds to old ocean (age > 100 m.y.). In the continents, 'p' represents 'Phanerozoic platforms'; 'q', 'Phanerozoic orogenic zones and magmatic belts'; and 's' is used for 'Precambrian shields and platforms'. The model of

Lévêque (1980) shows the following symbols: 'N', for oceanic areas with age ranging from 0 to 30 m.y., '=' for oceanic areas older than 30 m.y.. In addition, '0' is used for shield areas in the continents, and '⊬' is used for 'tectonic areas'. Finally, the model of Okal (1977) uses symbols 'N', '#', '=', and '-' for oceanic areas. These areas are bounded by the 30, 80, and 135 m.y. age contours, respectively. Other symbols are '0', for shield areas, '.' for 'Phanerozoic mountains', and '⊬' for 'trenches and marginal seas'. The above symbols were also used in Tables 3.1 thru 3.3, and Figures 3.15 thru 3.17.

Figures 3.11b, 3.12b, and 3.13b - Discretized representation of the regionalized Earth models of Jordan (1981), Lévêque (1980), and Okal (1977) respectively, to be used for waves with period greater than 50 sec.

Figure 3.14 - Coordinate systems used in tracing the greatcircle ray path.

Figures 3.15 thru 3.17 - Plot of the average phase velocity value $\bar{c}(T)$ measured for each region of the Earth models shown in Figures 3.11 thru 3.13, respectively.

FIGURE 3.1

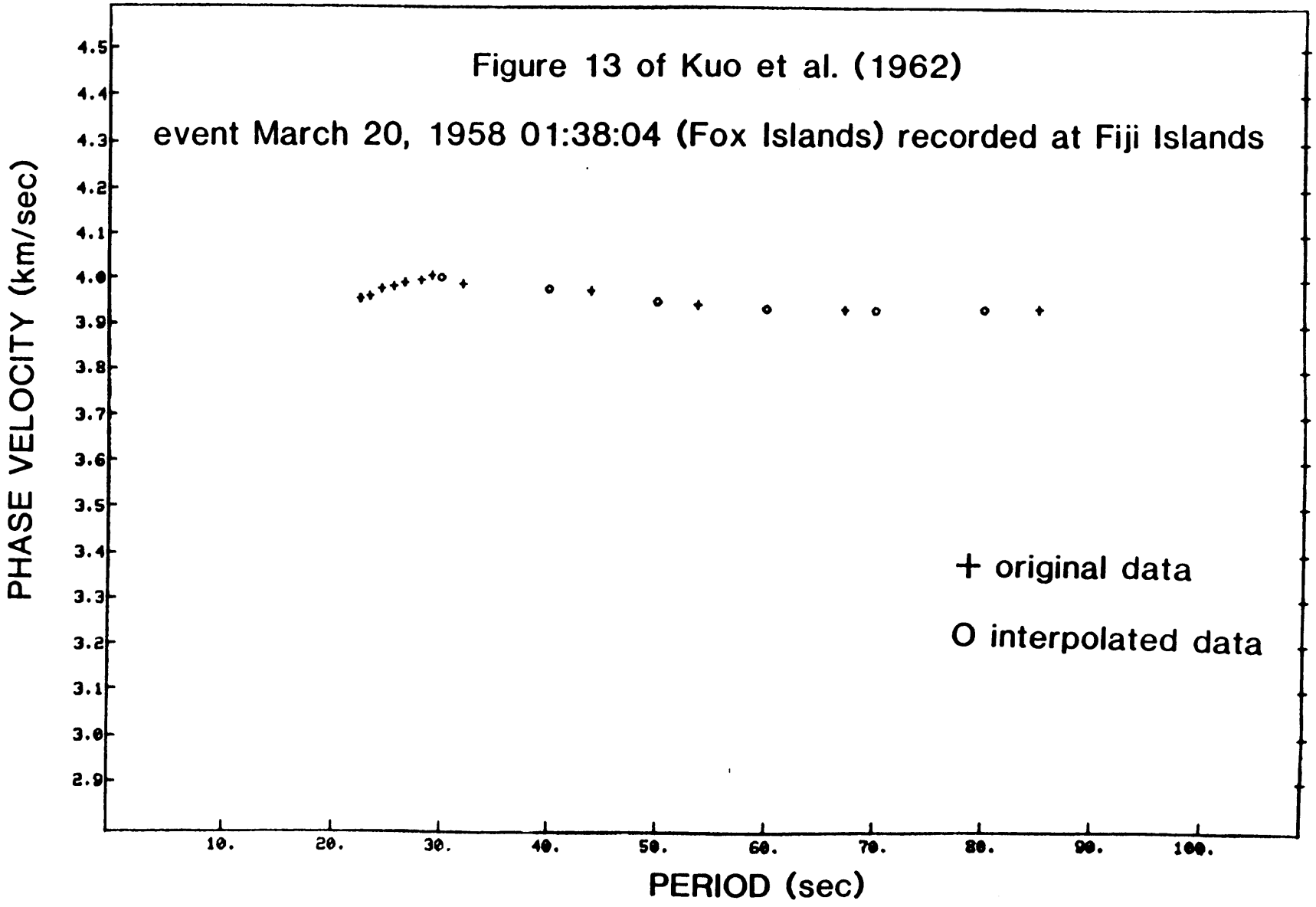
Figure 13 of Kuo et al. (1962)
event March 20, 1958 01:38:04 (Fox Islands) recorded at Fiji Islands
PHASE VELOCITY (km/sec)
4.5
4.4
4.3
4.2
4.1
4.0
3.9
3.8
3.7
3.6
3.5
3.4
3.3
3.2
3.1
3.0
2.9
10.
20.
30.
40.
50.
60.
70.
80.
90.
100.
PERIOD (sec)
+ original data
O interpolated data

FIGURE 3.2

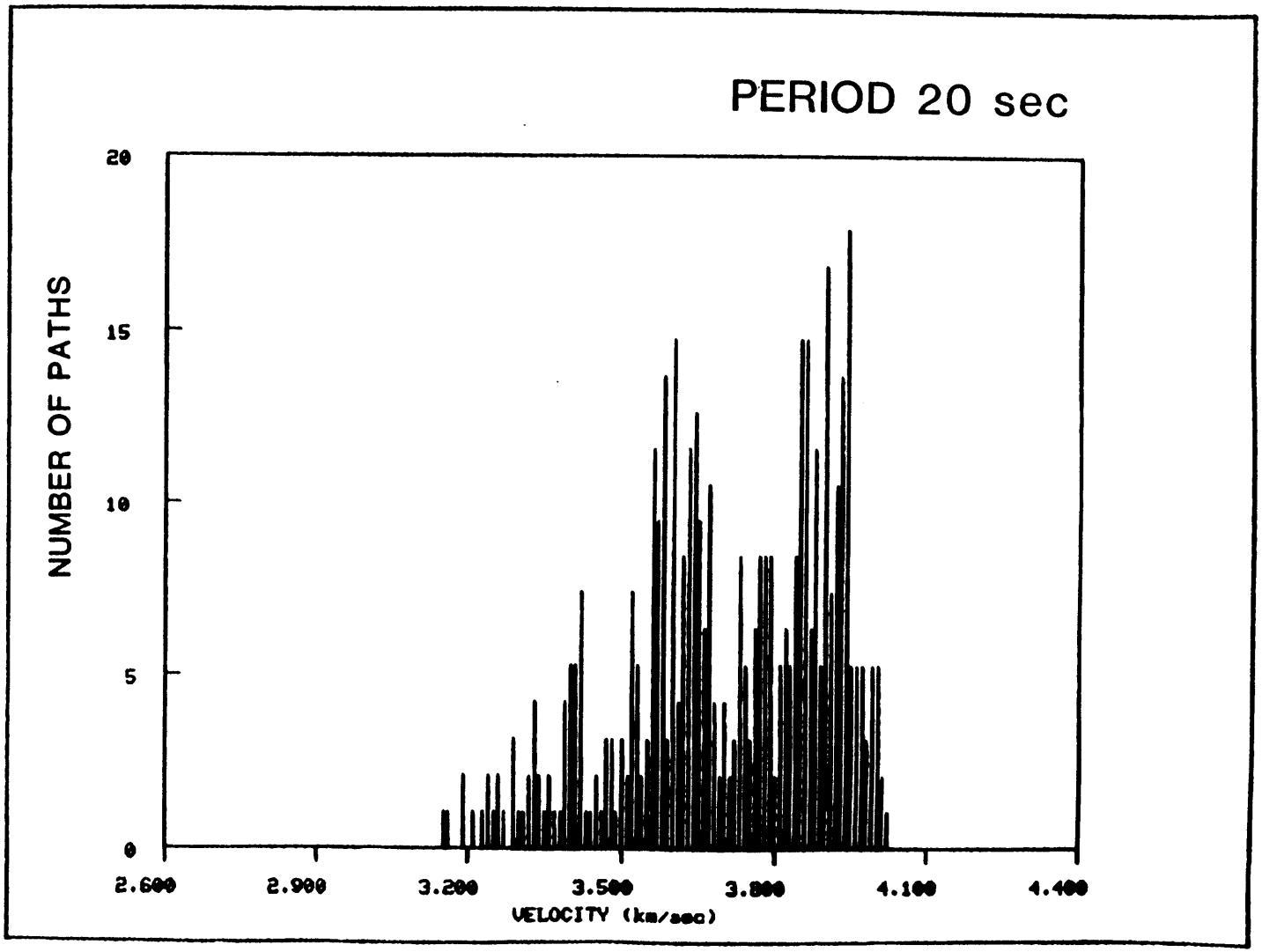
PERIOD 20 sec
NUMBER OF PATHS
20
15
10
5
0
2.600
2.900
3.200
3.500
3.800
4.100
4.400
VELOCITY (km/sec)

FIGURE 3.3

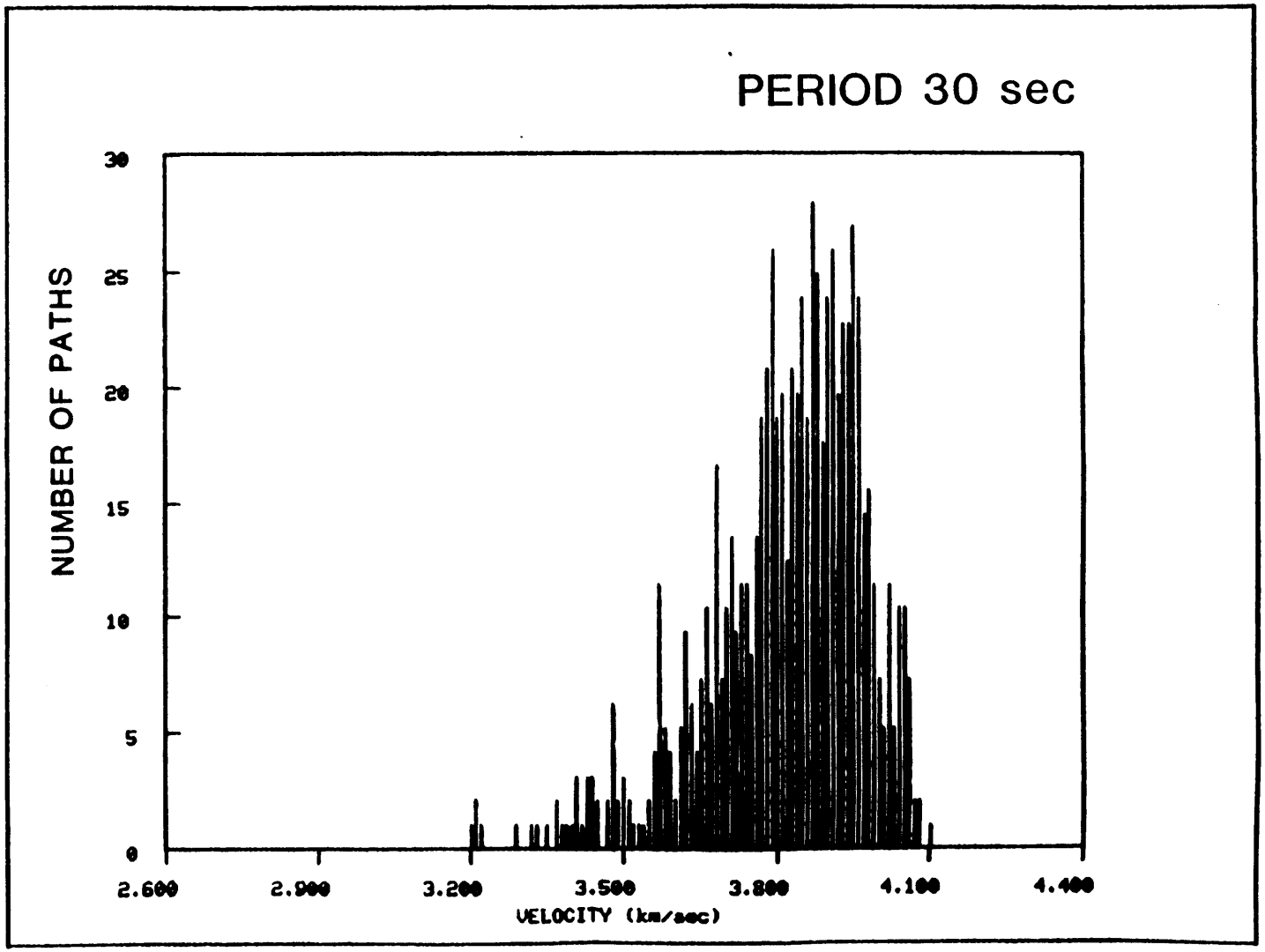
PERIOD 30 sec
NUMBER OF PATHS
30
25
20
15
10
5
0
2.600
2.900
3.200
3.500
3.800
4.100
4.400
VELOCITY (km/sec)

FIGURE 3.4

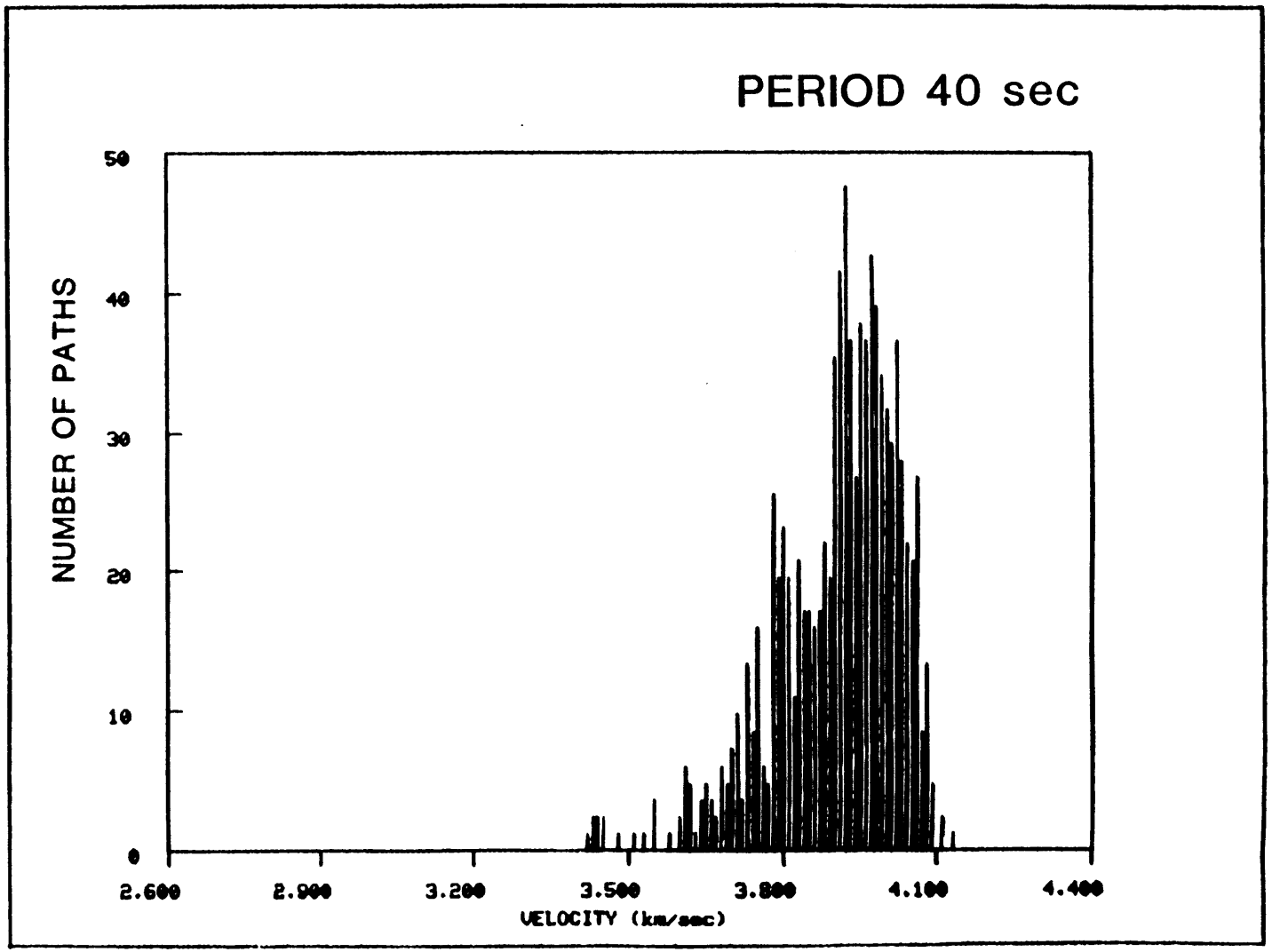
PERIOD 40 sec
NUMBER OF PATHS
50
40
30
20
10
0
2.600
2.900
3.200
3.500
3.800
4.100
4.400
VELOCITY (km/sec)

FIGURE 3.5

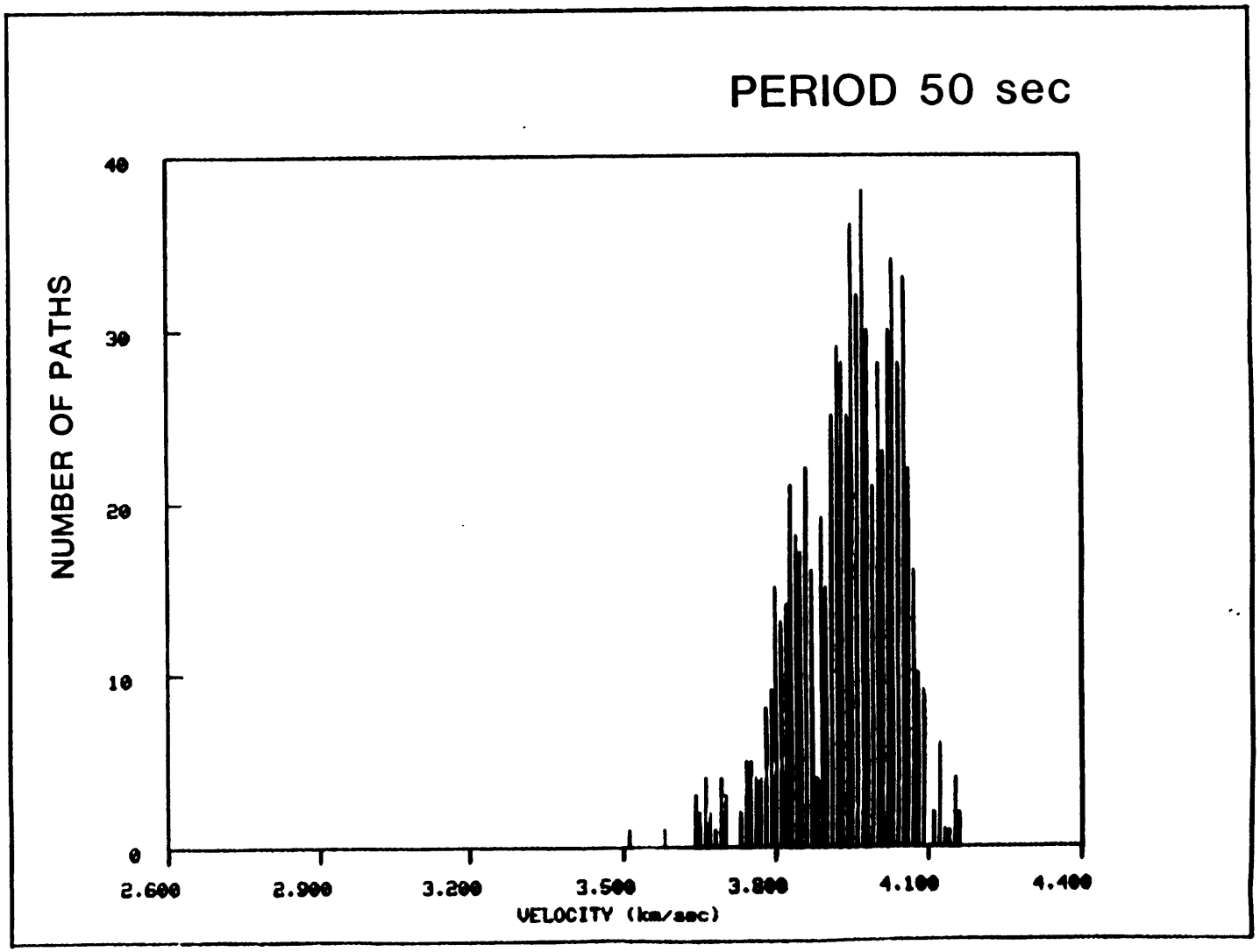
PERIOD 50 sec
NUMBER OF PATHS
40
30
20
10
0
2.600
2.900
3.200
3.500
3.800
4.100
4.400
VELOCITY (km/sec)

FIGURE 3.6

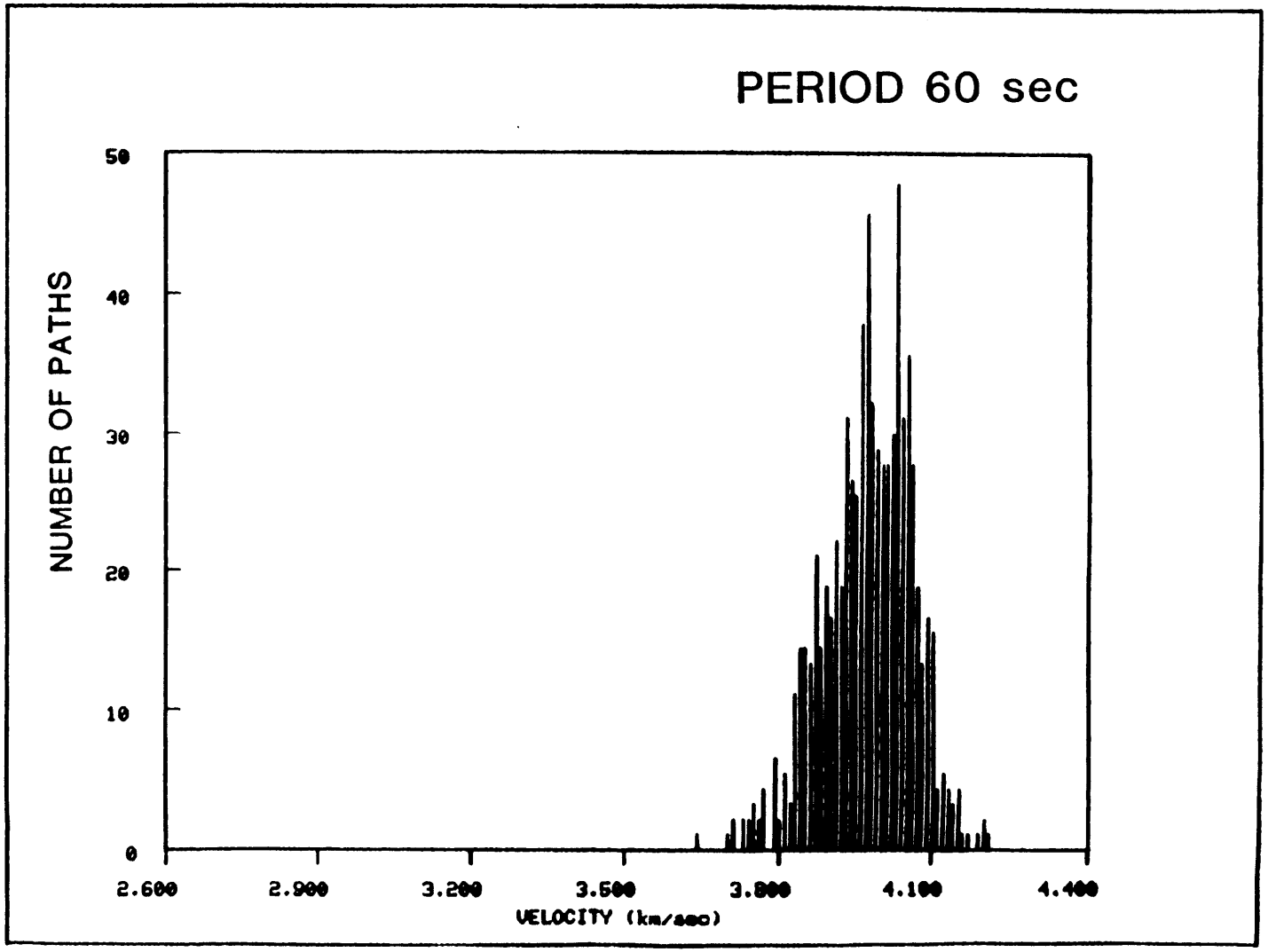
PERIOD 60 sec
NUMBER OF PATHS
50
40
30
20
10
0
2.600
2.900
3.200
3.500
3.800
4.100
4.400
VELOCITY (km/sec)

FIGURE 3.7

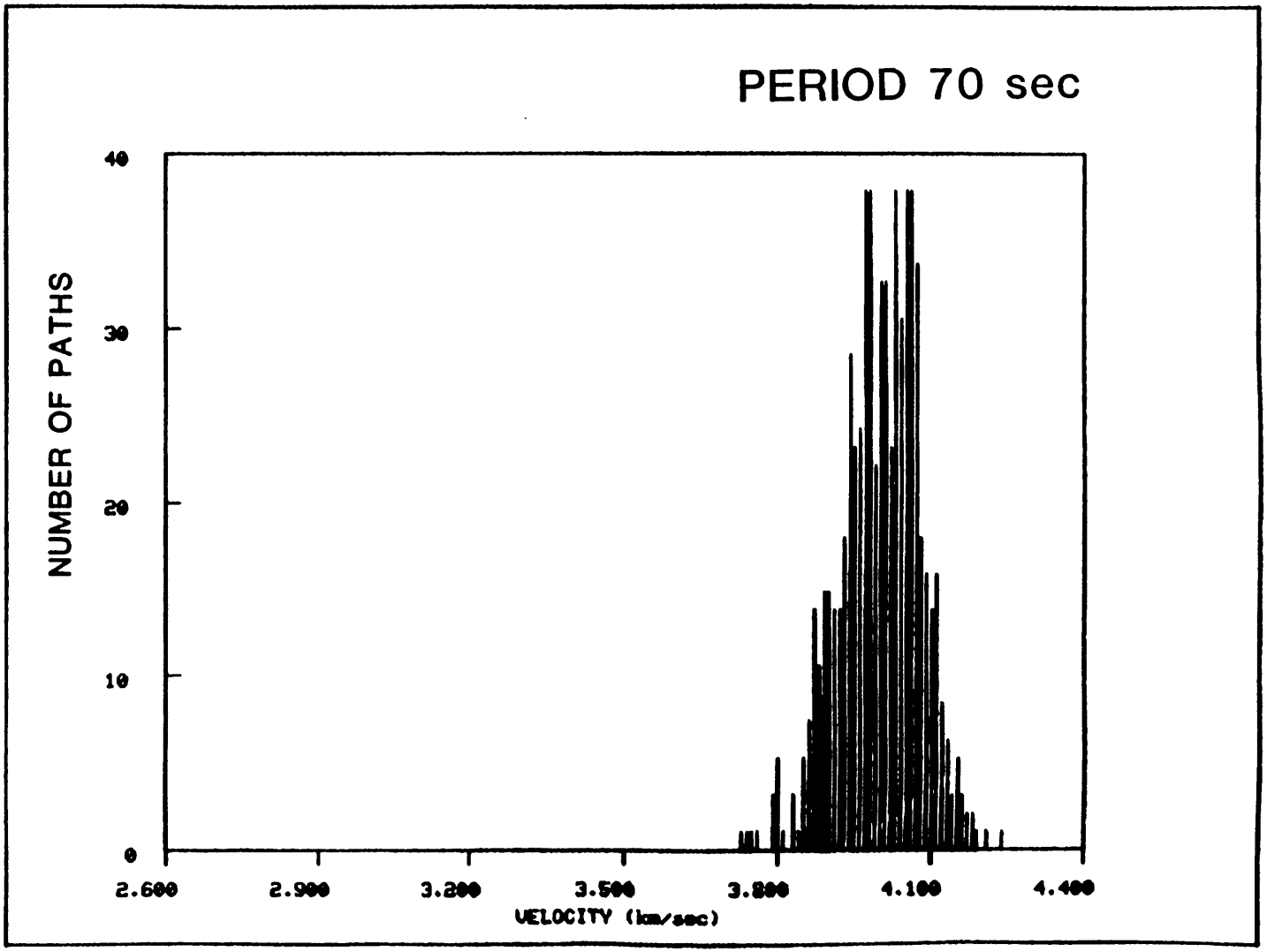
PERIOD 70 sec
NUMBER OF PATHS
40
30
20
10
0
2.600
2.900
3.200
3.500
3.800
4.100
4.400
VELOCITY (km/sec)

FIGURE 3.8

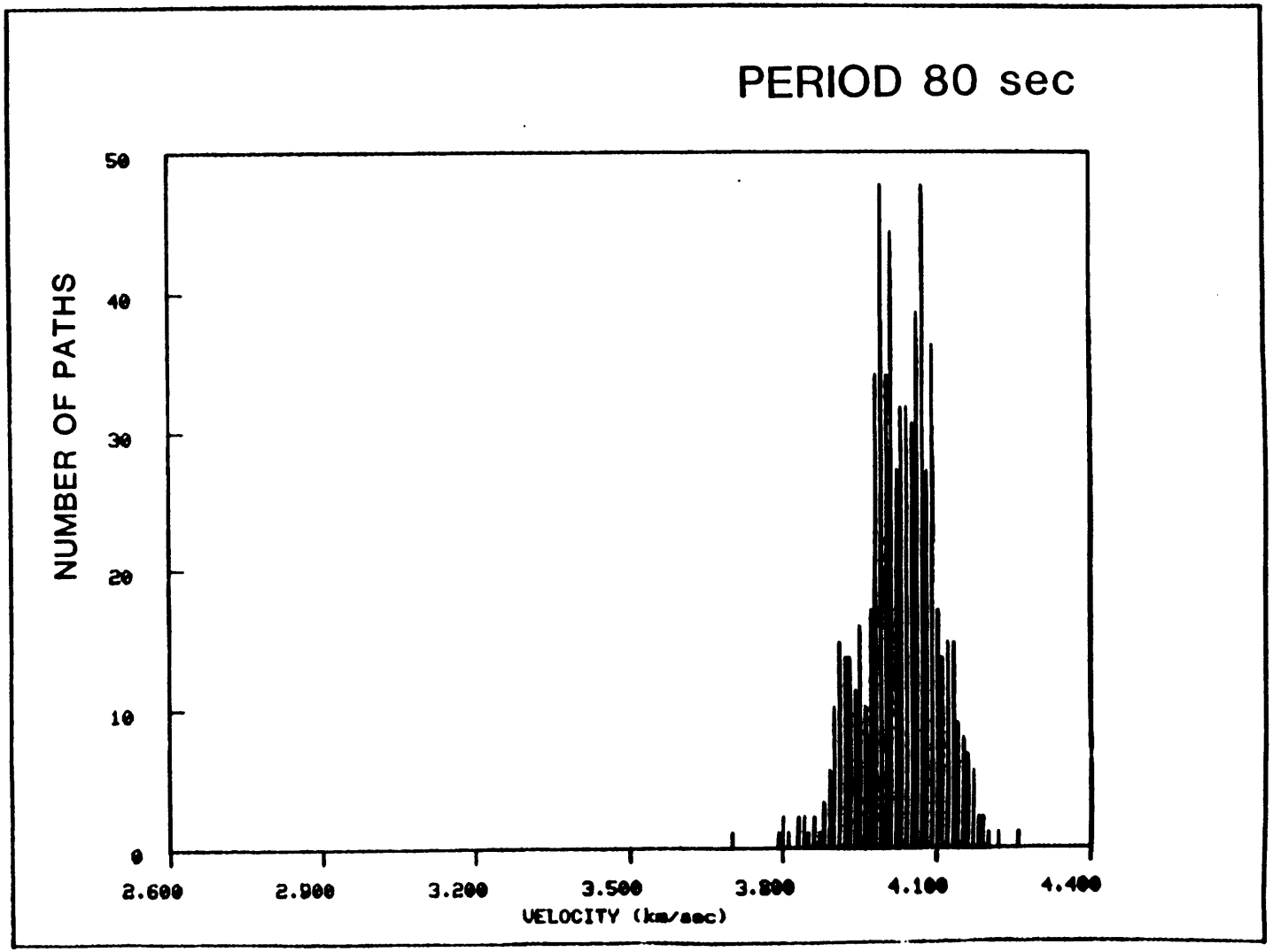
PERIOD 80 sec
NUMBER OF PATHS
50
40
30
20
10
0
2.600
2.900
3.200
3.500
3.800
4.100
4.400
VELOCITY (km/sec)

FIGURE 3.9

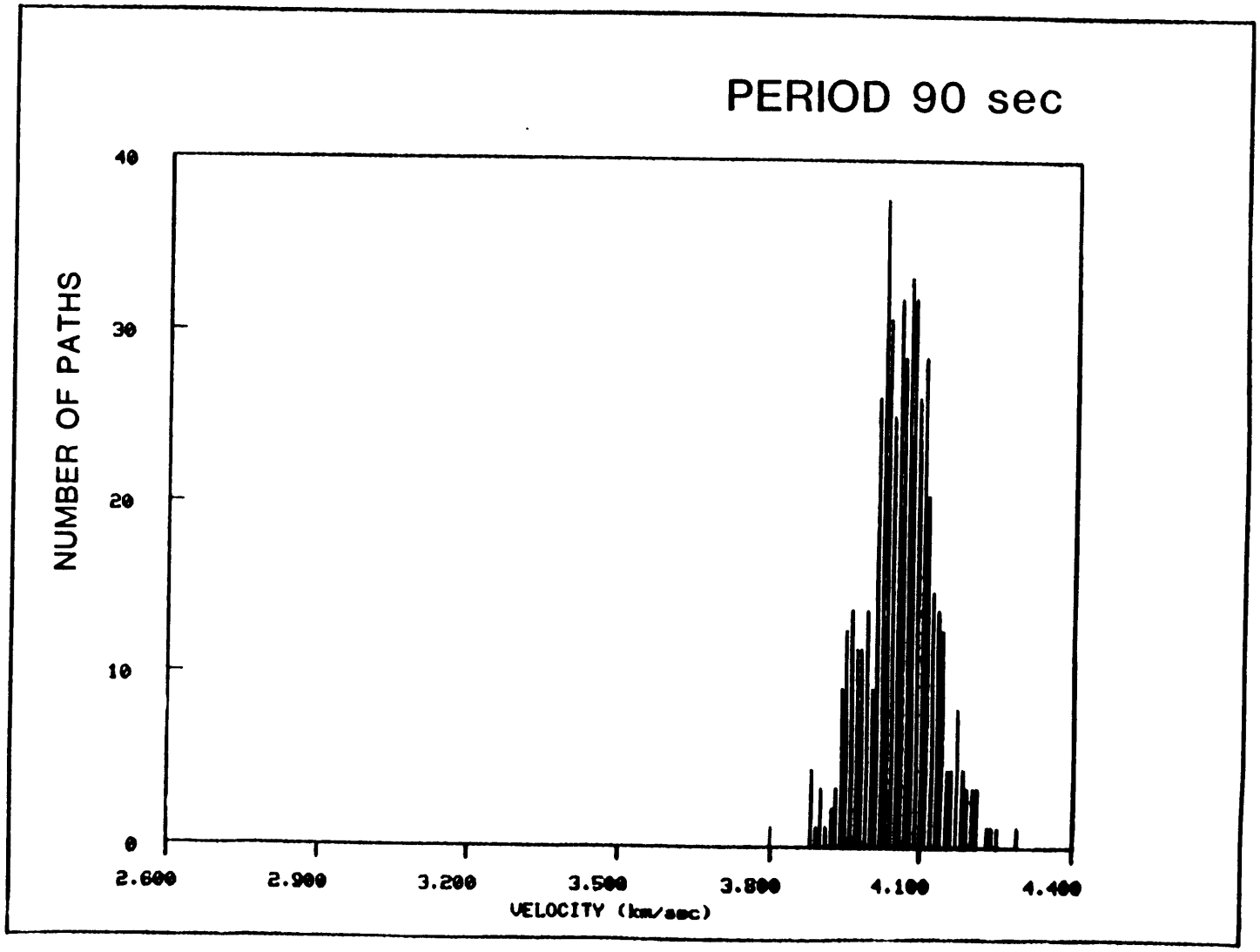
PERIOD 90 sec
NUMBER OF PATHS
40
30
20
10
0
2.600
2.900
3.200
3.500
3.800
4.100
4.400
VELOCITY (km/sec)

FIGURE 3.10

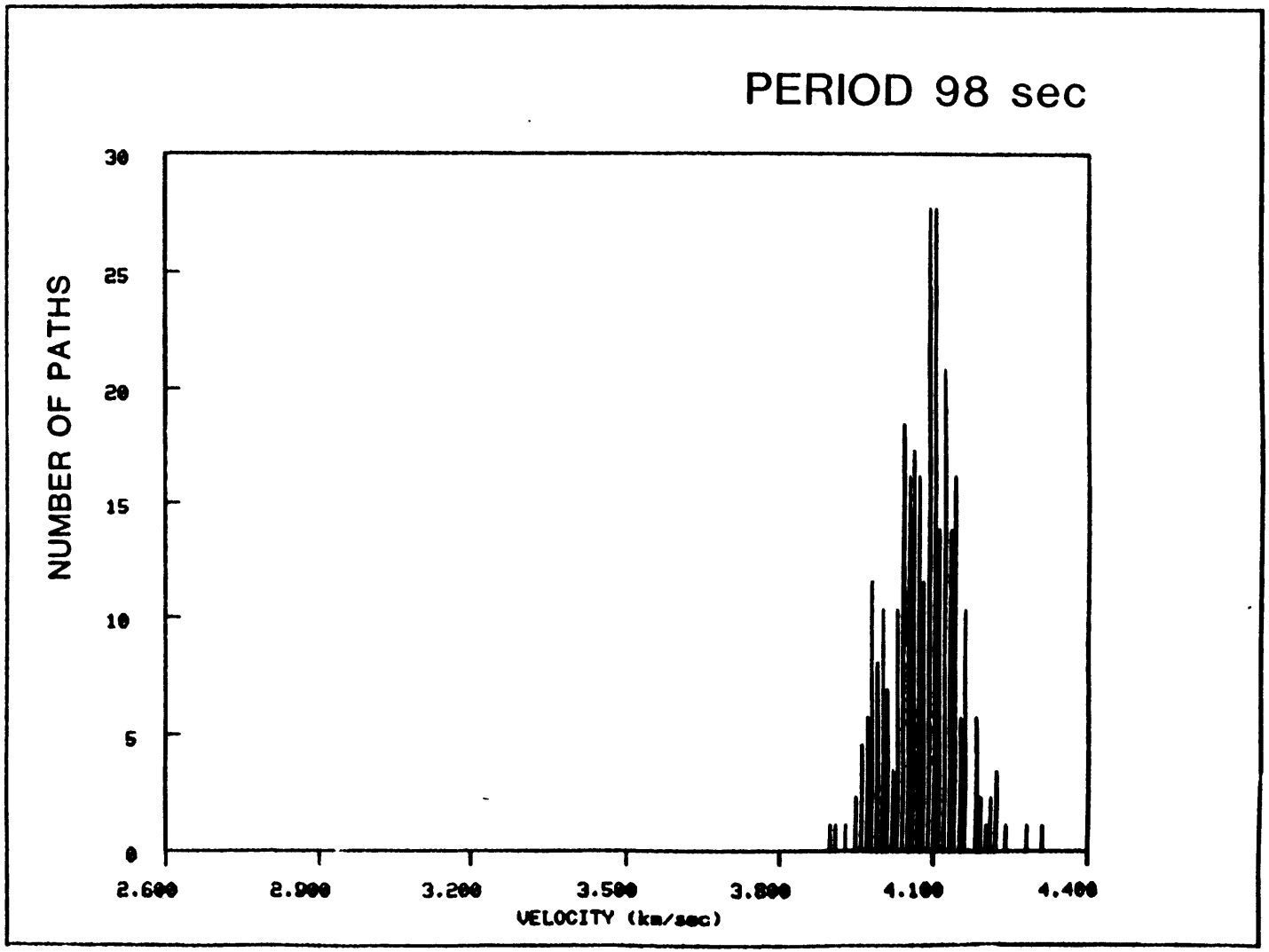
PERIOD 98 sec
NUMBER OF PATHS
30
25
20
15
10
5
0
2.600
2.900
3.200
3.500
3.800
4.100
4.400
VELOCITY (km/sec)

FIGURE 3.11a

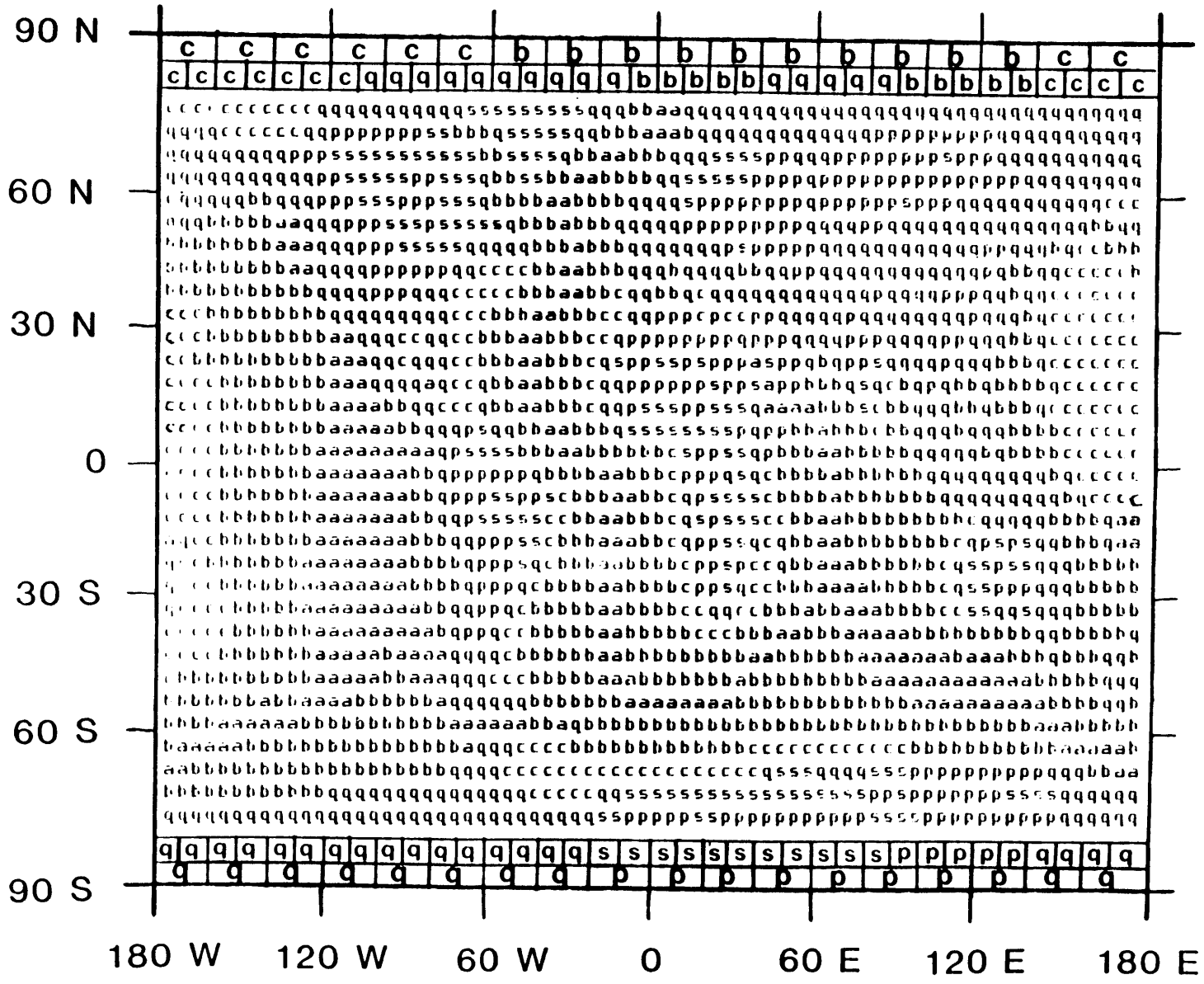

FIGURE 3.11b

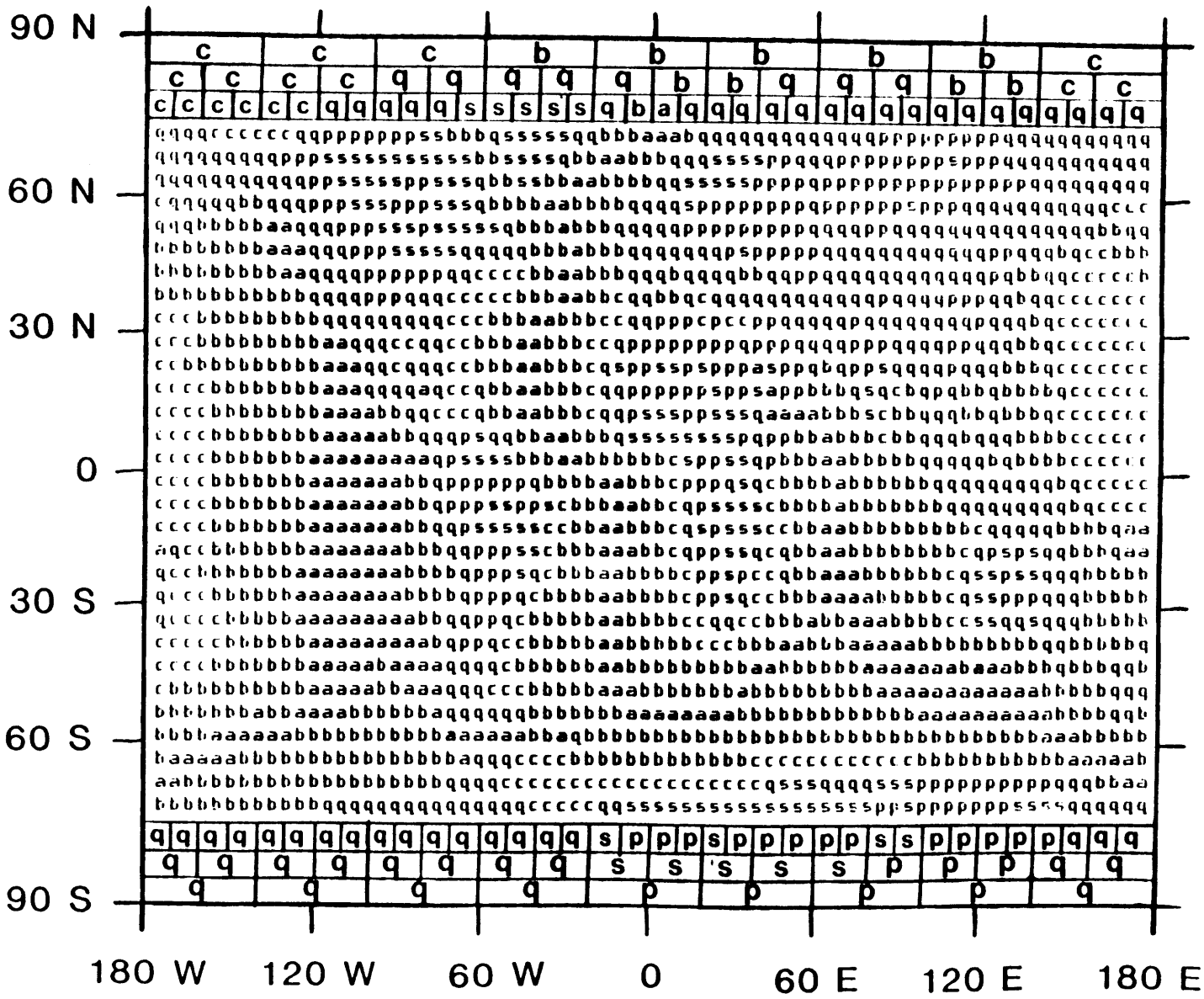

FIGURE 3.12a

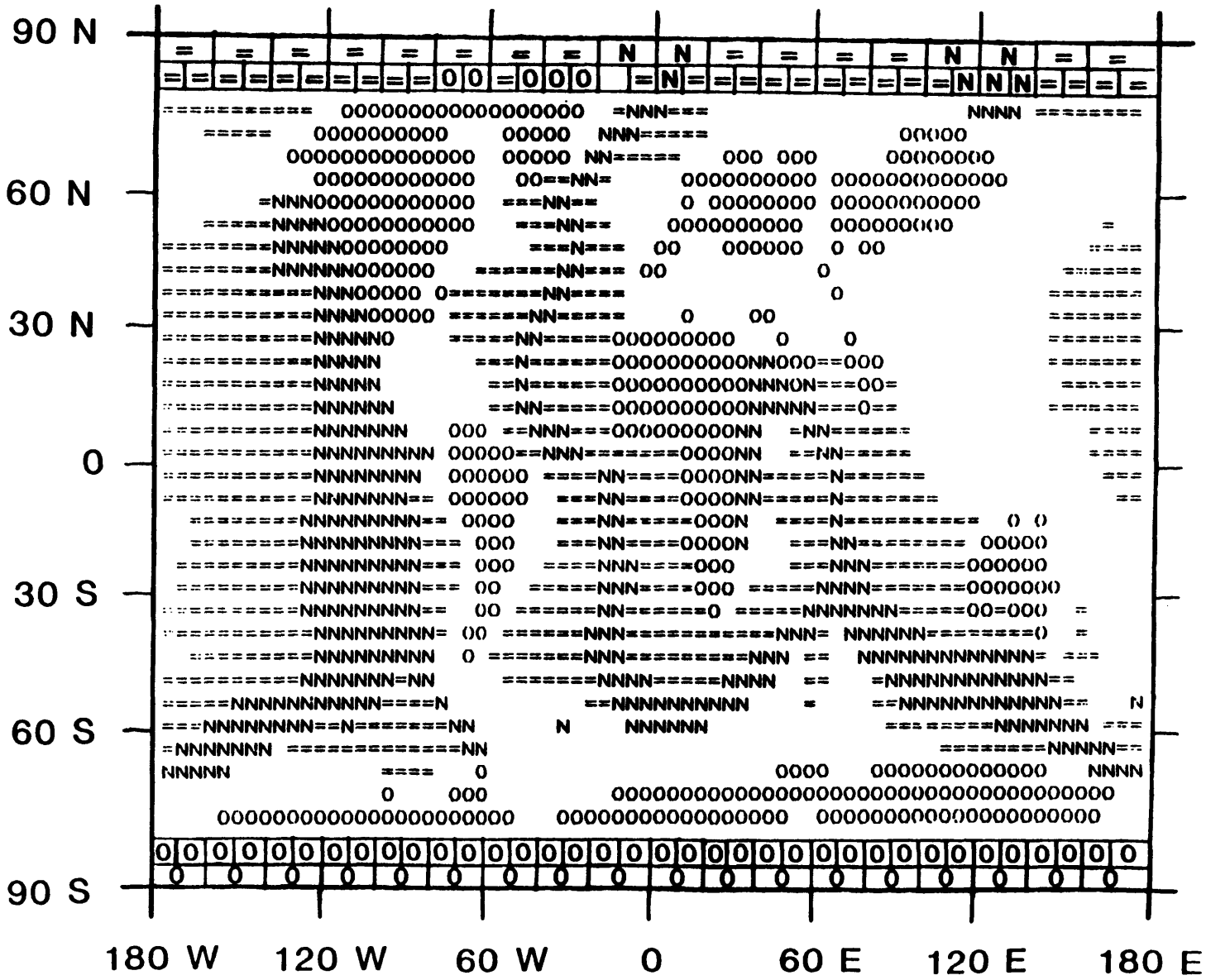

FIGURE 3.12b

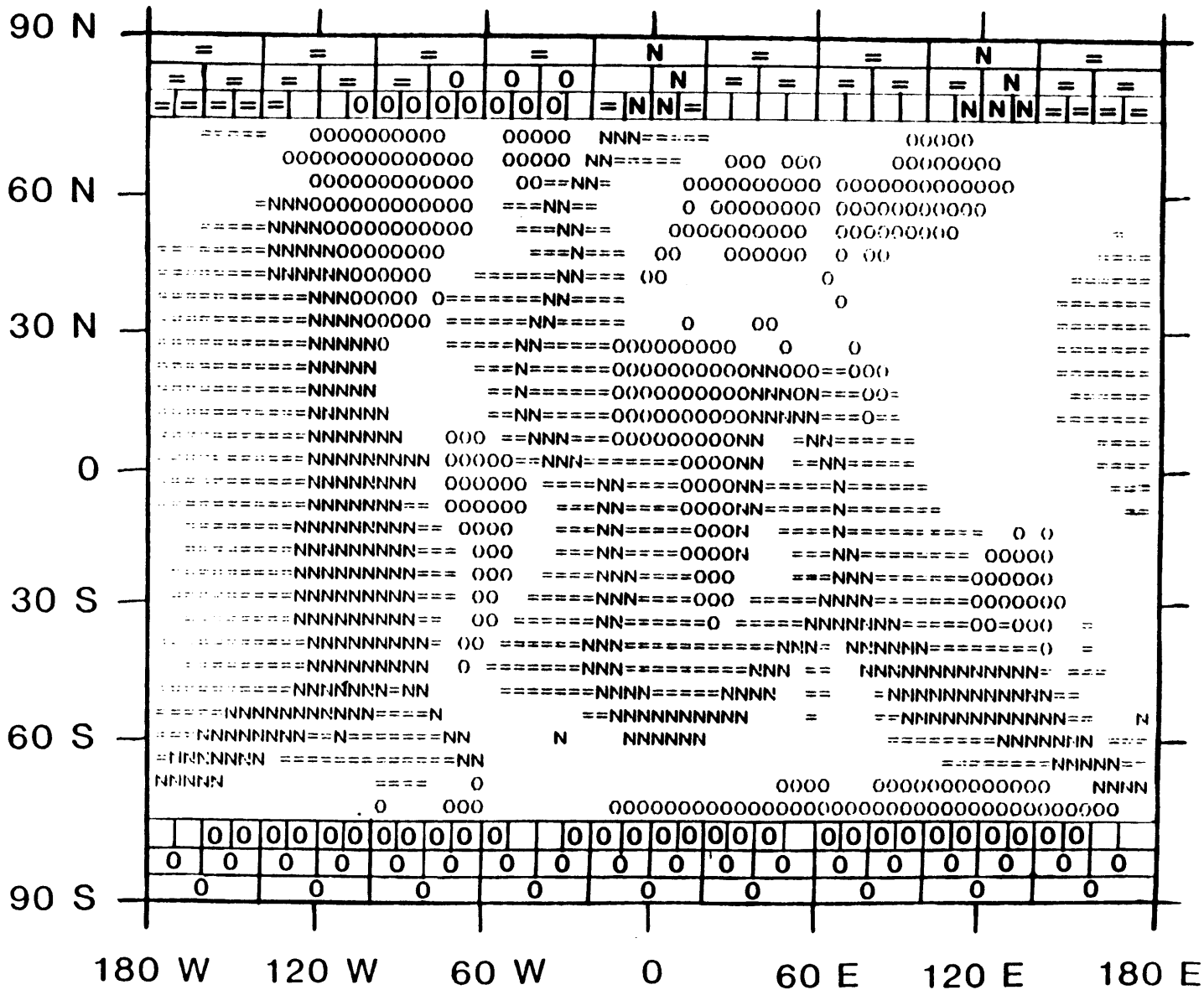

FIGURE 3.13a

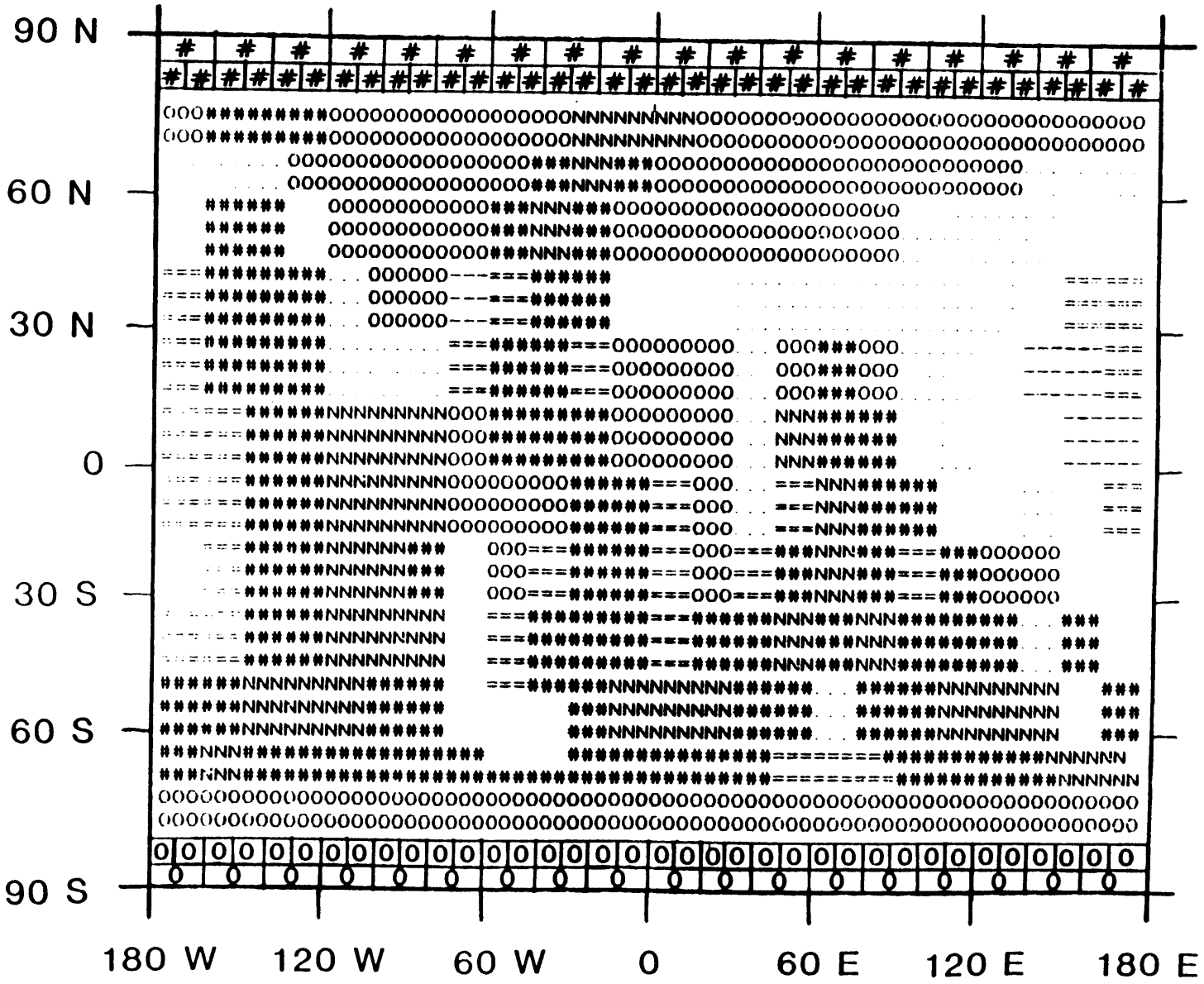

FIGURE 3.13b

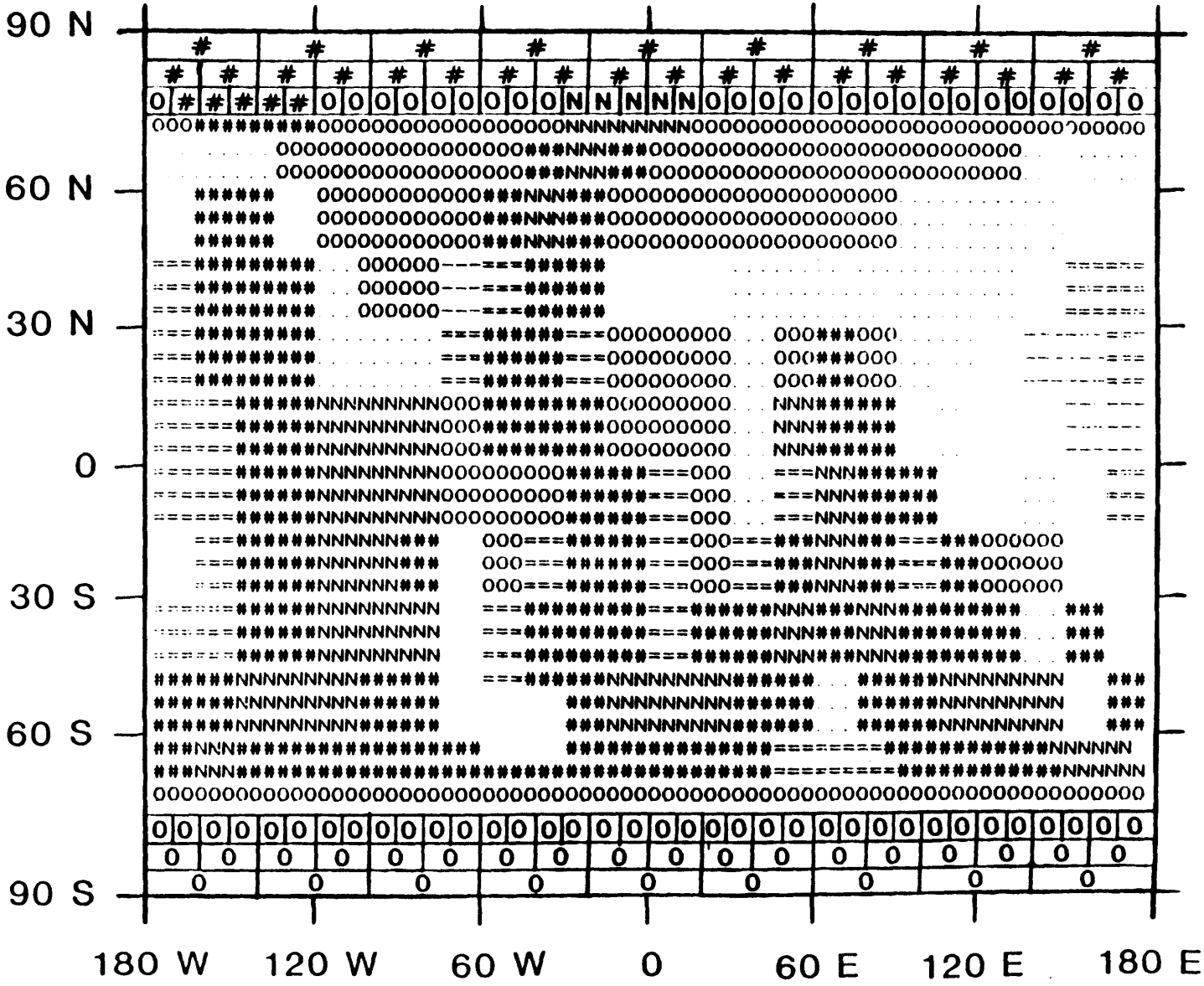

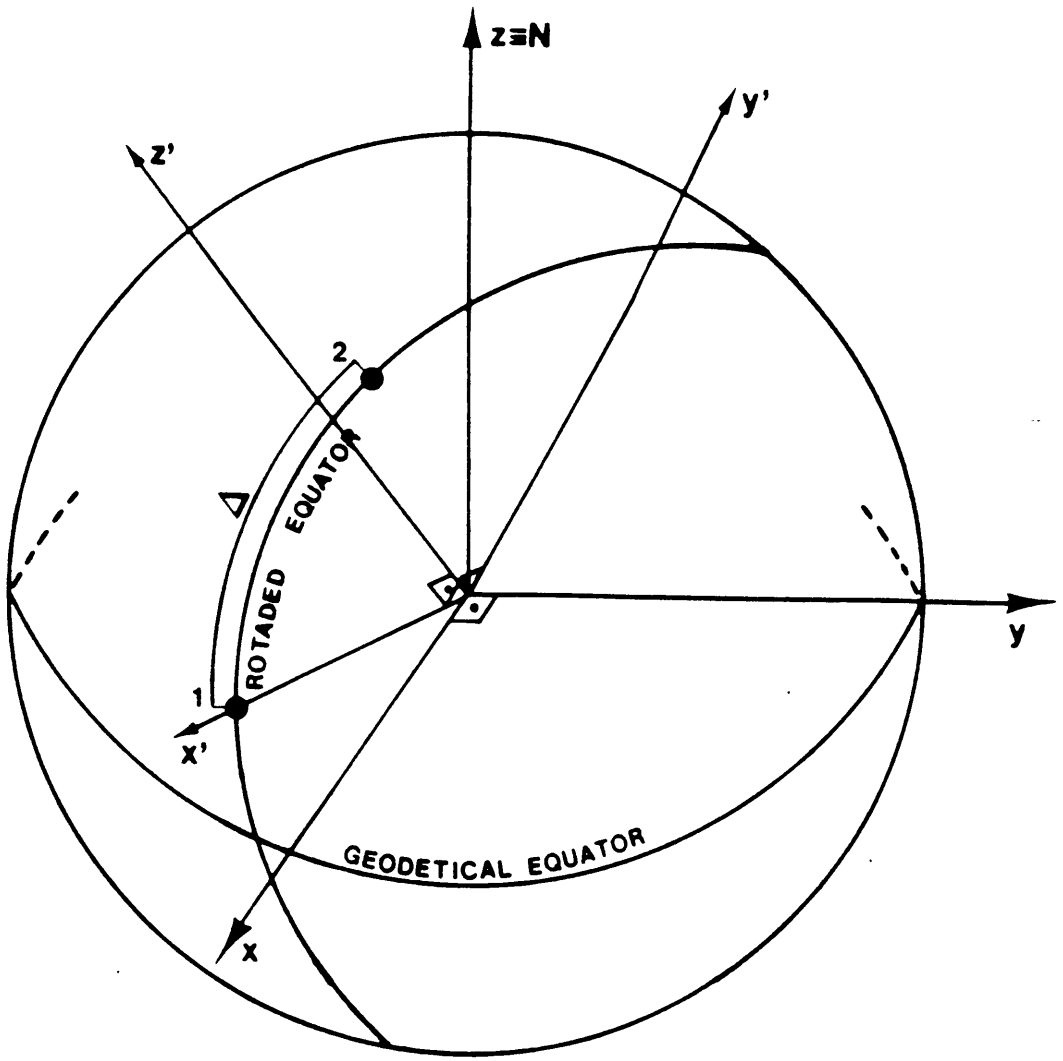
z≡N
y'
z'
2
ROTADED EQUATOR
Δ
y
1
x'
GEODETICAL EQUATOR
x

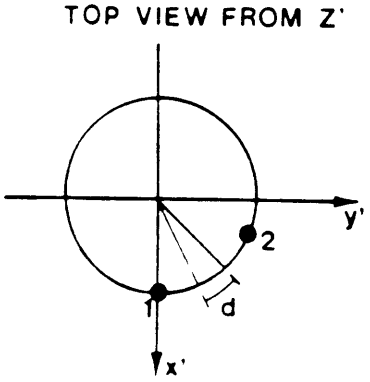
TOP VIEW FROM Z'
y'
2
d
1
x'

FIGURE 3.14

FIGURE 3.15

PHASE VELOCITY - JORDAN'S MODEL

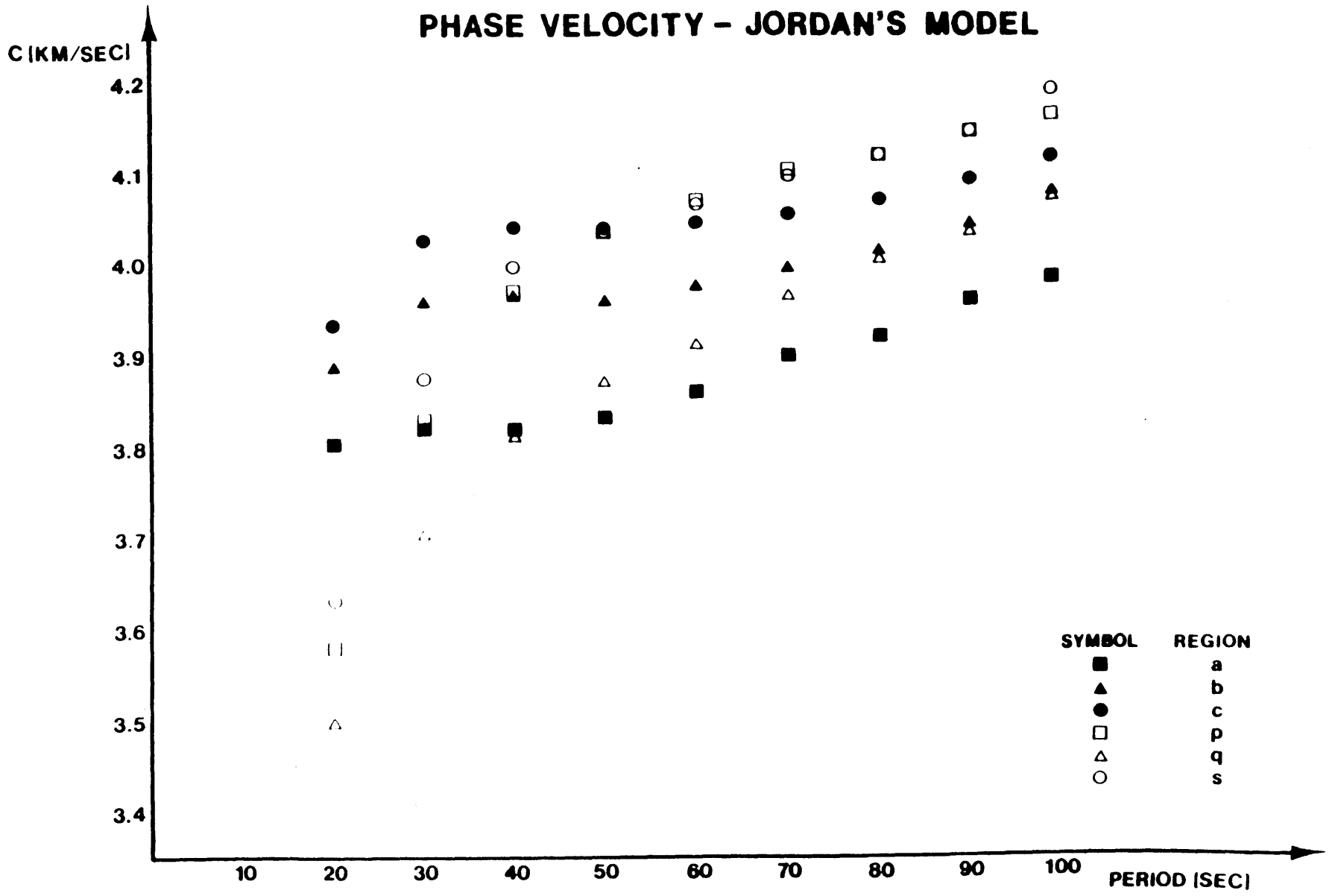

FIGURE 3.16

PHASE VELOCITY - LÉVÊQUE'S MODEL

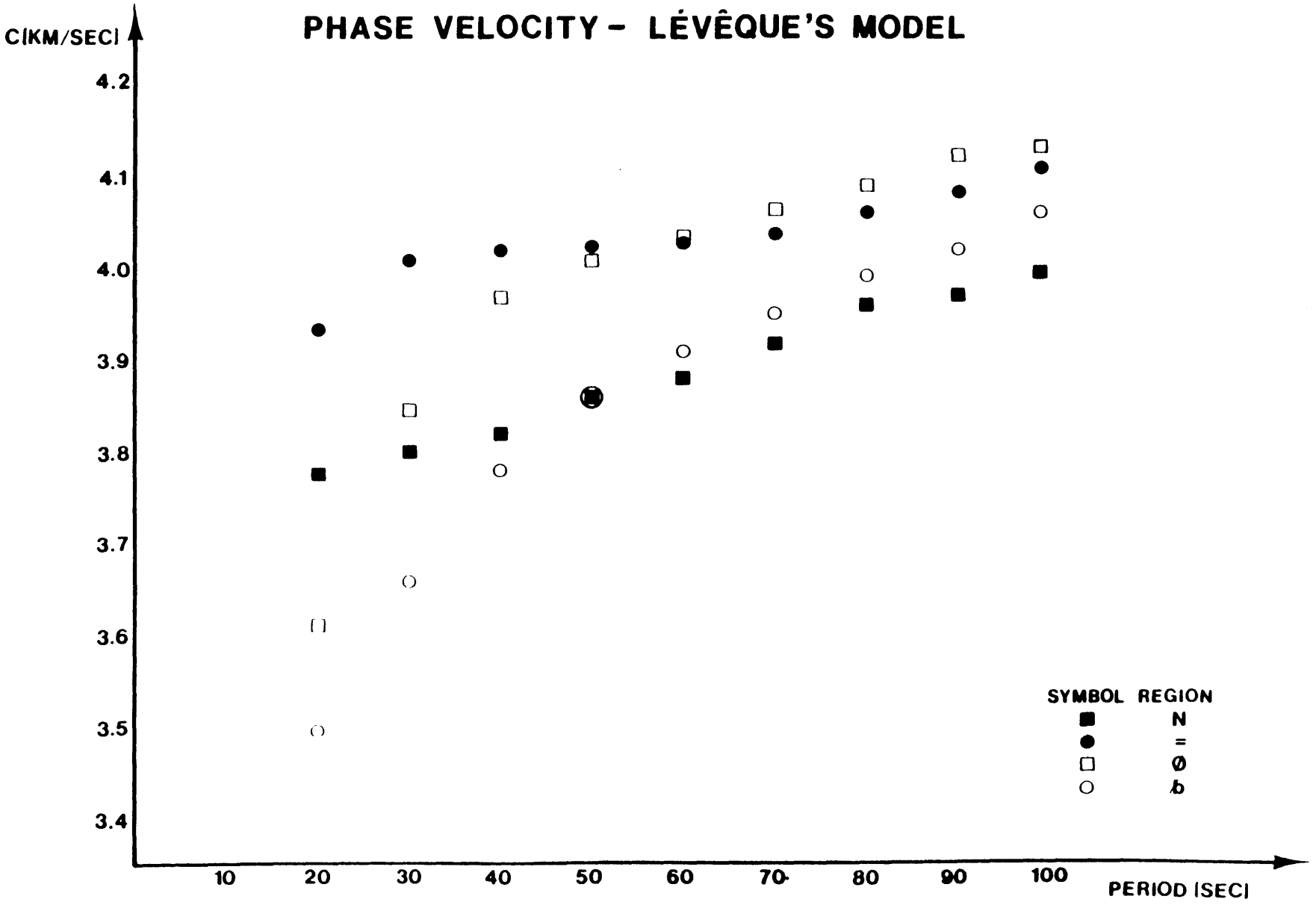

FIGURE 3.17

PHASE VELOCITY - OKAL'S MODEL

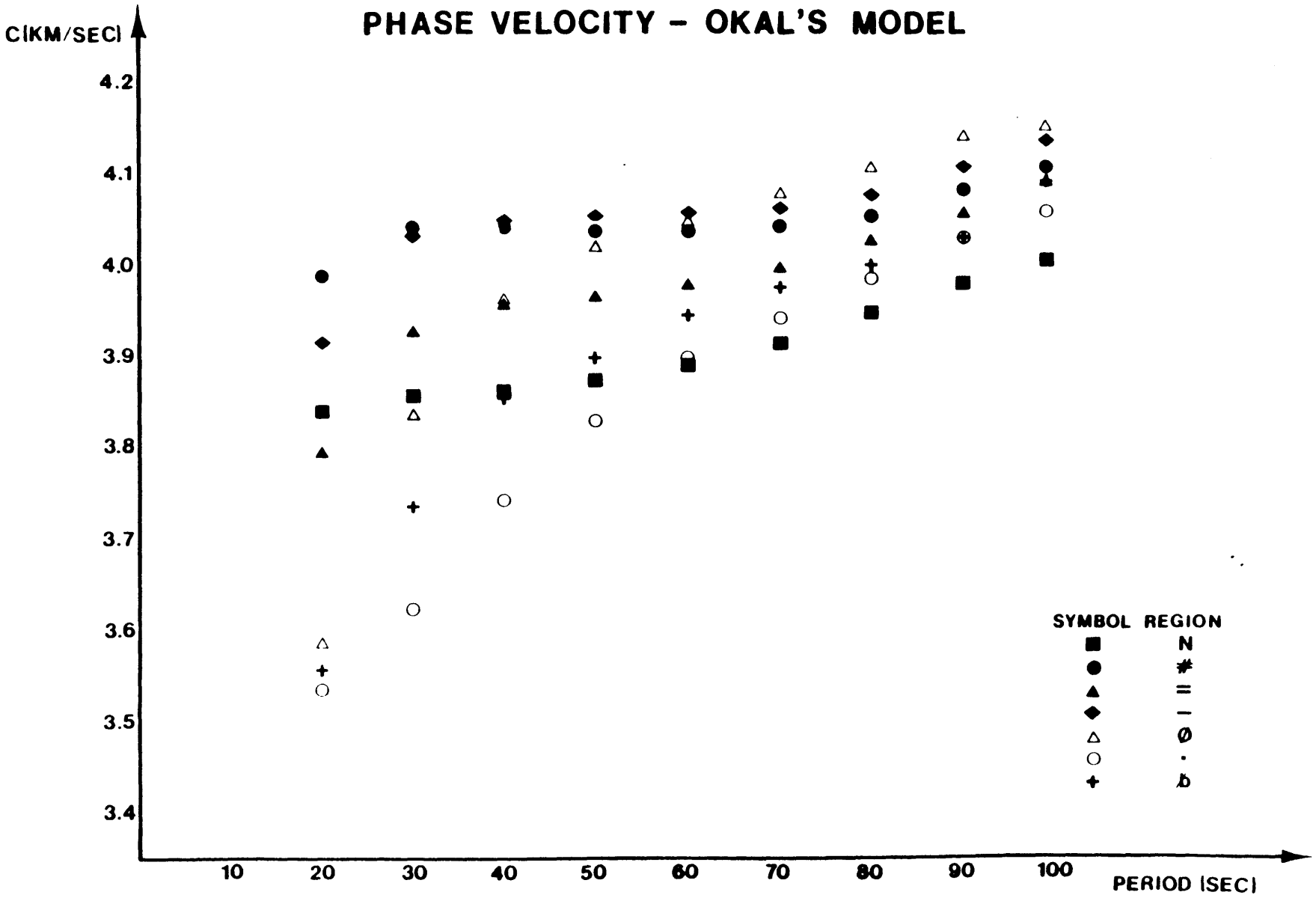

CHAPTER 4

Additional worldwide measurement of phase velocity of fundamental mode Rayleigh waves for the period range 20 to 100 sec.

4.1 - Introduction:

The data set collected from the literature and described in Chapter 2 provided the initial model for the lateral distribution of the phase velocity of fundamental mode Rayleigh waves obtained in Chapter 3. As can be seen in Figures A.1a thru A.9a, where we showed the greatcircle paths of the collected data, the coverage is far from ideal in many parts of the Earth. In order to increase our data set, we decided to apply the one-station method to a set of earthquakes, for which source parameters have been determined recently by seismologists at M.I.T. using the body waveform data. Our work more than doubled the number of paths for which the phase velocities of Rayleigh waves are measured for the above period range.

We describe in this chapter the data analysis procedure applied to the surface wave records in order to determine the

phase velocity for the path between a given earthquake and a recording station, and discuss the possible causes of error on these measurements.

4.2 - Data processing:

We used a set of about 1500 seismograms obtained by the vertical long-period seismograph of the W.W.S.S.N. from 45 worldwide distributed earthquakes as shown in Figure 4.1. Their epicenter information is listed in Table 4.1. The focal mechanism and depth of these earthquakes were obtained by a number of authors (Bergman and Solomon, 1984, 1985; Bergman *et al.*, 1984, 1985; Bergman, 1985; Huang, 1985; Huang *et al.*, 1986; Jemsek *et al.*, 1985), who used a computer program developed by Nábělek (1984) for fitting the synthetic teleseismic P and SH waveform to the observed. Fortunately, the new epicenters are conveniently located so that their paths to W.W.S.S.N. stations cover areas which were not covered well in earlier studies, such as the Indian Ocean, South America, South Atlantic, and western Africa regions (see Figure A.1a through A.9d). The above authors have also chosen earthquakes with epicenter in oceanic areas, which provide records of waves that travelled a considerable part of their

paths on a simple oceanic structure, which also helped to provide records of fundamental mode Raleigh waves relatively uncontaminated by other modes.

The above set of seismograms was selected based on the overall quality of the record which was examined on a microfiche viewer. We avoided those records which showed modulated amplitude. Beating was more frequently observable for shorter period waves. The time window we selected for our study was determined from the range of arrival time corresponding to the range of group velocity curves of Oliver (1962). The end of the window was, in many cases, determined by the appearance of the beating phenomenon. Stations that were farther than 150 degrees from the epicenter were not used because of possible contamination of the direct waves by waves approaching from the antipode (*i.e.*, R_2).

The above seismograms were then digitized, in the window set for each case, using a 9000 series CALCOMP table-top digitizer, which can read the coordinates of a point indicated by a cross-hair cursor with an accuracy of 0.001 inch. During the digitizing procedure, we tried to keep the seismic trace parallel to the horizontal axis of the digitizer. We have digitized two reference points in the trace so that we could

correct for any eventual tilt between the horizontal axis of the digitizer and the trace in the record. The correction is done by rotating all the points about the misalignement angle.

If θ is this tilt angle between the horizontal axis x' in the digitizer table, and the horizontal line in the seismic trace, x than,

$$\begin{cases} x' = x\cos\theta + y\sin\theta \\ y' = y\cos\theta - x\sin\theta \end{cases} \qquad (4.1)$$

where x' and y' are the corrected time and amplitude of each digitized point, respectively.

The amplitude and time of each digitized point were also corrected for the fact that the movement of the galvanometer is not perpendicular to the seismic trace due to the helical movement of the recording drum. We calculated β, the angle between the trace and the true horizontal on the seismogram, by considering the vertical distance d between two consecutive lines in the seismogram (that represent two minute marks separated in time by 30 minutes or one hour, depending on the rotation speed of the drum), and the length of the seismic

trace separating these two minute marks, the horizontal distance L,

$$\beta = \tan^{-1}\left[\frac{d}{L}\right] \qquad (4.2)$$

So, the coordinate pair (x', y') can be further corrected to account for this angle between the galvanometer movement, and the normal to the horizontal digitizing axis,

$$\begin{cases} a = \sqrt{d^2 + y'^2} \\ t = x' + d \end{cases} \qquad (4.3)$$

The corrections summarized by (4.1) and (4.3) were shown by James and Linde (1971) to be necessary when analyzing data digitized from seismograms recorded on a helical drum.

Finally, the corrected amplitude and time (a, t) pair for each digitized point, was used in the interpolation process to determine the amplitude at every second. The interpolation was needed because we digitized at an irregular rate, with a larger number of samples taken at the peaks and troughs, as suggested by Wiggins (1976). The following formula based on

the cubic spline interpolation was used.

$$a(t) = a_1'(t_1)\,\frac{(t_2 - t)^2\,(t - t_1)}{(t_2 - t_1)^2} - a_2'(t_2)\,\frac{(t - t_1)^2\,(t_2 - t)}{(t_2 - t_1)^2} + a_1'(t_1)\,\frac{(t_2 - t)^2\,[2\,(t - t_1) + (t_2 - t_1)]}{(t_2 - t_1)^3} + a_2'(t_2)\,\frac{(t - t_1)^2\,[2\,(t_2 - t) + (t_2 - t_1)]}{(t_2 - t_1)^3} \qquad (4.4)$$

where

$$a_i'(t_i) = \frac{(w_i\,m_i + w_{i+1}\,m_{i+1})}{(w_i + w_{i+1})} \qquad (4.5)$$

with

$$w_i = \frac{1}{\max(|m_i|, \varepsilon)}$$

and

$$m_i = \frac{(a_i\ (t_i) - a_{i-1}\ (t_{i-1}))}{(t_i - t_{i-1})}$$

(ε is a small number, as explained in Chapter 3). The above method has been shown by Wiggins (1976) to be the most appropriate for the interpolation of digitized seismogram.

In the next step of the data processing, we have applied the moving window analysis of Landisman *et al.* (1969). This technique starts with the multiplication of the digitized seismogram a(t) by a rectangular time window $\omega(t)$. The center of the window is set at a time t_n, which is equal to the epicentral distance divided by the group velocity U_n. The window limits are then set to be $t_n - 2T < t < t_n + 2T$, for each period T that we want to analyze ($\omega(t) = 1$ for values of t in this interval and zero otherwise). After multiplying the seismogram a(t) by this rectangular time window, we detrend the result using the least-squares fit of a linear trend to the points inside the window. We then multiply the detrended data by the cosine taper. Finally, we evaluate the Fourier transform of the output of the above step, and correct the

amplitude for the instrument response, using the formulas of Hagiwara (1958). We repeat the above procedure for different choices of U_n as shown in Figures 4.2a thru 4.4a where we plot the absolute value of Fourier Transform at an interval of the decimal logarithm for each period T and group velocity U_n. In each of these figures, we have marked by closed squares the group velocity which correspond to the maximum energy arrival for each period. This technique has been used by Weidner (1972), Forsyth (1973), and later M.I.T. researchers. The usual procedure included the design of a time-variable filter from these group velocity dispersion curves, to eliminate contamination of the observed spectra by waves other than Rayleigh waves. We chose, however, not to use this step in our data processing sequence, because some tests showed that it was commom to have a phase shift in the phase spectra resultant from such windowing, relative to the phase spectrum of the original signal. Instead, we eliminated the data outside the period bands for which a smooth and reasonable group velocity was obtained in the moving window analysis (by 'reasonable' we mean that the group velocity values were compatible with the bounds published by Oliver, 1962 for this period band). As an example, we show the lower and upper

boundary for the period band separated for each of the group velocity dispersion curves in Figures 4.2a thru 4.4a. Further elimination of data was necessary while checking the outcome of the application of Fourier transform to each seismogram,

$$A_{obs}(T)\, e^{-i\varphi^{o}(T)} = \int_{t_1}^{t_2} a(t)\, e^{-i\frac{2\pi}{T}t}\, dt \qquad (4.6)$$

where t_1 and t_2 are the time limits of the window. We have plotted the observed amplitude $A_{obs}(T)$ and phase delay $\varphi^{o}(T)$ (after application of the formulas of Hagiwara, 1958, for the instrument response correction) for each path, and eliminated the period range in which phase spectra varied irregularly, as shown in Figures 4.2b thru 4.4b. In these, we also show the digitized waveform, which was checked against the original seismogram. We found that the selection of the period band through analysis of the group velocity dispersion curves in general produces good results, with the amplitude and phase spectra showing smooth and then mostly noise-free variations. These spectral plots have been used by a number of authors (*e.g.* Forsyth, 1973, Romanowicz, 1981, Suarez, 1982), and the quality of our data is comparable to theirs.

We show in Table 4.2 some values of group velocity, phase velocity, and also the corresponding values of the integer N(T) used in the measurement of the latter by Equation (4.10), which will be discussed in the next section. These measurements correspond to the paths which records are shown in Figures 4.2 thru 4.4.

At this point, a total of 1242 seismograms remained from our original set of about 1500.

4.3 - Determination of the phase velocity values:

In the next step of our data analysis, an extensive use was made of a formula for vertical component (upward positive) of the fundamental mode Rayleigh wave spectrum for a point source specified by the moment tensor buried in a laterally

homogeneous layered medium

$$a(\Delta, \theta, \omega)\, e^{i\omega t} = Y_1(0, \omega) \left[\frac{1}{8\, c^2\, U^2\, I_1^2\, \pi\, k} \right]^{1/2}$$

$$\frac{1}{\left[R \sin\left[\frac{\Delta}{R} \right] \right]^{1/2}}\, e^{i(\omega t - \omega\Delta/c + 3\pi/4)}\, e^{-\gamma\Delta}\, G(\omega) \left[(M_{xx} + \right.$$

$$+ M_{yy}) \frac{kY_3}{2} - M_{zz} \frac{(Y_2 + \lambda k Y_3)}{\lambda + 2\mu} - (M_{yy} - M_{xx}) \frac{k\, Y_3 \cos 2\theta}{2} +$$

$$\left. + M_{xy}\, k\, Y_3 \sin 2\theta - i \frac{Y_4}{\mu} (M_{xz} \cos\theta + M_{yz} \sin\theta) \right] \qquad (4.7)$$

Equation (4.7) above has been derived by Saito (1967) and conveniently rearranged by Pujol (1982). In the above equation, c and U are , respectively, the phase and the group velocity of the Rayleigh wave with angular frequency ω and wavenumber k observed at time t. The path is defined by spherical surface coordinates (Δ, θ), with the epicenter at Δ = 0, the epicentral distance Δ given in km, and the azimuthal angle θ measured counter-clockwise from the East. $\omega^2 I_1$ is the kinetic energy of the Rayleigh wave integrated over the

depth. The term $1/[R \sin(\Delta/R)]^{1/2}$, where R (in km) represents the radius of the Earth, accounts for the geometric spreading on a spherical surface, as they propagate away from the source. The variable γ is a function of ω and represents the attenuation coefficient. $G(\omega)$ is the Fourier transform of the source time function g(t),

$$G(\omega) = \int_{-\infty}^{\infty} g(t)\, e^{-i\omega t}\, dt \qquad (4.8)$$

We assume that the source time function g(t) is a unit step, which is justified if the earthquake magnitude is small, and its source size is much smaller than the wavelength of the signal we are studying. Then,

$$G(\omega) = \frac{1}{\omega}\, e^{i3\pi/2} \qquad (4.8a)$$

The variables designated Y_i are the stress-motion eigenfunctions, Y_1 corresponds to the vertical component of displacement, and Y_3 is the horizontal component. The other two components, Y_2 and Y_4, correspond to the components of

traction in the x-y plane (Saito, 1967; Takeuchi and Saito, 1972). These eigenfunctions are calculated for a structure for the source region, given in terms of the P and S velocity and density for the free surface boundary condition and zero displacement at infinite depth boundary conditions. The resultant components Y_i are normalized so that $Y_1(0, \omega) = 1$ (*i.e.* the vertical component of displacement at zero depth is equal to one). The calculation was made by computer program written originally by M. Saito and modified later by M.I.T. researchers. We shall refer to the Earth model structure whenever we use eigenfunctions Y_i. The variables M_{ij} in Equation (4.7) represent the components of the moment tensor, with respect to coordinate with origin at the source, and the positive x-, y-, and z- axes in the East, North, and up directions, respectively. We assume that $\Sigma M_{ii} = 0$ (corresponding to no volume change in the source region). For a fault with dip angle δ, slip angle ψ, and strike ϕ,

Mendiguren (1977) gives the expressions for each component M_{ij},

$$\begin{cases} M_{xy} = M_o[\frac{1}{2}\sin2\phi\sin2\delta\sin\psi + \cos2\phi\cos\psi\sin\delta] \\ M_{yz} = M_o[\sin\phi\cos\delta\cos\psi - \cos\phi\sin\psi\cos2\delta] \\ M_{zx} = M_o[\cos\phi\cos\delta\cos\psi + \sin\phi\sin\psi\cos2\delta] \\ M_{xx} = M_o[-\sin2\phi\cos\psi\sin\delta - \sin^2\phi\sin2\delta\sin\psi] \\ M_{yy} = M_o[-\sin2\phi\cos\psi\sin\delta - \cos^2\phi\sin2\delta\sin\psi] \\ M_{zz} = M_o[\sin2\delta\sin\psi] \end{cases} \quad (4.9)$$

Equation (4.7) has been used by several authors (*e.g.* Weidner, 1972, Forsyth, 1973, Patton, 1978, and others) in the determination of phase velocity by the one-station method, in which the source phase, $\varphi^s(T)$ of Equation (2.5) is calculated by Equation (4.7) for a given set (M_o, δ, ψ, ϕ) of source parameters, the source depth h, and the azimuth θ. The phase velocity c(T) for the path between a given station and the corresponding epicenter for each of those earthquakes can then be determined from the observed phase delay $\varphi^o(T)$ that has

been corrected for the instrument response,

$$c(T) = \frac{\Delta}{t + \frac{T}{2\pi}\left[\varphi^{s}(T) + \varphi^{o}(T) + \frac{\pi}{4} + 2\pi\, N(T)\right]} \qquad (4.10)$$

Here, t represents the starting time for calculating the Fourier transform for each record of Rayleigh waves. We should also clarify that the term $\pi/4$ corresponds to the phase correction that resulted from the $3\pi/4$ term of Equation (4.7) combined with the $3\pi/2$ term of Equation (4.8a). The first of these, $3\pi/4$, corresponds to the term originated from the asymptotic expansion of the Hankel function in the derivation of Equation (4.7), while the second, $3\pi/2$, represents the convention chosen for the source phase $\varphi^{s}(T)$ (Patton, 1978, Pujol, 1982). This correction should not be confused with the phase shift introduced by Brune (1962a), and discussed in Aki and Richards (1980), which we used in Equation (2.5). This latter correction is only needed when the peak and trough method (and not Fourier analyses) is used to measure the phase velocity by the one-station method.

The phase velocity was calculated by Equation (4.10) for the paths shown in Figures B.1a thru B.45a. Before describing

the procedure, we shall first test the reliability of the source mechanism and centroid depth derived using the body wave modelling inversion method of Nábělek (1984). We shall calculate the theoretical amplitude spectral density of Rayleigh waves using Equation (4.7) and compare the result with the observed spectral density. The absolute value of spectral density is given by the following equation,

$$A^t(T, \theta) = \left[\frac{1}{8\, c^2\, U^2\, I_1^2\, \pi\, k\, \Delta'}\right]^{1/2} \left|\left|(M_{xx} + M_{yy})\, \frac{kY_3}{2} - \right.\right.$$

$$- M_{zz}\, \frac{(Y_2 + \lambda k Y_3)}{\lambda + 2\mu} - (M_{yy} - M_{xx})\, \frac{kY_3 \cos 2\theta}{2} +$$

$$\left.\left. + M_{xy}\, k\, Y_3 \sin 2\theta - i\, \frac{Y_4}{\mu} (M_{xz} \cos\theta + M_{yz} \sin\theta)\right|\right| \qquad (4.11)$$

where Δ' is the reference epicentral distance, chosen to be 4000 km here, and the other variables are the same as defined for Equation (4.7). The theoretical amplitude data, calculated using the above equation, are then compared with the observed amplitude data for the whole azimuth range, at four reference periods: 30, 50, 70 and 98 sec. These observed

values were corrected for the geometrical spreading effect and the attenuation effect by the use of the following relation, which reduces the observed amplitude $A^{o}(T, \theta)$ to $A'(T, \theta)$ at the reference epicentral distance Δ',

$$A'(T, \theta) = A^{o}(T, \theta)\, e^{\eta\Delta} \left[\frac{R \sin(\Delta/R)}{\Delta'}\right]^{1/2} \qquad (4.12)$$

Such reduction was first used by Tsai (1969), who used a reference distance of 2000 km.

We calculated, for a given Earth structure (for which the P and S wave velocities, together with the density ρ and the Lame's coefficients λ and μ are specified), the phase and group velocities (U and c), and the kinetic energy $\omega^2 I_1$ of the Rayleigh waves for a given period T. The eigenfunctions Y_i are computed for each period at predetermined depths, and the value at the focal depth was estimated by an interpolation.

We used two Earth models: one for a continental region, used by Pujol (1982) based on the P-wave velocity distribution taken from tables of Herrin (1968), the S-wave velocity from the work of Randall (1971), and the density from the relation of Birch (1961) between P-wave velocity and density. Our

model for oceanic structure was taken from the paper by Harkrider and Anderson (1966). Although the dependence of the Rayleigh wave spectrum at far-field (Equation 4.7) has been known to be fairly independent of the eigenfunctions Y_i (Forsyth, 1973), we tried to use the eigenfunction for a structure appropriate for the source region for each event. So, we have used a different Earth structure to calculate the eigenfunctions Y_i for each earthquake, depending on whether the event was located in a continental or an oceanic region. In the case of an oceanic region, there was the problem related to the thickness of the water layer used: the original model of Harkrider and Anderson (1966) includes a 5 km thick water layer, that cannot be used for all of our oceanic events, because some of these have fairly shallow centroid depth, and their epicenters are in regions where the water layer is known to be much thinner than 5 km (Table 4.1).

We have calculated the phase and group velocities, the kinetic energy, and the eigenfunctions Y_i for five different oceanic models, all based on the model of Harkrider and Anderson (1966), but with the water layer varying from 1 to 5 km thick, using 1 km depth increments between each case. We have obtained from the M.I.T. researchers who determined the

source mechanism, and the centroid depth of each earthquake, the water depth used in their body waveform inversion. Some of these data have been published in the corresponding references we cited at the beginning of this chapter, others were not. These are all listed in Table (4.1), where the water depth was given to the nearest km.

For the correction of the observed amplitude spectrum at each period, $A^{o}(T, \theta)$, of Equation (4.12), we adopted two different sets of attenuation coefficient values, $\eta(T)$ for continental and oceanic regions. The set for waves propagating in mostly continental regions was taken from the work of Tsai and Aki (1969). The other set for paths in oceanic regions was taken from the work of Canas and Mitchell (1978). For each path, we identified the portions of oceanic and continental path using Jordan's regionalization, and applied the attenuation correction appropriate for the path.

The resultant observed and theoretical amplitude radiation pattern were plotted for four periods for each of the 45 earthquakes listed in Table 4.1 in Appendix B. From these plots, we can see that, whenever the data is well distributed in azimuth, we have a good agreement between the calculated and the theoretical curves. The agreement implies

that the source mechanism and focal depth determined from the body wave can also be applicable to the surface wave. This result encouraged us to use all the focal mechanisms and centroid depths given in Table 4.1 to calculate the initial source phase, $\varphi^s(T)$ using Equation (4.7). The source phase is determined from the real and imaginary parts of Equation (4.7), by setting $a(\Delta, \delta, \omega) = |A| e^{i\varphi^s(\omega)}$. In calculating the source phase, we used the same set of eigenfunctions used for calculating amplitude.

In order to find the value of N(T), one must refer to some reference phase velocity dispersion curve. If we are dealing with a single period, the natural choice for the reference curve is the predicted value for the particular ray path using the initial model of phase velocity distribution obtained in Chapter 3. If we are dealing with a range of periods (which is our case), we should use the most reliable period to find N(T). Once N(T) is found for the period, the continuity of phase with ω will determine N(T) for other periods. The problem with this procedure is that it is difficult to tell which is the most reliable period. Longer periods show less regional variation, but their signal to noise ratio is usually poorer. So, we decided to apply the

first procedure (*i.e.* to treat each reference period independently). This will avoid the above problem, but introduces another by violating the continuity of the observed phase in some cases. We chose nevertheless the more conservative approach of this procedure, which will give as result the dispersion curve that is less deviated from an initial model.

Thus, in the determination of the value of N(T), we made use of the phase velocity estimate for the particular path calculated using the initial model derived in Chapter 3. First, we determine the region type, of the model by Jordan (1981), that was sampled by the points on a given ray at equal interval of 0.1 degrees. The predicted phase velocity c^p for each path is calculated using the phase velocity value $\bar{c}_i$, tabulated in Chapter 3 for the i-th region and the portion of the greatcircle path Δ_i in the i-th region as

$$c^p(T) = \frac{1}{\sum_{i=1}^{6} \left[\frac{\Delta_i}{\Delta} \frac{1}{\bar{c}_i(T)} \right]} \qquad (4.13)$$

We selected the value of N(T), which gives the closest value of c(T) (from Equation 4.10) to the value of $c^{p}(T)$ given by Equation (4.13). The resultant phase velocity value c(T) and the integer N(T) were then printed for each period and each path. The above phase unwrapping gave, in general, satisfactory result except for the shortest periods, and provided us with the phase velocity data for 1242 new paths in addition to the data from previous works described in Chapter 2.

An example of the result from the above procedure is given in Table 4.2, where we list the group velocity, phase velocity, and the value of N(T) used in the calculation of the latter. These results are related to the spectral data shown in Figures 4.2b thru 4.4b. We have marked with an arrow the points of the phase velocity spectra that correspond to the reference periods considered. Notice that the process has correctly identified all the cycle changes. As we can see, these changes are more common to occur in the shortest periods studied, which will make the risk of an erroneous determination of N(T) to be higher in the analyses of these periods. We should recall this fact when we analyze the results of our study in the next chapter.

We will soon publish all the values of phase velocity referred in Chapter 2, and those measured in this chapter. When we publish the measured values for each path, we shall include the corresponding values of N(T). This information should be useful to alleviate the problem of eventual phase discontinuity in the future use of this data.

4.4 - Error analysis:

The data processing procedure used in this chapter are very similar to those used by Weidner (1972), Forsyth (1973), Patton (1978), Romanowicz (1981, 1982b), Suarez (1982), and Pujol (1982). The portions of the data processing in our study that differ from the earlier works are: avoiding the use of time-variable filter, and unwrapping of the observed phase spectra using an automated process based on the initial model. There may be differences in the errors in phase velocity due to differences in uncertainties in the focal mechanism and depth of each earthquake. These uncertainties depend on several factors. Different types of fault mechanism and depth can cause different sources of uncertainty. For example, it seems that the strike-slip events are the ones which we have more problems with the strike uncertainty, due to the

four-lobed azimuthal variation of the radiation pattern for the events of this type of mechanism. This causes phase changes more often than, for example, dip slip mechanism.

The ideal approach would be the simultaneous inversion, in which both the phase velocity distribution and the source parameters are adjusted to improve the agreement between the observed and predicted amplitude and phase spectra. Such an approach was taken by Weidner (1972), Patton (1978) and others, and is known as the reference point technique, which we referred in Chapter 2. The reference point technique, however, requires many records from events close to each other with different source mechanisms. Our data are not adequate for the application of the reference point method for most regions, and we are interested in constructing the global distribution of phase velocity in this thesis. We, therefore, gave up on an attempt to improve the focal mechanism and centroid depth of our earthquakes.

The errors in our phase velocity data are probably of the same magnitude as those in Forsyth (1973), and better than most works we reviewed in Chapter 2, but they are by no means comparable to the error level achieved by a work such as Weidner (1972), who accomplished an almost complete separation

of source and propagation effects on these waves and the accuracy of phase velocity as good as ±0.02 km/sec in the period range 20-100 sec.

Some of the event-station pairs we studied were also used by previous workers, whose work we reviewed in Chapter 2. We have searched our database and found that we had 14 pairs already studied by other authors. Two of these pairs are from the work of Forsyth (1973), six are from Patton's (1973) work, and the remaining six were studied by Chang (1979). The phase velocity data from these workers, interpolated for the reference periods, are listed in Table 4.3, where we compare them with our measurements. As we can see, despite some difference in the focal mechanism and depth used by our study and theirs, there is a good agreement between the two phase velocity values in most cases.

To confirm the source of these differences, we have compared the phase velocity values obtained by Forsyth (1973) with our measurements, this time using the same focal mechanism used by Forsyth (1973) for each of the two events considered. We have also used the oceanic model of Harkrider and Anderson (1966) with a 5 km thick water layer, which has been used by Forsyth (1973). This comparison is shown in

Table 4.4. As we can see from these values, specially for the path to station GIE (located in the Galapagos Islands), we obtain a better agreement between the two results. This is probably due to the fact that the azimuthal direction of this station is closer to the strike direction of the fault, which makes it more dependent on changes in the focal mechanism. The remaining differences between the values are probably due to slight differences in data processing (***e.g.*** we have not used the time variable filter of Landisman ***et al.***, 1969).

TABLE 4.1 - SOURCE INFORMATION RELATIVE TO THE EVENTS USED IN THIS WORK

event no	date	origin time	lat. °N	lon. °E	m_b	M_o[a]	mechanism[b]	depth[c] (km)	water layer[d] (km)	ref[e]
1	May 25, 1964	19:44:05.9	-9.08	88.89	5.7	9.6	177/87/005	17	5	iii
2	Aug 25, 1964	13:47:19	78.15	126.65	6.2	125	171/46/277	5	2	vii
3	Oct 23, 1964	01:56:05.1	19.80	-56.11	6.2	50	283/54/151	30	5	iv
4	Sep 09, 1965	10:02:25.7	6.51	-84.44	5.8	24	173/88/180	8	2	ii
5	Sep 12, 1965	22:02:37.7	-6.46	70.76	6.1	33	263/44/246	18	4	ii
6	Oct 07, 1965	03:36:01.4	12.46	114.45	5.8	5.4	220/44/085	3	4	iv
7	Oct 31, 1965	17:24:09.5	-14.22	95.27	5.3	6.1	165/68/009	24	5	iii
8	Dec 19, 1965	22:06:33.0	-32.24	78.87	5.5	13	300/68/304	11	4	i
9	Feb 17, 1966	11:47:57.3	-32.20	78.93	6.0	84	276/59/290	11	4	i
10	Jan 07, 1967	00:27:23.0	-48.80	112.76	5.5	12	016/41/236	9	2	ii
11	Nov 10, 1967	18:38:34	-6.03	71.34	5.2	3	234/76/191	18	3	ii
12	Nov 11, 1967	11:55:56	-6.01	71.36	5.3	3.7	264/50/261	17	2	ii
13	Mar 02, 1968	22:02:24.2	-6.09	71.41	5.5	7.7	284/52/280	13	1	ii
14	Sep 03, 1968	15:37:00.3	20.58	-62.30	5.6	6.4	169/77/005	27	5	iv
15	Oct 08, 1968	07:43:22.8	-39.85	87.74	5.8	22.8	006/54/269	9	4	i
16	Mar 31, 1969	07:15:54.4	27.61	33.91	6.1	106.3	294/37/271	6	n.a.	v
17	Apr 07, 1969	20:26:30	76.55	130.86	5.4	2	163/42/285	11	n.a.	vii
18	Aug 08, 1969	11:08:13.2	-47.76	-15.66	5.7	15	008/67/215	7	3	ii
19	Sep 20, 1969	05:08:57.8	58.35	-32.08	5.6	15	023/42/261	2	2	vi
20	Jan 21, 1970	17:51:37.4	7.03	-104.24	6.1	140	332/41/106	6	3	ii
21	Mar 31, 1970	18:18:28.0	-3.78	69.70	5.5	8	043/83/187	13	4	ii
22	Apr 25, 1970	03:43:31	-6.29	69.84	5.1	1.6	248/85/192	11	4	ii
23	May 09, 1971	08:25:01.1	-39.78	-104.87	6.0	53	025/46/104	9	4	ii
24	May 31, 1971	03:46:50.6	72.21	1.09	5.5	6.8	051/51/284	2	3	vi
25	Jun 26, 1971	19:27:11	-5.18	96.90	5.9	54	014/67/019	29	5	iii
26	Sep 30, 1971	21:24:10.8	-0.45	-4.89	6.0	10	081/59/074	13	5	iv
27	May 02, 1972	06:56:23.2	5.22	-100.32	5.9	18	332/49/280	11	3	ii
28	May 21, 1972	06:01:54.3	-27.10	174.97	5.6	4.8	333/72/157	13	4	iv
29	Oct 20, 1972	04:33:49.9	20.60	-29.69	5.7	28	250/80/170	18	5	iv
30	Apr 26, 1973	20:26:27	20.05	-155.16	5.9	37	087/64/346	41	1	iv
31	Aug 30, 1973	19:50:03.9	7.15	84.33	5.8	3.7	290/52/118	27	4	iii
32	Jul 01, 1974	23:11:14.5	-22.57	-10.68	5.5	3.3	068/29/092	3	4	ii
33	Nov 20, 1974	13:21:41.6	-53.59	-28.26	5.8	6.6	298/87/005	5	5	iv
34	Sep 11, 1975	22:00:01.3	7.05	-104.18	6.3	11	307/44/093	5	3	ii
35	Sep 19, 1975	03:37:11	-34.74	81.88	5.9	48.5	241/63/275	18	3	i
36	Mar 29, 1976	05:39:36.3	3.96	-85.88	5.8	92	199/82/181	8	3	ii
37	Aug 30, 1976	08:37:54.4	1.03	147.56	5.8	24	334/77/173	25	5	iv
38	Nov 02, 1976	07:13:17	-29.36	77.65	5.8	76.4	230/37/282	14	4	i
39	Feb 05, 1977	03:29:19	-66.49	-82.45	6.1	40	003/43/073	14	4	iv
40	Jun 28, 1977	19:18:36	22.68	-45.11	5.9	11	001/44/255	2	4	vi
41	Aug 26, 1977	19:50:02.3	-59.54	-20.59	6.3	540	091/85/175	9	5	ii
42	Oct 17, 1977	17:26:40.4	-27.93	173.13	6.2	200	274/78/010	13	3	iv
43	Dec 13, 1977	01:14:20.5	17.33	-54.91	5.7	44	240/60/050	22	5	iv
44	Mar 24, 1978	00:42:36.7	29.68	-67.45	6.0	20	331/46/089	8	5	iv
45	Jan 28, 1979	19:45:21	11.92	-43.70	5.7	6.3	020/46/270	2	4	vi

NOTES ON TABLE 4.1:

a) Seismic moment x 10^{24} dyne cm (units equivalent to 10^{17} N m).

b) Focal mechanism: strike, slip, and dip angles (in degrees), according to the convention of Aki and Richards (1980).

c) Centroid depth (km below seafloor).

d) Approximate water depth at the epicentral region.

e) Reference body-wave studies:

i) Bergman et al. (1984, 1985)
ii) Bergman and Solomon (1984)
iii) Bergman and Solomon (1985)
iv) Bergman (1985)
v) Huang (1985)
vi) Huang et al. (1986)
vii) Jemsek et al. (1985)

TABLE 4.2a - GROUP VELOCITY MEASURED FOR THE FIRST THREE PATHS STUDIED IN THIS CHAPTER

path	052564 to AAE	052564 to ANP	052564 to BAG
period (sec)	U (km/sec)	U (km/sec)	U (km/sec)
109.9	3.64	3.64	3.62
97.5	3.66	3.68	3.62
86.4	3.72	3.72	3.64
76.7	3.78	3.72	3.68
68.0	3.80	3.72	3.70
60.3	3.84	3.72	3.72
53.5	3.86	3.74	3.72
47.5	3.86	3.76	3.74
42.1	3.86	3.74	3.74
37.4	3.84	3.72	3.72
33.1	3.80	3.66	3.68
29.4	3.66	3.62	3.60
26.1	----	3.56	3.52
23.1	----	3.22	3.48
20.5	----	----	3.44
18.2	----	----	3.42

TABLE 4.2b - PHASE VELOCITY MEASURED FOR THE FIRST THREE PATHS STUDIED IN THIS CHAPTER

path	052564 to AAE		052564 to ANP		052564 to BAG	
period (sec)	c (km/sec)	N	c (km/sec)	N	c (km/sec)	N
98	4.070	0	4.038	0	4.046	0
90	4.023	0	3.991	0	4.015	0
80	3.980	0	3.982	0	3.979	0
70	3.963	0	3.965	0	3.943	0
60	3.951	0	3.931	0	3.923	0
50	3.943	0	3.896	0	3.899	0
40	3.932	1	3.884	0	3.874	0
30	3.919	1	3.835	1	3.841	1
20	-----	-	-----	-	3.714	4

TABLE 4.3 - COMPARISON BETWEEN PHASE VELOCITY VALUES INTERPOLATED FROM PREVIOUS WORKS WITH THOSE VALUES MEASURED IN THIS WORK

REFERENCE: Forsyth, 1973

path	05/09/71 to GIE		05/09/71 to LPB	
period (sec)	reference values	this work	reference values	this work
98	4.055	3.983	4.071	-----
90	4.020	3.952	4.042	-----
80	3.959	3.919	4.010	3.970
70	3.935	3.893	3.980	3.940
60	3.907	3.876	3.952	3.912
50	3.877	3.848	3.928	3.891
40	3.872	3.849	3.910	3.871
30	3.886	3.856	3.899	3.857
20	-----	3.807	3.862	3.760

REFERENCE: Patton, 1973

path	09/12/65 to NAI		09/12/65 to SHI	
period (sec)	reference values	this work	reference values	this work
98	-----	-----	4.147	4.093
90	-----	-----	4.082	4.079
80	-----	-----	4.033	4.052
70	-----	-----	3.992	4.027
60	-----	3.961	3.976	4.006
50	3.897	3.954	3.957	3.808
40	3.905	3.945	3.925	3.822
30	3.911	3.941	3.864	3.812
20	3.850	-----	3.738	3.712

path	12/19/65 to BUL		12/19/65 to SHL	
period (sec)	reference values	this work	reference values	this work
98	-----	-----	4.107	-----
90	-----	-----	4.084	4.081
80	-----	-----	4.061	4.065
70	-----	-----	4.037	4.031
60	-----	3.960	4.027	4.018
50	4.039	3.994	4.012	4.004
40	4.022	3.974	4.004	3.991
30	3.983	3.958	3.971	3.963
20	3.883	3.814	3.830	-----

(TO BE CONTINUED)

TABLE 4.3 (CONTINUED)

path	02/17/66 to AAE		02/17/66 to BUL	
period (sec)	reference values	this work	reference values	this work
98	4.054	4.092	-----	-----
90	4.029	4.062	-----	-----
80	3.995	4.031	-----	-----
70	3.965	4.000	-----	-----
60	3.946	3.979	-----	4.054
50	3.942	3.853	4.037	3.903
40	3.925	3.861	4.010	3.917
30	3.884	3.850	3.974	3.928
20	3.799	-----	3.886	3.818

REFERENCE: Chang, 1973

path	08/25/64 to ATU		08/25/64 to HKC	
period (sec)	reference values	this work	reference values	this work
98	4.170	4.182	4.105	4.102
90	4.148	4.162	4.083	4.086
80	4.119	4.129	4.054	4.047
70	4.089	4.093	4.025	4.017
60	4.057	4.063	3.994	3.985
50	4.017	3.891	3.960	3.951
40	3.947	3.854	3.923	3.911
30	-----	3.740	-----	3.738
20	-----	-----	-----	-----

path	08/25/64 to HOW		08/25/64 to KEV	
period (sec)	reference values	this work	reference values	this work
98	4.123	4.141	4.148	4.176
90	4.095	4.106	4.124	4.147
80	4.060	4.076	4.094	4.107
70	4.019	4.026	4.064	4.077
60	3.970	3.971	4.035	4.048
50	3.904	3.912	4.003	4.000
40	3.795	3.892	3.953	3.732
30	-----	3.767	-----	3.668
20	-----	-----	-----	-----

(TO BE CONTINUED)

TABLE 4.3 (CONTINUED)

path	08/25/64 to NHA		08/25/64 to SHI	
period (sec)	published values	this work	published values	this work
98	4.108	4.065	4.145	4.154
90	4.085	4.031	4.121	4.127
80	4.057	4.012	4.092	4.096
70	4.027	3.985	4.063	4.066
60	3.997	3.957	4.038	4.033
50	3.962	3.921	4.007	3.989
40	3.908	3.867	3.916	-----
30	3.775	3.758	3.775	-----
20	-----	-----	-----	-----

TABLE 4.4 - COMPARISON BETWEEN PHASE VELOCITY VALUES INTERPOLATED FROM FORSYTH'S WORK WITH THOSE VALUES MEASURED IN THIS WORK ASSUMING THE SAME FOCAL MECHANISM FOR THE EVENT

REFERENCE: Forsyth, 1973

path	05/09/71 to GIE		05/09/71 to LPB	
period (sec)	reference values	this work	reference values	this work
98	4.055	4.021	4.071	-----
90	4.020	3.987	4.042	-----
80	3.959	3.950	4.010	3.965
70	3.935	3.921	3.980	3.936
60	3.907	3.901	3.952	3.908
50	3.877	3.870	3.928	3.888
40	3.872	3.869	3.910	3.869
30	3.886	3.874	3.899	3.855
20	-----	3.814	3.862	3.825

Chapter 4 - Figure Captions

Figure 4.1 - Geographical distribution of the earthquakes studied in this chapter. Note that we have used the mercator projection between latitudes 80°N and 80°S, compared to the same projection between latitudes 75°N and 70°S used in Appendices A, B, and C.

Figures 4.2a thru 4.4a - Group velocity dispersion curves corresponding to paths from the epicenter of the event 052564 to the W.W.S.S.N. stations AAE, ANP, and BAG, determined by the moving window analyses of the records.

Figures 4.2b thru 4.4b - Plot of the digitized seismogram, and observed amplitude and phase spectra for each of the first three paths studied (from event 052564 to W.W.S.S.N. stations AAE, ANP, and BAG, respectively). The hatched and dotted bands of the amplitude and phase spectra represent the portion of the data which was found unsuitable for use in our study. Arrows in the phase spectra plots indicate the selected points for phase velocity measurements.

FIGURE 4.1 EVENTS STUDIED

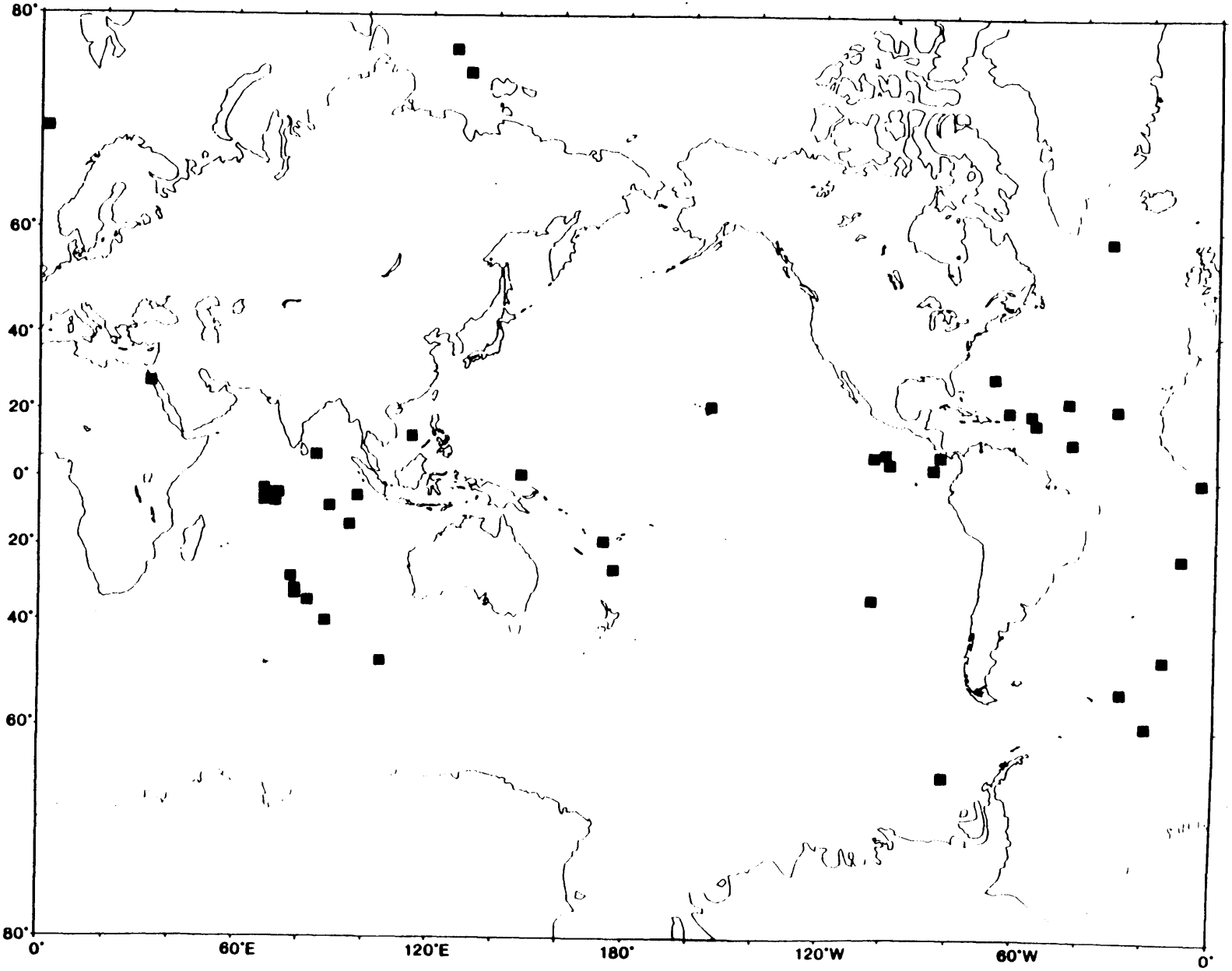

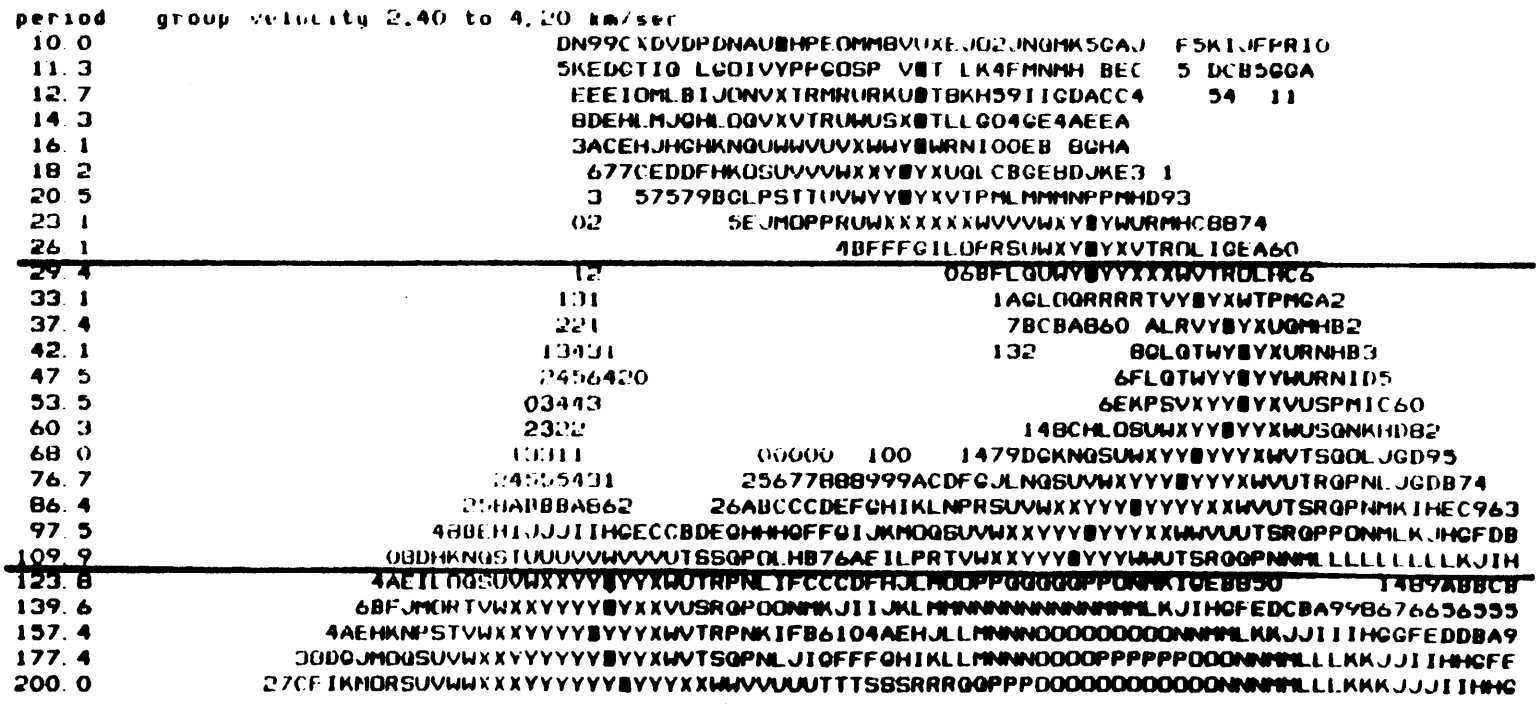
period group velocity 2.40 to 4.20 km/sec
10.0
11.3
12.7
14.3
16.1
18.2
20.5
23.1
26.1
29.4
33.1
37.4
42.1
47.5
53.5
60.3
68.0
76.7
86.4
97.5
109.9
123.8
139.6
157.4
177.4
200.0
PERIOD (sec)
GROUP VELOCITY (km/sec)

FIGURE 4.2a

FIGURE 4.2b

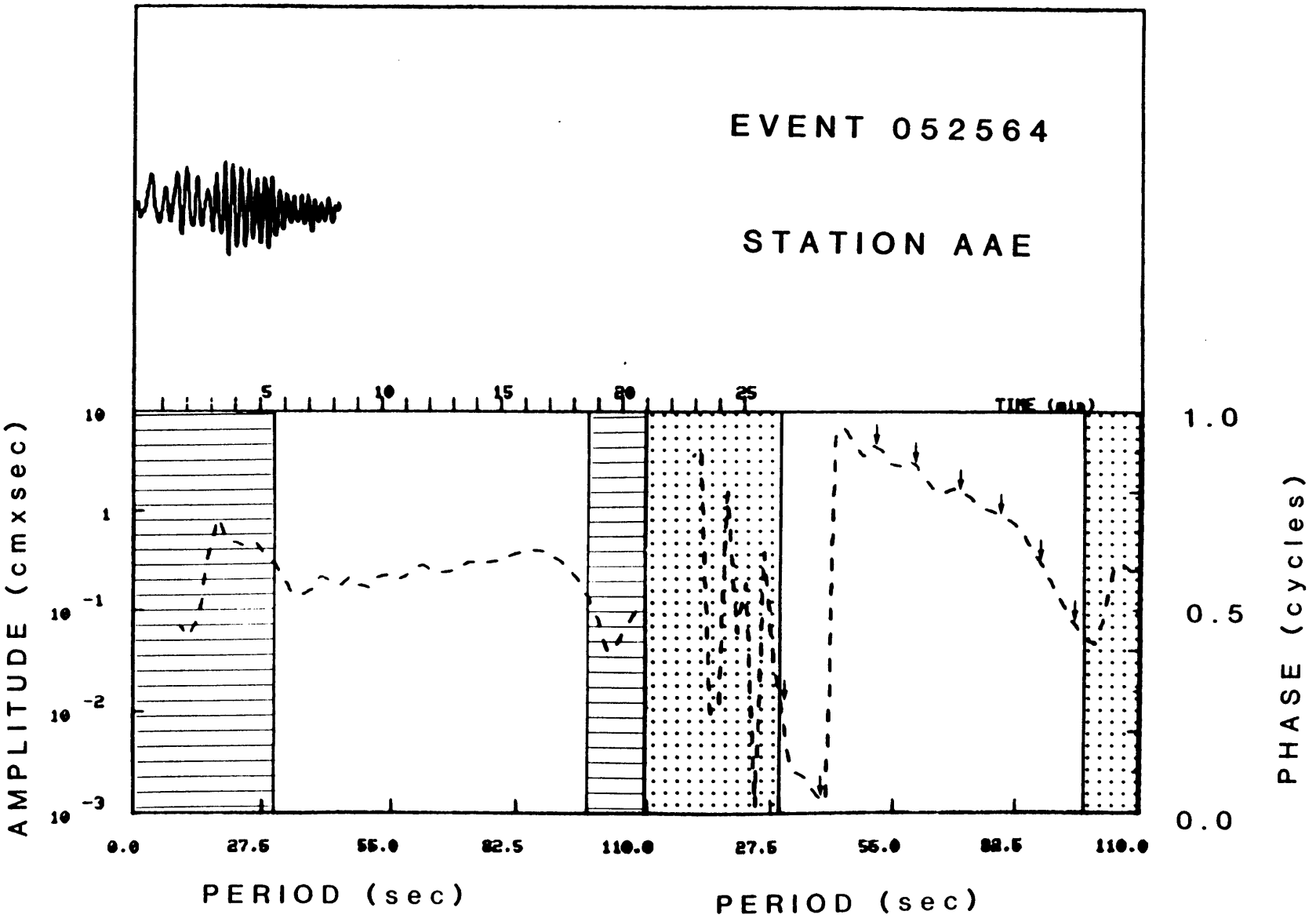
EVENT 052564
STATION AAE
5
10
15
20
25
TIME (min)
AMPLITUDE (cmxsec)
10
1
10 -1
10 -2
10 -3
0.0
27.5
55.0
82.5
110.0
PERIOD (sec)
1.0
0.5
0.0
PHASE (cycles)


period group velocity 2.40 to 4.20 km/sec
10.0
11.3
12.7
14.3
16.1
18.2
20.5
23.1
26.1
29.4
33.1
37.4
42.1
47.5
53.5
60.3
68.0
76.7
86.4
97.5
109.9
123.8
139.6
157.4
177.4
200.0
<2222222222222222222222222222223333333333333333333333333333333333333333333333333333333344444444444>
<4444455555666667777788888999990000011111222223333344444555556666677777888889999900000111112>
<0246802468024680246802468024680246802468024680246802468024680246802468024680246802468024680246802468024680>
PERIOD (sec)
GROUP VELOCITY (km/sec)

FIGURE 4.3a

FIGURE 4.3b

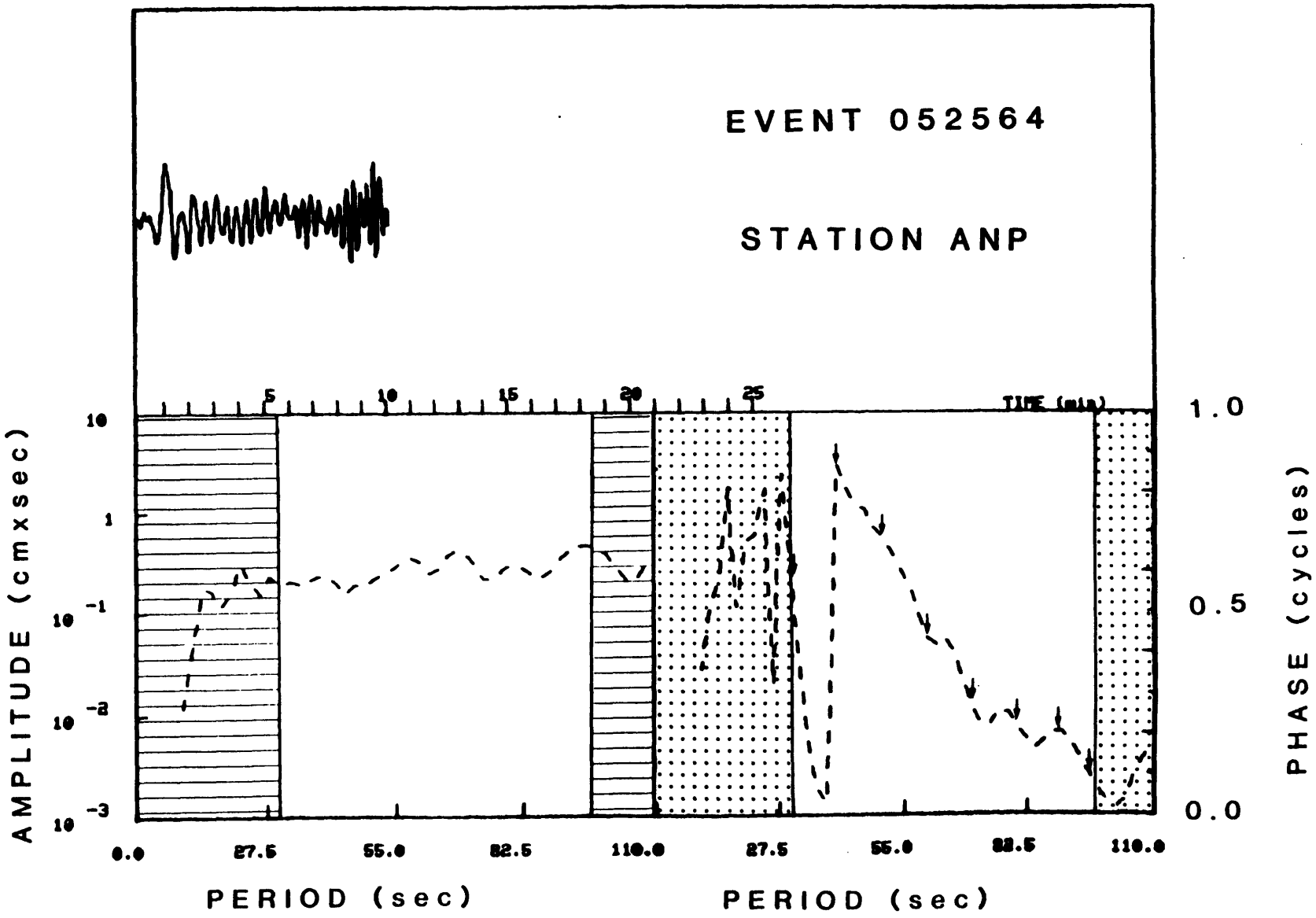
EVENT 052564
STATION ANP
5
10
15
20
25
TIME (min)
AMPLITUDE (cmxsec)
10
1
10 -1
10 -2
10 -3
1.0
0.5
0.0
PHASE (cycles)
0.0
27.5
55.0
82.5
110.0
27.5
55.0
82.5
110.0
PERIOD (sec)
PERIOD (sec)

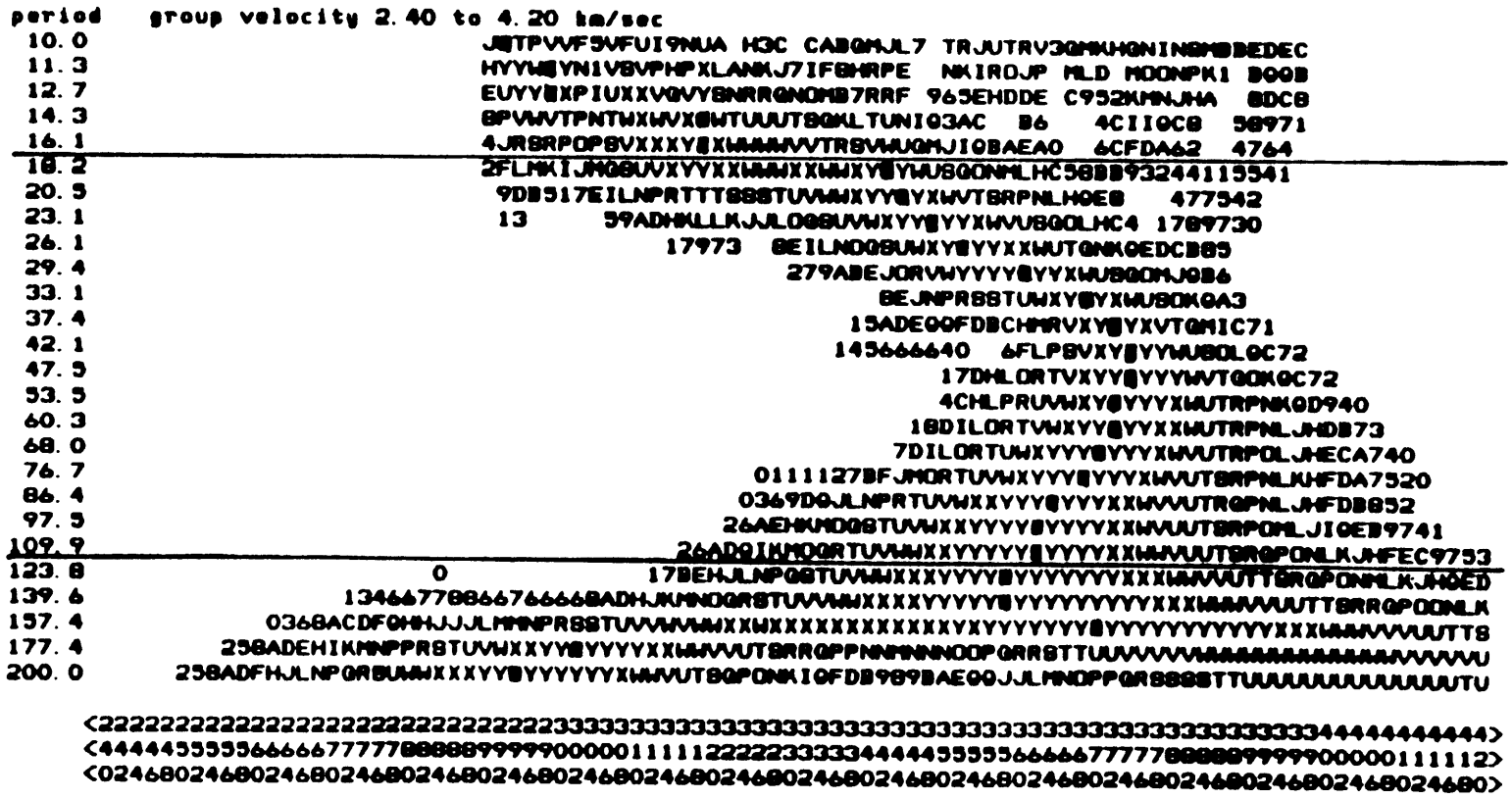
period group velocity 2.40 to 4.20 km/sec
10.0
11.3
12.7
14.3
16.1
18.2
20.5
23.1
26.1
29.4
33.1
37.4
42.1
47.5
53.5
60.3
68.0
76.7
86.4
97.5
109.9
123.8
139.6
157.4
177.4
200.0
<2222222222222222222222222222233333333333333333333333333333333333333333333333333444444444444>
<4444455555666667777788888999990000011111222223333344444555556666677777888889999900000111112>
<0246802468024680246802468024680246802468024680246802468024680246802468024680246802468024680>
PERIOD (sec)
GROUP VELOCITY (km/sec)

FIGURE 4.4a

FIGURE 4.4b

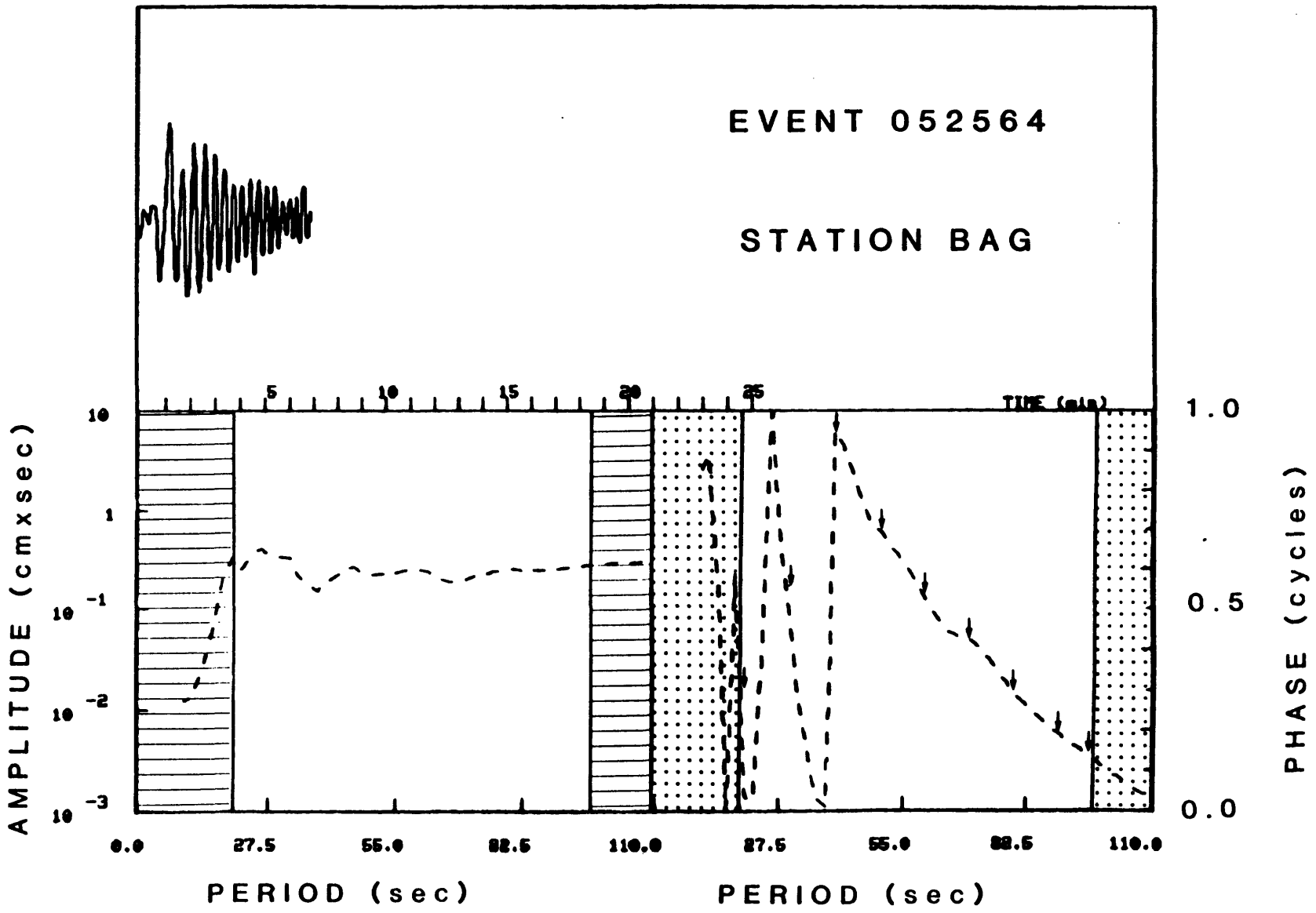
EVENT 052564
STATION BAG
5
10
15
20
25
TIME (min)
AMPLITUDE (cmxsec)
10
1
10 -1
10 -2
10 -3
1.0
0.5
0.0
PHASE (cycles)
0.0
27.5
55.0
82.5
110.0
87.5
55.0
82.5
110.0
PERIOD (sec)
PERIOD (sec)

CHAPTER 5

Inversion of travel time data for the global distribution of phase velocity of fundamental mode Rayleigh waves for the period range 20 to 100 sec

5.1 - Introduction:

The stochastic inverse for linear problems was introduced by Franklin (1970) and first used by Jordan (1972) in Seismology. It was then used by Aki *et al.* (1977) for determination of the three-dimensional velocity distribution underneath a seismic network using the travel time data observed for teleseismic events. This method has been further extended to the inversion of local earthquake travel time data by Aki and Lee (1976). Since then, it has been improved and widely used in various areas (see reviews by Aki (1977, 1979, 1981, and 1982b)).

In order to eliminate nonuniqueness of the solution Jackson (1979) included a priori information about the solutions in the formulation of the problem. More recently, Tarantola and Valette (1982) considered the stochastic inversion of data for nonlinear problems.

The method of Tarantola and Valette (1982) was applied to surface waves by Yomogida (1985). He inverted phase and amplitude data simultaneously, in an attempt to determine the distribution of phase velocity of Rayleigh waves in the 30 to 100 sec period range, in the Pacific region.

The purpose of this chapter is to apply the stochastic inverse to the dataset collected in Chapter 2, together with the new data obtained in Chapter 4, in order to determine the worldwide distribution of phase velocity of fundamental mode Rayleigh waves for the 20 to 100 sec period range.

We shall first describe the inversion method in detail, comment on the analysis of error, and discuss the appropriate choice for the damping constant. The effect of the damping constant used in the stochastic inversion is discussed in terms of the assumed a priori model variance. In this discussion, we shall make use of abundant examples of three-dimensional inversion of body wave travel time data, in order to arrive at the appropriate damping constant. Finally, we present our stochastic inverse solution, namely, the global map of phase velocity in the period range from 20 to 100 sec using computer color graphics.

In the final part of this chapter, we compare our results with other global geophysical data which have become available recently, and discuss the possibility of routinely using our models in the application of the moment tensor inversion technique to any earthquake on the Earth.

5.2 - Inversion method:

We follow the inversion procedure using a block model introduced by Aki *et al.* (1977). Assuming ray theory, the phase arrival time t^c for a path between two points x_1 and x_2 can be calculated in terms of the phase velocity c(x) at a point x along the path as

$$t^c = \int_{x_1}^{x_2} \frac{dx}{c(x)} \qquad (5.1)$$

where dx is the incremental path length.

Let us designate the observed phase arrival time for the i-th path as t_i^o, and the calculated arrival time for the initial model t_i^c. We shall use the phase velocity assigned to Jordan's regionalization as obtained in Chapter 3 as our

initial model. The residual travel time Δt_i is then defined as

$$\Delta t_i = t_i^o - t_i^c \qquad (5.2)$$

We attribute the cause of these travel time residuals to the perturbation in velocity along the path. Dividing the Earth's surface into blocks, we can write

$$\Delta t_i = \sum_j g_{ij} m_j + e_i \qquad (5.3)$$

where g_{ij} is the time spent by the i-th ray path in the j-th block, and m_j is the fractional slowness pertubation for this block. Notice that ray theory was used to define Equation (5.3). This brings up the usual restrictions of ray theory to the problem (*i.e.* the block size is constrained by the wavelength of the seismic waves used). g_{ij} is obtained by calculating the length of the ray in each block and the velocity value assigned to the region to which the block belongs. Our block model corresponds to the discretized model of Jordan, 1981, with block size of $10^o \times 10^o$ size, as shown in Figures 5.1a and 5.1b, for periods less or equal 50 sec, and

for periods greater than 50 sec, respectively. e_i represents the errors due to measurement errors and higher order terms neglected in the linearization of the problem.

In matrix form, Equation (5.3) can be written as

$$\mathbf{d} = \mathbf{G}\,\mathbf{m} + \mathbf{n} \qquad (5.4)$$

where d is a vector containing the residual time Δt_i observed for the i-th path, G is a matrix with elements g_{ij}. m is the vector consisting of elements m_j, and n is the error vector with elements e_i.

5.3 - Stochastic inverse:

We follow Aki and Richards (1980), who describe how to obtain a solution for Equation (5.4) using the stochastic inverse method (Franklin, 1970). The assumptions involved in this method are that both m and n are stochastic processes and that their means are zero,

$$\langle \mathbf{m} \rangle = \langle \mathbf{n} \rangle = 0$$

We define the covariance matrices of **m** and **n** by

$$\langle \mathbf{m}\mathbf{m}^t \rangle = \mathbf{R}_{mm}$$

$$\langle \mathbf{n}\mathbf{n}^t \rangle = \mathbf{R}_{nn}$$

where the suffix t means taking the transpose of a matrix.

An inverse operator L is then calculated in a way that the averaged differences between **m** and **Ld** are minimized in the least squares sense,

$$\langle |\mathbf{m} - \mathbf{L}\mathbf{d}|^2 \rangle = \text{MINIMUM}$$

this leads to the equation

$$\langle \mathbf{m}\mathbf{d}^t \rangle = \mathbf{L}\langle \mathbf{d}\mathbf{d}^t \rangle$$

$$\text{or} \quad \mathbf{L} = \mathbf{R}_{md}\,\mathbf{R}_{dd}^{-1} \qquad (5.5)$$

where $\mathbf{R}_{dd}$ can be written using Equation (5.4) as

$$\mathbf{R}_{dd} = \langle \mathbf{d}\mathbf{d}^t \rangle = \langle (\mathbf{G}\mathbf{m} + \mathbf{n})\,(\mathbf{G}\mathbf{m} + \mathbf{n})^t \rangle$$

if we assume that **m** and **n** are statistically independent,

$$R_{dd} = G R_{mm} G^t + R_{nn} \qquad (5.6)$$

Likewise, we obtain

$$R_{md} = \langle \mathbf{m} d^t \rangle = \langle \mathbf{m} (G\mathbf{m} + n)^t \rangle = R_{mm} G^t \qquad (5.7)$$

Using Equations (5.6) and (5.7) in Equation (5.5), we obtain

$$L = R_{mm} G^t (G R_{mm} G^t + R_{nn})^{-1} \qquad (5.8)$$

that is the stochastic inverse operator or 'minimum variance' estimator in the notation of Jackson (1979). It can also be obtained in the form

$$L = (G^t R_{nn}^{-1} G + R_{mm}^{-1})^{-1} G^t R_{nn}^{-1} \qquad (5.9)$$

This form is more convenient to use in this problem, where the data set is larger than the set of variables, so that the dimension of the matrix to be inverted in Equation (5.9) is smaller than in Equation (5.8).

Aki *et al.* (1977) assume that

$$R_{nn} = \sigma_n^2 I \qquad (5.10)$$

and $$R_{mm} = \sigma_m^2 I \qquad (5.11)$$

Equation (5.10) means that the measurement errors are independent and share the common variance and Equation (5.11) implies that all the parameters to be determined share the same model variance σ_m^2; and they are all statistically independent.

Using Equations (5.10) and (5.11) in Equation (5.9) and introducing damping constant $\vartheta^2 = \sigma_n^2/\sigma_m^2$, we can rewrite

$$L = (G^t G + \vartheta^2 I)^{-1} G^t \qquad (5.12)$$

The estimate **m'** of the solution is obtained by operating L on the data vector d,

$$\mathbf{m'} = L\,\mathbf{d} \qquad (5.13)$$

The same estimate can also be obtained by the minimization of weighted sum of squares:

$$(|d - Gm|^2/\sigma_n^2) + (|m|^2/\sigma_m^2) \qquad (5.14)$$

Let us now assess the stability and the errors of the solution. This is based on the work of Backus and Gilbert (1967, 1968, and 1970) who introduced the concepts of resolution and trade-off between errors and resolution of a particular solution.

5.4 - Error analysis of the inversion result:

The resolution matrix is calculated by applying the inverse operator L on the matrix G,

$$R = L\,G \qquad (5.15)$$

and the covariance matrix for the error in the solution m' due to random noise is given by

$$C = \sigma_n^2\, LL^t \qquad (5.16)$$

The above equation represents only the errors due to the noise in the data. The total error of the solution should also include errors due to imperfect resolution of the inversion process. We describe now how this total error covariance can be calculated, following Jackson (1979).

The total error in the solution $\mathbf{m}'$ is given by

$$\mathbf{m}' - \mathbf{m} = L(G\mathbf{m} + \mathbf{n}) - \mathbf{m} = (LG - I)\mathbf{m} + L\mathbf{n} \qquad (5.17)$$

$$\text{or} \qquad \mathbf{m}' - \mathbf{m} = (R - I)\mathbf{m} + L\mathbf{n} \qquad (5.18)$$

We notice that for a perfect resolution ($R = I$) there is only the second term in the right hand side of Equation (5.18) (we then have only errors due to random noise). We define the covariance matrix that includes all the errors in the solution. Using Equation (5.18),

$$\langle(\mathbf{m}' - \mathbf{m})(\mathbf{m}' - \mathbf{m})^t\rangle = (R - I)\langle\mathbf{m}\mathbf{m}^t\rangle(R - I)^t + L\langle\mathbf{n}\mathbf{n}^t\rangle L^t \qquad (5.19)$$

Since $\langle\mathbf{m}\mathbf{m}^t\rangle = R_{\mathbf{mm}}$ and $\langle\mathbf{n}\mathbf{n}^t\rangle = R_{\mathbf{nn}}$, we see that the right hand side of Equation (5.19) includes Equation (5.16) (the

contribution of the random error in the data), and contains also the contribution due to imperfect resolution.

From Equation (5.15) we have

$$\begin{aligned}(R - I) &= (G^t R_{nn}^{-1} G + R_{mm}^{-1})^{-1} G^t R_{nn}^{-1} G - I \\ &= -(G^t R_{nn}^{-1} G + R_{mm}^{-1})^{-1} R_{mm}^{-1}\end{aligned} \tag{5.20}$$

Using Equation (5.20), we can obtain

$$(R - I)\, R_{mm}\, (R - I)^t = -(G^t R_{nn}^{-1} G + R_{mm}^{-1})^{-1} (R - I)^t \tag{5.21}$$

From Equation (5.9),

$$L R_{nn} L^t = (G^t R_{nn}^{-1} G + R_{mm}^{-1})^{-1} G^t R_{nn}^{-1} R_{nn} L^t$$

or,

$$L R_{nn} L^t = (G^t R_{nn}^{-1} G + R_{mm}^{-1})^{-1} R^t \tag{5.22}$$

Finally, using Equations (5.21) and (5.22) in Equation (5.19) and rearranging, the final form for the covariance matrix

including all errors is obtained,

$$\langle (\mathbf{m}' - \mathbf{m})\,(\mathbf{m}' - \mathbf{m})^t \rangle = (G^t R_{nn}^{-1} G + R_{mm}^{-1})^{-1} \qquad (5.23)$$

For the special case $R_{nn} = \sigma_n^2 I$ and $R_{mm} = \sigma_m^2 I$, it simplifies to

$$\langle (\mathbf{m}' - \mathbf{m})\,(\mathbf{m}' - \mathbf{m})^t \rangle = \sigma_n^2 (G^t G + \beta^2 I)^{-1}$$

5.5 - Selection of a damping constant:

In the previous section it was shown that the best choice for the damping constant is given by $\beta^2 = \sigma_n^2 / \sigma_m^2$.

The error in the solution due to the linearization of the problem together with measurement errors have to be considered in the estimation of the noise variance σ_n^2. This is estimated from the residual for the estimated solution $\mathbf{m}'$,

$$\mathbf{e} = \mathbf{d} - G\mathbf{m}'$$

and its magnitude

$$\mathbf{e}^t\mathbf{e} = \mathbf{d}^t\mathbf{d} - 2\mathbf{m}'^t\mathbf{G}^t\mathbf{d} + \mathbf{m}'^t\mathbf{G}^t\mathbf{G}\mathbf{m}' \qquad (5.24)$$

σ_n^2 is estimated by dividing $|\mathbf{e}|^2$ by the number of degrees of freedom, that is, the number of data minus the number of model parameters, as done by Aki and Lee (1976) and Zandt (1978). On the other hand, σ_m^2 must be specified with an a priori assumption of the model. This introduces some subjectivity to the inversion process.

Table 5.1 shows the data variance, model variance and the damping constant used in several three-dimensional inversion studies of travel time data for body-waves, using the method of Aki *et al.* (1977). The studies of Hirahara (1977 and 1981) are related to the three-dimensional velocity structure underneath Japan and Sea of Japan. Zandt (1981) studied the Coast Range area in Central California. He processed the data separately for the three regions: Santa Rosa, San Jose, and Bear Valley. Horie and Aki (1982) studied the seismic velocity structure underneath the Kanto district in Japan. Taylor (1983) used the data from underground nuclear explosions at the Nevada Test Site for determination of the

local structure, and Biswas (written communication, 1983) studied south-central Alaska using teleseismic data.

The damping constant θ^2 assumed by these authors are shown in Table 5.1. They are obtained by the relation $\theta^2 = \sigma_n^2 / \sigma_m^2$ where σ_n^2 was, in some cases, estimated from the reading error in the measurements of arrival time, and σ_m was assumed by the author.

We were initially puzzled by a considerable discrepancy between the assumed value of σ_m and the root mean square of the solution, listed at the 6th and 7th lines of Table 5.1 for crust and mantle, respectively.

Examining the residual, $\mathbf{e} = \mathbf{d} - \mathbf{Gm}'$, we soon realized that some of the authors have underestimated σ_n^2 by considering only the reading error. The square root σ_n^* of the noise variance estimated from the residual is also listed in Table 5.1. The square root of the model variance corresponding to σ_n^* is calculated by the equation $\sigma_m^2 = \theta^2 / \sigma_n^{*2}$, and is listed at the 5th line of Table 5.1. Their values compare better with the root mean square of the solution.

An interesting feature of the inversion results may be observed in Table 5.1. It is clear that the velocity variations are greater in the crust than in the upper mantle,

and that the velocity variations increase with the decrease in block size as shown in Table 5.1. As shown in Table 5.2 for other studies, the crust presents, in general, a velocity variation greater than the mantle. We list also in Table 5.3 the root mean square velocity variations, the average diagonal element of the resolution matrix and the average standard error of the solution due to random error in the data. The depth range, lateral block size and number of resolved blocks are also listed for each layer. It is clear from these results that there is a decrease of the velocity variation with depth.

The above review of the results of three-dimensional velocity studies using the stochastic inversion is useful in our application to Rayleigh waves, since it shows how to estimate the noise variance, and how the lateral heterogeneities vary with depth. We have applied Equation (5.24) to estimate the noise variance in our data set, and found that different damping was needed while studying different periods, during the application of the stochastic inversion. We shall discuss the results of these analyses in the next section.

5.6 - Application of the stochastic inversion to the phase velocity data set:

The operator L of Equation (5.12) was obtained for each period, using the decomposition by the Cholesky algorithm (Strang, 1980). We have tried several damping constants for each period. In all cases, we required that each block was sampled by at least ten rays. In order to eliminate some anomalous observations, we rejected residual travel time data, with an absolute value more than four percent of the total travel time. For each run, corresponding to a given damping constant, we calculated the following parameters for each block; the number of hits in each block studied, the percentage velocity perturbation; the diagonal element of the resolution matrix, calculated using Equation (5.15); the standard deviation due to random noise, given by Equation (5.16); and the standard error due to poor resolution of the inversion (taken from the difference between the total variance of the solution and the variance due to random noise in the data).

In Tables 5.4 thru 5.12 we show the above parameters averaged for each region symbol of the initial model of Jordan (1981), for a number of inversions using different values for

the damping constant (which is specified for each run). At the top of each of these Tables, we indicated the period studied; the initial data variance, the number of observations used, the number of blocks solved, and the average path length, all for the period in question. For each run, we showed the residual variance, and the variance improvement. Also shown is the square root of the model variance σ_m^2 corresponding to the choice of damping constant.

The damping constant selected for the final solution for each of the reference periods are underlined in each of these Tables. The selection was made considering the trade-off between errors and resolution of each solution, so that an acceptable balance was achieved. The values of σ_m are, in many cases, comparable to those obtained earlier in Table 3.1.

An interesting comparison can be made between the standard deviation of our phase travel time residual data with that used by Yomogida (1985), which is shown in Table 5.13a. We can see that the two sets are very similar, although Yomogida (1985) studied paths restricted to the Pacific Basin. A more interesting comparison in Table 5.13b is between the residual standard deviation of the inversion results of our work and that of Forsyth (1975), by regionalization with four

oceanic, and two continental regions including the anisotropy. In the same table, we also show the result of Patton (1978), who used a regionalized model consisting of five regions: 'stable B', 'plains', 'tectonics', 'plateau', and 'ocean' to fit his observations of phase velocity for Rayleigh waves propagating in Eurasia. Also shown in Table 5.13b is the residual standard deviation reported by Patton (1984), for phase velocity data of Rayleigh waves in the Western U.S.. Patton (1984) used four major provinces, and three 'less distinct' provinces, to explain up to 40 percent of the initial variance of phase velocity data of Rayleigh waves with 40 sec period. Finally, we showed the residual standard deviation obtained by Yomogida (1985) by the inversion of phase data only.

From these data shown in Table 5.13b, we notice that the residual standard deviation achieved in our work is larger than that obtained by Forsyth (1975) and by Patton (1984), who studied much smaller regions. On the other hand, our results are comparable to those of Patton (1978) for shorter periods, probably because the regionalization used by Patton is not adequately detailed for shorter periods. Our residual standard deviation is comparable to the result of the phase

data inversion performed by Yomogida (1985) in the Pacific region, where he used a 5° by 5° regionalization grid.

The resulting phase velocity world maps (consisting of the initial velocity model plus perturbation) obtained by each computer run corresponding to a chosen damping constant, together with the velocity perturbation maps, the data density, the diagonal element of the resolution matrix, the total standard deviation, and the standard deviation due to random noise in the data, are all plotted in Figures 5.2 thru 5.10, for the reference periods 20 thru 98 sec. Each of these maps is shown in the mercator projection, with the same latitude range as in the maps of Appendices A, B, and C (*i.e.*, from 70°S to 75°N). We have used a bi-cubic spline interpolation scheme (de Boor, 1978) to interpolate between the values corresponding to each block studied. We expected to obtain some of the abnormal effects at the borders of the maps and in areas close to unresolved blocks (shown either as yellow or in black in these figures), due to the lack of continuity of values in such cases. So, we ignored anomalies which are too close to these borders. Other regions for which we kept some conservative view when analyzing the results are those too close to the polar regions. In these cases, the

lack of data affected both the resolution and error values, so that we usually obtained velocity perturbations which were smaller than the standard errors.

In general, the diagonal elements of the resolution matrix approaches unity for blocks with the largest number of hits. This increasing of resolution of the solution is also associated with a decrease in total standard deviation, and a decrease in the values of standard deviation associated with random error, in a way that the most reliable part of the result is in areas where the data coverage was the best (such as in North America, the East Pacific, the North Atlantic, western Europe, East Africa, northern portions of the Indian Ocean, and the Tibet region).

5.7 - Results:

Anomalies in phase velocity for the period range studied reflect possible differences in body wave seismic velocities and densities in the crust and upper mantle structure of the several regions considered. These differences can be caused by temperature anomalies, compositional variations, partial melting, and anisotropy.

We notice that negative anomalies in Figures 5.2b thru 5.10b are associated with the Tibet region, the back-arc regions in western Pacific and in the Aleutian Islands, with the Tonga trench and the Hawaiian Islands in the Pacific, and with subduction zones along the western Canadian coast, and western Mexican and Central America coast. Other regions of subduction tectonic activity where negative anomalies are observed are those along the southwestern South America coast, and the Caribbean Sea. We also observe negative anomalies in rifting zones (such as the Mid-Atlantic ridge, the East Pacific Rise, the Southwest and Southeast Indian Ocean Ridge, the Carlsberg Ridge, and the East African Rift). We showed some caution in the interpretation of some other small and isolated anomalies, since a large block size was used in our inversion.

Positive anomalies are generally associated with shield and other stable regions, such as the Canadian, the Guyana, and the Brazilian shields in the Western Hemisphere, and the Baltic, the Central Africa, and the West Australia regions in the Eastern Hemisphere. In the oceans, we observed positive anomalies associated with the northwestern Pacific, Nazca plate, as well as in other old oceanic regions which distribution is shown in the work of Sclater *et al.* (1981).

Many of the above features were noticeable by previous small-scale works, or were expected by the known tectonic setting of several regions. In these cases, our maps reassure these previous results and theories. On the other hand, there are areas where the tectonic setting is only now being revealed (*e.g.* the northeastern portion of China, recently studied by Shedlock, 1986). In these cases, our results are useful as additional evidence: in the case of China, we notice that its eastern portion has associated phase velocity values comparable to those found in western United States. This is in contrast with the higher velocities found in nortwestern China, where there is less tectonic activity. So, the tectonic environment in eastern China is probable closer to that found in active mountaneous areas such as western North America.

In the Pacific region, a comparison can be made between our results and those of Yomogida (1985) in the corresponding reference periods (model AP of his work, for the periods of 30, 40, 60, and 80 sec). We see that both maps corresponding to phase velocity changes, and maps of phase velocity distribution show much resemblance, with most of the major anomalies represented in both results. To be more specific,

we have included two of the resulting images of Yomogida's work in Figures 5.11a and 5.11b. These correspond to Figures 5.21b and 5.22d of his work, and represent the results he obtained for the phase velocity and velocity perturbations of the initial model used for the reference periods of 40 and 80 sec, respectively. These results were obtained by inverting both amplitude and phase observation data, and a $5^{\circ} \times 5^{\circ}$ grid was considered in contrast with the $10^{\circ} \times 10^{\circ}$ grid used here. Yomogida (1985) also solved the inverse problem using only the phase data. We have already referred to the latter results, and included some of the parameters in Table 5.13.

We will now compare the results of Figures 5.11a and 5.11b with those in Figures 5.4a, 5.4b and 5.8a, 5.8b, for the Pacific Ocean area. The most striking similarities between Figures 5.11a and 5.4a are the low velocity areas representing the back-arc regions in western Pacific, the Tonga trench, the western coast of North, Central, and South America; and the East Pacific Rise. High velocity anomalies in western Pacific, where old oceanic seafloor is present, and in the Nazca plate region, are also very similar in both maps. If we consider Figures 5.11b and 5.8a, we also notice a strong similarity between the two. The low velocity anomalies

corresponding to the back-arc regions are well represented in both maps, with the strong low velocity anomaly close to the Samoa Islands being remarkably well represented in the two results. The East Pacific Rise anomaly is also well characterized in both results, specially in its portion closest to the Gulf of California region, where a low velocity anomaly is well represented in both cases. Except for the high velocity anomaly located off the coast of Peru in Yomogida's map, we notice that the agreement between the two maps is very good. The other high velocity anomalies representing areas of old oceanic crust are similar in both maps. Some differences can be found in areas such as the Hawaiian Islands chain, where we have detected a low velocity region that is not present in the result of Yomogida (1985).

Some of the velocity anomalies shown in Figures 5.2a thru 5.10a and 5.2b thru 5.10b are present in all periods we studied (such as those related to the back-arc regions in western Pacific, and that corresponding to the Tibet area). This indicates that our initial model does not represent these areas well, and require finer regionalization distinguishing back-arc regions from other active regions.

In regard to anomalies correlated to hot-spot zones, we can consider those located in islands such as Hawaii and Galapagos. In the proximities of these two islands, we observe low velocity anomalies in most periods. This could indicate the presence of partial melting or high temperature zones in the upper mantle.

5.8 - Comparison with other global geophysical data:

5.8.1 - Phase velocities of Love and Rayleigh waves at longer periods:

As we have summarized in Chapter 1, there have been a number of recent works on the global distribution of phase and group velocity of Rayleigh and Love waves with period greater than the period range studied in this thesis. We will review these efforts here in more detail. We will also compare our results with some of the phase velocity results.

Nakanishi and Anderson (1982) studied the worldwide distribution of group velocity of mantle Rayleigh waves. The data (mainly R_2 and R_3 observations) were provided by the I.D.A. records of a set of 26 earthquakes. The velocity results obtained by the determination of spherical harmonics coefficients up to angular order 7 were presented for the reference periods of 152.34, 196.112, and 252.46 sec.

The worldwide distribution of fundamental mode Love and Rayleigh wave phase velocity was obtained by Nakanishi and Anderson (1983), who used the observed phase differences of multiple passages along greatcircle paths. The period range studied from 100 to 330 sec. They inverted the observations for regional phase velocities and for an even-order harmonic expansion of the lateral heterogeneities. These latter results were obtained from the application of spherical harmonics up to degree 6 to the data set, which contained information generated by 28 earthquakes that were recorded at I.D.A., S.R.O., A.S.R.O., and D.W.W.S.S.N. stations, totalling 200 paths for Love waves, and 250 paths for Rayleigh waves. In two other papers, Nakanishi and Anderson (1984a,b) present the results of a similar analysis, this time using measurements of both phase and group velocities of Love and Rayleigh waves (G_2, G_3, R_2, R_3) in the period range 100-330 sec, which were made using the one-station method. They used a total of 200 paths in this work, corresponding to records of 17 large earthquakes ($M_s \geq 6.5$) that occurred in 1980. The focal mechanisms of these events were studied by Kanamori and Given (1982), and were also previously examined by Nakanishi and Kanamori (1984). This second part of their work

(Nakanishi and Anderson, 1984a,b) show more similarities to our work than the first part (Nakanishi and Anderson, 1983). As a continuation of this study, Nataf *et al.* (1984), Anderson (1984), and Nataf *et al.* (1986) have analyzed the results of Nakanishi and Anderson (1983, 1984a,b) to study the shear wave velocity structure of the upper mantle and to determine the crustal thickness in a global scale.

Tanimoto and Anderson (1984, 1985) studied the lateral variation of phase velocity of long period surface waves (R_2, R_3 and G_2, G_3) and the azimuthal dependence of these velocities (anisotropy effect). They inverted a data set larger than that of Nakanishi and Anderson (1983, 1984a,b), including a total of more than 500 paths for Rayleigh wave, and more than 300 Love wave paths corresponding to 15 earthquakes that occurred in 1980. The reference periods used were 100, 150, 200, and 250 sec. The parameterization of the problem was also based on spherical harmonics expansion. One of their major conclusions is related to the anisotropy effect on the propagation of these waves: they found that faster phase velocity is associated with the direction of plate motion. The variance reduction with relation to an initially laterally homogeneous model achieved in their work are as

follows: 40.5, 39.3, 44.1, and 36.7% for the Love waves solution, and the reference periods of 100, 150, 200, and 250 sec, respectively. For Rayleigh waves, it was 45.8, 64.9, 66.6, 54.5% for the same respective reference periods. We have reproduced their map (Figure 9 of Tanimoto and Anderson, 1985) showing the solution from Rayleigh wave data with period 100 sec in Figure 5.12. The solution was obtained by application of the method of Backus and Gilbert (1967, 1968, 1970), which is discussed in detail by Tanimoto (1985). The average error estimated for the resultant anomalies is about 1 percent. The maximum variations reported for the phase velocity values range between 3 and 4 percent. The resultant maps showing the perturbations in phase velocity distribution from Tanimoto and Anderson (1985) and Tanimoto (1985) were later used by Tanimoto (1986) in the determination of the SH and SV velocity structure of the upper mantle.

We can compare the variance reduction achieved by Tanimoto and Anderson (1985) for 100 sec period, with the variance improvement we obtained. As we recall, their inversion achieved about 46% variance improvement, compared to 59% of our results. One could argue that Tanimoto and Anderson (1985) used a smaller number of unknowns than we did

(since l_{max} in their work is 10, which corresponds to 121 unknowns, while we solved for 391 blocks). On the other hand, Tanimoto and Anderson (1985) used 497 observations of R_2 and R_3 in contrast with the 954 R_1 observations used here. Furthermore, the use of R_2 and R_3 involves complications due to the one or two polar passages, respectively. These difficulties were considered by Aki (1966) while studying the Love wave equivalents to these phases namely, G_2 and G_3. He found that G_3 phases were particularly more complicated, and we expect to find the same difficulties when analyzing Rayleigh waves.

For shorter periods, Nishimura and Forsyth (1985) have determined a map of lateral variations in the Pacific of phase velocity for fundamental mode Love waves with reference periods of 40, 67, 91, and 125 sec. They used both spherical harmonics and the pure path regionalization technique used by Forsyth (1973) to analyze a set of 115 surface wave paths (43 from Forsyth, 1973 and 72 new ones) using digitized seismograms of the W.W.S.S.N.. They found a strong dependence of the velocities with the age of the seafloor. The anomalies not related to the age of the seafloor were correlated with existing hot-spots. We present here the resultant maps

showing the slowness anomaly distribution for each of the reference periods in Figure 5.13 (this figure corresponds to Figure 8 of Nishimura and Forsyth, 1985).

Further studies using long period surface waves include those of Woodhouse and Dziewonski (1984), that used a method proposed by Woodhouse (1983) to simultaneously determine the global lateral heterogeneity distribution and the source parameters of 53 events, using the global digital network data on mantle surface waves and long period body waves. The main result of their work is a set of maps showing the global variation of shear-wave velocity at six reference depths (between 50 and 550 km). Further results from the application of this technique are shown in a later paper by Dziewonski and Anderson (1984).

5.8.2 - Comparison with long period results:

Before analyzing our results compared with the maps discussed in the previous section, it is important to note that most of these results we obtained from the geophysical literature were generated by the evaluation of the spherical harmonics coefficients. The main implication of this is the usually smooth variation observed in these results, in

comparison with the sometimes sharp changes in phase velocity of our results. It is not our concern here to point out differences between the methods of analysis, but to compare the results to which we referred in the previous section.

We begin comparing Figure 5.12 (the result obtained by Tanimoto and Anderson, 1985 for Rayleigh wave phase velocity for the reference period 100 sec), which corresponds to Figures 5.9b and 5.10b of our work (the maps corresponding to the largest reference periods which we studied namely, 90 and 98 sec). We notice that most major anomalies we found from our work are present in this map: the low velocity anomaly associated with the East Pacific Rise, and that in the western United States, the low velocity anomalies associated with the back-arc regions along the western Pacific rim (from the Sea of Okhotsk and Bering Sea all the way to the Tasman Sea). The low velocity anomaly associated with the Samoa Islands region which stands out in our results at all periods is also clear in their results. Also coincident are the high velocity anomalies observed along the eastern North America coast, and that observed in southern Africa. Most of other shield regions present high velocity anomalies, which is not new but reaffirms previous results. The low velocity anomaly located

in the Arabian Peninsula - Red Sea region is also present in both results.

The results of Nishimura and Forsyth (1985) on the Love wave phase velocity distribution on the Pacific basin provide us with another opportunity (in addition to the results of Yomogida, 1985), to check our results in this region. The information reproduced from their work is shown in Figures 5.13a thru d, which correspond to period values of 40, 67, 91, and 125 sec. Notice that slowness perturbations are shown. We can compare these with the velocity anomalies of our study in Figures 5.2b thru 5.10b. We refer first to Figures 5.13a and Figure 5.3b, corresponding to period 40 sec. Notice the similarity on the negative velocity anomaly near the Kuril Islands Trench, the positive velocity anomaly in the eastern side of the Mariana Trench, and the low velocity anomaly off the coast of Chile. There is a negative velocity anomaly located close to the French Polynesia in our results, although it is not as broad as the one shown in Figure 5.13a.

We can observe the same similarities on results in the western Pacific if we compare Figures 5.7b and 5.13b. Notice

again the negative velocity anomaly by the Kuril Islands, as well as the positive velocity anomaly located on the portion of the ocean floor by the Mariana Trench. The negative anomaly observed at the Chilean coast is now further north in our results when compared to Figure 5.13b, although the positive anomaly located in the Nazca plate is coincident in both results. The negative velocity anomaly by the French Polynesia region found by Nishimura and Forsyth (1985) is not very clear in our results.

We finally compare their results at 91 sec (shown in Figure 5.13c) with the ones shown in Figure 5.9b, that we obtained at 90 sec. Notice that the high velocity anomaly by the Mariana Trench was detected in both results. Another high velocity anomaly in the western Pacific, present in both results, is clearly shown off the coast of New Zealand. The low velocity anomaly by the French Polynesia is now clear in our results, as well as the positive anomaly off the southern coast of Peru. The low velocity anomaly off the Canadian coast is also present in both results.

5.9 - Implications for moment tensor inversion:

In this section, we discuss the possibility of using our phase velocity maps for application of the moment tensor inversion method to study the mechanism of any earthquake in the Earth.

As we discussed in Chapter 2, Weidner (1972), using the reference point method described by Weidner and Aki (1973), was able to almost completely separate the source and path effects of earthquakes in the Atlantic using event pairs. Patton (1978) achieved a similar goal, by using a group of events located around a reference point in Tibet.

From calculated phase radiation pattern for a variety of source mechanisms, it is easy to notice that we need an accuracy of about 0.1 cycle in our phase observations, in order to make a meaningful distinction between different mechanisms. This means that we need an accuracy of 3 sec for the period of 30 sec.

An early estimate of the accuracy needed for the phase velocity values in all paths connecting stations and source point, in order to separate the propagation effect from the phase observations prior to the linear moment tensor inversion method of Mendiguren (1977), was made by Aki and Patton

(1978). They estimated that, for this case, we need 0.5% accuracy in the phase velocity data. This corresponds to saying that, for a path measuring a few thousand kilometers, we have an error of a few seconds in the travel time of the observed phase.

Patton (1978) was able to achieve such accuracy with the application of the reference point method, but not with his regionalized map of phase velocity. Romanowicz (1982a) proposed an alternative to relax the high accuracy needed in the propagation correction envolved in the method used by Patton (1978). We have reviewed this advance in the moment tensor inversion method in Chapter 2. As we recall, Romanowicz (1982a) does not give any accuracy bounds needed in her new version of the method. Although, Romanowicz (1982a,c) states that, for a given reference point, the phase velocity curves to the observing seismographic stations can be used to corrected the observed phase spectra generated by earthquakes distancing up to 1000 km from the reference point (or to a somewhat lower distance, for regions with significant changes in tectonic structure).

In our work, we have collected most of the available phase velocity data, and have added a greater number of newly

measured data, to obtain the results shown in Figures 5.2a thru 5.10a. These correspond to the solution of the inverse problem, which was set up using a 10° X 10° global mesh. As shown in Table 5.13b, the prediction based on the phase velocity mapping with the 10° X 10° meshes gave residuals ranging between 13 and 16 sec for all periods. Clearly, our results cannot be used in the application of the moment tensor inversion method to any event using the waves with period 20 or 30 sec, because the phase uncertainty is more than 0.5 cycles. On the other hand, if we use long period, say 100 sec, the residual is equivalent to a 0.15 cycles error. As we will see, this accuracy is enough to obtain useful results in the seismic moment tensor inversion.

Kanamori and Given (1982) determined the moment tensor for 25 large shallow earthquakes that occurred in 1980 and recorded by the I.D.A. network, using the linear inversion method described by Kanamori and Given (1981). This includes the use of a laterally homogeneous Earth model to derive the initial phase at the source. The method is good for events larger than M_s = 6. Nakanishi and Kanamori (1982) used the same method, this time with the regionalized phase velocity curves of Dziewonski and Steim (1982), and a discretized world

map representation with grid size $5^{o} \times 5^{o}$ similar to those we used in Chapter 3. They used I.D.A. records of three earthquakes, corresponding to a period range between 196.92 and 256 sec. Their conclusion was that the simple regionalized phase velocity curves have improved the linear inversion for the moment tensor, in comparison with the use of a laterally homogeneous media of their first work. Furthermore, they suggest that a more detailed model may be needed for improvement of the results.

We have reproduced in Figure 5.14 the Figure 7b of the work of Patton (1980a). It represents the final fit obtained after the linear moment tensor inversion was applied to one of the events he studied. This is one of the best fits obtained in his work. Notice that the scatter of the observation points is usually within 10% of the calculated values. This shows that our results at longer periods can probably be used for studies of focal mechanism by the same method in most of the Earth. It is a very encouraging result, specially because we can now use the moment tensor inversion at 100 sec, which is a great improvement when we consider that the smallest period considered by Nakanishi and Kanamori (1982) was about 200 sec.

To lower the applicability of the moment tensor inversion method from 100 sec to about 30 sec, it is necessary to improve our phase velocity maps for the shorter periods. This can be done by increasing the phase velocity data set for these periods, so that we can obtain the phase velocity at a much finer mesh size than the $10^{\circ} \times 10^{\circ}$ mesh used in our work. Since $10^{\circ} \times 10^{\circ}$ mesh is needed for 100 sec period, we may assume that $3^{\circ} \times 3^{\circ}$ mesh may be needed for 30 sec period. This will require to solve for about 10 times greater number of unknowns. If we consider that we needed about 1800 rays to solve for an average of 480 unknowns at an acceptable resolution level (each block was sampled at least 10 times), we may need about 18000 rays to solve this new problem. This is even larger than the estimate of Aki and Patton (1978), who estimated that it would take around 10000 rays. For each earthquake we studied, we obtained an average of about 30 good phase velocity observations. This means that we need to know the mechanism of about 550 more events in addition to the present data set, so that we have the sufficient number of data for the moment tensor inversion for 30 sec period Rayleigh waves. It is not very difficult to locate such number of events with magnitude less than 6 during the time

covered by the W.W.S.S.N. operation. The difficulty comes if we require uniform coverage of all blocks with hitting rays. Considering the effort needed to study the mechanism of such a number of events, and to digitize the long period records, we believe that this task would take at least 10 times longer than we needed to complete this thesis (*i.e.* it would take at least the whole carreer of one scientist). We hope that the proposed denser global digital network will soon make this problem a much easier task.

In the discussion above, we have neglected the problem of solving an inverse problem with such a large number of unknowns. Clearly, the approach used in our work could not be used due to the size of the memory needed in the computer. This does not, however, pose a major difficulty, since we could choose another technique, probably one similar to those used in medical tomography.

A much more reasonable approach, solvable in a realistic time scale, would be the establishment of a global network of reference points in areas of tectonic interest, where a large number of earthquakes usually occur. Notice that, some areas such as the Tibet, North America, and other areas already have a very good data coverage. If we examine Figure 4.1, we also

notice that we have set up a considerable network of reference points on areas in the Indian Ocean, and Central Atlantic Ocean. With the phase velocity values measured for these events, which will soon be published, geophysicists have already a very useful tool to study future events in these areas.

TABLE 5.1

REF.	Hirahara 1977	Hirahara 1981	Zandt 1978	Zandt 1978	Zandt 1978	Horie and Aki, 1982	Taylor 1983	Biswas 1983
REGION	Japan	Japan	Santa Rosa	San Jose	Bear Valley	Kanto District	Nevada	Alaska
Θ^2 $(SEC/\%)^2$	0.15	0.10	0.005	0.005	0.005	0.01	0.01	0.005
READING ERROR (SEC)	1.0	0.7	0.1	0.1	0.1	0.05	0.05	0.1
σ_m (%) ASSUMED BY AUTHOR	2.58	2.21	1.41	1.41	1.41	0.50	0.50	1.41
σ_d^* FROM RESIDUAL (SEC)	0.78	1.01	0.14	0.26	0.14	0.20	0.34	0.36
σ_{m_*} FROM σ_d^* (%)	2.02	3.21	2.01	3.64	2.00	2.00	3.46	5.10
ΔV RMS CRUST (%)	1.96	2.40	2.92	3.24	3.00	3.50	3.17	4.16
ΔV RMS MANTLE (%)	1.45	1.57	2.71	1.90	2.26	1.35	2.54	1.80
BLOCK SIZE MAX	2°	2°	25 km	25 km	25 km	30 km	20 km	100 km
MIN	-	1°	10 km	10 km	10 km	-	10 km	65 km

where ΔV RMS = $\langle(\Delta V/V_0)^2\rangle^{1/2}$

TABLE 5.2

REFERENCE	REGION	ΔV RMS (%) CRUST	ΔV RMS (%) MANTLE	θ^2 $(SEC/\%)^2$	BLOCK SIZE (km) MAX	BLOCK SIZE (km) MIN
Aki et al., 1976	LASA, USA	1.29	0.82	0.02	20	-
Husebye et al., 1976	Central California	2.18	1.10	0.02	25	30
Aki et al., 1977	Norsar, Norway	1.20	1.20	0.02	20	-
Ellsworth and Koyanagi, 1977	Hawaii	3.92	1.31	0.005	7.5	-
Mitchell et al., 1977	New Madrid, USA	1.78	1.45	0.02	50	-
Raikes, 1980	Southern California	2.34	1.71	0.01	40	55
Hasemi et al., 1984	Tohoku district, NE Japan	3.19	1.19	0.05	30	-

where $\Delta V \text{ RMS} = \langle(\Delta V/V_o)^2\rangle^{1/2}$

TABLE 5.3

REFERENCE	LAYER	RMS VEL VARIATIONS (%)	AVERAGE RESOLUTION	AVER STD DEV DUE TO RANDOM ERROR (%)	DEPTH (KM)	BLOCK SIZE (KM)	RESOLVED BLOCKS
Aki et al. 1976	1	1.45	0.56	-	0-20	20 x 20	23
	2	1.11	0.59	-	20-50	20 x 20	40
	3	0.91	0.52	-	50-80	20 x 20	60
	4	0.77	0.52	-	80-110	20 x 20	77
	5	0.77	0.59	-	110-140	20 x 20	79
Husebye et al., 1976	1	2.18	0.54	-	0-25	25 x 25	29
	2	1.14	0.40	-	25-50	25 x 25	35
	3	1.18	0.40	-	50-75	30 x 30	37
	4	1.00	0.37	-	75-100	30 x 30	48
	5	1.09	0.38	-	100-125	30 x 30	55
Aki et al. 1977	1	1.36	0.46	-	0-17	20 x 20	36
	2	1.02	0.40	-	17-36	20 x 20	48
	3	1.09	0.52	-	36-66	20 x 20	70
	4	1.09	0.51	-	66-96	20 x 20	80
	5	1.39	0.55	-	96-126	20 x 20	81
Hirahara 1977	1	1.96	0.48	0.71	0-50	2° x 2°	31
	2	2.05	0.54	0.58	50-150	2° x 2°	40
	3	1.74	0.47	0.63	150-250	2° x 2°	39
	4	1.25	0.39	0.56	250-350	2° x 2°	43
	5	1.08	0.38	0.61	350-450	2° x 2°	47
	6	1.17	0.40	0.64	450-550	2° x 2°	54
	7	1.17	0.42	0.71	550-650	2° x 2°	61
Mitchell et al., 1977	1	2.05	0.37	0.25	0-20	50 x 50	15
	2	1.47	0.26	0.20	20-40	50 x 50	22
	3	1.34	0.65	0.24	40-97	50 x 50	33
	4	1.55	0.69	0.27	97-154	50 x 50	39
Zandt, 1978 Bear Valley	1	3.70	0.37	0.72	0-10	10 x 10	62
	2	2.06	0.57	0.70	10-30	20 x 20	43
	3	2.05	0.69	0.64	30-60	25 x 25	46
	4	2.44	0.66	0.69	60-90	25 x 25	53
Zandt, 1978 San Jose	1	4.02	0.43	1.45	0-10	10 x 10	63
	2	2.23	0.64	1.32	10-30	20 x 20	42
	3	2.05	0.75	1.12	30-60	25 x 25	45
	4	1.74	0.68	1.23	60-90	25 x 25	53
Zandt, 1978 Santa Rosa	1	2.57	0.27	0.70	0-10	10 x 10	39
	2	3.23	0.46	0.73	10-30	20 x 20	32
	3	3.08	0.65	0.66	30-60	25 x 25	33
	4	2.28	0.56	0.72	60-90	25 x 25	40

TO BE CONTINUED

TABLE 5.3 CONTINUED

REFERENCE	LAYER	RMS VEL VARIATIONS (%)	AVERAGE RESOLUTION	AVER STD DEV DUE TO RANDOM ERROR (%)	DEPTH (KM)	BLOCK SIZE (KM)	RESOLVED BLOCKS
Raikes 1980	1	2.34	-	0.39	0-40	40 x 40	87
	2	1.57	-	0.40	40-100	45 x 45	99
	3	1.84	-	0.33	100-180	55 x 55	88
Hirahara 1981	1	2.40	0.38	1.07	0-33	1° x 1°	79
	2	1.86	0.43	0.94	33-66	1° x 1°	98
	3	1.60	0.33	0.95	66-100	1° x 1°	101
	4	1.77	0.28	0.92	100-150	1° x 1°	105
	5	1.46	0.45	0.98	150-200	1° x 1°	98
	6	1.27	0.42	1.01	200-300	2° x 2°	27
	7	1.28	0.35	0.76	300-400	2° x 2°	27
	8	1.69	0.26	0.65	400-500	2° x 2°	14
	9	1.48	0.15	0.60	500-600	2° x 2°	8
Horie and Aki 1982	1	3.50	0.56	0.77	0-32	30 x 30	34
	2	2.30	0.49	0.87	32-65	30 x 30	32
	3	1.08	0.37	0.90	65-98	30 x 30	24
	4	0.91	0.15	0.66	98-131	30 x 30	18
	5	0.21	0.02	0.27	131-164	30 x 30	4
Taylor 1983	1	4.08	0.43	-	0-5	10 x 10	18
	2	2.69	0.55	-	5-17	10 x 10	35
	3	2.51	0.66	-	17-32	10 x 10	66
	4	2.06	0.67	-	32-70	10 x 10	67
	5	2.94	0.55	-	70-100	20 x 20	33
Hasemi et al 1984	1	3.19	0.63	0.95	0-32	30 x 30	52
	2	1.54	0.67	0.93	32-65	30 x 30	56
	3	1.23	0.59	0.99	65-98	30 x 30	55
	4	1.66	0.41	0.99	98-131	30 x 30	49
	5	0.69	0.23	0.78	131-164	30 x 30	24
	6	0.18	0.04	0.47	164-197	30 x 30	4

TABLE 5.4

PERIOD 20 sec FOR THIS PERIOD:
initial data variance= 683.8181 sec^2 no of observations= 751 no blocks=209
average path length = 5377.750 km

REGION	NUMBER OF BLOCKS STUDIED	RMS VEL VARIATIONS (%)	AVERAGE RESOLUTION	AVER TOTAL STD DEV (%)	AVER STD DEV DUE TO RANDOM ERROR (%)	AVER STD DEV DUE TO POOR RESOL (%)	% TOTAL ERROR DUE TO POOR RESOL
a	41	3.726	0.912	2.609	2.306	1.163	19.871
b	73	4.742	0.865	3.205	2.671	1.667	27.041
c	22	3.192	0.896	2.890	2.531	1.333	21.277
p	18	4.992	0.901	2.810	2.500	1.248	19.727
q	38	3.685	0.926	2.422	2.224	0.924	14.552
s	17	2.767	0.874	3.108	2.648	1.555	25.049
FOR THE ABOVE RUN: σ_m^2= 9.2%							
θ^2= 25,000 sec^2	residual variance= 213.6641 sec^2			variance improvement= 68.75%			
a	41	3.366	0.855	2.418	2.022	1.278	27.958
b	73	4.082	0.793	2.885	2.243	1.738	36.283
c	22	2.916	0.830	2.662	2.193	1.461	30.106
p	18	4.409	0.836	2.605	2.174	1.399	28.842
q	38	3.467	0.872	2.293	2.005	1.080	22.203
s	17	2.445	0.802	2.822	2.246	1.650	34.165
FOR THE ABOVE RUN: σ_m^2= 6.6%							
θ^2= 50,000 sec^2	residual variance= 218.6743 sec^2			variance improvement= 68.02%			
a	41	3.149	0.812	2.291	1.842	1.320	33.209
b	73	3.672	0.742	2.685	1.989	1.740	42.014
c	22	2.728	0.781	2.511	1.978	1.505	35.921
p	18	4.052	0.787	2.465	1.967	1.451	34.658
q	38	3.295	0.829	2.200	1.854	1.156	27.597
s	17	2.270	0.750	2.639	2.004	1.667	39.871
FOR THE ABOVE RUN: σ_m^2= 5.4%							
θ^2= 75,000 sec^2	residual variance= 223.5098 sec^2			variance improvement= 67.31%			
a	41	2.989	0.777	2.196	1.712	1.338	37.121
b	73	3.381	0.701	2.540	1.813	1.725	46.116
c	22	2.585	0.740	2.397	1.823	1.521	40.262
p	18	3.794	0.747	2.358	1.817	1.471	38.902
q	38	3.153	0.793	2.127	1.739	1.199	31.781
s	17	2.145	0.709	2.506	1.834	1.662	44.019
FOR THE ABOVE RUN: σ_m^2= 4.8%							
θ^2= 100,000 sec^2	residual variance= 228.1161 sec^2			variance improvement= 66.64%			
a	41	2.748	0.720	2.059	1.529	1.348	42.846
b	73	2.982	0.639	2.337	1.576	1.682	51.842
c	22	2.374	0.677	2.232	1.604	1.523	46.572
p	18	3.419	0.683	2.202	1.608	1.477	44.981
q	38	2.926	0.733	2.015	1.568	1.243	38.076
s	17	1.959	0.646	2.315	1.601	1.636	49.928
FOR THE ABOVE RUN: σ_m^2= 4.0%							
θ^2= 150,000 sec^2	residual variance= 236.7157 sec^2			variance improvement= 65.38%			

TABLE 5.5

PERIOD 30 sec FOR THIS PERIOD:
initial data variance= 418.0665 sec^2 no of observations= 1669 no blocks=448
average path length = 6176.123 km

REGION	NUMBER OF BLOCKS STUDIED	RMS VEL VARIATIONS (%)	AVERAGE RESOLUTION	AVER TOTAL STD DEV (%)	AVER STD DEV DUE TO RANDOM ERROR (%)	AVER STD DEV DUE TO POOR RESOL (%)	% TOTAL ERROR DUE TO POOR RESOL
a	54	2.839	0.926	1.982	1.738	0.869	19.251
b	137	3.420	0.864	2.689	2.141	1.505	31.316
c	62	2.977	0.834	2.898	2.162	1.764	37.082
p	51	2.991	0.825	2.927	2.067	1.890	41.663
q	110	3.800	0.860	2.583	1.981	1.494	33.454
s	34	2.223	0.873	2.505	2.007	1.367	29.789
			FOR THE ABOVE RUN:		σ_m^2= 7.9%		
θ^2= 25,000 sec^2			residual variance= 158.0148 sec^2			variance improvement= 62.20%	
a	54	2.497	0.882	1.841	1.549	0.934	25.732
b	137	2.811	0.801	2.386	1.791	1.486	38.803
c	62	2.566	0.771	2.520	1.781	1.667	43.759
p	51	2.327	0.767	2.510	1.717	1.692	45.427
q	110	3.322	0.805	2.274	1.674	1.413	38.623
s	34	1.910	0.816	2.234	1.707	1.333	35.576
			FOR THE ABOVE RUN:		σ_m^2= 5.7%		
θ^2= 50,000 sec^2			residual variance= 161.9616 sec^2			variance improvement= 61.26%	
a	54	2.288	0.846	1.750	1.428	0.916	30.159
b	137	2.469	0.756	2.206	1.592	1.452	43.363
c	62	2.341	0.727	2.306	1.571	1.594	47.797
p	51	2.035	0.726	2.288	1.530	1.587	48.100
q	110	3.057	0.764	2.101	1.503	1.361	41.997
s	34	1.754	0.774	2.077	1.536	1.304	39.416
			FOR THE ABOVE RUN:		σ_m^2= 4.7%		
θ^2= 75,000 sec^2			residual variance= 165.1805 sec^2			variance improvement= 60.49%	
a	54	2.135	0.817	1.681	1.338	0.974	33.571
b	137	2.238	0.720	2.078	1.455	1.419	46.850
c	62	2.186	0.693	2.159	1.429	1.537	50.689
p	51	1.855	0.693	2.140	1.405	1.517	50.245
q	110	2.870	0.732	1.981	1.386	1.323	44.573
s	34	1.648	0.740	1.966	1.417	1.280	42.370
			FOR THE ABOVE RUN:		σ_m^2= 4.1%		
θ^2= 100,000 sec^2			residual variance= 168.0143 sec^2			variance improvement= 59.81%	
a	54	1.916	0.768	1.580	1.208	0.983	38.711
b	137	1.935	0.664	1.901	1.271	1.362	51.330
c	62	1.973	0.640	1.959	1.243	1.450	54.791
p	51	1.628	0.641	1.944	1.235	1.423	53.625
q	110	2.605	0.681	1.818	1.227	1.266	48.479
s	34	1.503	0.687	1.812	1.254	1.240	46.844
			FOR THE ABOVE RUN:		σ_m^2= 3.4%		
θ^2= 150,000 sec^2			residual variance= 172.9529 sec^2			variance improvement= 58.63%	

TABLE 5.6

PERIOD 40 sec FOR THIS PERIOD:
initial data variance= 399.0022 sec^2 no of observations= 1865 no blocks=479
average path length = 6426.467 km

REGION	NUMBER OF BLOCKS STUDIED	RMS VEL VARIATIONS (%)	AVERAGE RESOLUTION	AVER TOTAL STD DEV (%)	AVER STD DEV DUE TO RANDOM ERROR (%)	AVER STD DEV DUE TO POOR RESOL (%)	% TOTAL ERROR DUE TO POOR RESOL
a	56	2.569	0.883	1.978	1.655	1.011	26.160
b	151	2.780	0.793	2.618	1.906	1.681	41.225
c	65	3.024	0.792	2.581	1.846	1.665	41.610
p	53	2.407	0.794	2.563	1.821	1.660	41.925
q	121	2.823	0.798	2.478	1.778	1.571	40.190
s	33	2.406	0.835	2.296	1.794	1.316	32.881
FOR THE ABOVE RUN: σ_m^2= 6.2%							
θ^2= 50,000 sec^2 residual variance= 190.5725 sec^2 variance improvement= 52.24%							
a	56	2.174	0.820	1.798	1.428	1.044	33.692
b	151	2.283	0.715	2.256	1.543	1.567	48.249
c	65	2.403	0.719	2.221	1.505	1.539	48.028
p	53	1.835	0.722	2.206	1.506	1.511	46.926
q	121	2.336	0.728	2.140	1.467	1.445	45.572
s	33	2.046	0.763	2.035	1.509	1.278	39.470
FOR THE ABOVE RUN: σ_m^2= 4.4%							
θ^2= 100,000 sec^2 residual variance= 196.6412 sec^2 variance improvement= 50.72%							
a	56	1.946	0.772	1.685	1.287	1.048	38.666
b	151	2.013	0.662	2.051	1.346	1.486	52.473
c	65	2.068	0.668	2.020	1.318	1.457	52.031
p	53	1.559	0.671	2.011	1.332	1.428	50.458
q	121	2.095	0.679	1.954	1.296	1.370	49.173
s	33	1.836	0.711	1.882	1.343	1.248	44.000
FOR THE ABOVE RUN: σ_m^2= 3.7%							
θ^2= 150,000 sec^2 residual variance= 201.3351 sec^2 variance improvement= 49.54%							
a	56	1.790	0.734	1.602	1.186	1.043	42.401
b	151	1.828	0.621	1.911	1.214	1.424	55.514
c	65	1.848	0.629	1.883	1.193	1.396	54.948
p	53	1.386	0.630	1.878	1.212	1.371	53.237
q	121	1.935	0.641	1.827	1.179	1.317	51.941
s	33	1.684	0.670	1.773	1.227	1.222	47.479
FOR THE ABOVE RUN: σ_m^2= 3.2%							
θ^2= 200,000 sec^2 residual variance= 205.3084 sec^2 variance improvement= 48.55%							
a	56	1.579	0.674	1.481	1.043	1.025	47.871
b	151	1.580	0.560	1.722	1.040	1.332	59.851
c	65	1.569	0.570	1.698	1.026	1.306	59.145
p	53	1.169	0.569	1.700	1.049	1.289	57.496
q	121	1.722	0.582	1.656	1.022	1.240	56.124
s	33	1.467	0.607	1.622	1.066	1.177	52.672
FOR THE ABOVE RUN: σ_m^2= 2.6%							
θ^2= 300,000 sec^2 residual variance= 211.9552 sec^2 variance improvement= 46.88%							

TABLE 5.7

PERIOD 50 sec — FOR THIS PERIOD:
initial data variance= 419.6517 sec^2 no of observations= 1867 no blocks=482
average path length = 6540.800 km

REGION	NUMBER OF BLOCKS STUDIED	RMS VEL VARIATIONS (%)	AVERAGE RESOLUTION	AVER TOTAL STD DEV (%)	AVER STD DEV DUE TO RANDOM ERROR (%)	AVER STD DEV DUE TO POOR RESOL (%)	% TOTAL ERROR DUE TO POOR RESOL
a	56	2.761	0.883	2.065	1.725	1.058	26.268
b	151	2.713	0.792	2.745	1.991	1.772	41.673
c	65	3.116	0.792	2.700	1.928	1.746	41.856
p	54	2.717	0.787	2.716	1.916	1.774	42.659
q	122	2.734	0.793	2.613	1.853	1.671	40.917
s	34	3.055	0.826	2.467	1.916	1.435	33.809
FOR THE ABOVE RUN: σ_m= 6.4%							
θ^2= 50,000 sec^2	residual variance= 208.3203 sec^2			variance improvement= 50.36%			
a	56	2.295	0.820	1.876	1.488	1.089	33.688
b	151	2.223	0.714	2.361	1.608	1.645	48.588
c	65	2.495	0.719	2.320	1.571	1.610	48.173
p	54	2.228	0.714	2.330	1.576	1.608	47.632
q	122	2.266	0.724	2.250	1.526	1.527	46.098
s	34	2.454	0.751	2.178	1.600	1.388	40.588
FOR THE ABOVE RUN: σ_m= 4.6%							
θ^2= 100,000 sec^2	residual variance= 214.7183 sec^2			variance improvement= 48.83%			
a	56	2.037	0.773	1.757	1.342	1.092	38.623
b	151	1.962	0.661	2.145	1.402	1.558	52.744
c	65	2.157	0.669	2.110	1.376	1.523	52.122
p	54	1.961	0.663	2.120	1.390	1.516	51.104
q	122	2.023	0.675	2.051	1.347	1.445	49.624
s	34	2.145	0.698	2.009	1.417	1.351	45.191
FOR THE ABOVE RUN: σ_m= 3.8%							
θ^2= 150,000 sec^2	residual variance= 219.7206 sec^2			variance improvement= 47.64%			
a	56	1.861	0.735	1.670	1.237	1.086	42.339
b	151	1.786	0.621	1.997	1.264	1.491	55.739
c	65	1.932	0.630	1.966	1.245	1.458	55.010
p	54	1.779	0.623	1.978	1.262	1.451	53.833
q	122	1.860	0.637	1.916	1.225	1.387	52.356
s	34	1.938	0.656	1.890	1.290	1.319	48.695
FOR THE ABOVE RUN: σ_m= 3.3%							
θ^2= 200,000 sec^2	residual variance= 223.9850 sec^2			variance improvement= 46.63%			
a	56	1.626	0.675	1.544	1.088	1.057	47.788
b	151	1.549	0.560	1.798	1.042	1.393	60.019
c	65	1.635	0.570	1.773	1.071	1.364	59.177
p	54	1.532	0.562	1.787	1.090	1.361	58.020
q	122	1.643	0.579	1.735	1.061	1.304	56.501
s	34	1.661	0.592	1.723	1.115	1.265	53.881
FOR THE ABOVE RUN: σ_m= 2.8%							
θ^2= 300,000 sec^2	residual variance= 231.1445 sec^2			variance improvement= 44.92%			

TABLE 5.8

PERIOD 60 sec — FOR THIS PERIOD:
initial data variance= 421.5191 sec^2 no of observations= 1779 no blocks=456
average path length = 6662.692 km

REGION	NUMBER OF BLOCKS STUDIED	RMS VEL VARIATIONS (%)	AVERAGE RESOLUTION	AVER TOTAL STD DEV (%)	AVER STD DEV DUE TO RANDOM ERROR (%)	AVER STD DEV DUE TO POOR RESOL (%)	% TOTAL ERROR DUE TO POOR RESOL
a	55	2.066	0.770	1.819	1.380	1.142	39.380
b	147	2.139	0.672	2.180	1.458	1.563	51.443
c	60	1.890	0.709	2.058	1.438	1.425	47.971
p	50	1.684	0.710	2.053	1.486	1.372	44.634
q	111	1.970	0.724	1.977	1.434	1.304	43.528
s	33	2.007	0.730	1.982	1.498	1.261	40.459
θ^2= 150,000 sec^2		FOR THE ABOVE RUN: σ_m^2= 3.9% residual variance= 231.6534 sec^2			variance improvement= 45.04%		
a	55	1.877	0.732	1.726	1.269	1.133	43.076
b	147	1.926	0.630	2.033	1.315	1.502	54.629
c	60	1.713	0.668	1.929	1.305	1.381	51.225
p	50	1.501	0.666	1.934	1.353	1.343	48.242
q	111	1.814	0.683	1.864	1.309	1.278	46.991
s	33	1.827	0.686	1.877	1.365	1.255	44.699
θ^2= 200,000 sec^2		FOR THE ABOVE RUN: σ_m^2= 3.4% residual variance= 235.9013 sec^2			variance improvement= 44.03%		
a	55	1.735	0.700	1.653	1.184	1.121	46.021
b	147	1.768	0.596	1.922	1.209	1.452	57.115
c	60	1.581	0.635	1.831	1.206	1.342	53.767
p	50	1.371	0.630	1.841	1.252	1.317	51.130
q	111	1.697	0.649	1.776	1.213	1.253	49.753
s	33	1.698	0.649	1.794	1.264	1.243	48.034
θ^2= 250,000 sec^2		FOR THE ABOVE RUN: σ_m^2= 3.1% residual variance= 239.6021 sec^2			variance improvement= 43.16%		
a	55	1.623	0.672	1.592	1.114	1.108	48.463
b	147	1.645	0.568	1.832	1.126	1.409	59.154
c	60	1.477	0.607	1.751	1.128	1.309	55.854
p	50	1.271	0.600	1.765	1.171	1.292	53.538
q	111	1.604	0.620	1.705	1.137	1.230	52.052
s	33	1.600	0.618	1.725	1.182	1.229	50.775
θ^2= 300,000 sec^2		FOR THE ABOVE RUN: σ_m^2= 2.8% residual variance= 242.8998 sec^2			variance improvement= 42.37%		
a	55	1.533	0.648	1.541	1.056	1.095	50.545
b	147	1.544	0.543	1.759	1.058	1.372	60.880
c	60	1.392	0.582	1.685	1.063	1.279	57.626
p	50	1.192	0.573	1.702	1.103	1.269	55.598
q	111	1.528	0.595	1.645	1.073	1.209	54.022
s	33	1.520	0.591	1.666	1.113	1.214	53.093
θ^2= 350,000 sec^2		FOR THE ABOVE RUN: σ_m^2= 2.6% residual variance= 245.8863 sec^2			variance improvement= 41.67%		

TABLE 5.9

PERIOD 70 sec — FOR THIS PERIOD:
initial data variance= 448.7001 sec^2 no of observations= 1650 no blocks=445
average path length = 6756.104 km

REGION	NUMBER OF BLOCKS STUDIED	RMS VEL VARIATIONS (%)	AVERAGE RESOLUTION	AVER TOTAL STD DEV (%)	AVER STD DEV DUE TO RANDOM ERROR (%)	AVER STD DEV DUE TO POOR RESOL (%)	% TOTAL ERROR DUE TO POOR RESOL
a	55	1.971	0.717	1.752	1.268	1.171	44.692
b	141	1.912	0.619	2.039	1.300	1.524	55.849
c	59	1.676	0.662	1.929	1.302	1.389	51.881
p	49	1.615	0.653	1.952	1.342	1.380	49.979
q	108	1.839	0.677	1.864	1.300	1.290	47.885
s	33	1.880	0.672	1.897	1.353	1.297	46.750
FOR THE ABOVE RUN: σ_m^2= 3.4%							
θ^2= 200,000 sec^2	residual variance= 229.8752 sec^2			variance improvement= 48.77%			
a	55	1.827	0.684	1.676	1.180	1.157	47.630
b	141	1.747	0.585	1.927	1.195	1.471	58.261
c	59	1.534	0.628	1.831	1.203	1.351	54.460
p	49	1.496	0.616	1.857	1.241	1.350	52.803
q	108	1.716	0.642	1.777	1.205	1.264	50.635
s	33	1.775	0.635	1.810	1.251	1.280	49.959
FOR THE ABOVE RUN: σ_m^2= 3.0%							
θ^2= 250,000 sec^2	residual variance= 233.9635 sec^2			variance improvement= 47.86%			
a	55	1.712	0.656	1.614	1.110	1.142	50.058
b	141	1.618	0.557	1.837	1.113	1.426	60.246
c	59	1.424	0.599	1.753	1.124	1.318	56.569
p	49	1.401	0.586	1.780	1.159	1.322	55.156
q	108	1.618	0.613	1.706	1.130	1.241	52.920
s	33	1.690	0.604	1.739	1.169	1.262	52.598
FOR THE ABOVE RUN: σ_m^2= 2.8%							
θ^2= 300,000 sec^2	residual variance= 237.6208 sec^2			variance improvement= 47.04%			
a	55	1.617	0.632	1.561	1.051	1.137	52.122
b	141	1.514	0.532	1.764	1.046	1.388	61.931
c	59	1.336	0.574	1.687	1.059	1.289	58.352
p	49	1.323	0.559	1.715	1.092	1.297	57.169
q	108	1.537	0.588	1.646	1.067	1.219	54.874
s	33	1.620	0.577	1.679	1.101	1.243	54.833
FOR THE ABOVE RUN: σ_m^2= 2.6%							
θ^2= 350,000 sec^2	residual variance= 240.9366 sec^2			variance improvement= 46.30%			
a	55	1.537	0.610	1.515	1.001	1.112	53.914
b	141	1.427	0.511	1.701	0.989	1.354	63.392
c	59	1.263	0.552	1.631	1.005	1.262	59.897
p	49	1.258	0.536	1.659	1.034	1.274	58.924
q	108	1.468	0.566	1.594	1.013	1.199	56.579
s	33	1.559	0.554	1.627	1.044	1.226	56.766
FOR THE ABOVE RUN: σ_m^2= 2.5%							
θ^2= 400,000 sec^2	residual variance= 243.9740 sec^2			variance improvement= 45.63%			

TABLE 5.10

PERIOD 80 sec — FOR THIS PERIOD:
initial data variance= 493.0962 sec^2 no of observations= 1533 no blocks=442
average path length = 6884.480 km

REGION	NUMBER OF BLOCKS STUDIED	RMS VEL VARIATIONS (%)	AVERAGE RESOLUTION	AVER TOTAL STD DEV (%)	AVER STD DEV DUE TO RANDOM ERROR (%)	AVER STD DEV DUE TO POOR RESOL (%)	% TOTAL ERROR DUE TO POOR RESOL
a	54	2.080	0.706	1.874	1.340	1.273	46.145
b	140	1.879	0.607	2.171	1.364	1.642	57.232
c	59	1.594	0.652	2.049	1.371	1.489	52.804
p	49	1.646	0.640	2.080	1.409	1.493	51.494
q	107	1.900	0.664	1.990	1.371	1.397	49.283
s	33	1.831	0.654	2.040	1.419	1.432	49.267
θ^2= 200,000 sec^2			FOR THE ABOVE RUN: σ_m^2= 3.5% residual variance= 251.1567 sec^2 variance improvement= 49.06%				
a	54	1.936	0.672	1.790	1.244	1.254	49.104
b	140	1.721	0.573	2.048	1.252	1.581	59.588
c	59	1.479	0.618	1.943	1.265	1.446	55.379
p	49	1.532	0.604	1.975	1.300	1.455	54.278
q	107	1.768	0.630	1.894	1.268	1.366	52.021
s	33	1.720	0.617	1.941	1.308	1.405	52.362
θ^2= 250,000 sec^2			FOR THE ABOVE RUN: σ_m^2= 3.2% residual variance= 255.5379 sec^2 variance improvement= 48.18%				
a	54	1.819	0.644	1.721	1.168	1.235	51.534
b	140	1.599	0.544	1.951	1.165	1.530	61.525
c	59	1.389	0.589	1.858	1.180	1.409	57.483
p	49	1.441	0.573	1.891	1.212	1.422	56.591
q	107	1.664	0.600	1.816	1.187	1.338	54.290
s	33	1.628	0.586	1.861	1.220	1.379	54.895
θ^2= 300,000 sec^2			FOR THE ABOVE RUN: σ_m^2= 2.9% residual variance= 259.4882 sec^2 variance improvement= 47.37%				
a	54	1.720	0.619	1.663	1.104	1.217	53.591
b	140	1.500	0.520	1.871	1.093	1.487	63.170
c	59	1.316	0.563	1.787	1.112	1.376	59.262
p	49	1.366	0.546	1.820	1.140	1.393	58.565
q	107	1.579	0.575	1.751	1.119	1.313	56.225
s	33	1.550	0.559	1.794	1.147	1.355	57.034
θ^2= 350,000 sec^2			FOR THE ABOVE RUN: σ_m^2= 2.7% residual variance= 263.0964 sec^2 variance improvement= 46.64%				
a	54	1.634	0.597	1.612	1.050	1.200	55.369
b	140	1.419	0.498	1.803	1.034	1.449	64.596
c	59	1.254	0.541	1.727	1.054	1.347	60.801
p	49	1.303	0.523	1.759	1.079	1.366	60.283
q	107	1.507	0.552	1.694	1.062	1.289	57.910
s	33	1.483	0.535	1.736	1.085	1.332	58.879
θ^2= 400,000 sec^2			FOR THE ABOVE RUN: σ_m^2= 2.6% residual variance= 266.4241 sec^2 variance improvement= 45.97%				

TABLE 5.11

PERIOD 90 sec FOR THIS PERIOD:
initial data variance= 551.8558 sec^2 no of observations= 1276 no blocks=424
average path length = 7220.475 km

REGION	NUMBER OF BLOCKS STUDIED	RMS VEL VARIATIONS (%)	AVERAGE RESOLUTION	AVER TOTAL STD DEV (%)	AVER STD DEV DUE TO RANDOM ERROR (%)	AVER STD DEV DUE TO POOR RESOL (%)	% TOTAL ERROR DUE TO POOR RESOL
a	53	2.002	0.653	1.784	1.216	1.278	51.305
b	131	1.579	0.560	2.015	1.219	1.570	60.747
c	58	1.471	0.590	1.948	1.224	1.490	58.480
p	46	1.795	0.570	1.997	1.258	1.525	58.296
q	103	1.663	0.603	1.904	1.242	1.408	54.716
s	33	1.618	0.552	2.039	1.266	1.574	59.609
FOR THE ABOVE RUN: σ_m^2= 3.1%							
θ^2= 250,000 sec^2	residual variance= 238.4564 sec^2			variance improvement= 56.79%			
a	53	1.880	0.624	1.716	1.140	1.258	53.730
b	131	1.466	0.531	1.921	1.134	1.521	62.689
c	58	1.393	0.561	1.862	1.142	1.448	60.447
p	46	1.682	0.539	1.909	1.171	1.485	60.483
q	103	1.560	0.573	1.825	1.160	1.378	56.961
s	33	1.494	0.521	1.947	1.173	1.532	61.900
FOR THE ABOVE RUN: σ_m^2= 2.8%							
θ^2= 300,000 sec^2	residual variance= 243.2100 sec^2			variance improvement= 55.93%			
a	53	1.780	0.599	1.659	1.077	1.239	55.769
b	131	1.376	0.506	1.844	1.064	1.479	64.332
c	58	1.330	0.536	1.791	1.075	1.411	62.107
p	46	1.590	0.513	1.836	1.099	1.449	62.334
q	103	1.477	0.547	1.760	1.093	1.350	58.867
s	33	1.394	0.495	1.870	1.098	1.494	63.810
FOR THE ABOVE RUN: σ_m^2= 2.6%							
θ^2= 350,000 sec^2	residual variance= 247.4798 sec^2			variance improvement= 55.15%			
a	53	1.695	0.577	1.609	1.024	1.220	57.523
b	131	1.302	0.484	1.779	1.006	1.442	65.754
c	58	1.276	0.514	1.730	1.018	1.379	63.544
p	46	1.515	0.490	1.773	1.039	1.418	63.935
q	103	1.409	0.524	1.703	1.036	1.325	60.522
s	33	1.310	0.472	1.805	1.035	1.460	65.441
FOR THE ABOVE RUN: σ_m^2= 2.5%							
θ^2= 400,000 sec^2	residual variance= 251.3674 sec^2			variance improvement= 54.45%			
a	53	1.557	0.539	1.525	0.937	1.186	60.422
b	131	1.185	0.448	1.672	0.913	1.380	68.119
c	58	1.189	0.477	1.630	0.927	1.324	65.941
p	46	1.395	0.452	1.670	0.942	1.363	66.595
q	103	1.300	0.486	1.609	0.944	1.280	63.285
s	33	1.180	0.434	1.697	0.934	1.400	68.113
FOR THE ABOVE RUN: σ_m^2= 2.3%							
θ^2= 500,000 sec^2	residual variance= 258.2618 sec^2			variance improvement= 53.20%			

TABLE 5.12

PERIOD 98 sec FOR THIS PERIOD:
initial data variance= 536.8802 sec^2 no of observations= 954 no blocks=391
average path length = 7734.103 km

REGION	NUMBER OF BLOCKS STUDIED	RMS VEL VARIATIONS (%)	AVERAGE RESOLUTION	AVER TOTAL STD DEV (%)	AVER STD DEV DUE TO RANDOM ERROR (%)	AVER STD DEV DUE TO POOR RESOL (%)	% TOTAL ERROR DUE TO POOR RESOL
a	52	1.571	0.584	1.711	1.088	1.302	57.925
b	115	1.312	0.507	1.865	1.076	1.501	64.758
c	55	1.173	0.529	1.823	1.073	1.453	63.556
p	41	1.606	0.498	1.886	1.095	1.517	64.739
q	97	1.617	0.529	1.816	1.103	1.418	60.934
s	31	1.420	0.446	1.982	1.077	1.647	69.059
FOR THE ABOVE RUN: σ_m^2= 2.7%							
θ^2= 300,000 sec^2	residual variance= 216.0930 sec^2			variance improvement= 59.75%			
a	52	1.483	0.558	1.653	1.026	1.280	59.887
b	115	1.231	0.482	1.793	1.011	1.460	66.355
c	55	1.115	0.504	1.754	1.011	1.415	65.089
p	41	1.523	0.472	1.813	1.028	1.477	66.388
q	97	1.535	0.503	1.751	1.038	1.387	62.755
s	31	1.323	0.421	1.899	1.006	1.596	70.641
FOR THE ABOVE RUN: σ_m^2= 2.5%							
θ^2= 350,000 sec^2	residual variance= 221.2085 sec^2			variance improvement= 58.80%			
a	52	1.410	0.535	1.604	0.974	1.258	61.564
b	115	1.164	0.460	1.732	0.957	1.425	67.736
c	55	1.066	0.483	1.696	0.959	1.382	66.422
p	41	1.453	0.450	1.751	0.972	1.442	67.822
q	97	1.466	0.480	1.695	0.984	1.359	64.334
s	31	1.244	0.400	1.830	0.946	1.552	71.993
FOR THE ABOVE RUN: σ_m^2= 2.4%							
θ^2= 400,000 sec^2	residual variance= 225.8989 sec^2			variance improvement= 57.92%			
a	52	1.349	0.515	1.560	0.930	1.239	63.025
b	115	1.107	0.441	1.679	0.910	1.394	68.952
c	55	1.024	0.463	1.645	0.914	1.353	67.600
p	41	1.393	0.430	1.698	0.924	1.411	69.087
q	97	1.405	0.460	1.646	0.936	1.334	65.724
s	31	1.177	0.381	1.769	0.895	1.514	73.170
FOR THE ABOVE RUN: σ_m^2= 2.3%							
θ^2= 450,000 sec^2	residual variance= 230.2374 sec^2			variance improvement= 57.11%			
a	52	1.296	0.498	1.522	0.891	1.220	64.316
b	115	1.057	0.423	1.632	0.869	1.366	70.035
c	55	0.987	0.446	1.601	0.875	1.326	68.654
p	41	1.341	0.412	1.651	0.881	1.383	70.218
q	97	1.351	0.442	1.603	0.895	1.312	66.963
s	31	1.119	0.365	1.717	0.852	1.479	74.211
FOR THE ABOVE RUN: σ_m^2= 2.2%							
θ^2= 500,000 sec^2	residual variance= 234.2789 sec^2			variance improvement= 56.36%			

TABLE 5 13a
STANDARD DEVIATION OF THE TRAVEL TIME RESIDUAL DATA (sec)

PERIOD (sec)	Yomogida (1985)	this work
20	----	23.15
30	18.7	20.45
40	17.0	19.97
50	----	20.48
60	16.5	20.53
70	----	21.18
80	14.9	22.20
90	----	23.49
98	----	23 17

TABLE 5 13b
RESIDUAL STANDARD DEVIATION AFTER INVERSION (sec)

PERIOD (sec)	Forsyth (1975)	Patton (1978)
26	6.5	15.8
34	5 5	11.9
40	4.8	9.7
66	5.1	8.0
90	6.2	8.3

PERIOD (sec)	Patton (1984)	Yomogida (1985)	this work
20		----	14.79 (68.02%)
30		13.8 (45.5%)	12.85 (60.49%)
40		12.3 (47.6%)	14.02 (50.72%)
50	4-6 (40%)	----	14.82 (47.64%)
60		13.1 (36 5%)	15.36 (44.03%)
70		----	15.29 (47.86%)
80		12 9 (24.8%)	16.11 (47.37%)
90		----	15.73 (55.15%)
98		----	14.87 (58.80%)

in this last table we also show the variance improvement for each case

Chapter 5 - Figure Captions

Notice: We have specified here the range covered by the spectrum in each color picture in order to make it more clear.

Figures 5.1a and 5.1b - Discretized representation of the regionalized Earth model of Jordan (1981) used for waves with period less than of equal 50 sec, and greater than 50 sec, respectively. Symbols representing the region-types are the same ones used in Chapter 3.

Figures 5.2a thru 5.10a - Resulting phase velocity global maps for the reference periods from 20 thru 98 sec, respectively.

Figures 5.2b thru 5.10b - Velocity perturbation maps for the reference periods from 20 thru 98 sec, respectively.

Period 20 sec: from -14 to +14%

30 sec: from -13 to +13%

40 sec: from -8 to +8%

50 sec: from -6 to +6%

60 sec: from -5 to +5%

70 sec: from -4 to +4%

80 sec: from -5 to +5%

90 sec: from -4 to +4%

98 sec: from -4 to +4%

Figures 5.2c thru 5.10c - Data density maps (number of hits in each block) for the reference periods from 20 thru 98 sec, respectively.

Period 20 sec: from 0 to 68

30 sec: from 0 to 124

40 sec: from 0 to 140

50 sec: from 0 to 143

60 sec: from 0 to 141

70 sec: from 0 to 136

80 sec: from 0 to 133

90 sec: from 0 to 123

98 sec: from 0 to 108

Figures 5.2d thru 5.10d - Maps showing the diagonal elements of the resolution matrix for the reference periods from 20 thru 98 sec, respectively.

Values range from zero to one in all cases.

Figures 5.2e thru 5.10e - Maps showing the total standard deviation of the results, for the reference periods from 20 thru 98 sec, respectively.

Period 20 sec: from 0 to 5.5%

30 sec: from 0 to 4.3%

40 sec: from 0 to 4.1%

50 sec: from 0 to 3.7%

60 sec: from 0 to 3.0%

70 sec: from 0 to 2.7%

80 sec: from 0 to 2.5%

90 sec: from 0 to 2.5%

98 sec: from 0 to 2.3%

Figures 5.2f thru 5.10f - Maps showing the standard deviation of the results due to random noise in the data, for the reference periods from 20 thru 98 sec, respectively.

Period 20 sec: from 0 to 3.1%

30 sec: from 0 to 2.2%

40 sec: from 0 to 2.1%

50 sec: from 0 to 1.8%

60 sec: from 0 to 1.7%

70 sec: from 0 to 1.5%

80 sec: from 0 to 1.3%

90 sec: from 0 to 1.3%

98 sec: from 0 to 1.3%

Figures 5.11a and 5.11b - Phase velocity distribution, together with total velocity perturbation, obtained for the Pacific Ocean at periods 40 and 80 sec by Yomogida (1985). These figures were reproduced from his work.

Figure 5.12 - Global distribution of Rayleigh wave phase velocity heterogeneity results corresponding to the reference period of 100 sec. Contour interval is 0.5% in the map. The horizontal line pattern represent areas where the perturbation is positive, while the other represents the negative results. Reproduced from Tanimoto and Anderson (1985).

Figure 5.13 - Slowness anomaly distributions ($\times 10^3$ sec/km) for Love wave phase velocity in the Pacific, for the following reference periods: 40, 67, 91, and 125 sec (indices a thru d) obtained by Nishimura and Forsyth (1985). Contour interval is 0.001 sec/km, assuming an average velocity of 4.5 km/sec.

Figure 5.14 - Comparison between observed focal phase radiation patterns with the results of the linear inversion and logarithmic fitting for one event studied by Patton (1978). This figure was reproduced from Patton (1980a).

FIGURE 5.1a

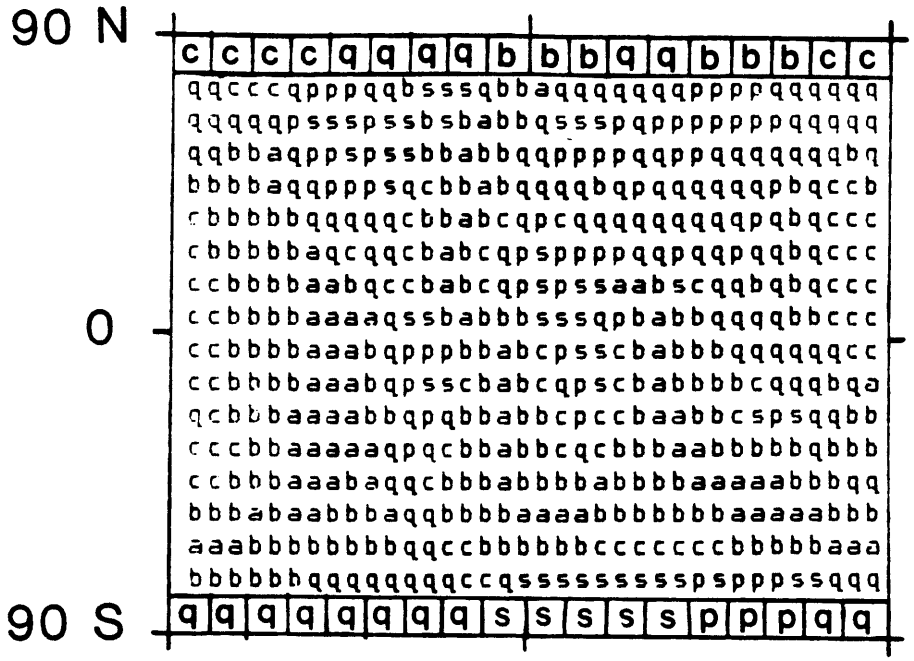

FIGURE 5.1b

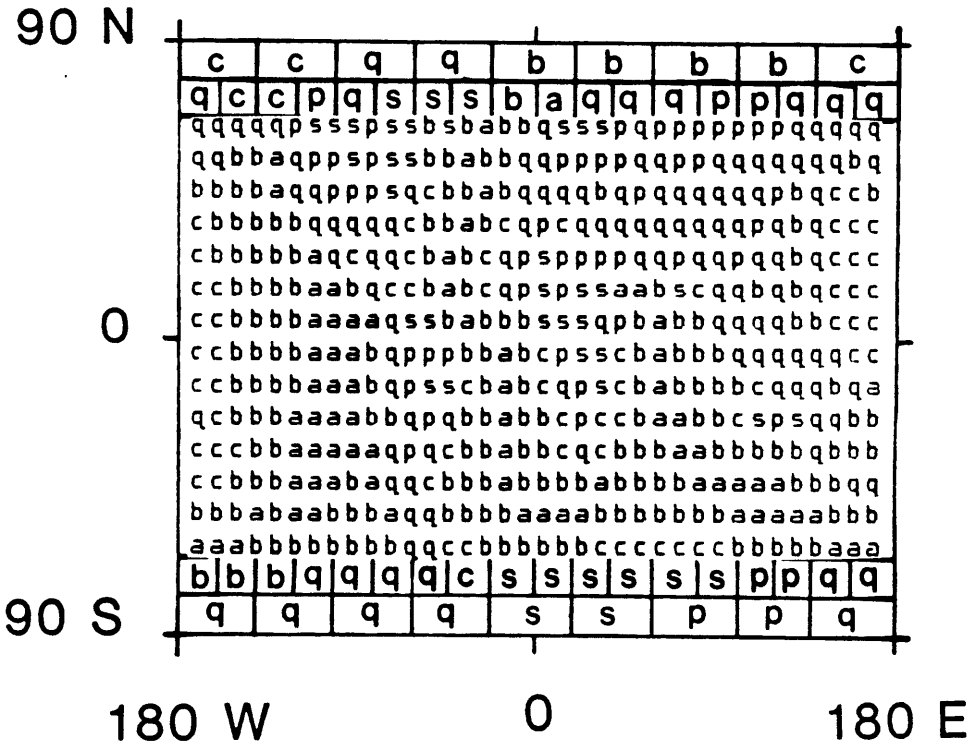

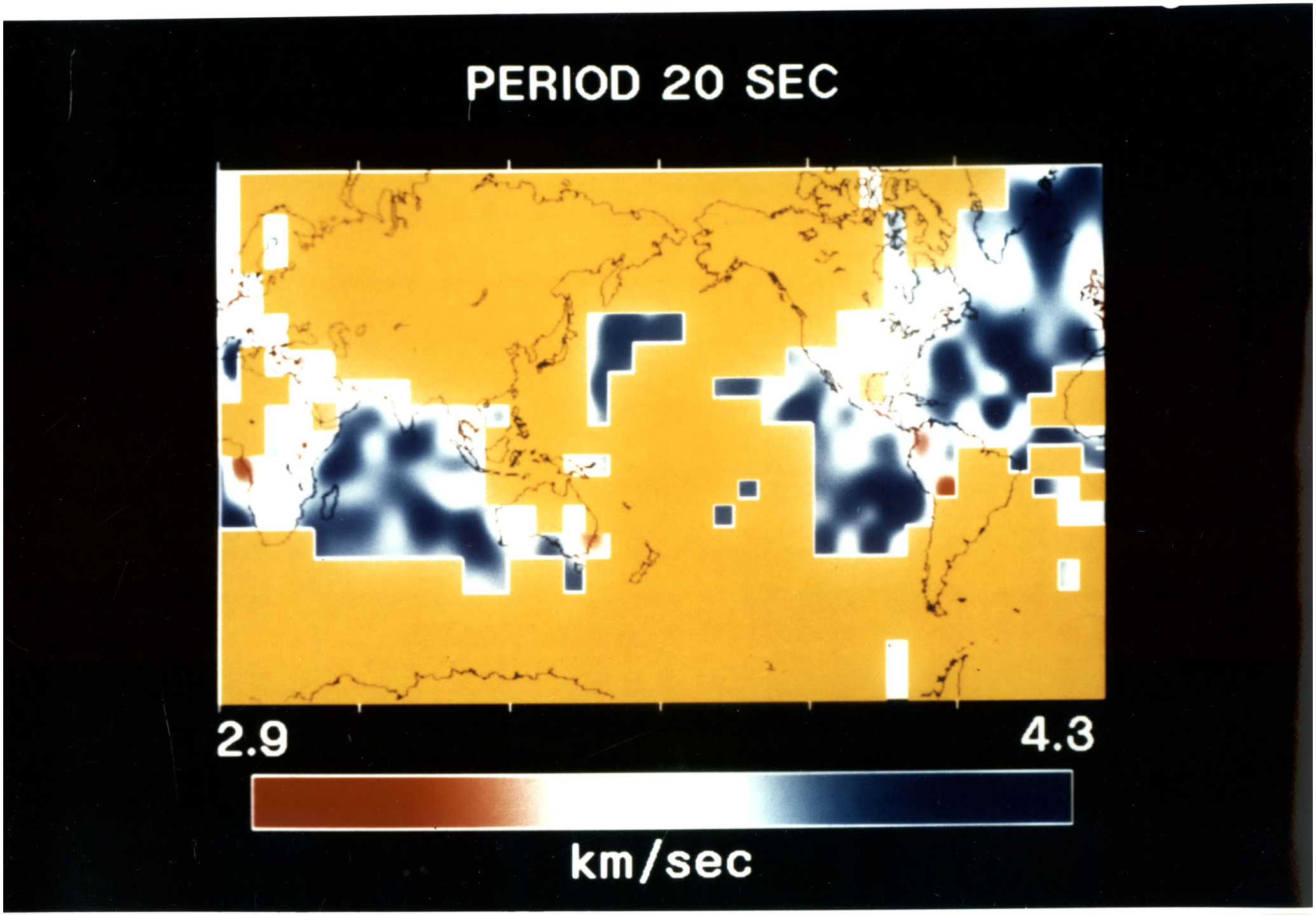

FIGURE 5.2a

FIGURE 5.2b

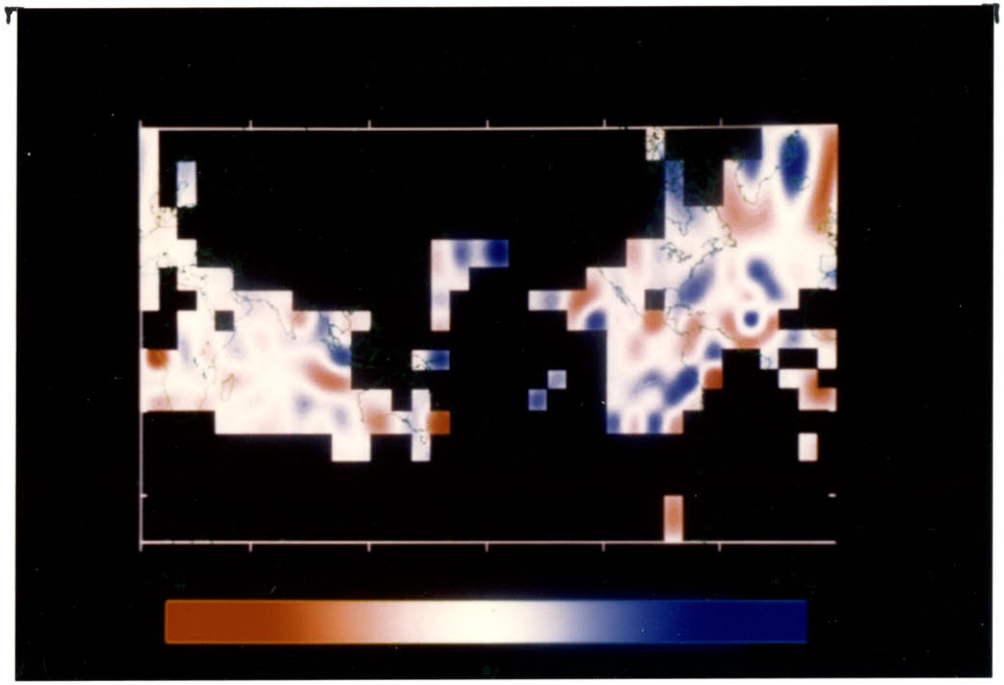

FIGURE 5.2c

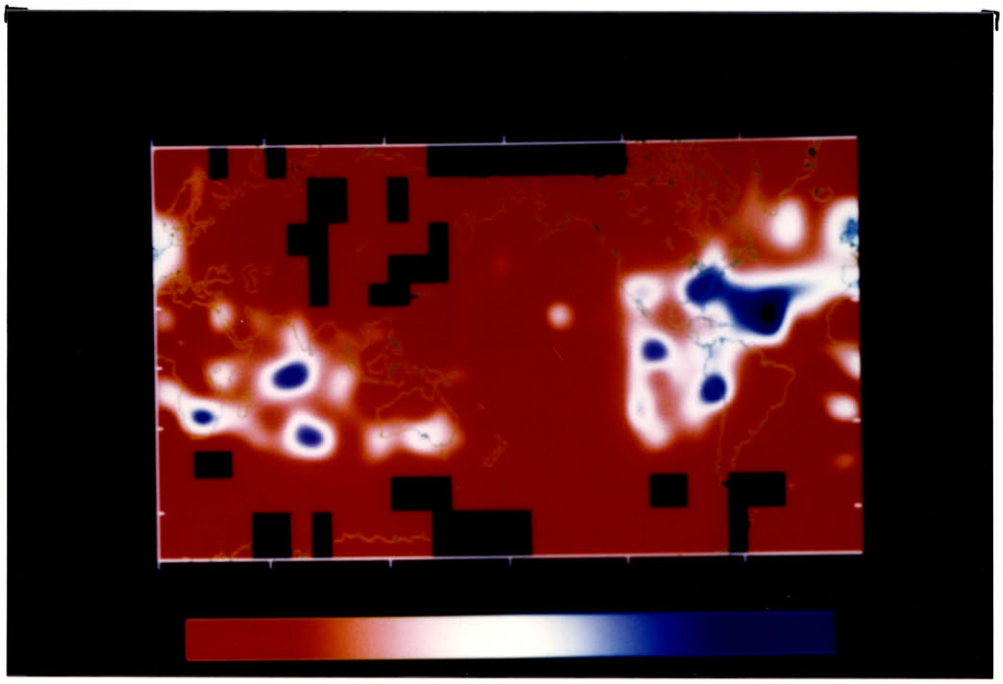

FIGURE 5.2d

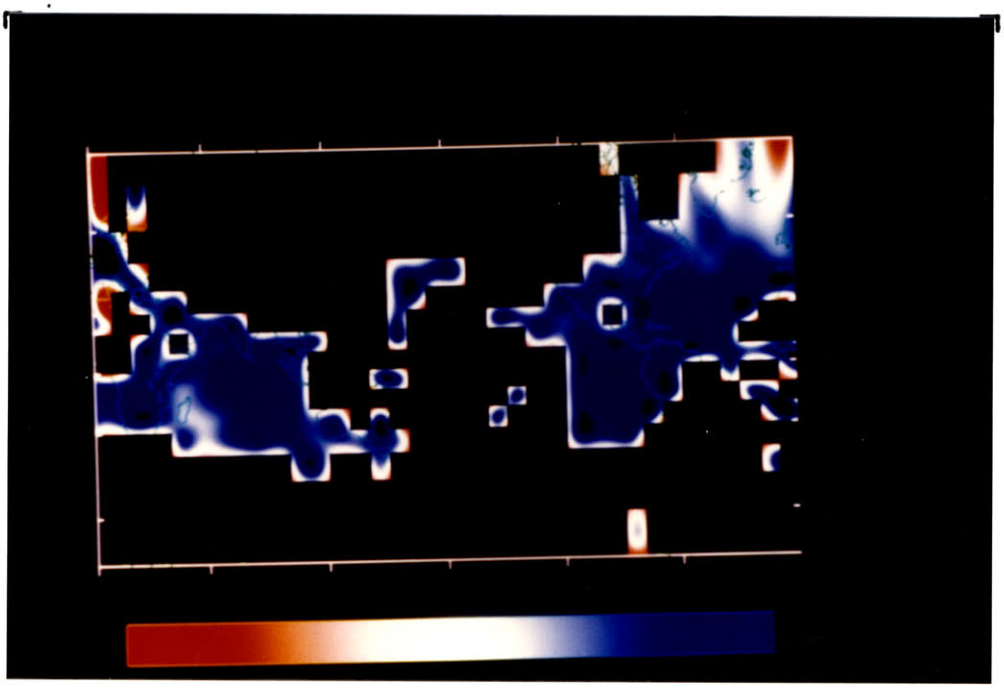

FIGURE 5.2e

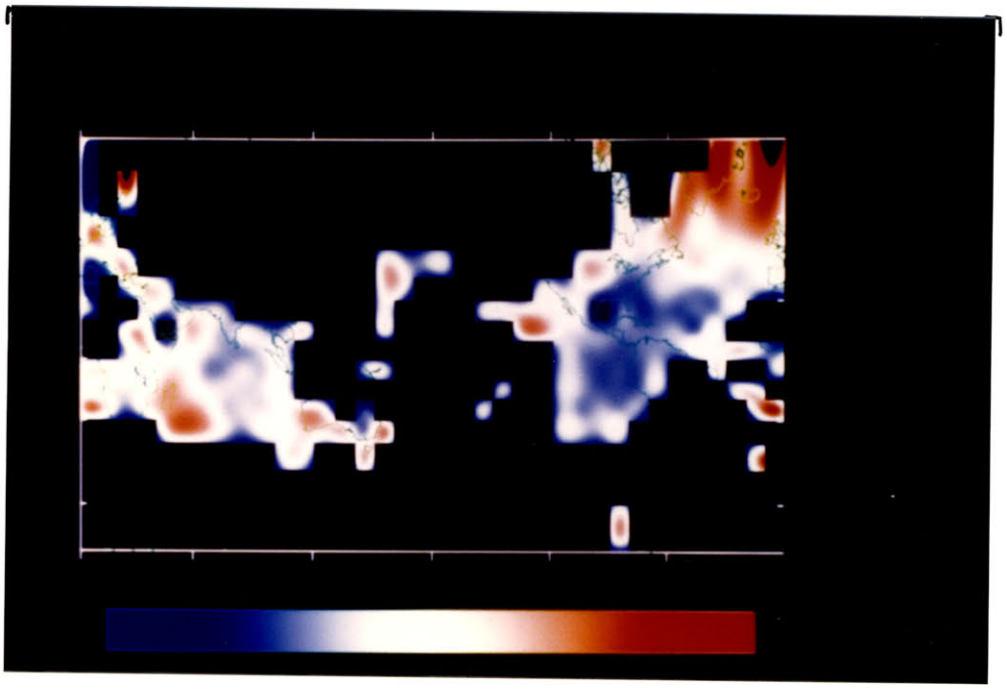

FIGURE 5.2f

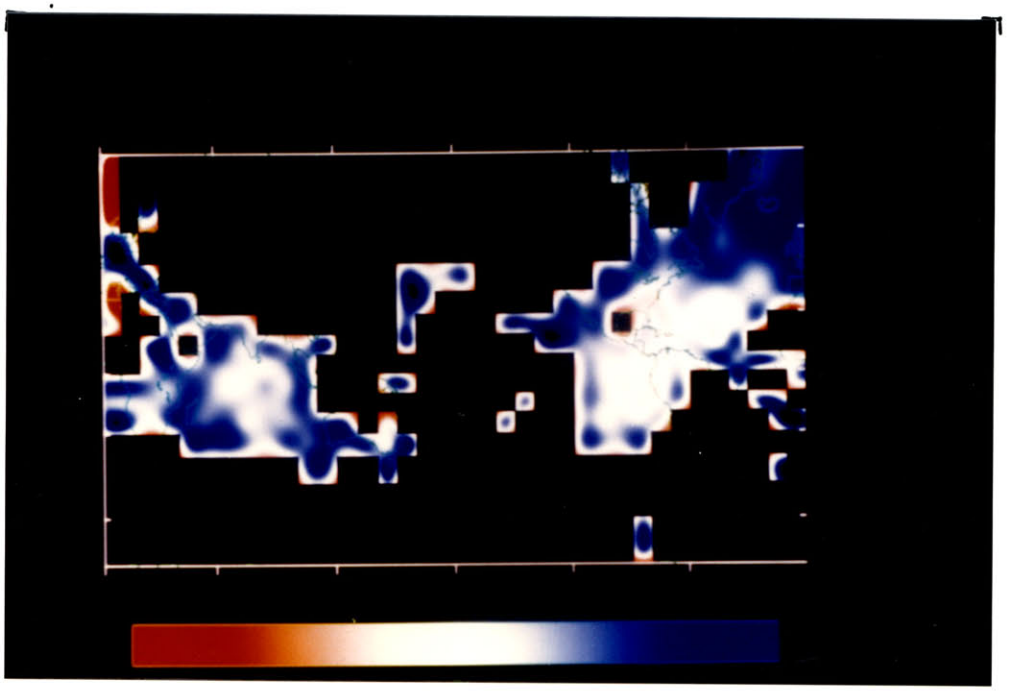

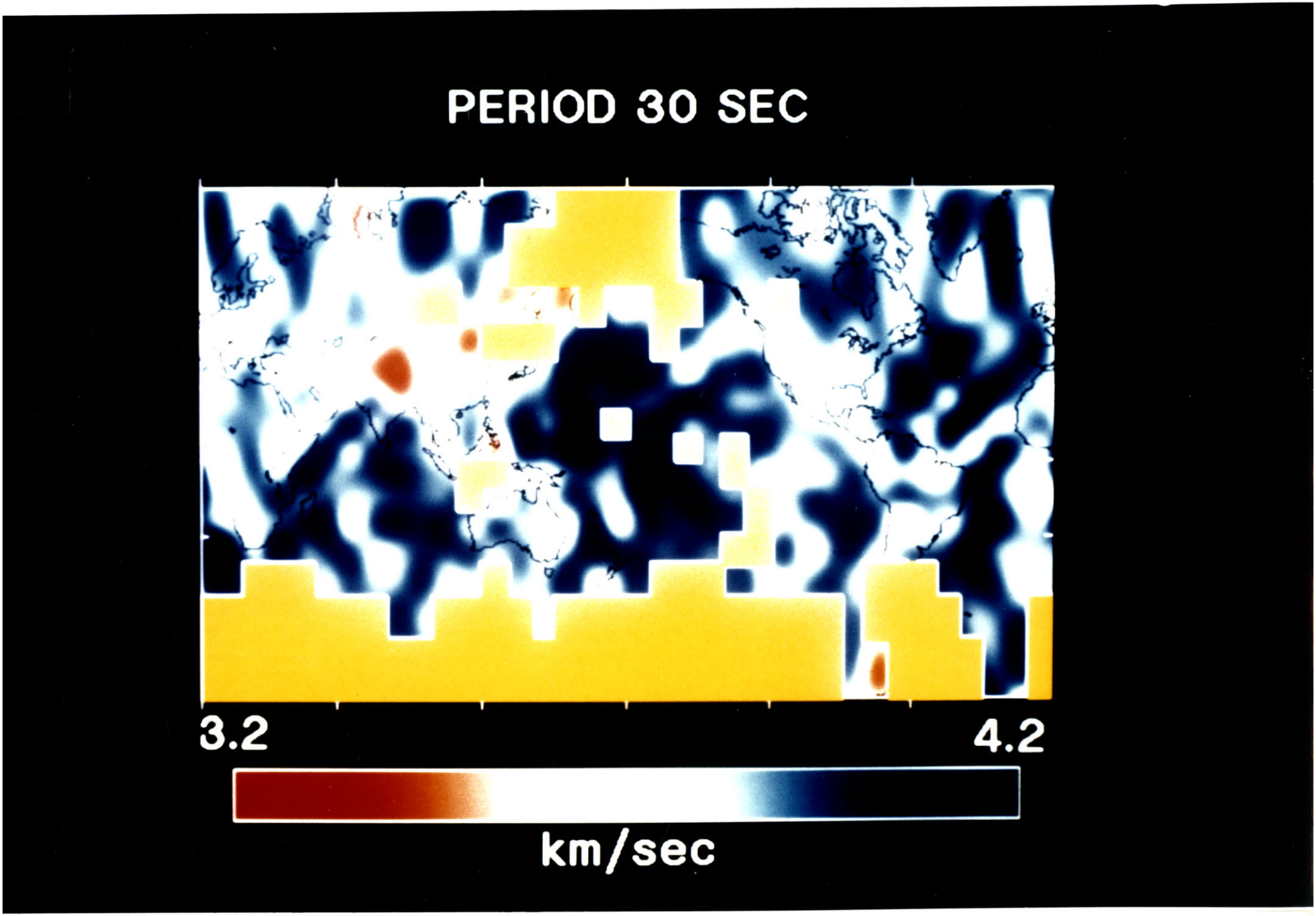

FIGURE 5.3a

FIGURE 5.3b

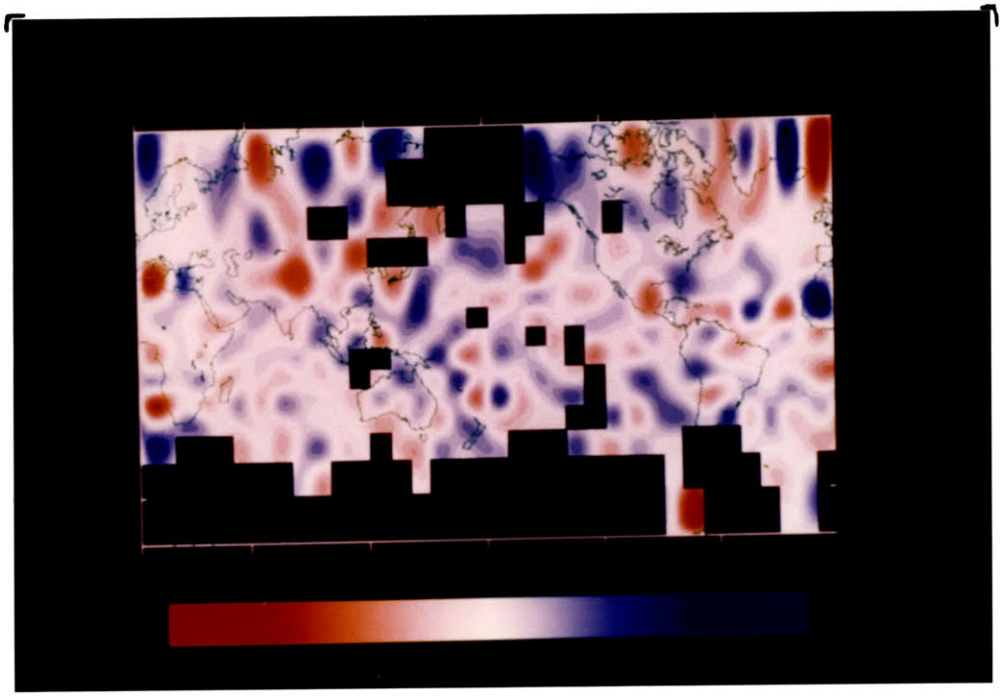

FIGURE 5.3c

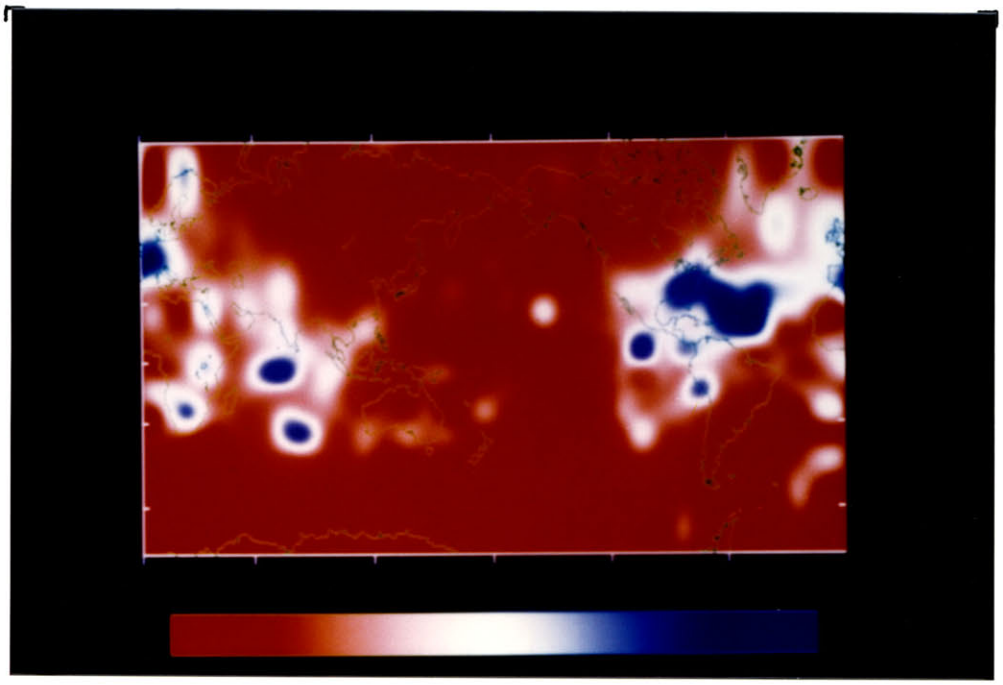

FIGURE 5.3d

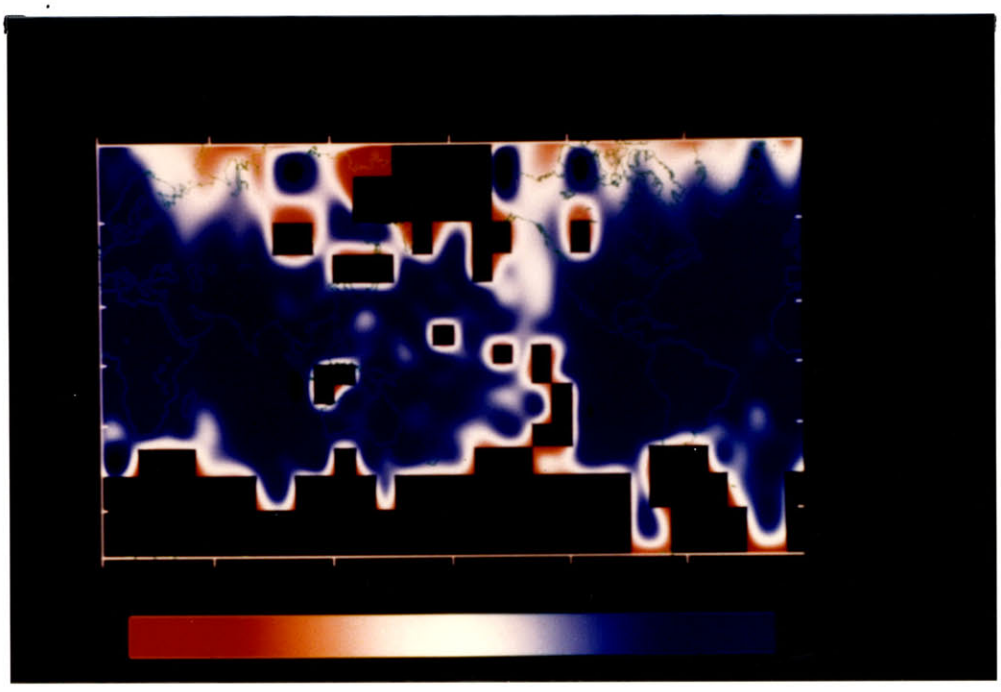

FIGURE 5.3e

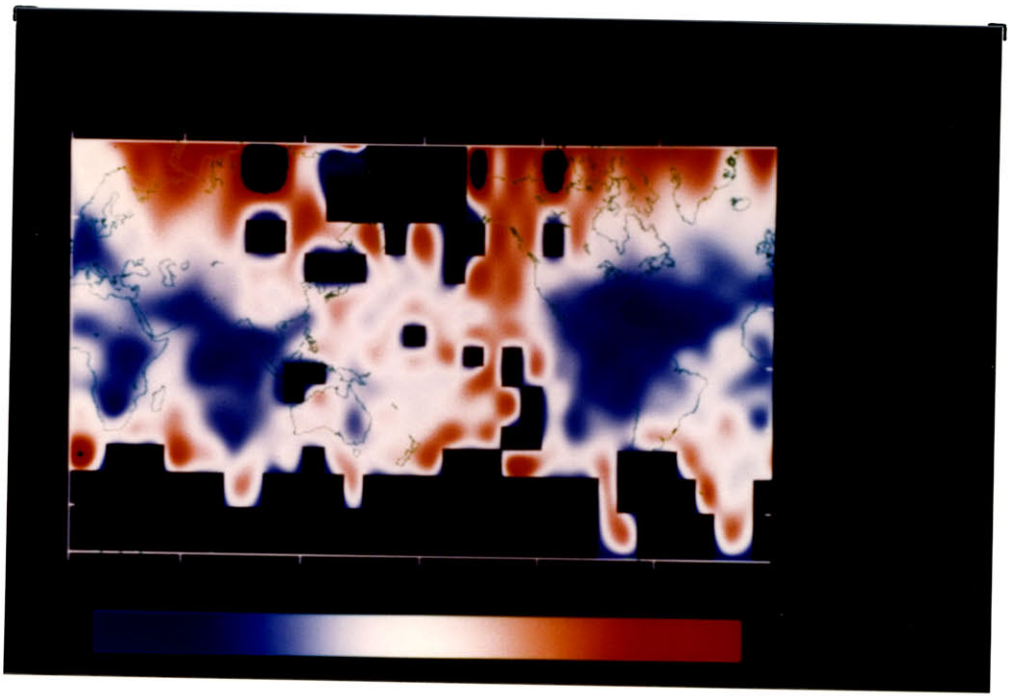

FIGURE 5.3f

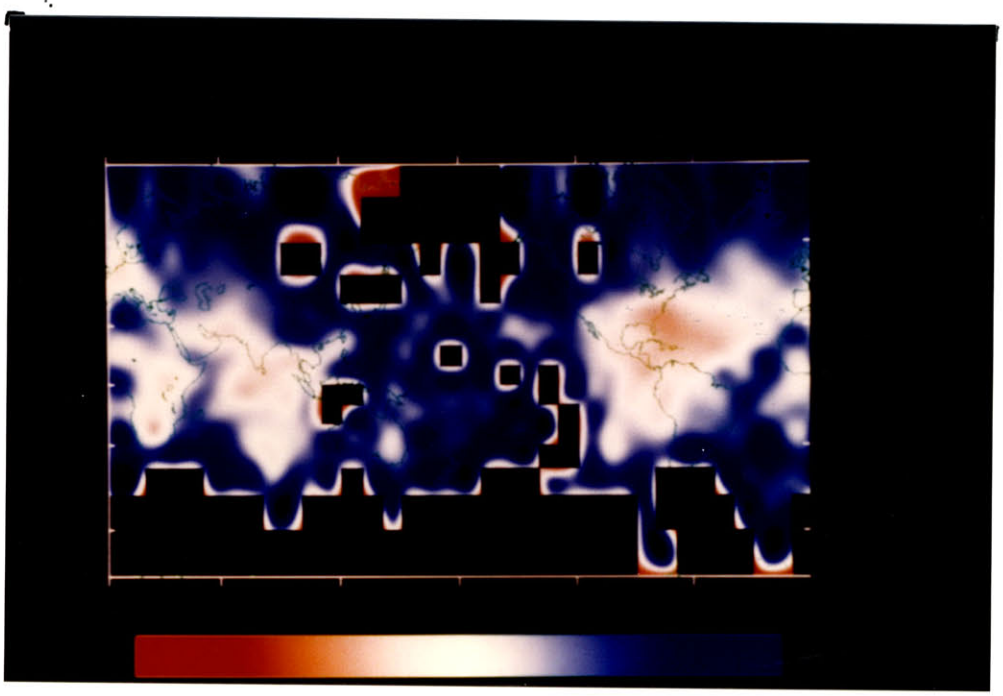

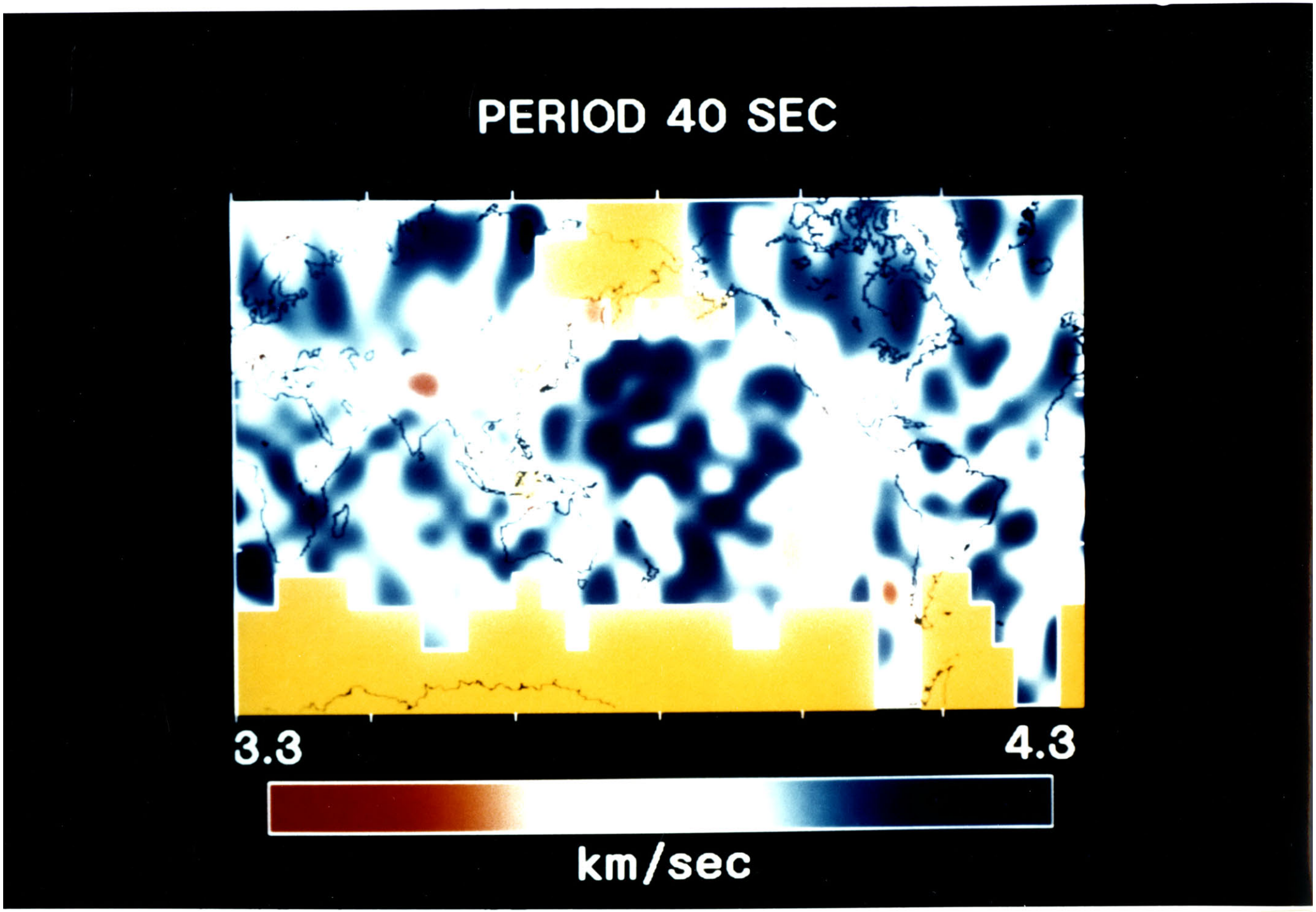

FIGURE 5.4a

FIGURE 5.4b

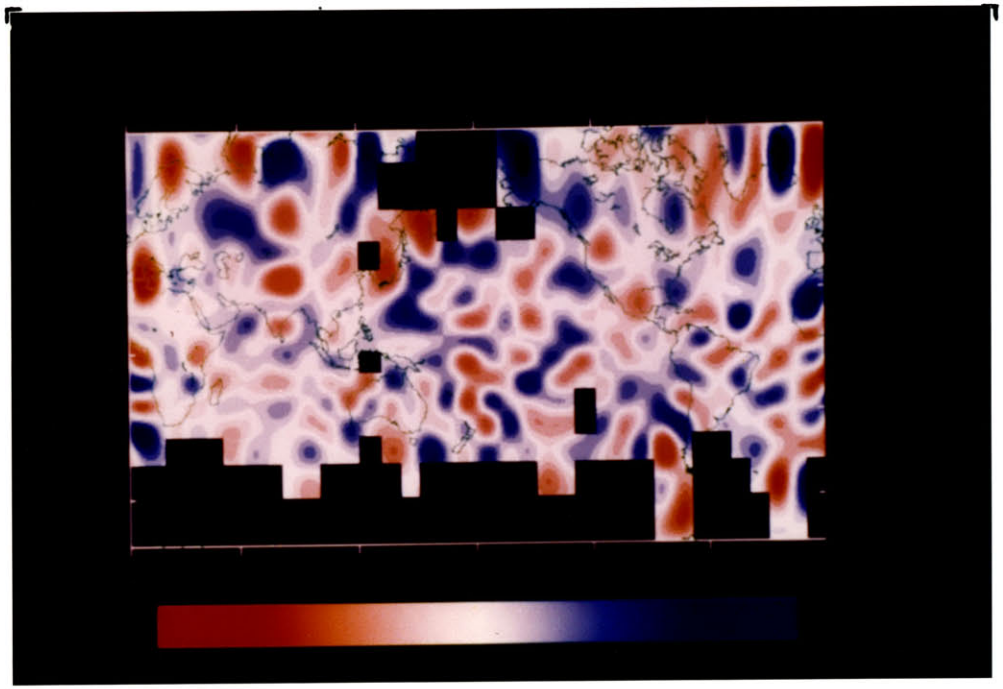

FIGURE 5.4c

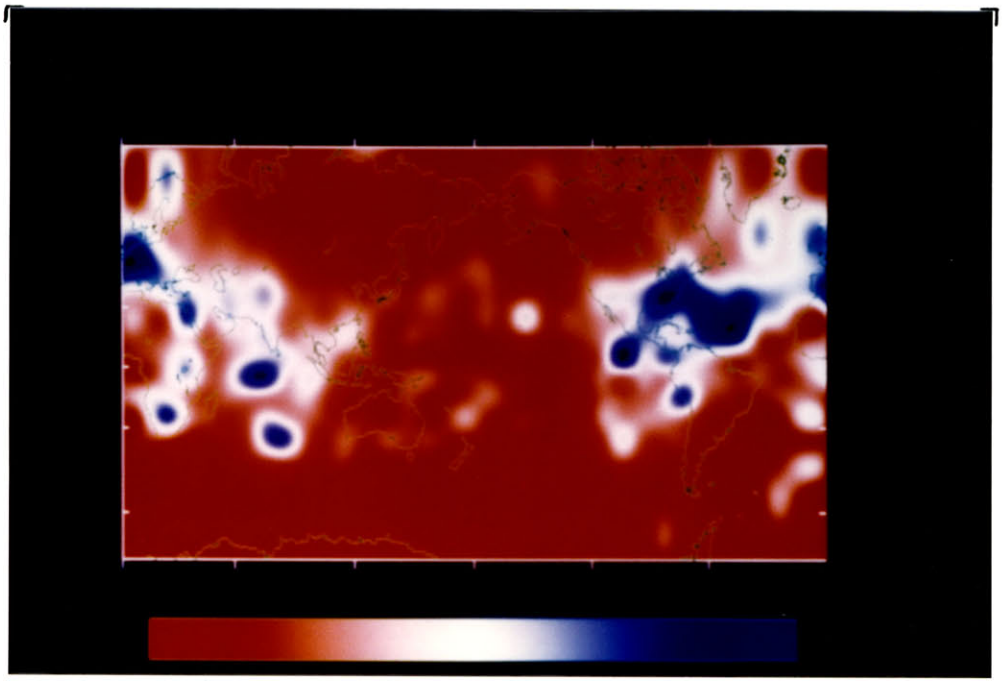

FIGURE 5.4d

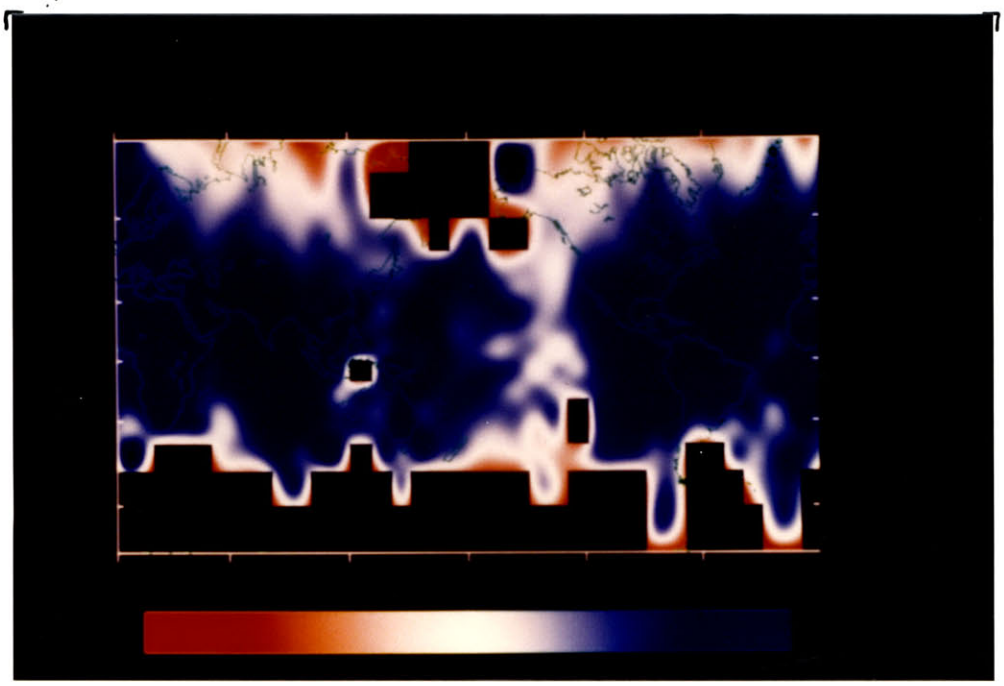

FIGURE 5.4e

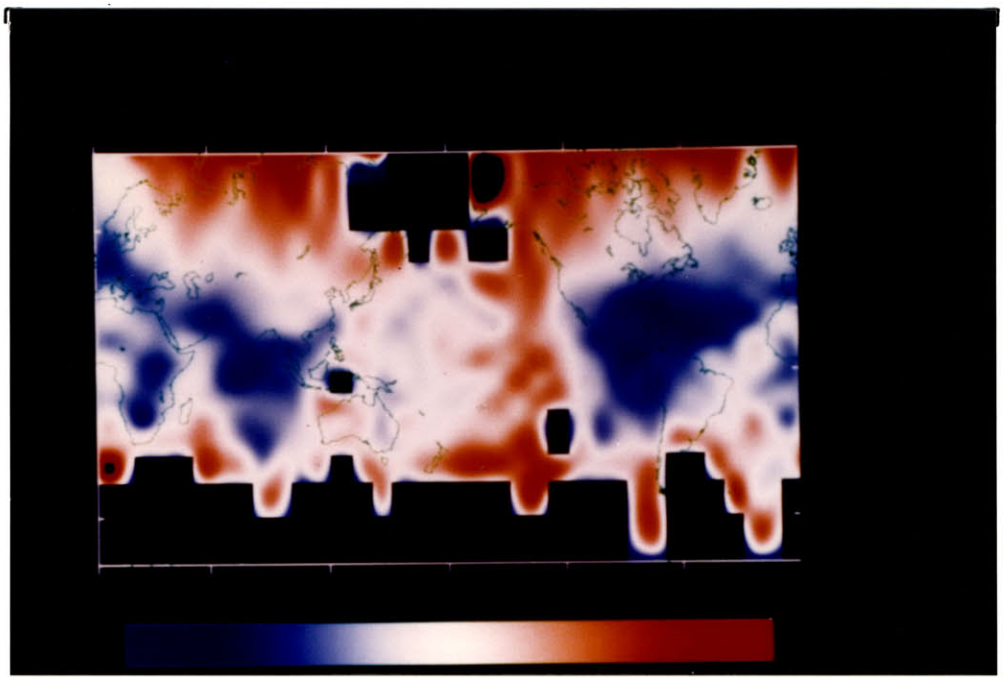

FIGURE 5.4f

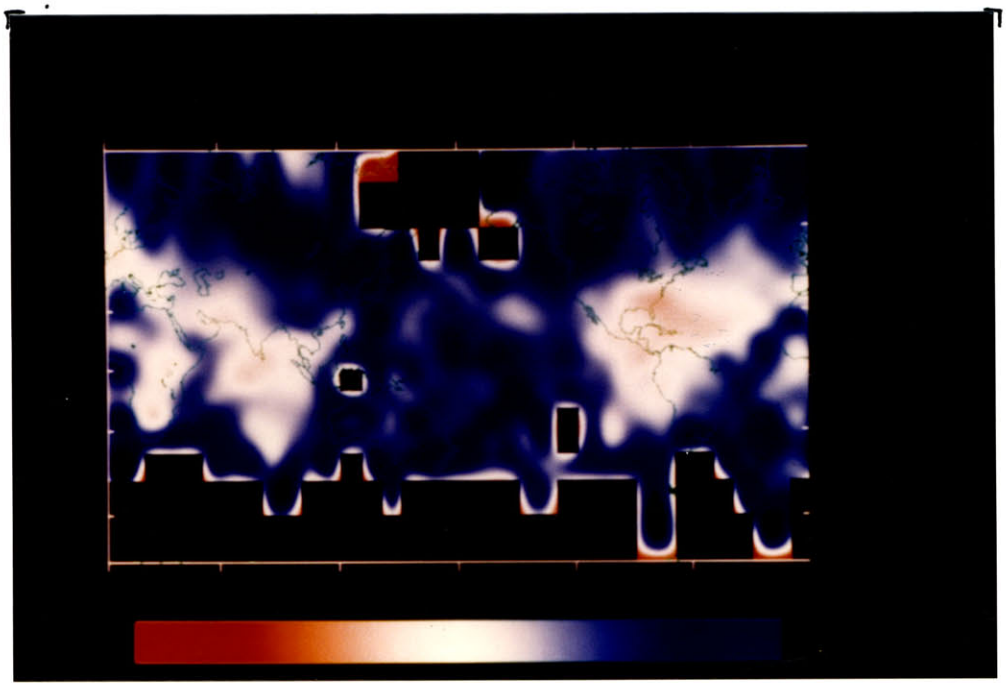

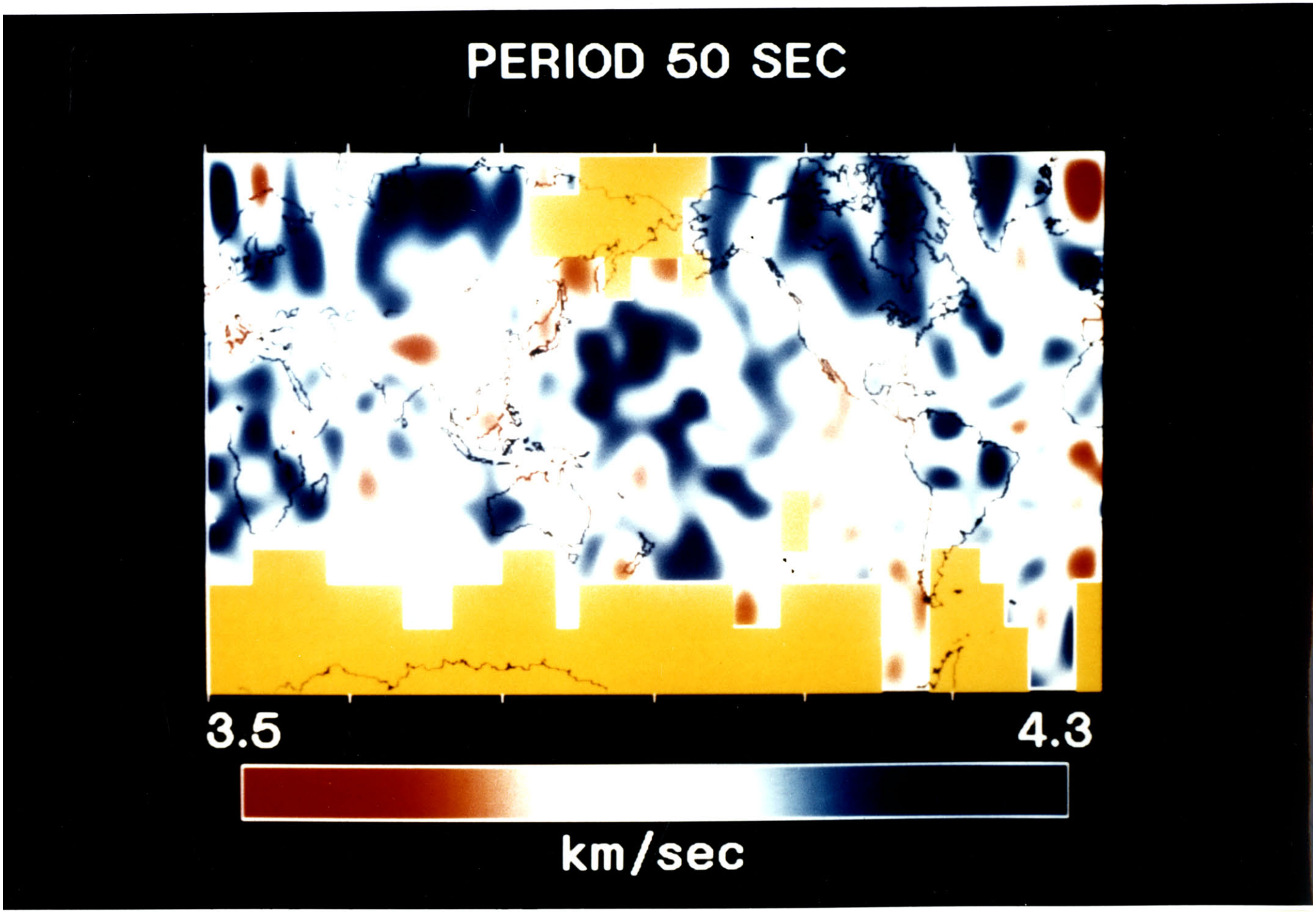

FIGURE 5.5a

FIGURE 5.5b

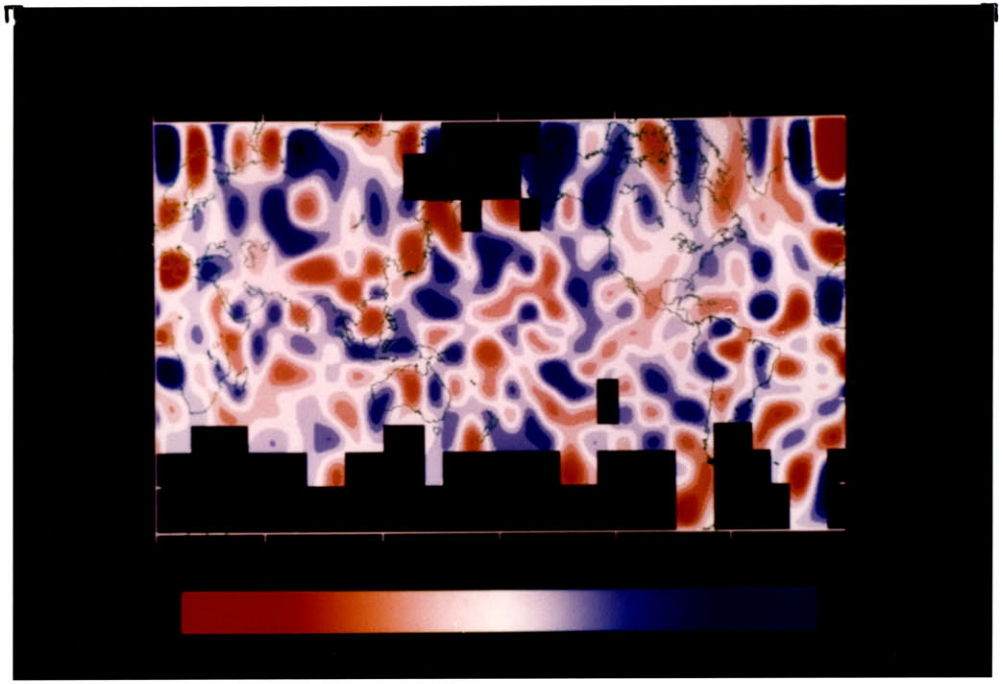

FIGURE 5.5c

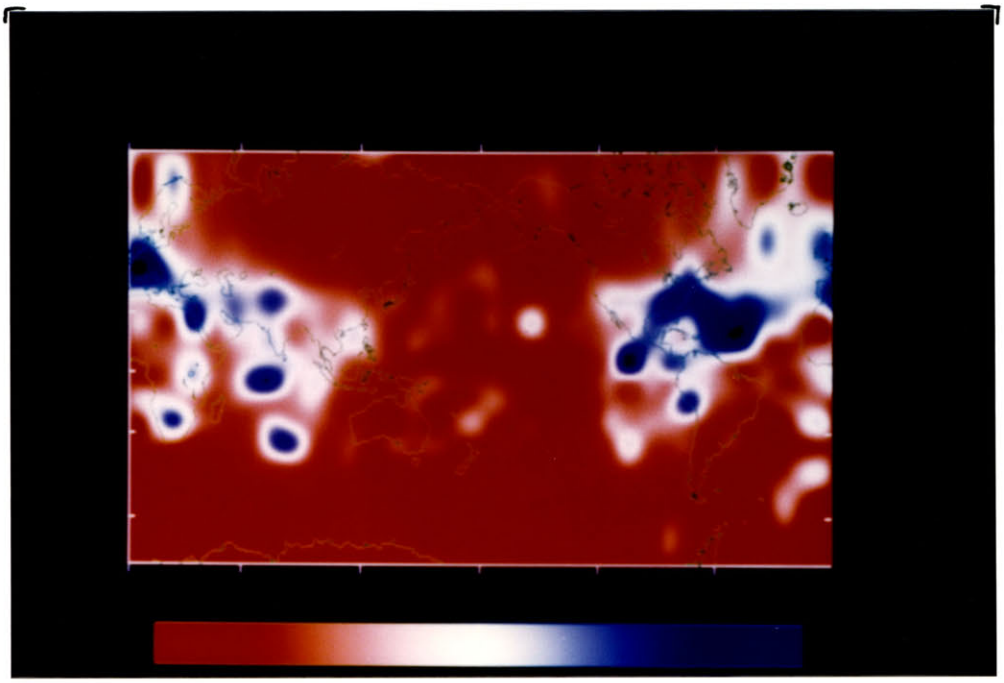

FIGURE 5.5d

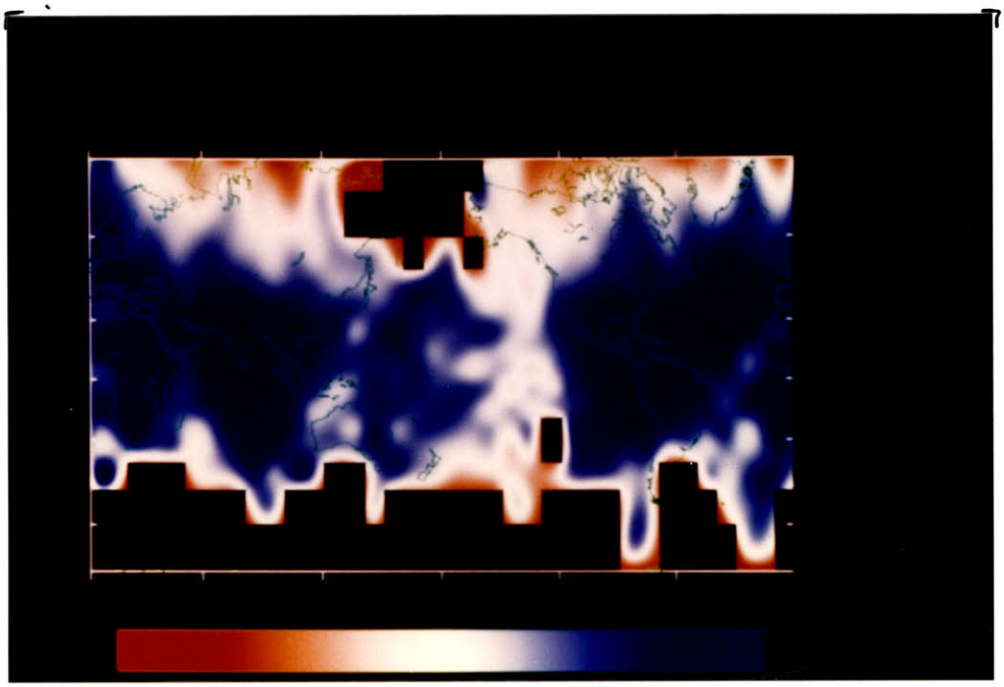

FIGURE 5.5e

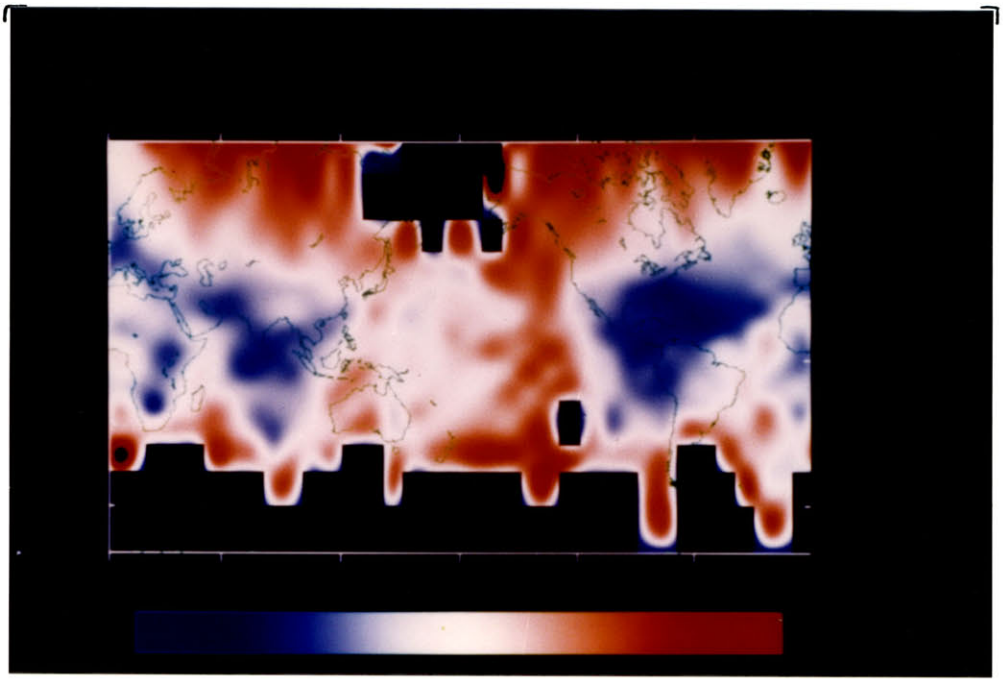

FIGURE 5.5f

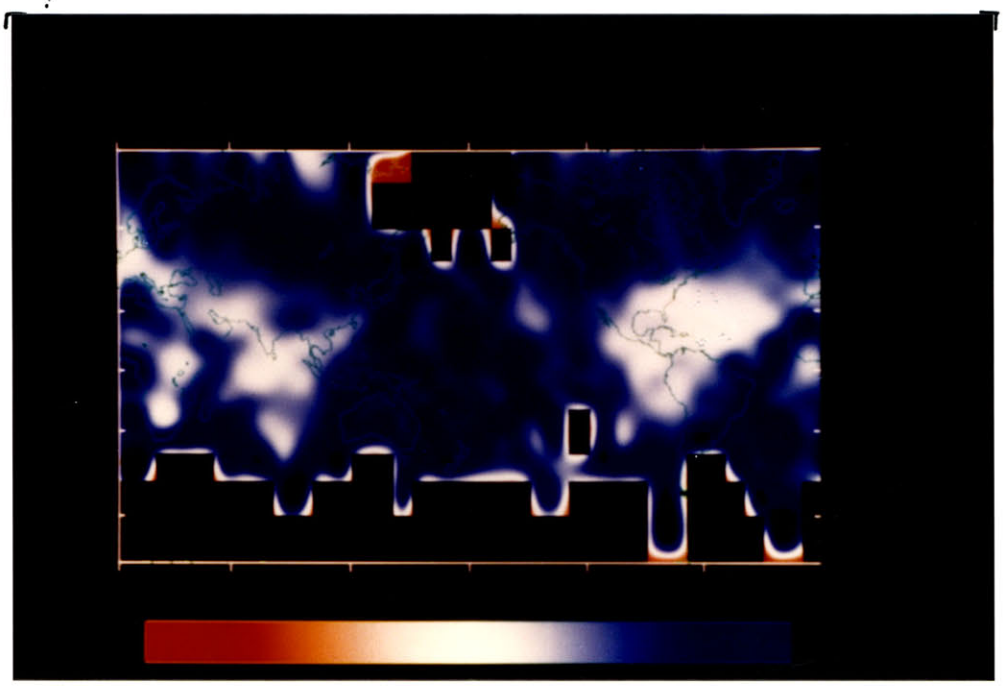

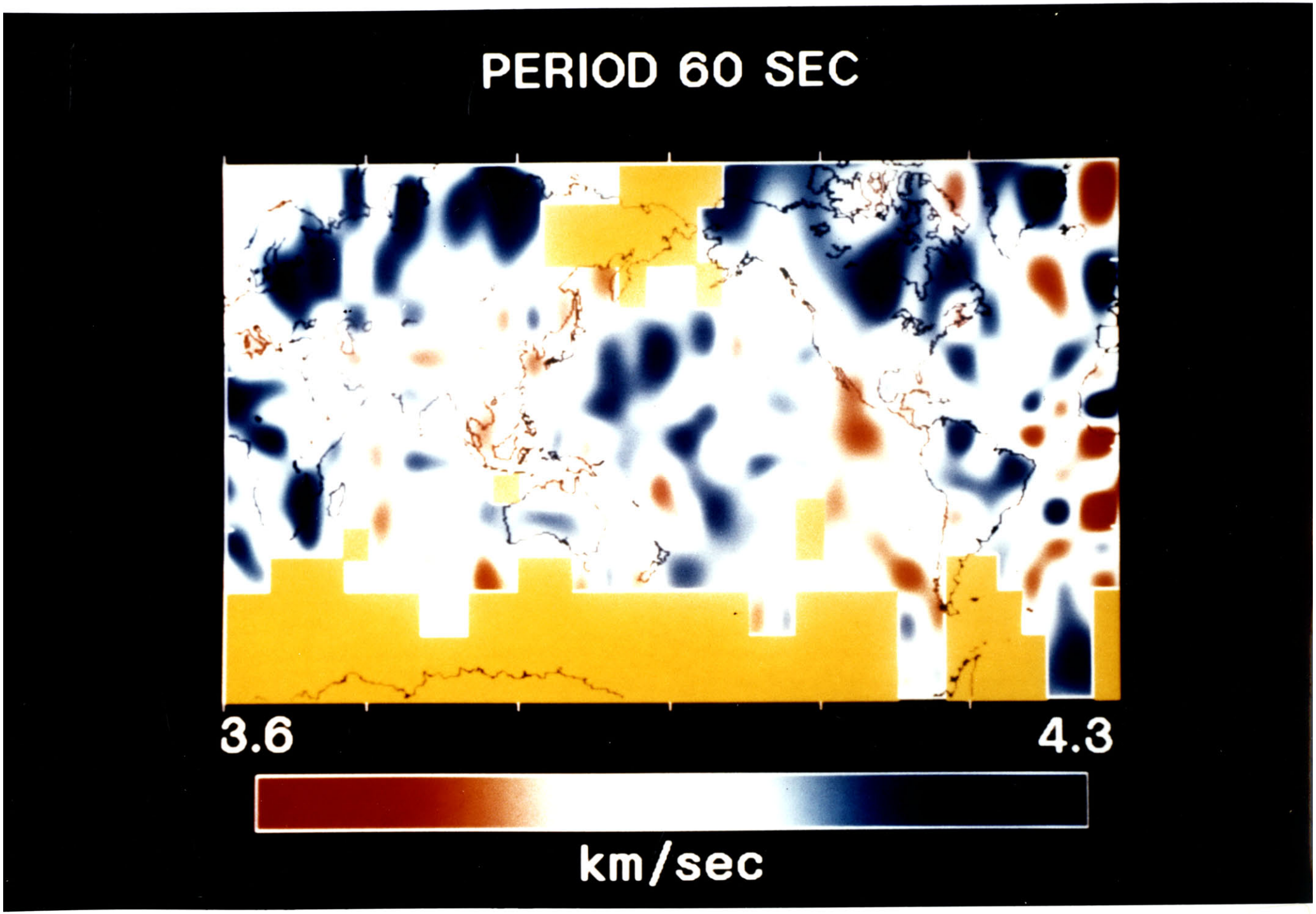

FIGURE 5.6a

FIGURE 5.6b

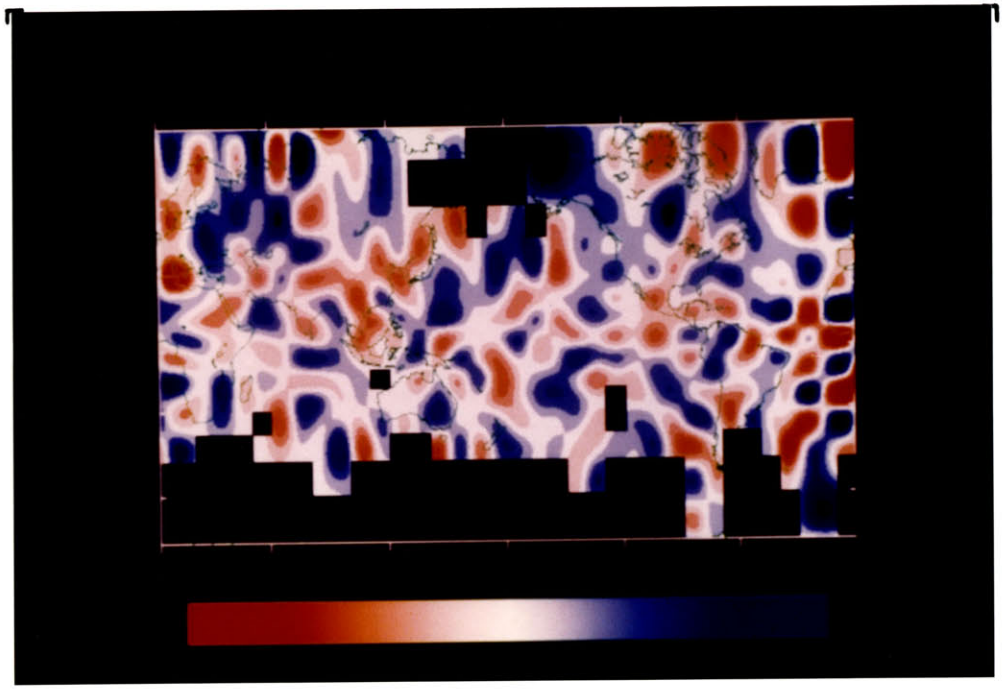

FIGURE 5.6c

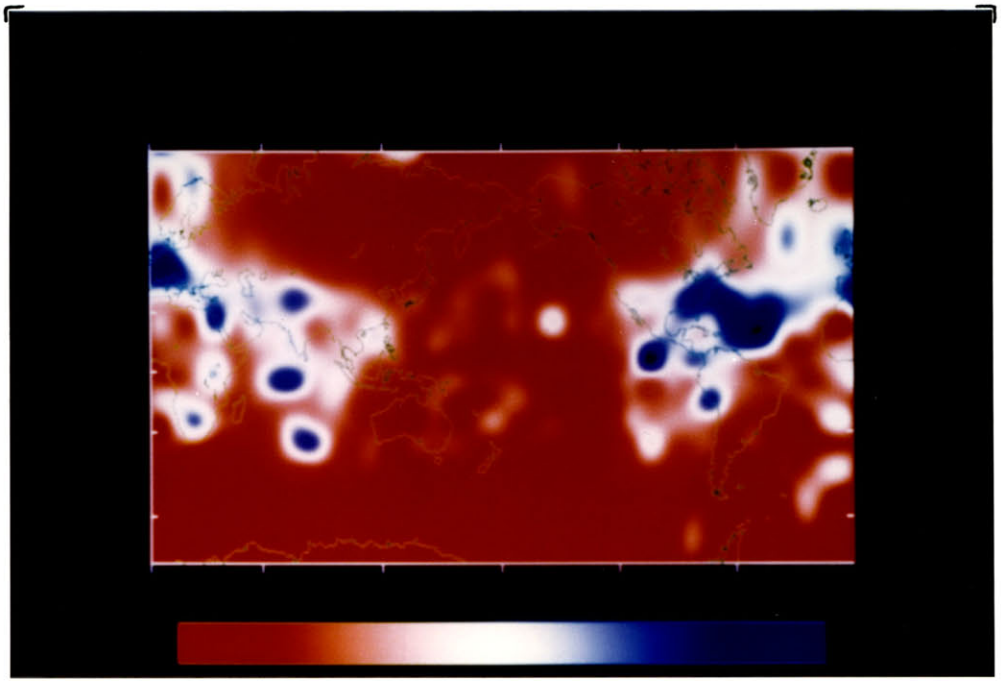

FIGURE 5.6d

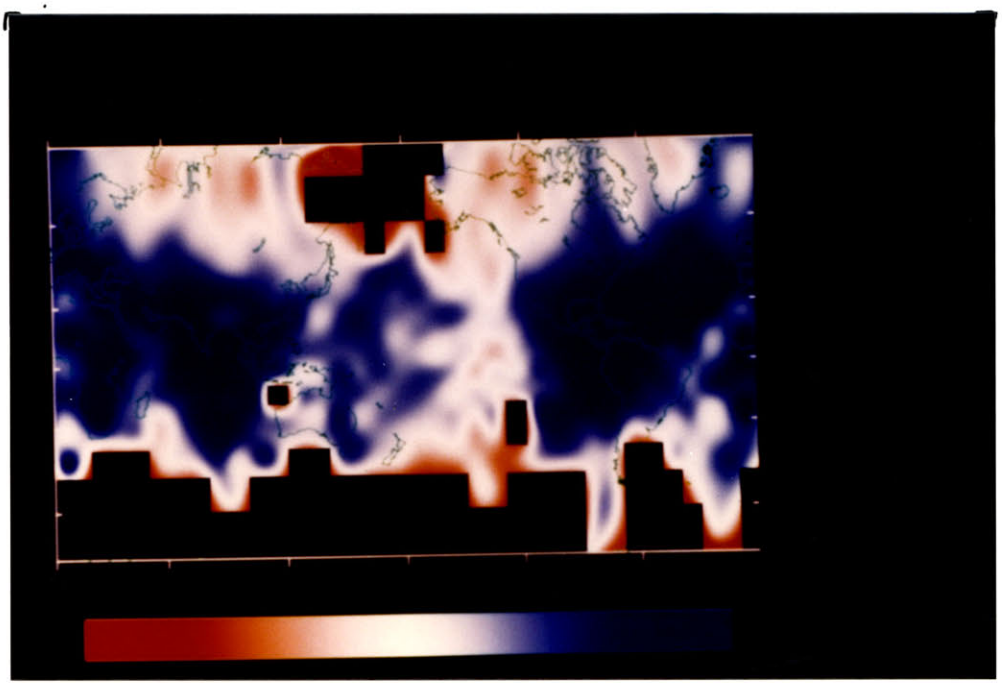

FIGURE 5.6e

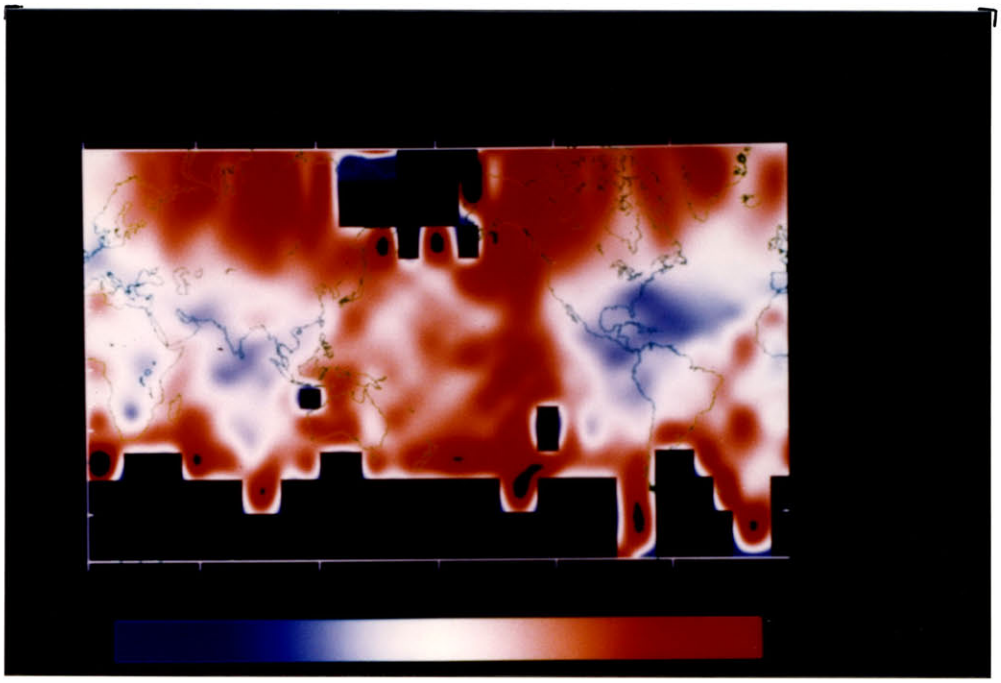

FIGURE 5.6f

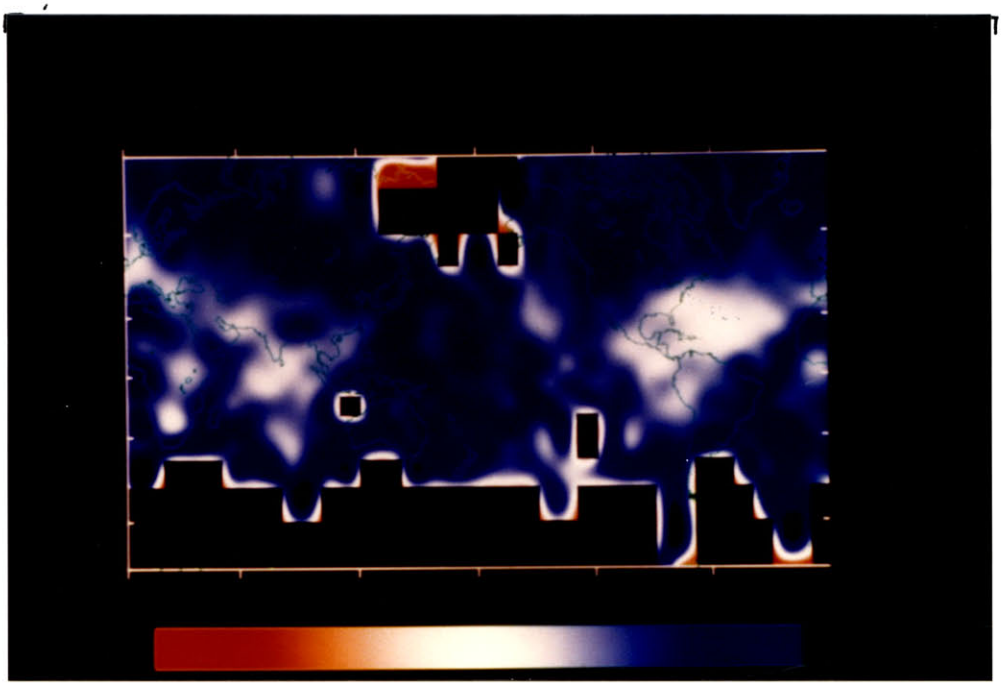

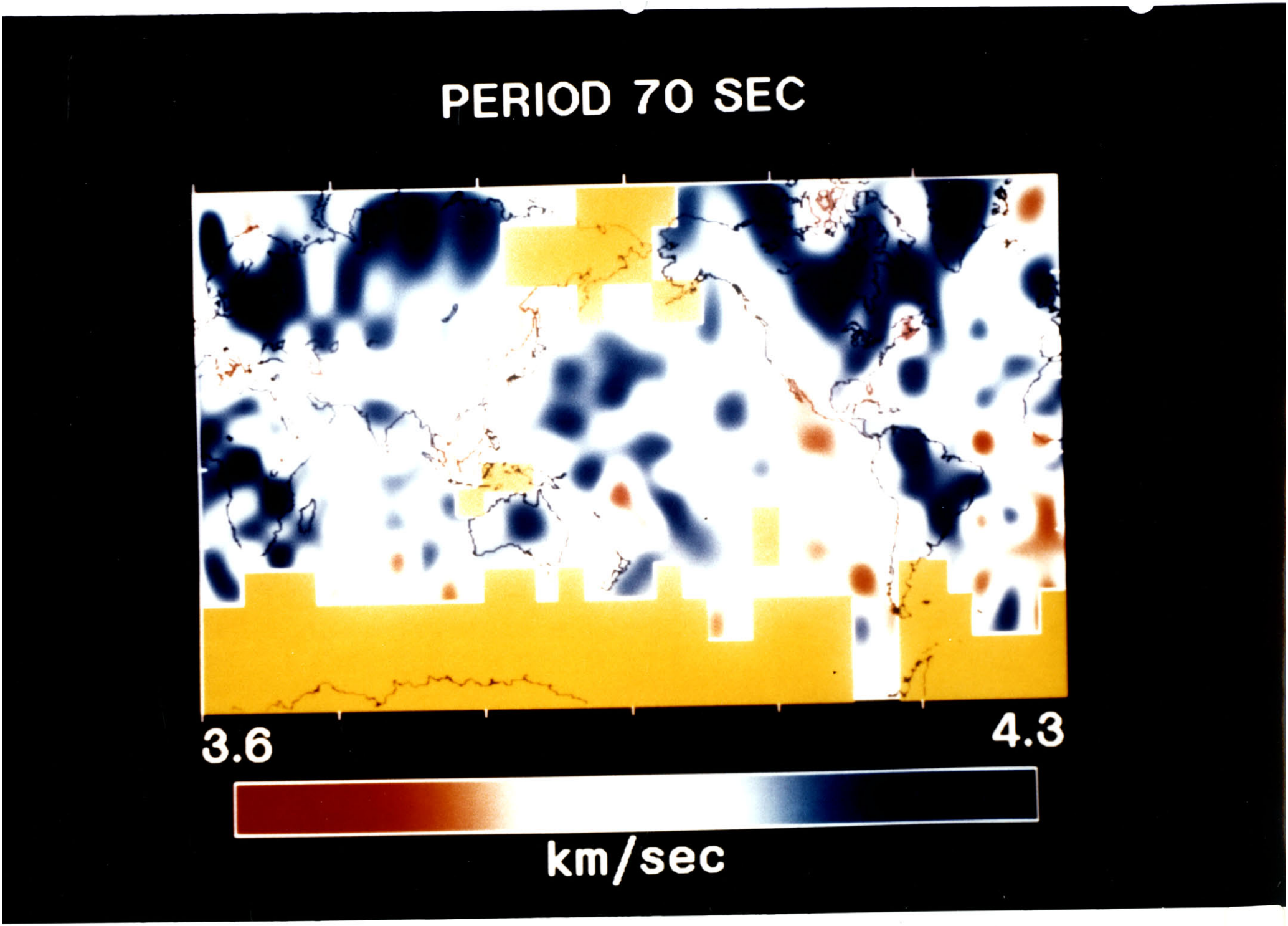

FIGURE 5.7a

FIGURE 5.7b

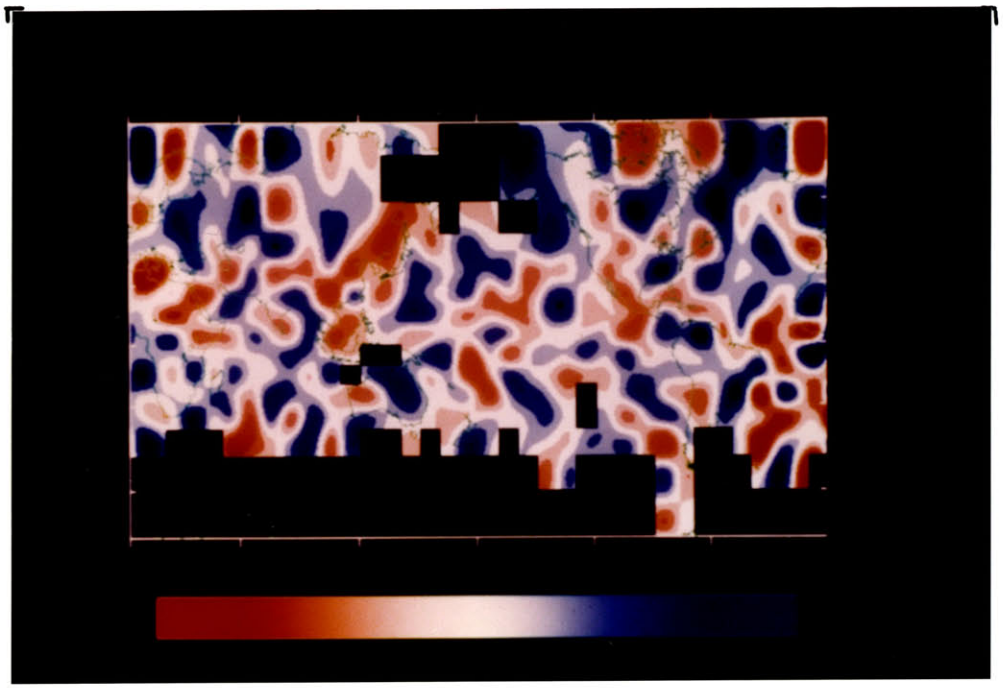

FIGURE 5.7c

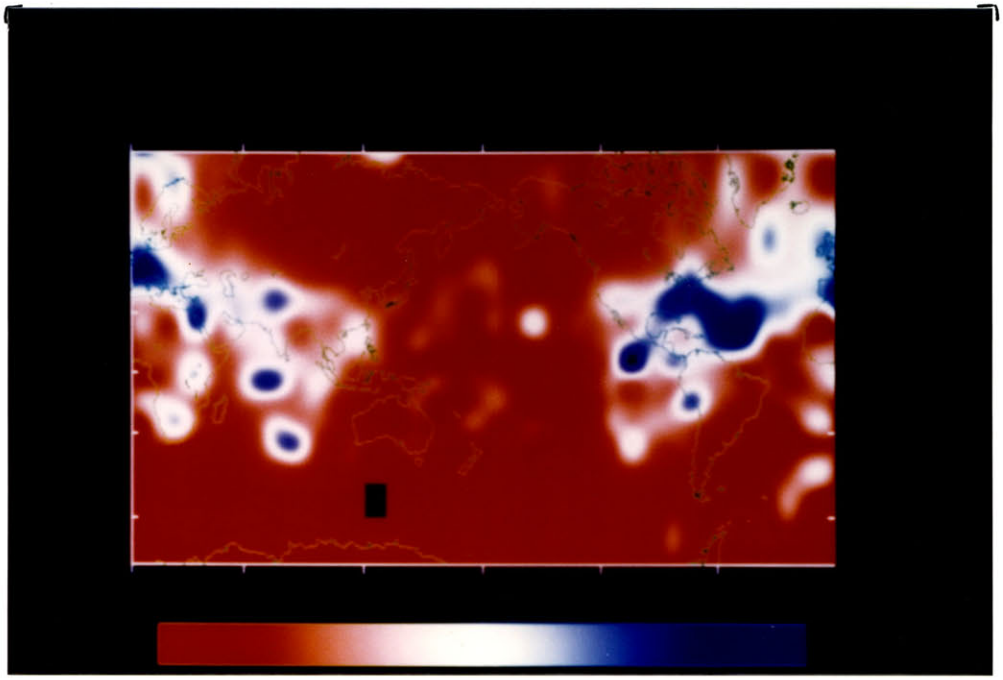

FIGURE 5.7d

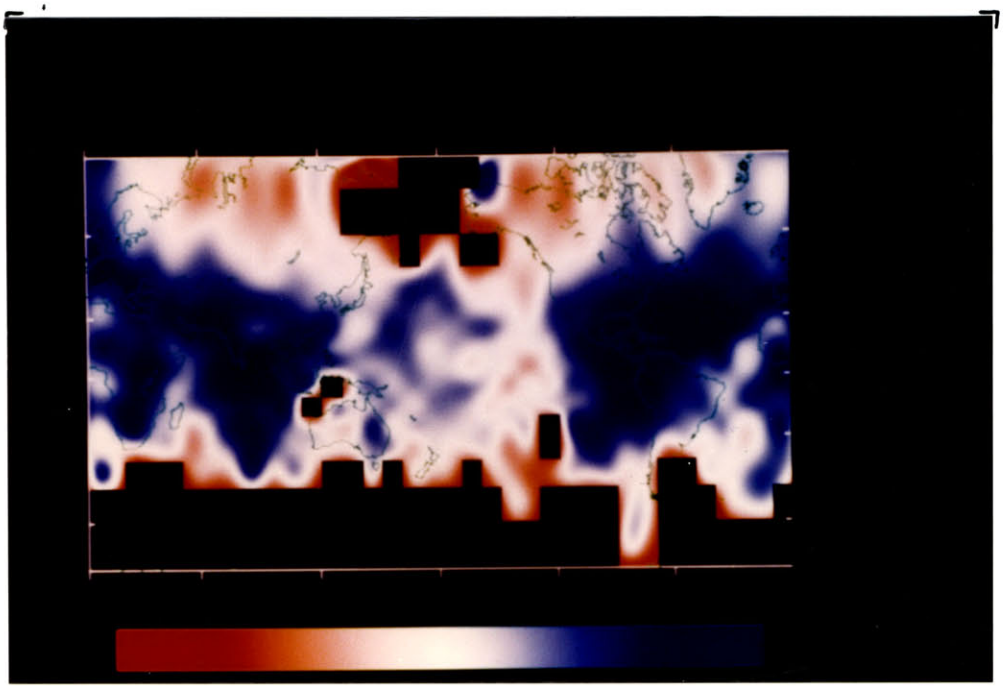

FIGURE 5.7e

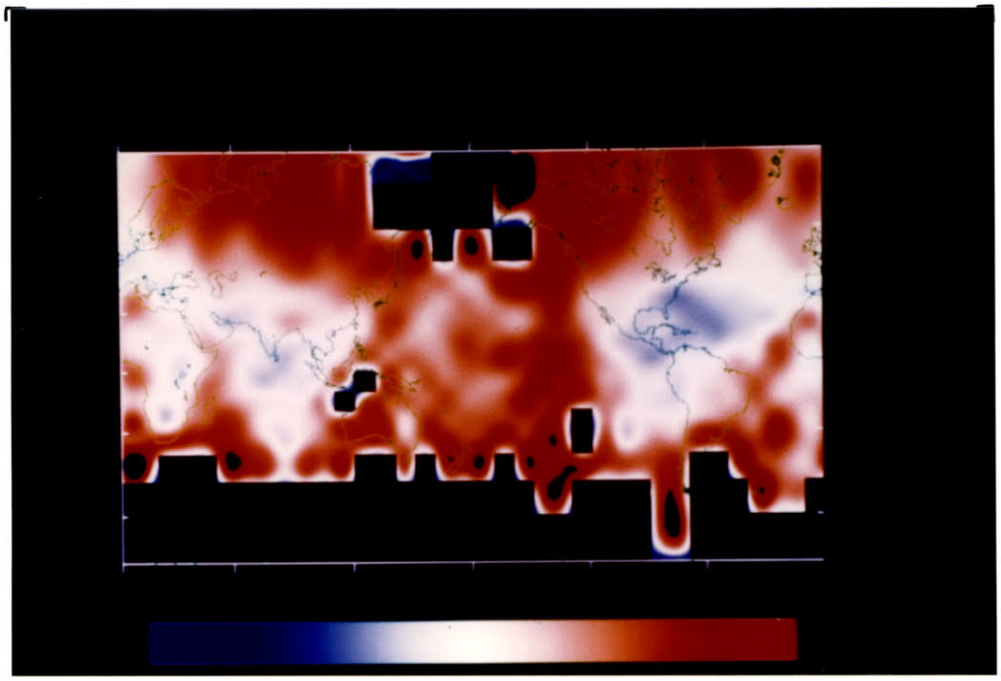

FIGURE 5.7f

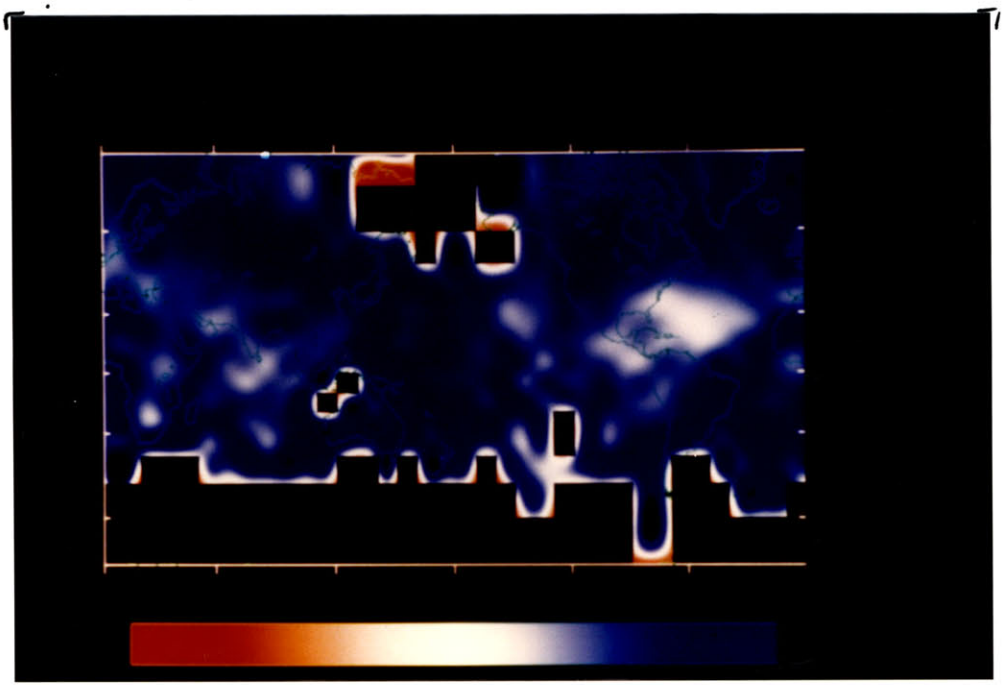

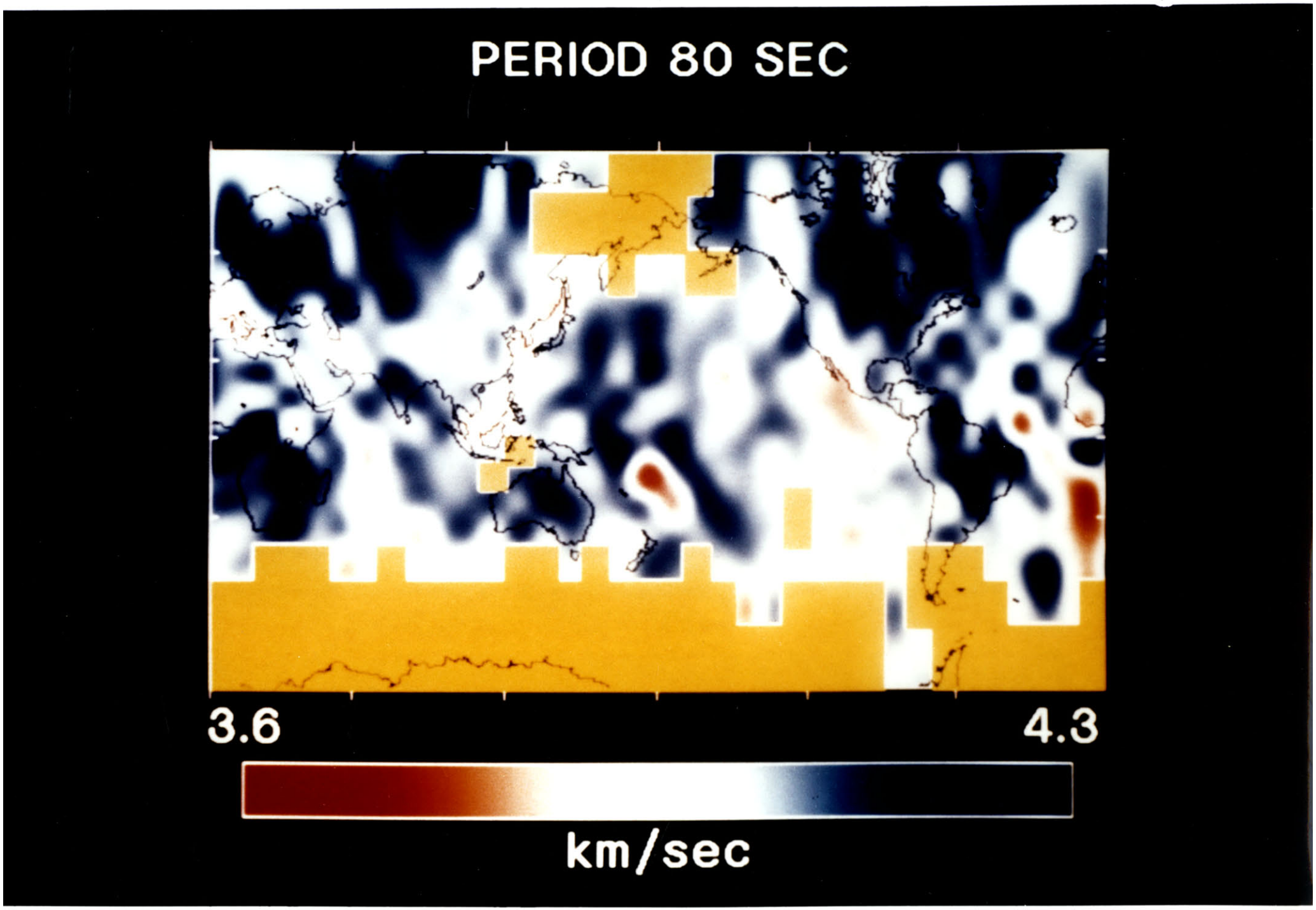

FIGURE 5.8a

FIGURE 5.8b

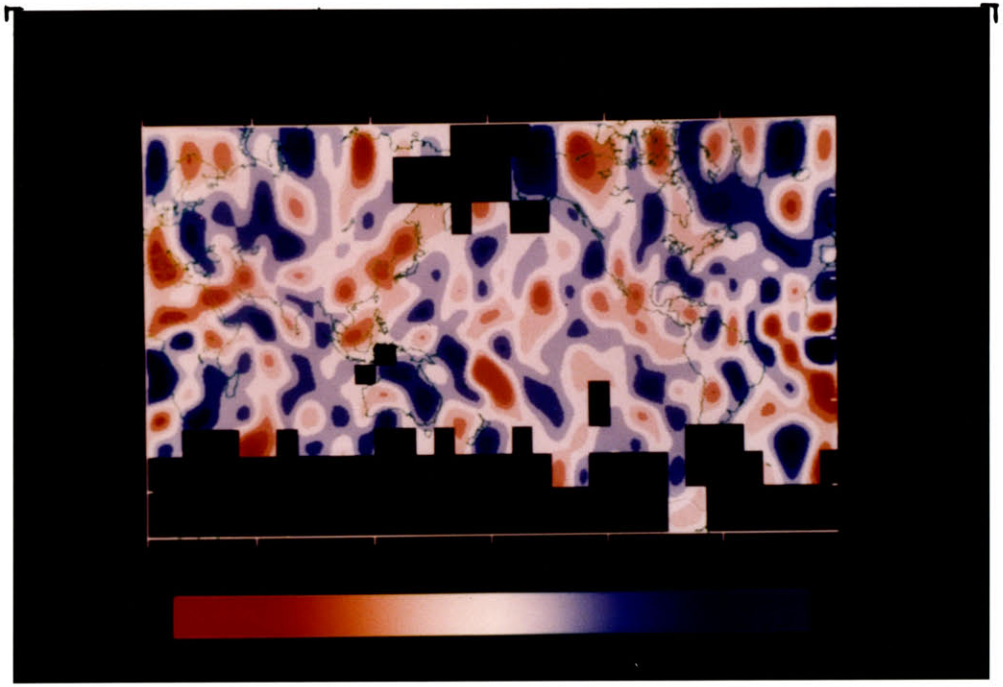

FIGURE 5.8c

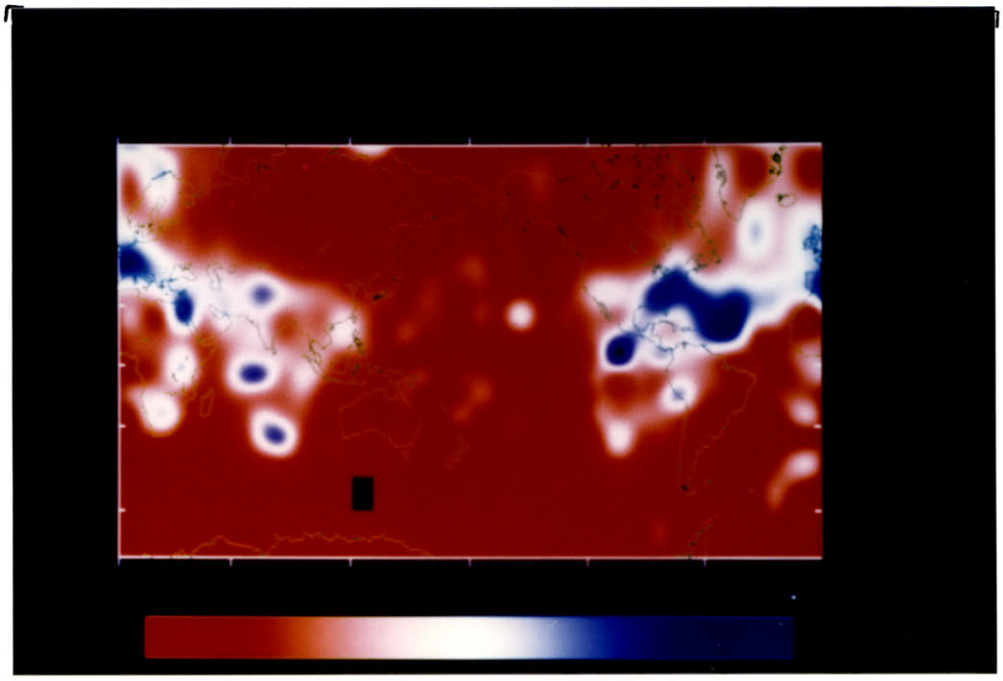

FIGURE 5.8d

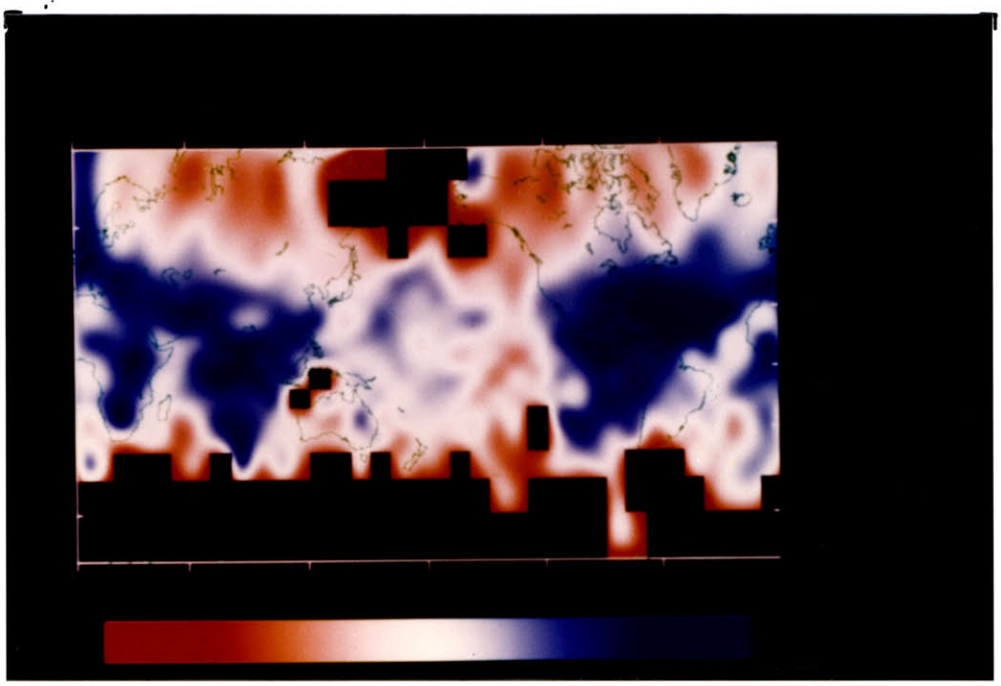

FIGURE 5.8e

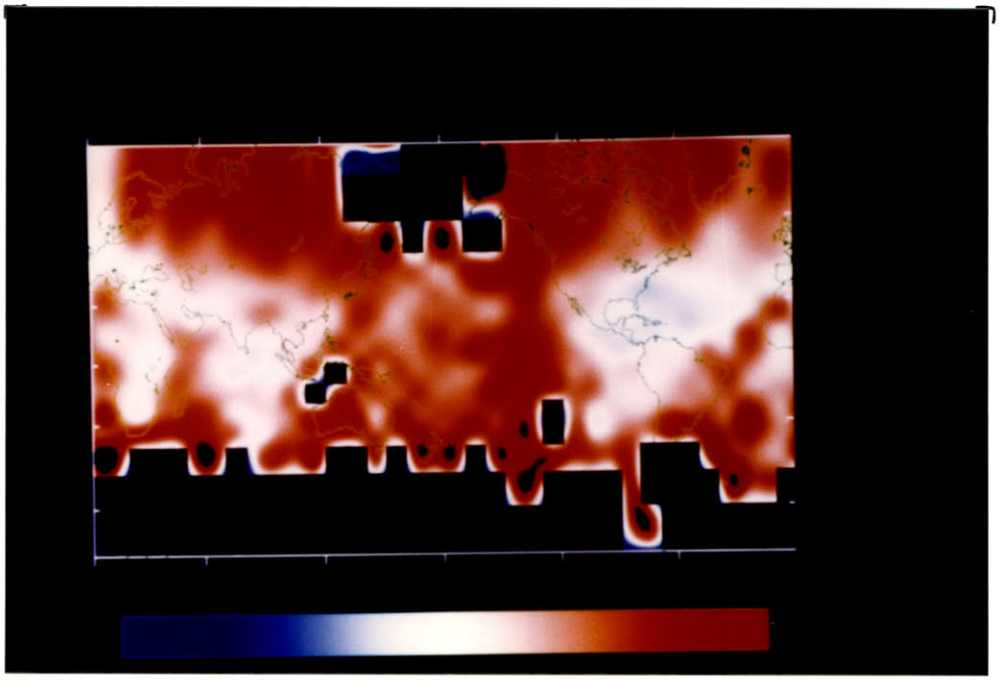

FIGURE 5.8f

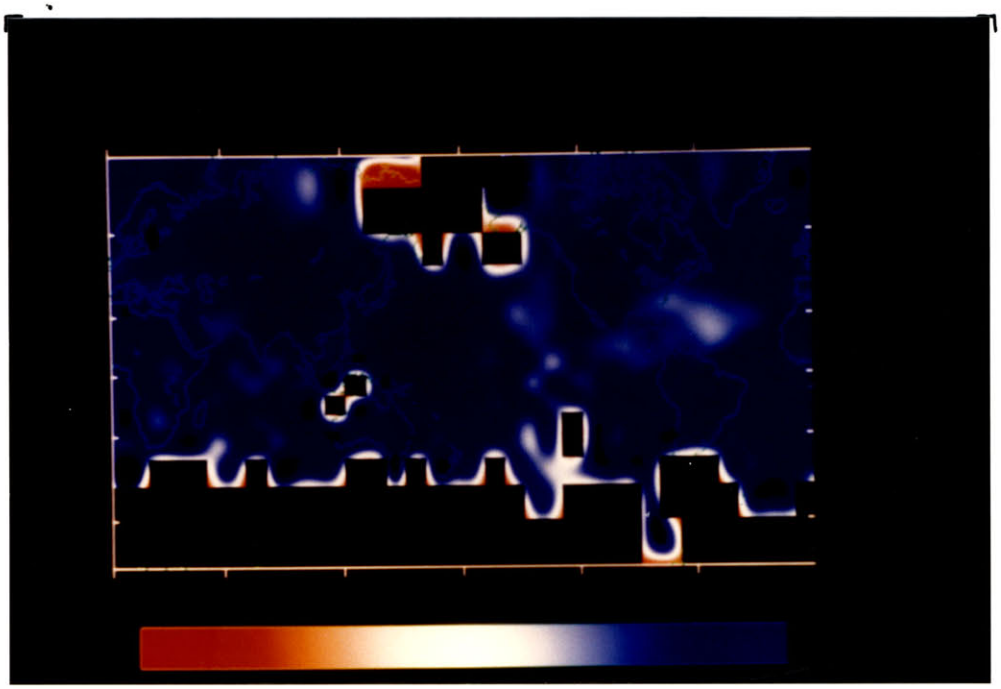

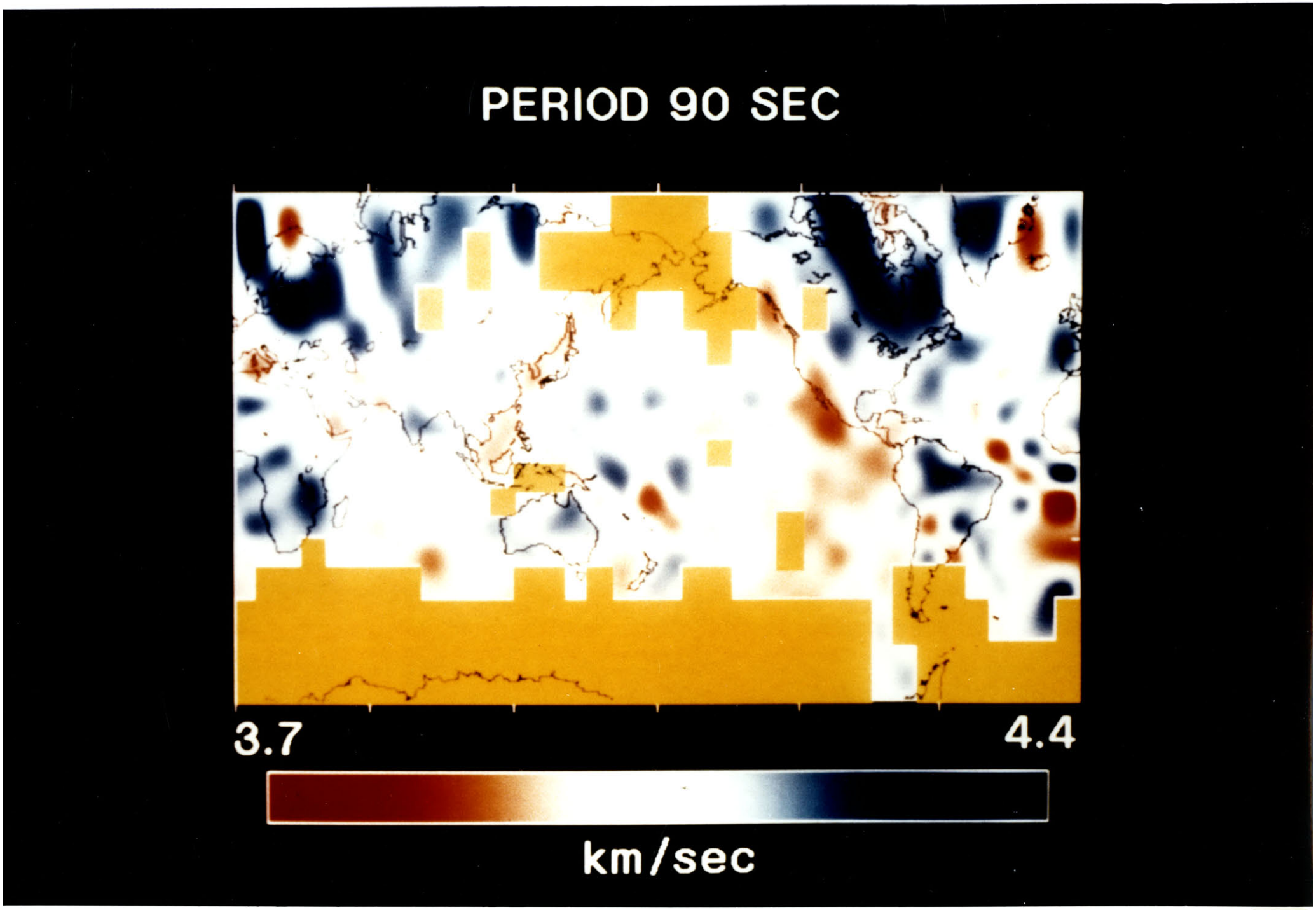

FIGURE 5.9a

FIGURE 5.9b

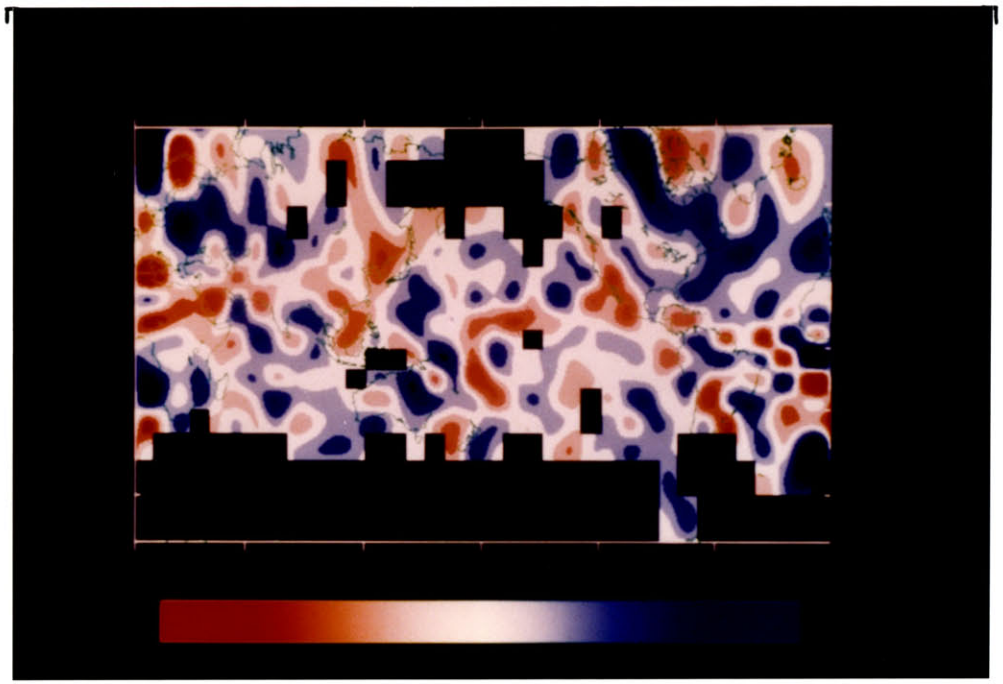

FIGURE 5.9c

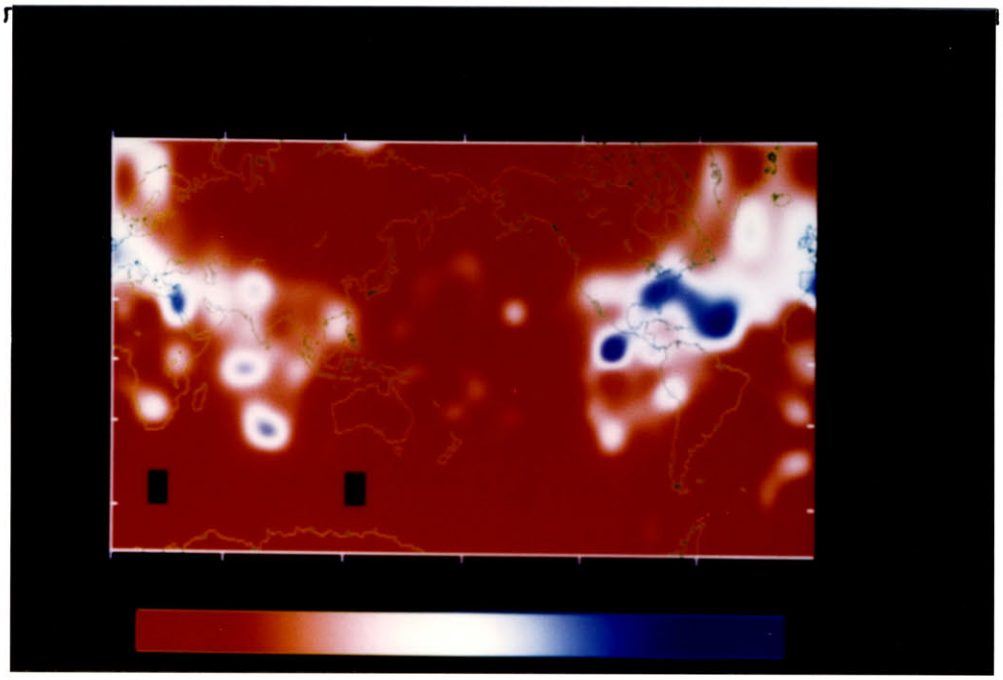

FIGURE 5.9d

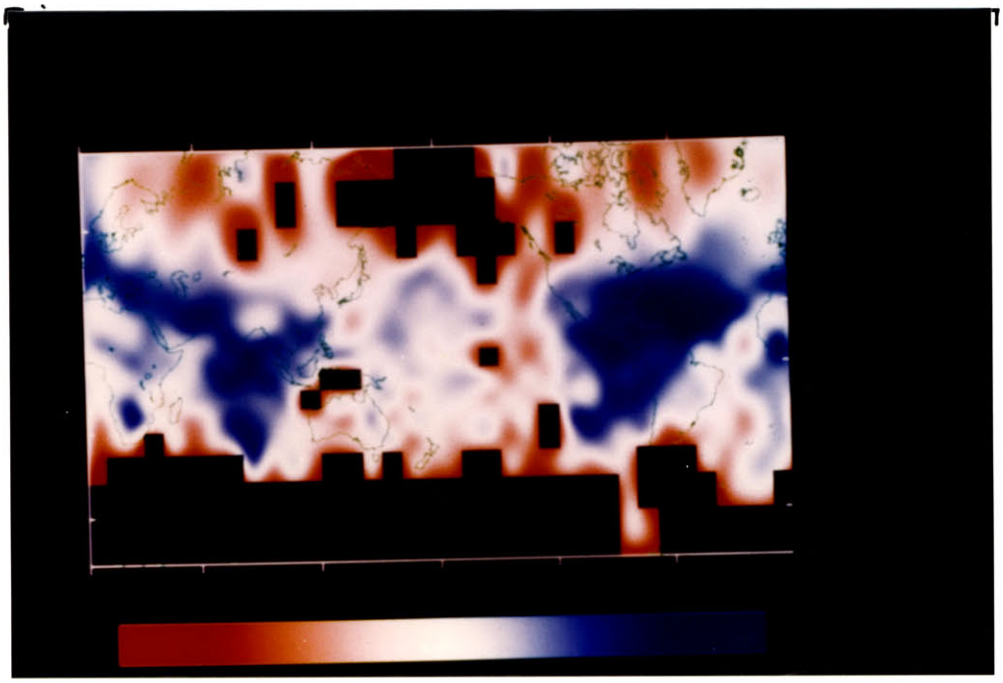

FIGURE 5.9e

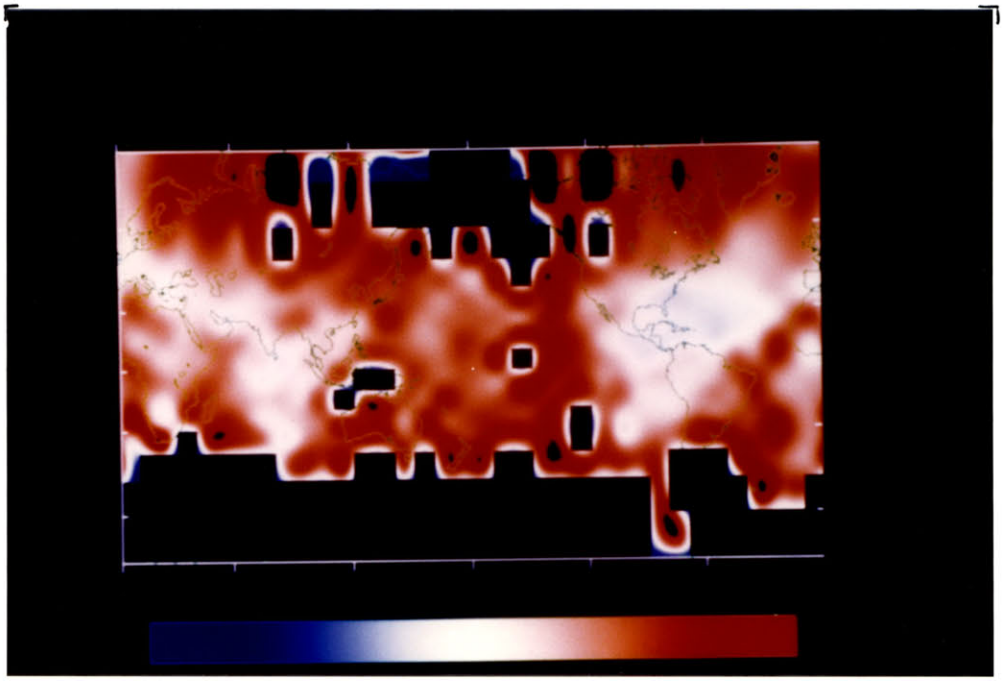

FIGURE 5.9f

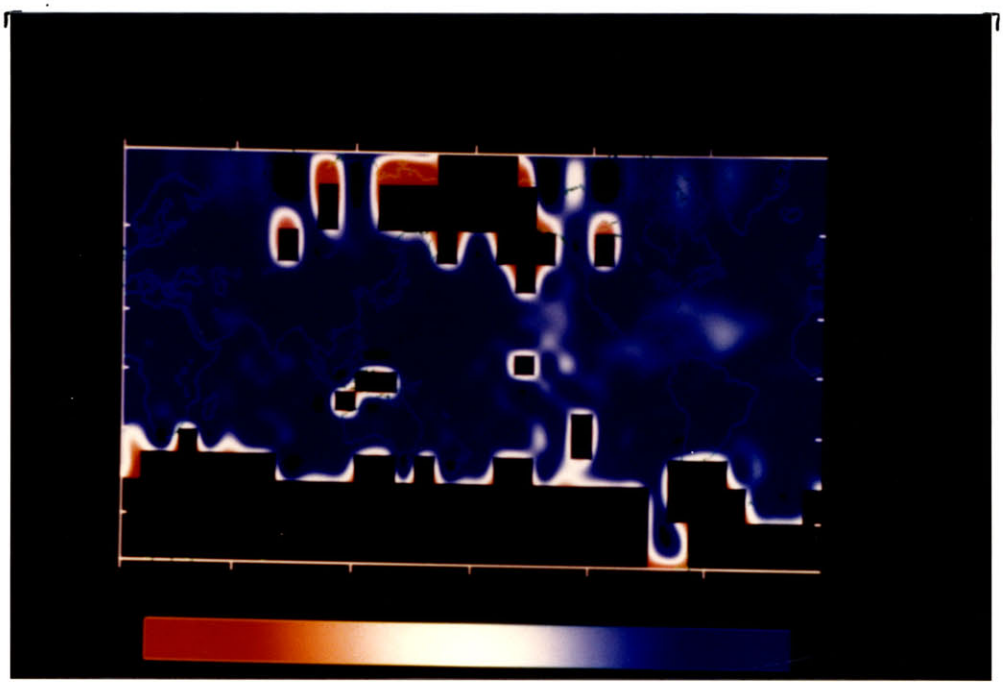

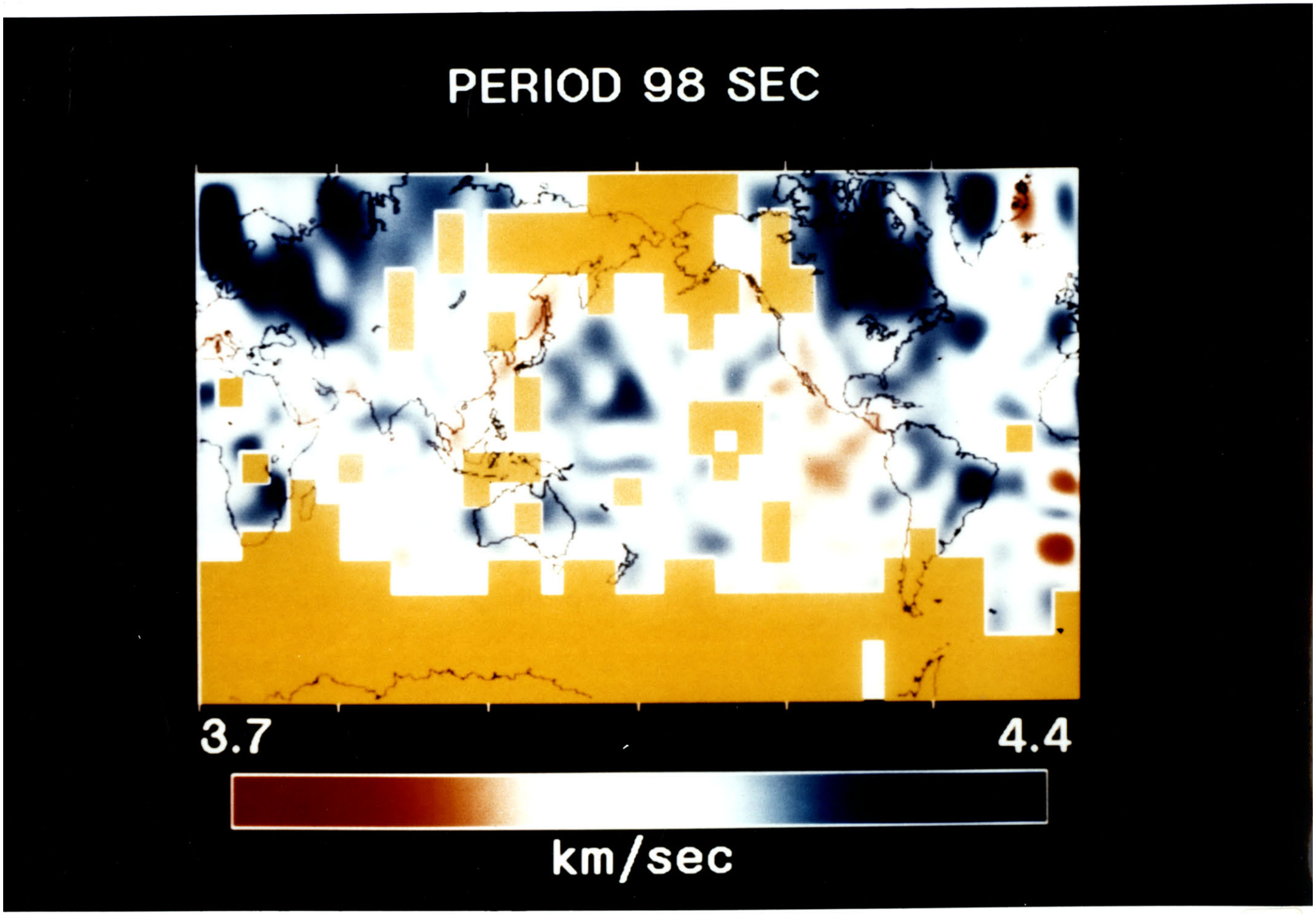

FIGURE 5.10a

FIGURE 5.10b

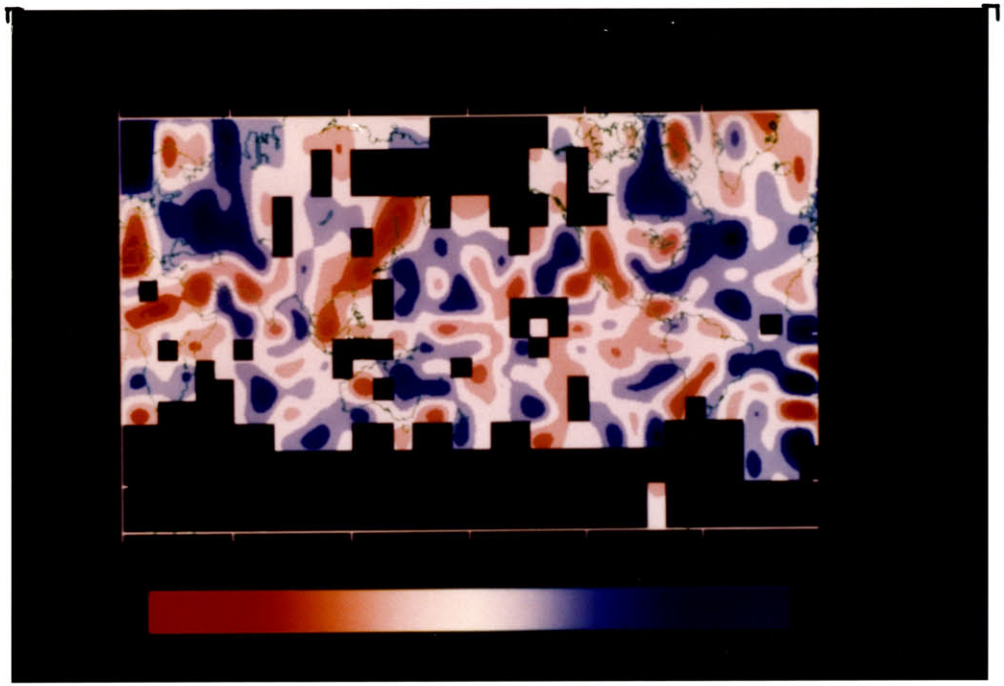

FIGURE 5.10c

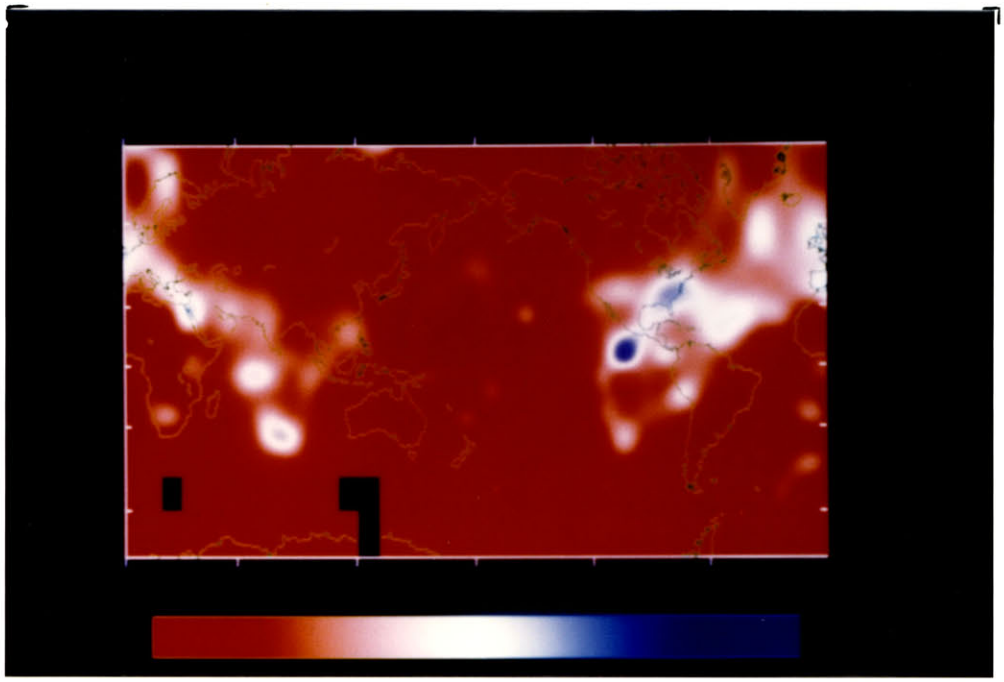

FIGURE 5.10d

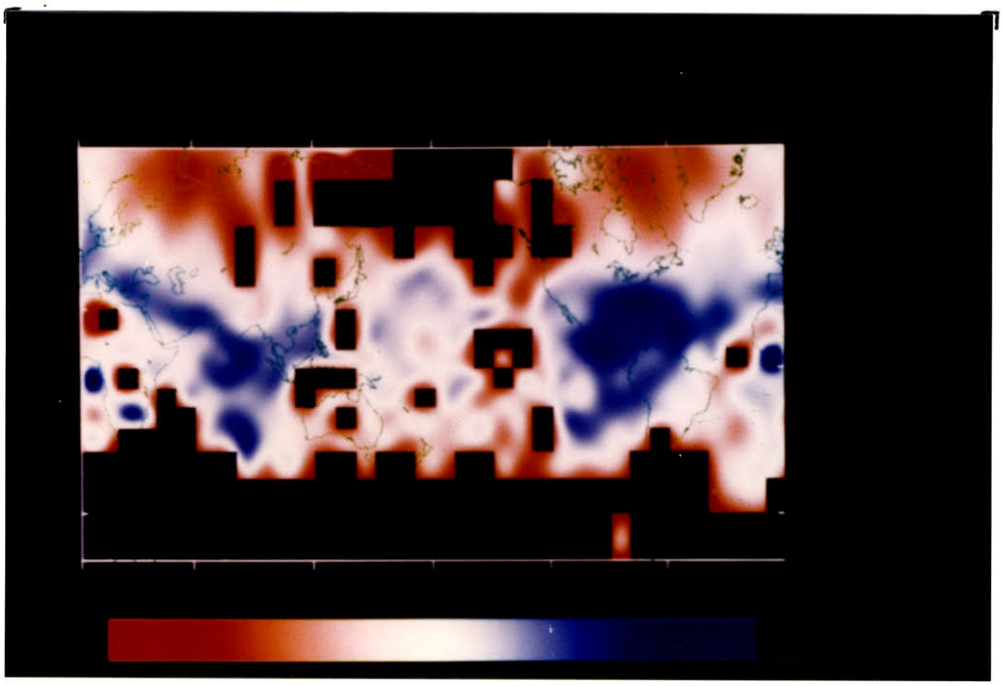

FIGURE 5.10e

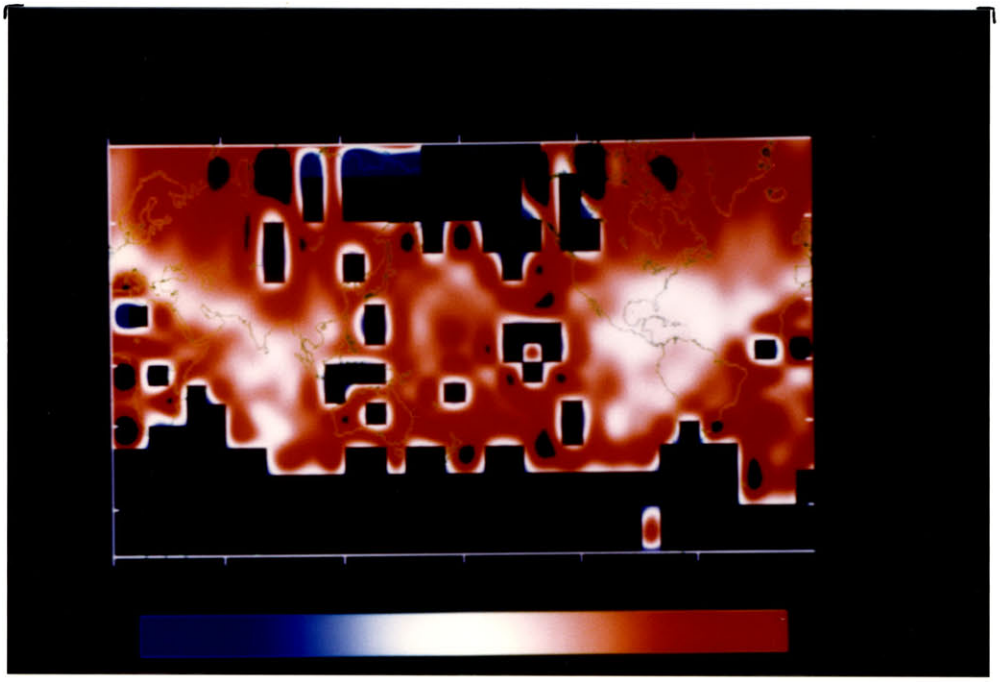

FIGURE 5.10f

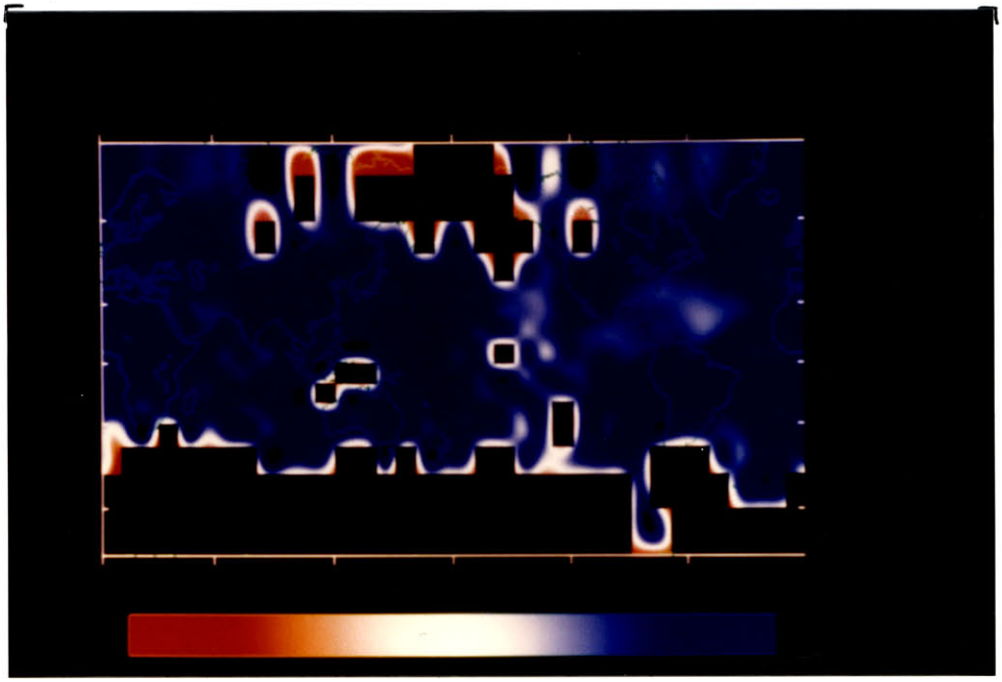

FIGURE 5.11a

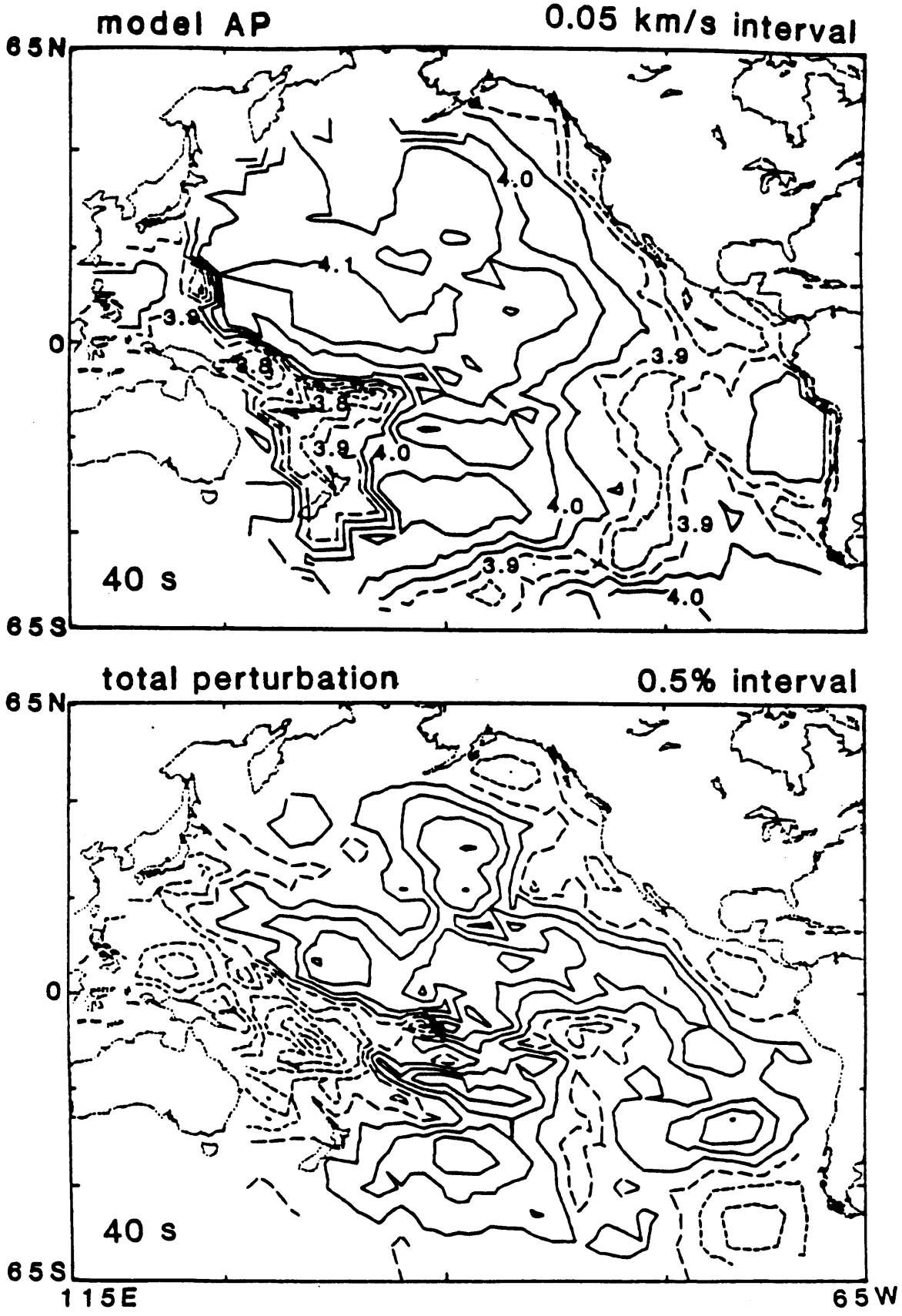
model AP
0.05 km/s interval
65N
0
65S
4.0
4.1
3.9
3.8
3.9
4.0
4.0
3.9
3.9
4.0
40 s
total perturbation
0.5% interval
65N
0
65S
40 s
115E
65W

FIGURE 5.11b

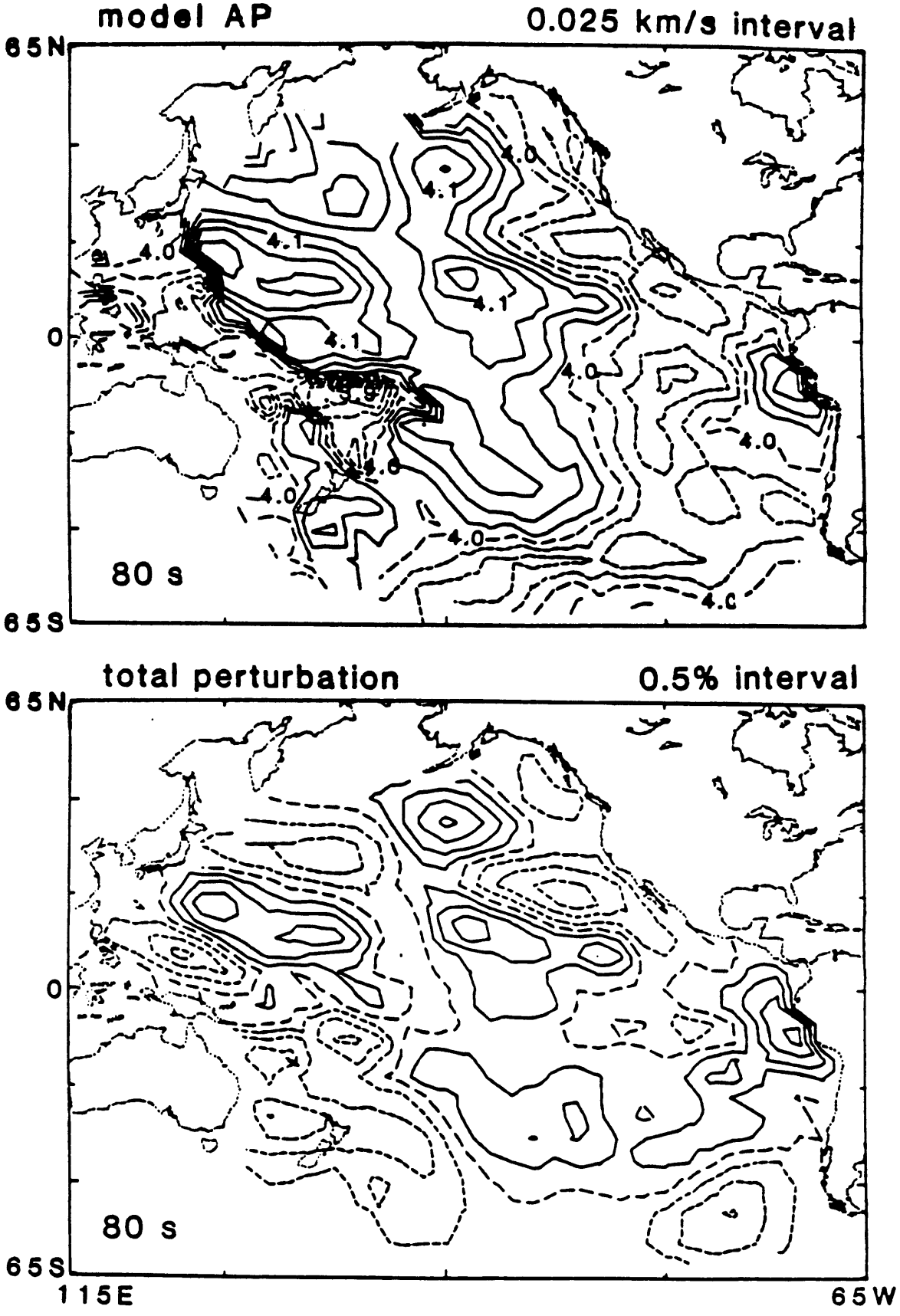
model AP
0.025 km/s interval
65N
0
65S
4.0
4.1
80 s
total perturbation
0.5% interval
65N
0
65S
80 s
115E
65W

FIGURE 5.12

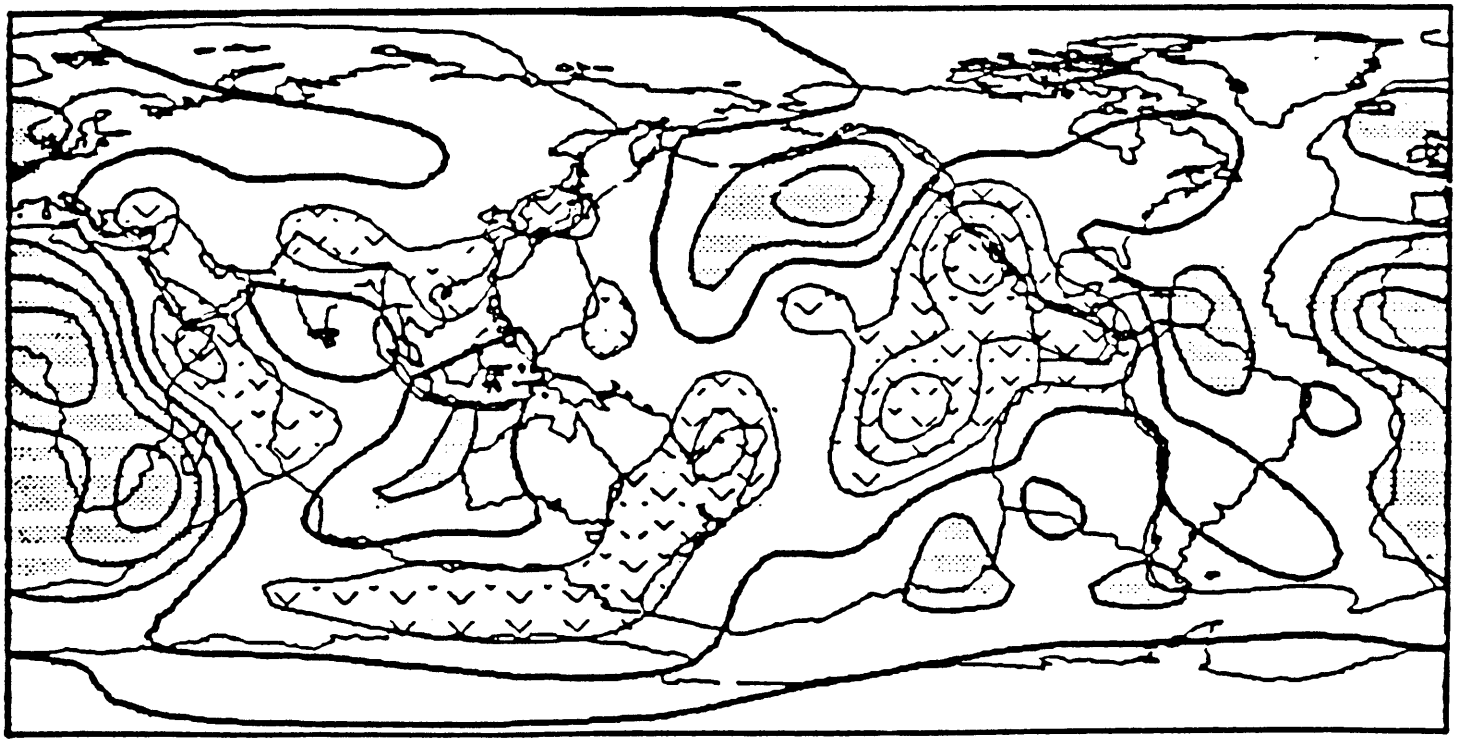

FIGURE 5.13

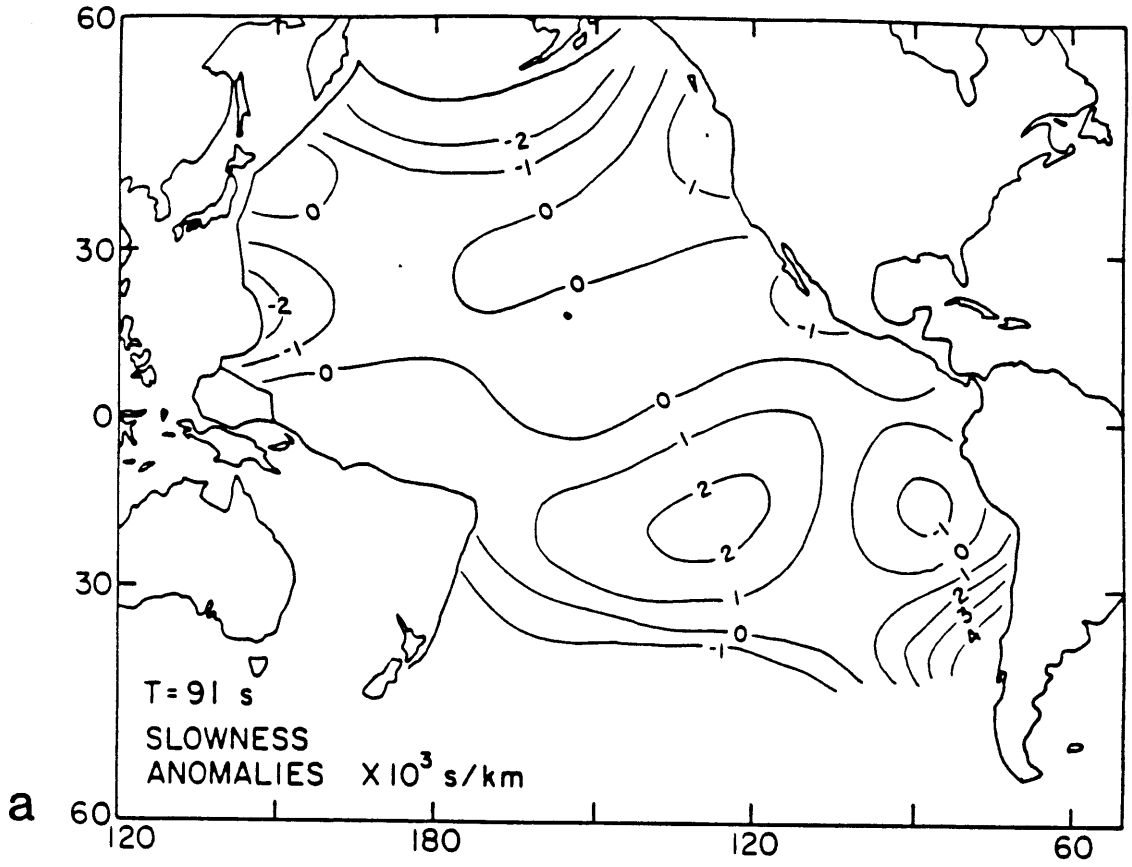

a

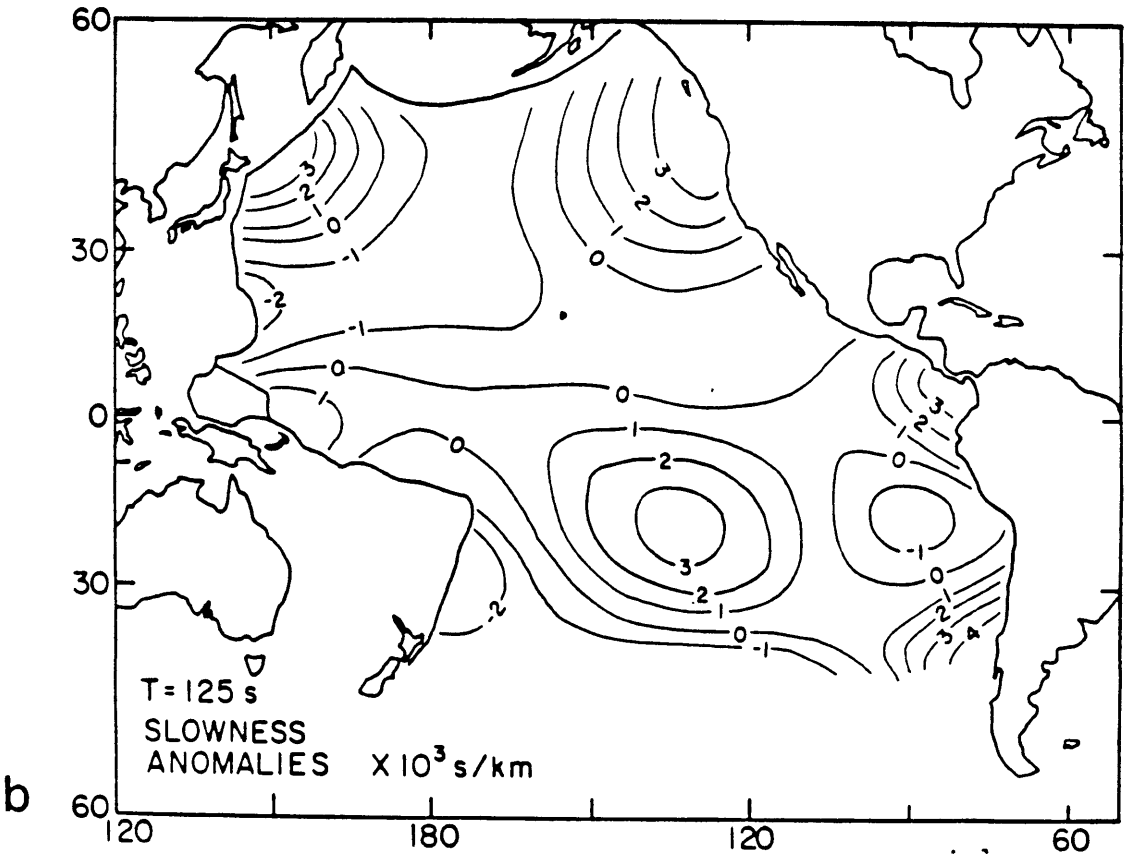

b

FIGURE 5.13 (continued)

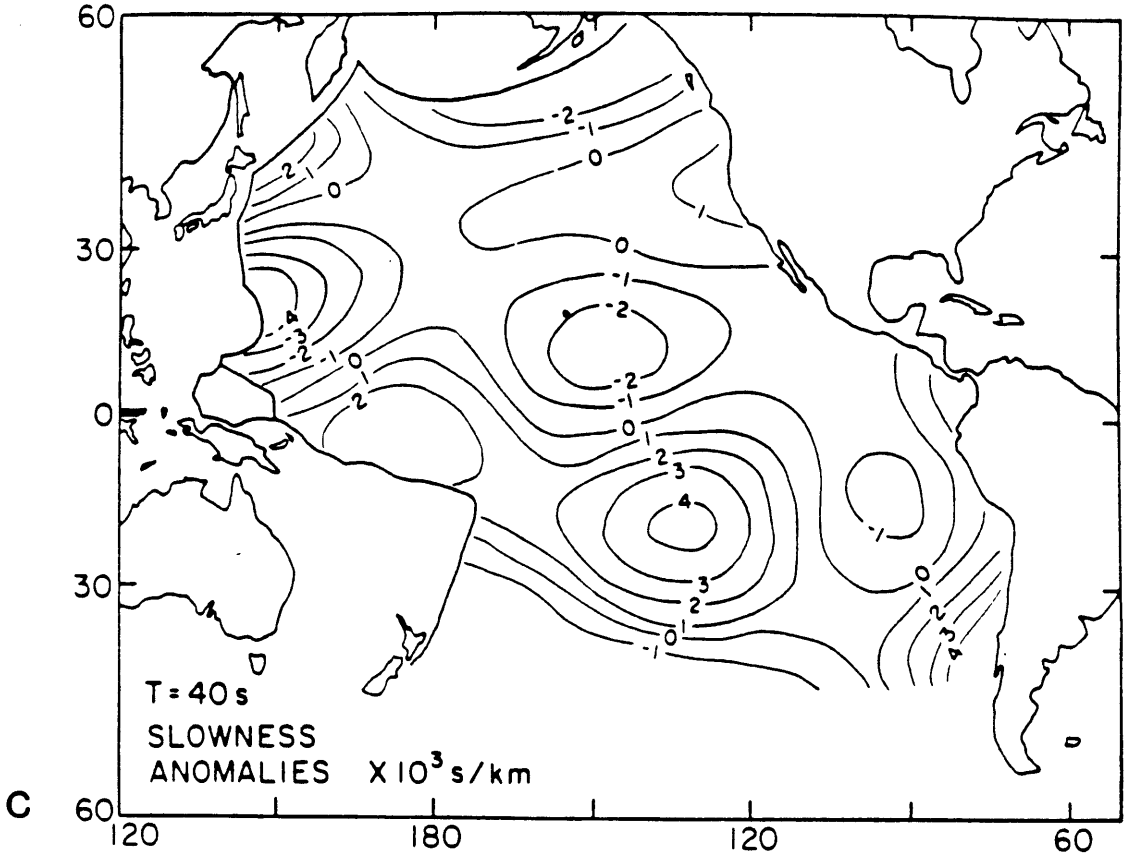

c

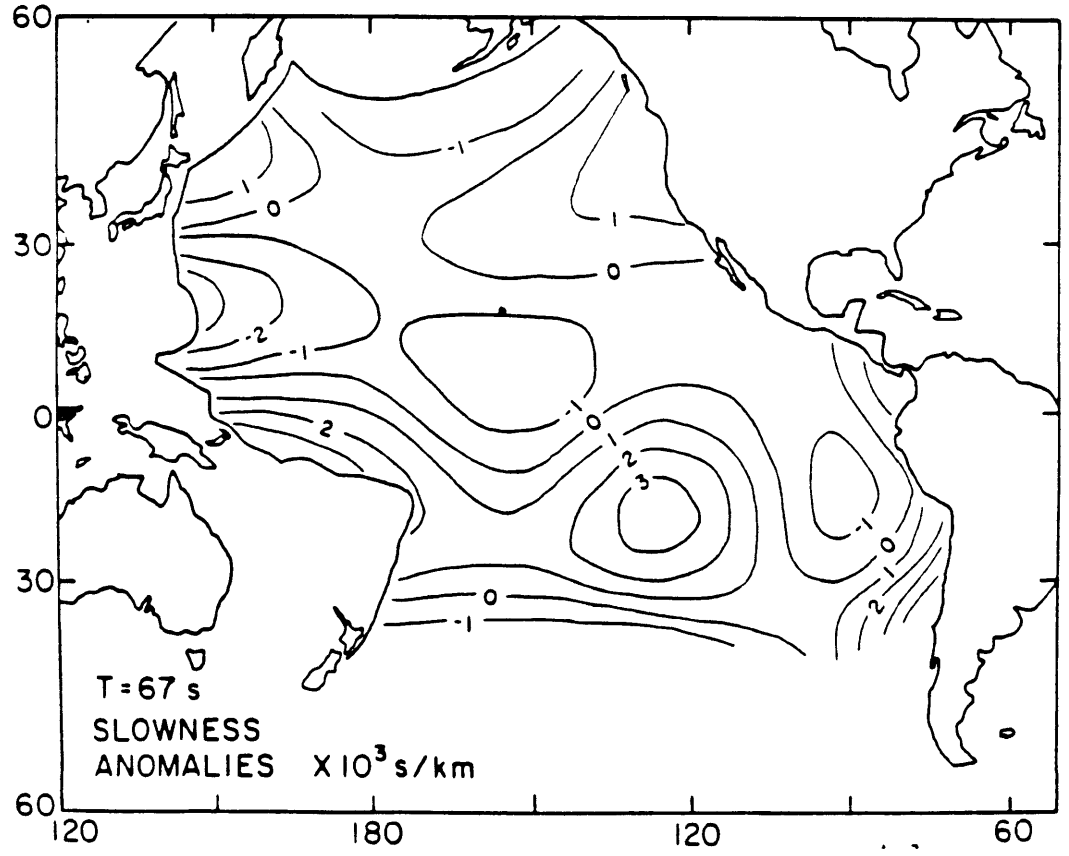

d

FIGURE 5.14

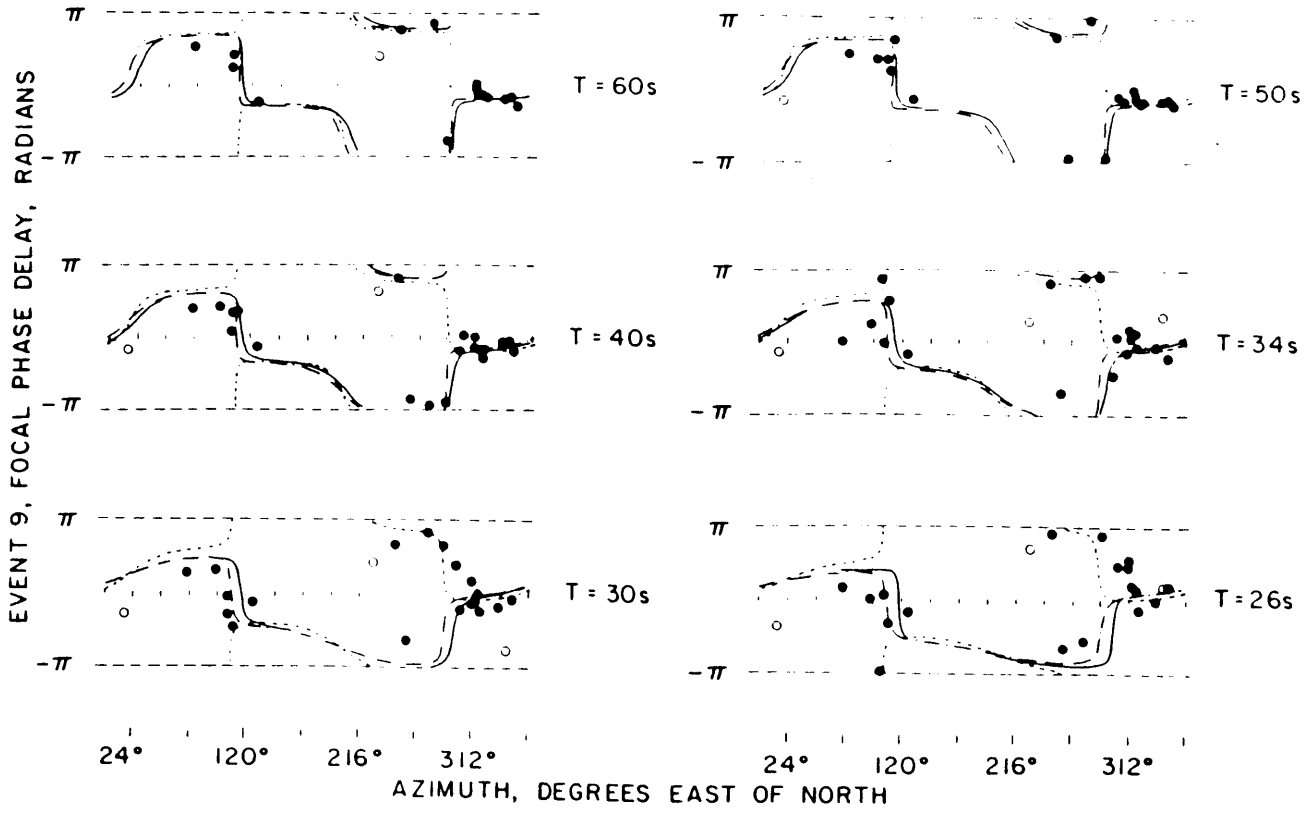
EVENT 9, FOCAL PHASE DELAY, RADIANS
π
-π
T = 60s
T = 50s
T = 40s
T = 34s
T = 30s
T = 26s
24°
120°
216°
312°
AZIMUTH, DEGREES EAST OF NORTH

CHAPTER 6

Global regionalization of group velocity of fundamental mode Rayleigh waves for the period range 20 to 100 sec.

6.1 - Introduction:

In this Chapter, we analyze the group velocity data gathered in Chapter 4. There, we used the group velocity measured for each path as a guide to determine which portions of the Rayleigh wave spectrum were suitable for the phase velocity measurement. This data will be used here to determine regional variation of group velocity for the period range 20 to 100 sec, in the same fashion we analyzed the phase velocity data in Chapter 3. We will also discuss an attempt made to invert the group velocity data, using the same method applied to the phase velocity data in Chapter 5.

Let us first review the studies of Tetsuo A. Santô, who used several long-period seismograph stations installed during the International Geophysical Year, and the W.W.S.S.N. stations, to determine the global distribution of the group velocity of fundamental mode Rayleigh waves.

He started with the determination of the group velocity dispersion curves in the 20 to 35 sec period range, for paths between earthquakes around the world and the station at Tsukuba, Japan (Santô, 1960a). He then studied the variation of group velocity in the Pacific area (Santô, 1960b). Santô (1961a) further examined the data measured in the above two works and compared these with dispersion curves published by other authors. A method for regionalization of the group velocity was developed by Santô (1961b) based on the least squares fit of the predicted to the observed times.

The method was then applied to the group velocity data for 78 paths in the period range between 22 and 35 sec to study the whole Pacific region (Santô, 1963) which was divided into seven regions. A similar analysis was extended to Eurasia, Africa, and the Atlantic and Indian Oceans by Santô (1965a), using approximately 200 greatcircle paths of Rayleigh waves in the 20 to 35 sec period range, and a set of seven different region types. The Eurasian continent was examined separetely by Santô (1965b). This time, four region types with the boundaries based on topographic lines, were used. The group velocity data used was separated from the data set of Santô (1965a). This data set was further explored by Santô

(1966), together with some newly measured data in the 20-35 sec period range, to study the Atlantic and Indian Oceans, and the African continent, in a similar fashion. A total of 77, 47, and 38 paths was used for each of the above regions, respectively. The study was extended later by Santô (1967) to the Gulf of Mexico and Caribbean Sea, and by Santô (1968) to the North American and Arctic Ocean regions.

All these group velocity data above, together with some additional information taken from the geophysical literature, were used by Santô and Sato (1966) to determine the group velocity of Rayleigh waves with period of 30 sec in a set of 12 region types globally distributed. This time, the least squares method was applied in the determination of the group velocity. They found a result that showed good agreement with the reference dispersion curves used previously in Santo's regionalization. A global map (mercator projection) was presented showing the distribution of the regional boundaries. Sato and Santô (1969) solved the same problem of the above paper, this time determining the coefficients of the spherical harmonic expansion.

Regionalization of group velocity for Rayleigh waves with longer periods was considered by other workers, such as Savage

and White (1969), who used 103 measurements in the Pacific Ocean; Tarr (1969), who considered a set of 112 group velocity measurements in the North Atlantic and Caribbean Sea. Forsyth (1973) considered several types of models and the anisotropy effects on the propagation of these waves, to regionalize a set of 78 newly measured paths in the Pacific (Nazca plate region). The group velocity of Rayleigh waves propagating in the Pacific was further studied by Yoshii (1975), who measured the dispersion curves for 27 paths in the 40 to 90 sec period range, and later by Yu and Mitchell (1979) and Mitchell and Yu (1980).

6.2 - Regionalization of the group velocity data:

In this section, we apply the method described in section 3.5 to regionalize the group velocity data.

We interpolated the group velocity values of each dispersion curve, so that the values corresponding to the same reference periods used in Chapters 3, 4, and 5, could be determined (we have used other reference period values when we measured these group velocity dispersion curves in the work summarized in Chapter 4). This interpolation process was made using Equations (3.1) and (3.2) (*i.e.* the same process that we

used to interpolate the phase velocity dispersion curves which we collected from the literature). The resulting histograms of all group velocity data for each of the reference periods of 20 thru 98 sec are shown in Figures 6.1 thru 6.9, respectively. We then grouped these data using the same three regionalized Earth models as discussed in section 3.3, with their discretized version shown in Figures 3.11 thru 3.13 for the models of Jordan (1981), Lévêque (1980), and Okal (1977), respectively. This time, we selected ray paths for which more than 40 percent of the total path length lies in one of the specified region, instead of the 70 percent limit used for the phase velocity estimation for each region.

The histogram of group velocity for each region is shown in Appendix C.

In the histograms in Appendix C we have used an increment of 0.01 km/sec of group velocity. We calculated the sample mean $\bar{u}(T)$, and the square root of the sample variance $s^2(T)$ for each region, of each regionalized model, from the distribution curves shown in Appendix C, using Equations (3.8) and (3.9), respectively. These values, together with the number of samples assigned to each region, are shown in Tables 6.1 thru 6.3, for the regionalized Earth models of Jordan

(1981), Lévêque (1980), and Okal (1977), respectively. The sample average and the standard deviation for the whole data set plotted in Figures 6.1 thru 6.9 are also shown in Table 6.1. The sample average values of Tables 6.1 thru 6.3 were plotted in Figures 6.10 thru 6.12, respectively.

6.3 - Statistical analysis of the results of regionalization:

We can compare the models of Jordan (1981), Lévêque (1980), and Okal (1977) in the same fashion as used to compare the regionalized phase velocity for these three models in section 3.6 (*i.e.* we make use again of the hypothesis testing procedure applied to the mean and variance of each region in the models shown in Tables 6.1 thru 6.3).

We chose the value of the significance level α to be again 2 percent in all cases. We also made all the testing procedure considering α to be 20 percent, and obtained almost the same results that we discuss here (just as in Chapter 3).

The results of the above tests for the value of α equal to 2 percent are shown in Tables 6.4 thru 6.6, for the models of Jordan (1981), Lévêque (1980), and Okal (1977), respectively. We can compare the performance of these tests

by considering the percentage of the cases treated which show the regions to have different mean: 76, 92, and 69 percent for the models of Jordan (1981), Lévêque (1980), and Okal (1977), respectively. As we can see, the performance of the models of Jordan (1981), and Okal (1977), have roughly the same effectiveness, in contrast with the much better performance of the four-region model of Lévêque (1980), which has the disadvantage of assuming a much coarser regionalization.

6.4 - Inversion of travel time data for the global velocity distribution:

In this section, we describe an attempt to invert the group velocity data by the same method as described in Chapter 5 to determine the global distribution of phase velocity for all nine reference periods considered.

Since most of the paths used in the phase velocity study of Chapter 5 are the same in the group velocity data set, the operator G of Equation (5.4) will be very similar between the two inverse problems.

We used Jordan's regionalization with group velocity given in Table 6.1 as our initial model. We have eliminated the rays which showed the absolute value of the residual

travel time larger than four percent of the total travel time, and required that only blocks with more than 20 ray crossings be included in the inversion process. For each run, we calculated the root mean square of the velocity variations, the average value of the diagonal element of the resolution matrix, the average total standard deviation, the average standard deviation due to random error in the data, the average standard deviation due to the poor resolution of the process, and the percentage of the total standard deviation which is represented by this latter variable.

We have considered the data corresponding to the 50 sec reference period. The most striking difference between this data set and the phase velocity data set is evident when we compare the initial data variance of these two: we found that $\langle d^2 \rangle$ is about four times greater for the group velocity data (Table 6.7). If we consider Equation (5.4), from the parameterization of our problem,

$$\mathbf{d} = \mathbf{Gm} + \mathbf{n}$$

we notice that the difference in $\langle d^2 \rangle$ can be due to difference in either **m** or in **n**. In other words, we need to

know if group velocity actually varies more than phase velocity, or if group velocity measurements have more errors than the phase velocity ones.

If we consider the first of these possibilities, we are assuming that $\sigma^2_{mU} > \sigma^2_{mc}$, but $\sigma^2_{nU} \cong \sigma^2_{nc}$. In this case, the damping constant for the group velocity inversion should be chosen four times smaller than in the phase velocity inversion procedure. We tried this possibility and found solutions with unacceptable error (*i.e.* the resulting velocity variations were in most cases smaller than the total error bound).

We can compare Tables 6.1 thru 6.3 with the corresponding phase velocity results of Tables 3.1 thru 3.3, and try to verify the possibility of $\sigma^2_{mU} > \sigma^2_{mc}$. Consider the particular case of 50 sec waves in Jordan's model. We chose this period because it is the one with larger amount of data, and the signal to noise ratio is larger than in other cases. The only significant difference found between σ_{mU} and σ_{mc} is for the cases of oceanic regions 'a', and 'c', which represent, respectively, very young and old oceanic areas. Note that, for the intermediate-age oceanic region, the model variance is basically the same for the phase and group velocity models. This is important due to the much denser sampling of this

region types compared to the other oceanic regions. In the continental regions, the agreement between the two model variances is very good, indicating that the first possibility is not the most likely.

Let us now examine the possibility if the noise variance (measurement error) may be different between group and phase velocity data. The phase velocity is defined as the velocity at which the phase of waves (peaks, zeros and troughs) propagates, and is given by

$$c = \frac{\omega}{k}$$

where ω is frequency and k is wave number. The group velocity on the other hand, is the velocity of propagation of wave packet or energy with frequency ω, and is given by

$$U = \frac{d\omega}{dk}$$

What we are considering in the measurement of these two is the observable phase difference $\Delta\varphi(\omega)$ between two points separated by a distance Δ. The expressions for the phase and group

velocities are then given by

$$\frac{1}{c} = \frac{1}{\Delta} \frac{\Delta\varphi(\omega)}{\omega}$$

$$\frac{1}{U} = \frac{1}{\Delta} \frac{d}{d\omega} (\Delta\varphi(\omega))$$

If we consider that the observed phase difference $\Delta\varphi(\omega)$ can be in error by $\Delta\varphi(\omega) \pm \delta\varphi(\omega)$, we see that the error in $\frac{1}{c}$ and $\frac{1}{U}$ are respectively,

$$\Delta\left[\frac{1}{c}\right] = \frac{1}{\Delta} \frac{\delta\varphi(\omega)}{\omega}$$

$$\Delta\left[\frac{1}{U}\right] = \frac{1}{\Delta} \frac{\partial}{\partial\omega} (\delta\varphi(\omega))$$

Thus, the error in group velocity measurement is related to the derivative of phase difference with respect to ω. If one tries to measure $\frac{1}{U}$ by the Fourier transform and estimating the derivative by finite difference, one can anticipate a greater error for $\frac{1}{U}$ than for $\frac{1}{c}$.

This basic difference between the accuracy of these two parameters has long been known. Evernden (1953, 1954) concluded that the phase velocity is the most important

parameter to study the Earth structure using surface wave data. The same point was emphasized by Ewing and Press (1959). Other authors, such as Pilant (1967), Weidner (1972), and Soriau-Thevenard (1976a), all concluded that their phase velocity measurements were much more accurate than the group velocity measurements performed the same paths which they studied.

It is then reasonable to accept that the initial data variance of the group velocity data is much larger than the initial data variance of the phase velocity data, due to the larger measurement errors for group velocity. We accepted this case and concluded that, for the group velocity inverse problem, a damping constant greater than the one used in the phase velocity study is needed in order to achieve acceptable error levels. We list the results of one run of our inversion computer program, performed to invert the data set for waves with 50 sec period. This run was performed using a constant damping constant for all blocks, as done in Chapter 5 while treating the phase velocity data. Notice that the average resolution is much lower than the level achieved in our phase velocity study. This is due to the stronger damping used here, which could not be enhanced by requiring that the blocks

used had more hits than in the phase velocity study. Even though the result of the inversion procedure summarized in Table 6.7 showed some similarity with some major tectonic features, we do not have enough confidence in the results due to the poor resolution associated with most of the blocks studied.

As we can see in Table 6.7, the residual variance obtained in the inversion process is about four times larger than that obtained in the inversion of the phase velocity data (Table 5.7). It is also of the same order of the residual variance obtained by Feng and Teng (1983b), who inverted a similar set of group velocity data in Eurasia, using a discretized model with the same block size of our work (10^{o} by 10^{o}). The standard deviation of their solution, listed in Table 4 of their work, is 29.68 sec for Rayleigh waves with period of 49.95 sec, while the standard deviation of our solution is about 30 sec for similar waves with period of 50 sec (considering the values for the residual variance listed in Table 6.7). The method used by Feng and Teng (1983b) to measure the group velocity values, discussed in a previous paper (Feng and Teng, 1983a) is of the same type of that used in our work, and show approximately the same error size. They

do not show the errors and resolution associated with the solution of the blocks they studied, but the similarity between our and their study indicates that the error may be greater than the variation of solution.

TABLE 6.1 - JORDAN'S MODEL - GROUP VELOCITY (includes also all data)

REGION / T (sec)	a	b	c	p	q	s	ALL DATA
20	3.646 51 0.170	3.544 183 0.187	3.487 20 0.174	3.072 10 0.162	3.169 51 0.177	3.194 11 0.101	3.440 414 0.237
30	3.787 95 0.126	3.770 427 0.145	3.735 55 0.177	3.336 41 0.178	3.457 184 0.199	3.452 19 0.092	3.647 1056 0.211
40	3.816 106 0.105	3.856 449 0.105	3.876 60 0.137	3.597 48 0.132	3.644 228 0.140	3.671 18 0.084	3.775 1163 0.143
50	3.802 104 0.083	3.868 444 0.090	3.901 60 0.113	3.729 49 0.065	3.733 234 0.107	3.819 18 0.068	3.824 1168 0.105
60	3.776 100 0.073	3.858 428 0.085	3.901 58 0.103	3.781 47 0.061	3.758 230 0.103	3.885 18 0.040	3.833 1137 0.094
70	3.748 96 0.065	3.832 375 0.081	3.871 53 0.089	3.792 44 0.062	3.763 218 0.100	3.903 18 0.034	3.822 1042 0.088
80	3.723 91 0.065	3.804 340 0.083	3.840 48 0.093	3.790 42 0.060	3.760 207 0.100	3.894 16 0.041	3.804 971 0.088
90	3.697 82 0.070	3.774 283 0.086	3.814 41 0.070	3.793 37 0.061	3.747 188 0.105	3.873 12 0.057	3.783 853 0.090
98	3.681 68 0.064	3.757 224 0.086	3.787 29 0.064	3.785 30 0.063	3.751 159 0.096	3.866 10 0.075	3.769 700 0.089

TABLE 6.2 - LÉVÊQUE'S MODEL - GROUP VELOCITY

REGION / T (sec)	N	=	U	
20	3.638 74 0.183	3.513 214 0.195	3.172 52 0.144	3.305 76 0.227
30	3.763 137 0.150	3.757 483 0.157	3.427 161 0.153	3.544 253 0.212
40	3.805 150 0.116	3.861 507 0.107	3.667 184 0.110	3.695 295 0.143
50	3.801 148 0.089	3.880 501 0.089	3.786 185 0.079	3.762 303 0.103
60	3.781 146 0.082	3.874 486 0.082	3.834 182 0.076	3.781 297 0.096
70	3.756 136 0.074	3.851 439 0.075	3.855 162 0.065	3.777 276 0.088
80	3.730 127 0.072	3.827 398 0.077	3.853 154 0.062	3.769 259 0.084
90	3.703 115 0.075	3.800 338 0.078	3.840 138 0.067	3.755 233 0.085
98	3.682 97 0.073	3.780 266 0.079	3.831 115 0.073	3.751 205 0.077

TABLE 6.3 - OKAL'S MODEL - GROUP VELOCITY

REGION / T (sec)	N	#	=	-	0	.	✗
20	3.593 57 0.204	3.514 161 0.208	3.501 32 0.158	3.540 4 0.124	3.167 68 0.164	3.233 19 0.191	3.331 14 0.225
30	3.755 95 0.124	3.739 354 0.174	3.778 58 0.147	3.789 9 0.138	3.436 213 0.166	3.483 73 0.202	3.665 45 0.165
40	3.802 100 0.088	3.843 376 0.113	3.897 60 0.099	3.884 9 0.129	3.666 244 0.120	3.617 94 0.138	3.757 55 0.107
50	3.795 101 0.072	3.866 376 0.087	3.929 53 0.067	3.913 9 0.121	3.785 250 0.080	3.691 95 0.101	3.771 57 0.103
60	3.779 100 0.064	3.862 361 0.075	3.919 50 0.066	3.947 9 0.119	3.831 246 0.076	3.709 93 0.096	3.770 55 0.100
70	3.755 94 0.060	3.837 325 0.074	3.879 40 0.060	3.900 7 0.090	3.845 228 0.072	3.712 86 0.093	3.752 47 0.095
80	3.732 88 0.057	3.812 296 0.075	3.844 33 0.075	3.875 6 0.085	3.842 220 0.070	3.705 80 0.089	3.729 45 0.090
90	3.707 75 0.059	3.783 256 0.081	3.813 26 0.073	3.862 5 0.102	3.828 198 0.073	3.692 71 0.095	3.705 40 0.093
98	3.688 60 0.052	3.764 203 0.086	3.785 20 0.076	3.810 2 0.099	3.819 162 0.071	3.699 60 0.081	3.703 32 0.089

TABLE 6.4 - JORDAN'S MODEL

T (sec)	REGIONS axb	axc	axp	axq	axs	bxc	bxp	bxq	bxs	cxp	cxq	cxs	pxq	pxs	qxs
20	N Y	N Y	N Y	N Y	N Y	N N	N Y	N Y	N Y	N Y	N Y	N Y	N N	N N	N N
30	N N	Y N	Y Y	Y Y	N Y	N N	N Y	Y Y	N Y	N Y	N Y	Y Y	N Y	Y Y	Y N
40	N Y	N Y	N Y	Y Y	N Y	Y N	N Y	Y Y	N Y	N Y	N Y	N Y	N N	N N	Y N
50	N Y	Y Y	N Y	Y Y	N N	N Y	Y Y	N Y	N N	Y Y	N Y	N Y	Y N	N Y	N Y
60	N Y	Y Y	N N	Y N	Y Y	N Y	Y Y	N Y	Y Y	Y Y	N Y	Y N	Y N	N Y	Y Y
70	N Y	Y Y	N Y	Y N	Y Y	N Y	N Y	Y Y	Y Y	Y Y	N Y	Y N	Y Y	Y Y	Y Y
80	Y Y	Y Y	N Y	Y Y	N Y	N Y	Y N	N Y	Y Y	Y Y	N Y	Y Y	Y Y	N Y	Y Y
90	N Y	N Y	N Y	Y Y	N Y	N Y	N N	N Y	N Y	N N	Y Y	N Y	Y Y	N Y	N Y
98	Y Y	N Y	N Y	Y Y	N Y	N N	N N	N N	N Y	N N	Y Y	N Y	Y Y	N Y	N Y

Example: null hypotheses when comparing regions i and ii:

Y<--- σ^2_i and σ^2_{ii} are different? Yes
N<--- m_i and m_{ii} are different? No

TABLE 6.5 - LÉVÊQUE'S MODEL

T (sec)	REGIONS Nx=	NxO	Nx∅	=xO	=x∅	Ox∅
20	N Y	N Y	N Y	Y Y	N Y	Y Y
30	N N	N Y	Y Y	N Y	Y Y	Y Y
40	N Y	N Y	N Y	N Y	Y Y	Y Y
50	N Y	N N	N Y	N Y	N Y	Y Y
60	N Y	N Y	N N	N Y	N Y	Y Y
70	N Y	N Y	N Y	N N	N Y	Y Y
80	N Y	N Y	N Y	Y Y	N Y	Y Y
90	N Y	N Y	N Y	N Y	N Y	Y Y
98	N Y	N Y	N Y	N Y	N Y	N Y

Example: null hypotheses when comparing regions i and ii:

Y<--- σ^2_i and σ^2_{ii} are different? Yes
N<--- m_i and m_{ii} are different? No

TABLE 6.6 - OKAL'S MODEL

T (sec)	REGIONS														
	Nx#	Nx=	Nx-	Nx0	Nx.	Nx/	#x=	#x-	#x0	#x.	#x/	=x-	=x0	=x.	=x/
20	N Y	N N	N N	N Y	N Y	N Y	N N	N N	N Y	N Y	N Y	N N	N Y	N Y	N Y
30	Y N	N N	N N	Y Y	Y Y	N Y	N N	N N	N Y	N Y	N Y	N N	N Y	Y Y	N Y
40	Y Y	N Y	N Y	Y Y	Y Y	N Y	N Y	N N	N Y	N Y	N Y	N N	N Y	Y Y	N Y
50	N Y	N Y	Y N	N N	Y Y	Y N	N Y	N N	N Y	N Y	N Y	Y N	N Y	Y Y	Y Y
60	N Y	N Y	Y Y	N Y	Y Y	Y N	N Y	N Y	N Y	Y Y	Y Y	Y N	N Y	Y Y	Y Y
70	N Y	N Y	N Y	N Y	Y Y	Y N	N Y	N N	N N	N Y	N Y	N N	N Y	Y Y	Y Y
80	Y Y	N Y	N Y	N Y	Y N	Y N	N N	N N	N Y	N Y	N Y	N N	N N	N Y	N Y
90	Y Y	N Y	N Y	N Y	Y N	Y N	N N	N N	N Y	N Y	N Y	N N	N N	N Y	N Y
98	Y Y	N Y	N Y	Y Y	Y N	Y N	N N	N N	N Y	N Y	N Y	N N	N N	N Y	N Y

TO BE CONTINUED

Example: null hypotheses when comparing regions i and ii:

Y<--- σ^2_i and σ^2_{ii} are different? Yes
N<--- m_i and m_{ii} are different? No

TABLE 6.6 - OKAL'S MODEL
(CONTINUED)

T (sec)	REGIONS -xØ	-x.	-xØ	Øx.	ØxØ	.xØ
20	N Y	N Y	N N	N N	N Y	N N
30	N Y	N Y	N N	N N	N Y	N Y
40	N Y	N Y	N Y	N Y	N Y	N Y
50	N Y	N Y	N Y	Y Y	N N	N Y
60	N Y	N Y	N Y	Y Y	Y Y	N Y
70	N N	N Y	N Y	Y Y	Y Y	N N
80	N N	N Y	N Y	N Y	N Y	N N
90	N N	N Y	N Y	Y Y	N Y	N N
98	N N	N N	N N	N Y	N Y	N N

Example: null hypotheses when comparing regions i and ii:

Y<--- σ^2_i and σ^2_{ii} are different? Yes
N<--- m_i and m_{ii} are different? No

TABLE 6.7

GROUP VELOCITY - PERIOD 50 sec FOR THIS PERIOD:
initial data variance= 1866.2941 sec^2 no of observations= 1077 no blocks=225
average path length = 7788.926 km

REGION	NUMBER OF BLOCKS STUDIED	RMS VEL VARIATIONS (%)	AVERAGE RESOLUTION	AVER TOTAL STD DEV (%)	AVER STD DEV DUE TO RANDOM ERROR (%)	AVER STD DEV DUE TO POOR RESOL (%)	% TOTAL ERROR DUE TO POOR RESOL
a	32	2.707	0.456	2.021	1.185	1.624	64.550
b	66	2.430	0.426	2.076	1.186	1.688	66.096
c	23	1.673	0.393	2.121	1.085	1.771	69.680
p	25	2.076	0.439	2.060	1.221	1.655	64.518
q	54	2.783	0.442	2.046	1.216	1.629	63.385
s	25	1.269	0.331	2.241	1.099	1.929	74.050

FOR THE ABOVE RUN: σ_m= 2.8%
θ^2=1,200,000 sec^2 residual variance= 910.6685 sec^2 variance improvement= 51.20%

Chapter 6 - Figure Captions

Figures 6.1 thru 6.9 - Histogram of the group velocity at reference periods from 20 thru 98 sec. A velocity increment of 0.01 km/sec was used to construct these histograms.

Figures 6.10 thru 6.12 - Plot of the average phase velocity value $\bar{c}(T)$ measured for each region of the Earth models shown in Figures 3.11 thru 3.13, respectively.

FIGURE 6.1

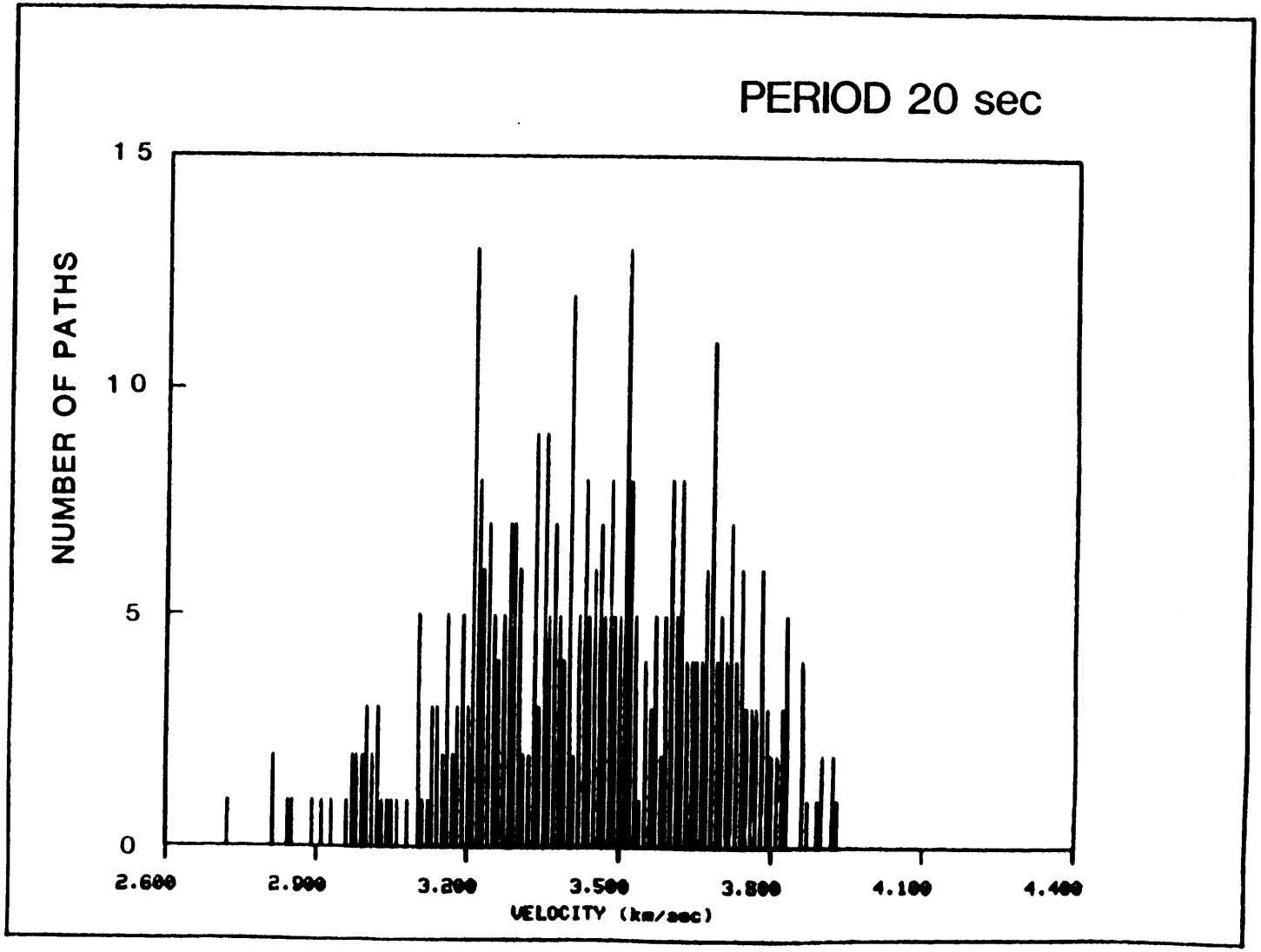
PERIOD 20 sec
NUMBER OF PATHS
15
10
5
0
2.600
2.900
3.200
3.500
3.800
4.100
4.400
VELOCITY (km/sec)

FIGURE 6.2

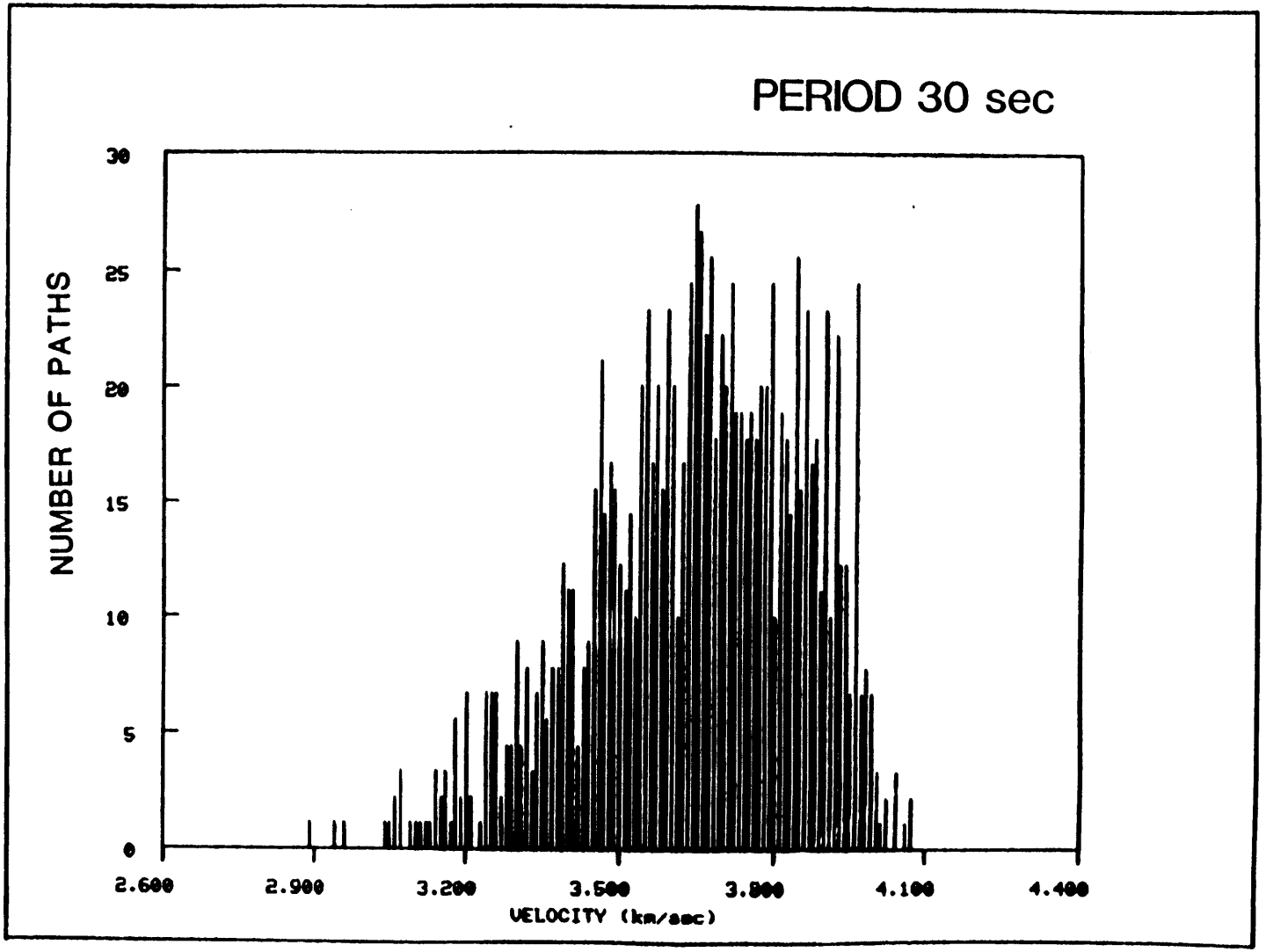
PERIOD 30 sec
NUMBER OF PATHS
30
25
20
15
10
5
0
2.600
2.900
3.200
3.500
3.800
4.100
4.400
VELOCITY (km/sec)

FIGURE 6.3

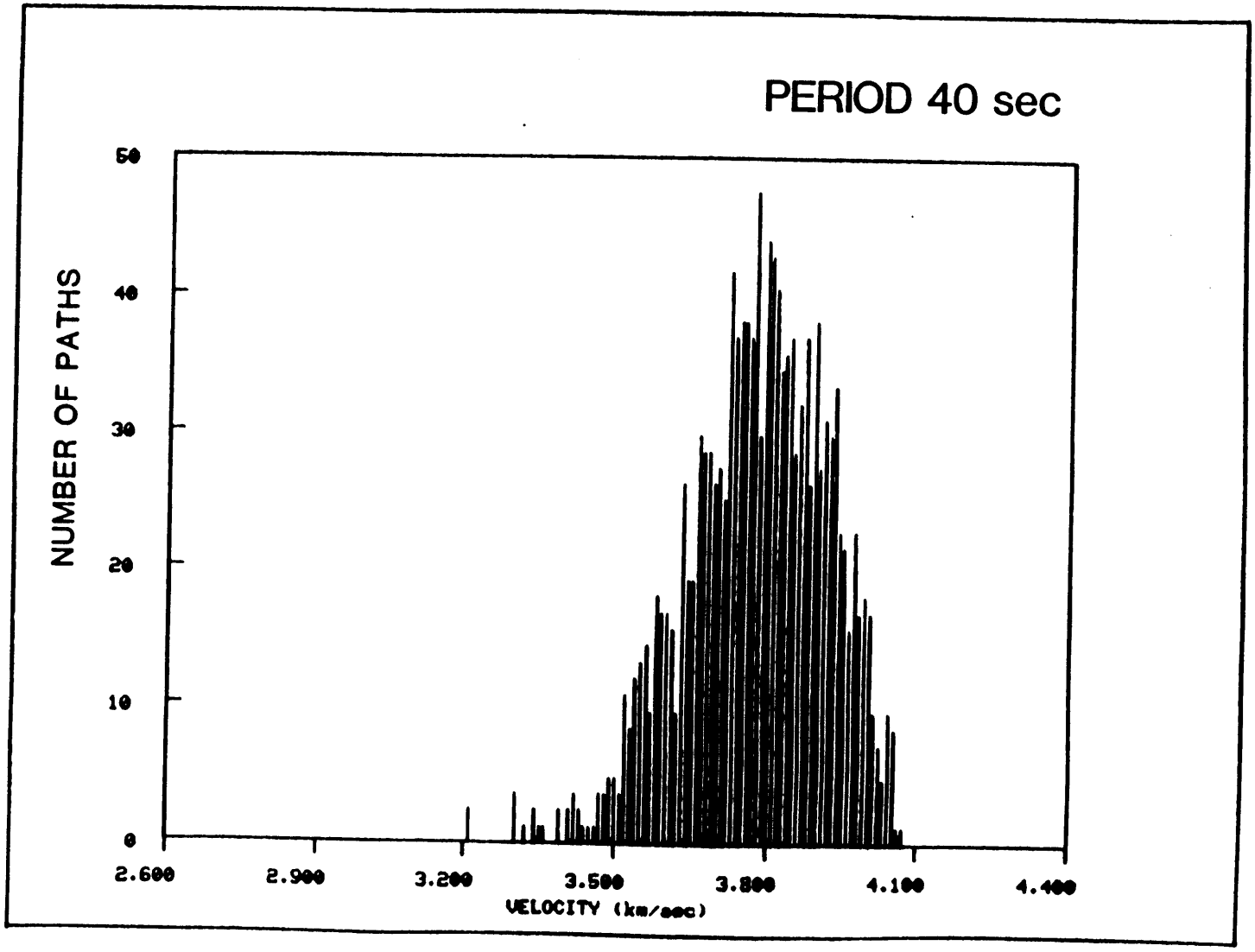
PERIOD 40 sec
NUMBER OF PATHS
50
40
30
20
10
0
2.600
2.900
3.200
3.500
3.800
4.100
4.400
VELOCITY (km/sec)

FIGURE 6.4

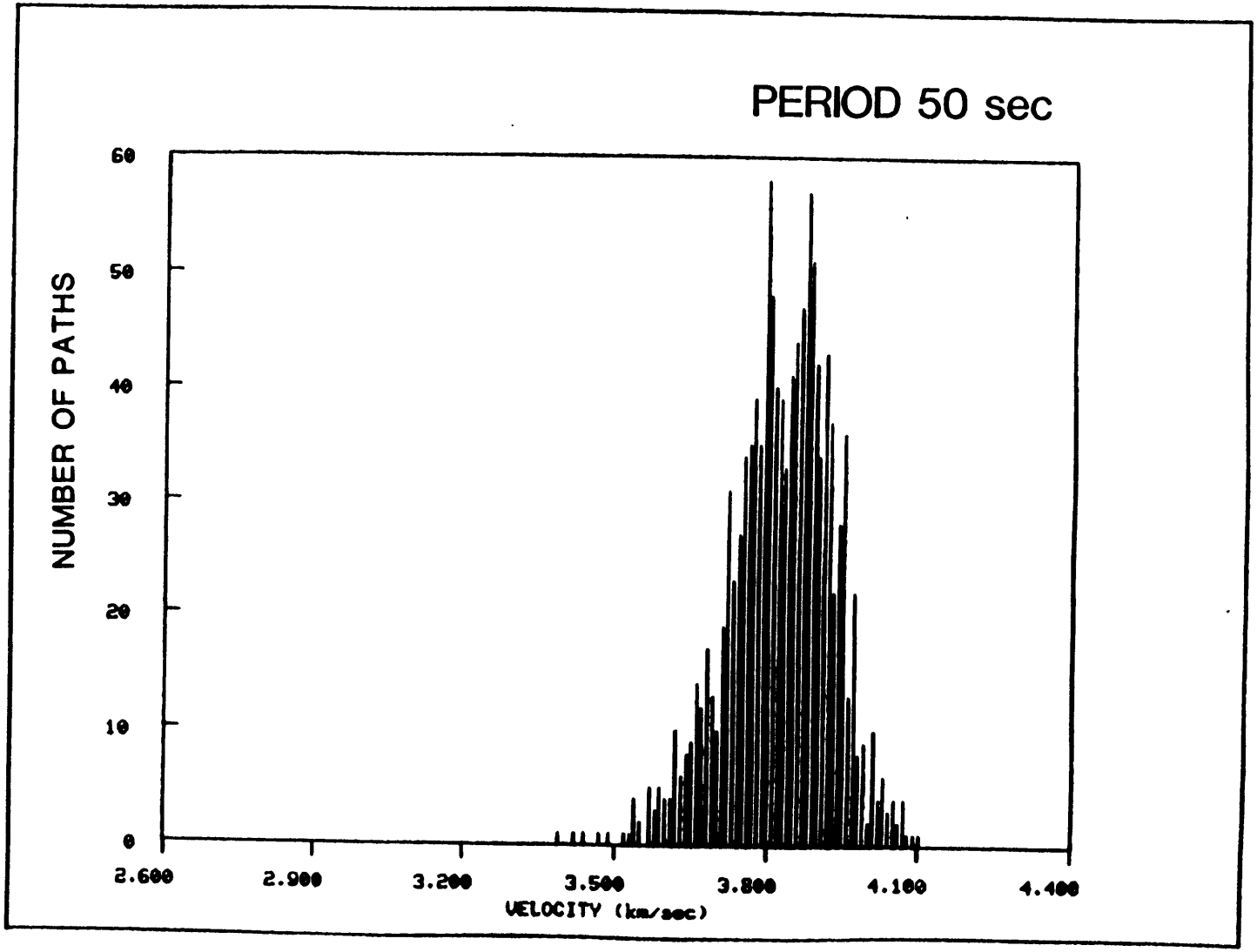
PERIOD 50 sec
NUMBER OF PATHS
60
50
40
30
20
10
0
2.600
2.900
3.200
3.500
3.800
4.100
4.400
VELOCITY (km/sec)

FIGURE 6.5

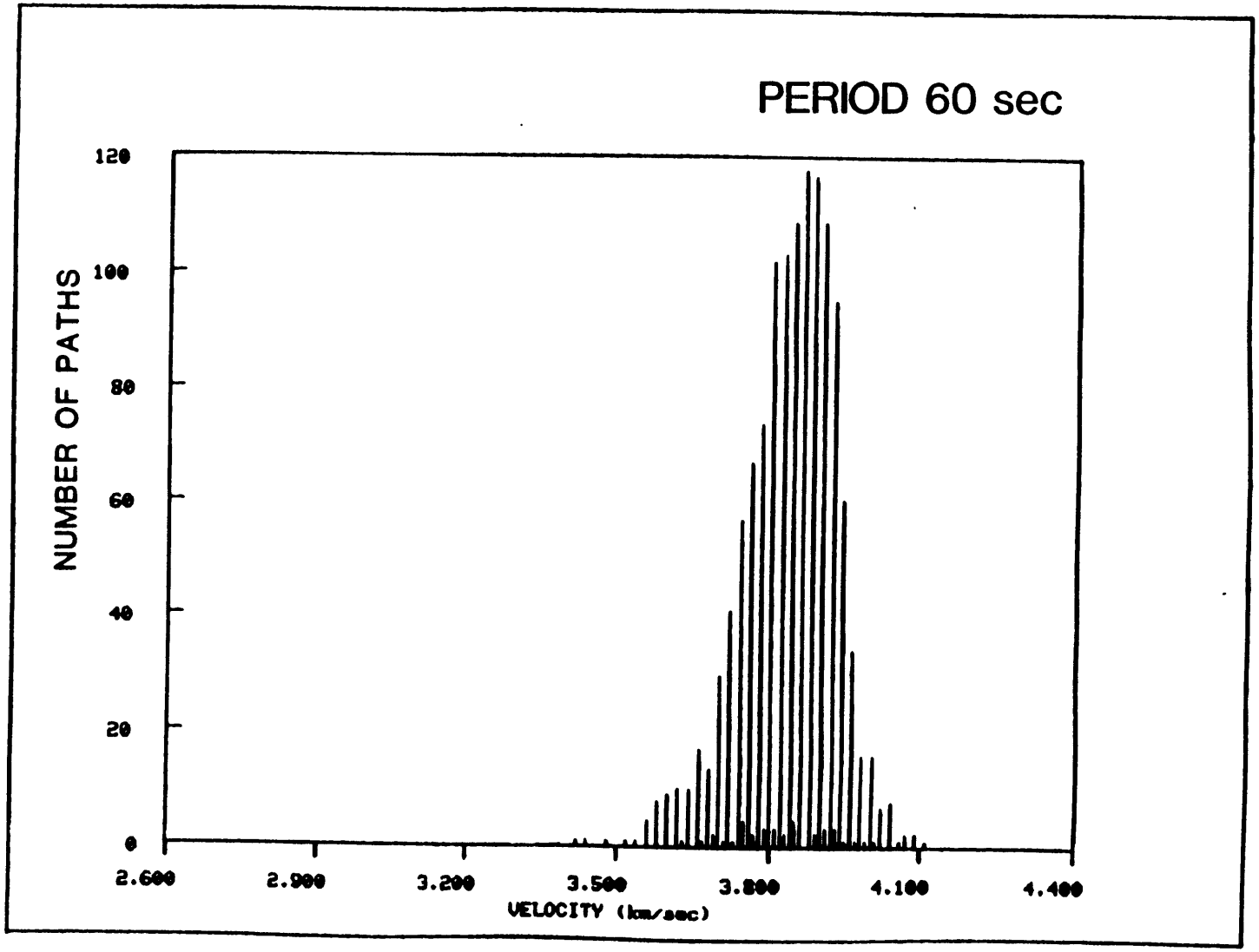
PERIOD 60 sec
NUMBER OF PATHS
120
100
80
60
40
20
0
2.600
2.900
3.200
3.500
3.800
4.100
4.400
VELOCITY (km/sec)

FIGURE 6.6

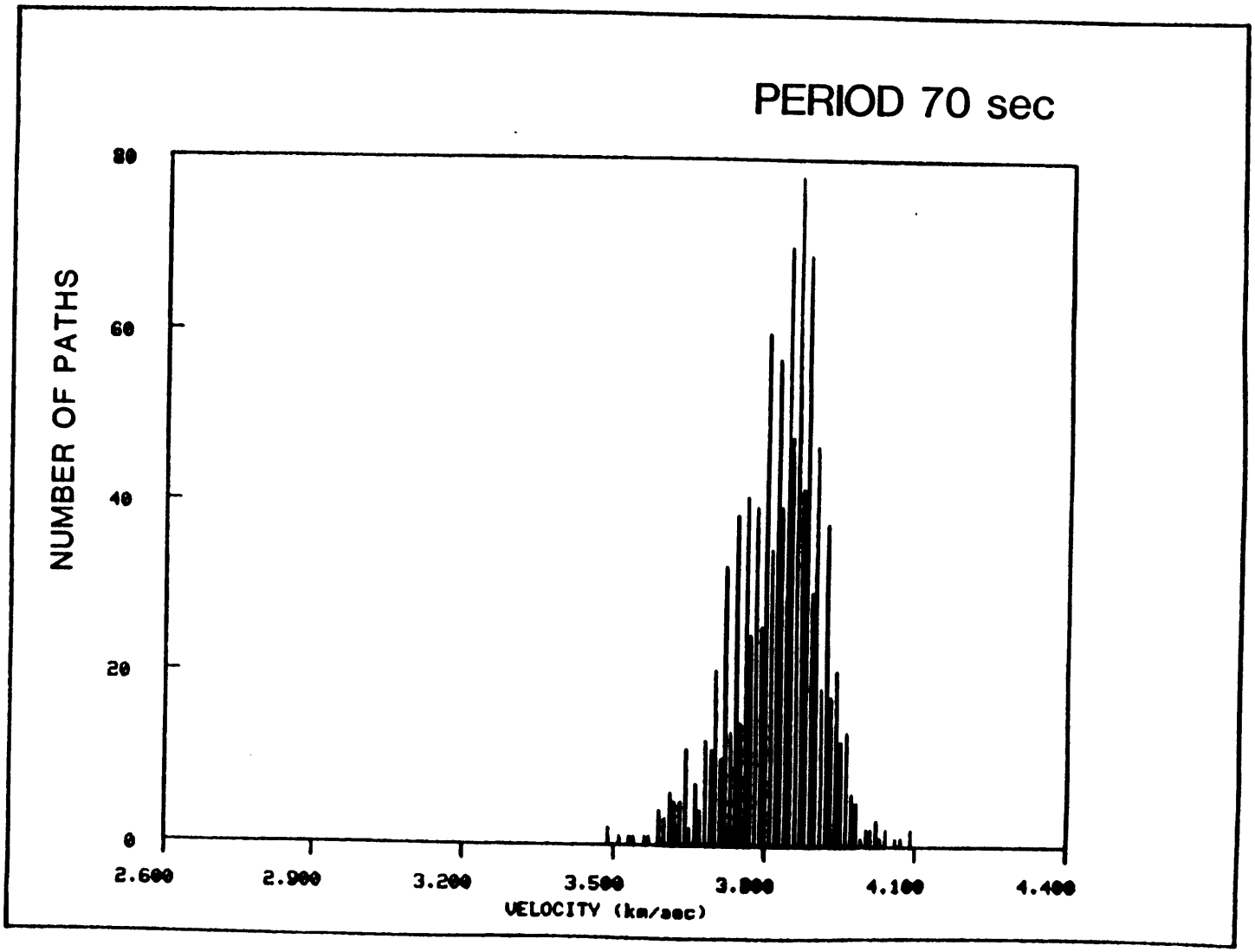
PERIOD 70 sec
NUMBER OF PATHS
80
60
40
20
0
2.600
2.900
3.200
3.500
3.800
4.100
4.400
VELOCITY (km/sec)

FIGURE 6.7

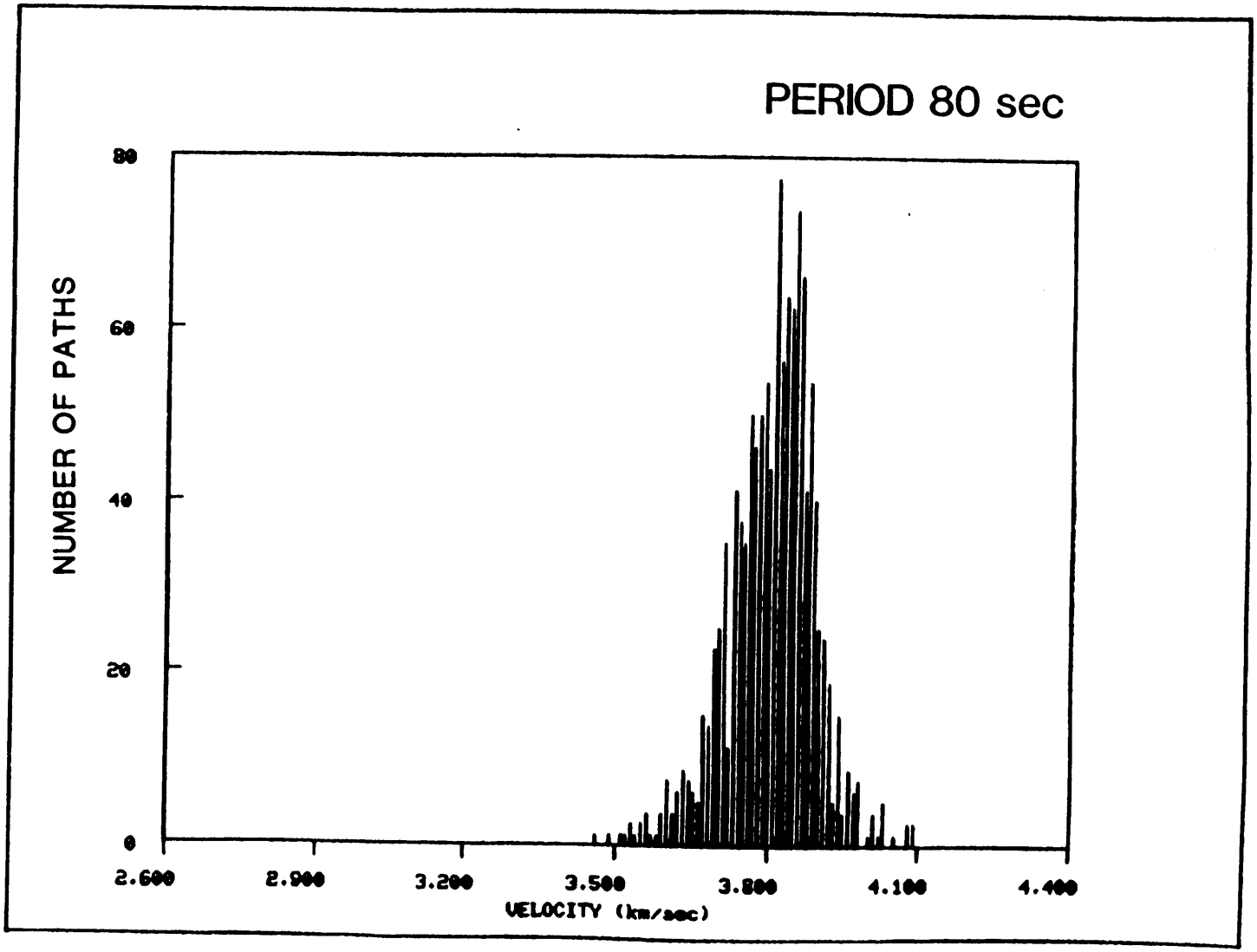
PERIOD 80 sec
NUMBER OF PATHS
80
60
40
20
0
2.600
2.900
3.200
3.500
3.800
4.100
4.400
VELOCITY (km/sec)

FIGURE 6.8

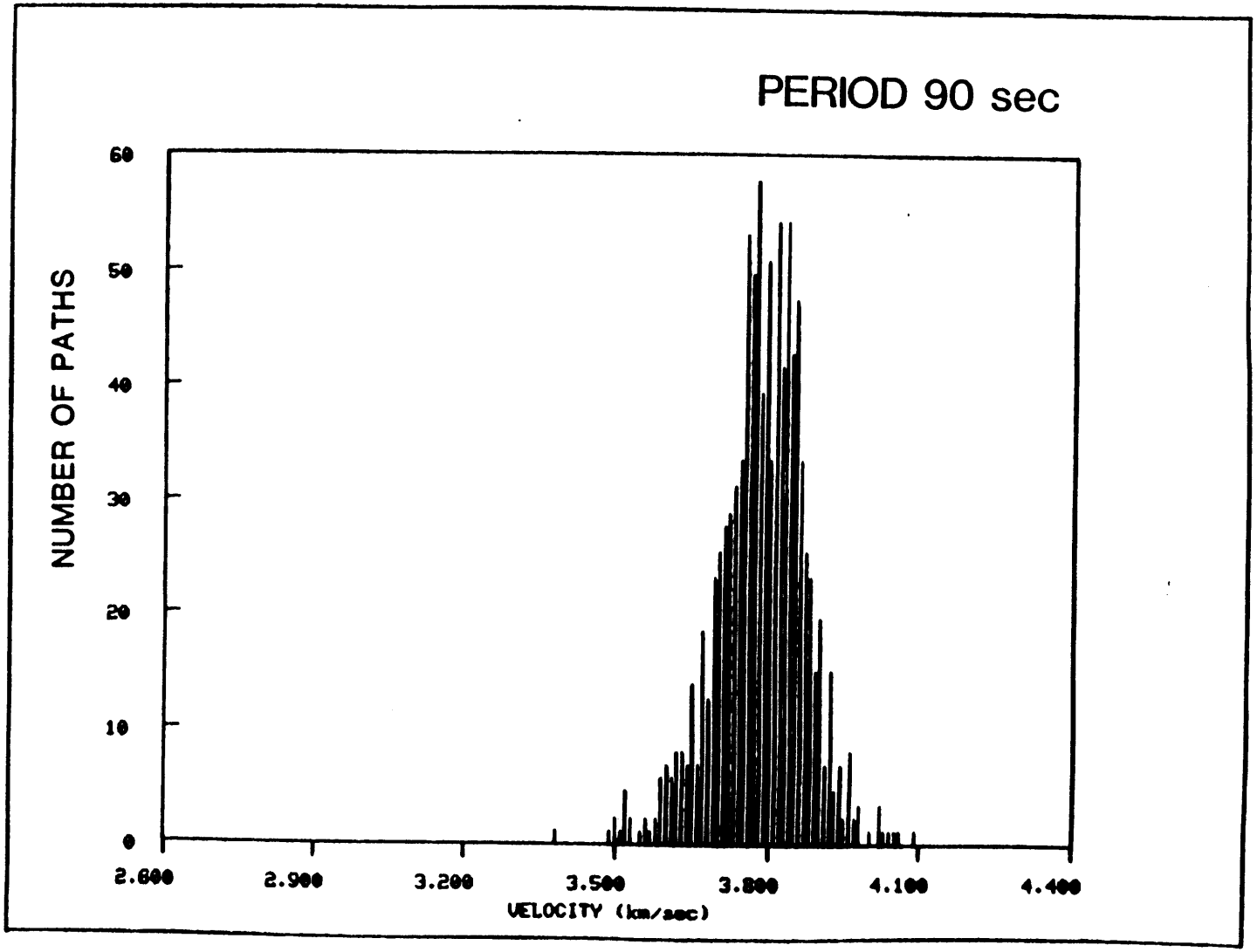
PERIOD 90 sec
NUMBER OF PATHS
60
50
40
30
20
10
0
2.600
2.900
3.200
3.500
3.800
4.100
4.400
VELOCITY (km/sec)

FIGURE 6.9

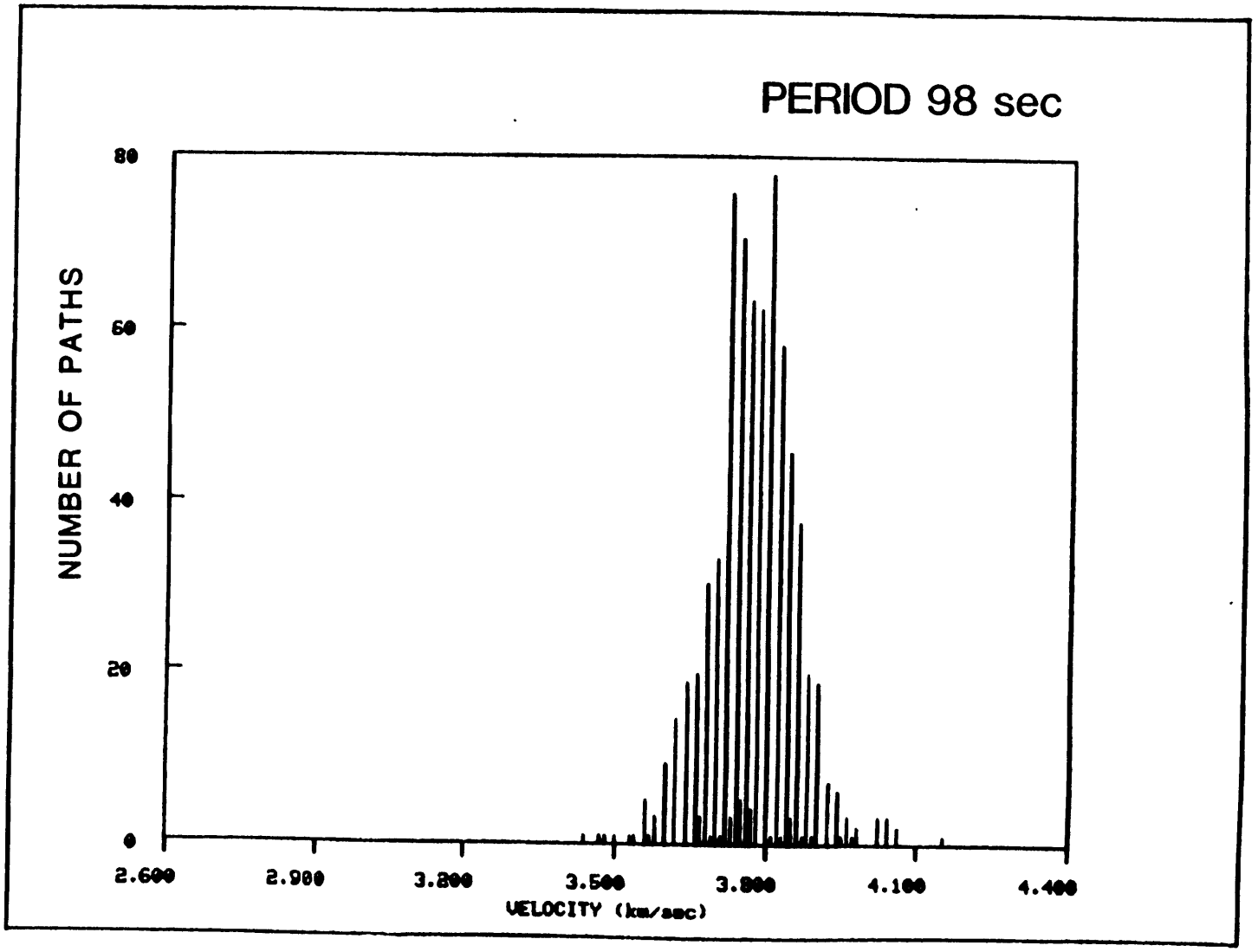
PERIOD 98 sec
NUMBER OF PATHS
80
60
40
20
0
2.600
2.900
3.200
3.500
3.800
4.100
4.400
VELOCITY (km/sec)

FIGURE 6.10

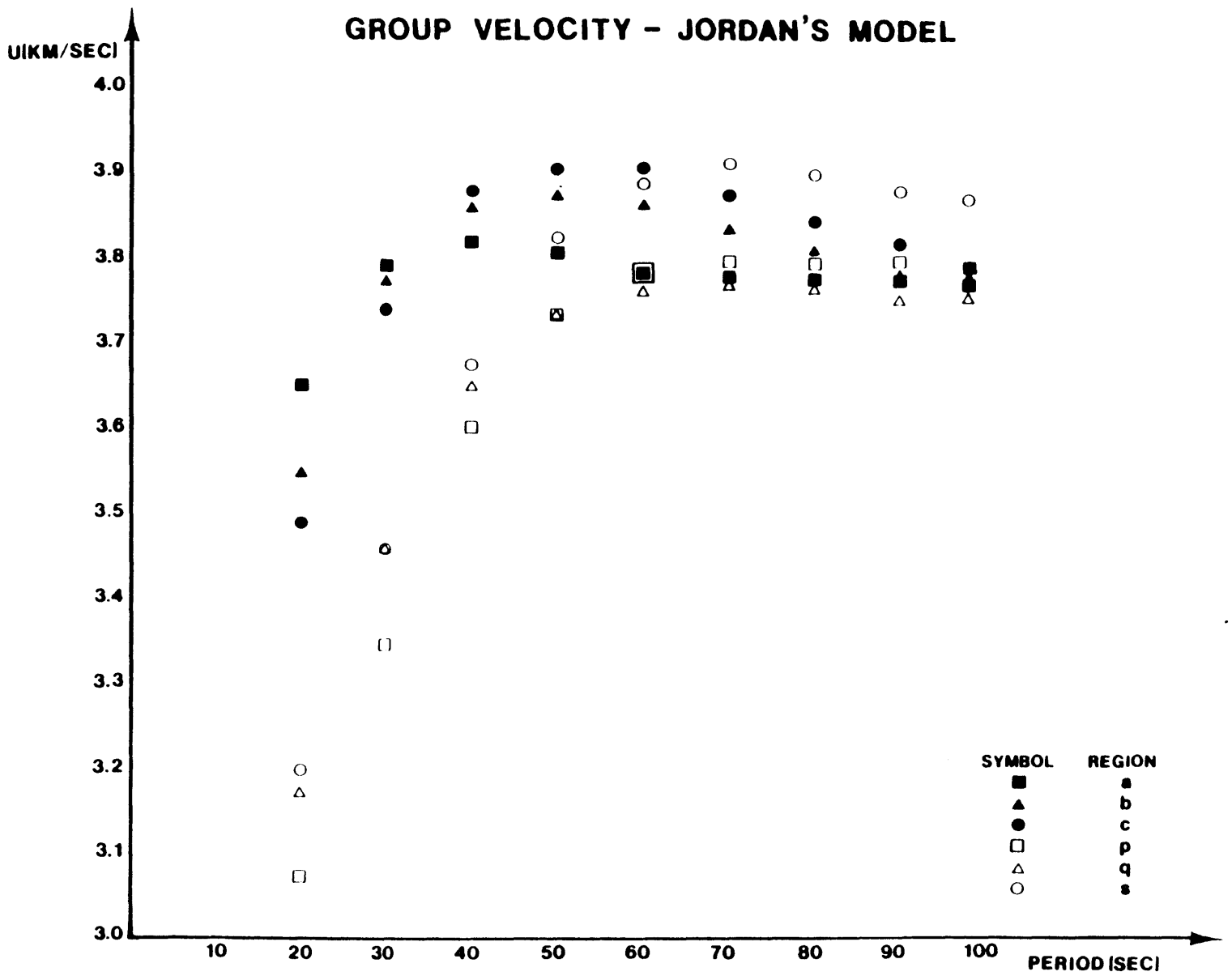
GROUP VELOCITY - JORDAN'S MODEL
U(KM/SEC)
4.0
3.9
3.8
3.7
3.6
3.5
3.4
3.3
3.2
3.1
3.0
10
20
30
40
50
60
70
80
90
100
PERIOD (SEC)
SYMBOL
REGION
a
b
c
p
q
s

FIGURE 6.11

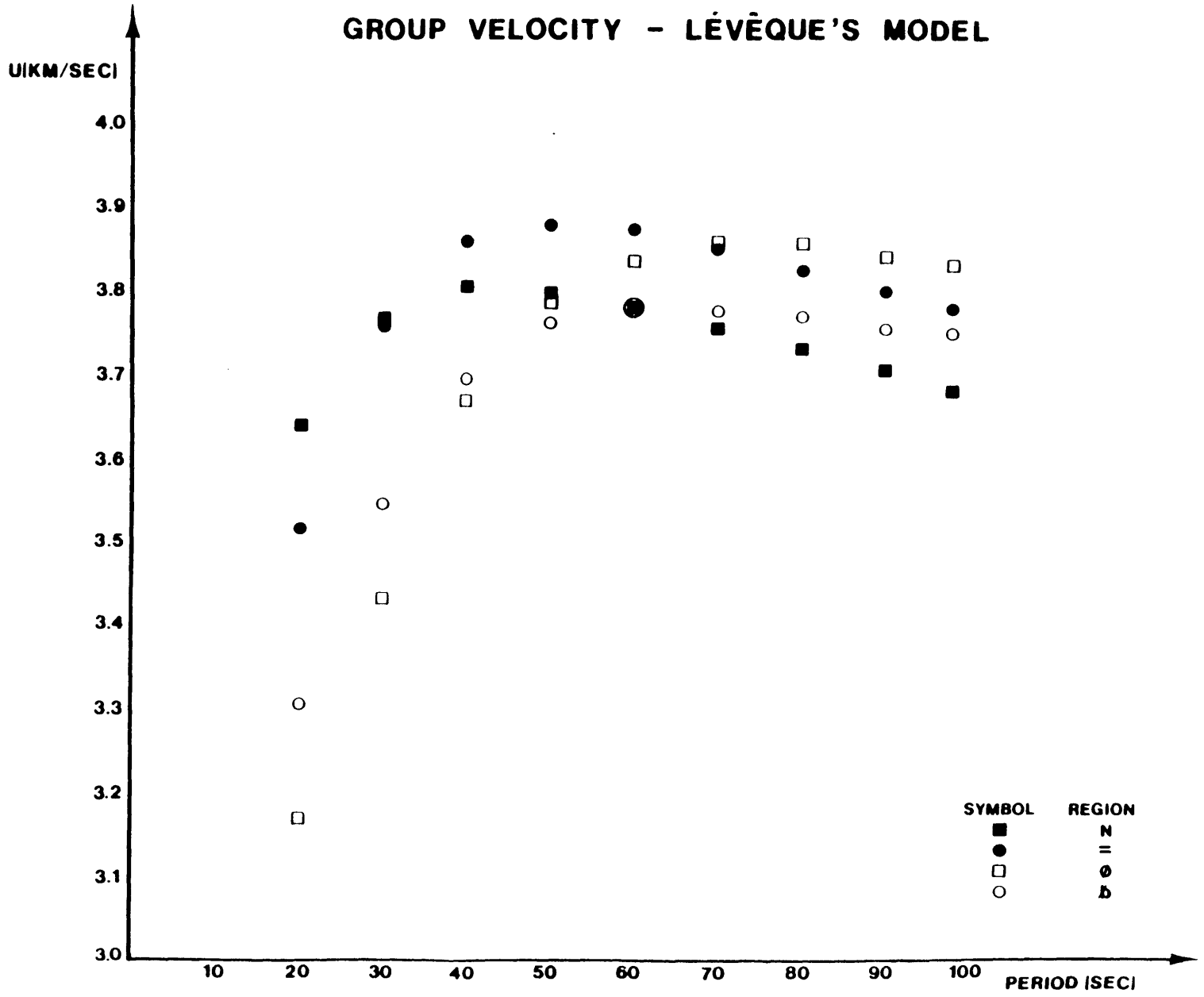
GROUP VELOCITY - LÉVÊQUE'S MODEL
U(KM/SEC)
4.0
3.9
3.8
3.7
3.6
3.5
3.4
3.3
3.2
3.1
3.0
10
20
30
40
50
60
70
80
90
100
PERIOD (SEC)
SYMBOL
REGION
N
=
Ø
Þ

FIGURE 6.12

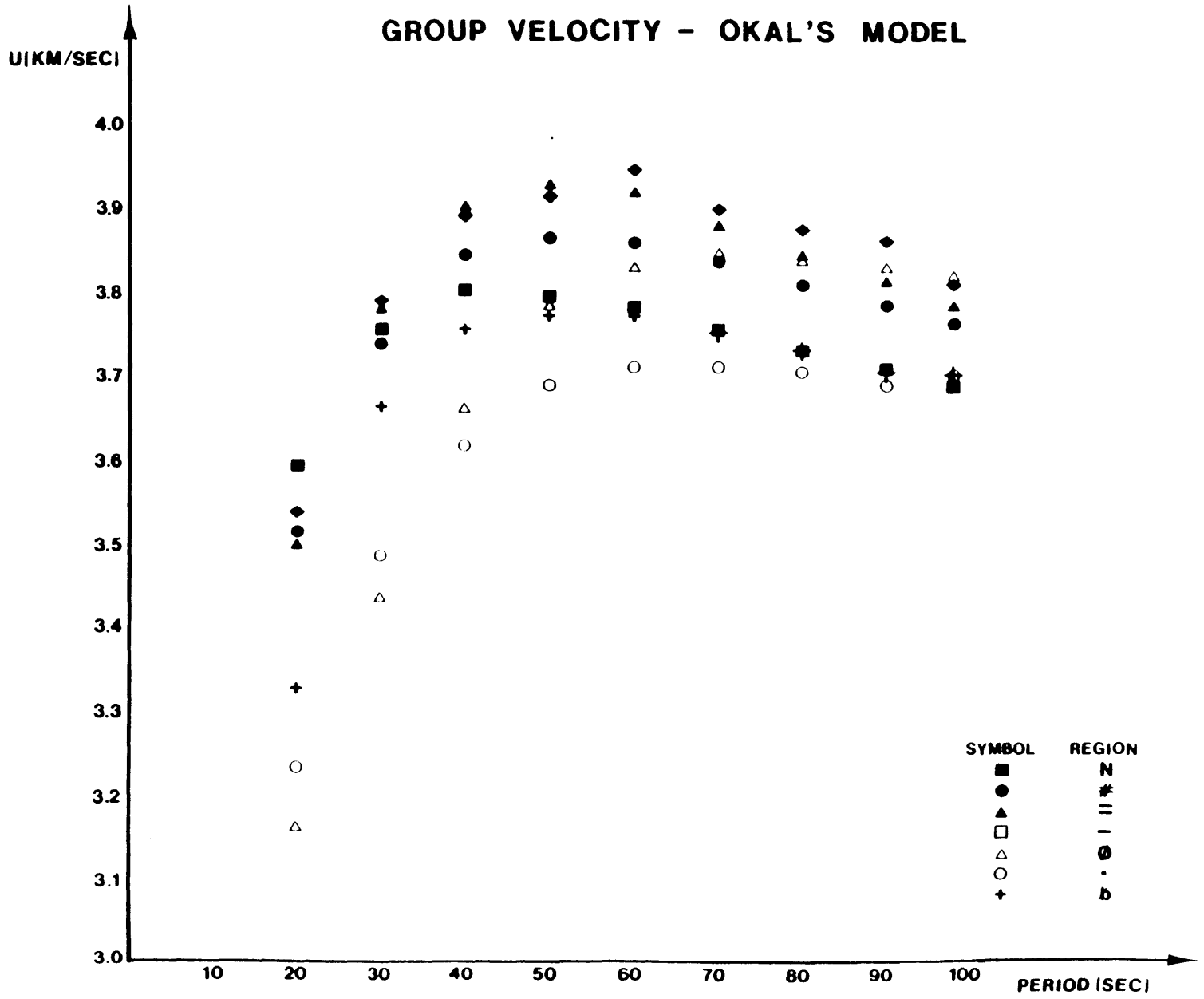
GROUP VELOCITY - OKAL'S MODEL
U(KM/SEC)
4.0
3.9
3.8
3.7
3.6
3.5
3.4
3.3
3.2
3.1
3.0
10
20
30
40
50
60
70
80
90
100
PERIOD (SEC)
SYMBOL
REGION
N

CHAPTER 7

Global regionalization of attenuation coefficients of fundamental mode Rayleigh waves for the period range 20 to 100 sec.

7.1 - Introduction:

We have regionalized the published phase velocity data in Chapter 3. The discretized Earth models used in the regionalization process were used again in Chapter 6 to establish a similar set of regionalized group velocity models. In this chapter, we attempt to do the same for the attenuation coefficient of fundamental mode Rayleigh waves.

In the next section we present a review of previous studies on the attenuation of fundamental mode Rayleigh waves. We assume a sequence based both on the evolution of the measurement methods, and on the chronological order in which the studies were made.

Section 7.3 is related to the data processing sequence which we used to measure the attenuation coefficient, for each of the regions of the model by Jordan (1981), and to the results obtained from these analyses.

7.2 - Previous studies:

Attenuation measurements studies were pioneered by Ewing and Press (1954a,b), who studied higher mode Rayleigh waves. Measurements for fundamental mode Rayleigh waves were only considered after the instalation of the W.W.S.S.N.. Early studies include those by Ben-Menahem (1965), by Tryggvason (1965) in the 10 to 100 sec period range, and by Marshall and Carpenter (1966) in the 20 to 40 sec range. The latter two studies used records of waves generated by nuclear explosions. Other study which used records of nuclear explosions was done later by Burton (1974). This procedure was convenient due to the difficulty of studying records from earthquakes, since the separation of the source and propagation effects was not then a simple problem. This difficulty could be avoided in some other studies (*e.g.* Solomon, 1971) by measuring the attenuation coefficient $\gamma(T)$ (or the quality factor, $Q(T)$), using the two-station method. This method is similar to that used to measure the phase velocity of these waves, which was introduced by Brune and Dorman (1963), and that was reviewed in Chapter 2. It consists of using the amplitude observations A_1 and A_2, at the corresponding stations labeled 1 and 2, respectively, of waves generated by an event which epicenter

lies in the same greatcircle joining the two stations. If these stations are at epicentral distances Δ_1 and Δ_2 (given in km) (or at distances Δ_1' and Δ_2', given in radians), we can obtain the attenuation coefficient $\gamma(T)$ by using,

$$\gamma(T) = \frac{\ln \left[\frac{A_1(T, \Delta_1)}{A_2(T, \Delta_2)} \sqrt{\frac{\sin \Delta_1'}{\sin \Delta_2'}} \right]}{\left[\Delta_2 - \Delta_1 \right]} \qquad (7.1)$$

where the amplitude observations $A_1(T, \Delta_1)$ and $A_2(T, \Delta_2)$ have been corrected for the instrumental response. The square-root term of Equation (7.1) represents the correction applied to account for the geometrical spreading effect.

The corresponding quality factor Q(T) can be obtained by using the observed group velocity U(T) (Brune, 1962b),

$$Q(T) = \frac{\pi}{U(T)\ T\ \gamma(T)} \qquad (7.2)$$

Another method, used to determine both the seismic moment M_o and the attenuation coefficients $\gamma(T)$, was introduced by Tsai and Aki (1969). It involves the use of a single

station-epicenter pair (in a similar fashion of the one-station method used to determine the phase velocity which was introduced by Brune *et al.*, 1960). Consider the observed amplitude at all the stations $A^{O}(T, \Delta)$, after they have been corrected for the instrument response, and the corresponding theoretical amplitude at these stations, $A^{T}(T, \Delta)$. We can then obtain the attenuation coefficient $\gamma(T)$, by fitting a straight line to the graph of observed logarithmic ratios of the observed to the theoretical amplitudes versus epicentral distance Δ (given in km),

$$\ln \left\{ \frac{A^{O}(T, \Delta)\ [R \sin\Delta']}{A^{T}(T, \Delta)} \right\} = b - a\Delta \qquad (7.3)$$

In the above expression, the term inside the brackets represent the correction applied to $A^{O}(T, \Delta)$ to account for the geometrical spreading effect. R is the radius of the Earth, and Δ' is the epicentral distance given in radians. The constants a and b, determined using the least-squares method, represent the attenuation coefficient $\gamma(T)$, and the logarithm of the correction needed for the seismic moment (*i.e.*, we correct the initially assumed seismic moment M_{o}, by

multiplying M_o by the factor e^b). The calculated amplitude $A^T(T, \Delta)$ can be obtained from Equation (4.7) without the term $e^{-\gamma\Delta}$, and without the term $1/[R \sin(\Delta/R)]^{1/2}$, which were used to account for the attenuation , and for the geometrical spreading effects, repectively (*i.e.* we used Equation 4.11). In the calculation of $A^T(T, \Delta)$, Tsai and Aki (1969), proceed in the same manner as in Chapter 4, using the results of the studies by Saito (1967) to evaluate the several terms needed in that equation, which are calculated using a laterally homogeneous layered medium, chosen according to the structure of the source region.

The above method was applied by Tsai and Aki (1969) to determine the attenuation coefficient of fundamental mode Rayleigh and Love waves for the North America region, since they used records of waves that had propagated mostly within that continent. The earthquake used occurred in Parkfield, California, and had the initially estimated seismic moment, M_o, corrected by the factor e^b determined from Equation (7.3).

Solomon (1971) applied the two station method to the path between stations LON and TUC, which are located in western U.S and to the path between stations RCD and ATL, which are in the east-central U.S.. Records from a total of 10 events were

used in the former case, while 6 events were used for the latter. The period range considered was from 15 to 50 sec. This data set was later used by Lee and Solomon (1975) to obtain the depth distribution of the quality factor in these two regions.

Bird and Toksoz (1977) applied the two-station method to Rayleigh waves with period 20 to 80 sec in Tibet. Soriau *et al.* (1980) studied the fundamental mode Rayleigh wave attenuation in the period range 20 to 90 sec for a profile between two stations located in France. Canas and Mitchell (1978) applied the two-station method to measure the attenuation coefficient values for Rayleigh waves in the 18 to 110 sec period range, propagating in the Pacific basin. They further divided this area into three regions according to the seafloor age, and found a systematic decrease of the attenuation coefficient values with age.

Applications of the one-station method of Tsai and Aki (1969) can be found in the work of Mitchell *et al.* (1976), for Rayleigh waves in the 15 to 110 sec period range propagating in the Pacific Ocean, and in the work of Mitchell *et al.* (1977), the latter involves waves with the same period range of the former. This time, they reviewed the previous studies

on the attenuation of the fundamental mode Rayleigh waves, and determined the attenuation coefficients of such waves propagating in the eastern Pacific (from five earthquakes studied by Forsyth (1973) to W.W.S.S.N. stations located in Pacific islands, and in North and South America).

A modification of the one-station measurement method of Tsai and Aki (1969) was introduced by Mitchell (1975), to study the attenuation coefficients of fundamental mode Rayleigh waves propagating in North America. He used records of waves generated by two nuclear explosions with epicenter in western Colorado, U.S., assuming that the amplitude radiation pattern generated by the source can be represented by a function, of which coefficients are obtained by non-linear inversion of the amplitude observations. This modified one-station method was applied by Yacoub and Mitchell (1977) to study the attenuation coefficient values in Eurasia, using records of Rayleigh waves in the 4 to 50 sec period range, generated by six earthquakes, and two nuclear explosions.

Patton (1978, 1980a) determined the attenuation coefficients of Rayleigh waves in the 26 to 60 sec period range for paths between the reference point of his work and W.W.S.S.N. seismographic stations at variable azimuthal

distances. He used the reference point technique, which we reviewed in Chapter 2, and involves the joint determination of perturbations to initially guessed source and propagation parameters from the observed Rayleigh wave spectra, recorded by stations located at different azimuthal directions. The phase velocity and quality factor results were used in a study of the crust and upper mantle structure of Eurasia, which are presented in another paper (Patton, 1980b).

Finally, Romanowicz (1984) used two events and two stations to determine the attenuation coefficient between the two events. The idea is the same as used by Brandon and Romanowicz (1984, 1986) for the establishment of the two-event method for the determination of the phase velocity. Romanowicz (1984) used this technique to study the attenuation of Rayleigh waves in Tibet for the 30 to 90 sec period range.

7.3 - Measurements of regionalized attenuation coefficients:

We took advantage of the large amplitude spectral data accumulated from the phase velocity measurement study summarized in Chapter 4, to determine the attenuation coefficient for six regions of the discretized model of Jordan (1981).

The procedure followed in these measurements make use of the one-station method of Tsai and Aki (1969). Like in the phase velocity measurement problem, the use of a one-station method has the disadvantage of requiring an initial knowledge of the focal mechanism and depth of the earthquakes used. On the other hand, this method does not involve any assumption on the character of regions outside the propagation path, as in the case of the two-station method in which, we have to assume that the waves are not signifficantly affected by inhomogeneities, that may exist in the regions travelled by the waves prior to their arrival at the first station.

We again used the greatcircle ray-tracing method described in Chapter 3 to separate all paths, from a given event and a given period, that had 40 percent of more of their total path length inside each of the six region-types of the discretized model of Jordan (1981) from Figure 3.11. After separation of the paths, we calculated the theoretical amplitude $A_i^T(T, \Delta_i)$ corresponding to the i-th observed amplitude $A_i^o(T, \Delta_i)$. This calculation followed the same fashion used in Section 4.3 during the calculation of the theoretical initial source phase (*i.e.* we used the information on the focal mechanism and depth, and on the type of the Earth

structure in the source region of Table 4.1, together with Equation 4.11).

Then, for each region of the discretized model of Jordan (1981), and most earthquakes of Table 4.1 (since in some events we had too few observations), we have a set of N linear equations, corresponding to N observations at each reference period T,

$$\ln \left\{ \frac{A_i^o(T, \Delta_i) \; [R \sin\Delta_i']}{A_i^T(T, \Delta_i)} \right\} = b' - a'\Delta_i \qquad (7.4)$$

where the other variables are the same as in Equation (7.3).

For each of these cases, we want to determine the constants (model parameters) a' and b' (the attenuation coefficient, and the correction to the initially assumed seismic moment, respectively). We can solve the problem for each case, using regression analysis (*e.g.* Draper and Smith, 1966). In this formulation, our model consists of a set of N equations of the type,

$$d_i = b - am_i + e_i \qquad (7.5)$$

were e_i represents the error due to the measurement error, and due to higher order terms neglected in the linearization of the problem (in other words, it also includes the effects due to scattering and interference by higher modes which could not be avoided in our observations). Notice that we have used a different notation for the model parameters a and b in Equation (7.5). We have not used a prime as in Equation (7.4) because a and b represent the exact model parameters for each observation. We want to estimate the values a' and b' in order to minimize s in the least squares sense,

$$s = \sum_{i=1}^{N} \varepsilon_i^2 = \sum_{i=1}^{N} (d_i - b + am_i)^2 \qquad (7.6)$$

If we assume that e_i is random variable with mean zero and unknown variance σ^2, and if we assume that e_i and e_j are uncorrelated (for $i \neq j$), we can calculate the estimated standard error of the slope a' using

$$\text{est. s. e. } (a') = \frac{s}{\left[\sum_{i=1}^{N} (m_i - \bar{m})^2\right]^{1/2}} \qquad (7.7)$$

where we have assumed that $s \simeq \sigma$. And we can also obtain the estimated standard error of the intercept b' using

$$\text{est. s. e. } (b') = \left\{ \frac{\sum_{i=1}^{N} m_i^2}{N \sum_{i=1}^{N} (m_i - \bar{m})^2} \right\}^{1/2} s \qquad (7.8)$$

The results obtained for each case considered in the study are listed in Table 7.1. In this table, we list the resulting slope a' and intercept b' for all the earthquakes studied as well as the corresponding estimated standard error values. Some region-types show very few observations, due both to the long length of the paths which we studied, and to the smaller areal distribution of some region-types when compared to others (such as region type 'b', which show a larger number of observations than the other ones). The fact that most earthquakes considered have their epicenter located in oceanic regions, also aids to the poor coverage of mostly continental region types (such as the region-type 's', which represents Precambrian shields and platforms, where we could not make any measurements). In Figure 7.1 we show one example of a resulting straight line fitted to the observed amplitude

variation as a function of distance. Whenever the data coverage is good, we obtain a result comparable with that shown in this figure. On the other hand, if only a few observations are available, the result is usually of poor quality. Sometimes we obtain a positive slope for the curve. These correspond to the cases where attenuation is small and focusing and interference increase the observed amplitude values. Some screening of the results could be done based on the statistical analysis of the regression results. We chose not to eliminate any other observations at this point, but to try to enhance the variation on the attenuation coefficients for each region, by averaging the values of Table 7.1 at each period, for a given region. The results of this averaging are shown in Table 7.2, together with the number of measurements, and the standard deviation of the average for each region-type and each period, in a similar fashion of that used for Table 3.1 and Table 6.1, which show the results for this regionalized model, from the phase and group velocity studies, respectively. As we can see, our attenuation coefficient results are still not enough to cover all the regions and all periods, for which we have a good density of phase and group velocity data. Notice that the separation between

region-types is still not clear in many cases. We hope that further analyses of observations from other earthquakes can aid to the completeness of these results in the future. This will only be possible with a data set far more extensive than the one used here, due to the much greater sensitivity of the amplitude part of the spectra to interference and multipath effects experienced by these waves in comparison to the more stable behavior of the phase spectra.

We took advantage of the Q values compiled from previous works and listed by Lee and Solomon (1975) to check our continental results of Table 7.2. Lee and Solomon (1975) list the Q values measured by Solomon (1971) in western and east-central United States (these correspond to symbols with indices (1) and (2) in Figure 7.2). We also used the values obtained for North America by Mitchell (1973a,b), and listed by Lee and Solomon (1975) in Figure 7.2 (these values are represented by the index (3) in Figure 7.2). Finally, we included the results from Tsai and Aki (1969), also from a study in North America. Our values for Q were computed by using the attenuation coefficient results of Table 7.2 for the region-type 'q' of the model by Jordan (1981) (that represents areas in both western and eastern United States). While

calculating these by Equation (7.2), we used the regionalized group velocity values obtained for this region-type in Table 6.1. Notice that our values are consistent with the range obtained by these other authors. The best agreement is found for the values of Tsai and Aki (1969) at higher frequencies.

With regard to the oceanic values, we chose to compare our results for the region-type 'b' of Jordan's (1981) model with the values of Q listed by Canas and Mitchell (1978). These latter values correspond to areas in the Pacific Ocean where the seafloor age ranges between 0 and 50 m.y. (represented by indices (1), (2), and (3) in Figure 7.3). Notice that our values are almost coincident with those for areas with age of the oceanic crust ranging between 50 and 100 m.y.. As we recall, the age range defined by Jordan (1981) for region 'b' is 25 to 100 m.y., which is almost the same as that of the region-type represented by index (2) of Figure 7.3. This is an important result and serves as a check of both works. Notice that the scatter of data in Figure 7.3 is much smaller than in Figure 7.2, which is consistent with the more homogeneous, oceanic, structures considered in the former.

The correction found for the seismic moment of each earthquake seems to be consistent for most of the periods within a given region-type. Although, some inconsistencies are present in some cases, as we can see in Table 7.1, specially when we compare results for different region-types for a given event.

The results of Table 7.1 are still useful, since many of the measurements for both attenuation coefficient, and seismic moment correction present small estimated standard error.

Yomogida (1985) has shown that amplitude of Rayleigh waves is very sensitive to lateral heterogeneities. Furthermore, he showed that only phase velocity variations affect the amplitude of these waves, in contrast with the minor role played by group velocity variations. In his method, he can make a better estimate of the geometrical spreading factor, so that more accurate measurements of the attenuation coefficient can be made. We can foresee a great improvement on this part of Seismology in the future. We believe that our phase velocity models of Chapter 5 will be useful on new attenuation studies by his method.

TABLE 7.1

REGION / PERIOD	a	b	c	p	q
			EVENT: 05/25/64, coefficient		(a)(x10^{-4} km^{-1})
20		1.535 (1.591)			----------
30		0.456 (0.480)			----------
40		0.343 (0.377)			0.342 (0.301)
50		0.375 (0.302)			0.211 (0.222)
60		0.380 (0.572)			0.300 (0.264)
70		0.471 (0.594)			1.048 (0.562)
80		0.591 (0.807)			0.305 (0.832)
90		0.669 (1.056)			----------
98		0.070 (0.531)			----------
			EVENT: 05/25/64, coefficient		(b)
20		0.436 (0.746)			----------
30		0.150 (0.247)			----------
40		0.052 (0.194)			-0.089 (0.164)
50		-0.029 (0.155)			-0.127 (0.121)
60		0.028 (0.294)			-0.047 (0.144)
70		0.104 (0.305)			0.339 (0.307)
80		0.116 (0.401)			-0.036 (0.327)
90		0.108 (0.524)			----------
98		0.002 (0.253)			----------
			EVENT: 08/25/64, coefficient		(a)(x10^{-4} km^{-1})
20				----------	----------
30				1.016 (1.092)	0.900 (1.000)
40				1.188 (0.606)	1.558 (0.565)
50				0.318 (0.503)	1.313 (0.519)
60				0.195 (0.614)	0.697 (0.462)
70				0.238 (0.547)	0.308 (0.418)
80				0.228 (0.421)	0.455 (0.394)
90				0.153 (0.469)	0.171 (0.406)
98				----------	-0.104 (0.384)
			EVENT: 08/25/64, coefficient		(b)
20				----------	----------
30				-0.150 (0.654)	-0.546 (0.605)
40				-0.113 (0.374)	0.301 (0.364)
50				-0.046 (0.313)	0.505 (0.335)
60				-0.038 (0.382)	0.298 (0.298)
70				-0.001 (0.340)	0.133 (0.278)
80				-0.002 (0.262)	0.287 (0.262)
90				-0.023 (0.291)	0.161 (0.273)
98				----------	0.104 (0.258)

TABLE 7.1 (TO BE CONTINUED)

where: $\ln[A^o(T,\Delta)\ (R \sin\Delta')/A^t(T,\Delta)] = b - a\Delta$

TABLE 7.1 (CONTINUED)

REGION / PERIOD	a	b	c	p	q
			EVENT: 10/23/64, coefficient (a)($\times 10^{-4}$ km^{-1})		
20		----------			----------
30		2.117 (0.877)			1.367 (1.255)
40		2.622 (1.164)			2.837 (1.956)
50		2.532 (0.686)			1.366 (0.969)
60		2.933 (0.531)			1.236 (1.010)
70		3.143 (0.776)			1.110 (0.448)
80		2.699 (0.467)			1.946 (0.444)
90		3.292 (0.868)			2.487 (1.187)
98		2.852 (0.908)			----------
			EVENT: 10/23/64, coefficient (b)		
20		----------			----------
30		0.250 (0.433)			0.243 (0.604)
40		0.376 (0.626)			0.428 (0.941)
50		0.326 (0.352)			0.126 (0.466)
60		0.355 (0.272)			0.054 (0.486)
70		0.607 (0.398)			0.027 (0.215)
80		0.338 (0.239)			0.032 (0.213)
90		0.576 (0.445)			0.187 (0.571)
98		0.453 (0.491)			----------
			EVENT: 09/09/65, coefficient (a)($\times 10^{-4}$ km^{-1})		
20					----------
30					-0.770 (0.497)
40					-0.573 (0.695)
50					-0.689 (0.423)
60					-0.341 (0.510)
70					0.050 (0.561)
80					0.061 (0.462)
90					0.393 (0.712)
98					0.491 (0.499)
			EVENT: 09/09/65, coefficient (b)		
20					----------
30					0.055 (0.220)
40					0.071 (0.301)
50					-0.021 (0.183)
60					0.061 (0.221)
70					0.201 (0.243)
80					0.348 (0.205)
90					0.435 (0.316)
98					0.145 (0.226)

TABLE 7.1 (TO BE CONTINUED)

where: $\ln[A^o(T,\Delta)\ (R \sin\Delta')/A^t(T,\Delta)] = b - a\Delta$

TABLE 7.1 (CONTINUED)

REGION / PERIOD	a	b	c	p	q
			EVENT: 09/12/65, coefficient (a)($\times 10^{-4}$ km^{-1})		
20		----------			
30		1.368 (1.176)			
40		0.525 (0.976)			
50		1.088 (0.940)			
60		1.923 (1.604)			
70		0.508 (1.520)			
80		0.525 (0.869)			
90		-0.147 (1.288)			
98		-0.397 (0.627)			
			EVENT: 09/12/65, coefficient (b)		
20		----------			
30		0.285 (0.613)			
40		-0.036 (0.508)			
50		0.051 (0.469)			
60		0.298 (0.801)			
70		-0.081 (0.757)			
80		0.183 (0.436)			
90		-0.121 (0.647)			
98		0.266 (0.327)			
			EVENT: 10/07/65, coefficient (a)($\times 10^{-4}$ km^{-1})		
20					----------
30					1.146 (0.547)
40					1.260 (0.369)
50					1.624 (0.460)
60					1.288 (1.058)
70					0.729 (0.870)
80					-0.751 (1.083)
90					----------
98					----------
			EVENT: 10/07/65, coefficient (b)		
20					----------
30					0.200 (0.193)
40					0.296 (0.163)
50					0.412 (0.203)
60					0.327 (0.388)
70					-0.034 (0.337)
80					0.039 (0.436)
90					----------
98					----------

TABLE 7.1 (TO BE CONTINUED)

where: $\ln[A^o(T,\Delta)\ (R \sin\Delta')/A^t(T,\Delta)] = b - a\Delta$

TABLE 7.1 (CONTINUED)

REGION / PERIOD	a	b	c	p	q
			EVENT: 10/31/65, coefficient (a)($\times 10^{-4}$ km^{-1})		
20		0.073 (1.570)			
30		0.123 (0.649)			
40		1.552 (0.812)			
50		1.360 (0.661)			
60		0.957 (0.959)			
70		1.406 (1.499)			
80		0.646 (0.676)			
90		0.297 (1.159)			
98		---			
			EVENT: 10/31/65, coefficient (b)		
20		-0.203 (0.633)			
30		-0.068 (0.303)			
40		0.063 (0.394)			
50		-0.115 (0.320)			
60		-0.274 (0.465)			
70		-0.254 (0.716)			
80		-0.309 (0.332)			
90		-0.271 (0.559)			
98		---			
			EVENT: 12/19/65, coefficient (a)($\times 10^{-4}$ km^{-1})		
20		1.480 (1.093)			
30		0.526 (0.911)			
40		0.682 (0.820)			
50		0.682 (0.711)			
60		0.730 (1.019)			
70		0.468 (0.771)			
80		0.391 (0.787)			
90		0.146 (0.921)			
98		0.244 (0.899)			
			EVENT: 12/19/65, coefficient (b)		
20		0.384 (0.607)			
30		-0.092 (0.549)			
40		-0.195 (0.494)			
50		-0.049 (0.429)			
60		-0.118 (0.613)			
70		0.086 (0.483)			
80		0.103 (0.483)			
90		0.089 (0.566)			
98		0.103 (0.547)			

TABLE 7.1 (TO BE CONTINUED)

where: $\ln[A^o(T,\Delta)\ (R \sin\Delta')/A^t(T,\Delta)] = b - a\Delta$

TABLE 7.1 (CONTINUED)

REGION / PERIOD	a	b	c	p	q
			EVENT: 02/17/66, coefficient (a)($\times 10^{-4}$ km^{-1})		
20		----------			
30		2.692 (0.927)			
40		1.934 (0.494)			
50		1.890 (0.403)			
60		1.087 (0.344)			
70		1.197 (0.443)			
80		0.779 (0.341)			
90		0.404 (0.341)			
98		0.639 (0.406)			
			EVENT: 02/17/66, coefficient (b)		
20		----------			
30		0.556 (0.618)			
40		0.451 (0.348)			
50		0.604 (0.284)			
60		0.218 (0.243)			
70		0.402 (0.298)			
80		0.313 (0.229)			
90		0.209 (0.229)			
98		0.412 (0.277)			
			EVENT: 01/07/67, coefficient (a)($\times 10^{-4}$ km^{-1})		
20		0.415 (0.381)			
30		1.172 (0.363)			
40		1.083 (0.261)			
50		1.242 (0.672)			
60		1.177 (0.523)			
70		0.919 (0.592)			
80		0.840 (0.683)			
90		0.676 (0.297)			
98		0.722 (0.520)			
			EVENT: 01/07/67, coefficient (b)		
20		0.264 (0.241)			
30		0.243 (0.305)			
40		0.046 (0.220)			
50		-0.113 (0.595)			
60		0.082 (0.463)			
70		0.167 (0.508)			
80		0.138 (0.586)			
90		0.004 (0.255)			
98		0.132 (0.447)			

TABLE 7.1 (TO BE CONTINUED)

where: $\ln[A^o(T,\Delta)\ (R \sin\Delta')/A^t(T,\Delta)] = b - a\Delta$

TABLE 7.1 (CONTINUED)

REGION / PERIOD	a	b	c	p	q
			EVENT: 11/10/67, coefficient (a)($\times 10^{-4}$ km^{-1})		
20		----------			
30		-0.964 (2.187)			
40		0.083 (1.351)			
50		1.186 (1.485)			
60		1.719 (1.235)			
70		1.017 (1.061)			
80		1.568 (2.250)			
90		-1.467 (1.857)			
98		----------			
			EVENT: 11/10/67, coefficient (b)		
20		----------			
30		0.550 (0.799)			
40		0.494 (0.528)			
50		0.646 (0.585)			
60		0.878 (0.486)			
70		0.617 (0.419)			
80		0.670 (0.926)			
90		-0.110 (0.686)			
98		----------			
			EVENT: 03/02/68, coefficient (a)($\times 10^{-4}$ km^{-1})		
20		-1.357 (1.429)			
30		1.548 (1.437)			
40		1.350 (1.100)			
50		1.157 (0.642)			
60		0.691 (0.804)			
70		0.510 (0.936)			
80		-0.549 (0.608)			
90		-0.223 (1.327)			
98		----------			
			EVENT: 03/02/68, coefficient (b)		
20		0.182 (0.583)			
30		0.634 (0.641)			
40		0.366 (0.531)			
50		0.412 (0.310)			
60		0.374 (0.392)			
70		0.426 (0.425)			
80		0.093 (0.257)			
90		-0.025 (0.478)			
98		----------			

TABLE 7.1 (TO BE CONTINUED)

where: $\ln[A^o(T,\Delta)\ (R \sin\Delta')/A^t(T,\Delta)] = b - a\Delta$

TABLE 7.1 (CONTINUED)

REGION / PERIOD	a	b	c	p	q
			EVENT: 09/03/68, coefficient (a)($\times 10^{-4}$ km^{-1})		
20		----------	-1.018 (3.208)		
30		0.877 (0.875)	-0.912 (1.410)		
40		1.527 (0.665)	0.059 (1.743)		
50		1.756 (0.647)	1.973 (3.252)		
60		----------	1.492 (2.282)		
70		----------	----------		
80		----------	----------		
90		----------	----------		
98		----------	----------		
			EVENT: 09/03/68, coefficient (b)		
20		----------	-0.395 (0.628)		
30		0.142 (0.479)	0.218 (0.318)		
40		-0.096 (0.364)	0.078 (0.384)		
50		0.076 (0.354)	-0.093 (0.698)		
60		----------	-0.058 (0.476)		
70		----------	----------		
80		----------	----------		
90		----------	----------		
98		----------	----------		
			EVENT: 10/08/68, coefficient (a)($\times 10^{-4}$ km^{-1})		
20	2.230 (1.211)	-0.980 (1.192)			
30	0.660 (0.682)	0.498 (0.785)			
40	1.049 (0.542)	0.540 (0.541)			
50	1.005 (0.410)	0.536 (0.666)			
60	0.934 (0.275)	0.353 (0.470)			
70	0.473 (0.346)	-0.215 (0.407)			
80	0.078 (0.197)	-0.537 (0.482)			
90	-0.013 (0.184)	-0.243 (0.527)			
98	-0.313 (0.254)	-0.690 (0.588)			
			EVENT: 10/08/68, coefficient (b)		
20	-0.074 (0.832)	-0.424 (0.547)			
30	-0.268 (0.521)	-0.005 (0.516)			
40	0.014 (0.413)	0.004 (0.366)			
50	0.035 (0.312)	0.142 (0.142)			
60	0.102 (0.209)	0.123 (0.318)			
70	-0.005 (0.263)	0.077 (0.275)			
80	-0.046 (0.150)	-0.045 (0.334)			
90	-0.083 (0.140)	0.154 (0.385)			
98	-0.214 (0.193)	0.022 (0.433)			

TABLE 7.1 (TO BE CONTINUED)

where: $\ln[A^o(T,\Delta)\ (R \sin\Delta')/A^t(T,\Delta)] = b - a\Delta$

TABLE 7.1 (CONTINUED)

REGION / PERIOD	a	b	c	p	q
			EVENT: 03/31/69, coefficient (a)($\times 10^{-4}$ km^{-1})		
20					----------
30					1.467 (0.870)
40					1.198 (0.523)
50					1.248 (0.556)
60					1.580 (0.505)
70					1.263 (0.429)
80					1.398 (0.436)
90					0.614 (0.342)
98					0.638 (0.296)
			EVENT: 03/31/69, coefficient (b)		
20					----------
30					-0.036 (0.694)
40					-0.245 (0.478)
50					0.112 (0.526)
60					0.382 (0.478)
70					0.406 (0.407)
80					0.701 (0.412)
90					0.133 (0.331)
98					0.432 (0.284)
			EVENT: 04/07/69, coefficient (a)($\times 10^{-4}$ km^{-1})		
20				----------	----------
30				-1.035 (2.045)	-0.506 (1.253)
40				0.153 (0.891)	0.658 (0.984)
50				-0.111 (0.515)	0.745 (1.322)
60				0.564 (0.845)	0.105 (0.950)
70				0.344 (1.975)	0.390 (1.488)
80				0.605 (1.170)	0.086 (1.499)
90				----------	0.155 (1.237)
98				----------	----------
			EVENT: 04/07/69, coefficient (b)		
20				----------	----------
30				-0.064 (1.074)	0.037 (0.681)
40				0.085 (0.468)	0.385 (0.573)
50				-0.015 (0.271)	0.440 (0.785)
60				-0.001 (0.444)	0.079 (0.564)
70				-0.025 (1.037)	0.236 (0.884)
80				0.004 (0.615)	0.274 (0.889)
90				----------	0.412 (0.715)
98				----------	----------

TABLE 7.1 (TO BE CONTINUED)

where: $\ln[A^o(T,\Delta)\ (R \sin\Delta')/A^t(T,\Delta)] = b - a\Delta$

TABLE 7.1 (CONTINUED)

REGION / PERIOD	a	b	c	p	q
			EVENT: 08/08/69, coefficient (a)($\times 10^{-4}$ km^{-1})		
20		----------			
30		0.432 (0.625)			
40		0.388 (0.414)			
50		0.128 (0.554)			
60		0.367 (0.302)			
70		0.617 (0.423)			
80		0.313 (0.280)			
90		0.190 (0.654)			
98		-0.207 (0.280)			
			EVENT: 08/08/69, coefficient (b)		
20		----------			
30		-0.179 (0.501)			
40		-0.033 (0.332)			
50		-0.340 (0.444)			
60		-0.015 (0.242)			
70		0.372 (0.337)			
80		0.298 (0.223)			
90		0.309 (0.454)			
98		0.104 (0.194)			
			EVENT: 09/20/69, coefficient (a)($\times 10^{-4}$ km^{-1})		
20		----------			1.562 (0.993)
30		-0.079 (0.863)			1.460 (0.565)
40		0.632 (1.162)			0.474 (0.548)
50		1.290 (1.504)			0.123 (0.656)
60		0.703 (1.022)			-0.249 (0.417)
70		0.225 (0.800)			-0.380 (0.357)
80		-0.315 (0.496)			-0.655 (0.434)
90		0.645 (0.695)			-0.524 (0.384)
98		0.398 (1.144)			-0.605 (0.371)
			EVENT: 09/20/69, coefficient (b)		
20		----------			0.128 (0.335)
30		0.081 (0.417)			0.398 (0.267)
40		0.282 (0.561)			-0.027 (0.353)
50		0.417 (0.727)			-0.174 (0.423)
60		0.345 (0.494)			-0.226 (0.277)
70		0.230 (0.301)			-0.252 (0.259)
80		-0.020 (0.236)			-0.464 (0.323)
90		0.397 (0.331)			-0.134 (0.286)
98		0.394 (0.580)			-0.432 (0.300)

TABLE 7.1 (TO BE CONTINUED)

where: $\ln[A^o(T,\Delta)\ (R \sin\Delta')/A^t(T,\Delta)] = b - a\Delta$

TABLE 7.1 (CONTINUED)

REGION / PERIOD	a	b	c	p	q
			EVENT: 01/21/70, coefficient (a)($\times 10^{-4}$ km^{-1})		
20		----------			----------
30		0.584 (0.610)			0.373 (0.434)
40		0.756 (0.489)			0.501 (0.377)
50		1.311 (0.730)			0.784 (0.300)
60		0.489 (0.449)			1.064 (0.402)
70		1.052 (0.345)			1.019 (0.285)
80		0.865 (0.454)			0.720 (0.153)
90		0.644 (0.285)			0.757 (0.220)
98		0.560 (0.422)			0.661 (0.272)
			EVENT: 01/21/70, coefficient (b)		
20		----------			----------
30		-0.251 (0.722)			-0.119 (0.442)
40		-0.137 (0.592)			-0.161 (0.460)
50		0.049 (0.851)			0.040 (0.367)
60		-0.069 (0.520)			0.283 (0.493)
70		0.143 (0.389)			0.190 (0.327)
80		-0.090 (0.511)			0.075 (0.175)
90		-0.055 (0.289)			0.193 (0.236)
98		-0.001 (0.410)			0.154 (0.293)
			EVENT: 03/31/70, coefficient (a)($\times 10^{-4}$ km^{-1})		
20		-0.894 (0.123)			
30		0.081 (0.613)			
40		0.075 (0.470)			
50		1.071 (0.389)			
60		0.968 (0.471)			
70		1.249 (0.394)			
80		0.444 (0.473)			
90		0.597 (0.555)			
98		0.043 (0.660)			
			EVENT: 03/31/70, coefficient (b)		
20		-0.175 (0.588)			
30		-0.040 (0.302)			
40		0.001 (0.234)			
50		0.349 (0.194)			
60		0.294 (0.232)			
70		0.573 (0.197)			
80		0.340 (0.229)			
90		0.359 (0.272)			
98		0.167 (0.325)			

TABLE 7.1 (TO BE CONTINUED)

where: $\ln[A^o(T,\Delta)\ (R \sin\Delta')/A^t(T,\Delta)] = b - a\Delta$

TABLE 7.1 (CONTINUED)

REGION / PERIOD	a	b	c	p	q
			EVENT: 04/25/70, coefficient (a)($\times 10^{-4}$ km^{-1})		
20		-0.092 (1.257)			
30		-0.348 (1.047)			
40		0.014 (0.898)			
50		0.253 (1.108)			
60		-0.390 (0.930)			
70		-1.460 (0.838)			
80		-1.871 (1.032)			
90		---			
98		---			
			EVENT: 04/25/70, coefficient (b)		
20		0.268 (0.383)			
30		0.272 (0.354)			
40		0.238 (0.304)			
50		0.270 (0.384)			
60		0.225 (0.322)			
70		-0.070 (0.311)			
80		-0.070 (0.380)			
90		---			
98		---			
			EVENT: 05/09/71, coefficient (a)($\times 10^{-4}$ km^{-1})		
20	1.476 (0.902)	-0.248 (0.897)			
30	0.393 (0.595)	0.922 (0.381)			
40	0.960 (0.404)	0.685 (0.284)			
50	0.813 (0.377)	1.425 (0.434)			
60	0.586 (0.335)	1.046 (0.408)			
70	0.334 (0.289)	0.979 (0.355)			
80	0.313 (0.334)	0.884 (0.336)			
90	0.169 (0.397)	0.515 (0.344)			
98	0.065 (0.509)	0.649 (0.428)			
			EVENT: 05/09/71, coefficient (b)		
20	0.092 (0.499)	-0.343 (0.553)			
30	0.083 (0.423)	0.099 (0.332)			
40	0.534 (0.310)	0.194 (0.260)			
50	0.698 (0.290)	0.672 (0.403)			
60	0.518 (0.257)	0.592 (0.379)			
70	0.574 (0.222)	0.563 (0.330)			
80	0.683 (0.259)	0.623 (0.299)			
90	0.668 (0.311)	0.342 (0.304)			
98	0.663 (0.387)	0.481 (0.377)			

TABLE 7.1 (TO BE CONTINUED)

where: $\ln[A^o(T,\Delta)\ (R \sin\Delta')/A^t(T,\Delta)] = b - a\Delta$

TABLE 7.1 (CONTINUED)

REGION / PERIOD	a	b	c	p	q
			EVENT: 05/31/71, coefficient (a)($\times 10^{-4}$ km^{-1})		
20		----------		----------	0.318 (0.860)
30		0.388 (0.452)		0.015 (2.260)	-0.189 (0.476)
40		-0.303 (0.227)		0.218 (1.523)	0.411 (0.416)
50		0.391 (0.515)		0.264 (0.816)	0.274 (0.272)
60		0.045 (0.440)		0.472 (0.781)	1.112 (0.334)
70		----------		0.725 (0.954)	1.785 (0.392)
80		----------		0.198 (0.891)	1.043 (0.530)
90		----------		0.992 (0.369)	0.205 (0.503)
98		----------		----------	0.225 (0.420)
			EVENT: 05/31/71, coefficient (b)		
20		----------		----------	-0.097 (0.264)
30		0.236 (0.162)		-0.775 (1.140)	0.077 (0.193)
40		0.100 (0.081)		-0.406 (0.768)	0.190 (0.187)
50		0.247 (0.184)		-0.194 (0.412)	0.180 (0.122)
60		0.168 (0.158)		-0.106 (0.394)	0.446 (0.150)
70		----------		-0.076 (0.481)	0.672 (0.176)
80		----------		-0.183 (0.449)	0.439 (0.253)
90		----------		0.076 (0.186)	0.343 (0.250)
98		----------		----------	0.237 (0.209)
			EVENT: 06/26/71, coefficient (a)($\times 10^{-4}$ km^{-1})		
20		----------			----------
30		2.952 (1.159)			0.263 (0.970)
40		2.133 (0.700)			-1.629 (0.938)
50		2.229 (1.123)			-1.166 (1.184)
60		1.554 (0.881)			-0.376 (0.810)
70		1.157 (0.738)			-0.279 (0.798)
80		1.284 (0.986)			-0.206 (0.621)
90		1.921 (1.653)			-0.297 (0.955)
98		----------			-0.435 (1.281)
			EVENT: 06/26/71, coefficient (b)		
20		----------			----------
30		0.912 (0.739)			-0.663 (0.635)
40		0.447 (0.457)			-1.446 (0.673)
50		0.427 (0.729)			-1.449 (0.851)
60		0.258 (0.548)			-0.889 (0.583)
70		0.136 (0.461)			-0.935 (0.545)
80		-0.003 (0.615)			-0.804 (0.424)
90		0.467 (0.106)			-0.660 (0.698)
98		----------			-0.752 (0.987)

TABLE 7.1 (TO BE CONTINUED)

where: $\ln[A^o(T,\Delta)\ (R \sin\Delta')/A^t(T,\Delta)] = b - a\Delta$

TABLE 7.1 (CONTINUED)

REGION / PERIOD	a	b	c	p	q
			EVENT: 09/30/71, coefficient (a)($\times 10^{-4}$ km^{-1})		
20		1.084 (0.926)			
30		0.414 (0.303)			
40		0.660 (0.336)			
50		1.302 (0.398)			
60		1.319 (0.728)			
70		0.708 (0.307)			
80		1.219 (0.827)			
90		----------			
98		----------			
			EVENT: 09/30/71, coefficient (b)		
20		0.104 (0.530)			
30		0.134 (0.204)			
40		-0.126 (0.231)			
50		-0.040 (0.284)			
60		-0.164 (0.536)			
70		-0.008 (0.225)			
80		0.001 (0.541)			
90		----------			
98		----------			
			EVENT: 05/02/72, coefficient (a)($\times 10^{-4}$ km^{-1})		
20		0.680 (0.220)			----------
30		0.777 (0.526)			-0.329 (1.068)
40		0.827 (0.299)			0.166 (0.645)
50		0.914 (0.362)			0.189 (0.665)
60		0.772 (0.696)			-0.114 (0.671)
70		0.753 (0.370)			0.102 (0.693)
80		----------			0.160 (0.759)
90		----------			0.081 (0.633)
98		----------			0.493 (0.515)
			EVENT: 05/02/72, coefficient (b)		
20		0.105 (0.131)			----------
30		0.064 (0.387)			0.260 (0.484)
40		0.096 (0.220)			0.414 (0.352)
50		0.240 (0.266)			0.374 (0.362)
60		-0.071 (0.512)			0.388 (0.376)
70		0.199 (0.292)			0.268 (0.404)
80		----------			0.438 (0.442)
90		----------			0.453 (0.368)
98		----------			0.145 (0.310)

TABLE 7.1 (TO BE CONTINUED)

where: $\ln[A^o(T,\Delta)\ (R \sin\Delta')/A^t(T,\Delta)] = b - a\Delta$

TABLE 7.1 (CONTINUED)

REGION / PERIOD	a	b	c	p	q
			EVENT: 05/21/72, coefficient (a)($\times 10^{-4}$ km^{-1})		
20		----------			
30		0.692 (0.262)			
40		0.990 (0.282)			
50		0.998 (0.289)			
60		1.227 (0.460)			
70		0.660 (0.403)			
80		0.766 (0.442)			
90		0.388 (0.284)			
98		0.128 (0.389)			
			EVENT: 05/21/72, coefficient (b)		
20		----------			
30		0.163 (0.201)			
40		0.034 (0.211)			
50		0.031 (0.235)			
60		0.239 (0.378)			
70		0.082 (0.331)			
80		0.123 (0.338)			
90		0.132 (0.217)			
98		0.006 (0.298)			
			EVENT: 10/20/72, coefficient (a)($\times 10^{-4}$ km^{-1})		
20		----------			
30		0.640 (0.794)			
40		0.667 (0.582)			
50		1.934 (0.616)			
60		1.548 (0.297)			
70		2.176 (0.697)			
80		1.870 (0.639)			
90		1.311 (0.838)			
98		1.039 (0.801)			
			EVENT: 10/20/72, coefficient (b)		
20		----------			
30		-0.261 (0.404)			
40		-0.270 (0.301)			
50		0.163 (0.319)			
60		0.056 (0.154)			
70		0.341 (0.365)			
80		0.447 (0.335)			
90		0.087 (0.458)			
98		0.119 (0.432)			

TABLE 7.1 (TO BE CONTINUED)

where: $\ln[A^o(T,\Delta)\ (R \sin\Delta')/A^t(T,\Delta)] = b - a\Delta$

TABLE 7.1 (CONTINUED)

REGION / PERIOD	a	b	c	p	q
			EVENT: 04/26/73, coefficient (a)($\times 10^{-4}$ km^{-1})		
20		0.810 (0.612)	----------		----------
30		1.423 (0.344)	0.869 (0.426)		----------
40		1.108 (0.360)	1.494 (0.469)		----------
50		0.900 (0.316)	1.536 (0.403)		1.078 (0.148)
60		1.124 (0.217)	2.140 (0.689)		1.150 (0.197)
70		1.163 (0.236)	1.488 (0.405)		1.120 (0.354)
80		1.382 (0.283)	1.874 (0.425)		1.501 (0.352)
90		1.076 (0.415)	1.707 (0.607)		----------
98		0.817 (0.374)	1.573 (0.495)		----------
			EVENT: 04/26/73, coefficient (b)		
20		0.420 (0.427)	----------		----------
30		0.465 (0.301)	0.073 (0.363)		----------
40		0.001 (0.327)	0.190 (0.402)		----------
50		-0.296 (0.286)	0.175 (0.346)		0.001 (0.159)
60		-0.154 (0.197)	0.322 (0.592)		-0.022 (0.213)
70		-0.287 (0.211)	0.017 (0.339)		-0.055 (0.383)
80		-0.191 (0.251)	0.145 (0.355)		0.031 (0.381)
90		-0.511 (0.361)	0.124 (0.497)		----------
98		-0.288 (0.357)	0.146 (0.392)		----------
			EVENT: 08/30/73, coefficient (a)($\times 10^{-4}$ km^{-1})		
20		----------			----------
30		0.899 (1.146)			0.237 (2.449)
40		0.667 (1.250)			1.264 (1.956)
50		1.394 (2.133)			1.334 (1.747)
60		----------			1.411 (1.586)
70		----------			----------
80		----------			----------
90		----------			----------
98		----------			----------
			EVENT: 08/30/73, coefficient (b)		
20		----------			----------
30		-0.473 (0.447)			-0.485 (0.947)
40		-0.686 (0.617)			-0.316 (0.756)
50		-0.638 (0.954)			-0.400 (0.771)
60		----------			-0.187 (0.621)
70		----------			----------
80		----------			----------
90		----------			----------
98		----------			----------

TABLE 7.1 (TO BE CONTINUED)

where: $\ln[A^o(T,\Delta)\ (R \sin\Delta')/A^t(T,\Delta)] = b - a\Delta$

TABLE 7.1 (CONTINUED)

REGION / PERIOD	a	b	c	p	q
			EVENT: 07/01/74, coefficient (a)($\times 10^{-4}$ km^{-1})		
20	----------	-0.885 (0.657)			
30	0.865 (0.798)	1.398 (0.510)			
40	0.679 (0.908)	2.557 (0.494)			
50	0.386 (0.403)	1.340 (0.396)			
60	0.468 (0.274)	1.305 (0.407)			
70	0.355 (0.251)	1.326 (0.813)			
80	0.305 (0.141)	0.197 (0.758)			
90	0.321 (0.547)	----------			
98	----------	----------			
			EVENT: 07/01/74, coefficient (b)		
20	----------	0.109 (0.217)			
30	-0.112 (0.617)	0.776 (0.322)			
40	-0.382 (0.738)	1.139 (0.312)			
50	-0.125 (0.327)	0.754 (0.250)			
60	0.010 (0.222)	0.836 (0.257)			
70	0.065 (0.203)	0.873 (0.438)			
80	-0.371 (0.923)	0.550 (0.400)			
90	0.142 (0.442)	----------			
98	----------	----------			
			EVENT: 11/20/74, coefficient (a)($\times 10^{-4}$ km^{-1})		
20		----------			
30		2.342 (0.744)			
40		1.846 (0.322)			
50		1.367 (0.354)			
60		1.150 (0.395)			
70		1.453 (0.474)			
80		-0.342 (0.445)			
90		-0.120 (0.851)			
98		----------			
			EVENT: 11/20/74, coefficient (b)		
20		----------			
30		0.718 (0.494)			
40		0.411 (0.214)			
50		0.339 (0.246)			
60		0.331 (0.269)			
70		0.628 (0.322)			
80		-0.027 (0.227)			
90		0.021 (0.426)			
98		----------			

TABLE 7.1 (TO BE CONTINUED)

where: $\ln[A^o(T,\Delta)\ (R \sin\Delta')/A^t(T,\Delta)] = b - a\Delta$

TABLE 7.1 (CONTINUED)

REGION / PERIOD	a	b	c	p	q
			EVENT: 09/11/75, coefficient (a)($\times 10^{-4}$ km^{-1})		
20	----------	----------			----------
30	-0.442 (1.865)	0.105 (0.759)			1.065 (0.627)
40	-0.423 (1.585)	0.063 (0.619)			1.162 (0.273)
50	-1.018 (1.172)	0.302 (0.730)			1.218 (0.313)
60	-1.187 (1.587)	0.230 (0.782)			0.771 (0.179)
70	-1.803 (1.525)	0.253 (0.597)			1.083 (0.254)
80	-1.425 (2.098)	0.028 (0.749)			1.045 (0.278)
90	-1.877 (1.912)	-0.143 (0.653)			0.422 (0.257)
98	----------	-0.133 (0.636)			0.404 (0.295)
			EVENT: 09/11/75, coefficient (b)		
20	----------	----------			----------
30	0.317 (0.673)	0.328 (0.789)			0.654 (0.340)
40	0.346 (0.600)	0.392 (0.657)			0.920 (0.222)
50	0.152 (0.458)	0.531 (0.733)			0.787 (0.277)
60	0.233 (0.620)	0.513 (0.785)			0.695 (0.159)
70	0.171 (0.574)	0.610 (0.600)			0.887 (0.244)
80	0.249 (0.790)	0.526 (0.752)			0.896 (0.268)
90	0.229 (0.720)	0.541 (0.656)			0.722 (0.253)
98	----------	0.573 (0.639)			0.709 (0.303)
			EVENT: 09/19/75, coefficient (a)($\times 10^{-4}$ km^{-1})		
20	----------	0.907 (0.950)			
30	1.598 (1.111)	0.206 (0.769)			
40	0.780 (0.861)	0.508 (0.586)			
50	0.840 (0.860)	0.310 (0.626)			
60	0.977 (0.264)	0.279 (0.505)			
70	1.383 (0.549)	1.022 (0.517)			
80	1.097 (0.499)	0.369 (0.493)			
90	0.907 (0.414)	-0.297 (0.408)			
98	0.754 (0.192)	-0.171 (0.610)			
			EVENT: 09/19/75, coefficient (b)		
20	----------	-0.275 (0.503)			
30	-0.219 (0.873)	-0.608 (0.569)			
40	-0.528 (0.677)	-0.576 (0.434)			
50	-0.376 (0.699)	-0.633 (0.468)			
60	0.075 (0.222)	-0.546 (0.378)			
70	0.149 (0.461)	0.125 (0.402)			
80	0.135 (0.419)	-0.283 (0.383)			
90	0.108 (0.348)	-0.372 (0.320)			
98	0.028 (0.161)	-0.406 (0.523)			

TABLE 7.1 (TO BE CONTINUED)

where: $\ln[A^o(T,\Delta)\ (R \sin\Delta')/A^t(T,\Delta)] = b - a\Delta$

TABLE 7.1 (CONTINUED)

REGION / PERIOD	a	b	c	p	q
			EVENT: 03/29/76, coefficient (a)($\times 10^{-4}$ km^{-1})		
20	----------	----------			----------
30	1.589 (0.159)	1.172 (0.585)			-0.579 (1.249)
40	2.134 (0.264)	1.280 (0.339)			-0.610 (0.931)
50	1.928 (0.381)	1.768 (1.102)			-1.088 (1.212)
60	----------	1.797 (0.595)			-0.906 (0.720)
70	----------	1.751 (1.136)			0.227 (0.850)
80	----------	1.098 (0.378)			-0.194 (0.843)
90	----------	0.781 (0.331)			-0.129 (0.762)
98	----------	0.744 (0.387)			-0.167 (0.805)
			EVENT: 03/29/76, coefficient (b)		
20	----------	----------			----------
30	-0.005 (0.170)	-0.050 (0.637)			-0.220 (0.920)
40	0.058 (0.283)	-0.040 (0.369)			-0.127 (0.686)
50	0.163 (0.408)	-0.056 (1.198)			-0.787 (0.861)
60	----------	0.222 (0.601)			-0.474 (0.511)
70	----------	0.205 (0.115)			0.167 (0.708)
80	----------	0.161 (0.382)			-0.002 (0.702)
90	----------	0.002 (0.334)			0.078 (0.635)
98	----------	0.005 (0.391)			0.123 (0.671)
			EVENT: 08/30/76, coefficient (a)($\times 10^{-4}$ km^{-1})		
20		----------			
30		0.890 (0.587)			
40		1.695 (0.510)			
50		0.611 (0.443)			
60		1.121 (0.439)			
70		0.959 (0.344)			
80		0.444 (0.280)			
90		0.026 (0.173)			
98		0.430 (0.321)			
			EVENT: 08/30/76, coefficient (b)		
20		----------			
30		-0.108 (0.228)			
40		-0.008 (0.209)			
50		-0.146 (0.214)			
60		0.074 (0.212)			
70		0.182 (0.173)			
80		-0.011 (0.141)			
90		-0.026 (0.089)			
98		0.071 (0.171)			

TABLE 7.1 (TO BE CONTINUED)

where: $\ln[A^o(T,\Delta)\ (R \sin\Delta')/A^t(T,\Delta)] = b - a\Delta$

TABLE 7.1 (CONTINUED)

REGION / PERIOD	a	b	c	p	q
			EVENT: 11/02/76, coefficient (a)($\times 10^{-4}$ km^{-1})		
20		----------			
30		0.898 (1.085)			
40		1.344 (1.103)			
50		0.814 (0.880)			
60		1.328 (1.548)			
70		0.041 (0.805)			
80		0.224 (1.306)			
90		0.365 (0.287)			
98		0.128 (0.533)			
			EVENT: 11/02/76, coefficient (b)		
20		----------			
30		-0.119 (0.629)			
40		0.029 (0.639)			
50		0.098 (0.536)			
60		0.066 (0.943)			
70		-0.249 (0.486)			
80		-0.171 (0.788)			
90		-0.036 (0.169)			
98		-0.056 (0.290)			
			EVENT: 02/05/77, coefficient (a)($\times 10^{-4}$ km^{-1})		
20	----------	1.285 (0.845)			----------
30	----------	0.506 (0.390)			1.183 (0.326)
40	----------	1.388 (0.488)			1.074 (0.855)
50	----------	1.000 (0.613)			0.323 (0.507)
60	----------	1.318 (0.436)			0.881 (0.652)
70	1.275 (0.351)	1.002 (0.398)			0.786 (0.944)
80	1.197 (0.177)	1.031 (0.468)			----------
90	----------	1.228 (0.567)			----------
98	----------	0.721 (0.522)			----------
			EVENT: 02/05/77, coefficient (b)		
20	----------	-0.335 (0.671)			----------
30	----------	-0.531 (0.393)			0.072 (0.298)
40	----------	0.184 (0.508)			-0.031 (0.780)
50	----------	-0.209 (0.638)			-0.463 (0.441)
60	----------	0.324 (0.453)			-0.193 (0.598)
70	0.072 (0.382)	0.385 (0.406)			-0.237 (0.873)
80	0.038 (0.193)	0.435 (0.488)			----------
90	----------	0.869 (0.591)			----------
98	----------	0.459 (0.533)			----------

TABLE 7.1 (TO BE CONTINUED)

where: $\ln[A^o(T,\Delta)\ (R \sin\Delta')/A^t(T,\Delta)] = b - a\Delta$

TABLE 7.1 (CONTINUED)

REGION / PERIOD	a	b	c	p	q
			EVENT: 06/28/77, coefficient (a)($\times 10^{-4}$ km^{-1})		
20	----------	1.367 (0.276)			
30	----------	1.730 (0.834)			
40	-0.238 (0.520)	1.416 (0.643)			
50	-0.074 (0.407)	1.835 (0.870)			
60	0.005 (0.820)	1.503 (0.574)			
70	0.213 (0.783)	1.179 (0.483)			
80	----------	0.988 (0.995)			
90	----------	0.788 (0.431)			
98	----------	0.900 (0.844)			
			EVENT: 06/28/77, coefficient (b)		
20	----------	-0.097 (0.164)			
30	----------	-0.047 (0.505)			
40	0.011 (0.257)	0.003 (0.389)			
50	0.061 (0.201)	0.245 (0.527)			
60	0.121 (0.406)	0.166 (0.348)			
70	0.152 (0.388)	0.261 (0.293)			
80	----------	0.055 (0.615)			
90	----------	0.095 (0.289)			
98	----------	0.150 (0.540)			
			EVENT: 08/26/77, coefficient (a)($\times 10^{-4}$ km^{-1})		
20		----------			
30		----------			
40		----------			
50		0.639 (1.311)			
60		0.842 (1.626)			
70		0.362 (1.078)			
80		----------			
90		----------			
98		----------			
			EVENT: 08/26/77, coefficient (b)		
20		----------			
30		----------			
40		----------			
50		-0.304 (1.417)			
60		-0.331 (1.757)			
70		-0.315 (1.164)			
80		----------			
90		----------			
98		----------			

TABLE 7.1 (TO BE CONTINUED)

where: $\ln[A^o(T,\Delta)\ (R \sin\Delta')/A^t(T,\Delta)] = b - a\Delta$

TABLE 7.1 (CONTINUED)

REGION / PERIOD	a	b	c	p	q
			EVENT: 10/17/77, coefficient (a)($\times 10^{-4}$ km^{-1})		
20		----------			----------
30		1.056 (0.575)			----------
40		1.143 (0.431)			0.501 (0.483)
50		1.119 (0.365)			1.106 (0.628)
60		1.287 (0.498)			0.857 (0.719)
70		0.658 (0.469)			0.600 (0.603)
80		0.602 (0.518)			0.022 (0.580)
90		0.513 (0.387)			0.564 (0.583)
98		0.530 (0.534)			0.781 (0.683)
			EVENT: 10/17/77, coefficient (b)		
20		----------			----------
30		0.208 (0.634)			----------
40		0.321 (0.473)			0.157 (0.438)
50		0.192 (0.400)			0.151 (0.570)
60		0.052 (0.559)			0.008 (0.653)
70		-0.069 (0.475)			0.259 (0.548)
80		-0.157 (0.524)			-0.417 (0.526)
90		-0.008 (0.391)			0.474 (0.529)
98		0.046 (0.554)			0.663 (0.620)
			EVENT: 12/13/77, coefficient (a)($\times 10^{-4}$ km^{-1})		
20	----------	----------			
30	1.439 (0.883)	1.622 (0.837)			
40	0.669 (0.545)	1.245 (1.005)			
50	----------	1.306 (1.074)			
60	----------	0.838 (0.726)			
70	----------	0.611 (0.852)			
80	----------	0.313 (0.633)			
90	----------	0.931 (1.255)			
98	----------	0.746 (1.080)			
			EVENT: 12/13/77, coefficient (b)		
20	----------	----------			
30	0.334 (0.553)	0.203 (0.543)			
40	0.135 (0.342)	0.148 (0.651)			
50	----------	0.260 (0.717)			
60	----------	0.118 (0.485)			
70	----------	0.192 (0.566)			
80	----------	0.053 (0.429)			
90	----------	0.037 (0.858)			
98	----------	0.025 (0.694)			

TABLE 7.1 (TO BE CONTINUED)

where: $\ln[A^o(T,\Delta)\ (R \sin\Delta')/A^t(T,\Delta)] = b - a\Delta$

TABLE 7.1 (CONTINUED)

REGION / PERIOD	a	b	c	p	q
			EVENT: 03/24/78, coefficient (a)($\times 10^{-4}$ km^{-1})		
20			----------		
30			0.526 (2.071)		
40			-0.679 (1.328)		
50			2.168 (1.807)		
60			1.128 (1.735)		
70			1.212 (1.621)		
80			----------		
90			----------		
98			----------		
			EVENT: 03/24/78, coefficient (b)		
20			----------		
30			0.554 (0.540)		
40			0.328 (0.346)		
50			0.662 (0.471)		
60			0.752 (0.453)		
70			0.743 (0.423)		
80			----------		
90			----------		
98			----------		
			EVENT: 01/28/79, coefficient (a)($\times 10^{-4}$ km^{-1})		
20			----------		
30			0.843 (0.681)		
40			1.227 (0.702)		
50			0.490 (0.509)		
60			0.408 (0.460)		
70			0.469 (0.789)		
80			-0.767 (1.046)		
90			----------		
98			----------		
			EVENT: 01/28/79, coefficient (b)		
20			----------		
30			0.113 (0.304)		
40			0.358 (0.313)		
50			0.192 (0.227)		
60			0.045 (0.205)		
70			0.284 (0.342)		
80			-0.040 (0.452)		
90			----------		
98			----------		

TABLE 7.1 (TO BE CONTINUED)

where: $\ln[A^o(T,\Delta)\ (R \sin\Delta')/A^t(T,\Delta)] = b - a\Delta$

TABLE 7.1 (CONTINUED)

REGION / PERIOD	s
	EVENT: 05/31/71, coefficient (a)($\times 10^{-4}$ km^{-1})
20	-0.995 (0.769)
30	-0.041 (0.730)
40	-0.068 (0.491)
50	0.338 (0.465)
60	0.160 (0.624)
70	0.232 (0.441)
80	0.331 (0.298)
90	0.404 (0.335)
98	0.915 (1.225)
	EVENT: 05/31/71, coefficient (b)
20	-0.324 (0.406)
30	-0.253 (0.416)
40	-0.272 (0.279)
50	-0.142 (0.265)
60	-0.200 (0.356)
70	-0.070 (0.251)
80	0.032 (0.164)
90	0.182 (0.180)
98	0.319 (0.646)

where: $\ln[A^{o}(T,\Delta)\ (R \sin\Delta')/A^{t}(T,\Delta)] = b - a\Delta$

TABLE 7.2 - JORDAN'S MODEL - ATTENUATION COEFFICIENT γ (X 10^{-4} km^{-1})

REGION T (sec)	a	b	c	p	q	s
20	1.853 2 0.533	0.324 16 0.251	-1.018 1 -----	----- -- -----	0.940 2 0.880	-0.995 1 -----
30	0.872 7 0.306	0.891 37 0.135	0.161 3 0.668	-0.001 3 0.725	0.472 15 0.215	-0.041 1 -----
40	0.701 8 0.299	1.007 37 0.115	0.291 3 0.781	0.520 3 0.410	0.623 17 0.249	-0.068 1 -----
50	0.554 7 0.378	1.112 38 0.094	1.892 3 0.229	0.157 3 0.165	0.555 18 0.207	0.338 1 -----
60	0.297 6 0.362	1.004 36 0.104	1.587 3 0.363	0.410 3 0.136	0.581 18 0.178	0.160 1 -----
70	0.319 7 0.428	0.851 35 0.126	1.350 2 0.195	0.436 3 0.181	0.645 17 0.147	0.232 1 -----
80	0.261 6 0.422	0.586 32 0.147	0.554 2 1.868	0.344 3 0.160	0.433 16 0.201	0.331 1 -----
90	-0.098 5 0.526	0.509 29 0.156	1.707 1 -----	0.573 2 0.593	0.377 13 0.211	0.404 1 -----
98	0.169 3 0.383	0.448 24 0.142	1.573 1 -----	----- -- -----	0.216 11 0.162	0.915 1 -----

Chapter 7 - Figure Captions

Figure 7.1 - Variation of the logarithmic ratios of the observed and calculated amplitudes with the epicentral distance at which the observation was taken. A straight line was fitted to these data, and the slope a' and the intercept value b' determined. This result is for fundamental mode Rayleigh waves with period 50 sec, generated by earthquake number 30 (April 26, 1973) of Table 4.1, and which travelled 40% or more of their total path length within areas represented by the region-type 'b' of the discretized model from Jordan (1981).

Figure 7.2 - Summary of values of Q for fundamental mode Rayleigh waves with period between 20 and 100 sec propagating in the United States. These values are compared with those obtained in our work for the region-type 'q' of the model by Jordan (1981). Frequency f is given in Hz.

Figure 7.3 - Summary of values of Q regionalized by Canas and Mitchell for fundamental mode Rayleigh waves with period between 20 and 100 sec propagating in the Pacific Ocean

(indices (1), (2), and (3) represent the age zones 0 - 50 m.y., 50 - 100 m.y., and older than 100 m.y., respectively). The values from our work are those corresponding to region-type 'b' of the model of Jordan (1981). Frequency f is given in Hz.

FIGURE 7.1

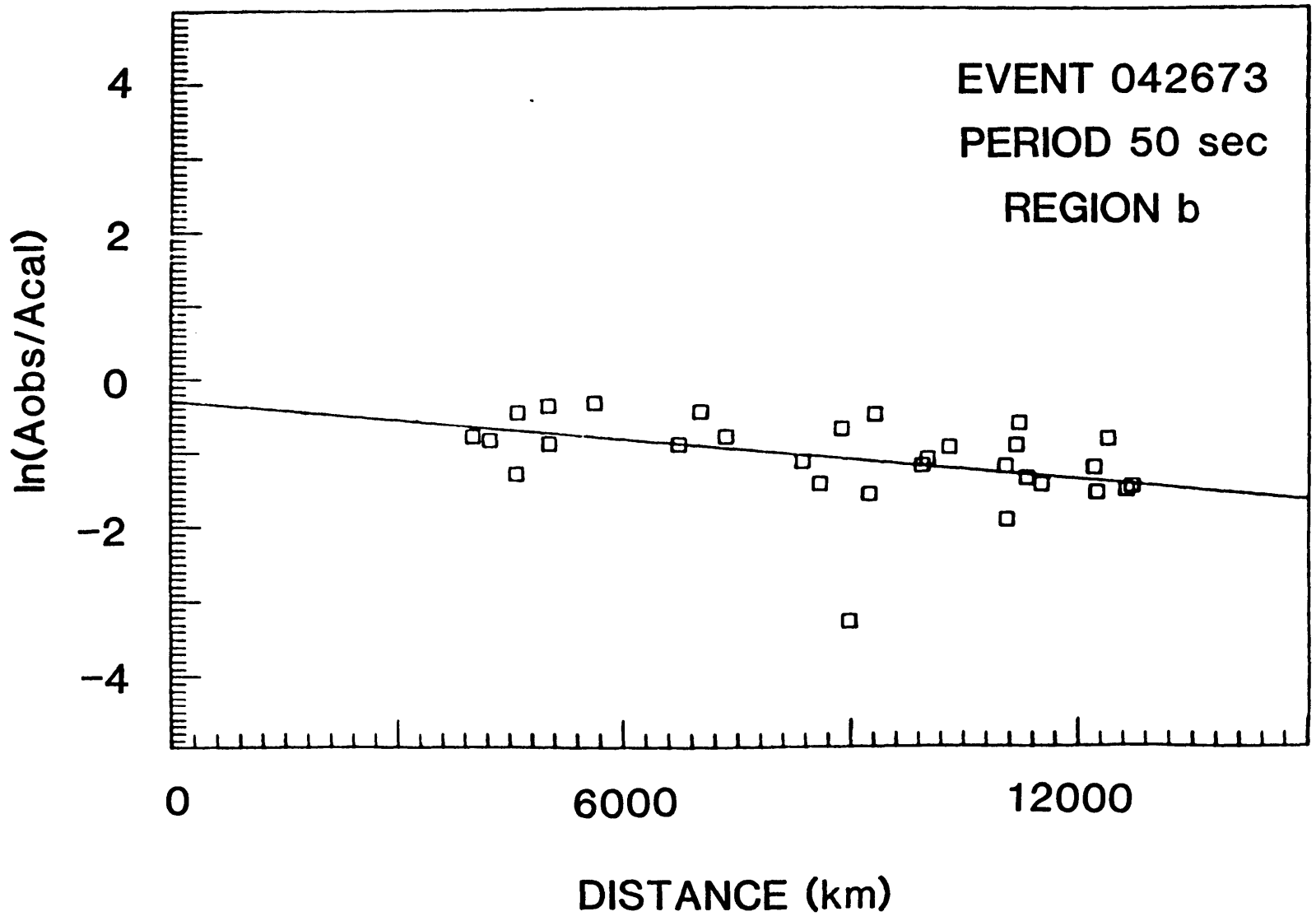
EVENT 042673
PERIOD 50 sec
REGION b
ln(Aobs/Acal)
4
2
0
−2
−4
0
6000
12000
DISTANCE (km)

FIGURE 7.2

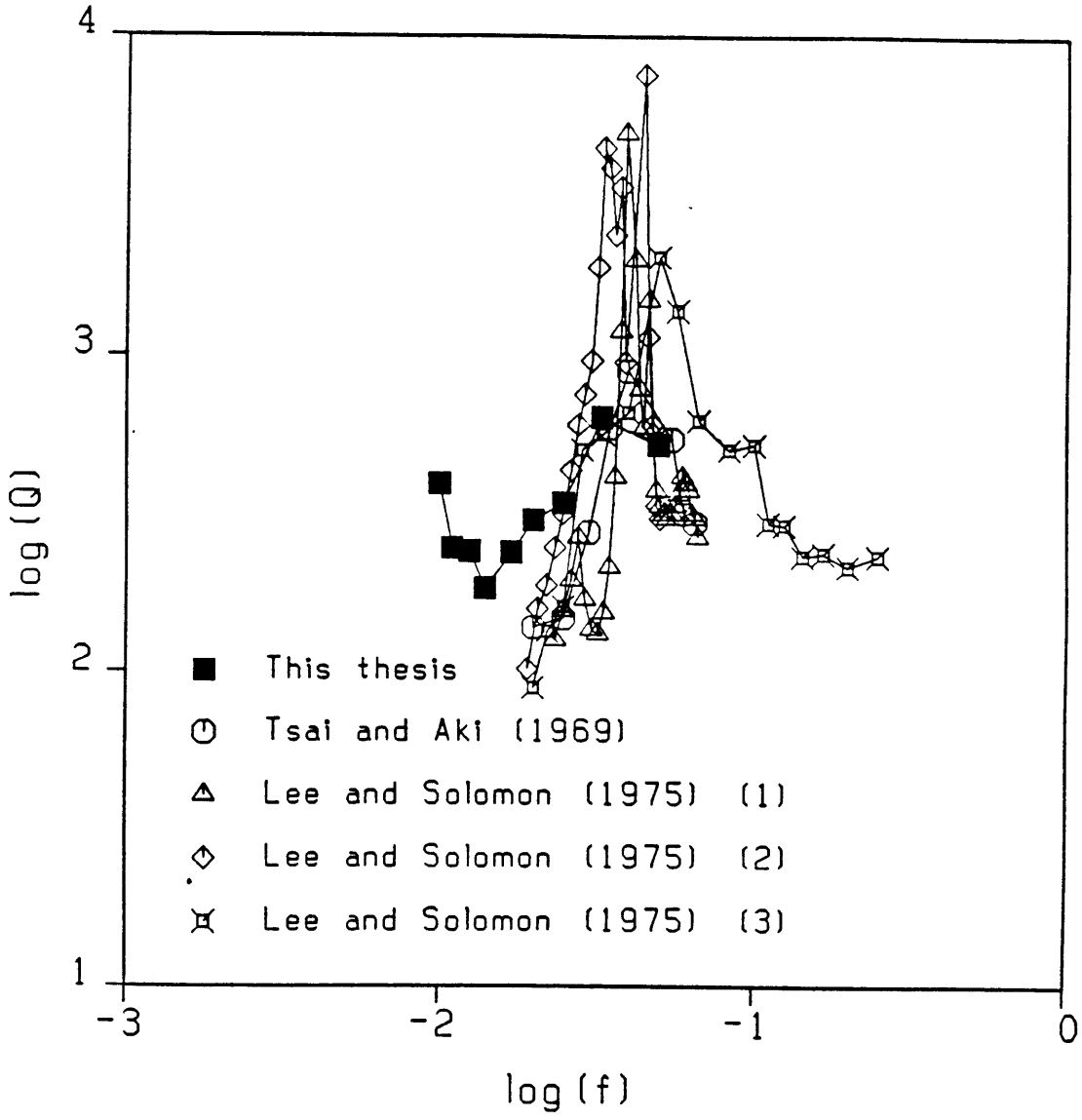
4
3
2
1
log (Q)
-3
-2
-1
0
log (f)
This thesis
Tsai and Aki (1969)
Lee and Solomon (1975) (1)
Lee and Solomon (1975) (2)
Lee and Solomon (1975) (3)

FIGURE 7.3

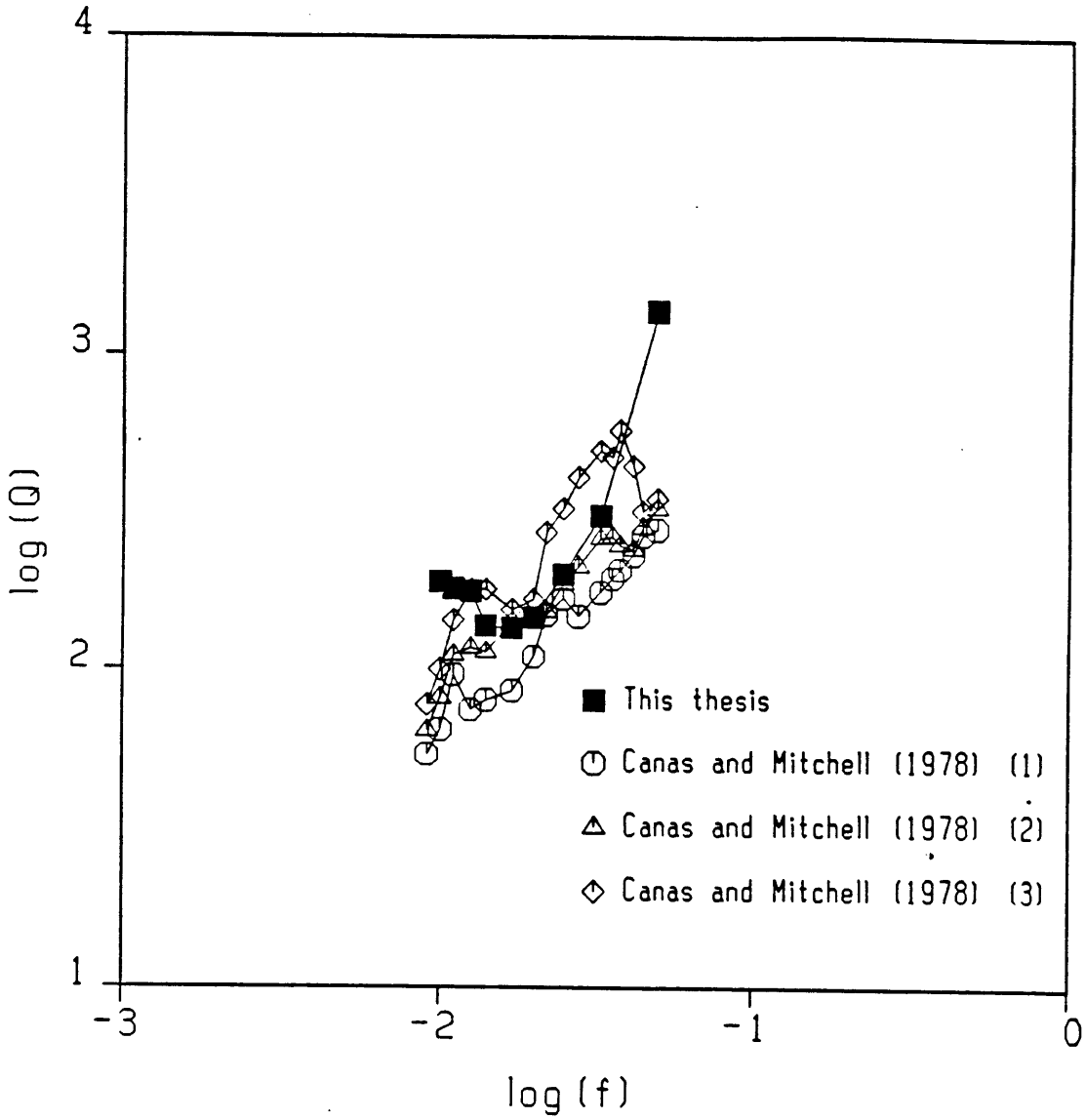
4
3
2
1
log (Q)
-3
-2
-1
0
log (f)
This thesis
Canas and Mitchell (1978) (1)
Canas and Mitchell (1978) (2)
Canas and Mitchell (1978) (3)

CHAPTER 8:

Conclusions:

We have gathered from the literature a large amount of phase velocity data for fundamental mode Rayleigh waves with period ranging between 20 and 100 sec, and organized a database of these values so that they can be effectively and routinely used for various purposes. The error bounds estimated by each author were included in our review of each paper. These error estimates were made using different criteria, and the data quality differs greately, in a way that a regionalization process was necessary.

The collected data were used to determine the mean phase velocity for the regionalized Earth models of Jordan (1981), Leveque (1980), and Okal (1977). These values serve as an initial model used in the unwrapping process of the phase spectra measured in a second part of our study. These observations correspond to Rayleigh waves generated by a set of 45 earthquakes, which had their source mechanism and focal depth determined by other authors. They used body-waveform data matching in their work, and their results agree well with our surface wave amplitude data. The newly measured phase

velocity data were used to increase our original phase velocity data, which was more than doubled.

The three regionalized Earth models above can also be used in a variety of fields in Geophysics to study areas located anywhere on the Earth. We hope that this newly available and well-catalogued set of information will significantly increase the use of fundamental mode Rayleigh waves in the period range considered, in present geophysical studies.

We have applied to our data the stochastic inverse method in order to obtain the global distribution of Rayleigh wave phase velocity values. Although this method is not new in Geophysics, its application to surface wave global studies is innovative. The method includes a simple and robust error analysis, as well as the possibility of checking the resolution of our solution, which are very useful tools while analyzing the resulting anomalies. The resultant anomalies of our studies correlate well with major tectonic features, in a way that our results can be effectively used in studies on the structure of the crust and upper mantle. This is important since the period range considered here has not been included in previous global surface wave studies. Our results

correlate well with previous regional studies made with similar period band (*e.g.* Yomogida, 1985 and, Nishimura and Forsyth, 1985). The results for 90 and 98 sec correlate well with those obtained by Tanimoto and Anderson (1985) at 100 sec. In this case, we showed that our results represent an improvement on their analysis, since more data and more variables were used, and a higher improvement in the initial data variance was achieved. It is also important to mention the significance of our results for use in the moment tensor inversion of other events. As we demonstrated before, our results at longer periods can be applied to correct Rayleigh wave phase observations from other earthquakes for the propagation effect, in a way that these can be used to obtain the moment tensor solution of events in most regions around the globe. On the other hand, shorter period results cannot be applied in this fashion, due to still large residual data variance obtained from the inversion. The application of the moment tensor inversion method, in this case, is limited to areas close to the reference points. Further improvements of the results for these periods require the addition of a much larger number of such reference points. This can be done in two ways: by studying events with epicenter near these

reference points at first, and then expanding the network of such points by considering the phase velocity dispersion curves to the epicenter of these events, in an iterative fashion as that proposed by Patton (1978). The second approach is the application of the body waveform inversion method to new events, for which dispersion curves would then be studied to obtain more phase velocity data. Maybe the most reasonable approach is to undertake both of these simultaneously. In any case, it is clear that the problem is best treated on a global scale, and that the phase velocity dispersion curves are the key elements needed to correct Rayleigh wave observations for the propagation effect.

Other propagation parameters measured in this thesis namely, the group velocity and attenuation coefficient data, also represent an advance in the study of Rayleigh waves, despite the fact that they include larger measurement errors than the phase velocity data. In the case of our group velocity study, we found that the standard deviation of the regionalized values were very similar to those obtained in the phase velocity regionalization. This showed that the large, unacceptable error bounds achieved after application of the stochastic inversion to the group velocity data, are related

to the larger errors involved in the measurement of group velocity. This makes it much harder to obtain useful results from such analysis involving group velocity data.

In the case of our study on the attenuation coefficient, we verified that the attenuation data is even poorer, mainly due to the effect of focusing, defocusing, and multipath interference on the amplitude of these waves. We suggest that another approach should be taken while studying attenuation, this time including our phase velocity maps and regionalized group velocity models while calculating the theoretical amplitude value, which can then be compared with the observation.

References

Aki, K., Crustal structure in Japan from the phase velocity of Rayleigh waves. Part 1 - Use of the network of seismological stations operated by the Japan Meteorological Agency., Bull. Earthq. Res. Inst., 39, 255-283, 1961.

Aki, K., Generation and propagation of G waves from the Niigata earthquake of June 16, 1964. Part 1. A statistical analysis, Bull. Earthq. Res. Inst., 44, 23-72, 1966.

Aki, K., Three dimensional seismic velocity anomalies in the lithosphere - method and summary of results, J. Geophys., 43, 235-242, 1977.

Aki, K., Three-dimensional seismic anomalies and their relation to local seismicity, Tectonophysics, 56, 85-88, 1979.

Aki, K., 3-D inhomogeneities in the upper mantle, Tectonophysics, 75, 31-40, 1981.

Aki, K., Progress report on the determination of seismic moment tensor from long-period surface waves, Tectonophysics, 84, 1-2, 1982a.

Aki, K., Three-dimensional seismic inhomogeneities in the lithosphere and asthenosphere: evidence for decoupling in the lithosphere and flow in the asthenosphere, Rev. of Geophys. and Space Phy, 20, 161-170, 1982b.

Aki, K., A. Christofferson, and E. S. Husebye, Three-dimensional seismic structure of the lithosphere, J. Geophys. Res., 82, 277-296, 1977.

Aki, K., and W. H. K. Lee, Determination of three-dimensional velocity anomalies under a seismic array using first P arrival times from earthquakes, 1, A homogeneous initial model, J. Geophys. Res., 81, 4381-4399, 1976.

Aki, K., J. A. Mendiguren, and Y. B. Tsai, Reply on A. McGarr's 'Comments on some papers concerning amplitudes of seismic surface waves', J. Geophys. Res., 77, 3827-3830, 1972.

Aki, K., and J. M. Nordquist, Automatic computation of impulse response seismograms of Rayleigh waves for mixed paths., Bull. Seismol. Soc. Am., 51, 29-34, 1961.

Aki, K., and H. J. Patton, Determination of seismic moment tensor using surface waves, Tectonophysics, 49, 213-222, 1978.

Aki, K., and P. G. Richards, Quantitative Seismology, Theory and Methods, vols. 1 and 2, W. H. Freeman, San Francisco, 1980.

Alexander, S., S., Surface wave propagation in the western United States, PhD thesis, Cal. Inst. of Technol., p. 242, Pasadena, 1963.

Anderson, D., L., Surface wave tomography, Eos, Trans. Am. geophys. Un., 65, 147-148, 1984.

Bache, T., C., W. L. Rodi, and D. G. Harkrider, Crustal structures inferred from Rayleigh-wave signatures of NTS explosions, Bull. Seismol. Soc. Am., 68, 1399-1413, 1978.

Backus, G., E., and J. F. Gilbert, Numerical applications of a formalism for geophysical inverse problems, Geophys. J. R. astr. Soc., 13, 247-276, 1967.

Backus, G., E., and J. F. Gilbert, The resolving power of gross earth data, Geophys. J. R. astr. Soc., 16, 169-205, 1968.

Backus, G., E., and J. F. Gilbert, Uniqueness in the inversion of inaccurate gross Earth data, Phil. Trans. R. Soc. Lon., A, 266, 123-192, 1970.

Baldi, P., G. Ferrari, and F. Mantovani, Evidence of rifting in the Tyrrhenian Sea observing Rayleigh wave dispersion, Bolletino di Geofisica Teorica, 21, 94-104, 1979.

Baldi, P., M. Gasperini, and E. Mantovani, Rayleigh wave velocities in Central Northern Italy, Annali di Geofisica, 31, 181-196, 1978.

Ben-Menahem, A., Observed attenuation and Q values of seismic surface waves in the upper mantle, J. Geophys. Res., 70, 4641-4651, 1965.

Bergman, E., A., Intraplate earthquakes and the state of stress in oceanic lithosphere, submitted to Tectonophysics, 1985.

Bergman, E., A., J. L. Nábělek, and S. C. Solomon, An extensive region of off-ridge normal-faulting earthquakes in the southern Indian Ocean, J. Geophys. Res., 89, 2425-2443, 1984.

Bergman, E., A., J. L. Nabelek, and S. C. Solomon, Correction to "An extensive region of off-ridge normal-faulting earthquakes in the southern Indian Ocean", J. Geophys. Res., 90, 2066-2067, 1985.

Bergman, E., A., and S. C. Solomon, Source mechanisms of earthquakes near mid-ocean ridges from body waveform inversion: implications for the early evolution of oceanic lithosphere, J. Geophys. Res., 89, 11415-11441, 1984.

Bergman, E., A., and S. C. Solomon, Earthquake source mechanisms from body-waveform inversion and intraplate tectonics in the northern Indian Ocean, Phys. Earth Planet. Inter., 40, 1-23, 1985.

Berry, M., J., and L. Knopoff, Structure of the upper mantle under the Western Mediterranean Basin, J. Geophys. Res., 72, 3613-3626, 1967.

Birch, F., The velocity of compressional waves in rocks to 10 kilobars, part 2, J. Geophys. Res., 66, 2199-2224, 1961.

Bird, P., and M. N. Toksoz, Strong attenuation of Rayleigh waves in Tibet, Nature, 266, 161-163, 1977.

Biswas, N., N., The upper mantle structure of the United States from the dispersion of surface waves, PhD thesis, University of California, p. 175, Los Angeles, 1971.

Biswas, N., N., and L. Knopoff, The structure of the upper mantle under the United States from the dispersion of Rayleigh waves, Geophys. J. R. astr. Soc., 36, 519-539, 1974.

Bloch, S., and A. L. Hales, New techniques for the determination of surface wave phase velocities, Bull. Seismol. Soc. Am., 58, 1021-1034, 1968.

Bloch, S., A. L. Hales, and M. Landisman, Velocities in the crust and upper mantle of southern Africa from multi-mode surface wave dispersion, Bull. Seismol. Soc. Am., 59, 1599-1629, 1969.

Bolt, B., A., and J. Dorman, Phase and group velocities of Rayleigh waves in a spherical, gravitating Earth, J. Geophys. Res., 66, 2965-2981, 1961.

Bolt, B., A., and M. Niazi, Dispersion of Rayleigh waves across Australia, Geophys. J. R. astr. Soc., 9, 21-35, 1964.

Brandon, C., and B. A. Romanowicz, Pure path phase velocities of Rayleigh waves in Tibet: evidence for north-south and east-west variations of crust and upper mantle structure, Eos, Trans. Am. geophys. Un., 65, 1000, 1984.

Brandon, C., and B. A. Romanowicz, A "no-lid" zone in the central Chang-Thang platform of Tibet: evidence from pure path phase velocity measurements of long period Rayleigh waves, J. Geophys. Res., 91, 6547-6564, 1986.

Brooks, J., A., Rayleigh waves in southern New Guinea II - A shear velocity profile, Bull. Seismol. Soc. Am., 59, 2017-2038, 1969.

Brune, J., N., Correction of initial phase measurements for the southeast Alaska earthquake of July 10, 1958, and for certain nuclear explosions, J. Geophys. Res., 67, 3643-

3644, 1962a.

Brune, J., N., Attenuation of dispersed wave trains, Bull. Seismol. Soc. Am., 52, 109-112, 1962b.

Brune, J., N., Surface waves and crustal structure, in The Earth's Crust and Upper Mantle, Geophysical Monograph 13, edited by P. Hart, pp. 230-242, Amer. Geophys. Union, Washington, D. C., 1969.

Brune, J., N., and J. Dorman, Seismic waves and Earth structure in the Canadian Shield, Bull. Seismol. Soc. Am., 53, 167-210, 1963.

Brune, J., N., J. E. Nafe, and J. E. Oliver, A simplified method for the analysis and synthesis of dispersed wave trains, J. Geophys. Res., 65, 287-304, 1960.

Bungum, H., and J. Capon, Coda pattern and multipath propagation of Rayleigh waves at NORSAR, Phys. Earth Planet. Inter., 9, 111-127, 1974.

Burkhard, N., R., Upper mantle structure of the Pacific basin from inversion of gravity and seismic data, PhD thesis, University of California, p. 169, Los Angeles, 1977.

Burkhard, N., R., and D. D. Jackson, Density and surface wave inversion, Geophys. Res. Lett., 3, 637-638, 1976.

Burton, P., W., Estimations of Q from seismic Rayleigh waves, Geophys. J. R. astr. Soc., 36, 167-189, 1974.

Calcagnile, G., The lithosphere-asthenosphere system in Fennoscandia, Tectonophysics, 90, 19-35, 1982.

Calcagnile, G., U. Mascia, V. del Gaudio, and G. F. Panza, Deep structure of southeastern Europe from Rayleigh waves, Tectonophysics, 110, 189-200, 1984.

Calcagnile, G., and G. F. Panza, Crust and upper mantle structure under the Baltic Shield and Barents Sea from the dispersion of Rayleigh waves, Tectonophysics, 47, 59-71, 1978.

Calcagnile, G., and G. F. Panza, Central and upper mantle structure beneath the Apennines region as inferred from the study of Rayleigh waves, J. Geophys., 45, 319-327, 1979.

Calcagnile, G., and G. F. Panza, Upper mantle structure of the Apulian plate from Rayleigh waves, Pure and Applied Geophysics, 118, 823-830, 1980.

Calcagnile, G., G. F. Panza, and L. Knopoff, Upper-mantle structure of north-central Italy from the dispersion of Rayleigh waves, Tectonophysics, 56, 51-63, 1979.

Canas, J., and B. J. Mitchell, Lateral variation of surface-wave anelastic attenuation across the Pacific, Bull. Seismol. Soc. Am., 68, 1637-1650, 1978.

Capon, J., Analysis of Rayleigh-wave multipath propagation at LASA, Bull. Seismol. Soc. Am., 60, 1701-1731, 1970.

Caputo, M., L. Knopoff, E. Mantovani, S. Mueller, and G. F. Panza, Rayleigh wave phase velocities and upper mantle structure in the Apennines, Annali di Geofisica, 4, 199-214, 1976.

Chang, F., The structure of the upper mantle of Eurasia and tectonic interpretation from a study of Rayleigh wave dispersion, PhD thesis, University of California, p. 209, Los Angeles, 1979.

Chaudhury, H., M., Seismic surface wave dispersion and the crust across the Gangetic basin, Indian Jour. Meteorology and G, 17, 385-394, 1966.

Cisternas, A., Crustal structure of the Andes from Rayleigh wave dispersion, Bull. Seismol. Soc. Am., 51, 381-388, 1961.

de Boor, C., A practical guide to splines, Spring-Verlag, New York, 1978.

de Groot, M., H., Probability and statistics, Addison-Wesley, Reading, 1975.

Dorman, J., .Seismic surface-wave data on the upper mantle, in The Earth's crust and upper mantle, Geophysical Monograph 13, edited by P. Hart, pp. 257-265, Amer. Geophys. Union, Washington, D. C., 1969.

Dorman, J., and M. Ewing, Numerical inversion of seismic surface wave dispersion data and crust-mantle structure in the New York-Pennsylvania area, J. Geophys. Res., 67, 5227-5241, 1962.

Dorman, J., M. Ewing, and J. Oliver, Study of shear-velocity distribution in the upper mantle by mantle Rayleigh waves, Bull. Seismol. Soc. Am., 50, 87-115, 1960.

Draper, N., R., and H. Smith, Applied regression analysis, John Wiley and Sons, New York, 1966.

Dziewonski, A., M., and D. L. Anderson, Seismic tomography of the Earth's interios, American Scientist, 72, 483-494, 1984.

Dziewonski, A., M., S. Bloch, and M. Landisman, A technique for the analysis of transient seismic signals, Bull. Seismol. Soc. Am., 59, 427-444, 1969.

Dziewonski, A., M., and A. L. Hales, Numerical analysis of dispersed seismic waves, in Methods of computational physics, edited by B. A. Bolt, pp. 39-85, Academic Press, New York and London, 1972.

Dziewonski, A., M., and J. M. Steim, Dispersion and attenuation of mantle waves through waveform inversion, Geophys. J. R. astr. Soc., 70, 503-527, 1982.

Evernden, J., F., Direction of approach of Rayleigh waves and related problems (Part I), Bull. Seismol. Soc. Am., 43, 335-374, 1953.

Evernden, J., F., Direction of approach of Rayleigh waves and related problems (Part II), Bull. Seismol. Soc. Am., 44, 159-184, 1954.

Ewing, M., and F. Press, An investigation of mantle Rayleigh waves, Bull. Seismol. Soc. Am., 44, 127-147, 1954a.

Ewing, M., and F. Press, Mantle Rayleigh waves from the Kamchatka earthquake of Nov. 4, 1952, Bull. Seismol. Soc. Am., 44, 471-479, 1954b.

Ewing, M., and F. Press, Determination of crustal structural from phase velocity of Rayleigh waves, Part III: The United States, Bull. Geol. Soc. Am., 70, 229-244, 1959.

Feng, C., and T. Teng, An error analysis of frequency-time analysis, Bull. Seismol. Soc. Am., 73, 143-155, 1983a.

Feng, C., and T. Teng, Three-dimensional crust and upper mantle structure of the Eurasian Continent, J. Geophys. Res., 88, 2261-2272, 1983b.

Forsyth, D., W., Anisotropy and the structural evolution of the oceanic upper mantle, PhD thesis, Mass. Inst. of Technol., p. 253, Cambridge, 1973.

Forsyth, D., W., The early structural evolution and anisotropy of the oceanic upper mantle, Geophys. J. R. astr. Soc., 43, 103-162, 1975.

Forsyth, D., W., The evolution of the upper mantle beneath mid-ocean ridges, Tectonophysics, 38, 89-118, 1977.

Fouda, A., A., The upper mantle structure under the stable regions, PhD thesis, University of California, p. 132, Los Angeles, 1973.

Franklin, J., N., Well-posed stochastic extension of ill-posed linear problems, J. Math. Anal. Appl., 31, 682-716, 1970.

Gabriel, V., G., and J. T. Kuo, High Rayleigh wave phase velocities for the New Delhi, India - Lahore, Pakistan profile, Bull. Seismol. Soc. Am., 56, 1137-1145, 1966.

Gilbert, F., Excitation of the normal modes of the Earth by earthquake source, Geophys. J. R. astr. Soc., 22, 223-226, 1970.

Glover, P., and S. S. Alexander, Lateral variations in crustal structure beneath the Montana LASA, J. Geophys. Res., 74, 505-531, 1969.

Goncz, J., H., A. L. Hales, and K. J. Muirhead, Analysis to extended periods of Rayleigh and Love wave dispersion across Australia, Geophys. J. R. astr. Soc., 41, 81-105, 1975.

Gregersen, S., Surface wave dispersion and crust structure in Greenland, Geophys. J. R. astr. Soc., 22, 29-39, 1970.

Gumper, F., and P. W. Pomeroy, Seismic wave velocities and Earth structure on the African continent, Bull. Seismol. Soc. Am., 60, 651-668, 1970.

Gupta, H., K., and J. G. Negi, Lateral variation of Rayleigh-wave dispersion characteristics in Australia, Bull. Seismol. Soc. Am., 60, 1897-1906, 1970.

Gupta, H., K., D. C. Nyman, and M. Landisman, Shield-like upper mantle velocity structure below the Indo-gangetic Plains: inferences drawn from long-period surface wave dispersion studies, Earth and Plan. Sci. Lett., 34, 51-55, 1977.

Hadiouche, O., N. Jobert, and B. A. Romanowicz, First two-station results for long-period surface waves velocity from the GEOSCOPE stations in Africa, Geophys. Res. Lett., 13, 547-550, 1986.

Hagiwara, T., A note on the theory of the eletromagnetic seismograph, Bull. Earthq. Res. Inst., 36, 139-164, 1958.

Harkrider, D., G., and D. L. Anderson, Surface wave energy from point sources in plane layered Earth models, J. Geophys. Res., 71, 2967-2980, 1966.

Haskell, N., A., The dispersion of surface waves on multilayered media, Bull. Seismol. Soc. Am., 43, 17-34, 1953.

Herrin, E. (editor), 1968 seismological tables for P phases, Bull. Seismol. Soc. Am., 58, 1193-1242, 1968.

Hildebrand, F., B., Introduction to numerical analysis, Second edition, McGraw-Hill, New York, 1974.

Hirahara, K., A large-scale three-dimensional seismic structure under the Japan Islands and the Sea of Japan, J. Phys. Earth, 25, 393-417, 1977.

Hirahara, K., Three-dimensional seismic structure beneath southwest Japan: The subducting Philippine Sea plate, Tectonophysics, 79, 1-44, 1981.

Horie, A., and K. Aki, Three-dimensional velocity structure beneath the Kanto district, Japan, J. Phys. Earth, 30, 255-281, 1982.

Huang, P., Y., Focal depths and mechanisms of mid-ocean ridge earthquakes from body waveform inversion, PhD thesis, Mass. Inst. of Technol., p. 301, Cambridge, 1985.

Huang, P., Y., S. C. Solomon, E. A. Bergman, and J. L. Nábělek, Focal depths and mechanisms of Mid-Atlantic ridge earthquakes from body waveform inversion, J. Geophys. Res., 91, 579-598, 1986.

Jackson, D., D., The use of a priori data to resolve non-uniqueness in linear inversion, Geophys. J. R. astr. Soc., 57, 137-157, 1979.

James, D., E., Andean crustal and upper mantle structures, J. Geophys. Res., 76, 3246-3271, 1971.

James, D., E., and A. Linde, A source of major error in the digital analysis of World Wide Standard Station seismograms, Bull. Seismol. Soc. Am., 61, 723-728, 1971.

Jemsek, J., P., E. A. Bergman, J. L. Náběl ek, and S. C. Solomon, Large earthquakes and tectonics of the Arctic Rift System, unpublished manuscript, 1985.

Jordan, T., H., Estimation of the radial variation of seismic velocities and density of the Earth, PhD thesis, Calif. Inst. of Technol., Pasadena, 1972.

Jordan, T., H., The deep structure of the continents, Scientific American, 240, 92-107, 1979a.

Jordan, T., H., Structural geology of the Earth's interior, Proc. Natl. Acad. Sci. USA, 76, 4192-4200, 1979b.

Jordan, T., H., Global tectonic regionalization for seismological data analysis, Bull. Seismol. Soc. Am., 71, 1131-1141, 1981.

Kaminuma, K., Crustal structure in Japan from the phase velocity of Rayleigh waves. Part 3 - Rayleigh waves from the Mindanao shock of Sept. 24, 1957, Bull. Earthq. Res. Inst., 42, 19-38, 1964.

Kaminuma, K., The crust and upper mantle structure in Japan. Part 1 - Phase velocities of Love and Rayleigh waves in central Japan, Bull. Earthq. Res. Inst., 44, 481-494, 1966a.

Kaminuma, K., The crust and upper mantle structure in Japan. Part 2 - Crustal structure in Japan from the phase velocity of Rayleigh waves, Bull. Earthq. Res. Inst., 44, 495-510, 1966b.

Kaminuma, K., The crust and upper mantle structure in Japan. Part 3 - An anisotropic model of the structure in Japan, Bull. Earthq. Res. Inst., 44, 511-518, 1966c.

Kaminuma, K., and K. Aki, Crustal structure in Japan from the phase velocity of Rayleigh waves. Part 2 - Rayleigh waves from the Aleutian shock of March 9, 1957, Bull. Earthq. Res. Inst., 41, 217-241, 1963.

Kanamori, H., and J. W. Given, Use of long-period surface waves for rapid determination of earthquake-source parameters, Phys. Earth Planet. Inter., 27, 8-31, 1981.

Kanamori, H., and J. W. Given, Use of long-period surface waves for fast determination of earthquake source parameters: 2. Preliminary determination of source mechanism of large earthquake (Ms>6.5) in 1980, Phys. Earth Planet. Inter., 30, 260-268, 1982.

Kausel, E., G., A. R. Leeds, and L. Knopoff, Variations of Rayleigh wave phase velocities across the Pacific Ocean, Science, 186, 139-141, 1974.

Knopoff, L., Observation and inversion of surface-wave dispersion, Tectonophysics, 13, 497-519, 1972.

Knopoff, L., The thickness of the lithosphere from the dispersion of surface waves, Geophys. J. R. astr. Soc., 74, 55-81, 1983.

Knopoff, L., M. J. Berry, and F. A. Schwab, Tripartite phase velocity observations in laterally heterogeneous regions, J. Geophys. Res., 72, 2595-2601, 1967.

Knopoff, L., and A. A. Fouda, Upper-mantle structure under the Arabian Peninsula, Tectonophysics, 26, 121-134, 1975.

Knopoff, L., S. Mueller, and W. L. Pilant, Structure of the crust and upper mantle in the Alps from the phase velocity of Rayleigh waves, Bull. Seismol. Soc. Am., 56, 1009-1044, 1966.

Knopoff, L., and J. W. Schlue, Rayleigh wave phase velocities for the path Addis Ababa-Nairobi, Tectonophysics, 15, 157-163, 1972.

Knopoff, L., J. W. Schlue, and F. A. Schwab, Phase velocities of Rayleigh waves across the East Pacific Rise, Tectonophysics, 10, 321-334, 1970.

Knopoff, L., and F. A. Schwab, Apparent initial phase of a source of Rayleigh waves, J. Geophys. Res., 73, 755-760, 1968.

Knopoff, L., F. A. Schwab, and J. W. Schlue, The dispersion of Rayleigh waves south of the Gulf of California, Geofisica Internac., 9, 39-52, 1969.

Knopoff, L., and G. Vane, Age of East Antarctica from surface wave dispersion, Pure and Applied Geophysics, 117, 806-815, 1978.

Kovach, R., L., Seismic surface waves and crustal and upper mantle structure, Rev. of Geophys. and Space Phy, 16, 1-13, 1978.

Kuo, J., J. N. Brune, and M. Major, Rayleigh wave dispersion in the Pacific Ocean for the period range 20 to 140 seconds, Bull. Seismol. Soc. Am., 52, 333-357, 1962.

Landisman, M., A. M. Dziewonski, and Y. Sato, Recent improvements in the analysis of surface wave observations, Geophys. J. R. astr. Soc., 17, 369-403, 1969.

Langston, C., A., and D. V. Helmberger, A procedure for modeling shallow dislocation sources, Geophys. J. R. astr. Soc., 42, .117-130, 1975.

Lass, H., and P. Gottlieb, Probability and statistics, Addison-Wesley, Reading, 1971.

Lee, W., B., and S. C. Solomon, Inversion schemes for surface wave attenuation and Q in the crust and the mantle, Geophys. J. R. astr. Soc., 43, 47-71, 1975.

Leeds, A., R., Rayleigh wave dispersion in the Pacific basin, PhD thesis, University of California, p. 100, Los Angeles, 1973.

Leeds, A., R., Lithospheric thickness in the western Pacific, Phys. Earth Planet. Inter., 11, 61-64, 1975.

Leeds, A., R., L. Knopoff, and E. F. Kausel, Variations of upper mantle structure under the Pacific Ocean, Science, 186, 141-143, 1974.

Lévêque, J., J., Regional upper mantle S-velocity models from phase velocities of great-circle Rayleigh waves, Geophys. J. R. astr. Soc., 63, 23-43, 1980.

Levshin, A., L., T. M. Sabitova, and V. P. Valus, Joint interpretation of body and surface waves data for a district in Middle Asia, Geophys. J. R. astr. Soc., 11, 57-66, 1966.

Liao, A., H., Anisotropy in the upper mantle of Eurasia, PhD thesis, University of California, p. 177, Los Angeles, 1981.

Long, R., E., R. W. Backhouse, P. K. H. Maguire, and K. Sundarlingham, The structure of East Africa using surface wave dispersion and Durham seismic array data, Tectonophysics, 15, 165-178, 1972.

Luosto, U., Phase velocities of Rayleigh waves in southern Fennoscandia, Geophysica, 9, 167-172, 1965.

Lyon-Caen, H., Rayleigh waves phase velocities curves for paths across Europe and Africa, unpublished manuscript, 1980.

Marshall, P., D., and E. W. Carpenter, Estimates of Q for Rayleigh waves, Geophys. J. R. astr. Soc., 10, 549-550, 1966.

McCowan, D., W., Moment tensor representation of surface wave sources, Geophys. J. R. astr. Soc., 44, 595-599, 1976.

McEvilly, T., V., Central U.S. crust-upper mantle structure from Love and Rayleigh wave phase velocity inversion, Bull. Seismol. Soc. Am., 54, 1997-2015, 1964.

McGarr, A., Amplitude variations of Rayleigh waves-propagation across a continental margin, Bull. Seismol. Soc. Am., 59, 1281-1305, 1969a.

McGarr, A., Amplitude variations of Rayleigh waves - Horizontal refraction, Bull. Seismol. Soc. Am., 59, 1307-1334, 1969b.

McGarr, A., Comments on some papers concerning amplitudes of seismic surface waves, J. Geophys. Res., 77, 3823-3826, 1972.

Mendiguren, J., A., Focal mechanism of a shock in the middle of the Nazca plate, J. Geophys. Res., 76, 3861-3879, 1971.

Mendiguren, J., A., Inversion of surface wave data in source mechanism studies, J. Geophys. Res., 82, 889-894, 1977.

Mitchel, R., G., The structure of the upper mantle of western North America from multimode Rayleigh wave dispersion, PhD thesis, University of California, p. 177, Los Angeles, 1977.

Mitchell, B., J., Radiation and attenuation of Rayleigh waves from the southeastern Missouri earthquake of October 21, 1965, J. Geophys. Res., 78, 886-899, 1973a.

Mitchell, B., J., Surface wave attenuation and crustal enaslicity in central North America, Bull. Seismol. Soc. Am., 63, 1057-1071, 1973b.

Mitchell, B., J., Regional wave attenuation in North America, J. Geophys. Res., 80, 4904-4916, 1975.

Mitchell, B., J., L. W. B. Leite, Y. K. Yu, and R. B. Herrmann, Attenuation of Love and Rayleigh waves across the Pacific at periods between 15 and 110 seconds, Bull. Seismol. Soc. Am., 66, 1189-1201, 1976.

Mitchell, B., J., N. K. Yacoub, and A. M. Correig, A summary of seismic surface wave attenuation and its regional variation across continents and oceans, in The Earth's Crust, its nature and physical properties, Geophysical Monograph 20, edited by J. G. Heacock, pp. 405-425, Amer. Geophys. Union, Washington, D. C., 1977.

Mitchell, B., J., and G. Yu, Surface wave dispersion, regionalized velocity models, and anisotropy of the Pacific crust and upper mantle, Geophys. J. R. astr. Soc., 63, 497-514, 1980.

Mitrovas, W., Global and regional phase velocities of long-period fundamental mode Rayleigh waves, J. Geophys., 43, 287-298, 1977.

Moazami-Goudarzi, K., La vitesse de phase des ondes de Rayleigh et les structures de la croute et du manteau superieur entre Machhad et Chiraz (Iran), Pure and Applied Geophysics, 112, 675-681, 1974.

Mueller, S., and C. Sprecher, Upper mantle structure along a profile through the eastern Alps from Rayleigh wave dispersion, in Alps, Apennines, Hellenides, edited by H. Closs, pp. 40-44, Intern. Geodyn. Comm., sci. report, 1978.

Náběl̆ek, J., L., Determination of earthquake source parameters from inversion of body waves, PhD thesis, Mass. Inst. of Technol., p. 361, Cambridge, 1984.

Nakanishi, I., and D. L. Anderson, Worldwide distribution of group velocity of mantle Rayleigh waves as determined by spherical harmonic inversion, Bull. Seismol. Soc. Am., 72, 1185-1194, 1982.

Nakanishi, I., and D. L. Anderson, Measurements of mantle wave velocities and inversion for lateral heterogeneity and anisotropy, 1. Analysis of great circle phase velocities, J. Geophys. Res., 88, 10267-10283, 1983.

Nakanishi, I., and D. L. Anderson, Measurements of mantle wave velocities and inversion for lateral heterogeneity and anisotropy, 2. Analysis by the single-station method, Geophys. J. R. astr. Soc., 78, 573-617, 1984a.

Nakanishi, I., and D. L. Anderson, Aspherical heterogeneity of the mantle from phase velocities of mantle waves, Nature, 307, 117-121, 1984b.

Nakanishi, I., and H. Kanamori, Effects of lateral heterogeneity and source process time on the linear moment tensor inversion of long-period Rayleigh waves, Bull. Seismol. Soc. Am., 72, 2063-2080, 1982.

Nakanishi, I., and H. Kanamori, Source mechanisms of twenty-six large shallow earthquakes (Ms>6.5) during 1980 from P-wave first motion and long-period Rayleigh wave data, Bull. Seismol. Soc. Am., 74, 805-818, 1984.

Nataf, H., C., I. Nakanishi, and D. L. Anderson, Anisotropy and shear-velocity heterogeneities in the upper mantle, Geophys. Res. Lett., 11, 109-112, 1984.

Nataf, H., C., I. Nakanishi, and D. L. Anderson, Measurements of mantle wave velocities and inversion for lateral heterogeneities and anisotropy, 3. Inversion, J. Geophys. Res., 91, 7261-7308, 1986.

Niazi, M., Crustal thickness in the central Saudi Arabian Peninsula, Geophys. J. R. astr. Soc., 15, 545-547, 1968.

Nishimura, C., E., and D. W. Forsyth, Anomalous Love-wave phase velocities in the Pacific: sequential pure-path and spherical harmonic inversion, Geophys. J. R. astr. Soc., 81, 389-407, 1985.

Noponen, I., Surface wave phase velocities in Finland, Bull. Seismol. Soc. Am., 56, 1093-1104, 1966.

Okal, E., and J. Talandier, Rayleigh-wave phase velocities in French Polynesia, Geophys. J. R. astr. Soc., 63, 719-733, 1980.

Okal, E., A., The effect of intrinsic oceanic upper-mantle heterogeneity on regionalization of long-period Rayleigh-wave phase velocities, Geophys. J. R. astr. Soc., 49, 357-370, 1977.

Oliver, J., A summary of observed seismic surface wave dispersion, Bull. Seismol. Soc. Am., 52, 81-86, 1962.

Oliver, J., R. Kovach, and J. Dorman, Crustal structure of the New York-Pennsylvania area, J. Geophys. Res., 66, 215-225, 1961.

Panza, G., F., and G. Calcagnile, Crustal structure along the coast of California from Rayleigh waves, Phys. Earth Planet. Inter., 9, 137-140, 1974.

Panza, G., F., H. Neunhofer, and G. Calcagnile, Contribution to phase velocity investigations of Rayleigh-waves in Middle Europe, Pure and Applied Geophysics, 116, 1299-1306, 1978.

Papazachos, B., C., Dispersion of Rayleigh waves in the Gulf of Mexico and Carabbean Sea, Bull. Seismol. Soc. Am., 54, 909-925, 1964.

Papazachos, B., C., Phase velocities of Rayleigh waves in southeastern Europe and eastern Mediterranean Sea, Pure and Applied Geophysics, 75, 47-55, 1969.

Patton, H., J., Rayleigh wave phase velocities in the Indian ocean, unpublished manuscript, 1973.

Patton, H., J., Source and propagation effects of Rayleigh waves from central Asian earthquakes, PhD thesis, Mass. Inst. of Tech., p. 342, Cambridge, 1978.

Patton, H., J., Reference point equalization method for determining the source and path effects of surface waves, J. Geophys. Res., 85, 821-848, 1980a.

Patton, H., J., Crust and upper mantle structure of the Eurasian continent from the phase velocity and Q of surface waves, Rev. of Geophys. and Space Phy, 18, 605-625, 1980b.

Patton, H., J., Measurements of Rayleigh-wave phase velocities in Nevada: implications for explosion sources and the Massachusetts Mountain earthquake, Bull. Seismol. Soc. Am., 72, 1329-1349, 1982.

Patton, H., J., Regionalization of surface wave phase velocities in the western United States, Earthquake Notes, 55, 23-24, 1984.

Patton, H., J., and K. Aki, Bias in the estimate of seismic moment tensor by the linear inversion method, Geophys. J. R. astr. Soc., 59, 479-495, 1979.

Payo, G., Iberian Peninsula crustal structure from surface waves dispersion, Bull. Seismol. Soc. Am., 55, 727-743, 1965.

Payo, G., Crustal structure of the Mediterranean Sea. Part II - Phase velocity and travel times, Bull. Seismol. Soc. Am., 59, 23-42, 1969.

Payo, G., Structure of the crust and upper mantle in the Iberian Shield by means of a long period triangular array, Geophys. J. R. astr. Soc., 20, 493-508, 1970.

Payo, G., and E. Ruiz de la Parte, Dispersion of surface waves in the Iberian Peninsula and the adjacent Atlantic and Mediterranean areas, Geofisica Internac., 14, 89-102, 1974.

Pilant, W., L., Tectonic features of the Earth's crust and upper mantle, Semi-Annual Technical Report, Air Force Off. Sci. Res., 1966a.

Pilant, W., L., Tectonic features of the Earth's crust and upper mantle, Semi-Annual Technical Report, Air Force Off. Sci. Res., 1966b.

Pilant, W., L., Tectonic features of the Earth's crust and upper mantle, Final Technical Report, AFOSR 67 - 1797, Air Force Off. Sci. Res., 1967.

Pilant, W., L., and L. Knopoff, Observations of multiple seismic events, Bull. Seismol. Soc. Am., 54, 19-39, 1964.

Pomeroy, P., W., Long period seismic waves from large, near-surface nuclear explosions, Bull. Seismol. Soc. Am., 53, 109-149, 1963.

Press, F., Crustal structure determined by the phase velocity method, Eos, Trans. Am. geophys. Un., 37, 356, 1956a.

Press, F., Determination of crustal structure from phase velocity of Rayleigh waves, Part I: Southern California, Bull. Geol. Soc. Am., 67, 1647-1658, 1956b.

Press, F., Determination of crustal structure from phase velocity of Rayleigh waves, Part II: San Francisco Bay region, Bull. Seismol. Soc. Am., 47, 87-88, 1957.

Press, F., Crustal structure in the California-Nevada region, J. Geophys. Res., 65, 1039-1051, 1960.

Press, F., M. Ewing, and J. Oliver, Crustal structure and surface-wave dispersion in Africa, Bull. Seismol. Soc. Am., 46, 97-103, 1956.

Priestley, K., and J. N. Brune, Surface waves and the structure of the Great Basin of Nevada and western Utah, J. Geophys. Res., 83, 2265-2272, 1978.

Proskuryakova, T., A., I. B. Ovchnnikova, and E. B. Voronina, The Earth's structure in the region of Crimea according to the Rayleigh waves observations, Pure and Applied Geophysics, 82, 98-107, 1970.

Pujol, J., M., Rayleigh waves spectral studies of some Alaskan intraplate earthquakes, M. S. thesis, University of Alaska, p. 78, Fairbanks, 1982.

Randall, M., A revised travel-time for S, Geophys. J. R. astr. Soc., 22, 229-234, 1971.

Romanowicz, B., A., Depth resolution of earthquakes in central Asia by moment tensor inversion of long-period Rayleigh waves: effects of phase velocity variations across Eurasia and their calibration, J. Geophys. Res., 86, 5963-5984, 1981.

Romanowicz, B., A., Moment tensor inversion of long period Rayleigh waves: a new approach, J. Geophys. Res., 87, 5394-5407, 1982a.

Romanowicz, B., A., Constraints on the structure of the Tibet plateau from pure path phase velocities of Love and Rayleigh waves, J. Geophys. Res., 87, 6865-6883, 1982b.

Romanowicz, B., A., Lateral heterogeneity in continents: moment-tensor inversion of long-period surface waves and depth resolution of crustal events; body-wave modeling and phase-velocity calibrations, Phys. Earth Planet. Inter., 30, 269-271, 1982c.

Romanowicz, B., A., Pure path attenuation measurements of long-period Rayleigh waves across the Tibet Plateau, Phys. Earth Planet. Inter., 36, 116-121, 1984.

Romanowicz, B., A., and G. Suarez, On an improved method to obtain the moment tensor and depth of earthquakes from the amplitude spectrum of Rayleigh waves, Bull. Seismol. Soc. Am., 73, 1513-1526, 1983.

Saito, M., Excitation of free oscillations and surface waves by a point source in a vertically heterogeneous Earth, J. Geophys. Res., 72, 3689-3699, 1967.

Santô, T., A., Observation of surface waves by Columbia-type seismograph installed at Tsukuba Station, Japan (Part I) - Rayleigh wave dispersions across the oceanic basin, Bull. Earthq. Res. Inst., 38, 219-240, 1960a.

Santô, T., A., Rayleigh wave dispersions across the oceanic basin around Japan (Part II), Bull. Earthq. Res. Inst., 38, 385-401, 1960b.

Santô, T., A., Rayleigh wave dispersions across the oceanic basin around Japan (Part III) - On the crust of the south-western Pacific Ocean, Bull. Earthq. Res. Inst., 39, 1-22, 1961a.

Santô, T., A., Division of the south-western Pacific area into several regions in each of which Rayleigh waves have the same dispersion characters, Bull. Earthq. Res. Inst., 39, 603-630, 1961b.

Santô, T., A., Division of the Pacific area into seven regions in each of which Rayleigh waves have the same group velocities, Bull. Earthq. Res. Inst., 41, 719-741, 1963.

Santô, T., A., Lateral variation of Rayleigh wave dispersion character. Part I: Observational data, Pure and Applied Geophysics, 62, 49-66, 1965a.

Santô, T., A., Lateral variation of Rayleigh wave dispersion character. Part II: Eurasia, Pure and Applied Geophysics, 62, 67-80, 1965b.

Santô, T., A., Lateral variation of Rayleigh wave dispersion character. Part III: Atlantic Ocean, Africa and Indian Ocean, Pure and Applied Geophysics, 63, 40-59, 1966.

Santô, T., A., Lateral variation of Rayleigh wave dispersion character. Part IV: The Gulf of Mexico and Caribbean Sea, Bull. Earthq. Res. Inst., 45, 963-971, 1967.

Santô, T., A., Lateral variation of Rayleigh wave dispersion character. Part V: North American Continent and Arctic Ocean, Bull. Earthq. Res. Inst., 46, 431-456, 1968.

Santô, T., A., and Y. Satô, World-wide survey of the regional characteristics of group velocity dispersion of Rayleigh waves, Bull. Earthq. Res. Inst., 44, 939-964, 1966.

Satô, Y., and T. A. Santô, World-wide distribution of the group velocity of Rayleigh wave as determined by dispersion data, Bull. Earthq. Res. Inst., 47, 31-41, 1969.

Savage, J., C., and W. R. H. White, A map of Rayleigh-wave dispersion in the Pacific, Canadian J. Earth Sci., 6, 1289-1300, 1969.

Savarenski, E., F., G. N. Bozhko, T. I. Kukhtikova, A. B. Peshkov, I. I. Popov, B. N. Shechkov, O. I. Yurkevich, and L. M. Yudakova, On the Earth structure in some regions of the USSR from surface waves data, Pure and Applied Geophysics, 73, 99-119, 1969.

Schlue, J., W., Anisotropy of the upper mantle of the Pacific basin, PhD thesis, University of California, p. 129, Los Angeles, 1975.

Schlue, J., W., and L. Knopoff, Shear wave anisotropy in the upper mantle of the Pacific basin, Geophys. Res. Lett., 3, 359-362, 1976.

Schlue, J., W., and L. Knopoff, Shear-wave polarization anisotropy in the Pacific Basin, Geophys. J. R. astr. Soc., 49, 145-165, 1977.

Schlue, J., W., P. J. Singer, and C. L. Edwards, Shear wave structure of the upper crust of the Albuquerque-Belen Basin from Rayleigh wave phase velocities, J. Geophys. Res., 91, 6277-6281, 1986.

Sclater, J., G., B. E. Parsons, and C. Jaupart, Oceans and continents: similarities and differences in the mechanisms of heat loss, J. Geophys. Res., 86, 11535-11552, 1981.

Shedlock, K., M., Structure and tectonics of north China, PhD thesis, Mass. Inst. of Technol., p. 194, Cambridge, 1986.

Sherburne, R., W., and S. S. Alexander, Crust and upper mantle structure in continental South America from surface wave measurements, Eos, Trans. Am. geophys. Un., 52, 281, 1971.

Shudofsky, G., N., Source mechanisms and focal depths of east african earthquakes and Rayleigh wave phase velocities in Africa, PhD thesis, Princeton University, p. 178, Princeton, 1984.

Silver, P., G., and T. H. Jordan, Fundamental spheroidal mode observations of aspherical heterogeneity, Geophys. J. R. astr. Soc., 64, 605-634, 1981.

Sinno, Y., A., and G. R. Keller, A Rayleigh wave dispersion study between El Paso, Texas and Albuquerque, New Mexico, J. Geophys. Res., 91, 6168-6174, 1986.

Sobel, P., A., and D. H. von Seggern, Applications of surface-wave ray tracing, Bull. Seismol. Soc. Am., 68, 1359-1380, 1978.

Solomon, S., C., Seismic-wave attenuation and the state of the upper mantle, PhD thesis, Mass. Inst. of Technol., p. 321, Cambridge, 1971.

Soriau, A., Upper mantle beneath the Paris Basin and Benelux including possible volcanic anomalies in Belgium, Tectonophysics, 57, 167-188, 1979.

Soriau, A., A. M. Correig, and M. Soriau, Attenuation of Rayleigh waves across the volcanic area of the Massif Central, France, Phys. Earth Planet. Inter., 23, 62-71, 1980.

Soriau, A., and M. Soriau, Test of tectonic models by great circle Rayleigh waves, Geophys. J. R. astr. Soc., 73, 533-551, 1983.

Soriau, A., and M. Vadell, The crust and upper mantle beneath the Pyrenees, from surface waves. Tectonic implications, Ann. Geophys., 36, 159-166, 1980.

Soriau-Thevenard, A., Structure of the crust and the upper mantle in the southwest of France, from surface waves, Ann. Geophys., 32, 63-69, 1976a.

Soriau-Thevenard, A., Structure profonde sous la France obtenue a partir des ondes de surface, Bull. Soc. Geol. France, 18, 1085-1093, 1976b.

Strang, G., Linear algebra and its applications, Second Edition, Academic Press, New York, 1980.

Stuart, G., W., The upper mantle structure of the North Sea region from Rayleigh wave dispersion, Geophys. J. R. astr. Soc., 52, 367-382, 1978.

Suarez, G., Seismicity, tectonics, and surface wave propagation in the Central Andes, PhD thesis, Mass. Inst. of Technol., p. 260, Cambridge, 1982.

Takeuchi, H., and M. Saito, Seismic surface waves, in Methods of computational physics, edited by B. A. Bolt, pp. 217-295, Academic Press, New York, 1972.

Tanimoto, T., The Backus-Gilbert approach to the three-dimensional structure in the upper mantle - I. Lateral variation of surface wave phase velocity with its error and resolution, Geophys. J. R. astr. Soc., 82, 105-123, 1985.

Tanimoto, T., The Backus-Gilbert approach to the three-dimensional structure in the upper mantle - II. SH and SV velocity, Geophys. J. R. astr. Soc., 84, 49-70, 1986.

Tanimoto, T., and D. L. Anderson, Mapping convection in the mantle, Geophys. Res. Lett., 11, 287-290, 1984.

Tanimoto, T., and D. L. Anderson, Lateral heterogeneity and azimuthal anisotropy of the upper mantle: Love and Rayleigh waves 100-250 sec, J. Geophys. Res., 90, 1842-1858, 1985.

Tarantola, A., and B. Valette, Generalized nonlinear inverse problems solved using the least squares criterion, Rev. of Geophys. and Space Phy, 20, 219-232, 1982.

Tarr, A., C., Rayleigh-wave dispersion in the North Atlantic Ocean, Caribbean Sea, and Gulf of Mexico, J. Geophys. Res., 74, 1591-1607, 1969.

Taylor, S., R., Three-dimensional crust and upper mantle structure at the Nevada Test Site, J. Geophys. Res., 88, 2220-2232, 1983.

Thomas, L., Rayleigh wave dispersion in Australia, Bull. Seismol. Soc. Am., 59, 167-182, 1969.

Thomson, A., A., and F. F. Evison, Thickness of the Earth's crust in New Zealand, N. Z. J. Geol. Geophys., 5, 29-45, 1962.

Trehú, A., M., J. L. Nábělek, and S. C. Solomon, Source characterization of two Reykjanes Ridge earthquakes: surface waves and moment tensors; P waveform and nonorthogonal nodal planes, J. Geophys. Res., 86, 1701-1724, 1981.

Tryggvason, E., Crustal thickness in Fennoscandia from phase velocities of Rayleigh waves, Annali di Geofisica, 14, 267-297, 1961.

Tryggvason, E., Dissipation of Rayleigh wave energy, J. Geophys. Res., 70, 1449-1455, 1965.

Tsai, Y., B., Determination of focal depths of earthquakes in mid-oceanic ridges from amplitude spectra of surface waves, PhD thesis, Mass. Inst. of Technol., p. 144, Cambridge, 1969.

Tsai, Y., B., and K. Aki, Simultaneous determination of the seismic moment and attenuation of seismic surface waves, Bull. Seismol. Soc. Am., 59, 275-287, 1969.

Tseng, J., and Z. Sung, Phase velocities of Rayleigh waves in China, Acta Geophys. Sinica, 12, 148-165, 1963.

Tubman, K., M., Structure and seismic properties of Iran and the Arabian Peninsula; effects of continental collision, unpublished manuscript, 1980.

Weidner, D., J., Rayleigh waves from mid-ocean ridge earthquakes: source and path effects, PhD thesis, Mass. Inst. of Technol., p. 256, Cambridge, 1972.

Weidner, D., J., Rayleigh wave phase velocities in the Atlantic Ocean, Geophys. J. R. astr. Soc., 36, 105-139, 1974.

Weidner, D., J., and K. Aki, Focal depth and mechanism of mid-ocean ridge earthquakes, J. Geophys. Res., 78, 1818-1831, 1973.

Wiggins, R., A., Interpolation of digitized waves, Bull. Seismol. Soc. Am., 66, 2077-2081, 1976.

Woodhouse, J., H., The joint inversion of seismic wave forms for lateral variations in earth structure and earthquake source parameters, Proc. Enrico Fermi Int. Sch. Phys., 85, 366-397, 1983.

Woodhouse, J., H., and A. M. Dziewonski, Mapping the upper mantle: Three-dimensional modeling of earth structure by inversion of seismic waveforms, J. Geophys. Res., 89, 5953-5986, 1984.

Yacoub, N., K., and B. J. Mitchell, Attenuation of Rayleigh-wave amplitudes across Eurasia, Bull. Seismol. Soc. Am., 67, 751-769, 1977.

Yomogida, K., Amplitude and phase variations of surface waves in a laterally heterogeneous Earth: ray- and beam-theoretical approach, PhD thesis, Mass. Inst. of Technol., p. 227, Cambridge, 1985.

Yoshii, T., Regionality of group velocities of Rayleigh waves in the Pacific and thickening of the plate, Earth and Plan. Sci. Lett., 25, 305-312, 1975.

Yu, G., and B. J. Mitchell, Regionalized shear velocity models of the Pacific upper mantle from observed Love and Rayleigh wave dispersion, Geophys. J. R. astr. Soc., 57, 311-341, 1979.

Zandt, G., Study of three-dimensional heterogeneity beneath seismic arrays in central California and Yellowstone, Wyoming, PhD thesis, Mass. Inst. of Technol., p. 490, Cambridge, 1978.

Zandt, G., Seismic images of the deep structure of the San Andreas fault system, Central Coast Range, California, J. Geophys. Res., 86, 5039-5052, 1981.

APPENDIX A

Distribution function of published phase velocity values of fundamental mode Rayleigh waves for the period range 20 to 100 sec.

Figures A.1a thru A.9a - Geographical distribution of greatcircle paths corresponding to the reference periods 20 thru 98 sec of our database of published phase velocity data. The latitude ranges from 75°N to 70°S in each map.

Figures A.1b thru A.9b - Histograms of published phase velocity data for periods of 20 thru 98 sec respectively, separated from our database of published values corresponding to paths that have a portion larger than 70% of their total length inside the region-type 'a' of the model of Jordan (1981). Each plot was made using an increment of 0.01 km/sec in the phase velocity value.

Figures A.1 thru A.9 - Indices c thru g - Same as above, for the region-types 'b', 'c', 'p', 'q', and 's', respectively, of the model of Jordan (1981).

Figures A.1 thru A.9 - Indices h thru k - Same as above, for the region-types 'N', '=', '0', and '⊅', respectively, of the model of Lévêque (1980).

Figures A.1 thru A.9 - Indices 1 thru r - Same as above, for the region-types 'N', '#', '=', '-', '0', '.', and '$\not\beta$', respectively, of the model of Okal (1977).

NOTE: As indicated in Table 3.1, the region 's' of the model of Jordan (1981), for periods 90 and 98 sec, was studied using paths that had more than 40% of their length in that region-type. The region-type '-' of the model of Okal (1977), for all reference periods, was studied in the same way. We have indicated this in Table 3.3.

FIGURE A.1a

PERIOD 20 sec

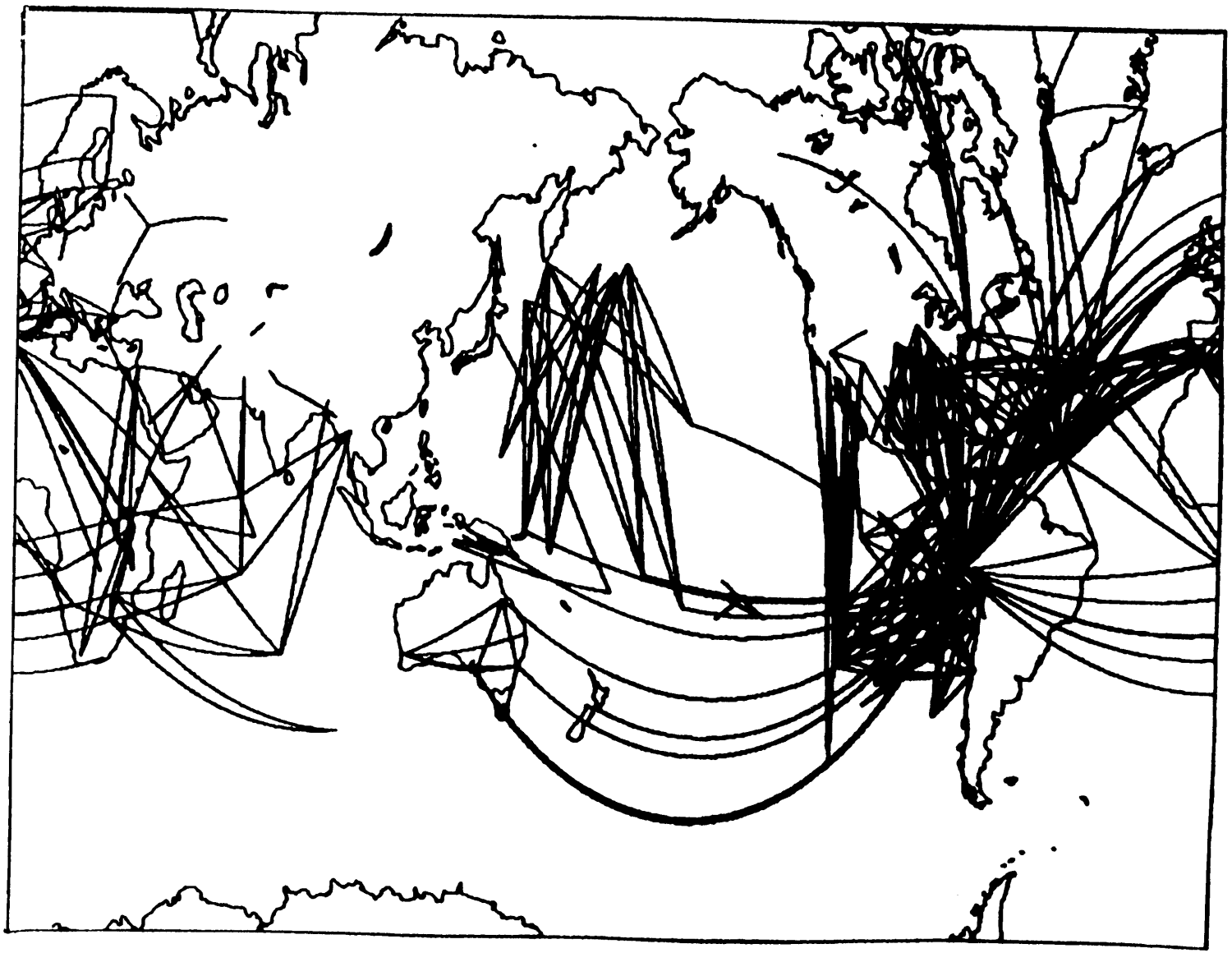

FIGURE A.1b REGION a

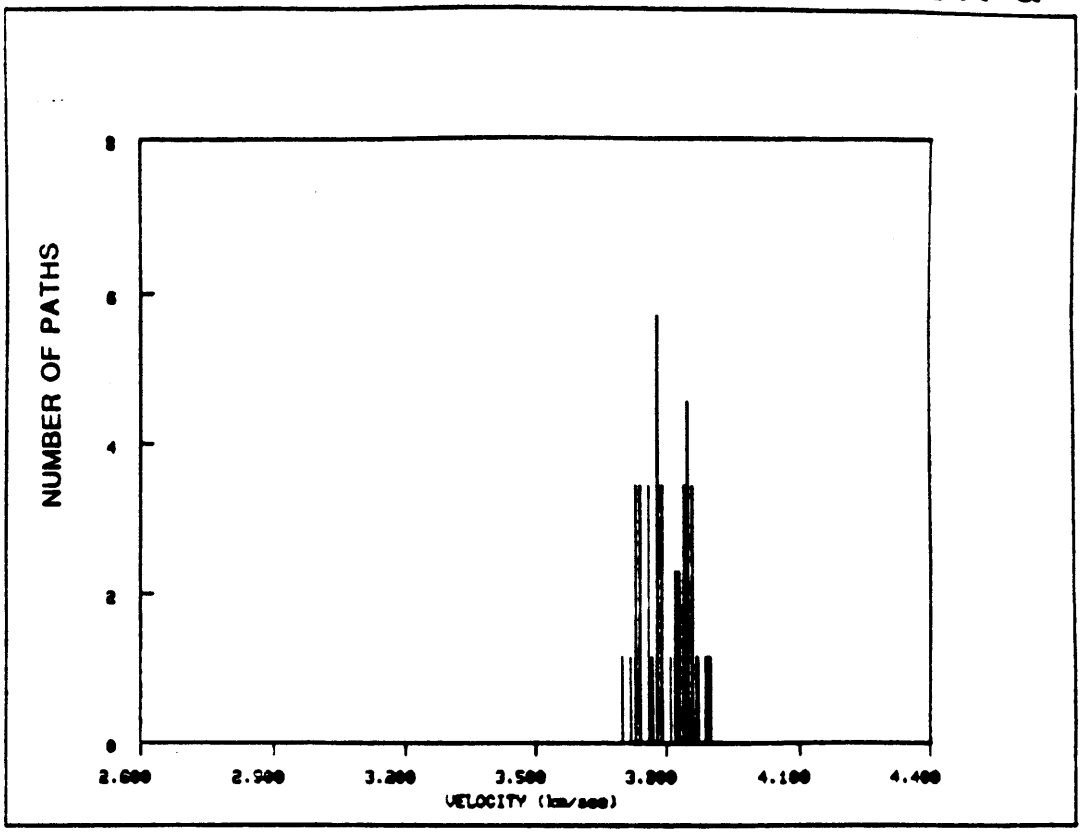

FIGURE A.1c REGION b

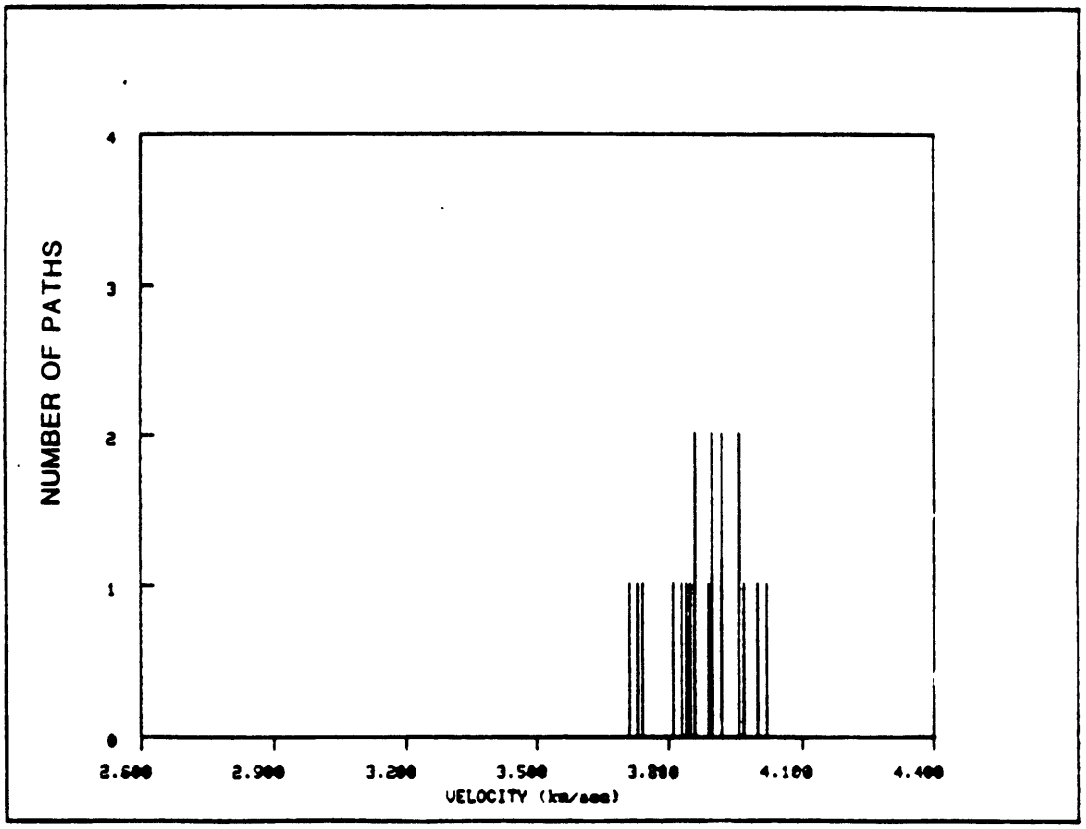

FIGURE A.1d REGION c

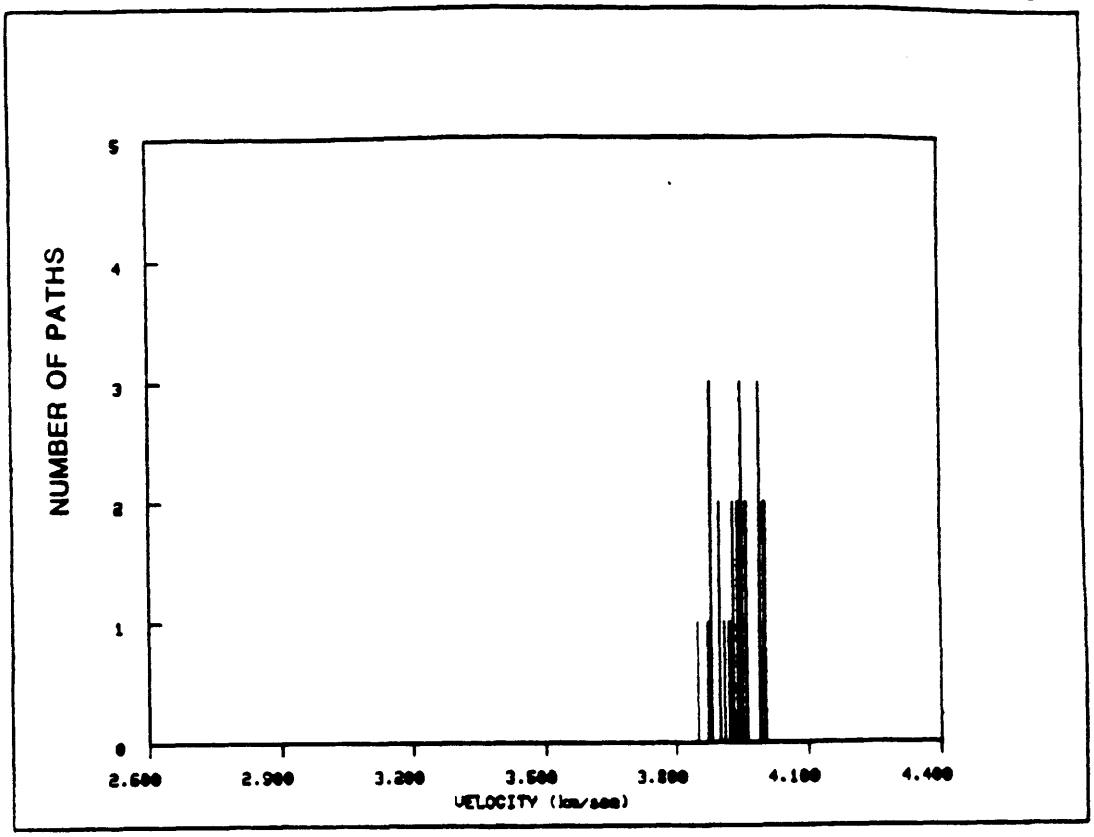

FIGURE A.1e REGION p

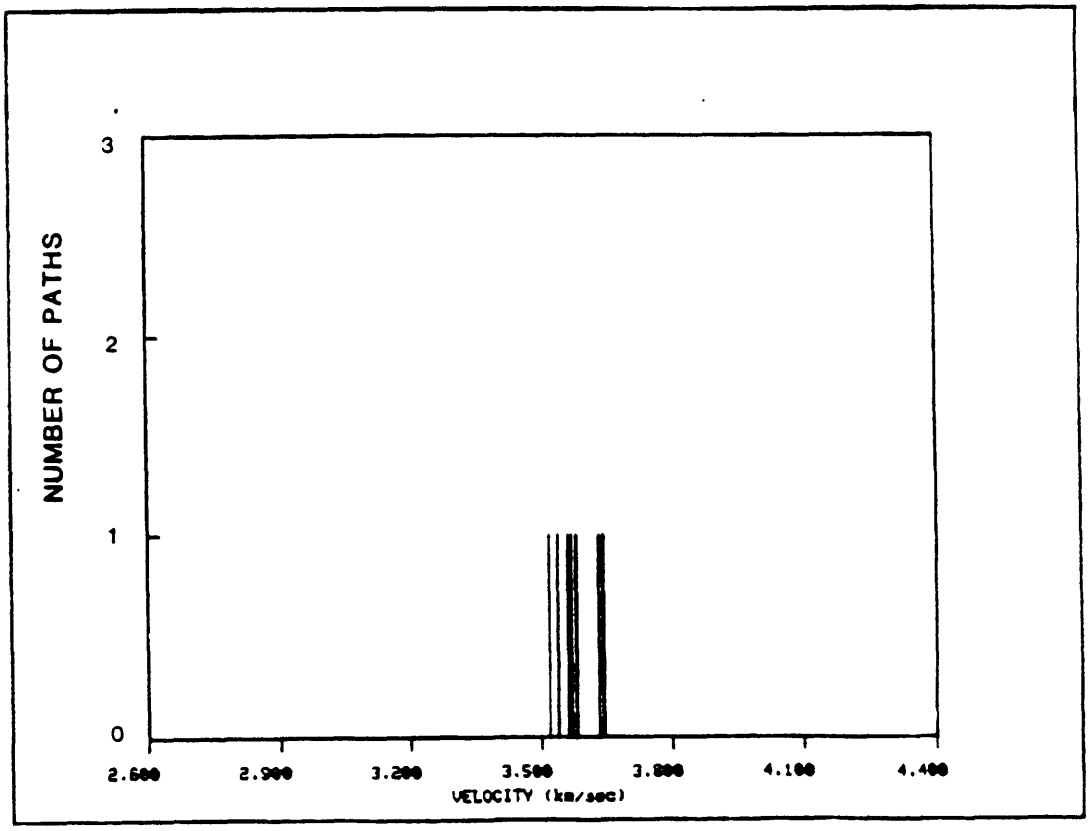

FIGURE A.1f REGION q

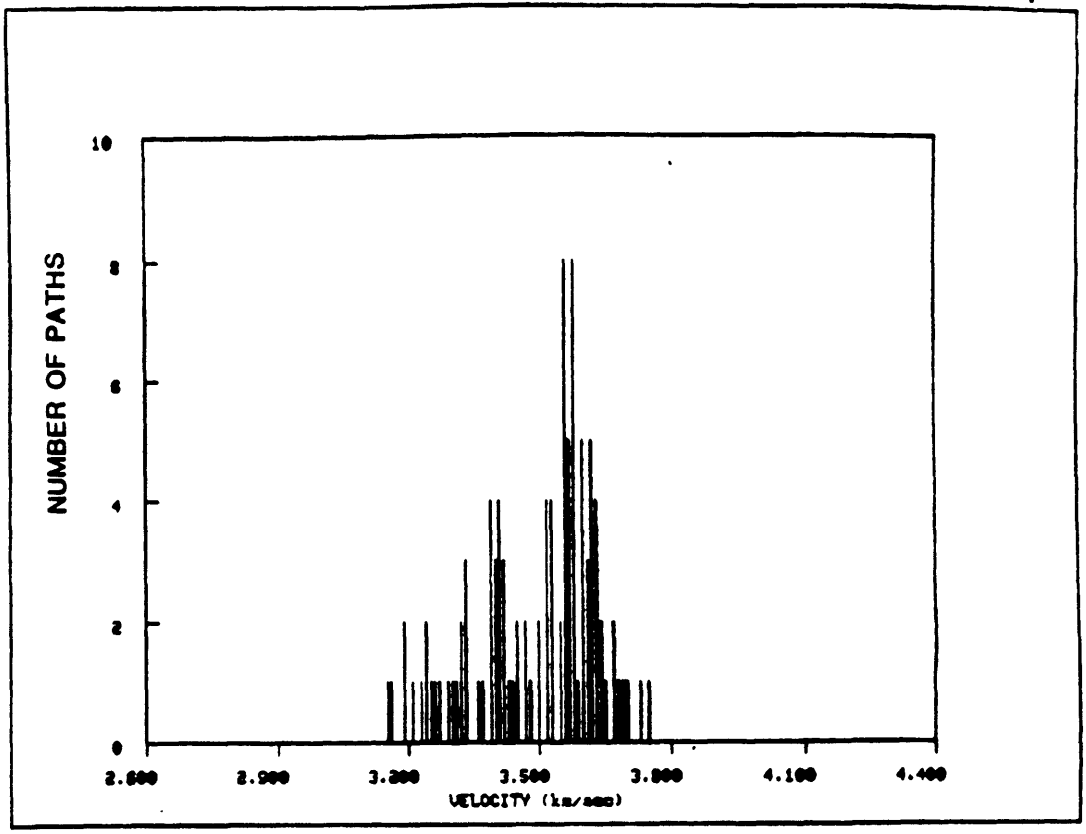

FIGURE A.1g REGION s

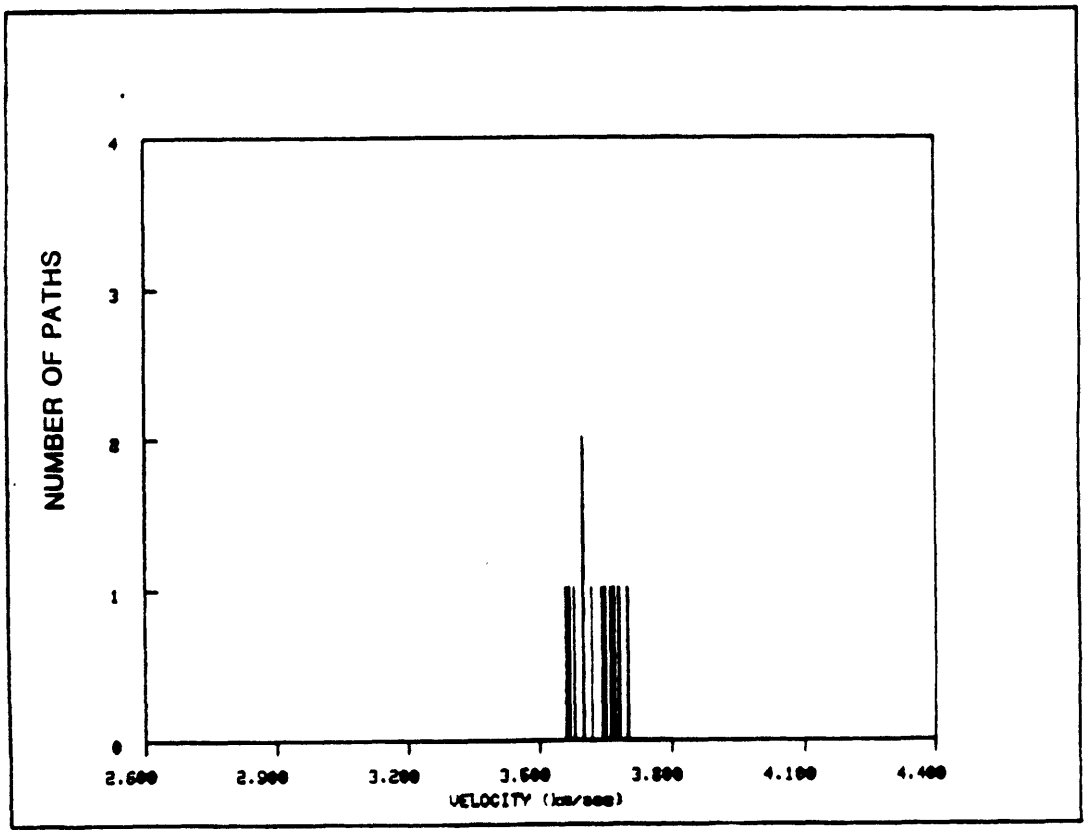

FIGURE A.1h REGION N

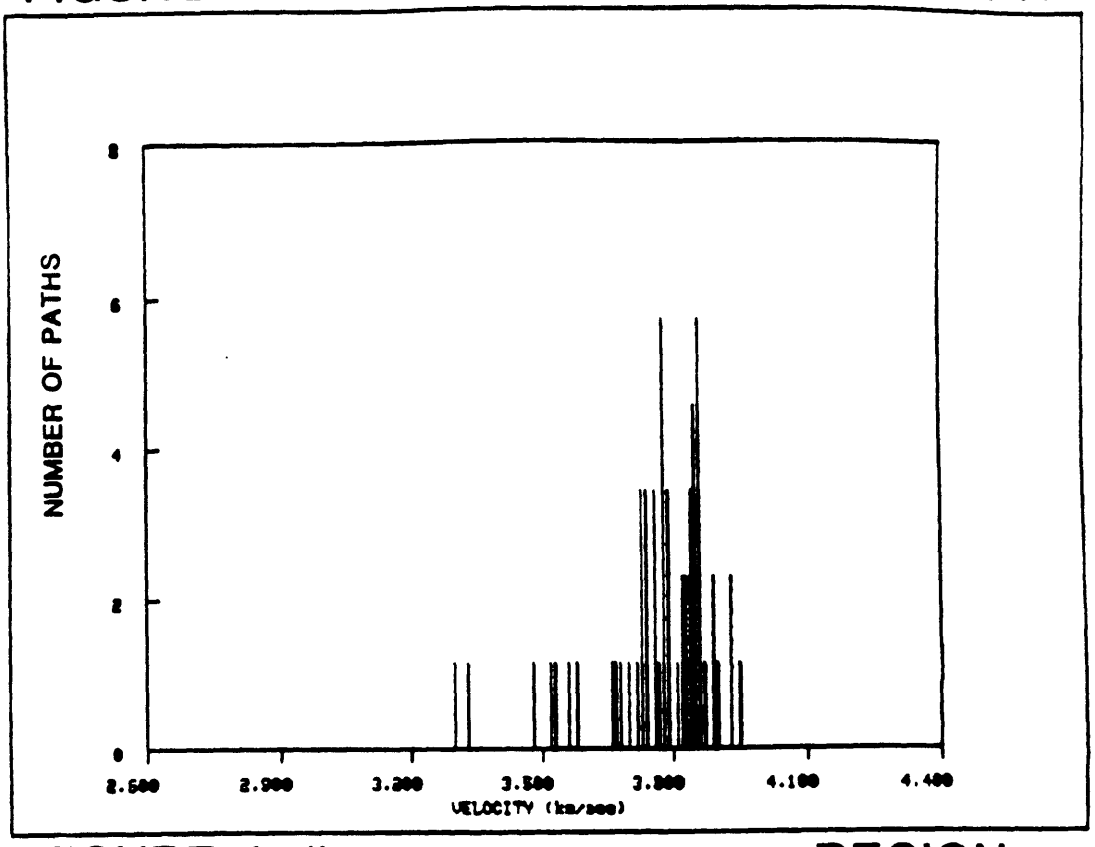

FIGURE A.1i REGION =

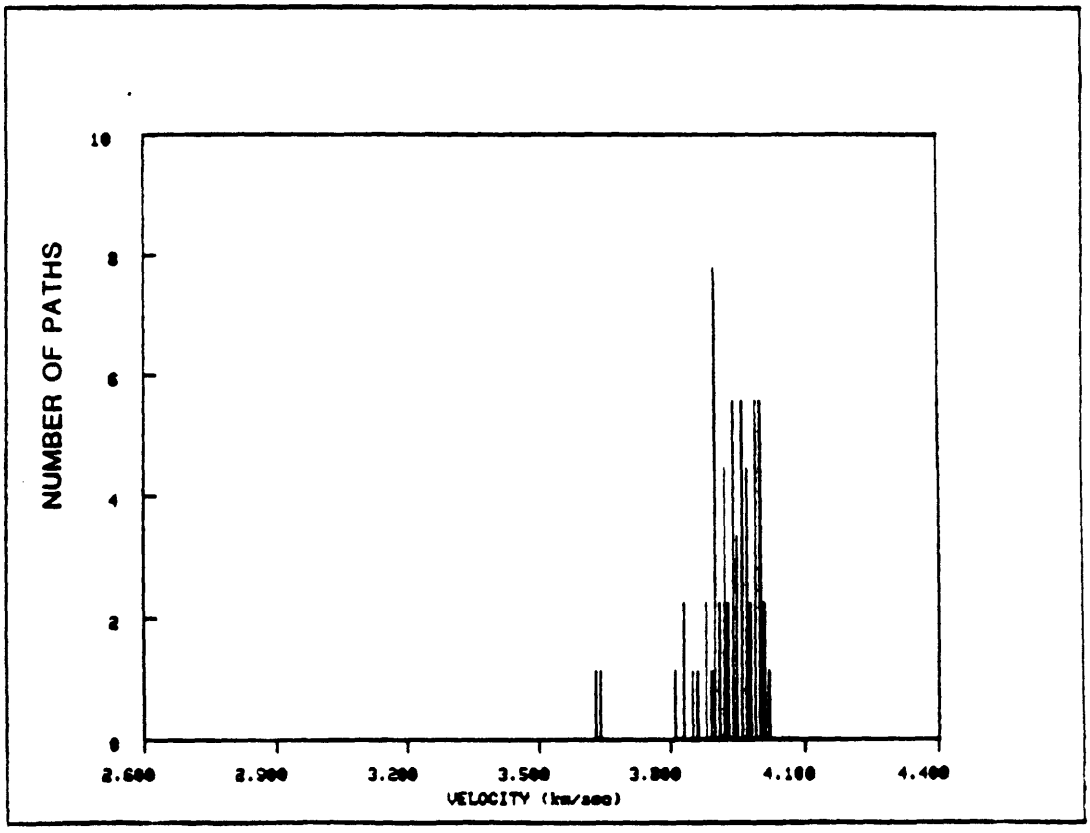

FIGURE A.1j REGION 0

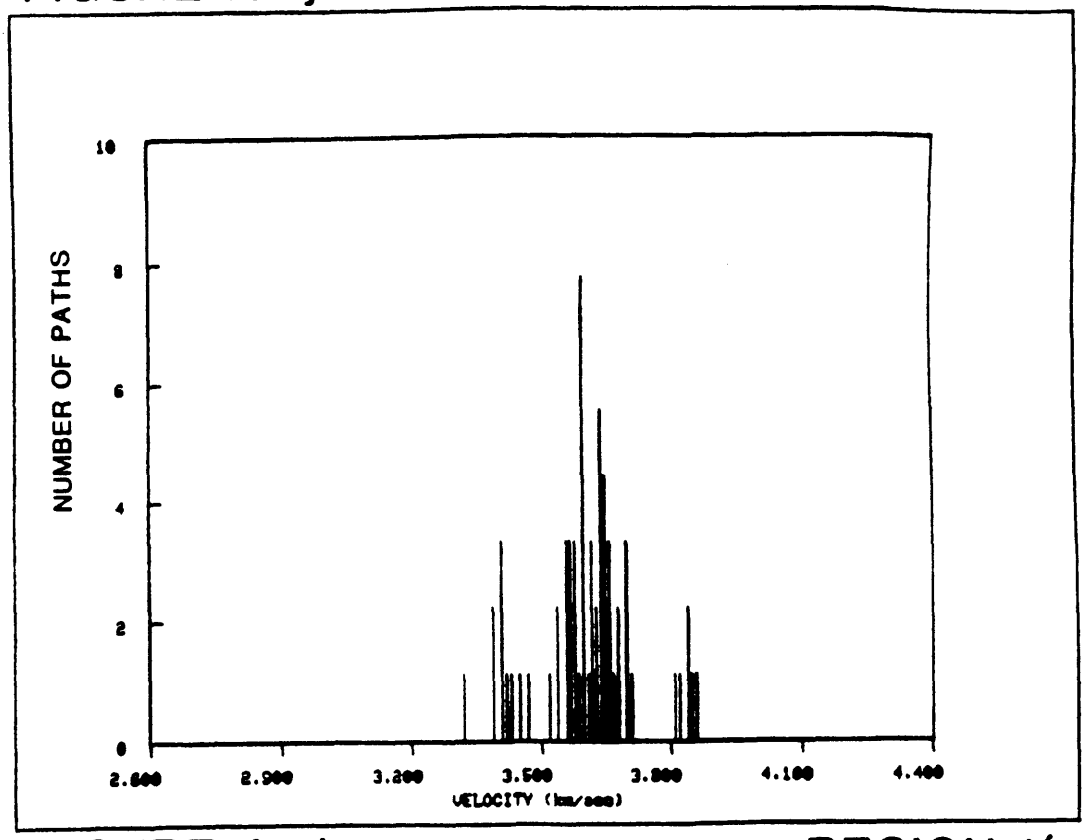

FIGURE A.1k REGION ~~0~~

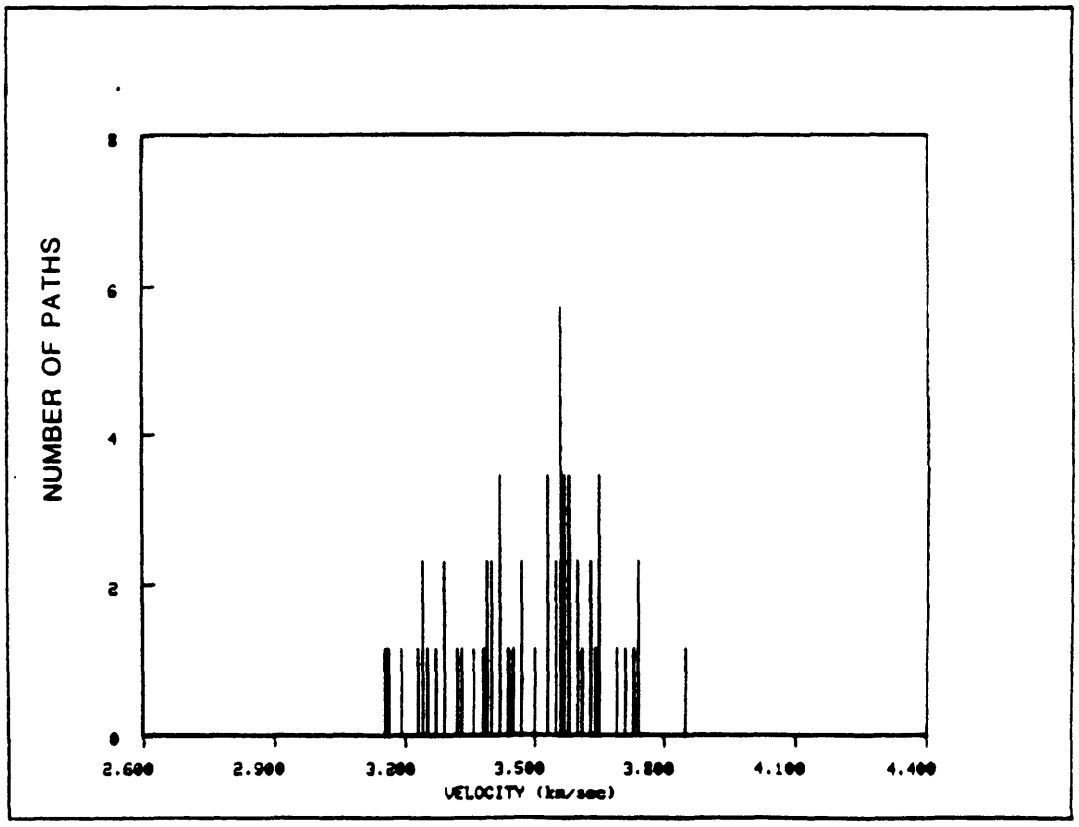

FIGURE A.1l REGION N

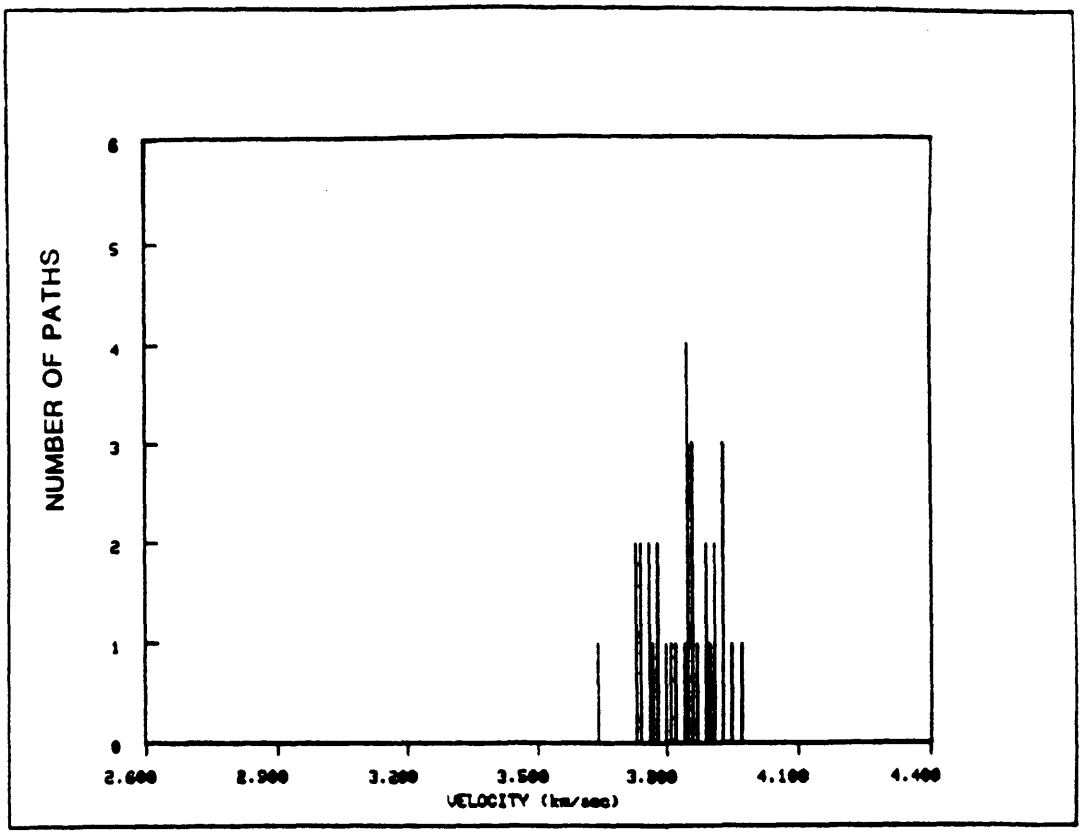

FIGURE A.1m REGION #

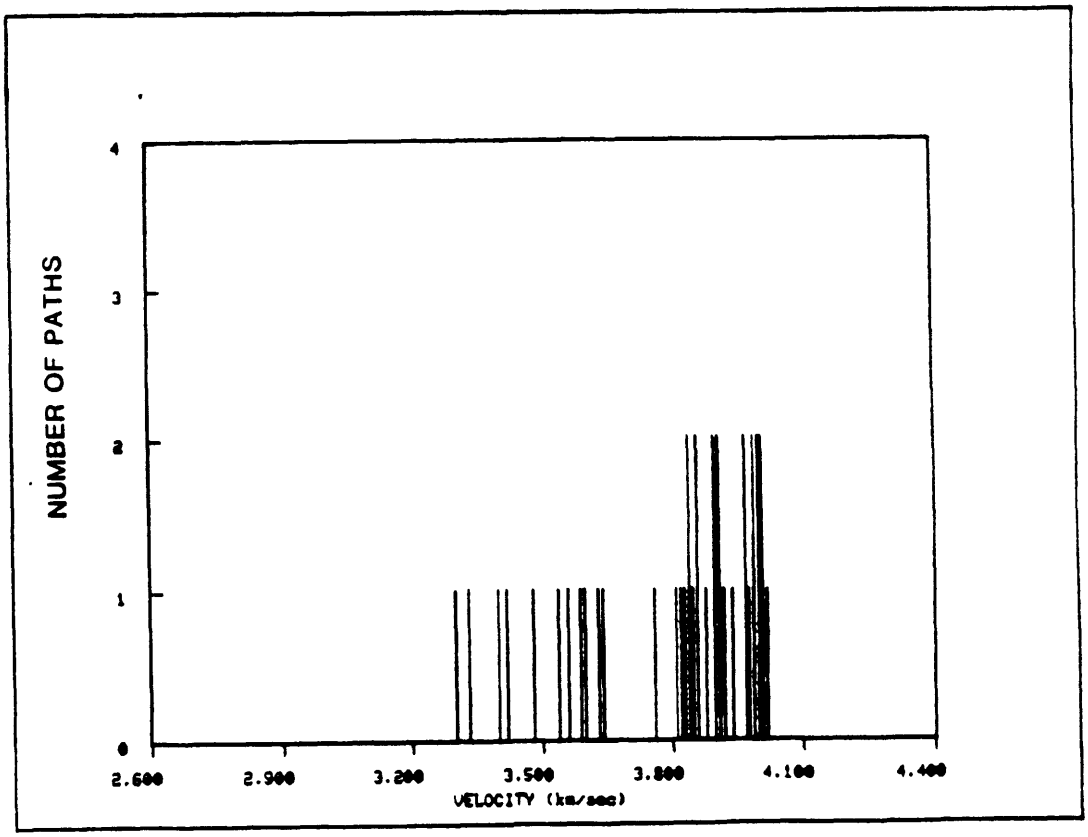

FIGURE A.1n REGION =

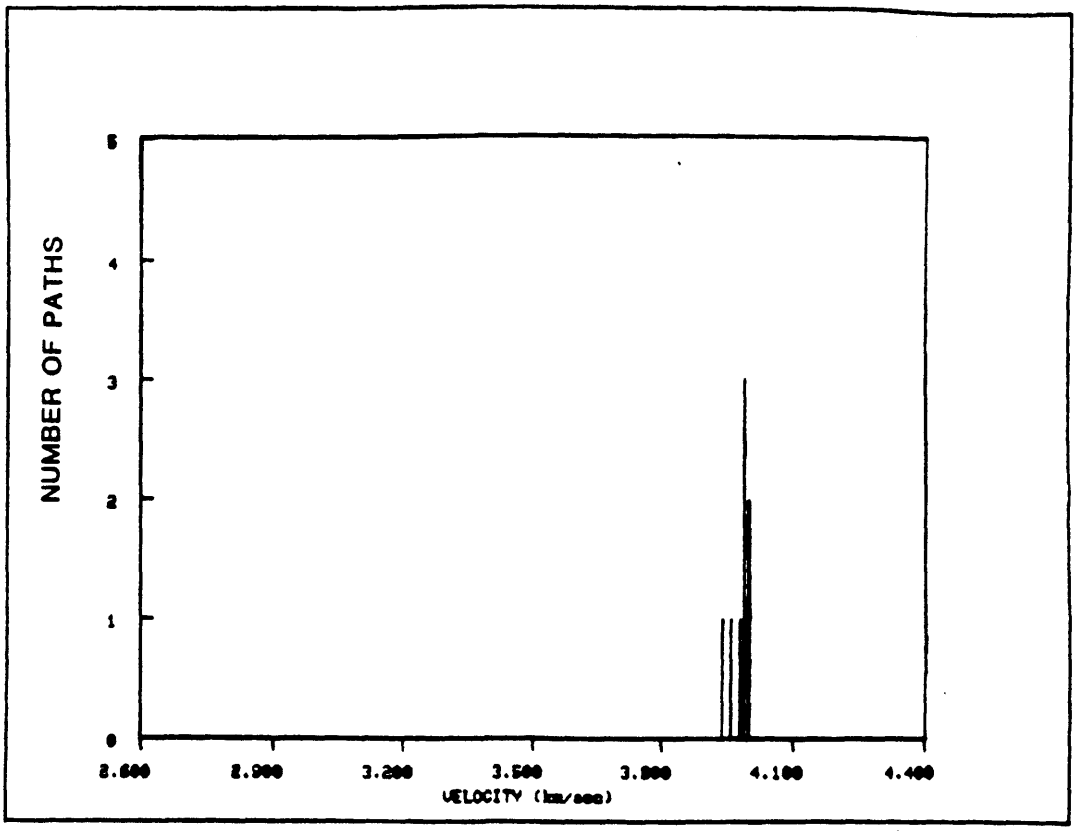

FIGURE A.1o REGION -

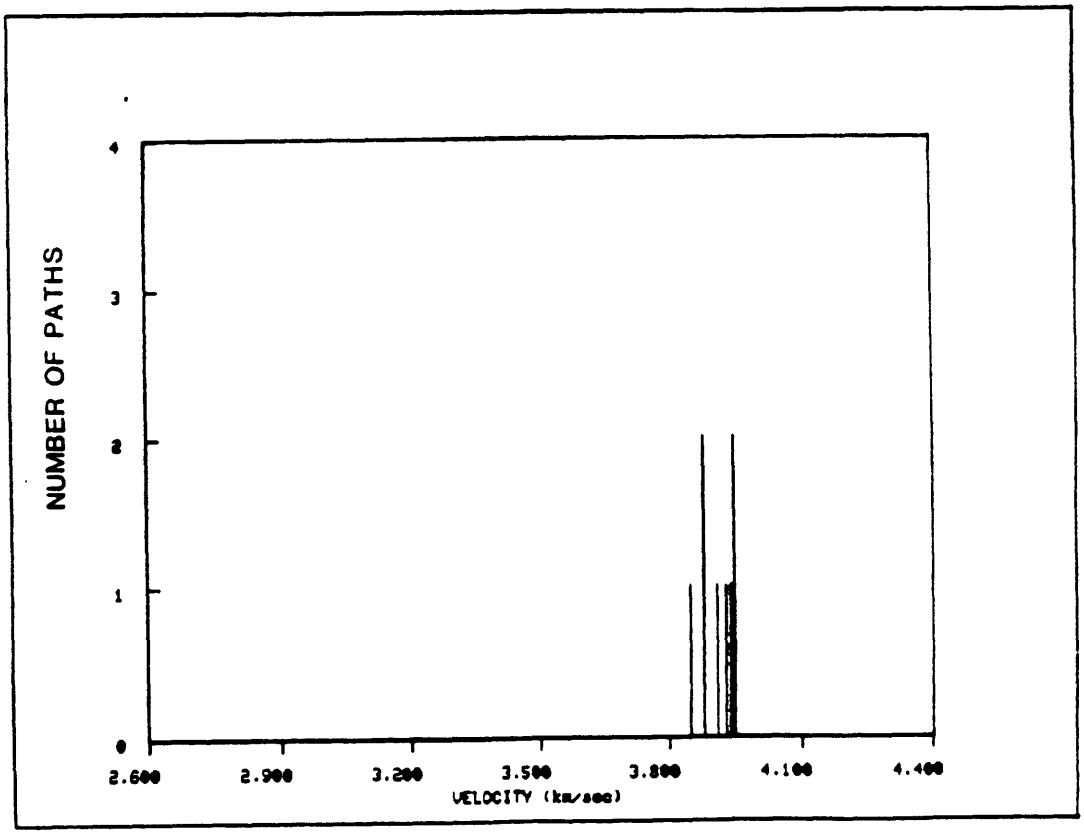

FIGURE A.1p REGION 0

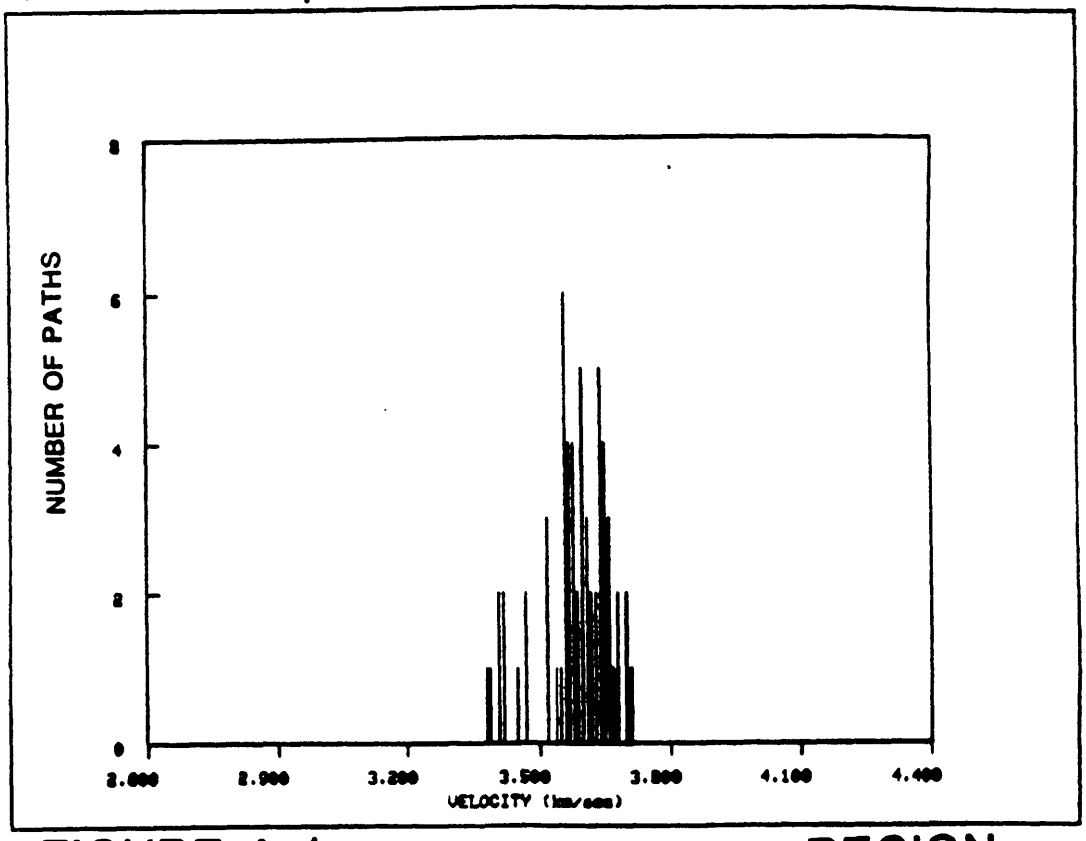

FIGURE A.1q REGION .

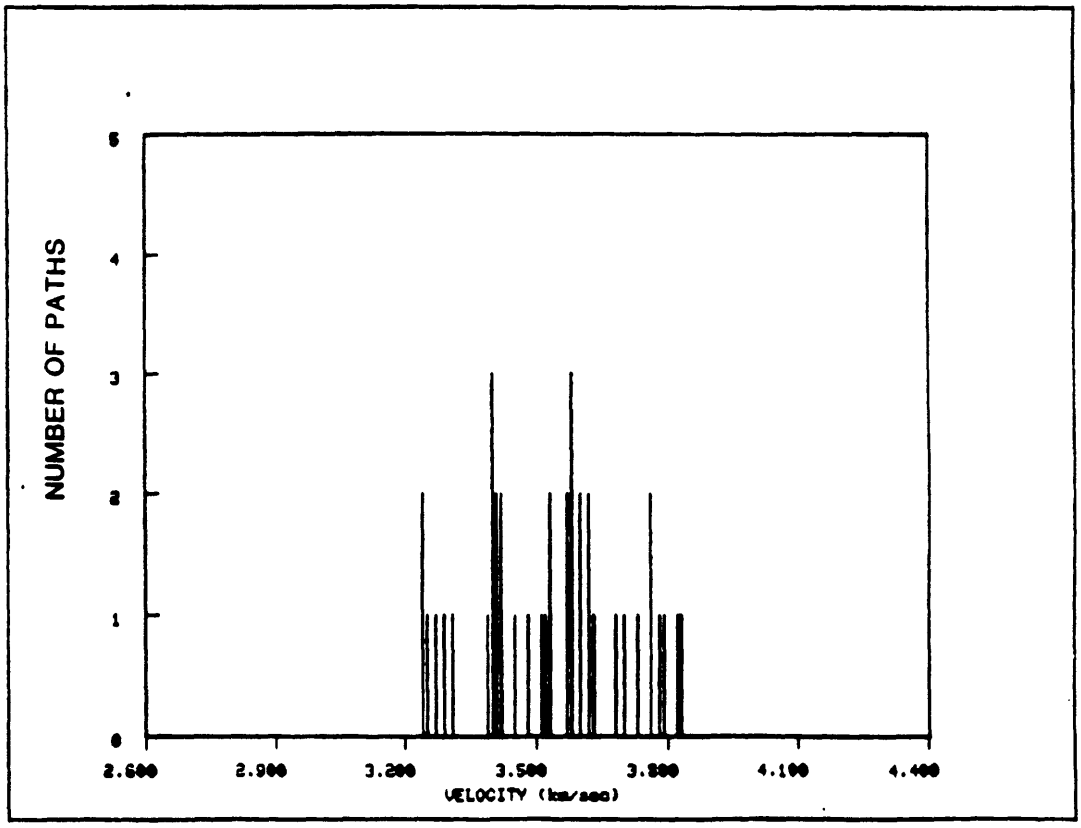

FIGURE A.1r REGION ø

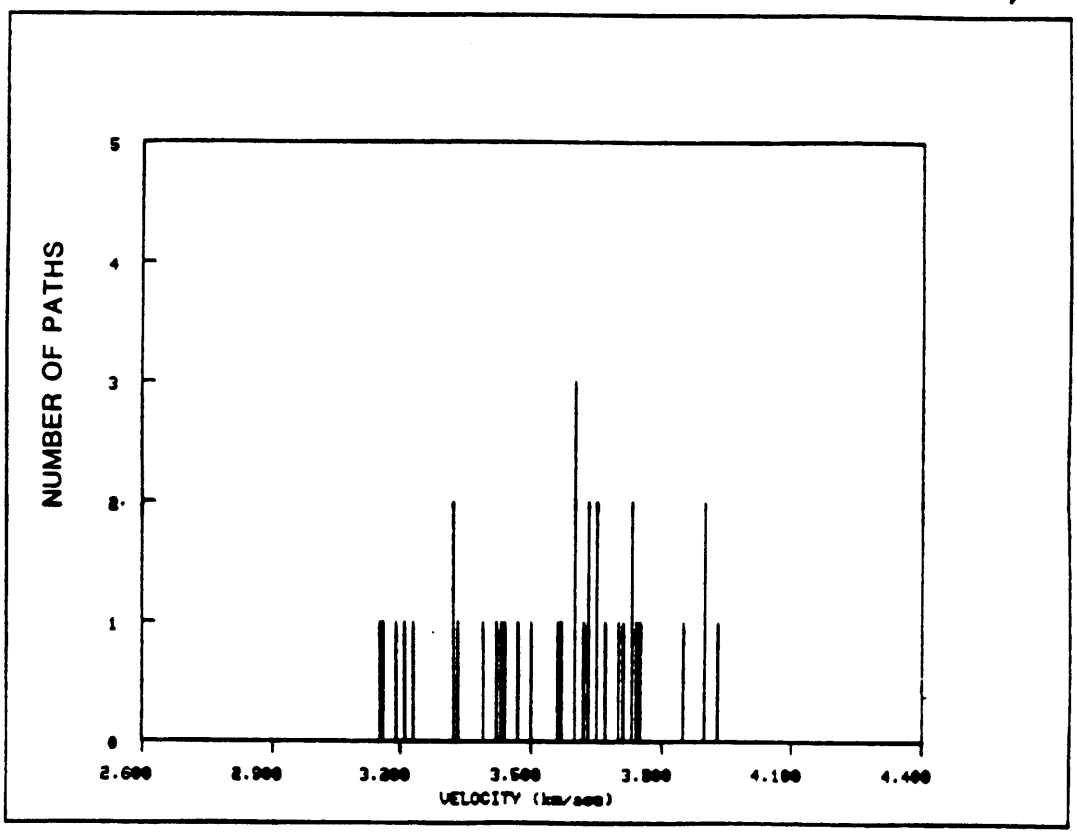

FIGURE A.2a

PERIOD 30 sec

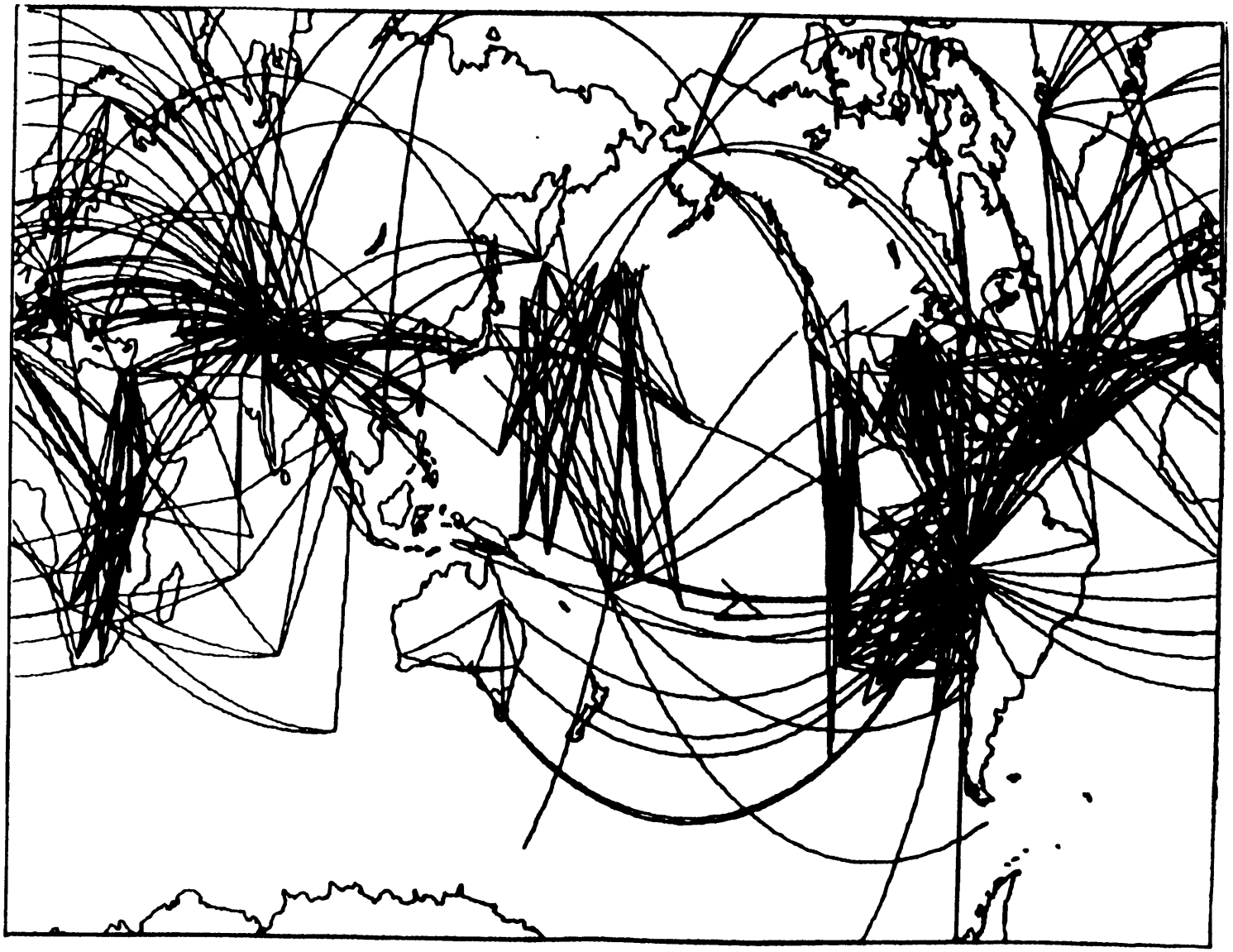

FIGURE A.2b REGION a

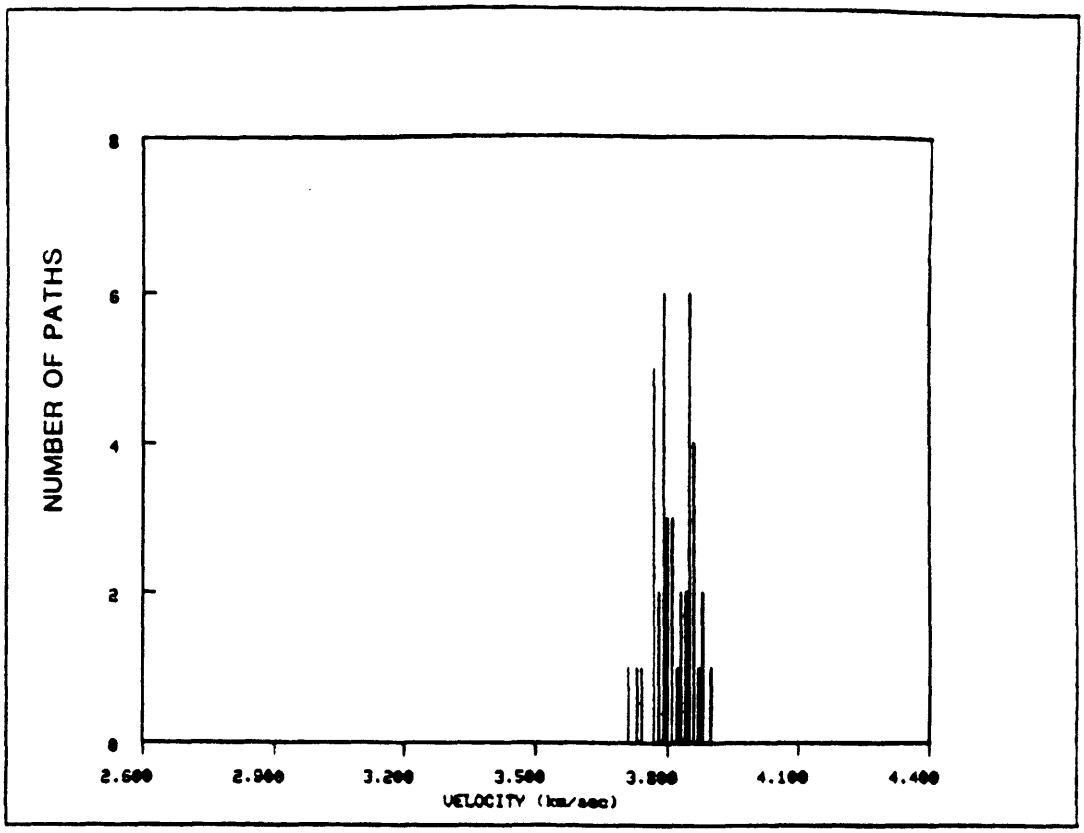

FIGURE A.2c REGION b

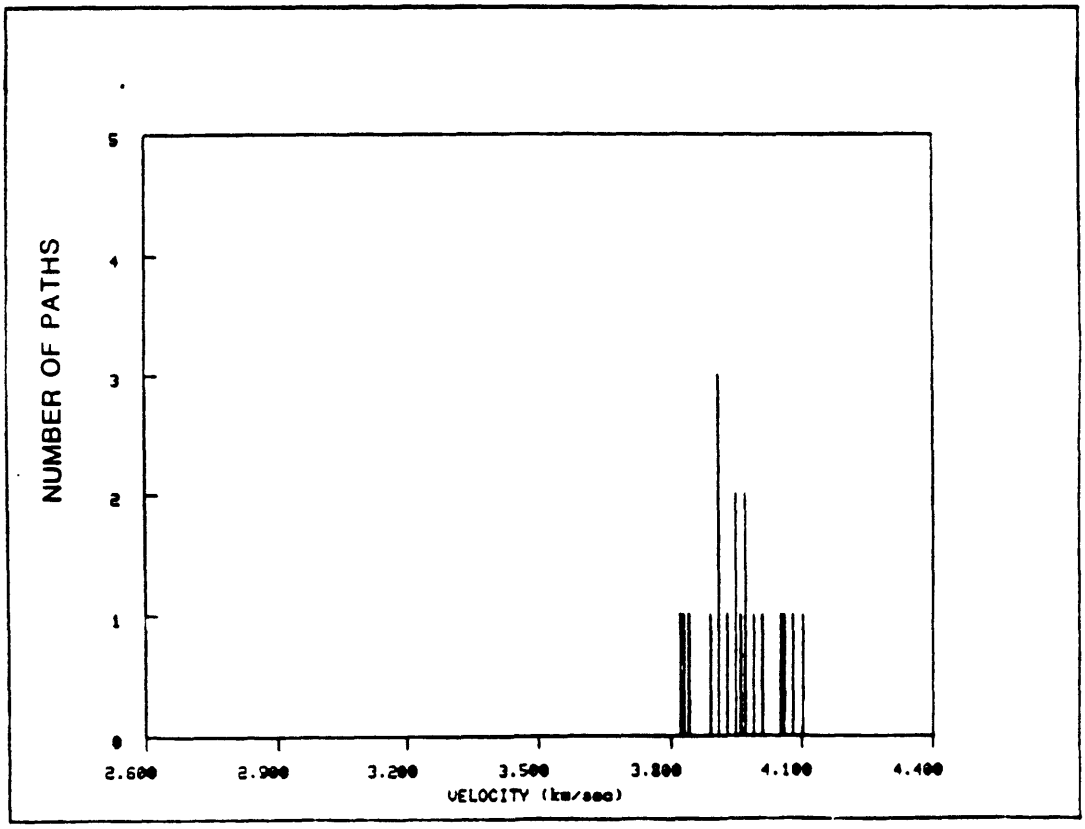

FIGURE A.2d REGION c

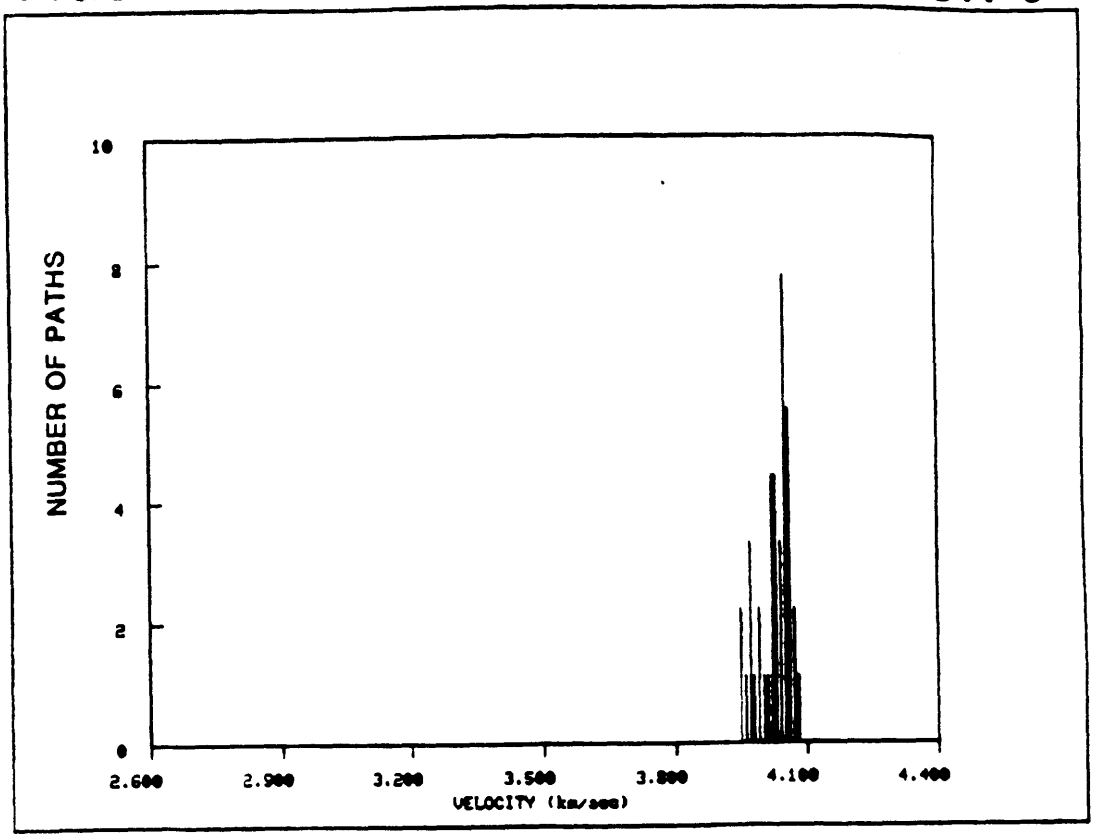

FIGURE A.2e REGION p

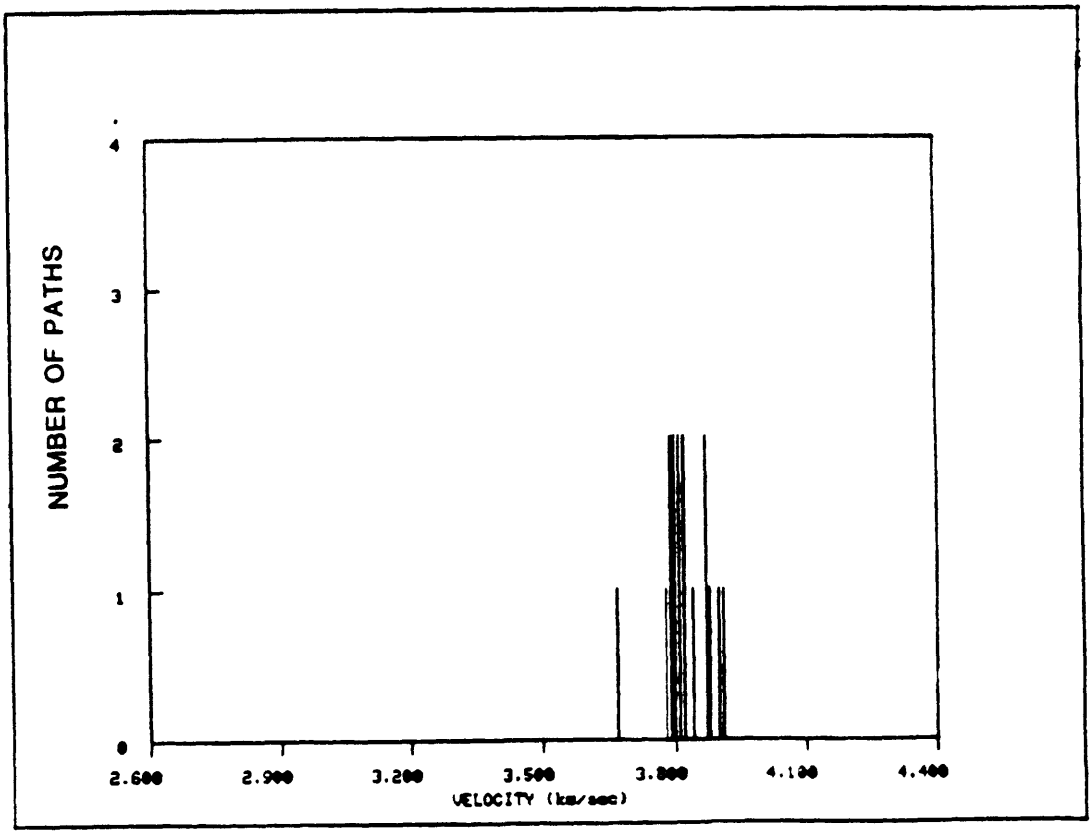

FIGURE A.2f REGION q

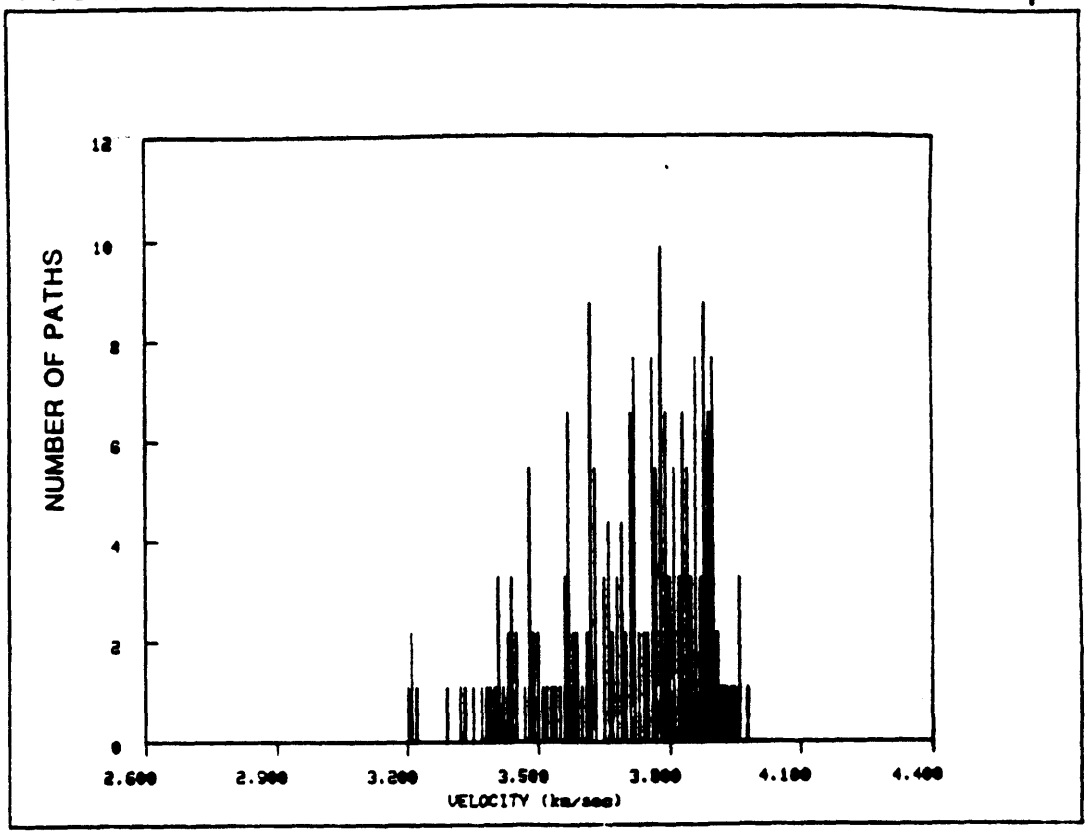

FIGURE A.2g REGION s

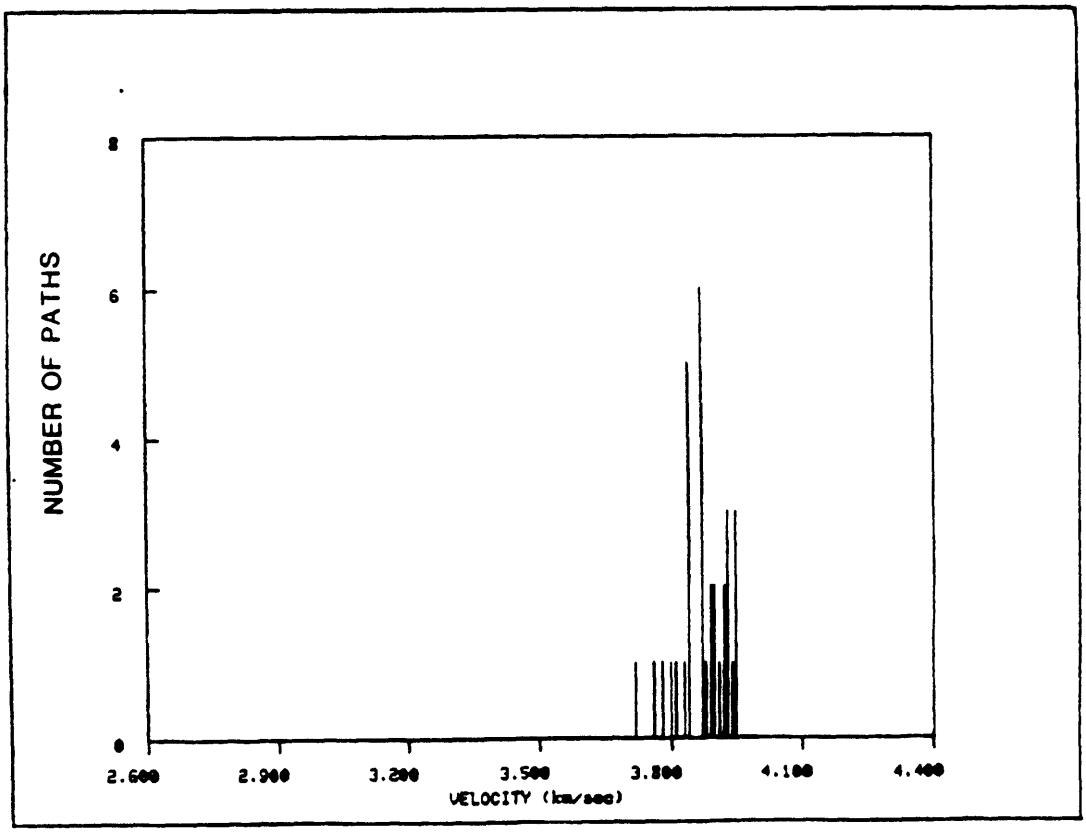

FIGURE A.2h REGION N

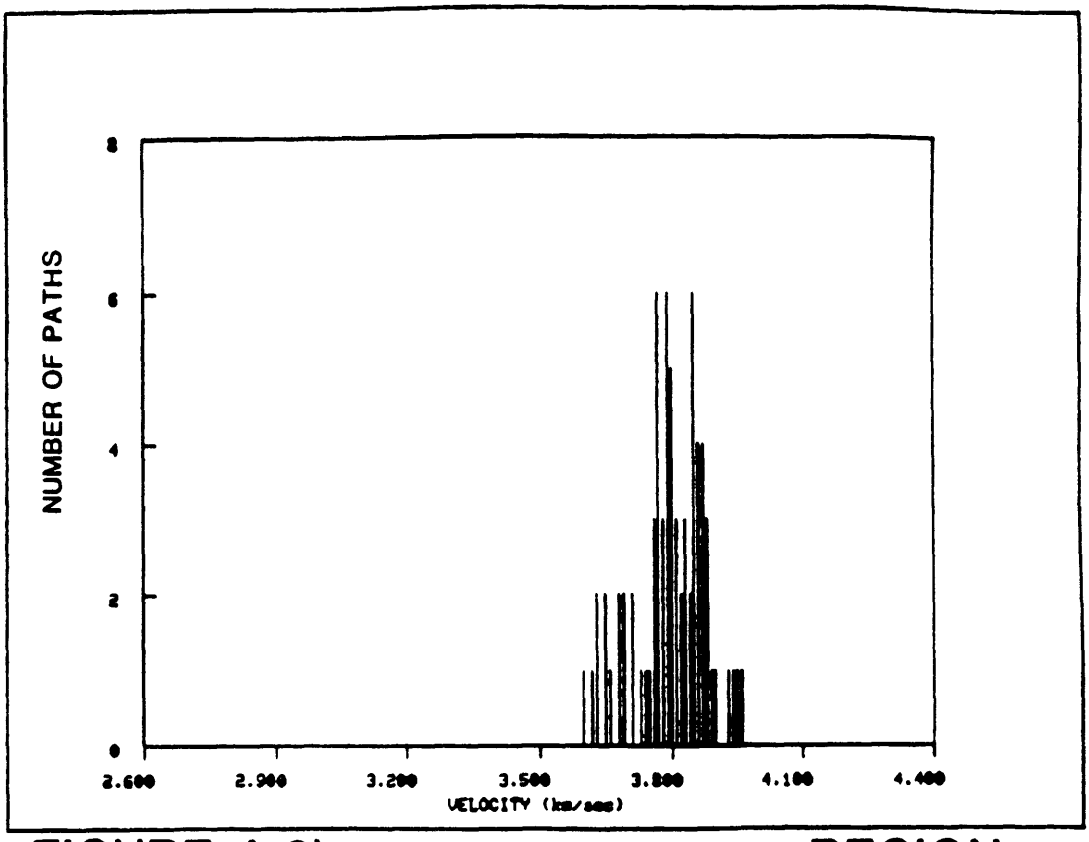

FIGURE A.2i REGION =

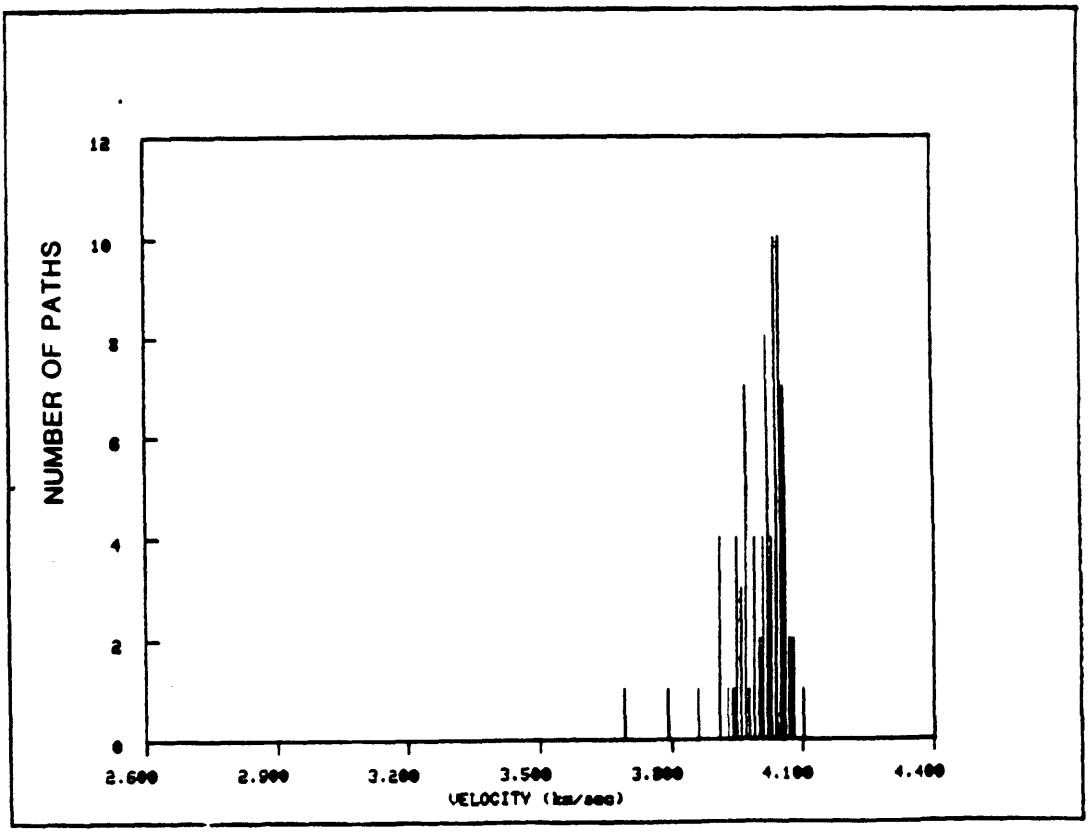

FIGURE A.2j REGION 0

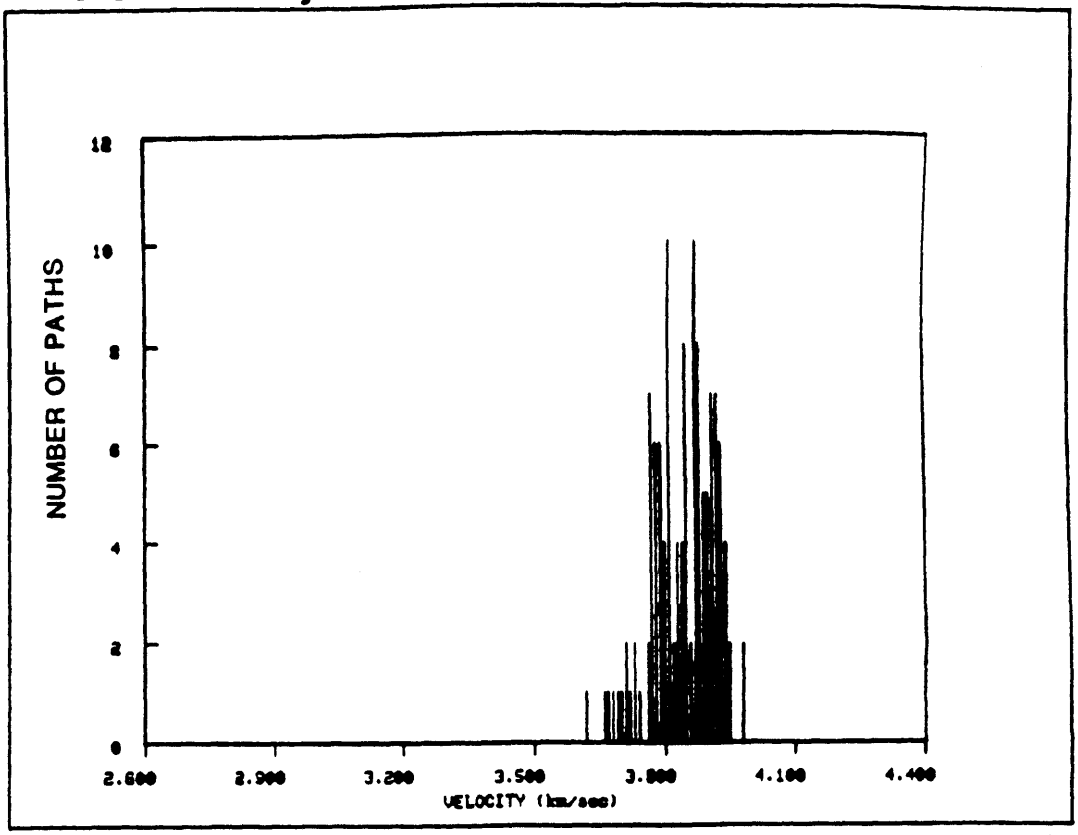

FIGURE A.2k REGION ~~0~~

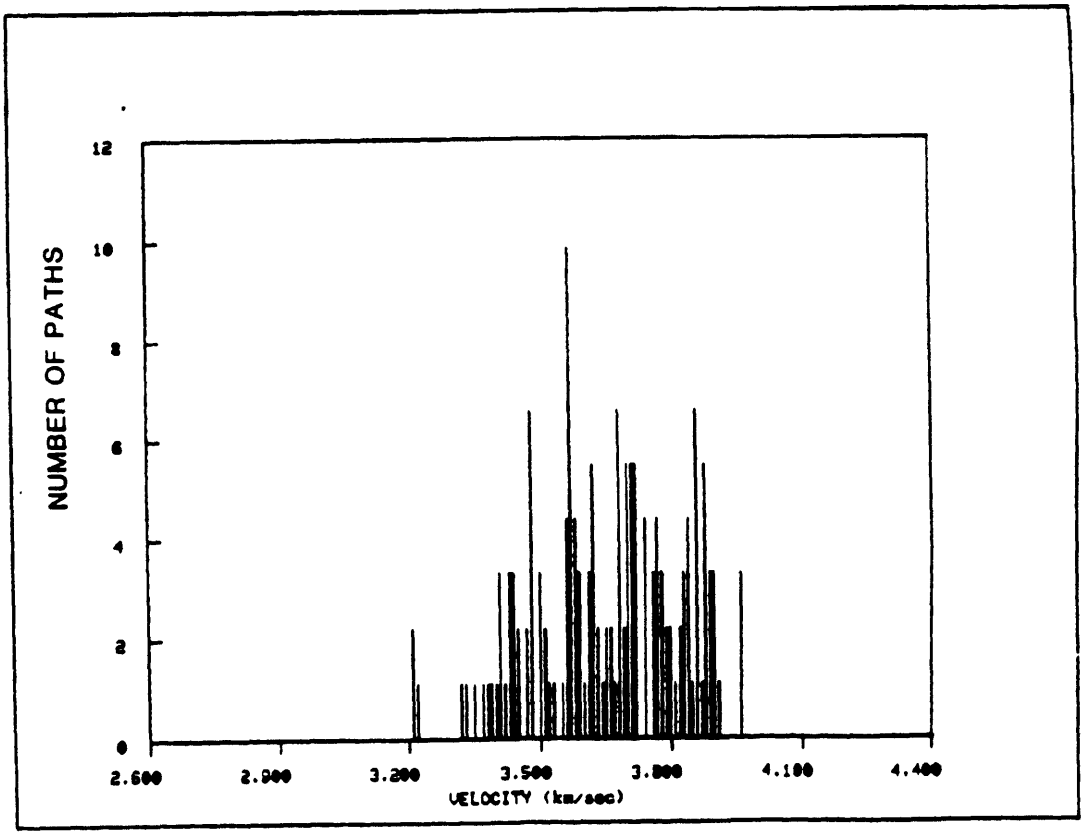

FIGURE A.2l REGION N

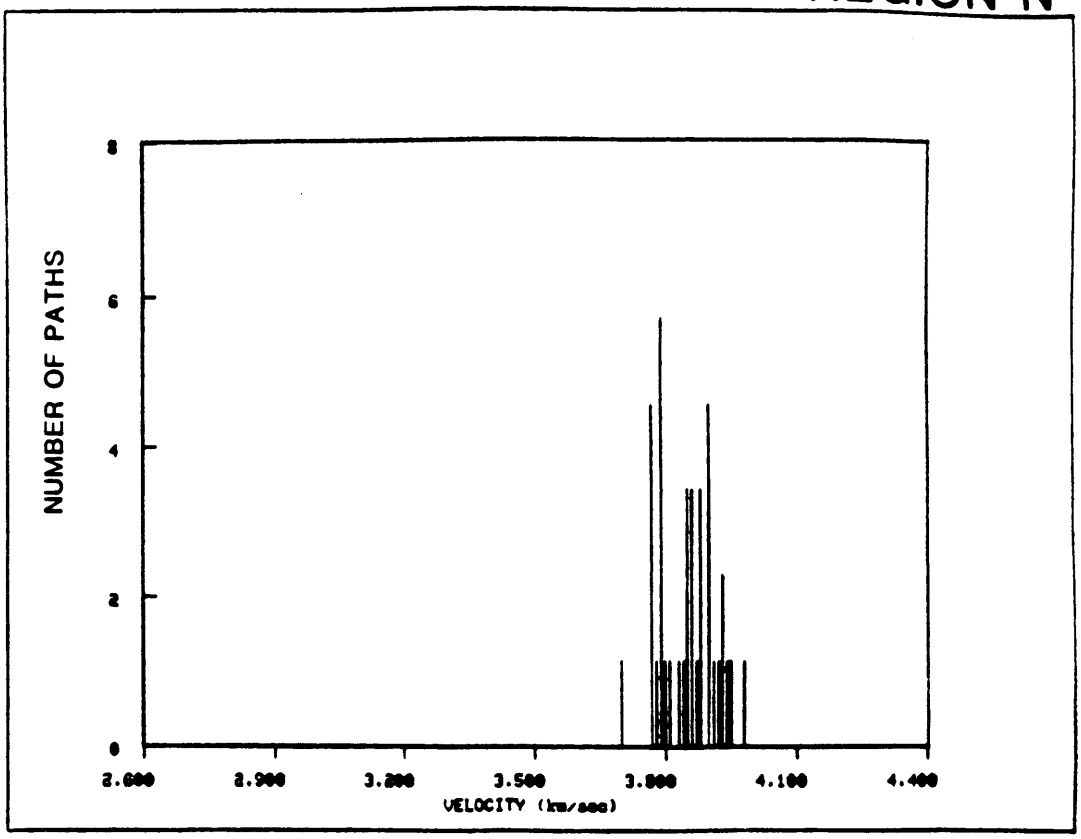

FIGURE A.2m REGION #

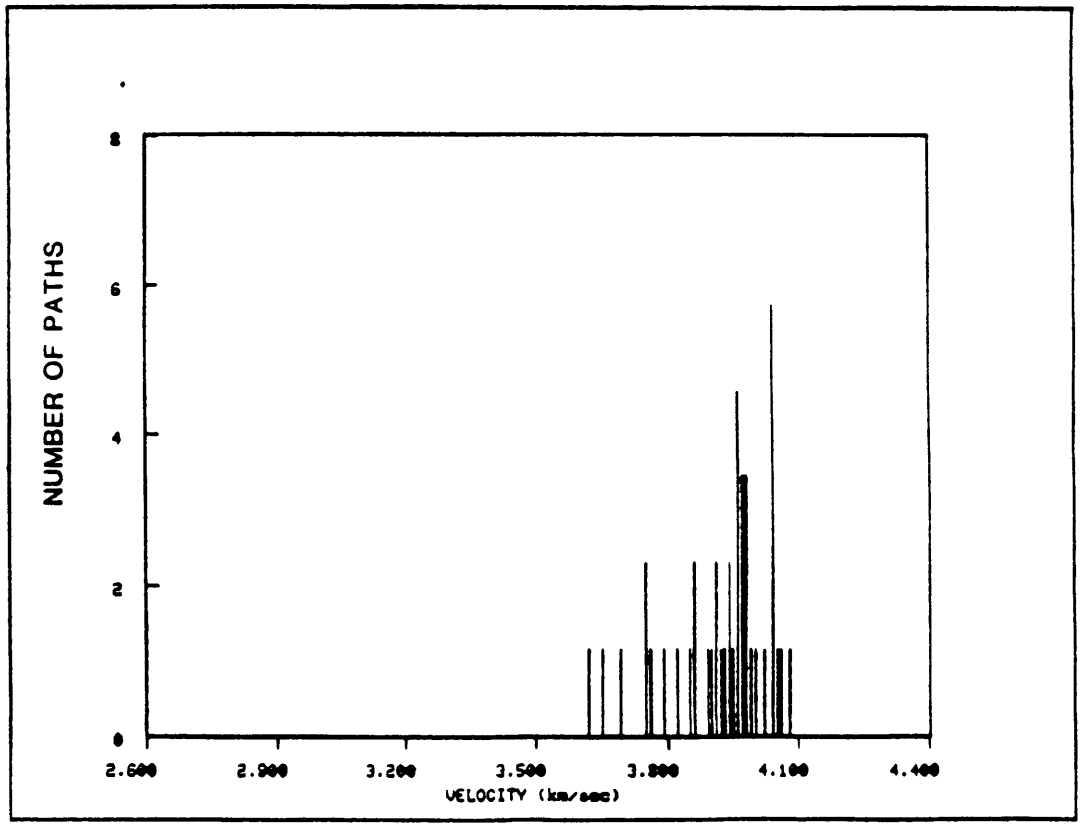

FIGURE A.2n REGION =

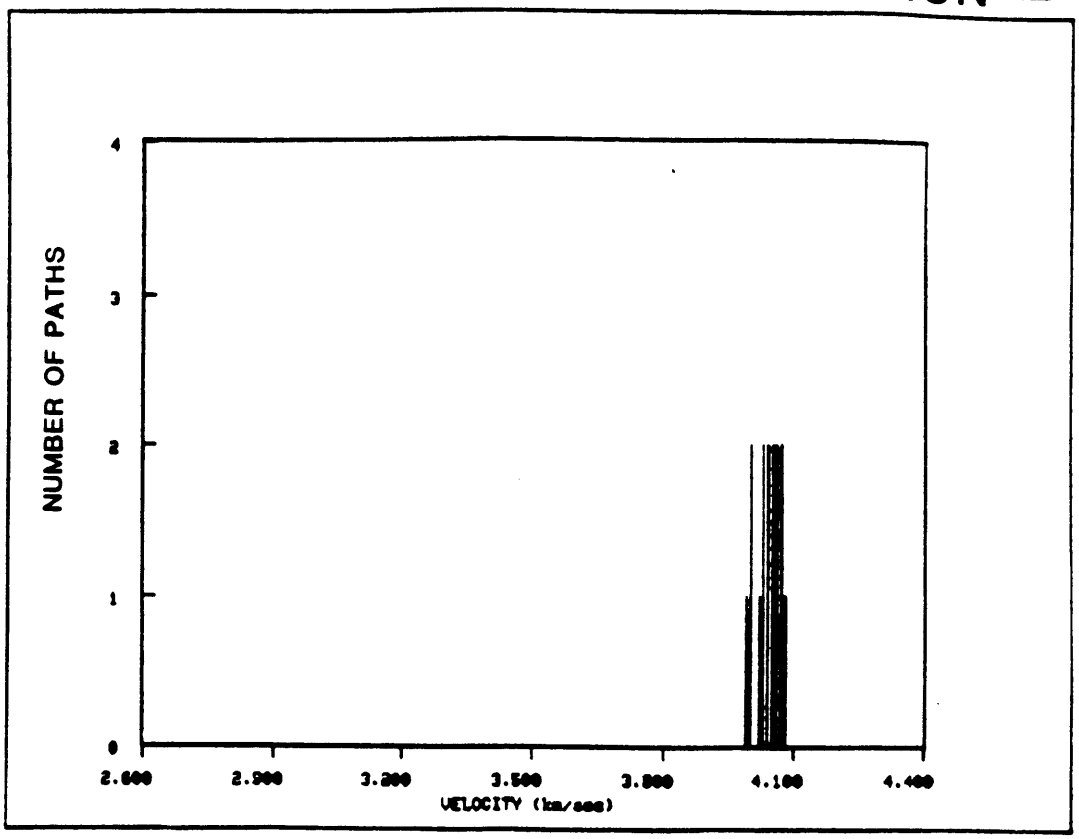

FIGURE A.2o REGION –

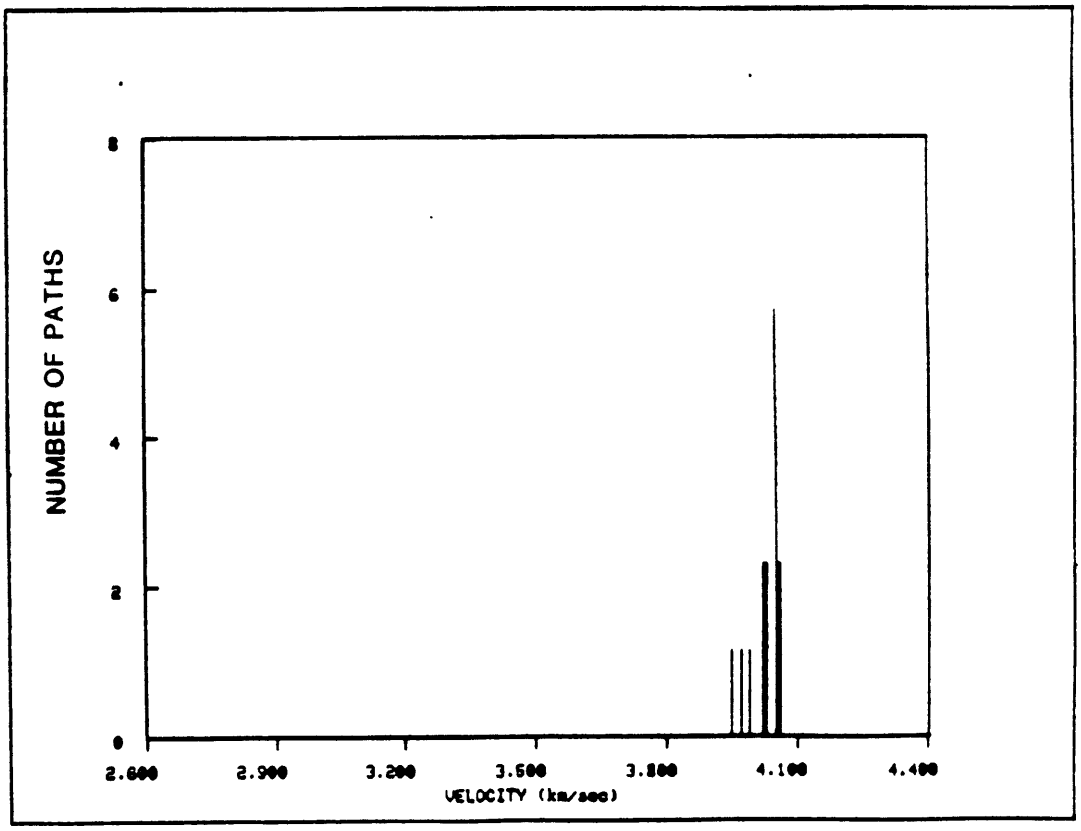

FIGURE A.2p REGION 0

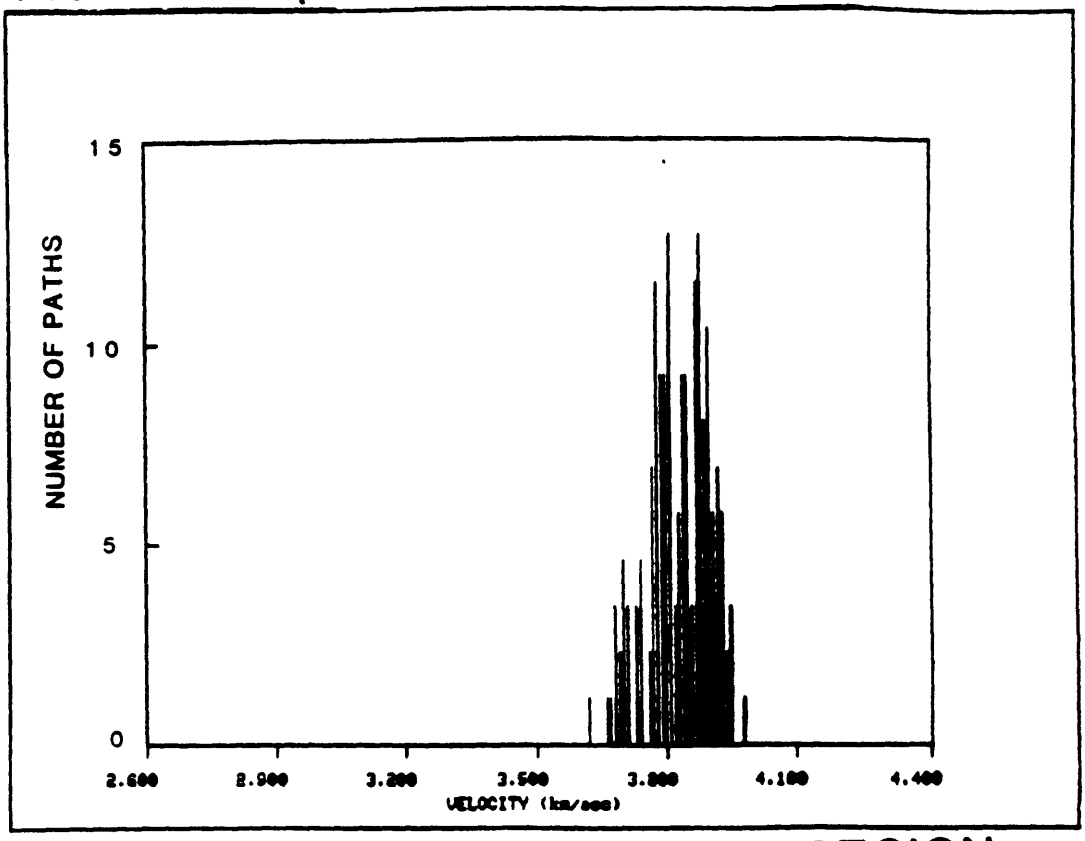

FIGURE A.2q REGION .

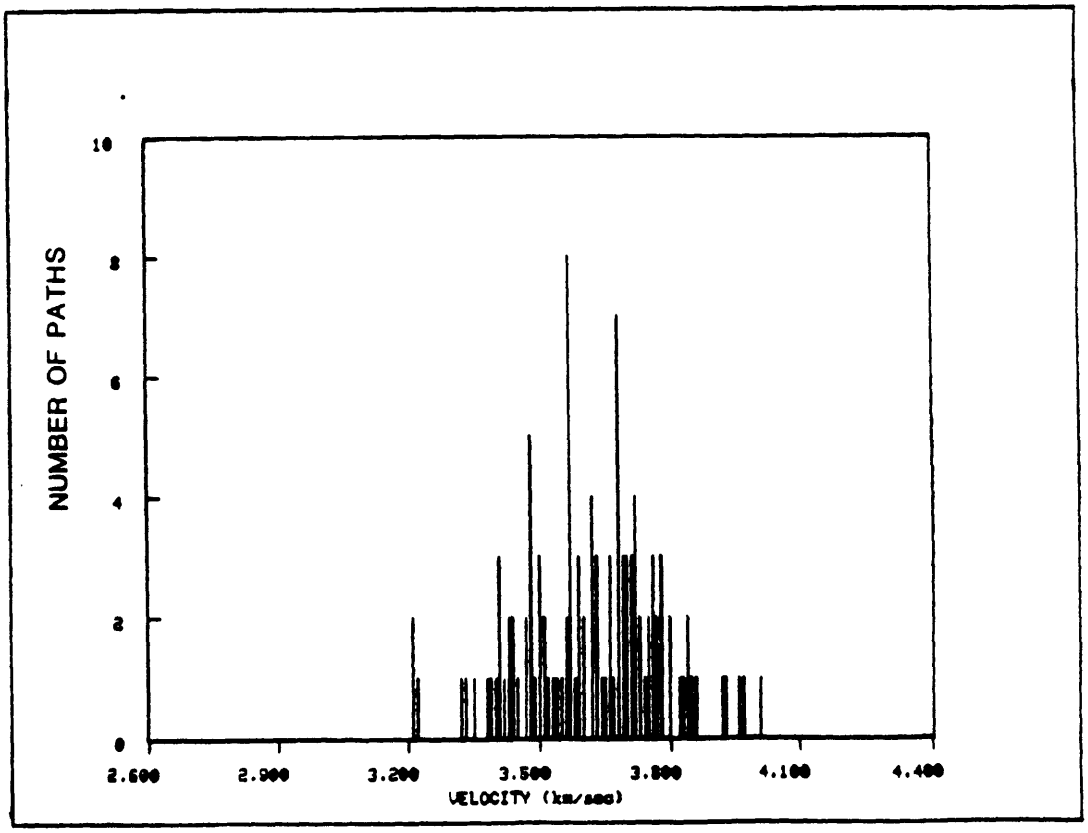

FIGURE A.2r

REGION ø

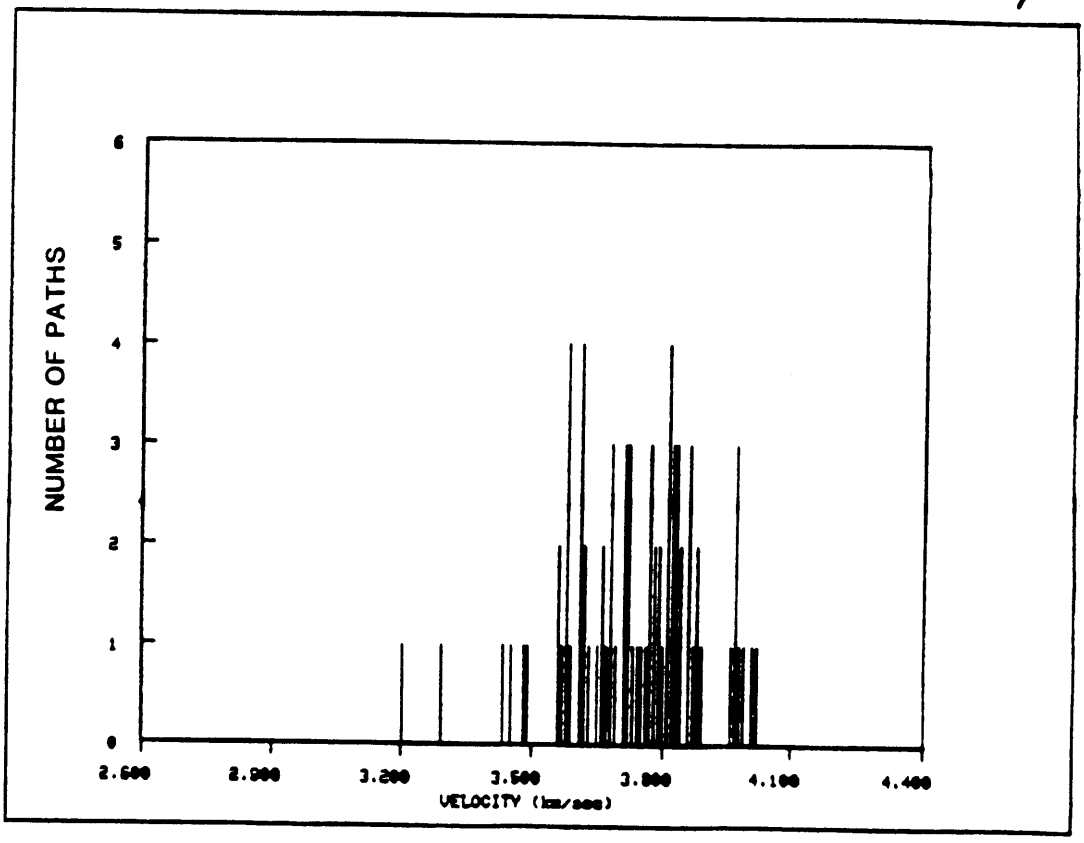

FIGURE A.3a

PERIOD 40 sec

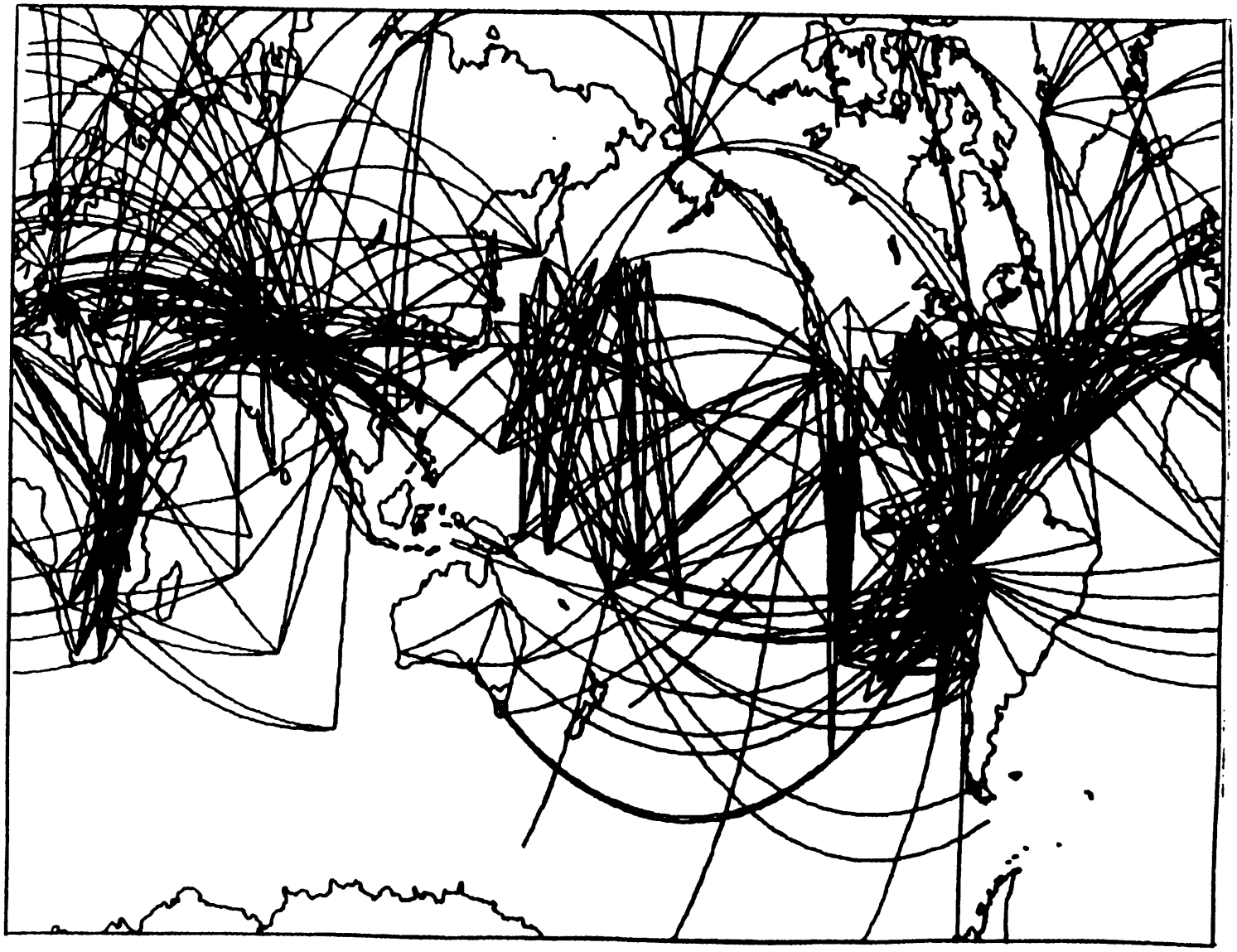

FIGURE A.3b REGION a

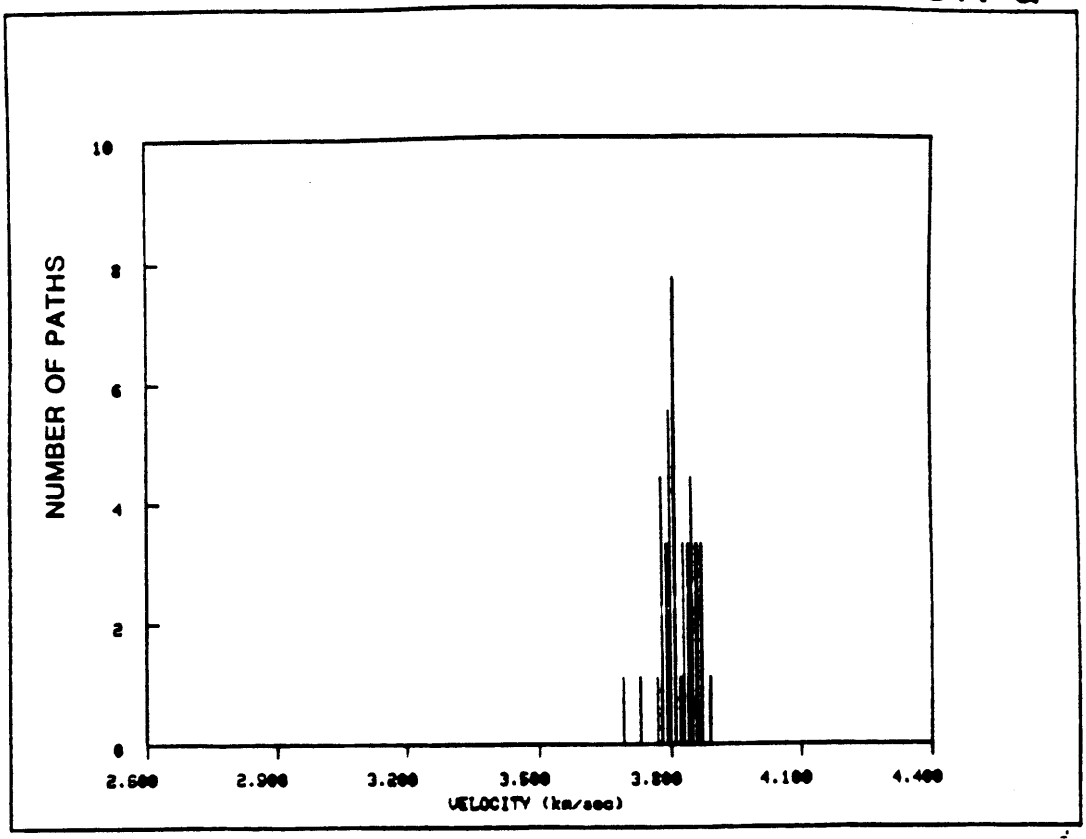

FIGURE A.3c REGION b

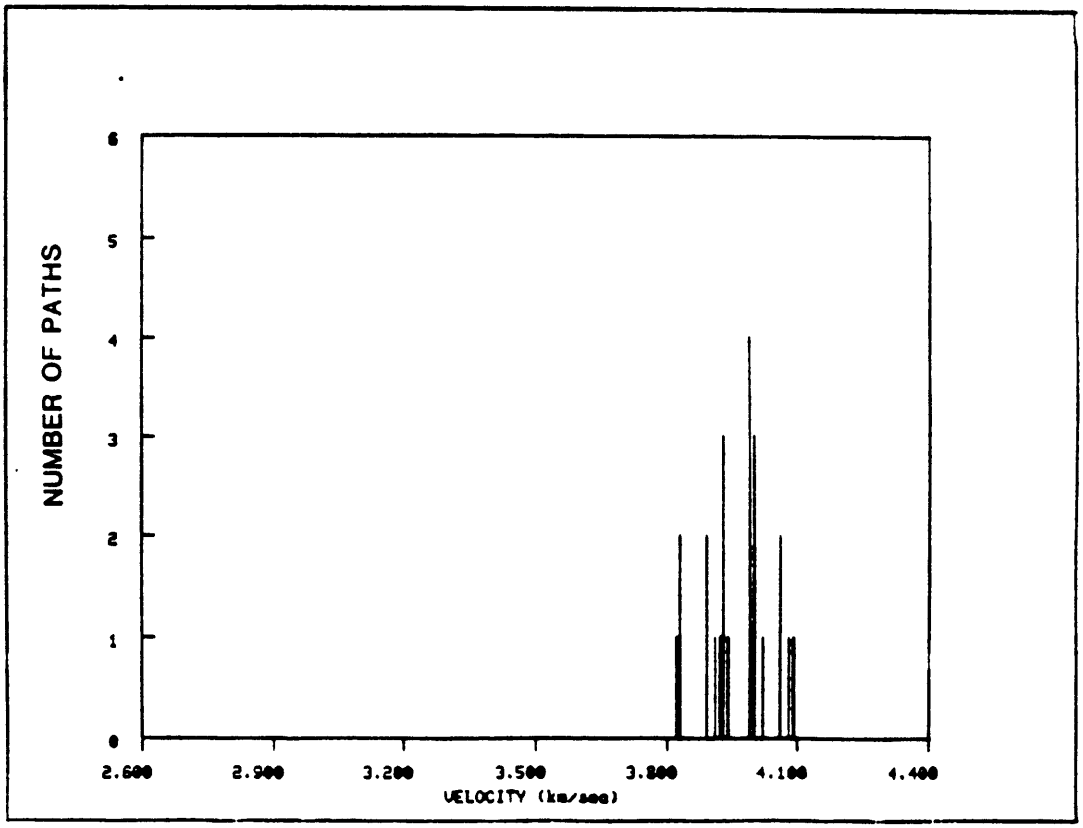

FIGURE A.3d REGION c

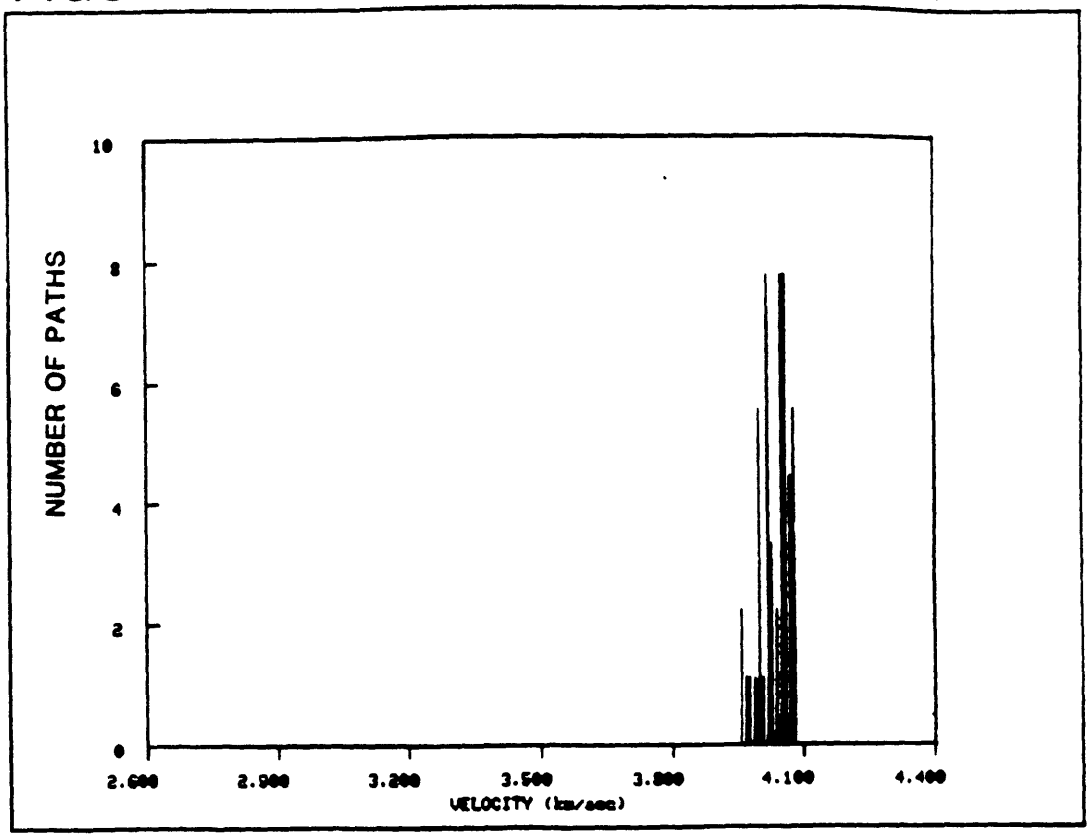

FIGURE A.3e REGION p

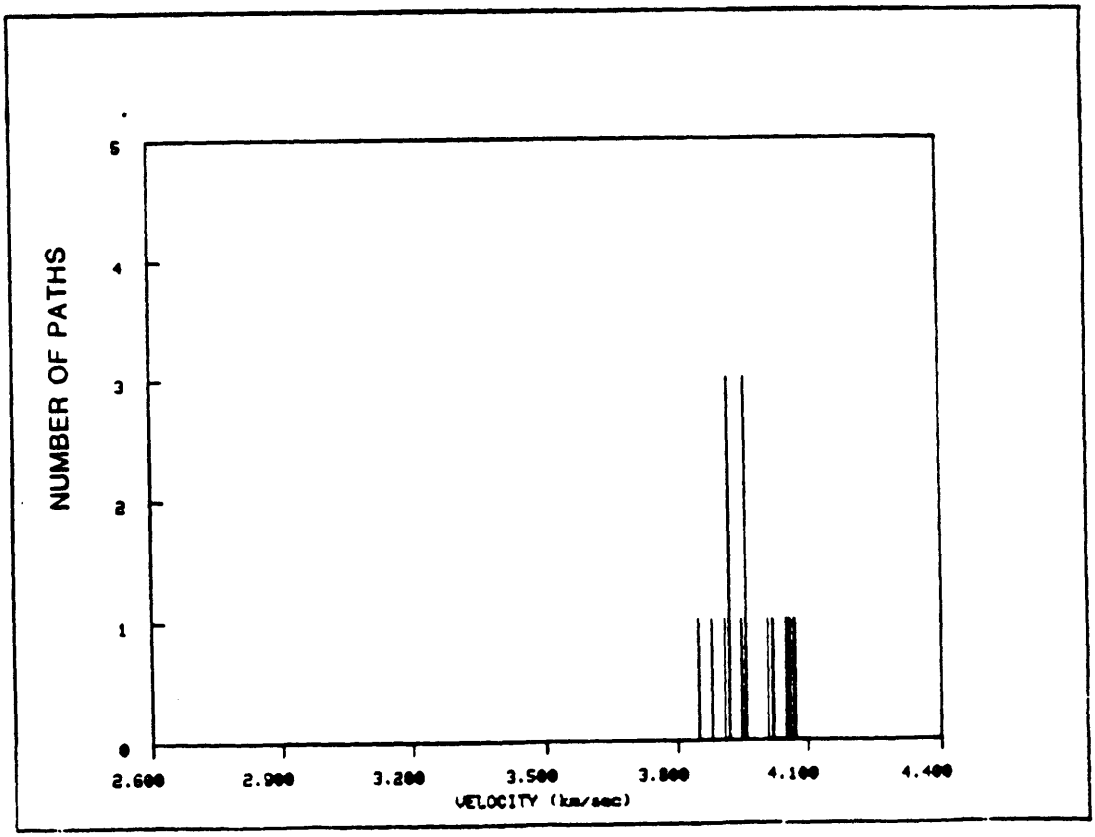

FIGURE A.3f REGION q

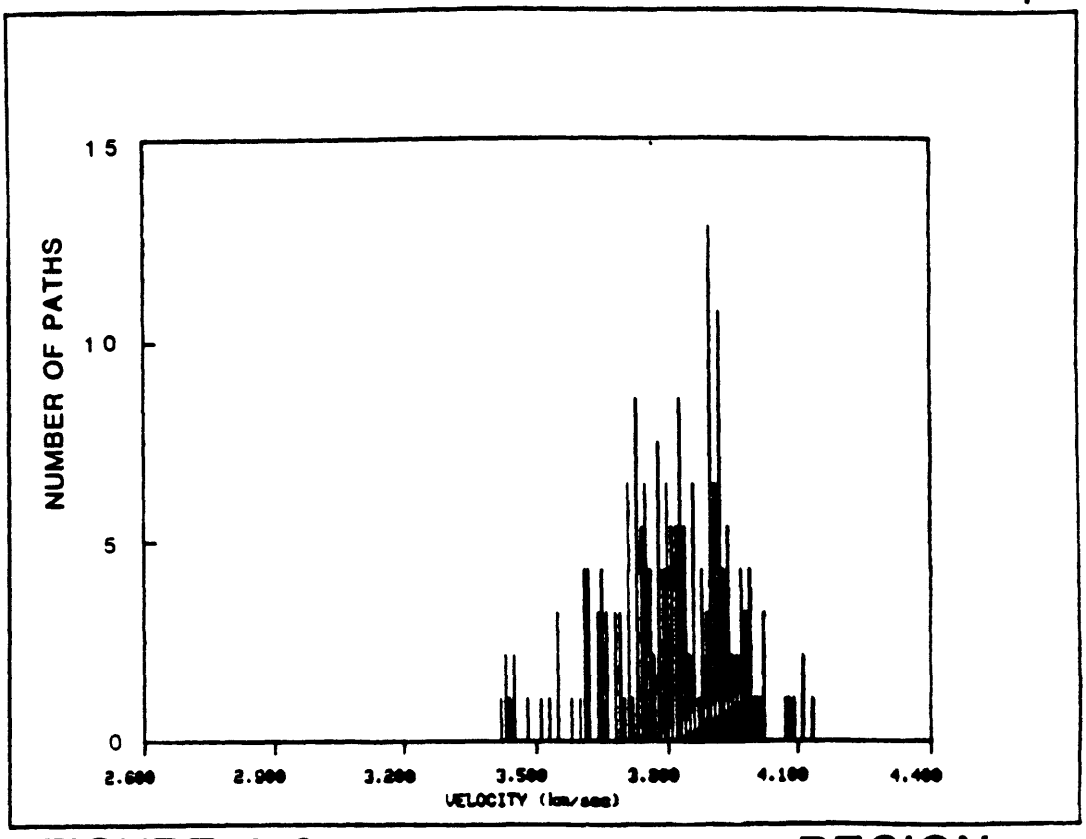

FIGURE A.3g REGION s

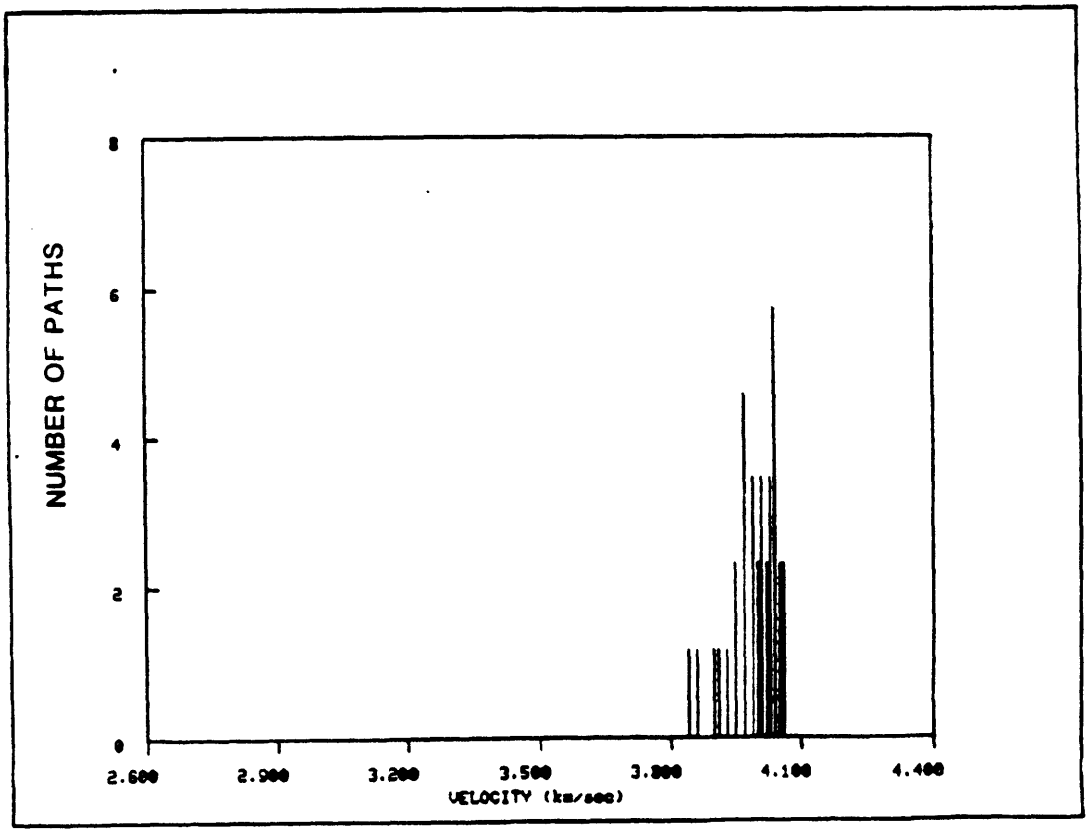

FIGURE A.3h REGION N

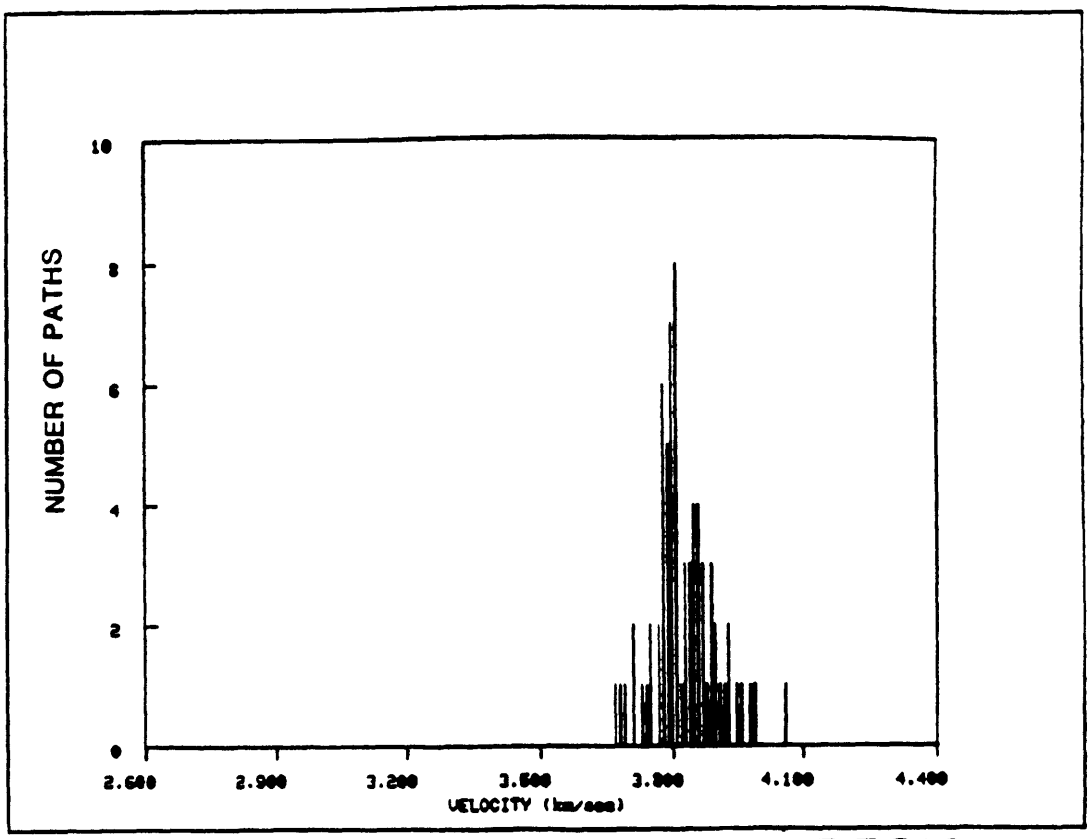

FIGURE A.3i REGION =

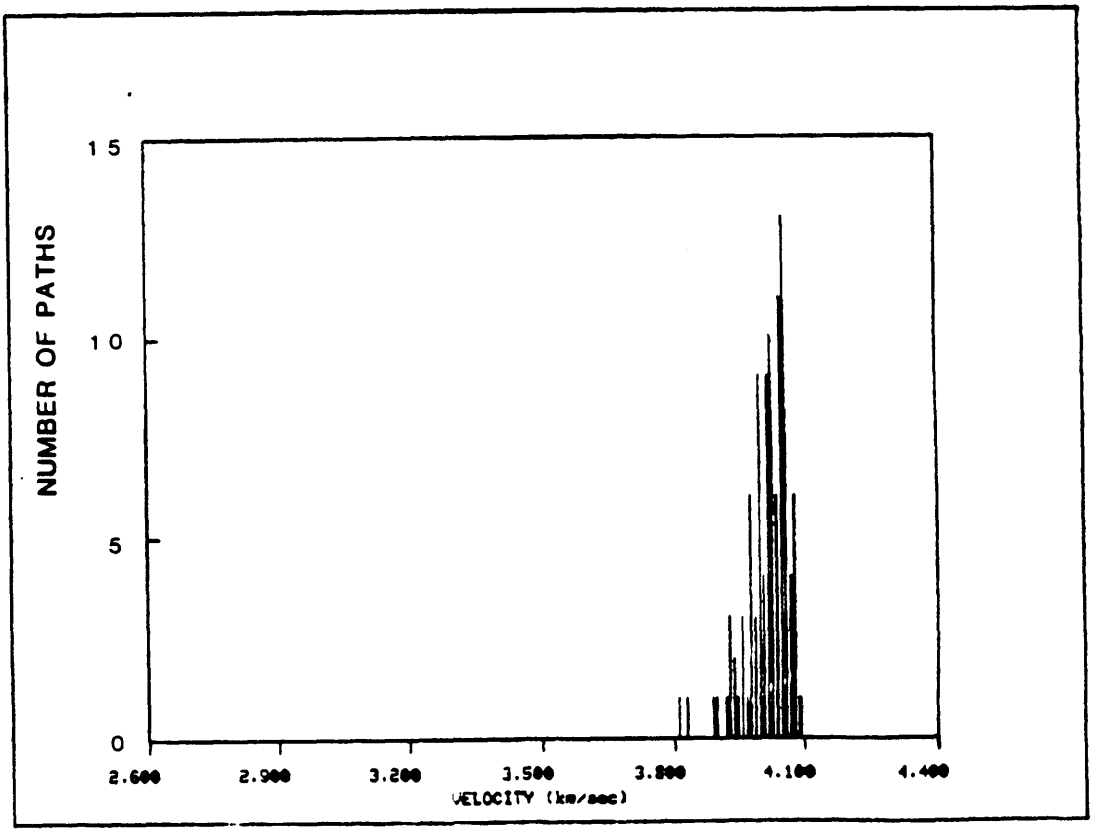

FIGURE A.3j REGION 0

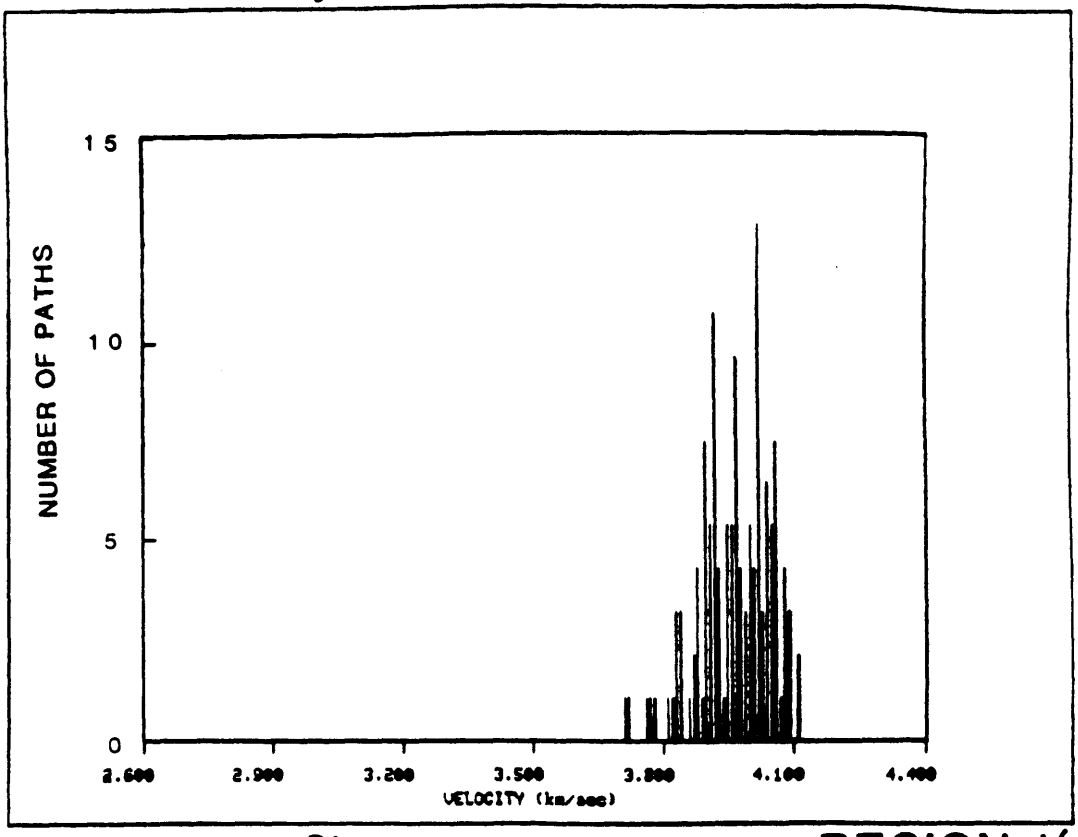

FIGURE A.3k REGION ~~0~~

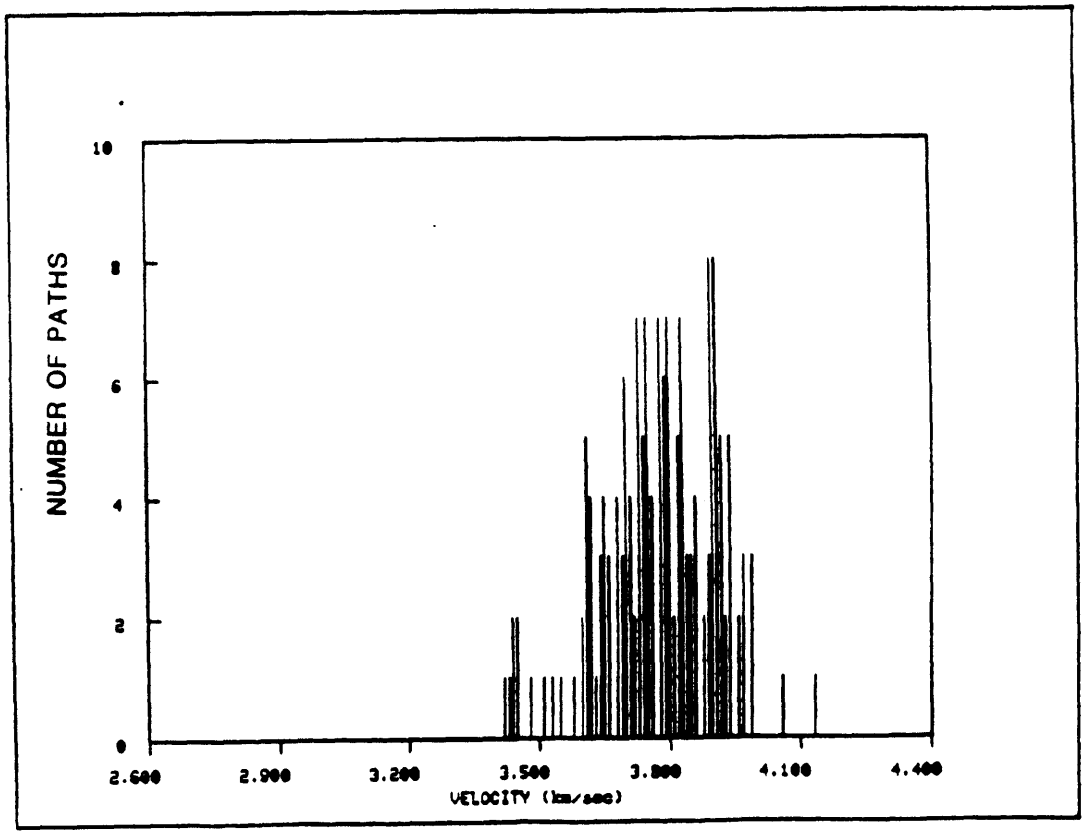

FIGURE A.3l REGION N

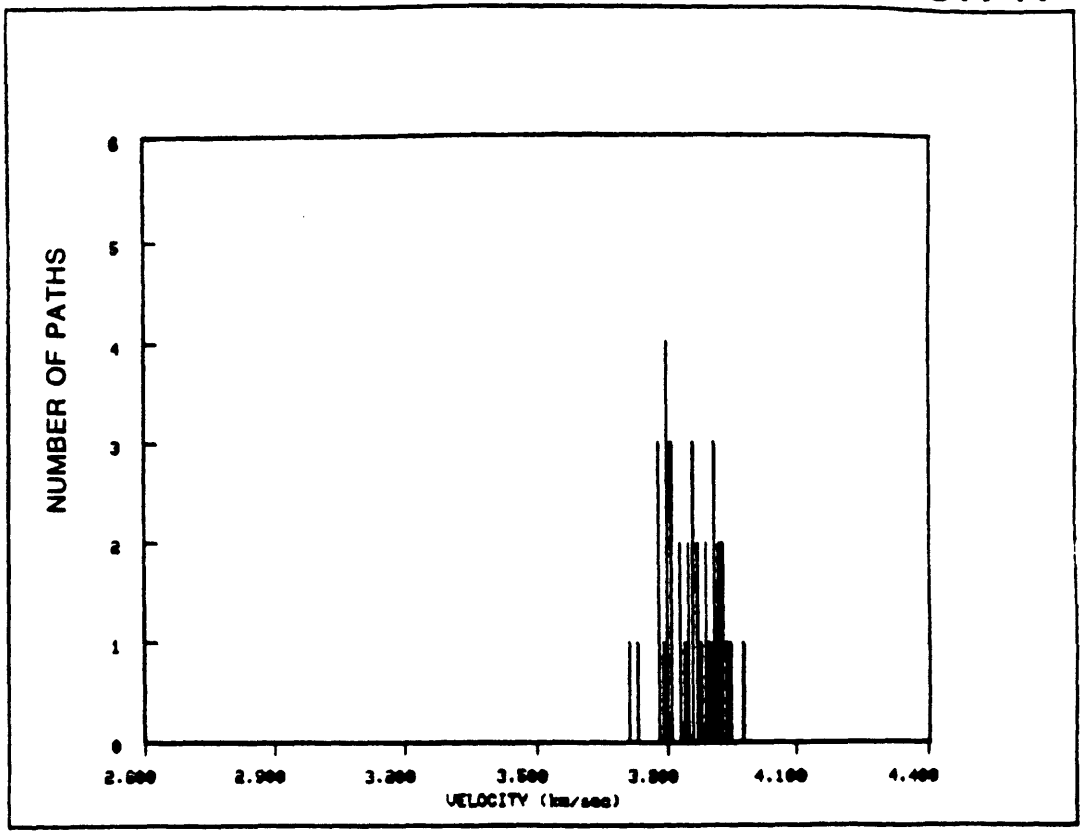

FIGURE A.3m REGION #

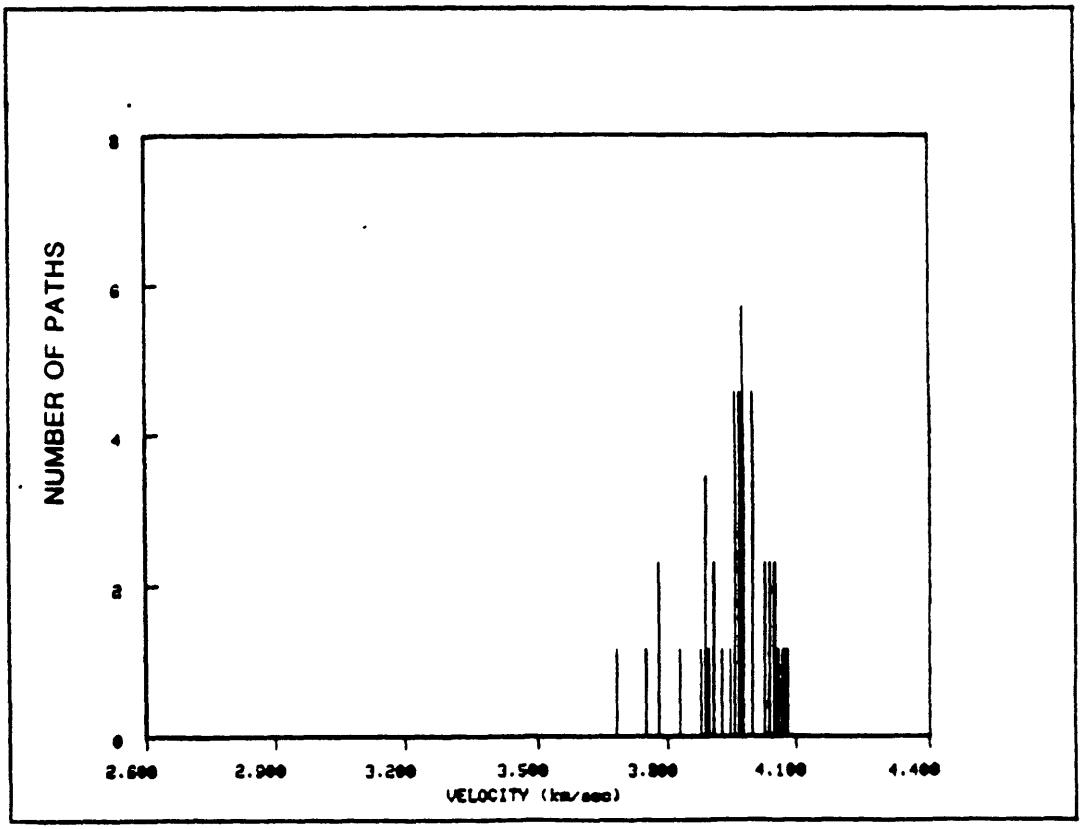

FIGURE A.3n REGION =

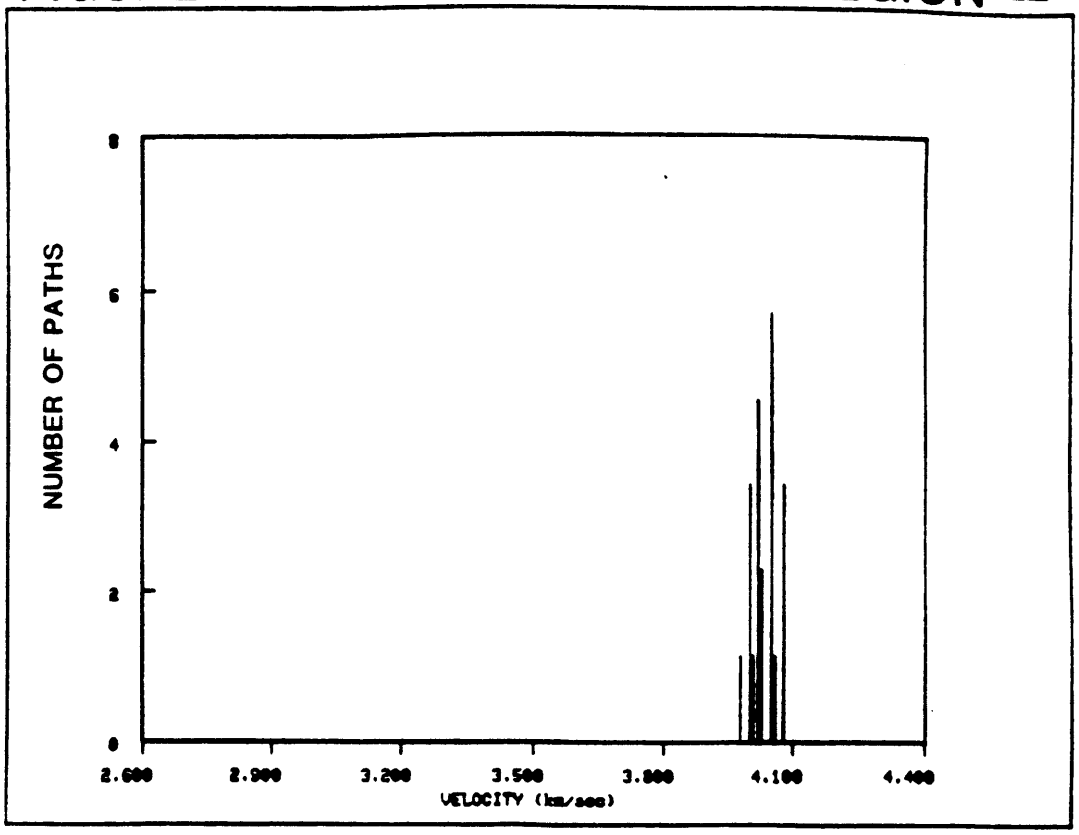

FIGURE A.3o REGION -

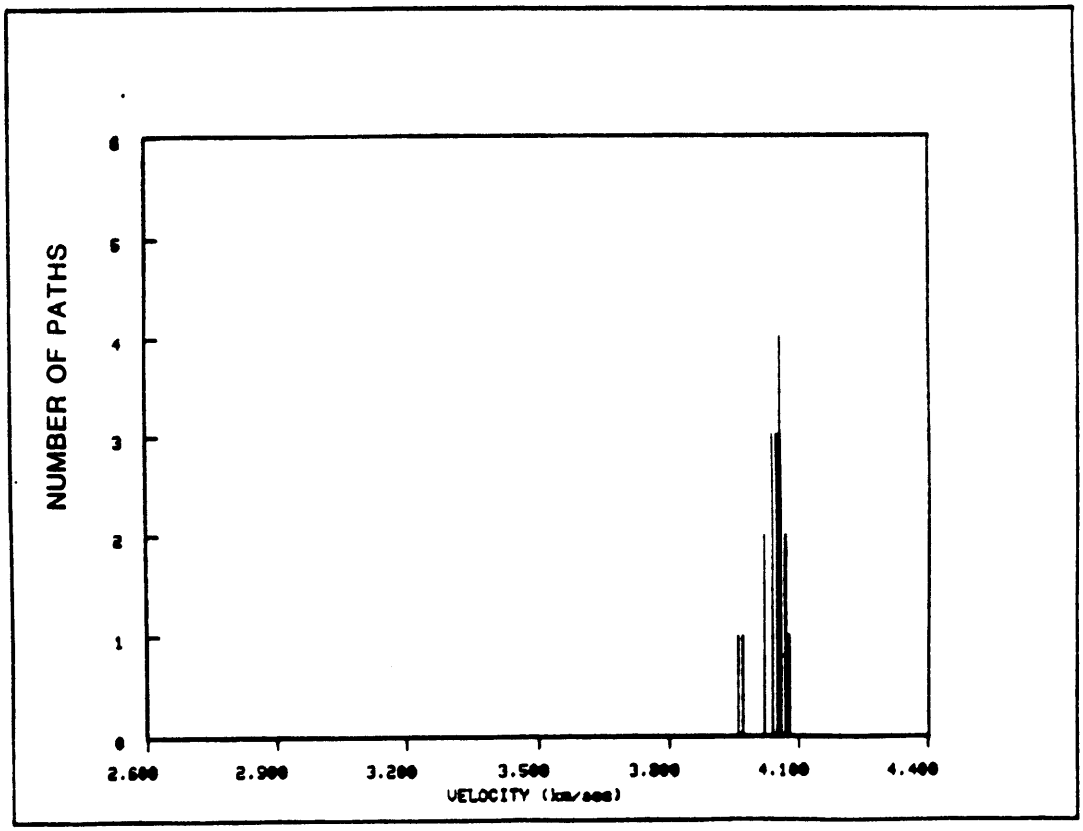

FIGURE A.3p REGION 0

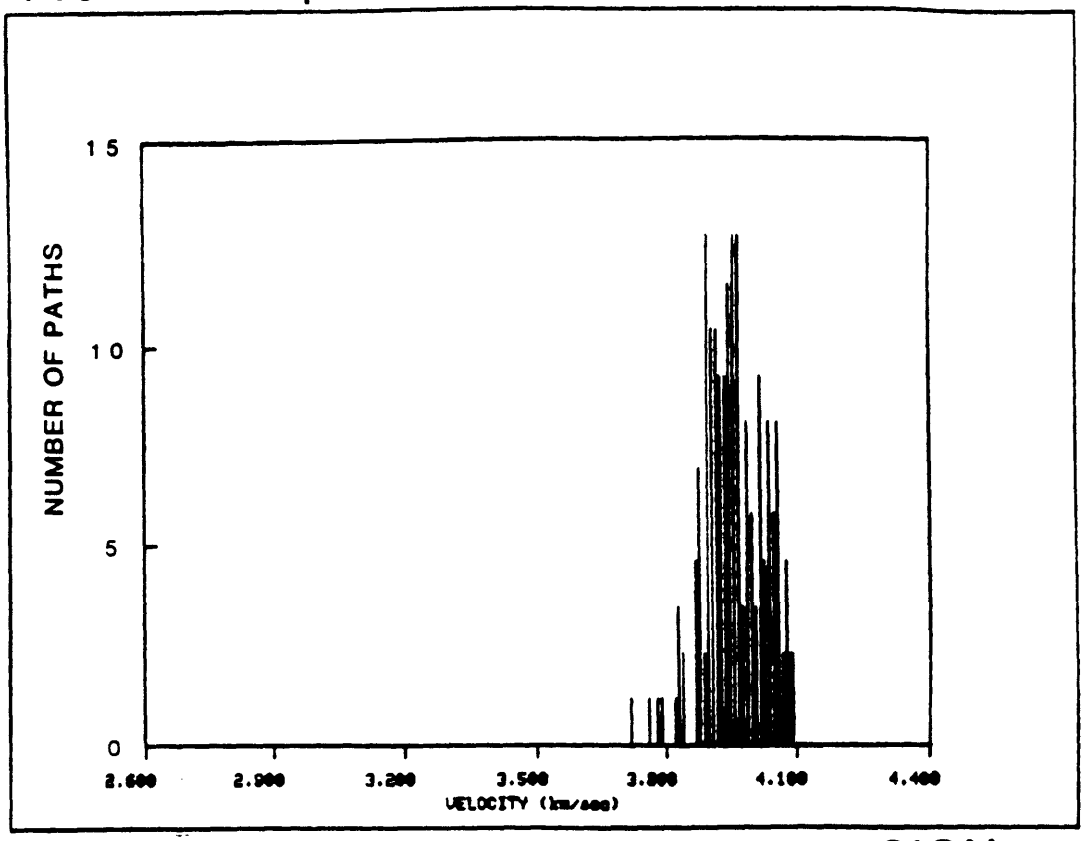

FIGURE A.3q REGION .

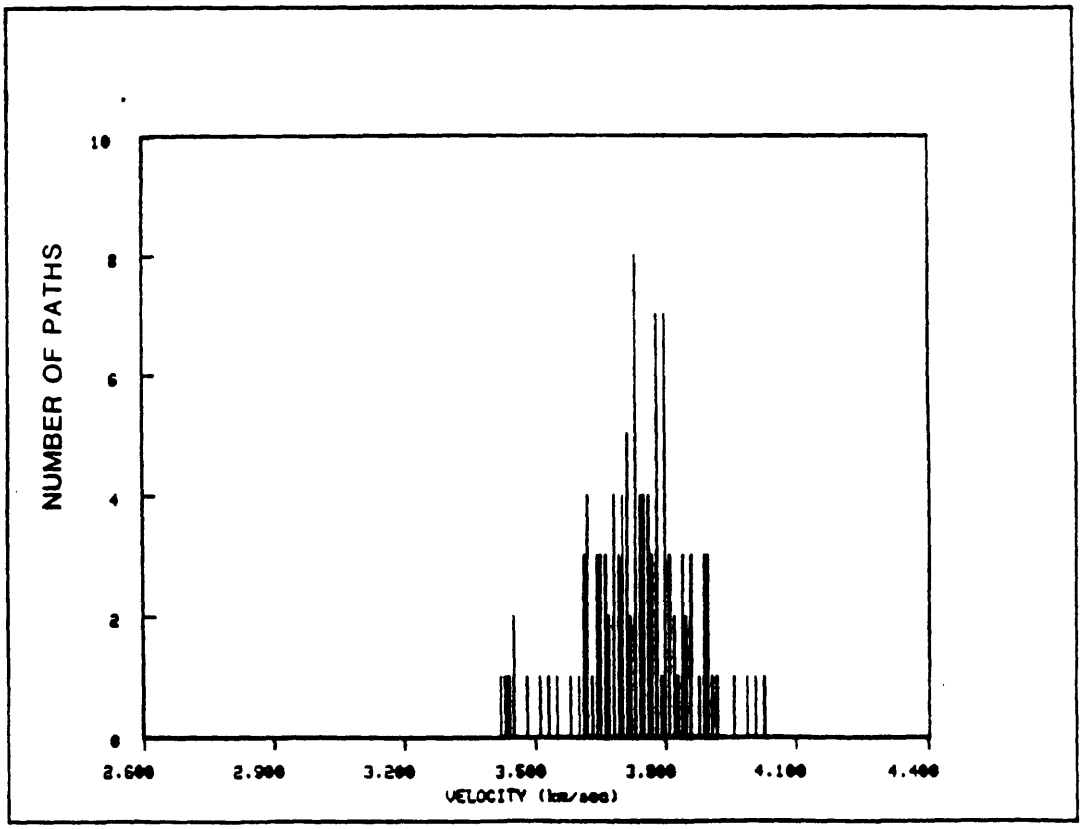

FIGURE A.3r REGION ø

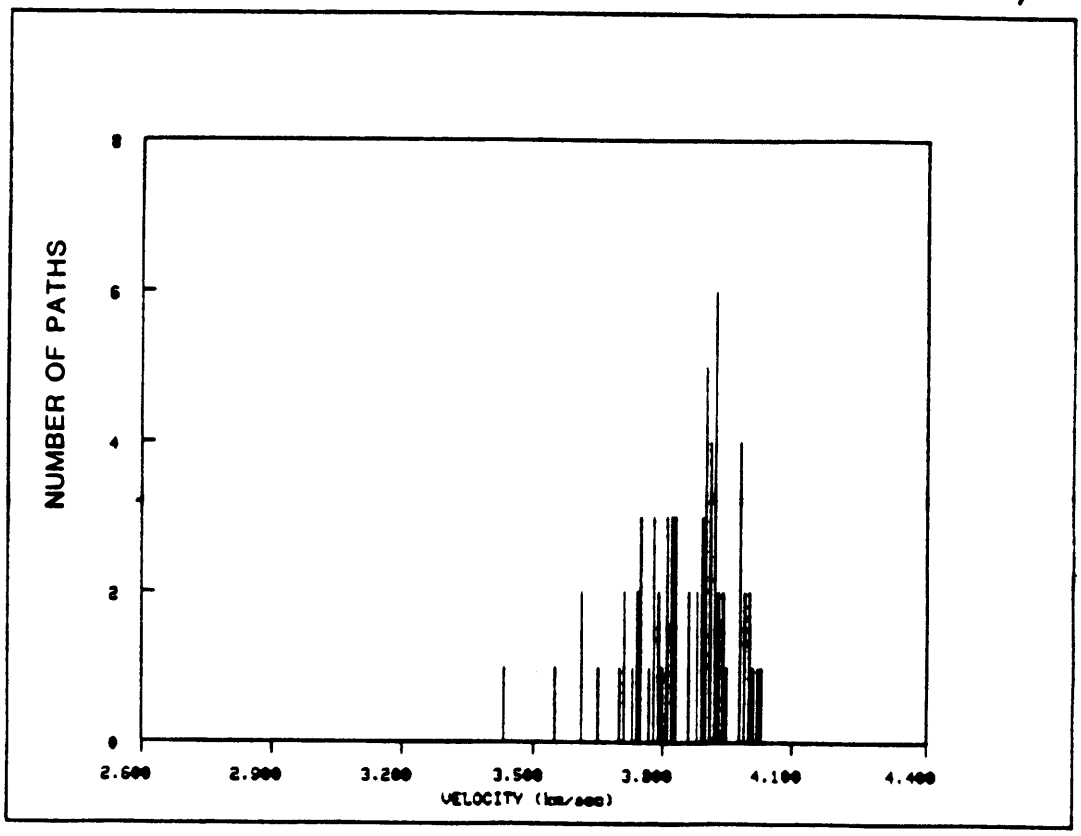

FIGURE A.4a

PERIOD 50 sec

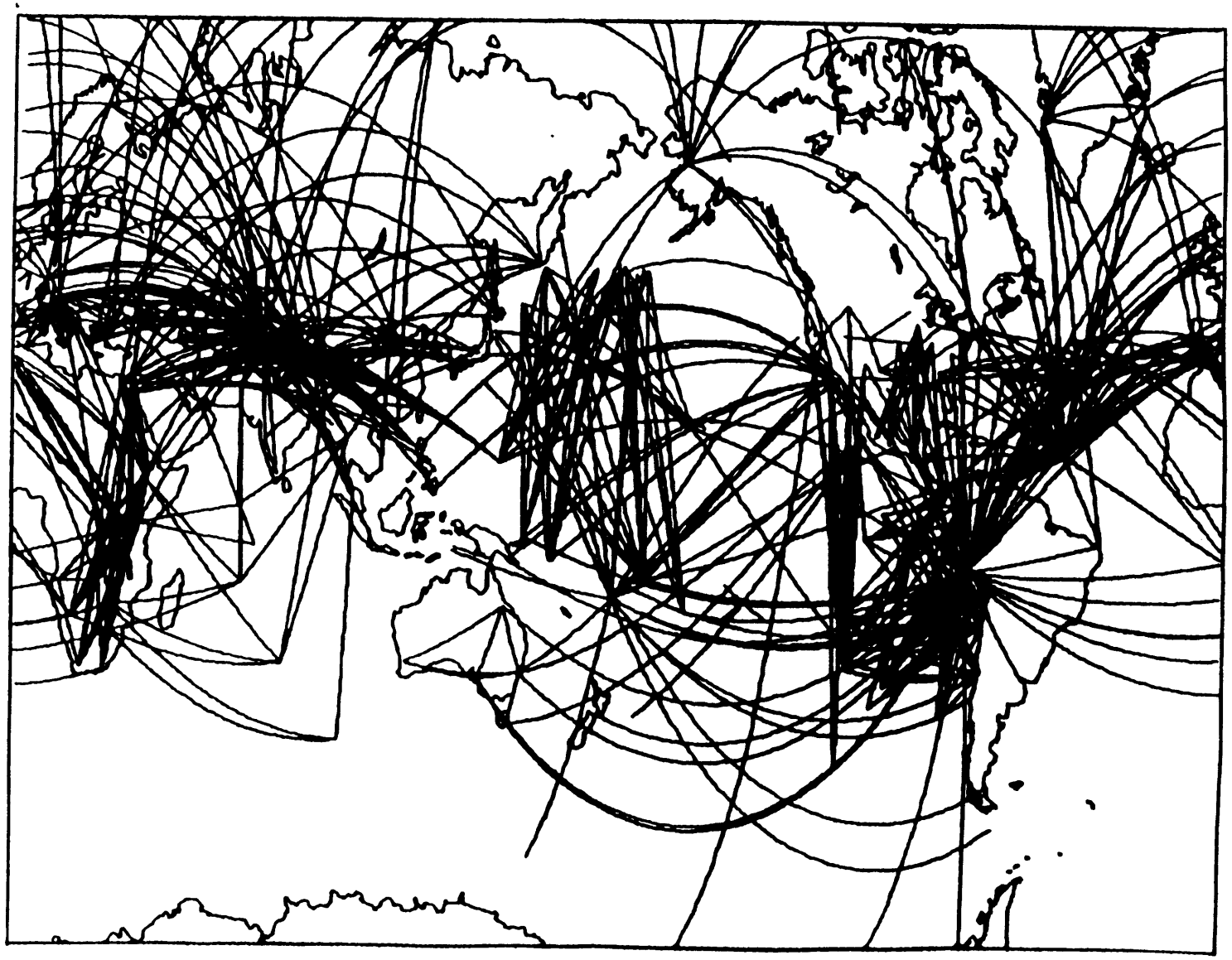

FIGURE A.4b REGION a

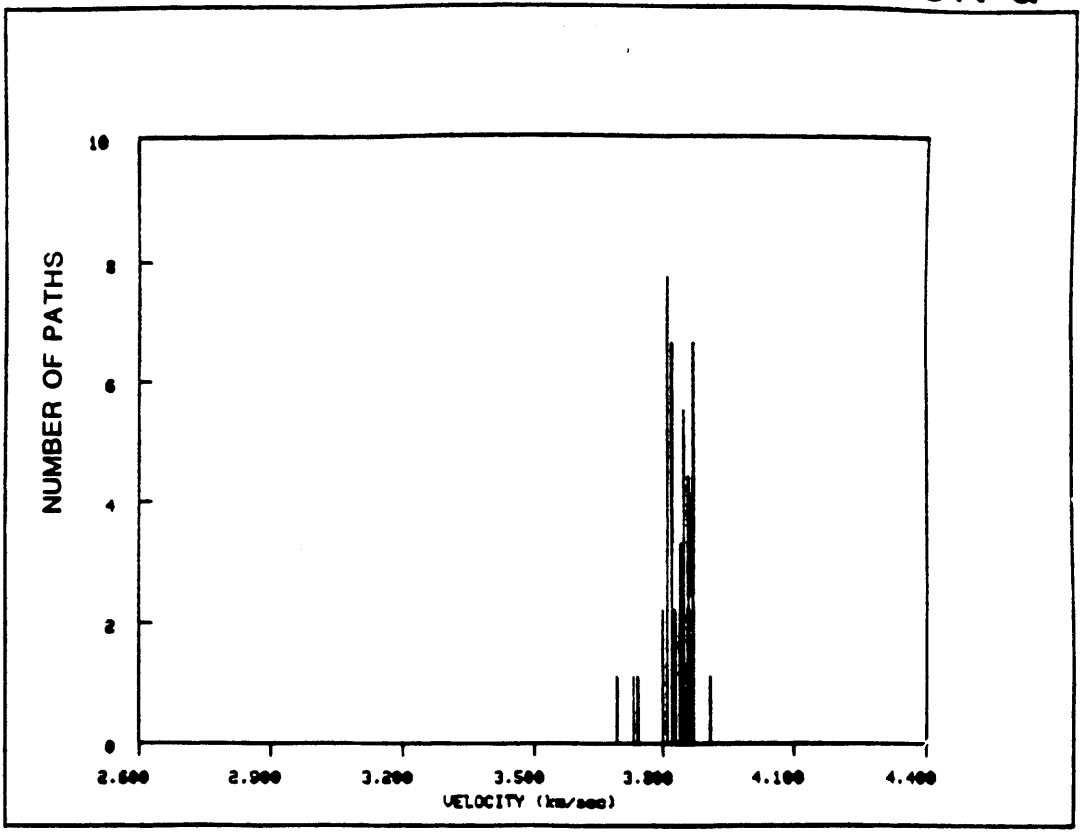

FIGURE A.4c REGION b

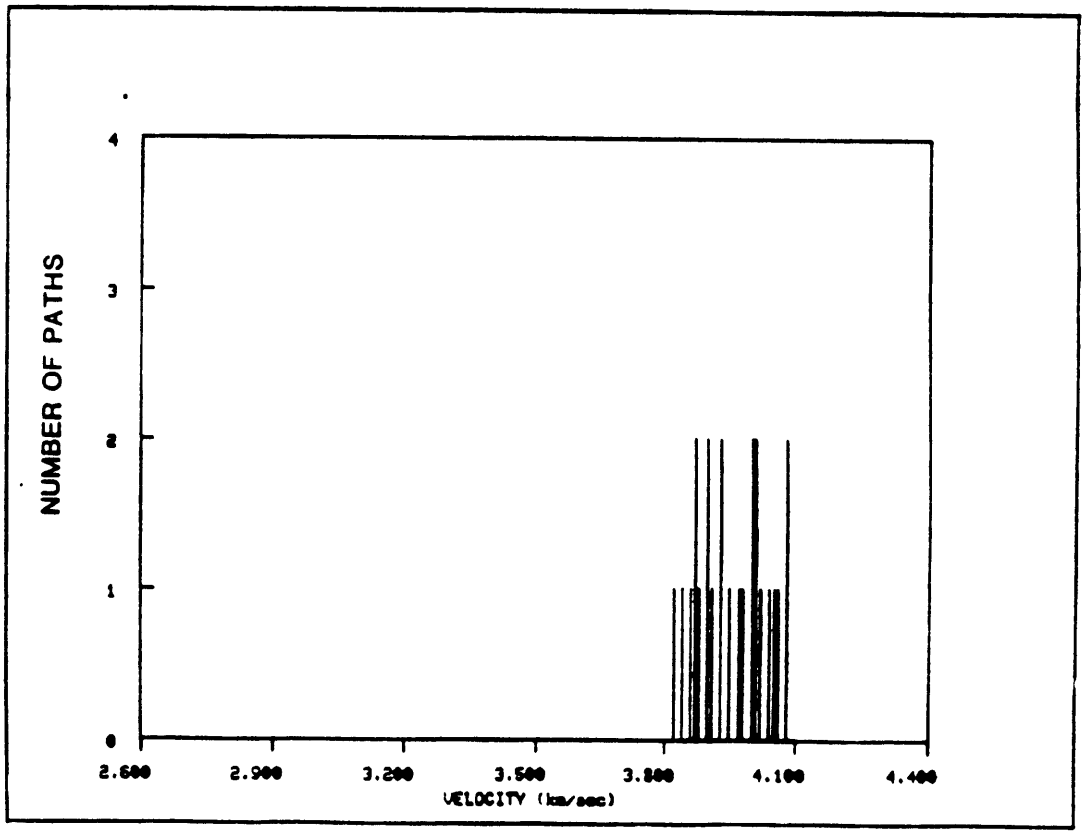

FIGURE A.4d REGION c

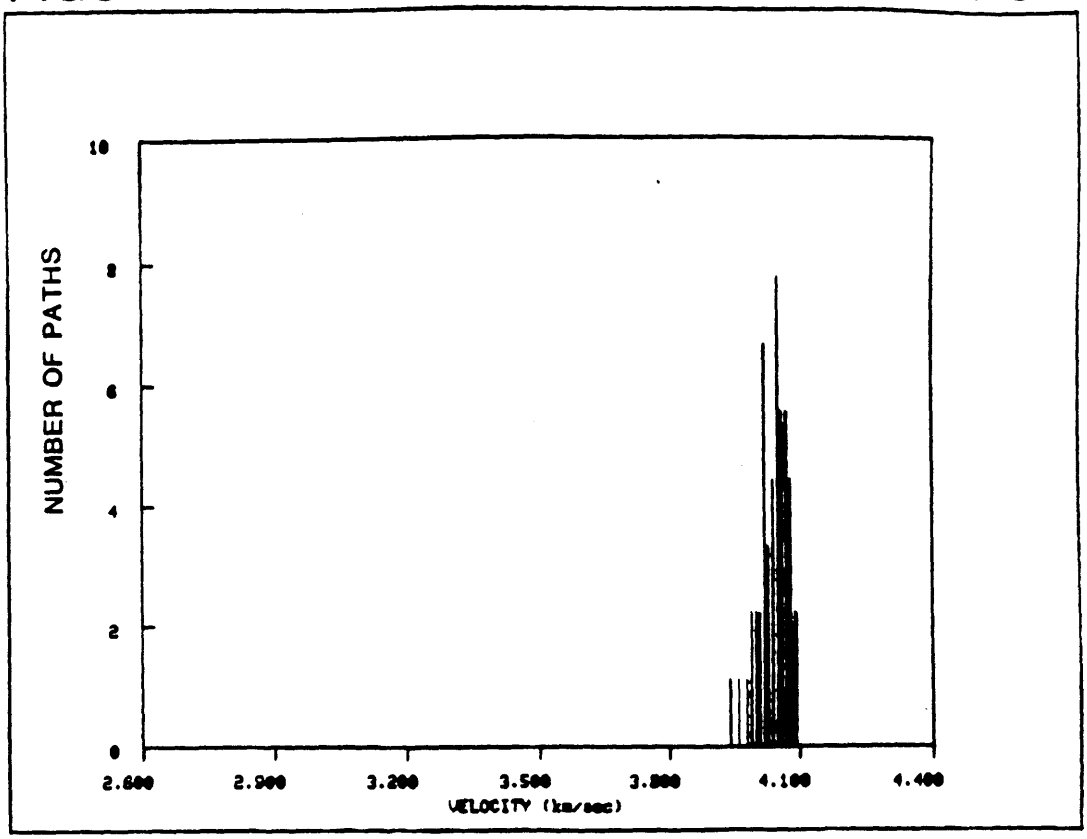

FIGURE A.4e REGION p

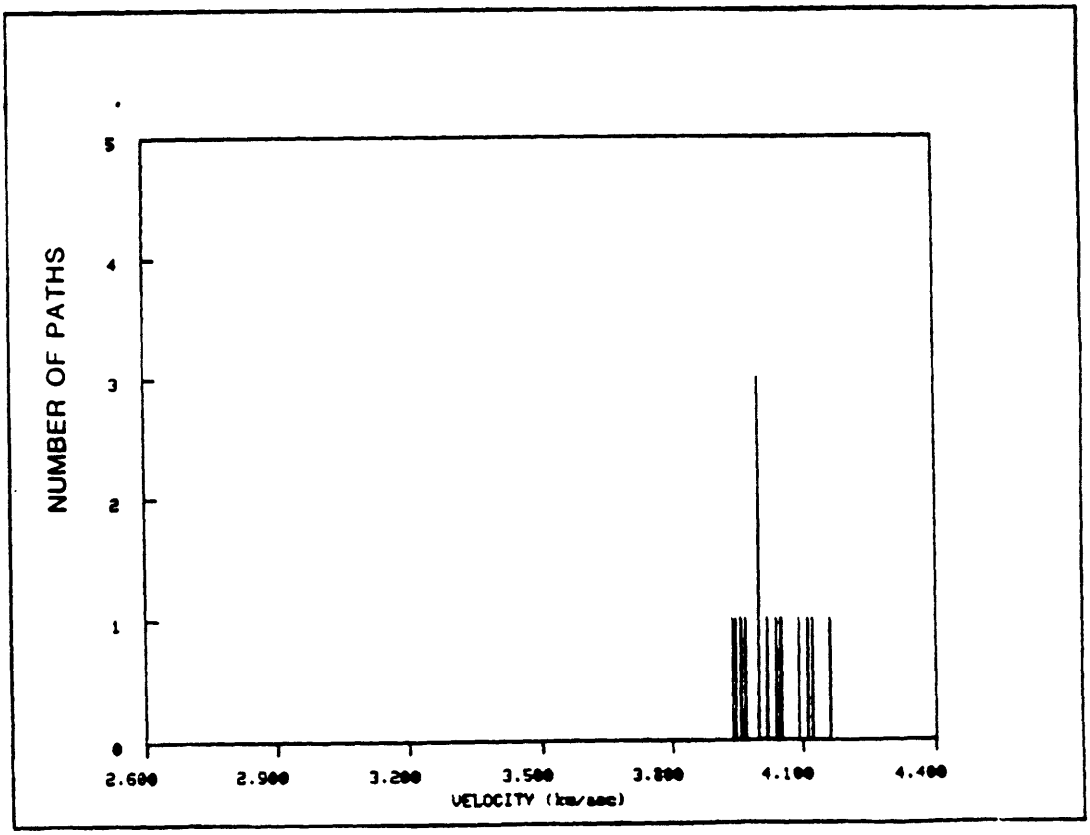

FIGURE A.4f REGION q

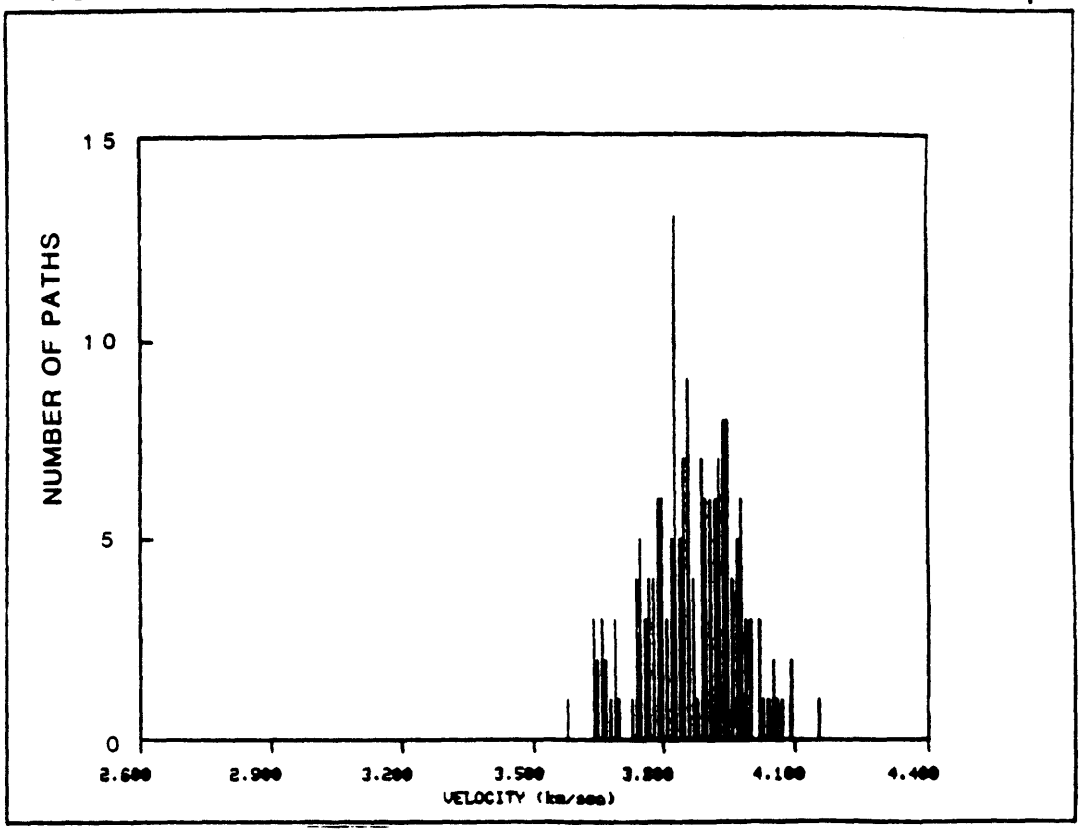

FIGURE A.4g REGION s

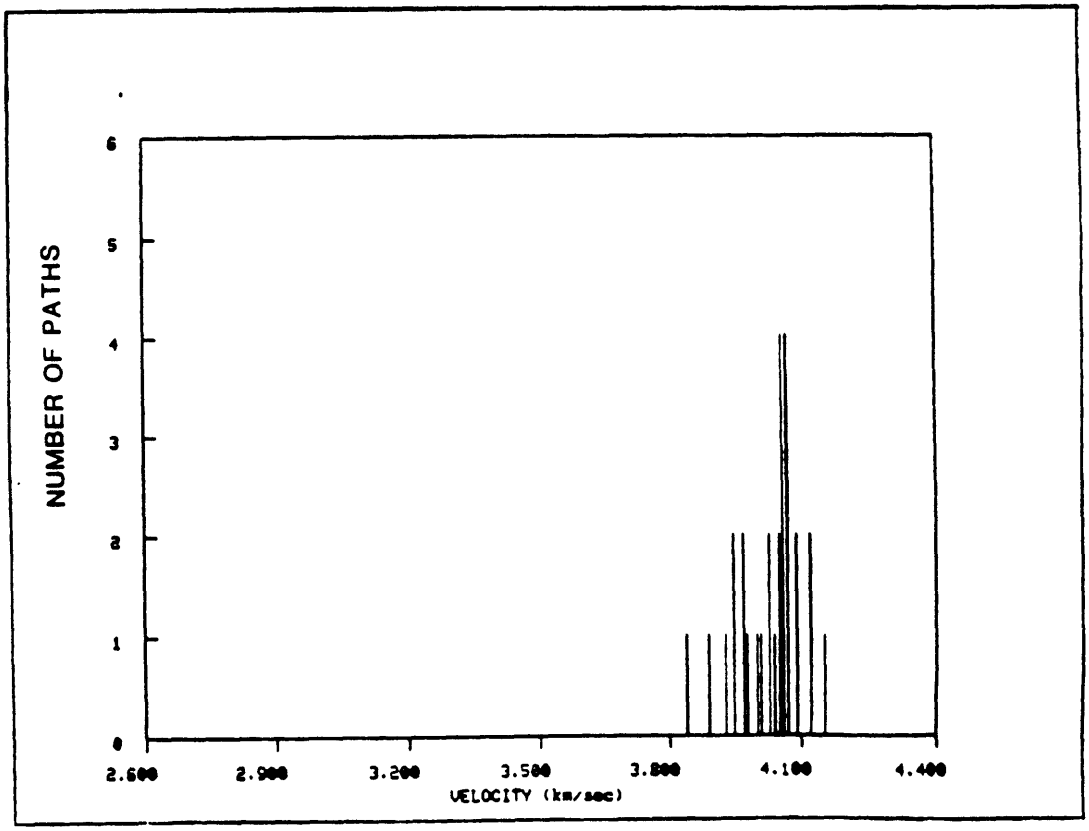

FIGURE A.4h REGION N

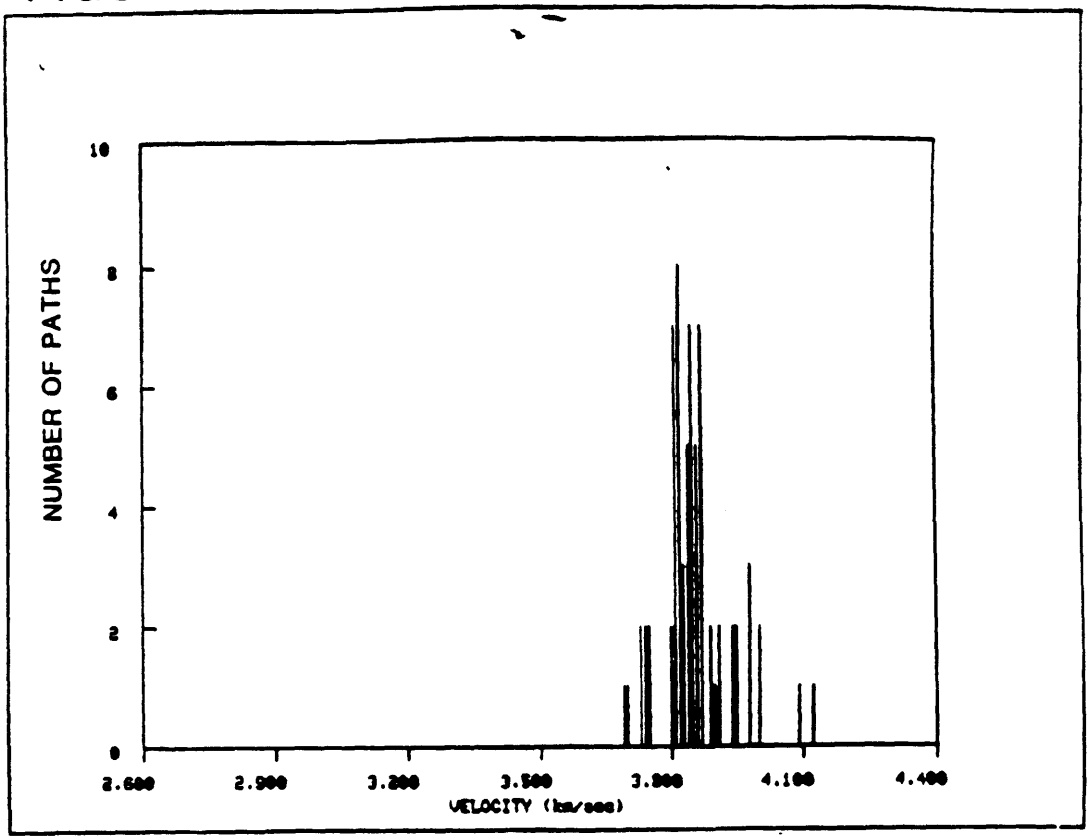

FIGURE A.4i REGION =

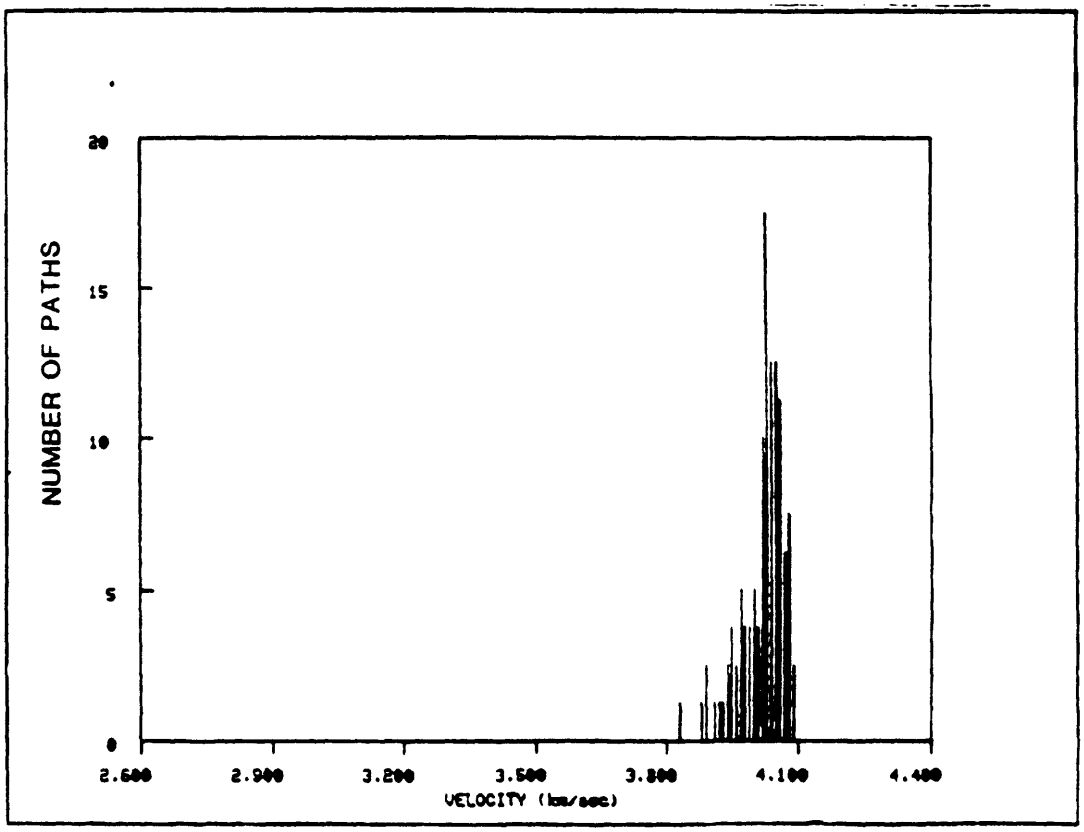

FIGURE A.4j REGION 0

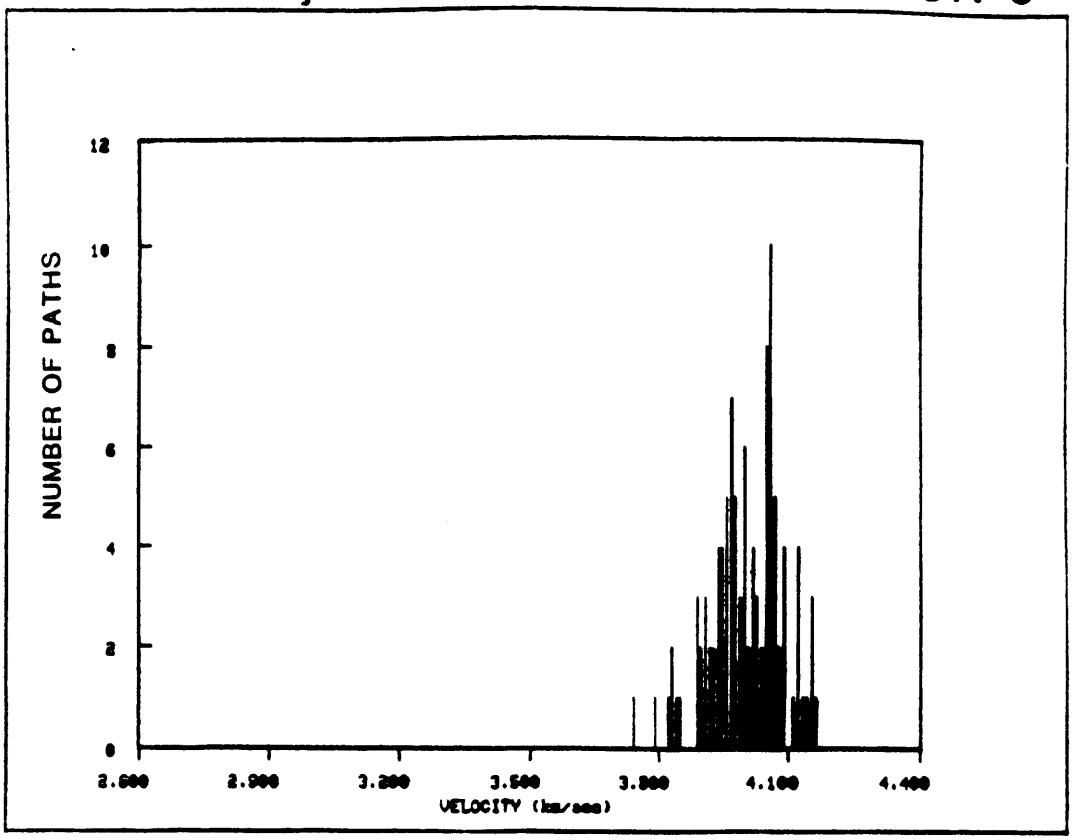

FIGURE A.4k REGION ~~0~~

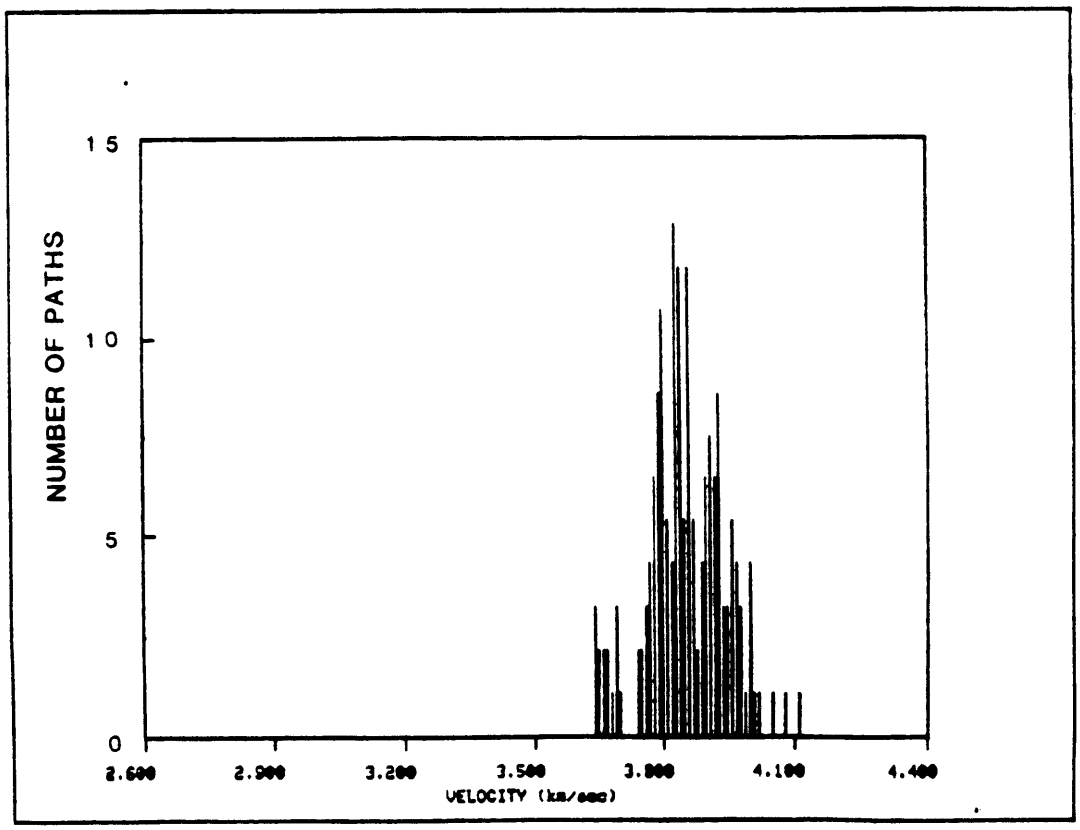

FIGURE A.4l REGION N

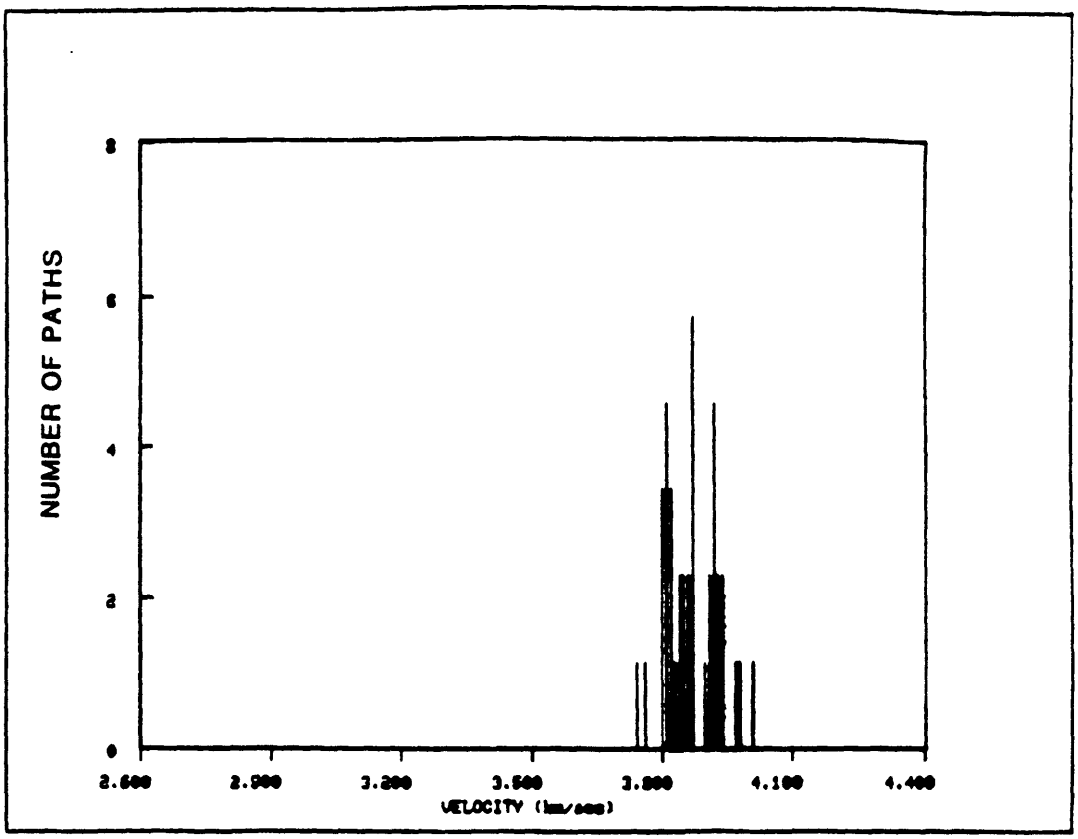

FIGURE A.4m REGION #

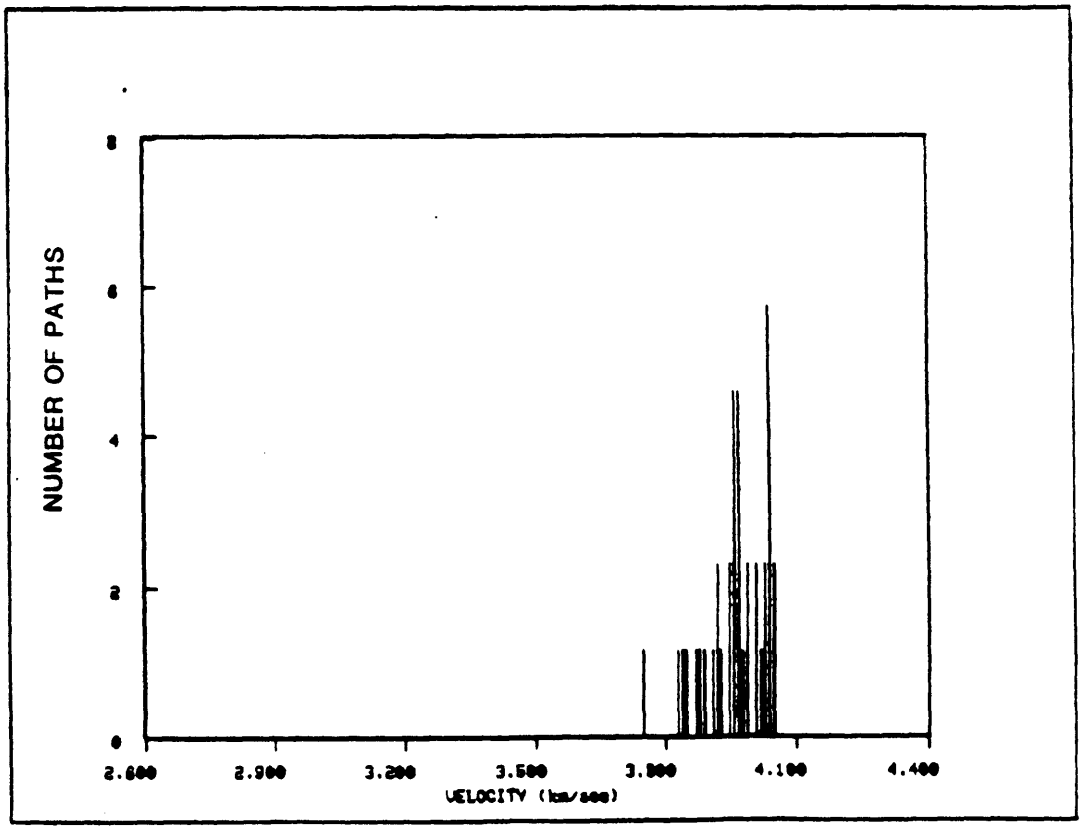

FIGURE A.4n REGION =

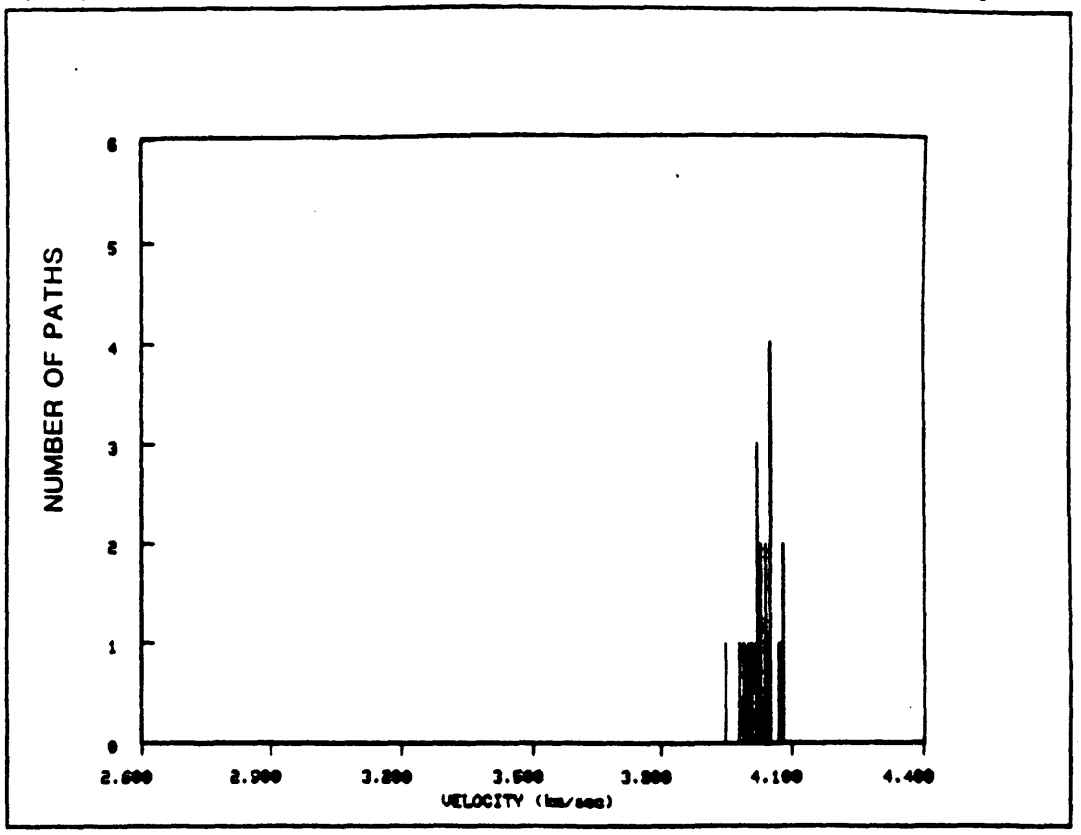

FIGURE A.4o REGION -

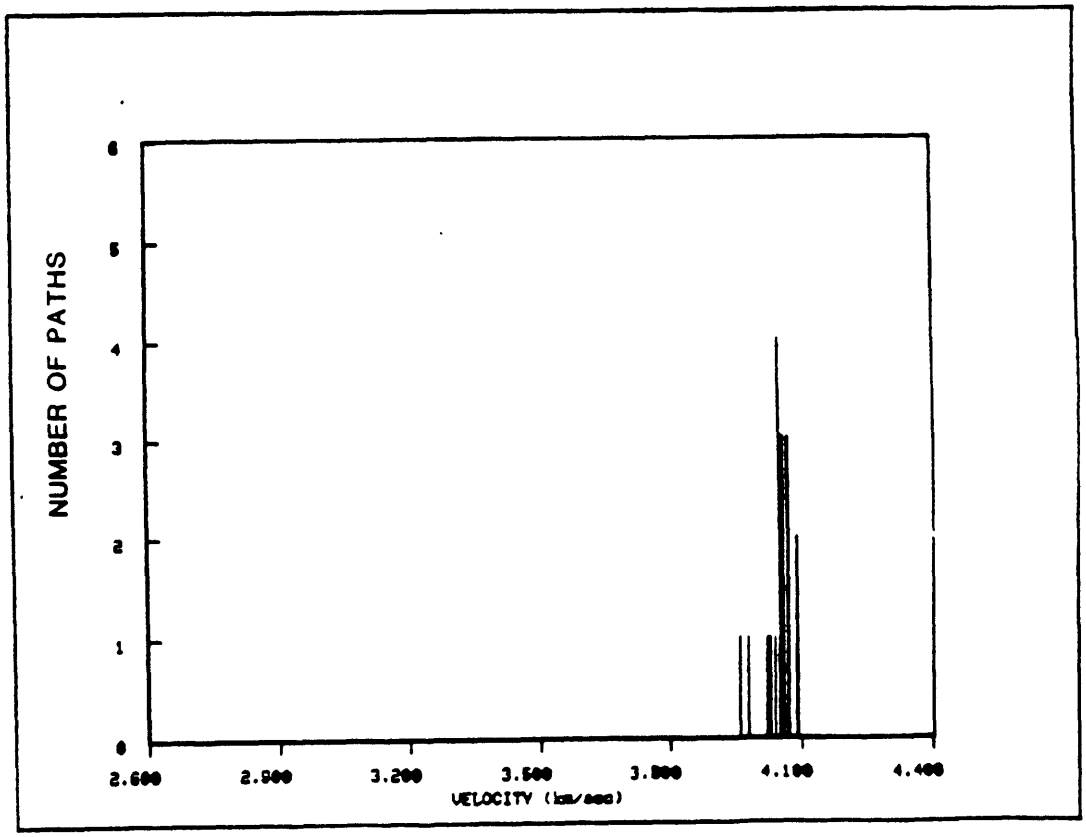

FIGURE A.4p REGION 0

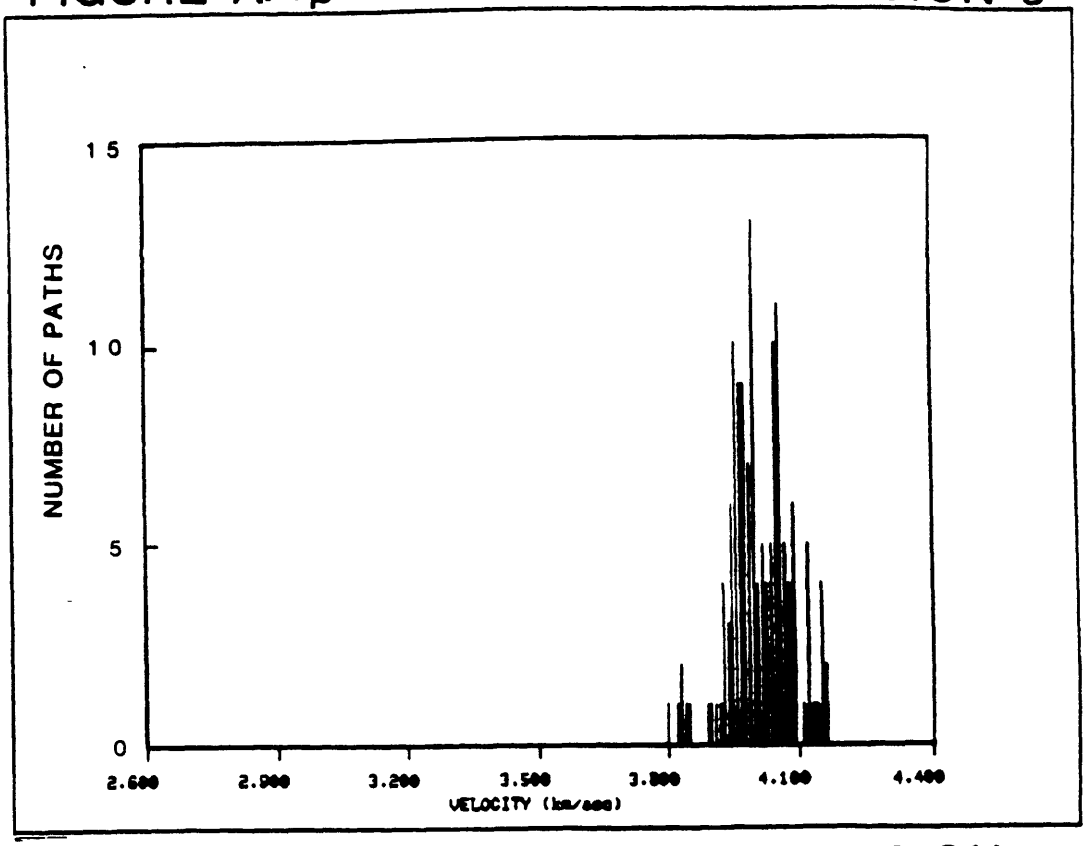

FIGURE A.4q REGION .

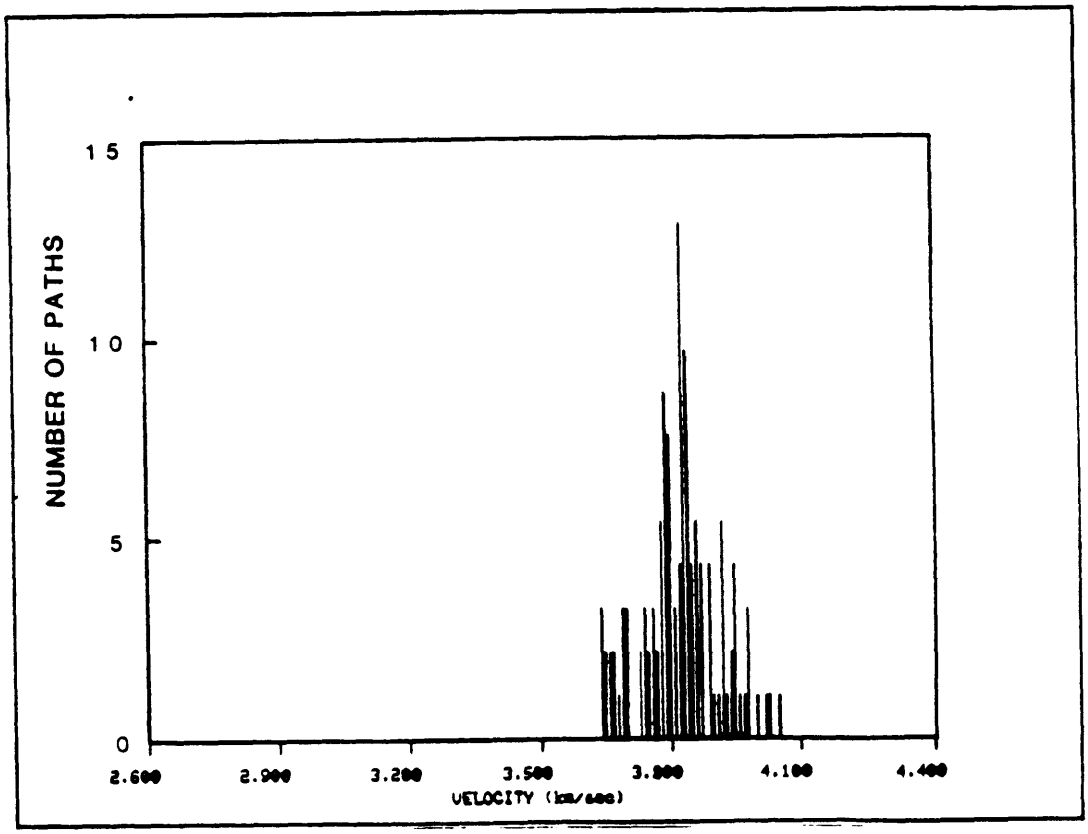

FIGURE A.4r

REGION ø

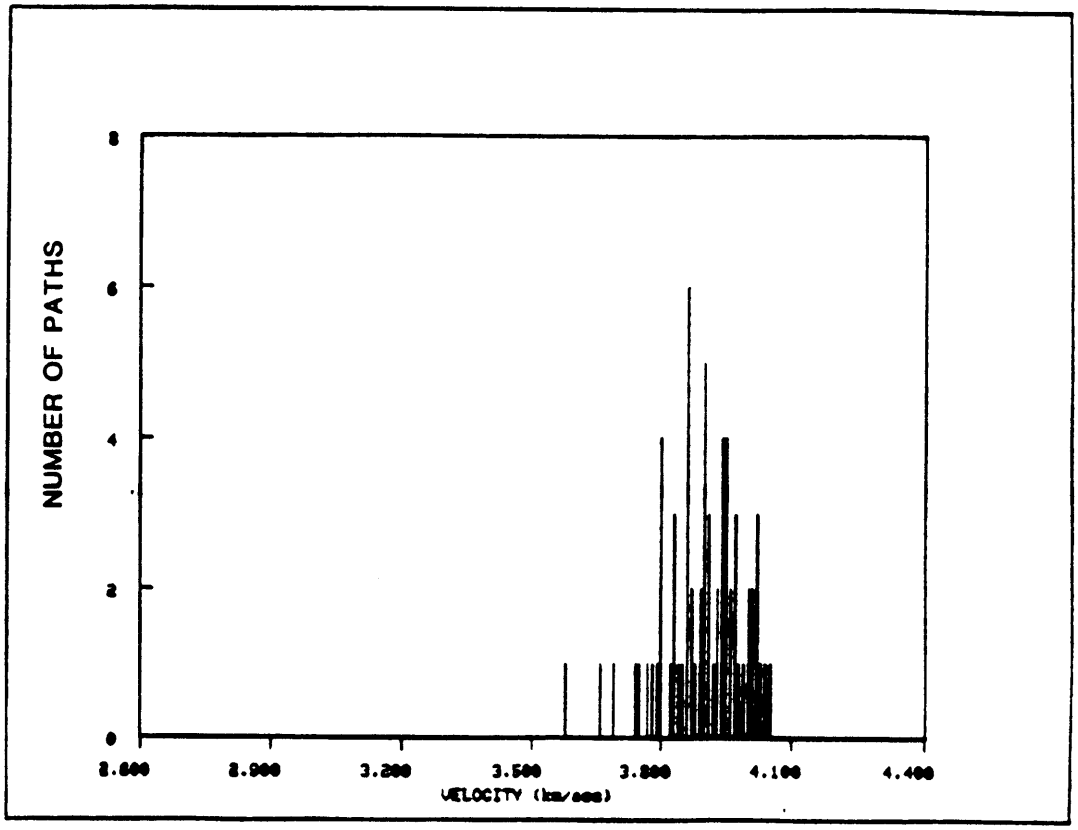

FIGURE A.5a

PERIOD 60 sec

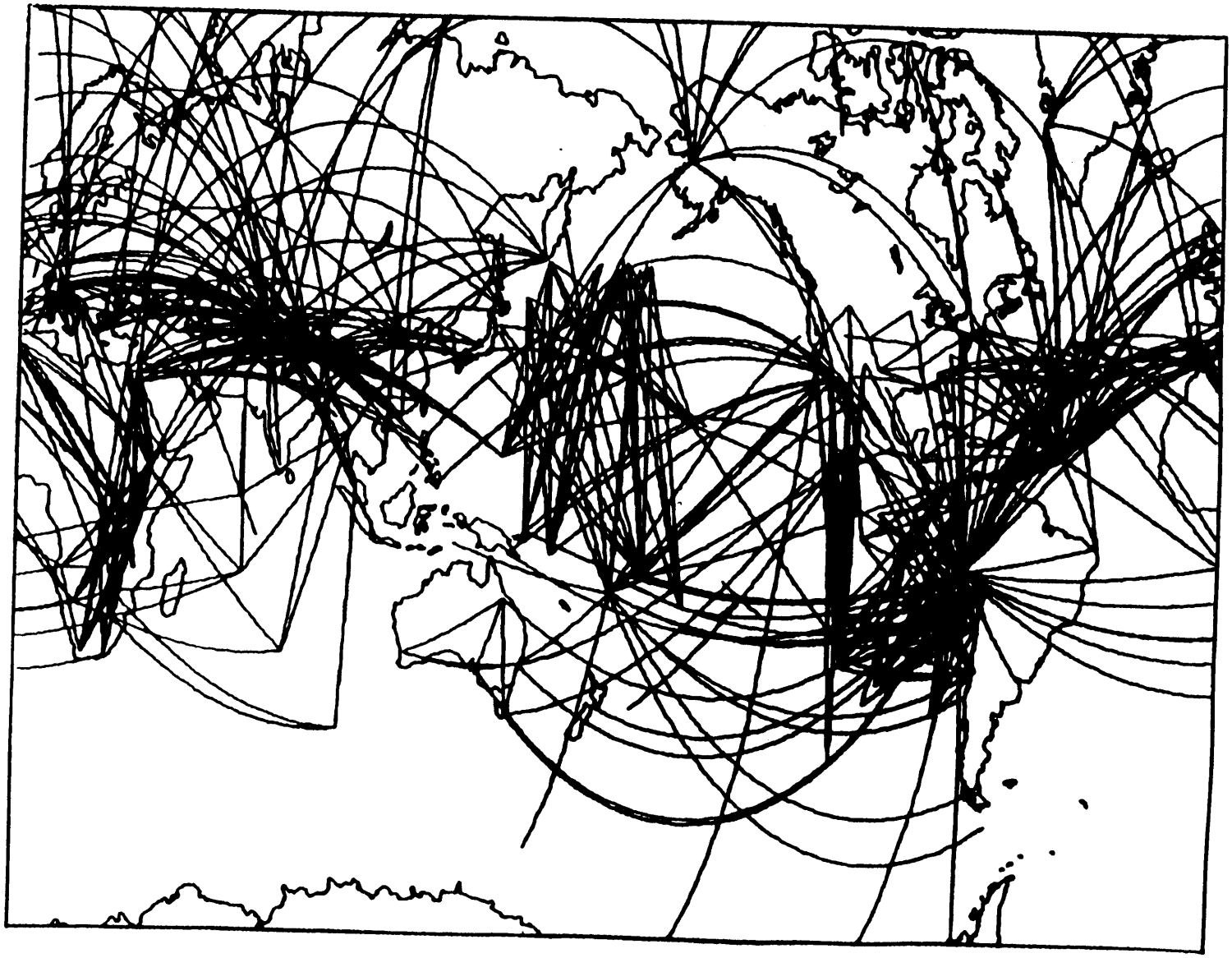

FIGURE A.5b REGION a

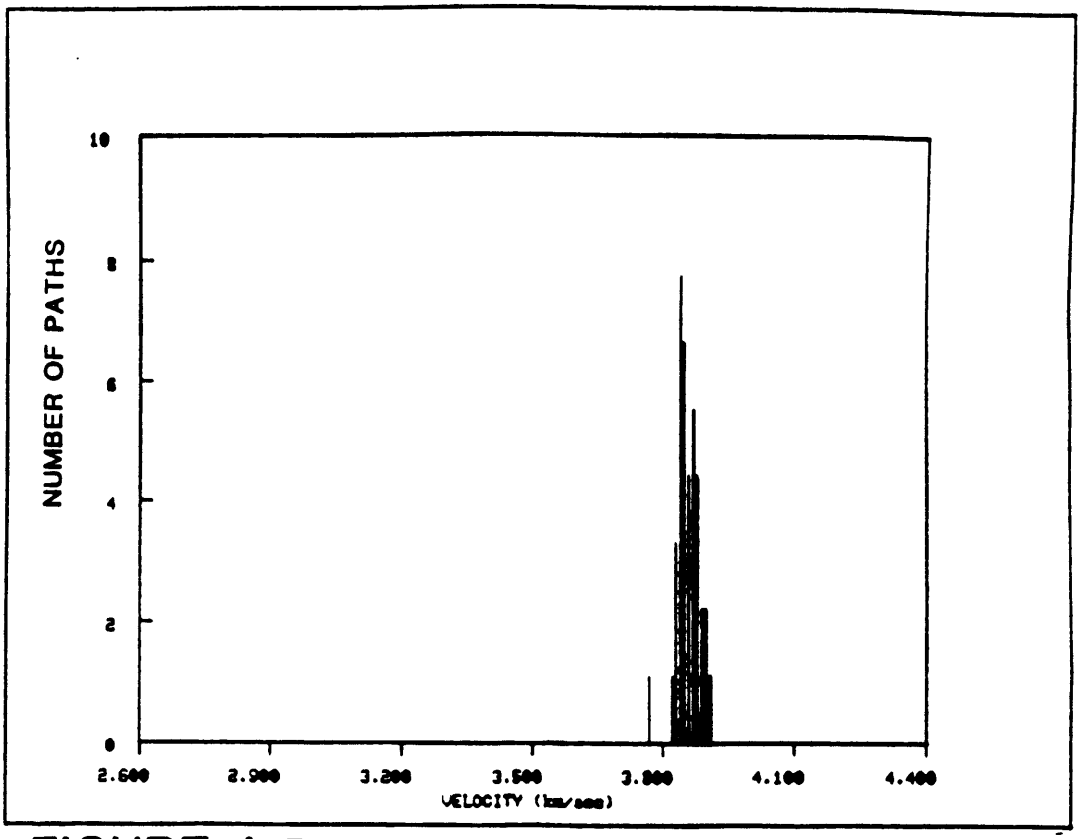

FIGURE A.5c REGION b

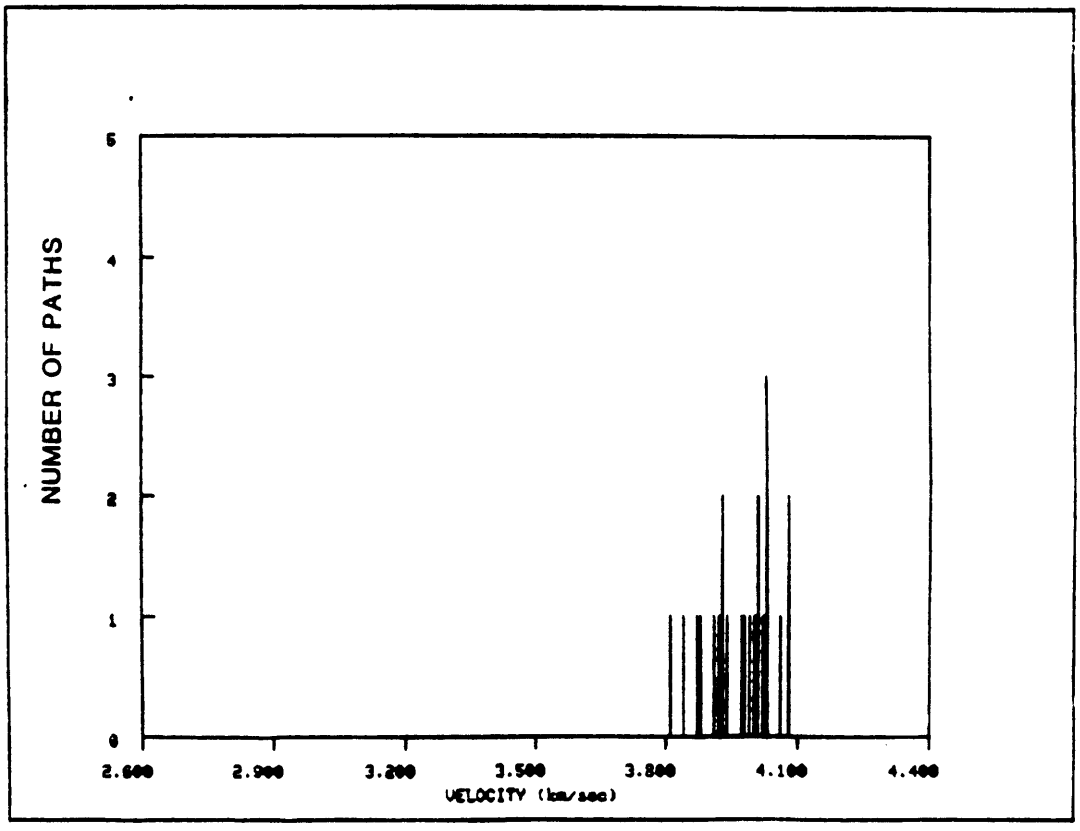

FIGURE A.5d REGION c

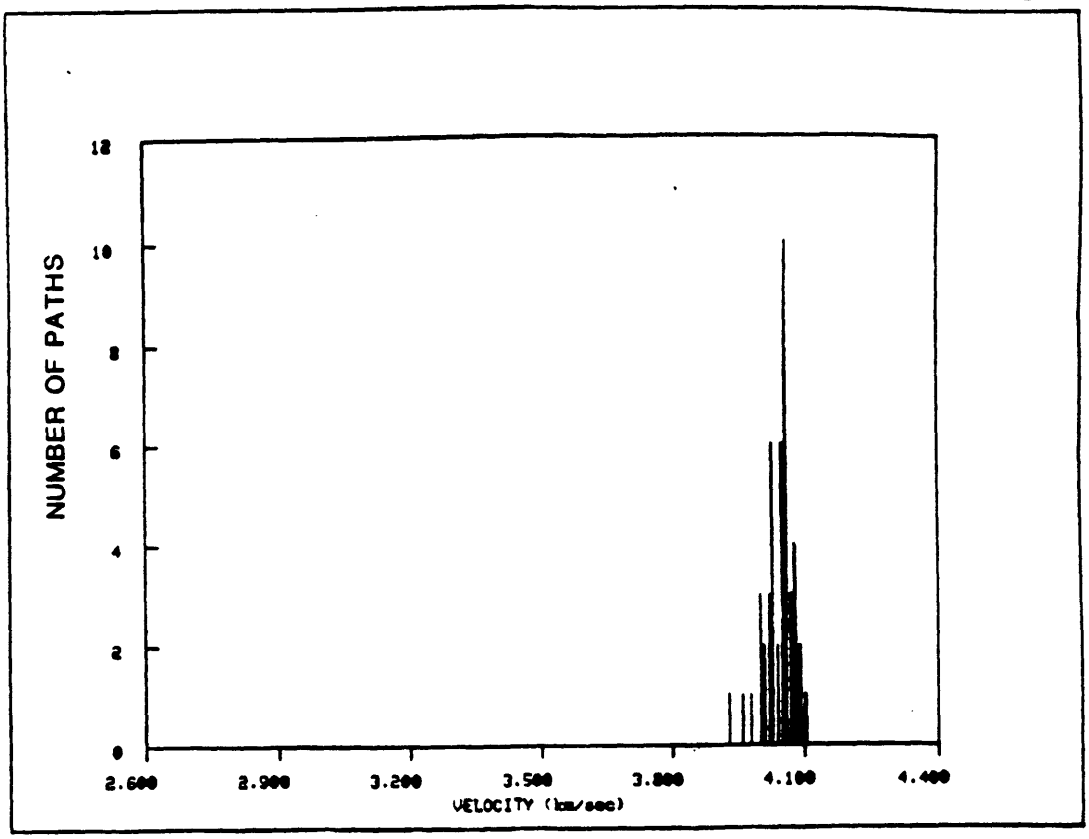

FIGURE A.5e REGION p

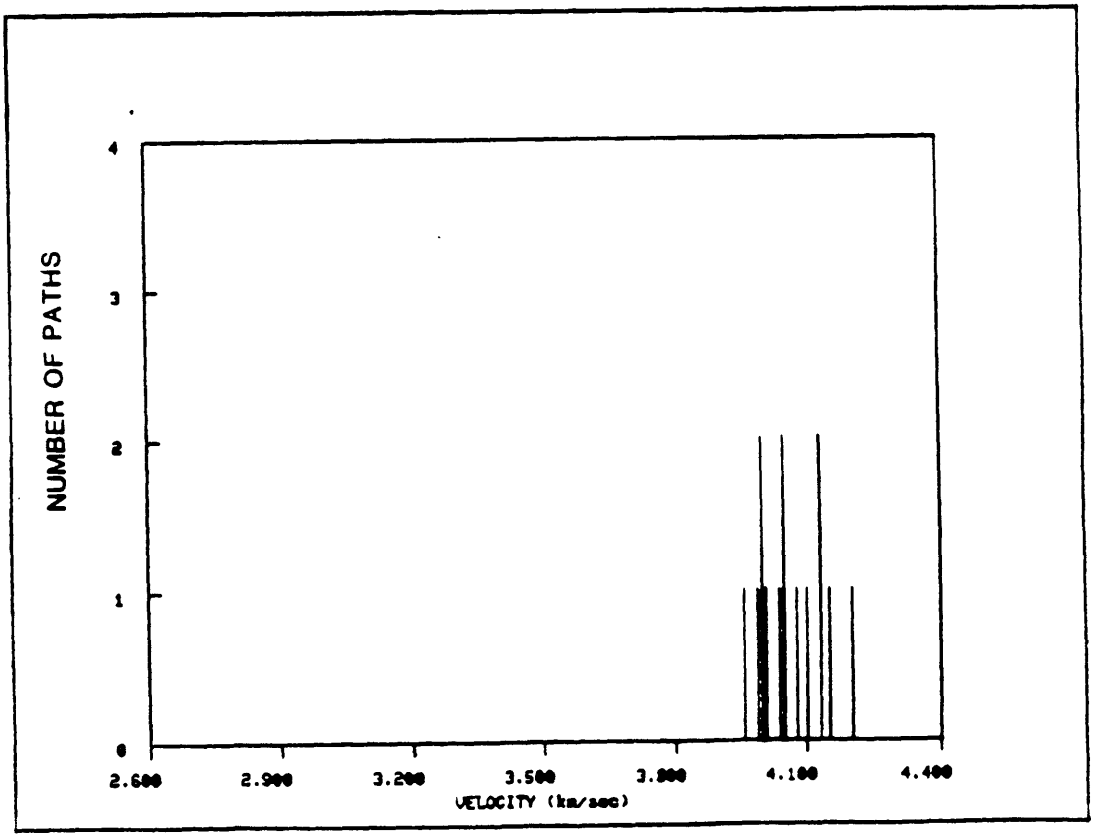

FIGURE A.5f REGION q

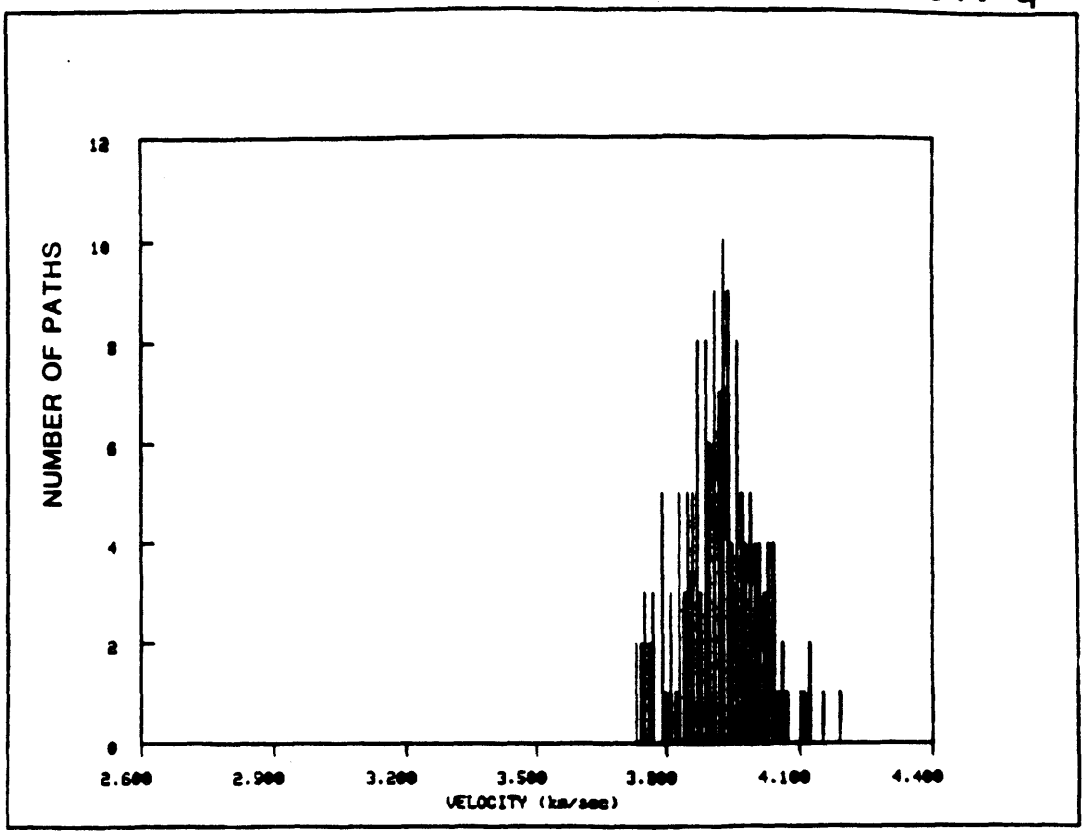

FIGURE A.5g REGION s

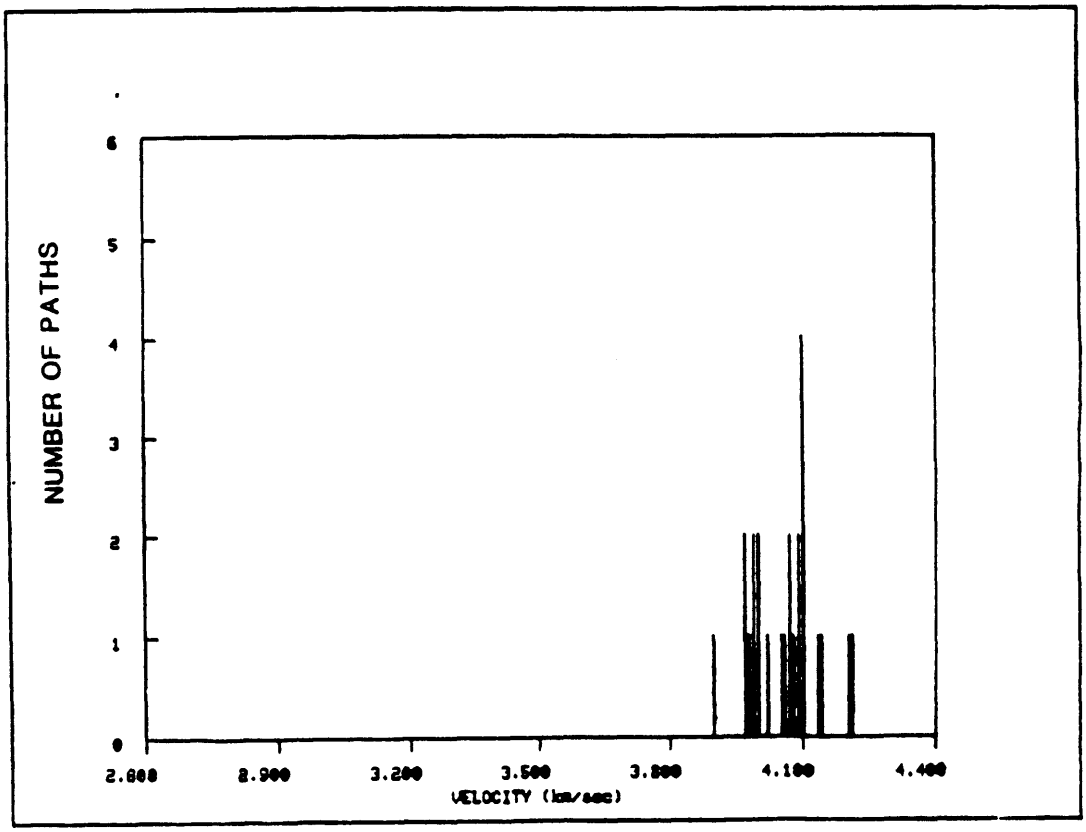

FIGURE A.5h REGION N

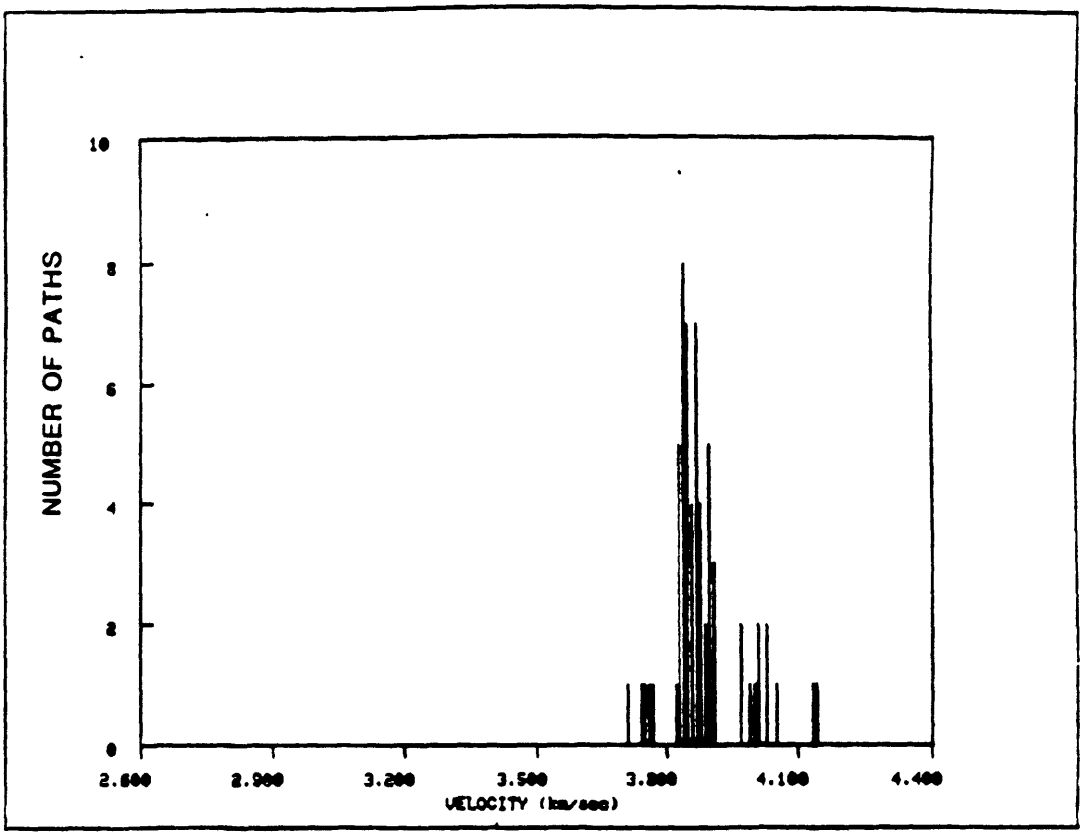

FIGURE A.5i REGION =

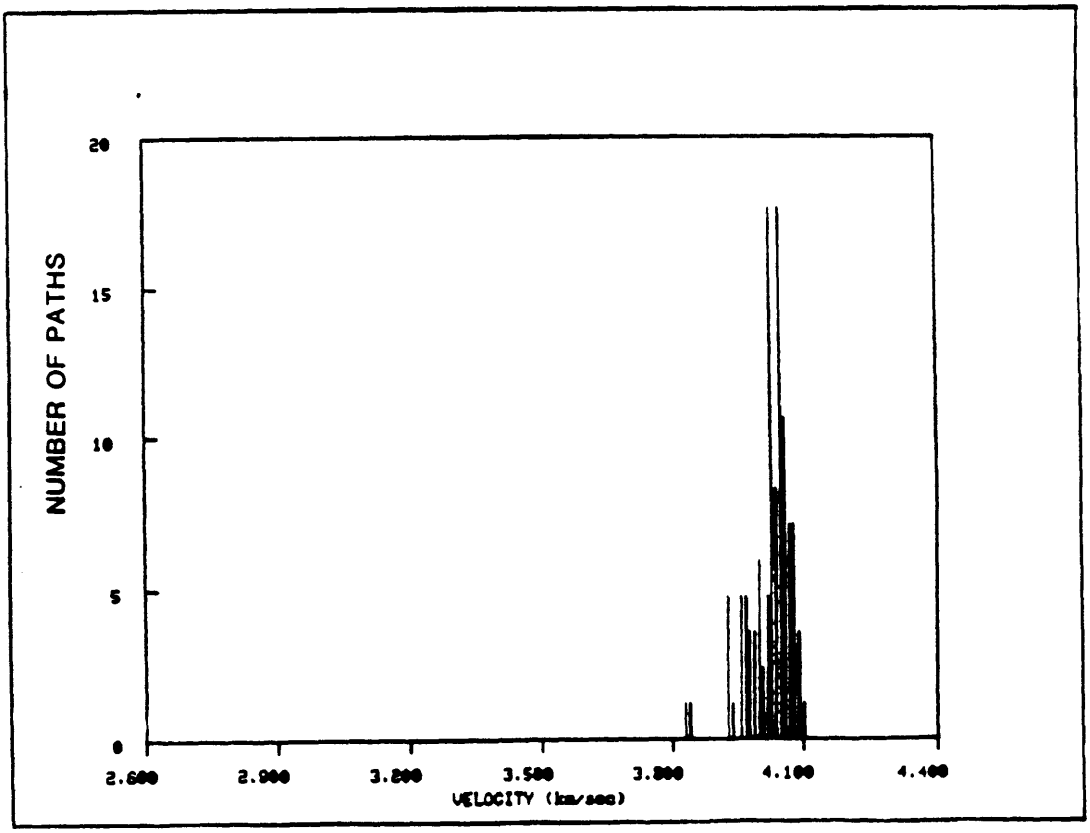

FIGURE A.5j REGION 0

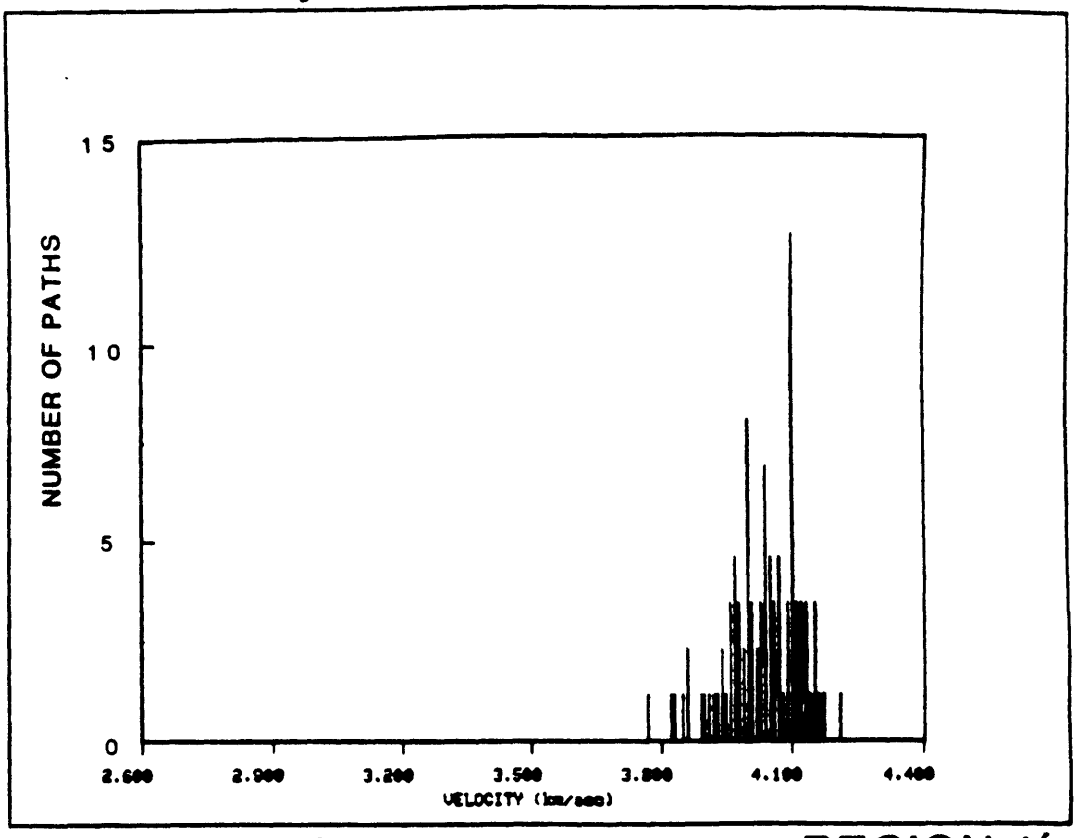

FIGURE A.5k REGION ~~0~~

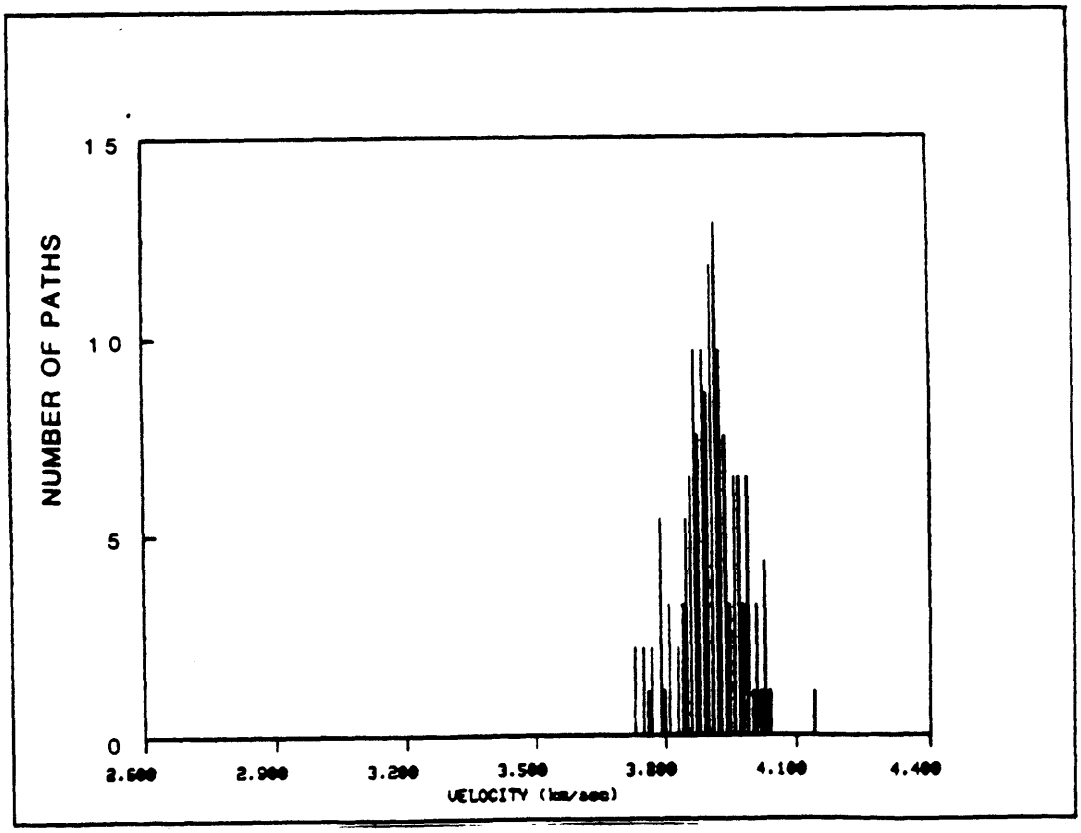

FIGURE A.5l REGION N

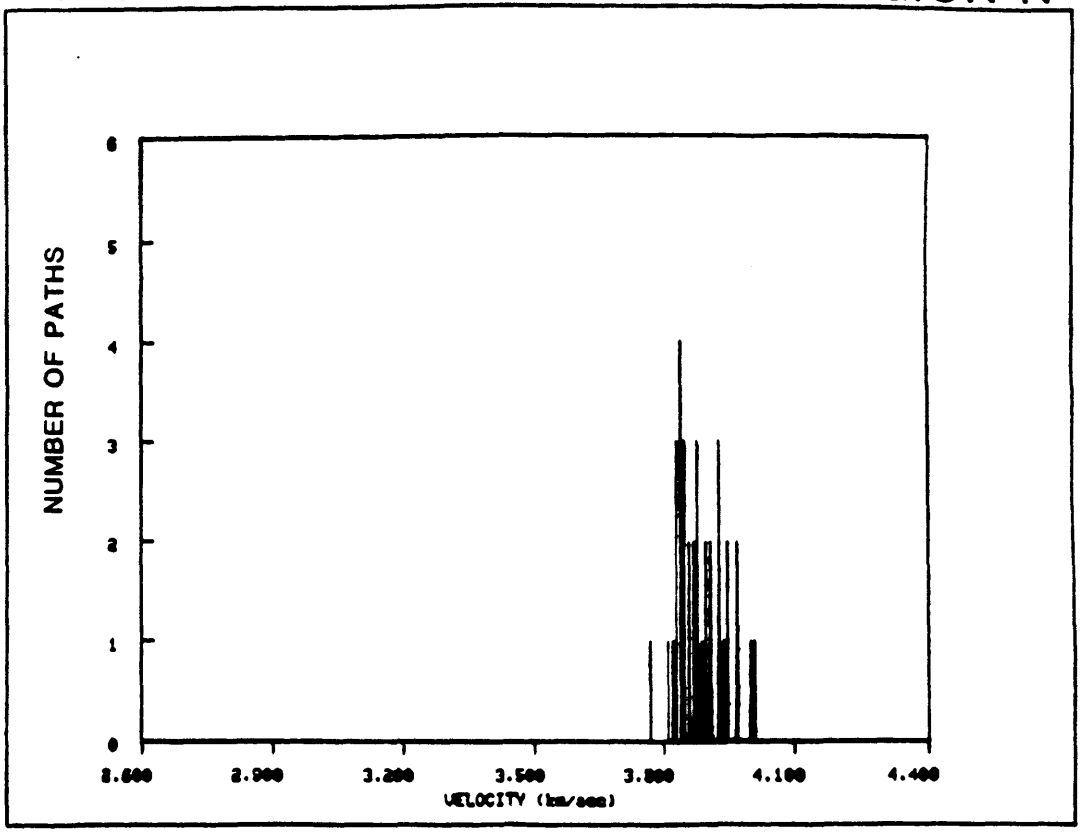

FIGURE A.5m REGION #

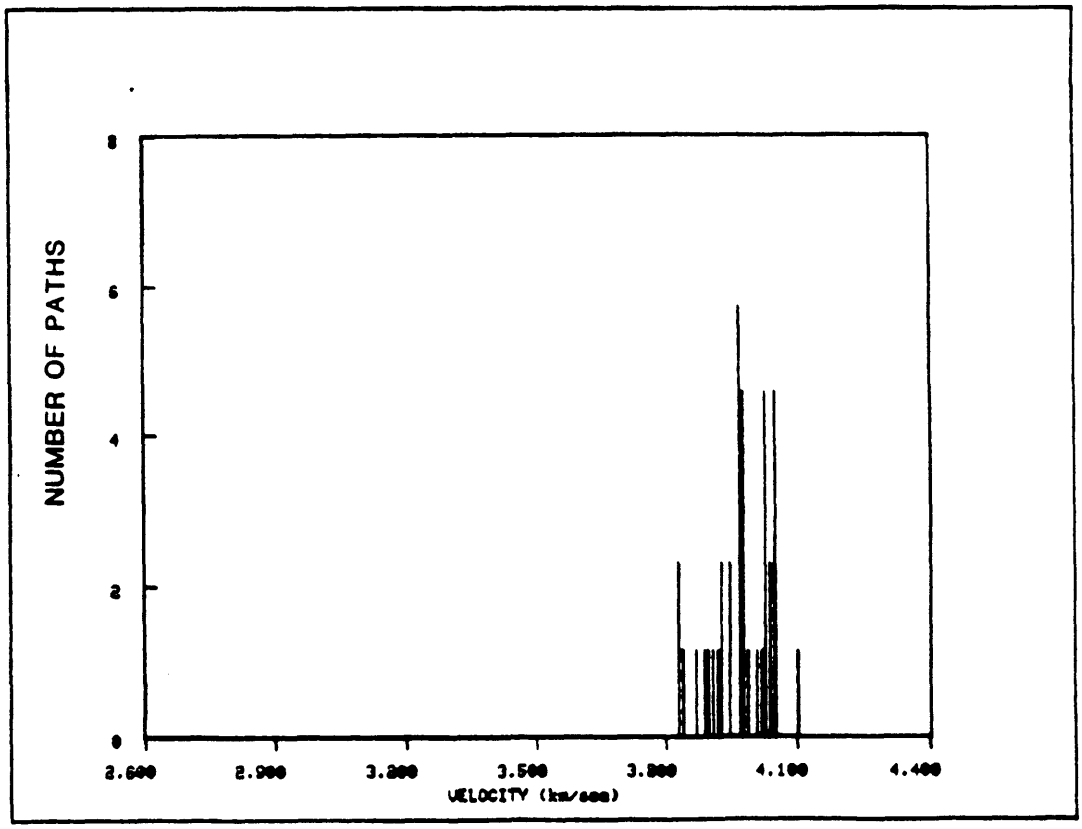

FIGURE A.5n REGION =

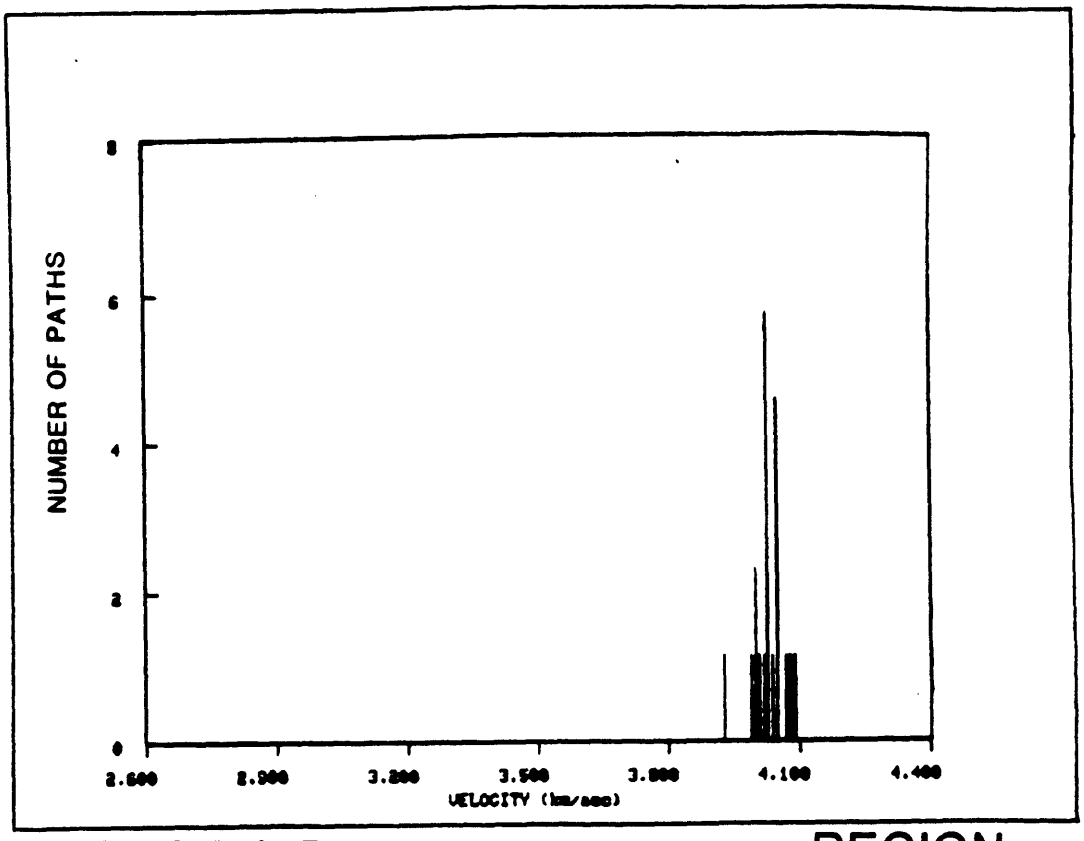

FIGURE A.5o REGION -

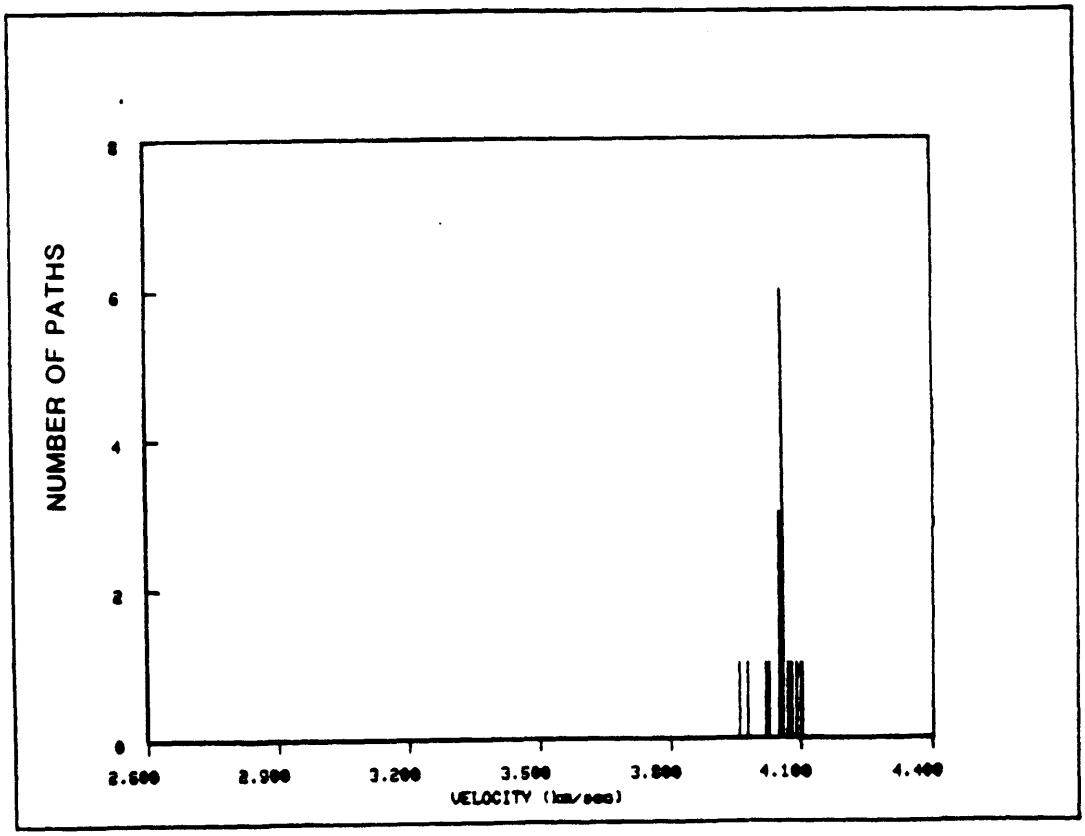

FIGURE A.5p REGION 0

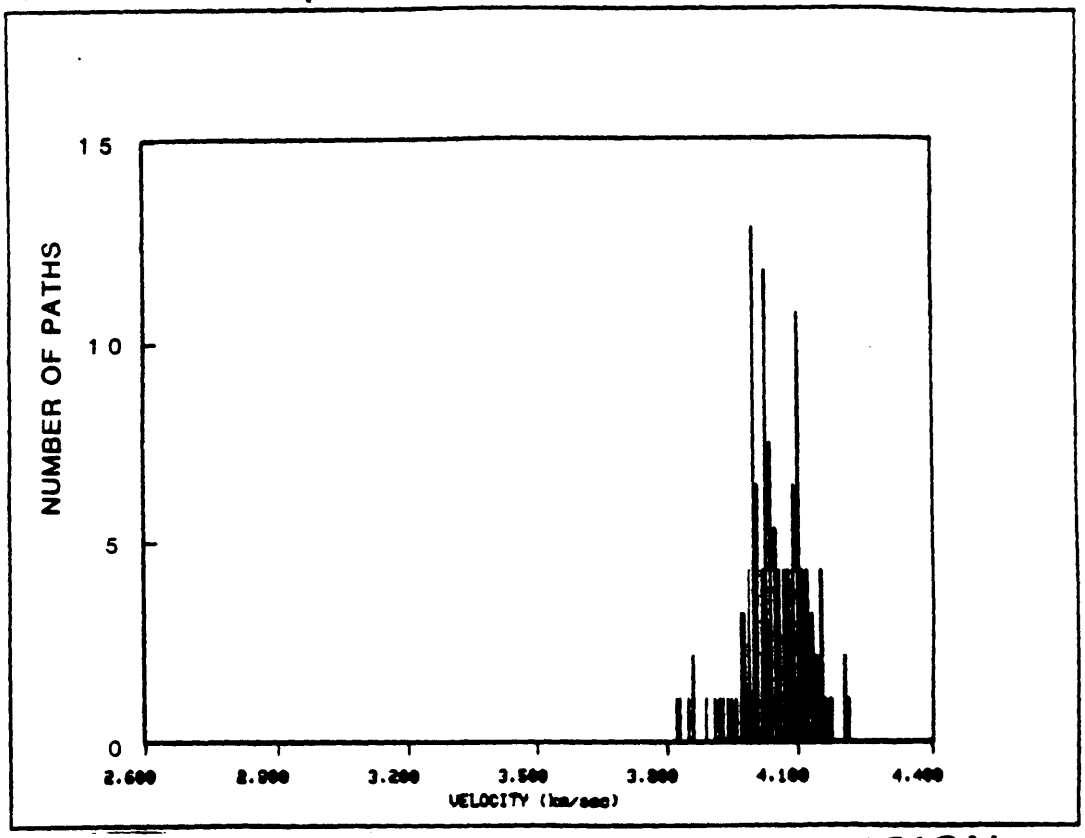

FIGURE A.5q REGION .

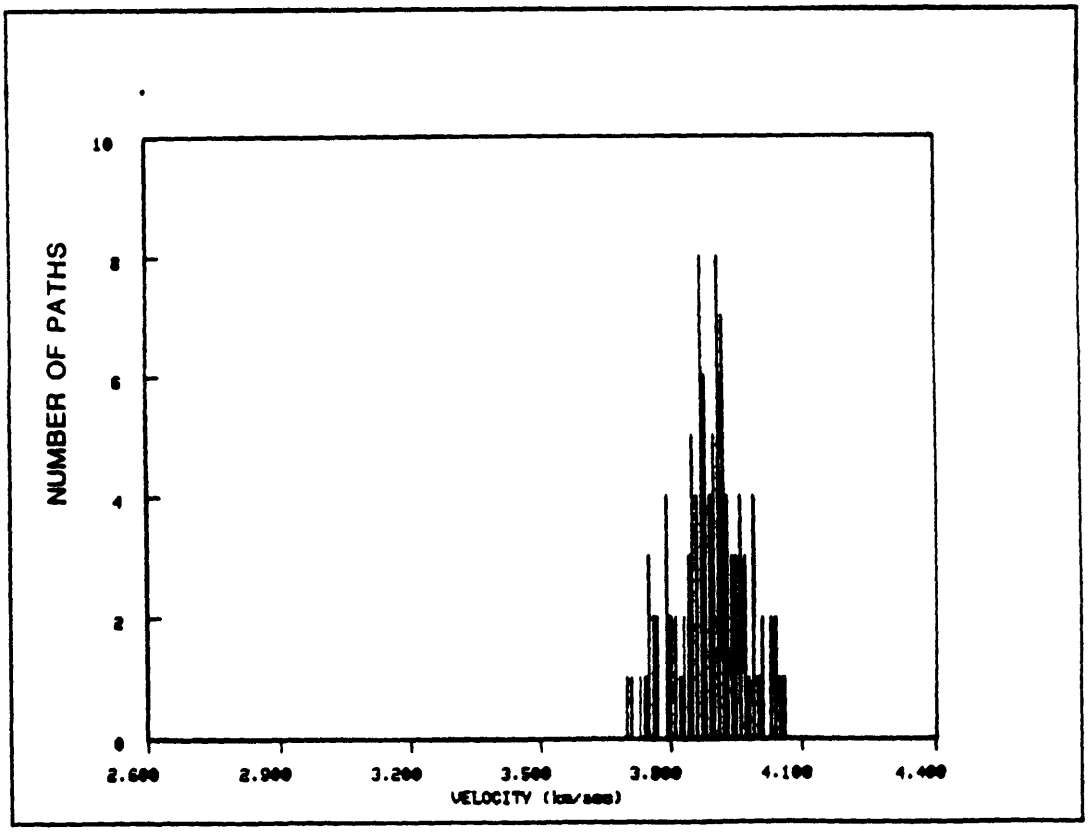

FIGURE A.5r REGION ø

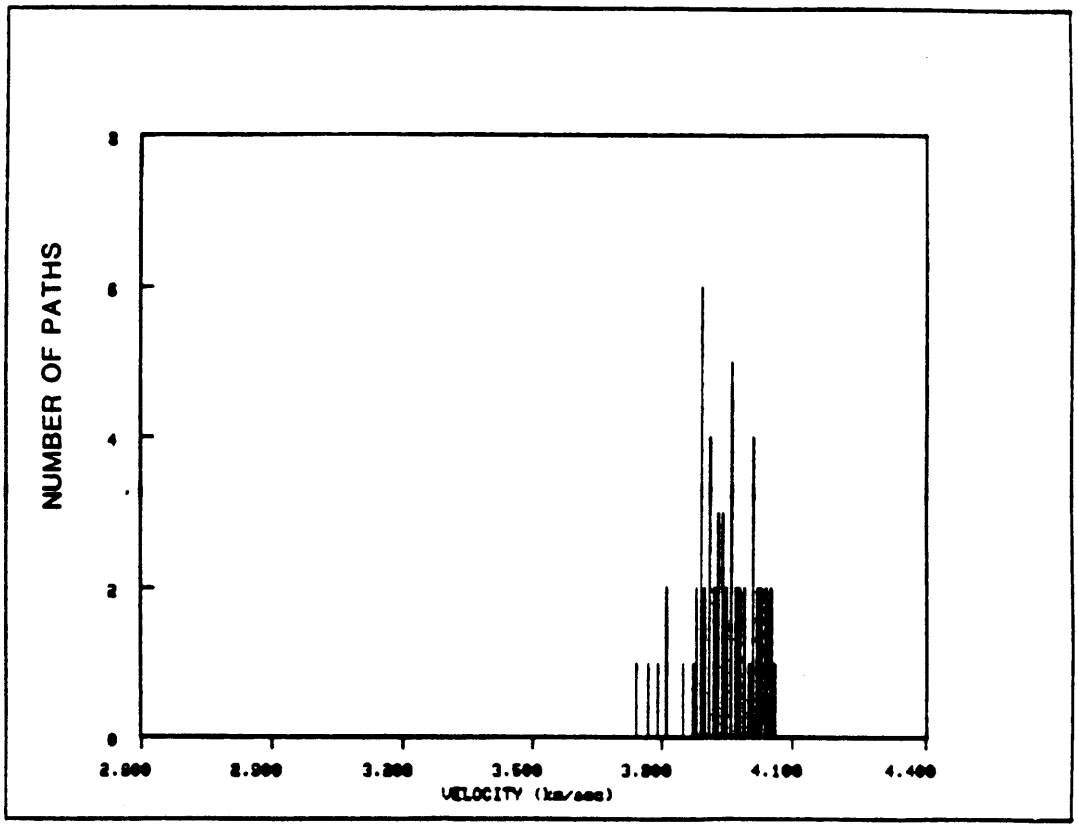

FIGURE A.6a

PERIOD 70 sec

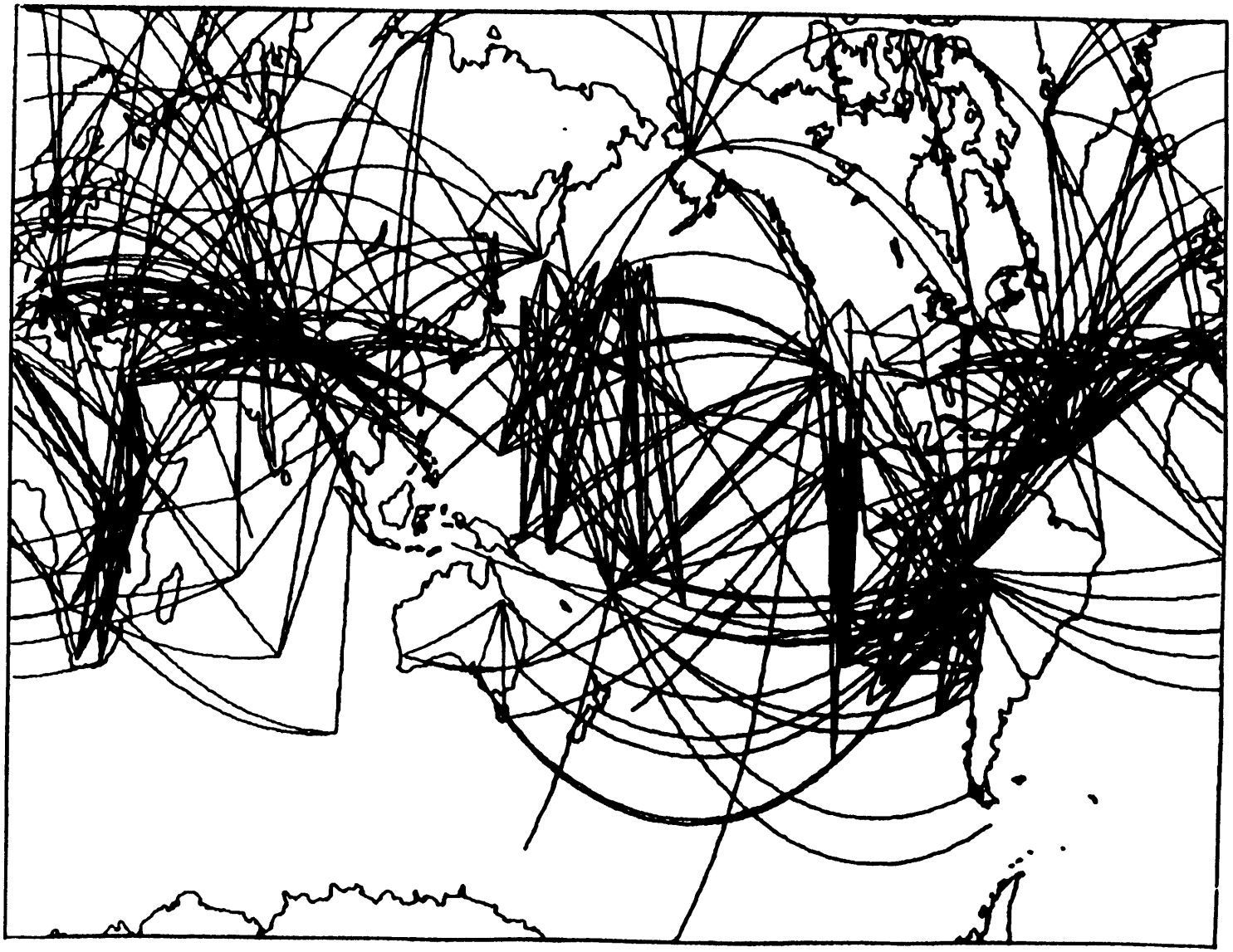

FIGURE A.6b REGION a

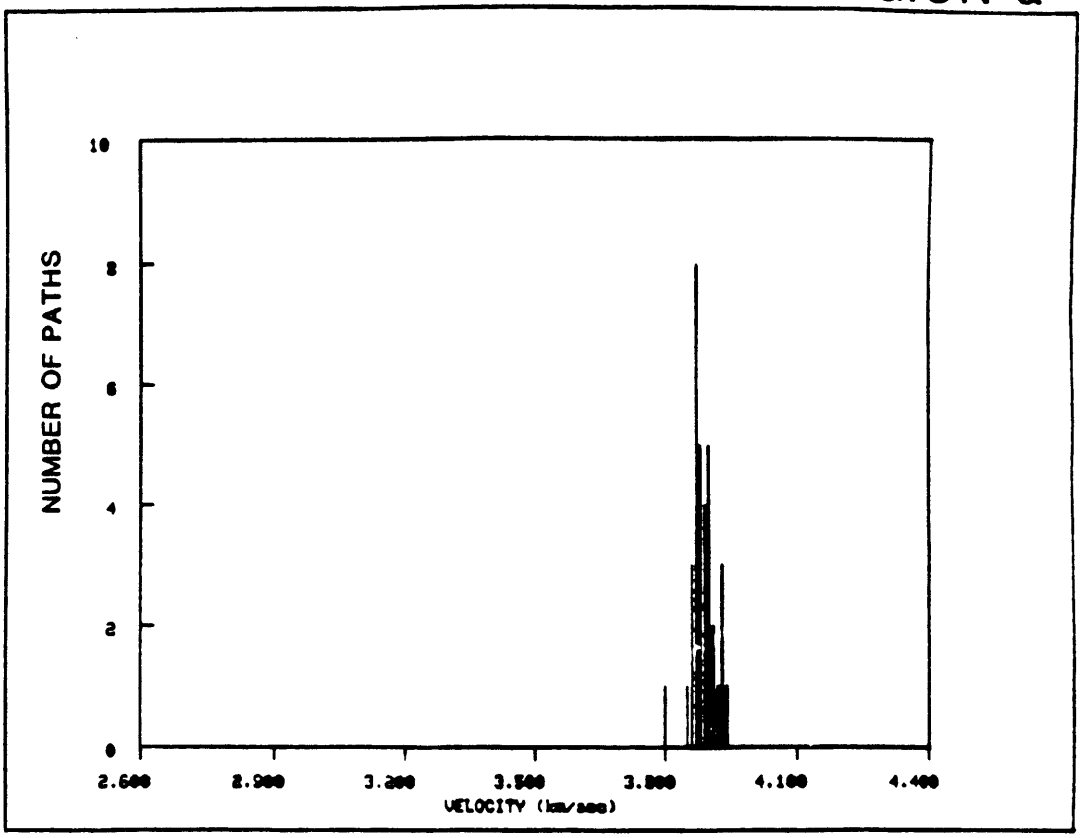

FIGURE A.6c REGION b

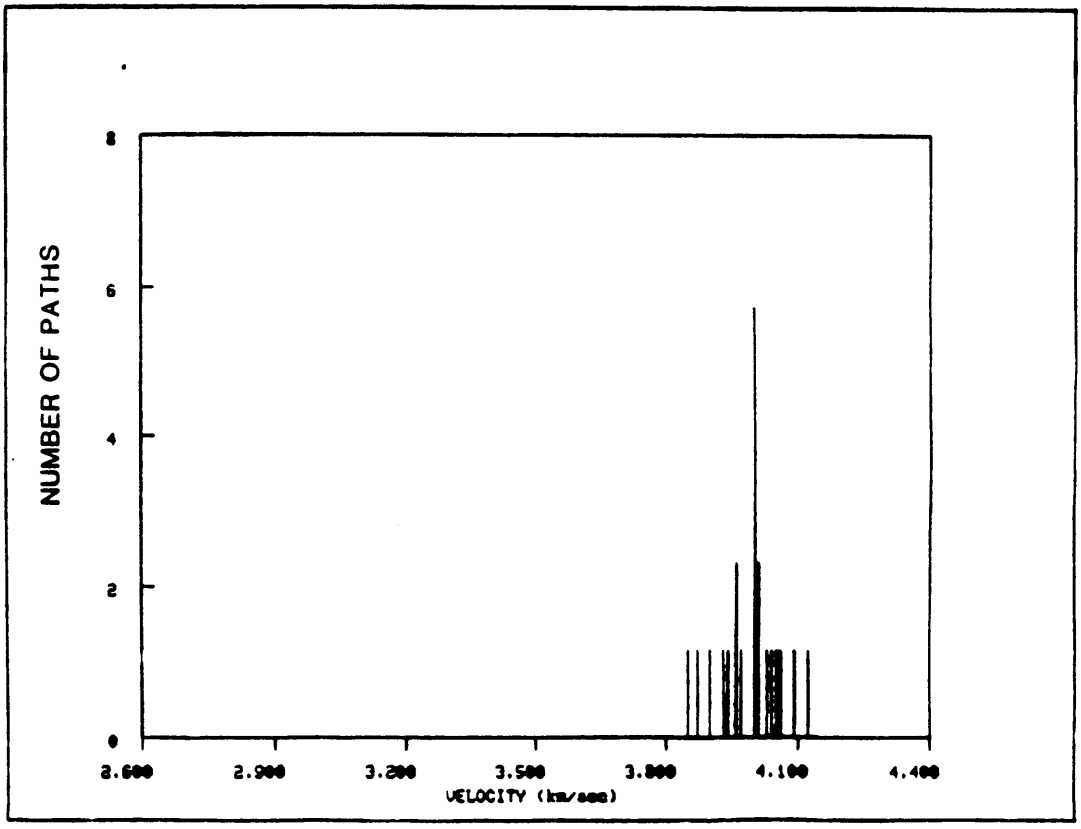

FIGURE A.6d REGION c

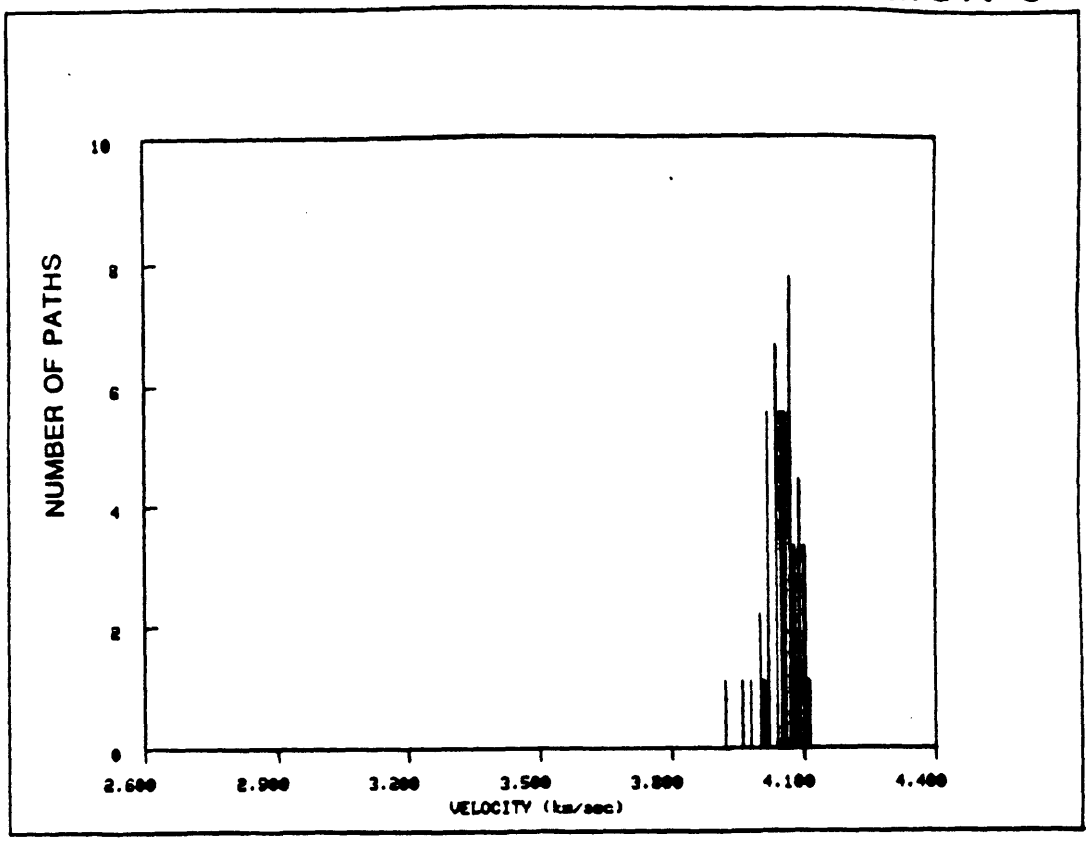

FIGURE A.6e REGION p

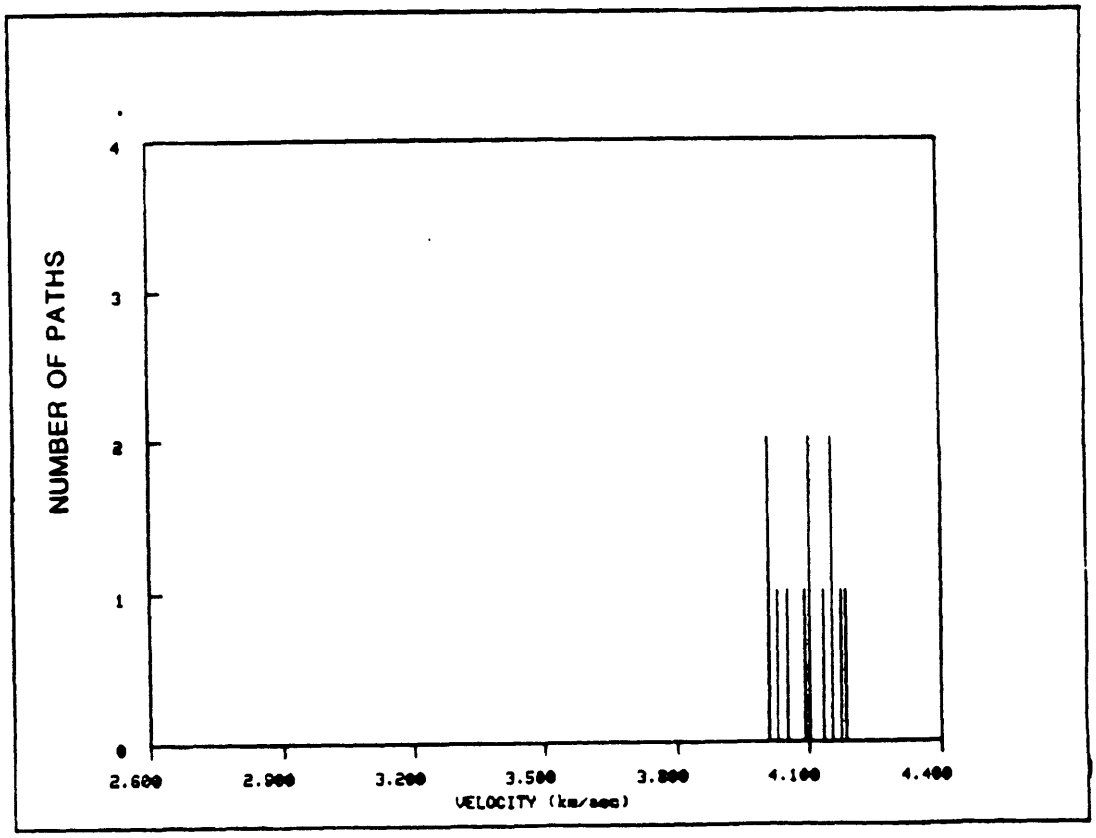

FIGURE A.6f REGION q

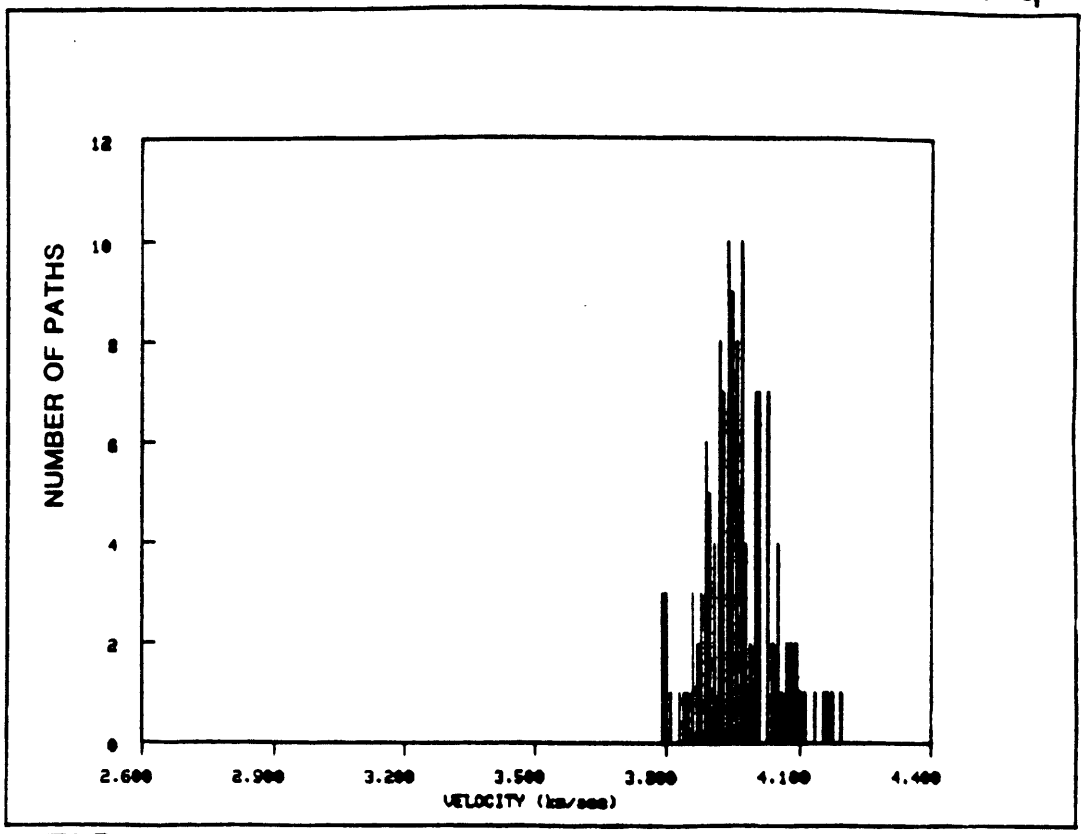

FIGURE A.6g REGION s

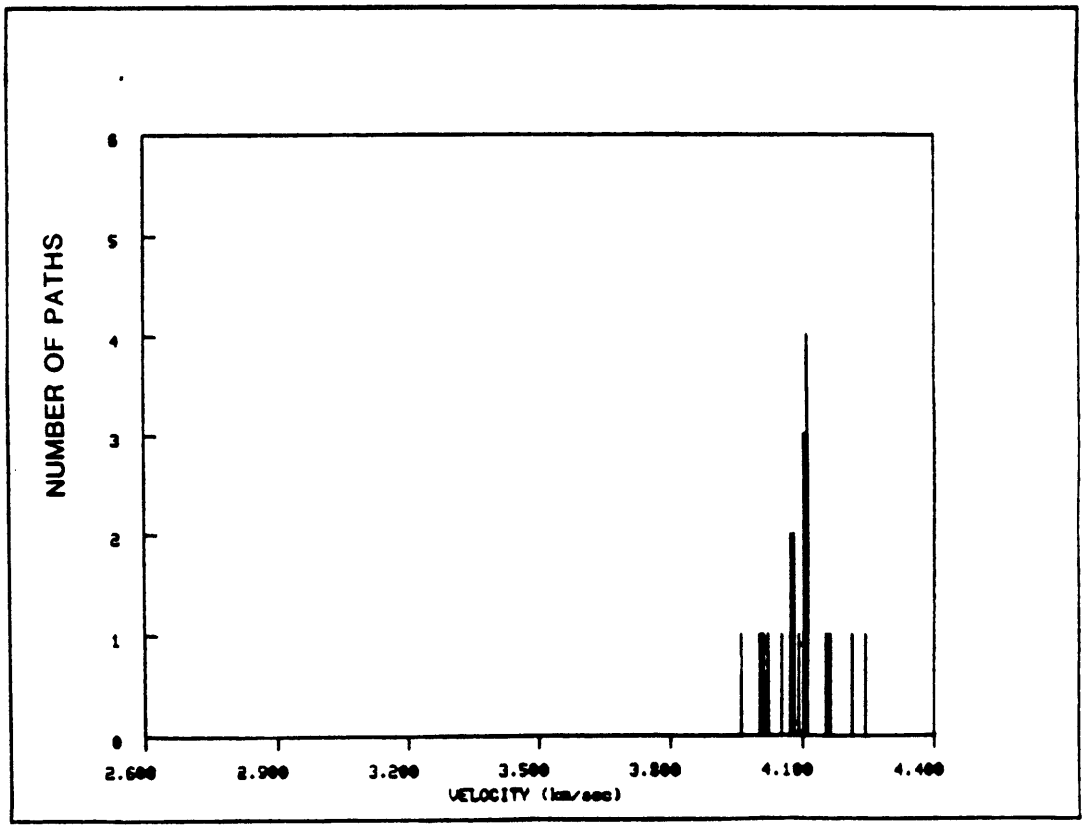

FIGURE A.6h REGION N

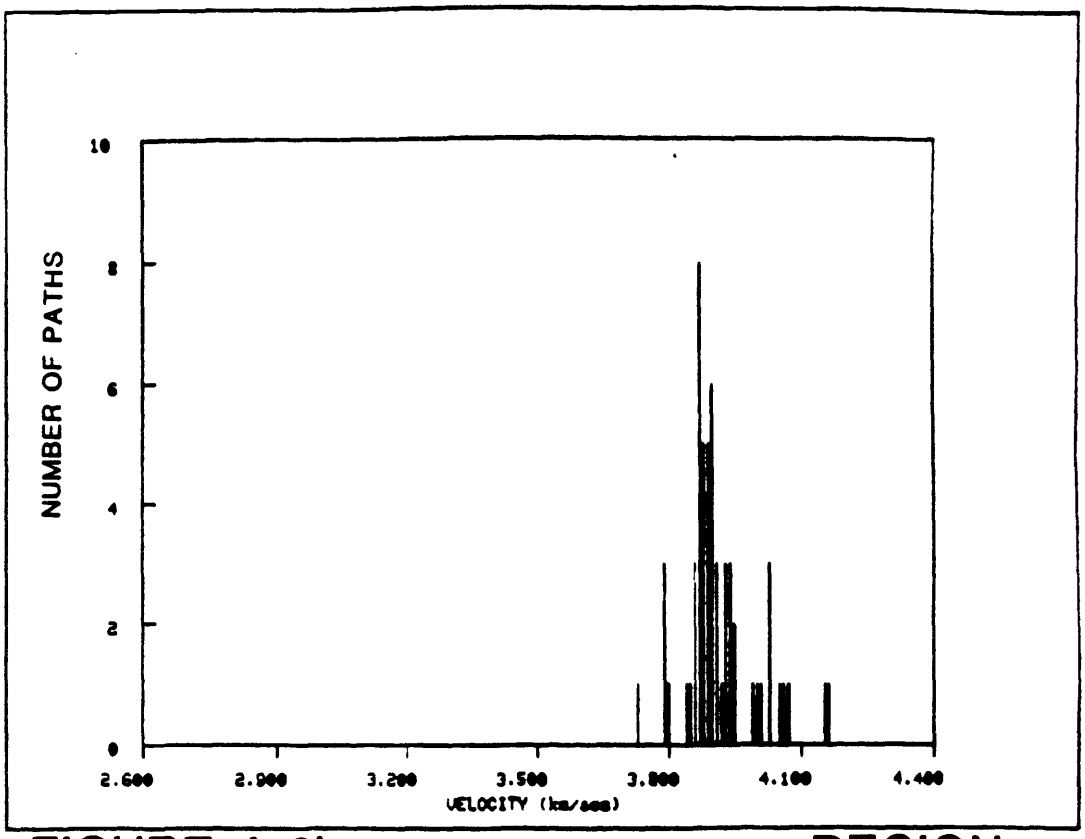

FIGURE A.6i REGION =

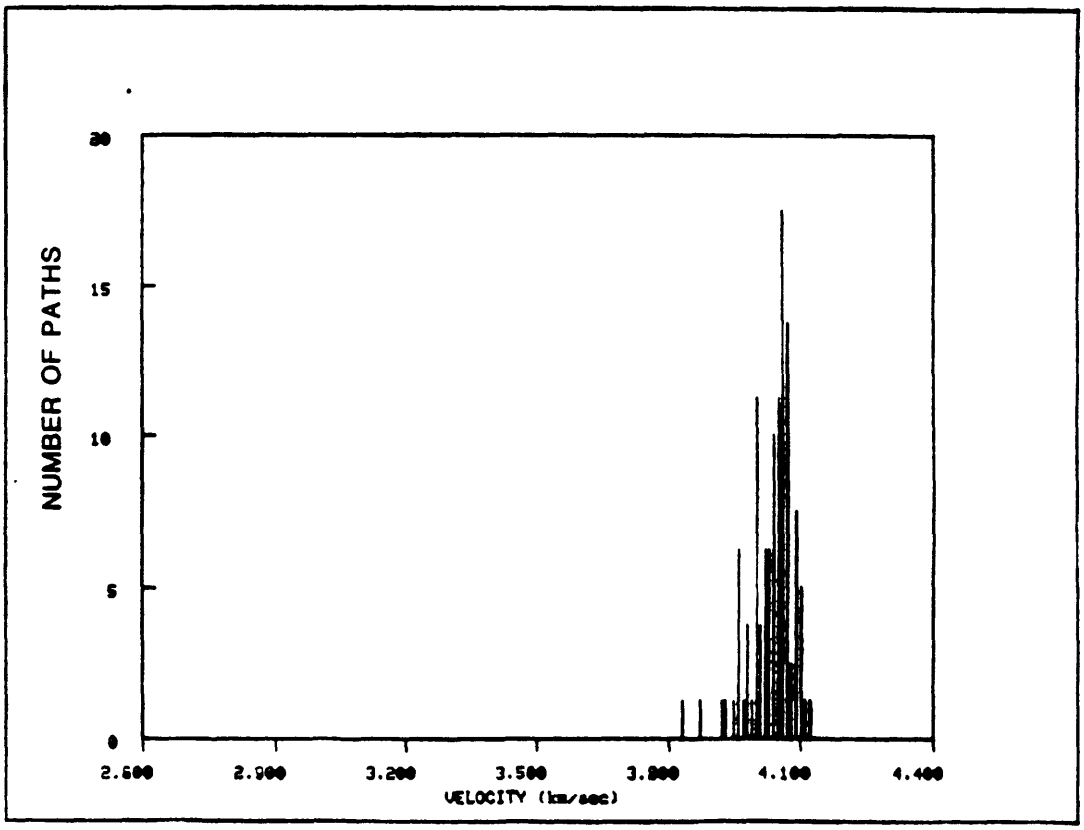

FIGURE A.6j REGION 0

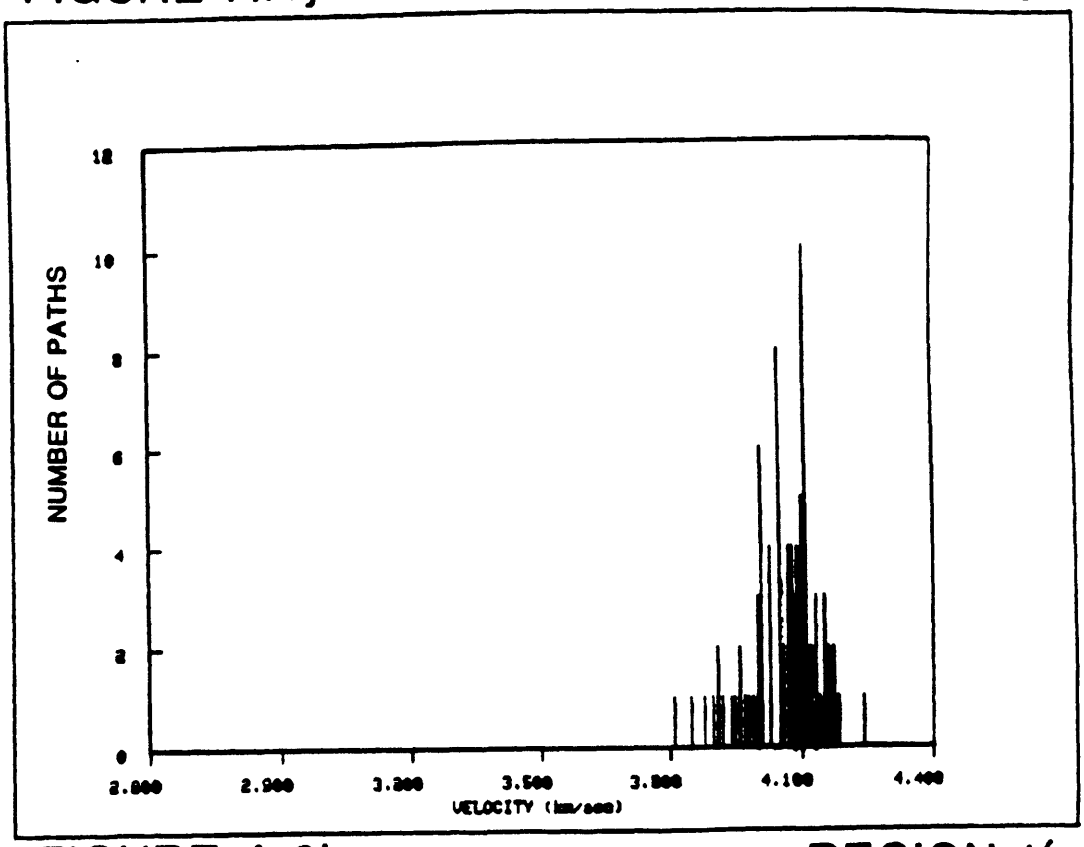

FIGURE A.6k REGION ~~0~~

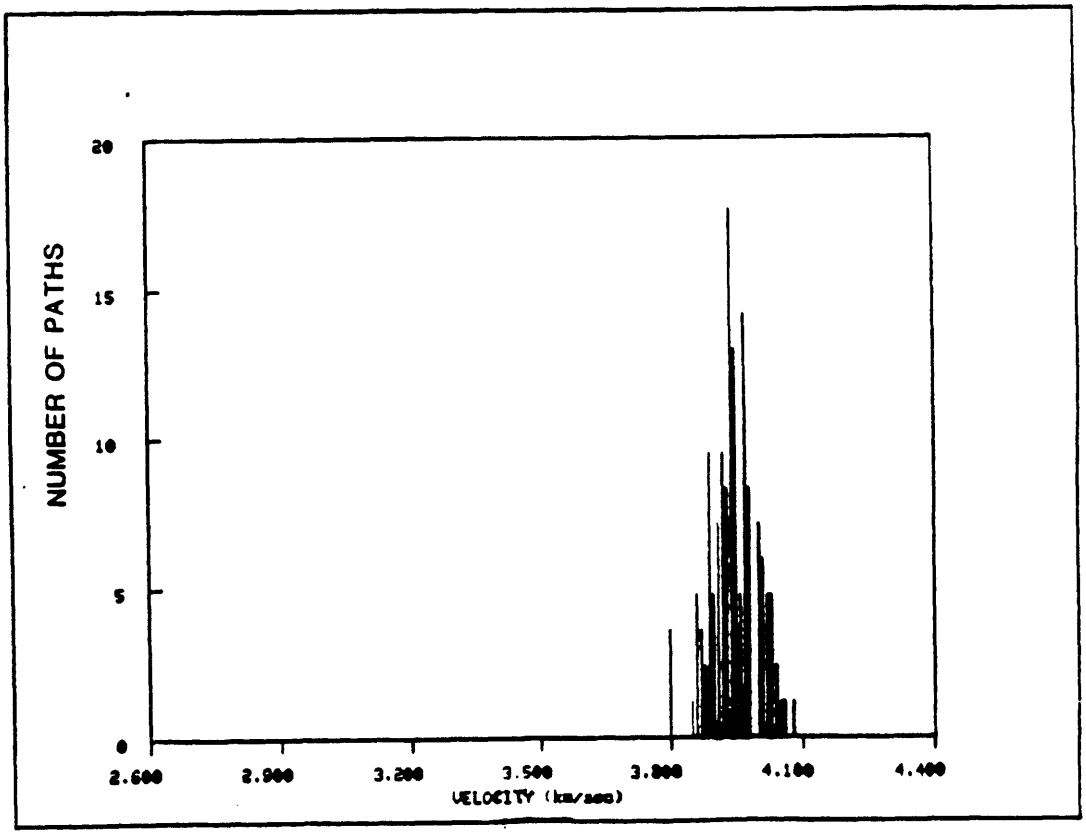

FIGURE A.6l REGION N

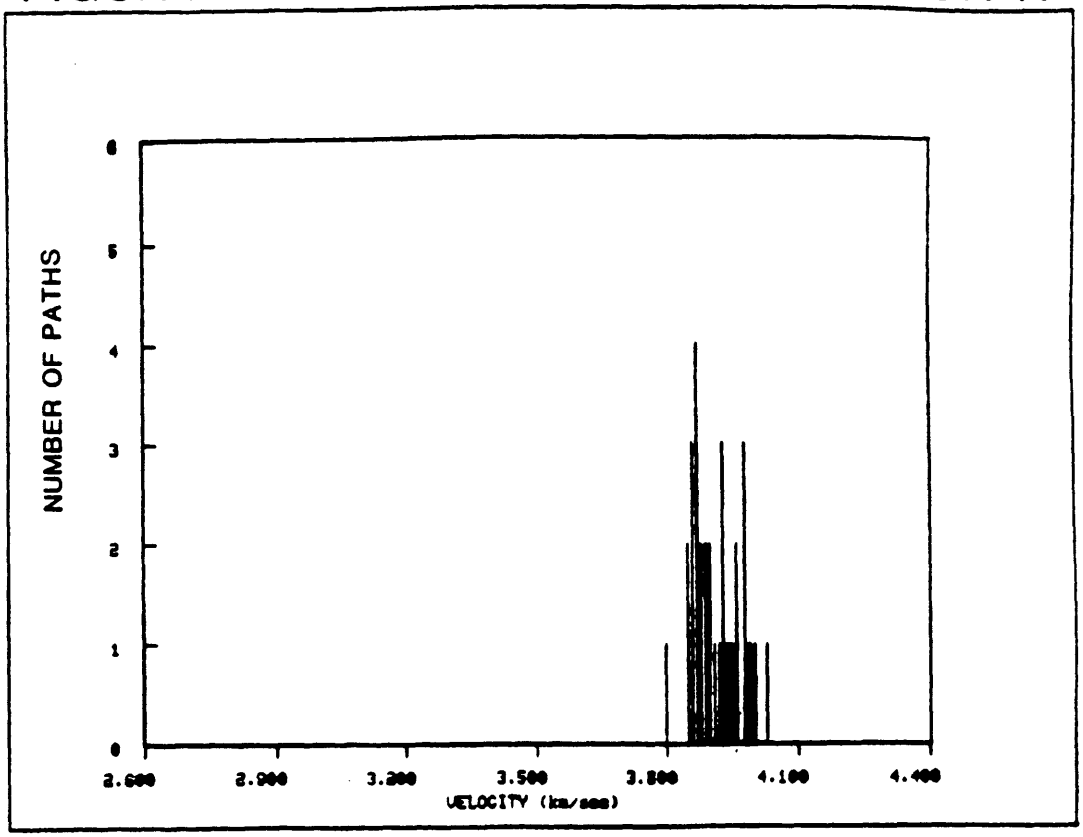

FIGURE A.6m REGION #

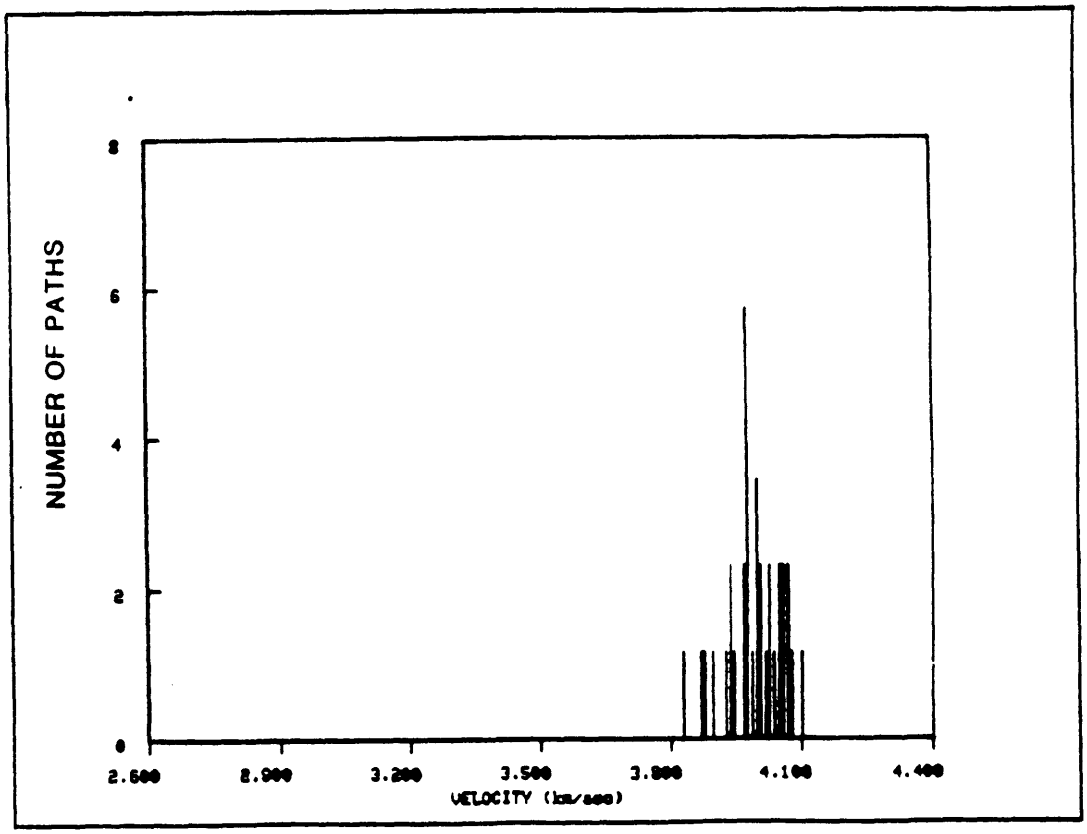

FIGURE A.6n REGION =

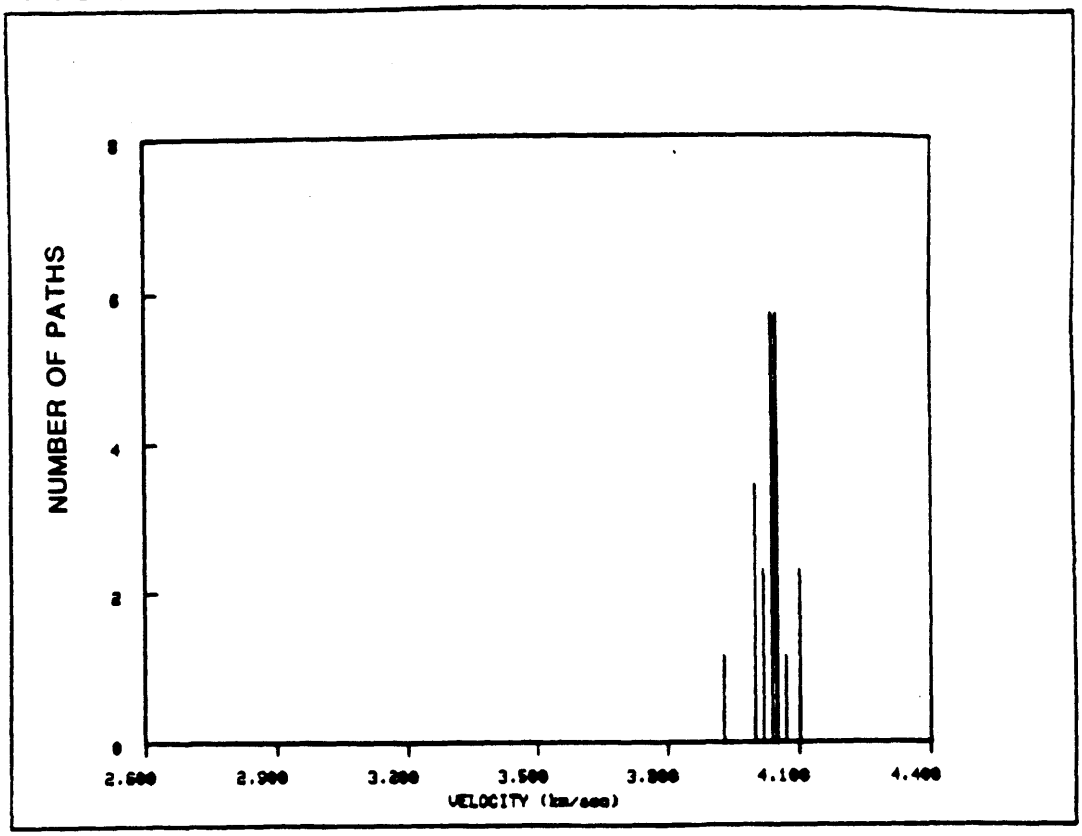

FIGURE A.6o REGION -

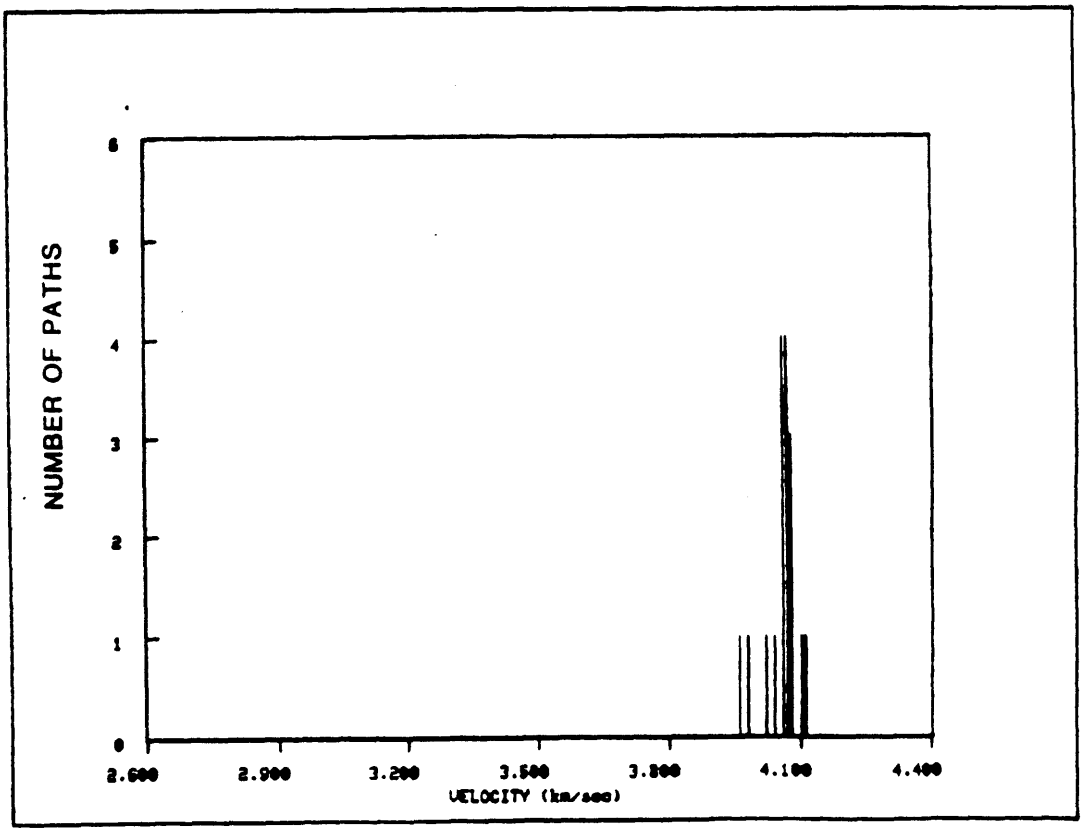

FIGURE A.6p REGION 0

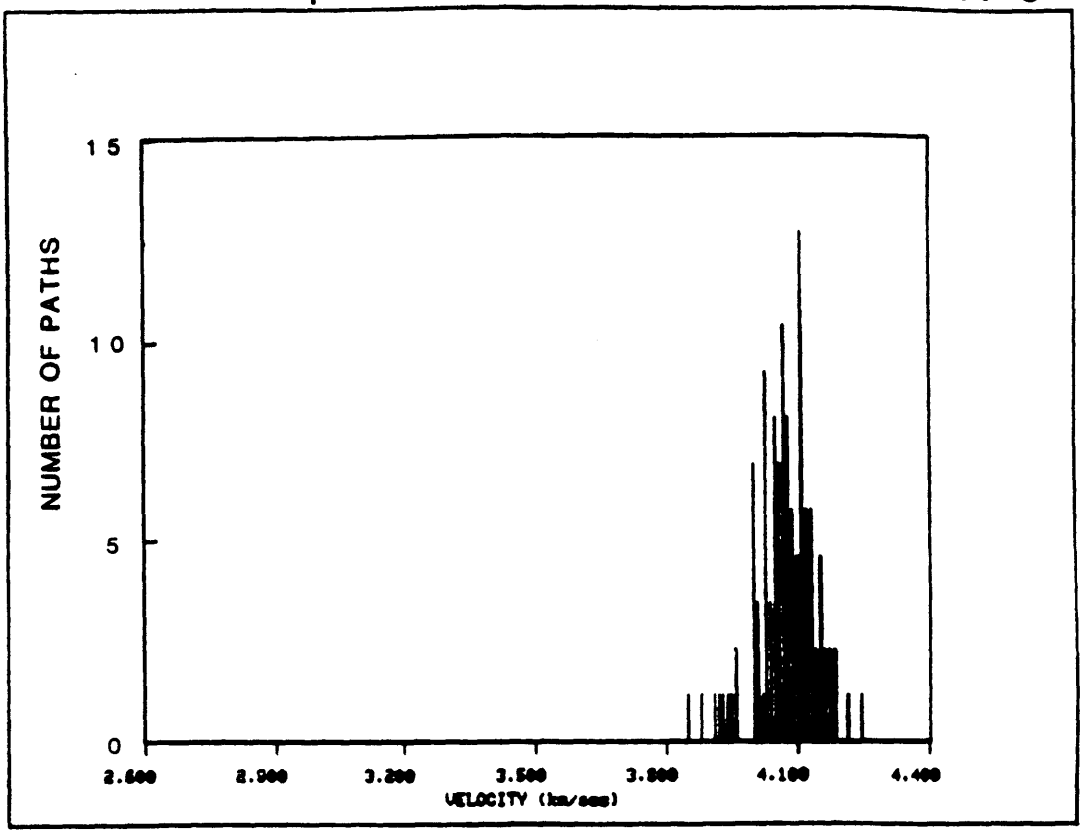

FIGURE A.6q REGION .

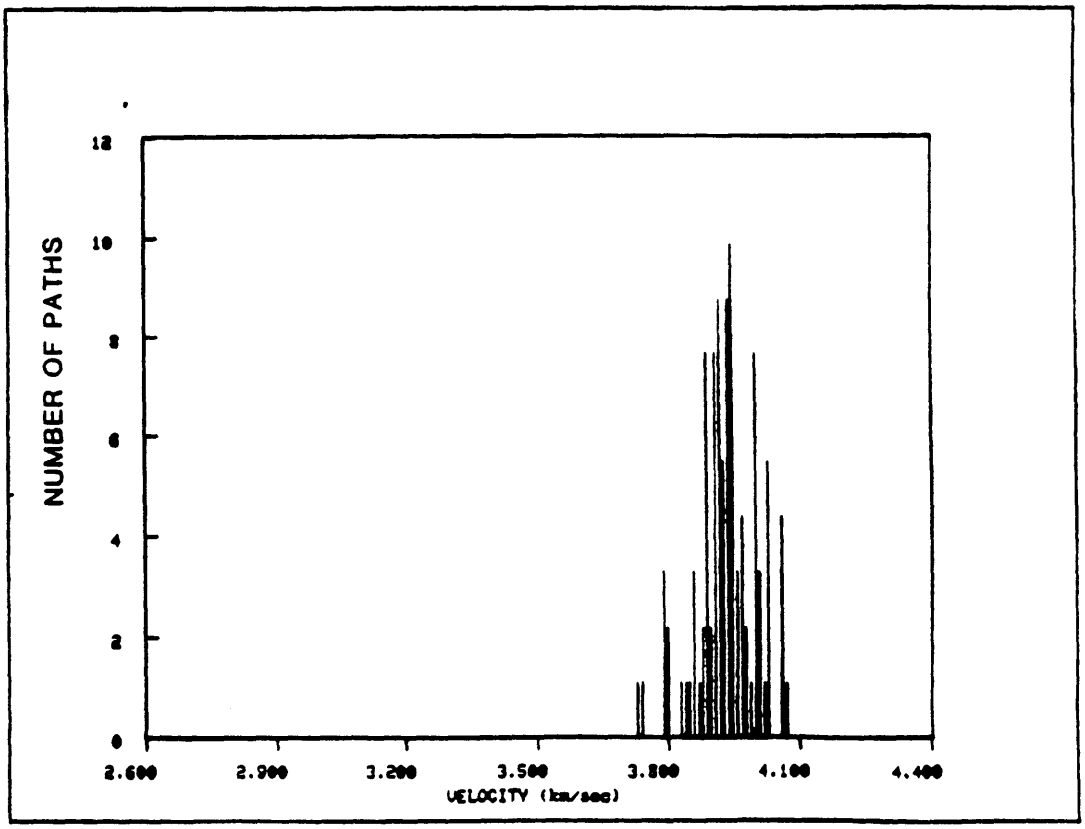

FIGURE A.6r

REGION ø

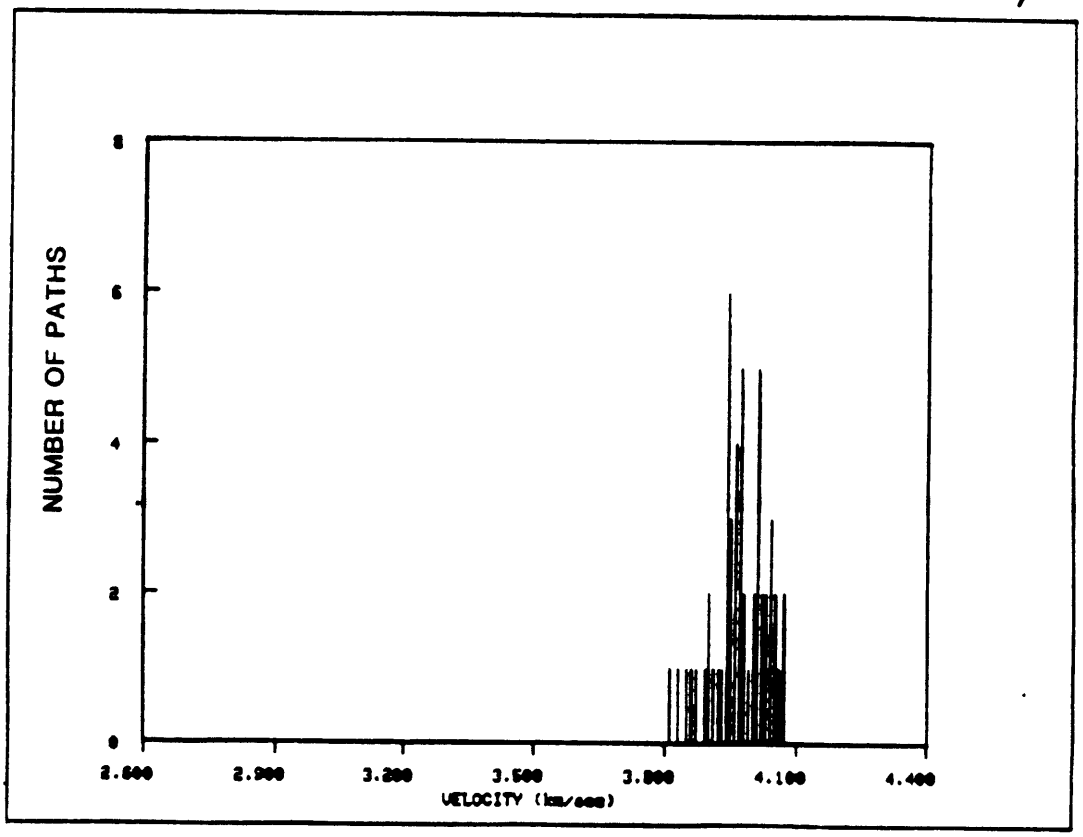

FIGURE A.7a

PERIOD 80 sec

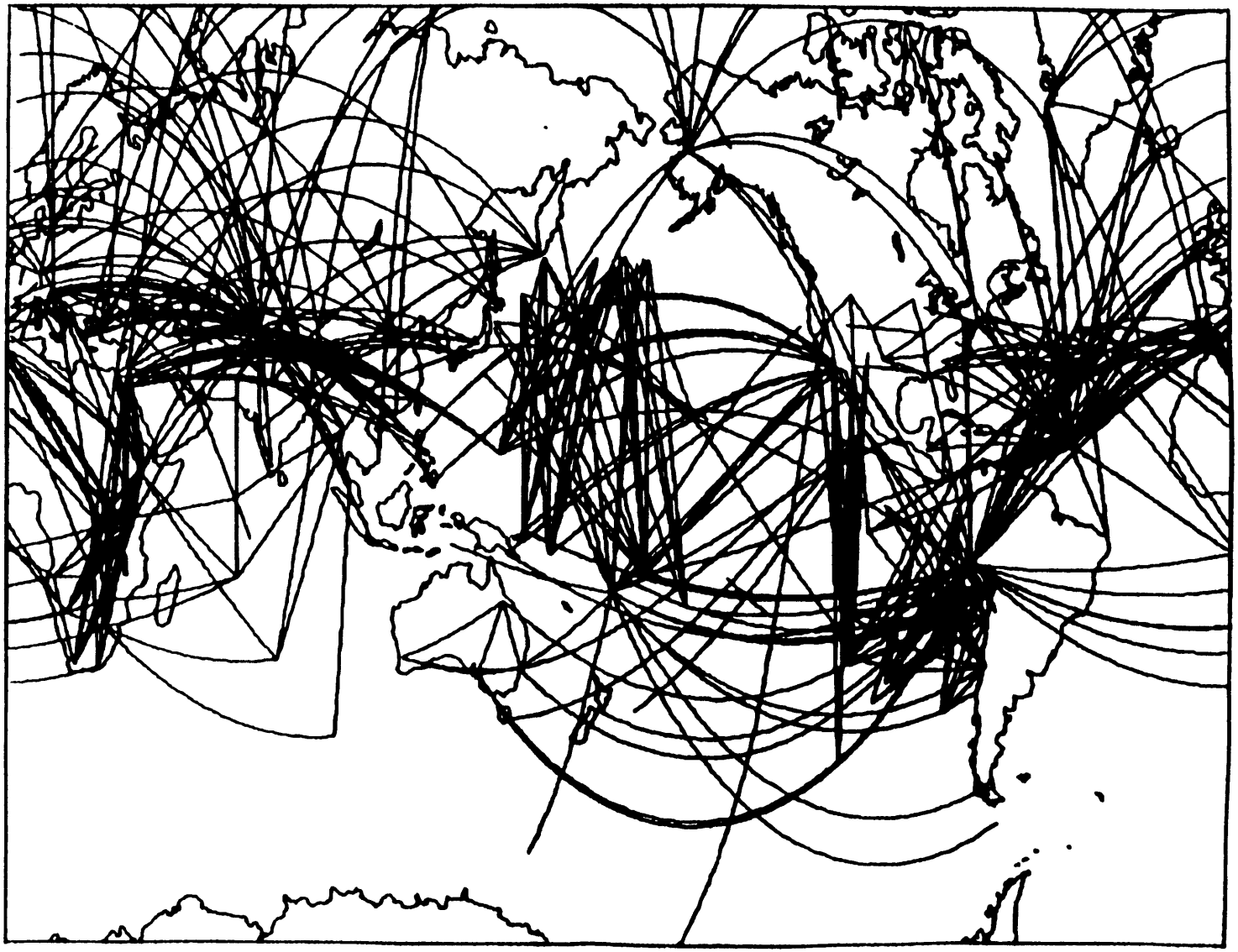

FIGURE A.7b REGION a

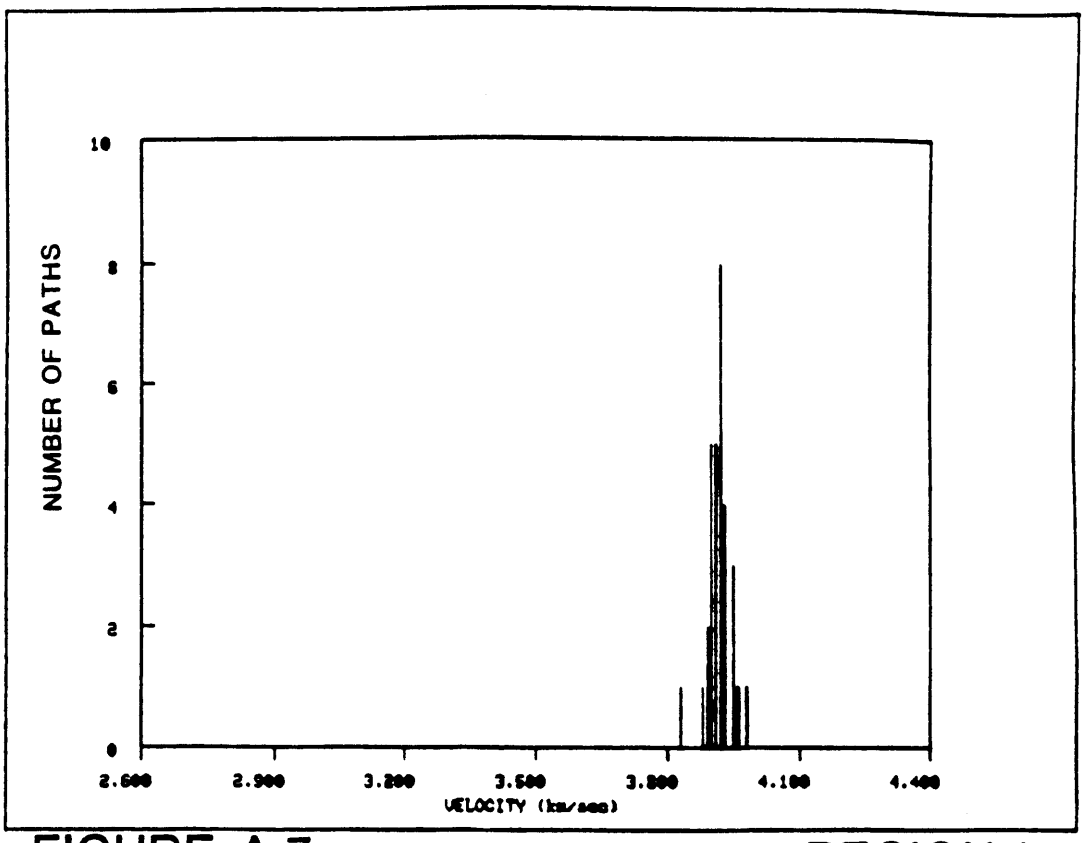

FIGURE A.7c REGION b

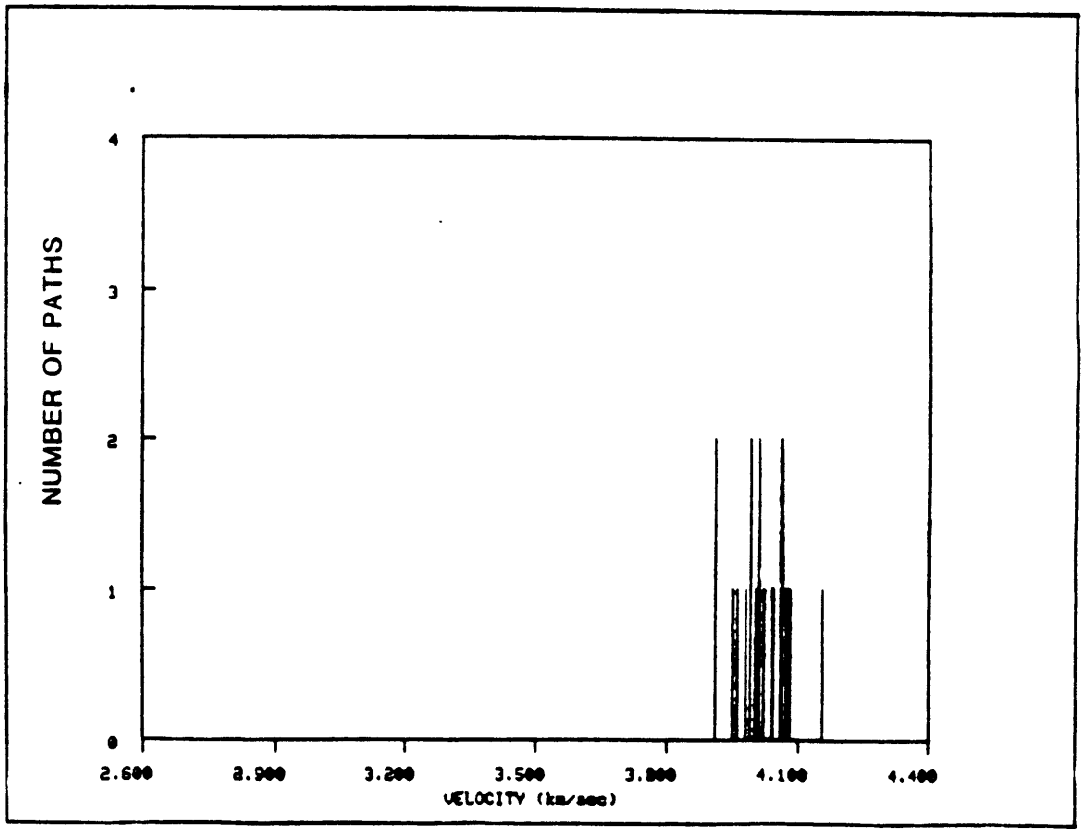

FIGURE A.7d REGION c

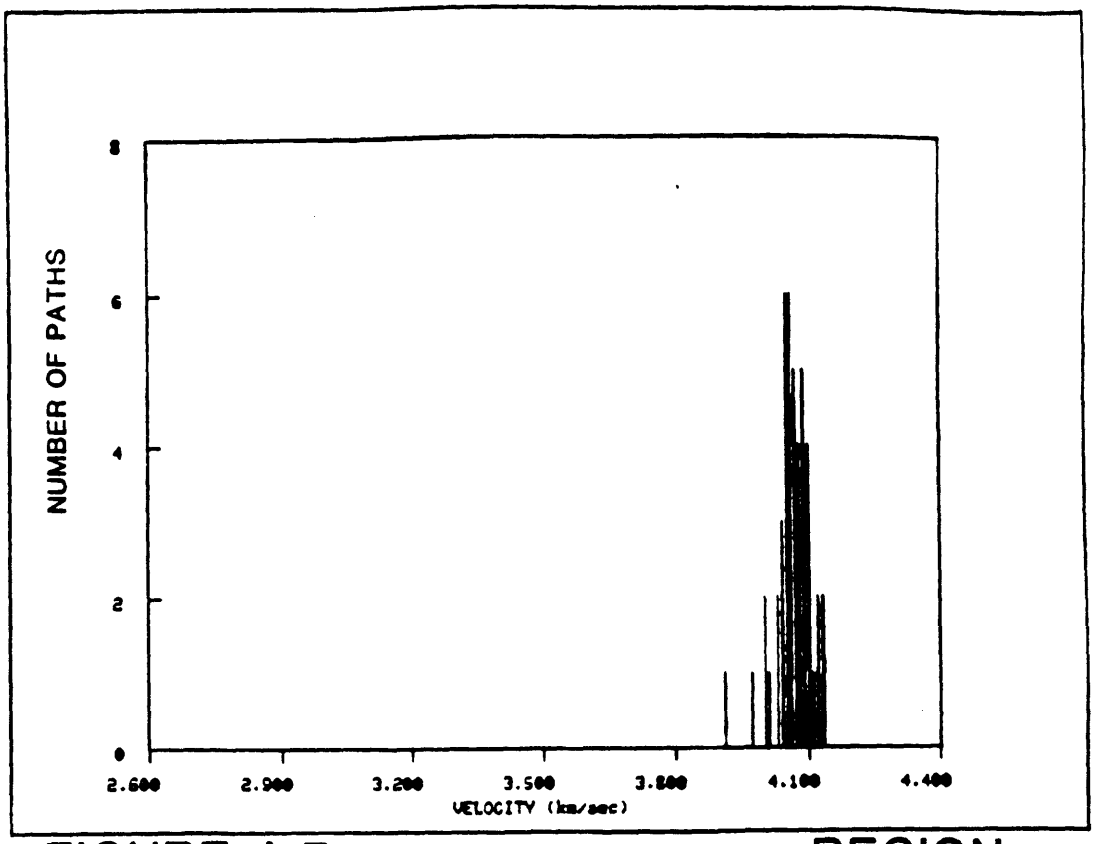

FIGURE A.7e REGION p

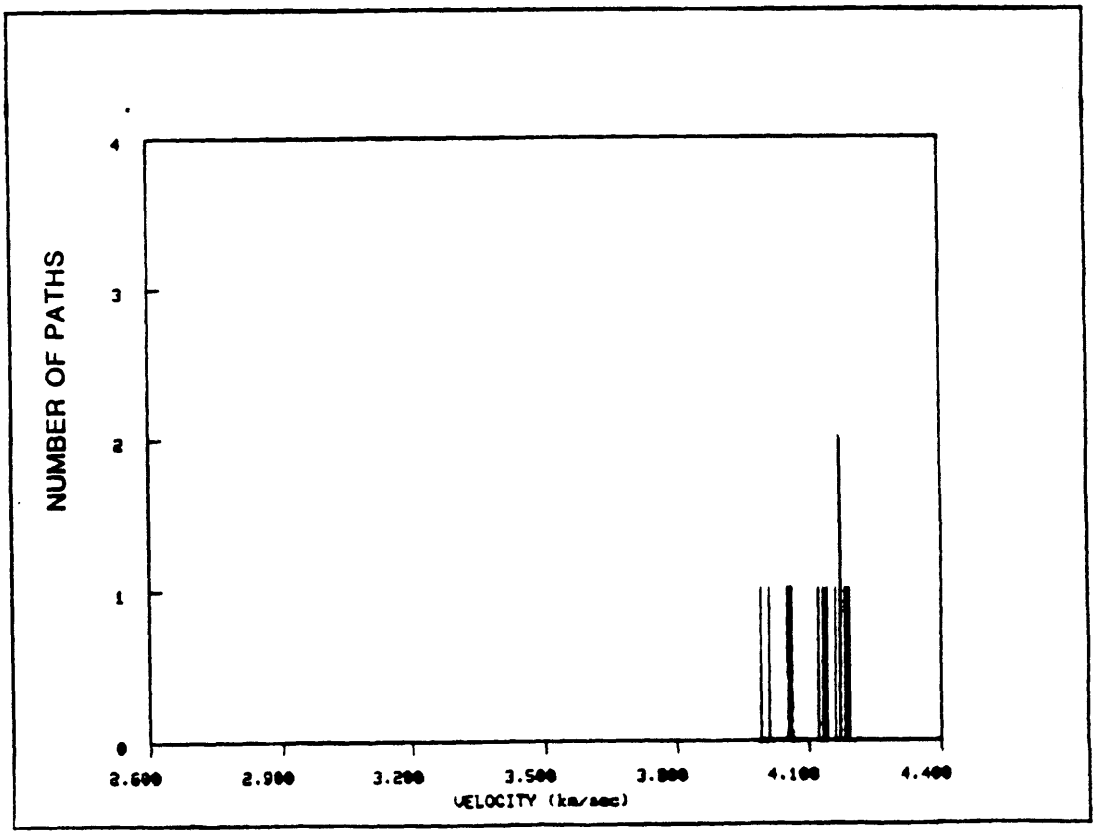

FIGURE A.7f REGION q

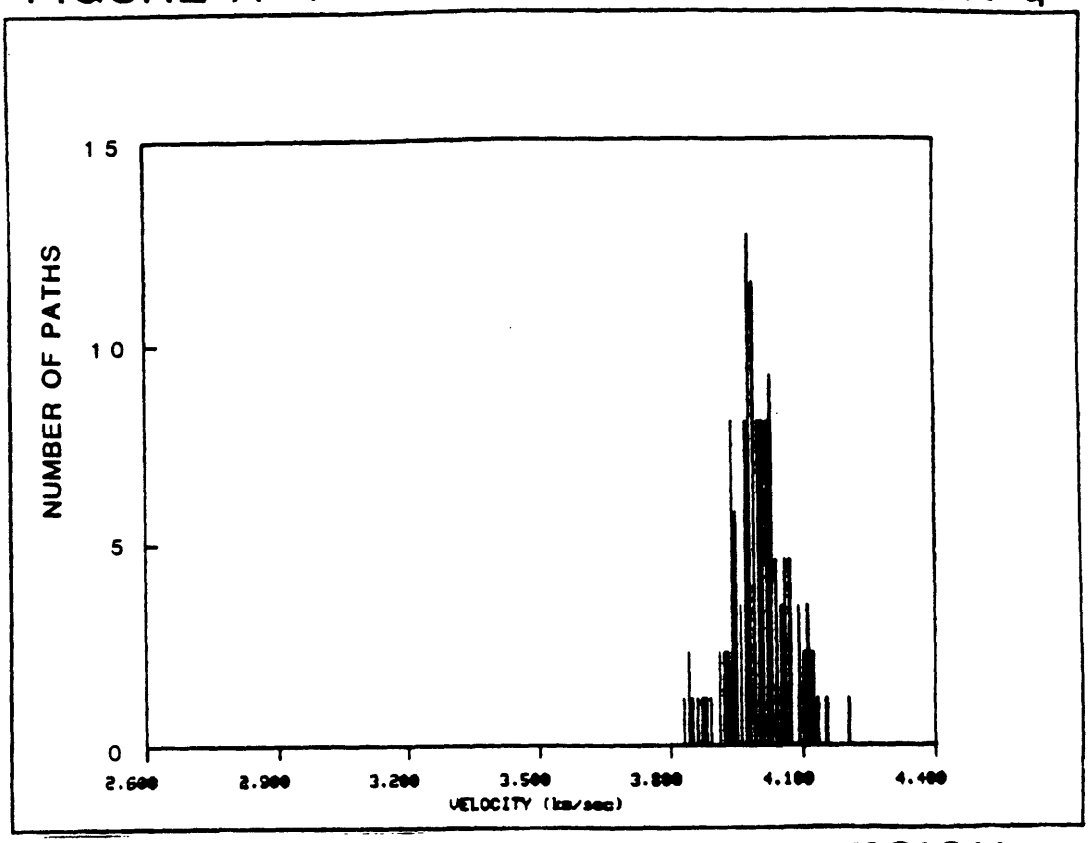

FIGURE A.7g REGION s

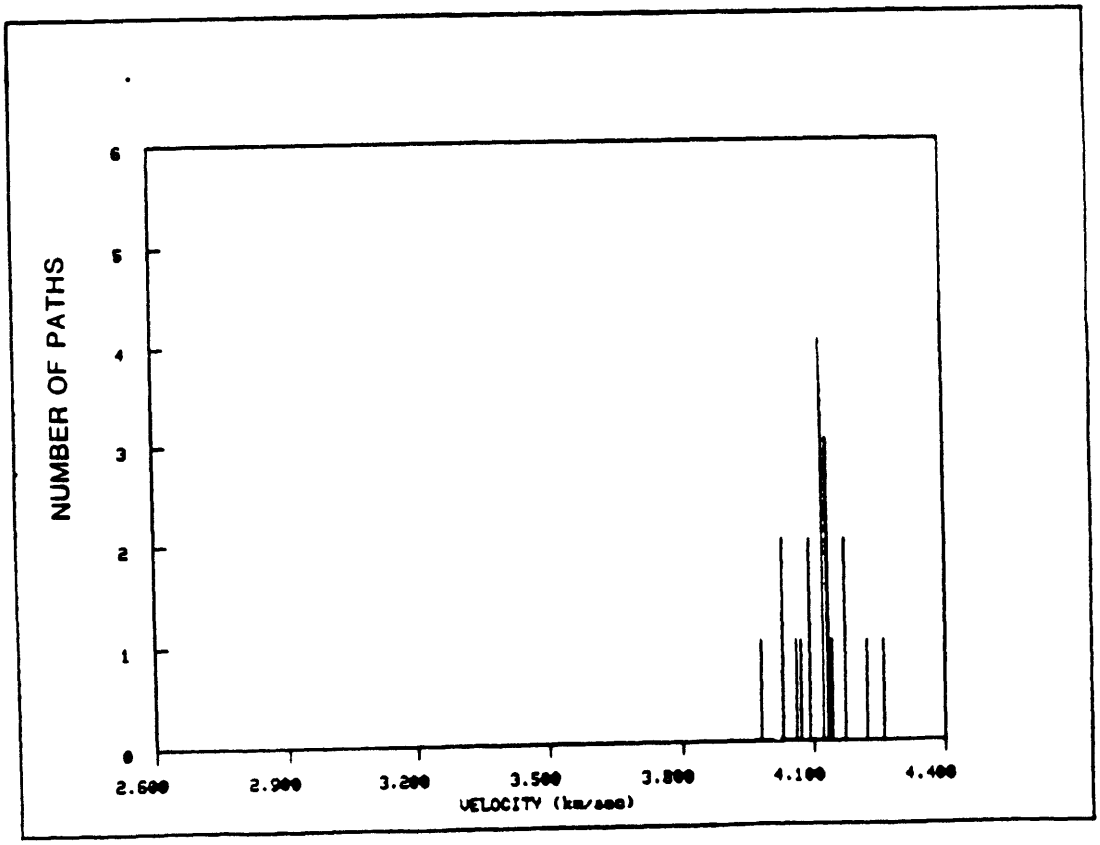

FIGURE A.7h REGION N

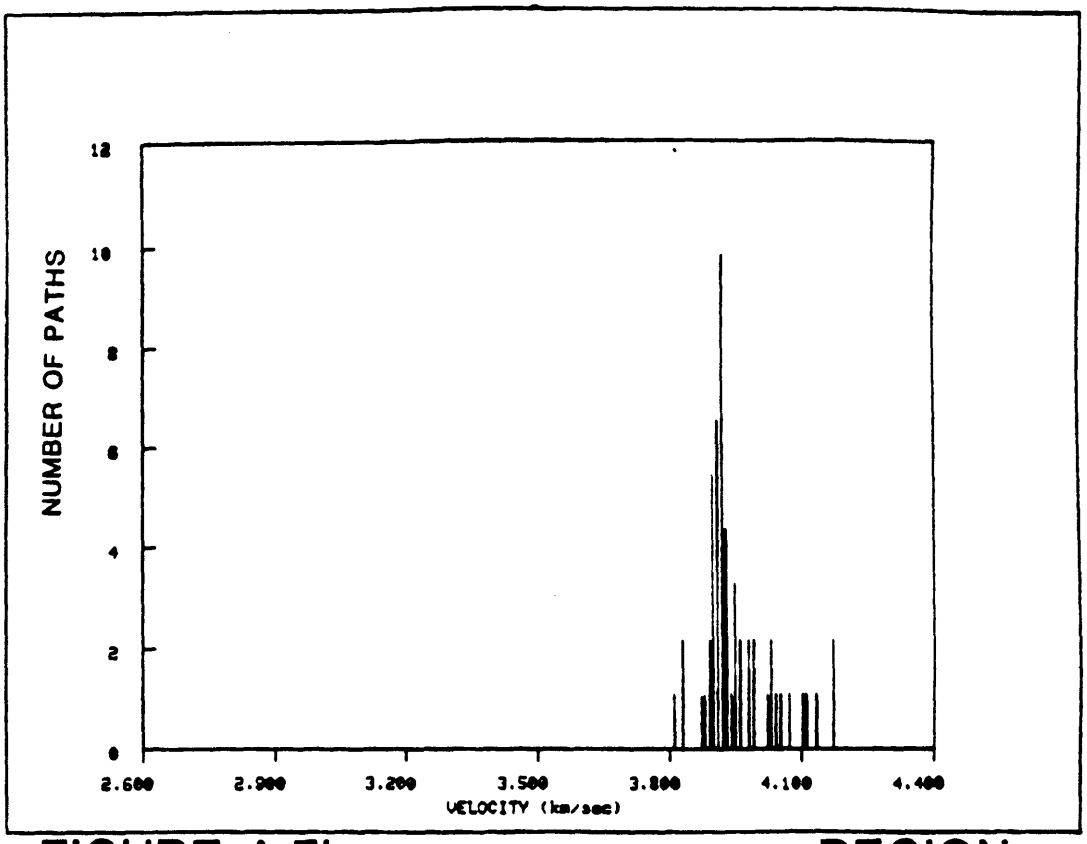

FIGURE A.7i REGION =

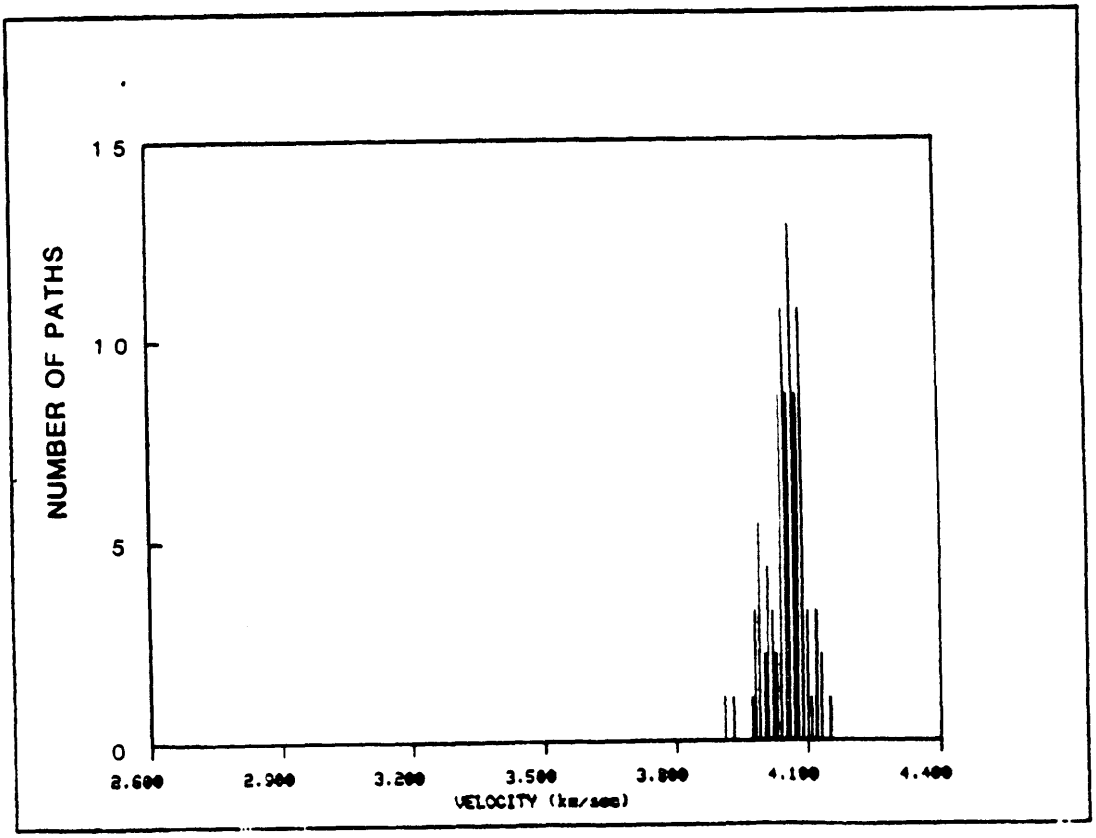

FIGURE A.7j REGION 0

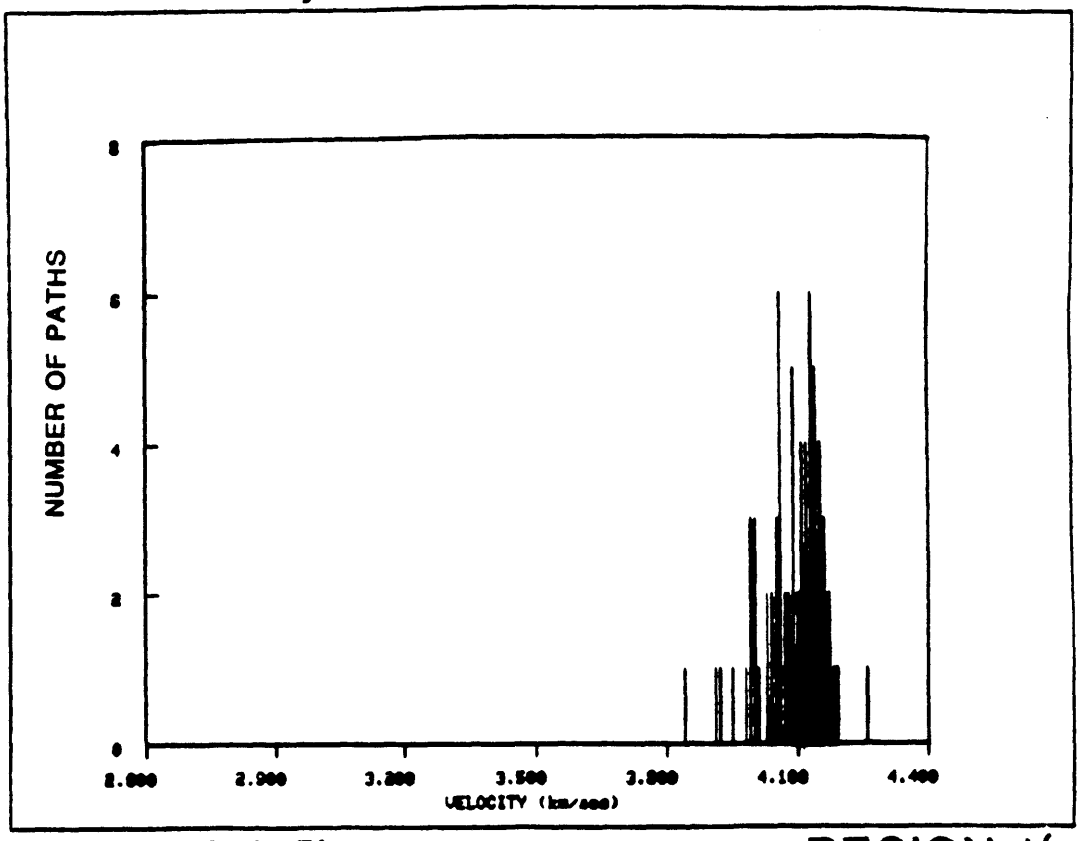

FIGURE A.7k REGION 0

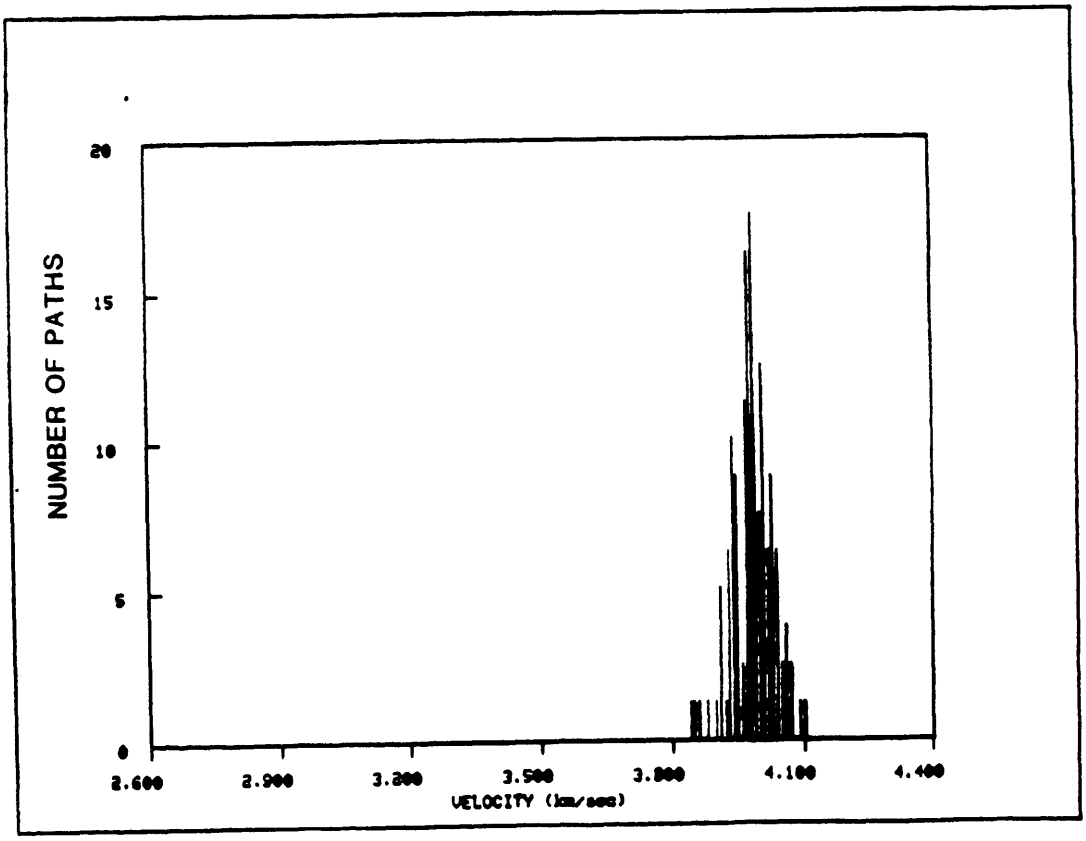

FIGURE A.7l REGION N

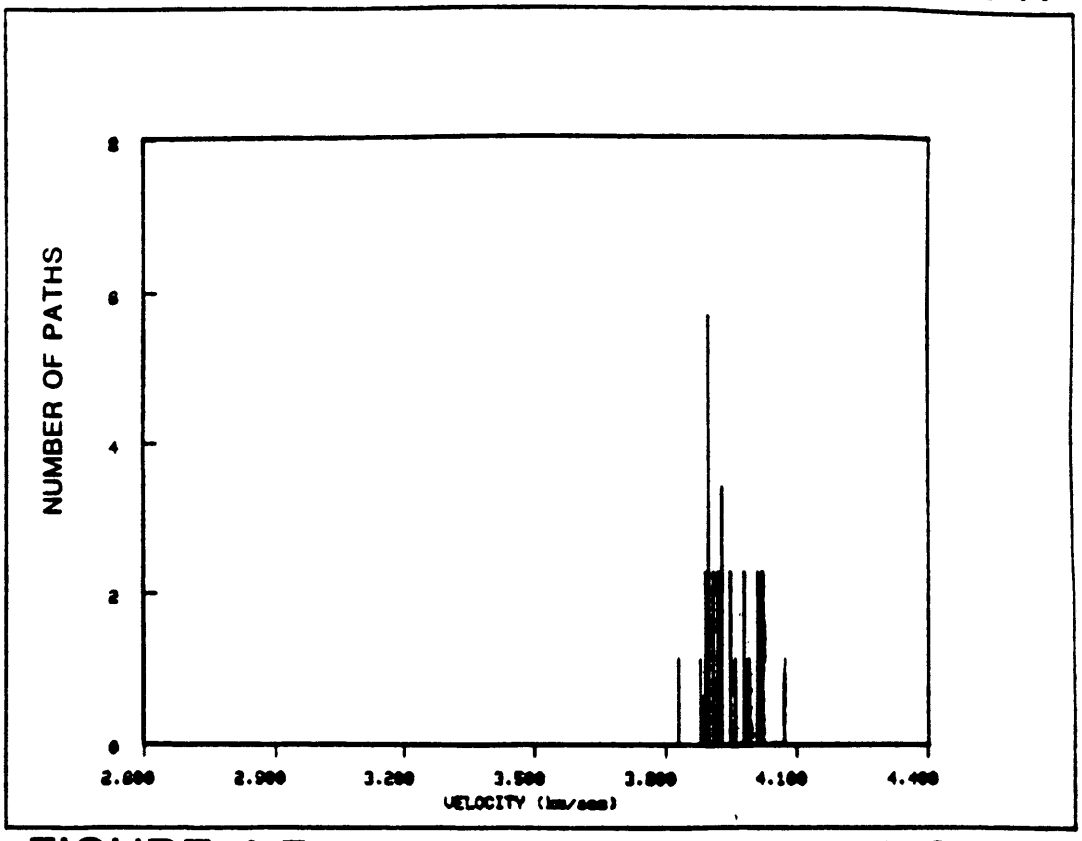

FIGURE A.7m REGION #

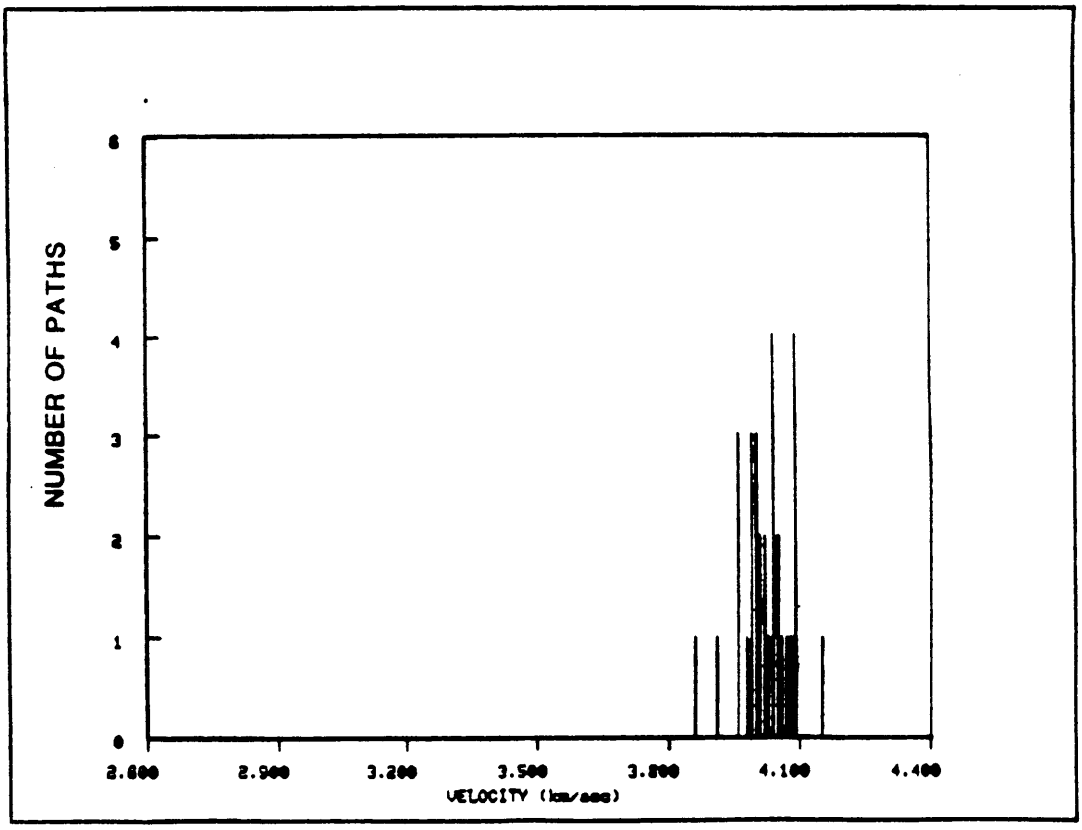

FIGURE A.7n REGION =

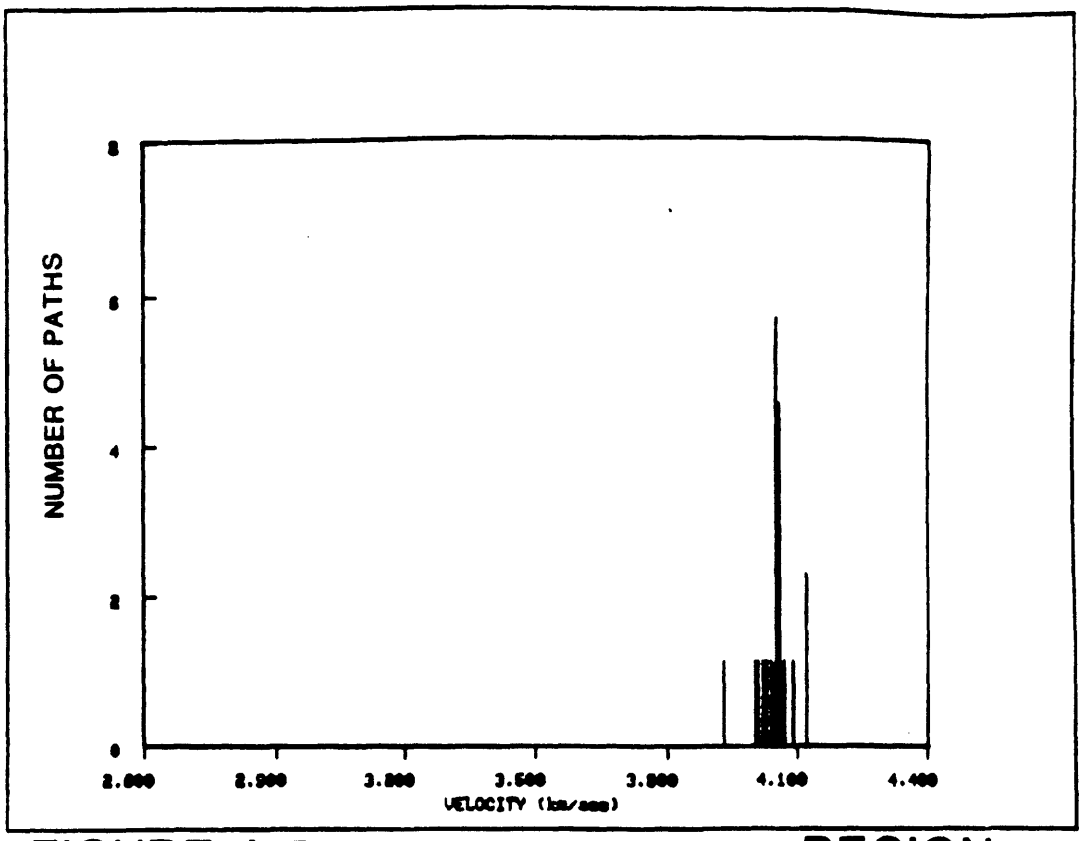

FIGURE A.7o REGION -

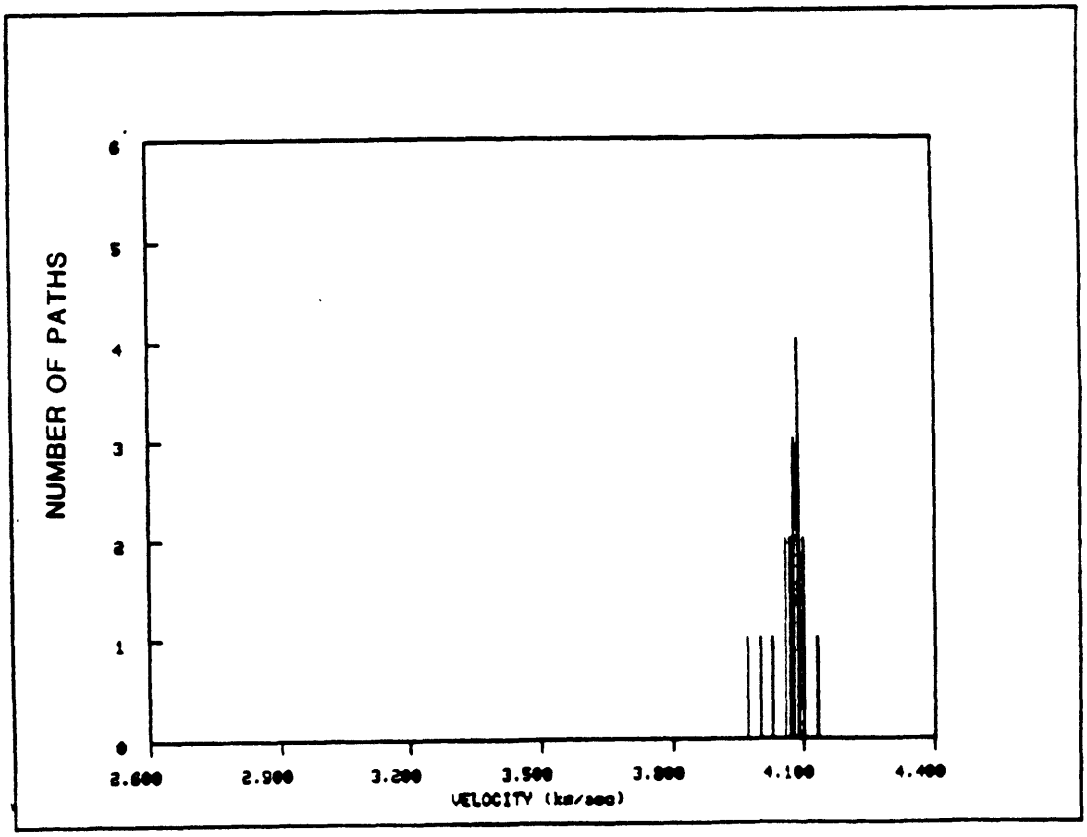

FIGURE A.7p REGION 0

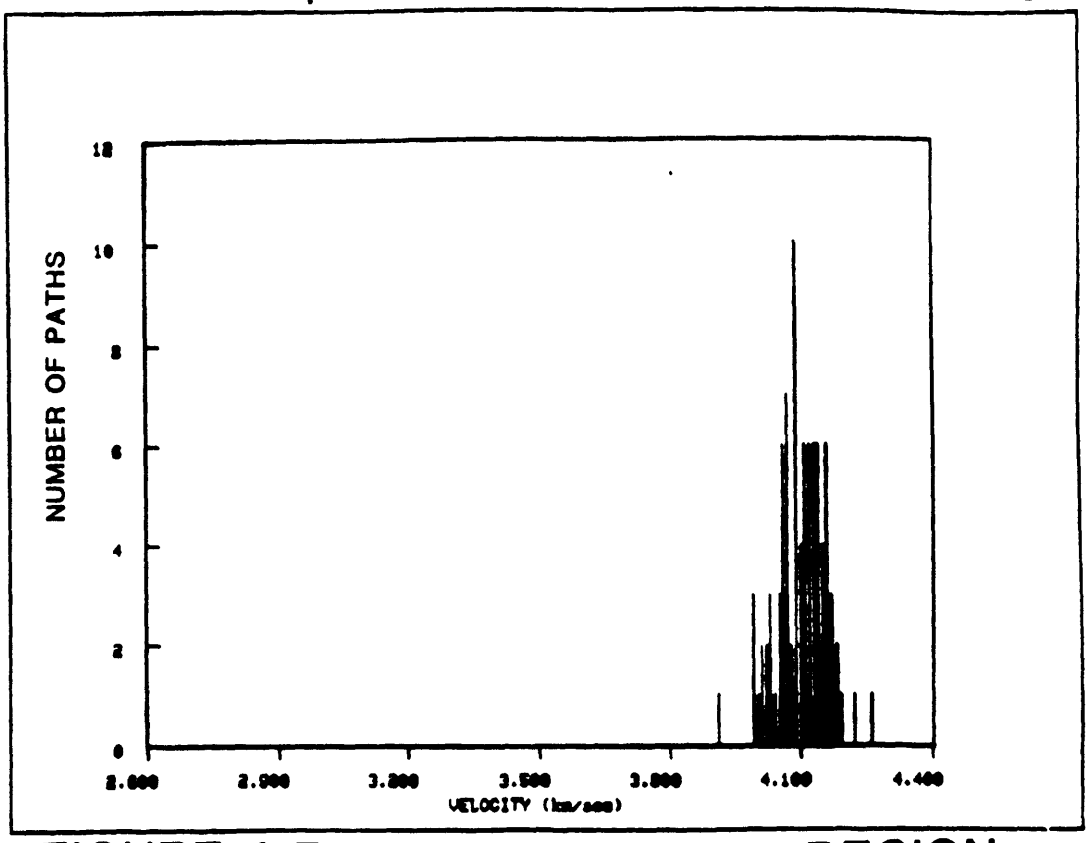

FIGURE A.7q REGION .

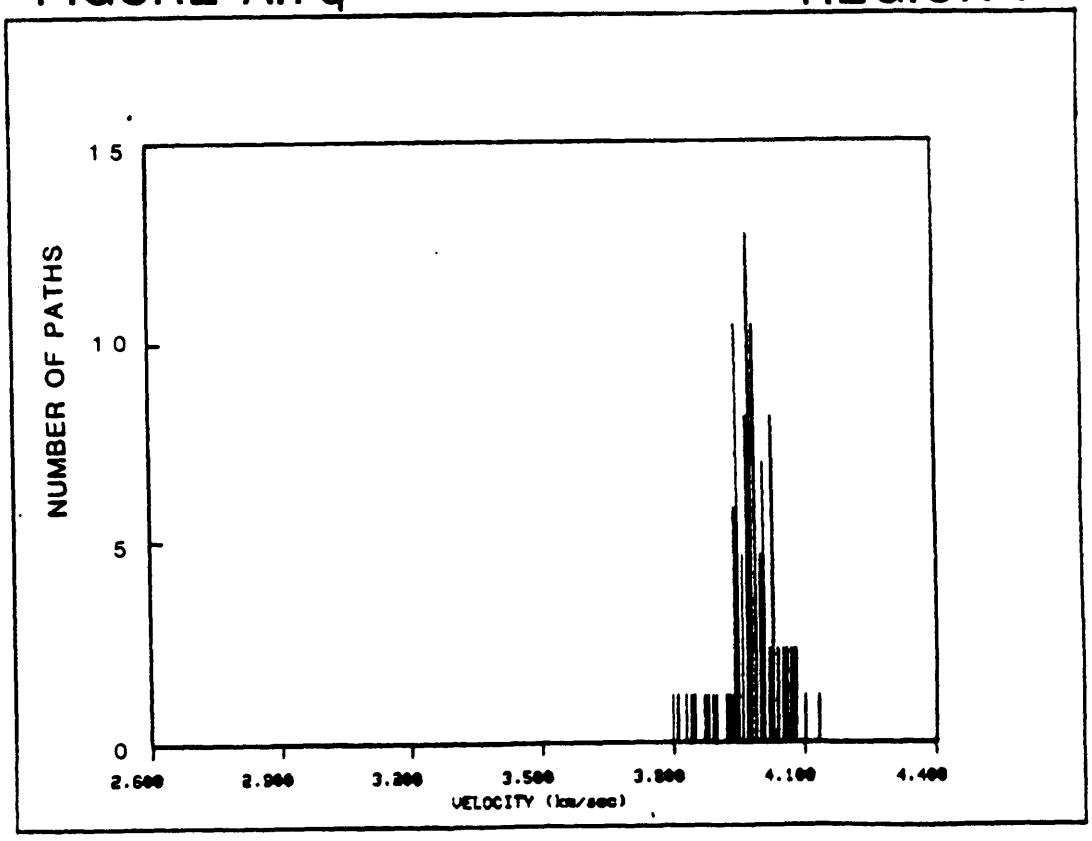

FIGURE A.7r

REGION ø

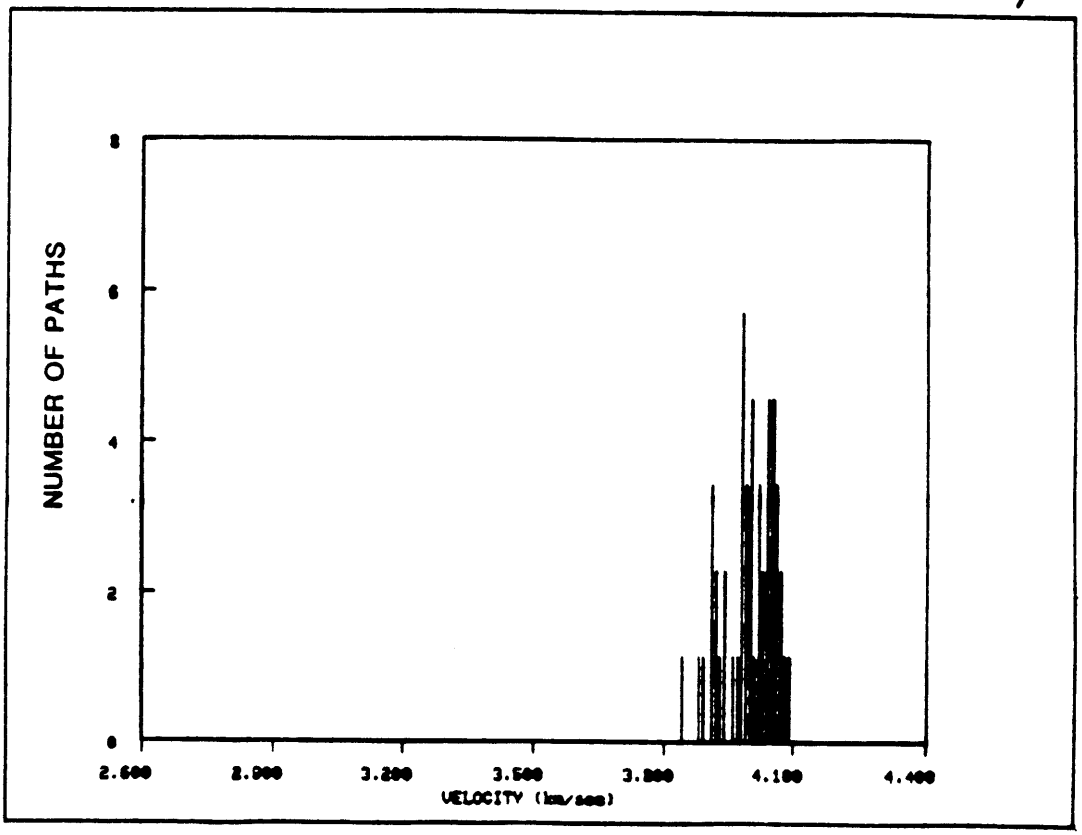

FIGURE A.8a

PERIOD 90 sec

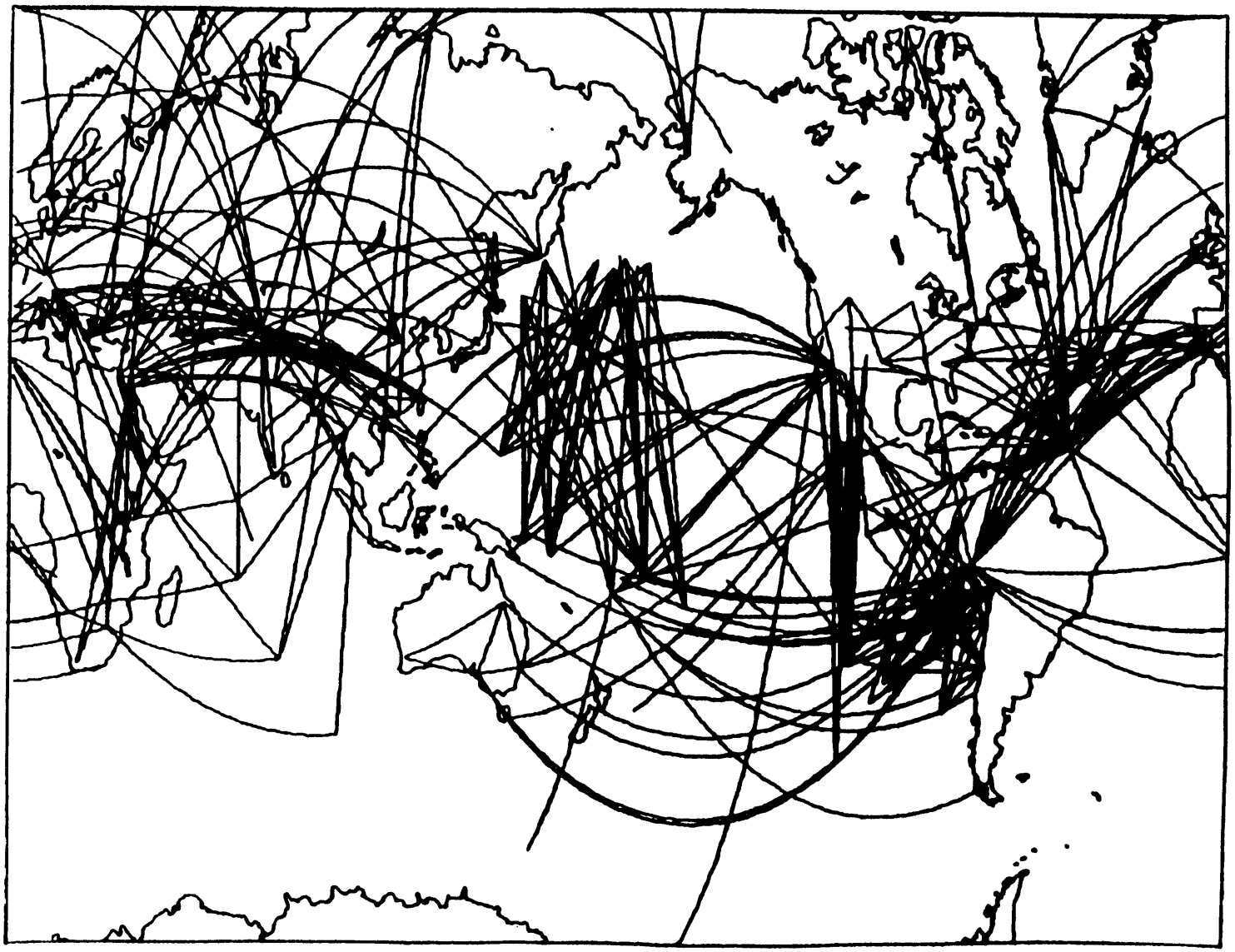

FIGURE A.8b REGION a

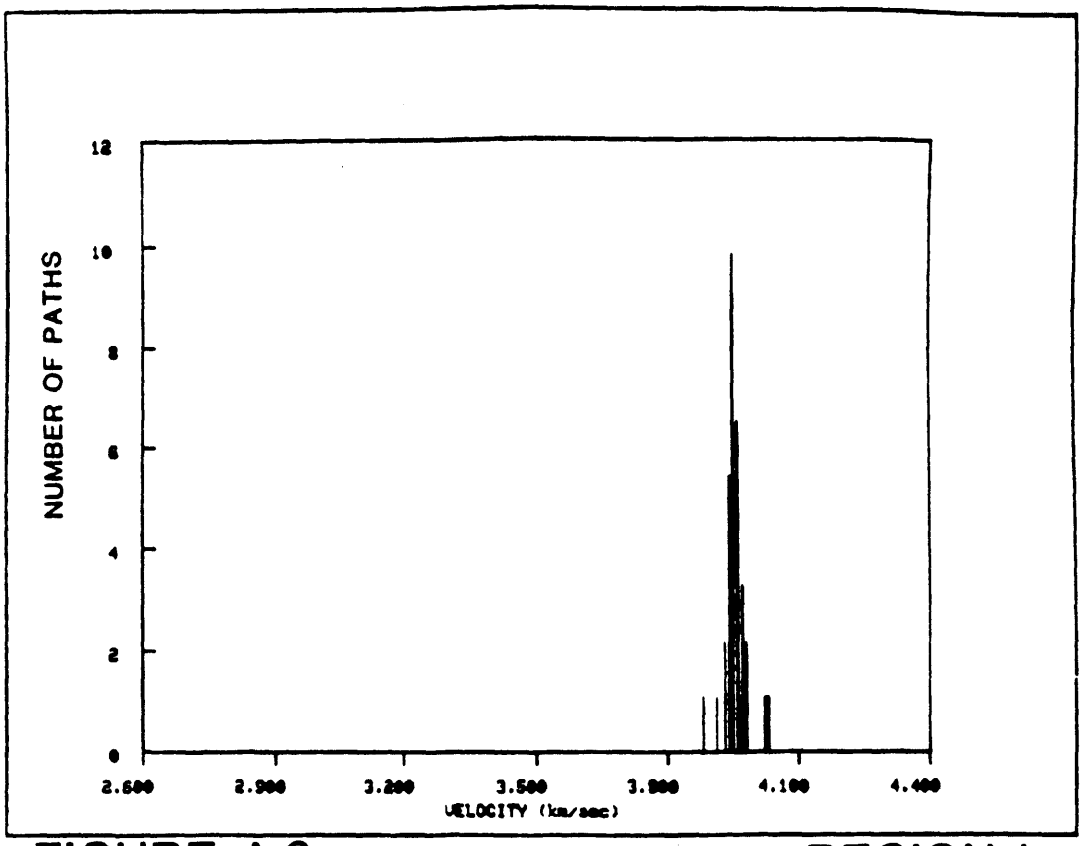

FIGURE A.8c REGION b

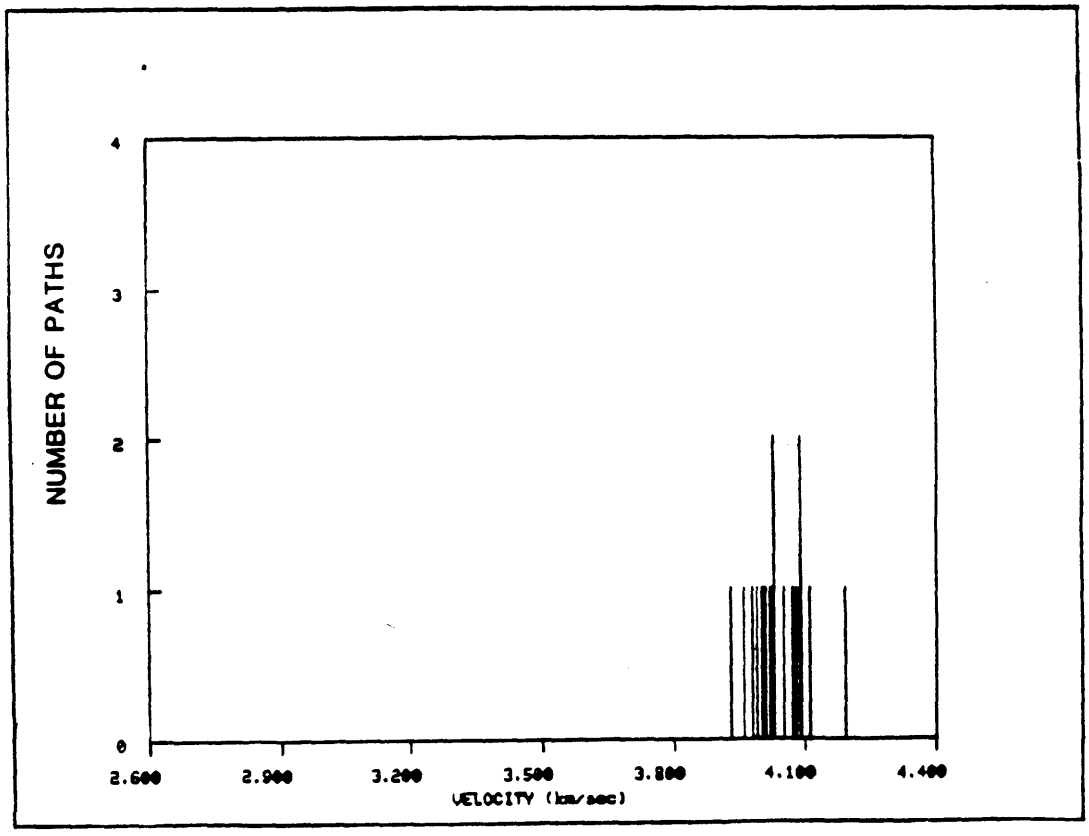

FIGURE A.8d REGION c

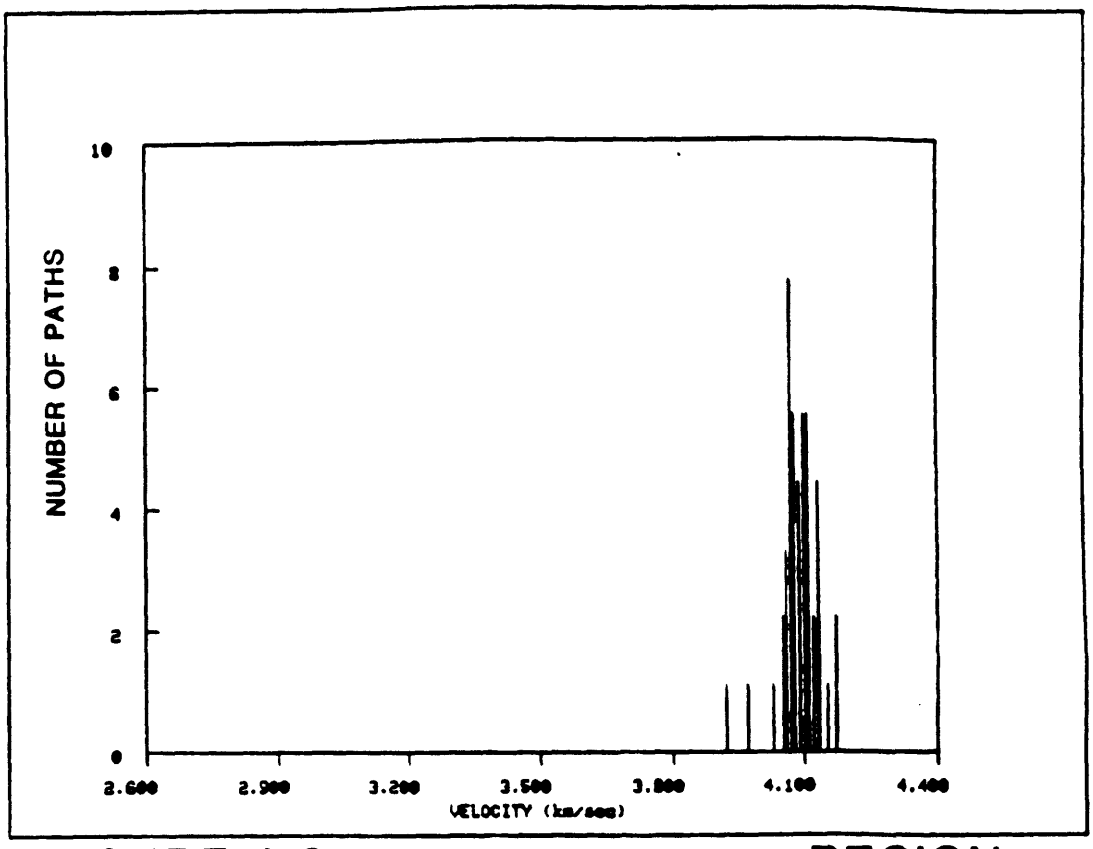

FIGURE A.8e REGION p

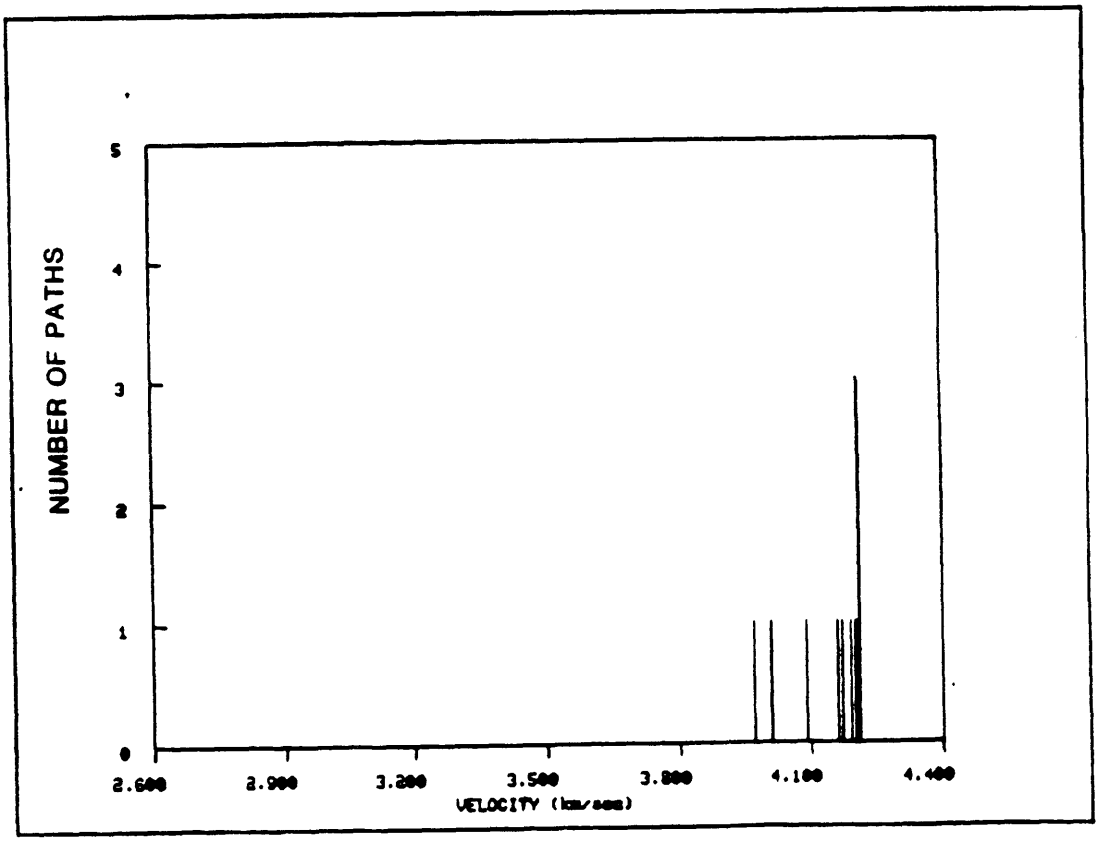

FIGURE A.8f REGION q

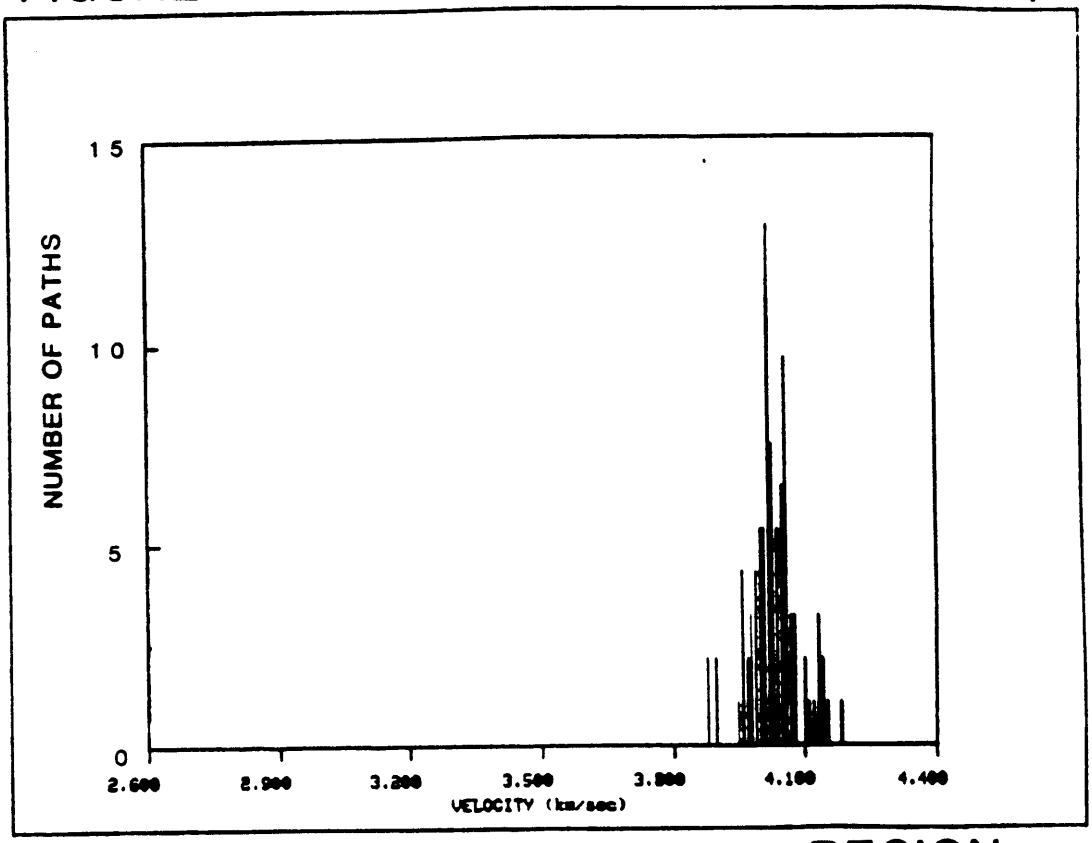

FIGURE A.8g REGION s

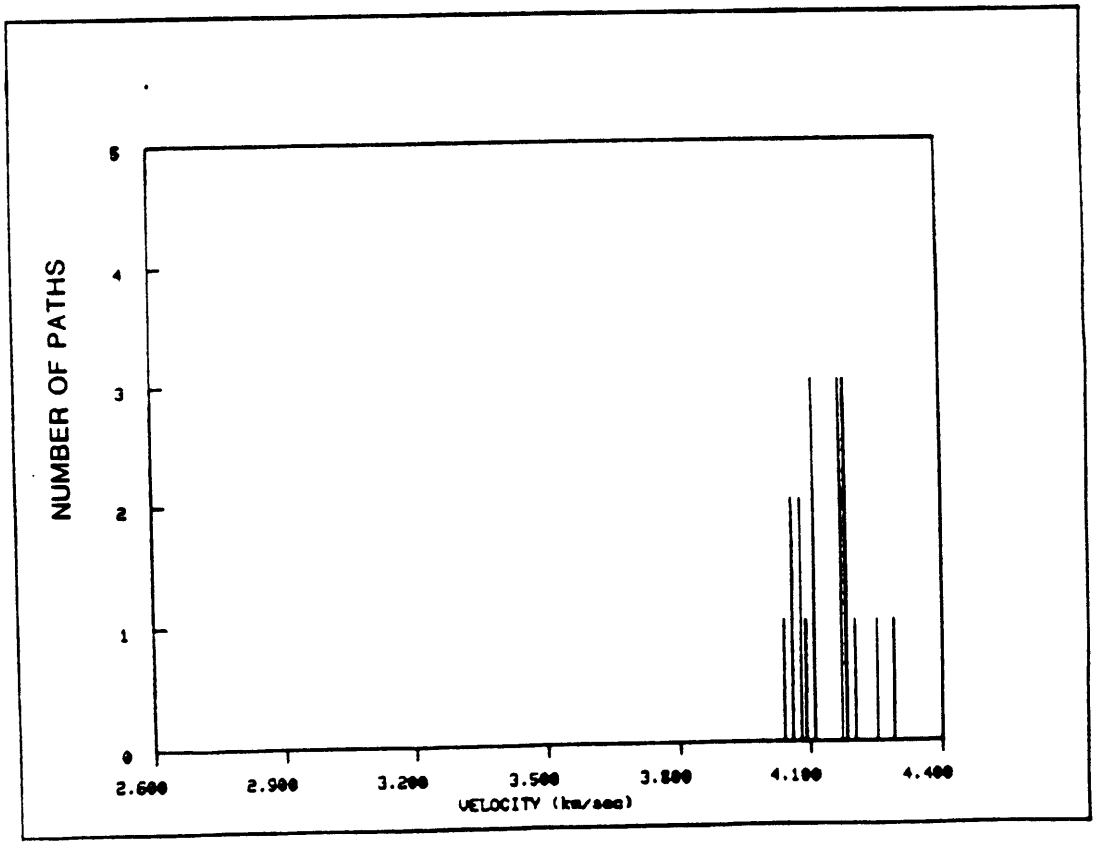

FIGURE A.8h REGION N

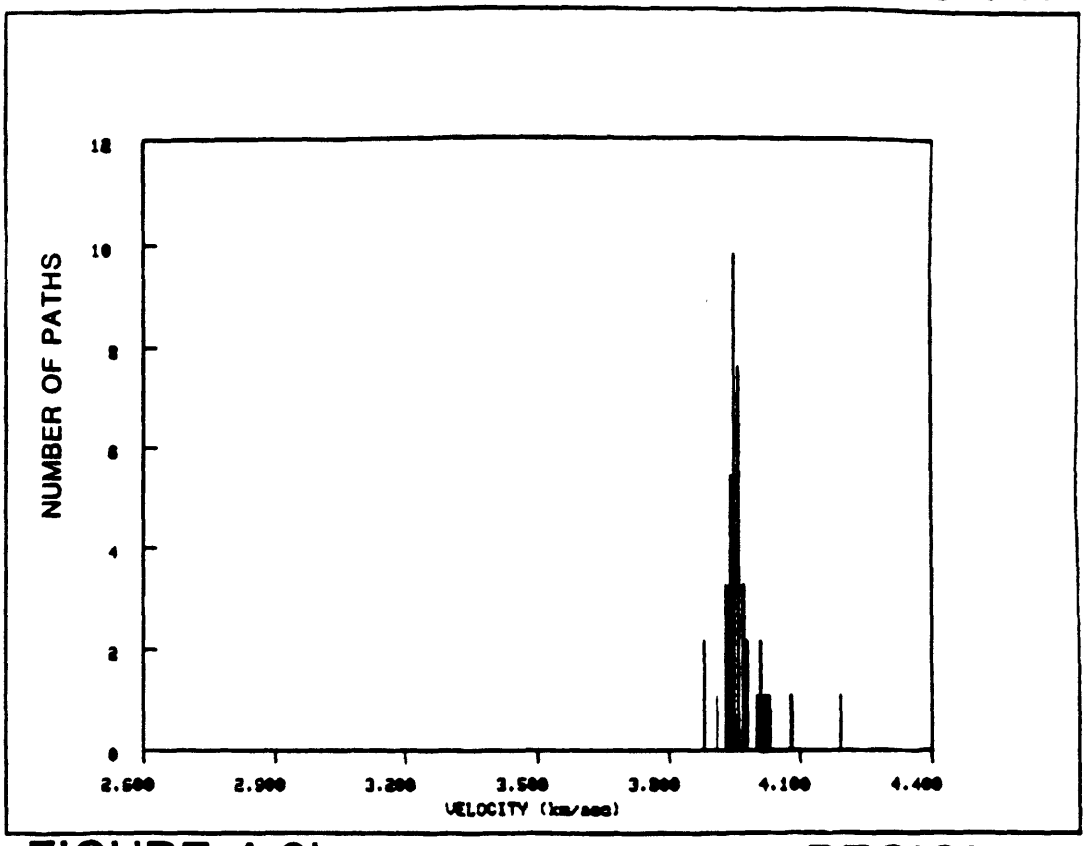

FIGURE A.8i REGION =

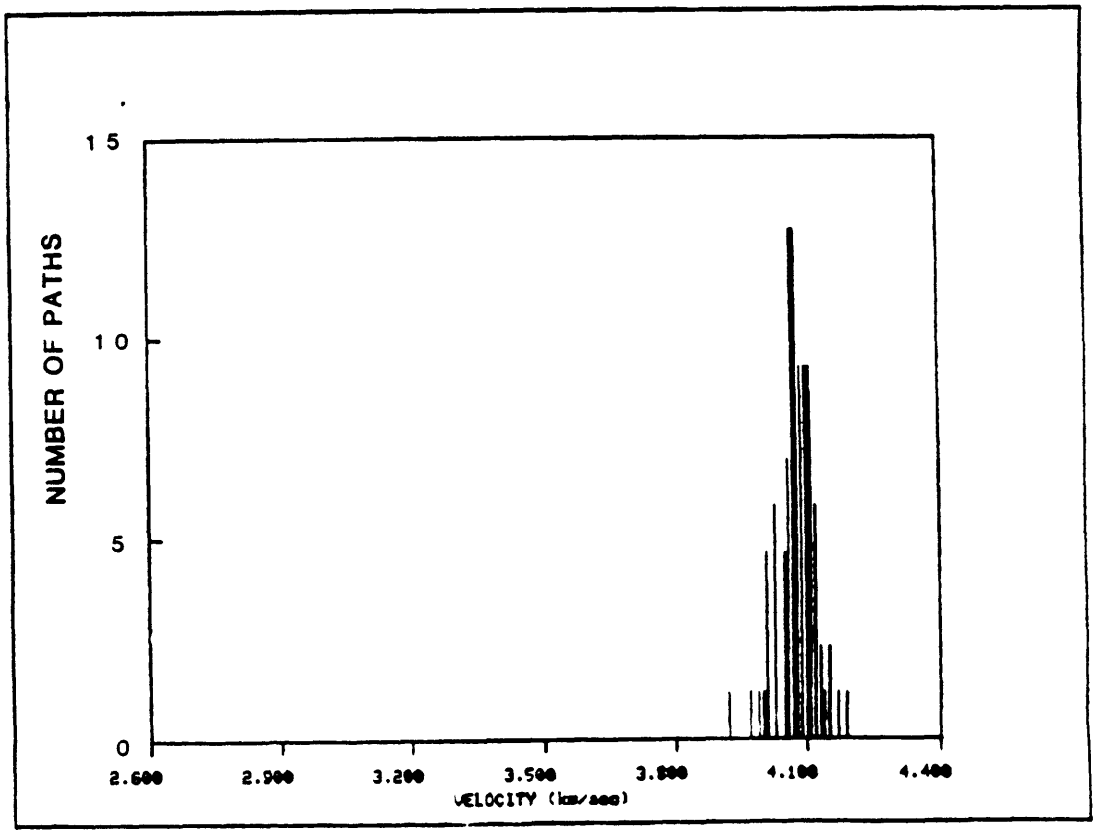

FIGURE A.8j REGION 0

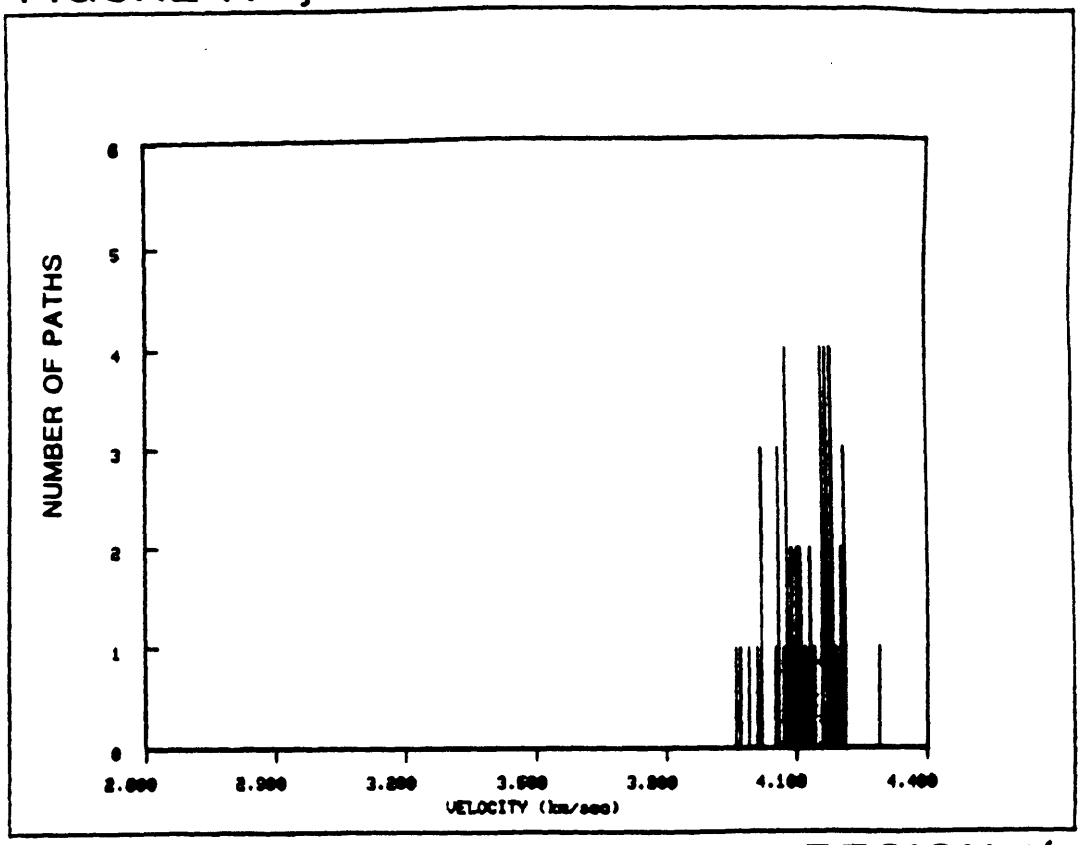

FIGURE A.8k REGION ~~0~~

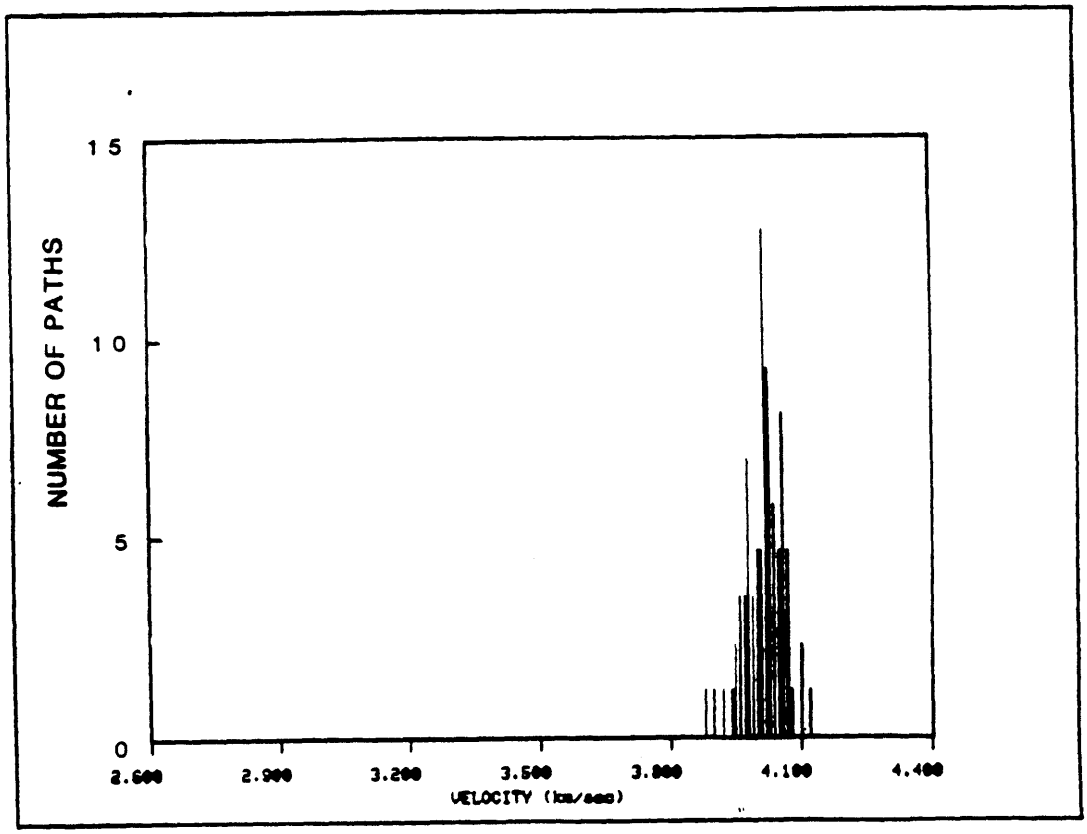

FIGURE A.8l REGION N

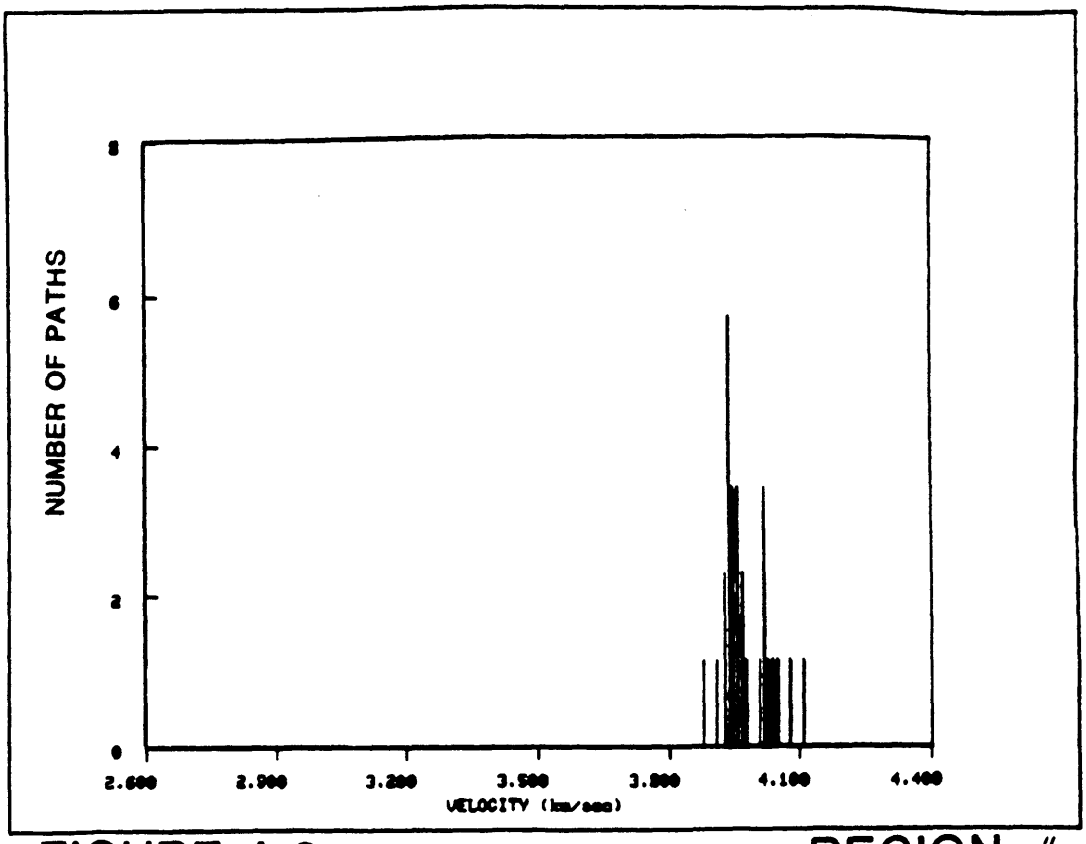

FIGURE A.8m REGION #

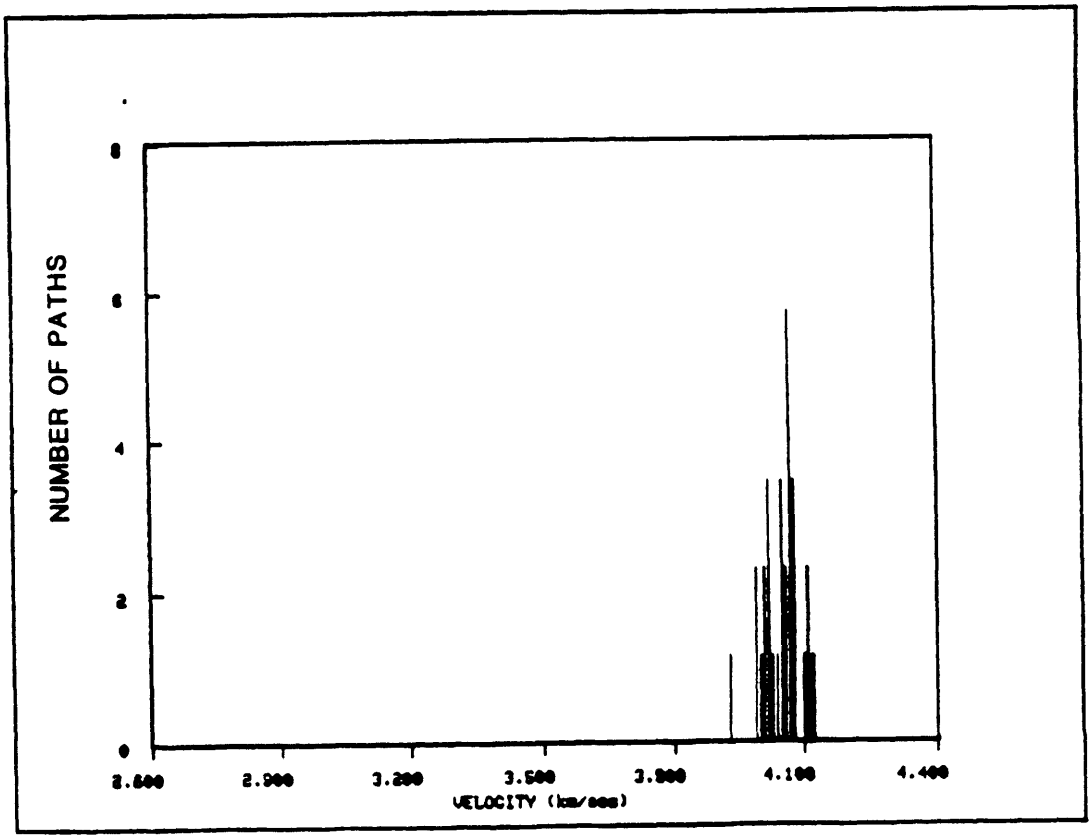

FIGURE A.8n REGION =

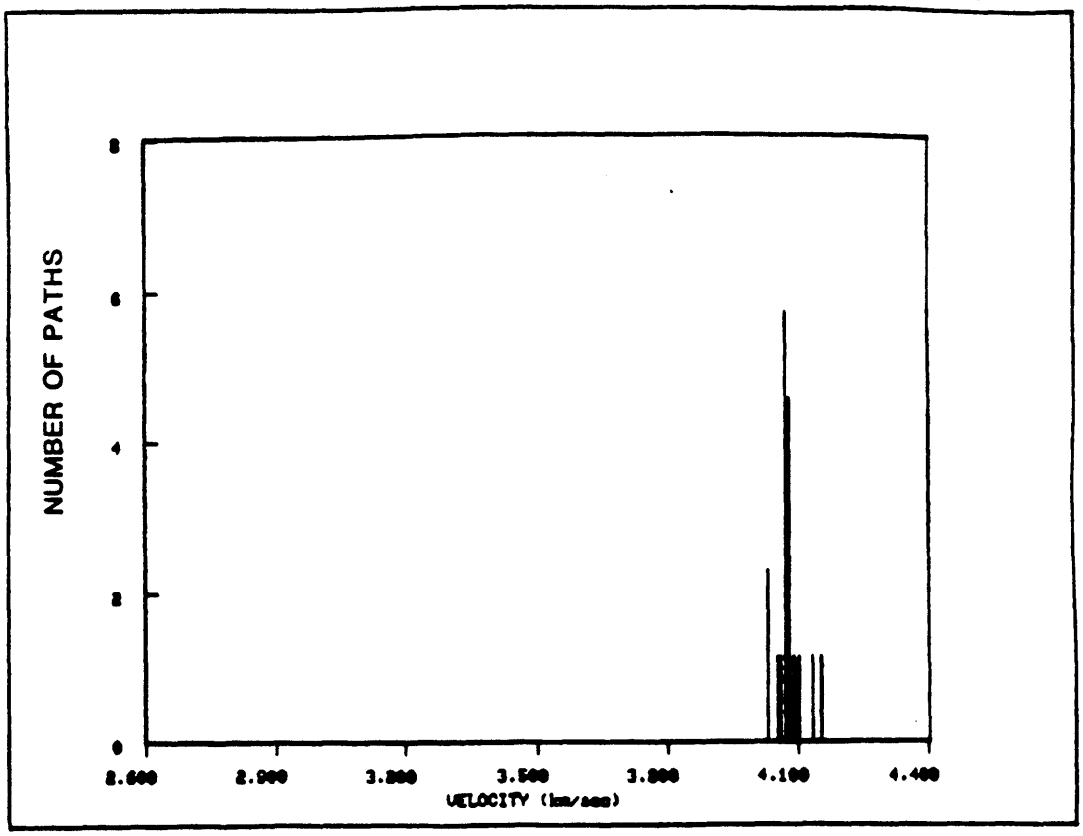

FIGURE A.8o REGION -

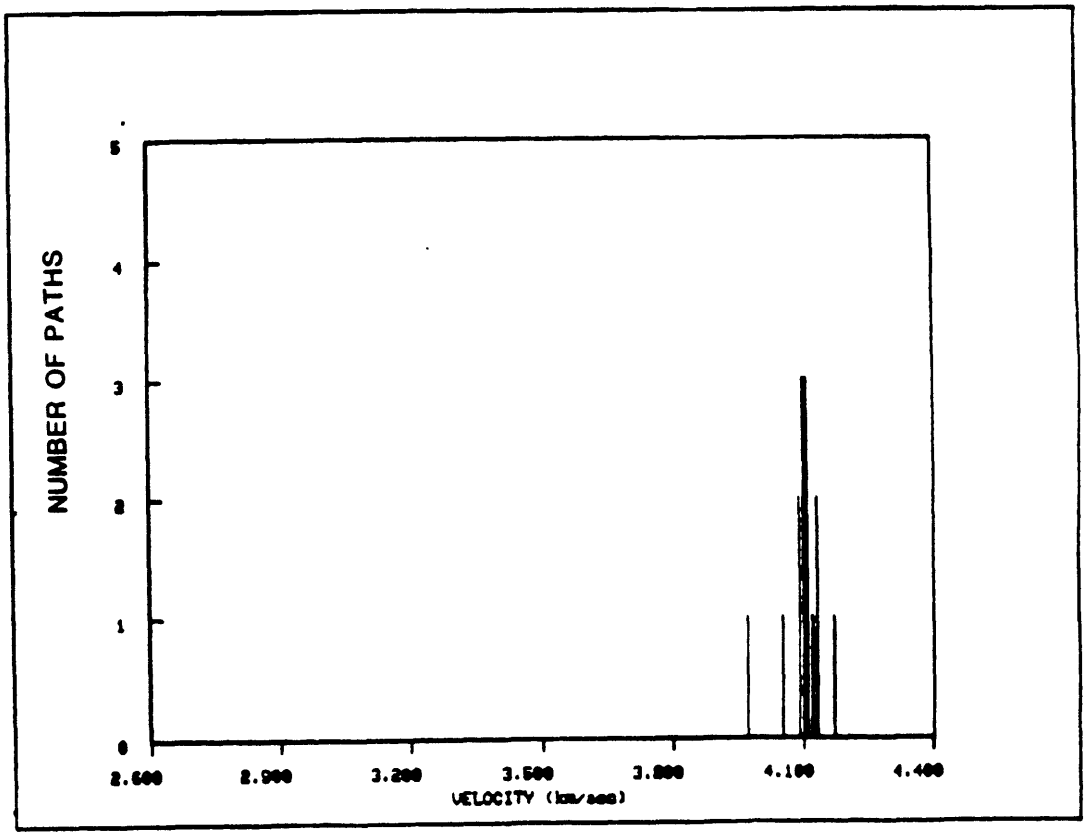

FIGURE A.8p REGION 0

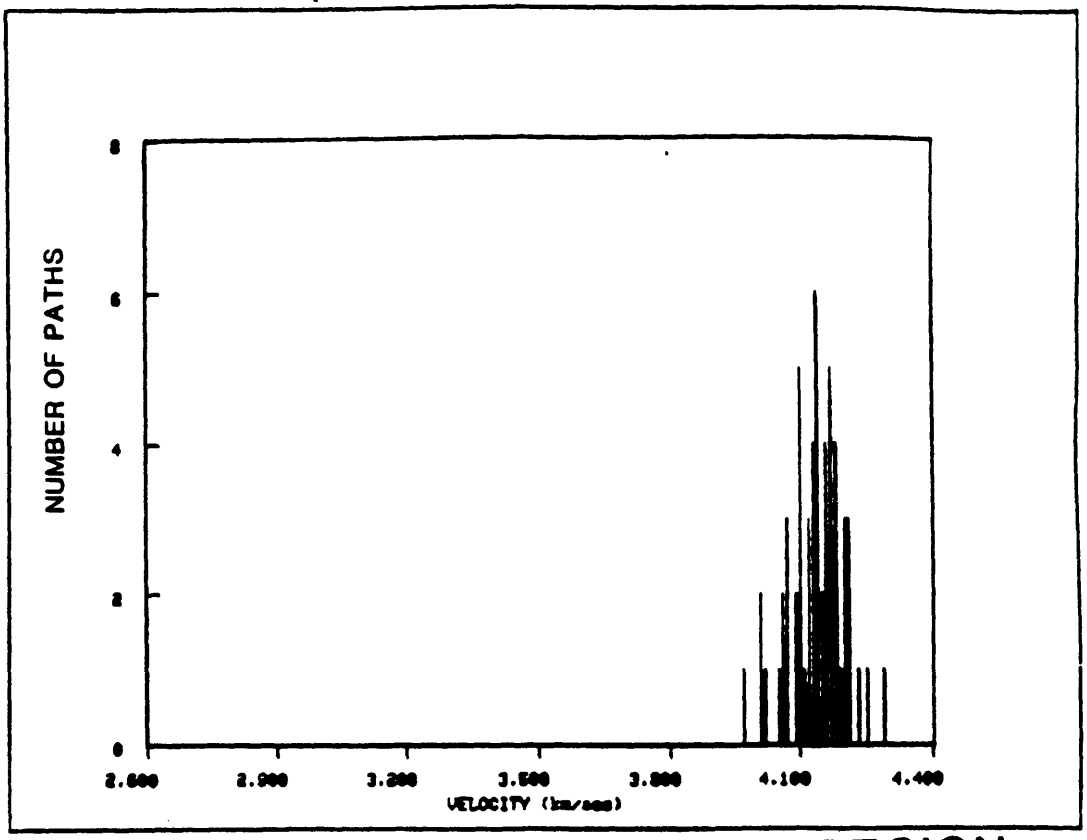

FIGURE A.8q REGION .

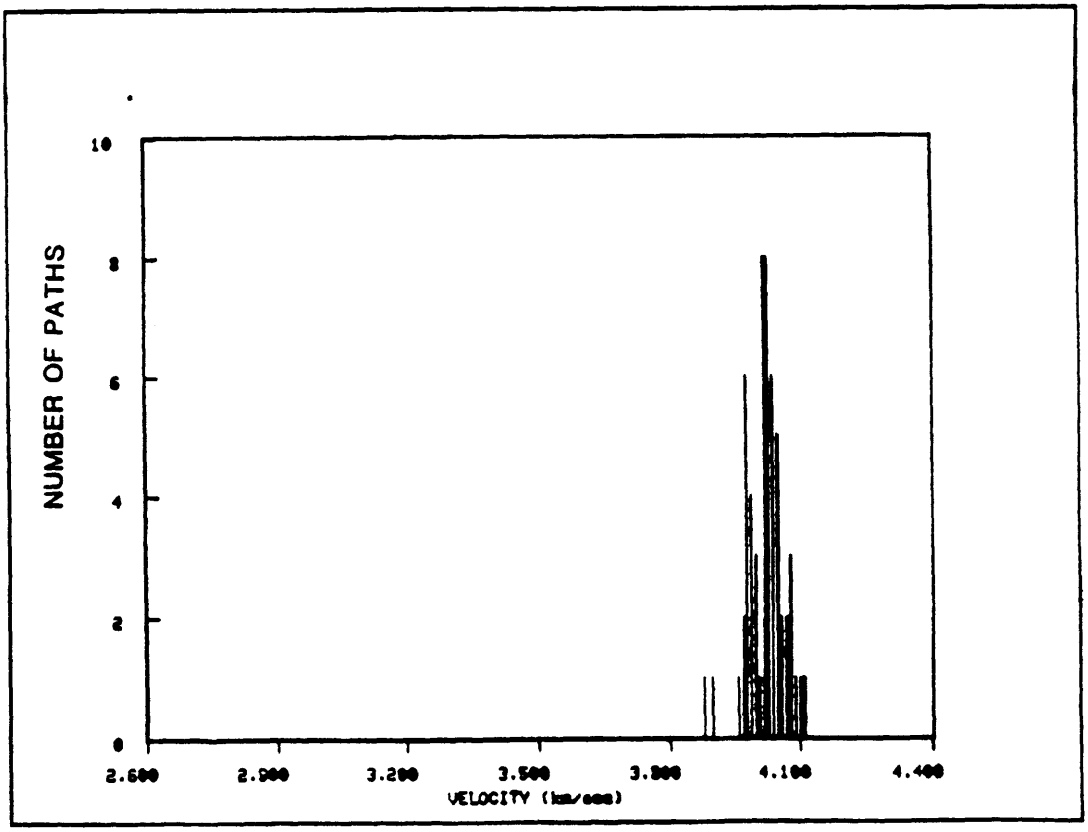

FIGURE A.8r REGION ø

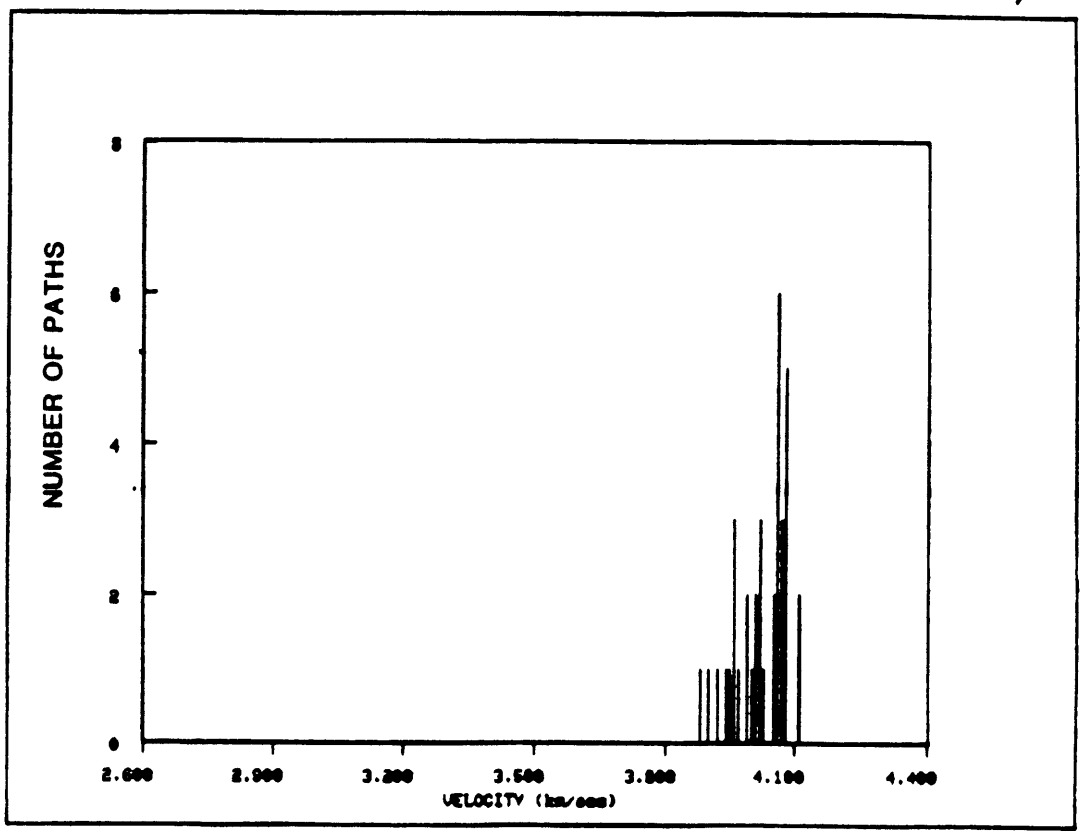

FIGURE A.9a

PERIOD 98 sec

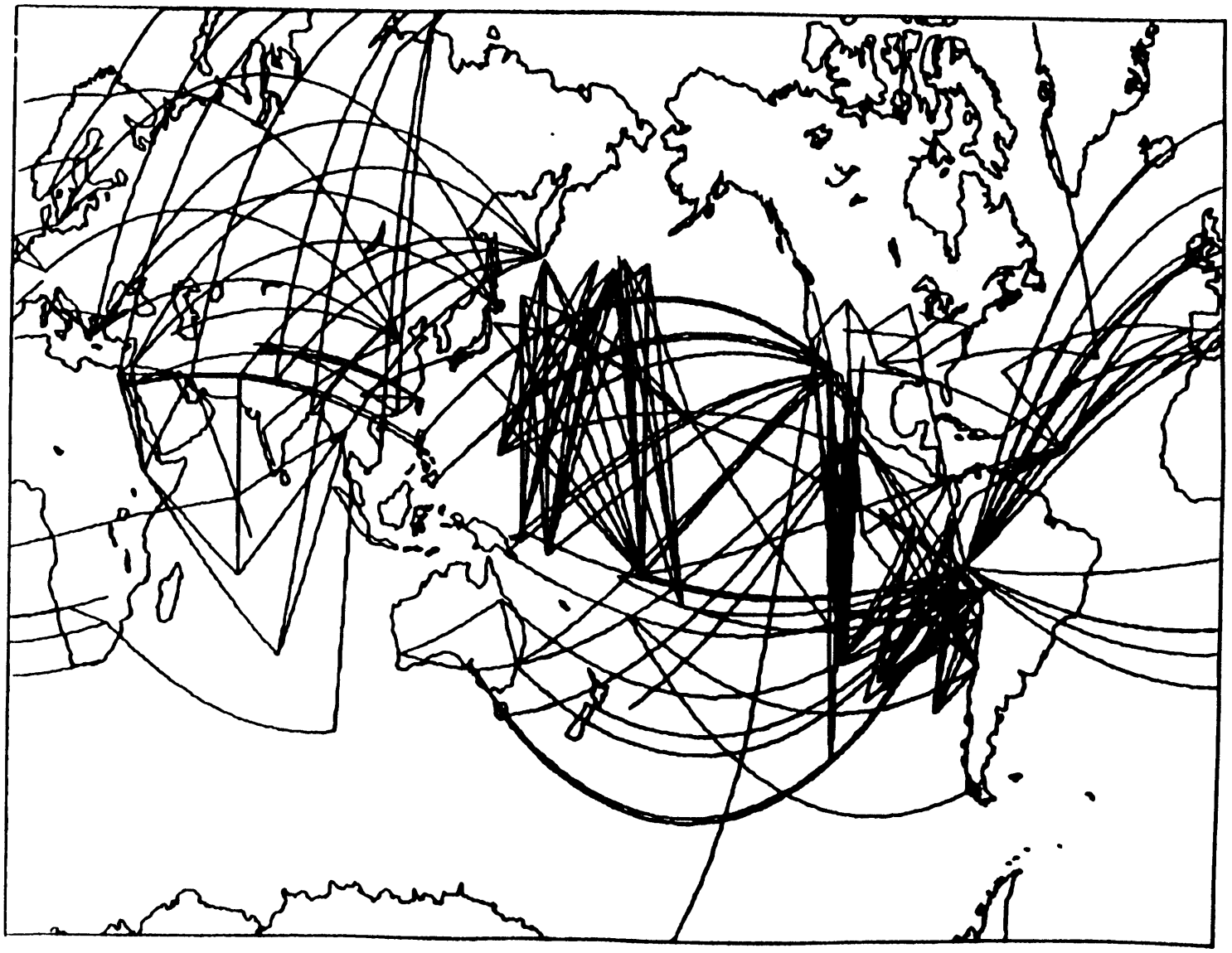

FIGURE A.9b REGION a

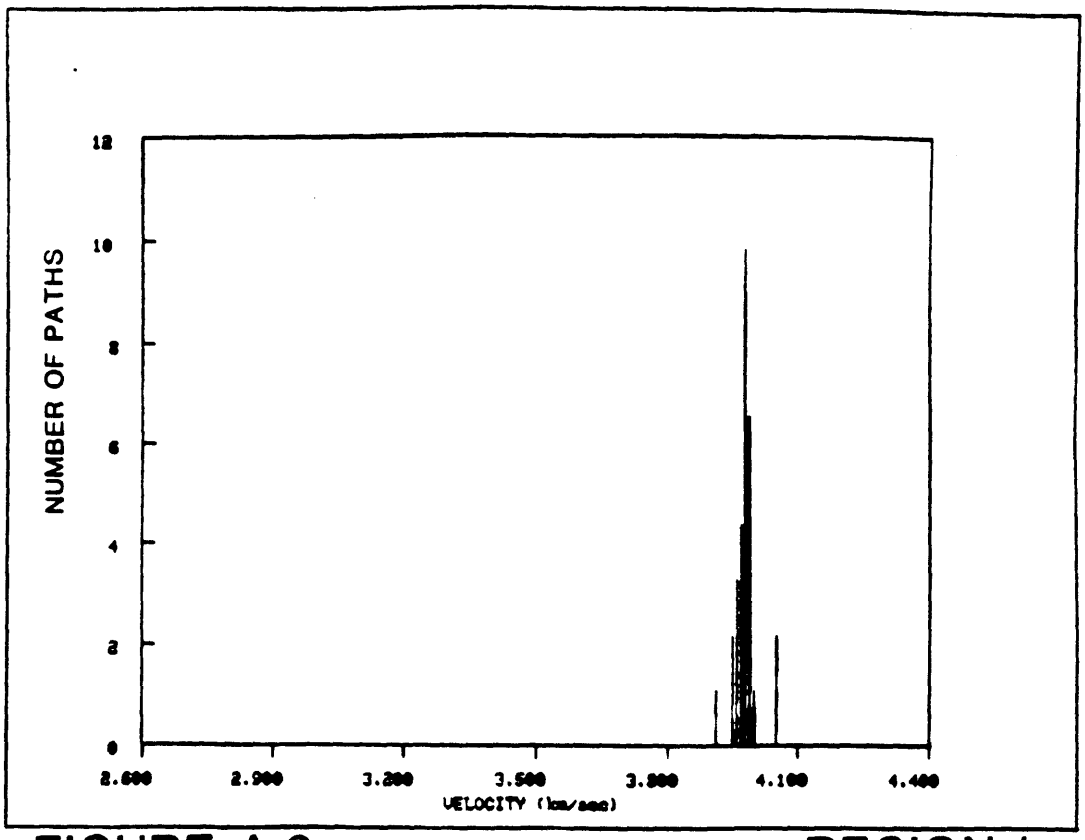

FIGURE A.9c REGION b

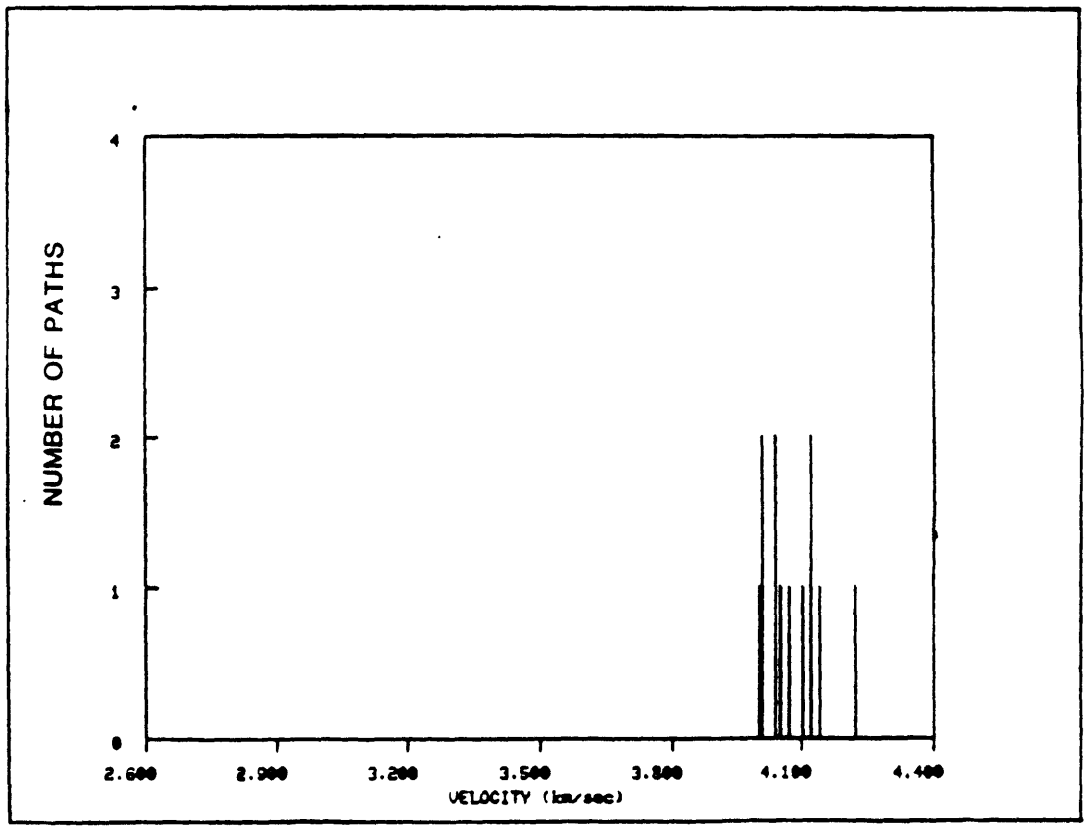

FIGURE A.9d REGION c

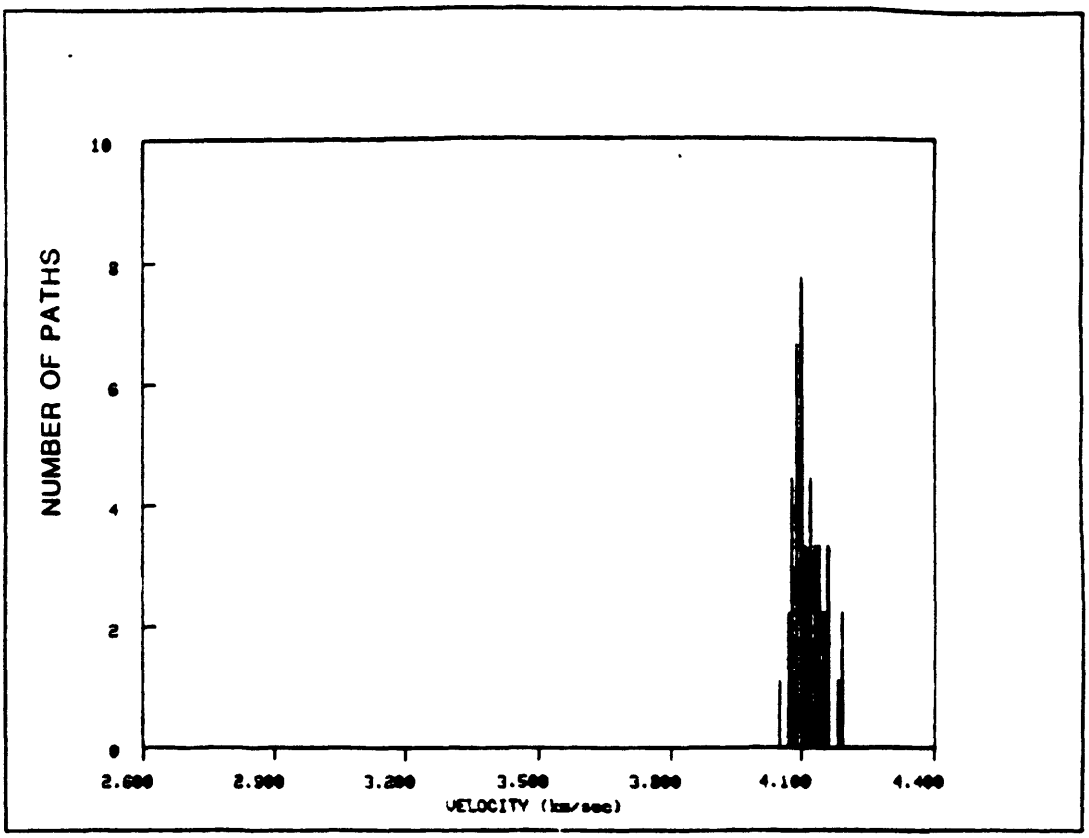

FIGURE A.9e REGION p

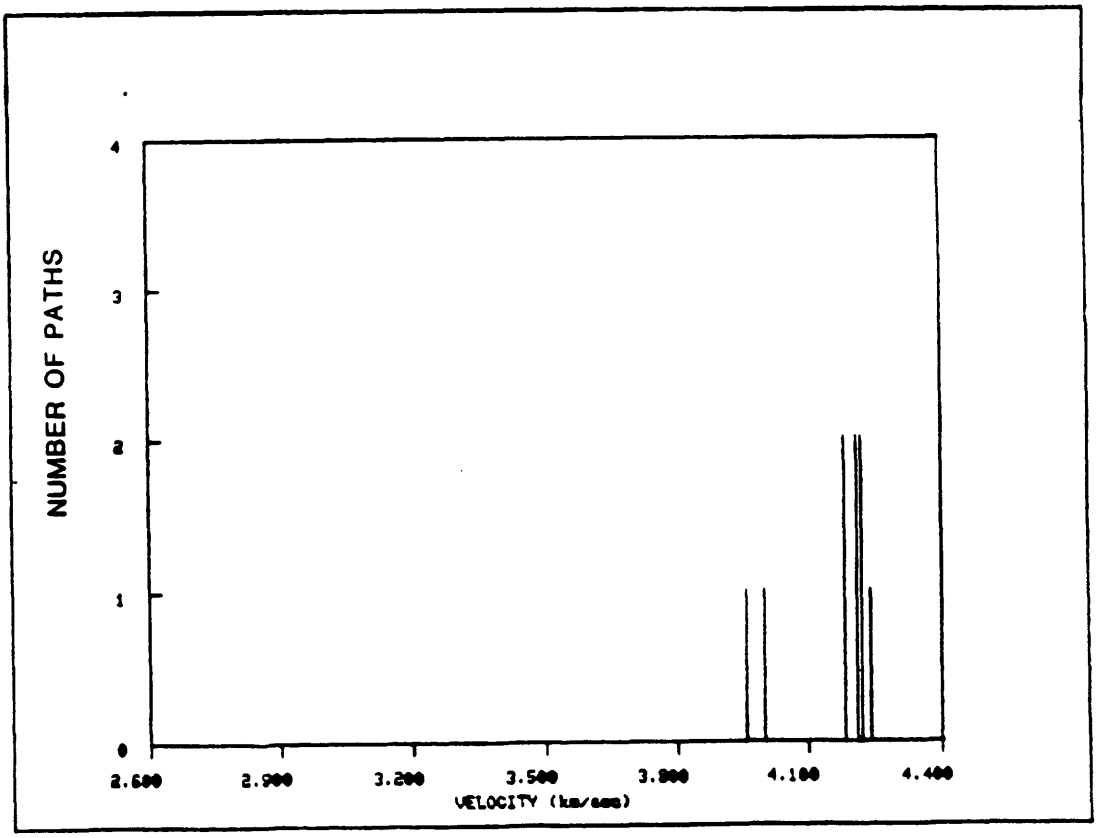

FIGURE A.9f REGION q

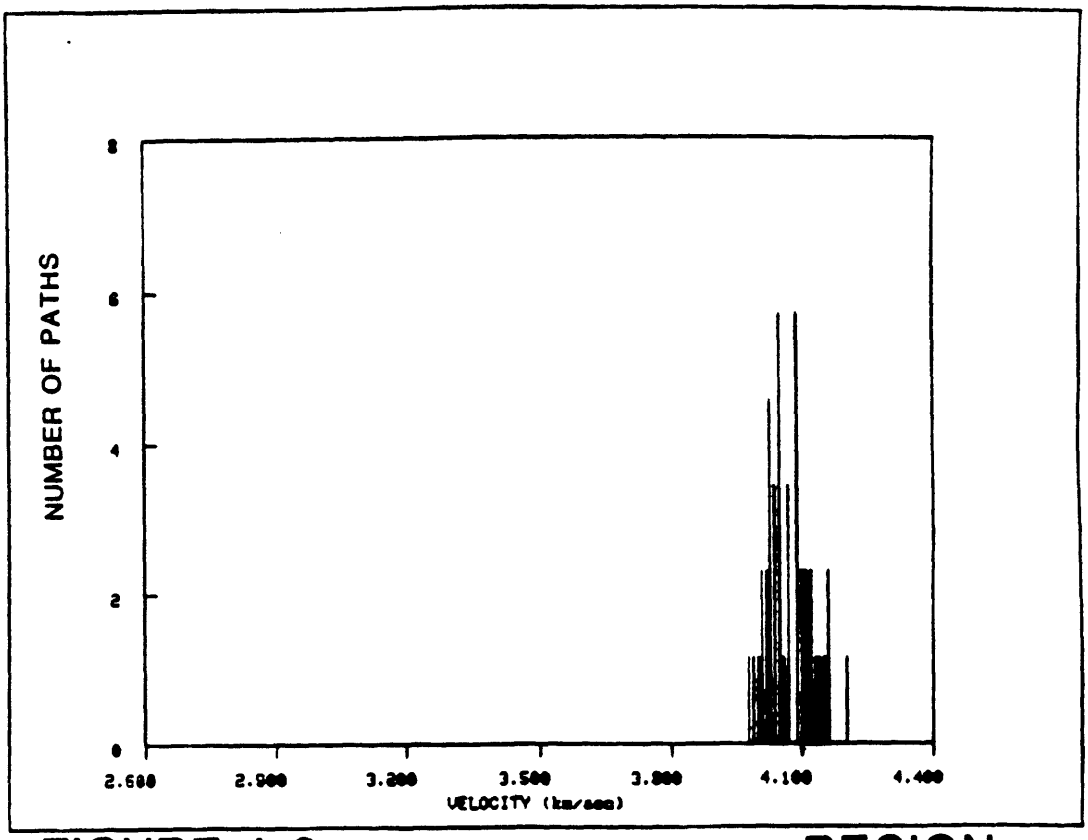

FIGURE A.9g REGION s

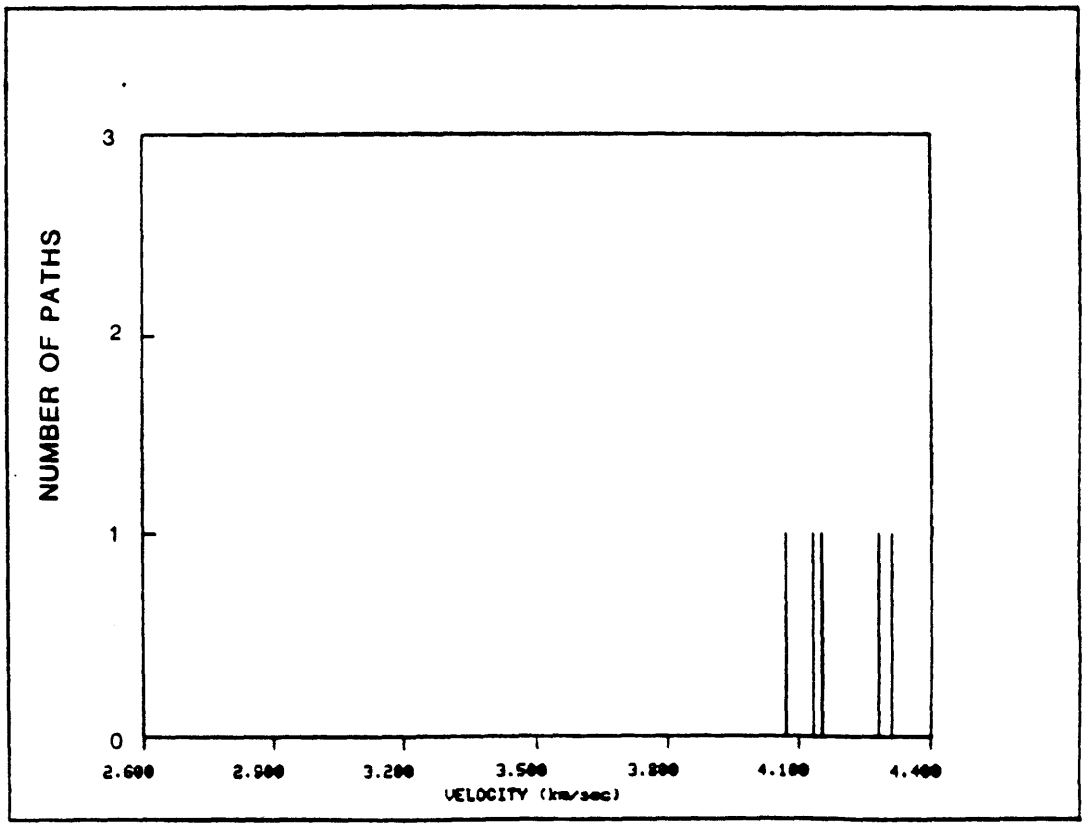

FIGURE A.9h REGION N

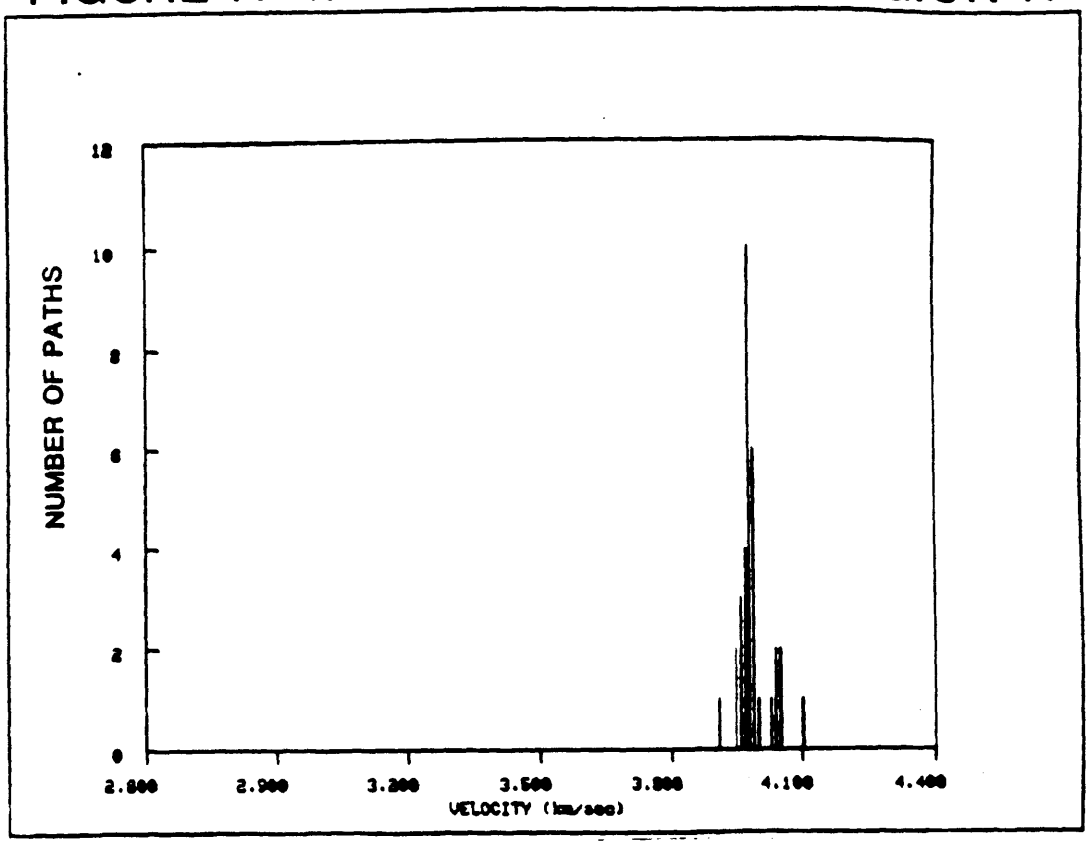

FIGURE A.9i REGION =

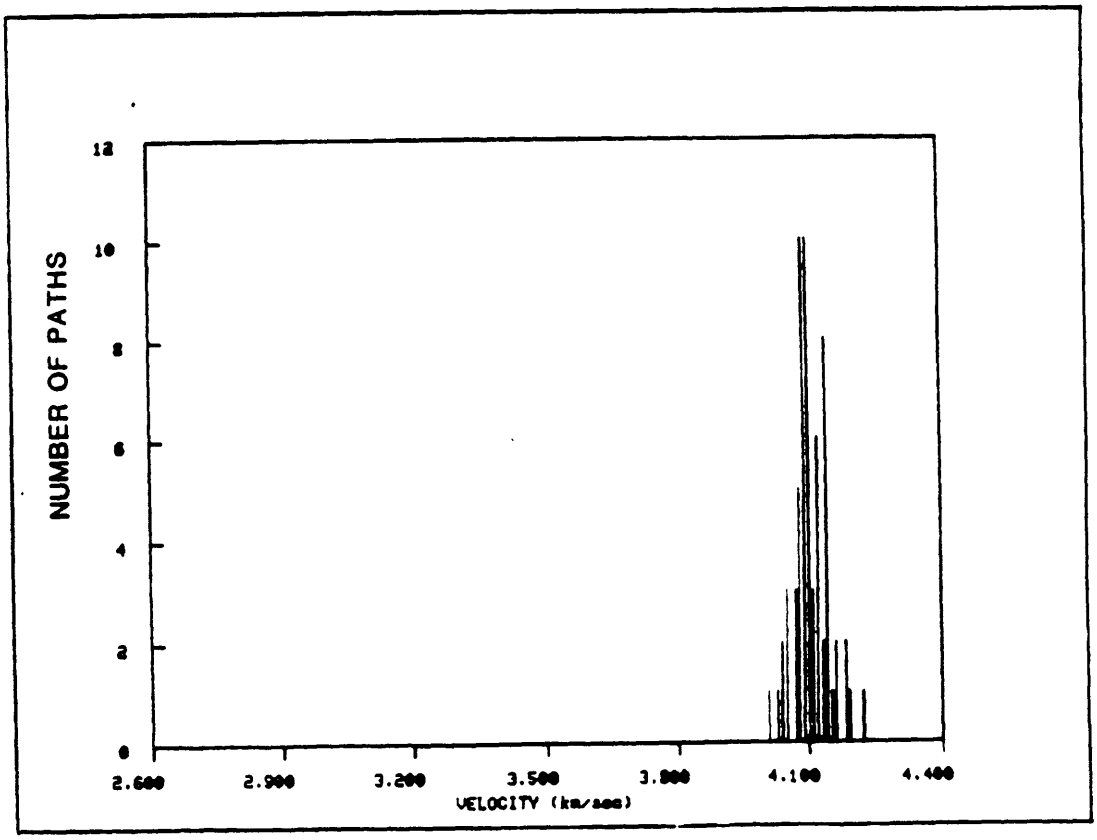

FIGURE A.9j REGION 0

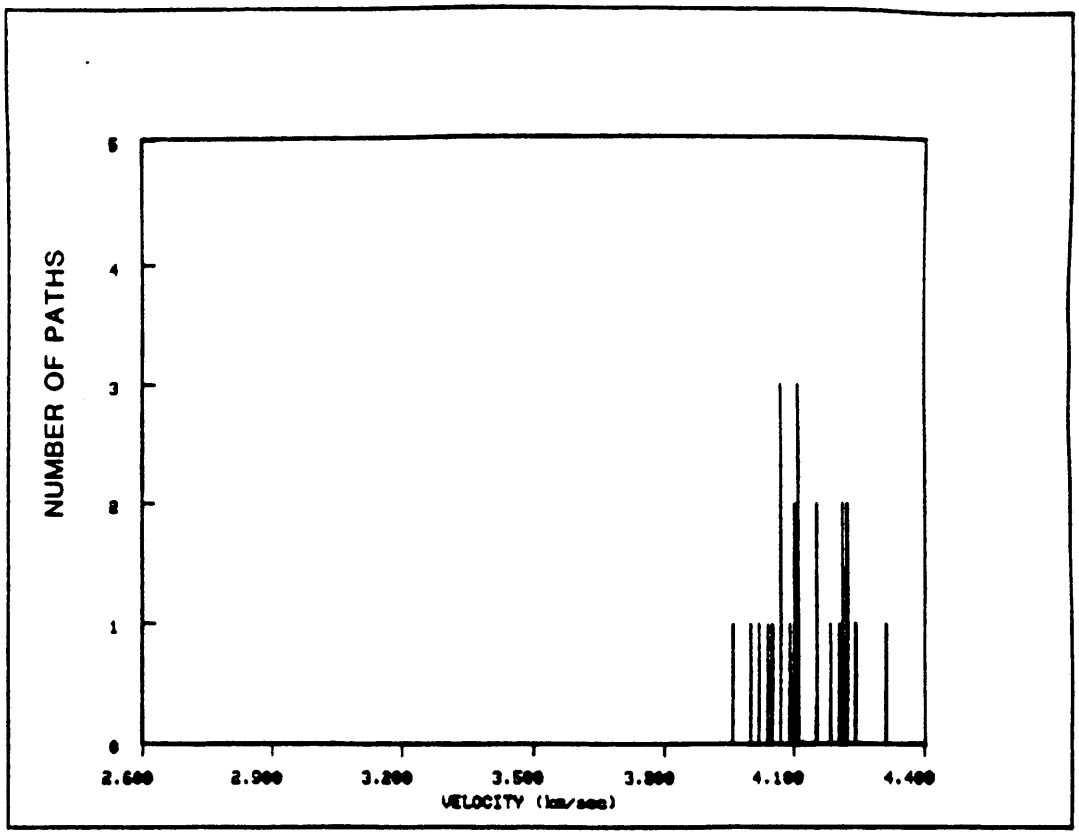

FIGURE A.9k REGION ~~0~~

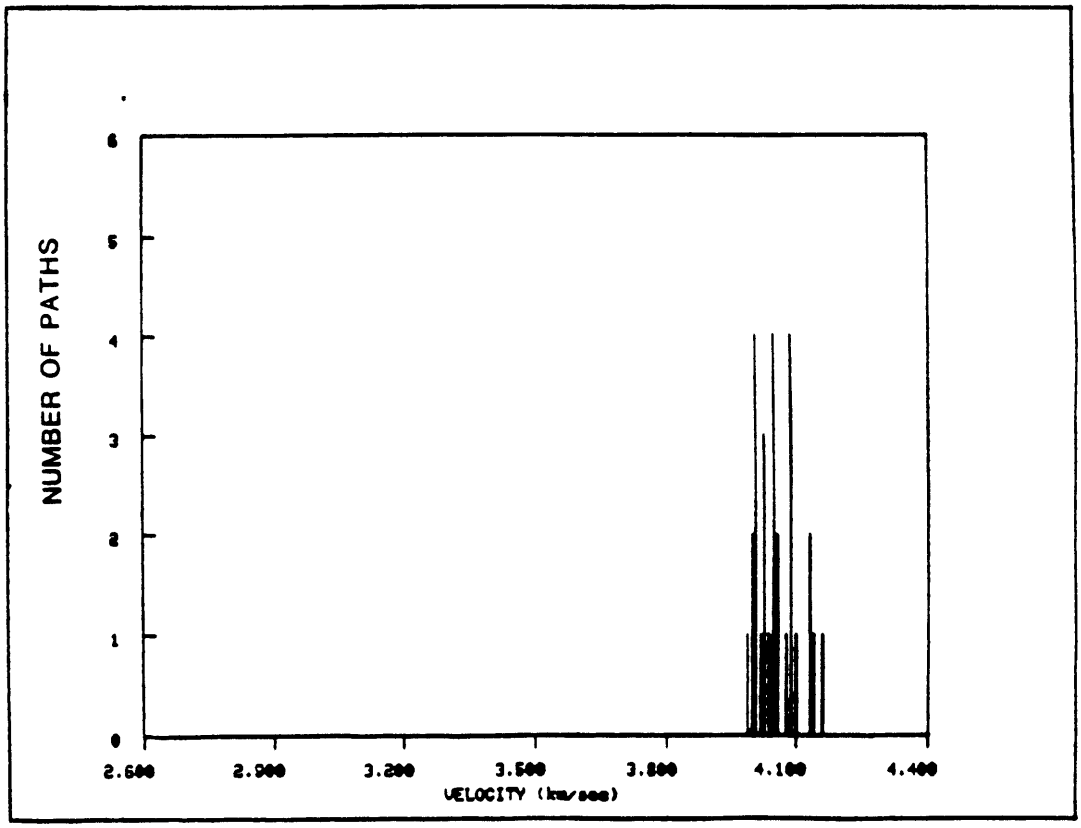

FIGURE A.9l REGION N

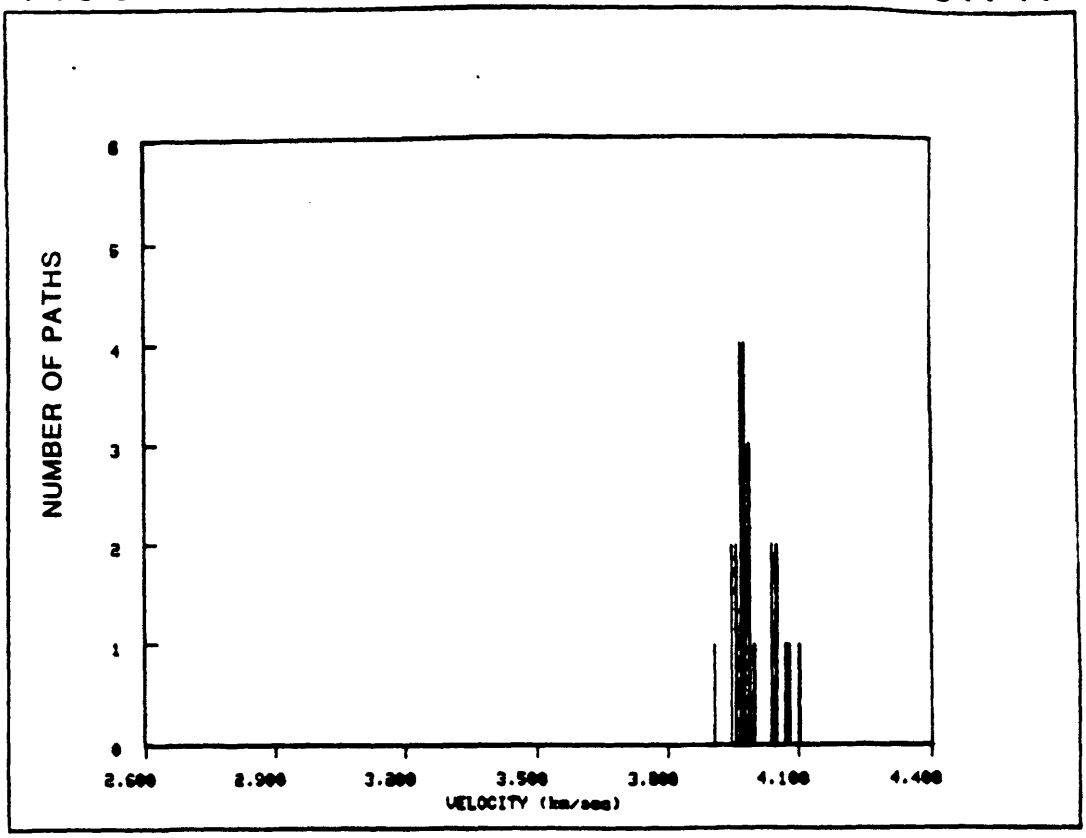

FIGURE A.9m REGION #

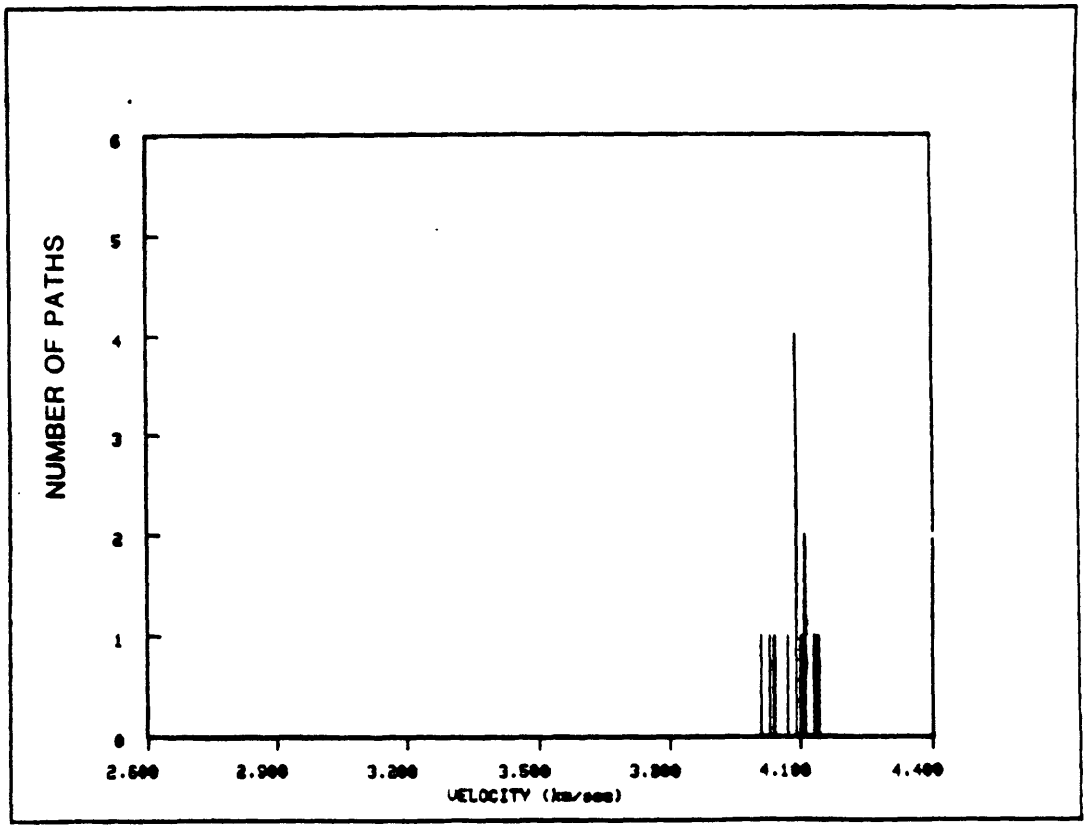

FIGURE A.9n REGION =

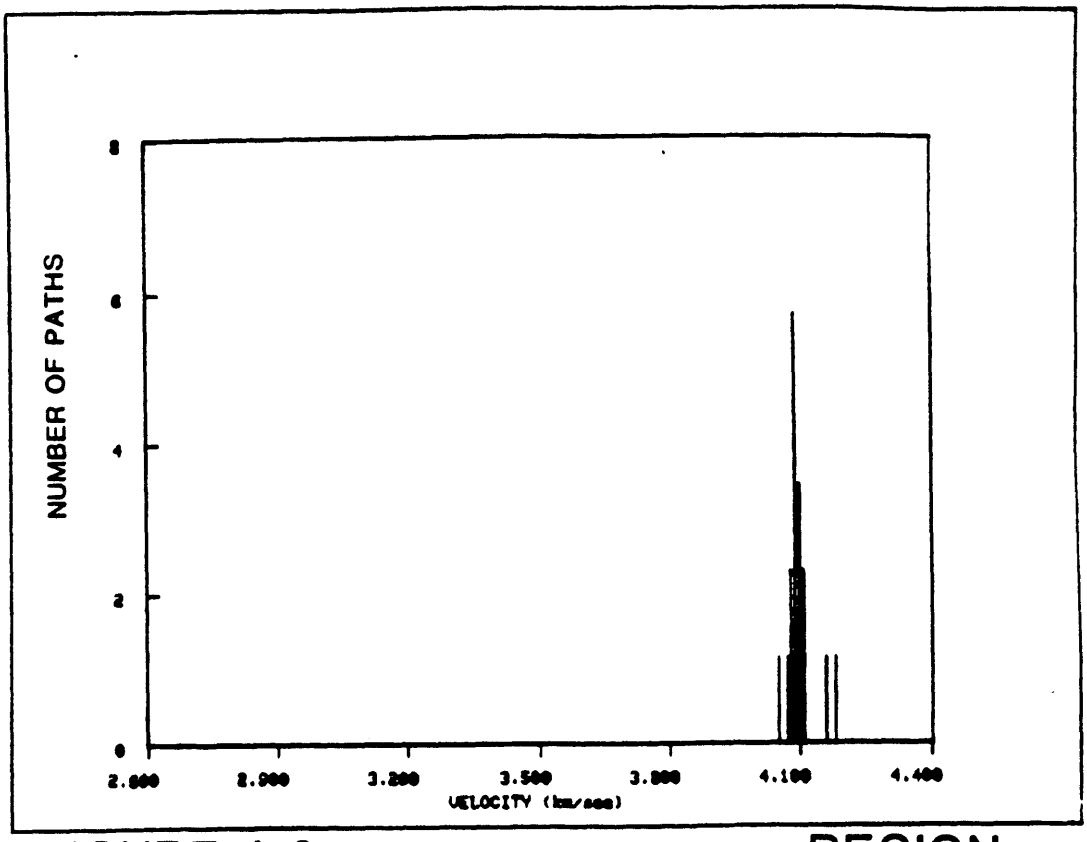

FIGURE A.9o REGION -

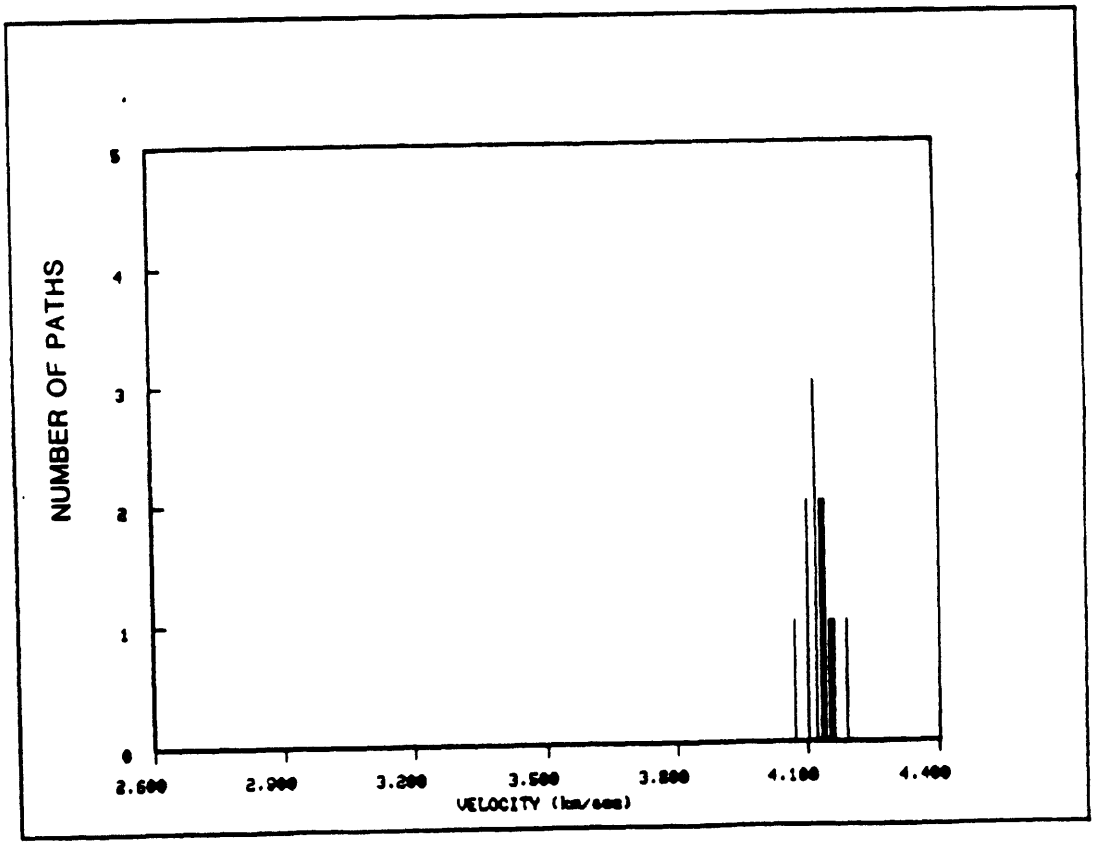

FIGURE A.9p REGION 0

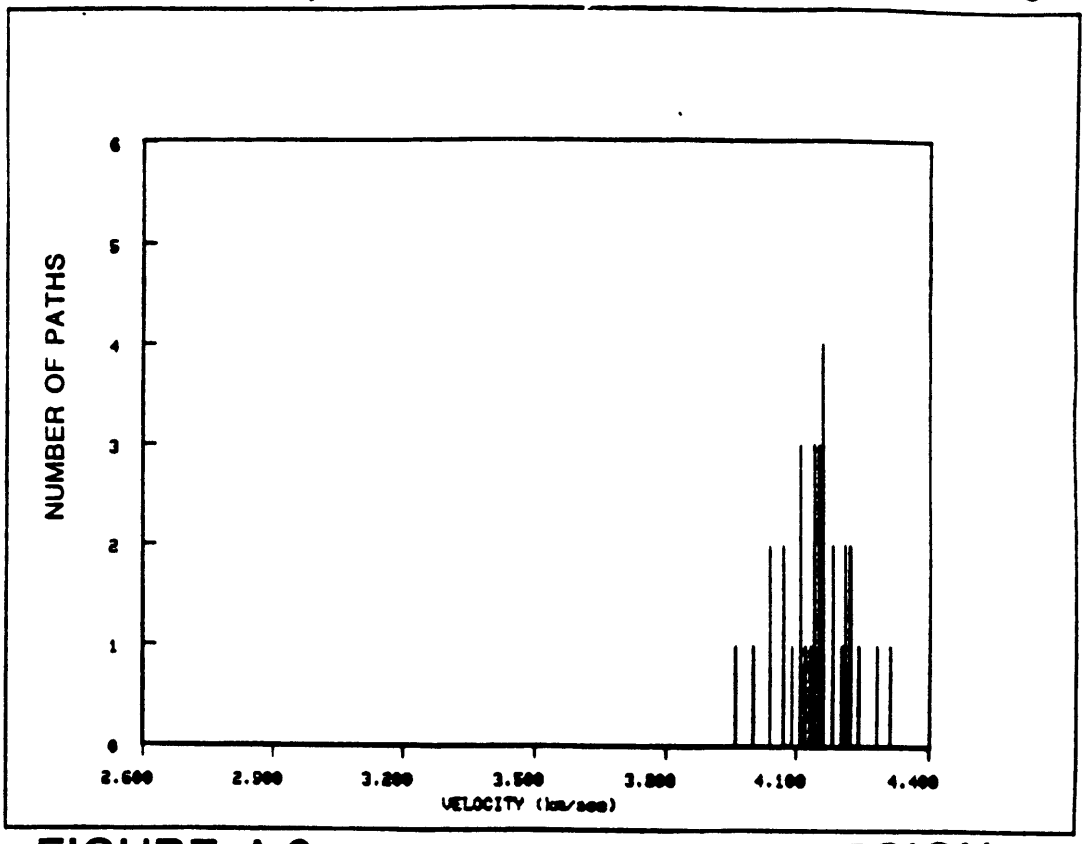

FIGURE A.9q REGION .

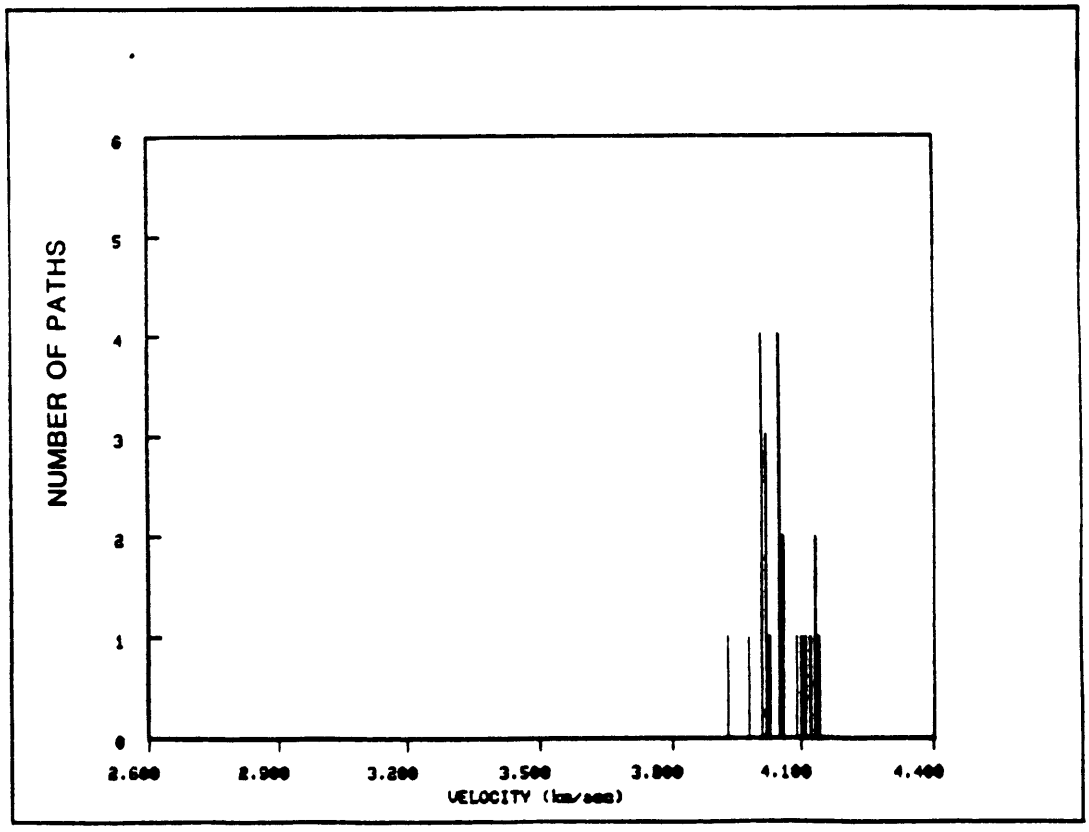

FIGURE A.9r

REGION ø

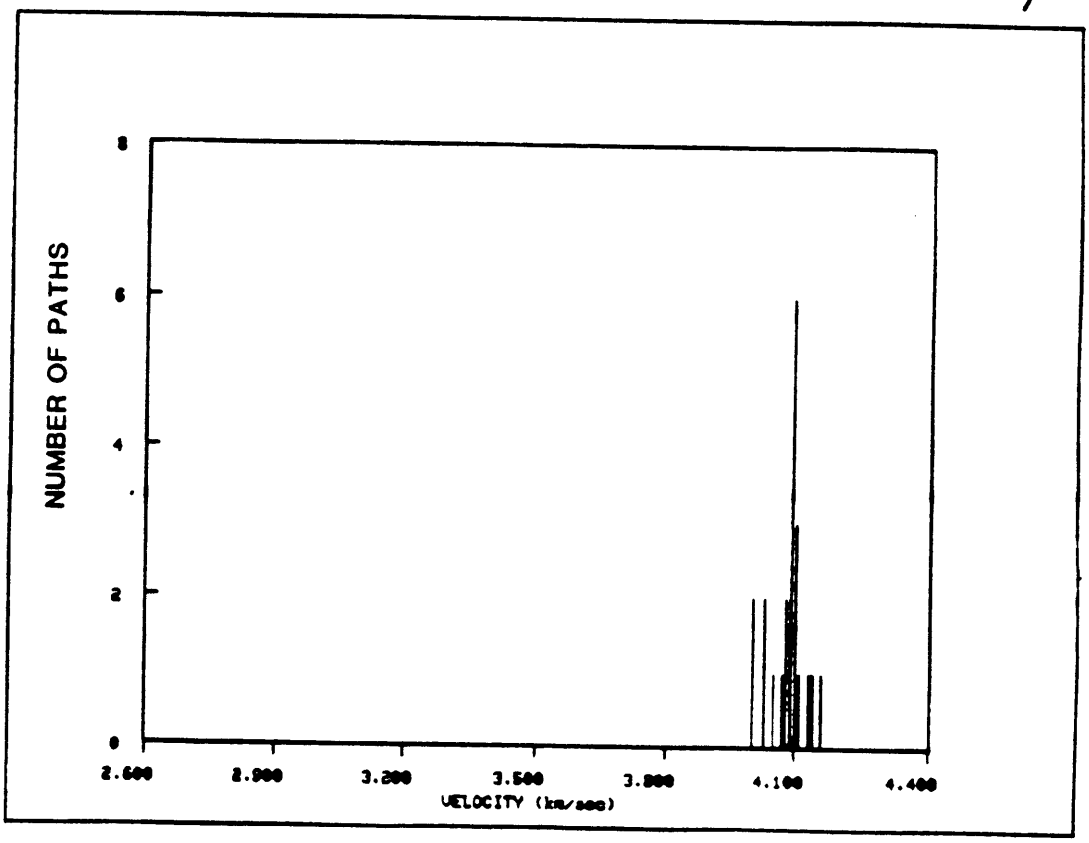

APPENDIX B

Comparison between observed and theoretical amplitude radiation pattern for each of the events studied

Figures B.1a thru B.45a - Geographical distribution of the greatcircle paths studied for earthquakes 1 thru 45 of Table 4.1. The latitude ranges from 75°N to 70°S in each map. The earthquake date is indicated on the top of each figure

Figures B.1 thru B.45 - indices b thru e - Comparison between calculated (dashed) amplitude radiation pattern, and observed amplitude at each station (which consecutive values are connected by a straight line). Calculated values were computed by Equation (4.11) and the source information of Table 4.1, and the observed values reduced using Equation (4.12). Indices b thru e refer to the reference periods 30, 50, 70, and 98 sec, respectively.

FIGURE B. 1a

05/25/64

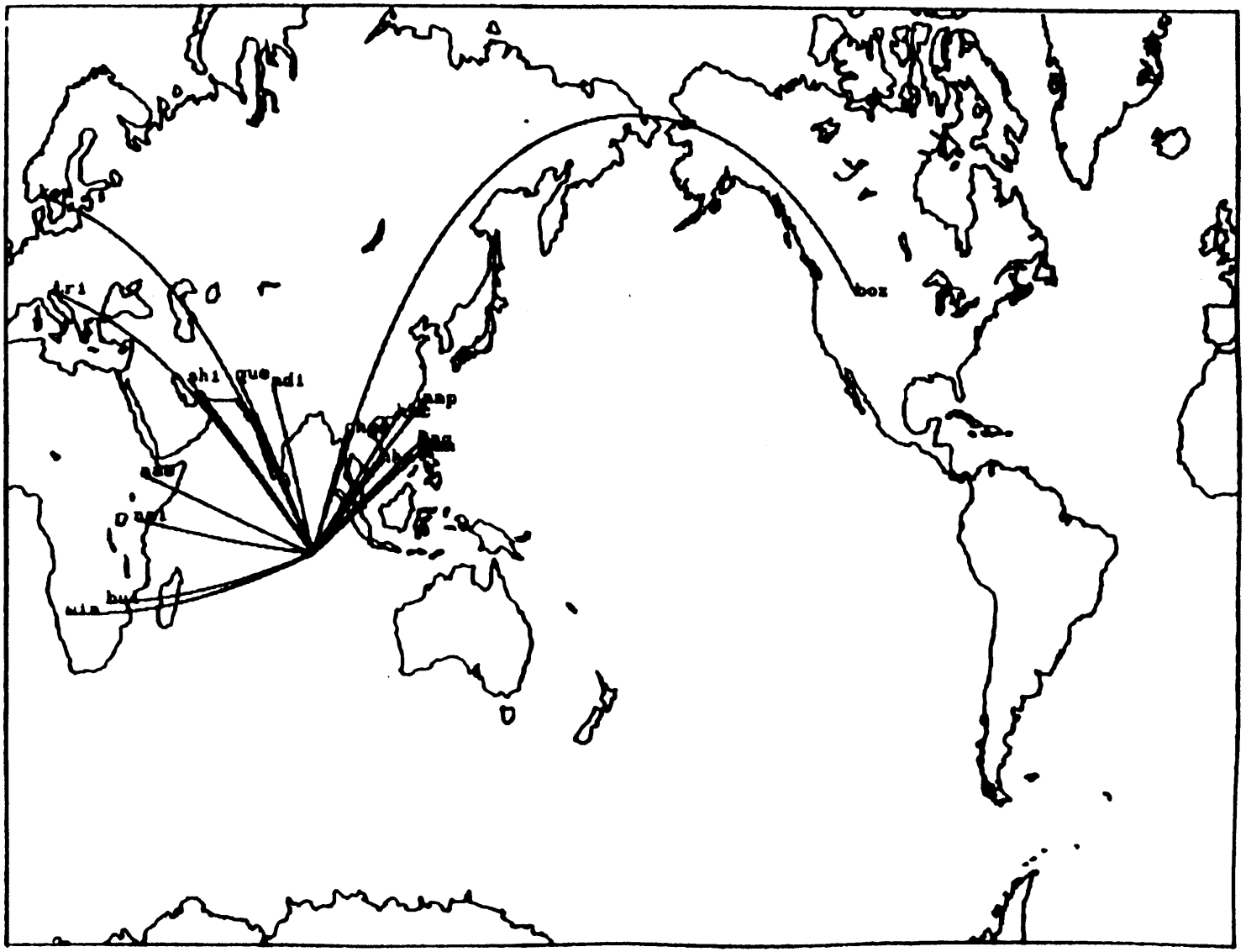

FIGURE B. 1b

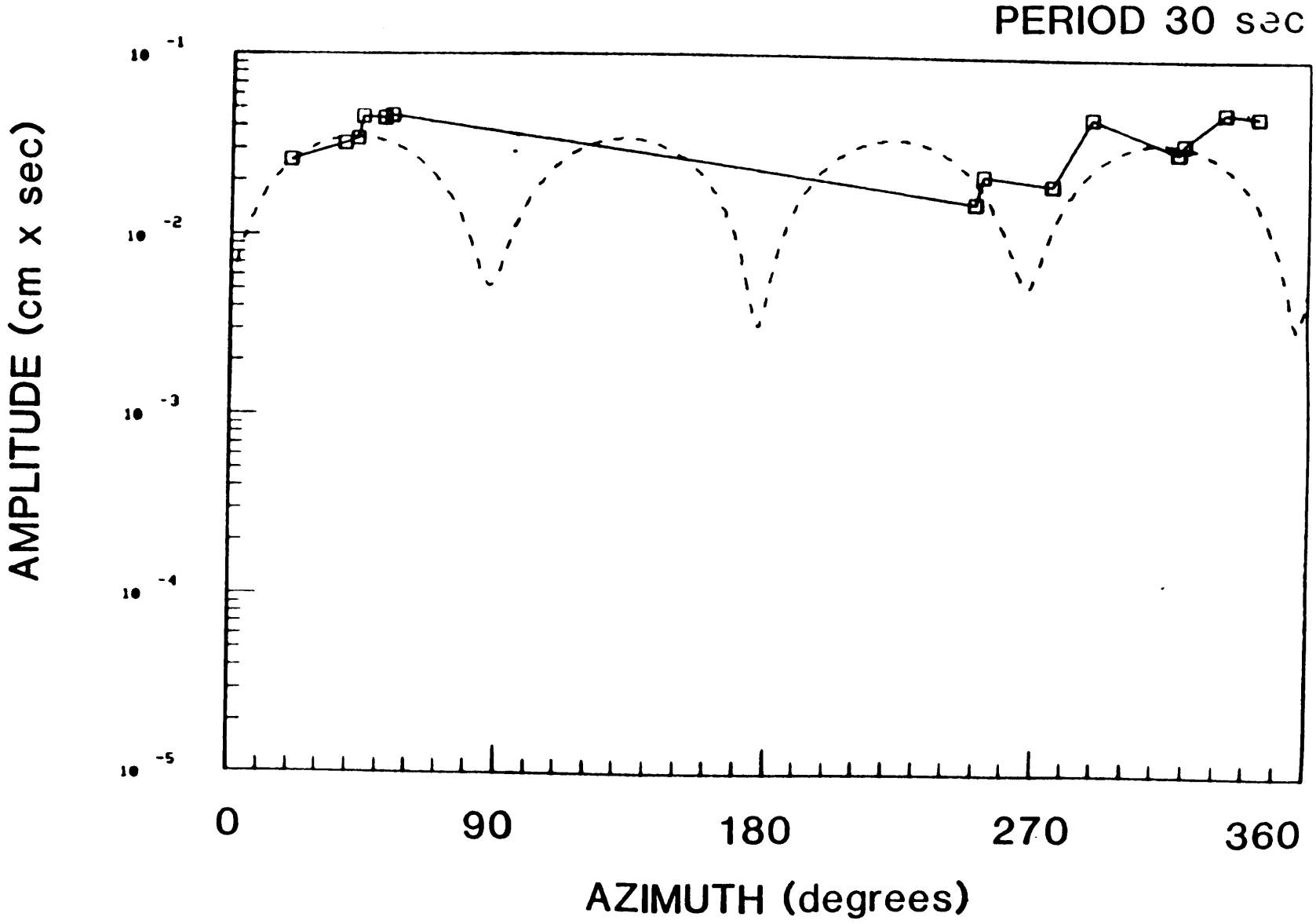
PERIOD 30 sec
AMPLITUDE (cm x sec)
10 -1
10 -2
10 -3
10 -4
10 -5
0
90
180
270
360
AZIMUTH (degrees)

FIGURE B. 1c

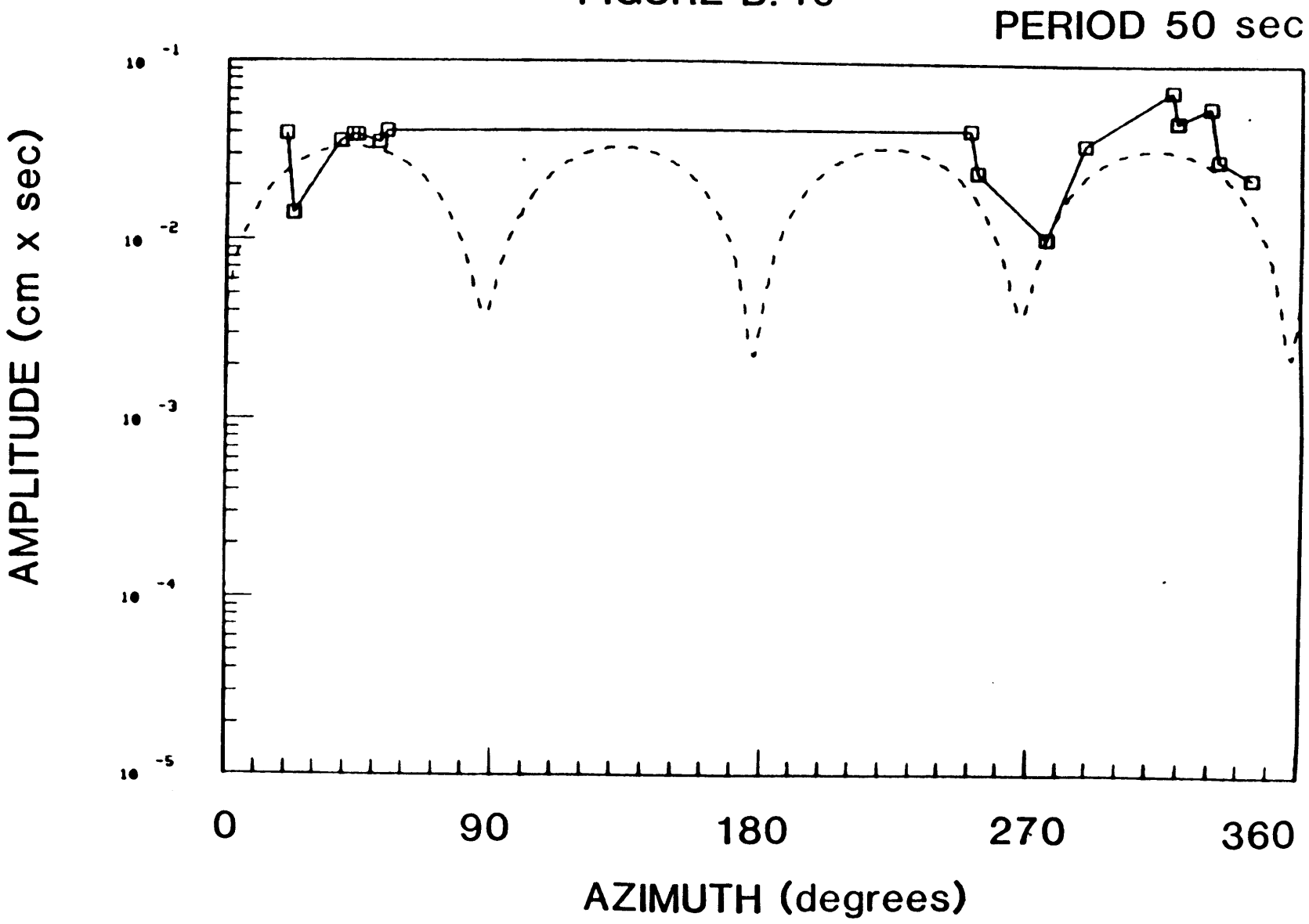
PERIOD 50 sec
AMPLITUDE (cm x sec)
10 -1
10 -2
10 -3
10 -4
10 -5
0
90
180
270
360
AZIMUTH (degrees)

FIGURE B. 1d

PERIOD 70 sec

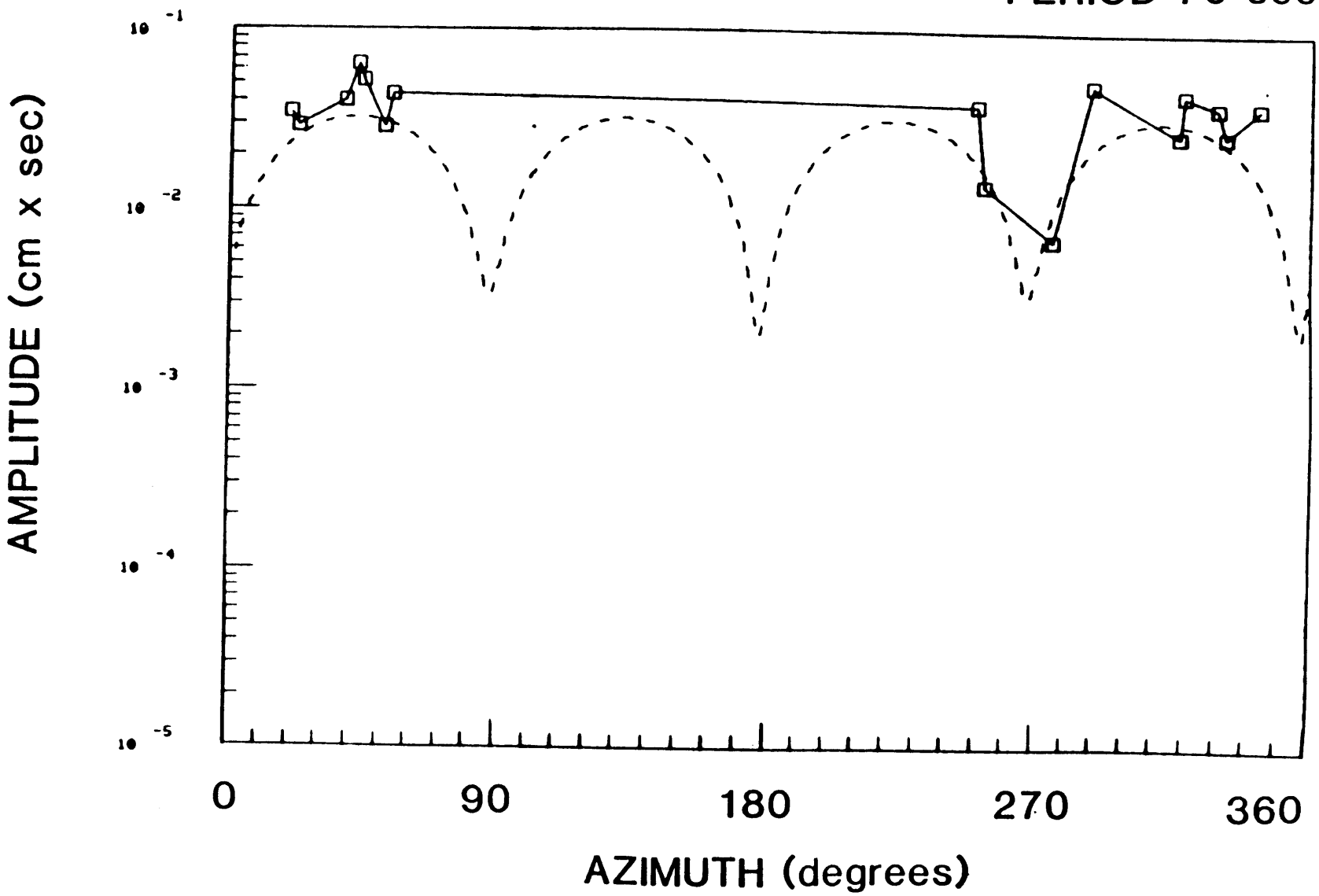

FIGURE B. 1e

PERIOD 98 sec

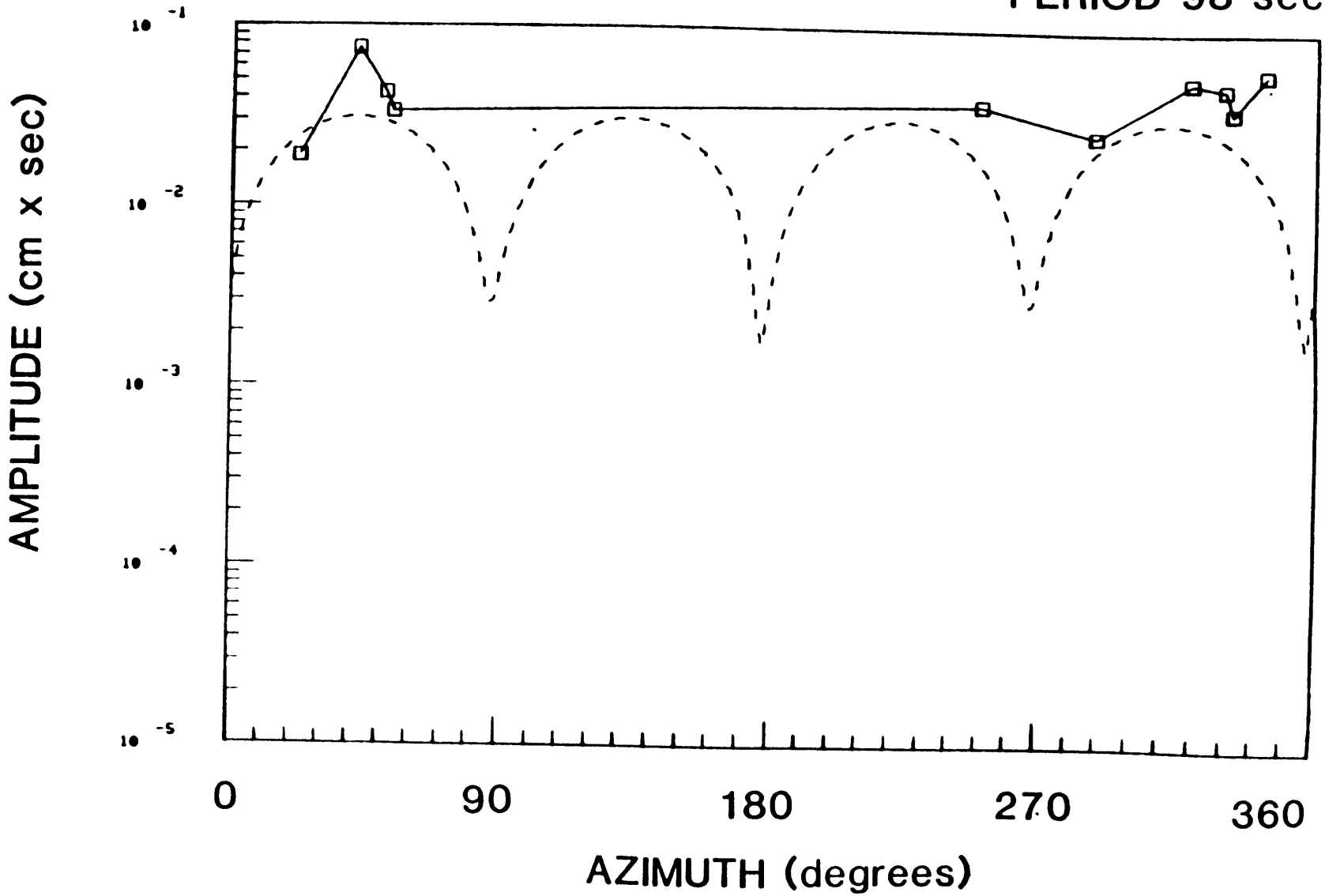

FIGURE B.2a

08/25/64

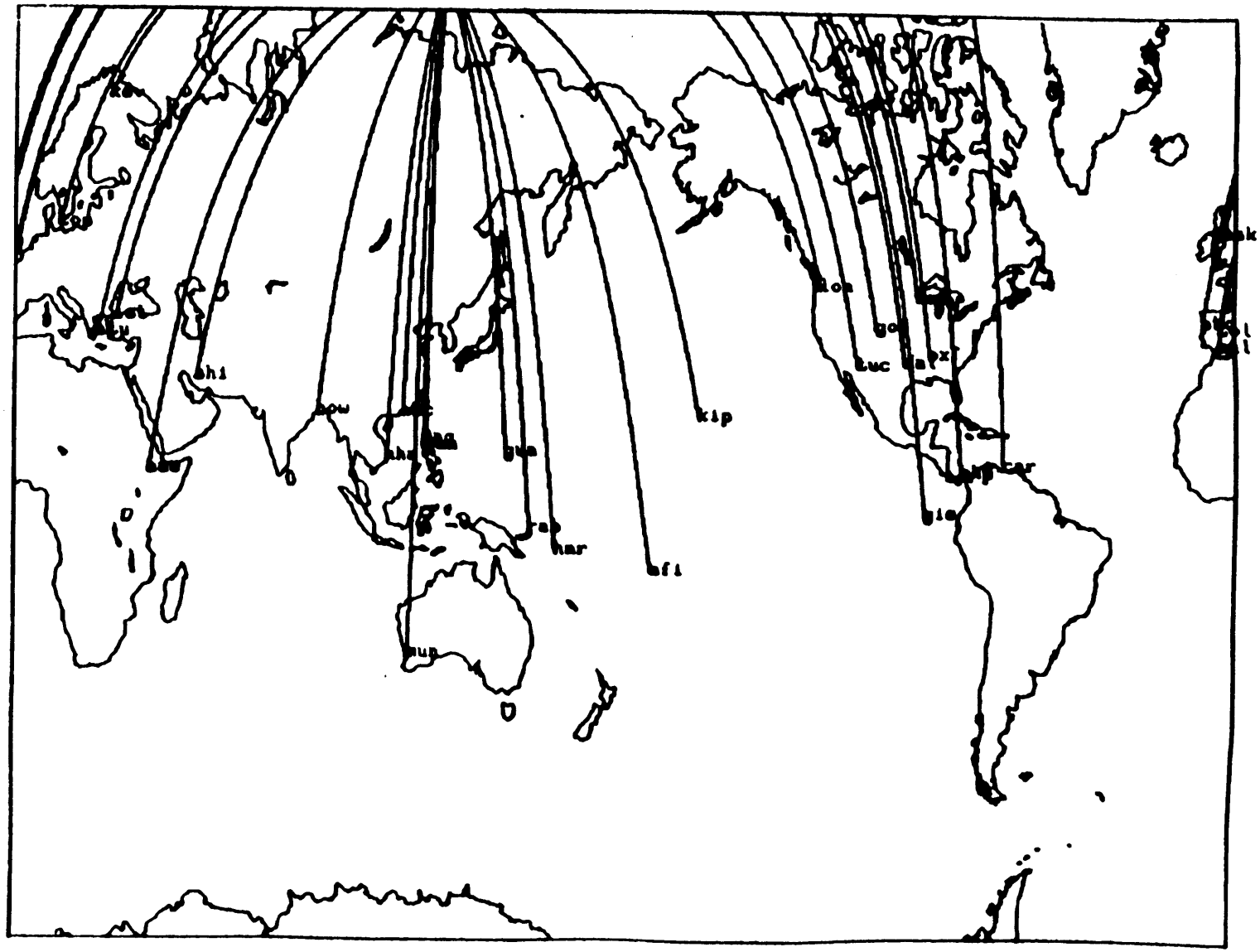

FIGURE B. 2b

PERIOD 30 sec

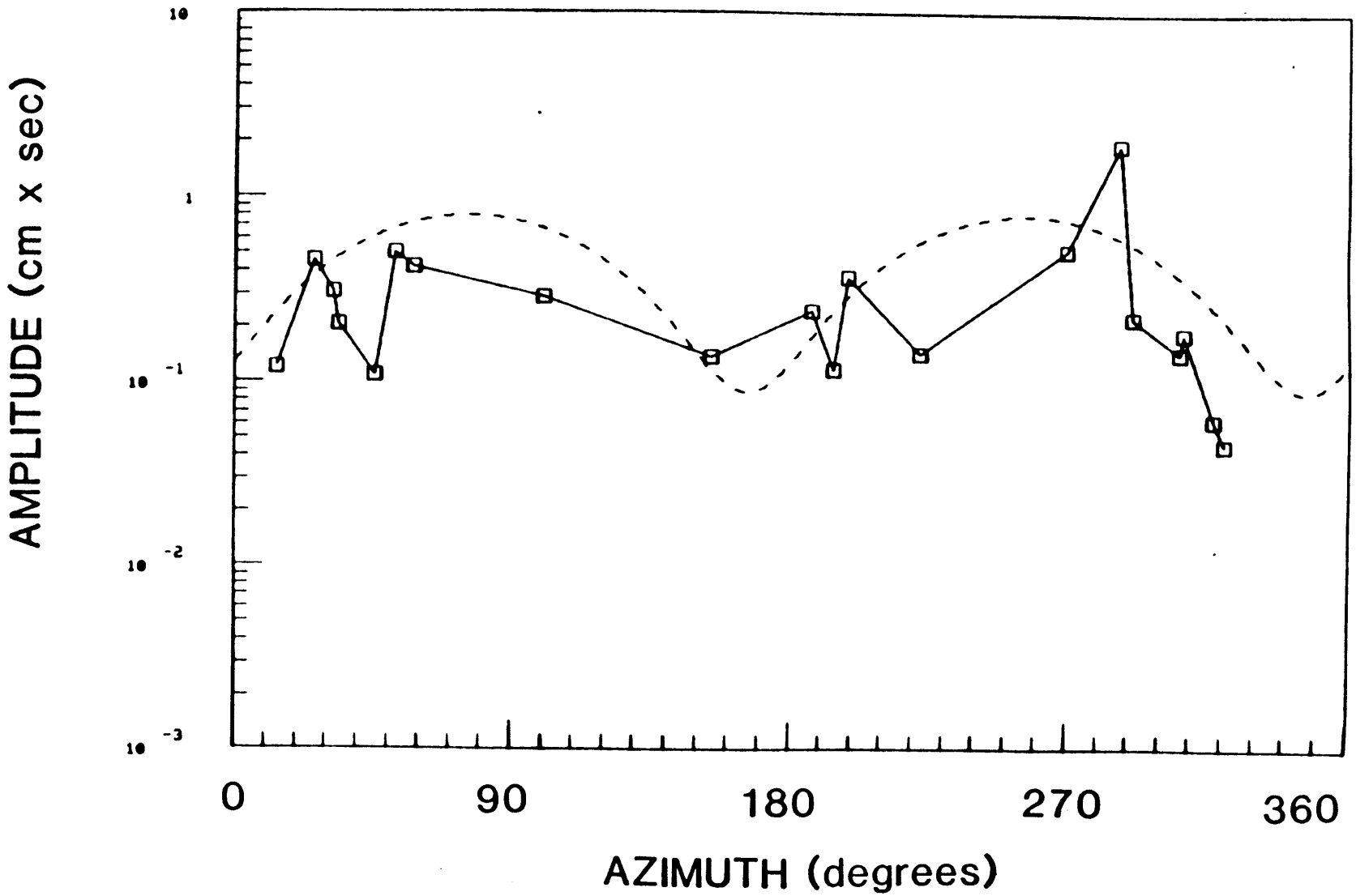

FIGURE B. 2c

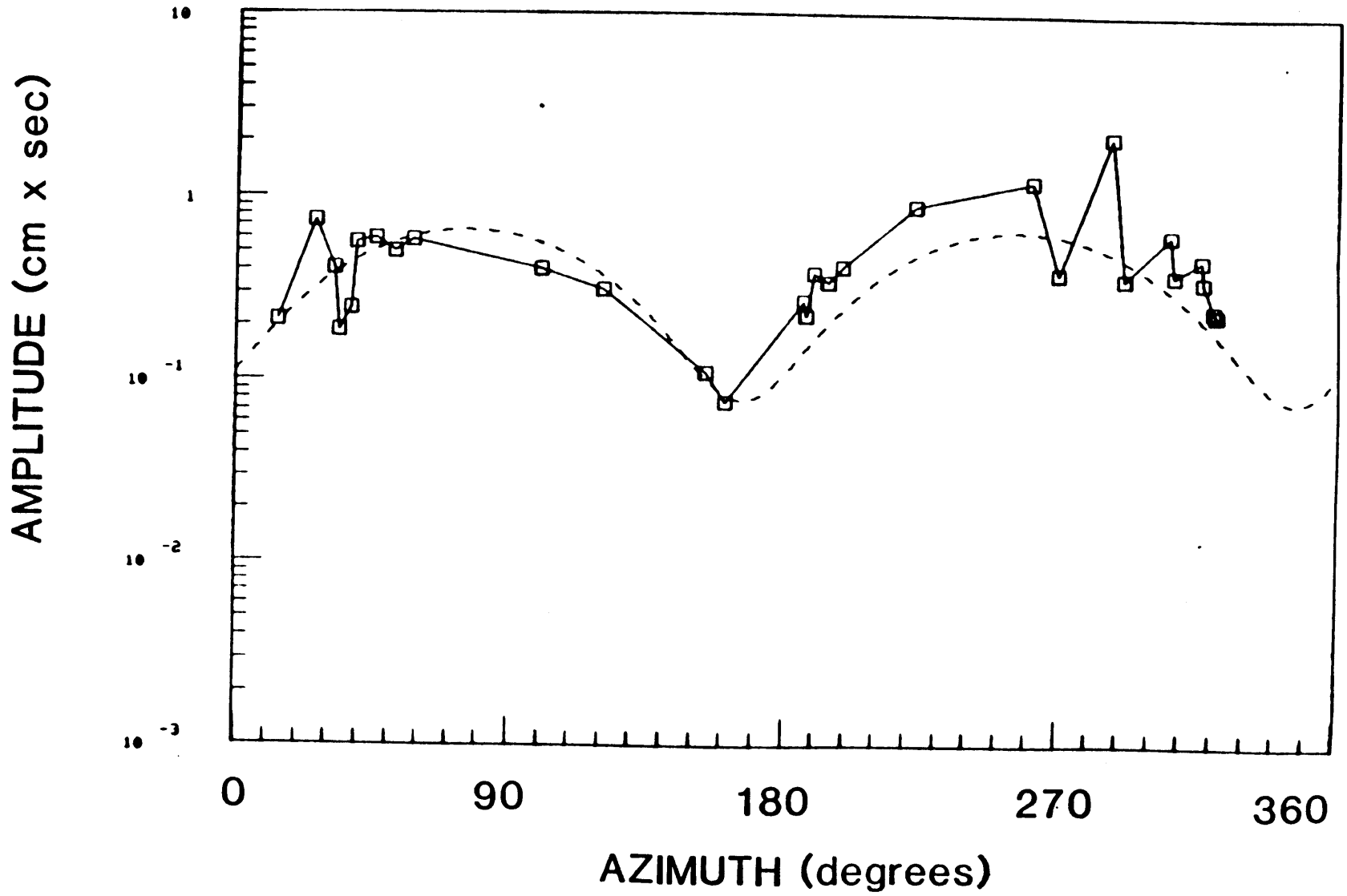
PERIOD 50 sec
AMPLITUDE (cm x sec)
10
1
10 -1
10 -2
10 -3
0
90
180
270
360
AZIMUTH (degrees)

FIGURE B.2d

PERIOD 70 sec

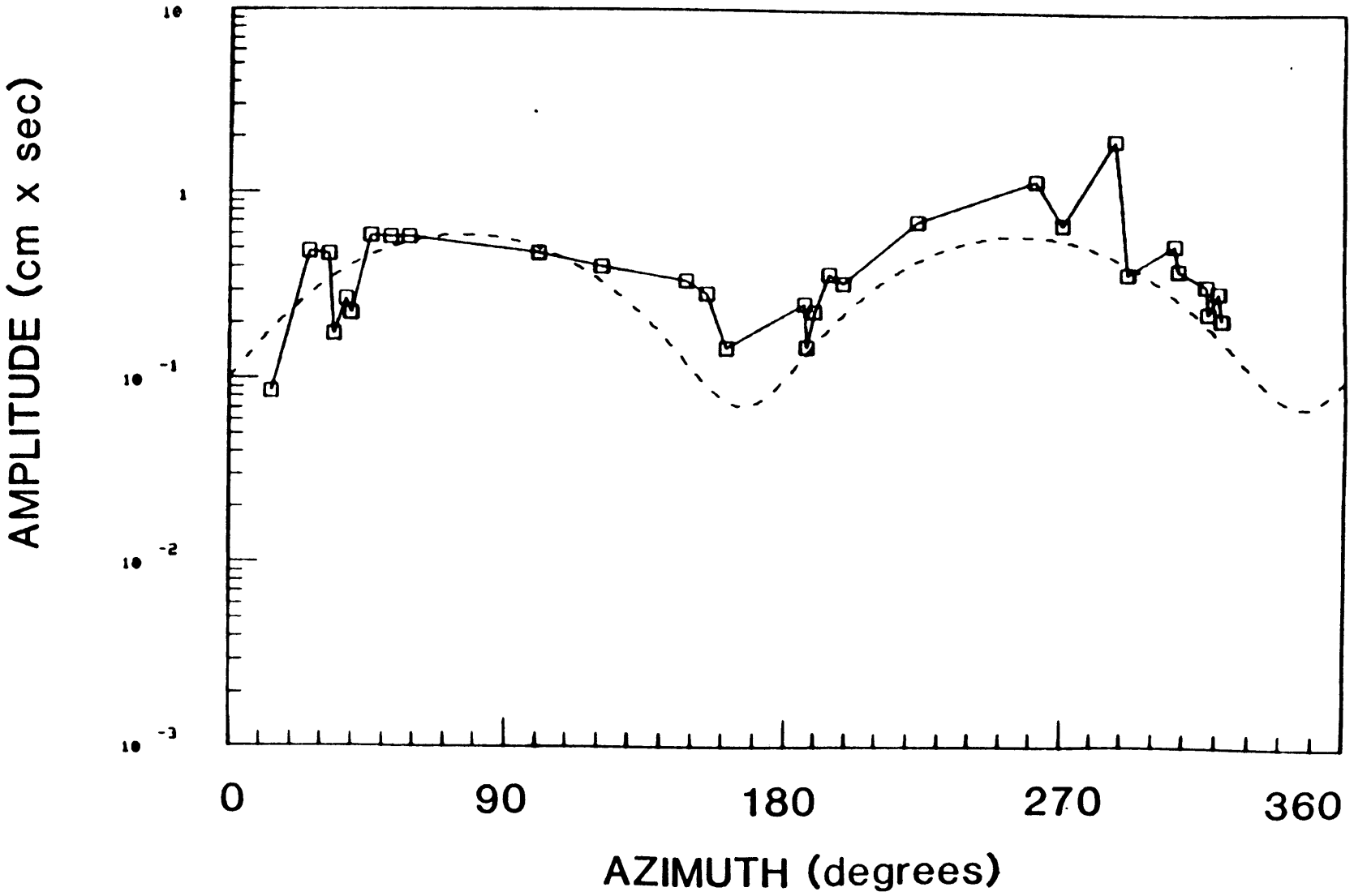

FIGURE B. 2e

PERIOD 98 sec

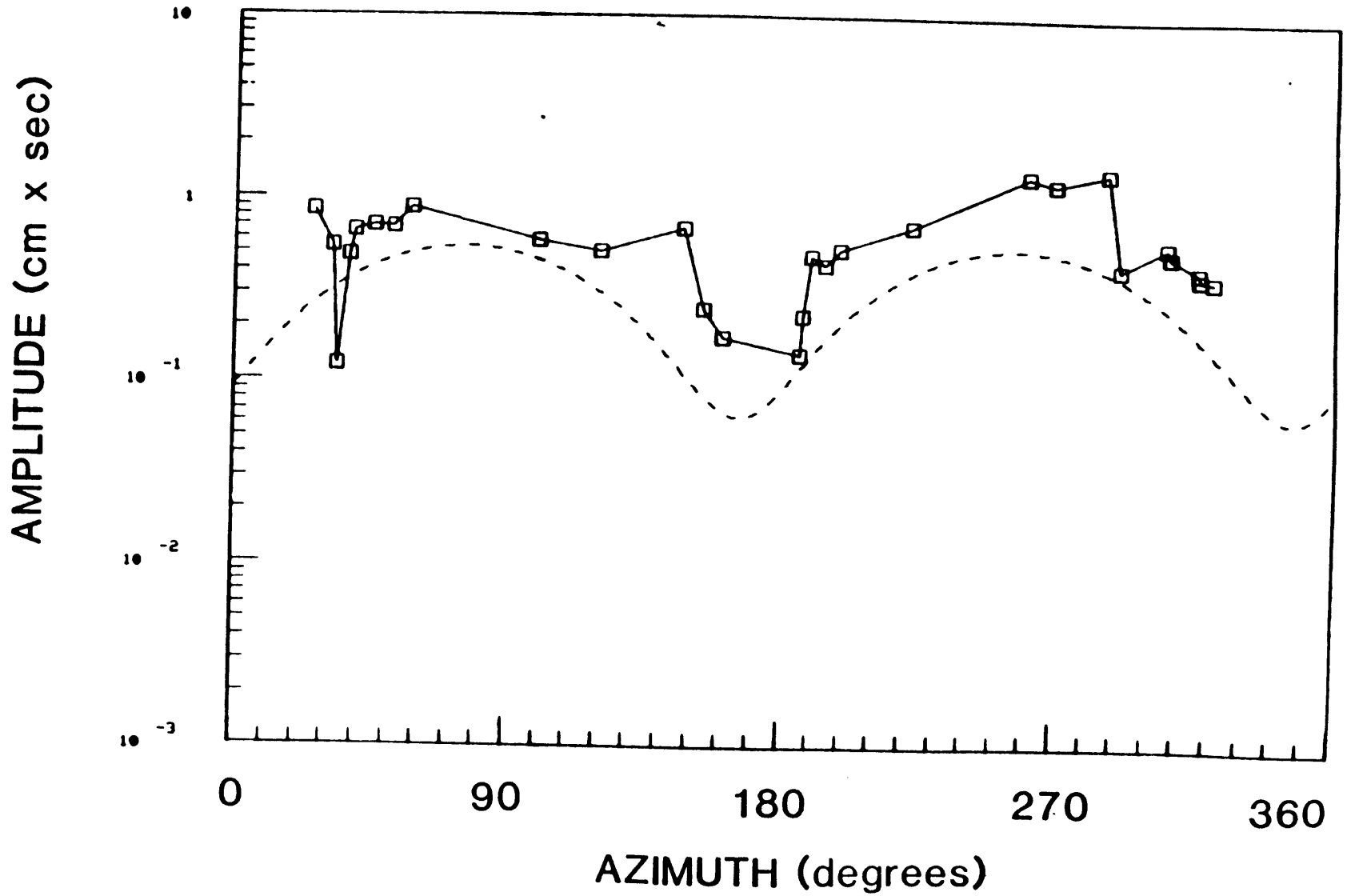

FIGURE B.3 a

10/23/64

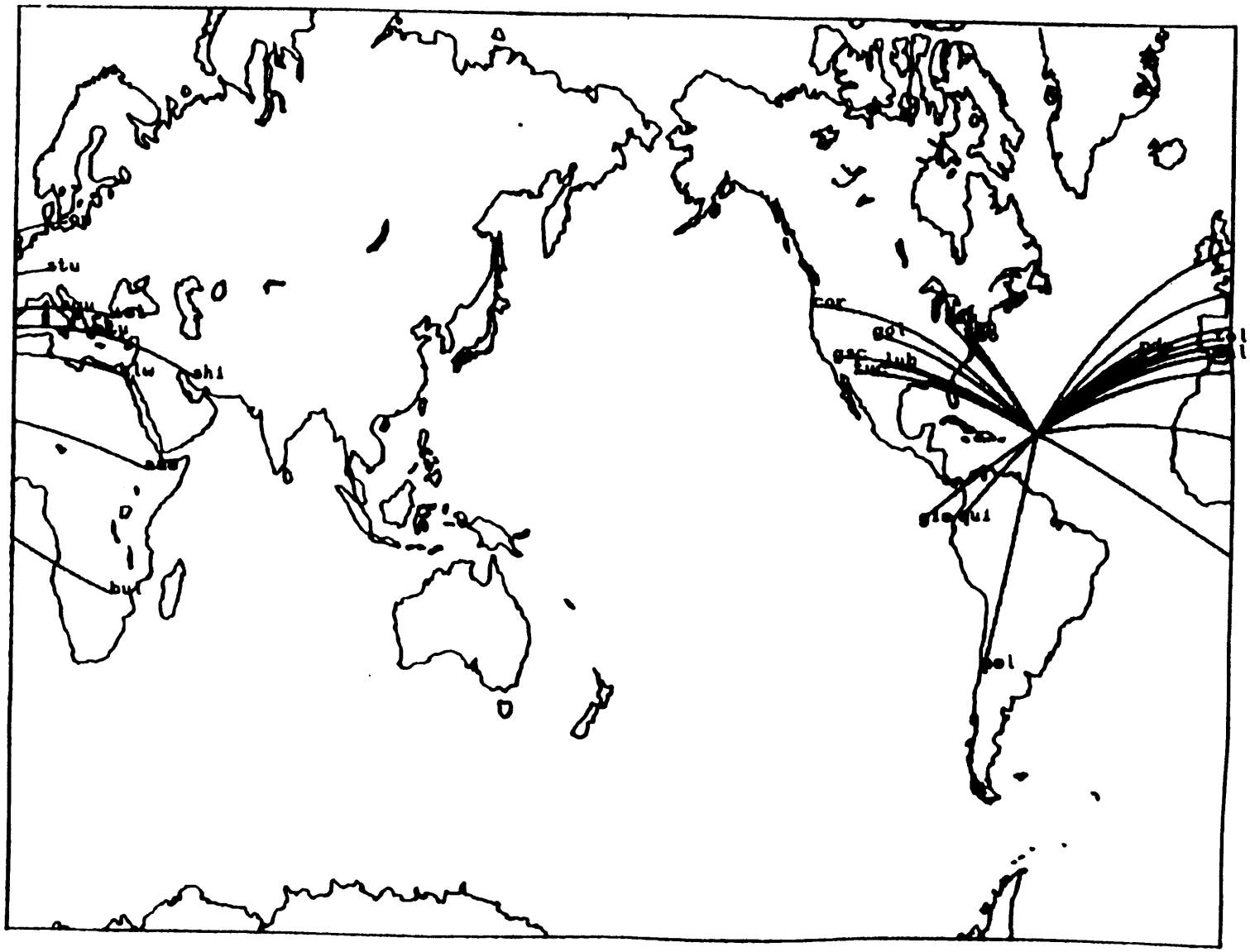

FIGURE B. 3b

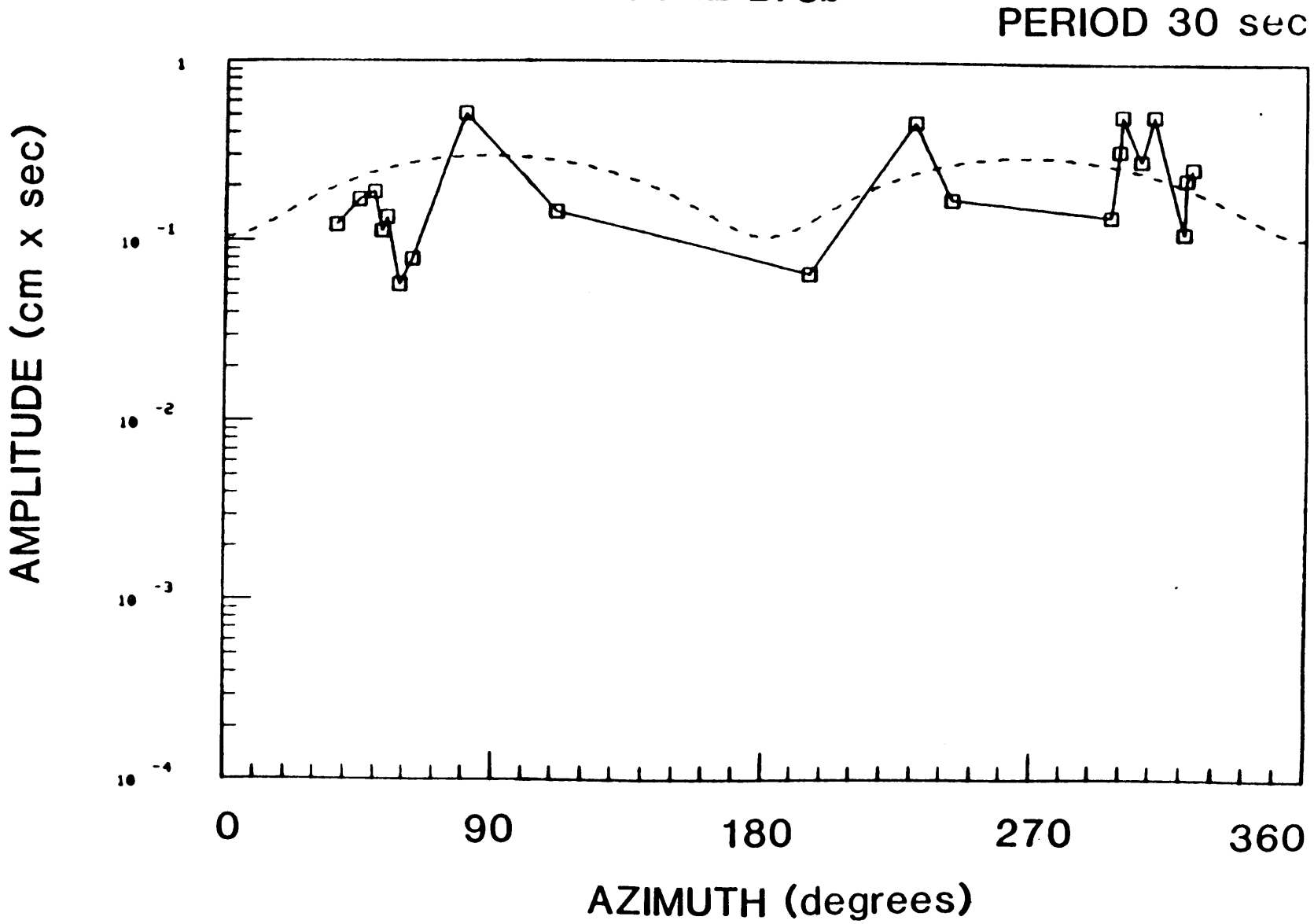
PERIOD 30 sec
AMPLITUDE (cm x sec)
1
10 -1
10 -2
10 -3
10 -4
0
90
180
270
360
AZIMUTH (degrees)

FIGURE B.3c

PERIOD 50 sec

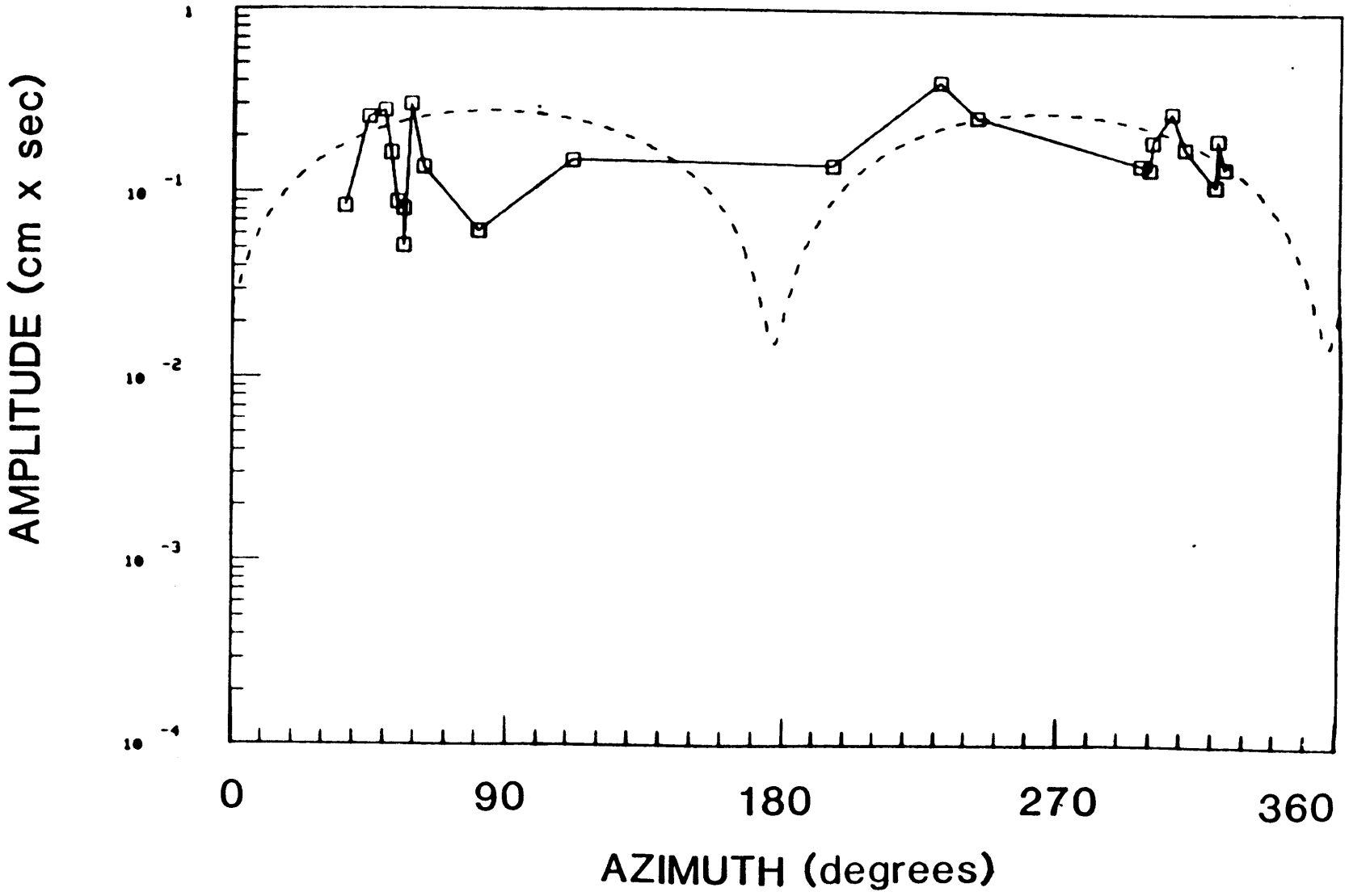

FIGURE B. 3d

PERIOD 70 sec

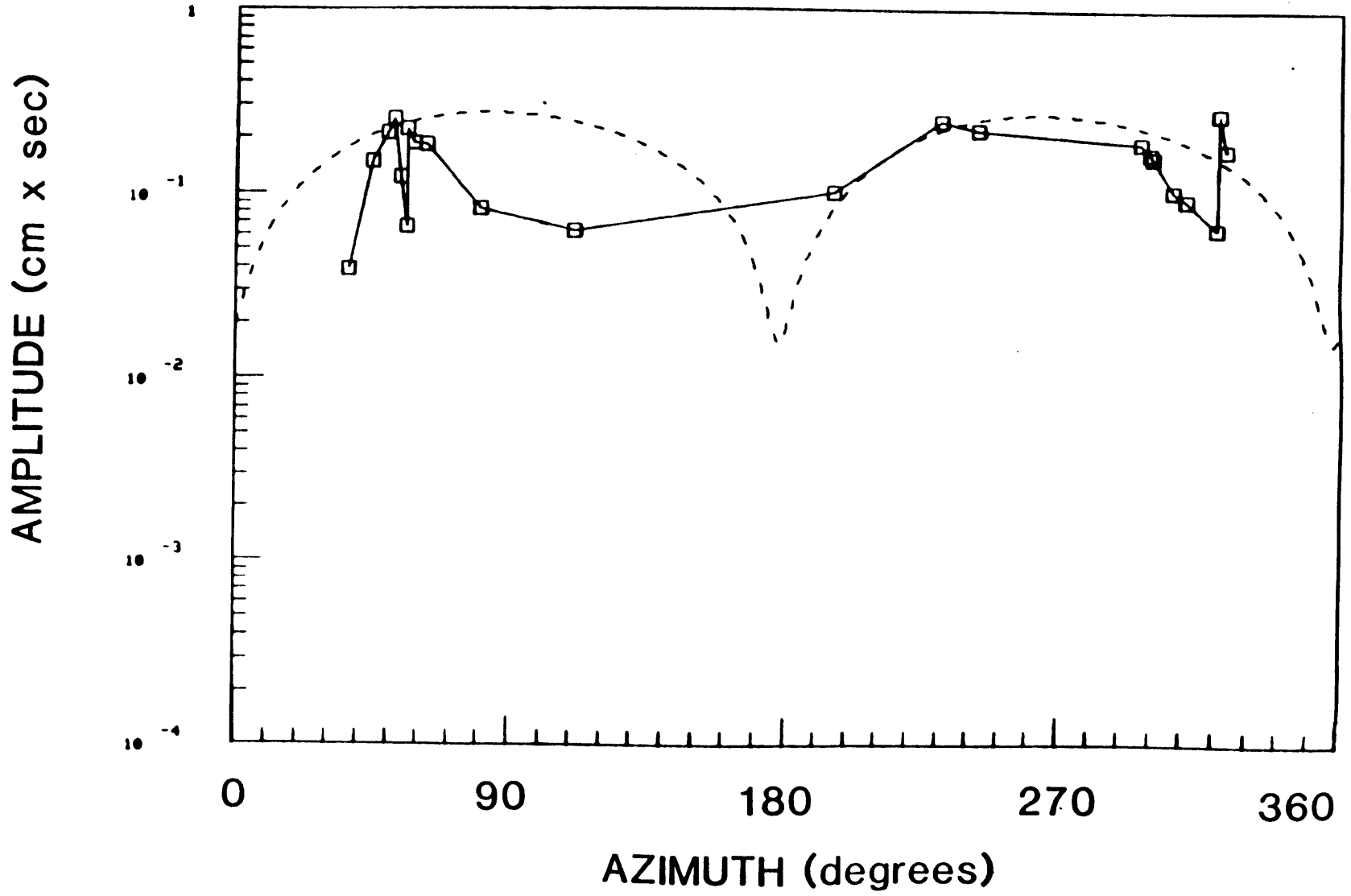

FIGURE B.3e

PERIOD 98 sec

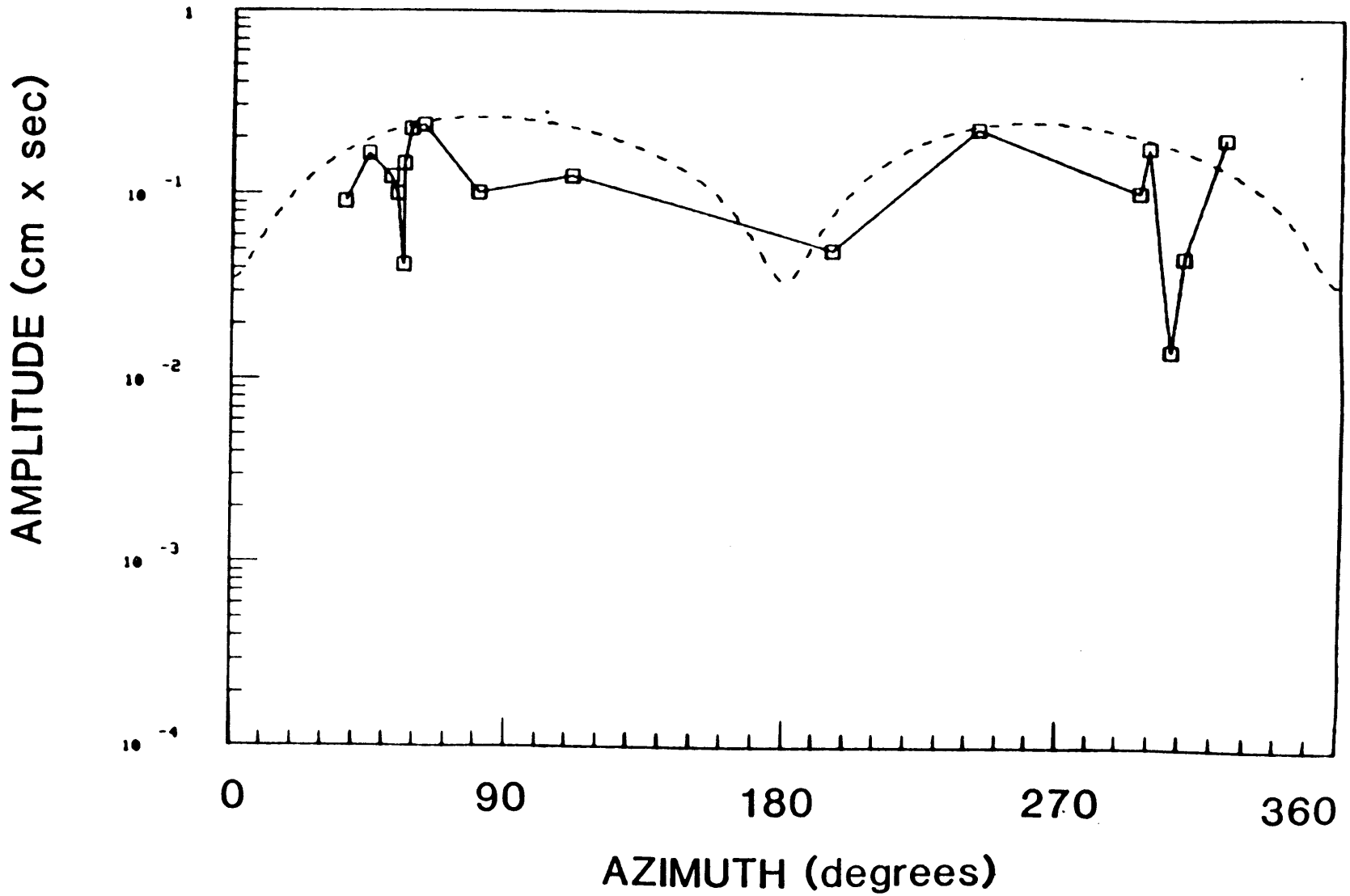

FIGURE B.4a

09/09/65

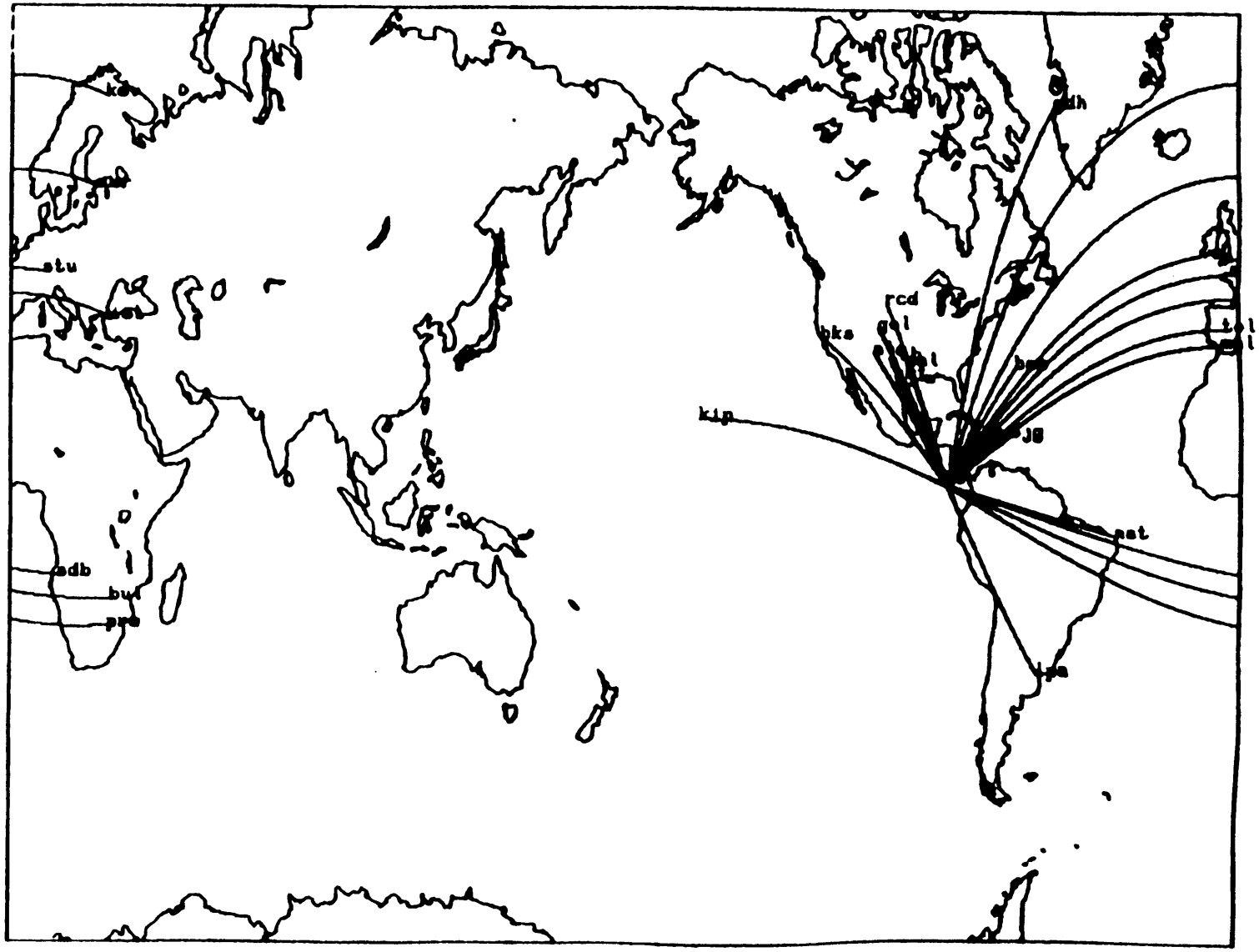

FIGURE B. 4b

PERIOD 30 sec

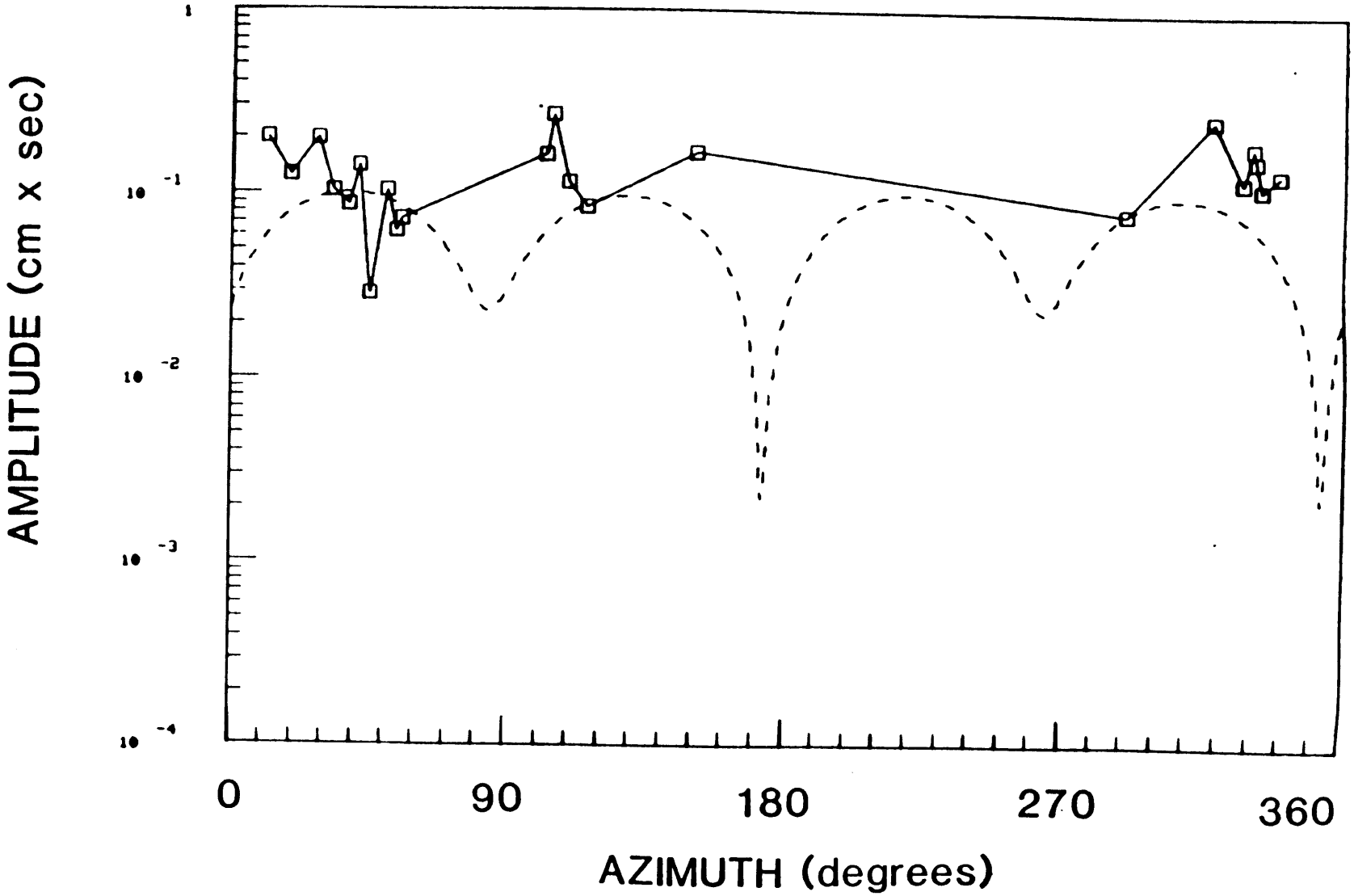

FIGURE B.4c

PERIOD 50 sec

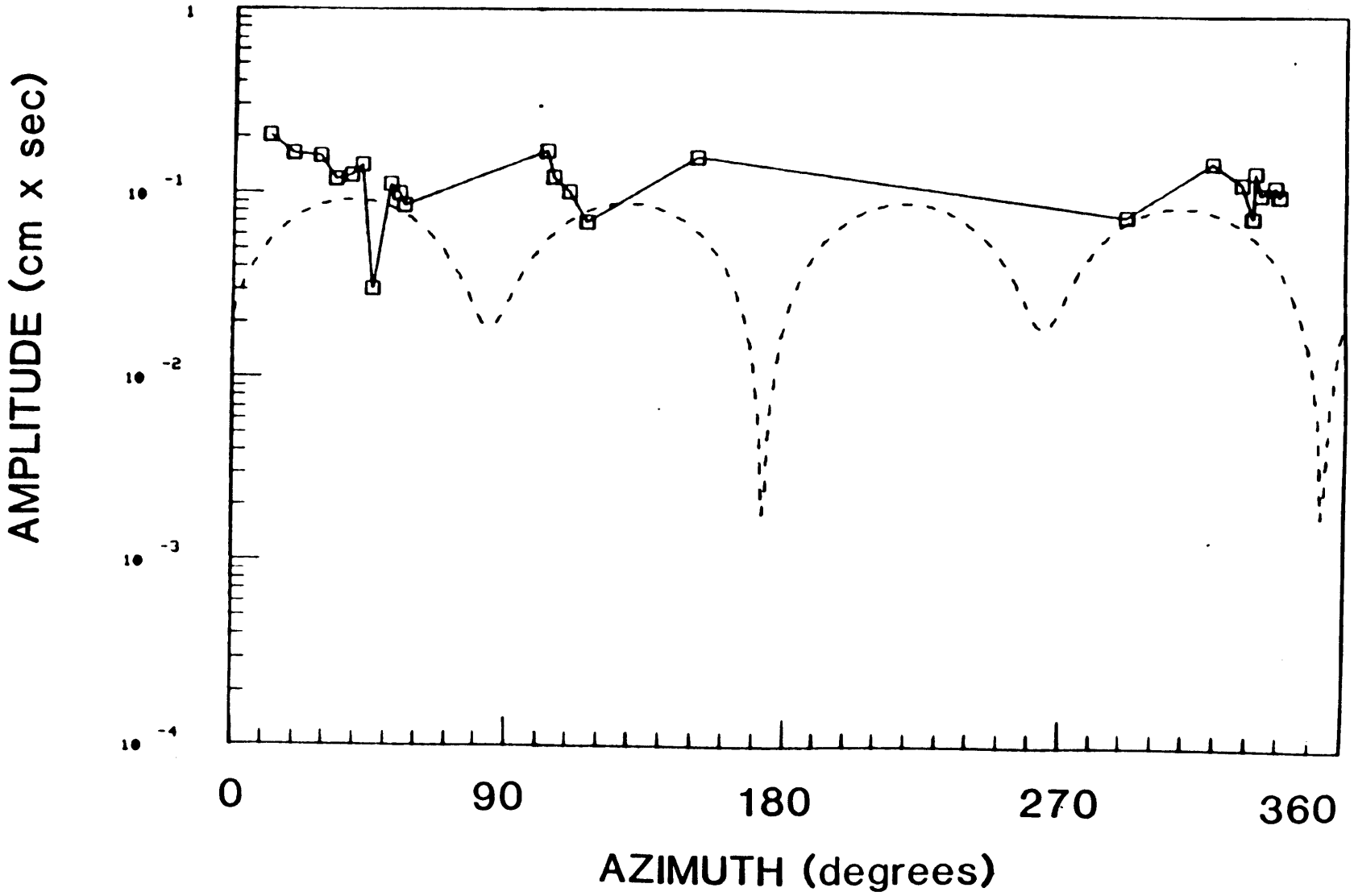

FIGURE B.4d

PERIOD 70 sec

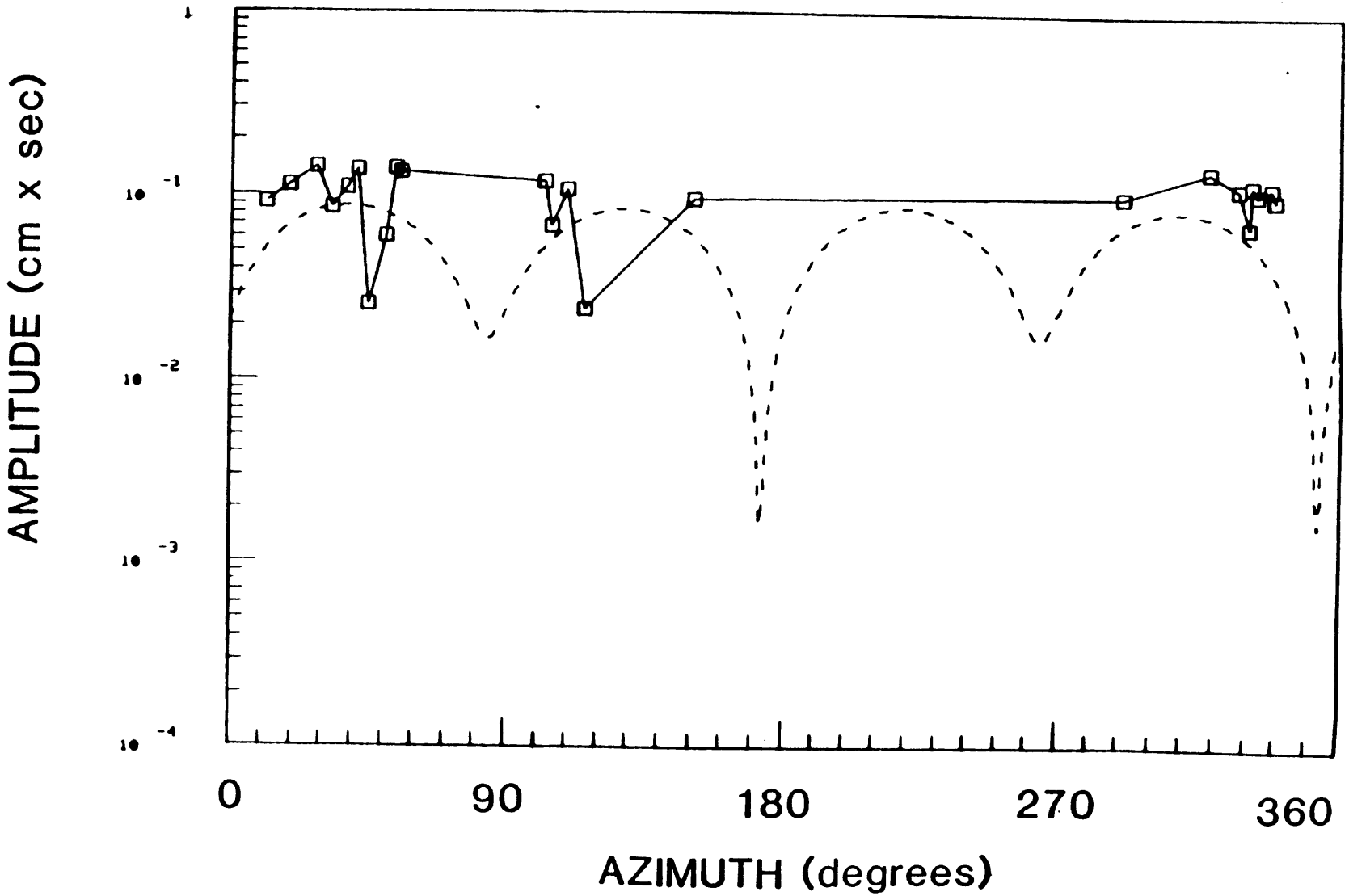

FIGURE B.4e

PERIOD 98 sec

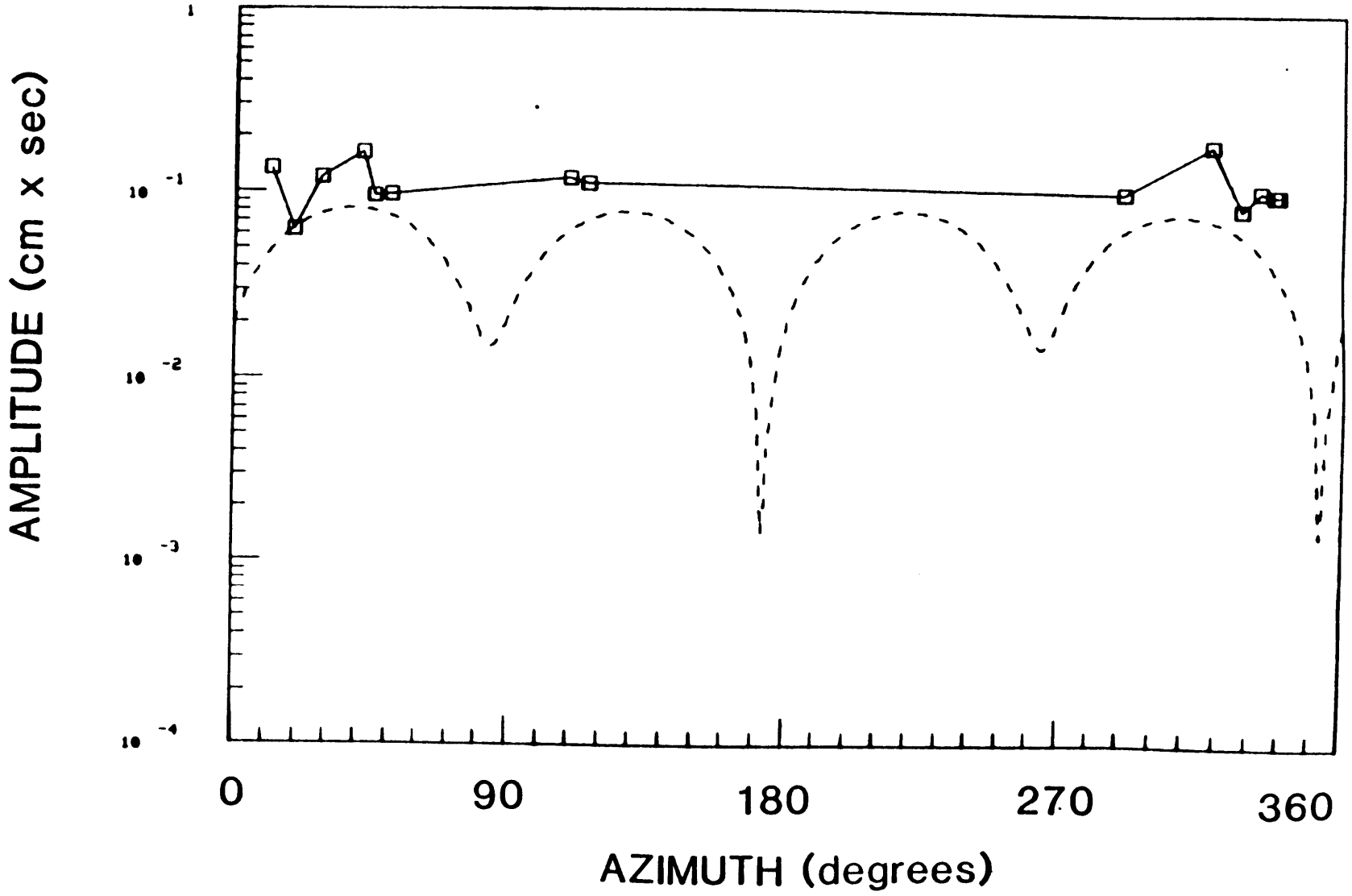

FIGURE B.5a

09/12/65

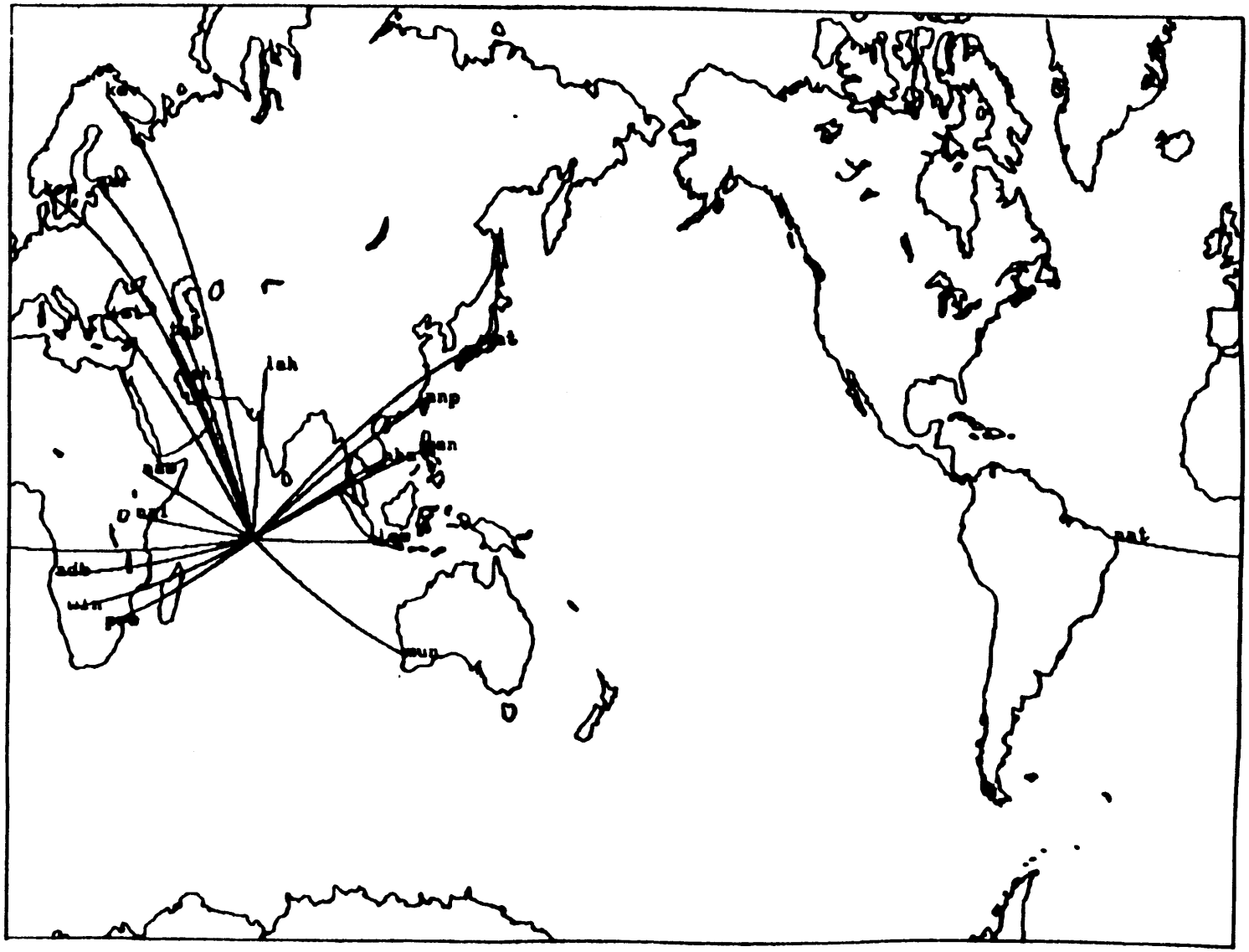

FIGURE B. 5b

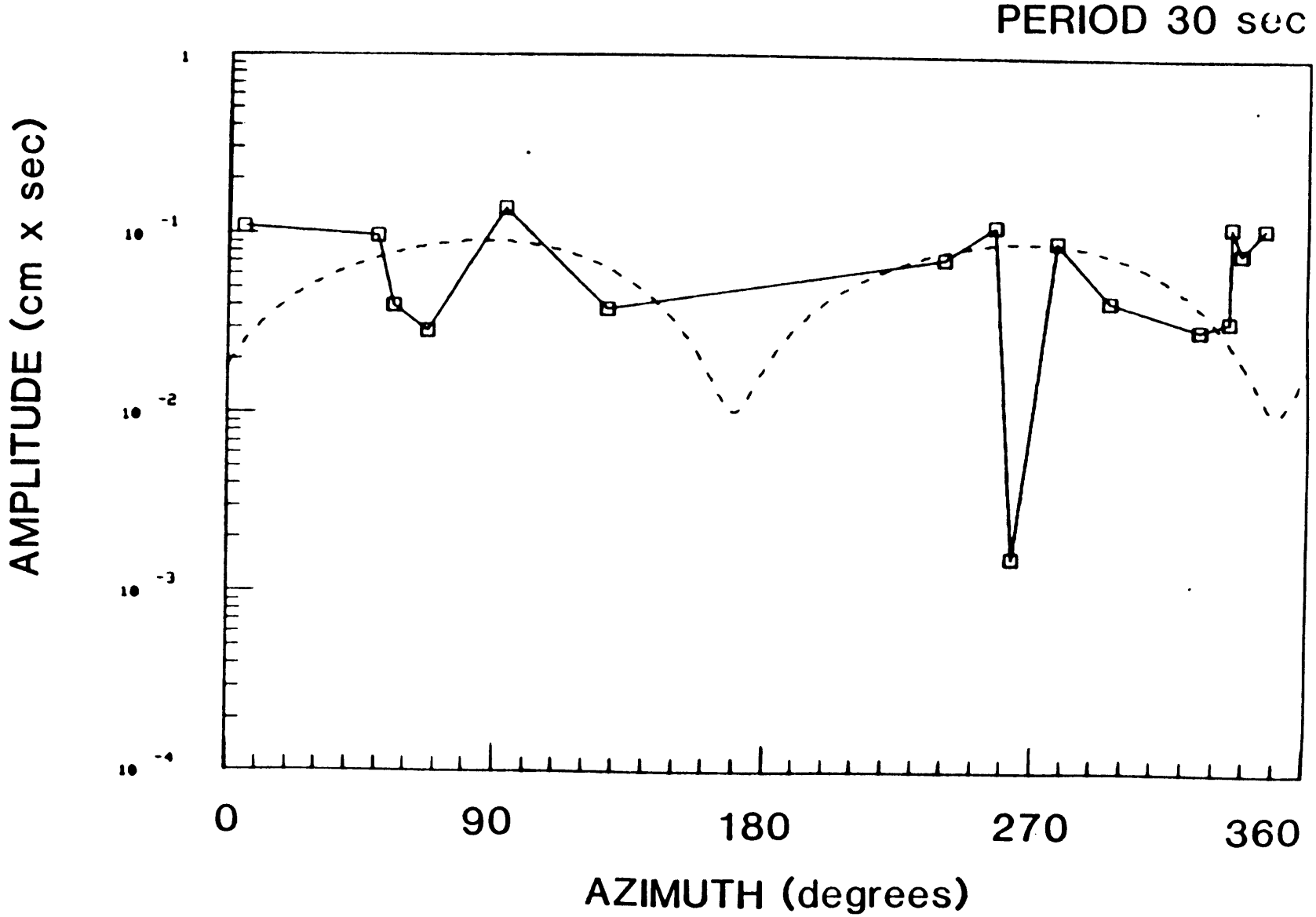
PERIOD 30 sec
AMPLITUDE (cm x sec)
1
10 -1
10 -2
10 -3
10 -4
0
90
180
270
360
AZIMUTH (degrees)

FIGURE B.5c

PERIOD 50 sec

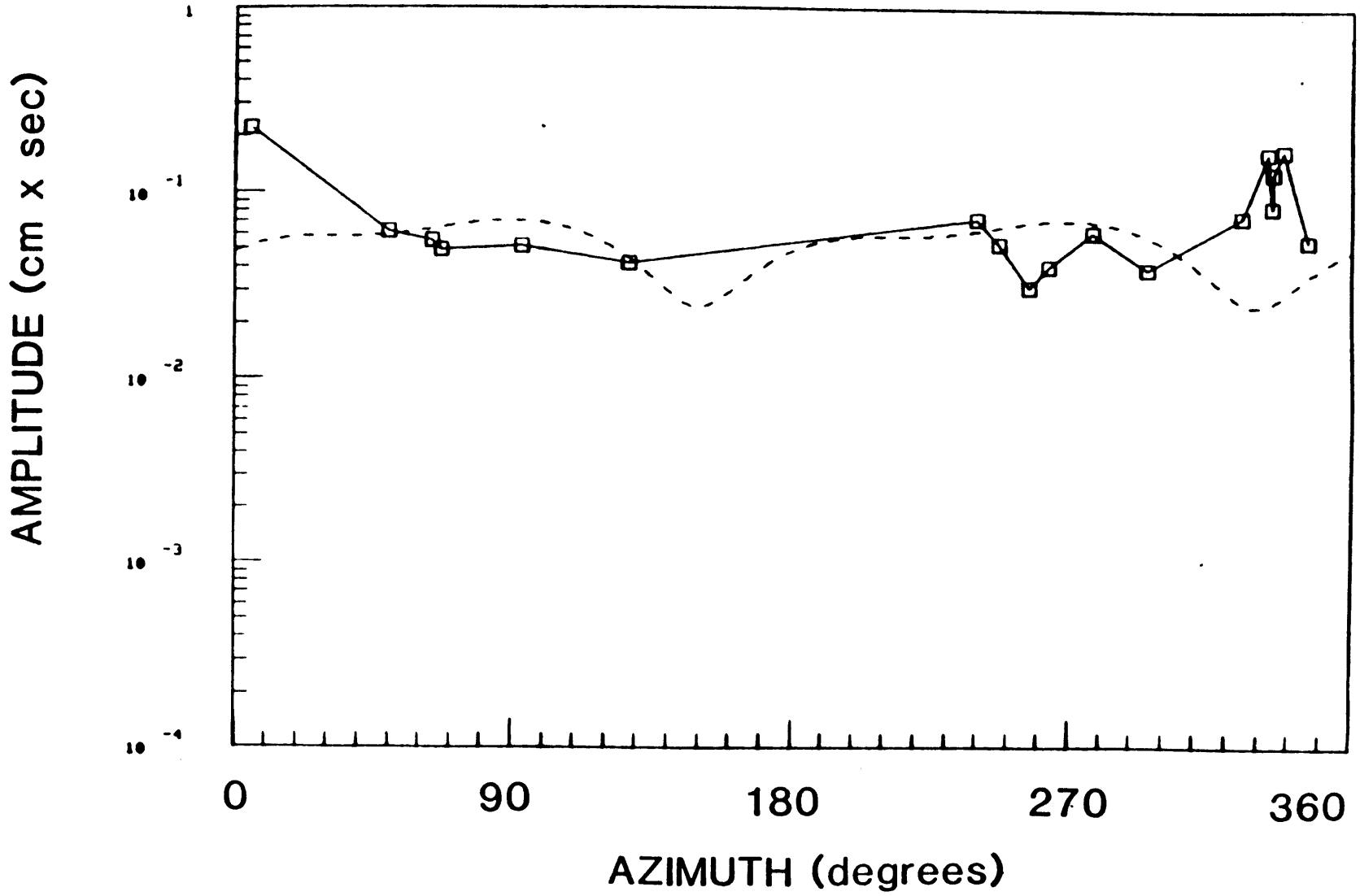

FIGURE B.5d

PERIOD 70 sec

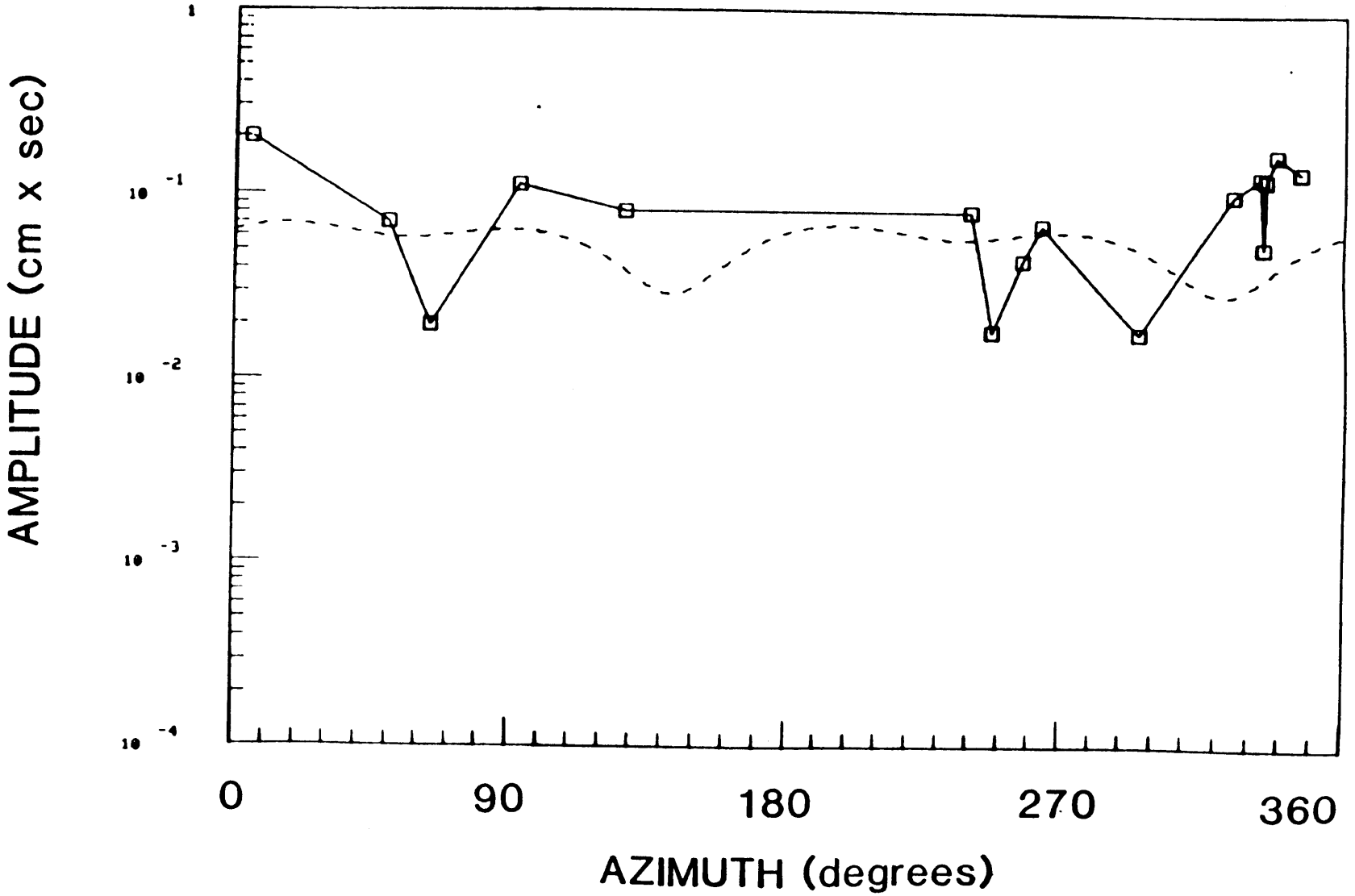

FIGURE B. 5e

PERIOD 98 sec

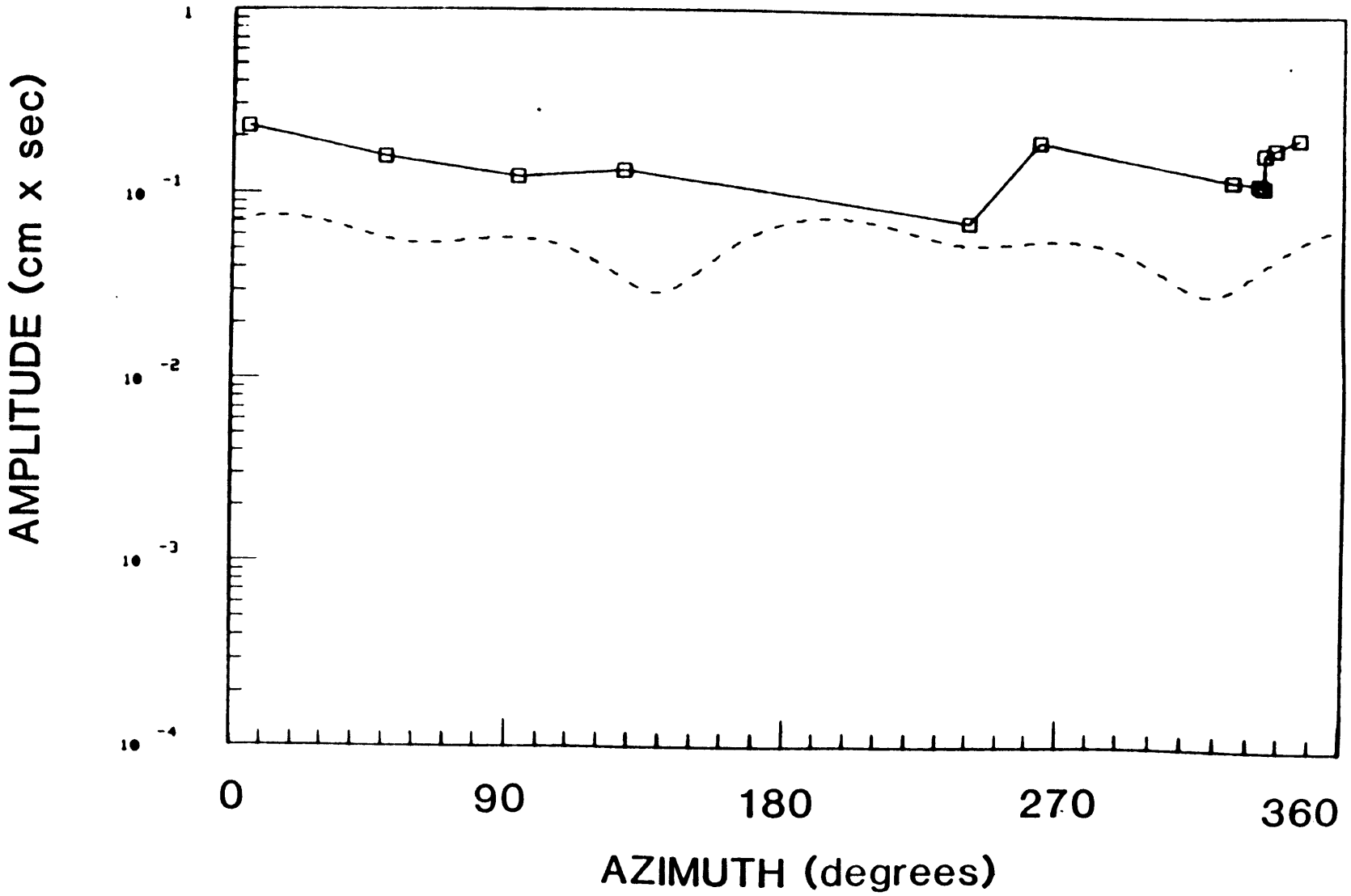

FIGURE B.6a

10/07/65

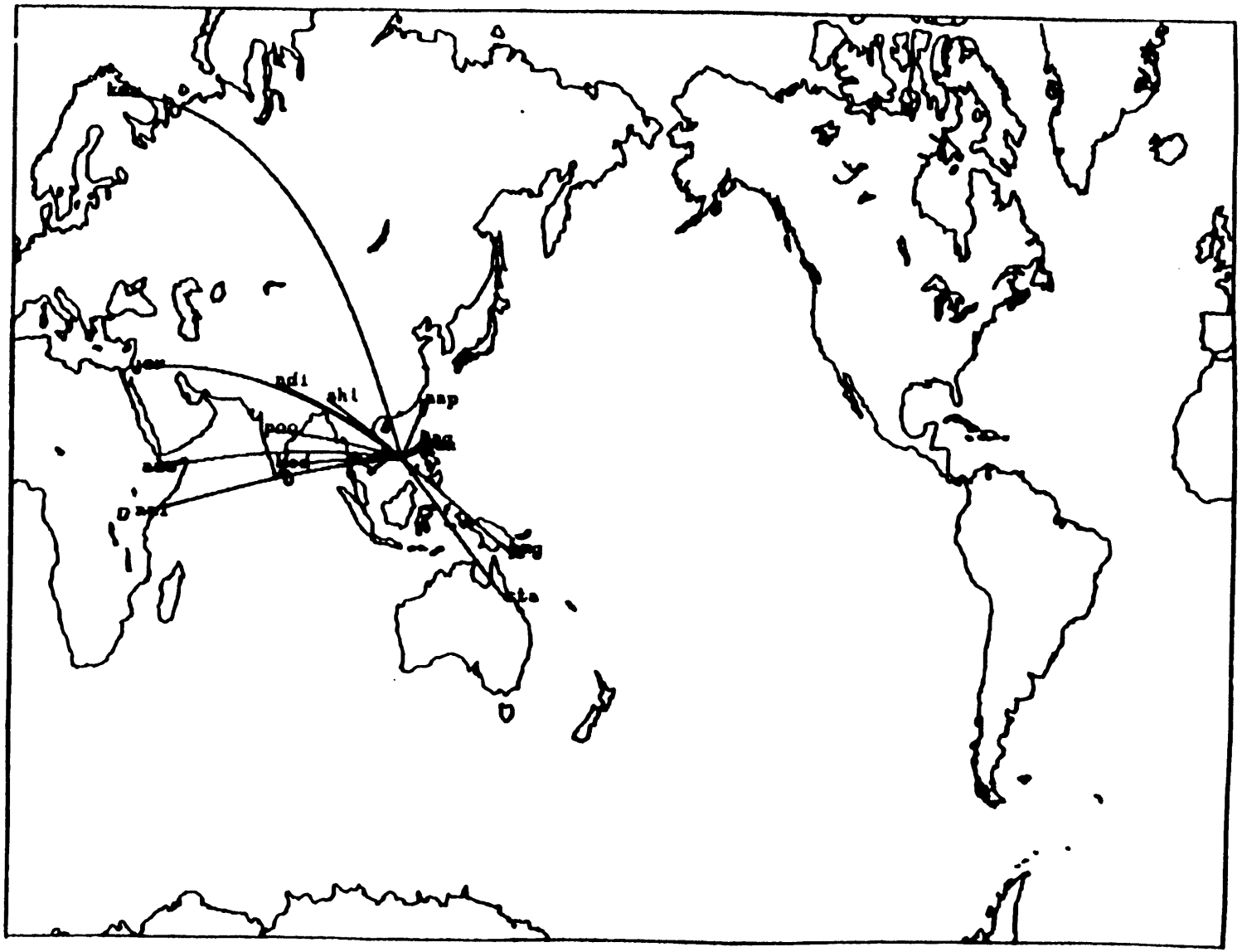

FIGURE B. 6b

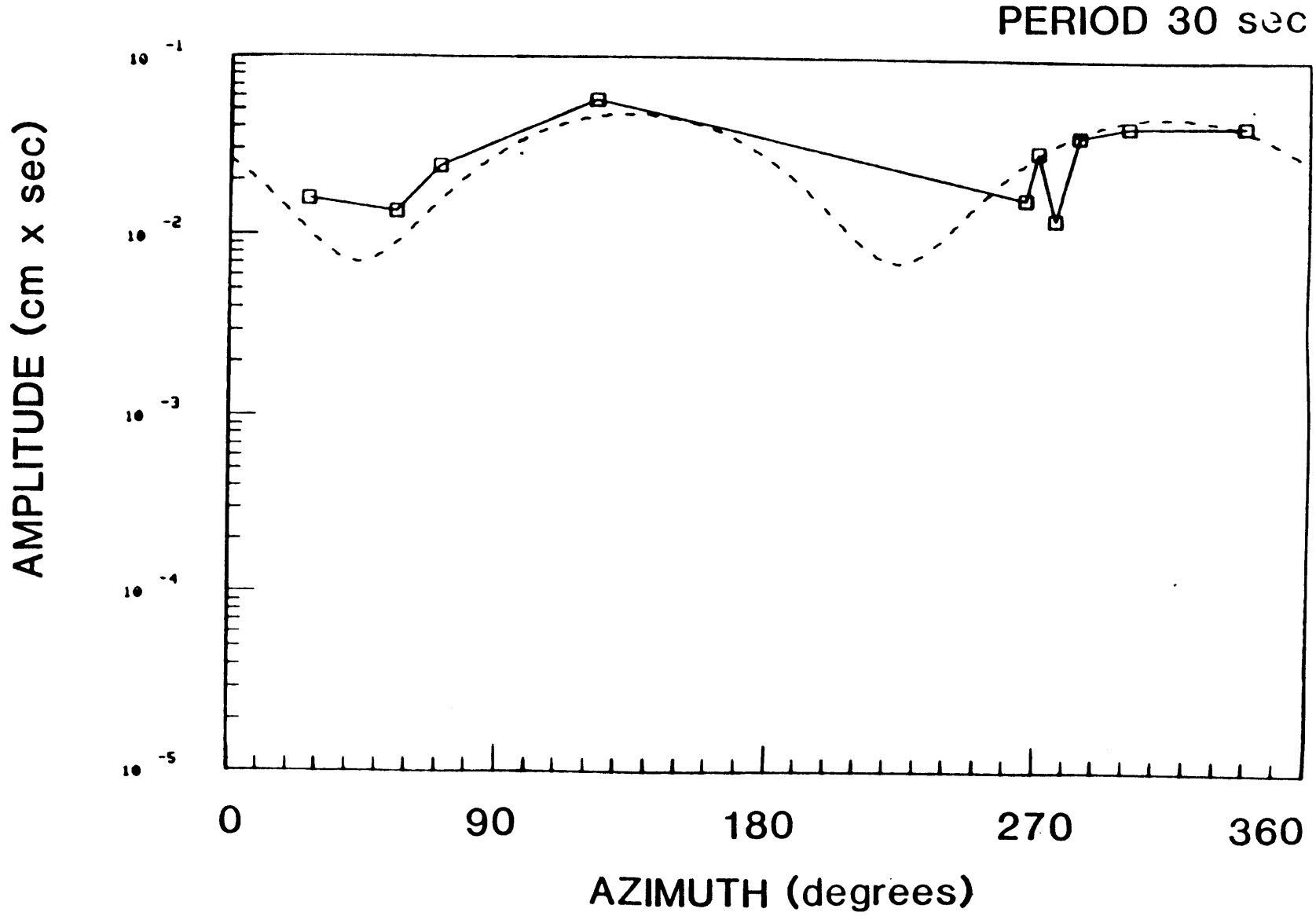
PERIOD 30 sec
AMPLITUDE (cm x sec)
10 -1
10 -2
10 -3
10 -4
10 -5
0
90
180
270
360
AZIMUTH (degrees)

FIGURE B. 6c

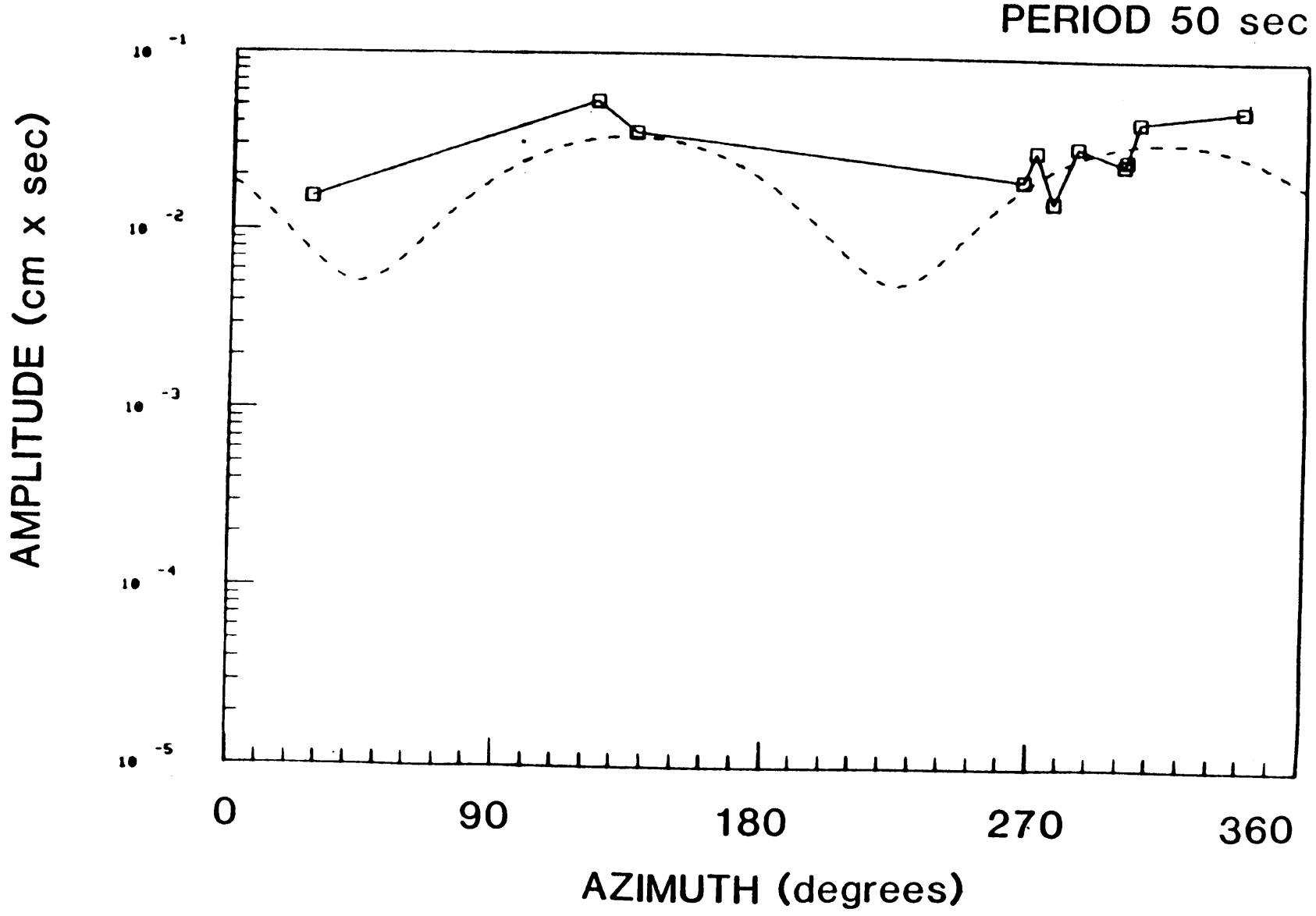
PERIOD 50 sec
AMPLITUDE (cm x sec)
10 -1
10 -2
10 -3
10 -4
10 -5
0
90
180
270
360
AZIMUTH (degrees)

FIGURE B. 6d

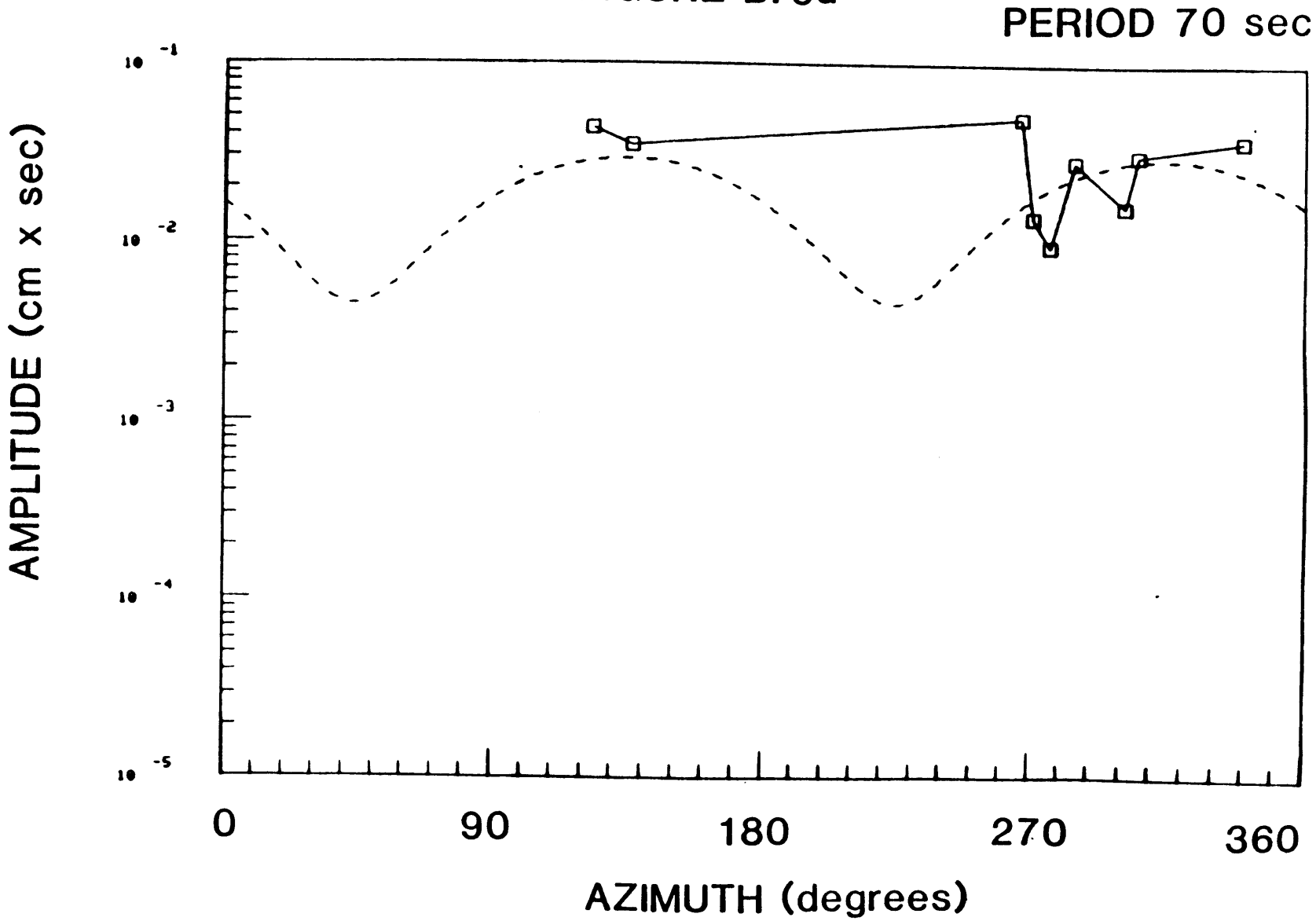
PERIOD 70 sec
AMPLITUDE (cm x sec)
10 -1
10 -2
10 -3
10 -4
10 -5
0
90
180
270
360
AZIMUTH (degrees)

FIGURE B.6e

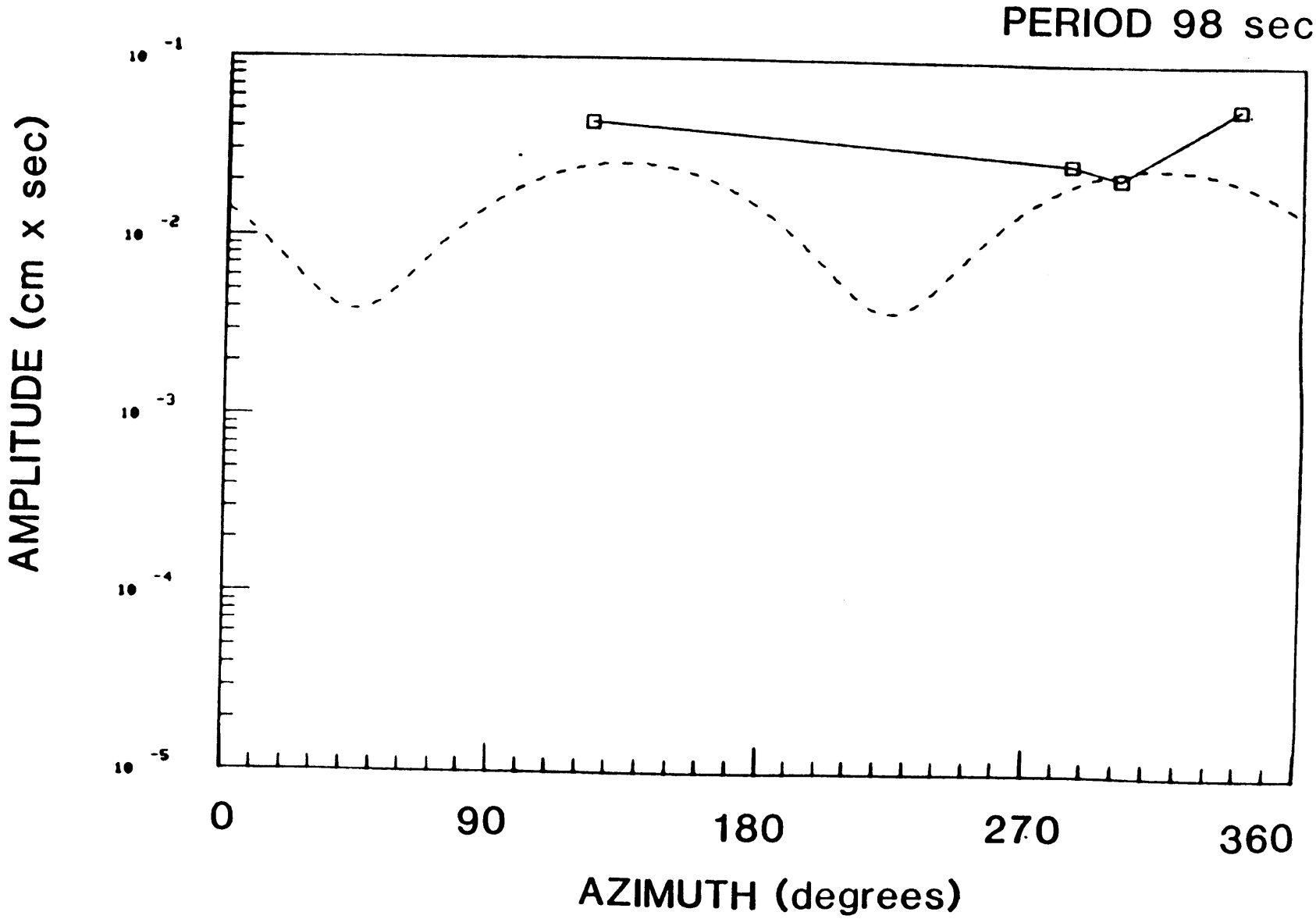
PERIOD 98 sec
AMPLITUDE (cm x sec)
10 -1
10 -2
10 -3
10 -4
10 -5
0
90
180
270
360
AZIMUTH (degrees)

FIGURE B.7a

10/31/65

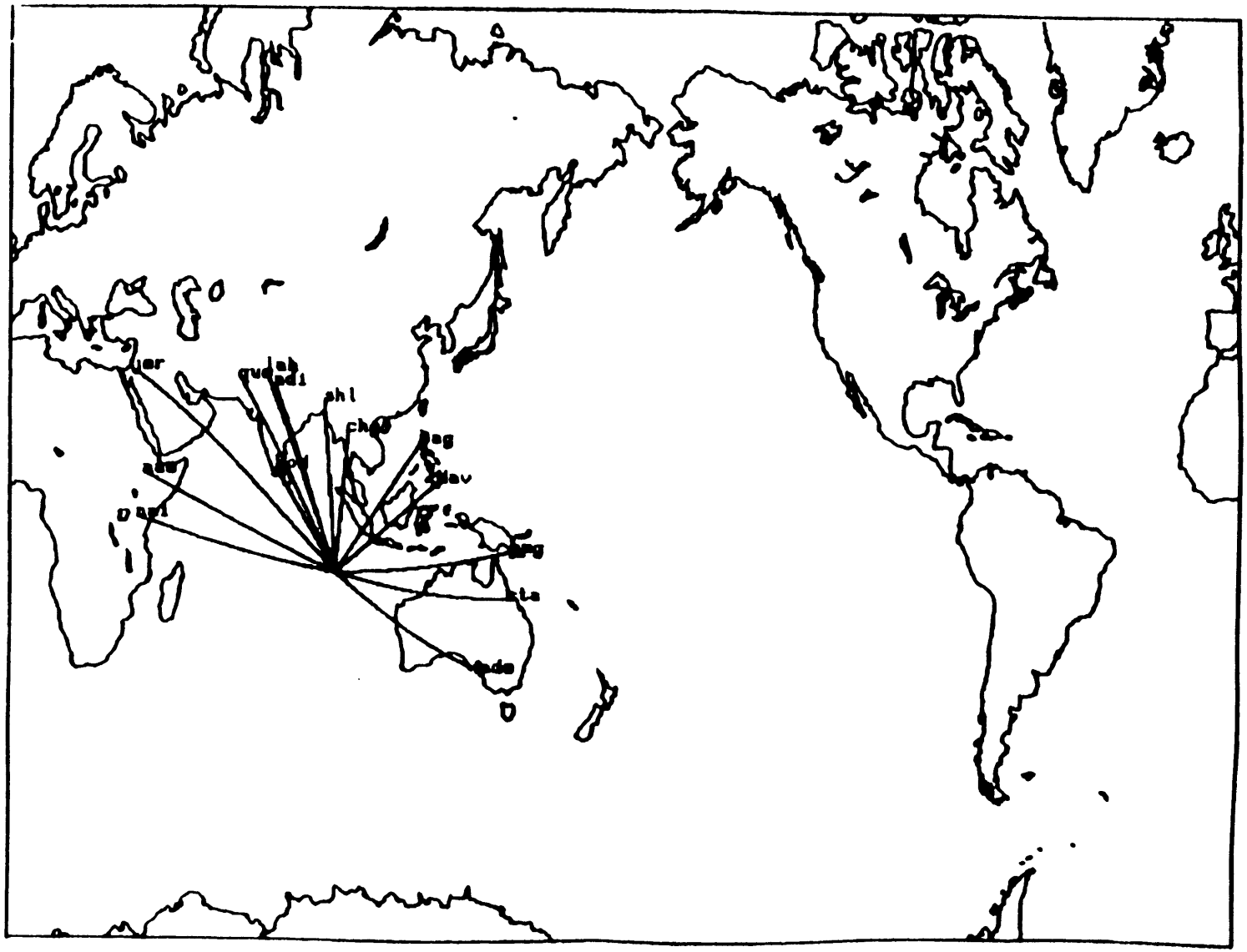

FIGURE B. 7b

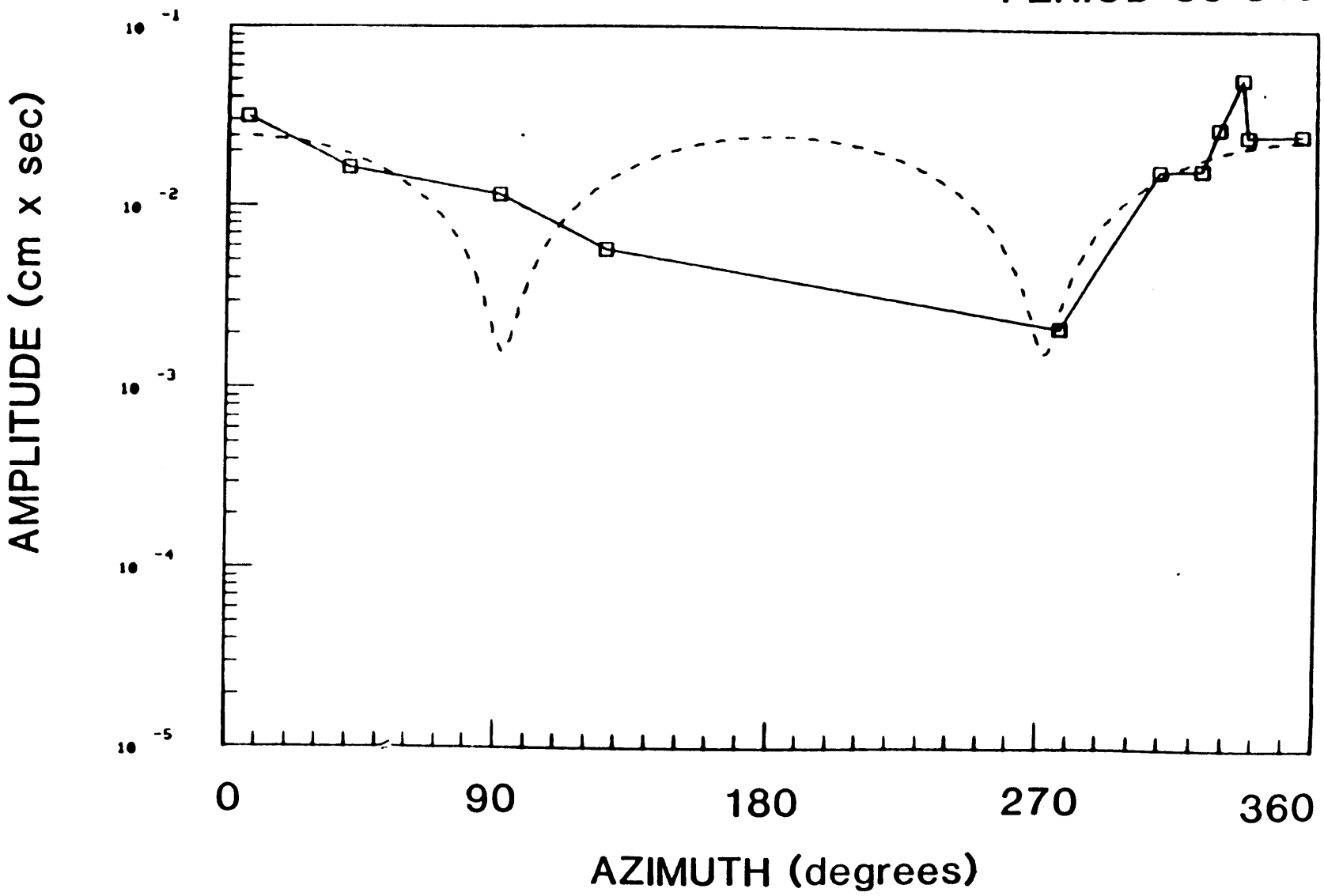
PERIOD 30 sec
AMPLITUDE (cm x sec)
10 -1
10 -2
10 -3
10 -4
10 -5
0
90
180
270
360
AZIMUTH (degrees)

FIGURE B.7c

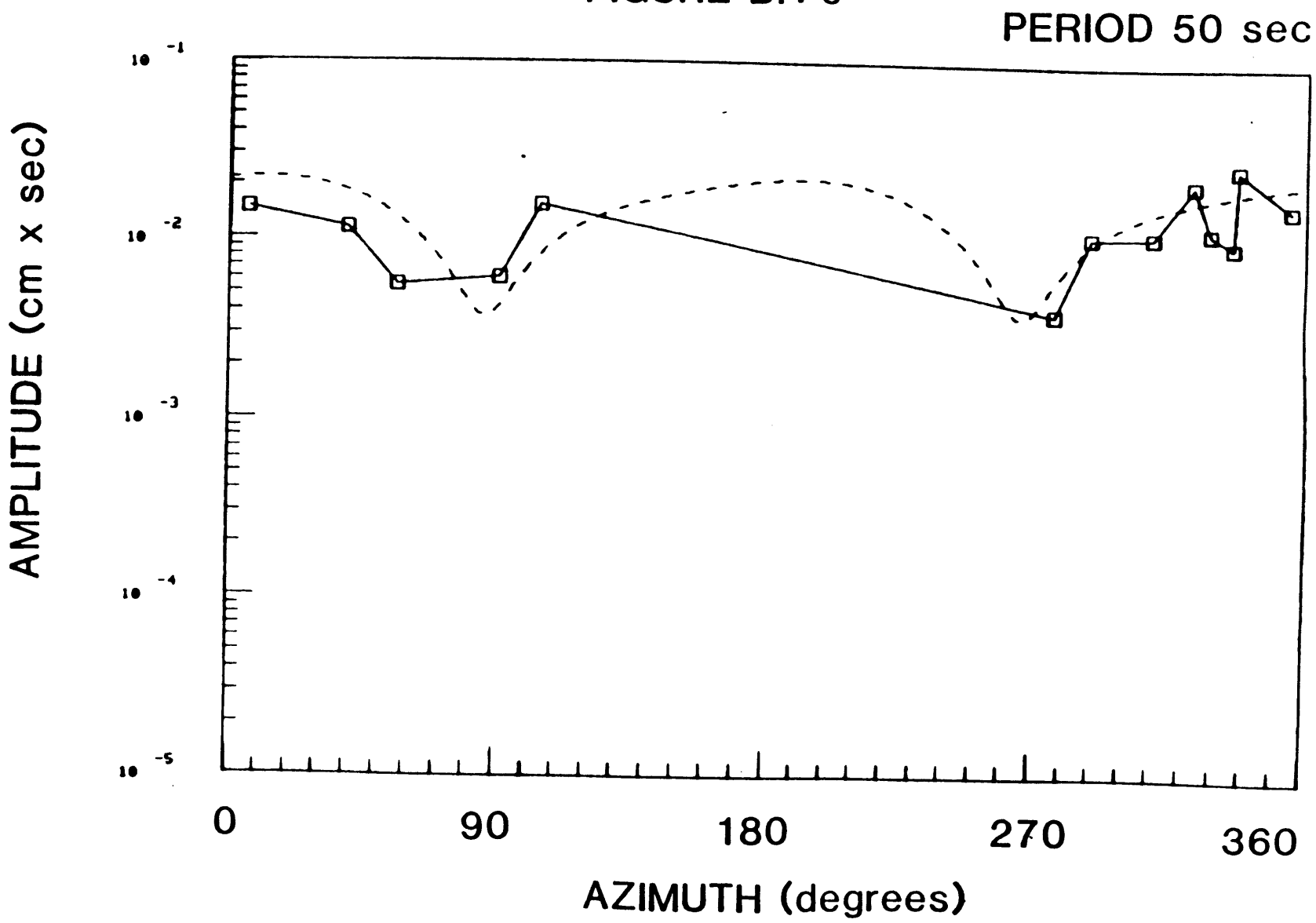
PERIOD 50 sec
AMPLITUDE (cm x sec)
10 -1
10 -2
10 -3
10 -4
10 -5
0
90
180
270
360
AZIMUTH (degrees)

FIGURE B. 7d

PERIOD 70 sec

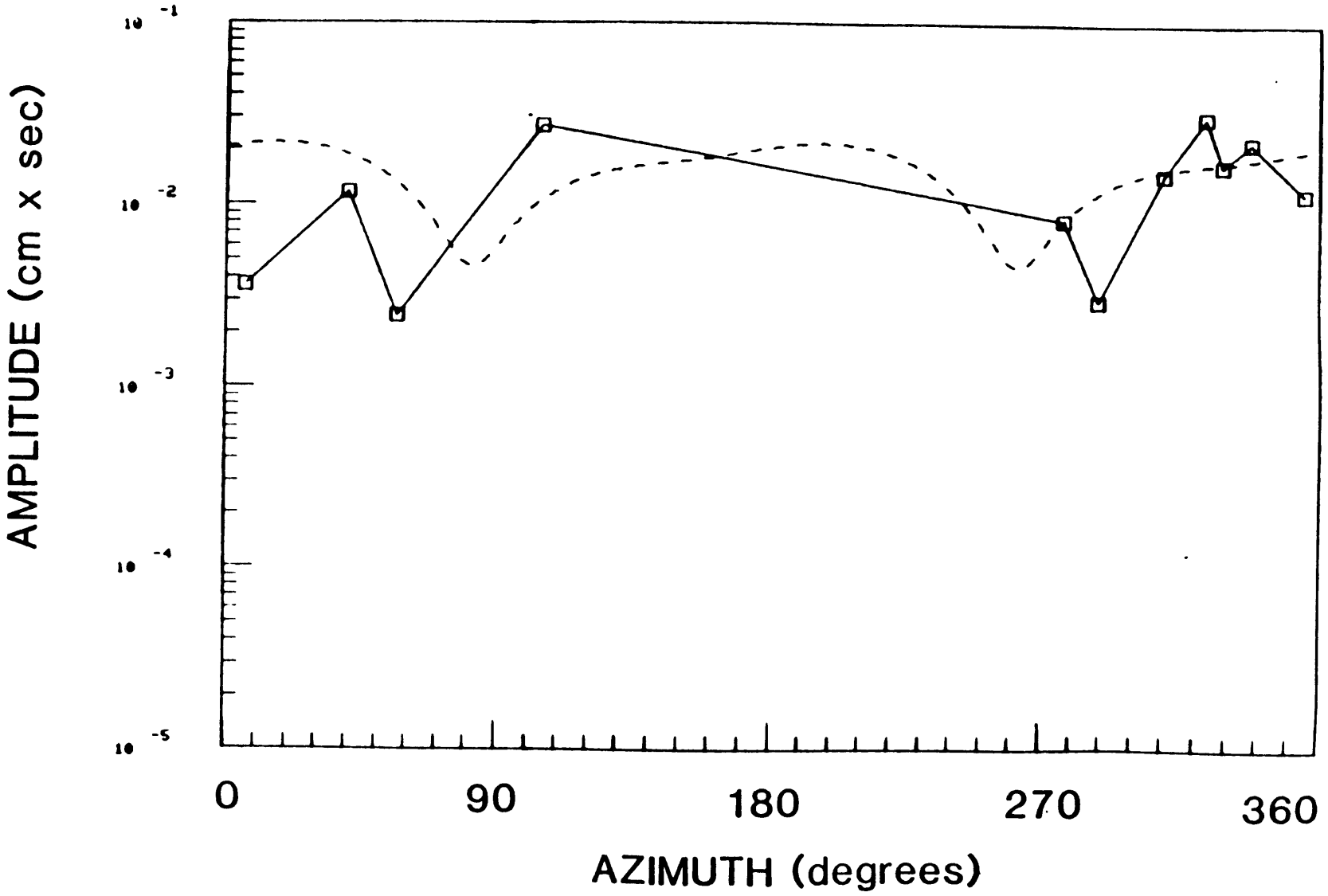

FIGURE B. 7e

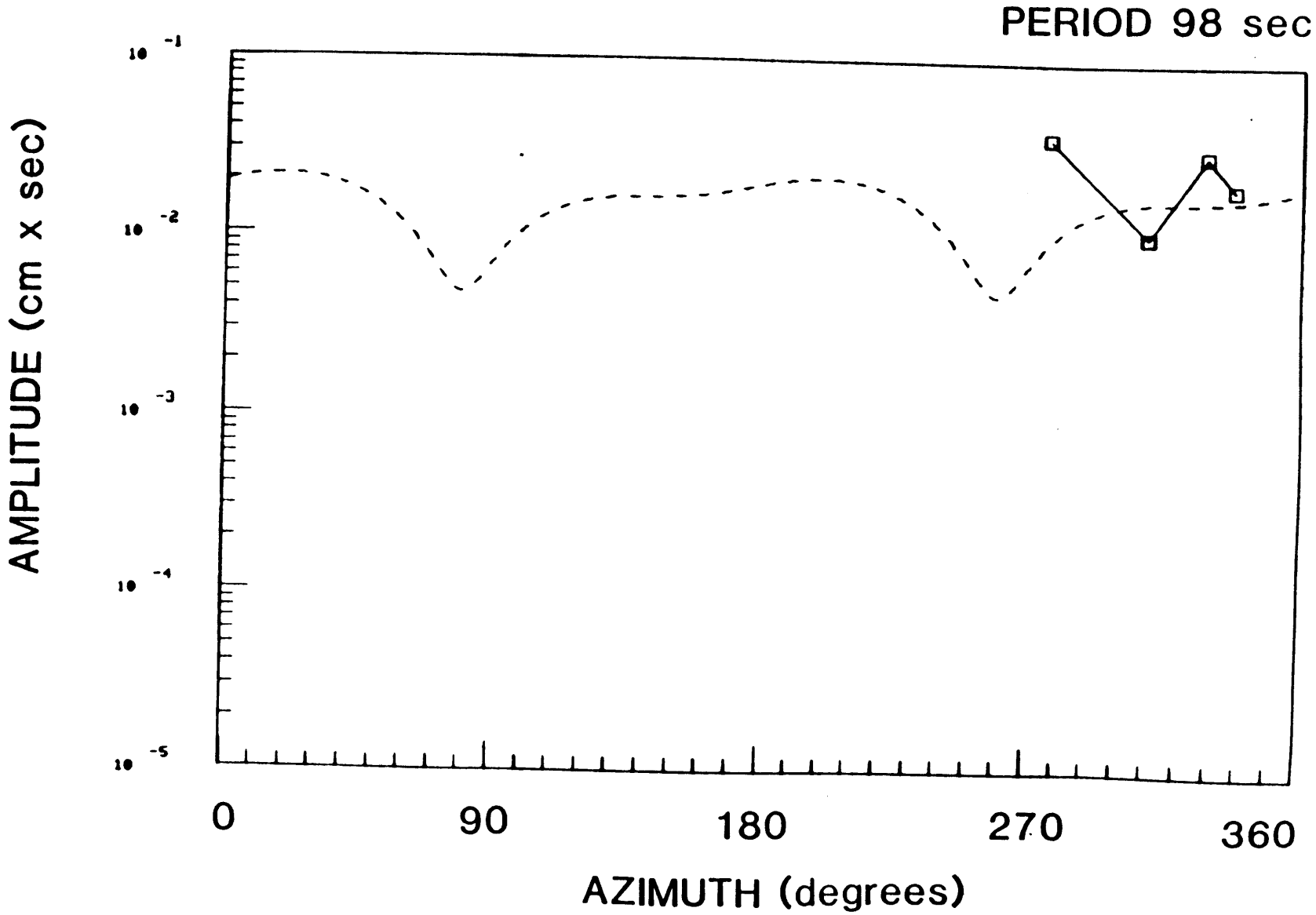
PERIOD 98 sec
AMPLITUDE (cm x sec)
10 -1
10 -2
10 -3
10 -4
10 -5
0
90
180
270
360
AZIMUTH (degrees)

FIGURE B.8a

12/19/65

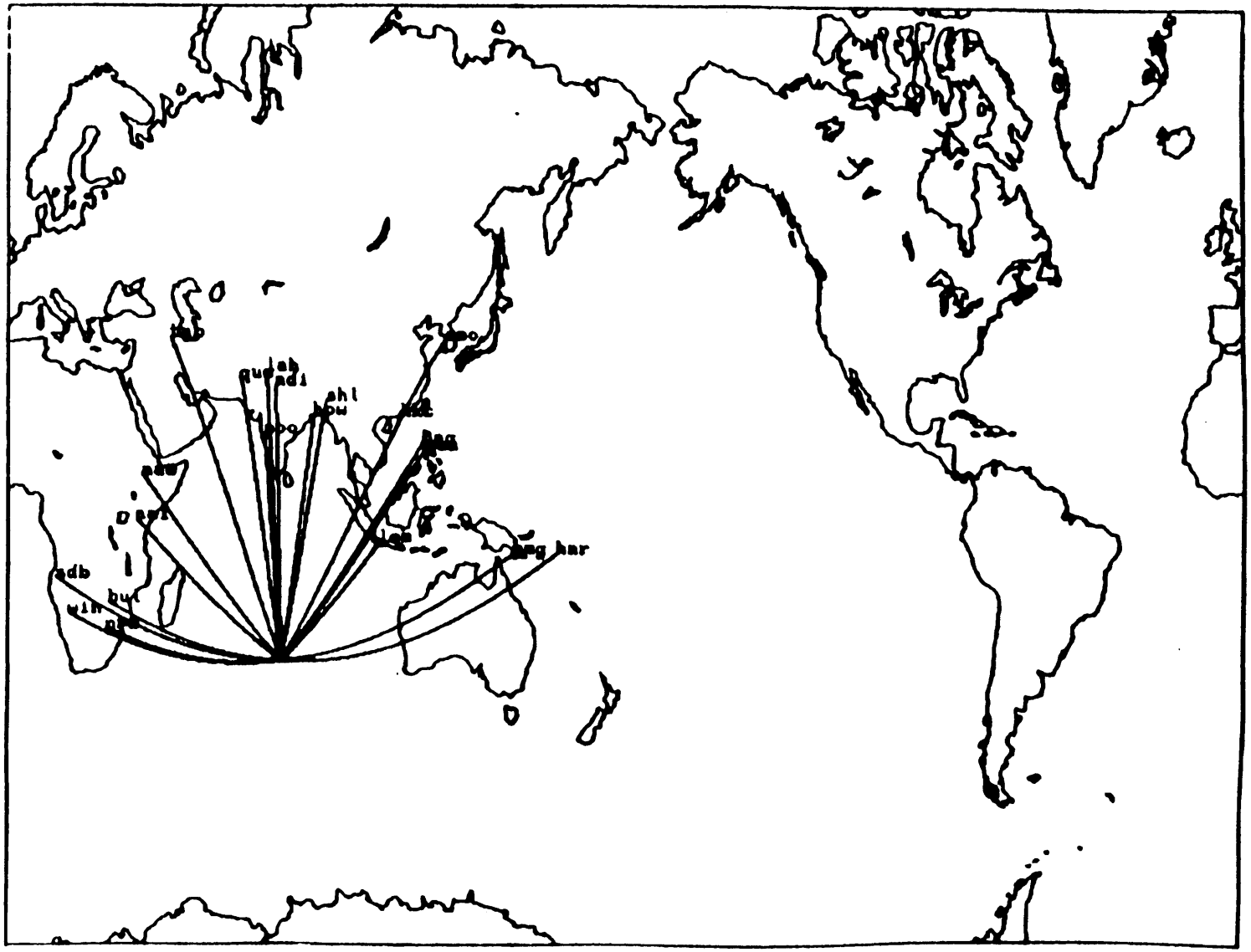

FIGURE B. 8b

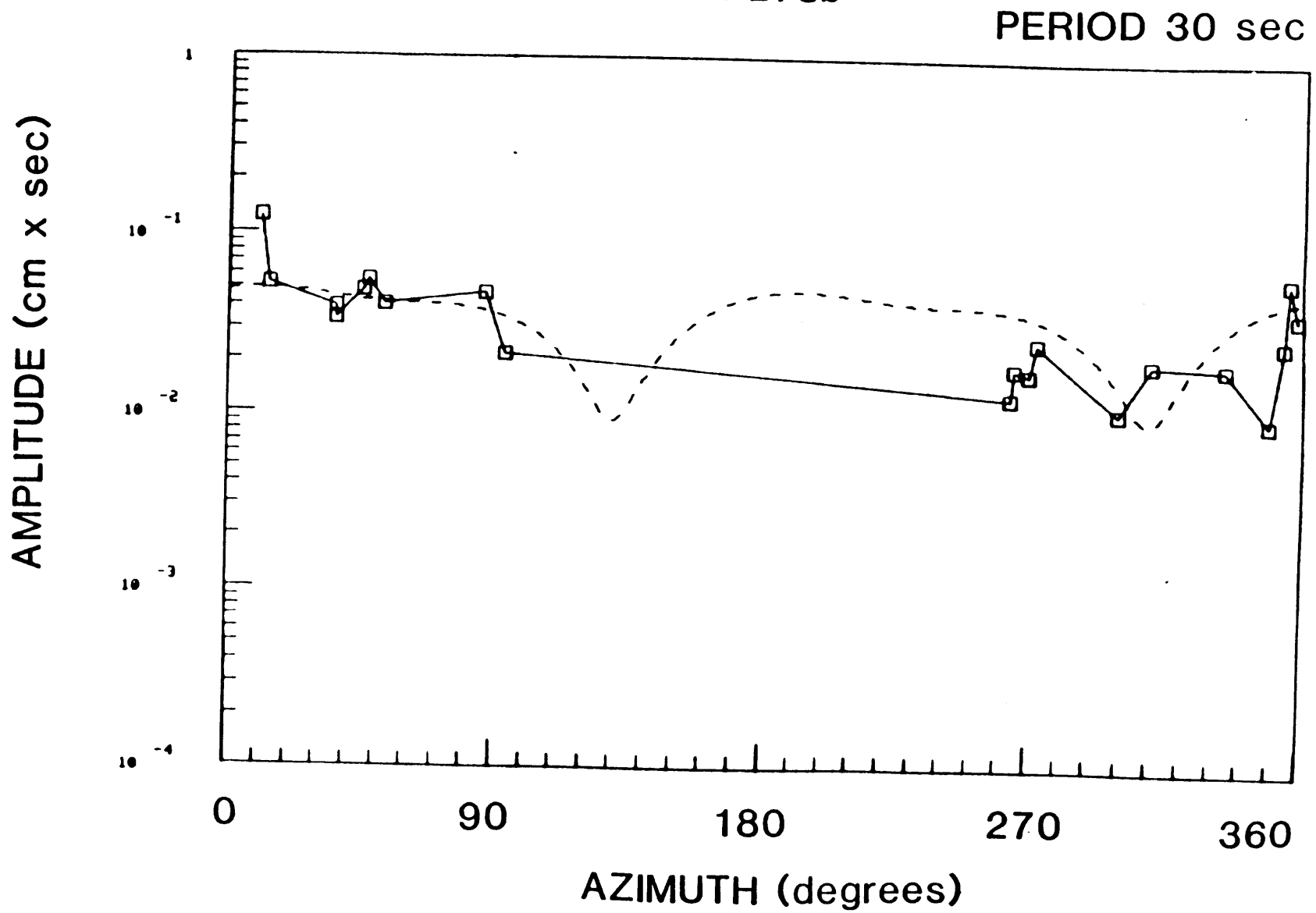
PERIOD 30 sec
AMPLITUDE (cm x sec)
1
10 -1
10 -2
10 -3
10 -4
0
90
180
270
360
AZIMUTH (degrees)

FIGURE B. 8c

PERIOD 50 sec

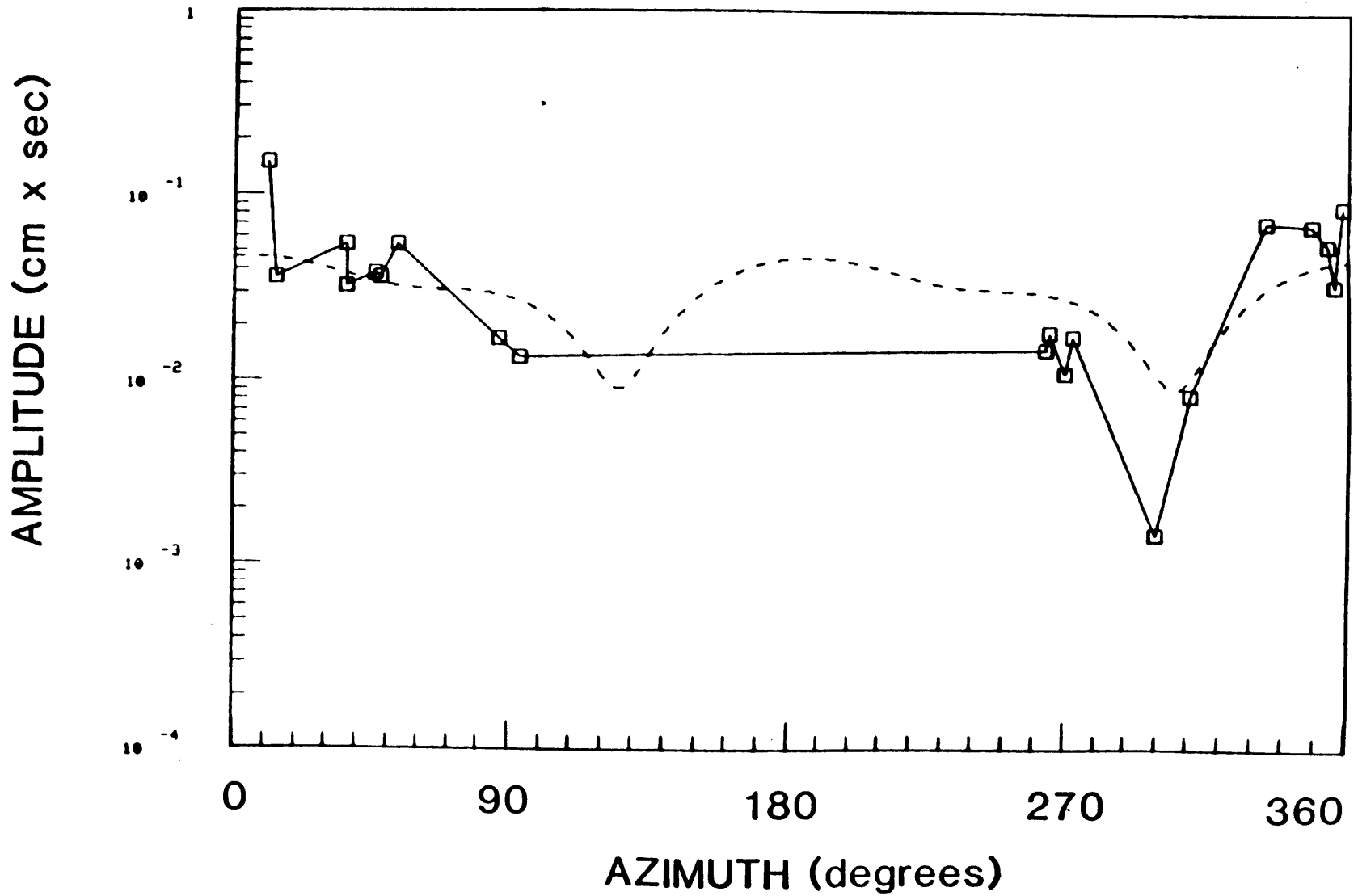

FIGURE B. 8d

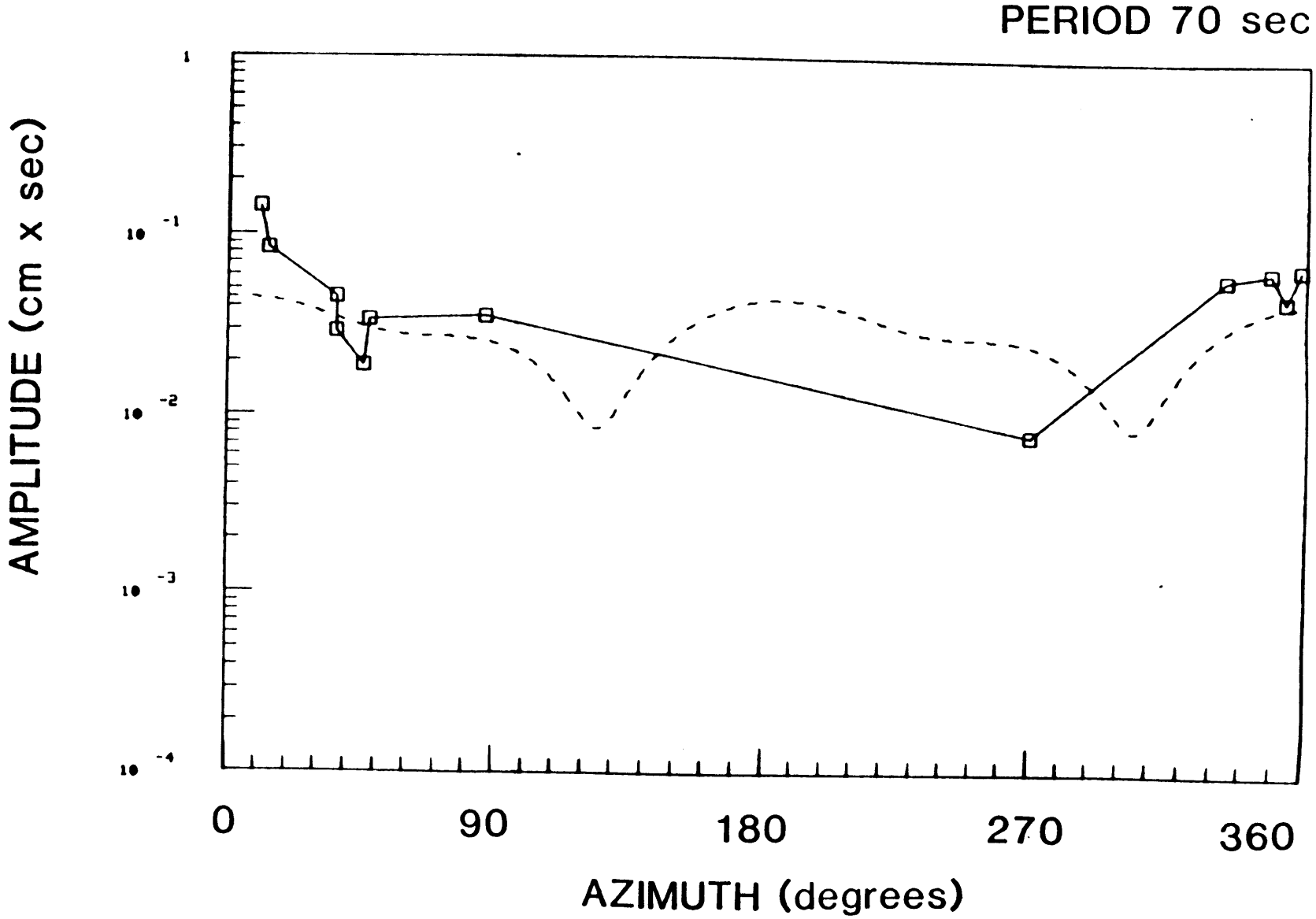
PERIOD 70 sec
AMPLITUDE (cm x sec)
1
10 -1
10 -2
10 -3
10 -4
0
90
180
270
360
AZIMUTH (degrees)

FIGURE B.8e

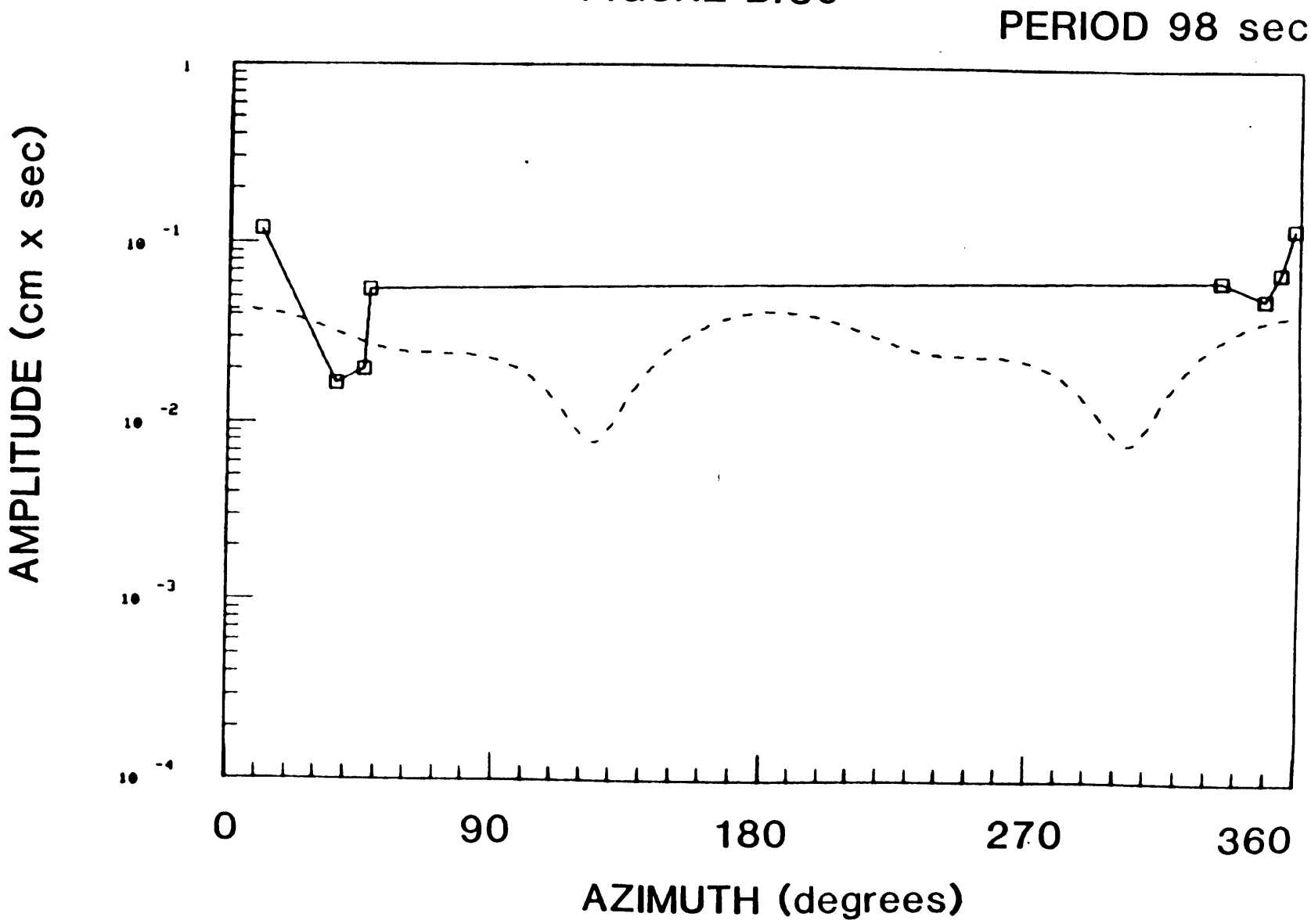
PERIOD 98 sec
AMPLITUDE (cm x sec)
1
10 -1
10 -2
10 -3
10 -4
0
90
180
270
360
AZIMUTH (degrees)

FIGURE B.9a

02/17/66

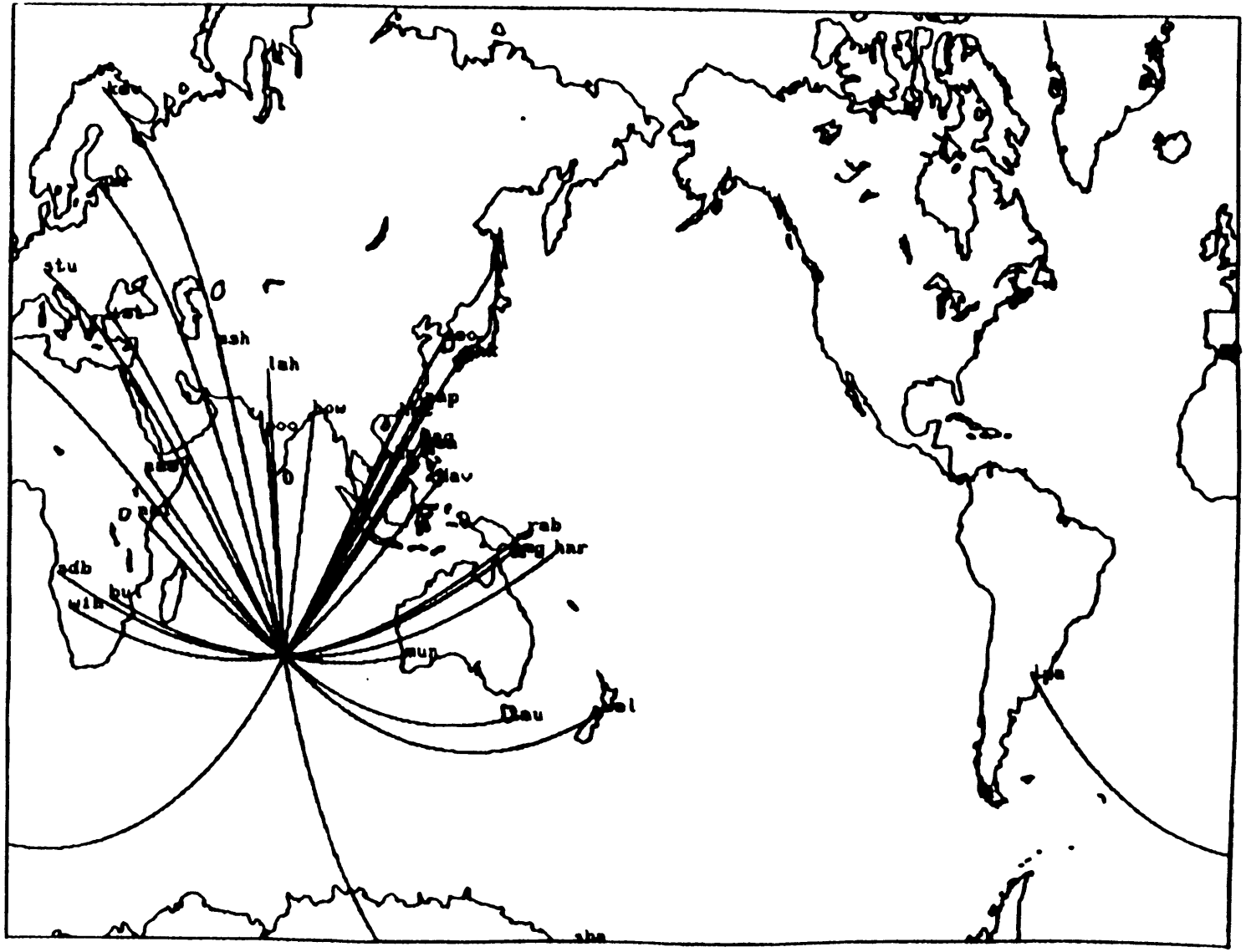

FIGURE B.9b

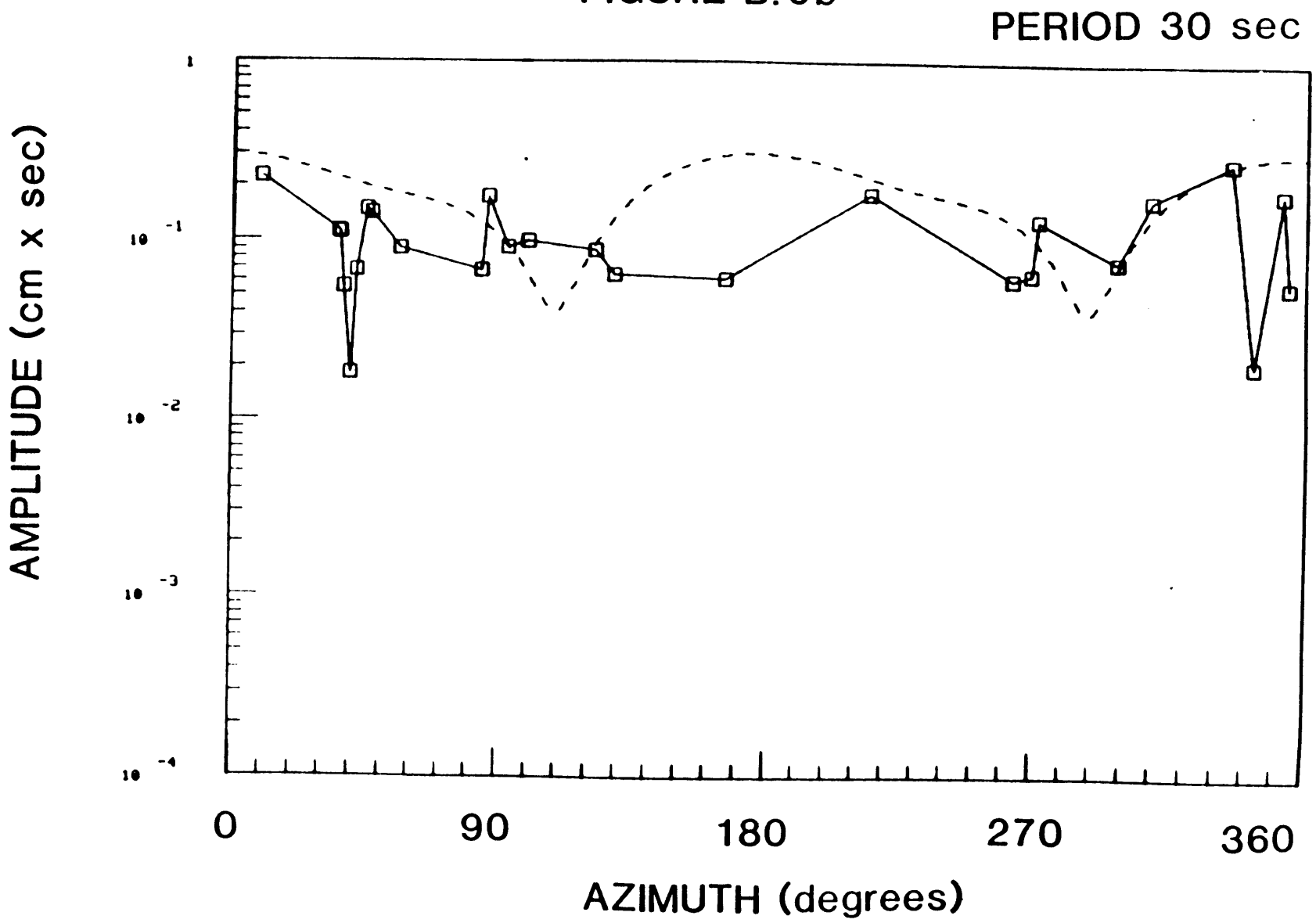
PERIOD 30 sec
AMPLITUDE (cm x sec)
1
10 -1
10 -2
10 -3
10 -4
0
90
180
270
360
AZIMUTH (degrees)

FIGURE B.9c

PERIOD 50 sec

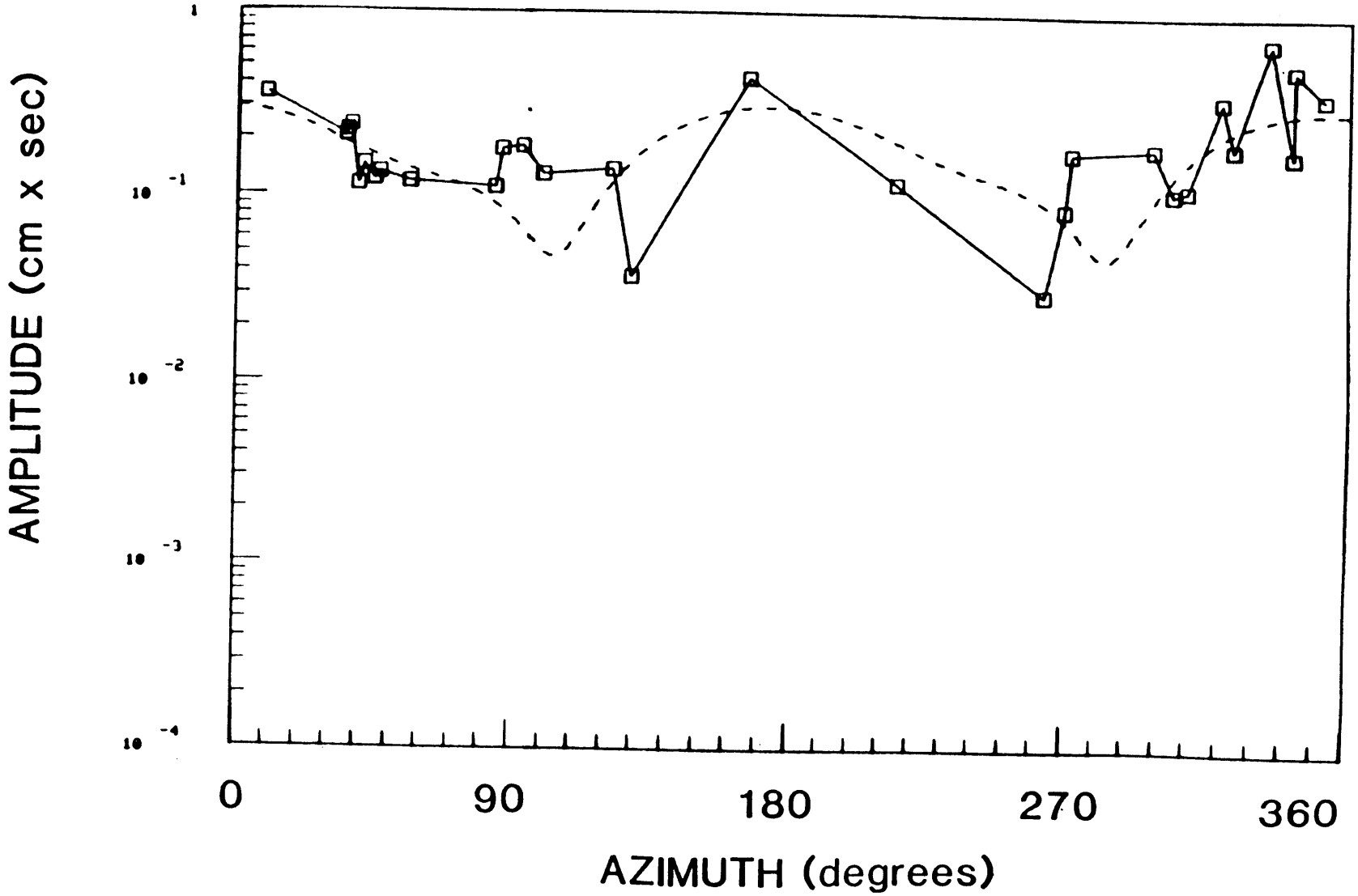

FIGURE B. 9d

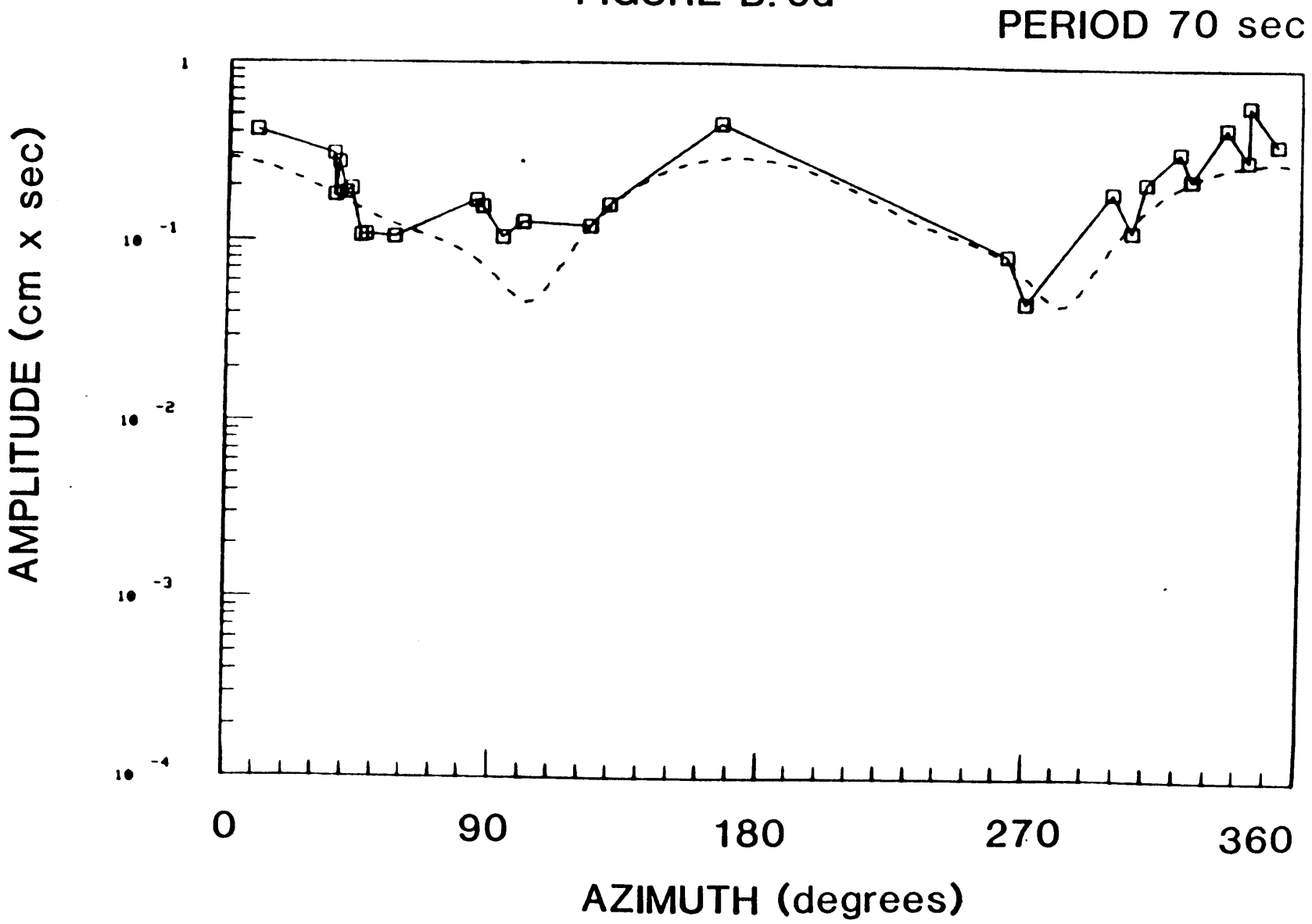
PERIOD 70 sec
AMPLITUDE (cm x sec)
1
10 -1
10 -2
10 -3
10 -4
0
90
180
270
360
AZIMUTH (degrees)

FIGURE B.9e

PERIOD 98 sec

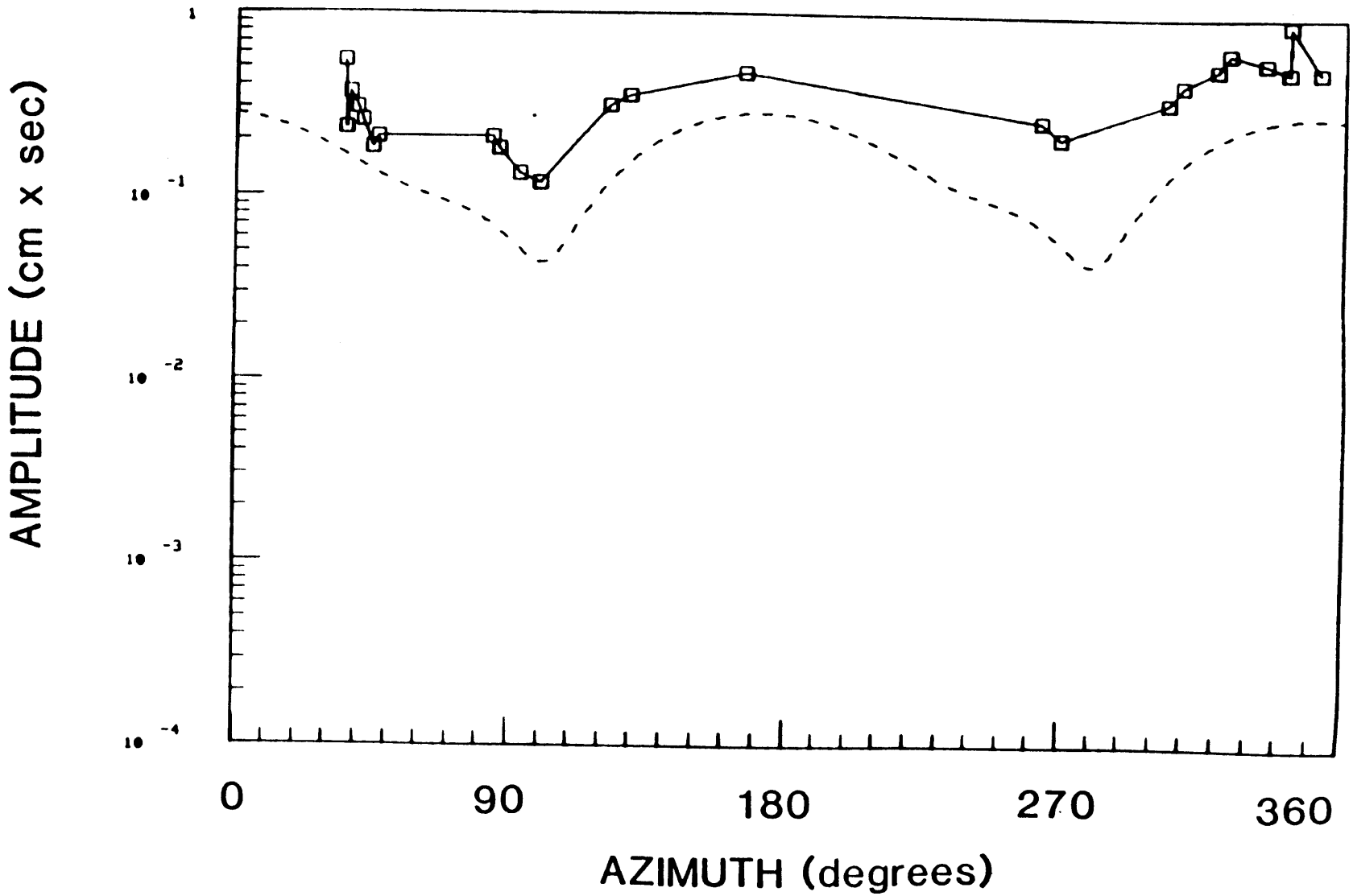

FIGURE B.10a

01/07/67

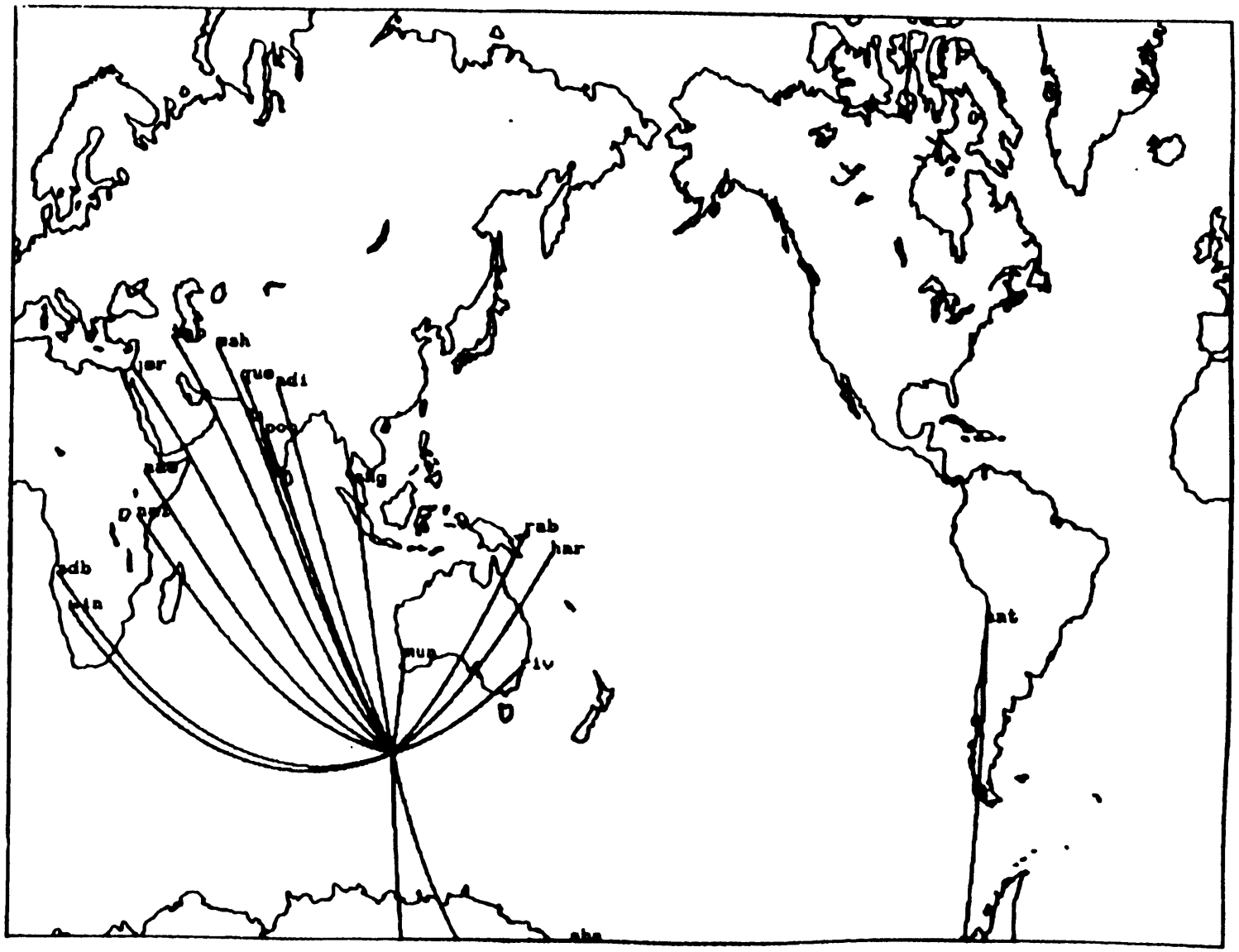

FIGURE B.10b

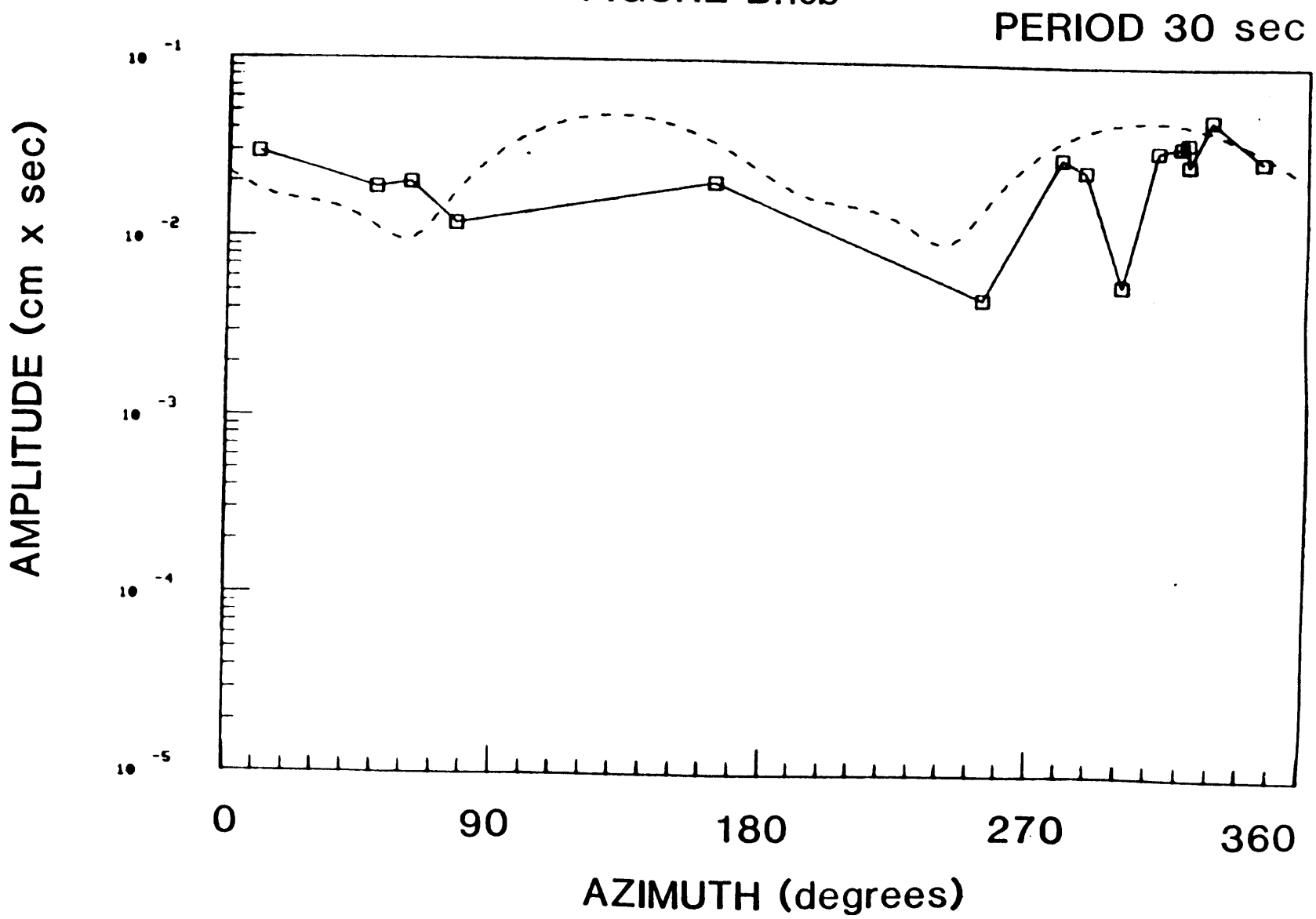
PERIOD 30 sec
AMPLITUDE (cm x sec)
10 -1
10 -2
10 -3
10 -4
10 -5
0
90
180
270
360
AZIMUTH (degrees)

FIGURE B.10C

PERIOD 50 sec

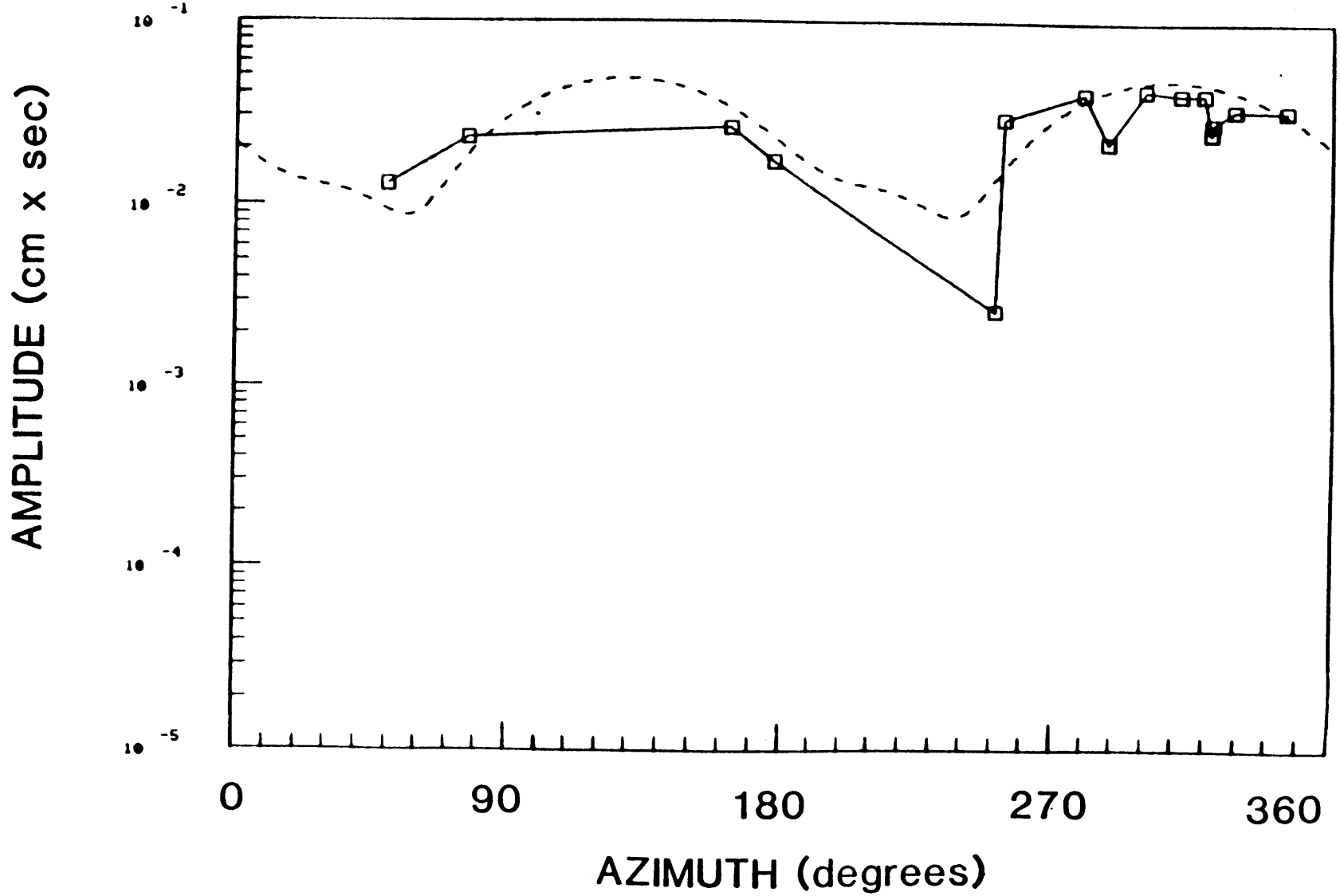

FIGURE B.10d

PERIOD 70 sec

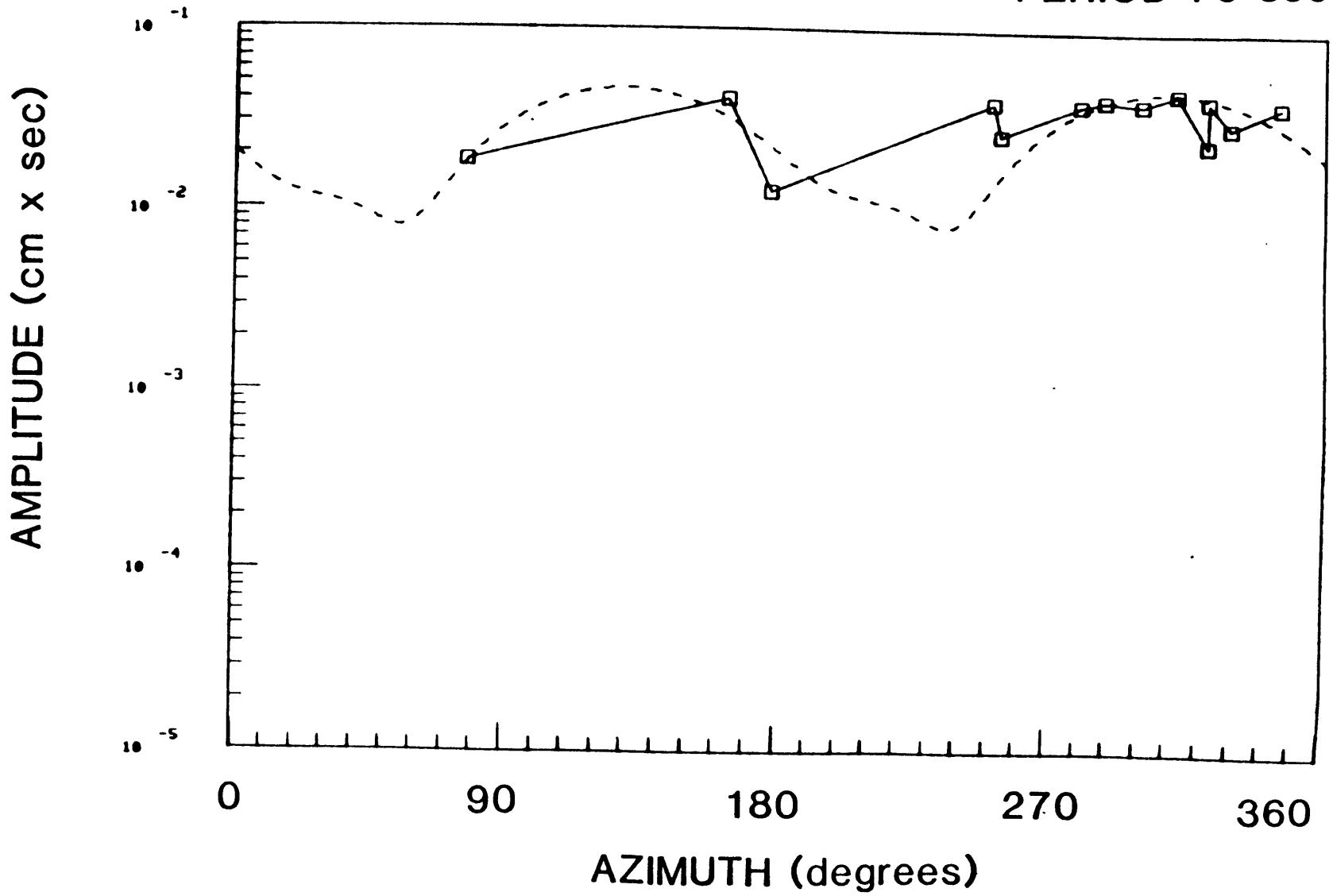

FIGURE B.10e

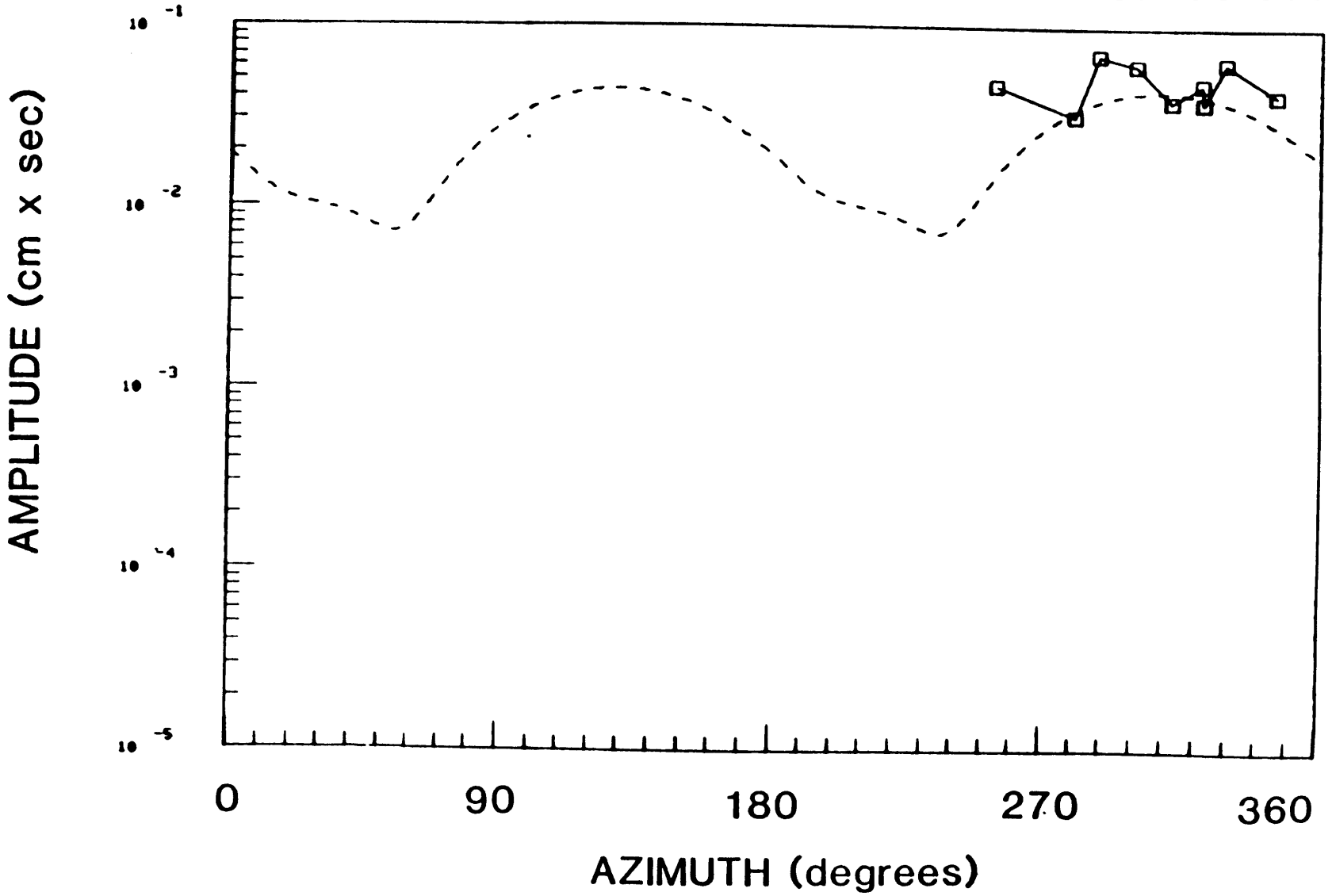
PERIOD 98 sec
AMPLITUDE (cm x sec)
10 -1
10 -2
10 -3
10 -4
10 -5
0
90
180
270
360
AZIMUTH (degrees)

FIGURE B.11a

11/10/67

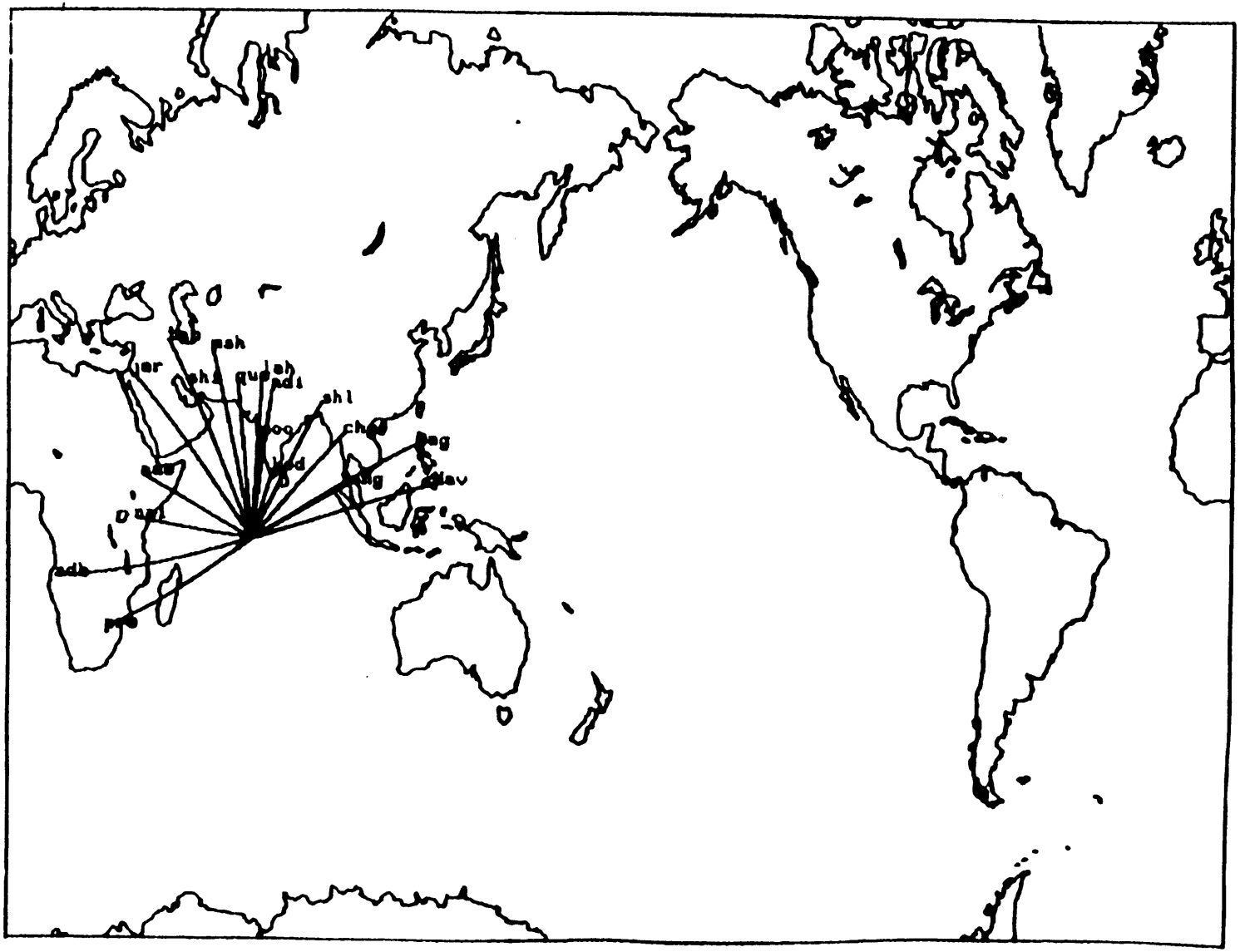

FIGURE B.11b

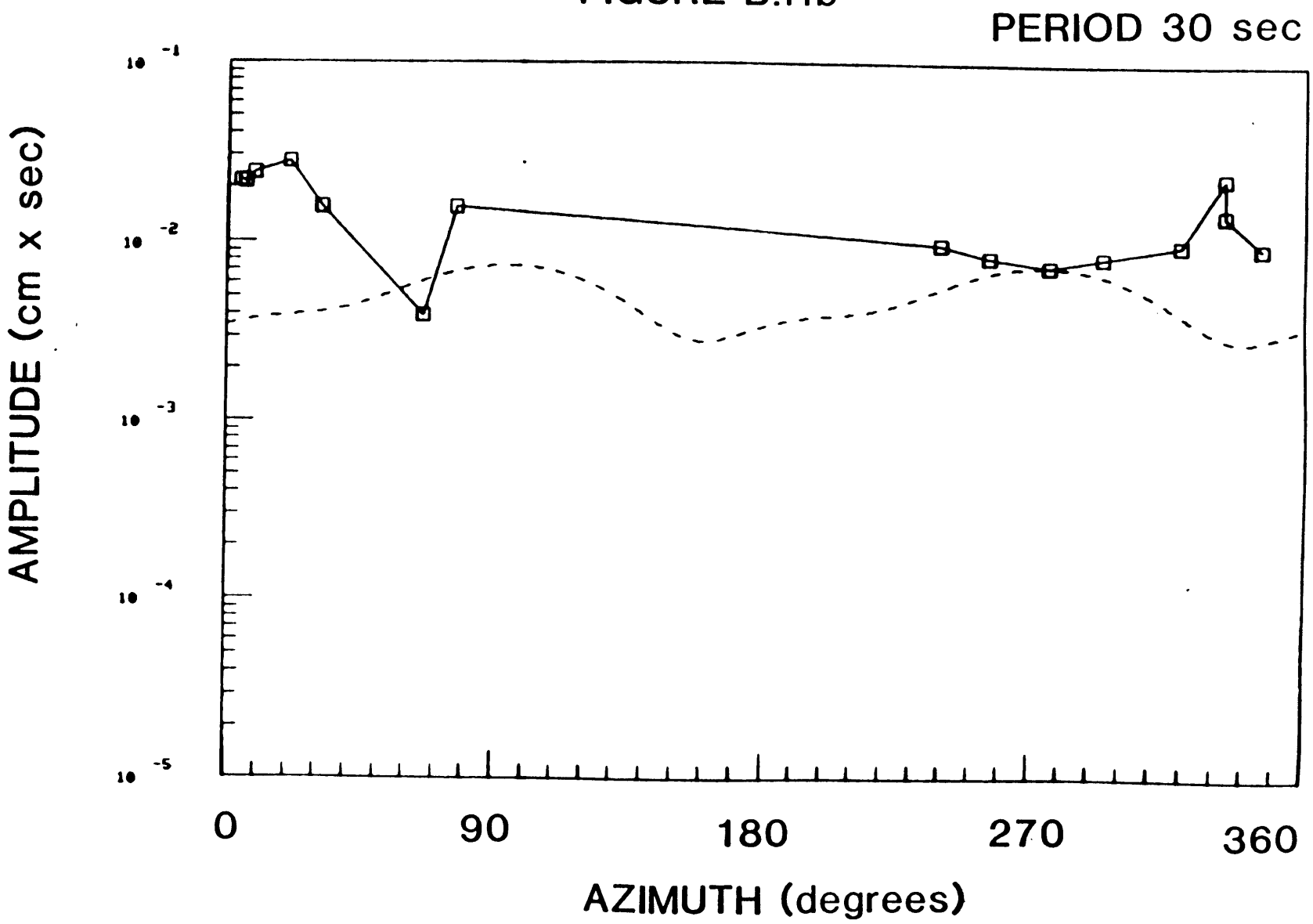
PERIOD 30 sec
AMPLITUDE (cm x sec)
10 -1
10 -2
10 -3
10 -4
10 -5
0
90
180
270
360
AZIMUTH (degrees)

FIGURE B.11c

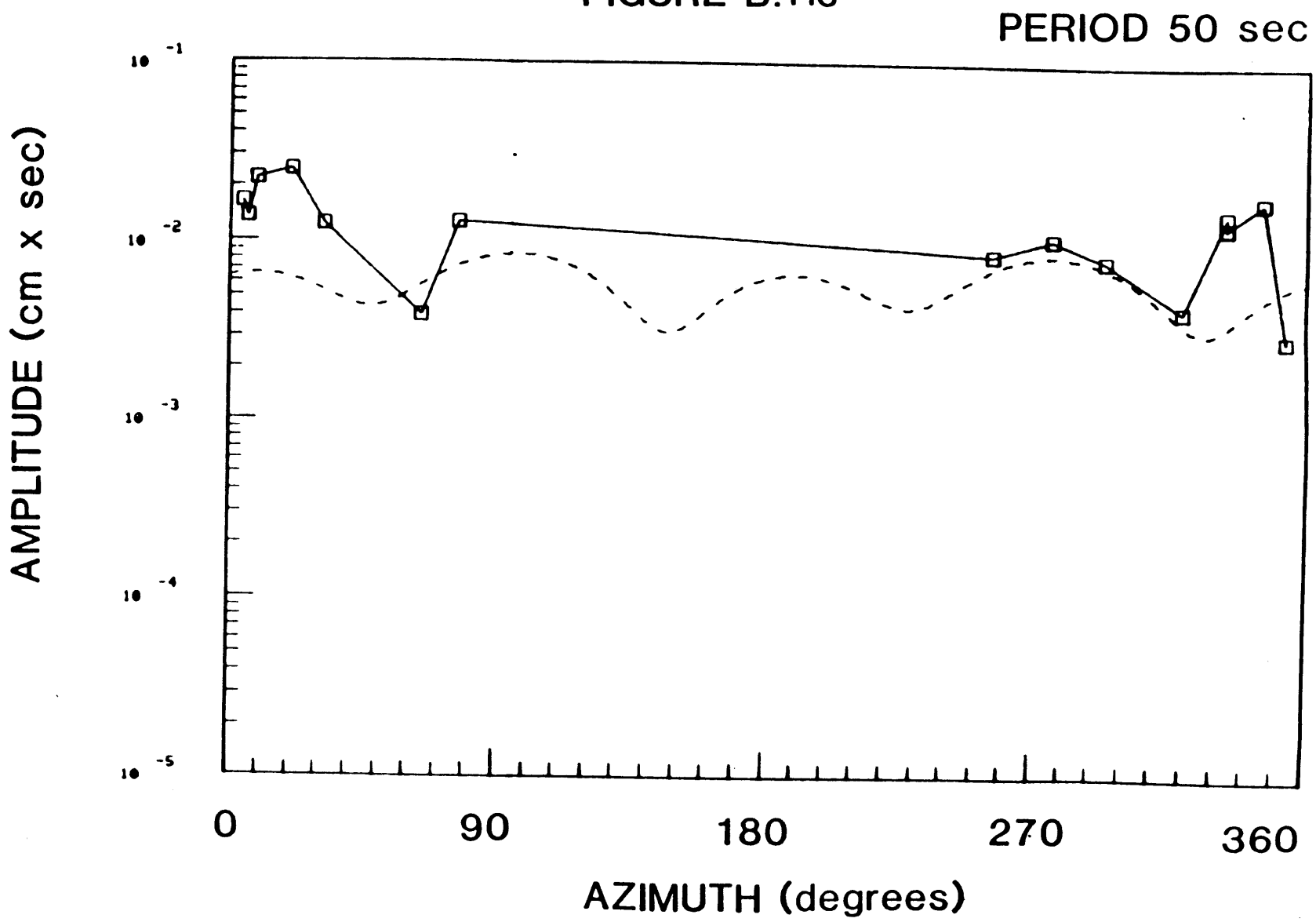
PERIOD 50 sec
AMPLITUDE (cm x sec)
10 -1
10 -2
10 -3
10 -4
10 -5
0
90
180
270
360
AZIMUTH (degrees)

FIGURE B.11d

PERIOD 70 sec

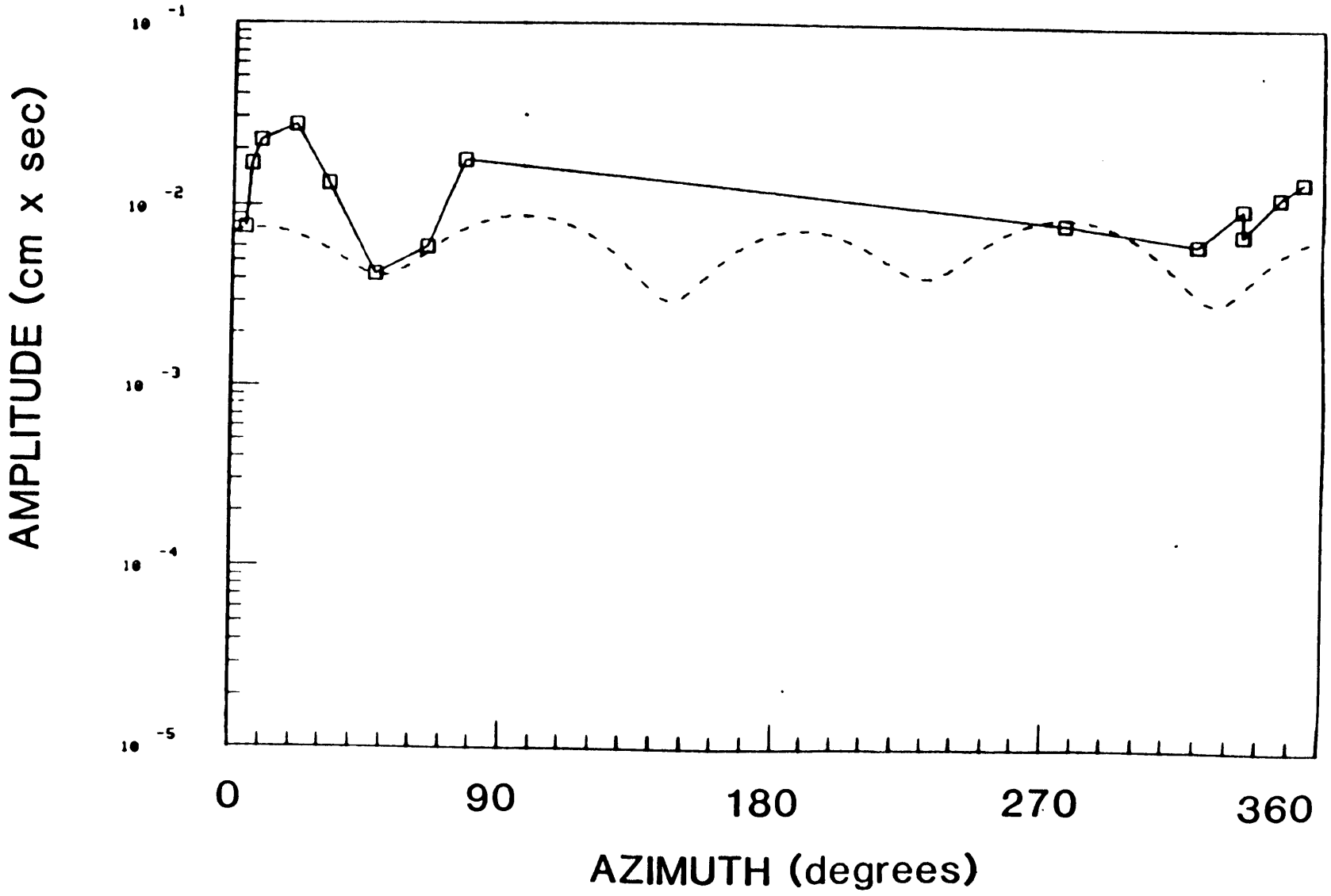

FIGURE B.11e

PERIOD 98 sec

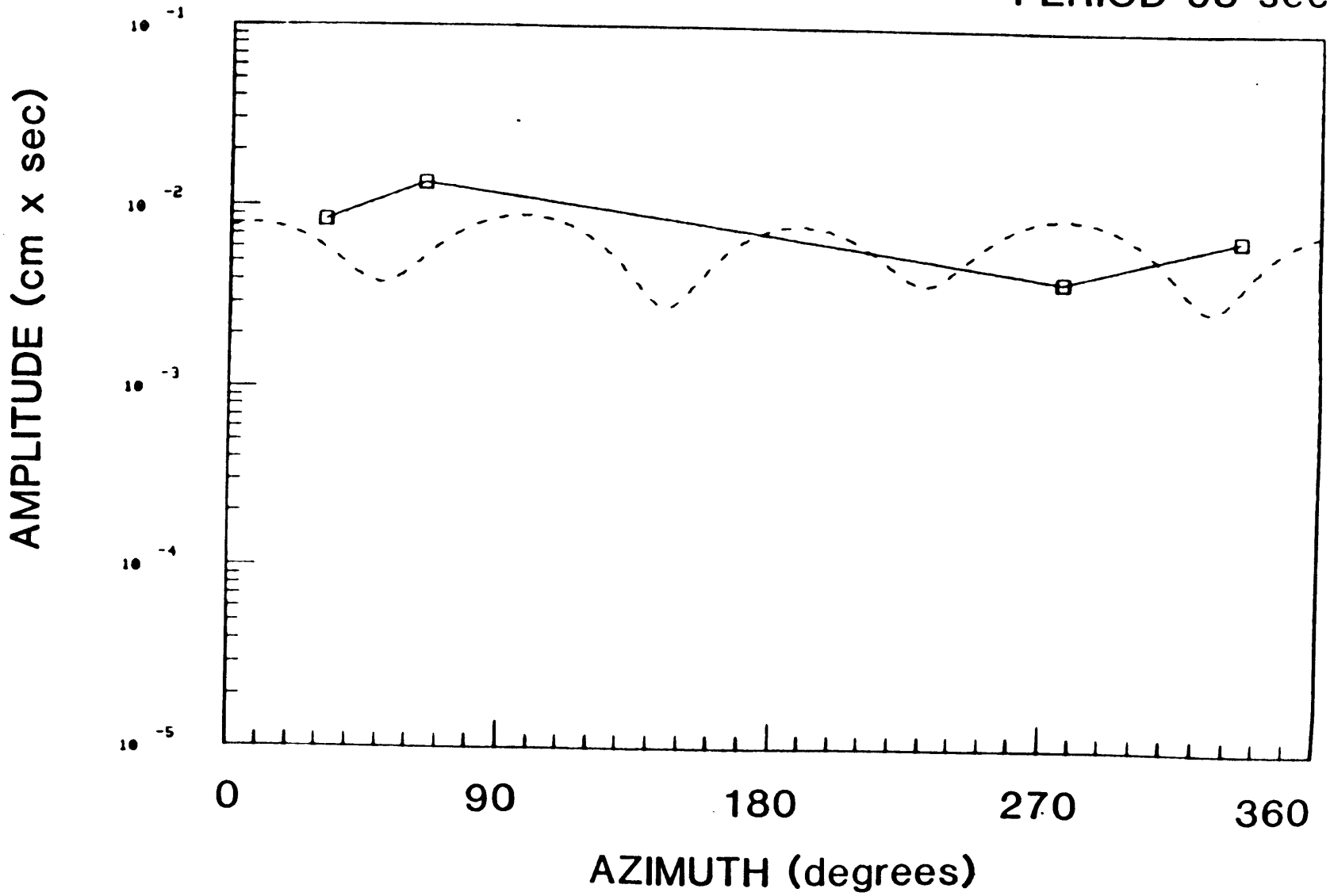

FIGURE B.12a 11/11/67

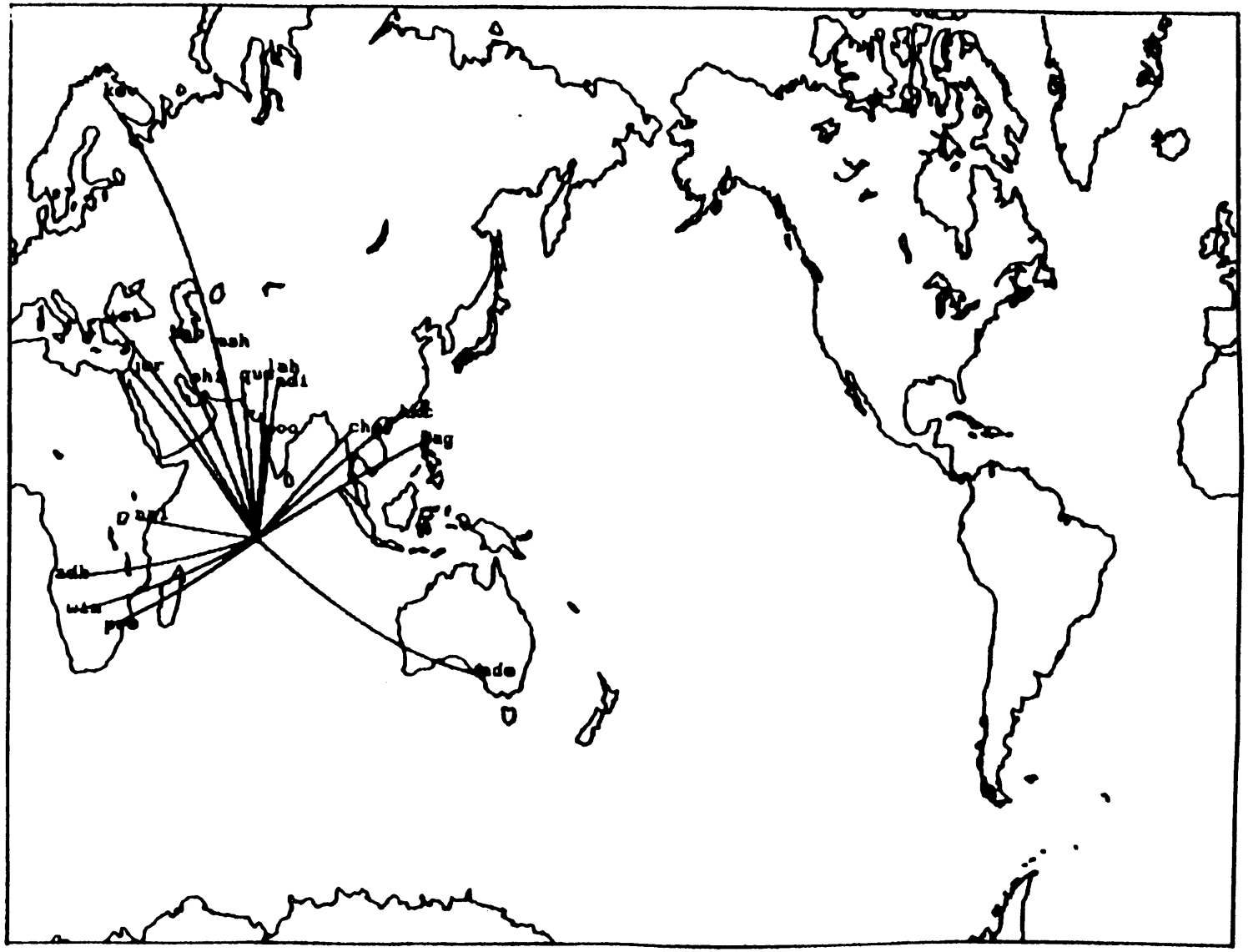

FIGURE B.12b

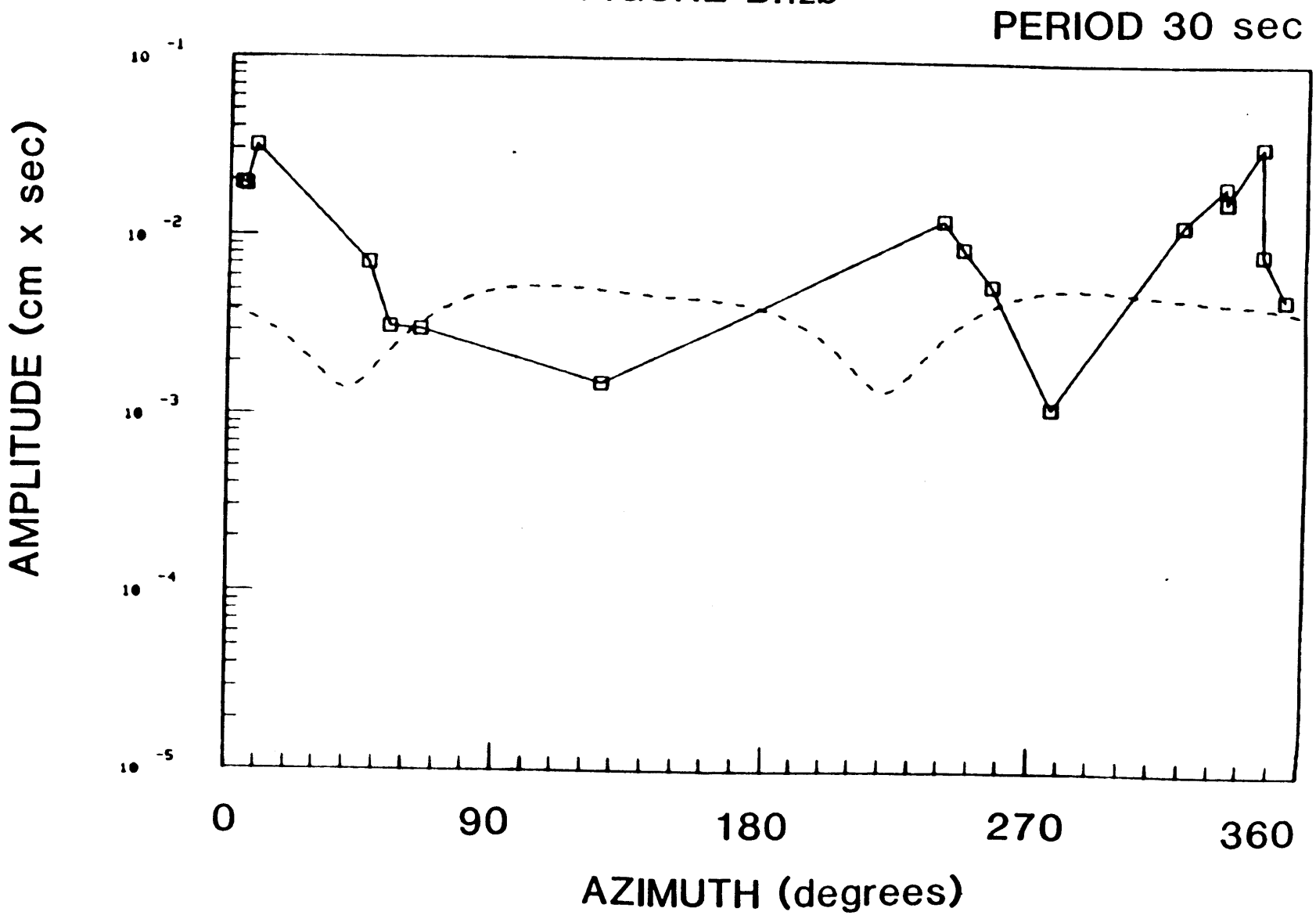
PERIOD 30 sec
AMPLITUDE (cm x sec)
10 -1
10 -2
10 -3
10 -4
10 -5
0
90
180
270
360
AZIMUTH (degrees)

FIGURE B.12c

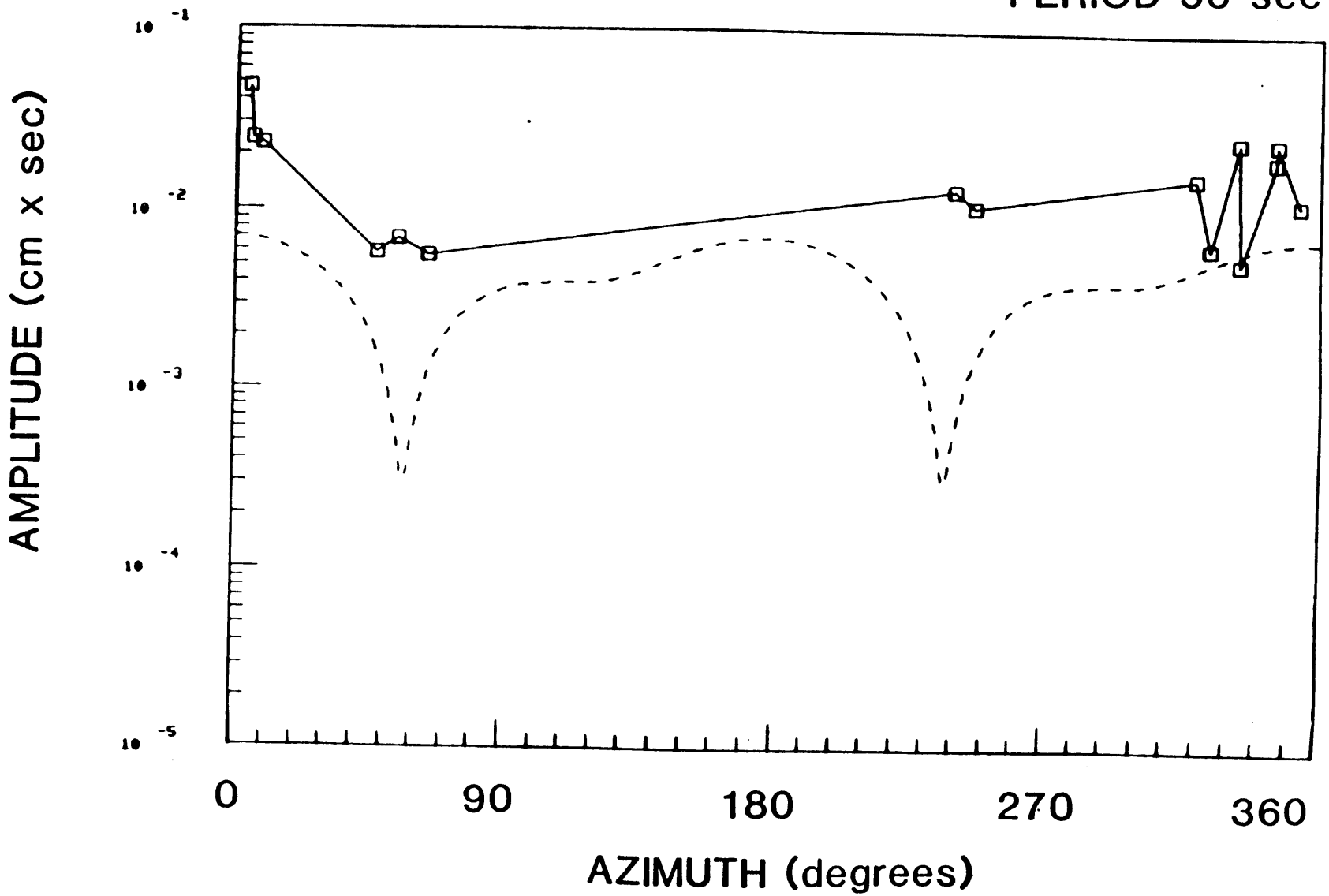
PERIOD 50 sec
AMPLITUDE (cm x sec)
10 -1
10 -2
10 -3
10 -4
10 -5
0
90
180
270
360
AZIMUTH (degrees)

FIGURE B.12d

PERIOD 70 sec

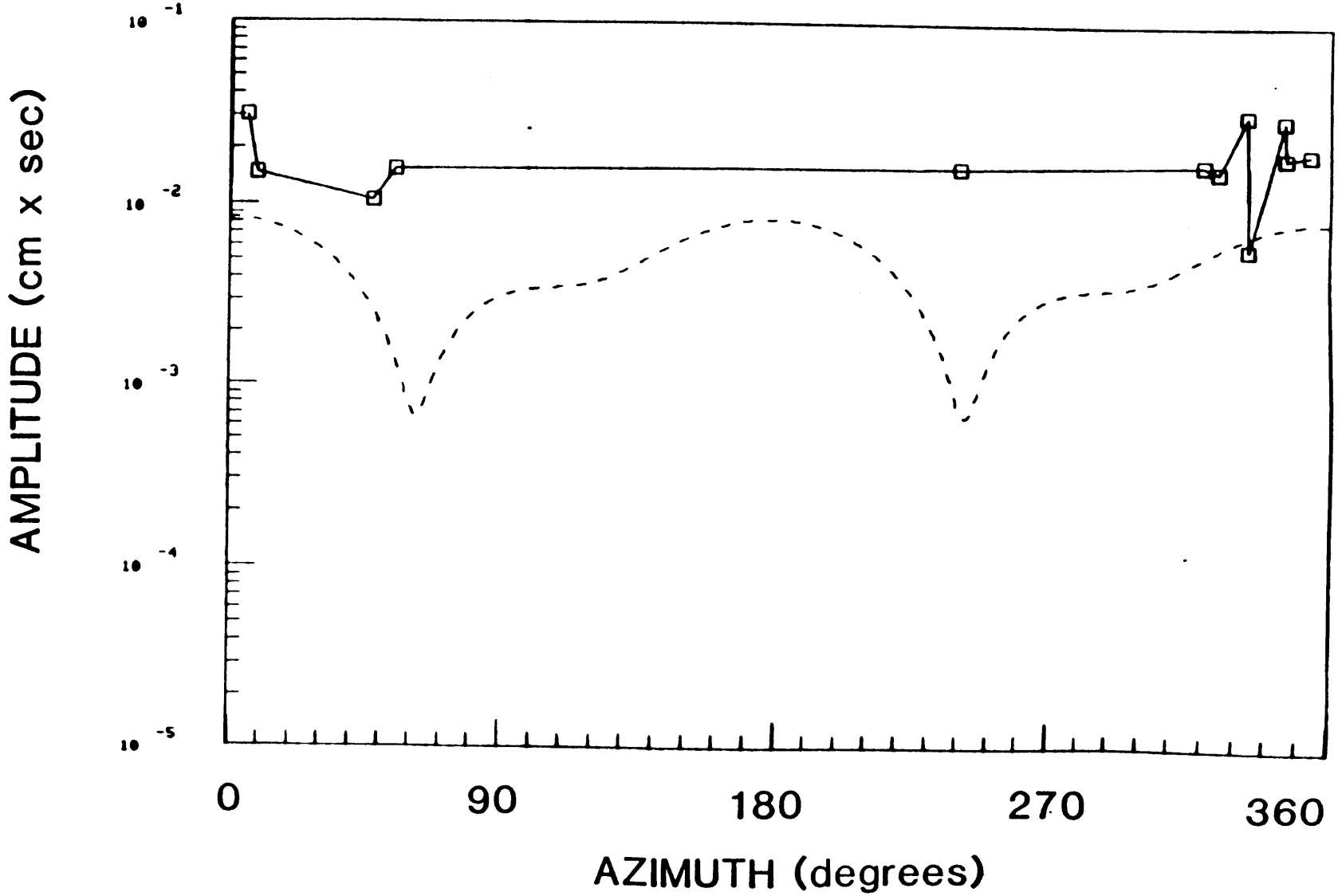

FIGURE B.12e

PERIOD 98 sec

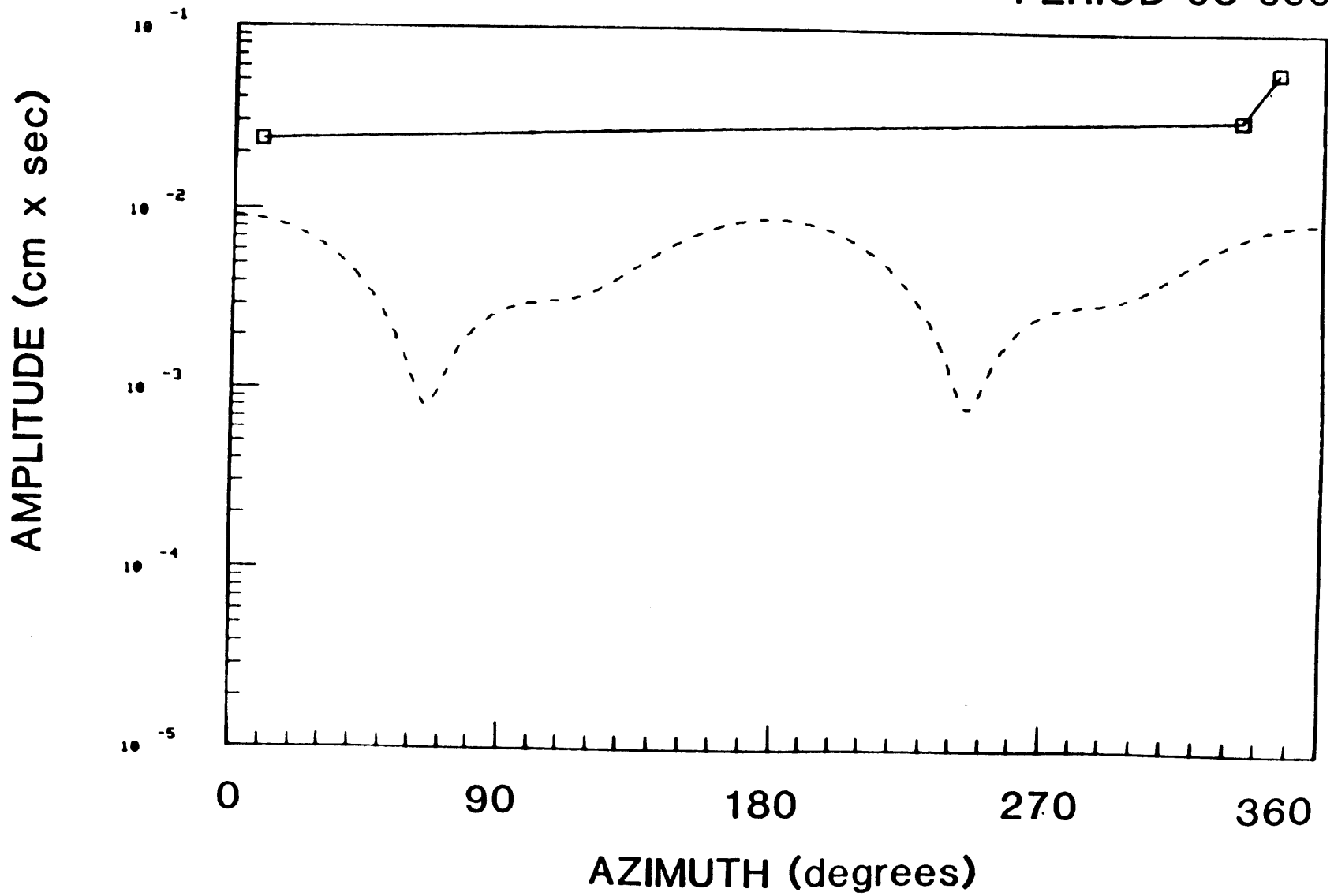

FIGURE B.13a

03/02/68

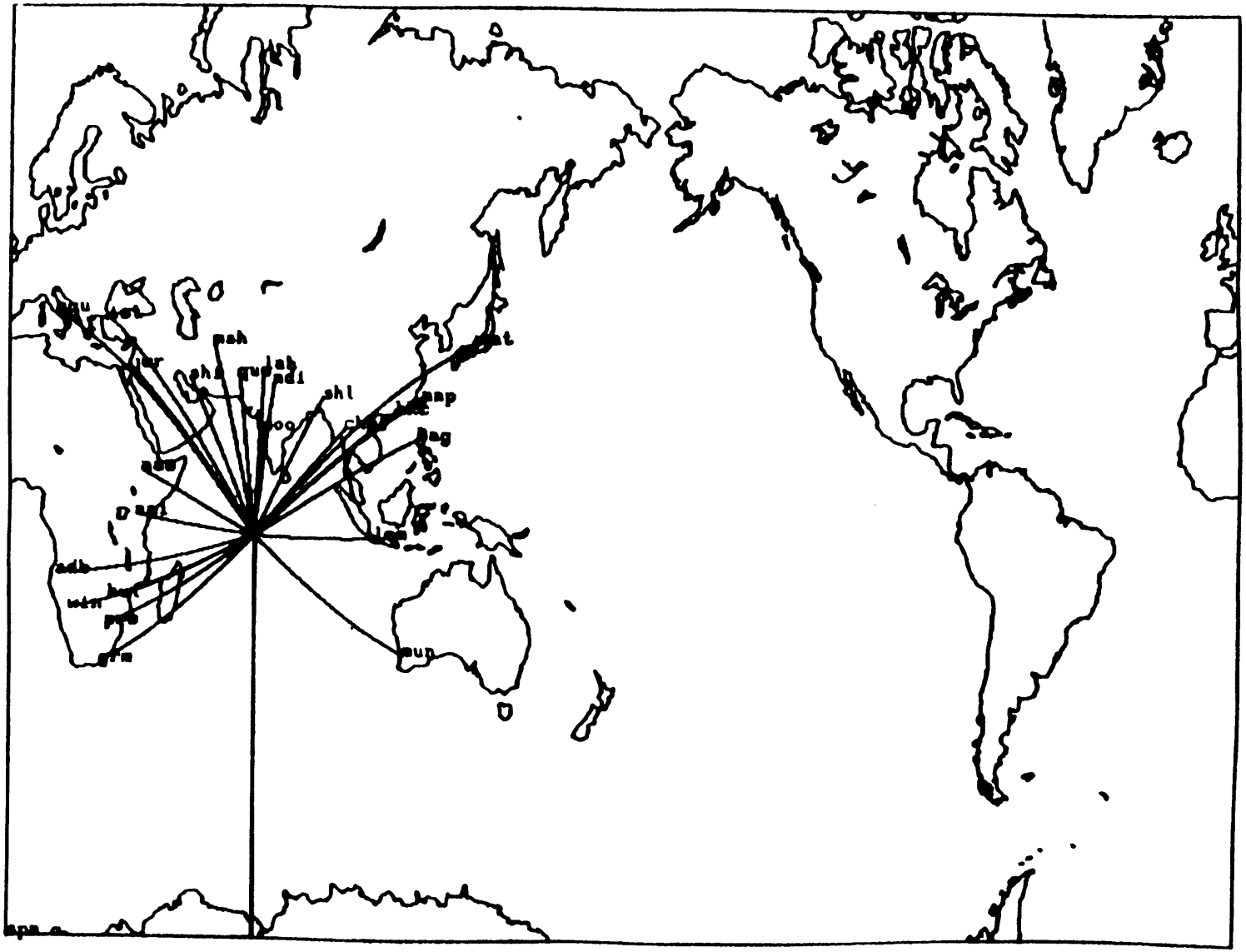

FIGURE B.13b

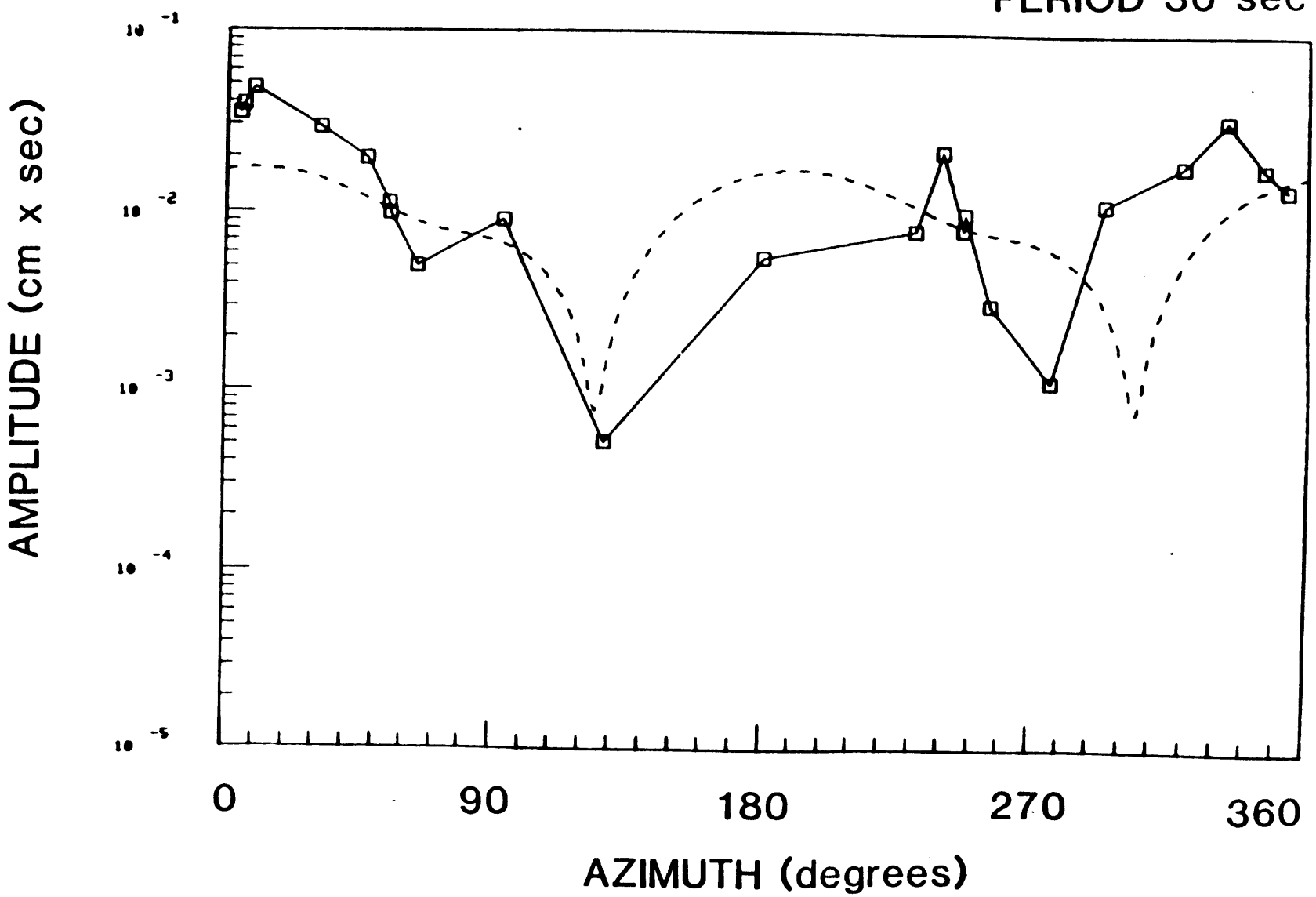
PERIOD 30 sec
AMPLITUDE (cm x sec)
10 -1
10 -2
10 -3
10 -4
10 -5
0
90
180
270
360
AZIMUTH (degrees)

FIGURE B.13C

PERIOD 50 sec

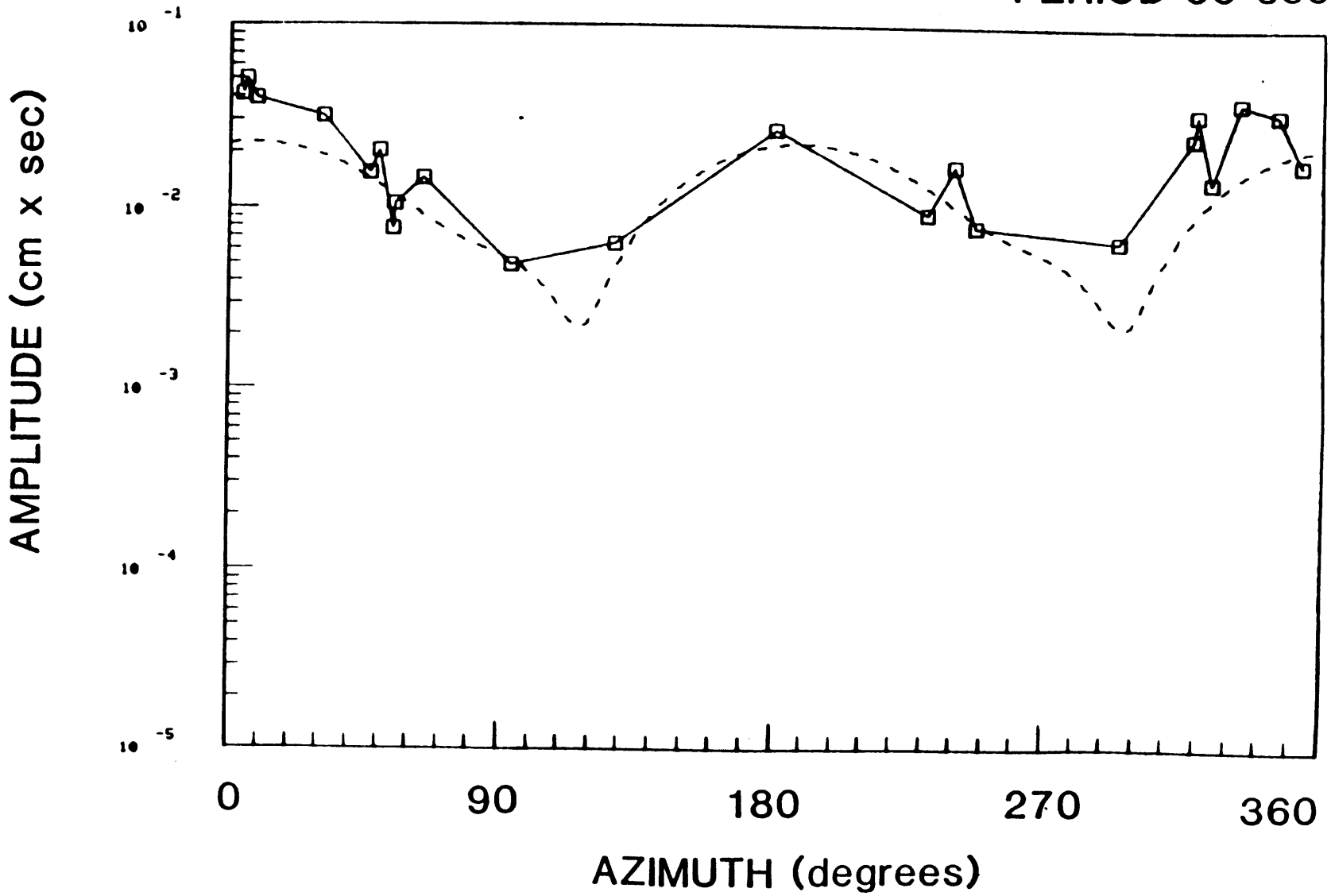

FIGURE B.13d

PERIOD 70 sec

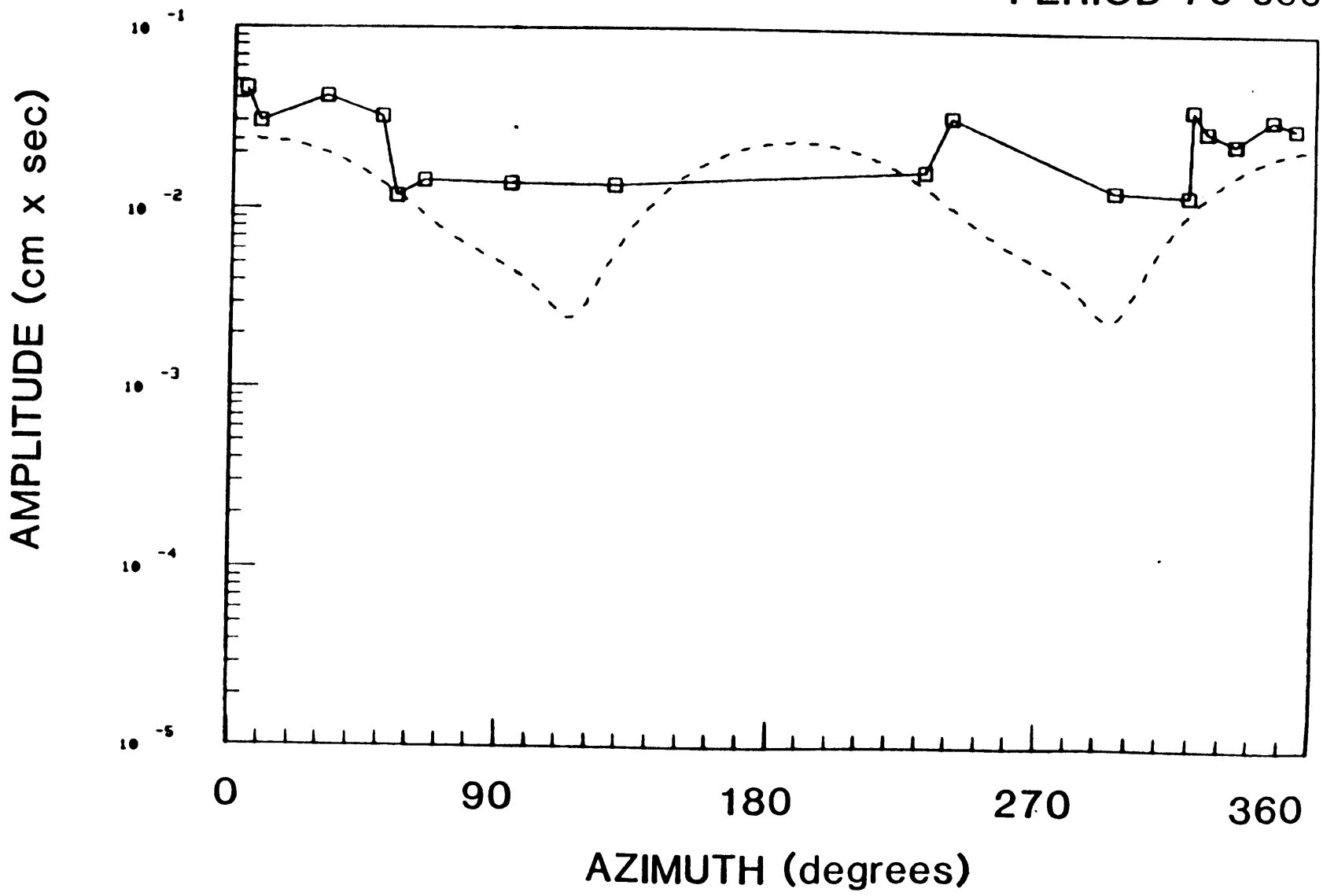

FIGURE B.13e

PERIOD 98 sec

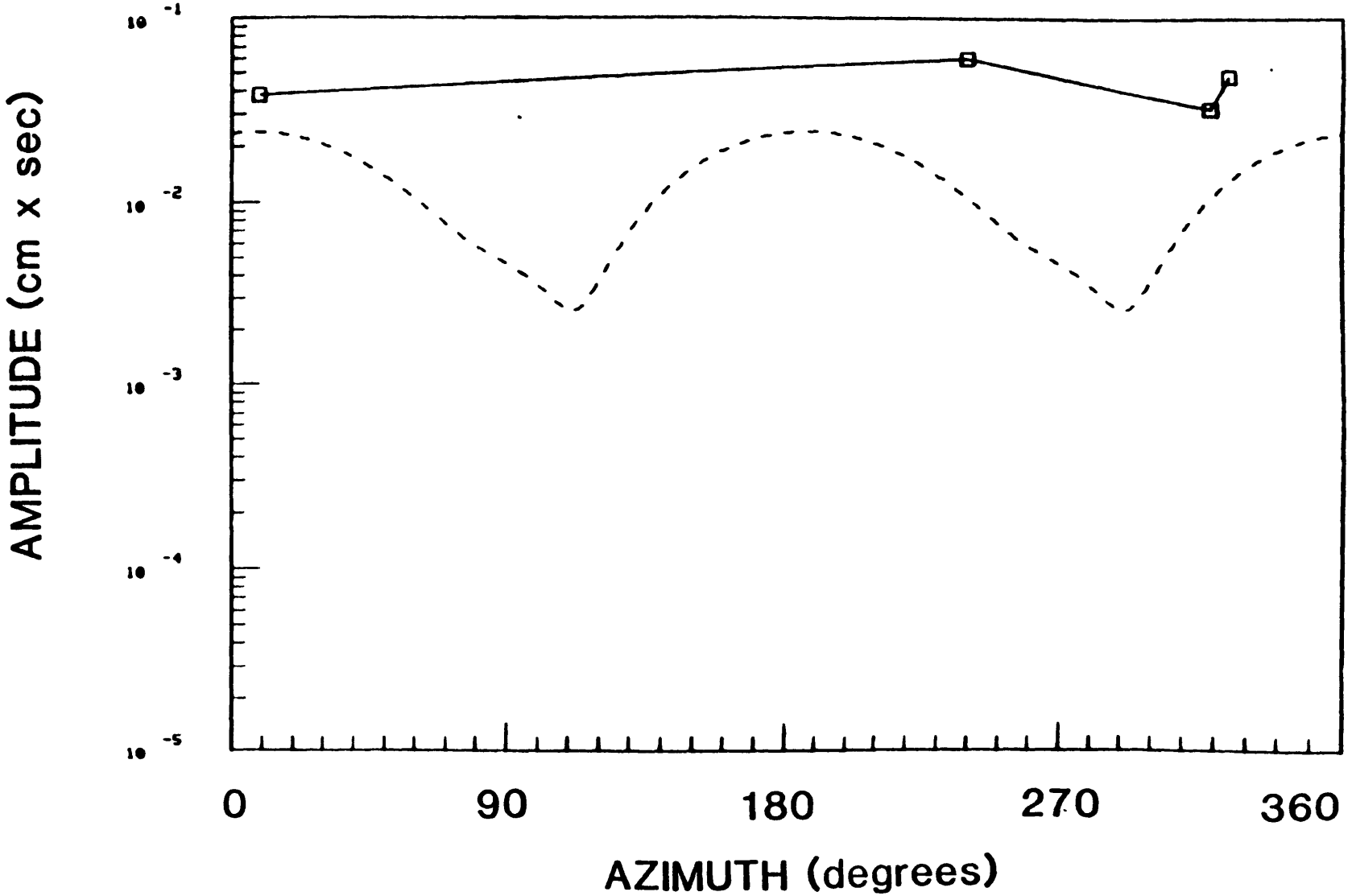

FIGURE B.14a

09/03/68

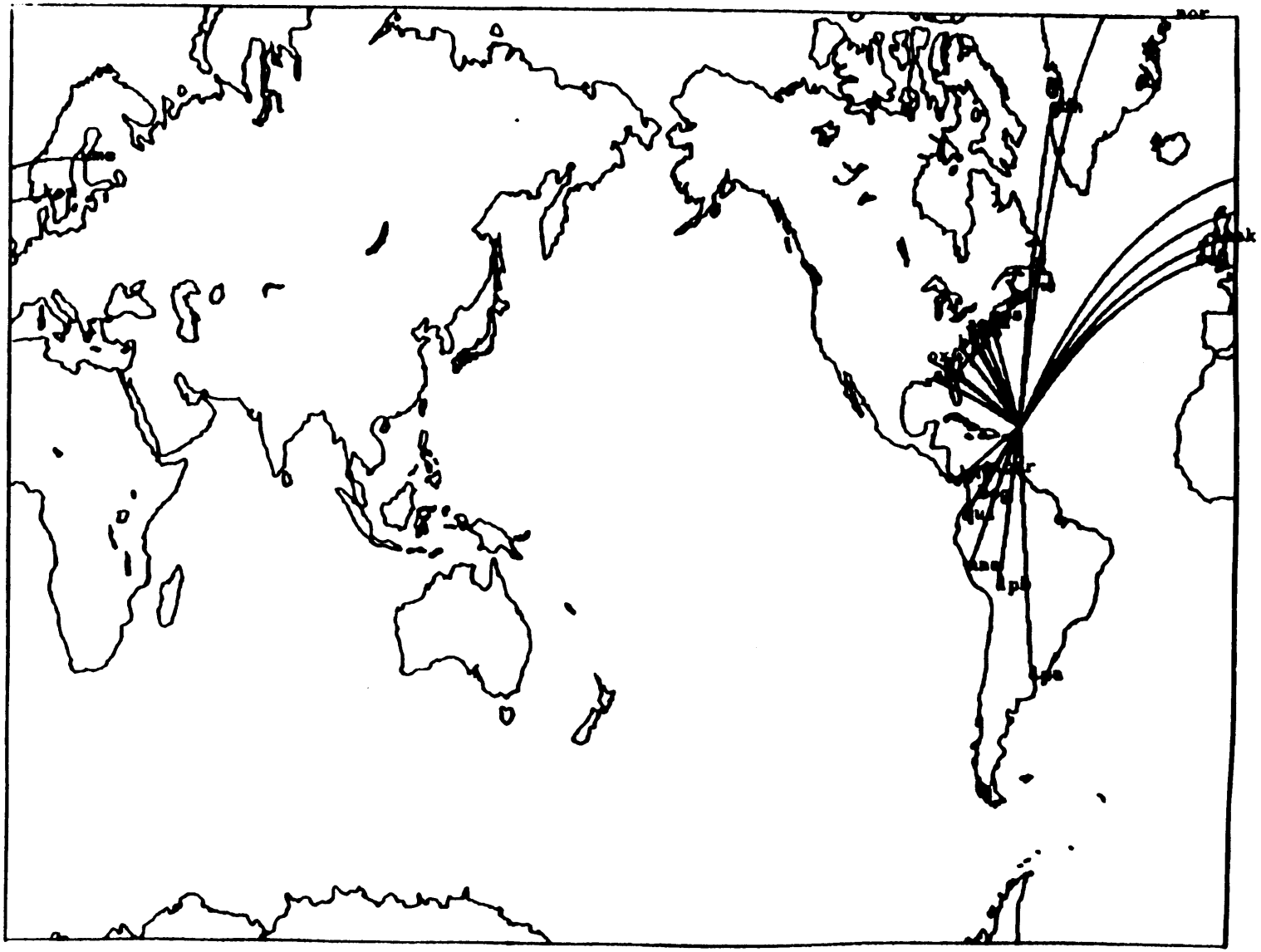

FIGURE B.14b

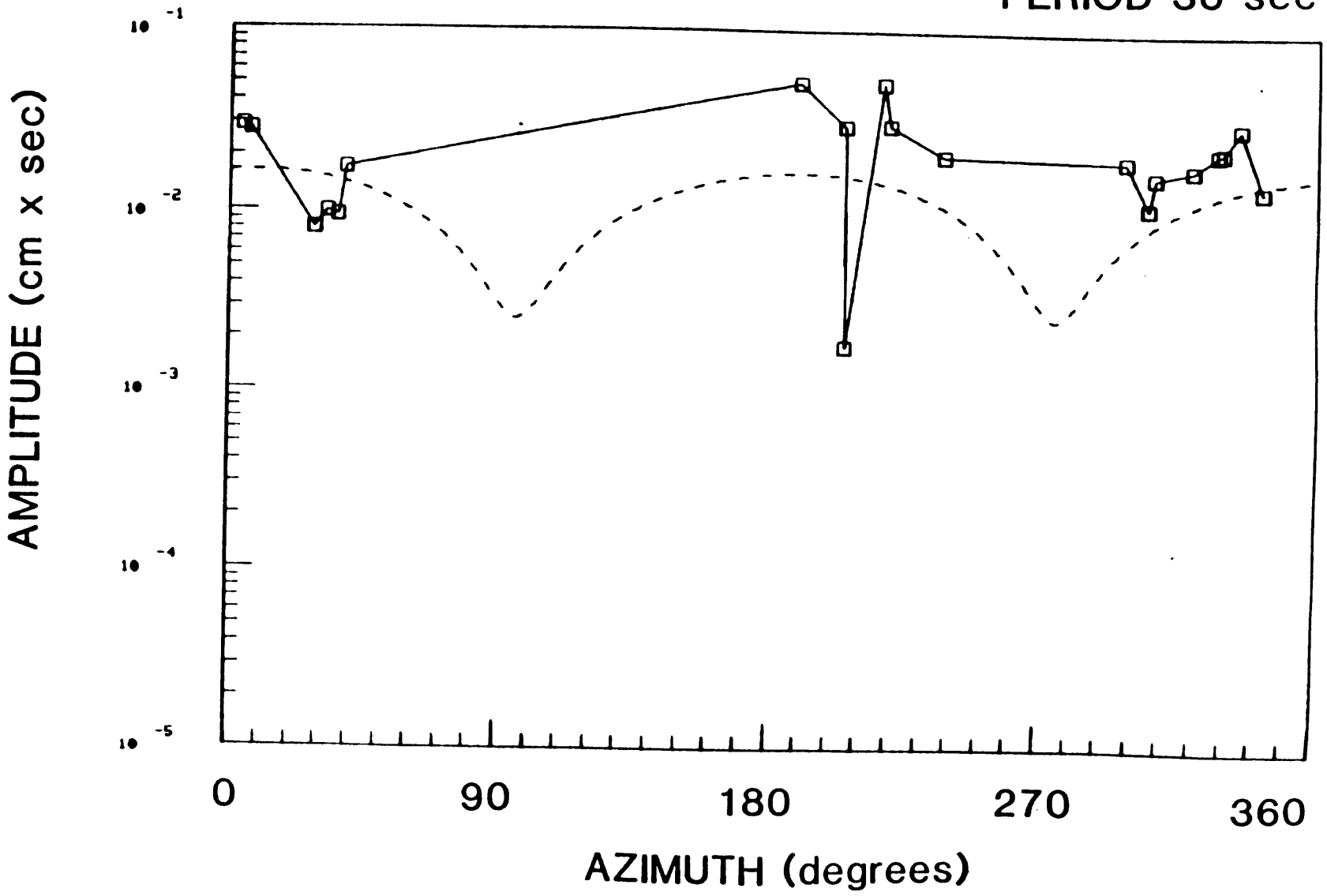
PERIOD 30 sec
AMPLITUDE (cm x sec)
10 -1
10 -2
10 -3
10 -4
10 -5
0
90
180
270
360
AZIMUTH (degrees)

FIGURE B.14c

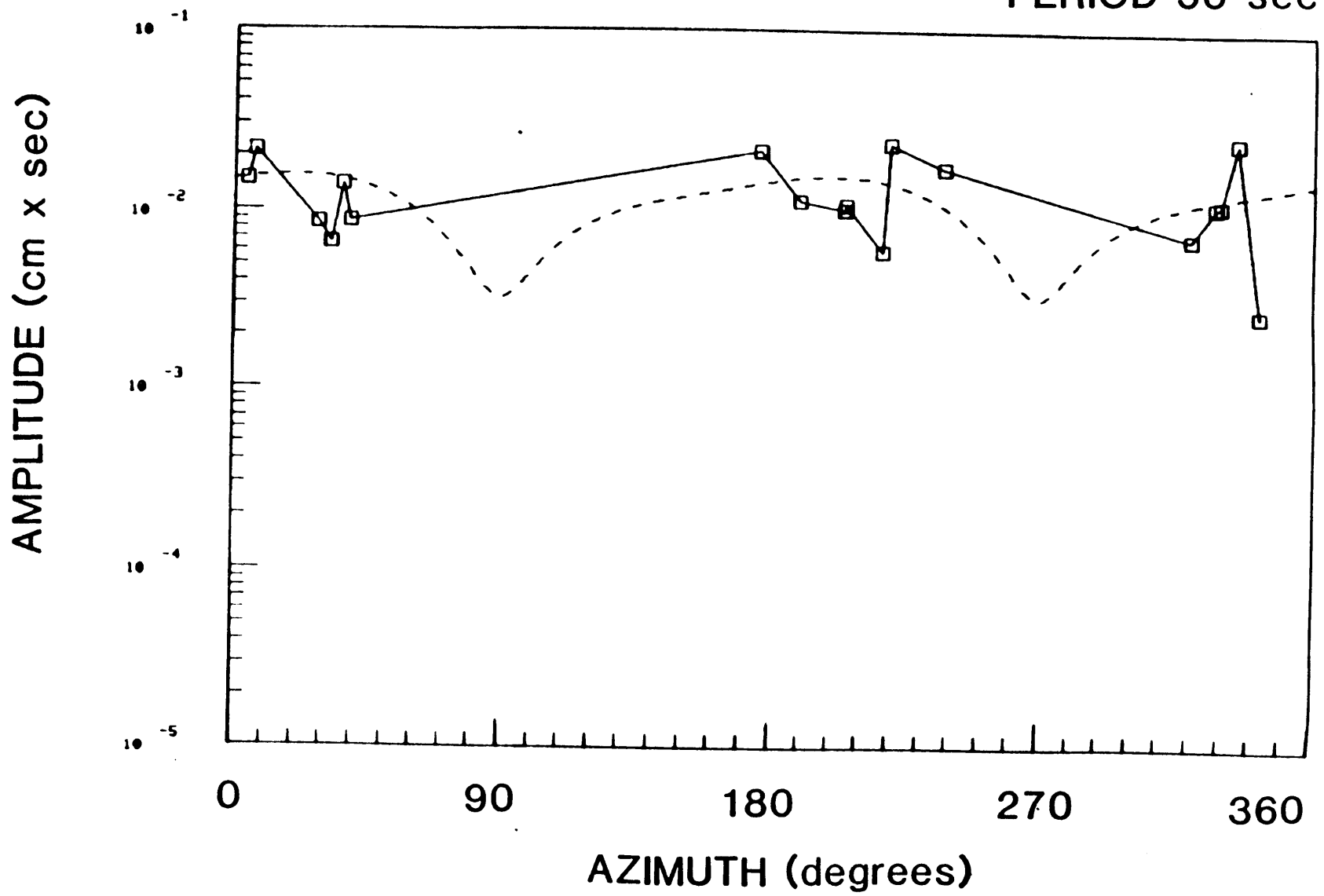
PERIOD 50 sec
AMPLITUDE (cm x sec)
10 -1
10 -2
10 -3
10 -4
10 -5
0
90
180
270
360
AZIMUTH (degrees)

FIGURE B.14d

PERIOD 70 sec

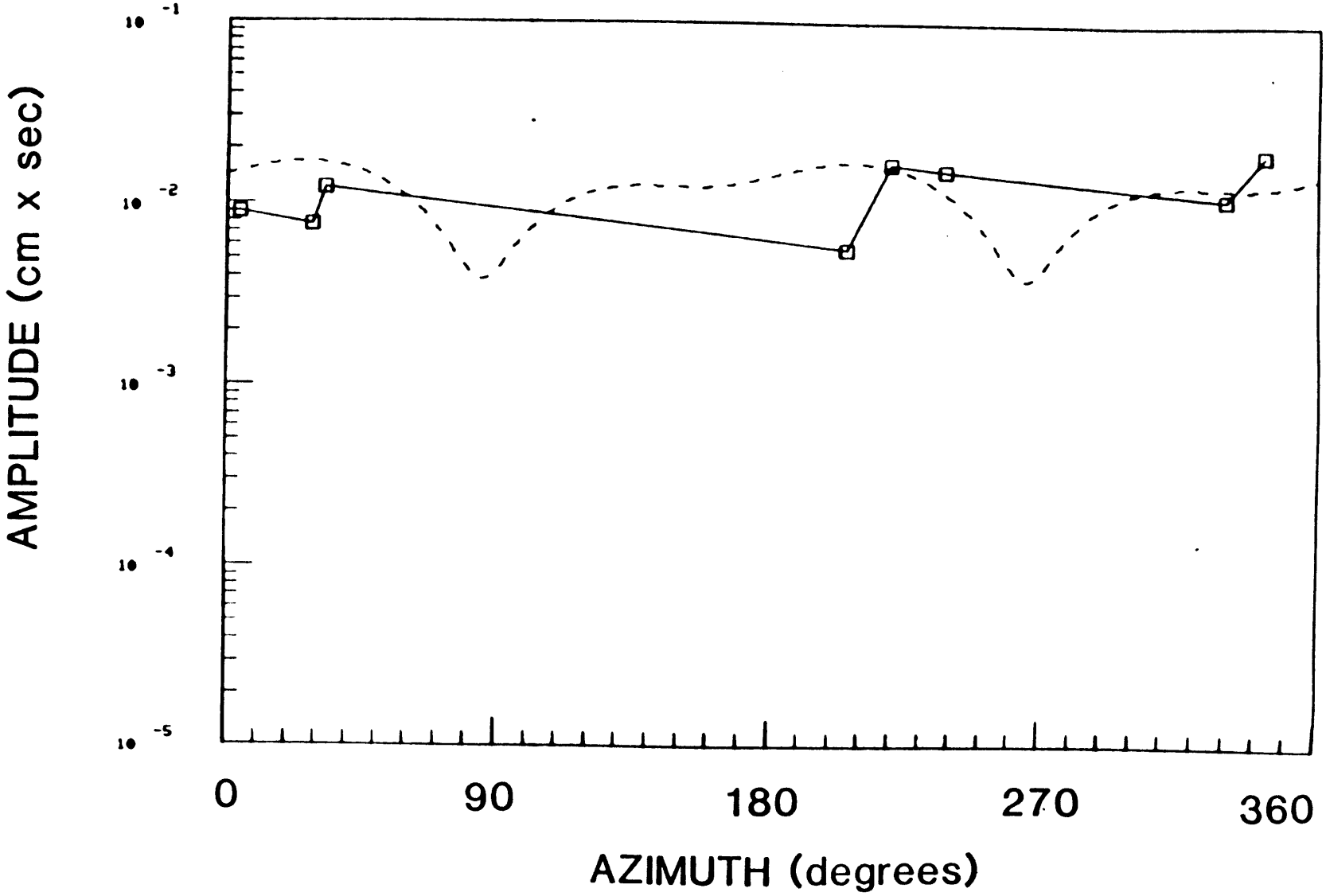

FIGURE B.14e

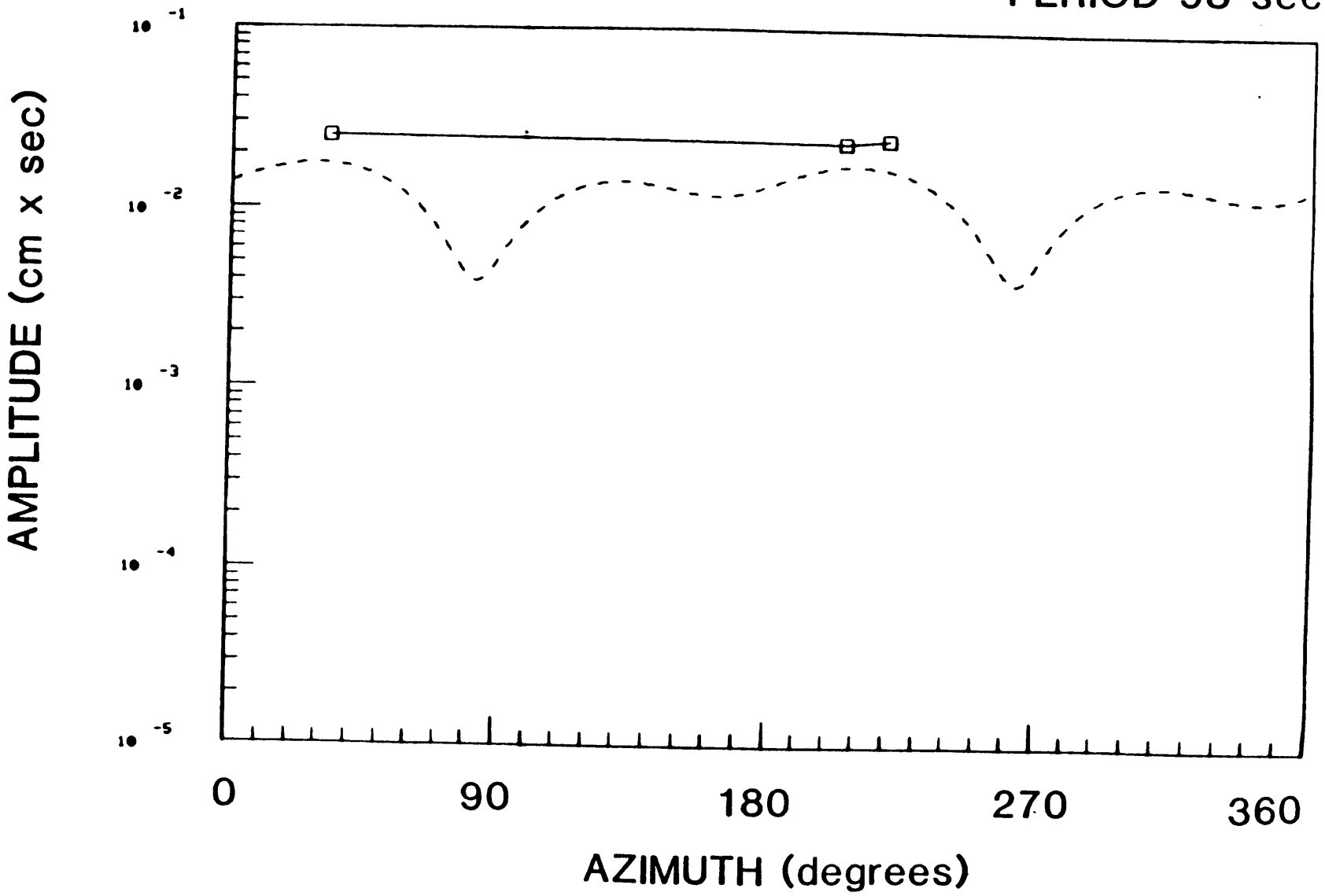
PERIOD 98 sec
AMPLITUDE (cm x sec)
10 -1
10 -2
10 -3
10 -4
10 -5
0
90
180
270
360
AZIMUTH (degrees)

FIGURE B.15a

10/08/68

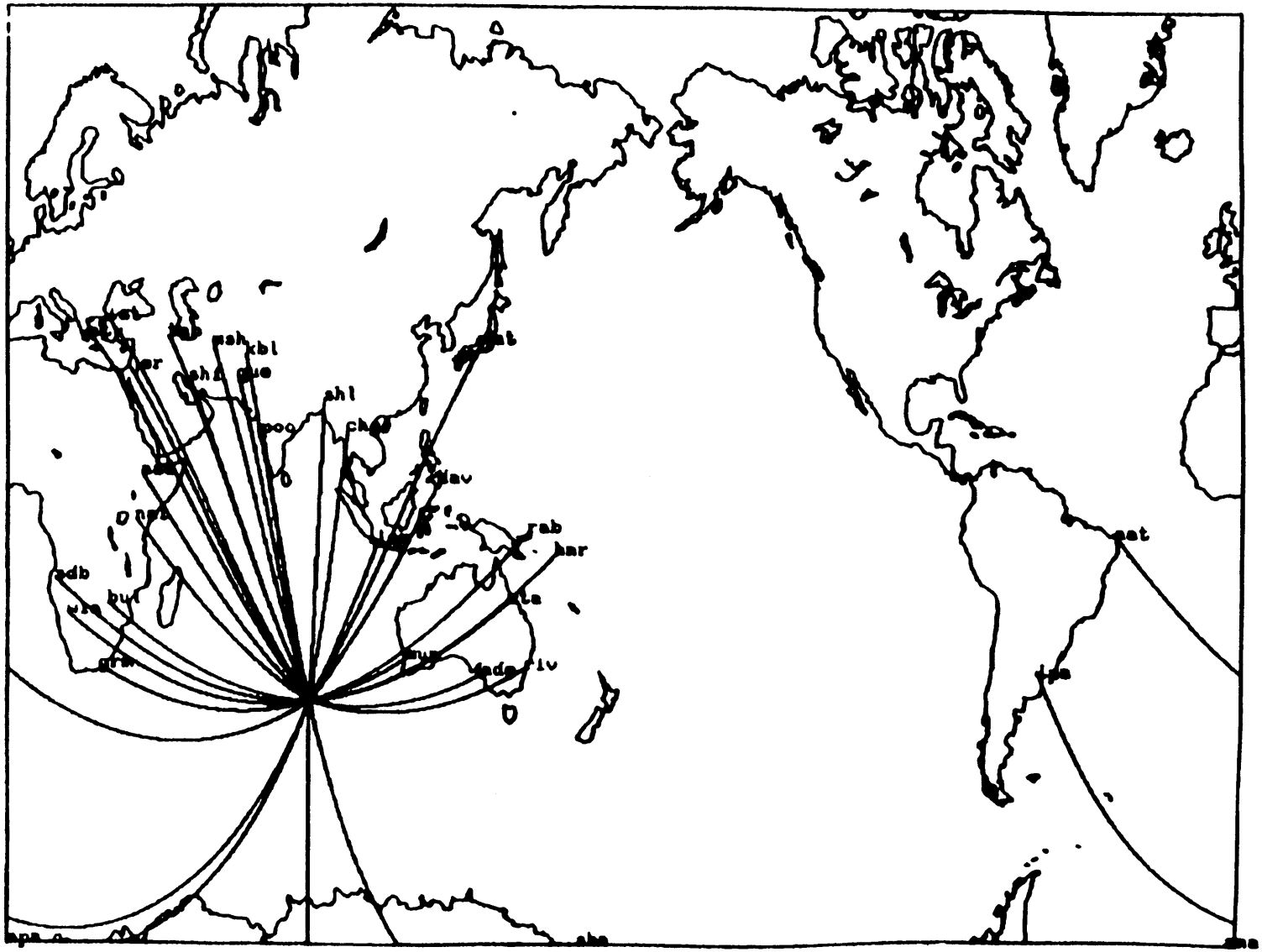

FIGURE B.15b

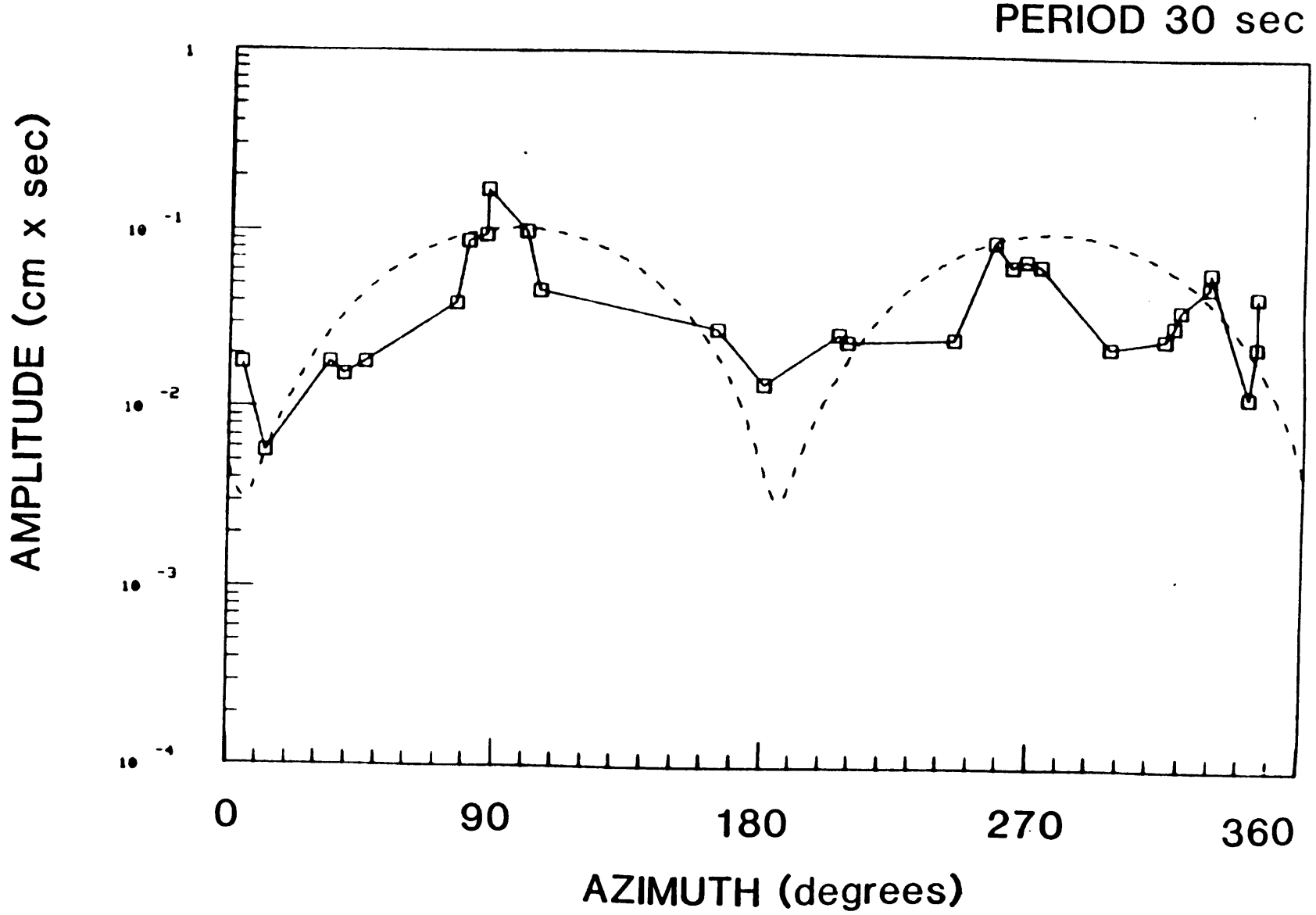
PERIOD 30 sec
AMPLITUDE (cm x sec)
1
10 -1
10 -2
10 -3
10 -4
0
90
180
270
360
AZIMUTH (degrees)

FIGURE B.15c

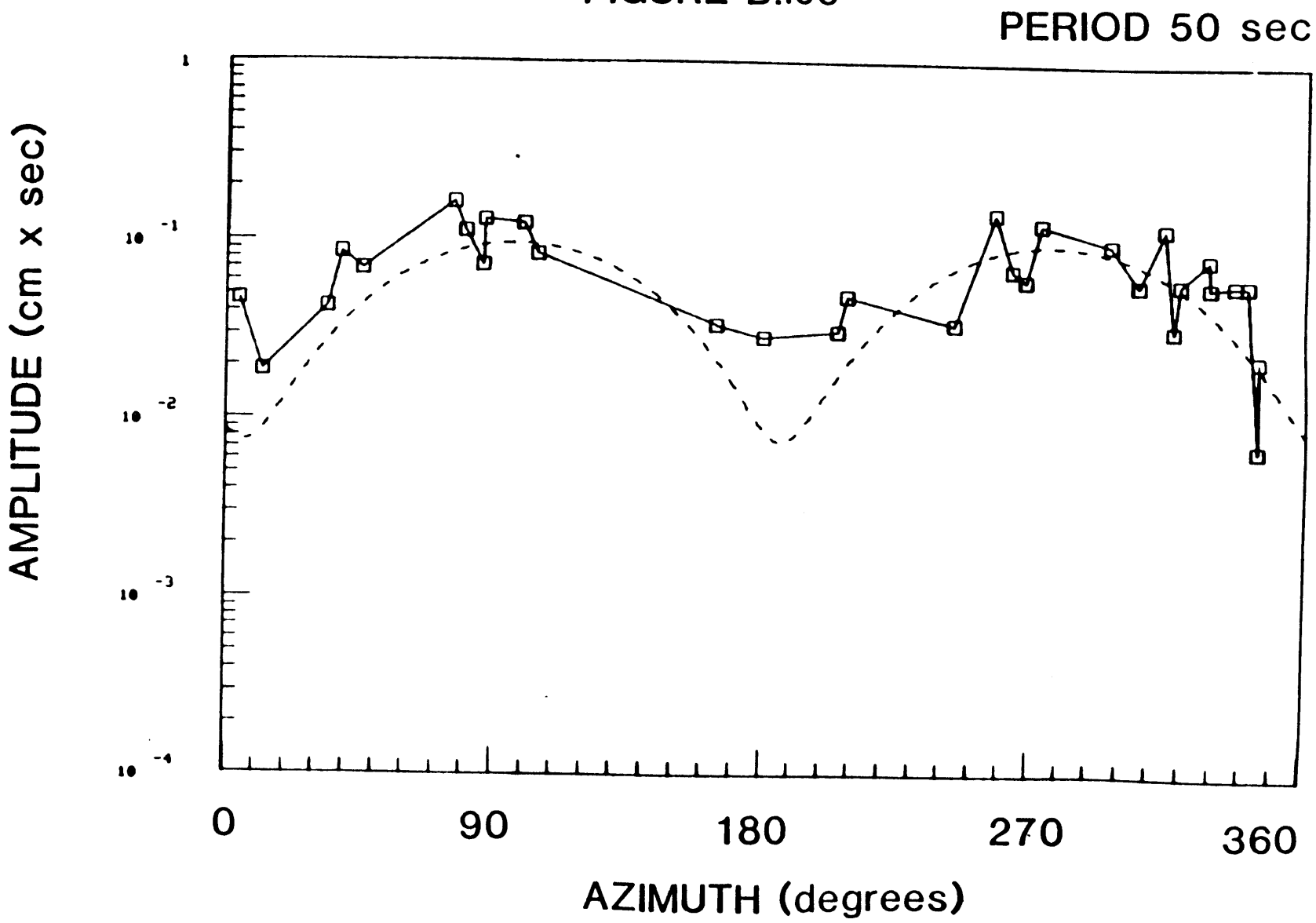
PERIOD 50 sec
AMPLITUDE (cm x sec)
1
10 -1
10 -2
10 -3
10 -4
0
90
180
270
360
AZIMUTH (degrees)

FIGURE B.15d

PERIOD 70 sec

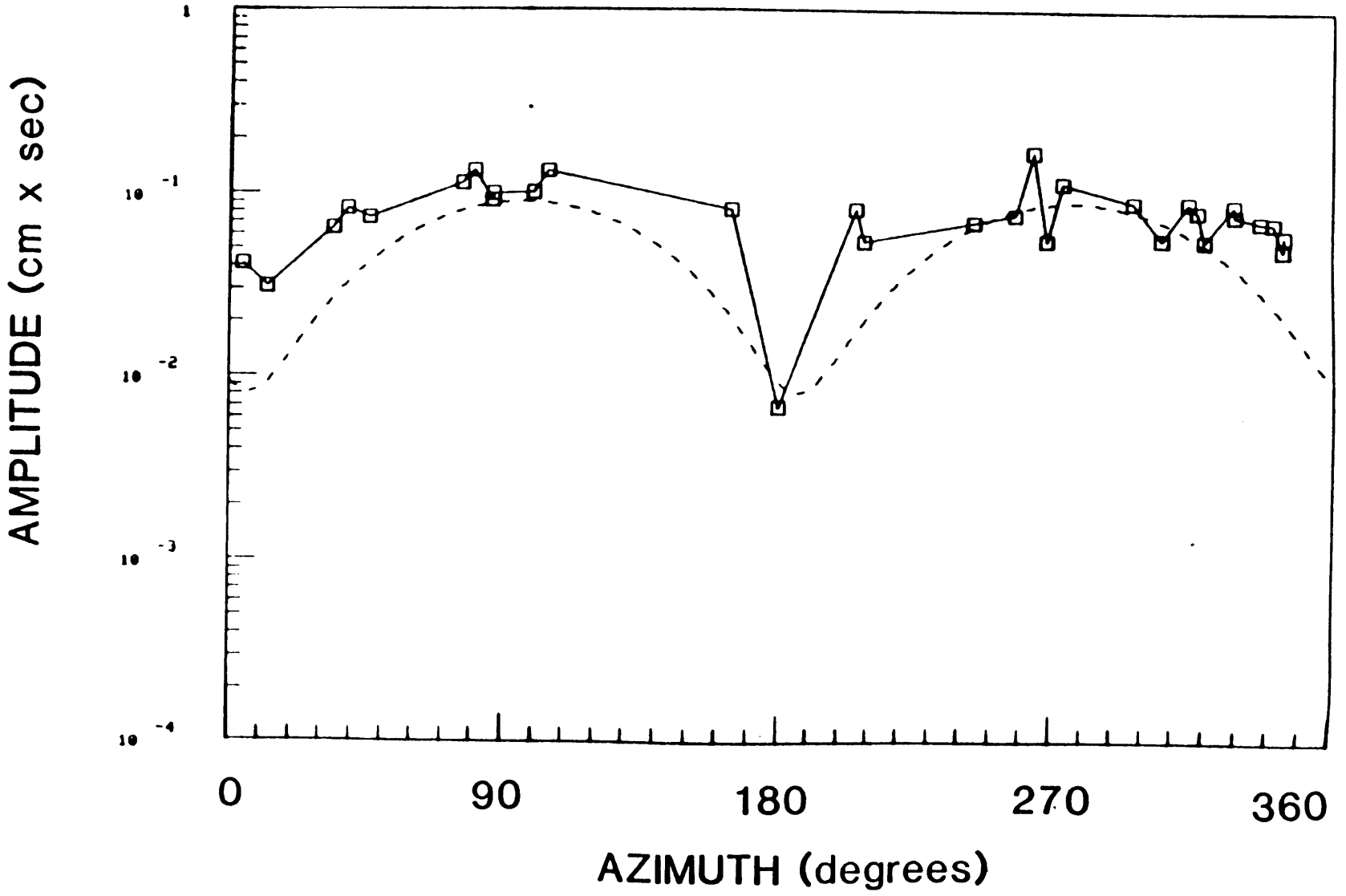

FIGURE B.15e

PERIOD 98 sec

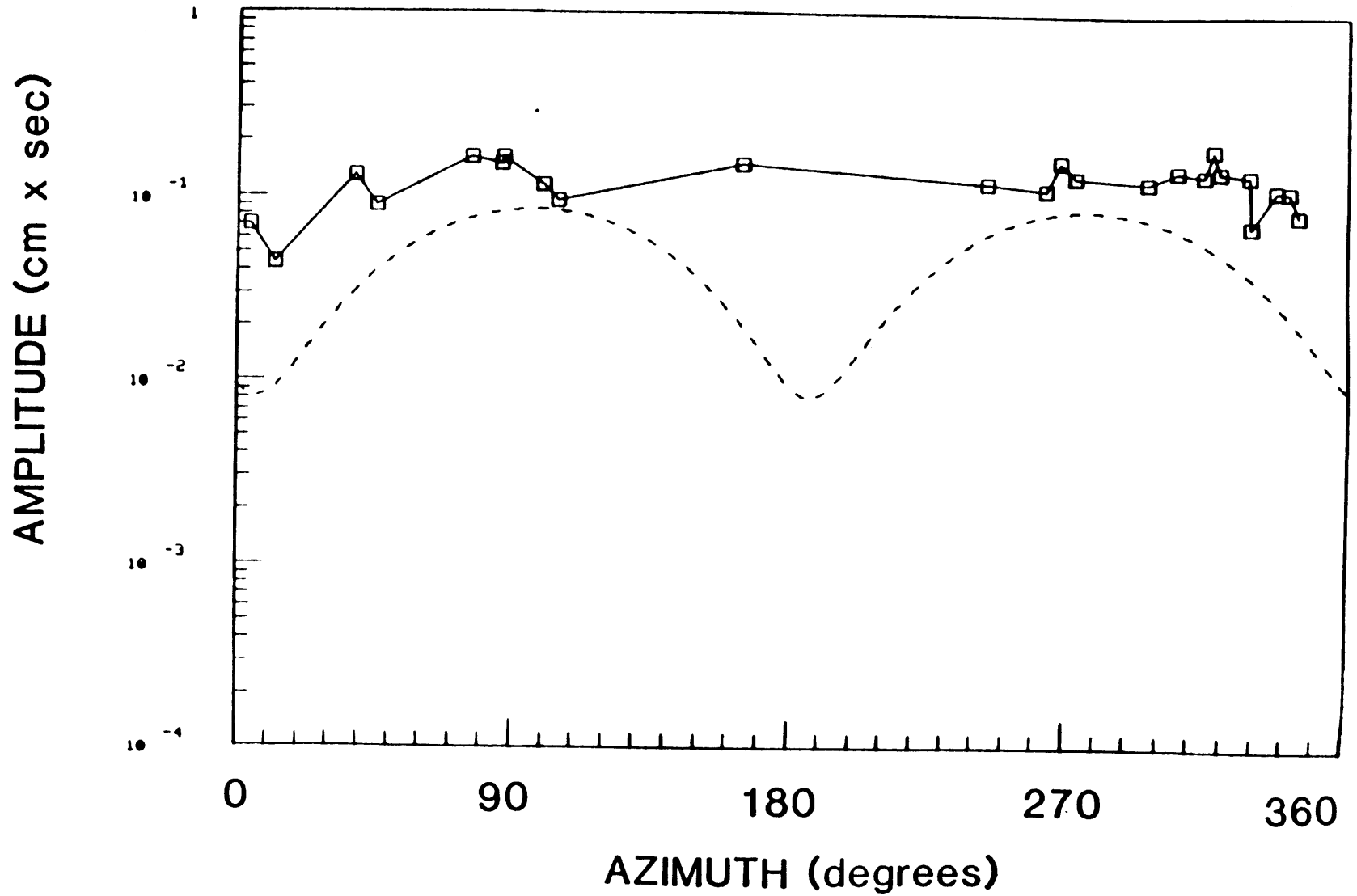

FIGURE B.16a

03/31/69

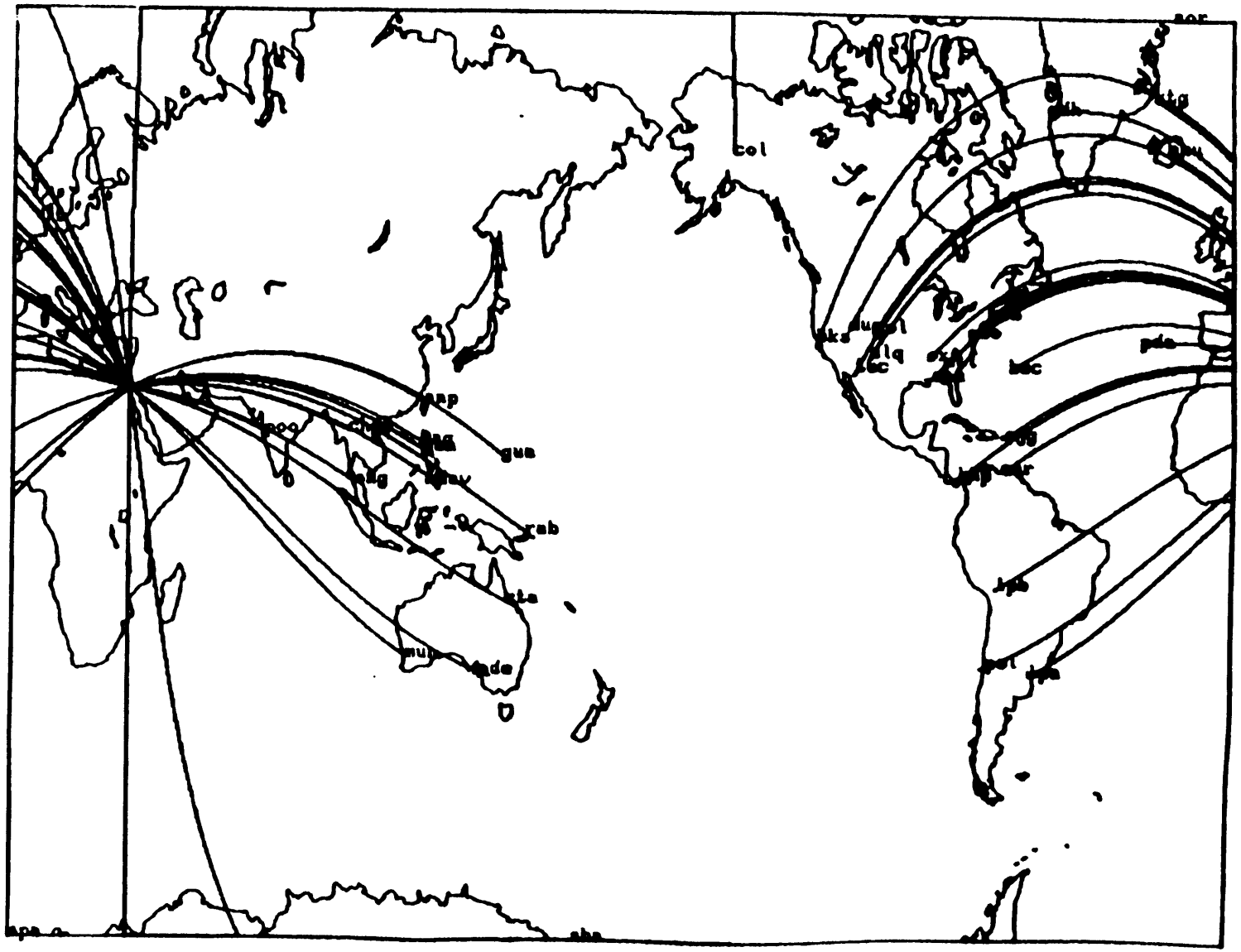

FIGURE B.16b

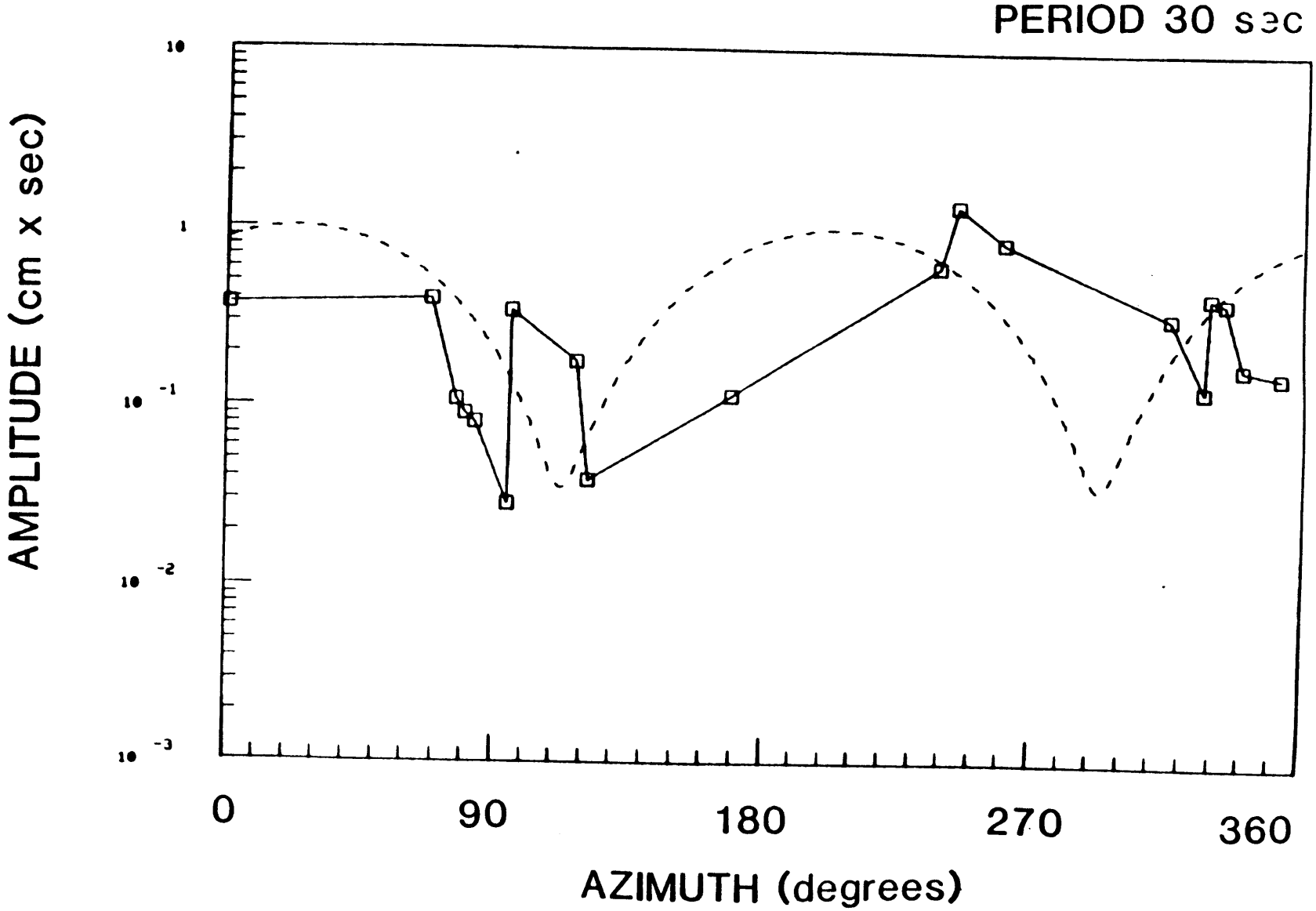
PERIOD 30 sec
AMPLITUDE (cm x sec)
10
1
10 -1
10 -2
10 -3
0
90
180
270
360
AZIMUTH (degrees)

FIGURE B.16C

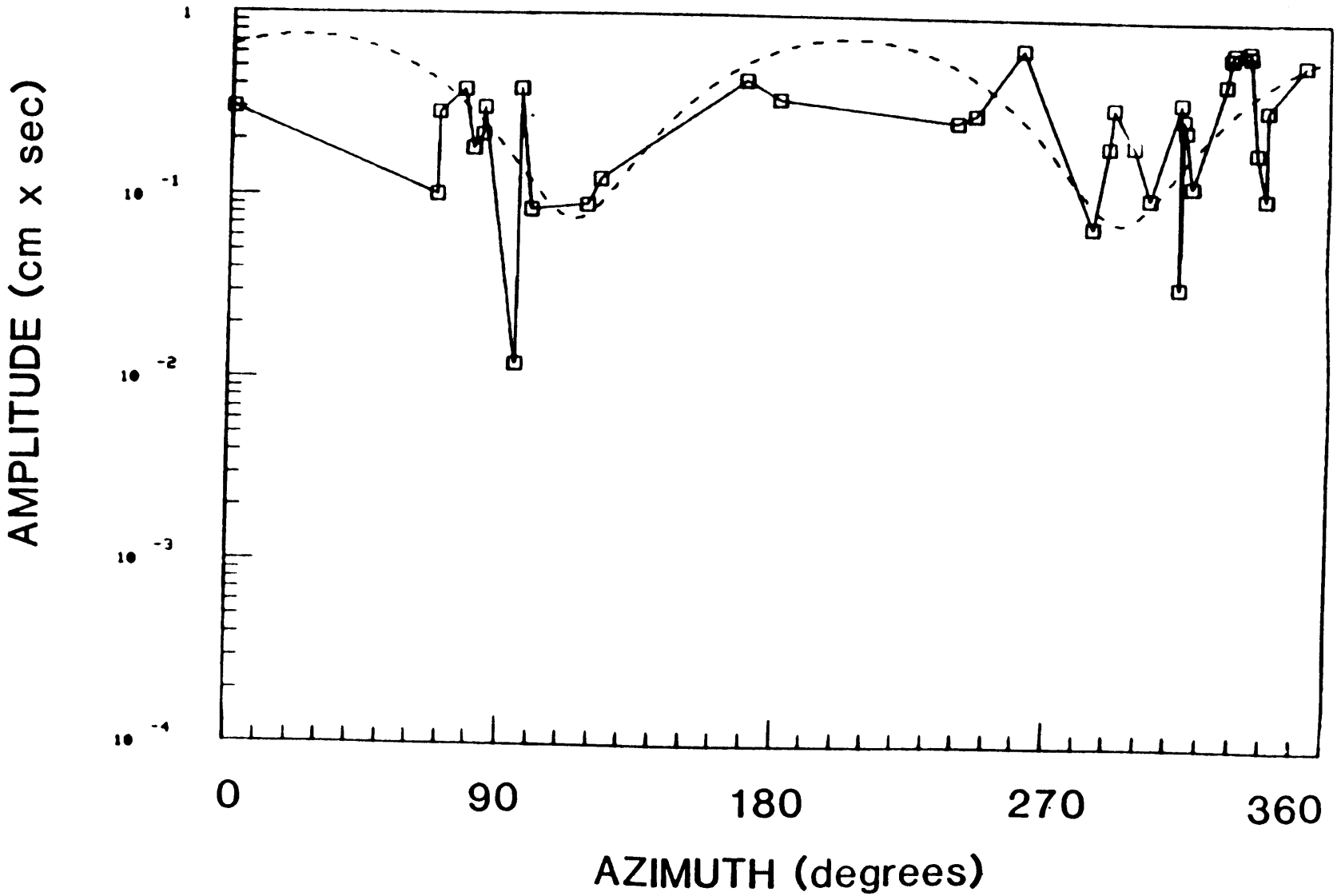
PERIOD 50 sec
AMPLITUDE (cm x sec)
1
10 -1
10 -2
10 -3
10 -4
0
90
180
270
360
AZIMUTH (degrees)

FIGURE B.16d

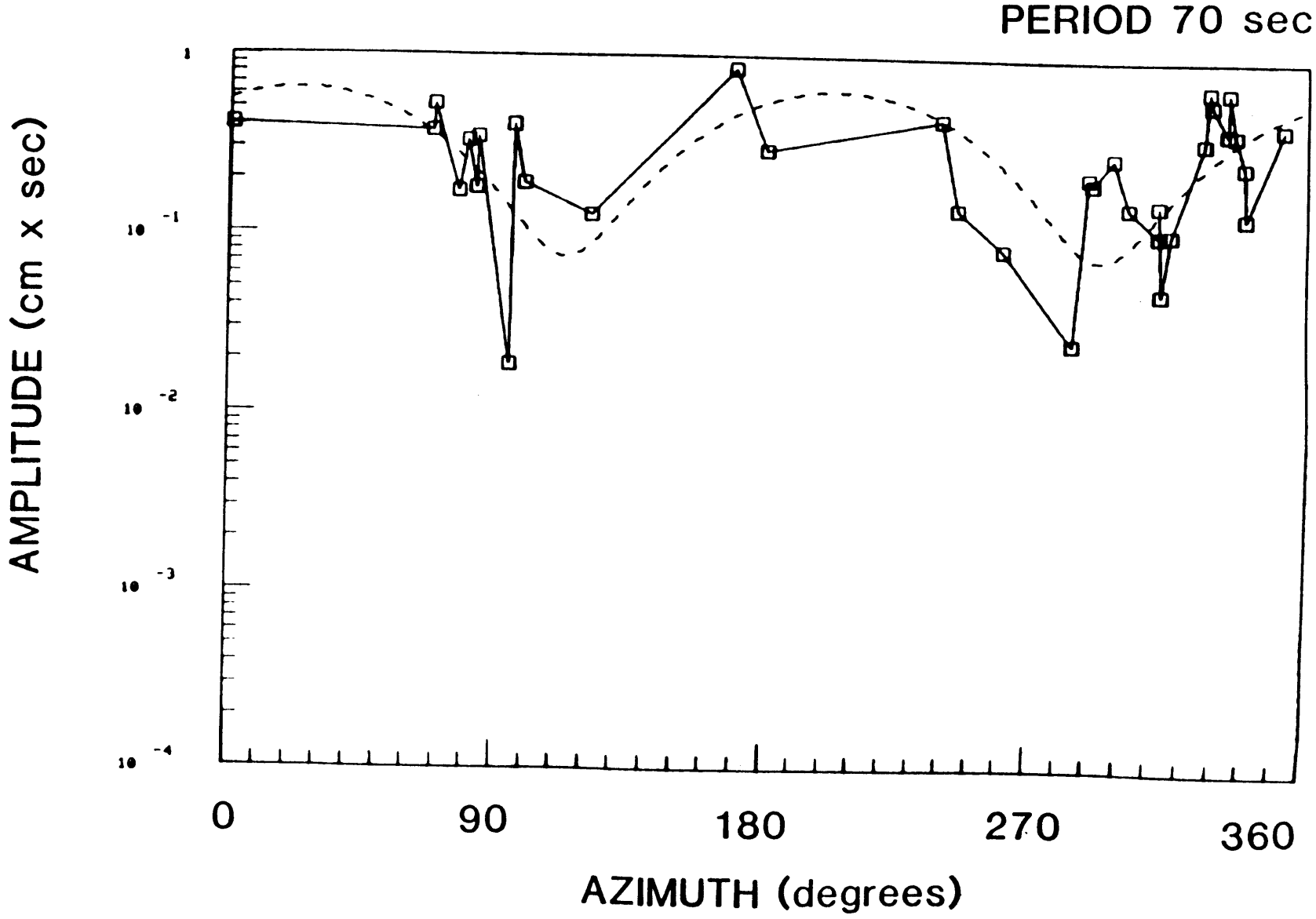
PERIOD 70 sec
AMPLITUDE (cm x sec)
1
10 -1
10 -2
10 -3
10 -4
0
90
180
270
360
AZIMUTH (degrees)

FIGURE B.16e

PERIOD 98 sec

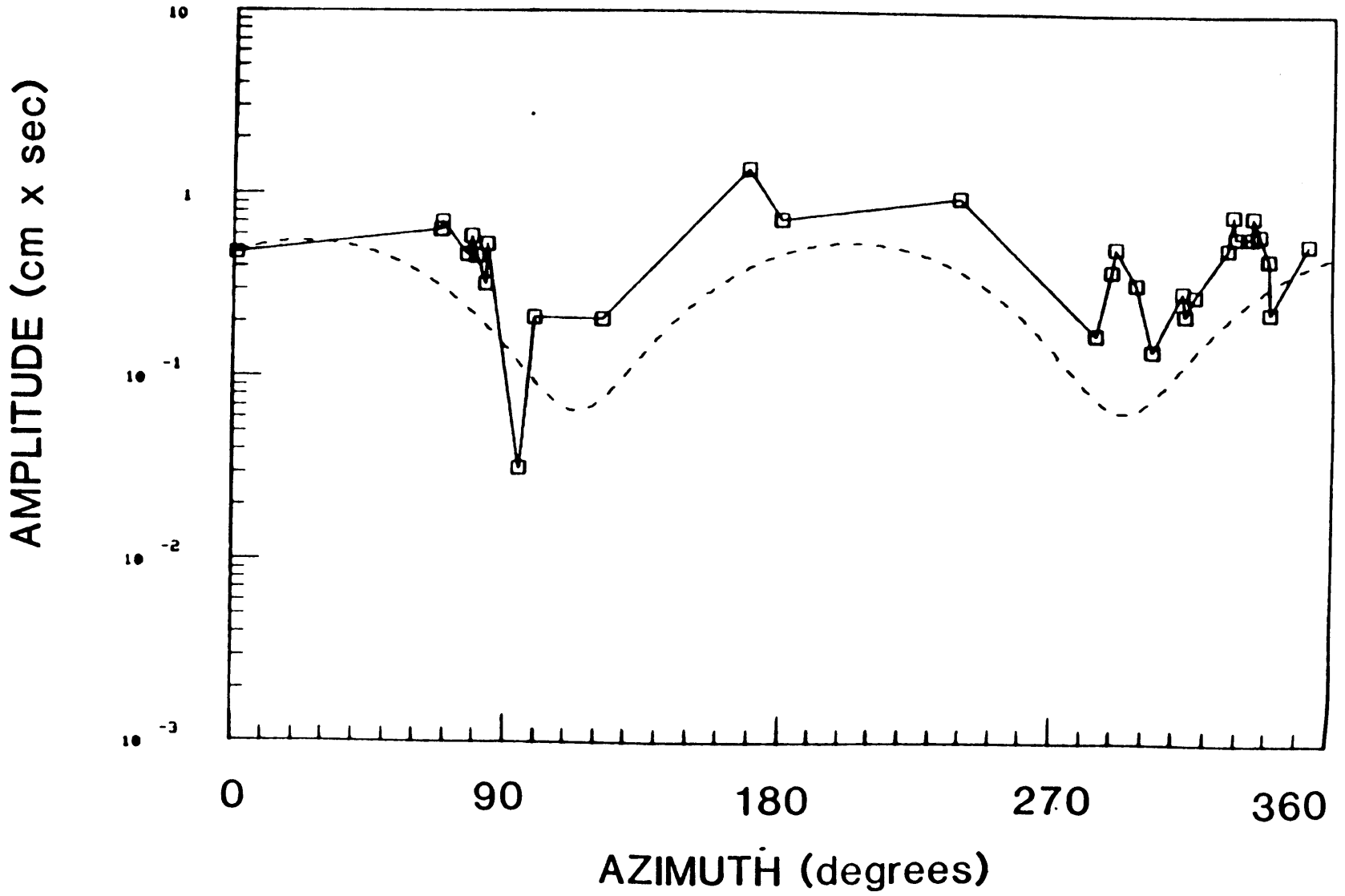

FIGURE B.17a

04/07/69

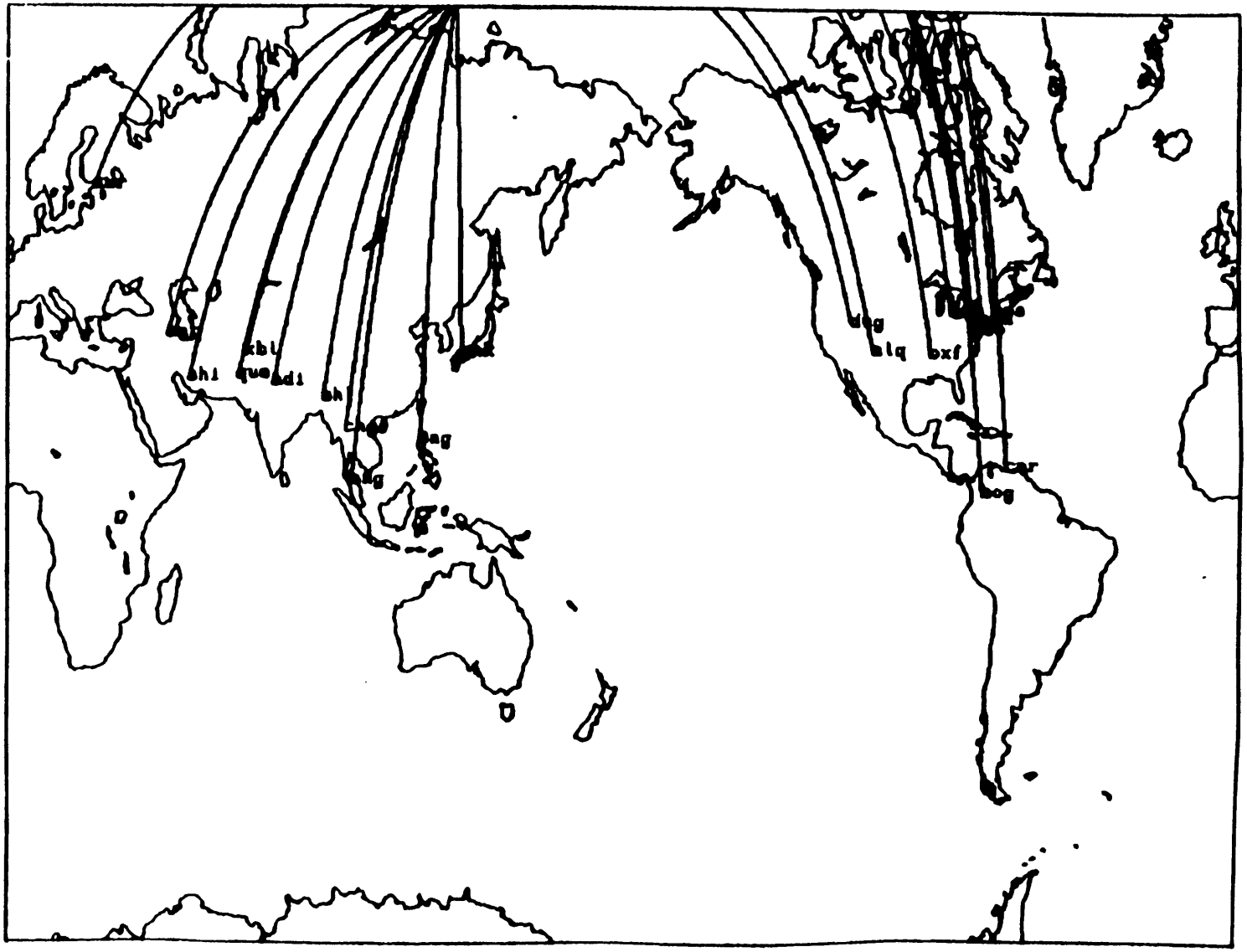

FIGURE B.17b

PERIOD 30 sec

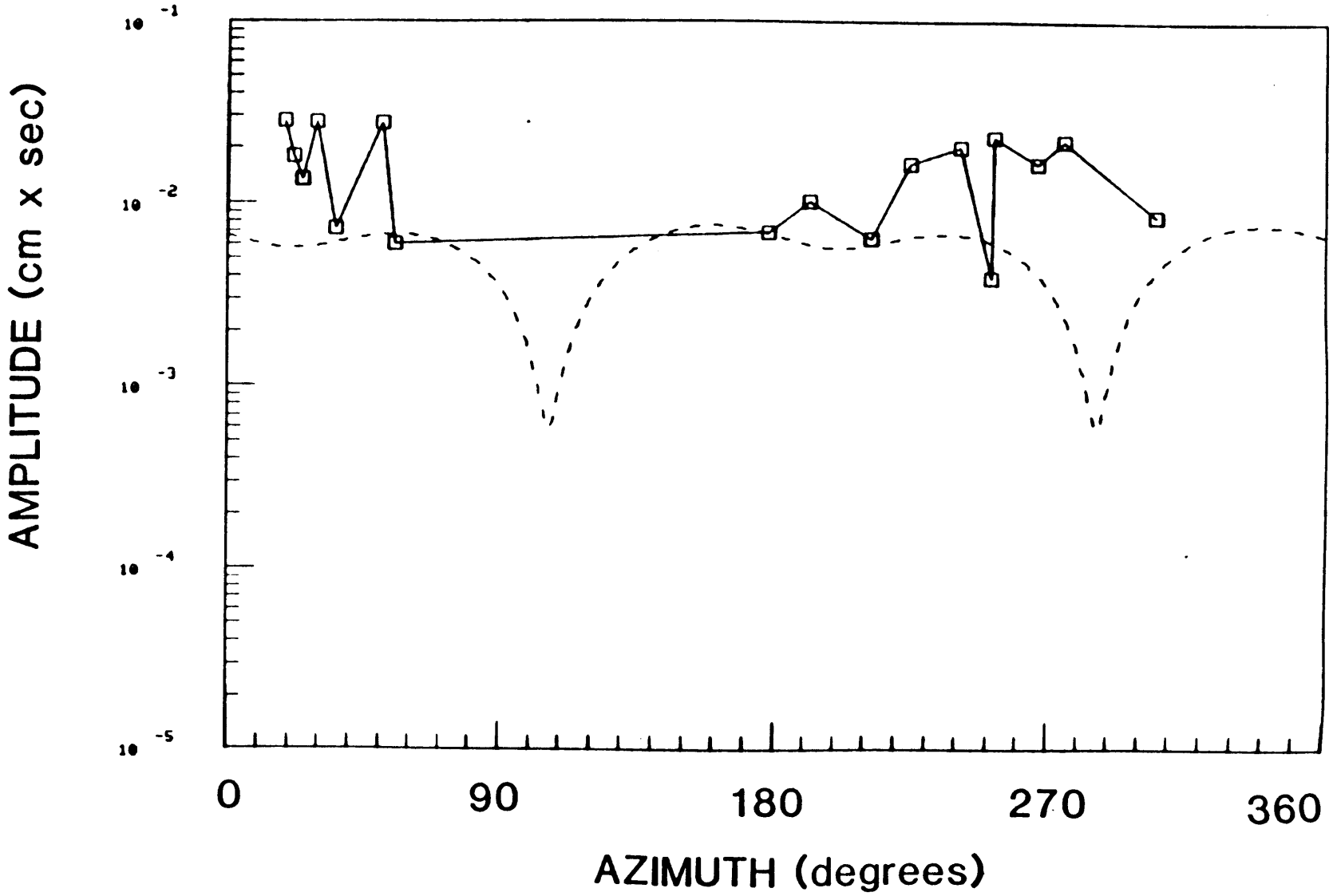

FIGURE B.17c

PERIOD 50 sec

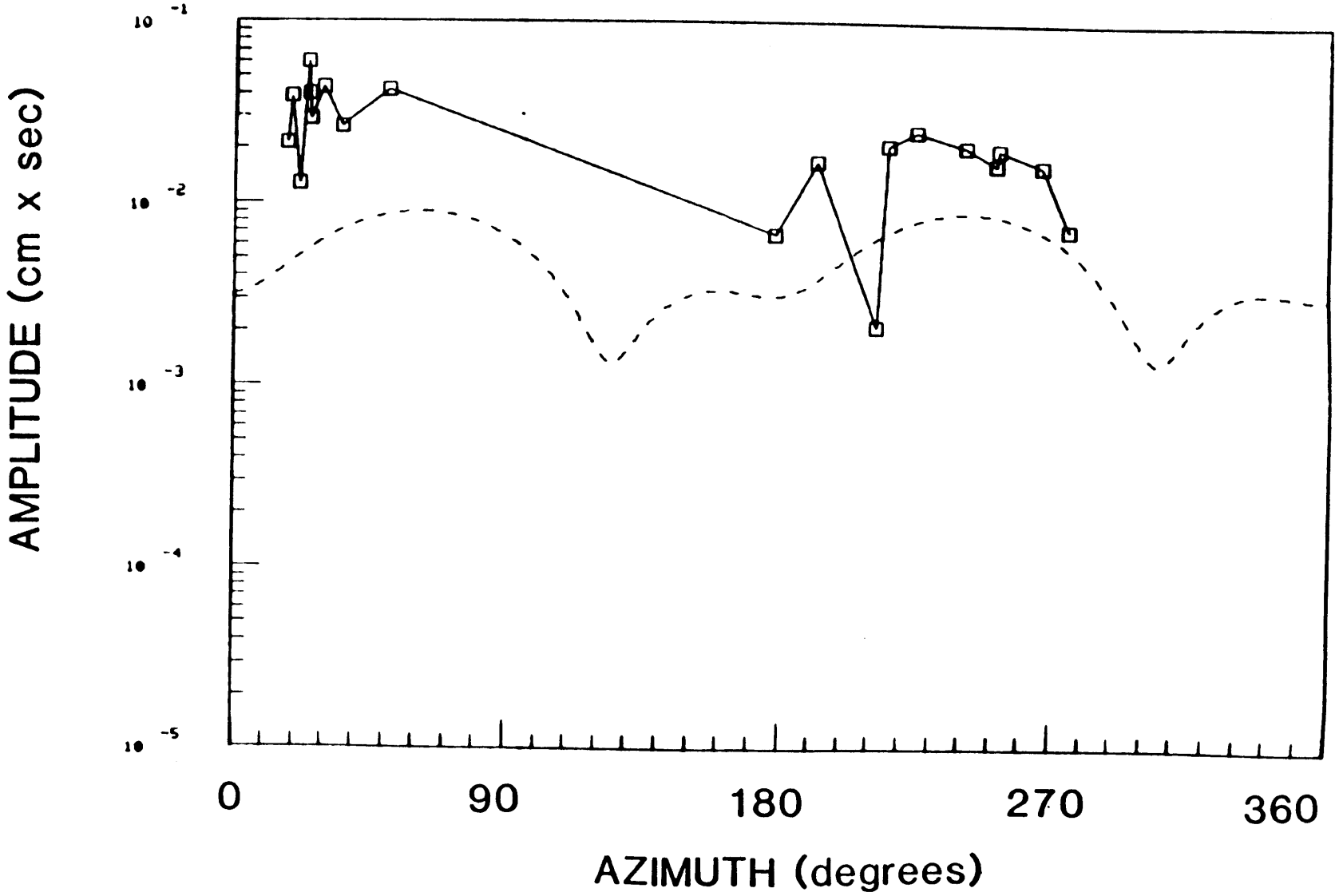

FIGURE B.17d

PERIOD 70 sec

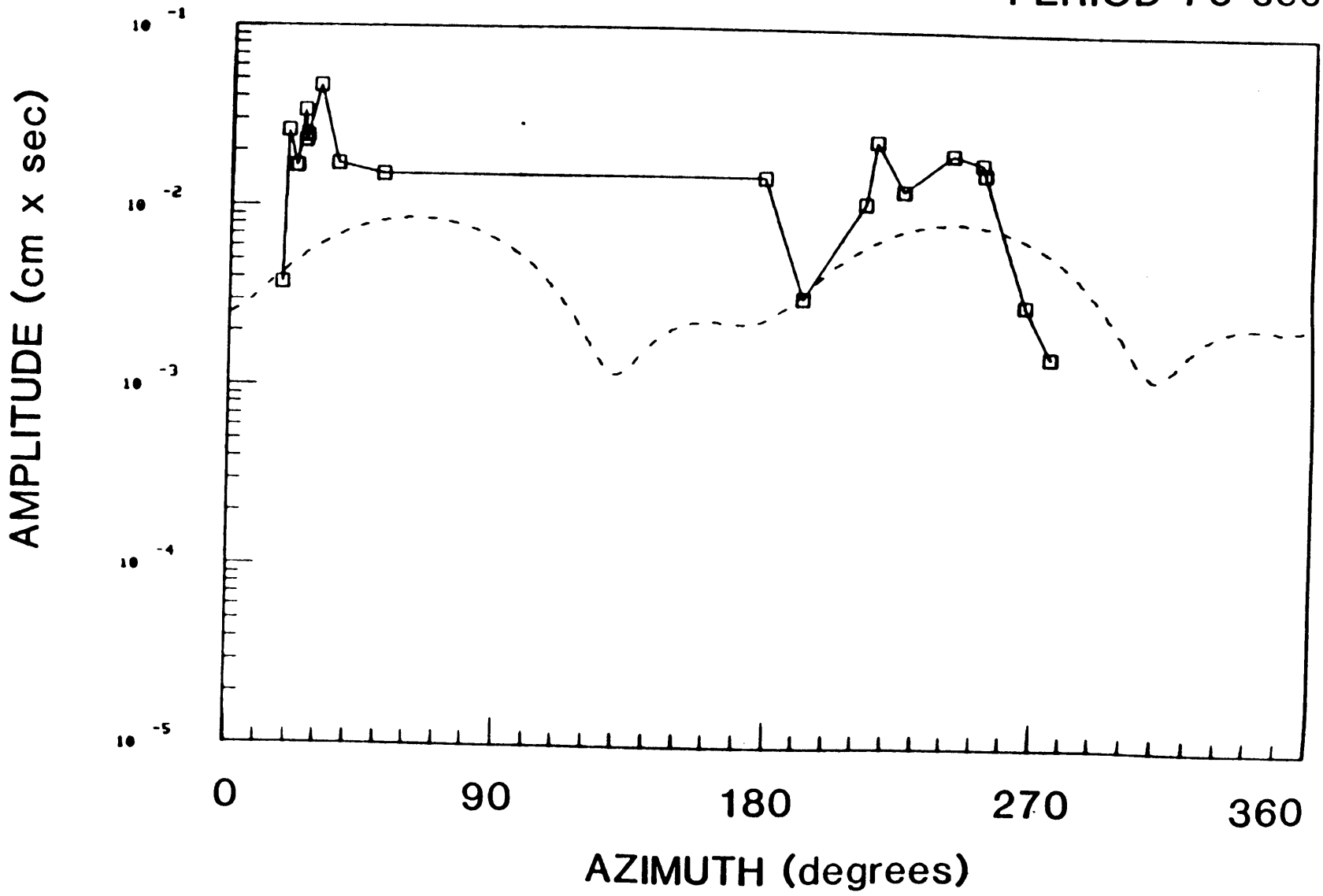

FIGURE B.17e

PERIOD 98 sec

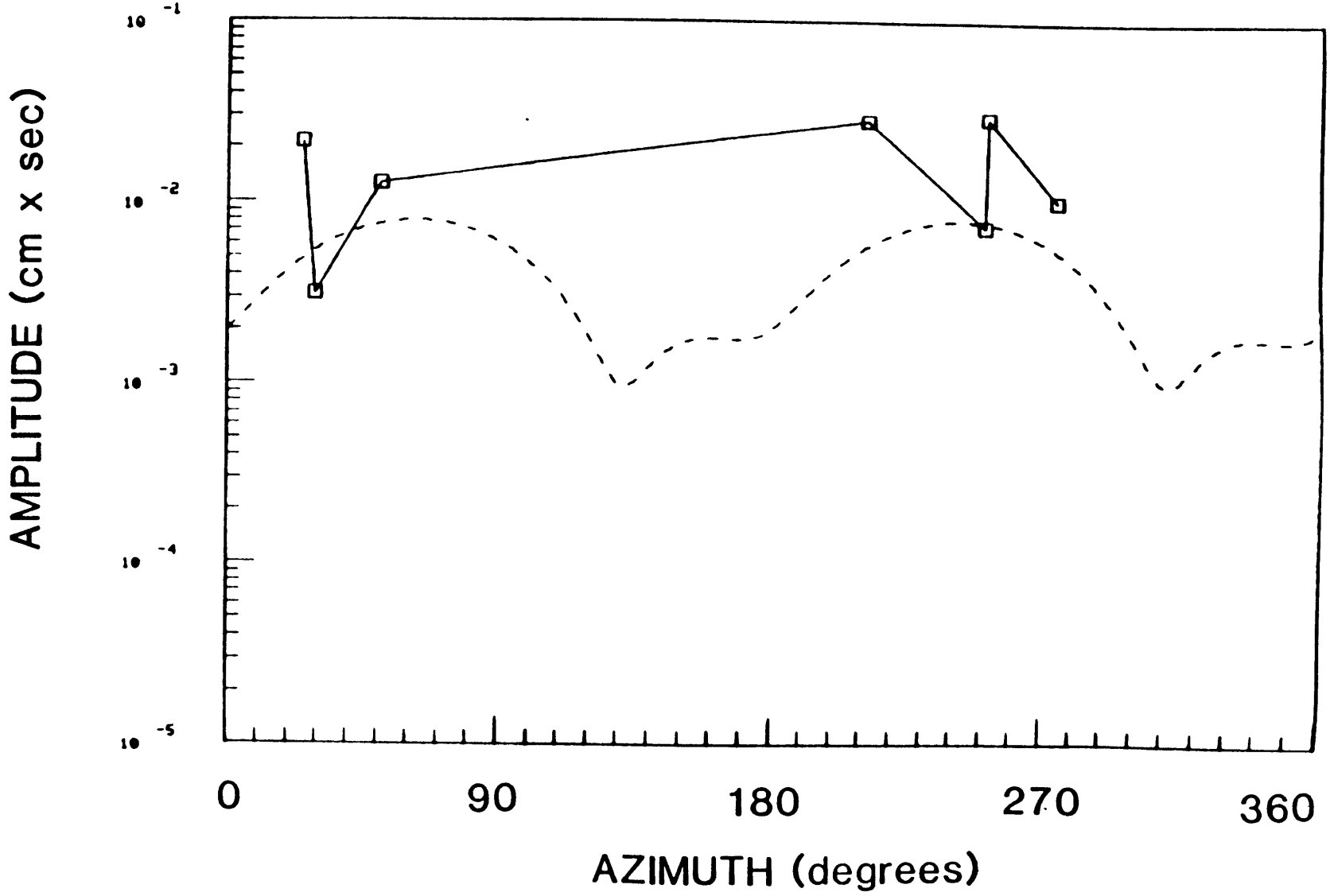

FIGURE B.18a

08/08/69

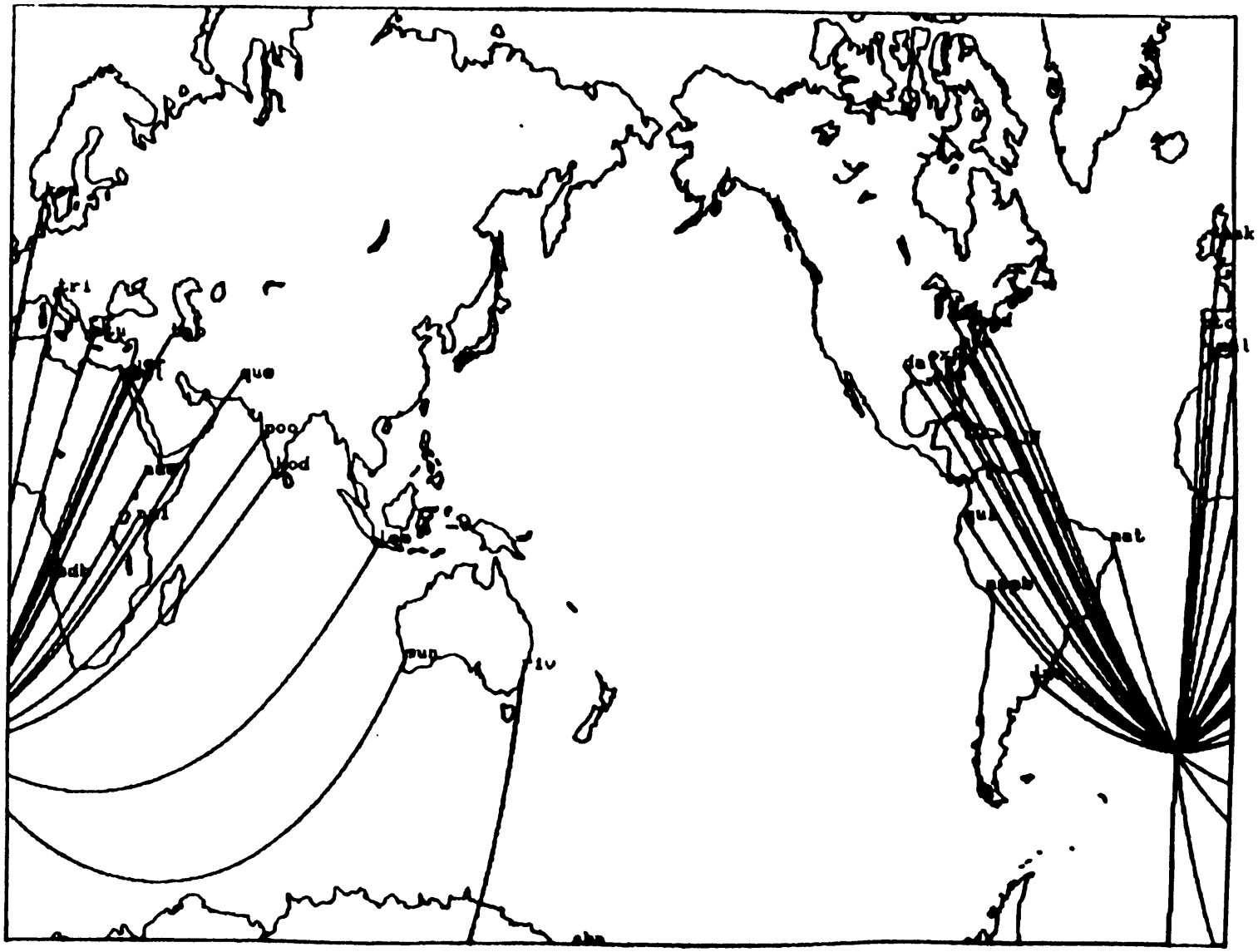

FIGURE B.18b

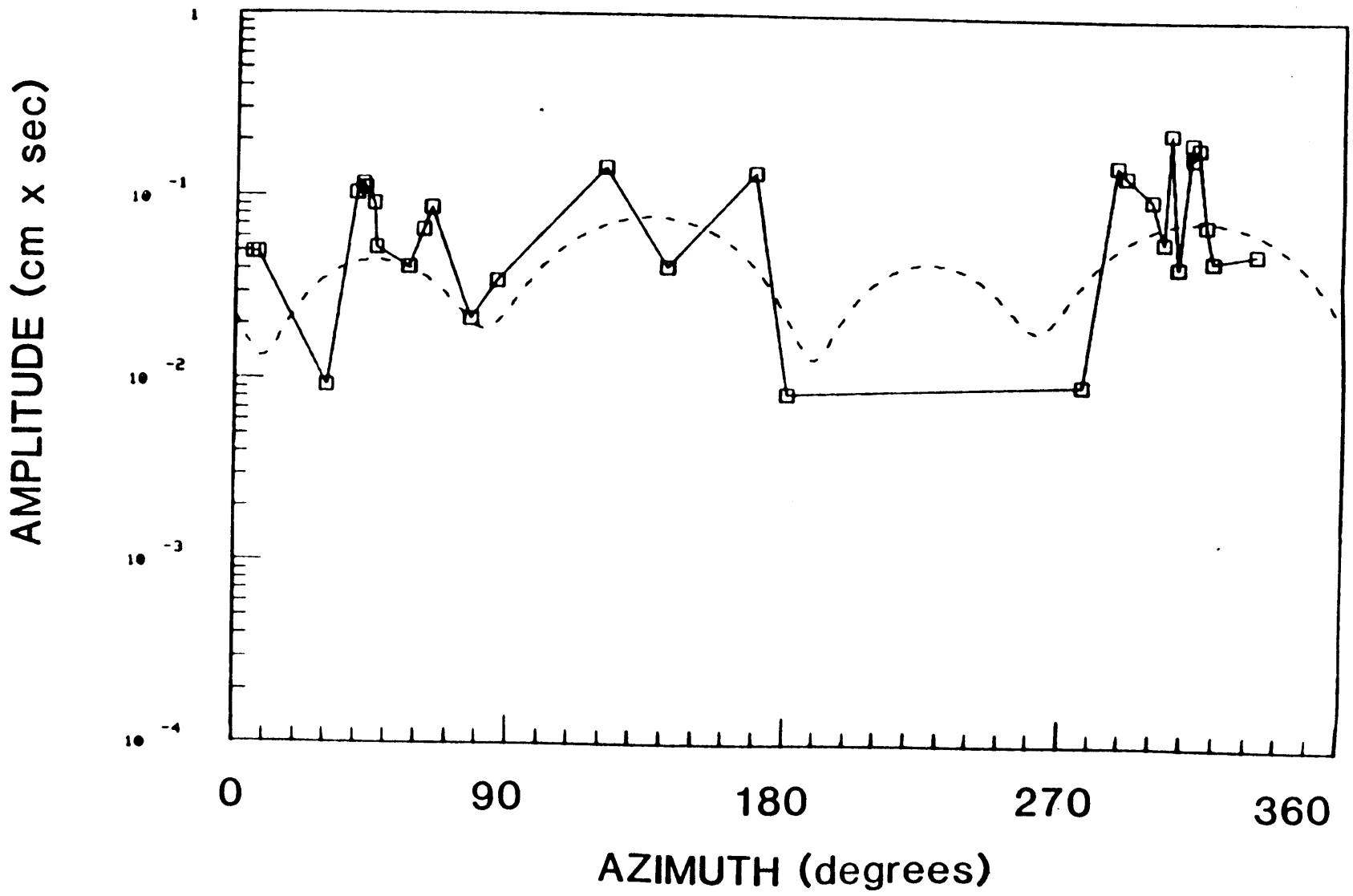
PERIOD 30 sec
AMPLITUDE (cm x sec)
1
10 -1
10 -2
10 -3
10 -4
0
90
180
270
360
AZIMUTH (degrees)

FIGURE B.18C

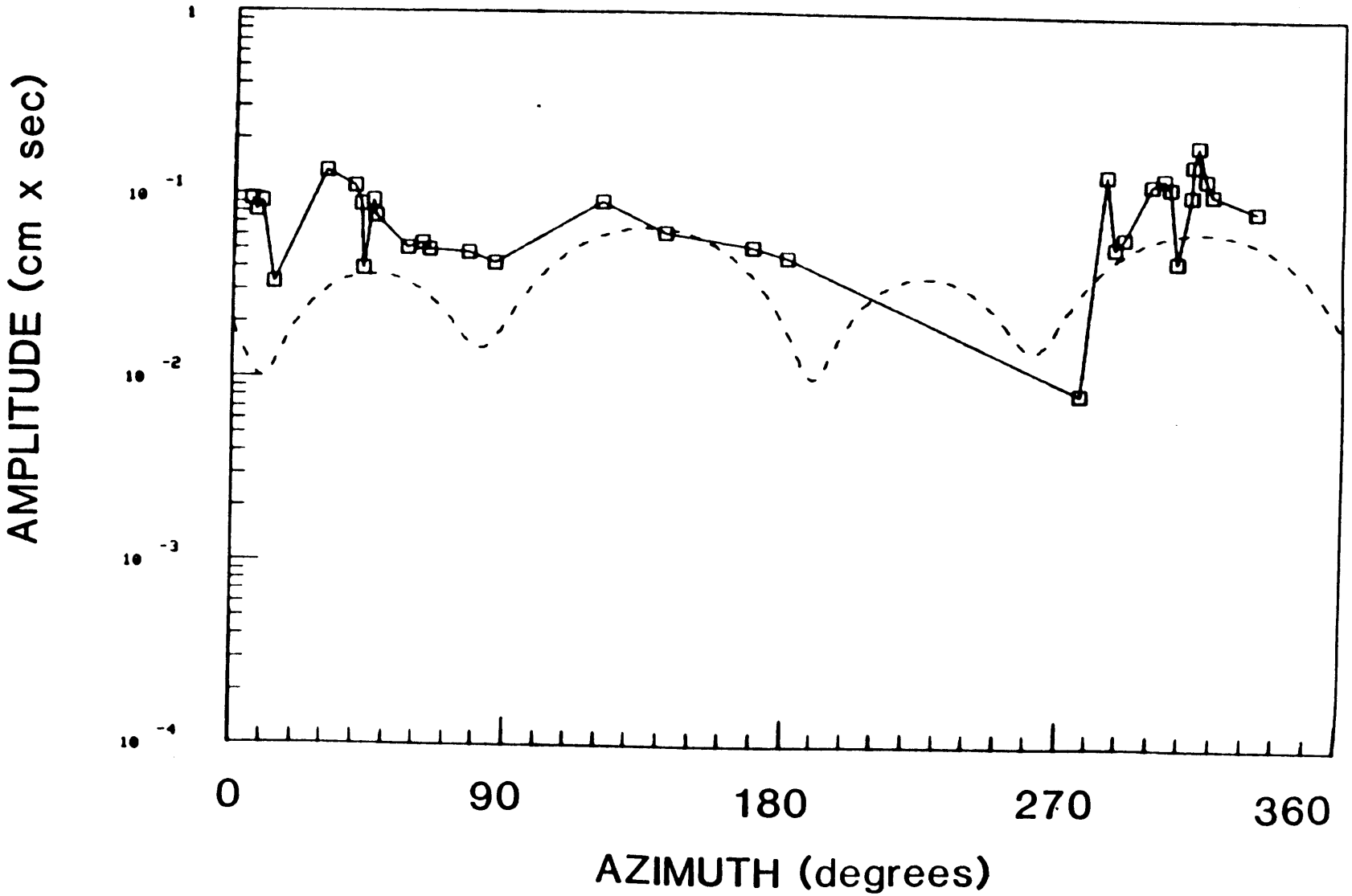
PERIOD 50 sec
AMPLITUDE (cm x sec)
1
10 -1
10 -2
10 -3
10 -4
0
90
180
270
360
AZIMUTH (degrees)

FIGURE B.18d

PERIOD 70 sec

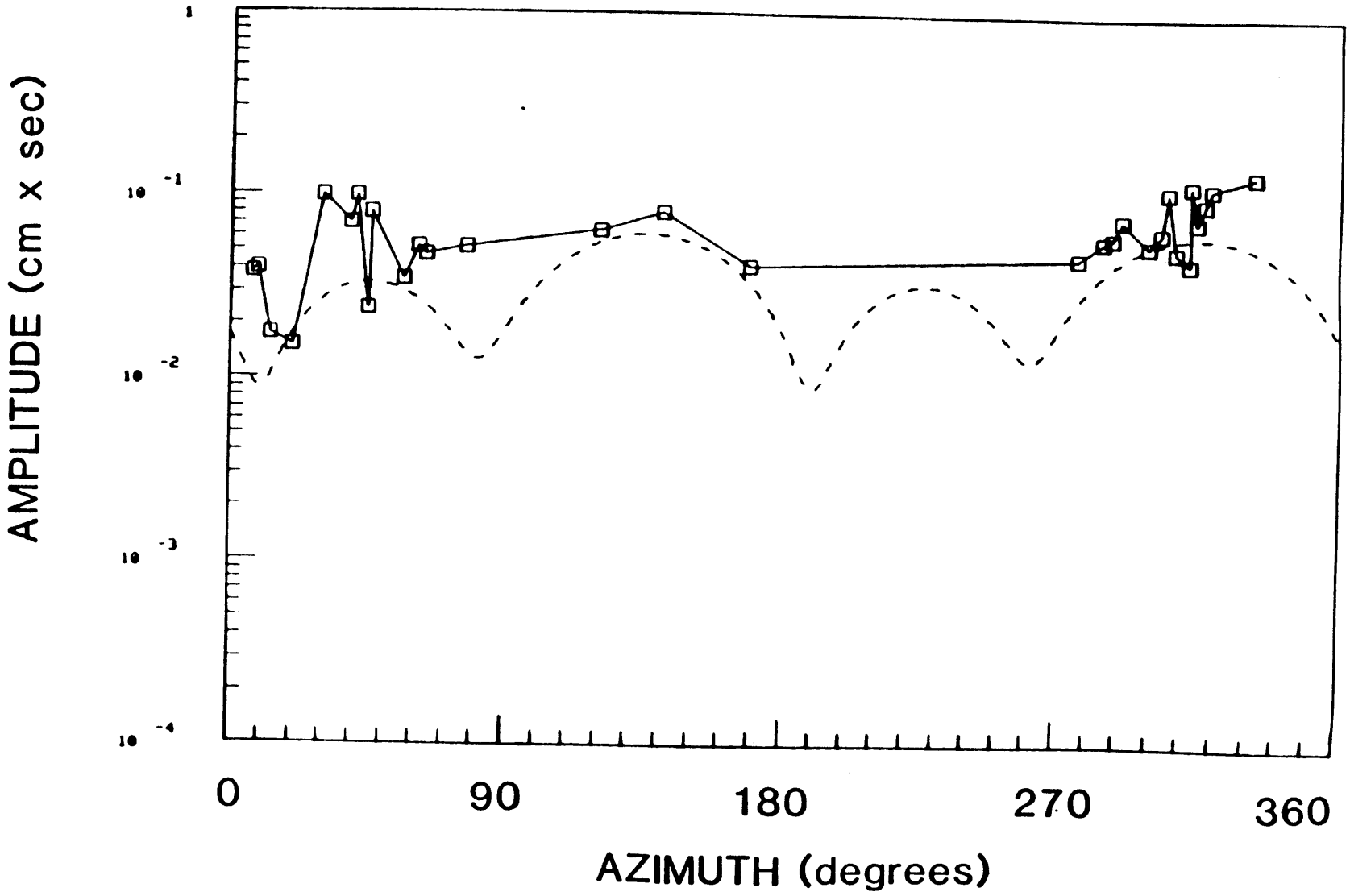

FIGURE B.18e

PERIOD 98 sec

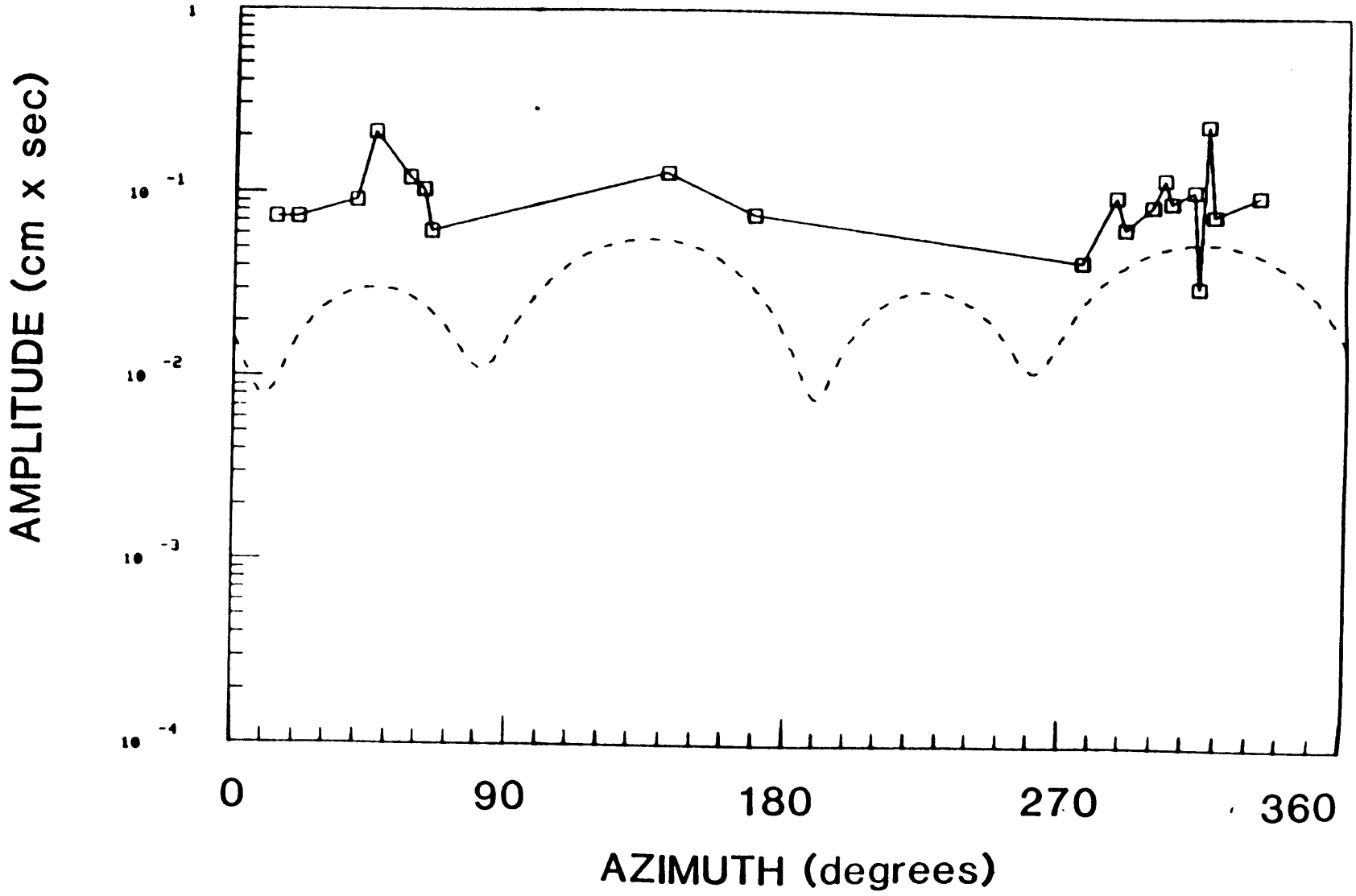

FIGURE B.19a

09/20/69

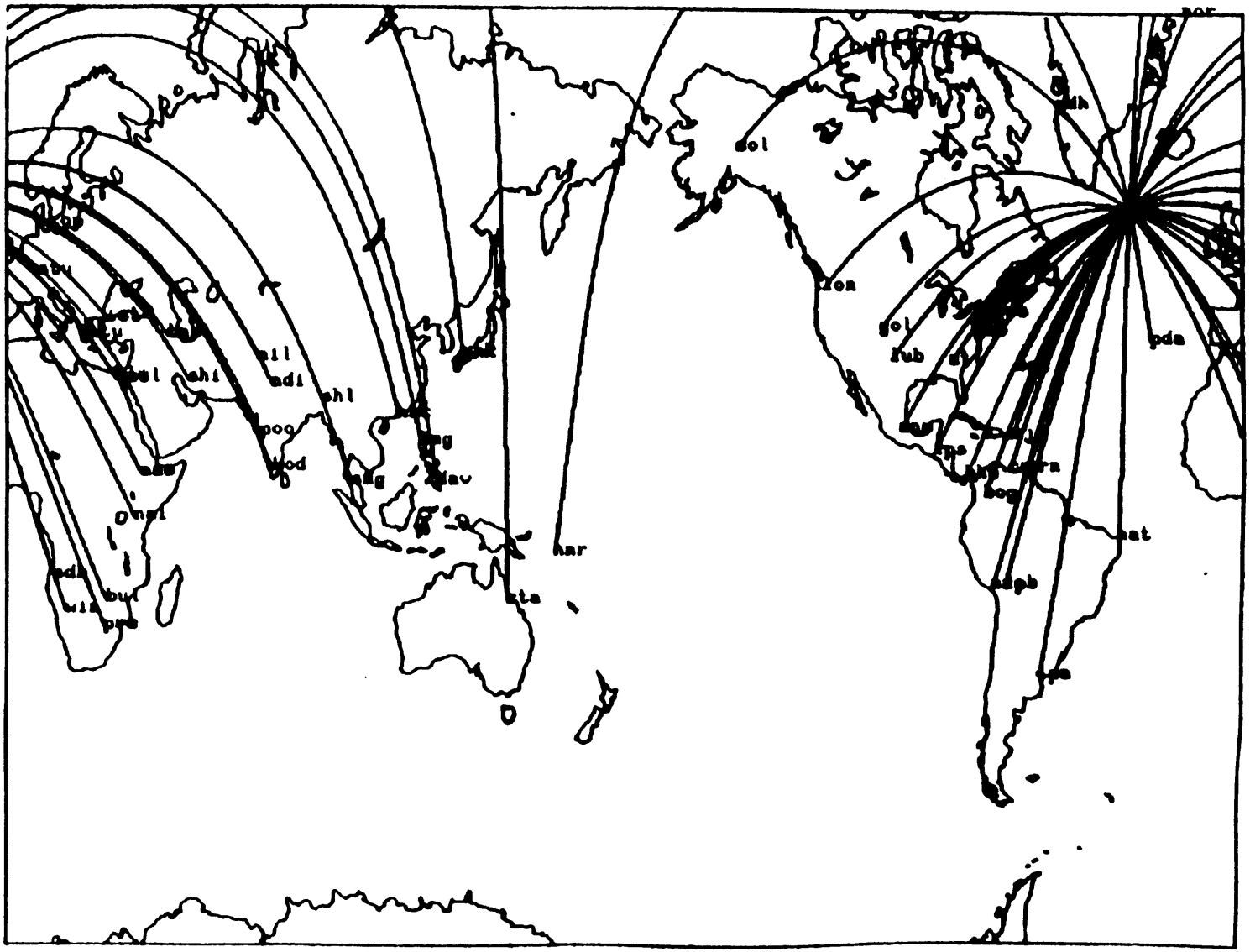

FIGURE B.19b

PERIOD 30 sec

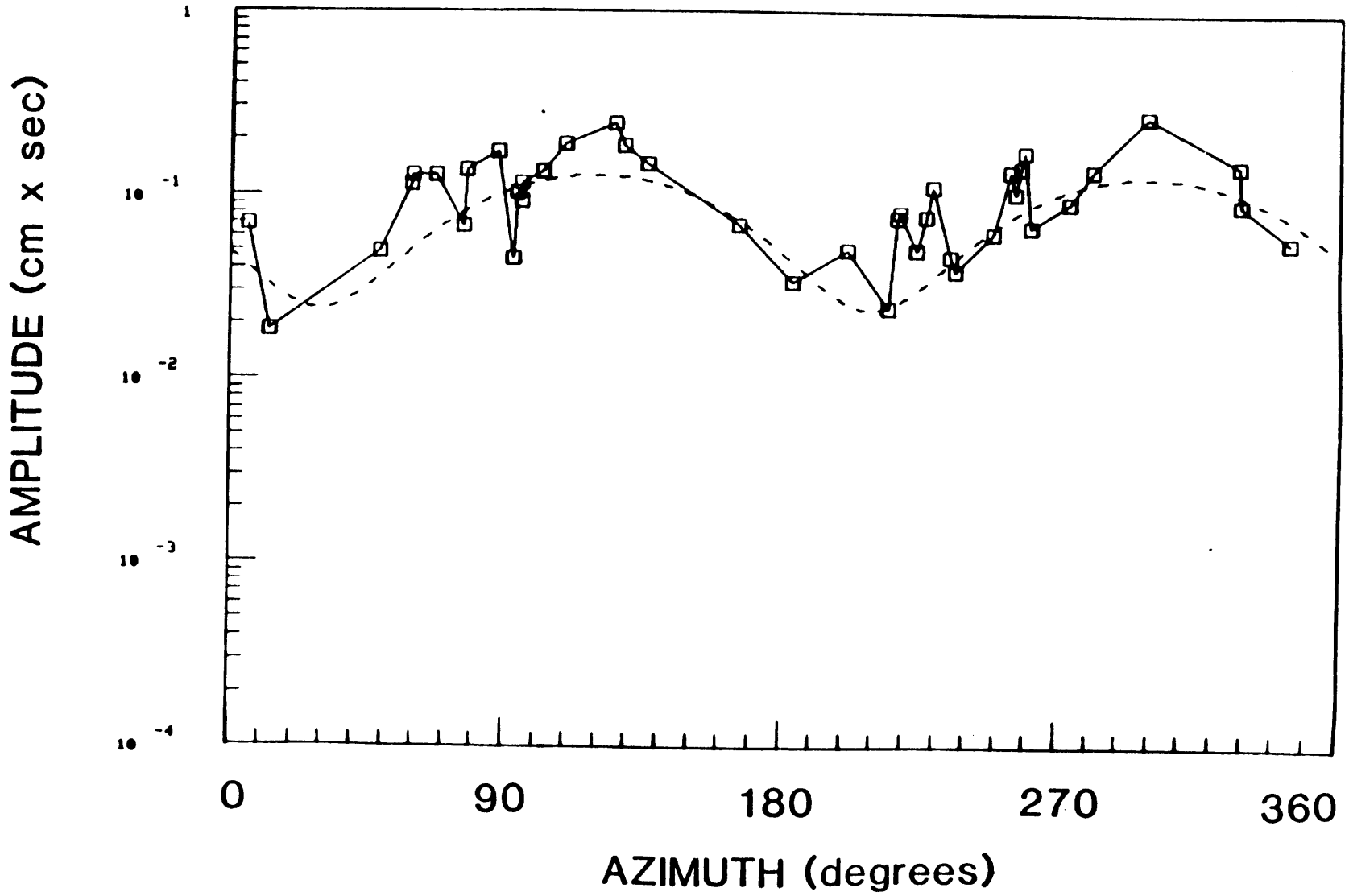

FIGURE B.19c

PERIOD 50 sec

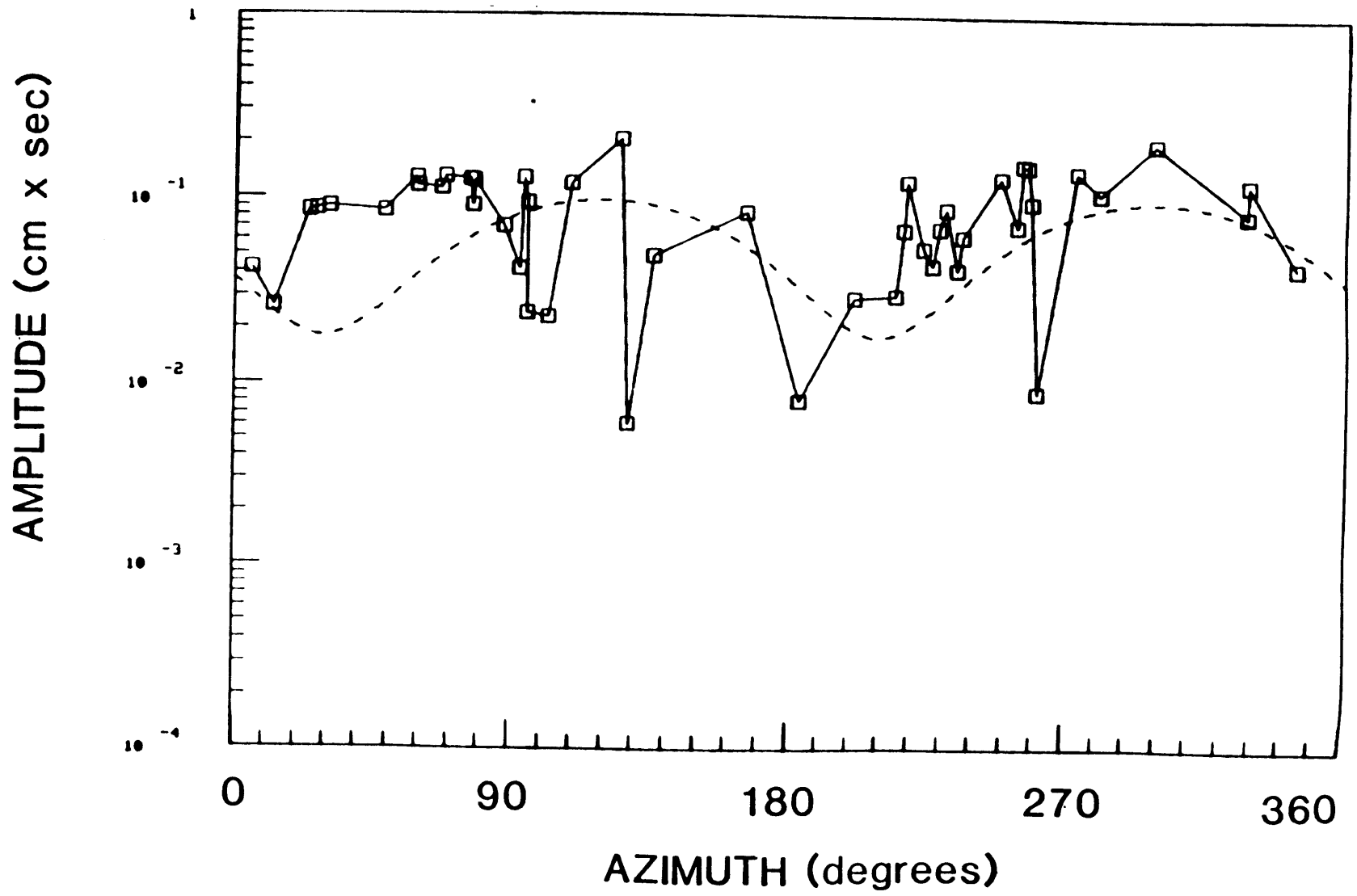

FIGURE B.19d

PERIOD 70 sec

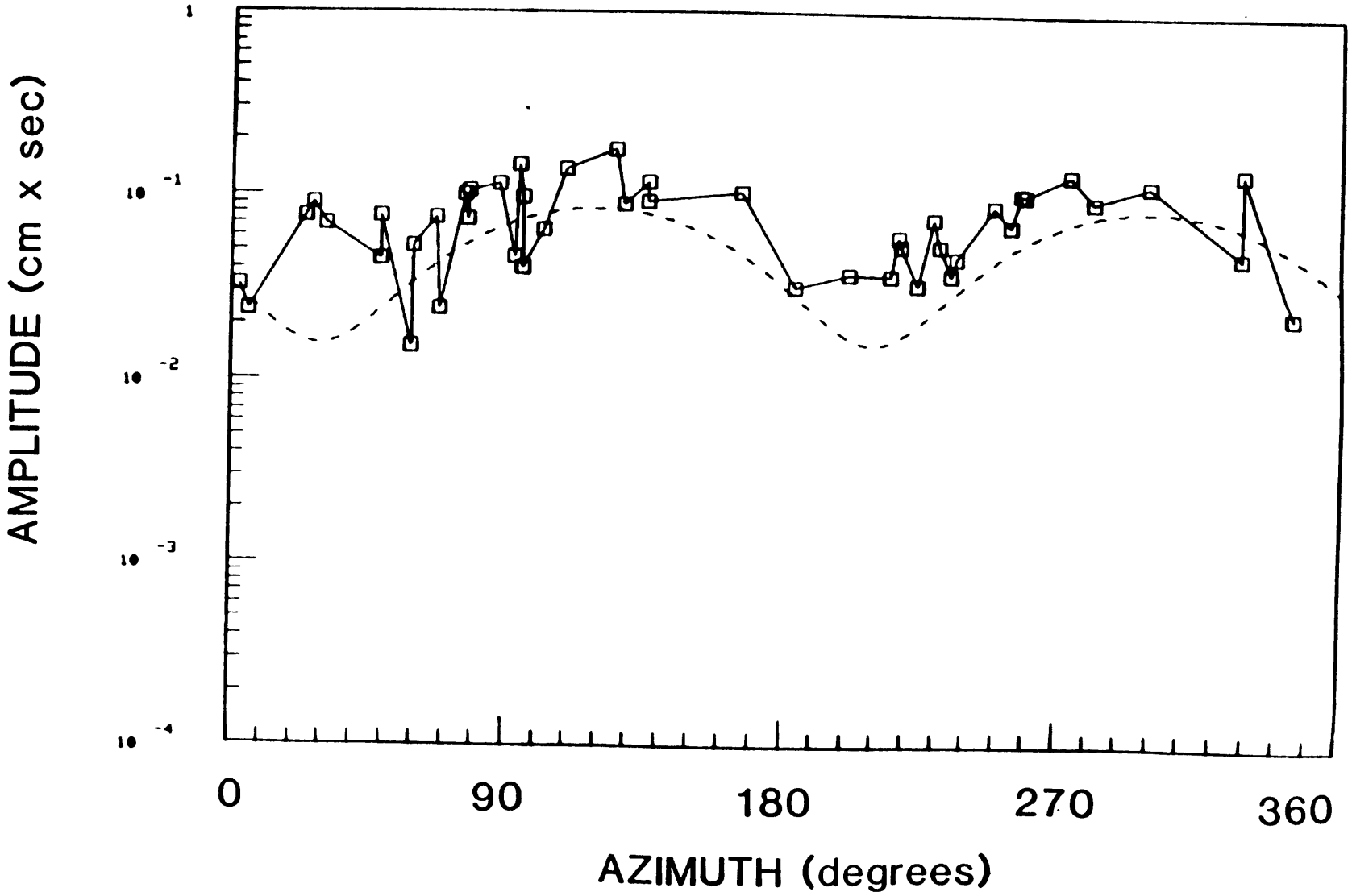

FIGURE B.19e

PERIOD 98 sec

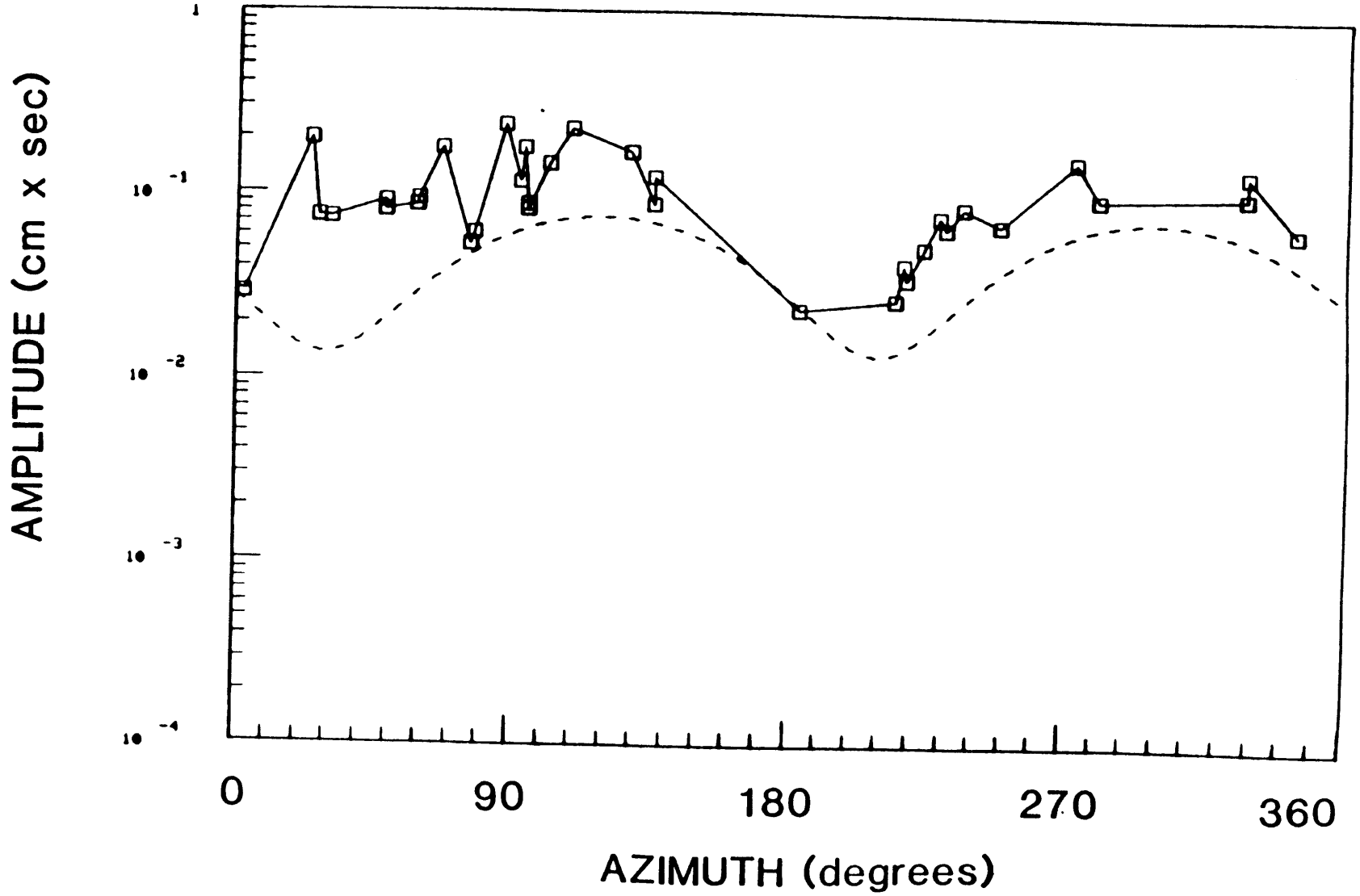

FIGURE B.20a

01/21/70

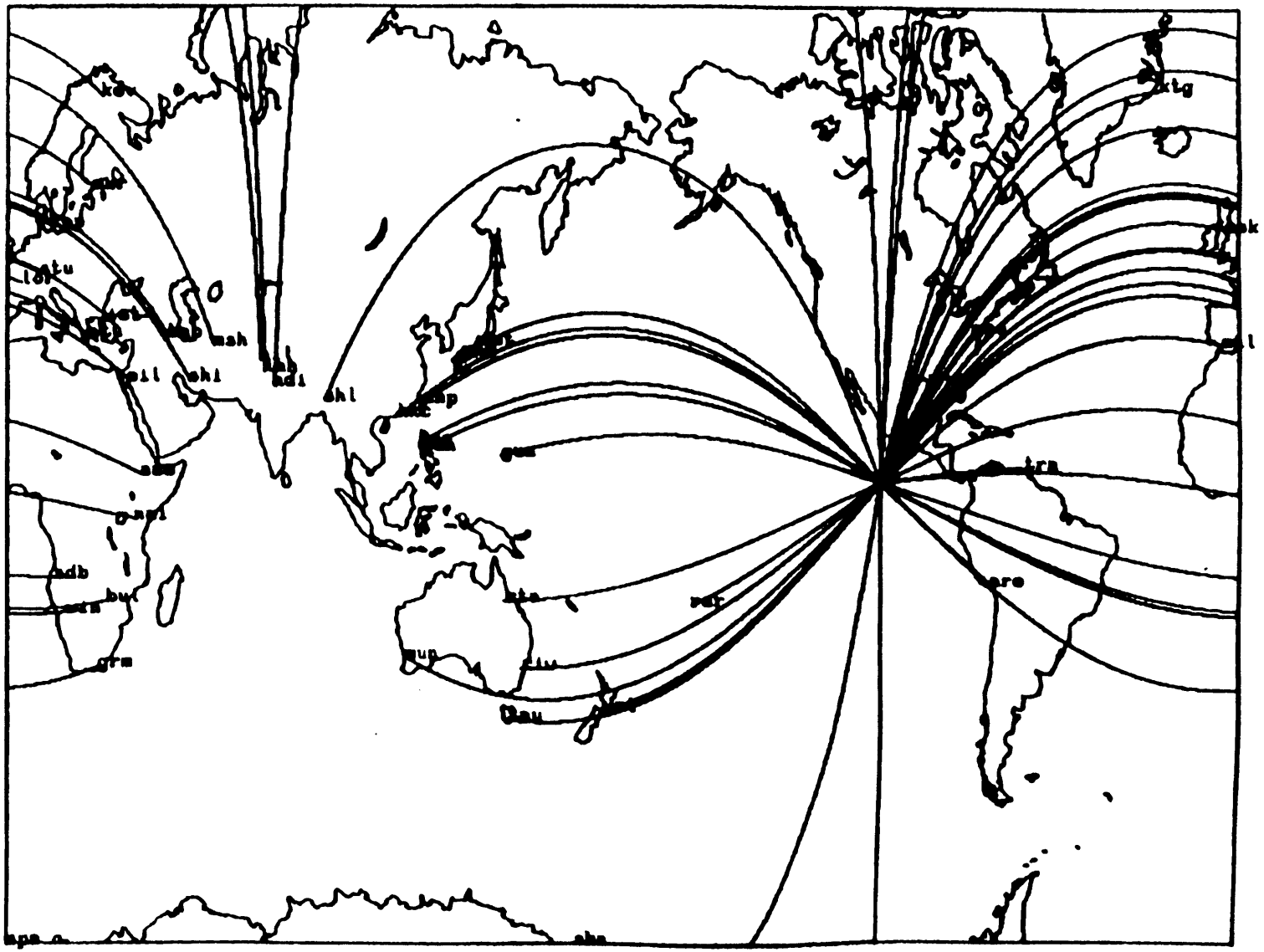

FIGURE B.20b

PERIOD 30 sec

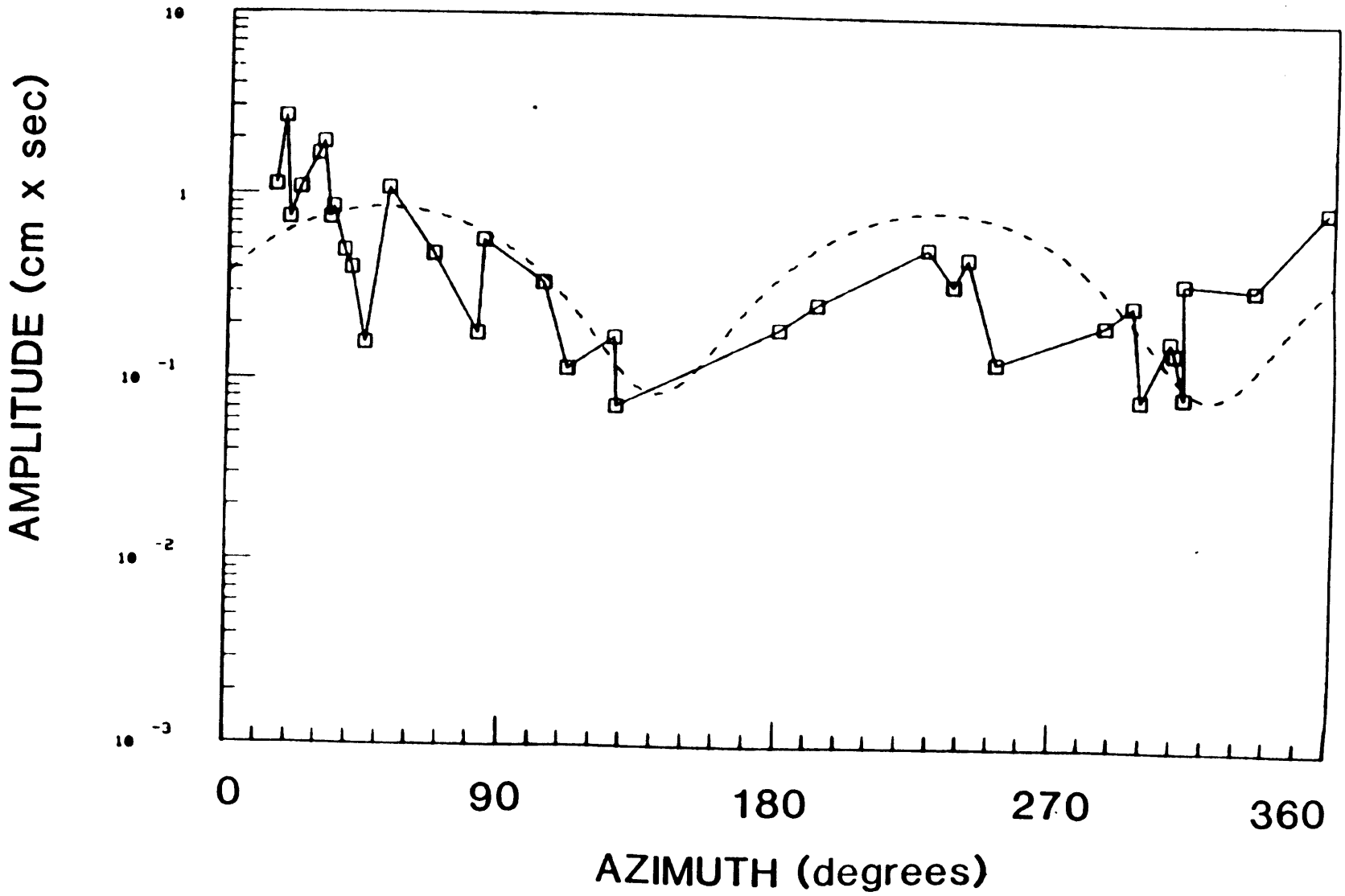

FIGURE B.20C

PERIOD 50 sec

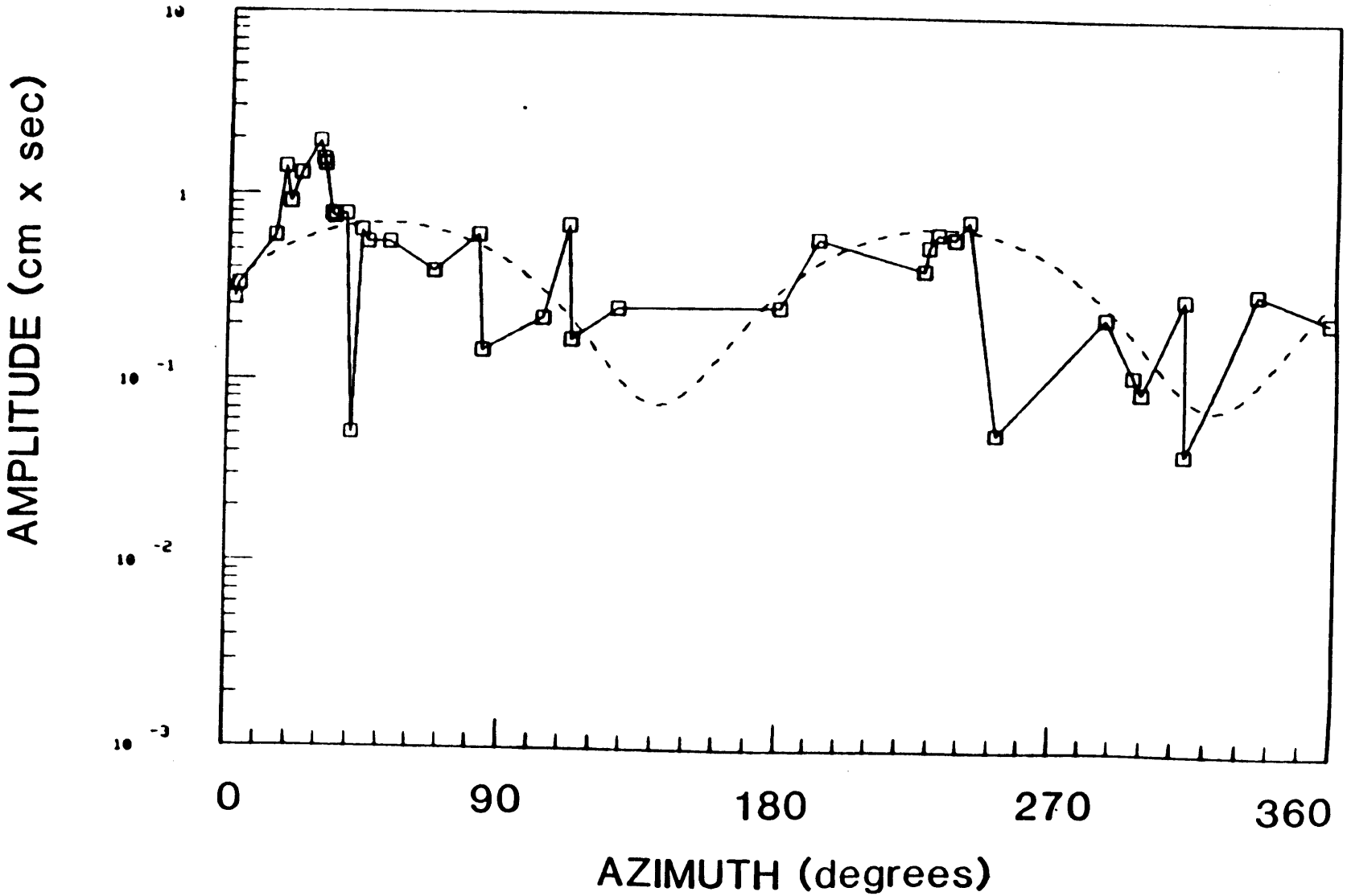

FIGURE B.20d

PERIOD 70 sec

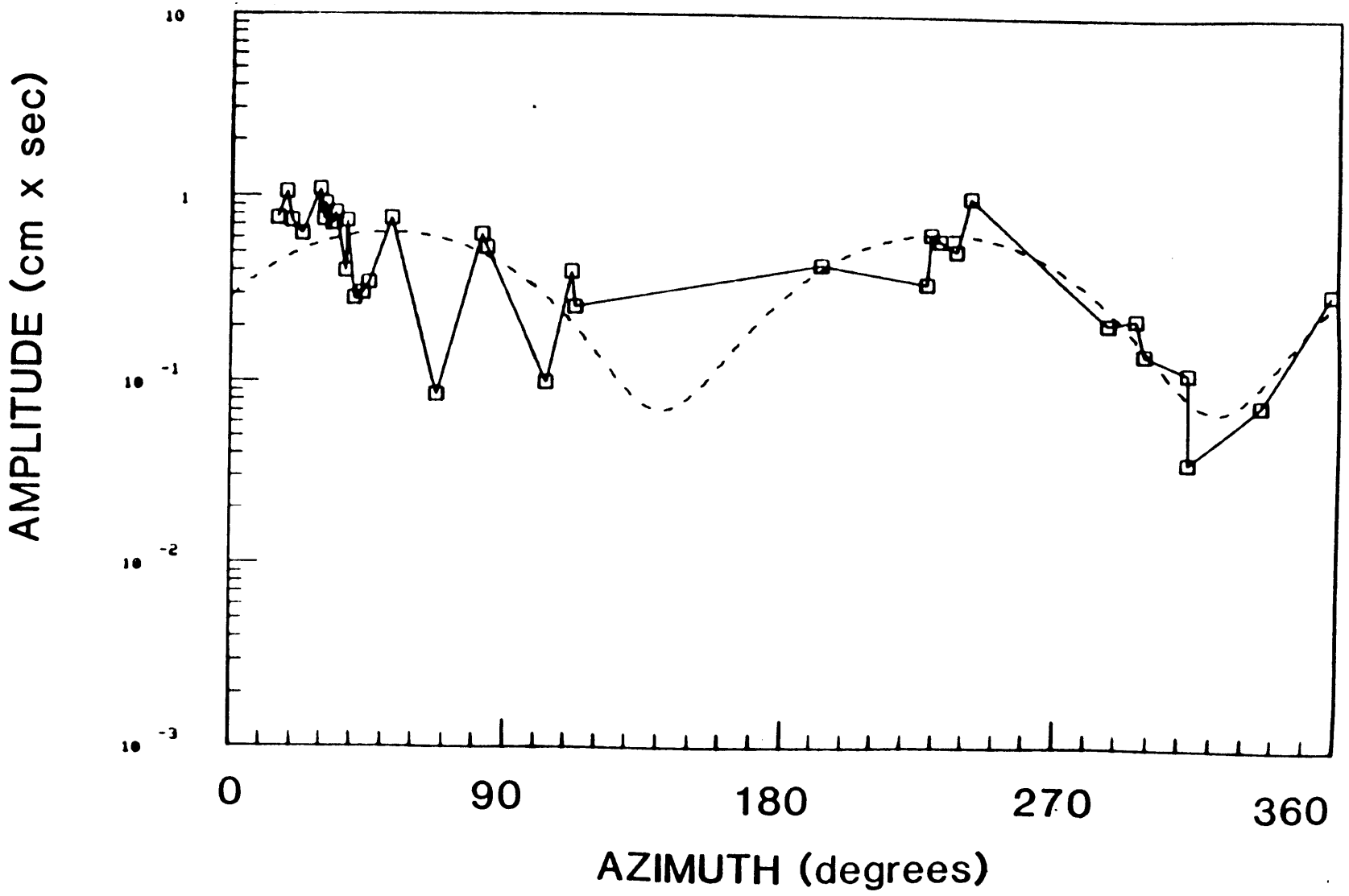

FIGURE B.20e

PERIOD 98 sec

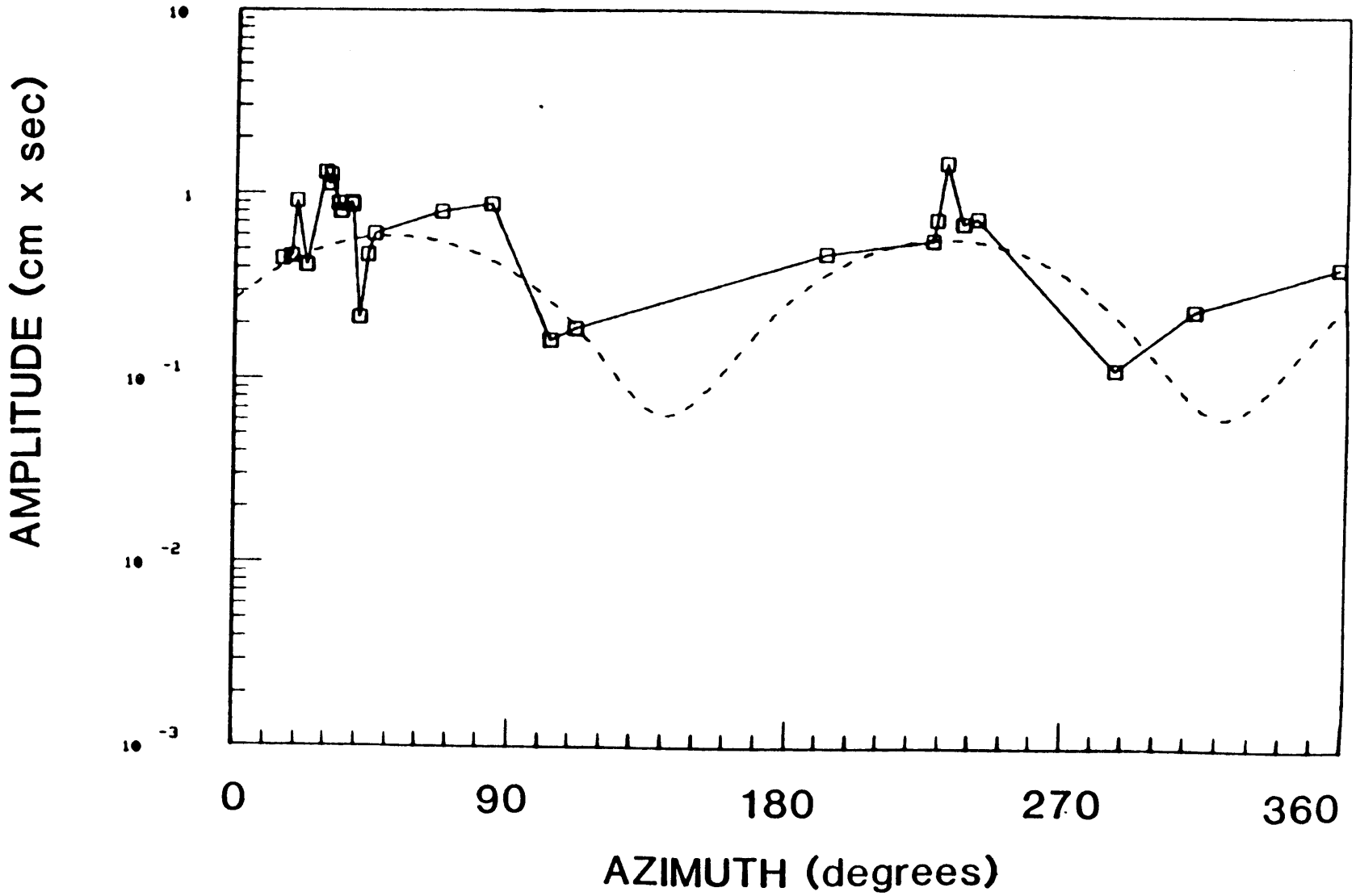

FIGURE B.21a

03/31/70

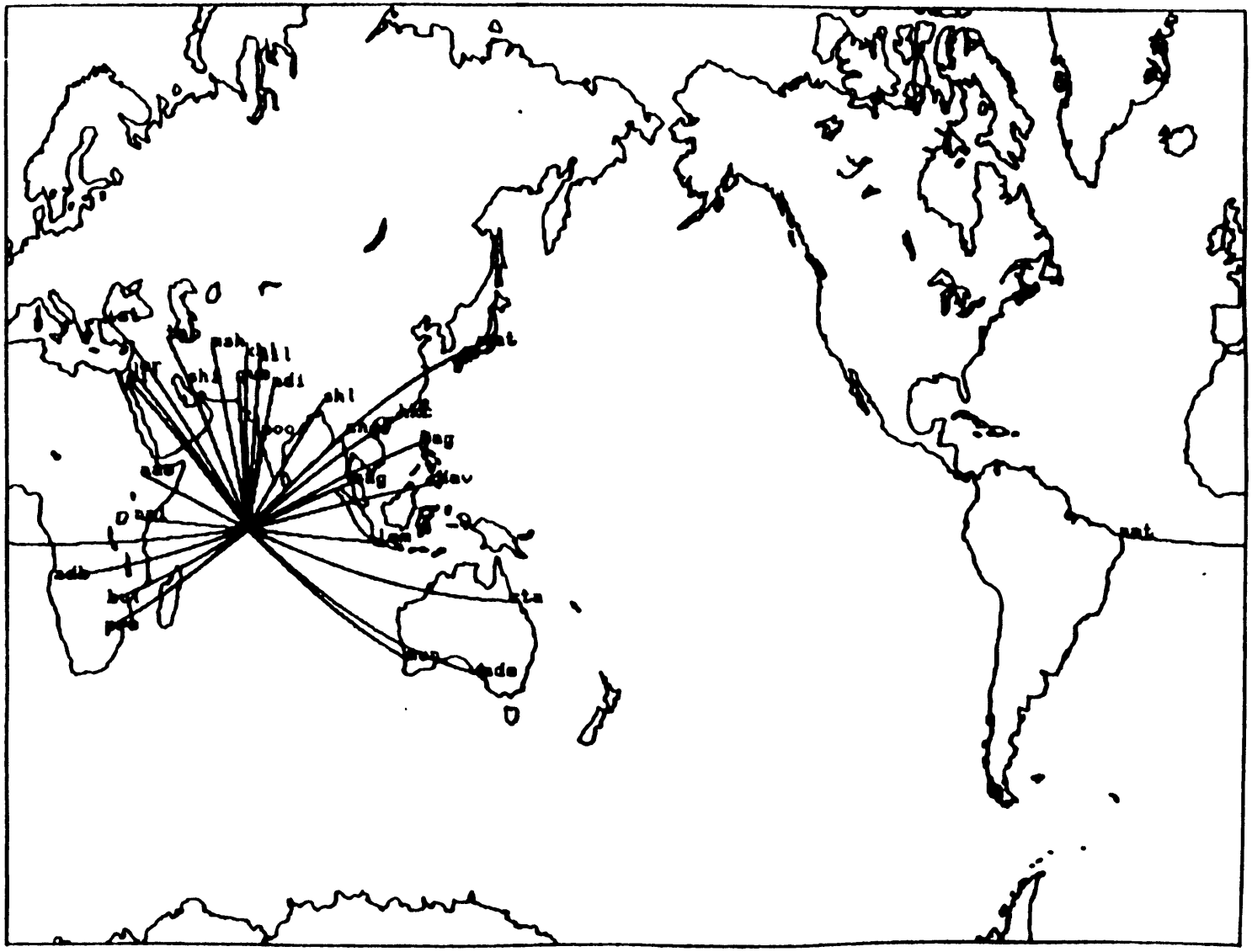

FIGURE B.21b

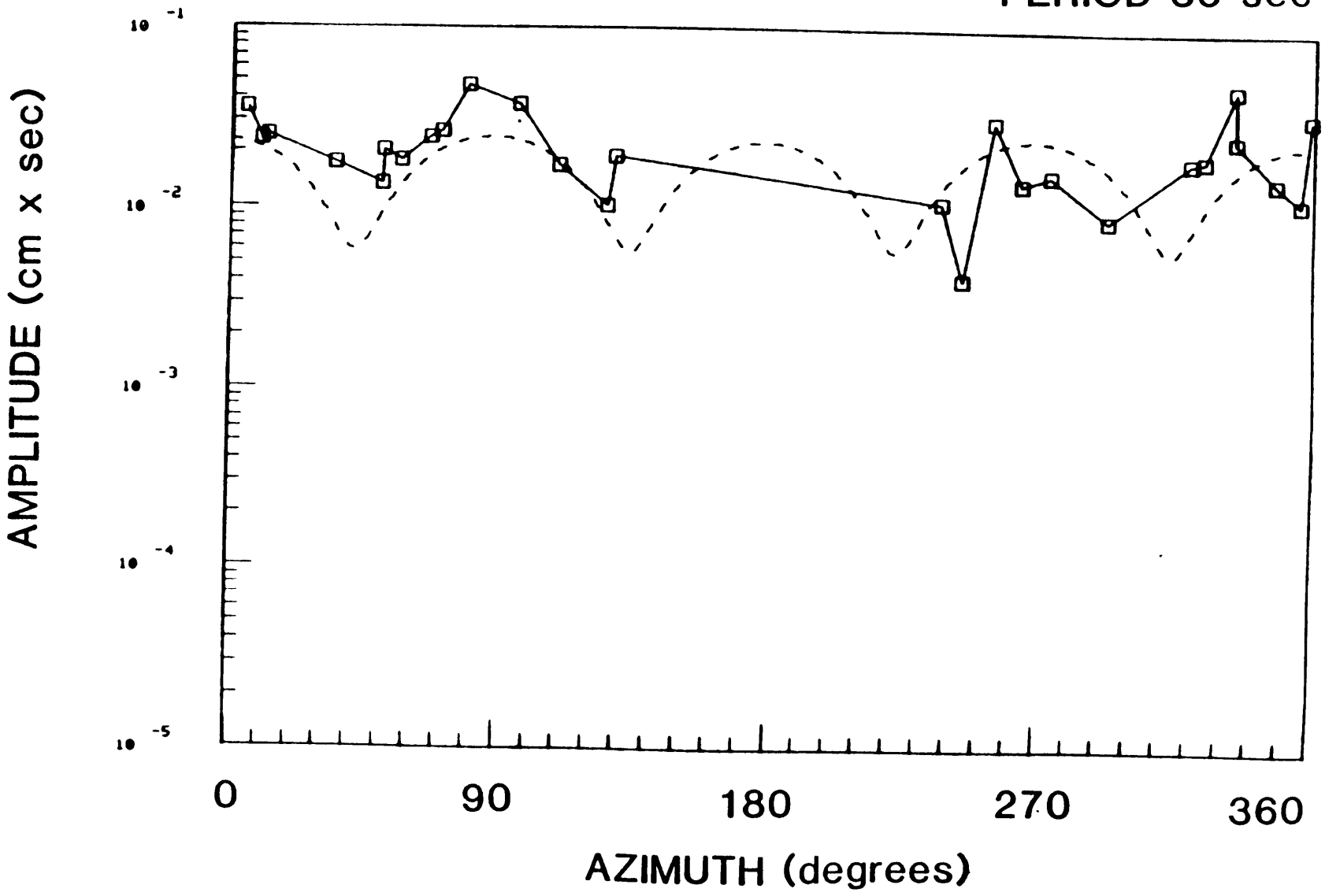
PERIOD 30 sec
AMPLITUDE (cm x sec)
10 -1
10 -2
10 -3
10 -4
10 -5
0
90
180
270
360
AZIMUTH (degrees)

FIGURE B.21c

PERIOD 50 sec

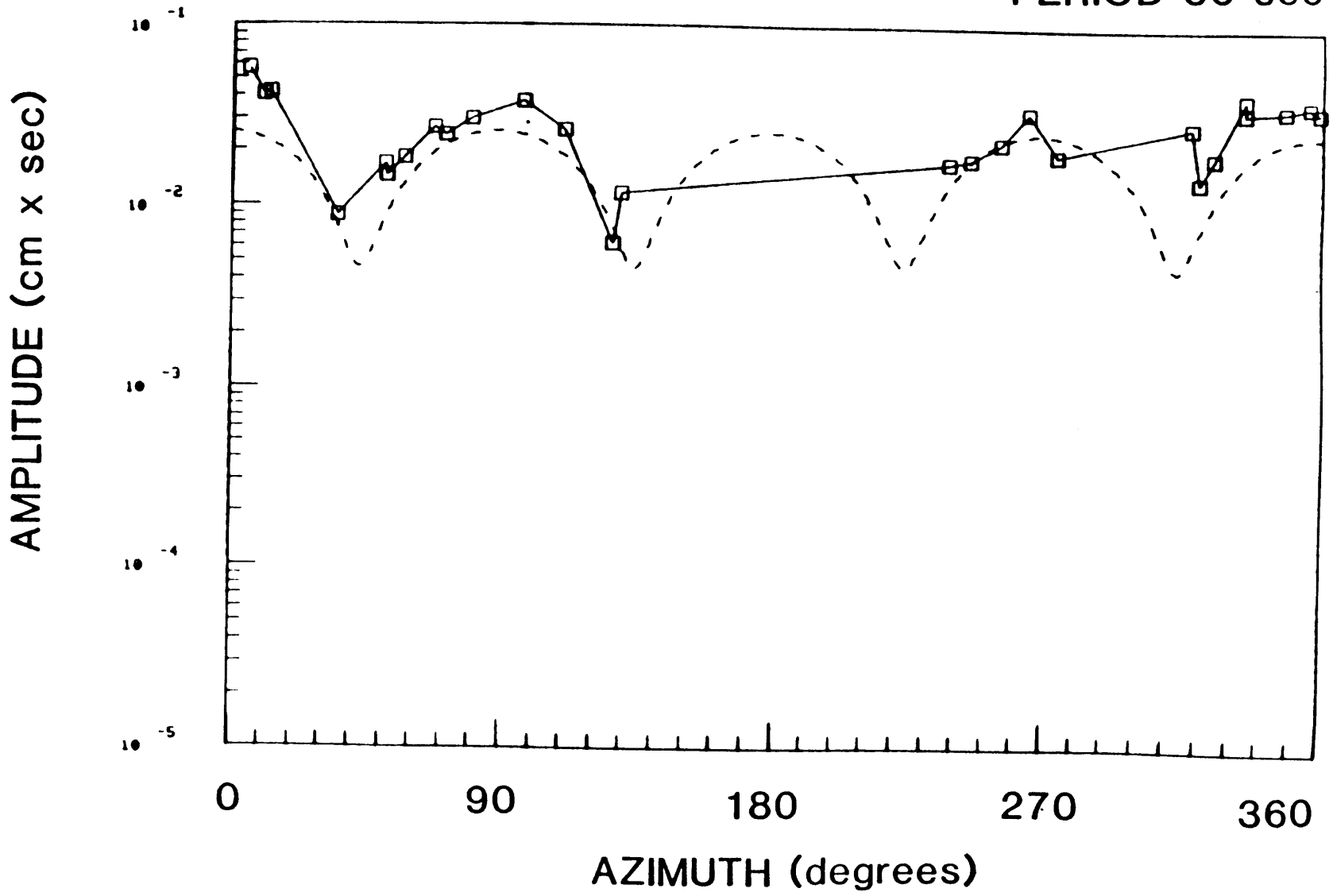

FIGURE B.21d

PERIOD 70 sec

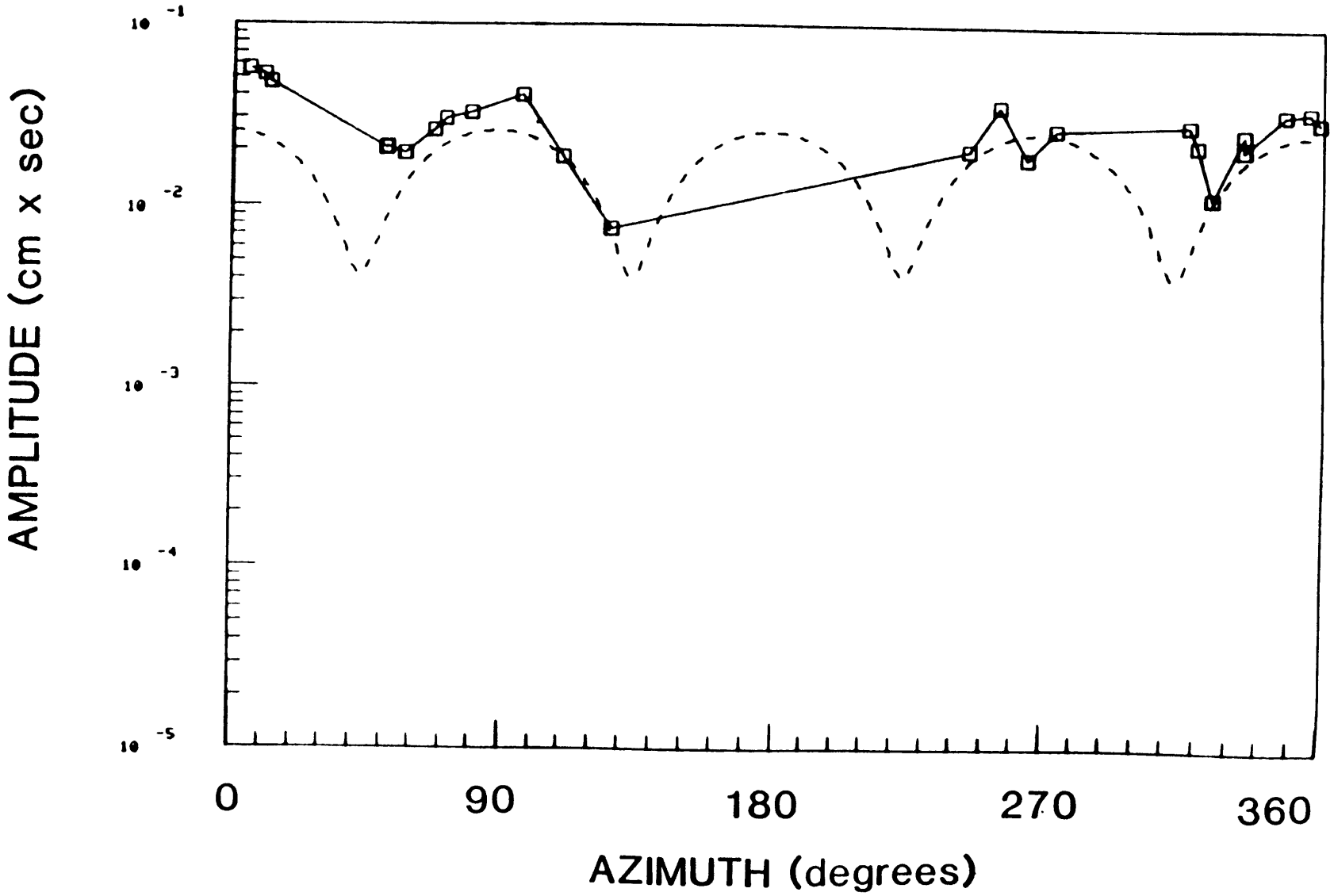

FIGURE B.21e

PERIOD 98 sec

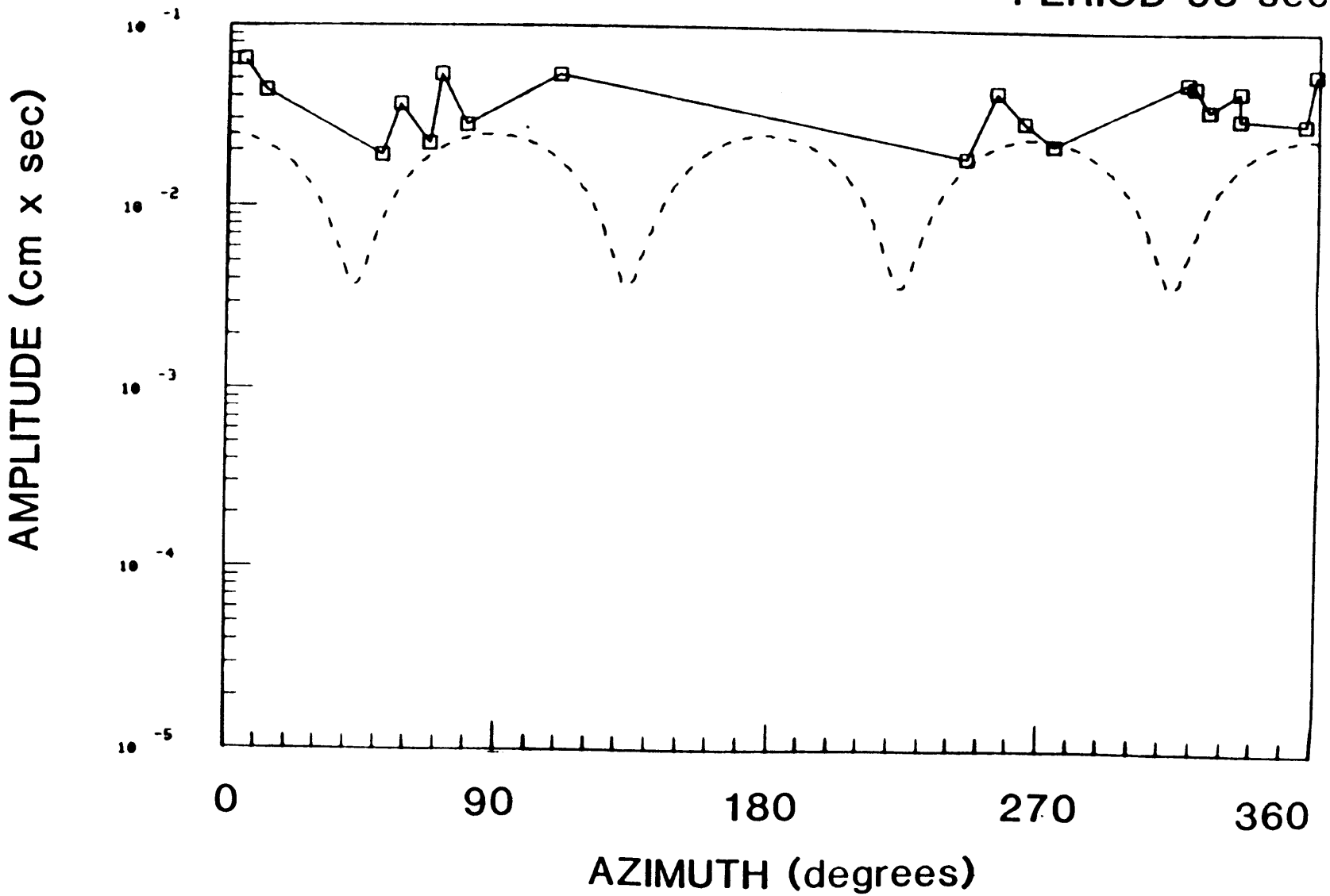

FIGURE B.22a

04/25/70

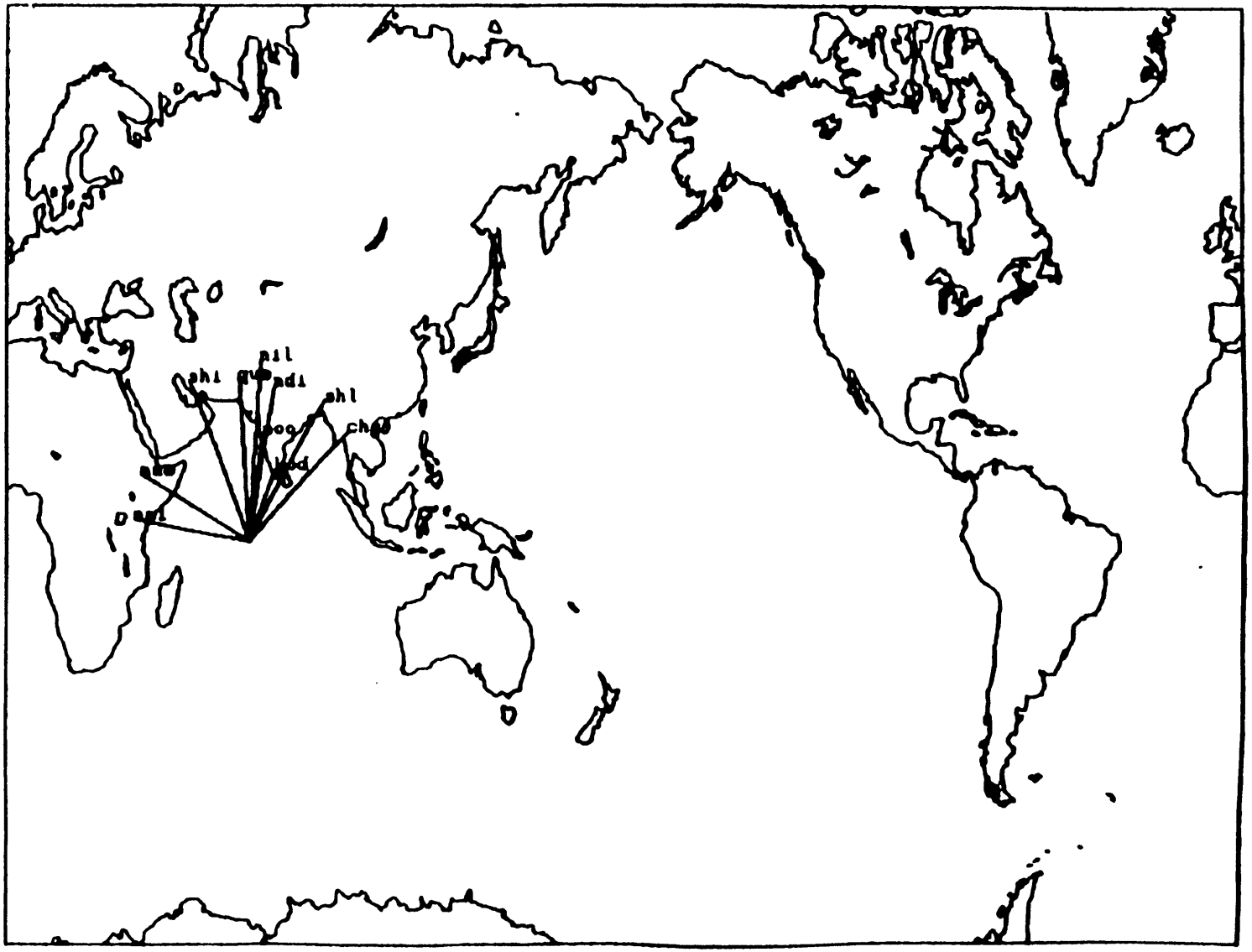

FIGURE B.22b

PERIOD 30 sec

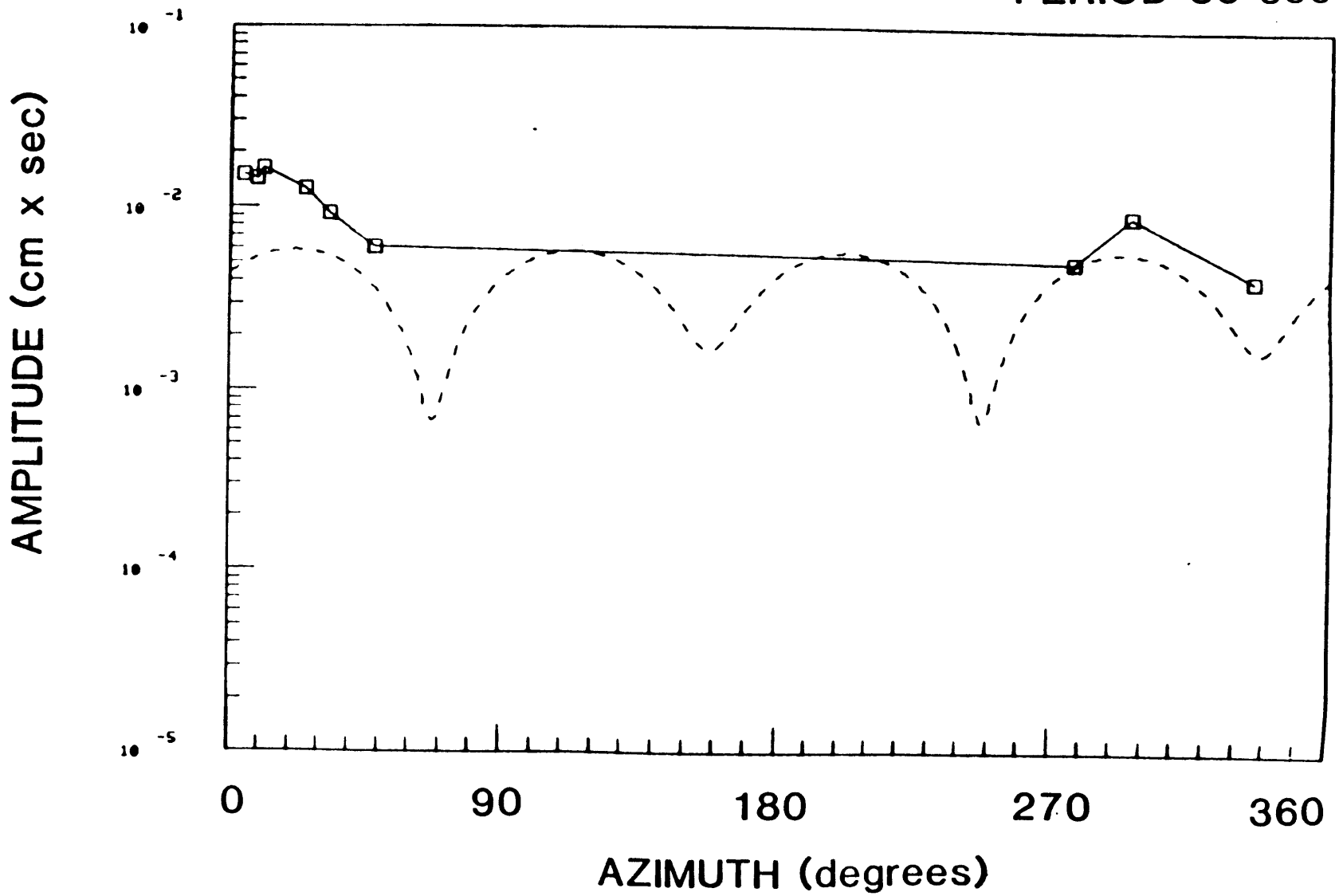

FIGURE B.22C

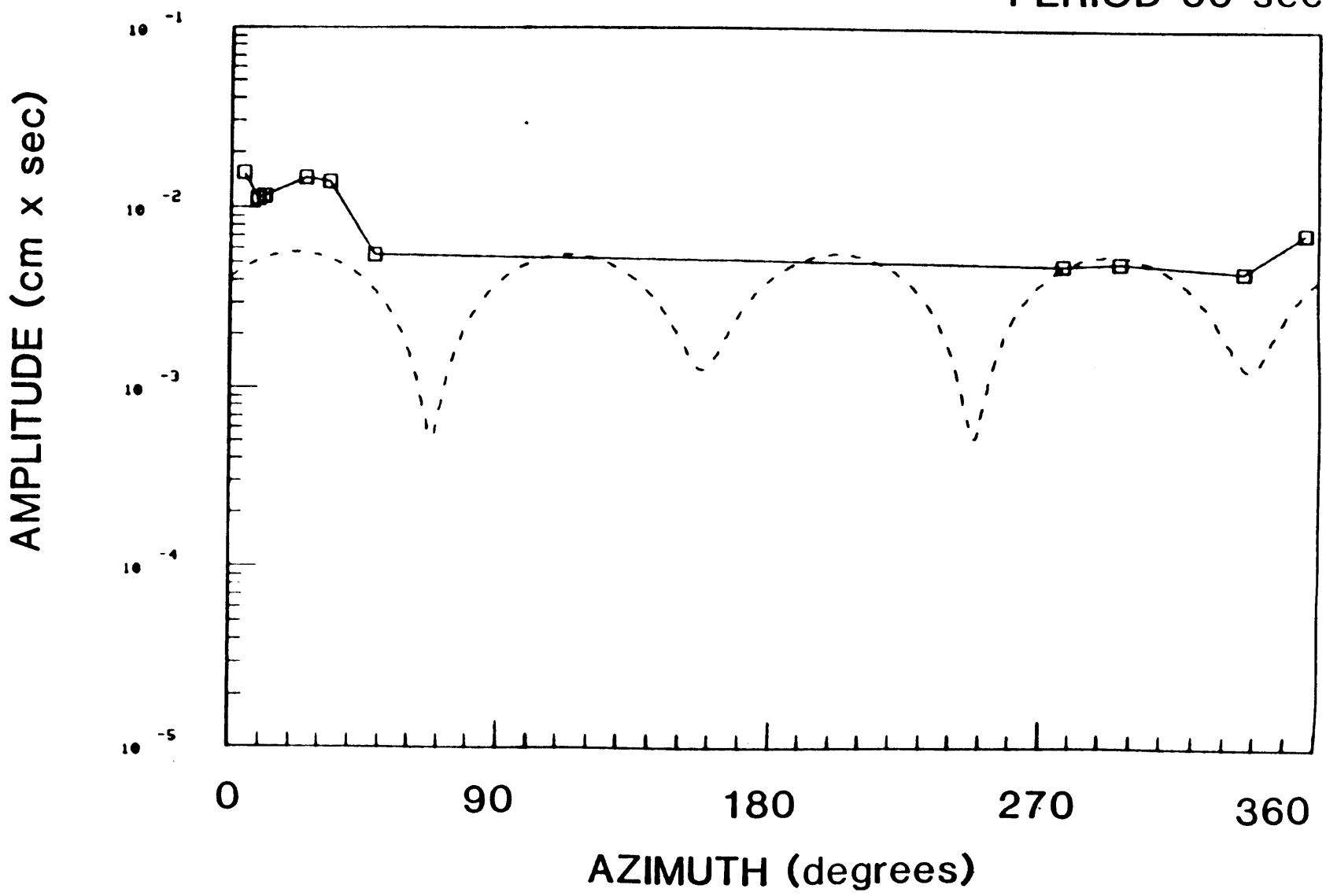
PERIOD 50 sec
AMPLITUDE (cm x sec)
10 -1
10 -2
10 -3
10 -4
10 -5
0
90
180
270
360
AZIMUTH (degrees)

FIGURE B.22d

PERIOD 70 sec

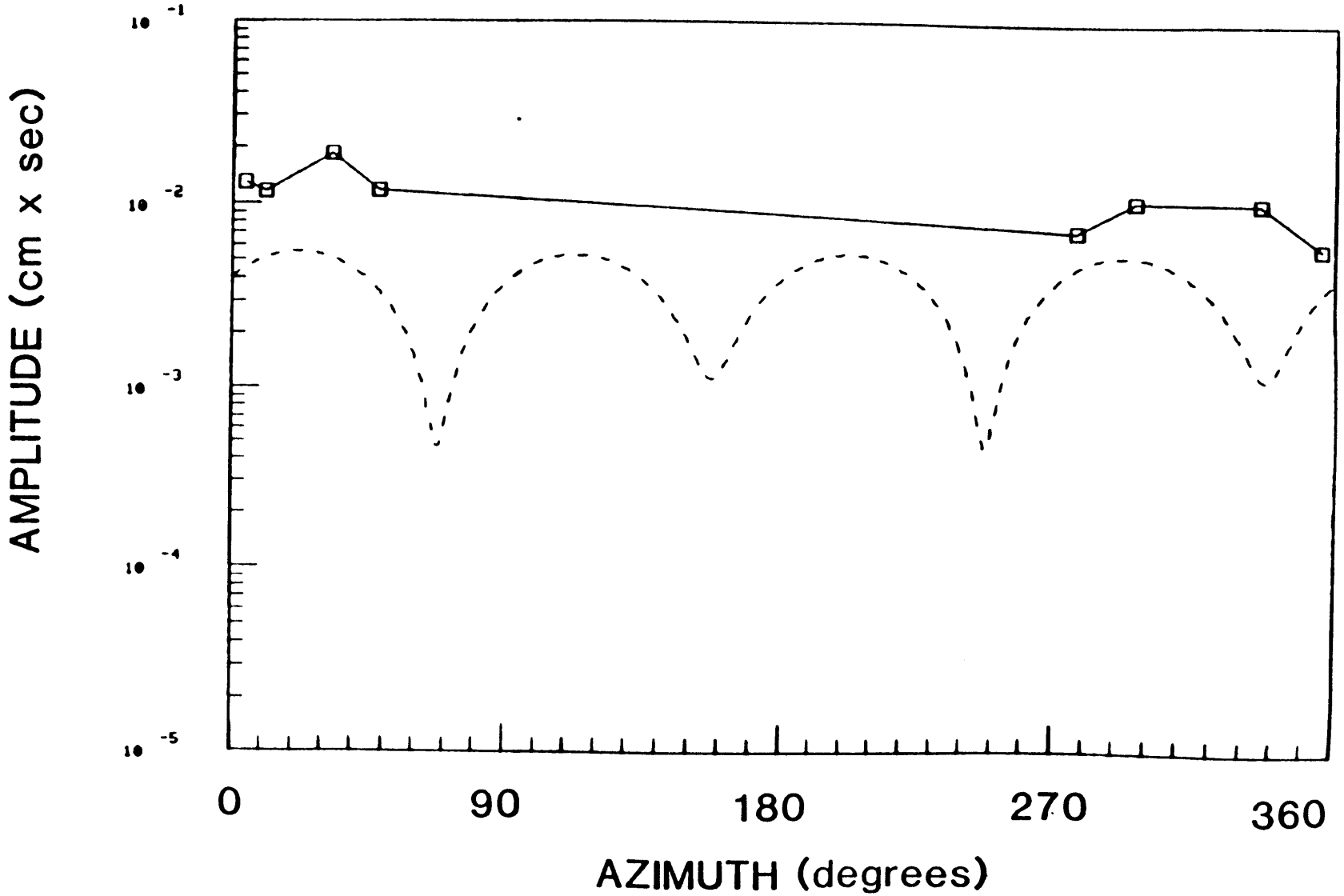

FIGURE B.22e

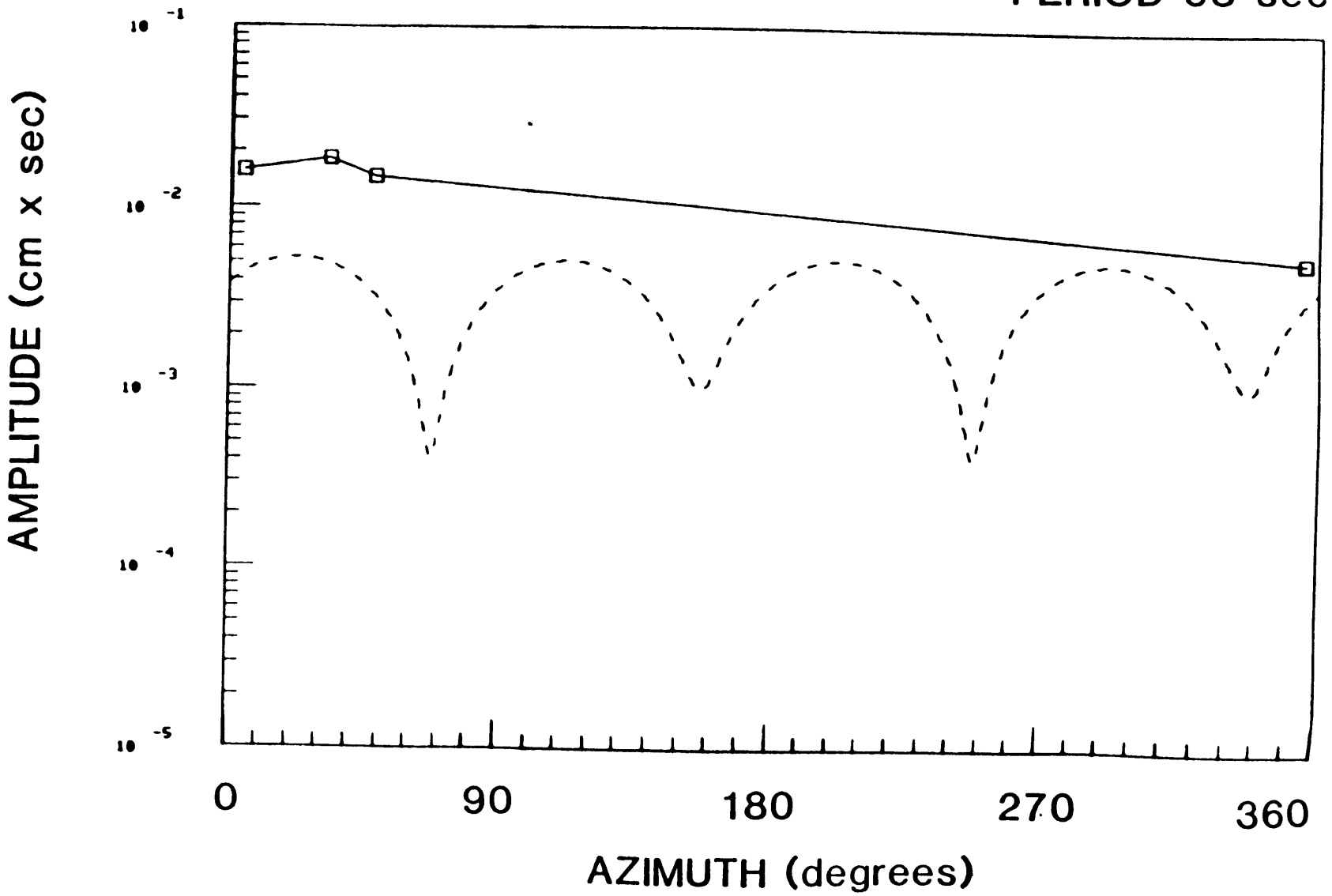
PERIOD 98 sec
AMPLITUDE (cm x sec)
10 -1
10 -2
10 -3
10 -4
10 -5
0
90
180
270
360
AZIMUTH (degrees)

FIGURE B.23a

05/09/71

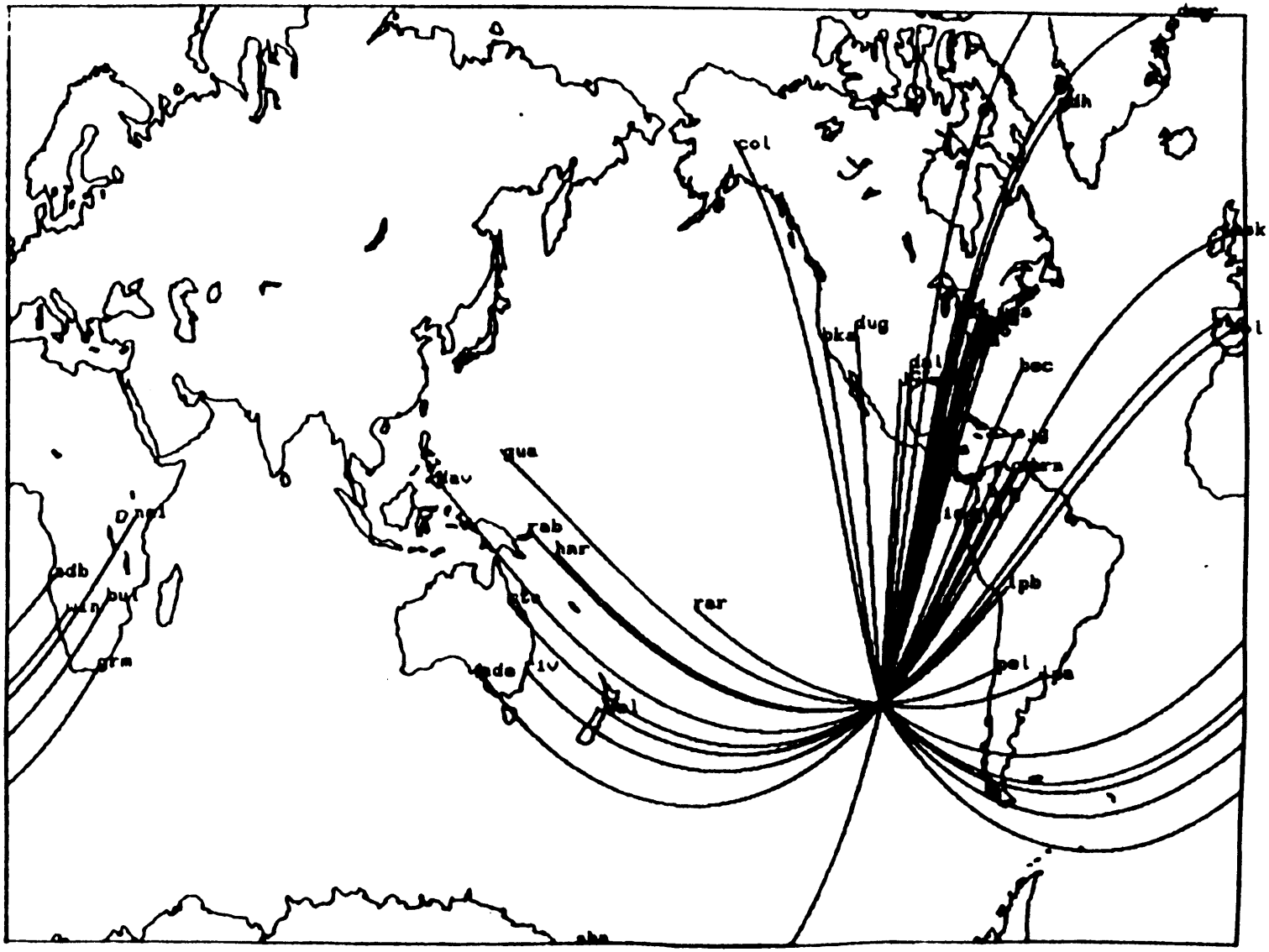

FIGURE B.23b

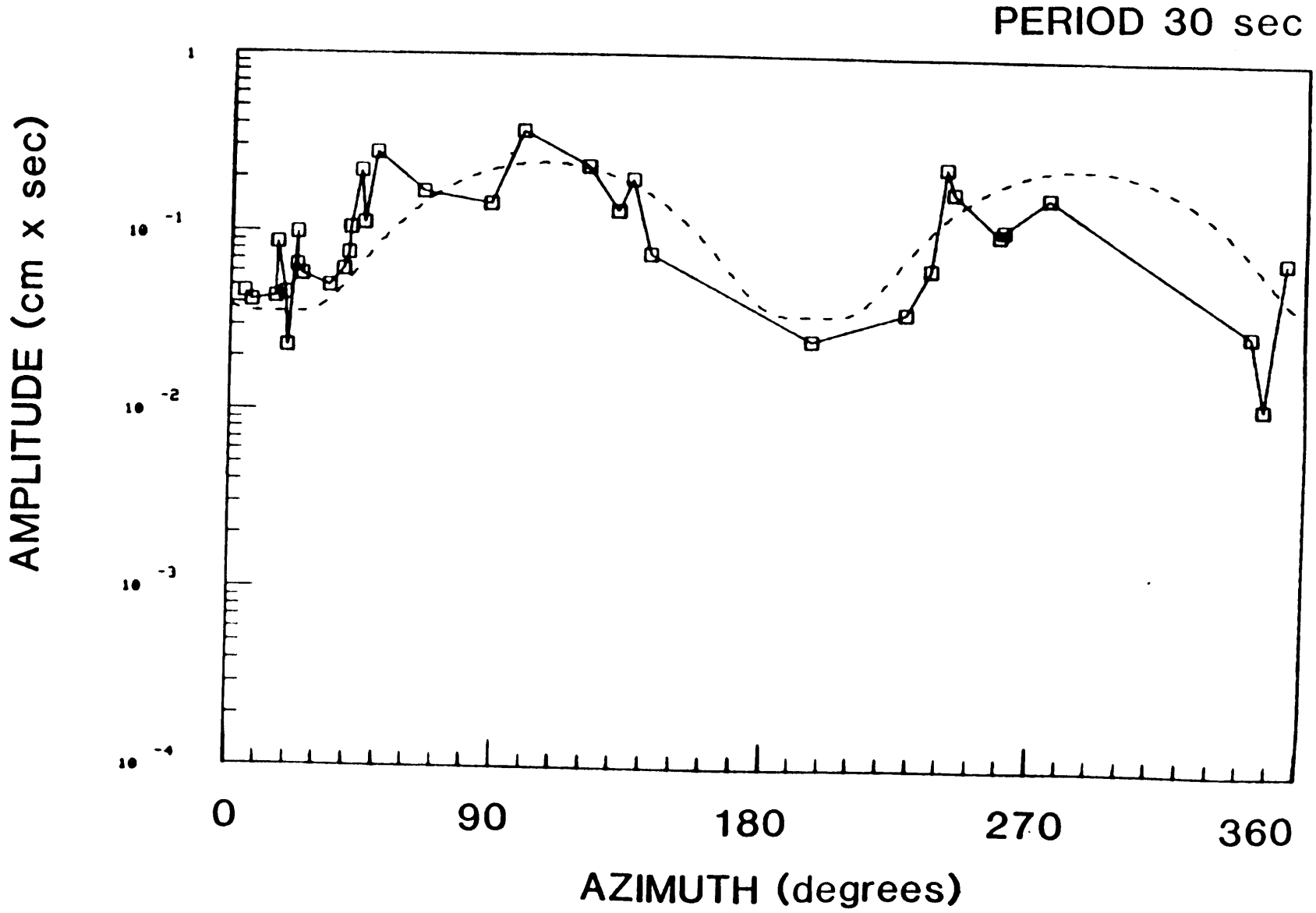
PERIOD 30 sec
AMPLITUDE (cm x sec)
1
10 -1
10 -2
10 -3
10 -4
0
90
180
270
360
AZIMUTH (degrees)

FIGURE B.23C

PERIOD 50 sec

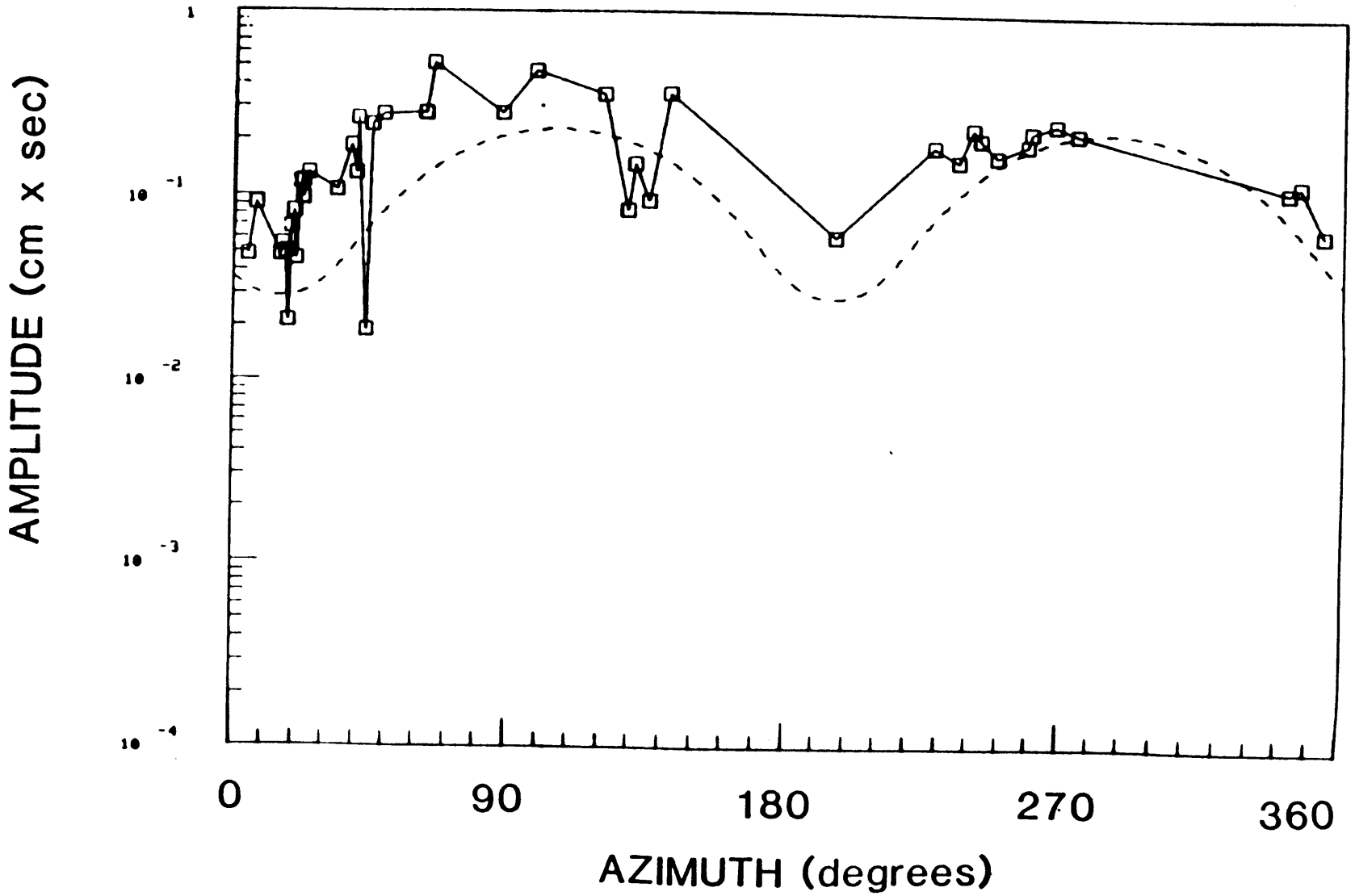

FIGURE B.23d

PERIOD 70 sec

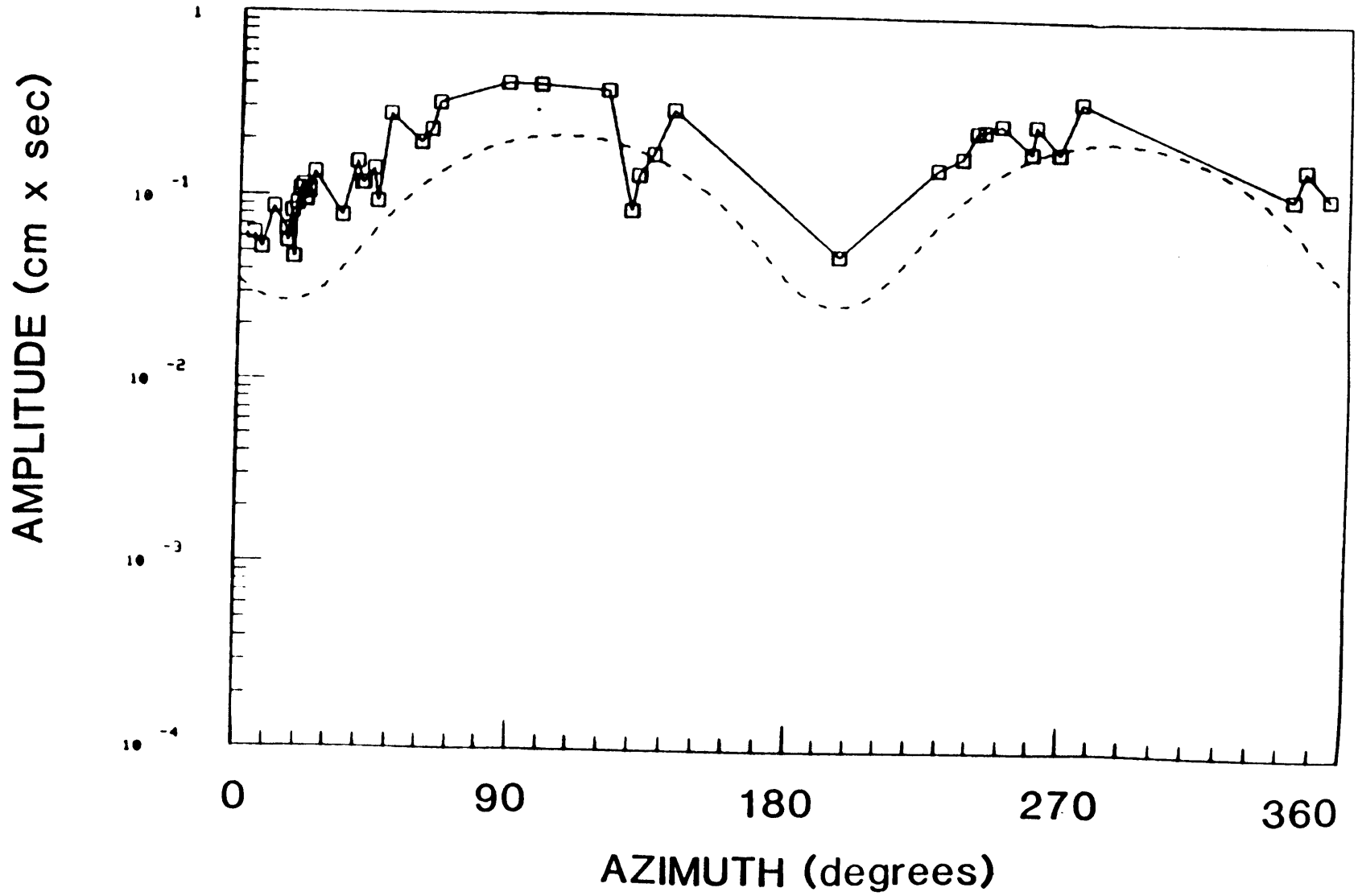

FIGURE B.23e

PERIOD 98 sec

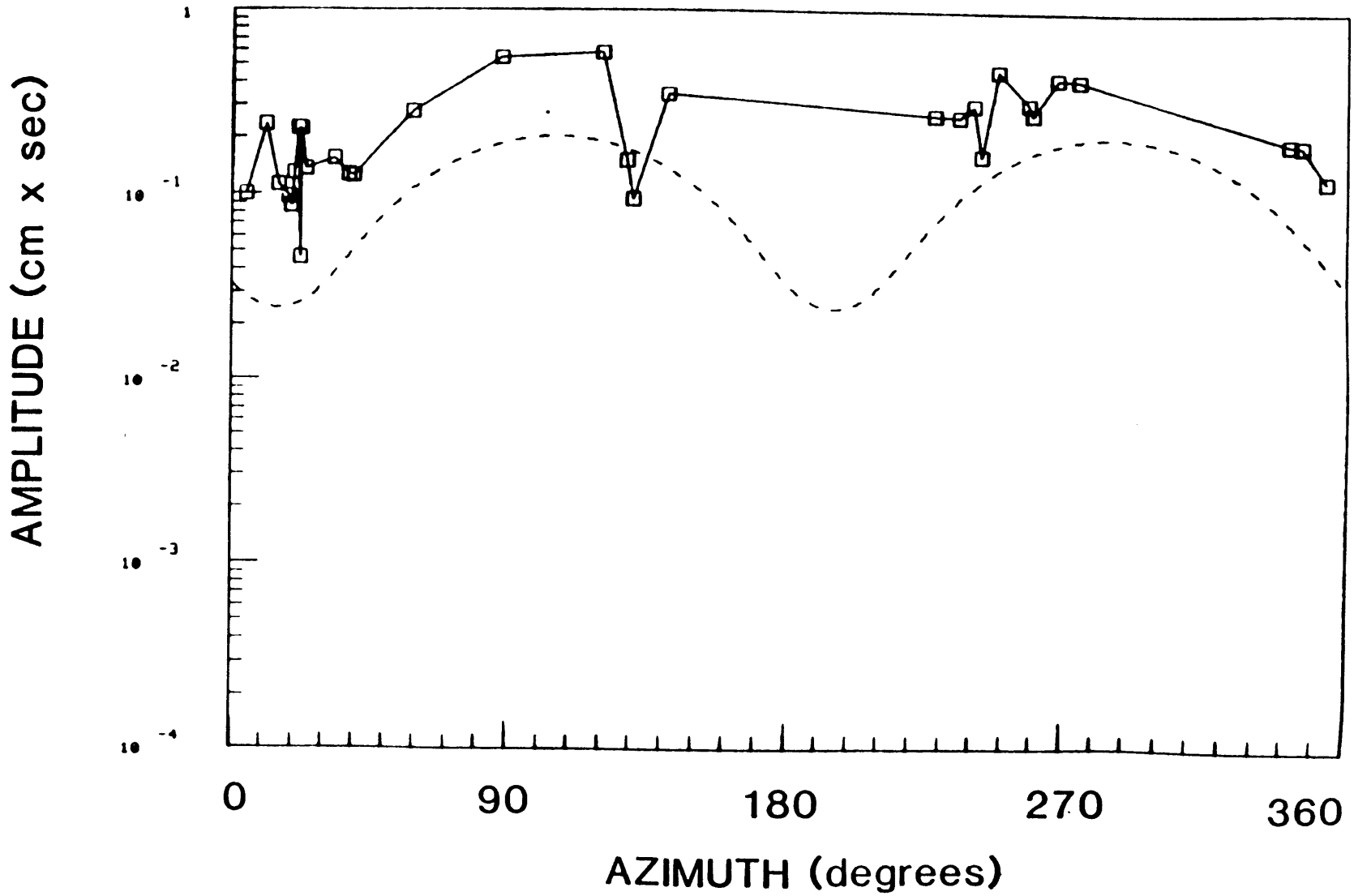

FIGURE B.24a

05/31/71

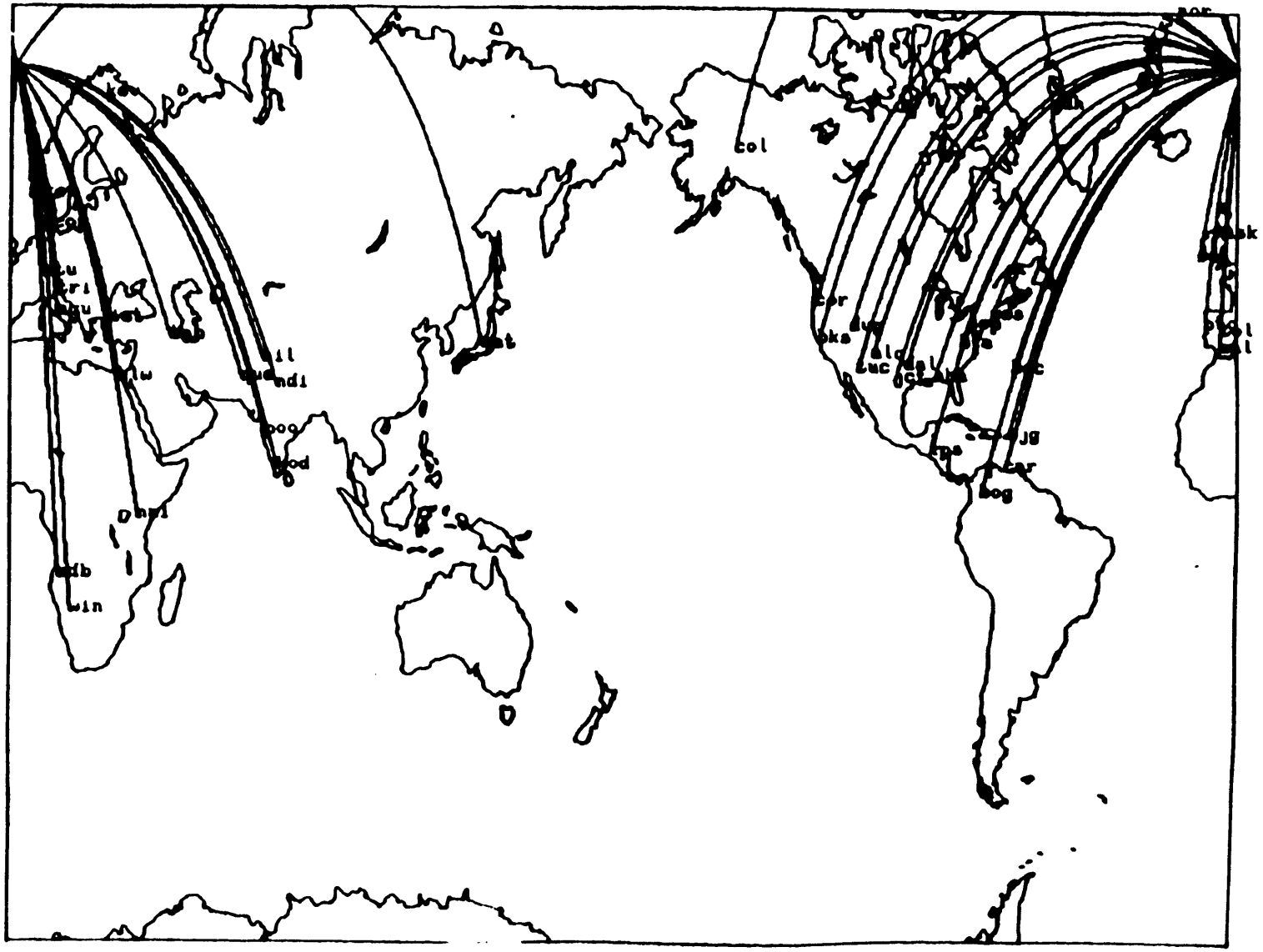

FIGURE B.24b

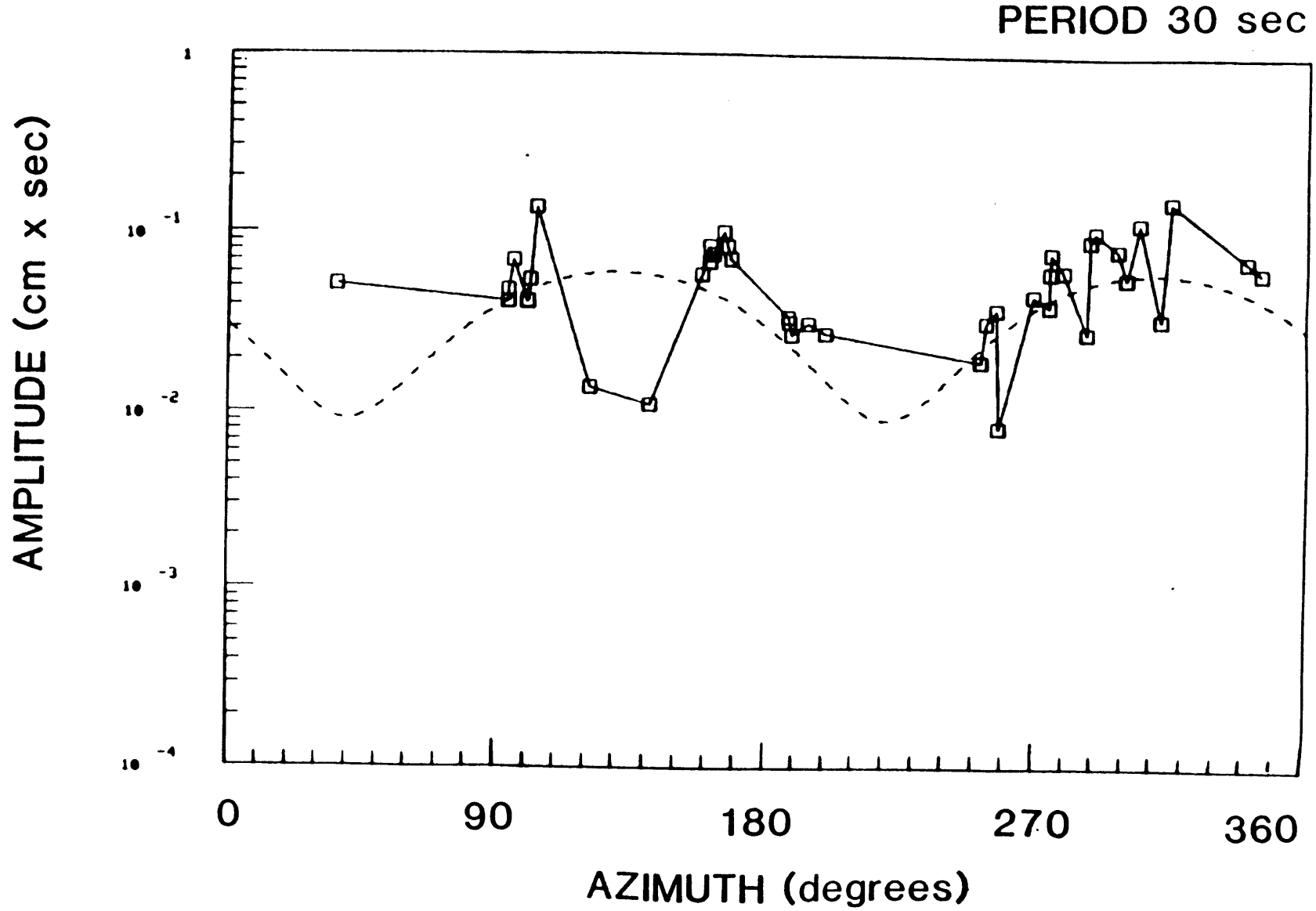
PERIOD 30 sec
AMPLITUDE (cm x sec)
1
10 -1
10 -2
10 -3
10 -4
0
90
180
270
360
AZIMUTH (degrees)

FIGURE B.24C

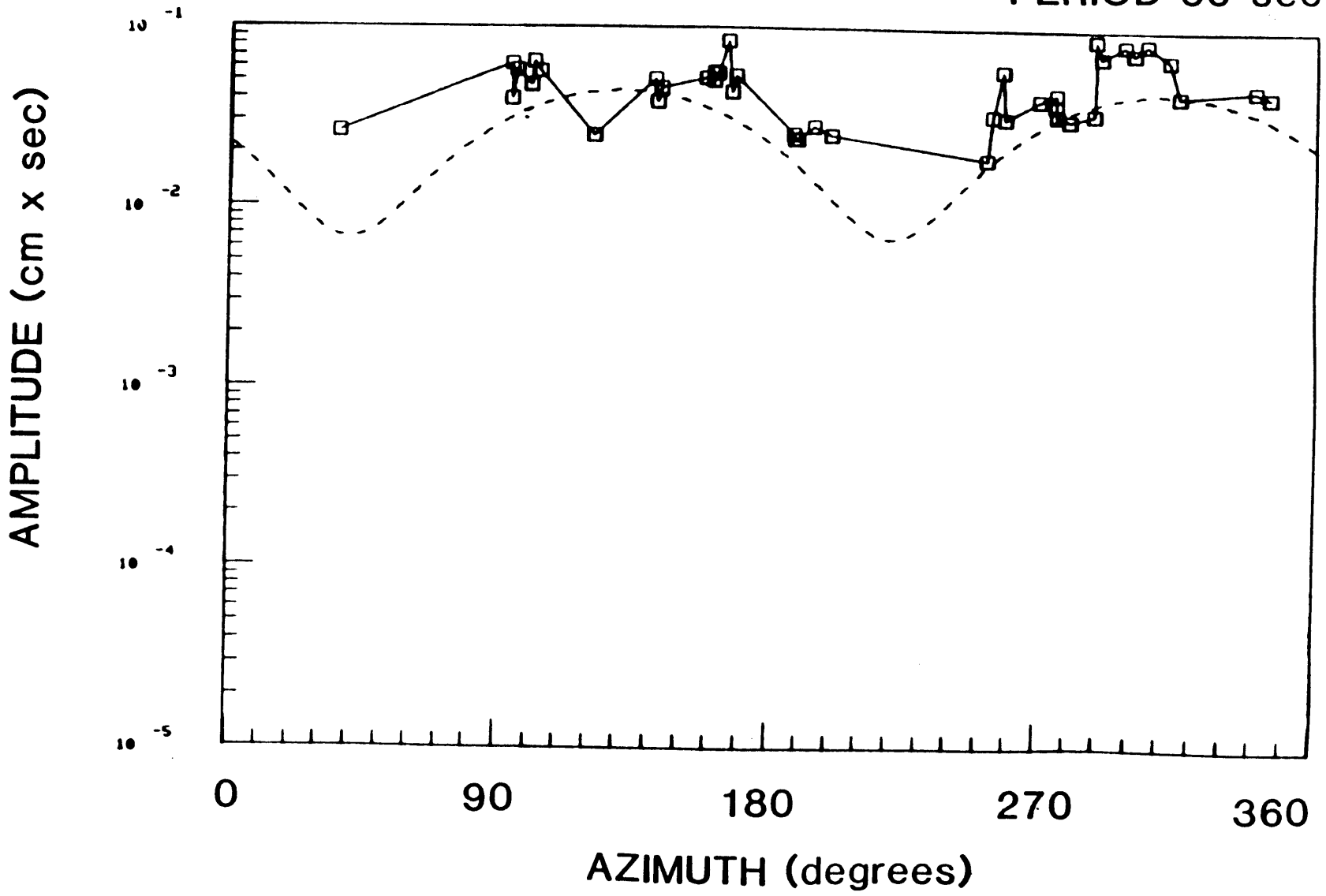
PERIOD 50 sec
AMPLITUDE (cm x sec)
10 -1
10 -2
10 -3
10 -4
10 -5
0
90
180
270
360
AZIMUTH (degrees)

FIGURE B.24d

PERIOD 70 sec

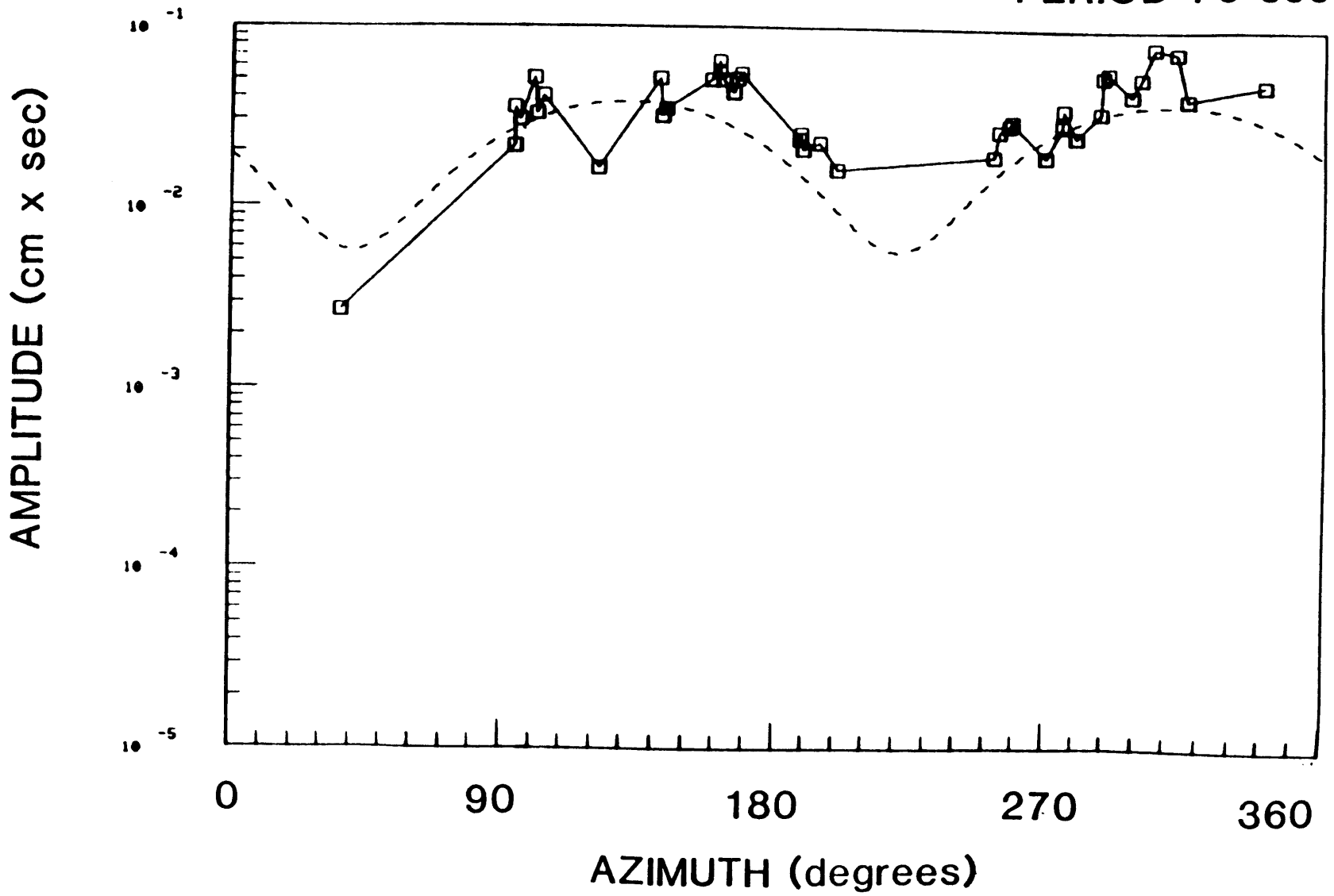

FIGURE B.24e

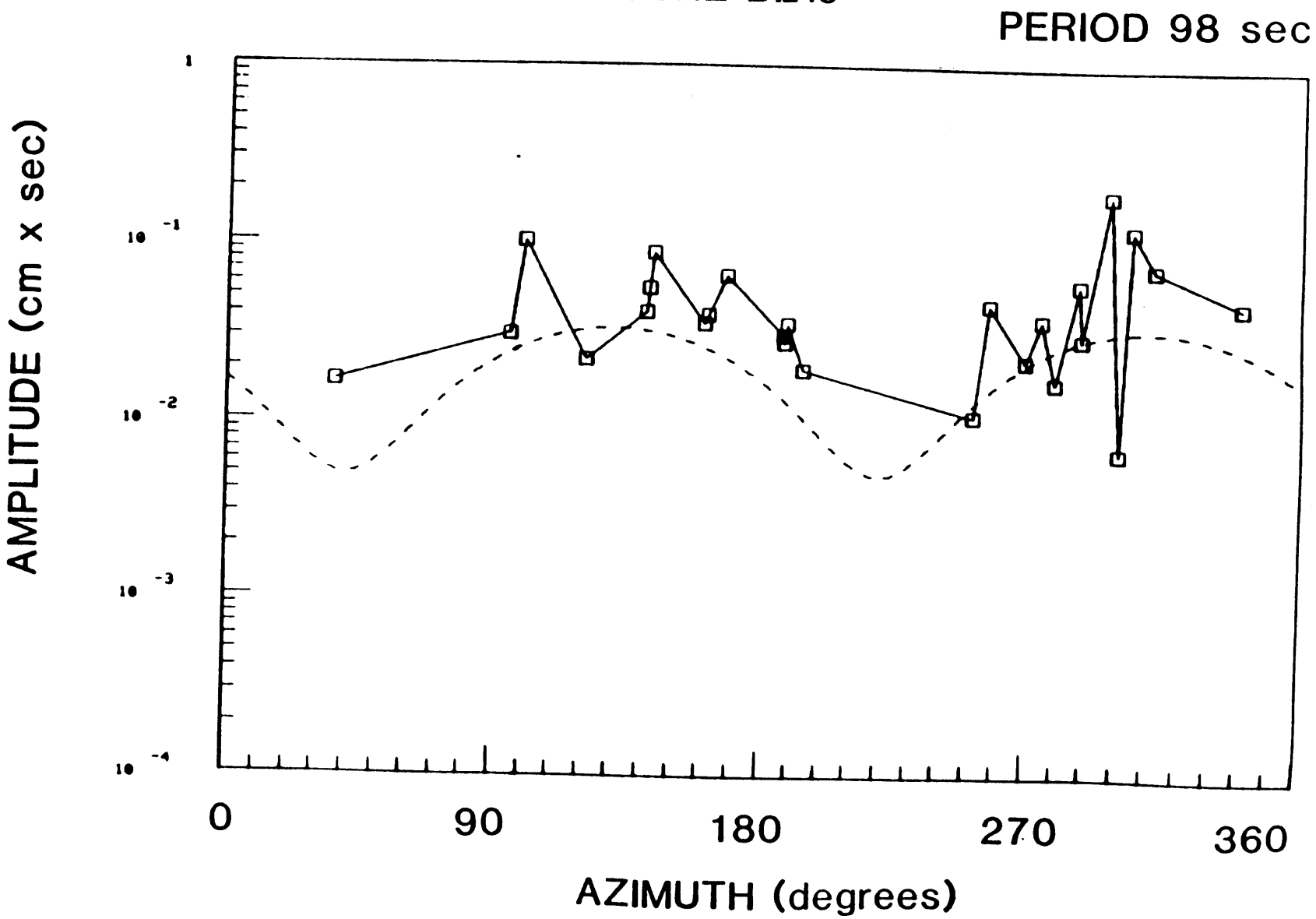
PERIOD 98 sec
AMPLITUDE (cm x sec)
1
10 -1
10 -2
10 -3
10 -4
0
90
180
270
360
AZIMUTH (degrees)

FIGURE B.25a

06/26/71

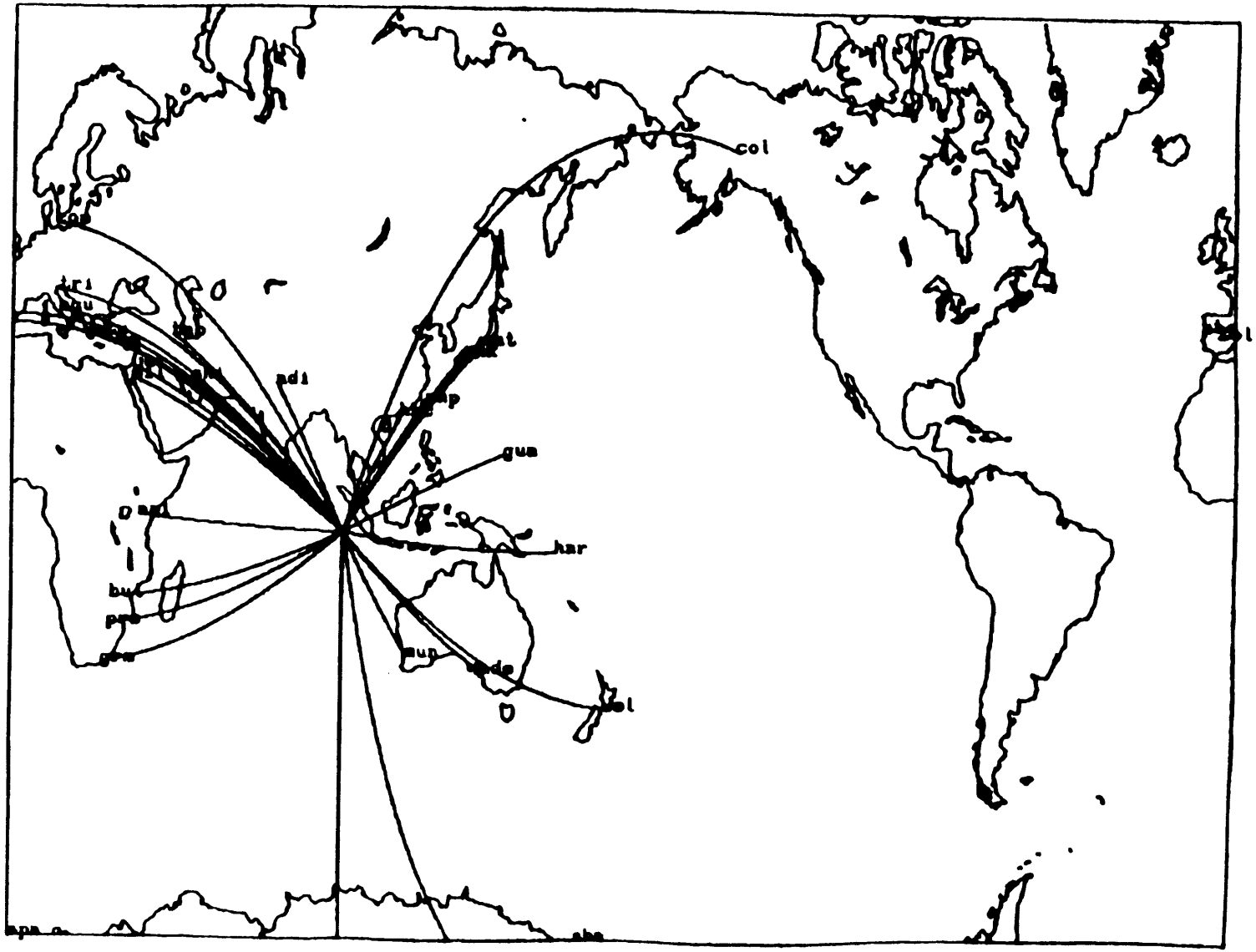

FIGURE B.25b

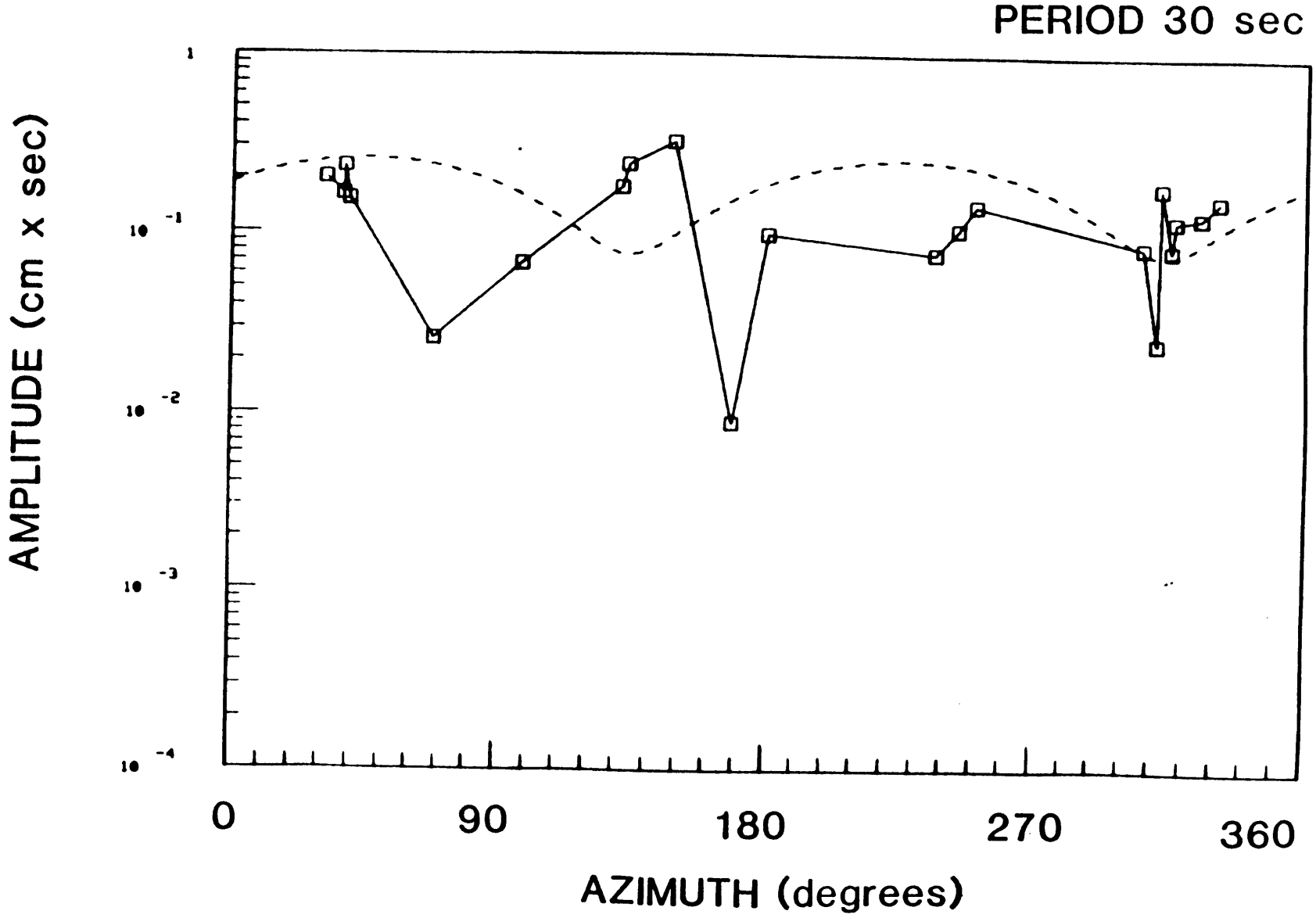
PERIOD 30 sec
AMPLITUDE (cm x sec)
1
10 -1
10 -2
10 -3
10 -4
0
90
180
270
360
AZIMUTH (degrees)

FIGURE B.25C

PERIOD 50 sec

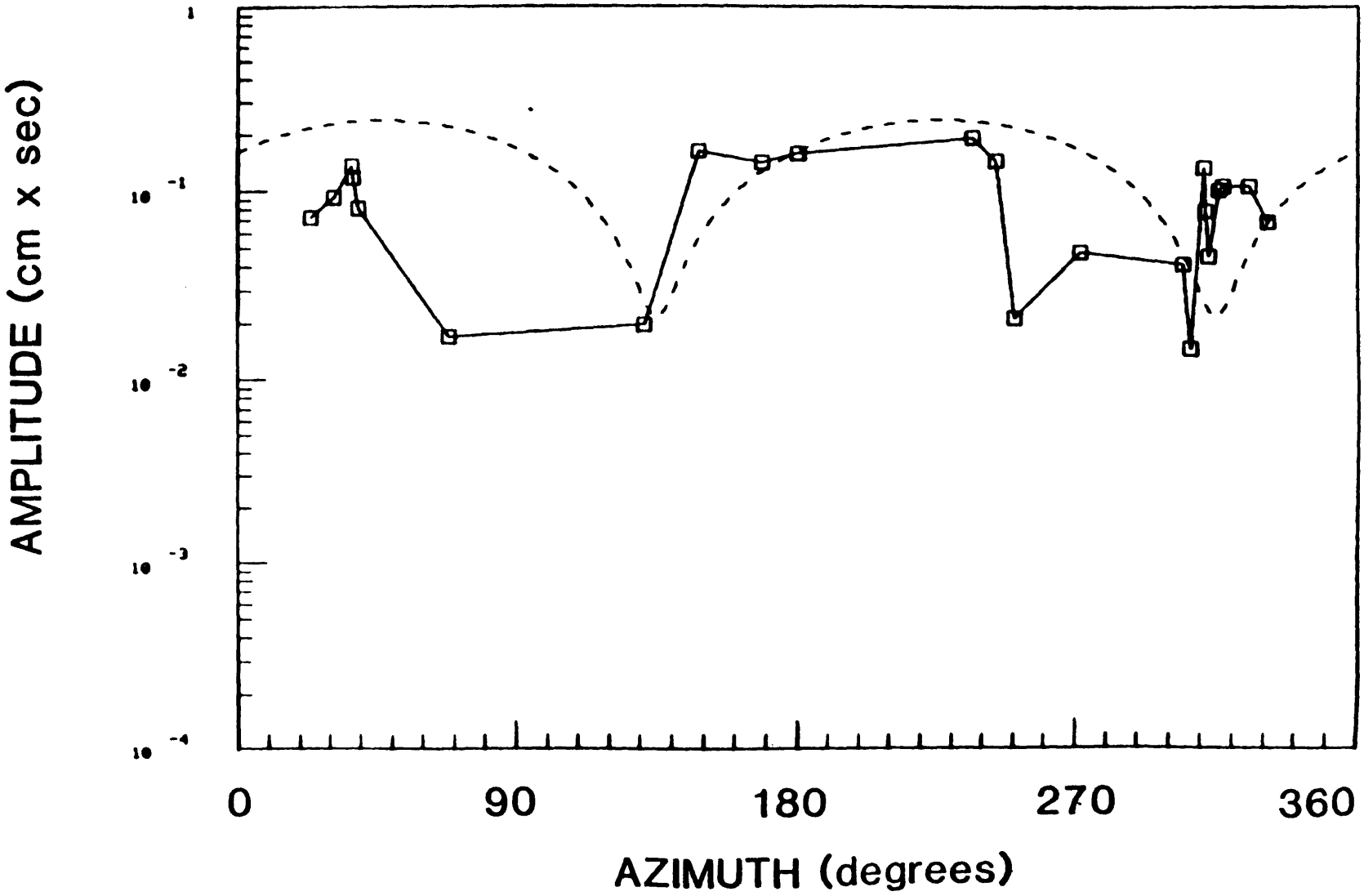

FIGURE B.25d

PERIOD 70 sec

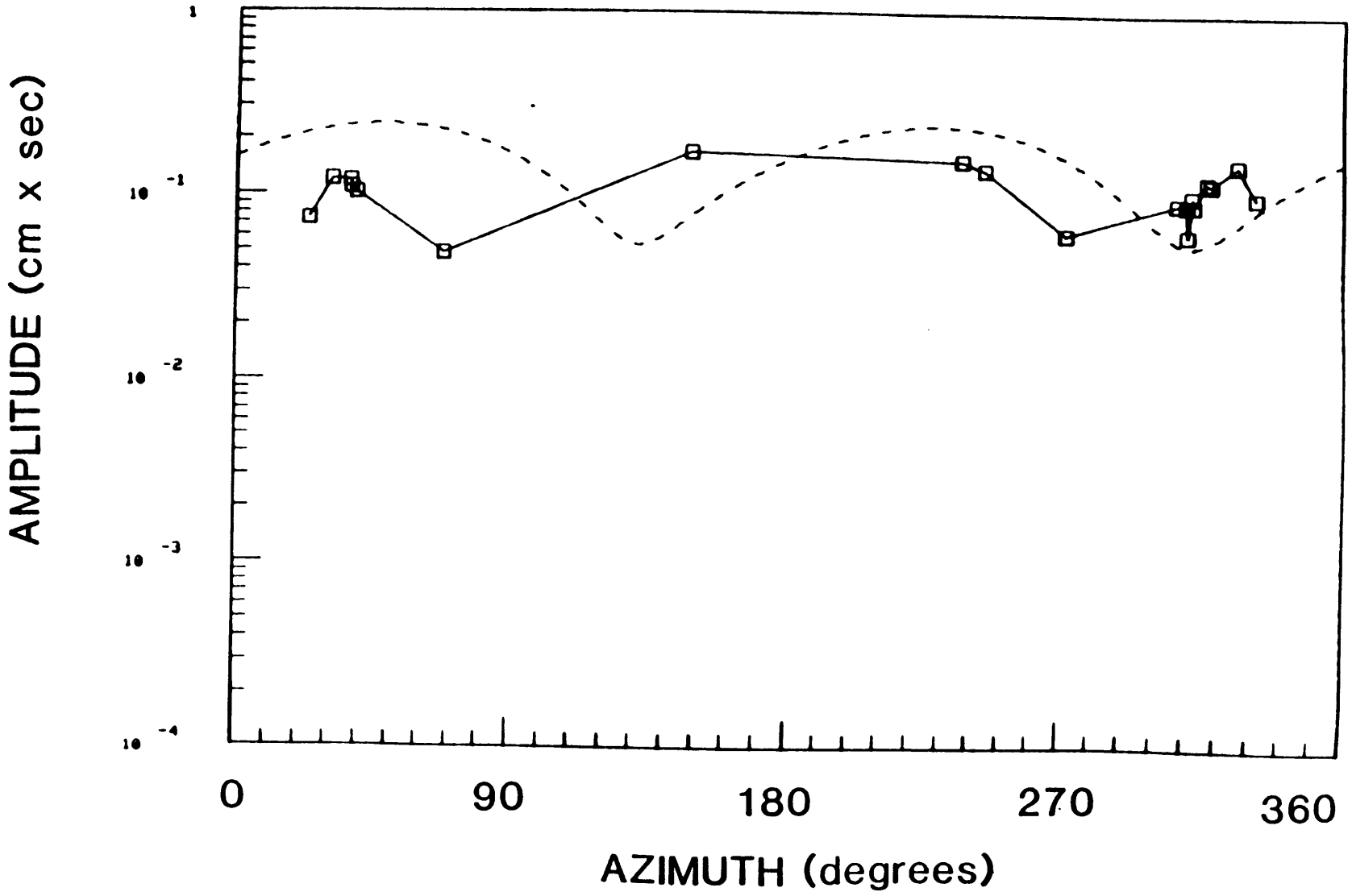

FIGURE B.25e

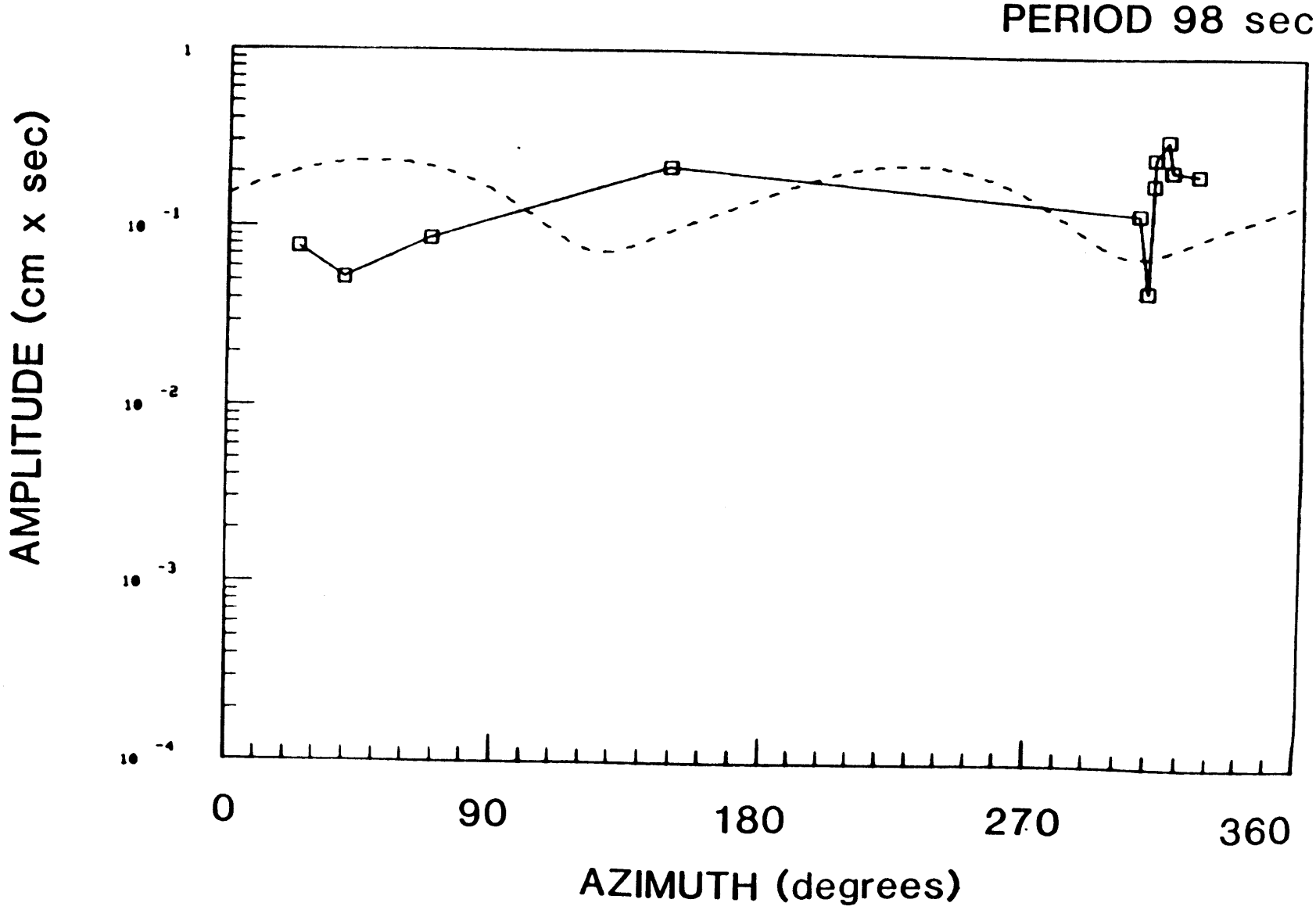
PERIOD 98 sec
AMPLITUDE (cm x sec)
1
10 -1
10 -2
10 -3
10 -4
0
90
180
270
360
AZIMUTH (degrees)

FIGURE B.26a

09/30/71

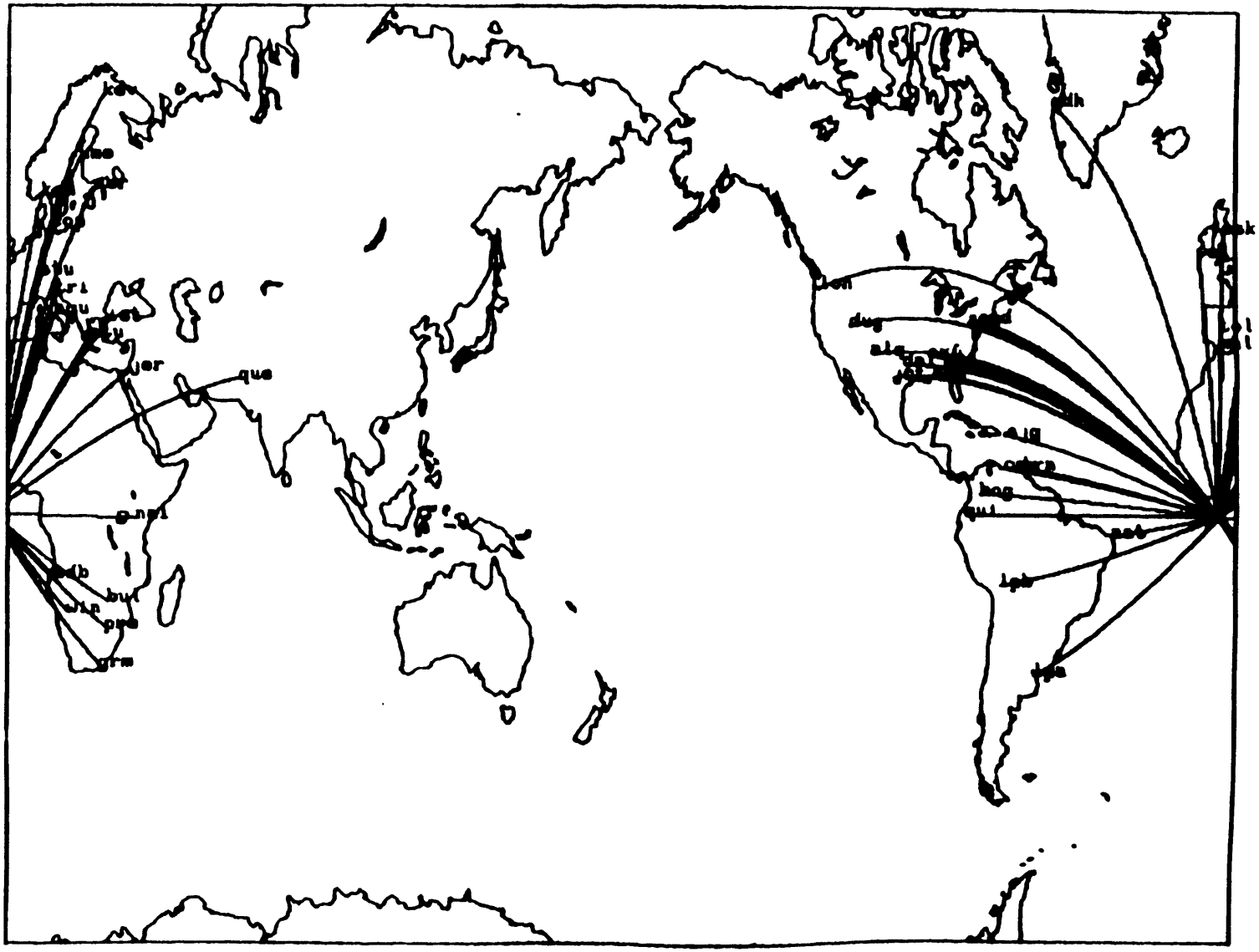

FIGURE B.26b

PERIOD 30 sec

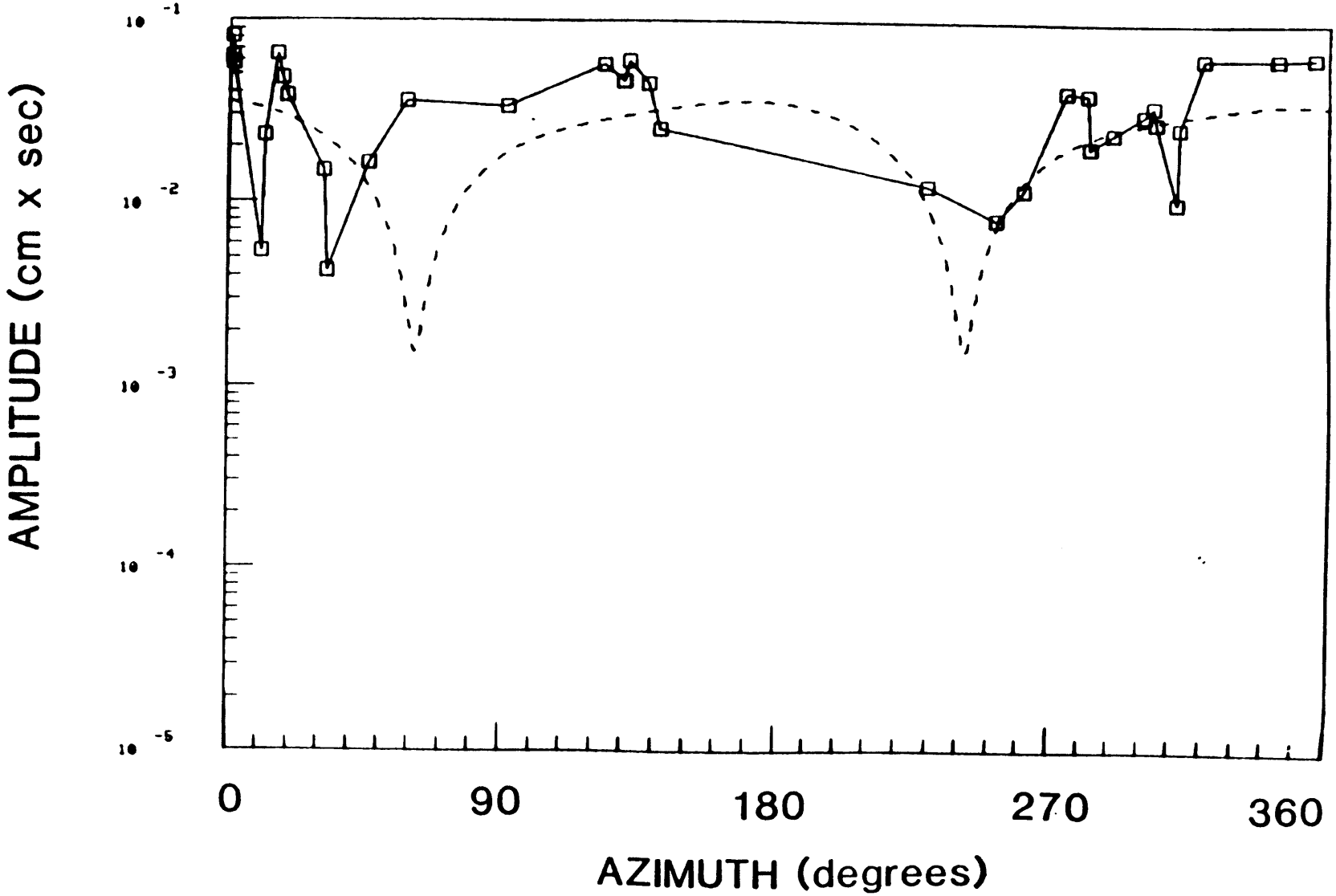

FIGURE B.26C

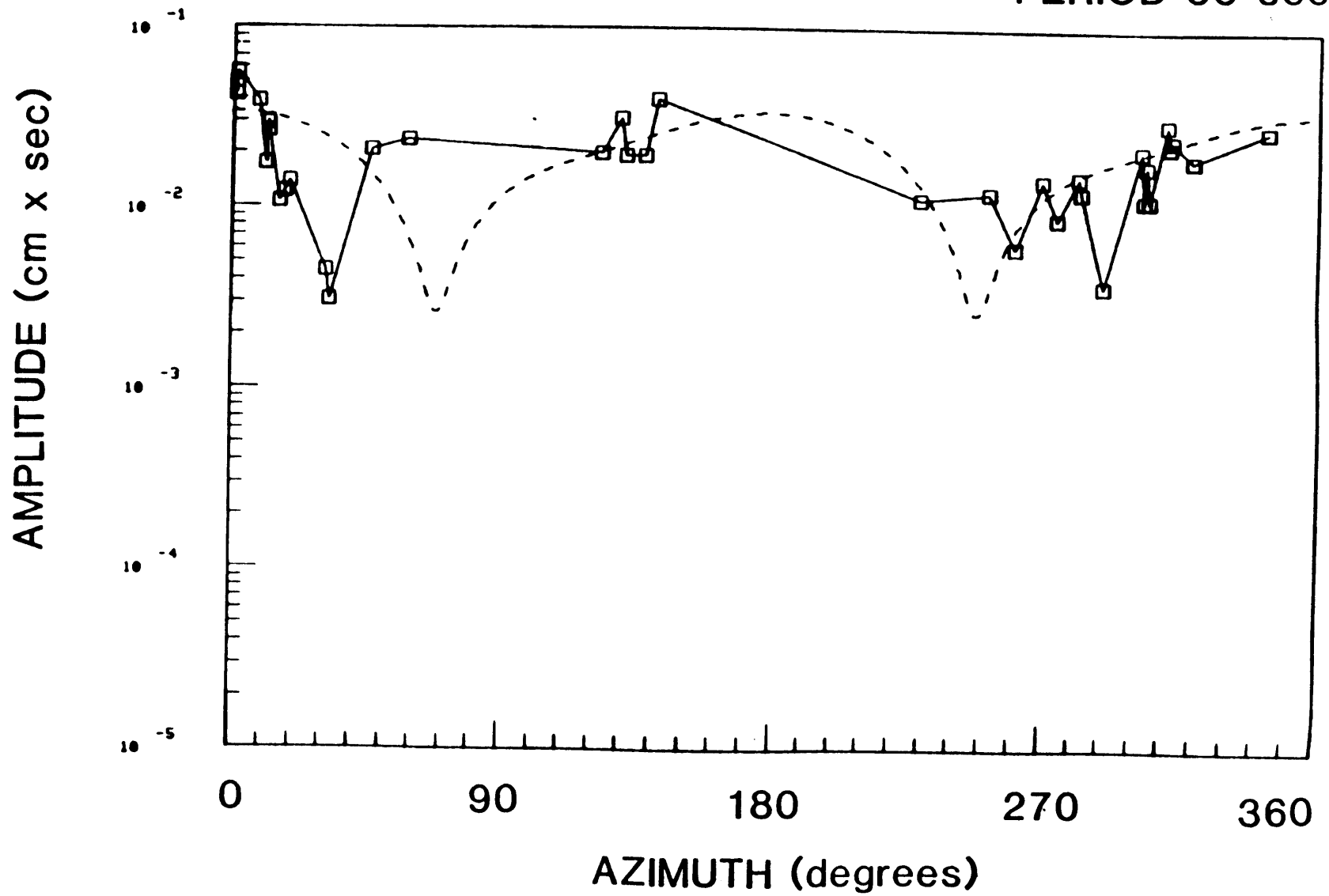
PERIOD 50 sec
AMPLITUDE (cm x sec)
10 -1
10 -2
10 -3
10 -4
10 -5
0
90
180
270
360
AZIMUTH (degrees)

FIGURE B.26d

PERIOD 70 sec

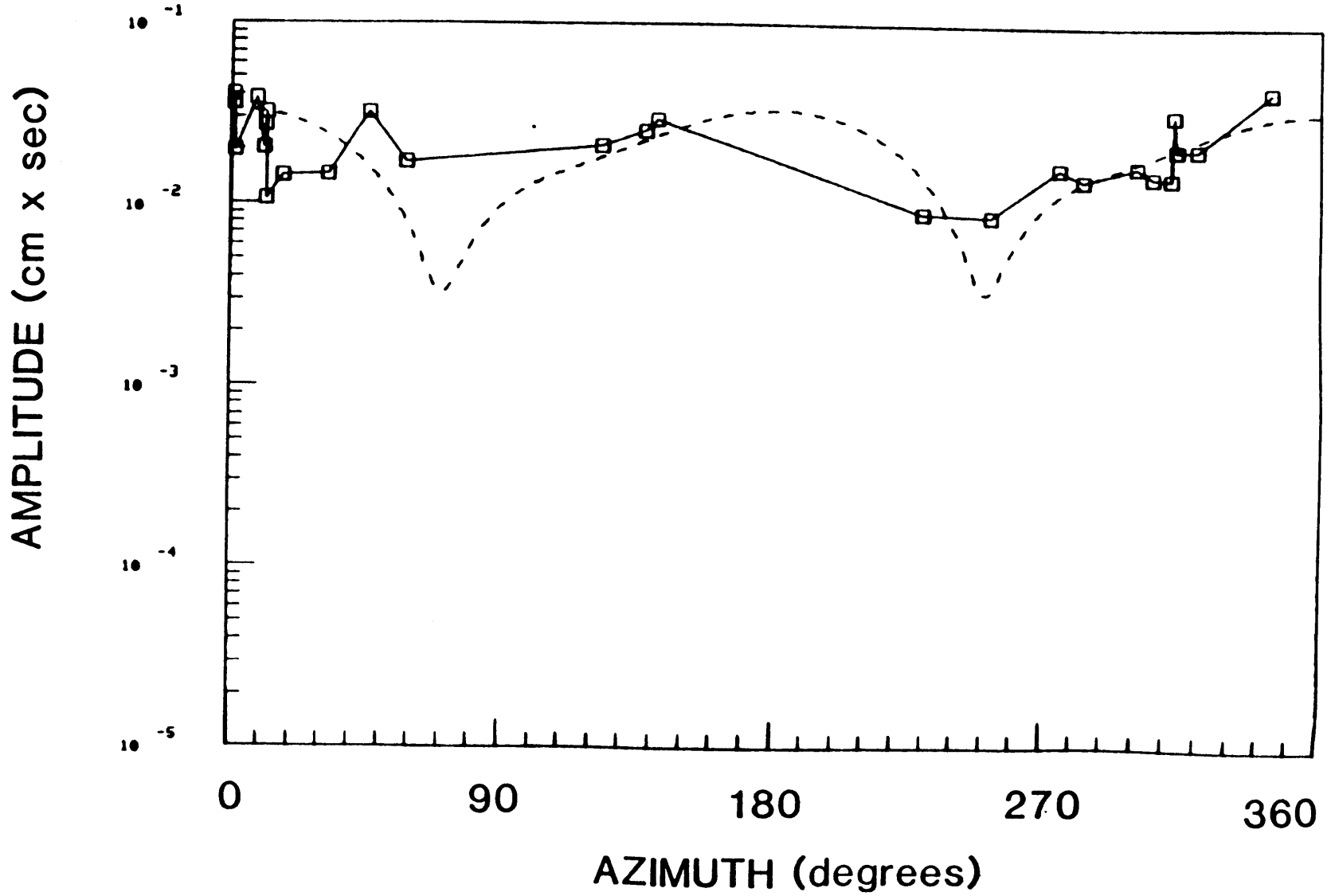

FIGURE B.26e

PERIOD 98 sec

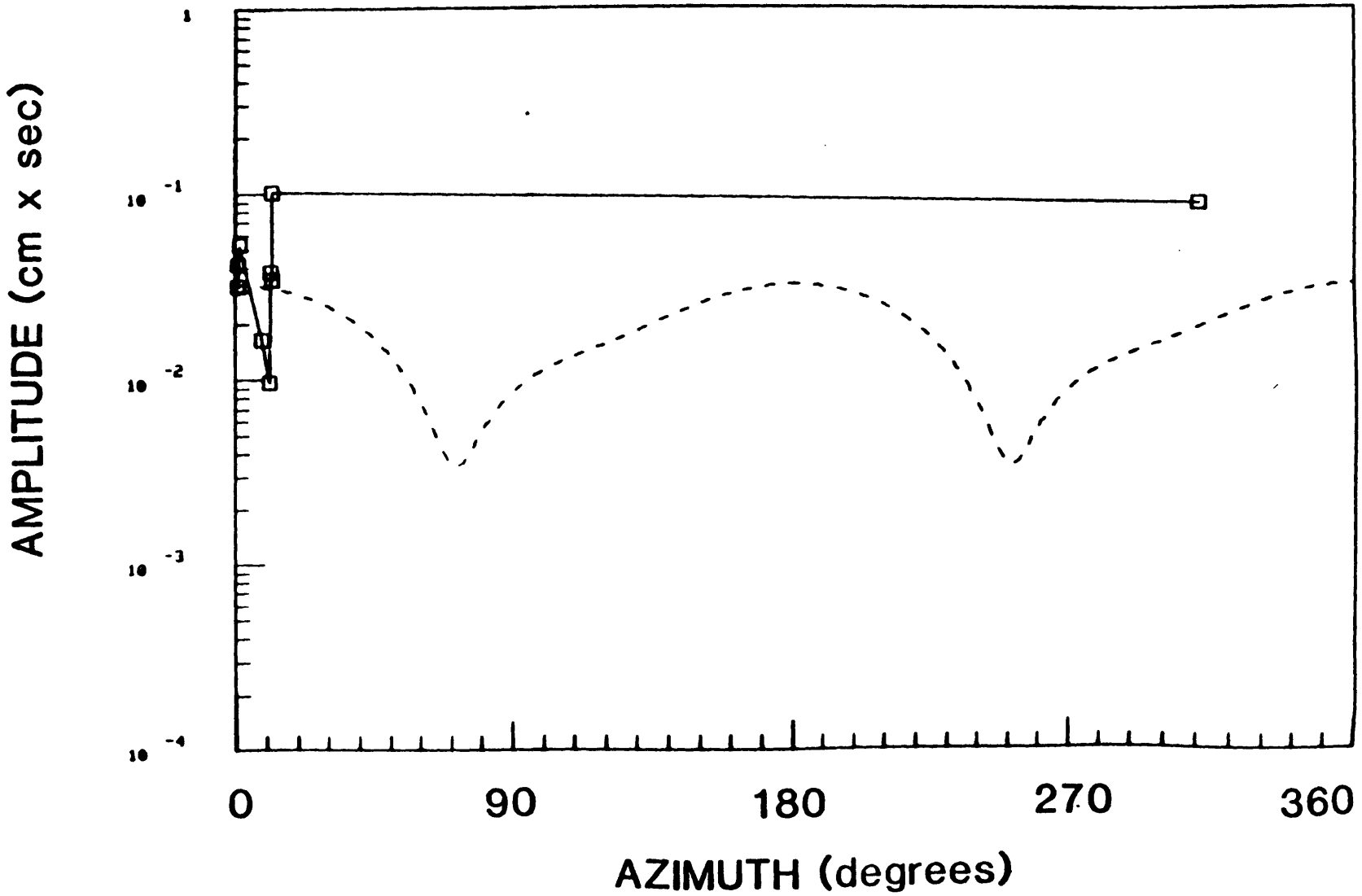

FIGURE B.27a

05/02/72

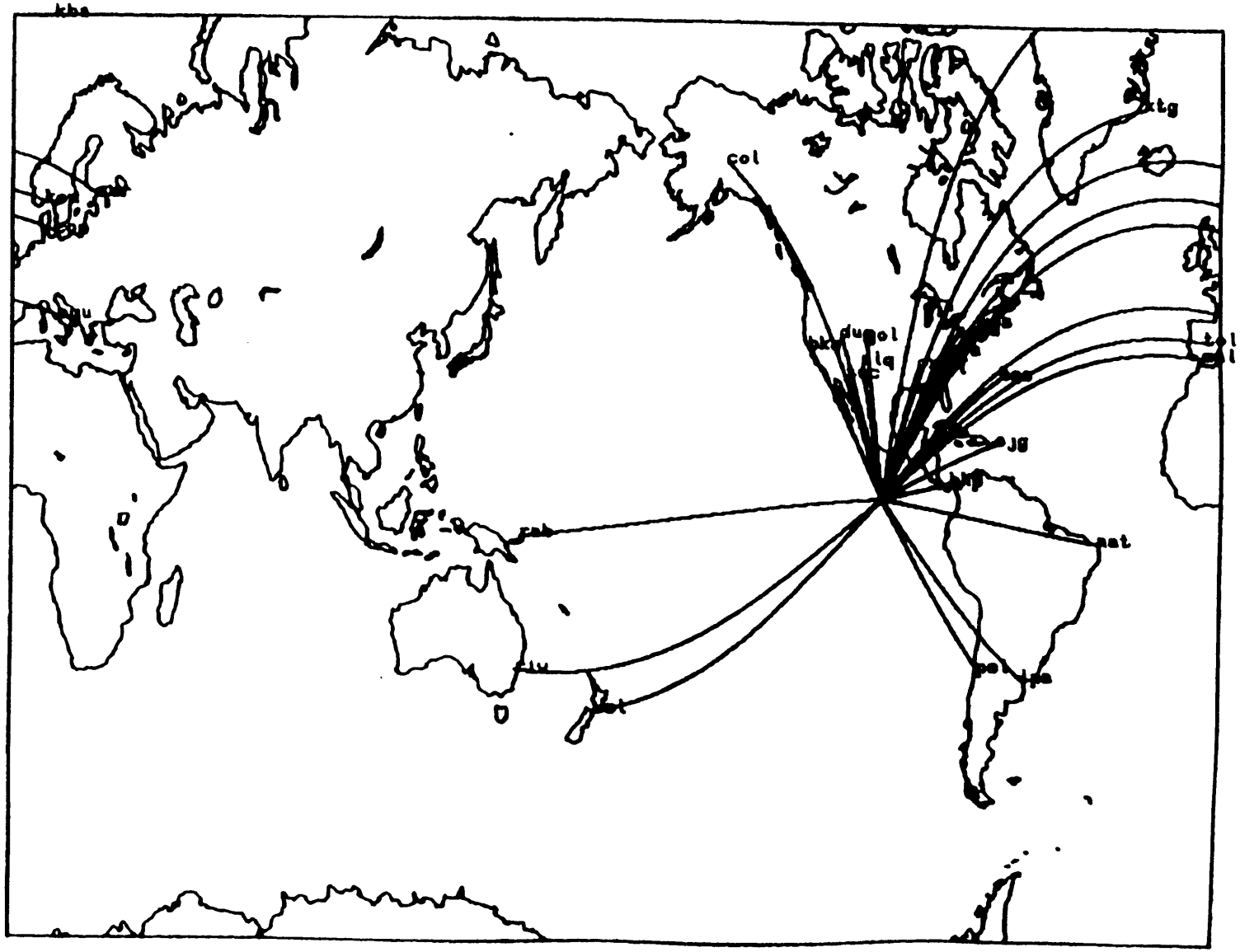

FIGURE B.27b

PERIOD 30 sec

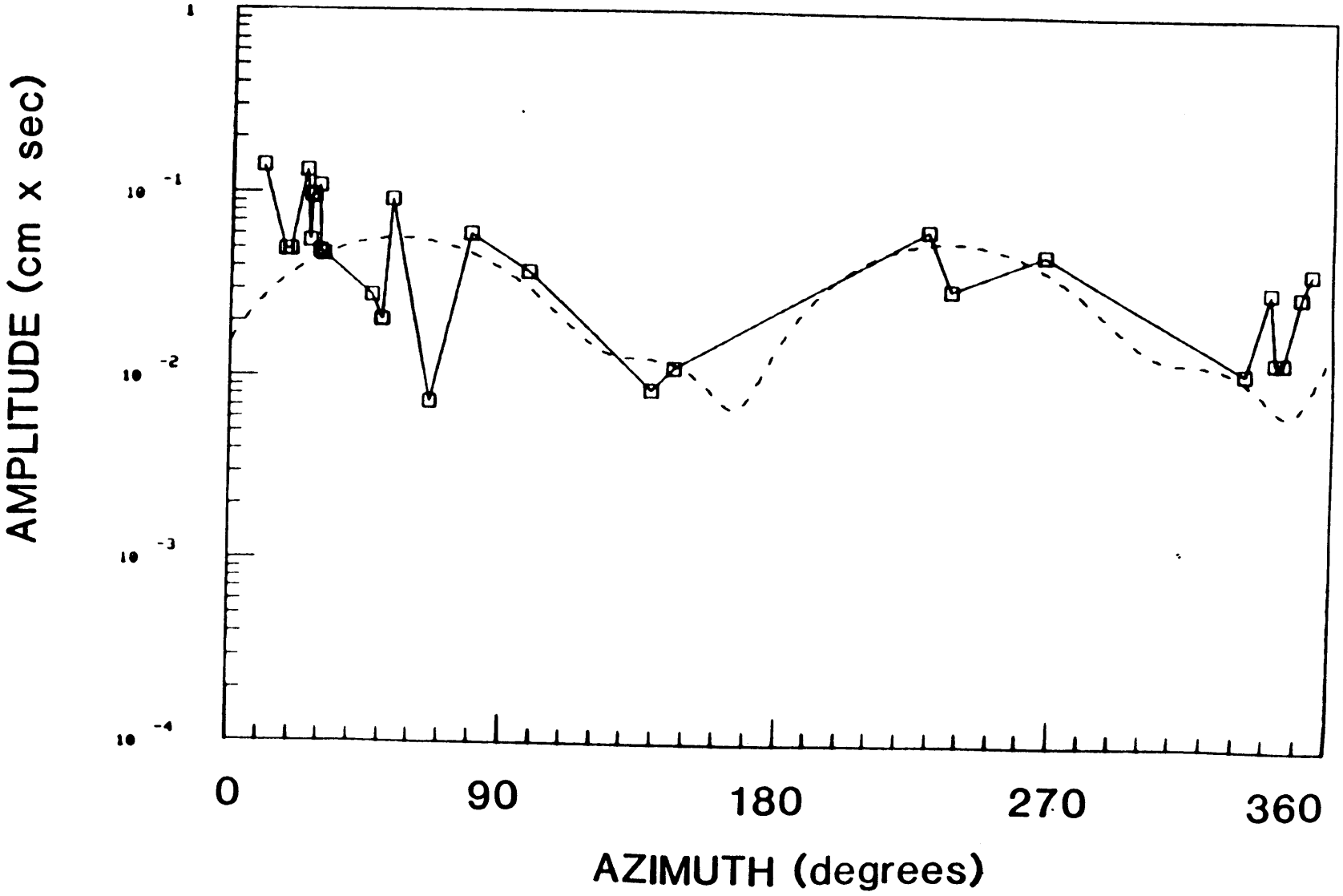

FIGURE B.27c

PERIOD 50 sec

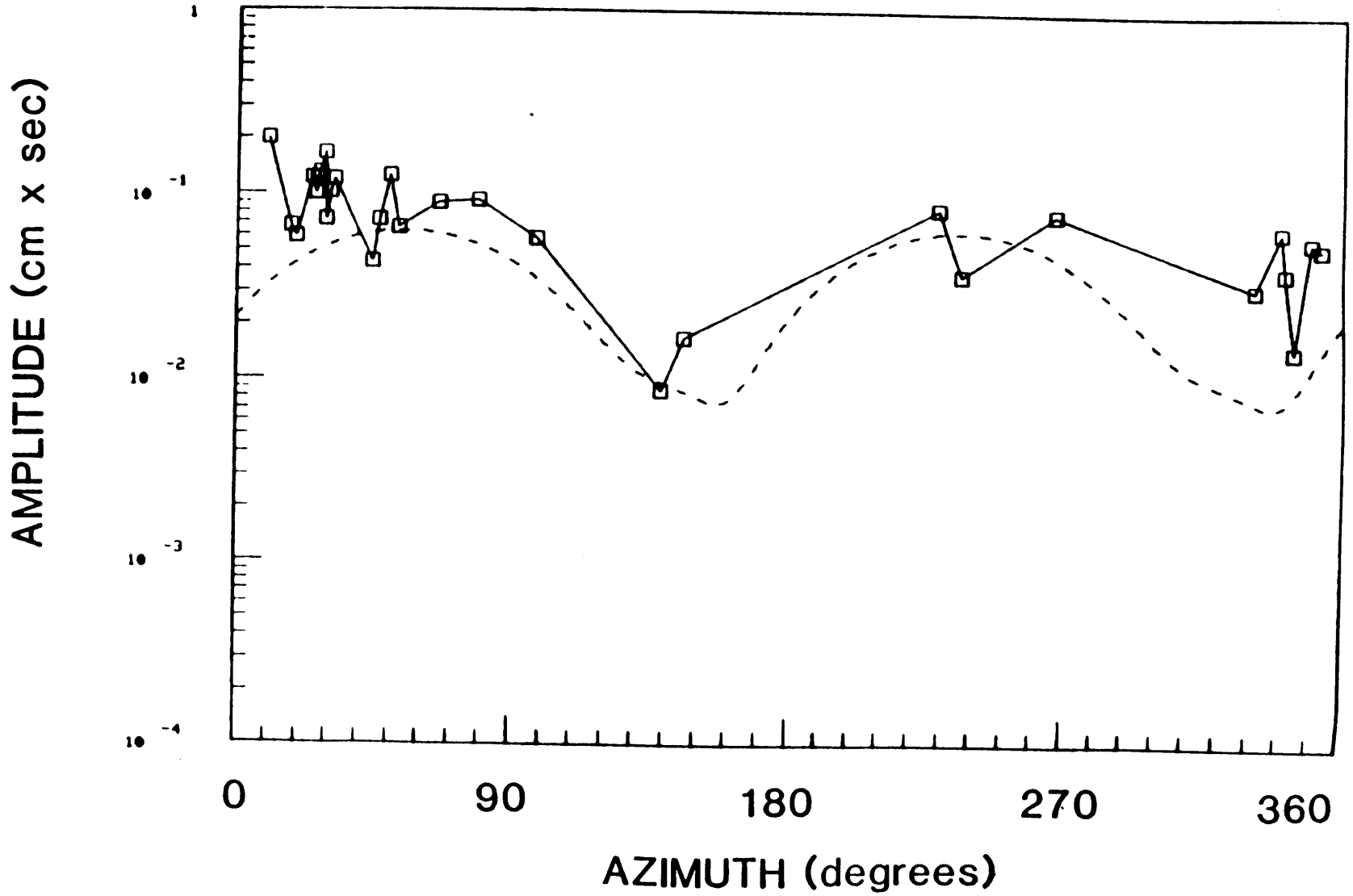

FIGURE B.27d

PERIOD 70 sec

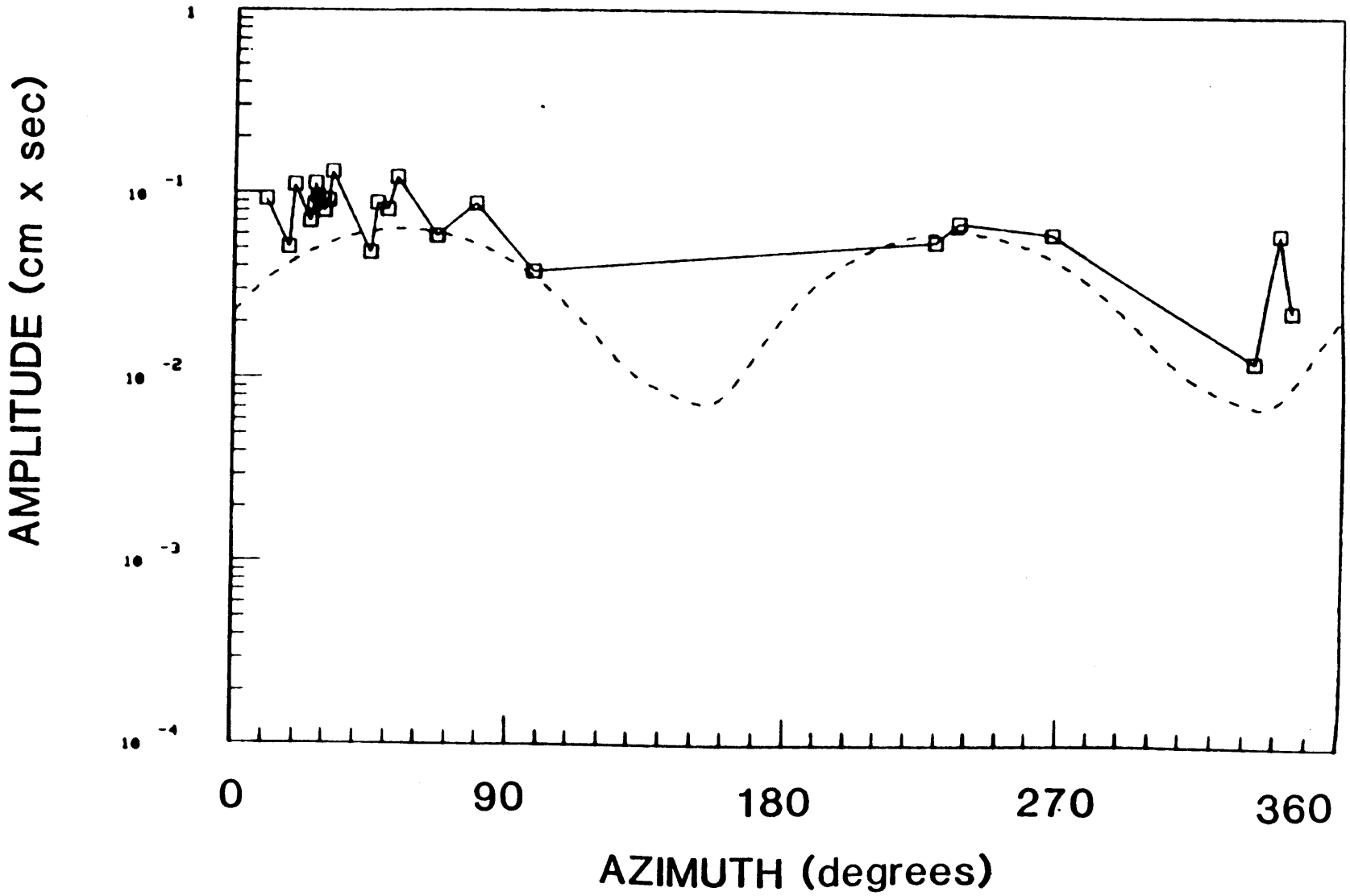

FIGURE B.27e

PERIOD 98 sec

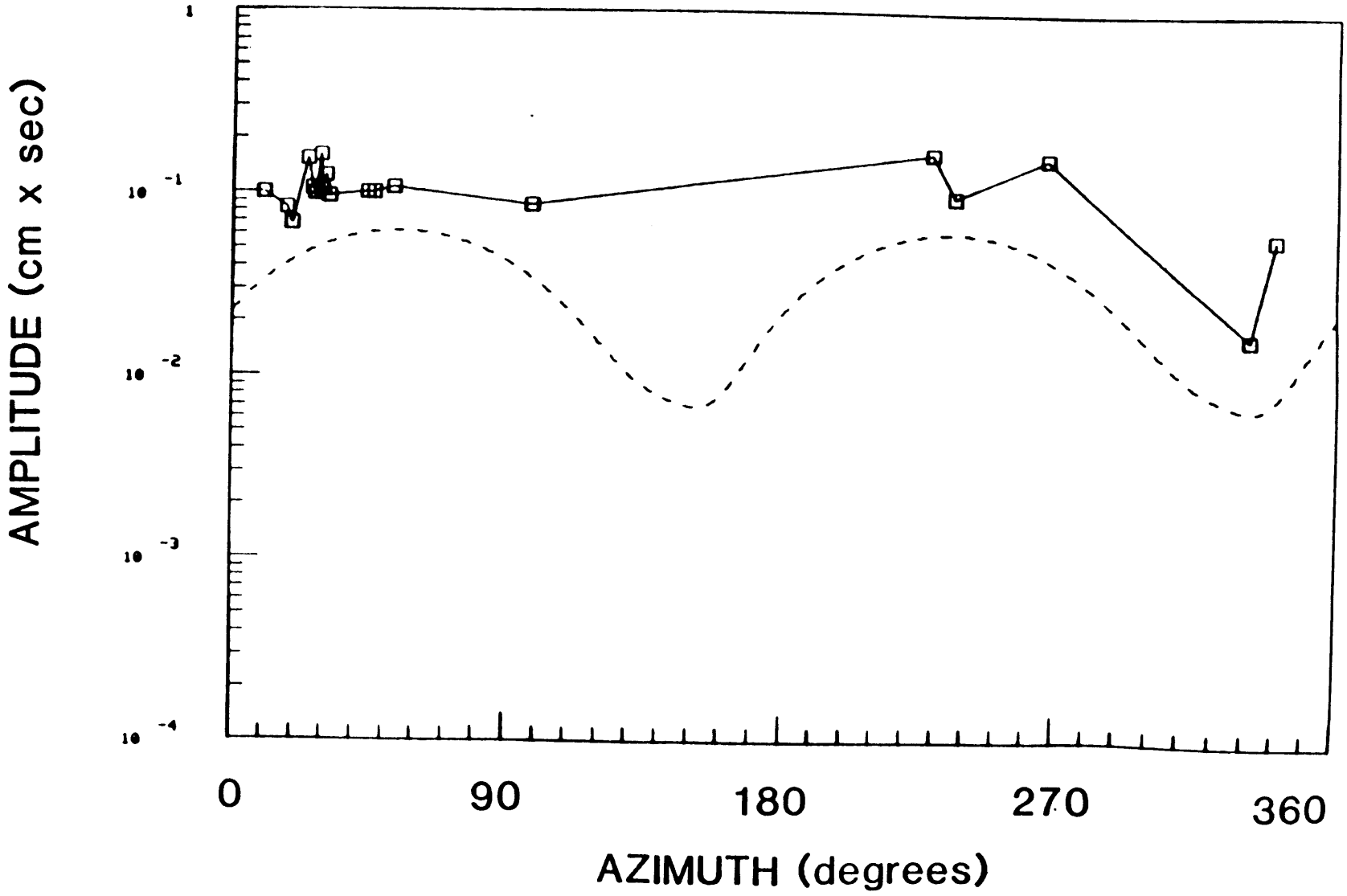

FIGURE B.28a

05/21/72

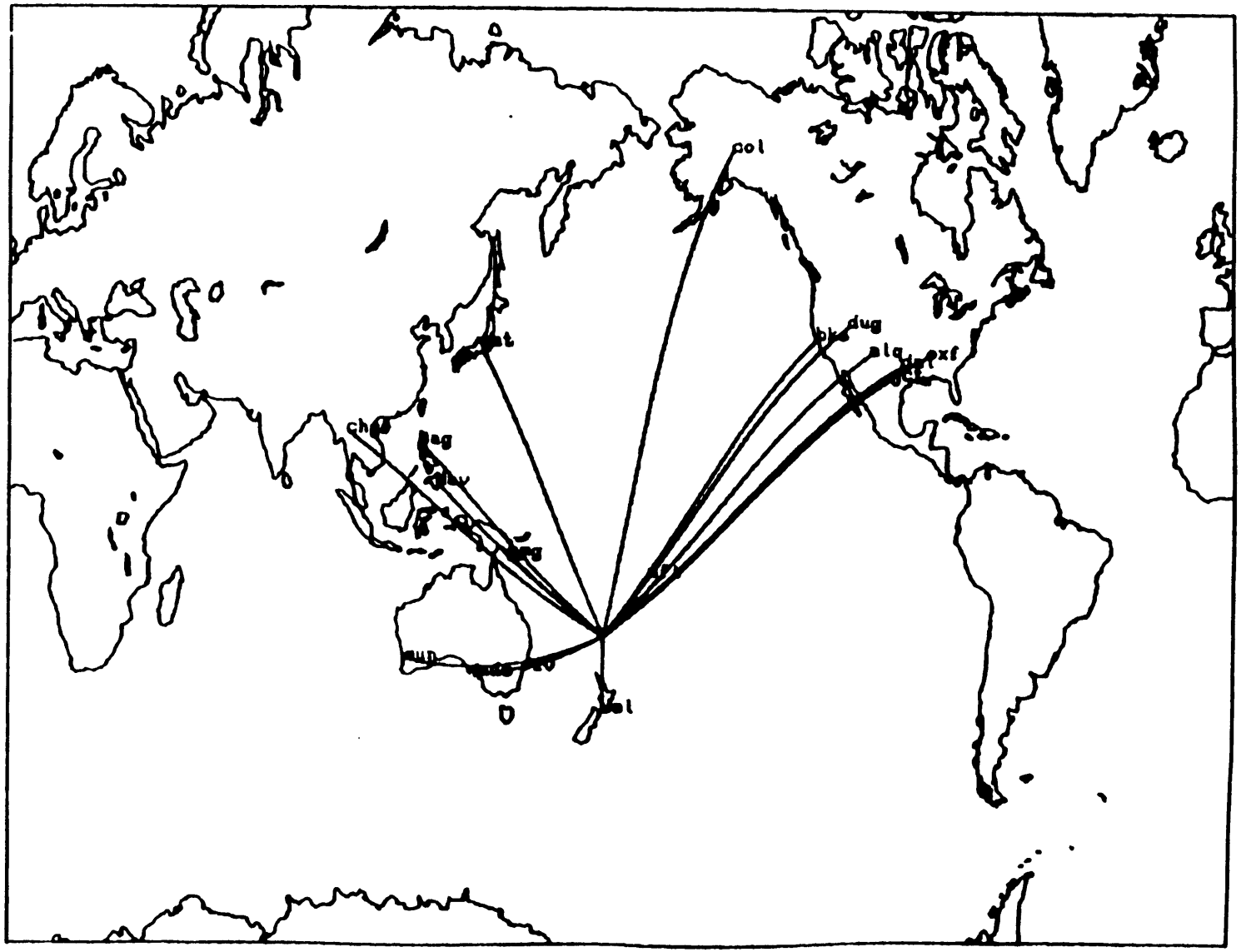

FIGURE B.28b

PERIOD 30 sec

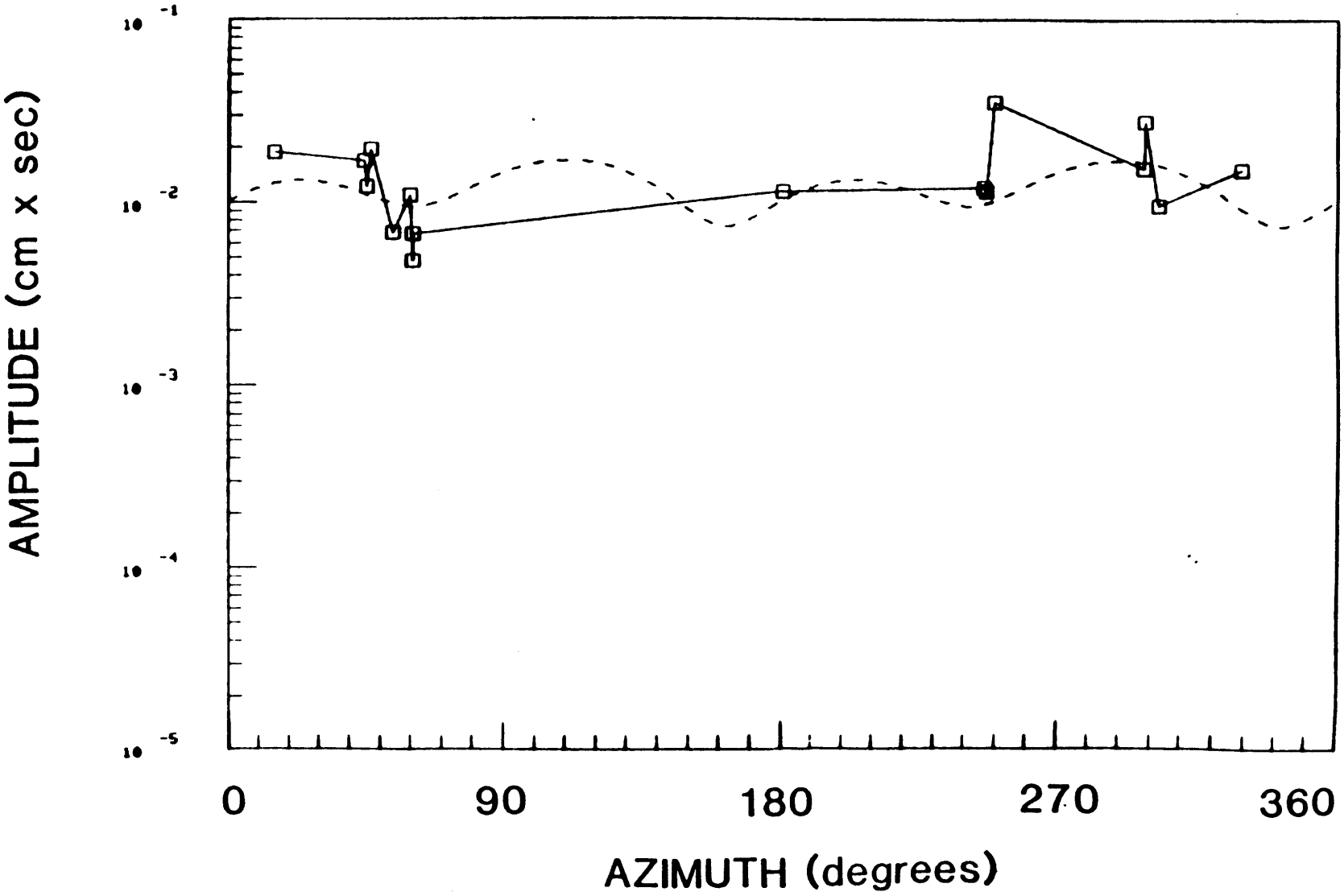

FIGURE B.28C

PERIOD 50 sec

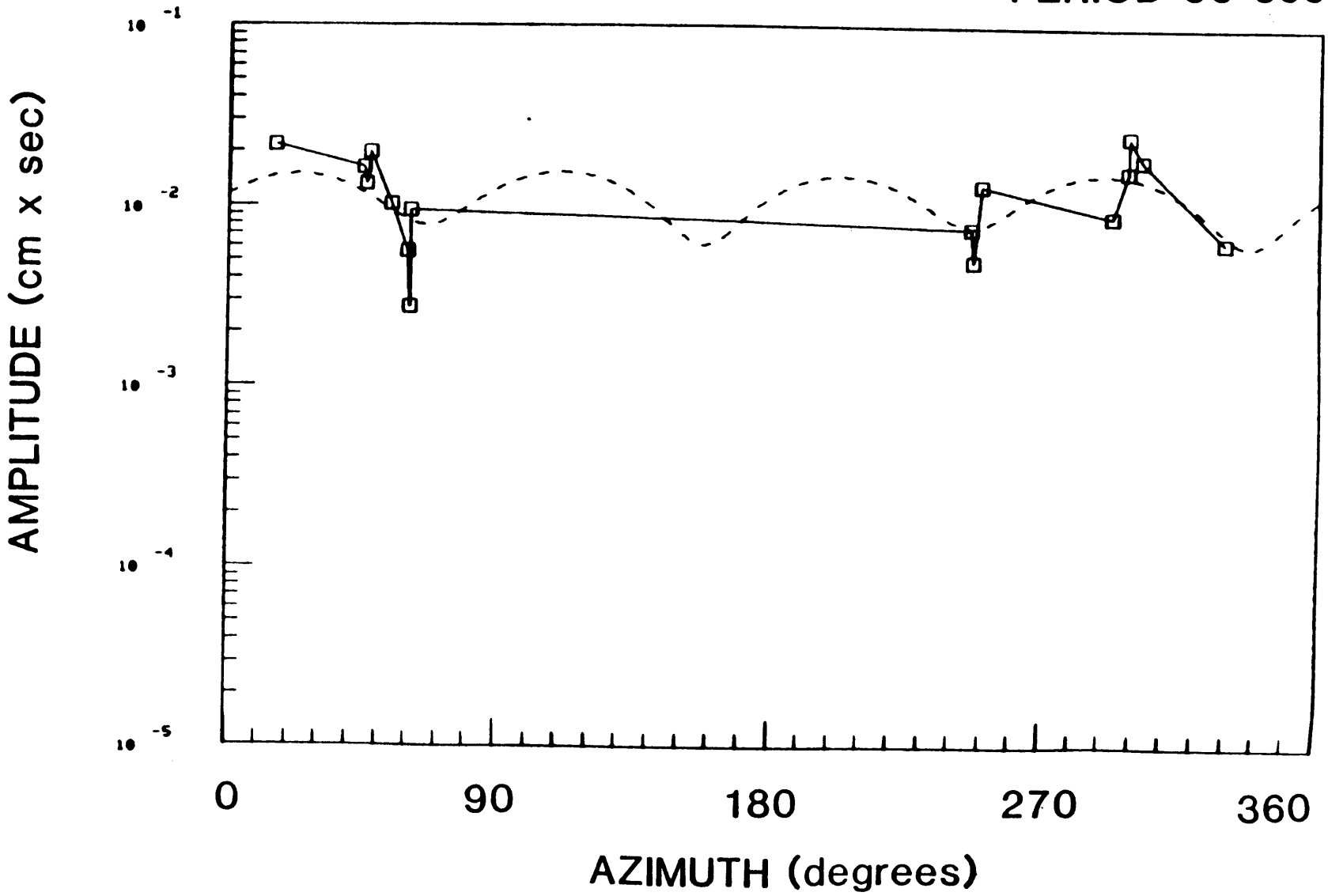

FIGURE B.28d

PERIOD 70 sec

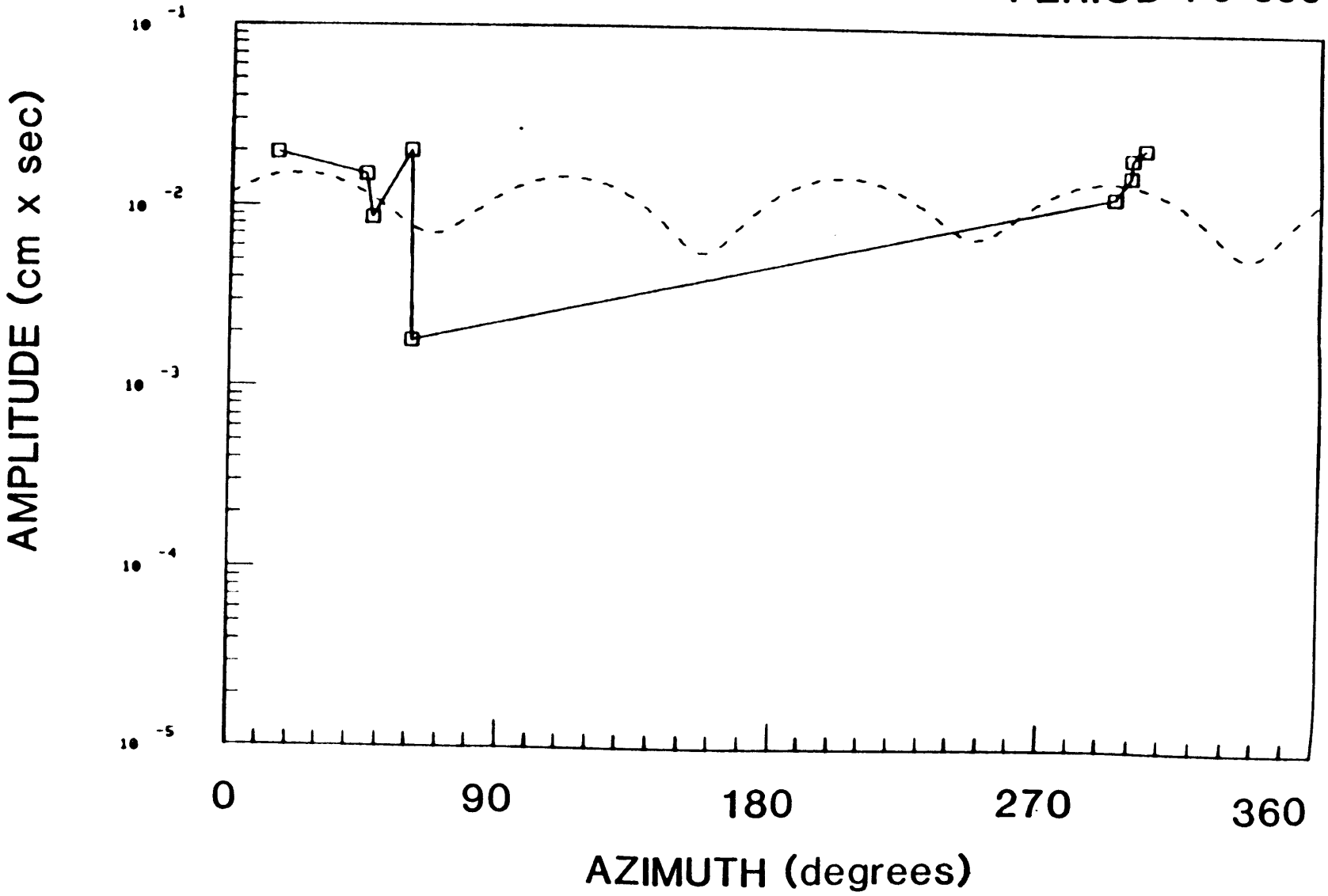

FIGURE B.28e

PERIOD 98 sec

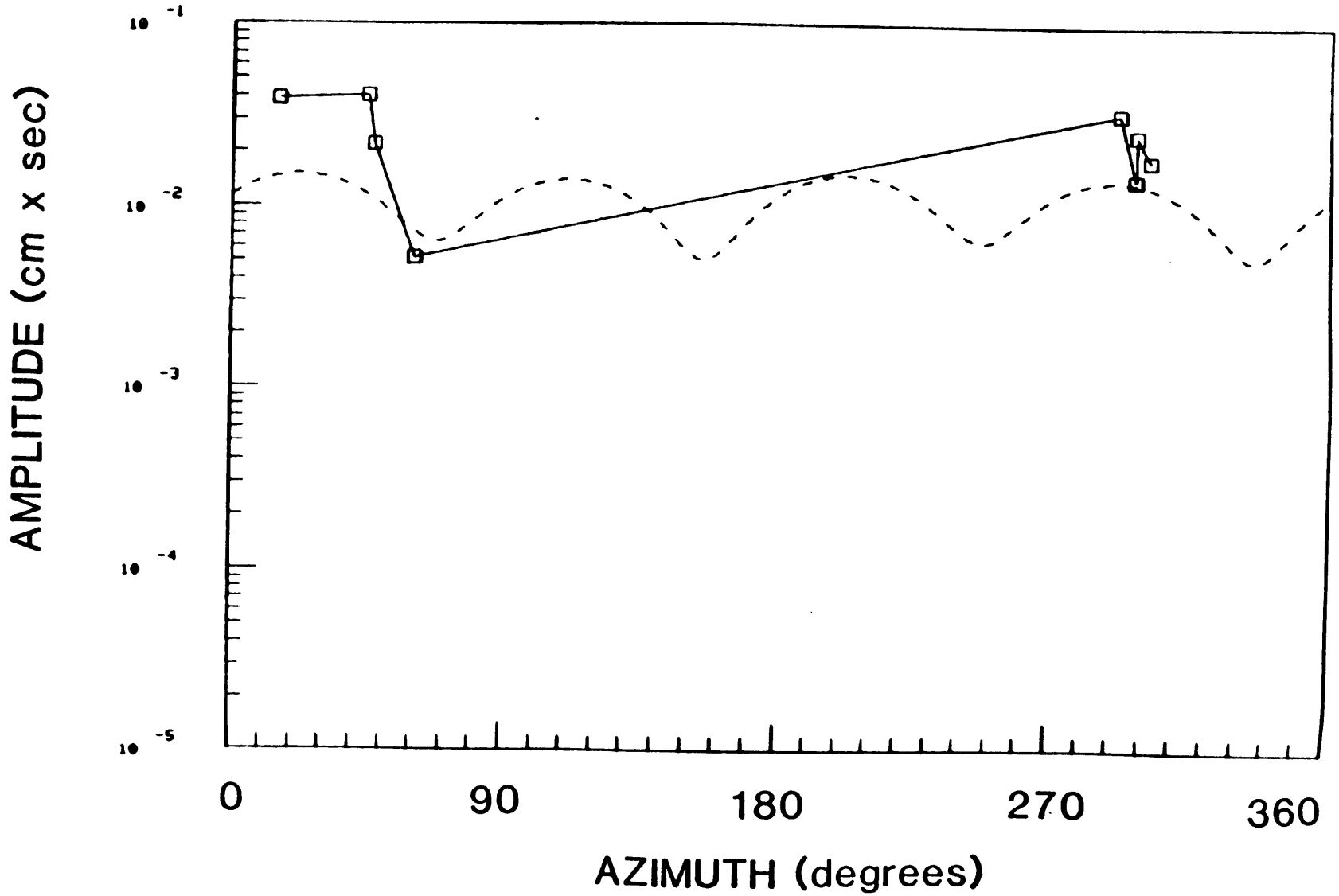

FIGURE B.29a

10/20/72

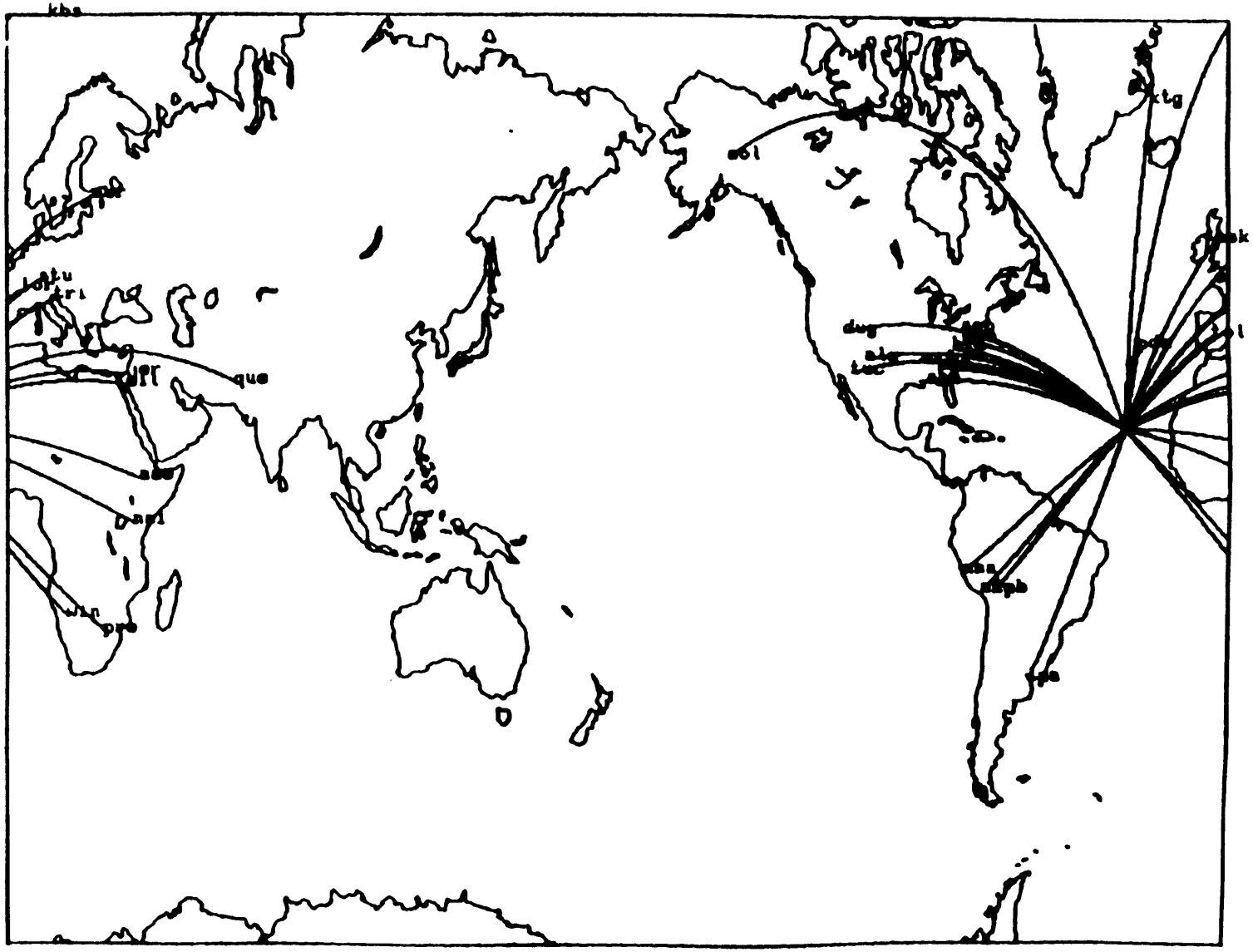

FIGURE B.29b

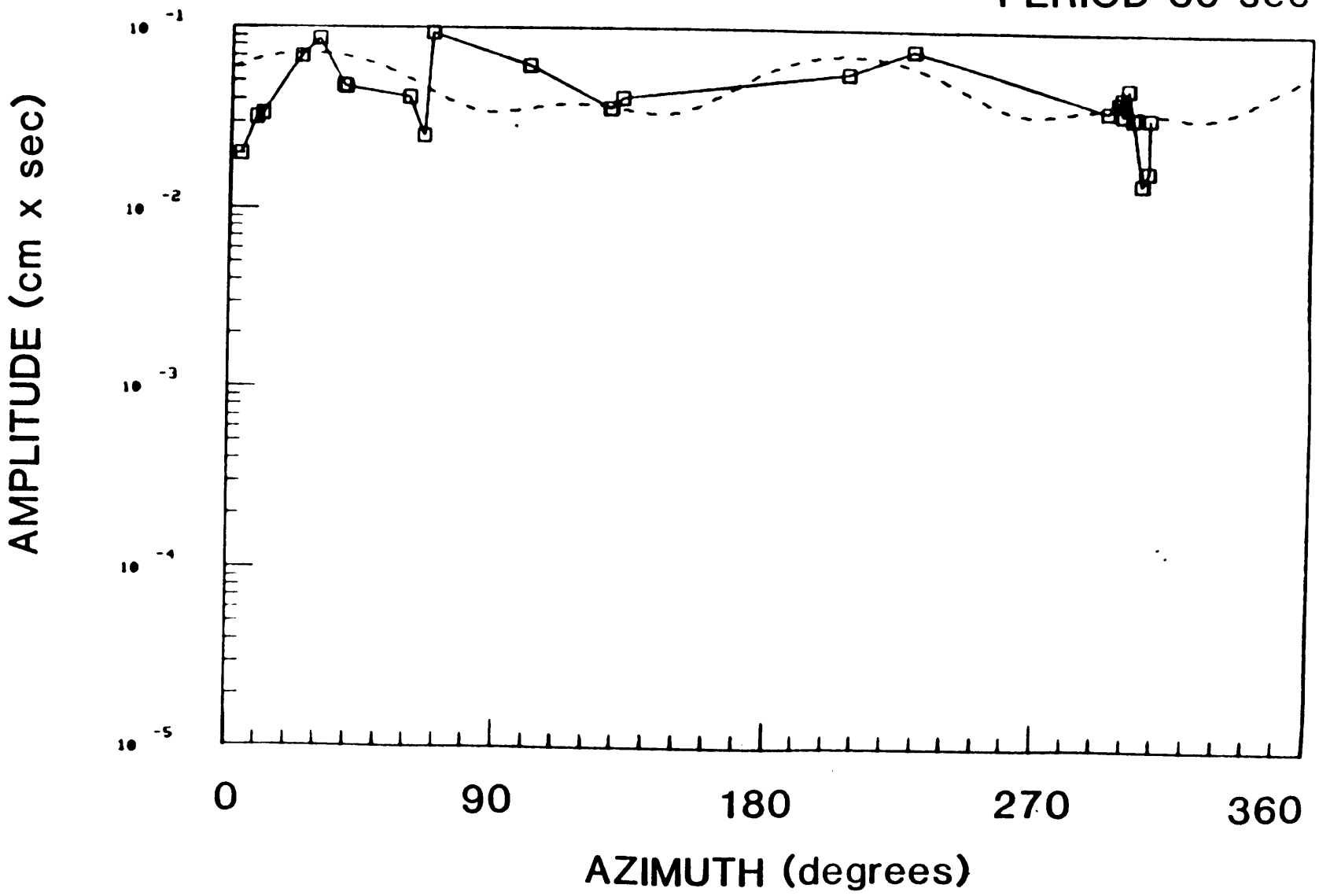
PERIOD 30 sec
AMPLITUDE (cm x sec)
10 -1
10 -2
10 -3
10 -4
10 -5
0
90
180
270
360
AZIMUTH (degrees)

FIGURE B.29C

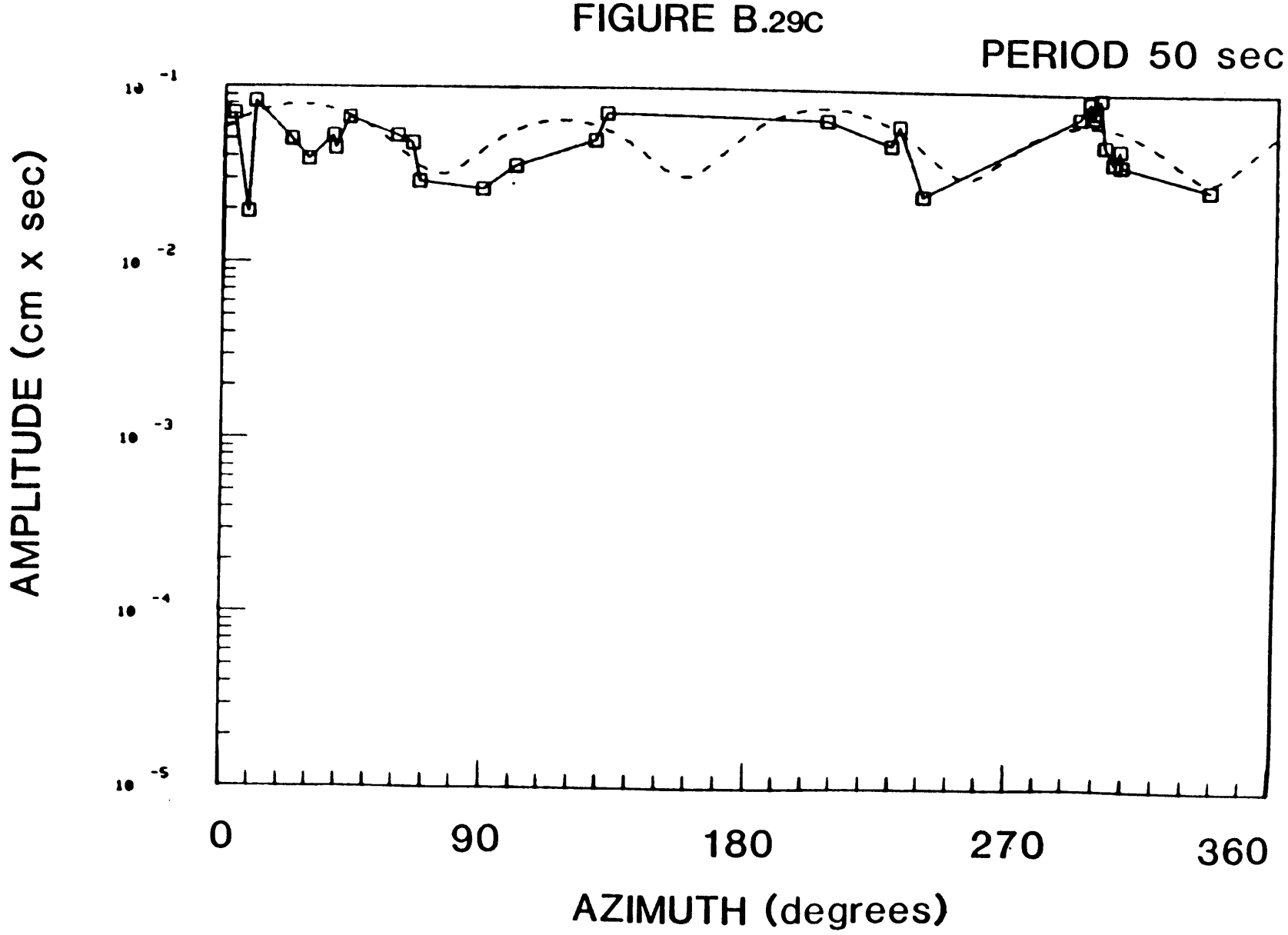
PERIOD 50 sec
AMPLITUDE (cm x sec)
10 -1
10 -2
10 -3
10 -4
10 -5
0
90
180
270
360
AZIMUTH (degrees)

FIGURE B.29d

PERIOD 70 sec

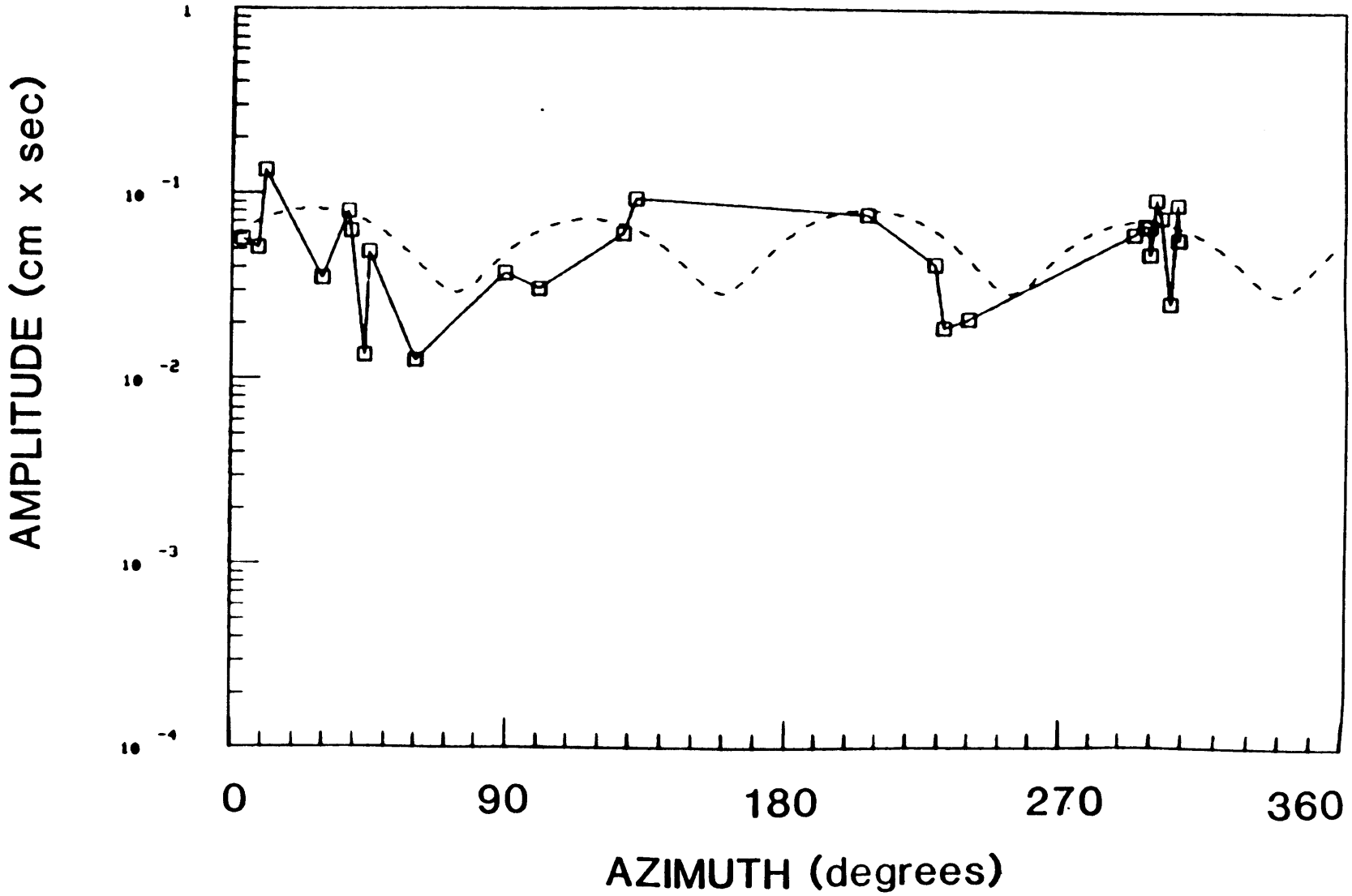

FIGURE B.29e

PERIOD 98 sec

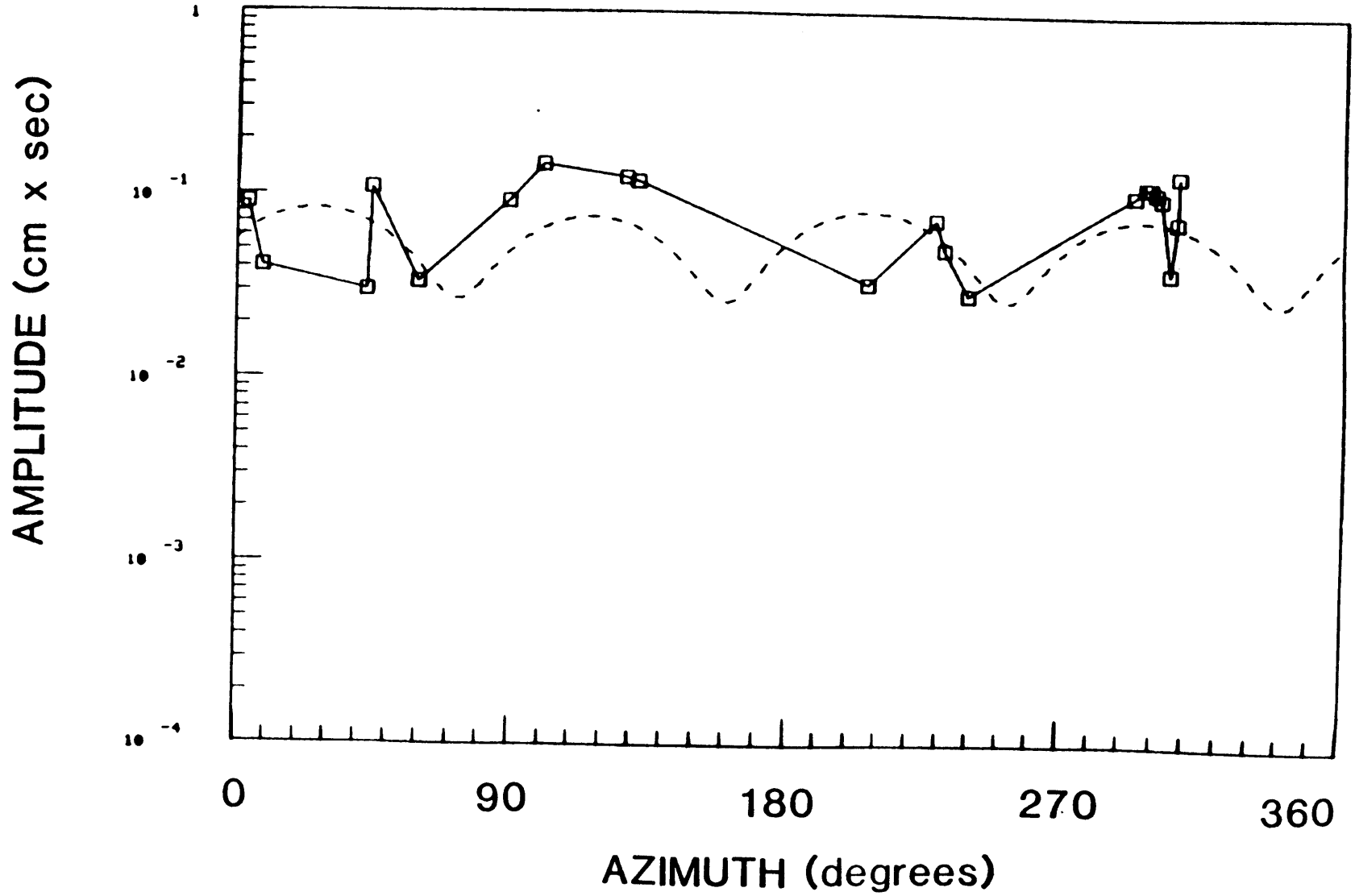

FIGURE B.30a 04/26/73

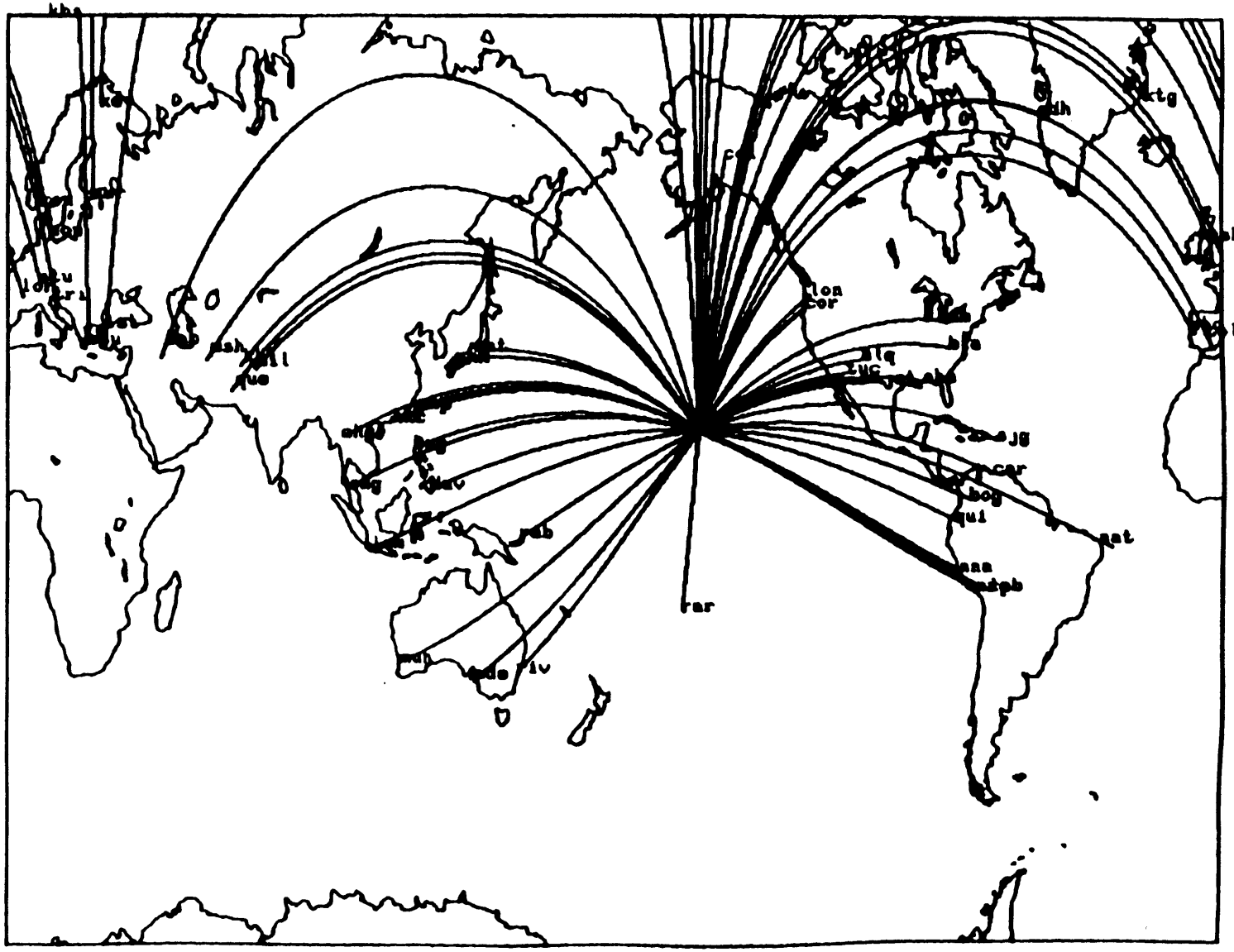

FIGURE B.30b

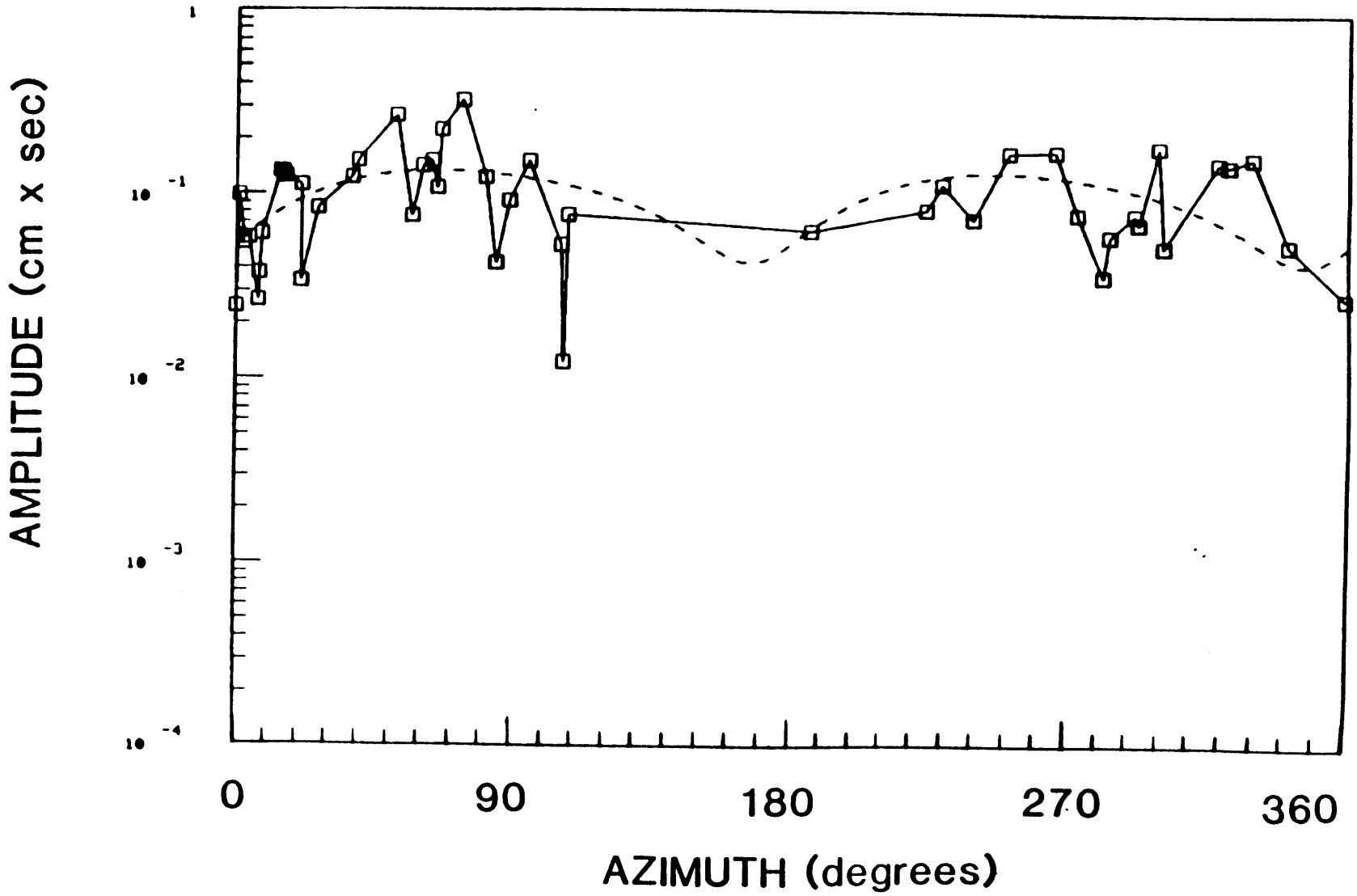
PERIOD 30 sec
AMPLITUDE (cm x sec)
1
10 -1
10 -2
10 -3
10 -4
0
90
180
270
360
AZIMUTH (degrees)

FIGURE B.30c

PERIOD 50 sec

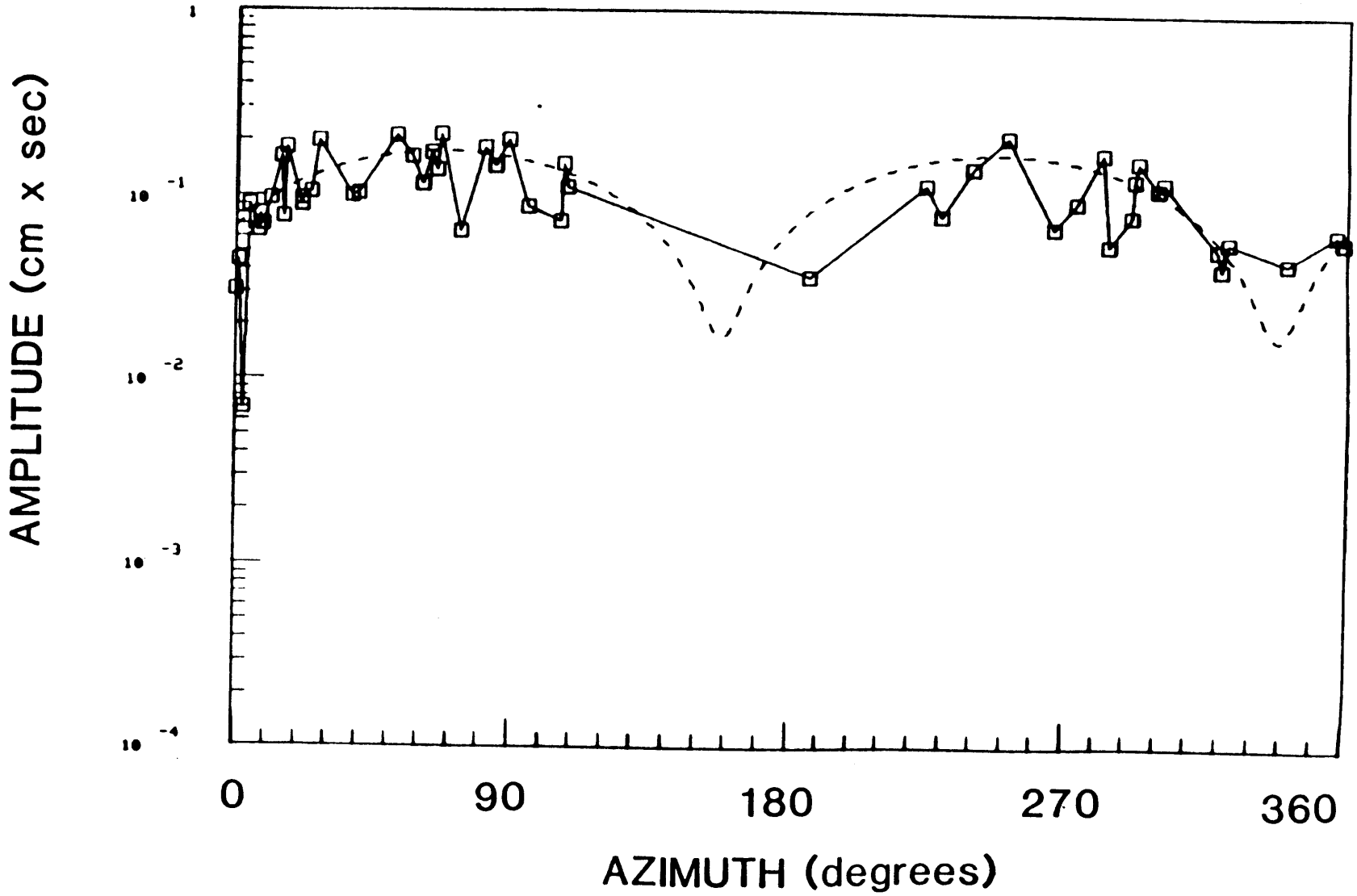

FIGURE B.30d

PERIOD 70 sec

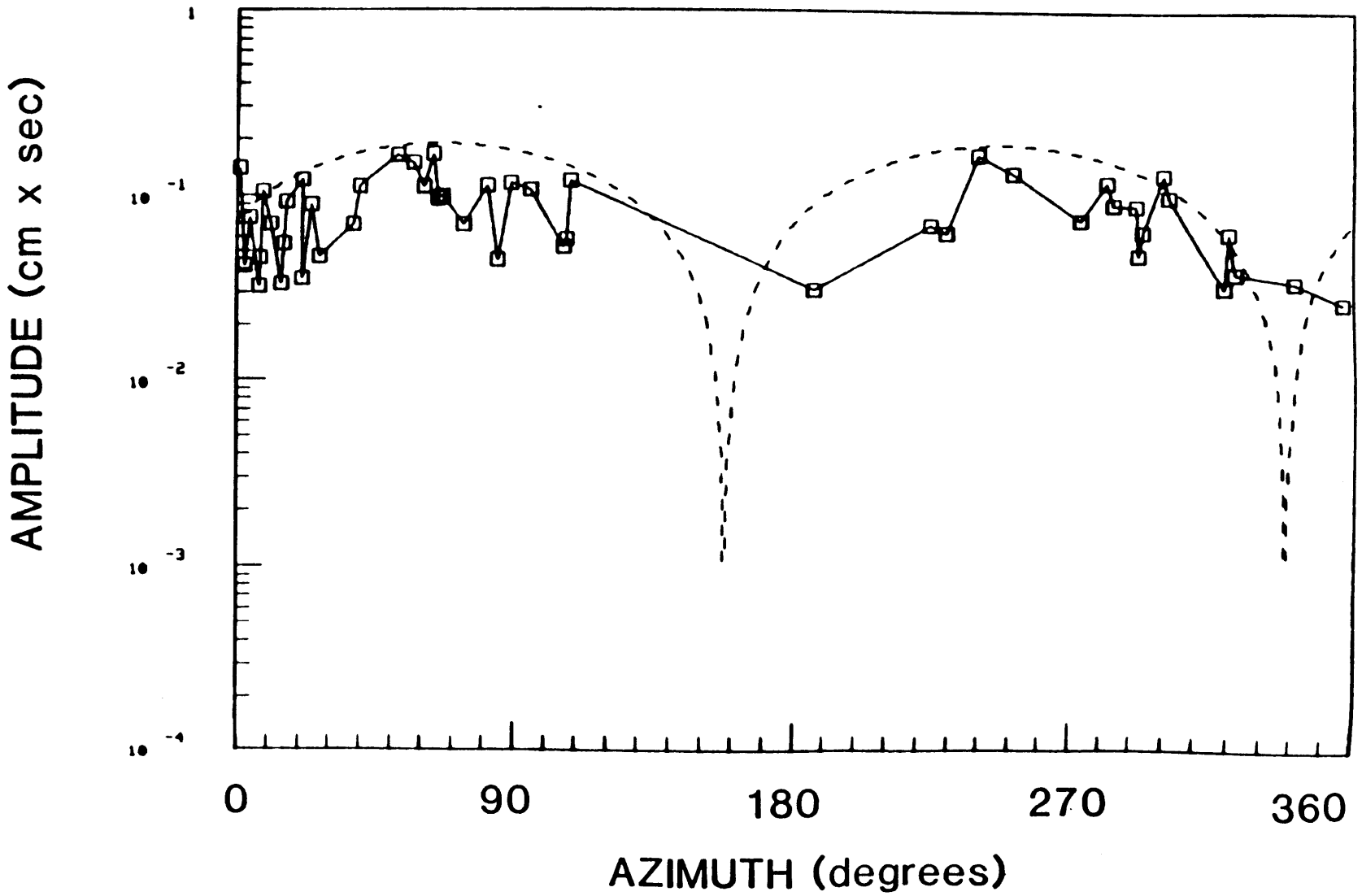

FIGURE B.30e

PERIOD 98 sec

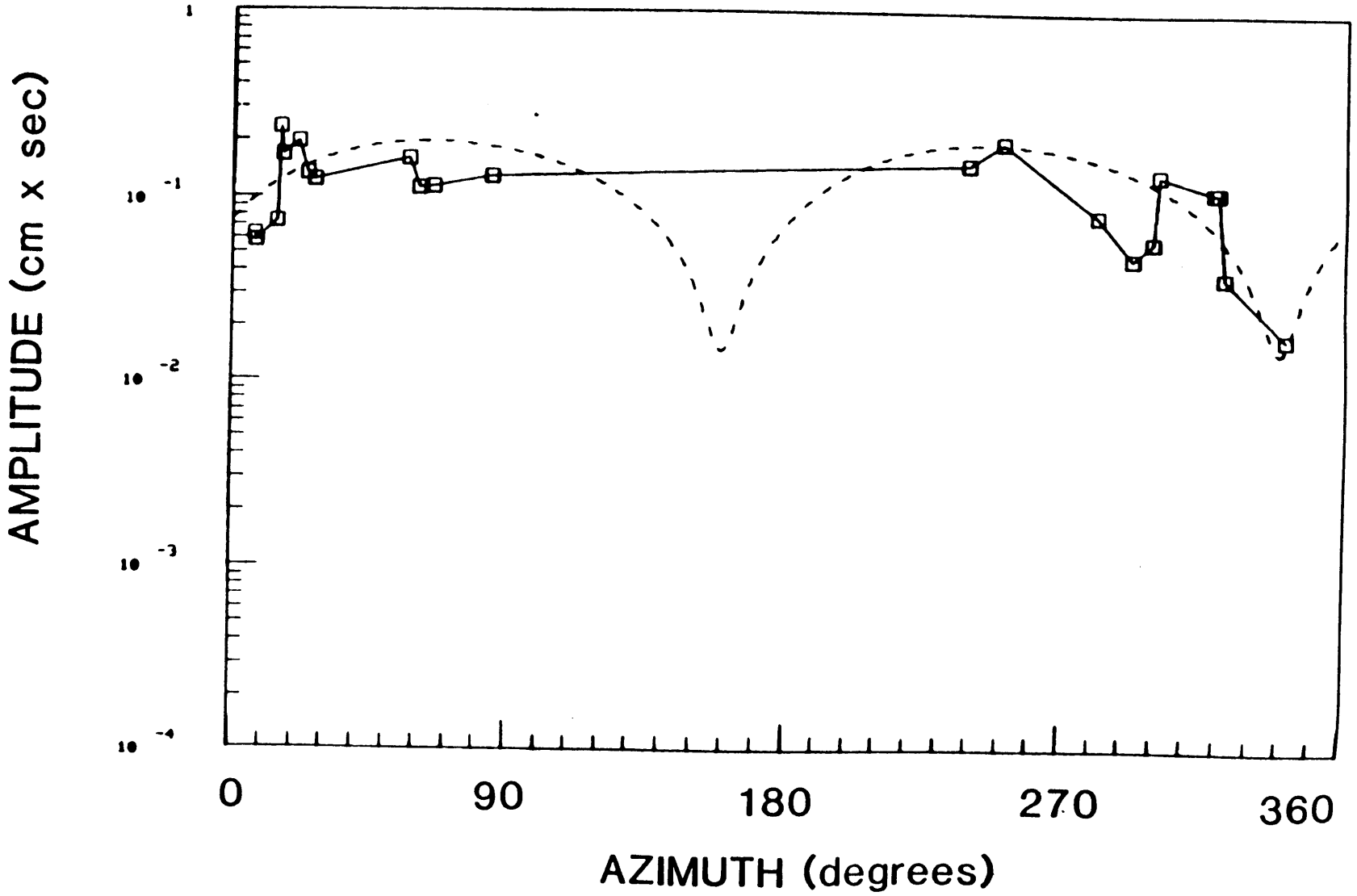

FIGURE B.31a

08/30/73

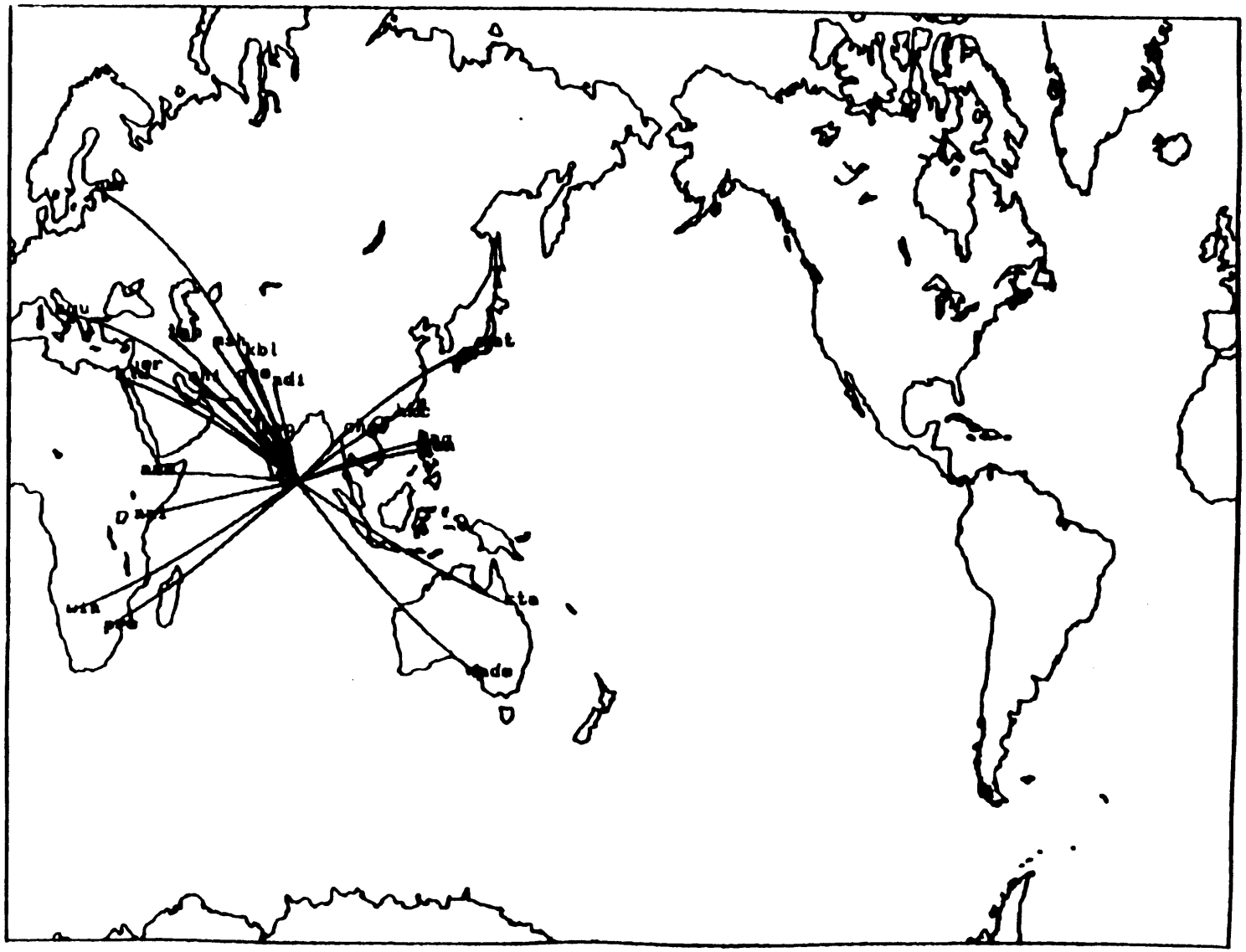

FIGURE B.31b

PERIOD 30 sec

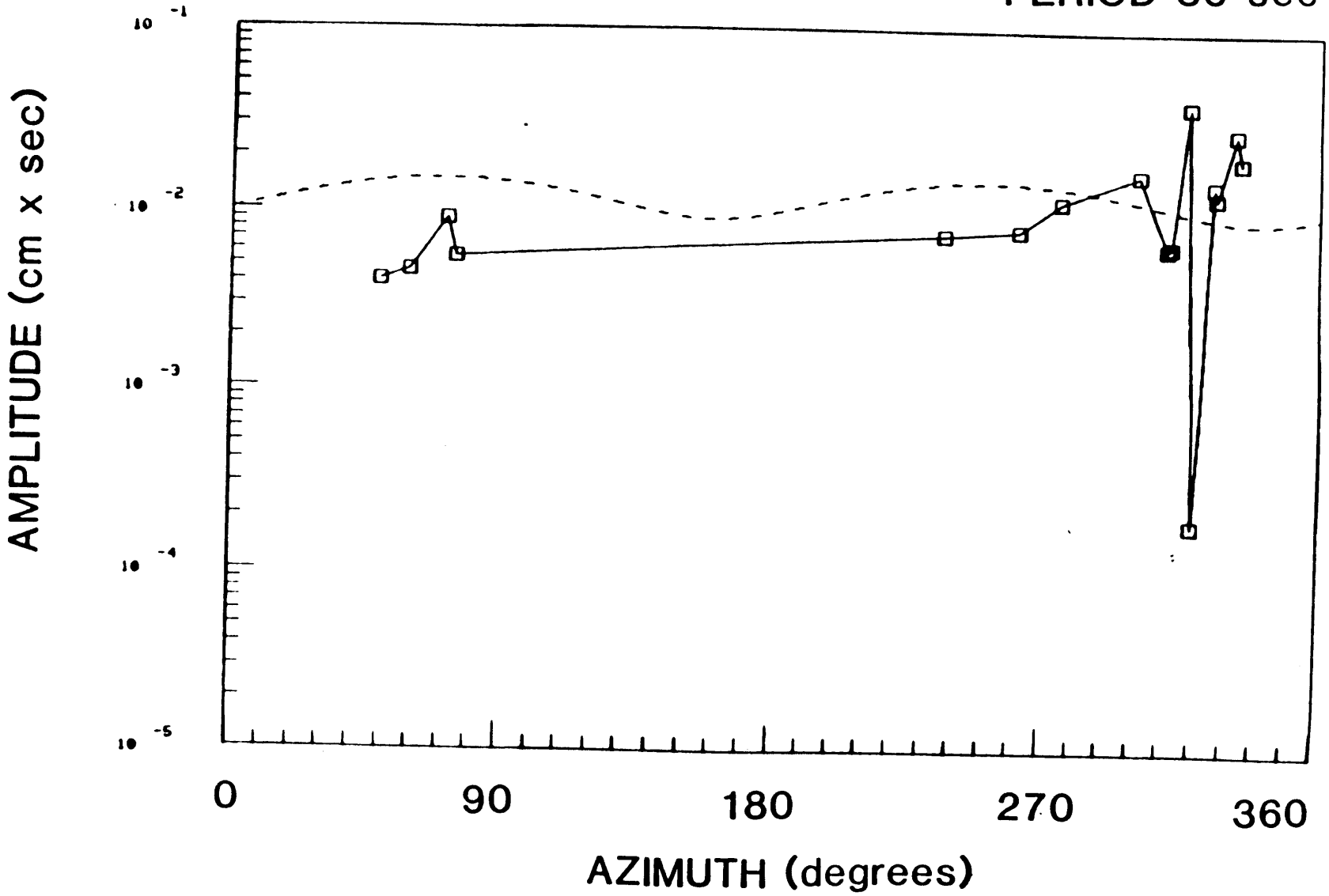

FIGURE B.31C

PERIOD 50 sec

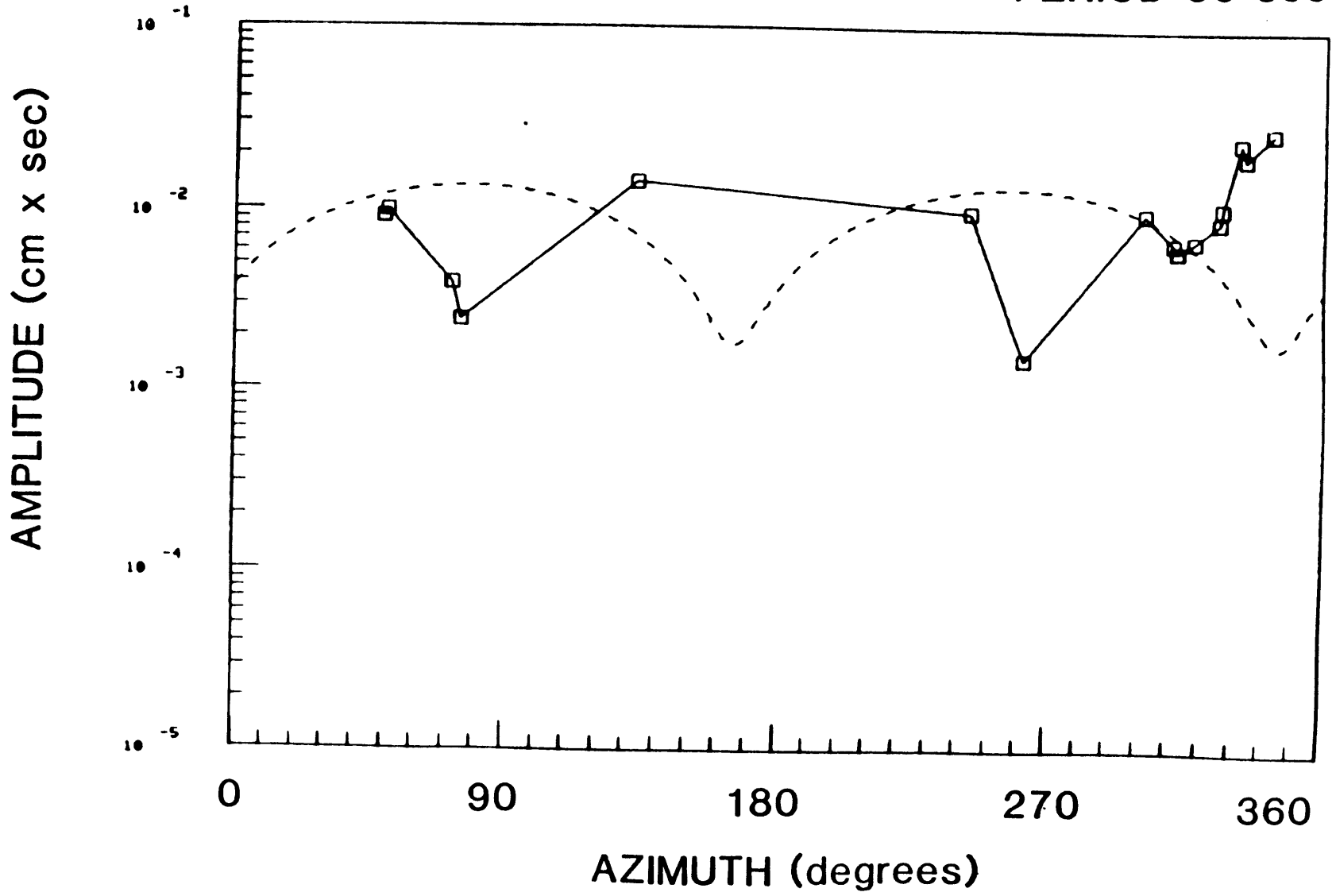

FIGURE B.31d

PERIOD 70 sec

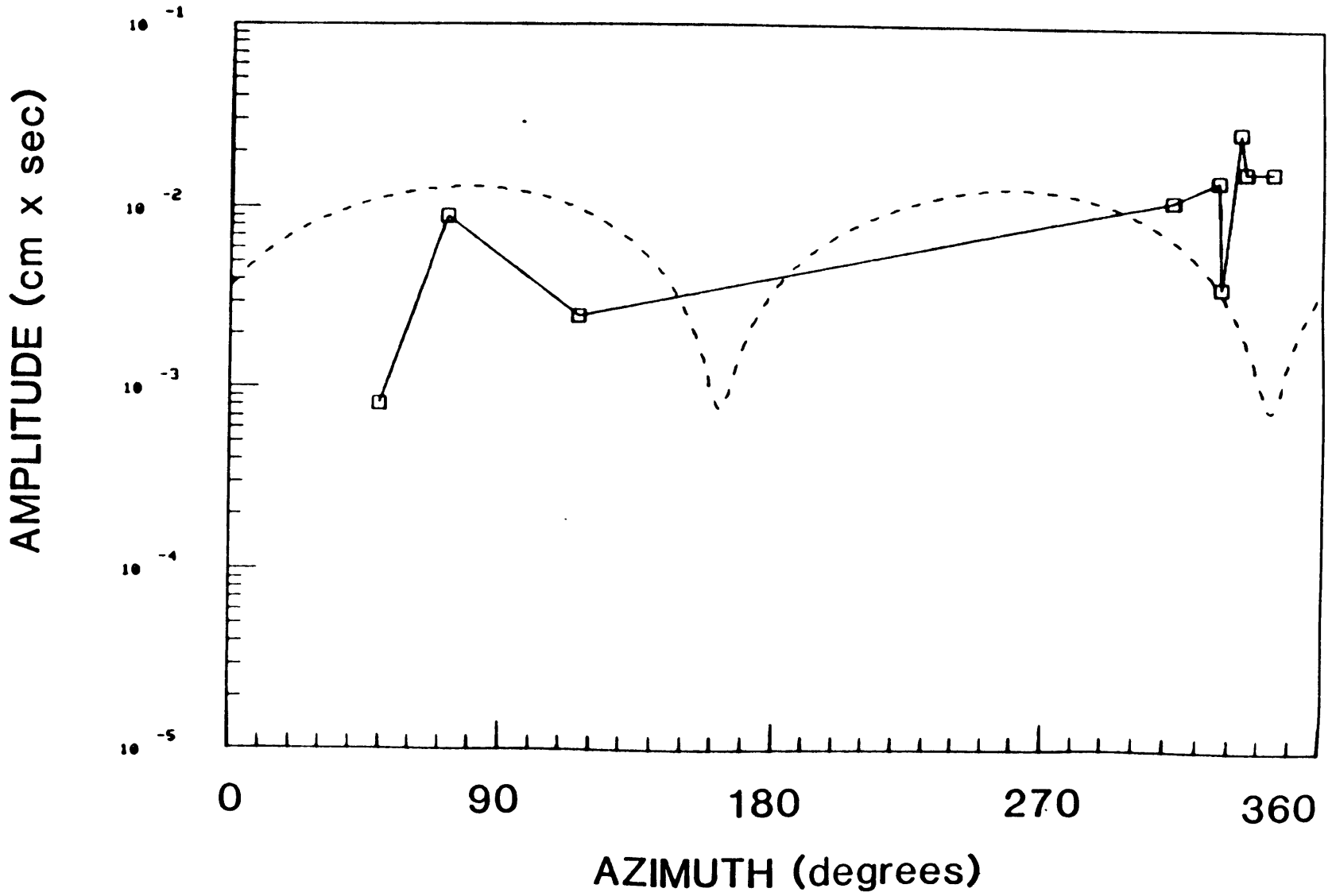

FIGURE B.31e

PERIOD 98 sec

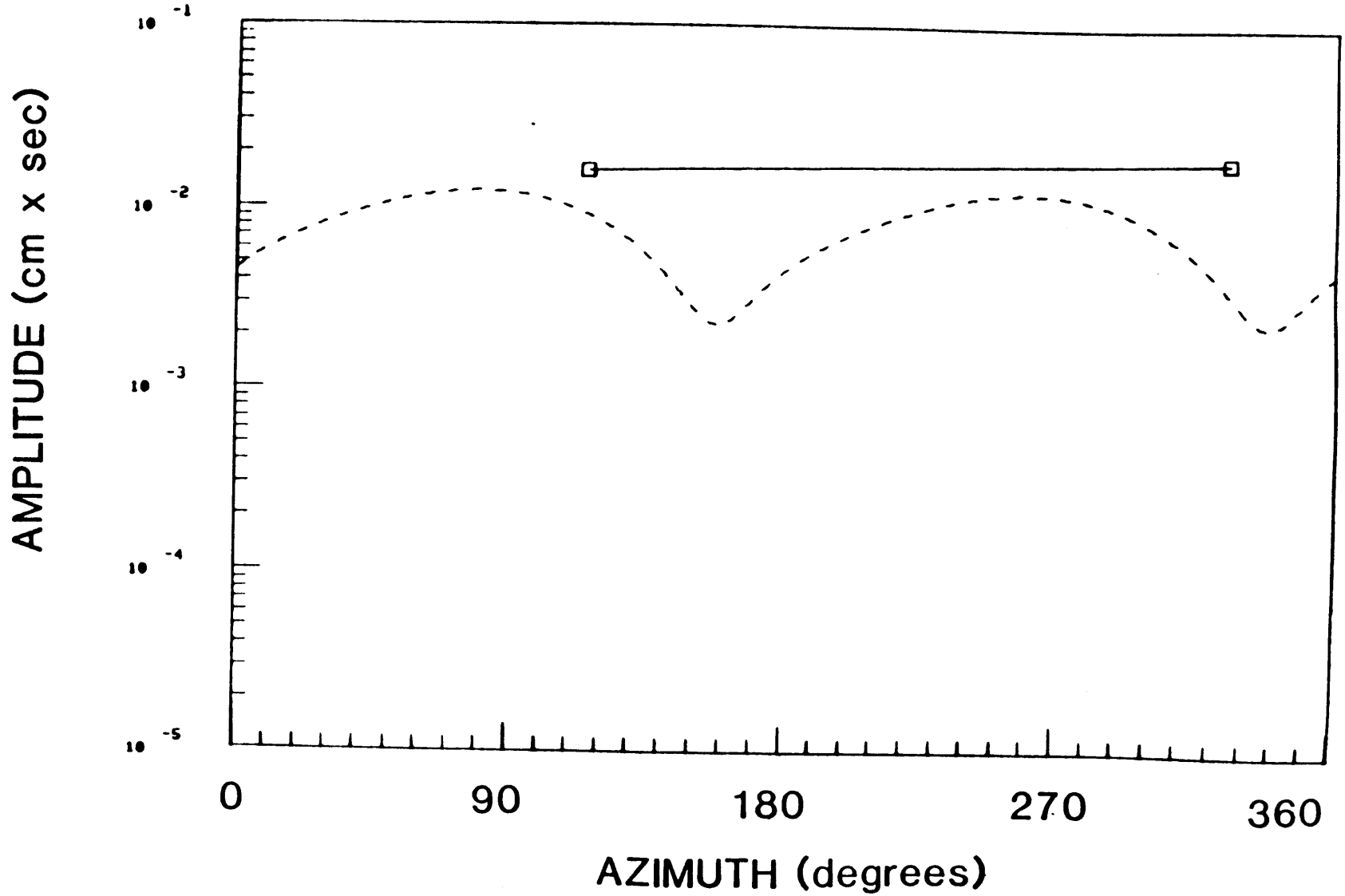

FIGURE B.32a

07/01/74

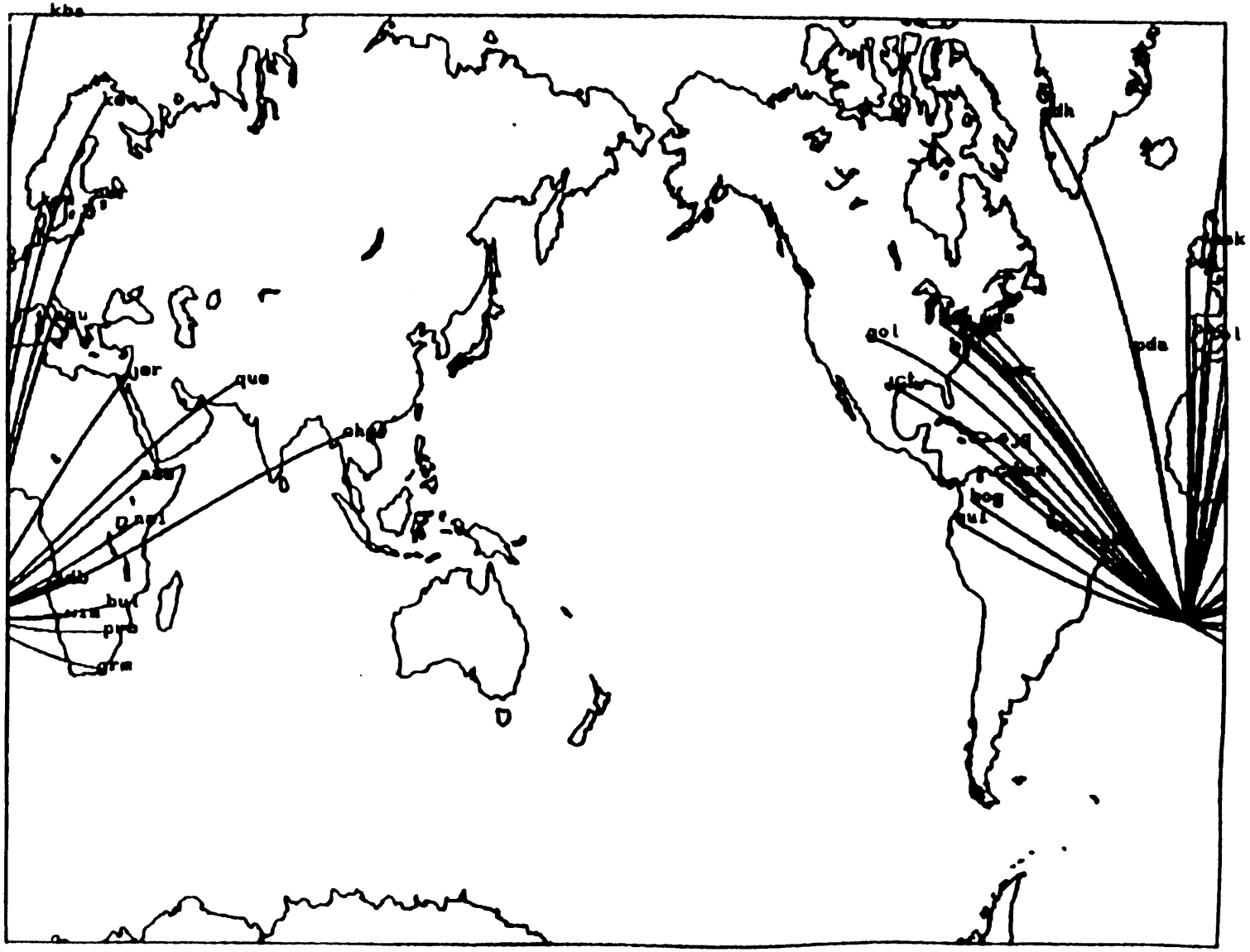

FIGURE B.32b

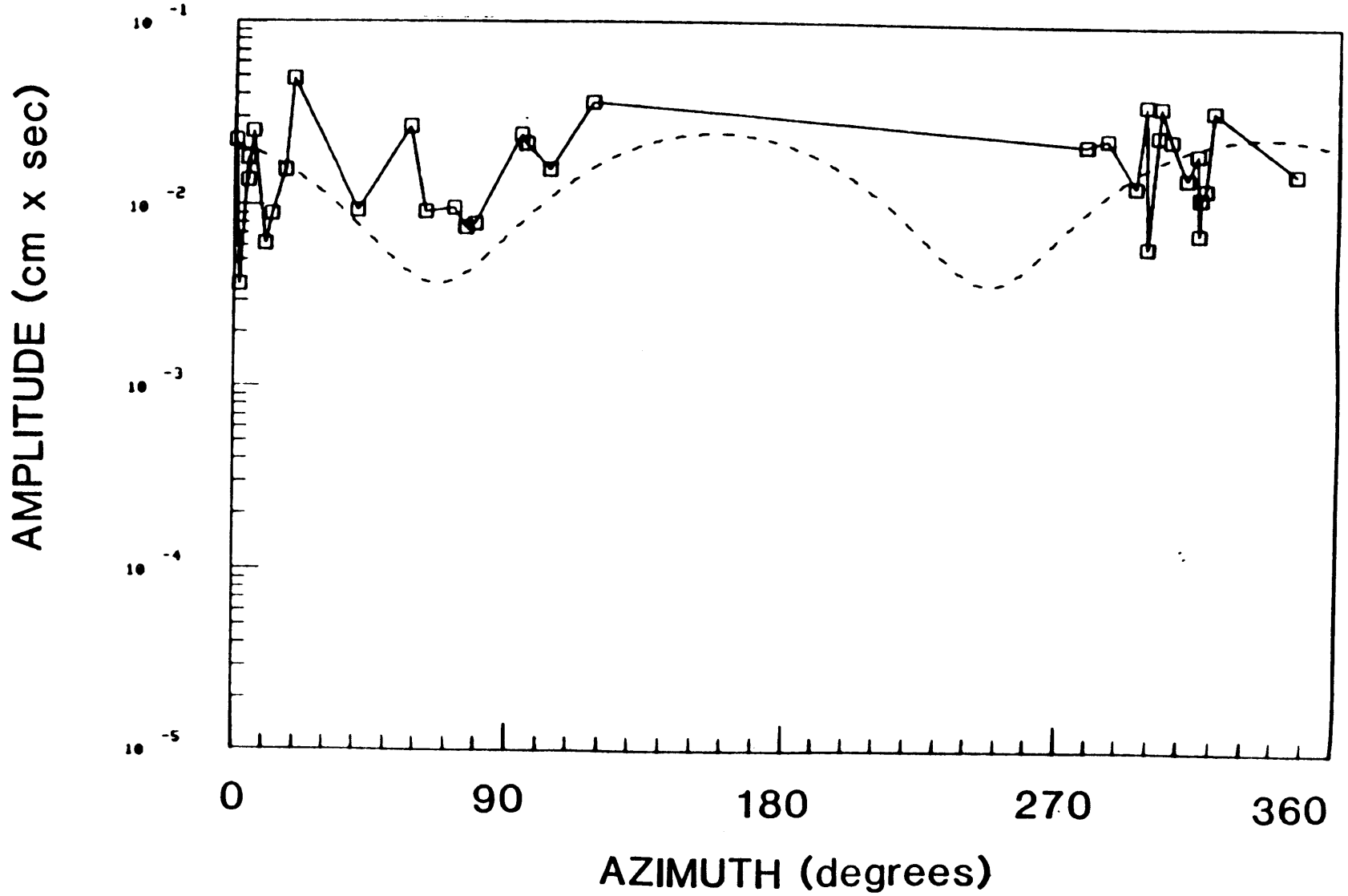
PERIOD 30 sec
AMPLITUDE (cm x sec)
10 -1
10 -2
10 -3
10 -4
10 -5
0
90
180
270
360
AZIMUTH (degrees)

FIGURE B.32C

PERIOD 50 sec

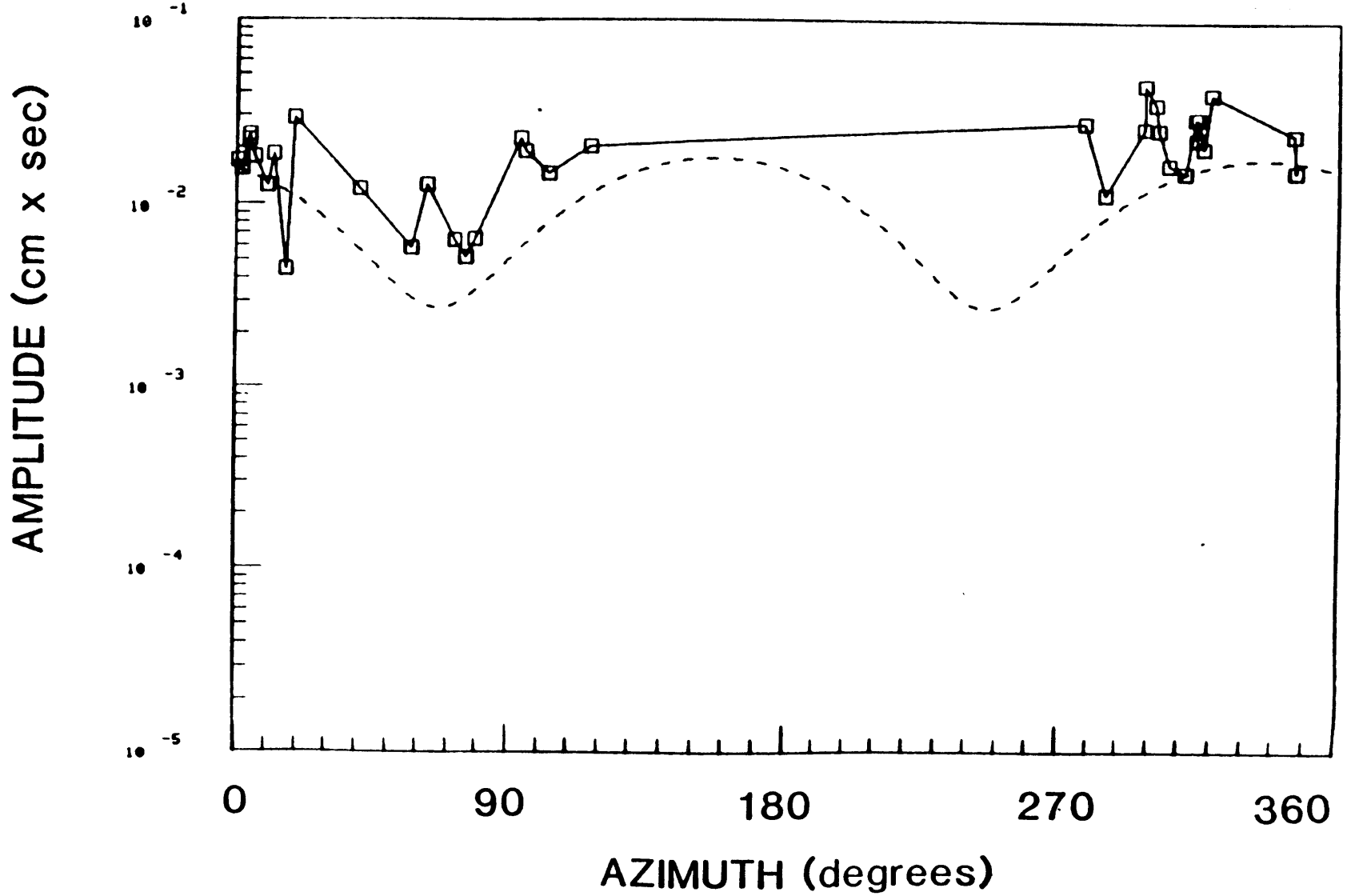

FIGURE B.32d

PERIOD 70 sec

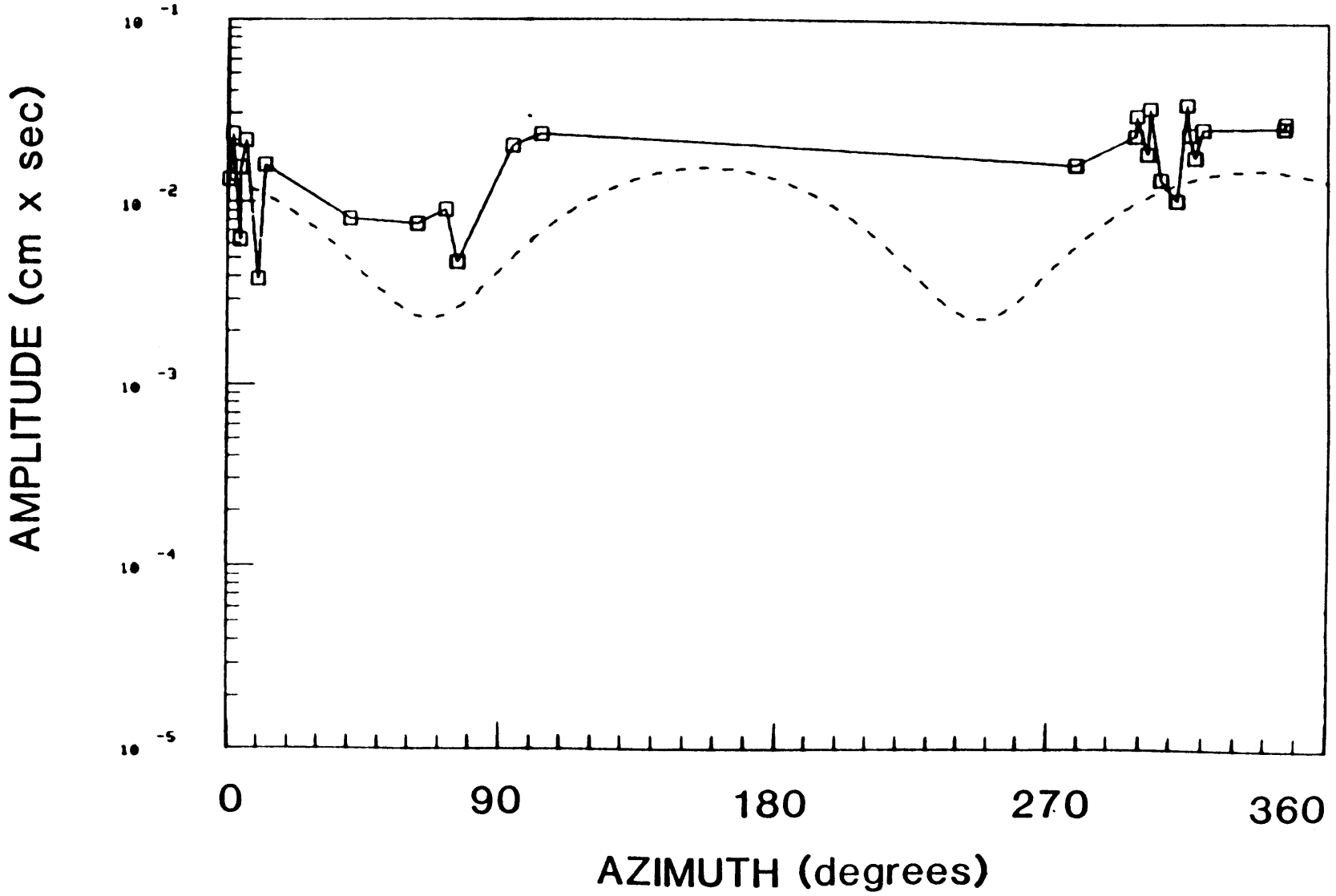

FIGURE B.32e

PERIOD 98 sec

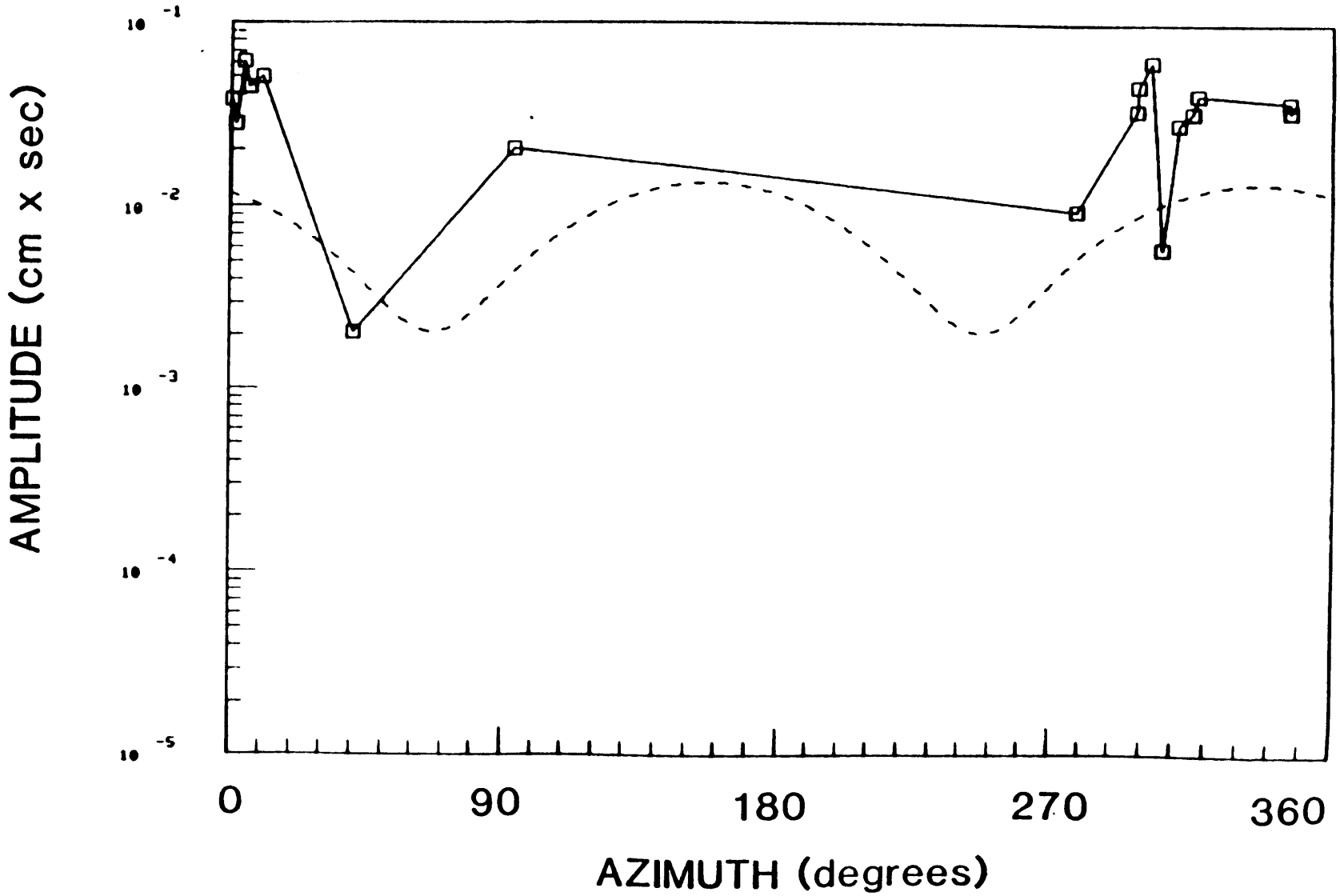

FIGURE B.33a

11/20/74

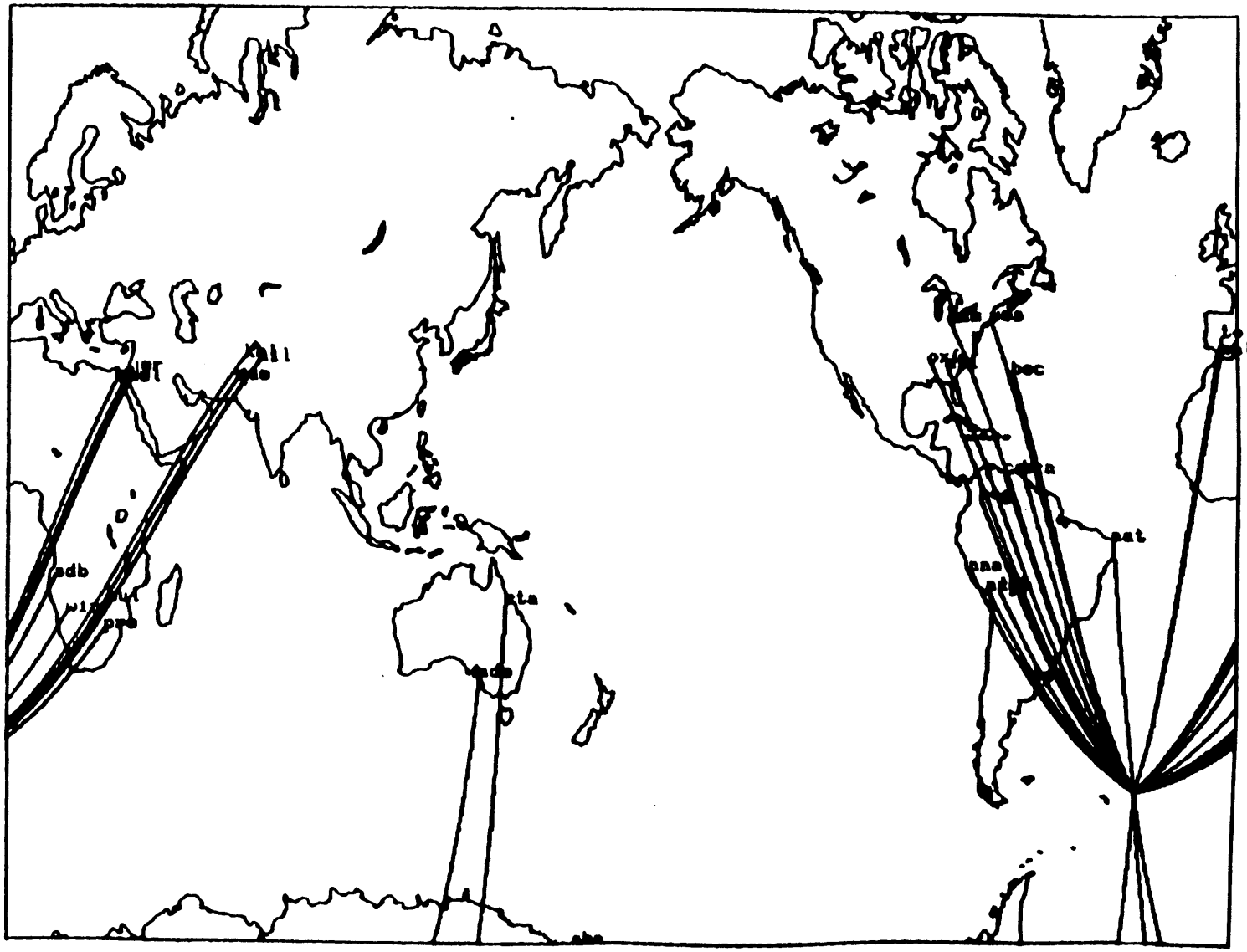

FIGURE B.33b

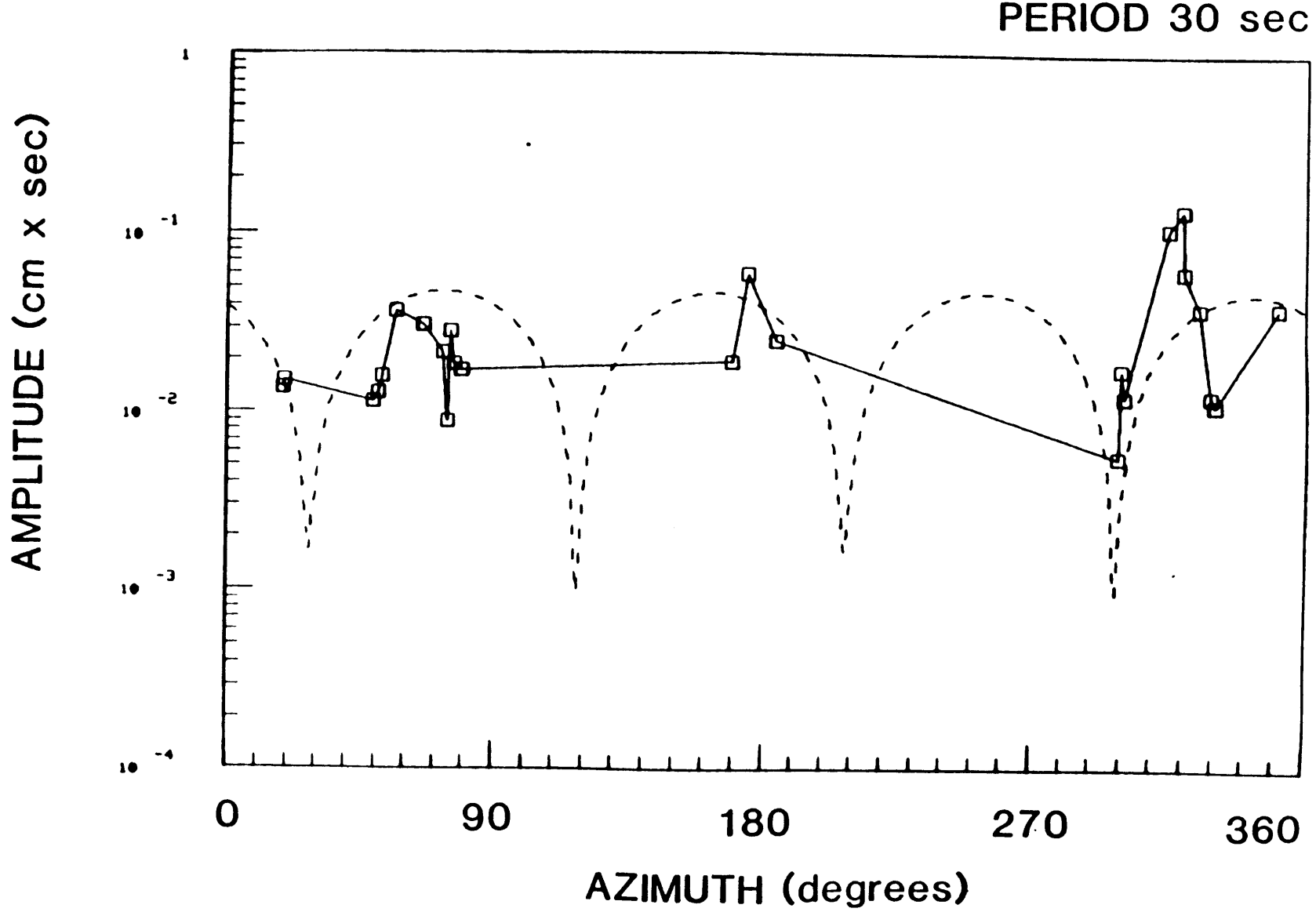
PERIOD 30 sec
AMPLITUDE (cm x sec)
1
10 -1
10 -2
10 -3
10 -4
0
90
180
270
360
AZIMUTH (degrees)

FIGURE B.33C

PERIOD 50 sec

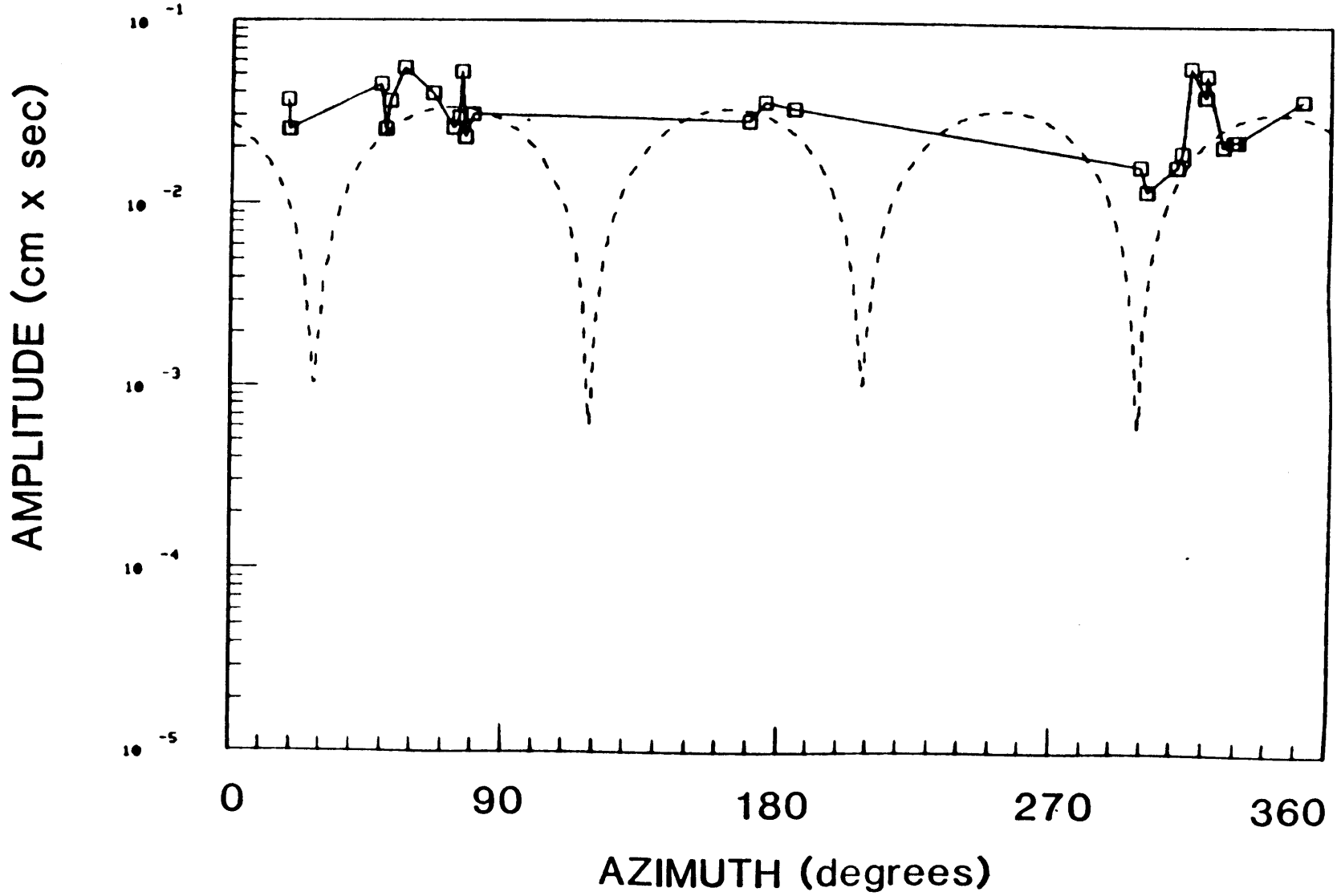

FIGURE B.33d

PERIOD 70 sec

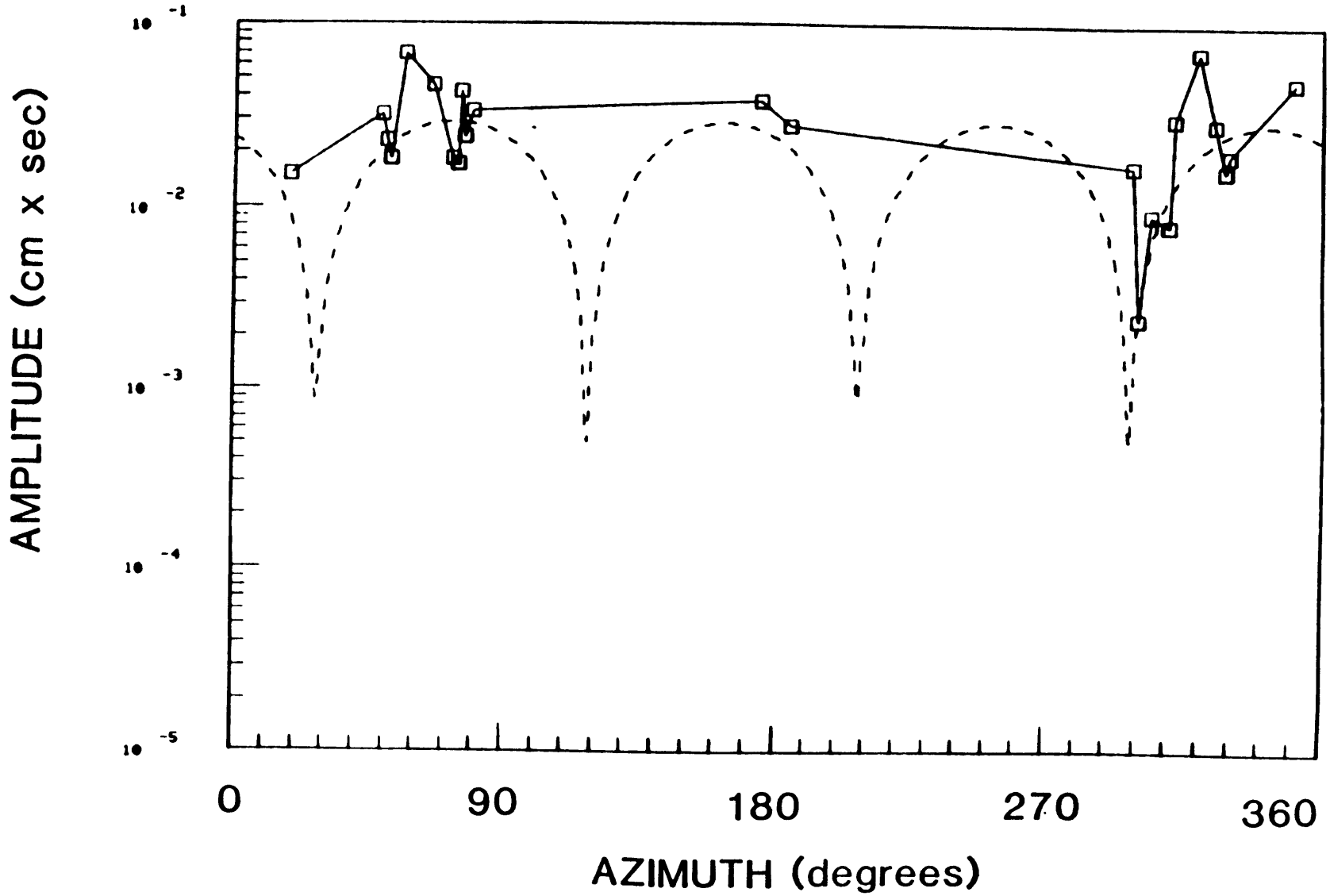

FIGURE B.33e

PERIOD 98 sec

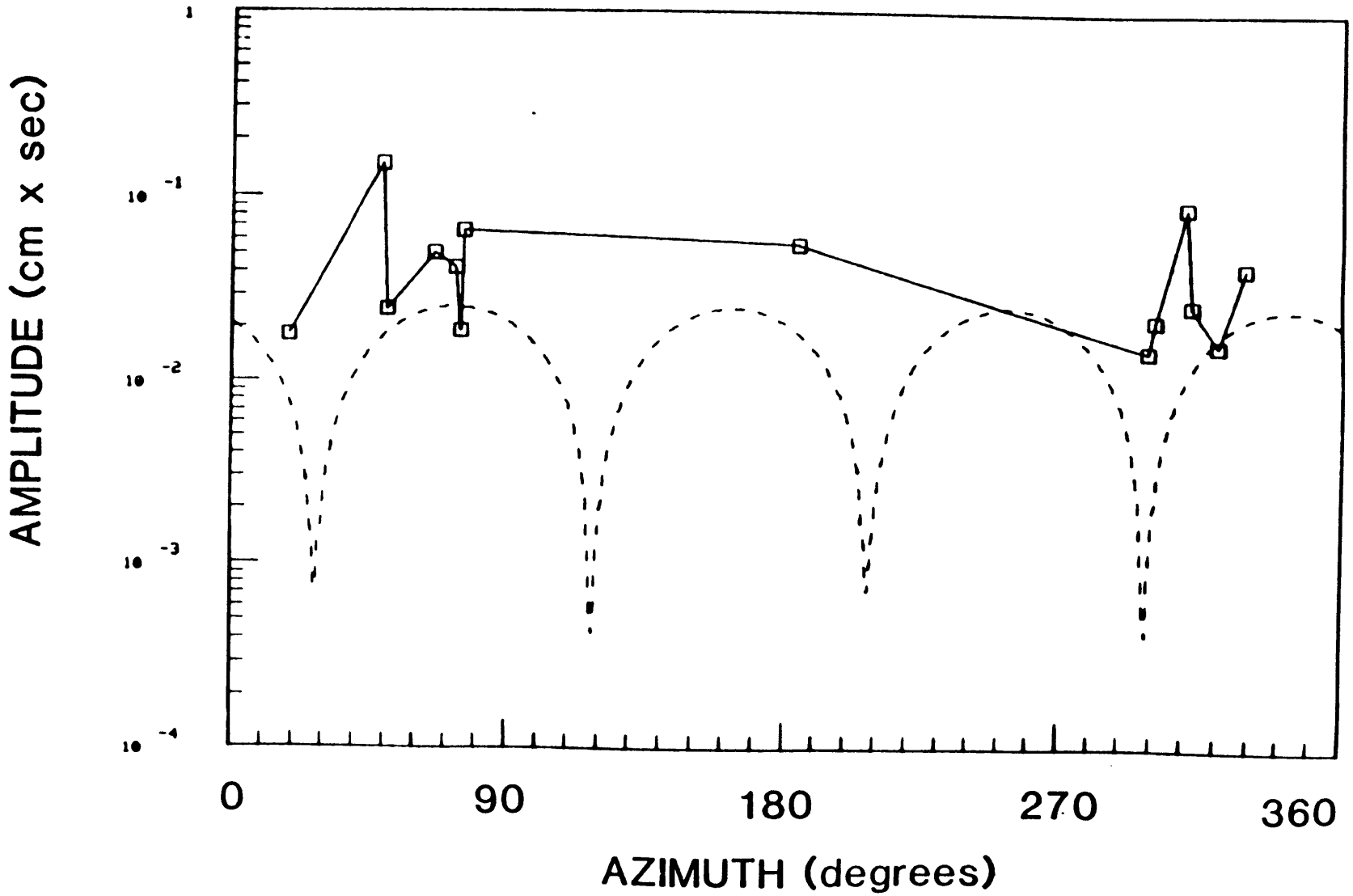

FIGURE B.34a

09/11/75

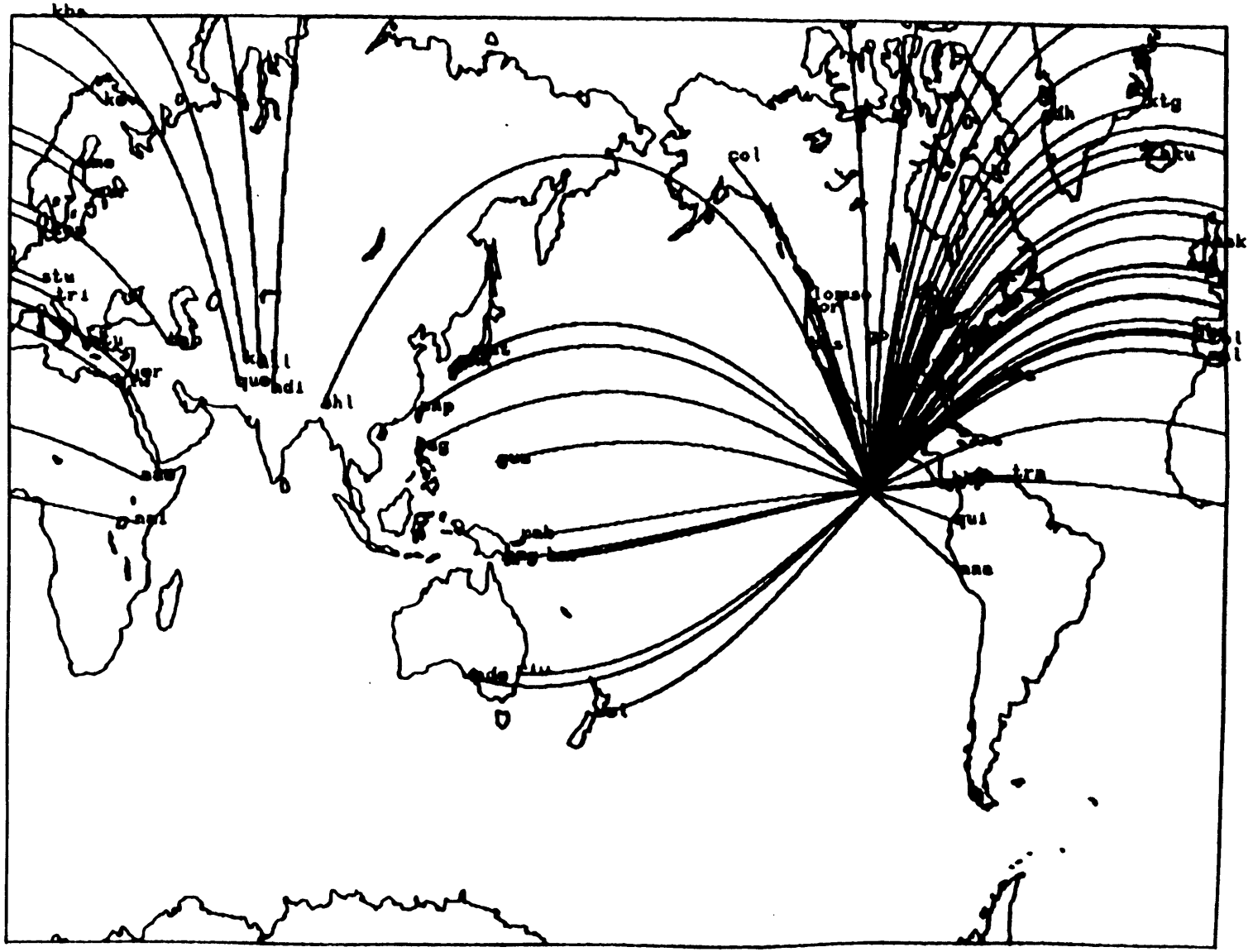

FIGURE B.34b

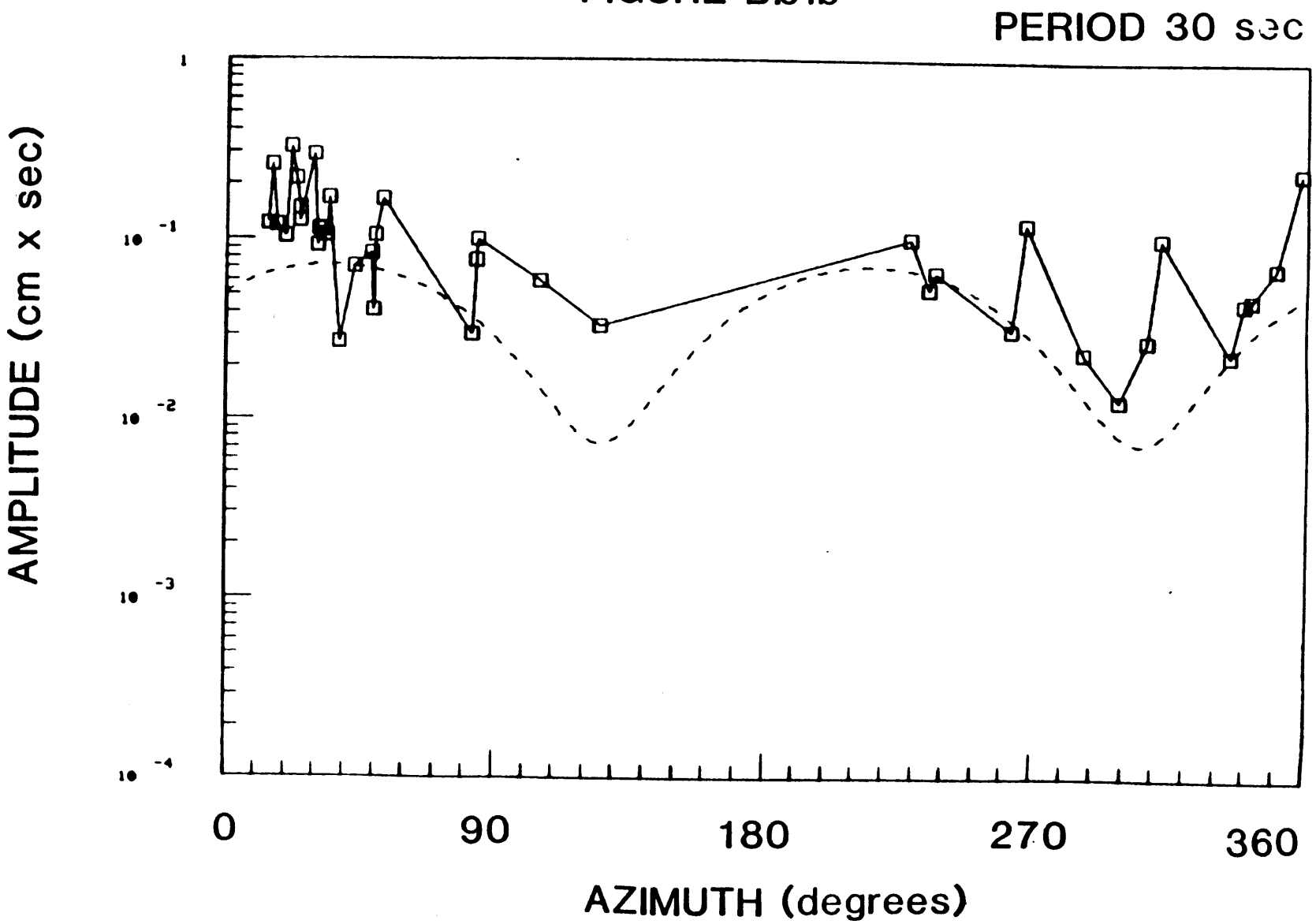
PERIOD 30 sec
AMPLITUDE (cm x sec)
1
10 -1
10 -2
10 -3
10 -4
0
90
180
270
360
AZIMUTH (degrees)

FIGURE B.34c

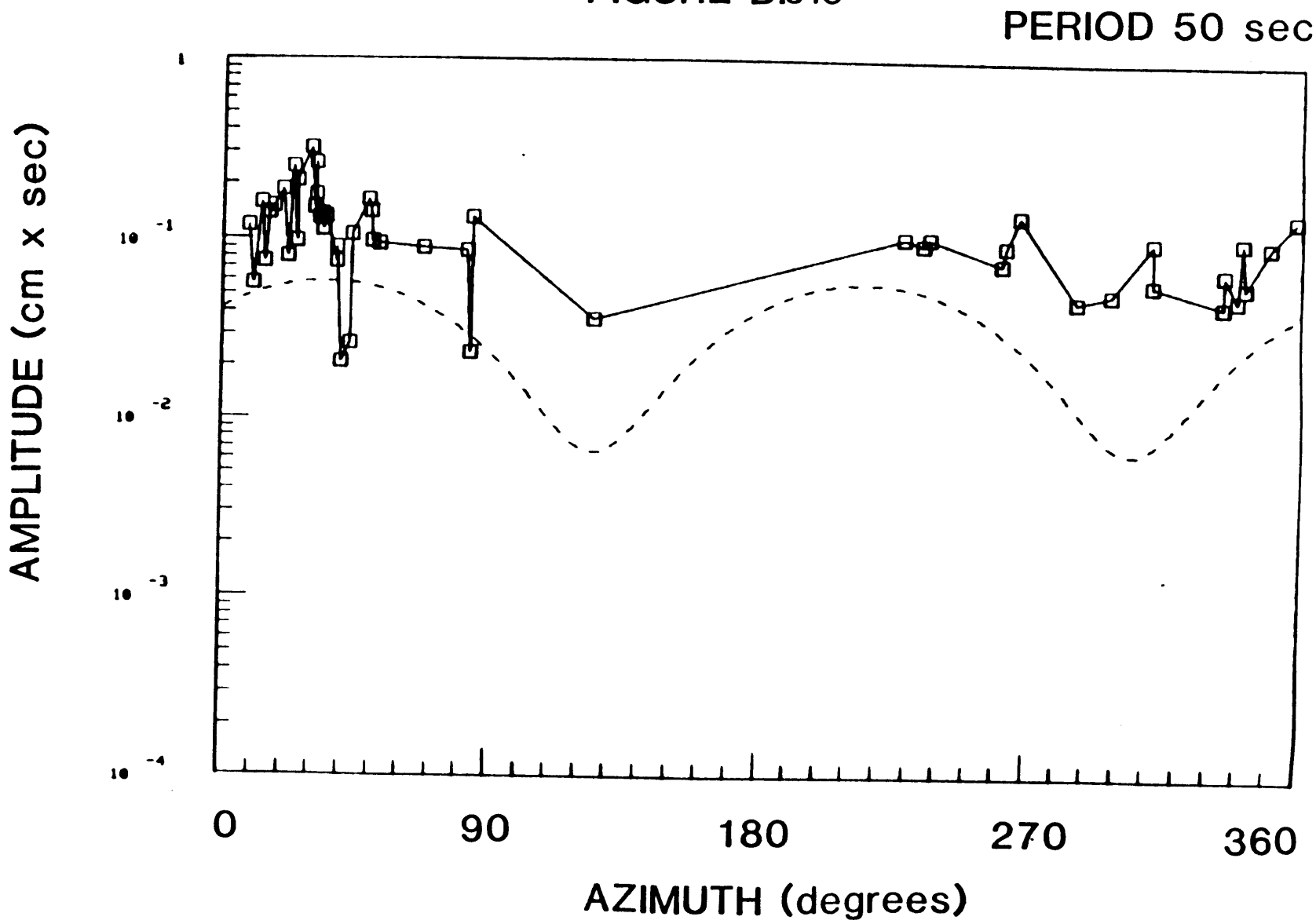
PERIOD 50 sec
AMPLITUDE (cm x sec)
1
10 -1
10 -2
10 -3
10 -4
0
90
180
270
360
AZIMUTH (degrees)

FIGURE B.34d

PERIOD 70 sec

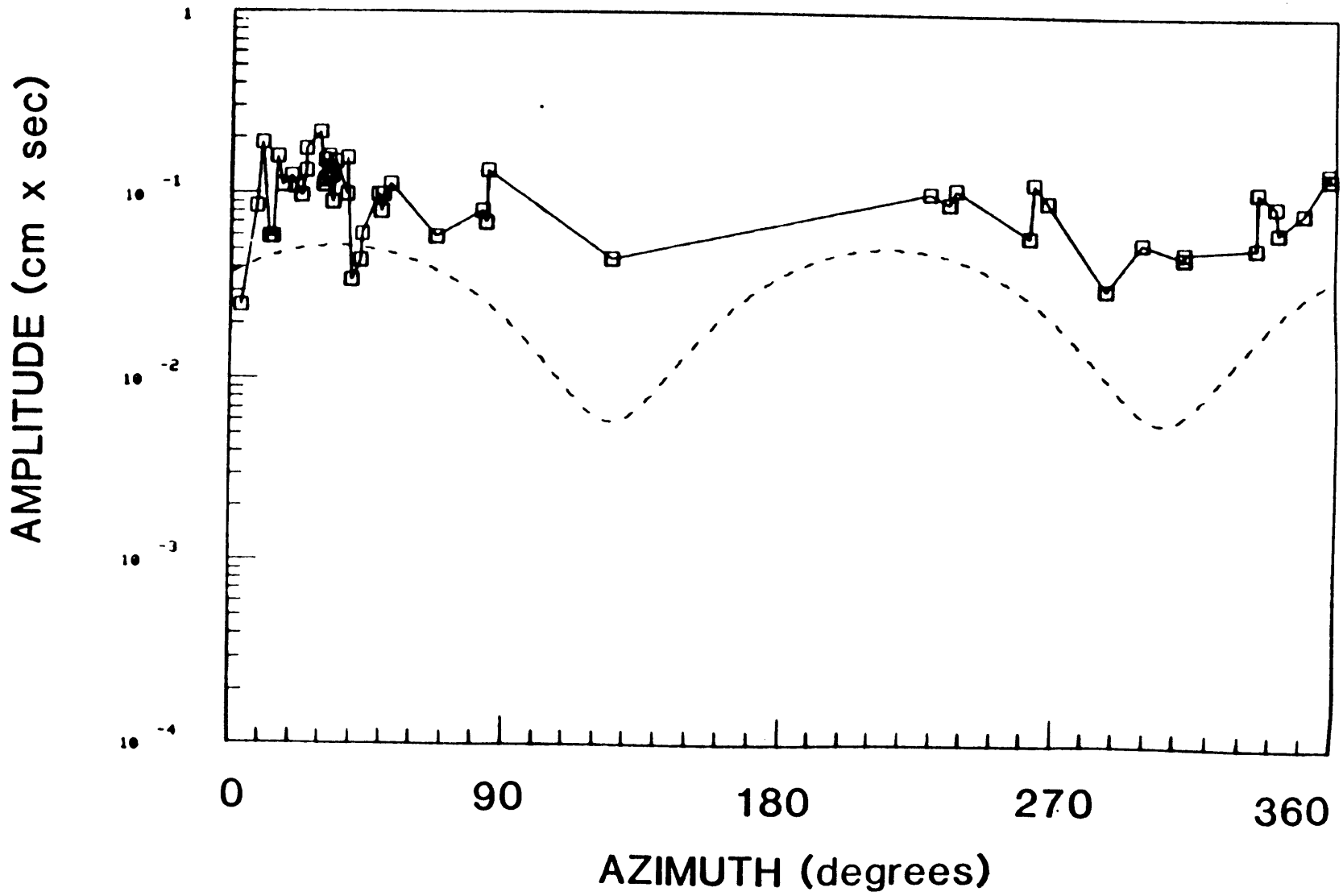

FIGURE B.34e

PERIOD 98 sec

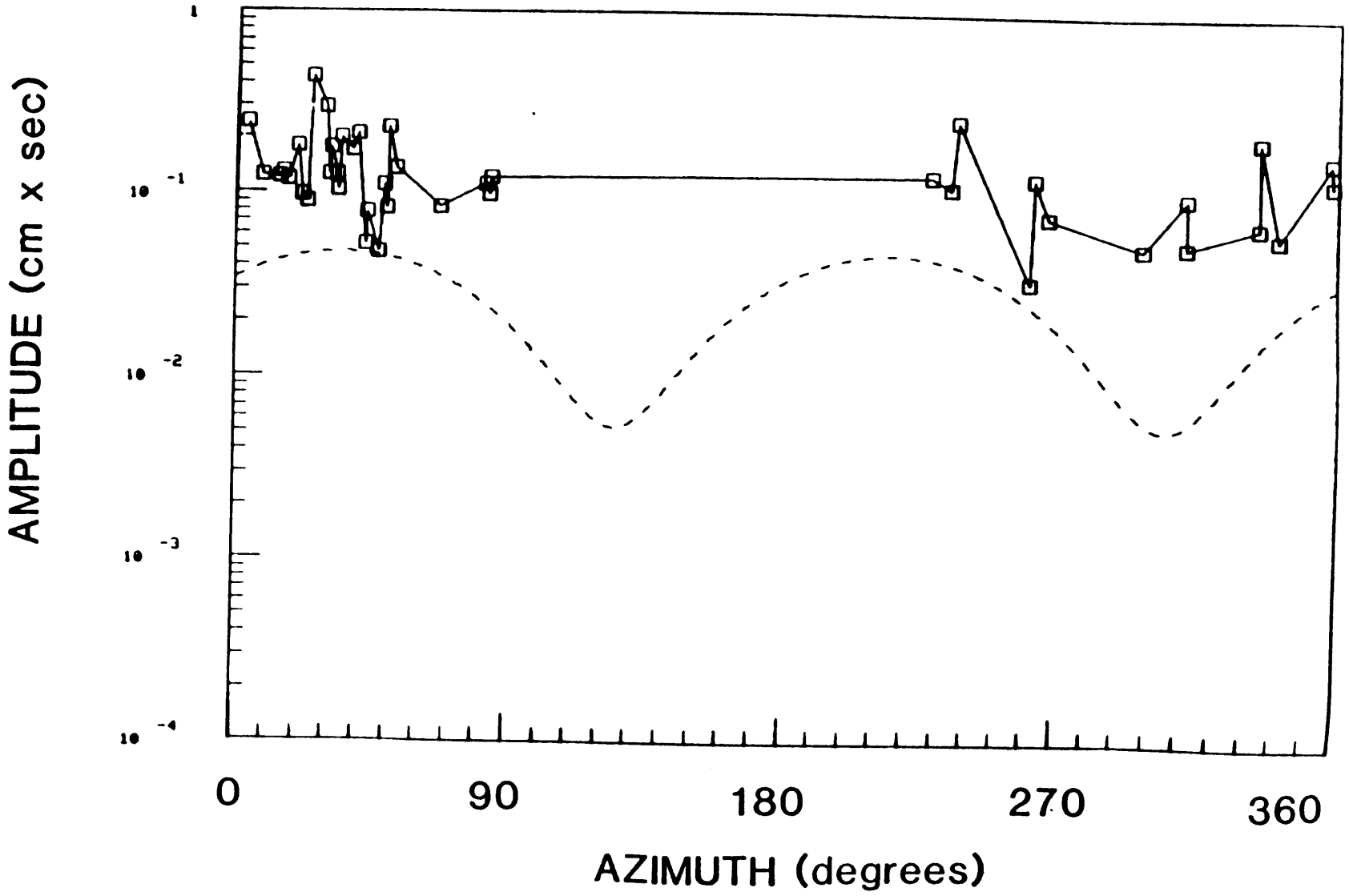

FIGURE B.35a

09/19/75

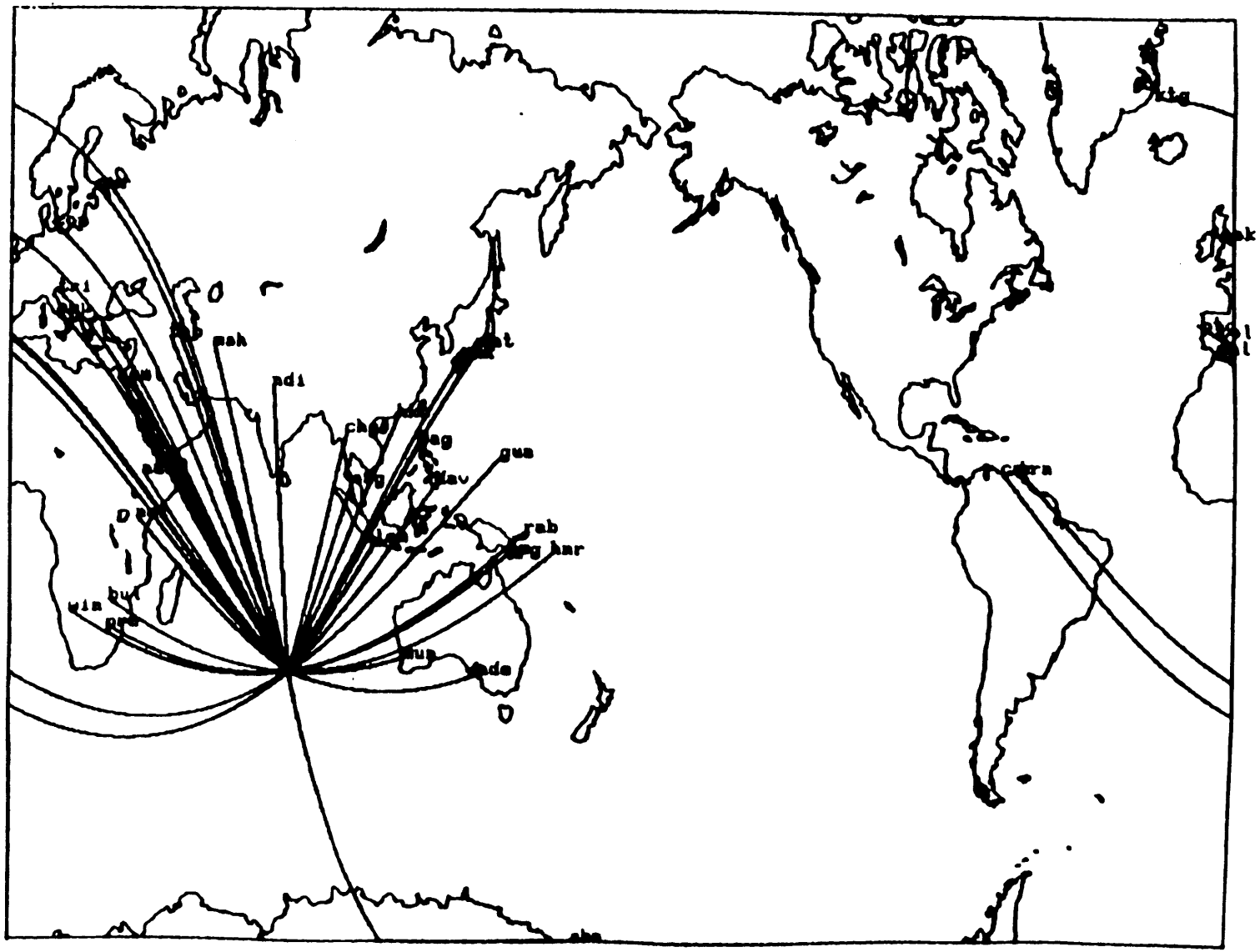

FIGURE B.35b

PERIOD 30 sec

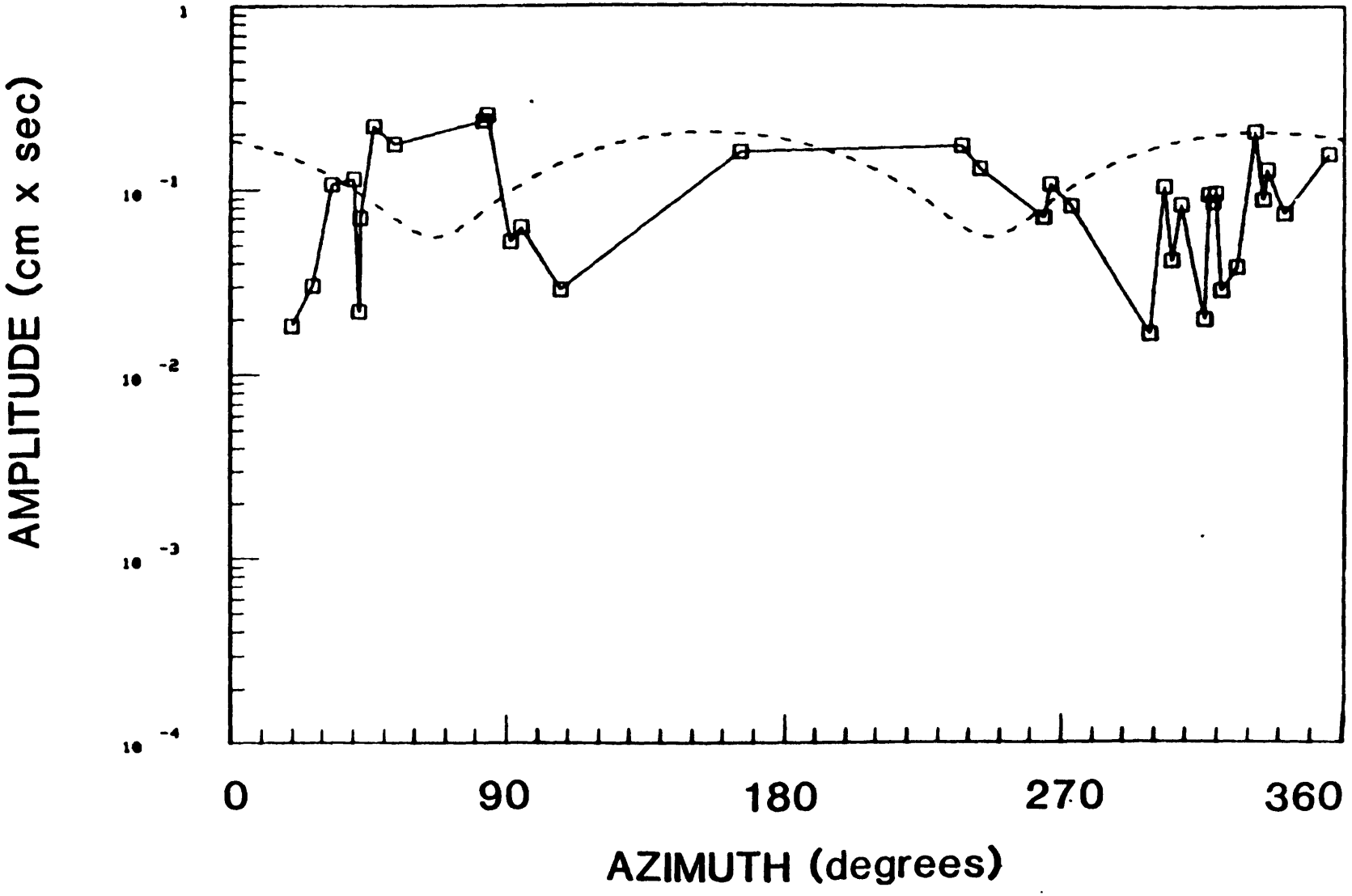

FIGURE B.35C

PERIOD 50 sec

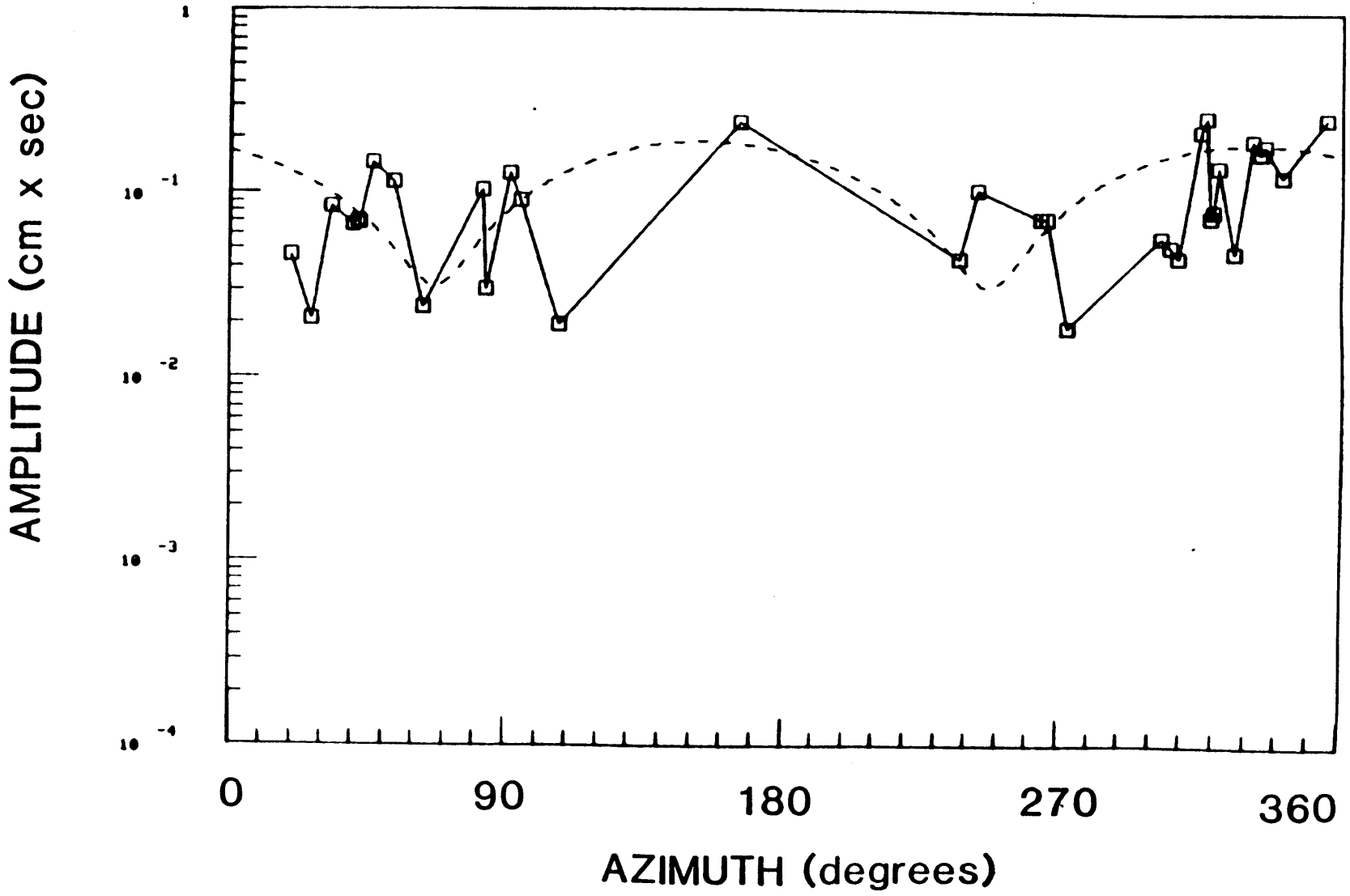

FIGURE B.35d

PERIOD 70 sec

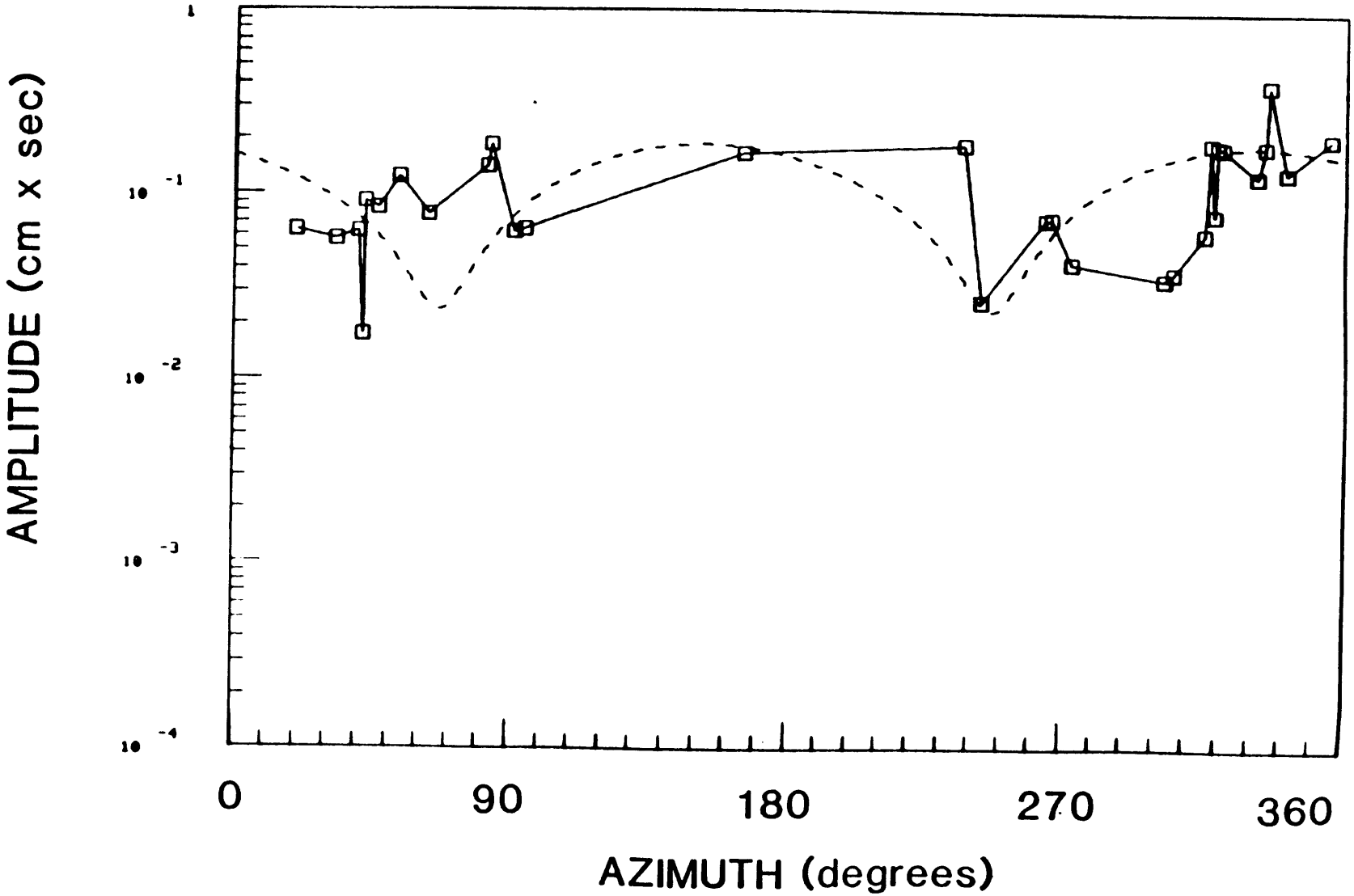

FIGURE B.35e

PERIOD 98 sec

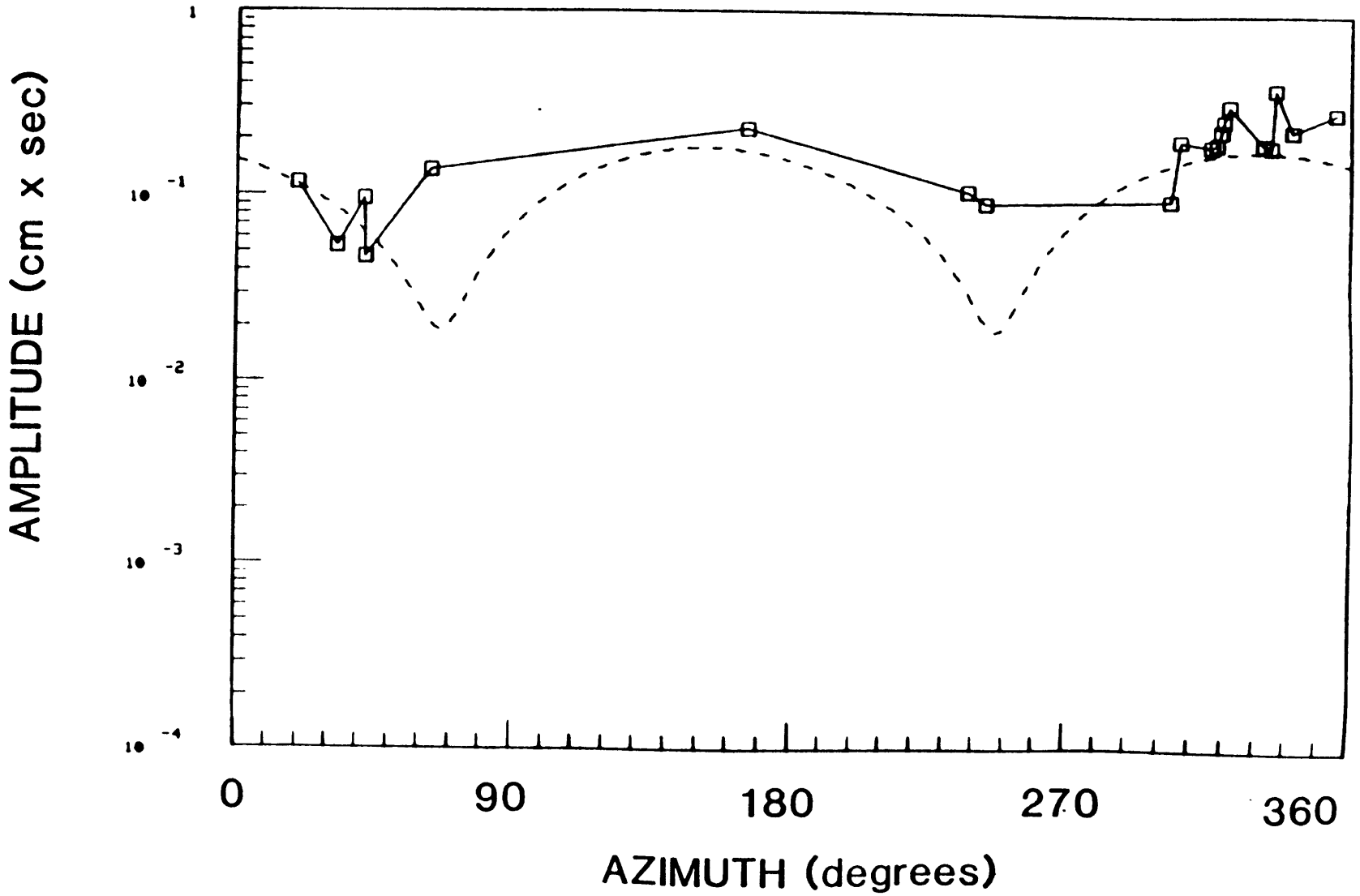

FIGURE B.36a

03/29/76

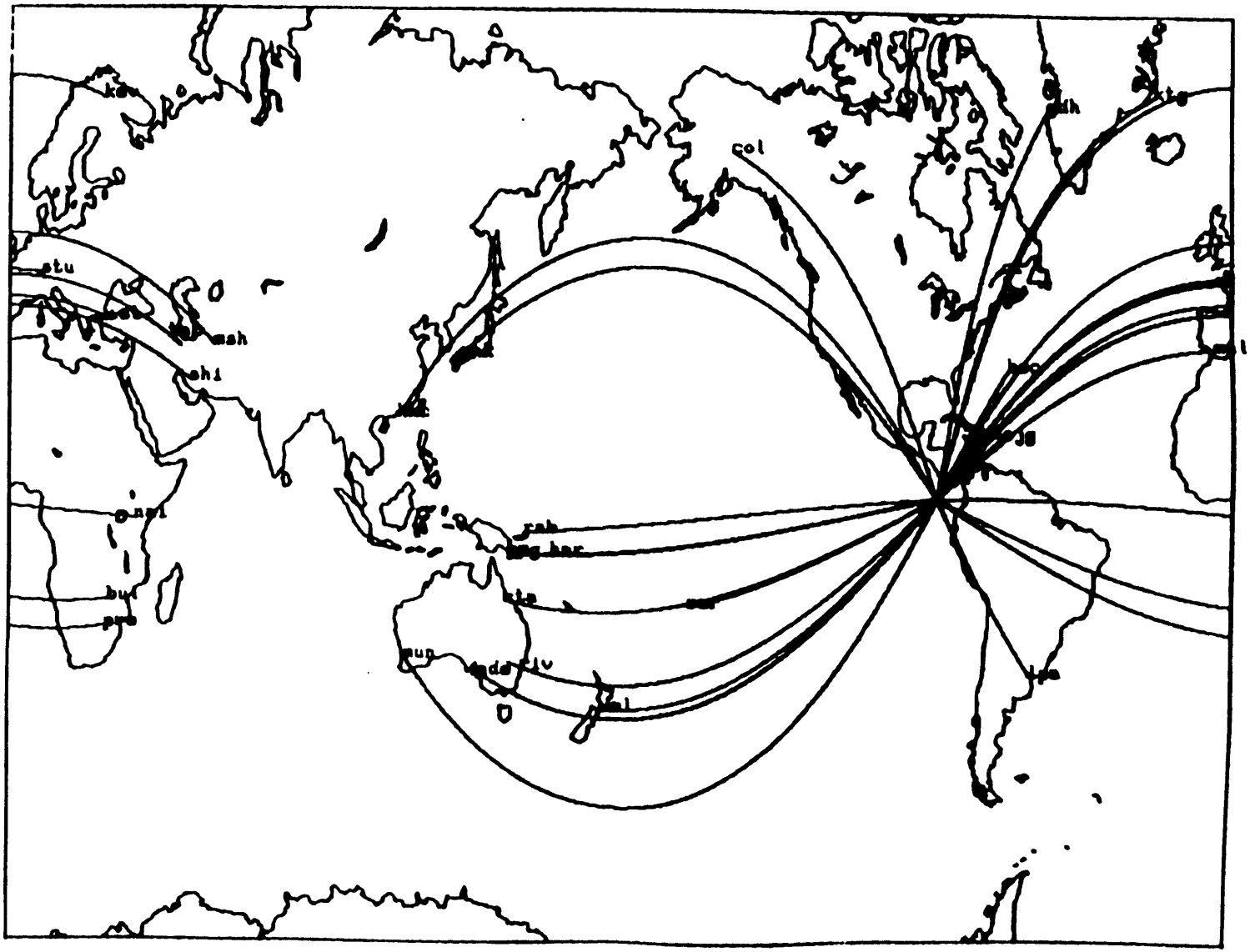

FIGURE B.36b

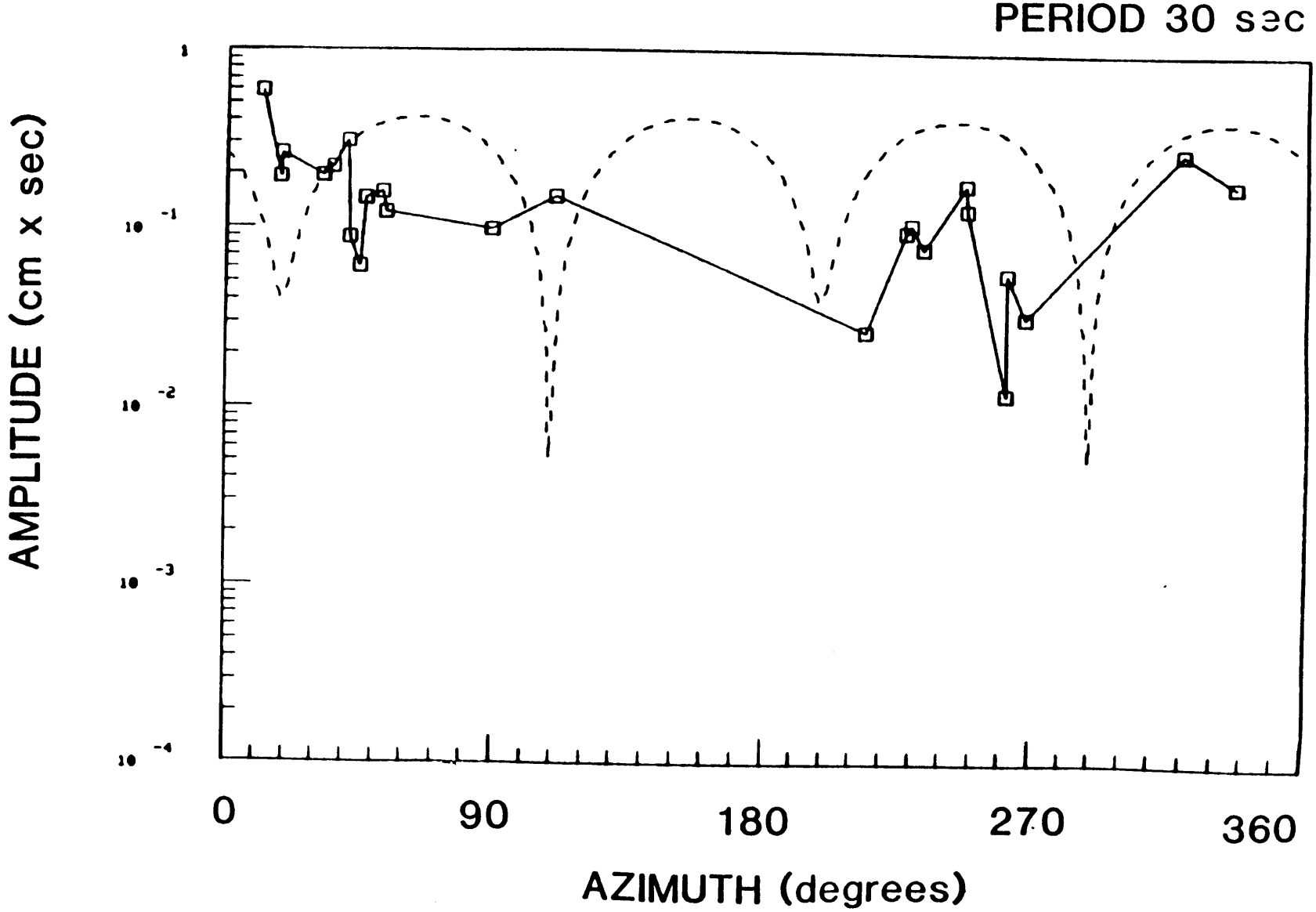
PERIOD 30 sec
AMPLITUDE (cm x sec)
1
10 -1
10 -2
10 -3
10 -4
0
90
180
270
360
AZIMUTH (degrees)

FIGURE B.36C

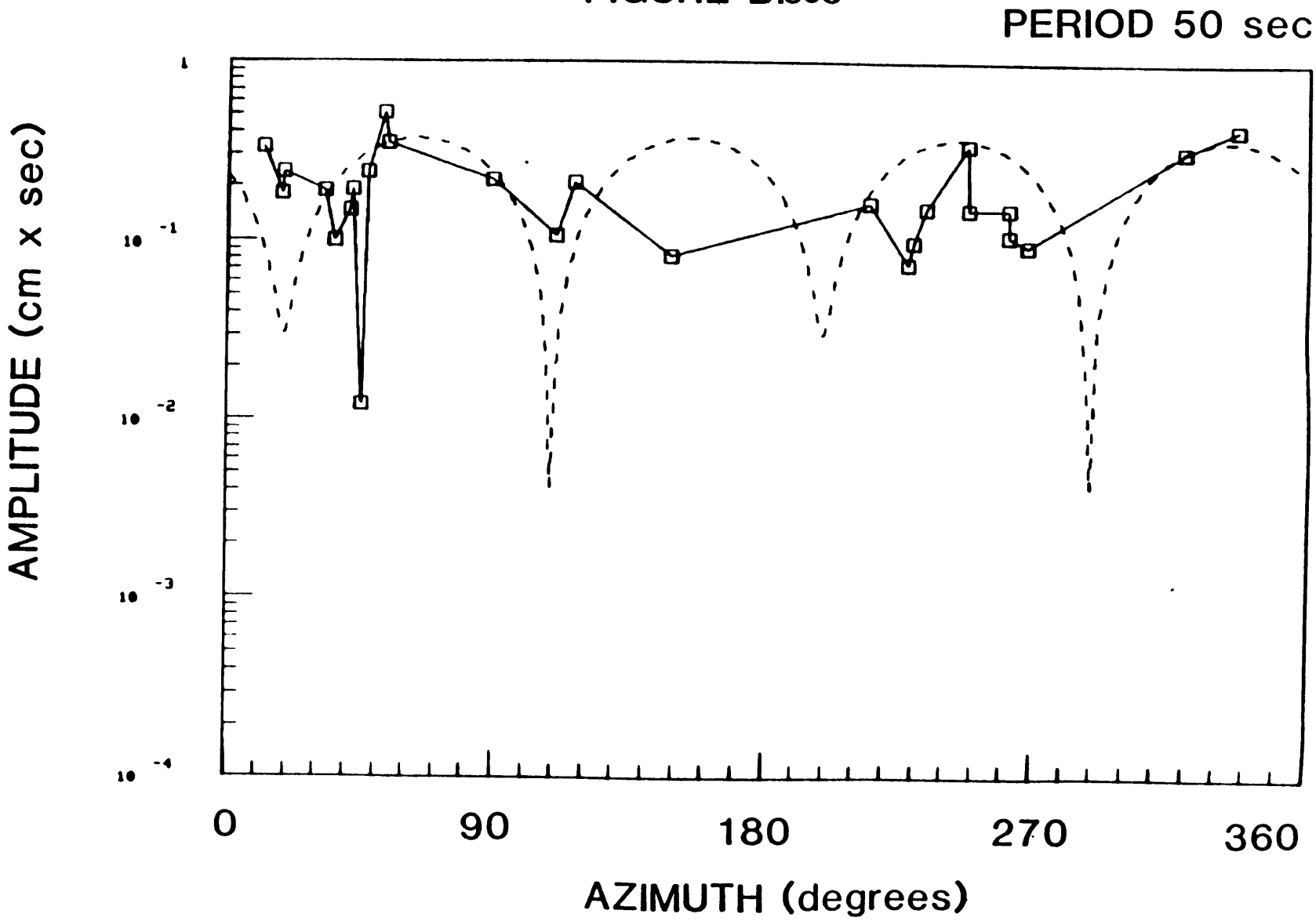
PERIOD 50 sec
AMPLITUDE (cm x sec)
1
10 -1
10 -2
10 -3
10 -4
0
90
180
270
360
AZIMUTH (degrees)

FIGURE B.36d

PERIOD 70 sec

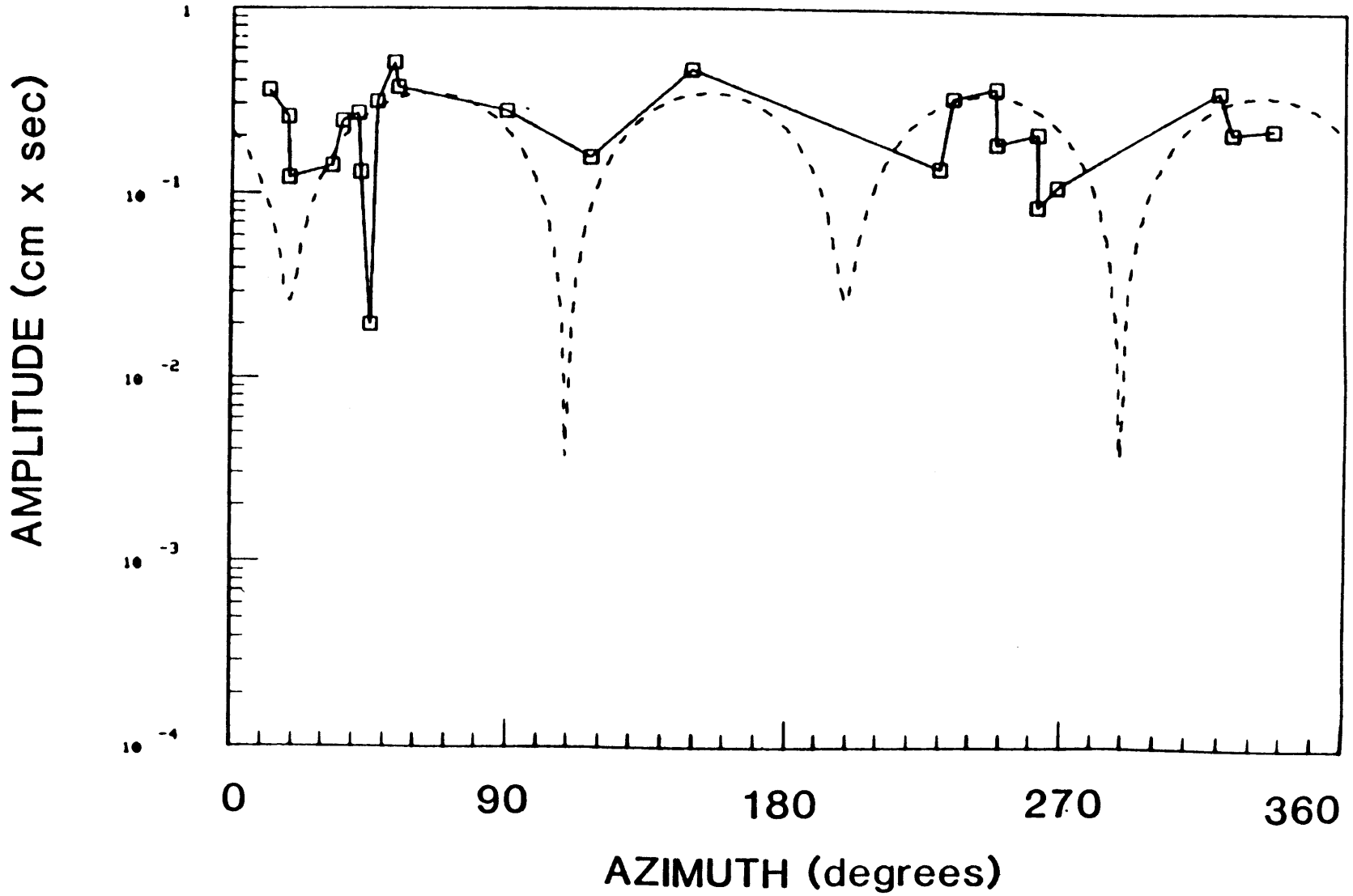

FIGURE B.36e

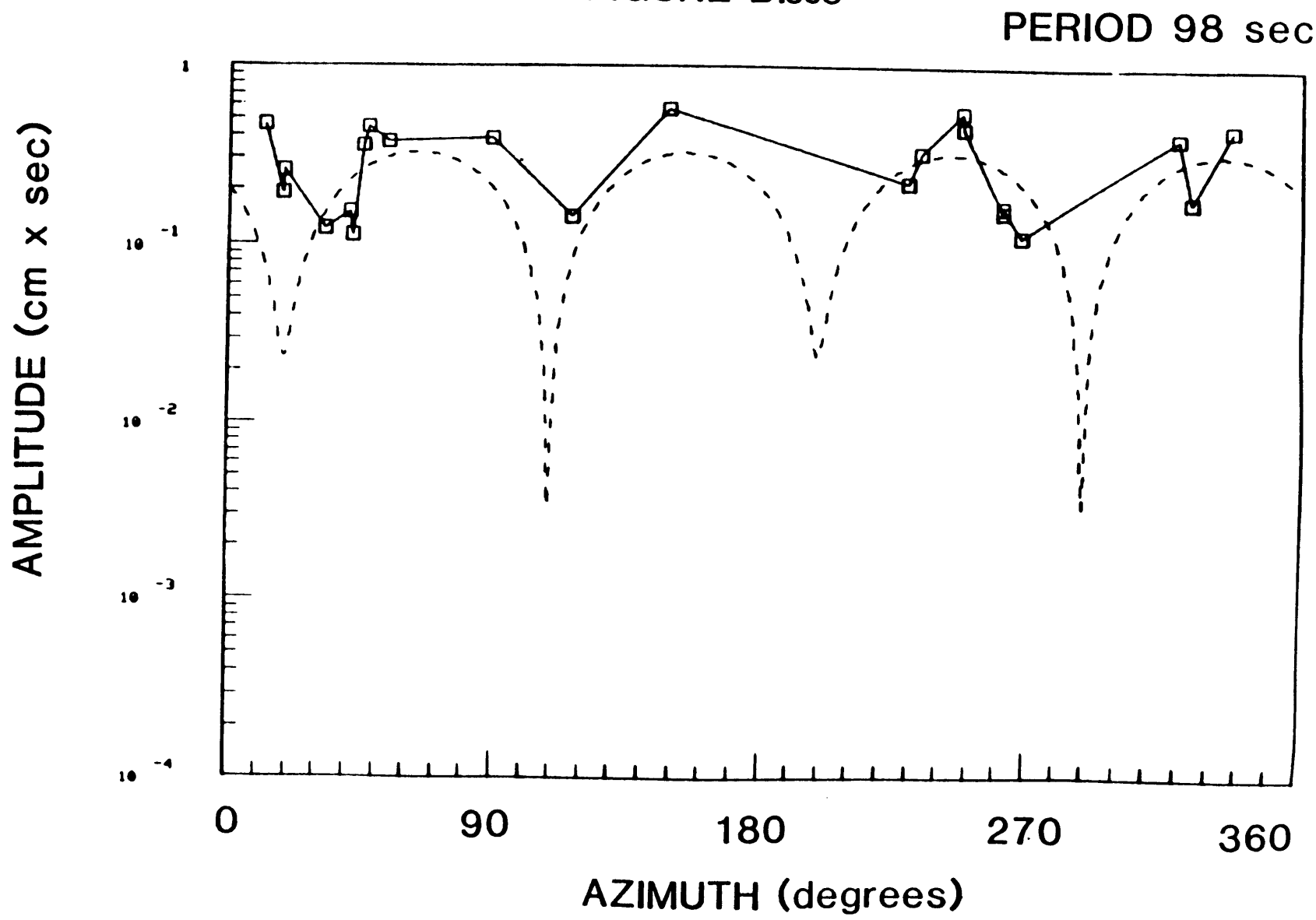
PERIOD 98 sec
AMPLITUDE (cm x sec)
1
10 -1
10 -2
10 -3
10 -4
0
90
180
270
360
AZIMUTH (degrees)

FIGURE B.37a

08/30/76

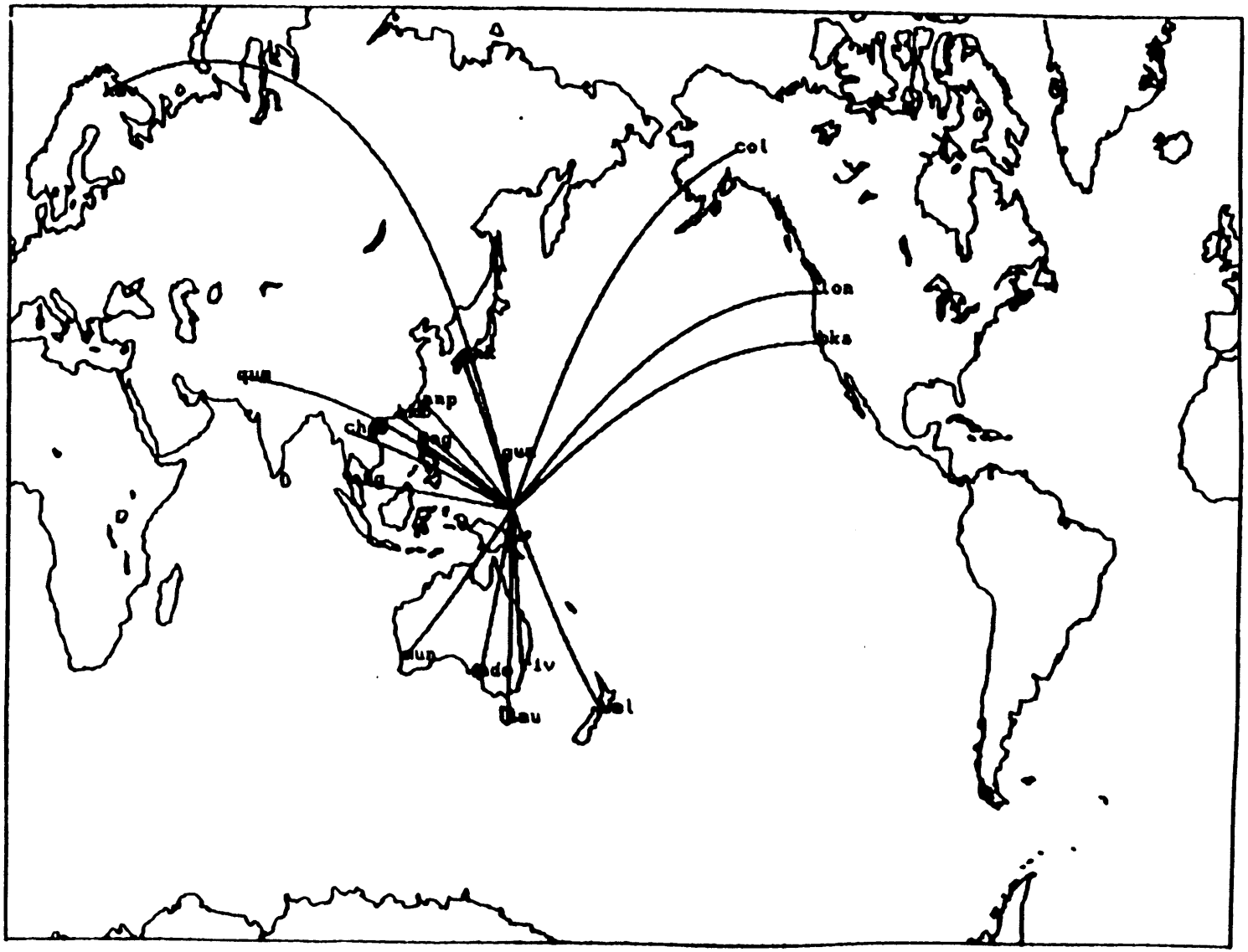

FIGURE B.37b

PERIOD 30 sec

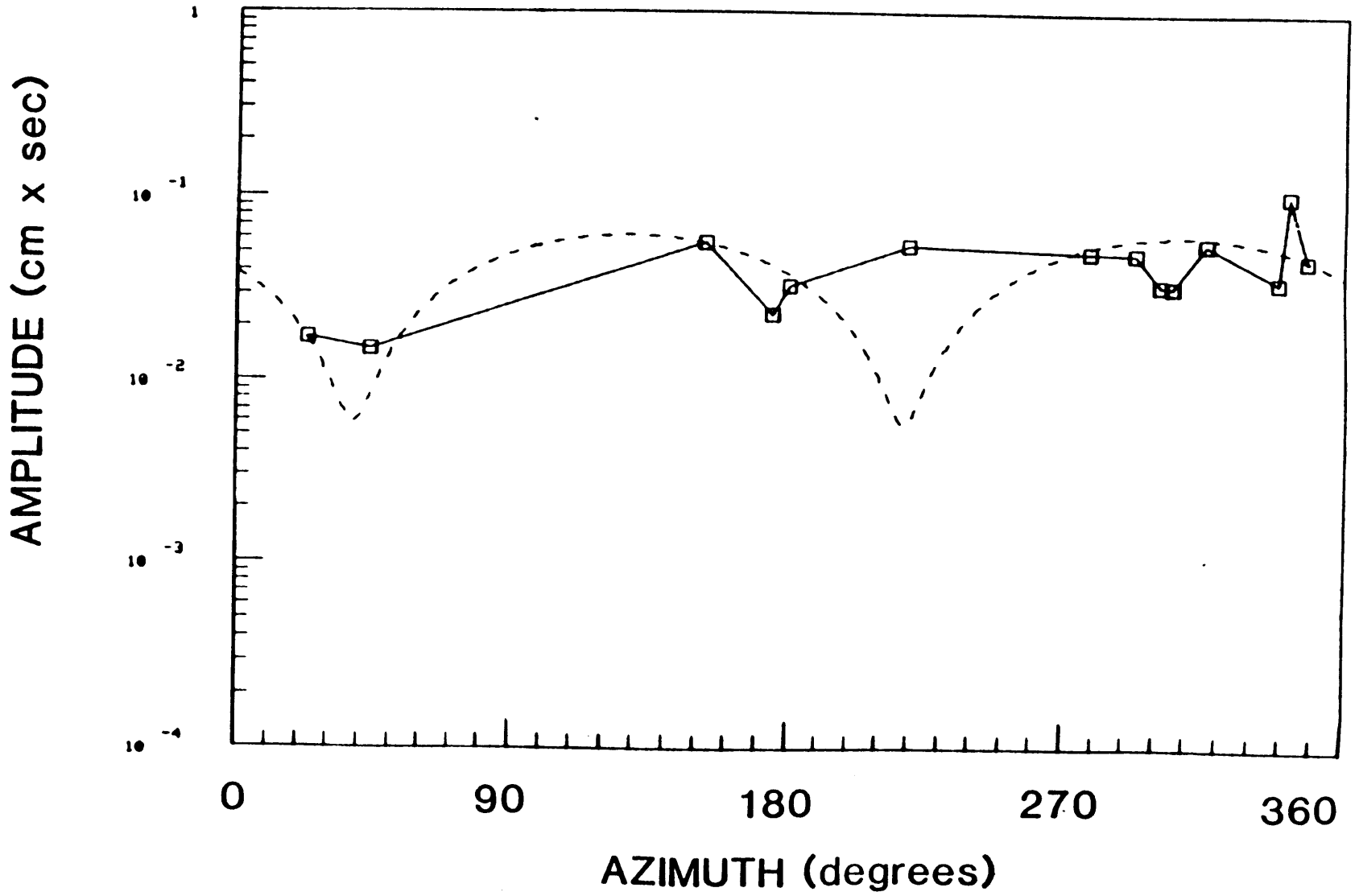

FIGURE B.37c

PERIOD 50 sec

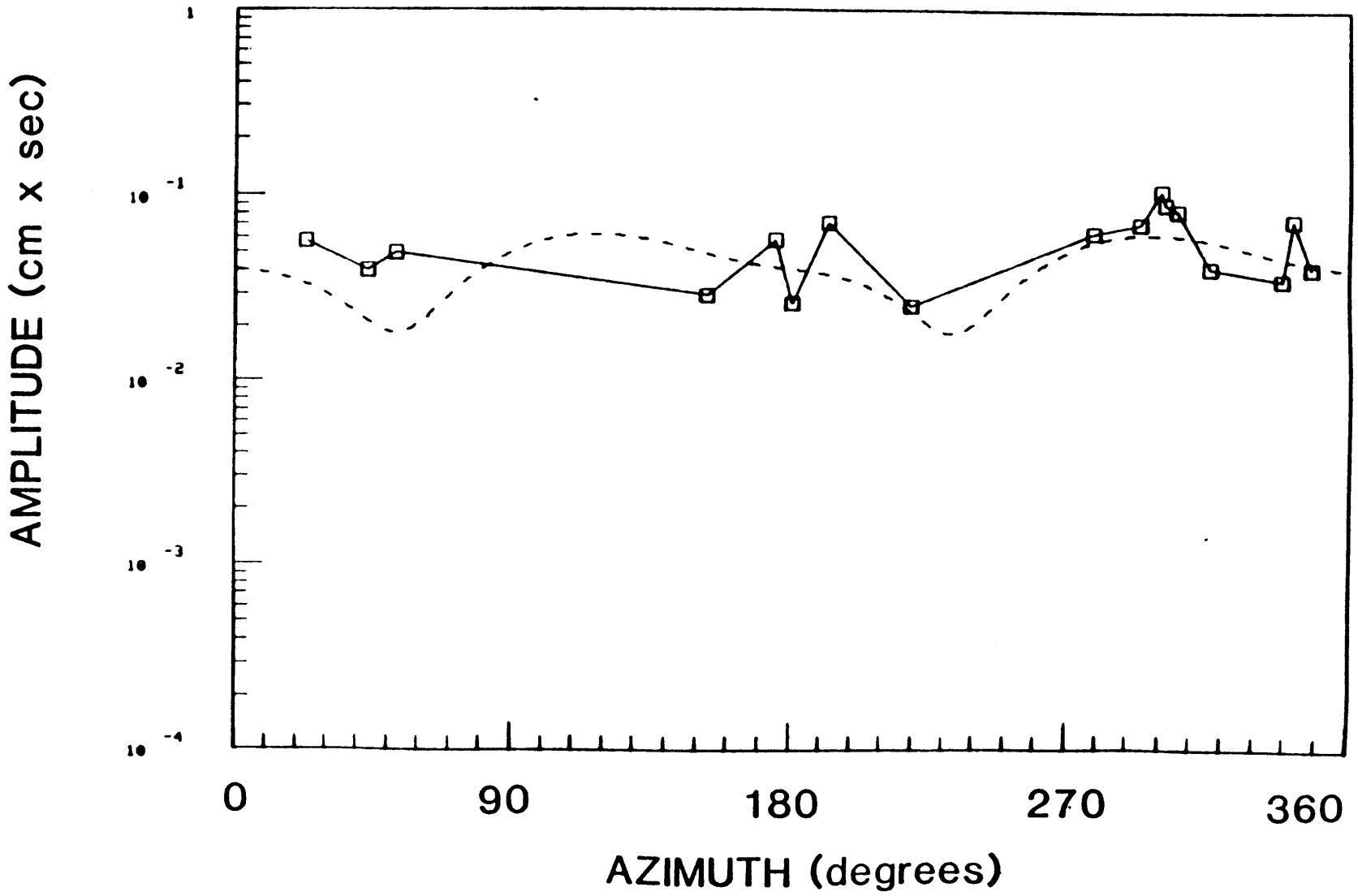

FIGURE B.37d

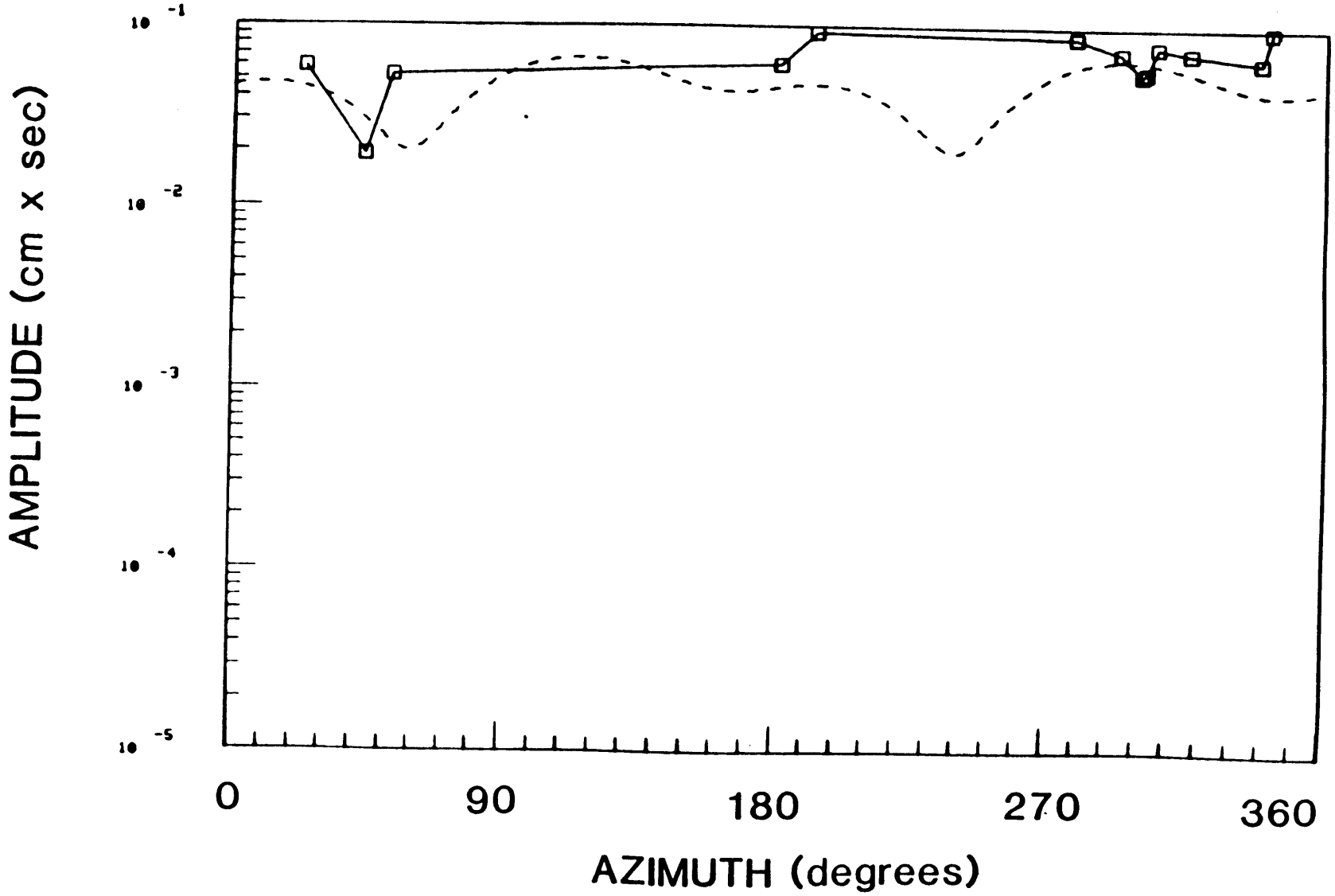
PERIOD 70 sec
AMPLITUDE (cm x sec)
10 -1
10 -2
10 -3
10 -4
10 -5
0
90
180
270
360
AZIMUTH (degrees)

FIGURE B.37e

PERIOD 98 sec

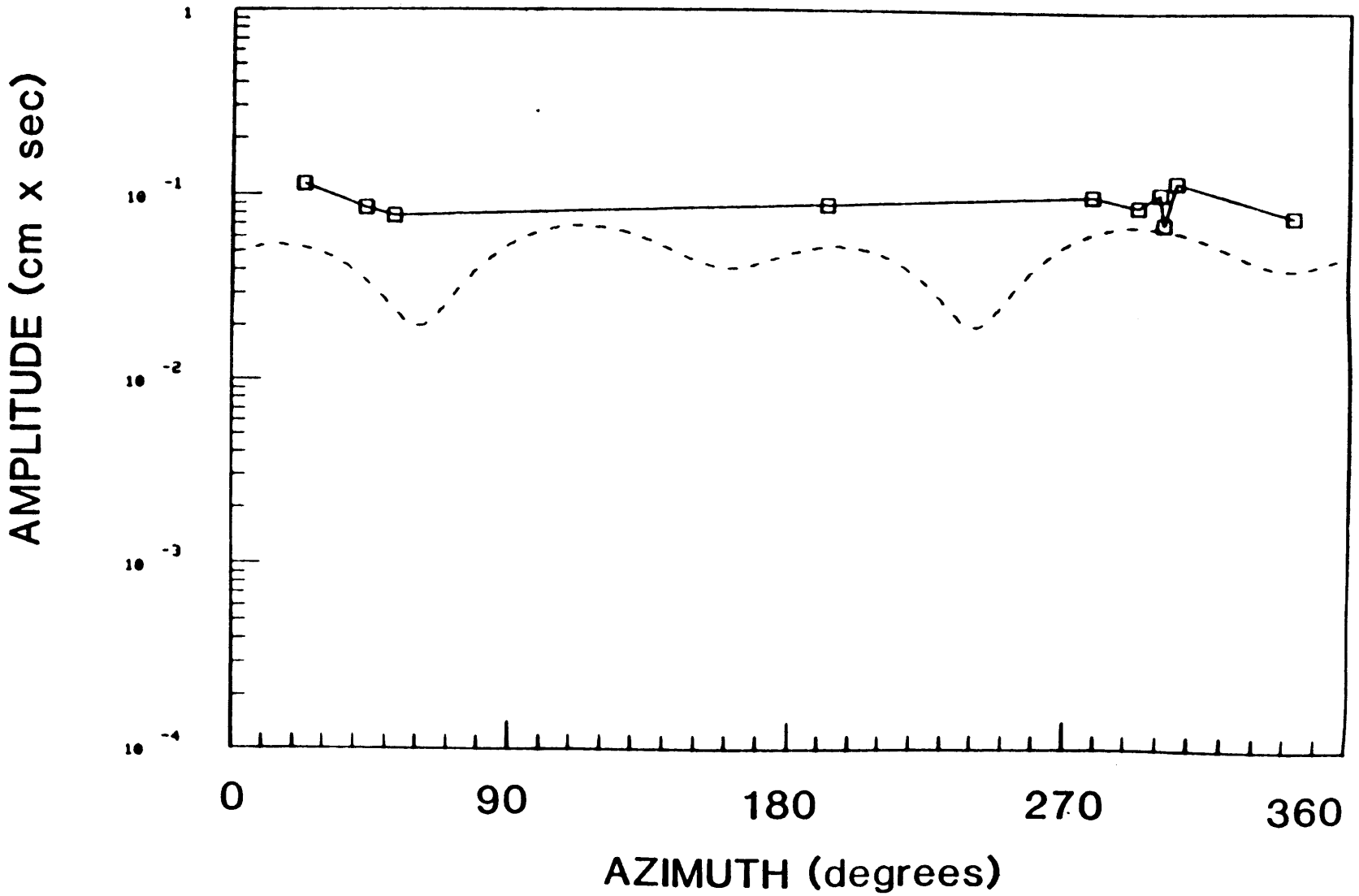

FIGURE B.38a

11/02/76

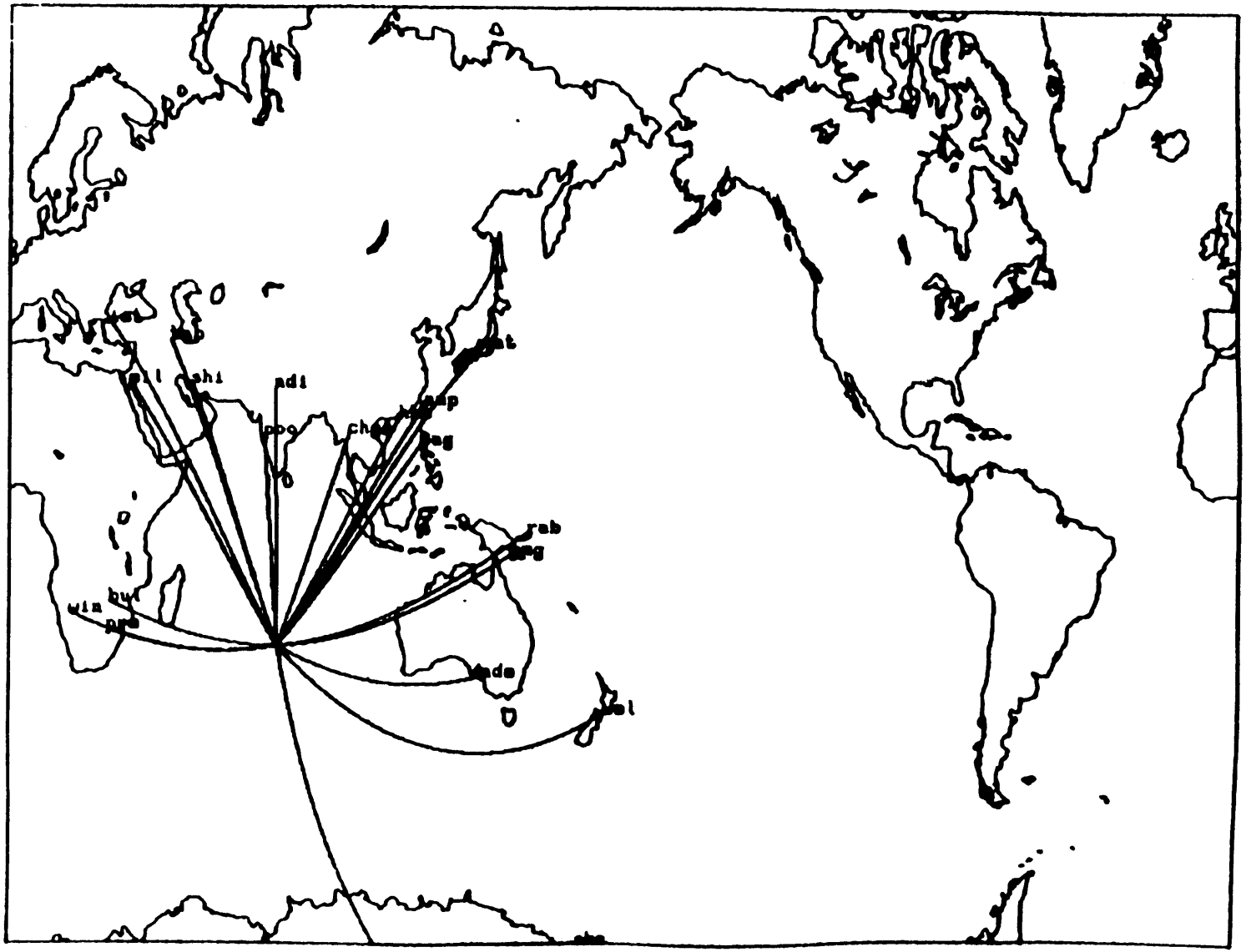

FIGURE B.38b

PERIOD 30 sec

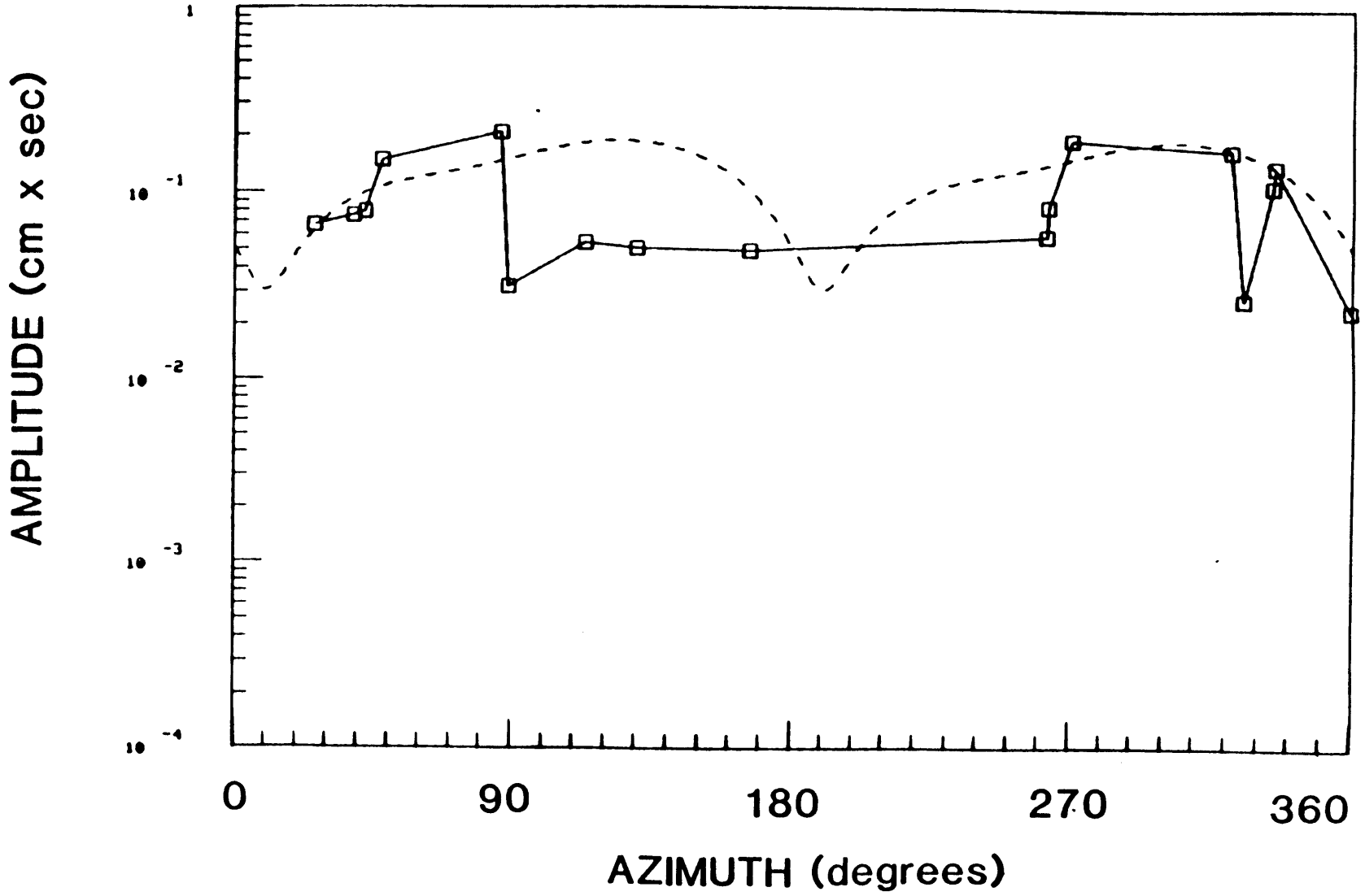

FIGURE B.38C

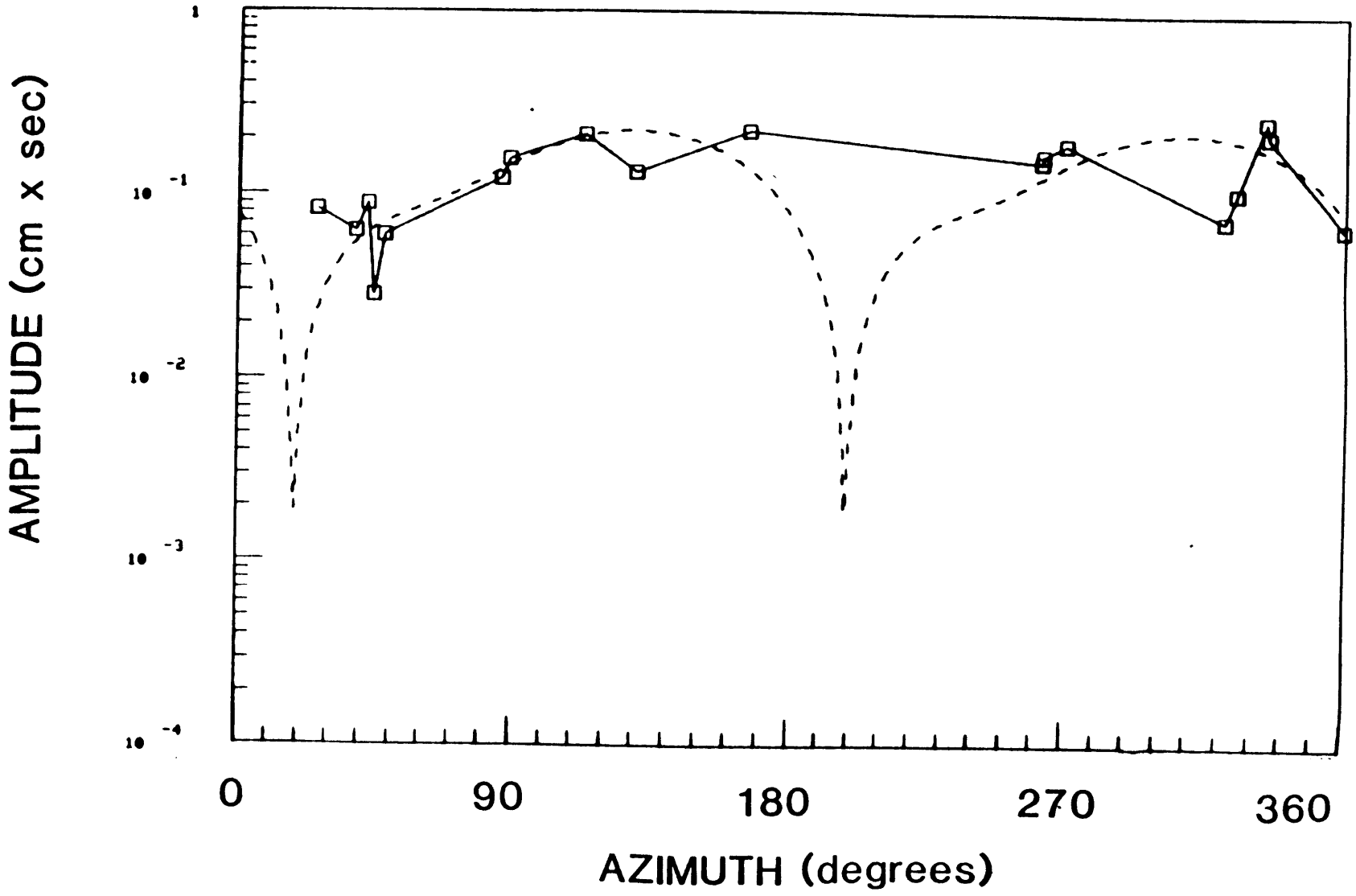
PERIOD 50 sec
AMPLITUDE (cm x sec)
1
10 -1
10 -2
10 -3
10 -4
0
90
180
270
360
AZIMUTH (degrees)

FIGURE B.38d

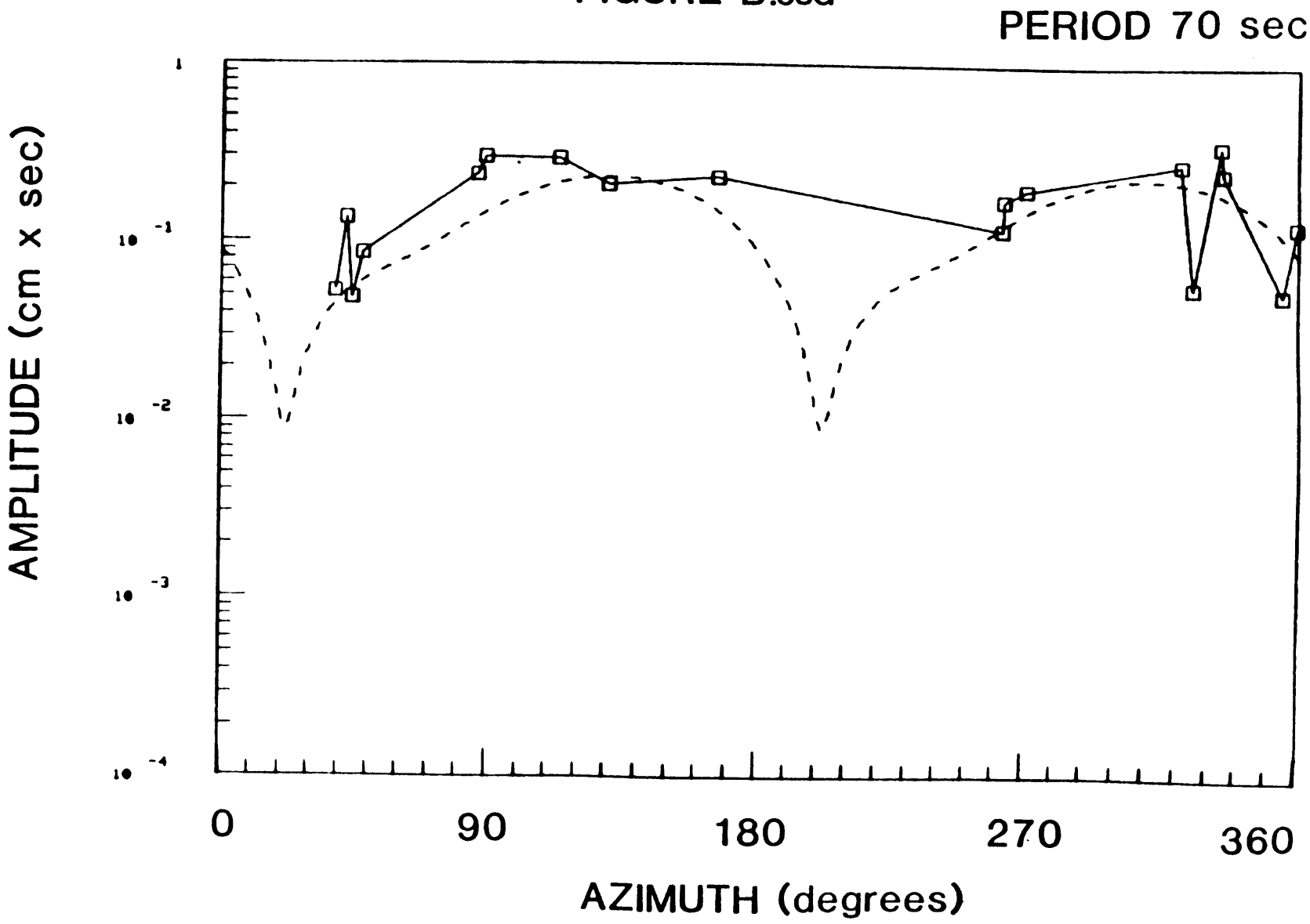
PERIOD 70 sec
AMPLITUDE (cm x sec)
1
10 -1
10 -2
10 -3
10 -4
0
90
180
270
360
AZIMUTH (degrees)

FIGURE B.38e

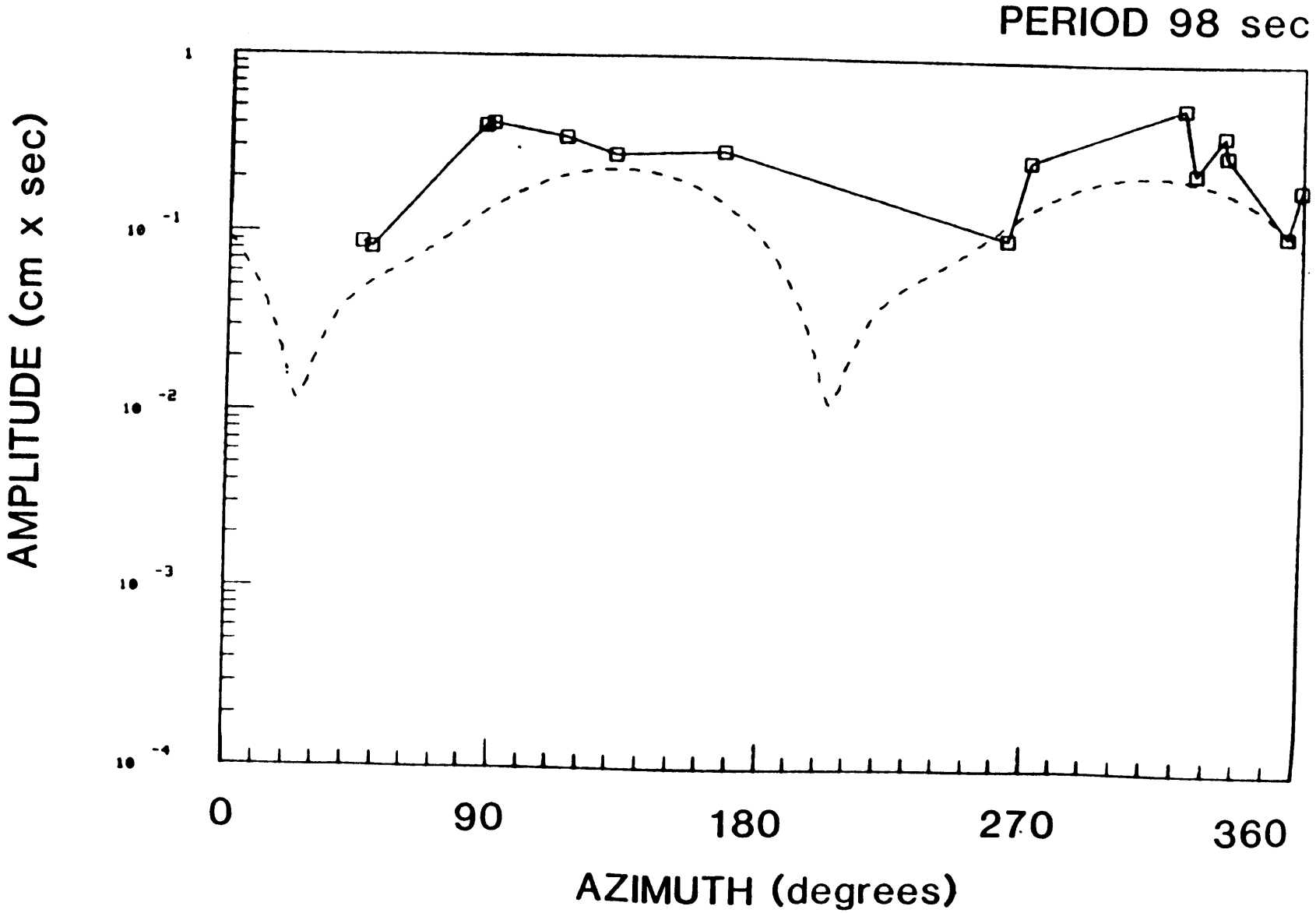
PERIOD 98 sec
AMPLITUDE (cm x sec)
1
10 -1
10 -2
10 -3
10 -4
0
90
180
270
360
AZIMUTH (degrees)

FIGURE B.39a

02/05/77

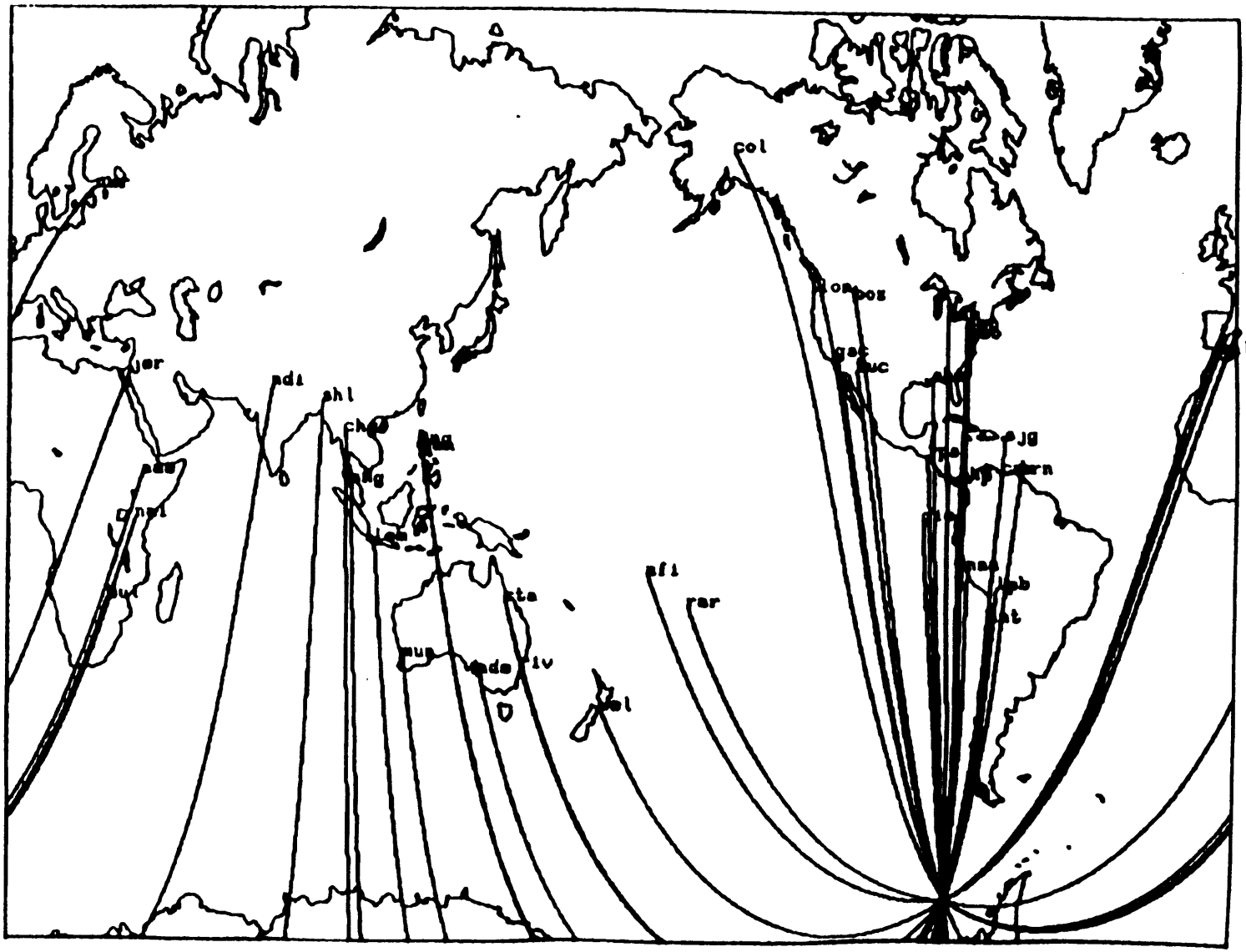

FIGURE B.39b

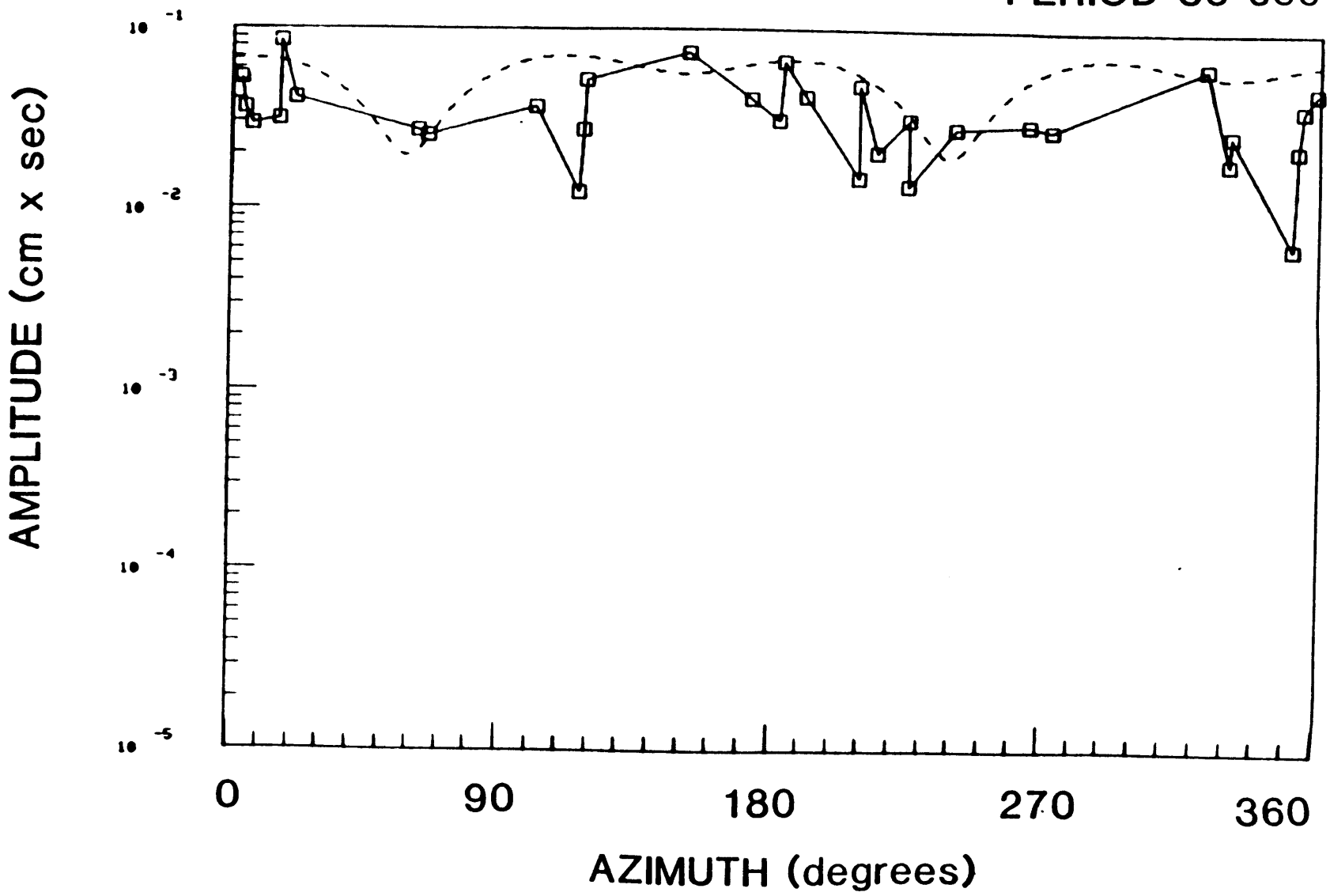
PERIOD 30 sec
AMPLITUDE (cm x sec)
10 -1
10 -2
10 -3
10 -4
10 -5
0
90
180
270
360
AZIMUTH (degrees)

FIGURE B.39C

PERIOD 50 sec

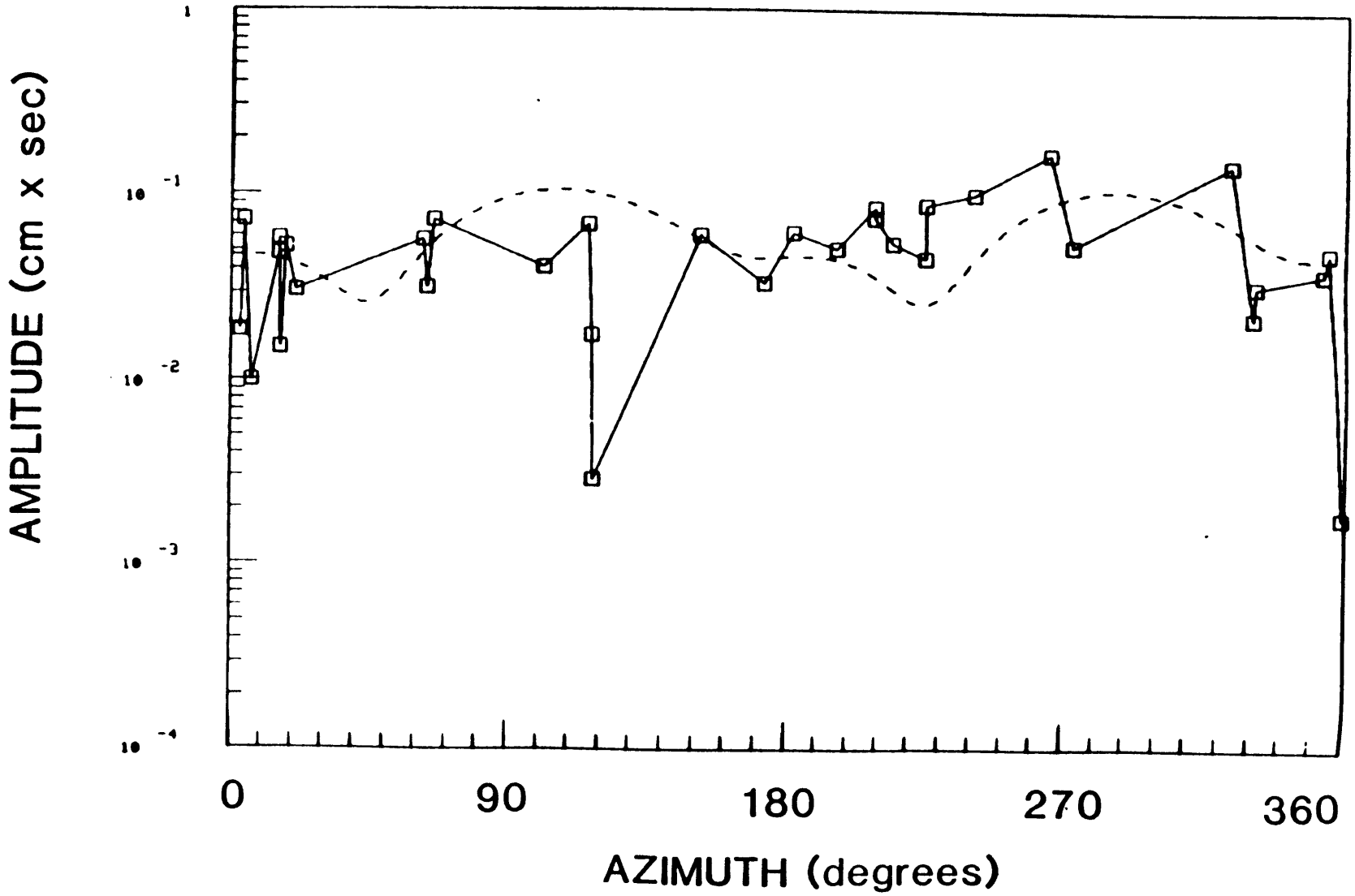

FIGURE B.39d

PERIOD 70 sec

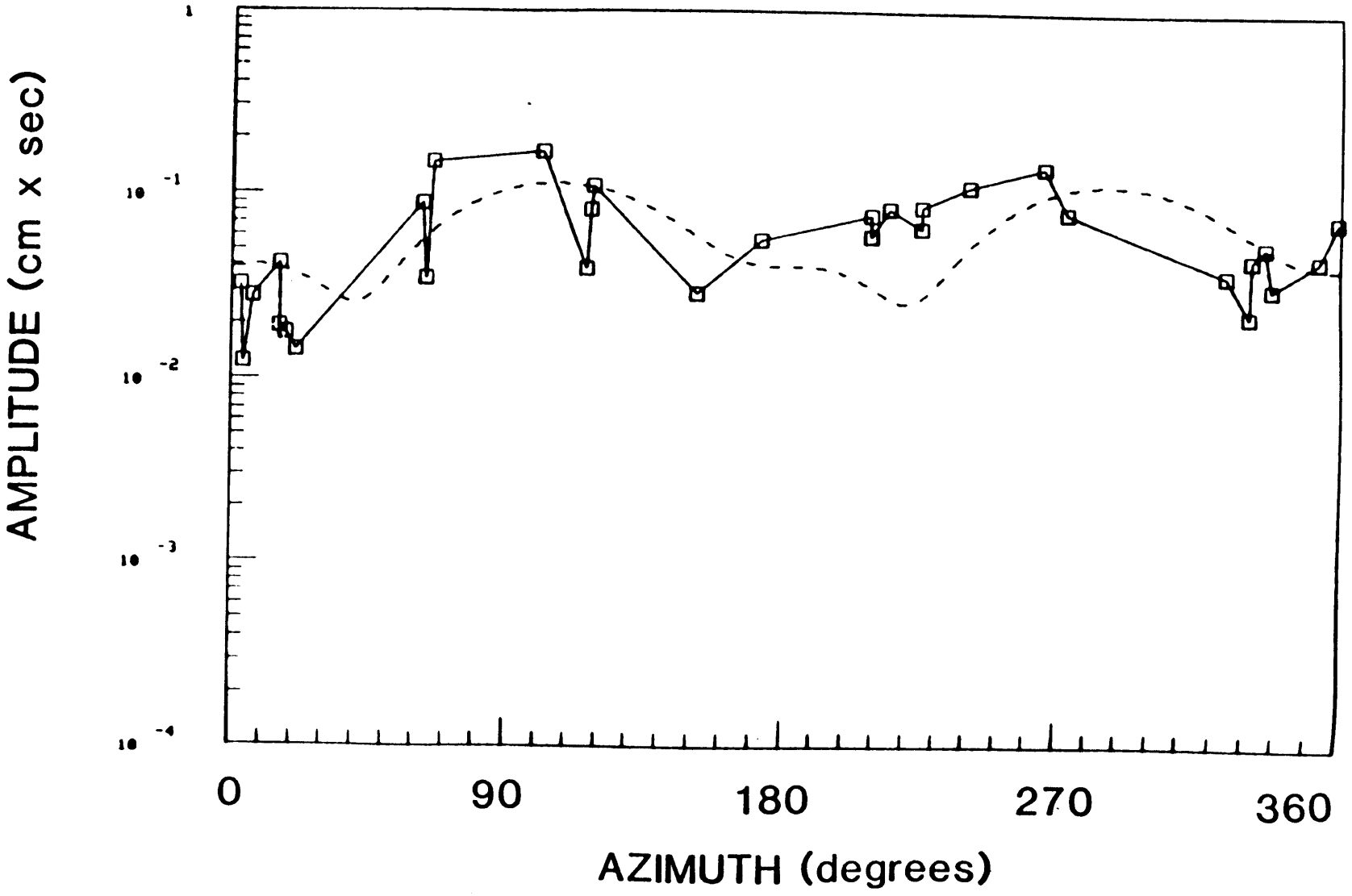

FIGURE B.39e

PERIOD 98 sec

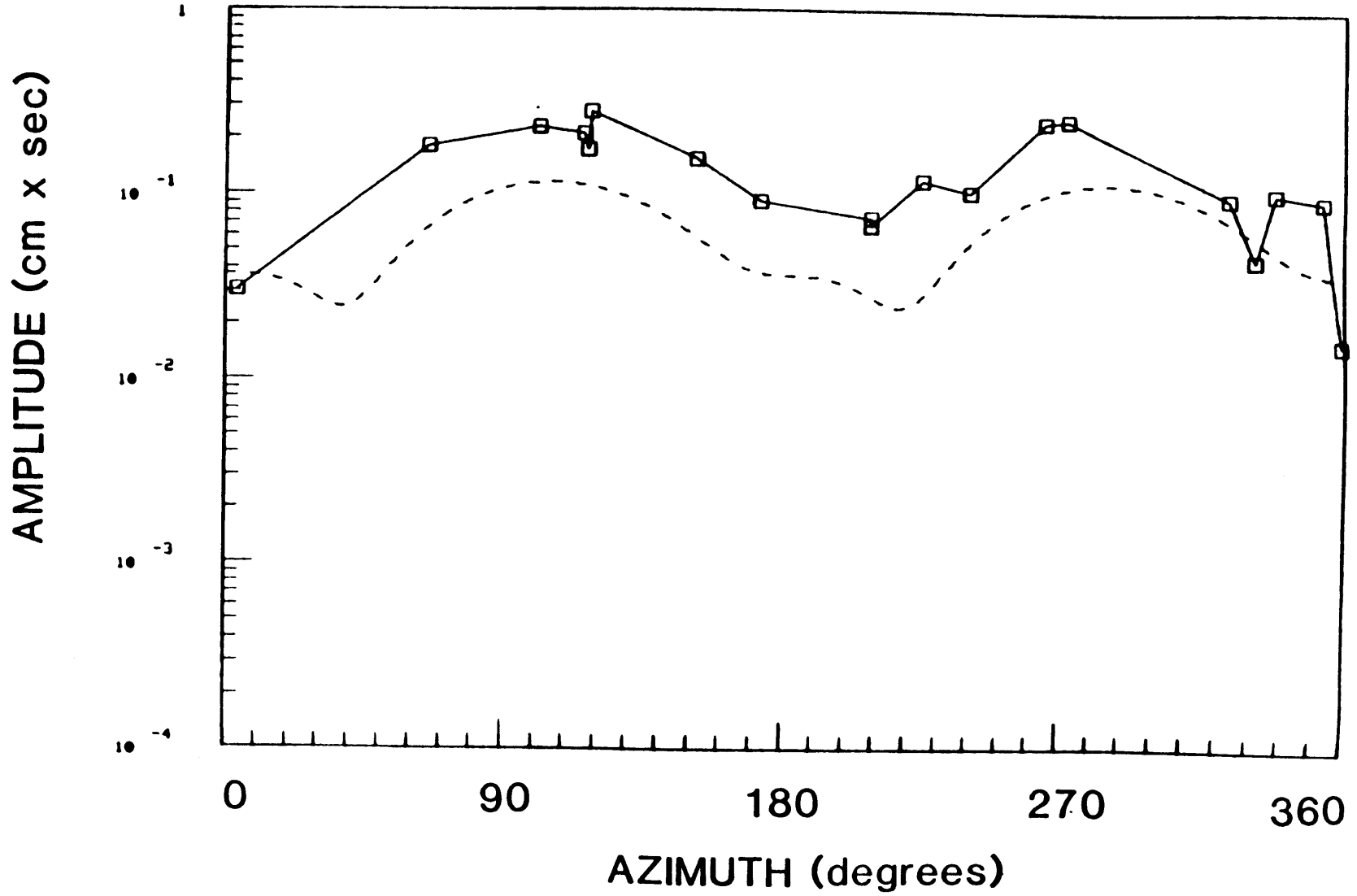

FIGURE B.40a

06/28/77

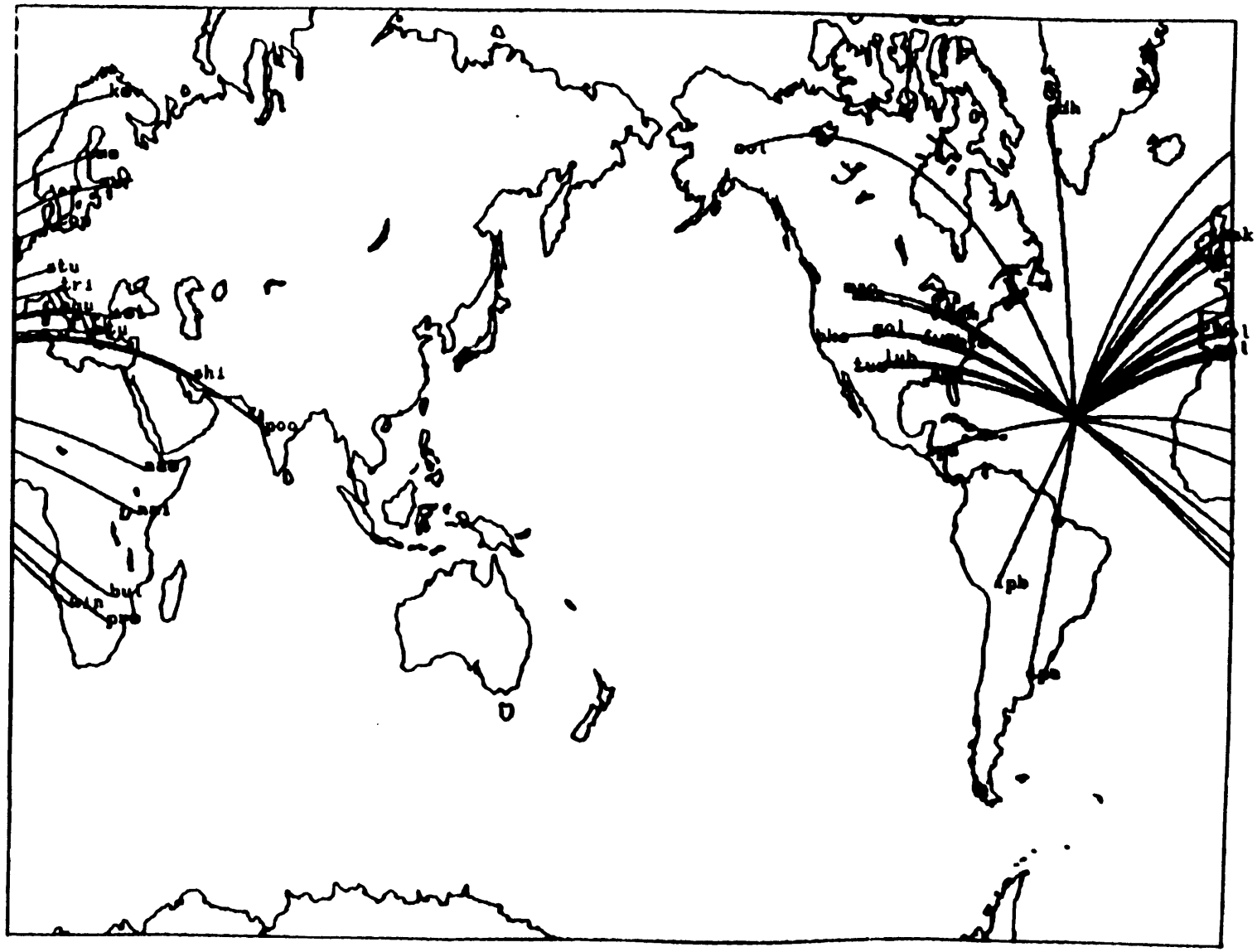

FIGURE B.40b

PERIOD 30 sec

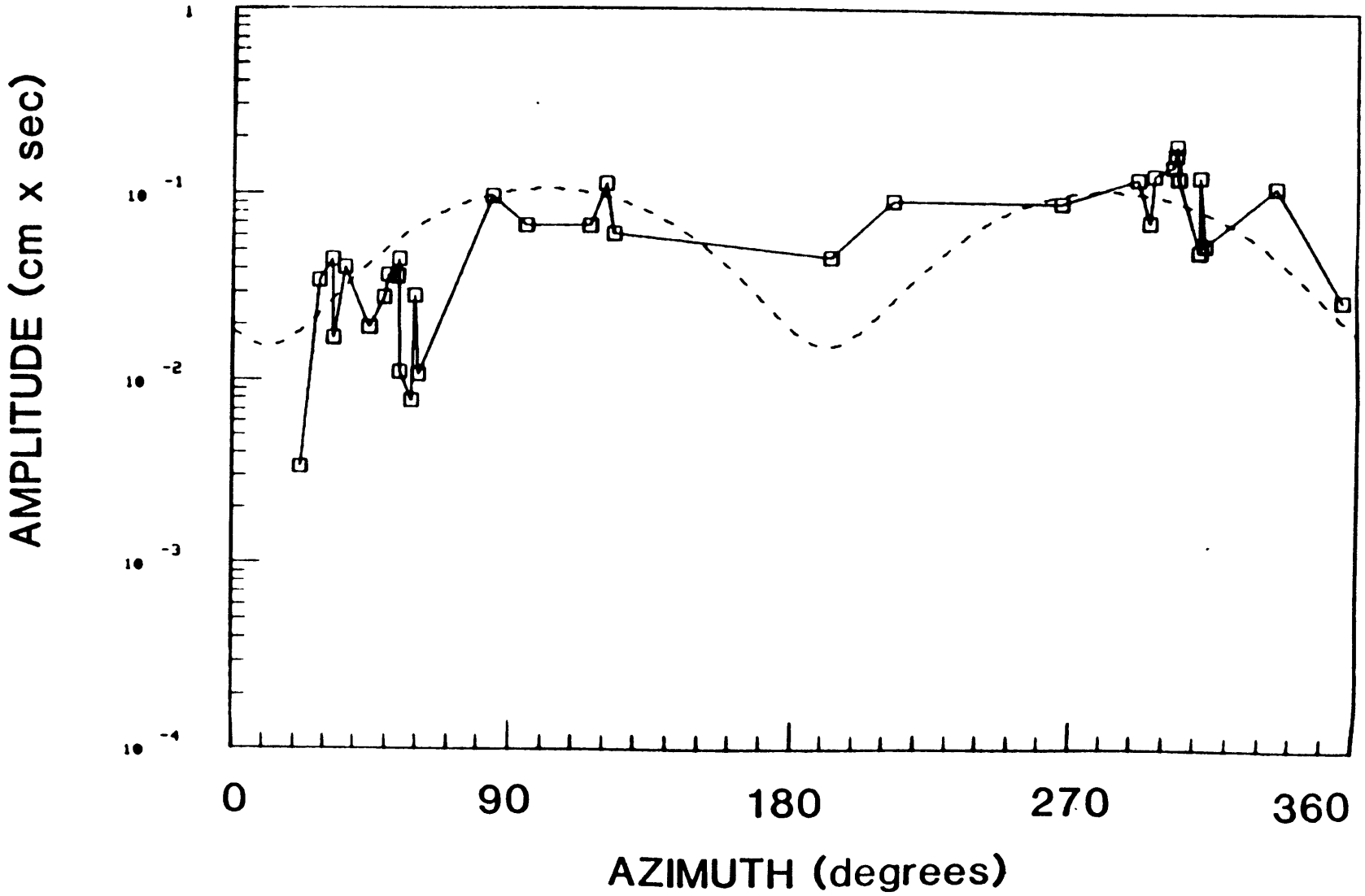

FIGURE B.40c

PERIOD 50 sec

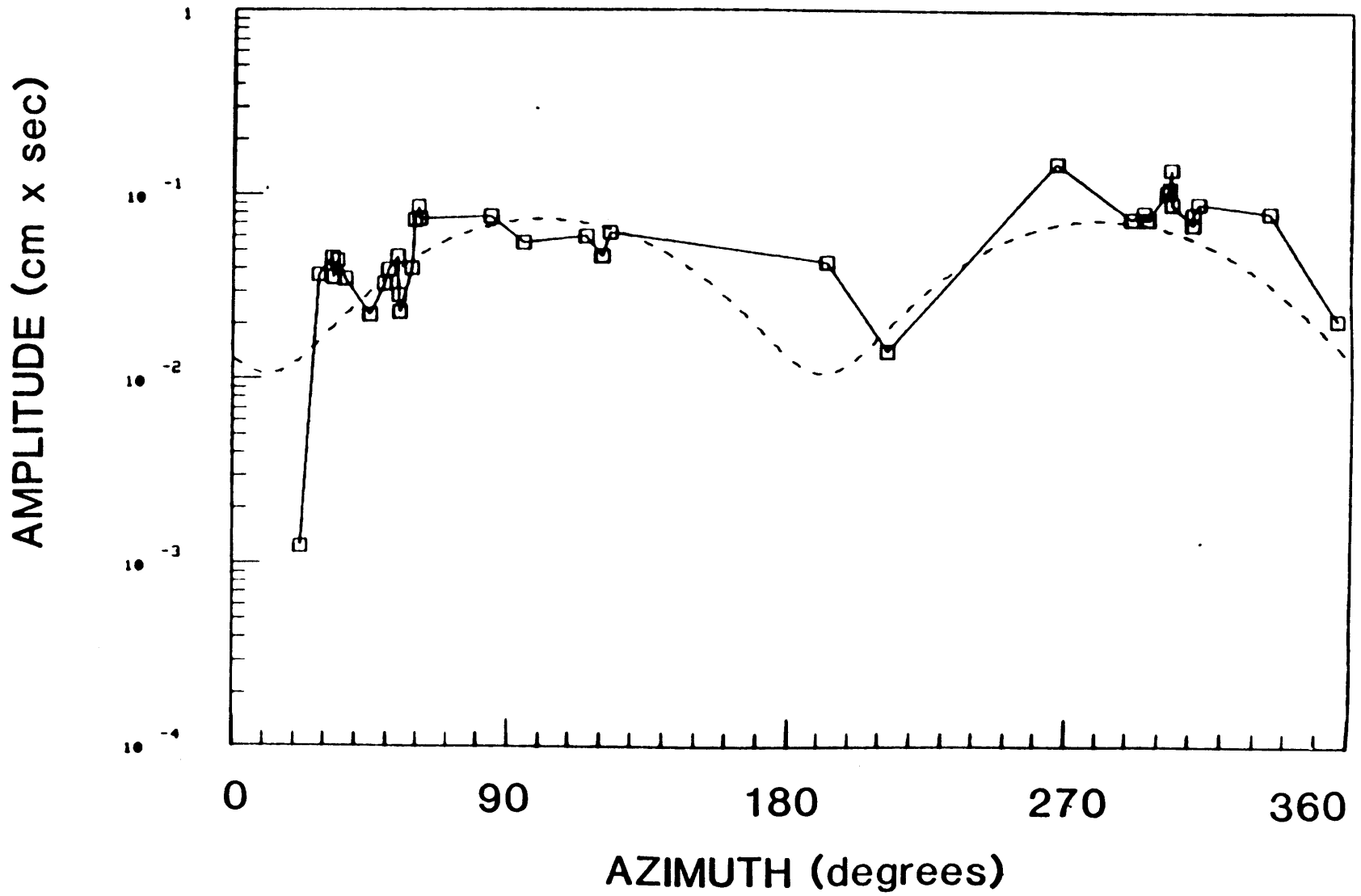

FIGURE B.40d

PERIOD 70 sec

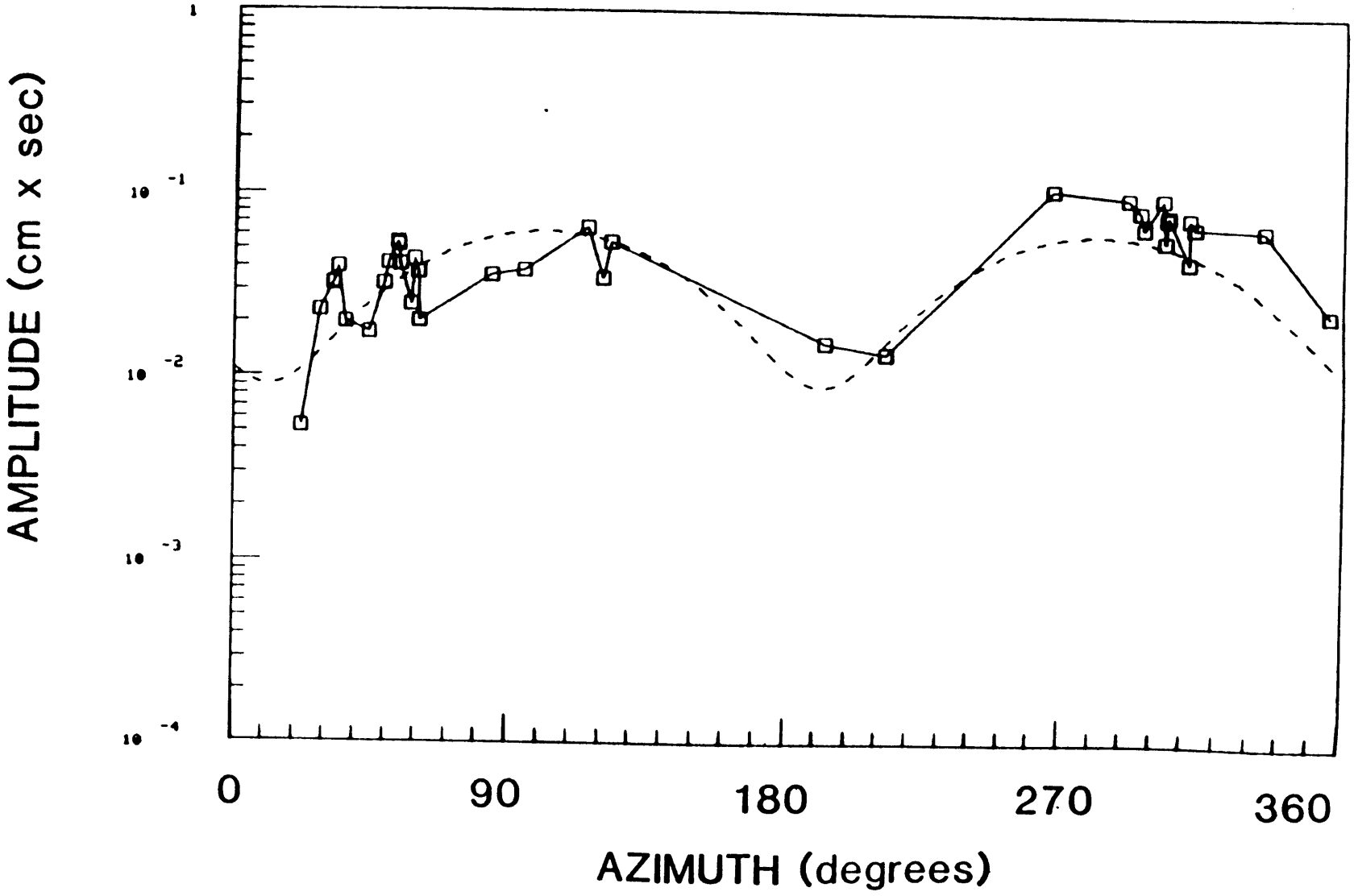

FIGURE B.40e

PERIOD 98 sec

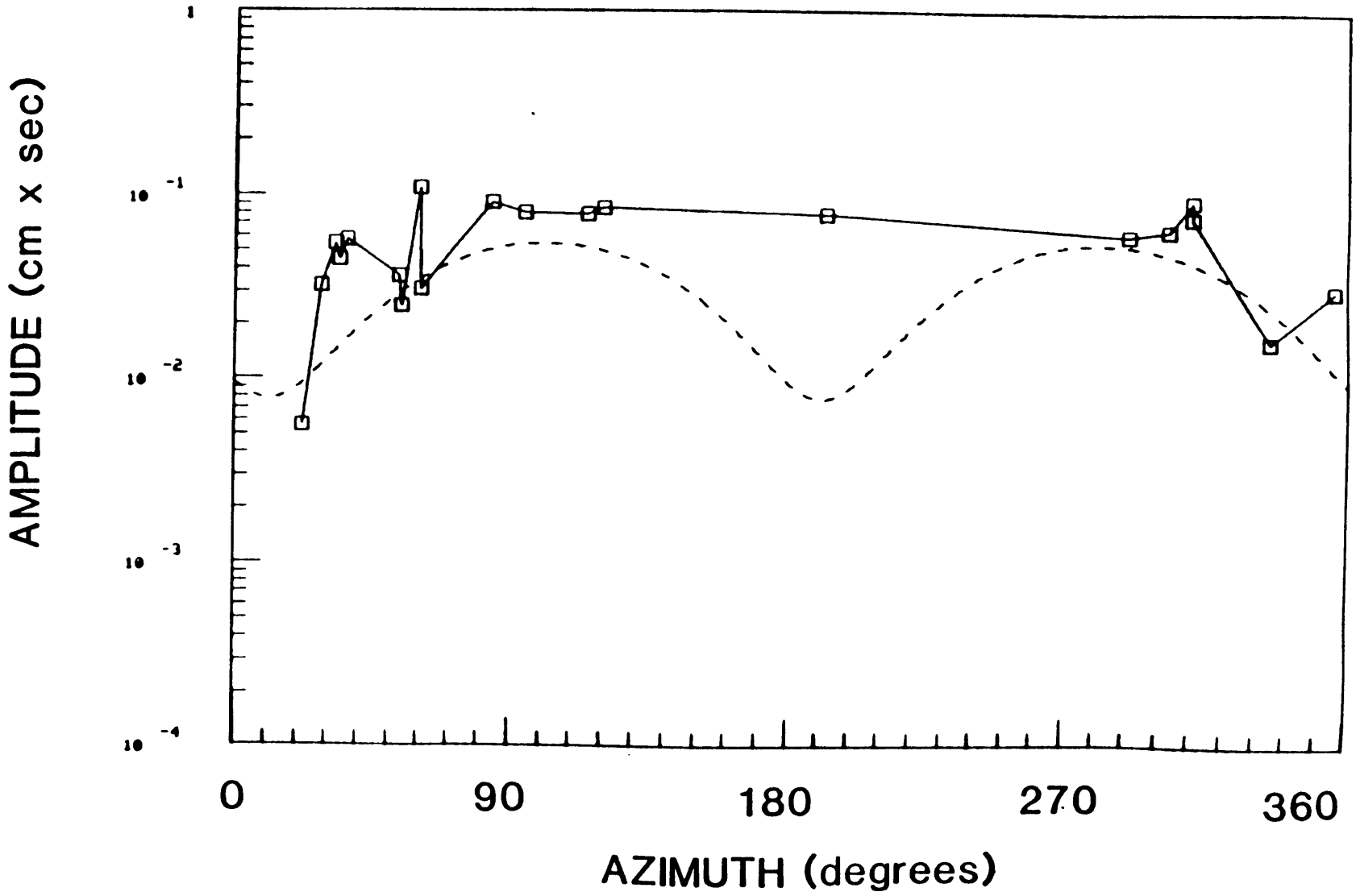

FIGURE B.41a

08/26/77

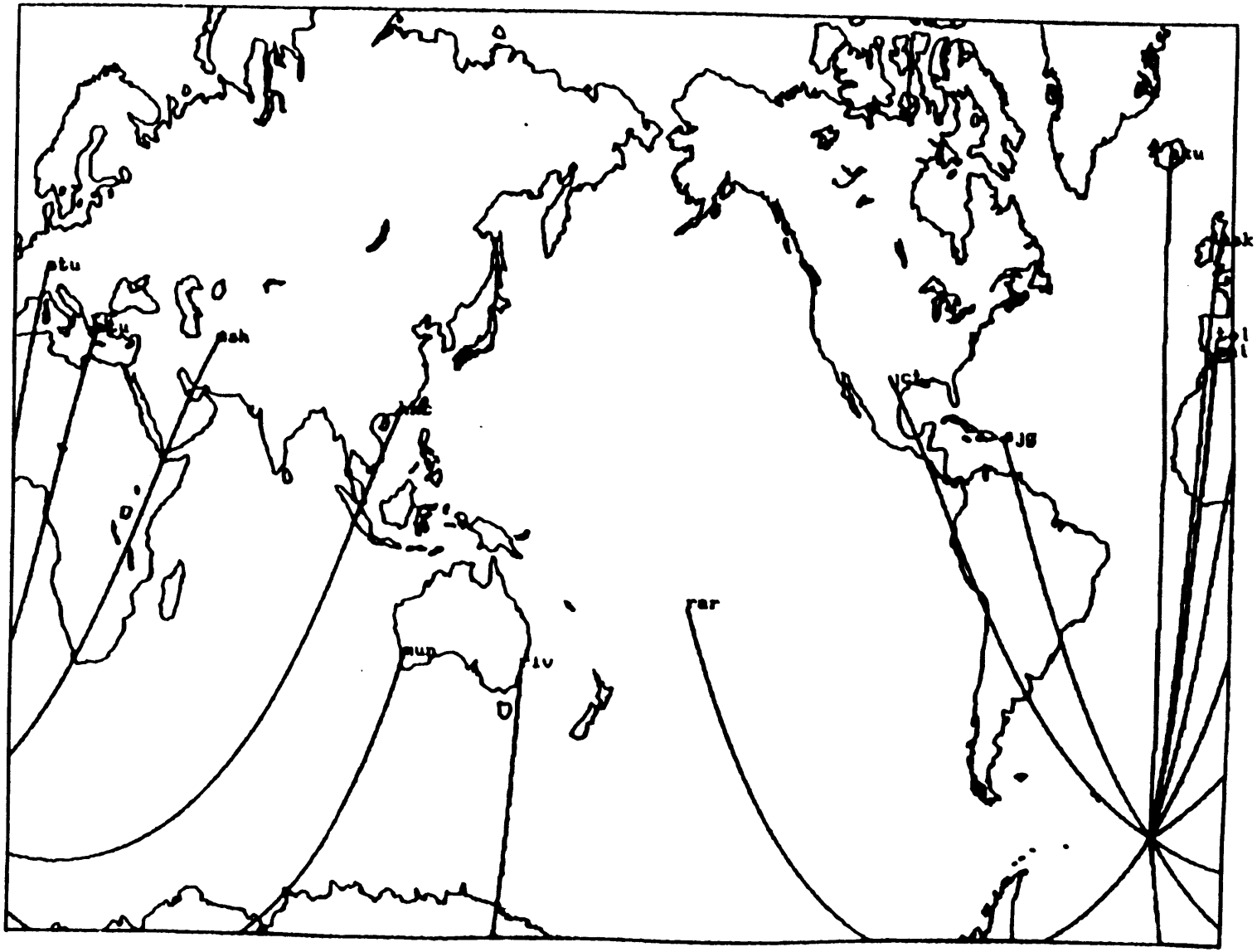

FIGURE B.41b

PERIOD 30 sec

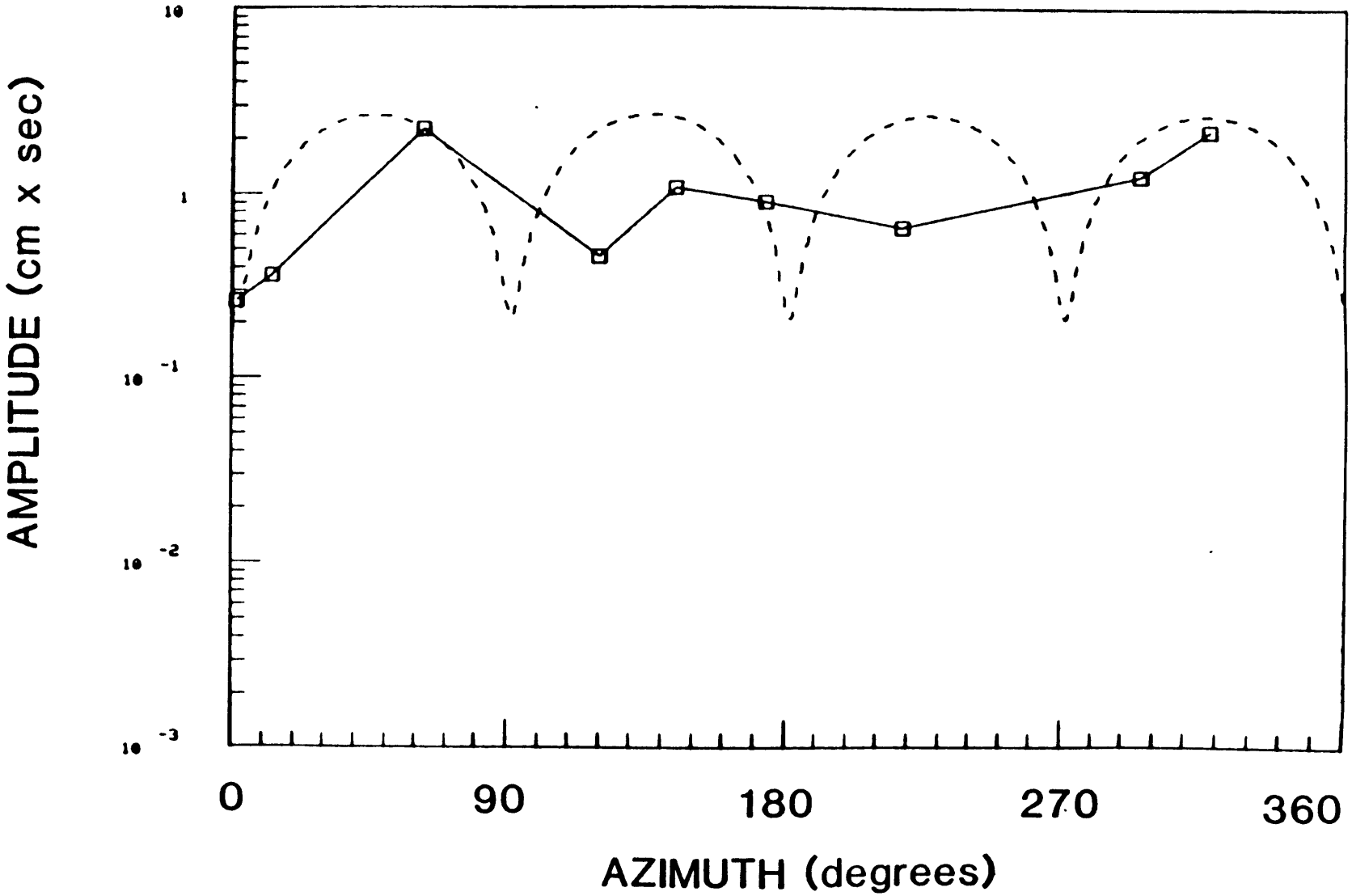

FIGURE B.41C

PERIOD 50 sec

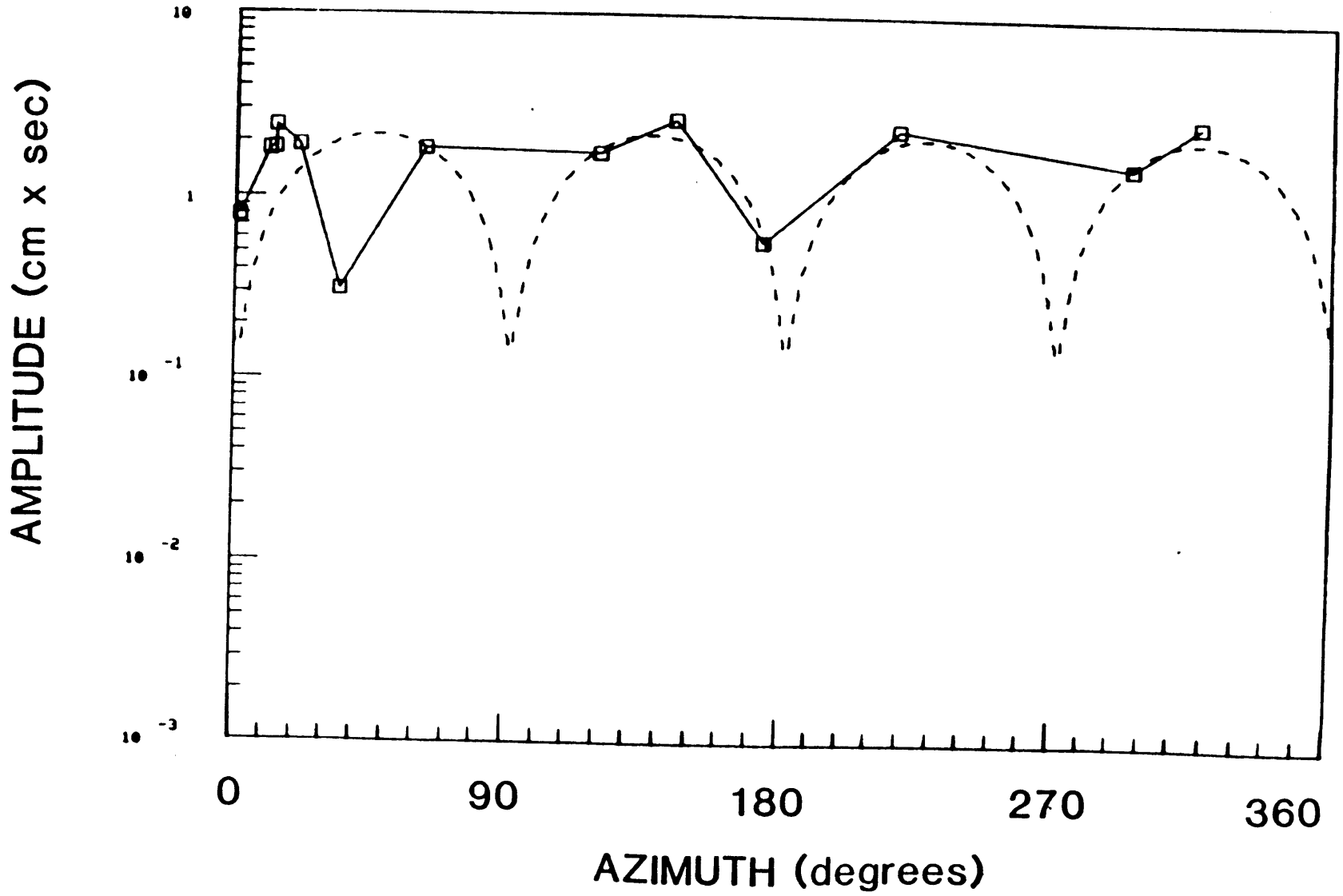

FIGURE B.41d

PERIOD 70 sec

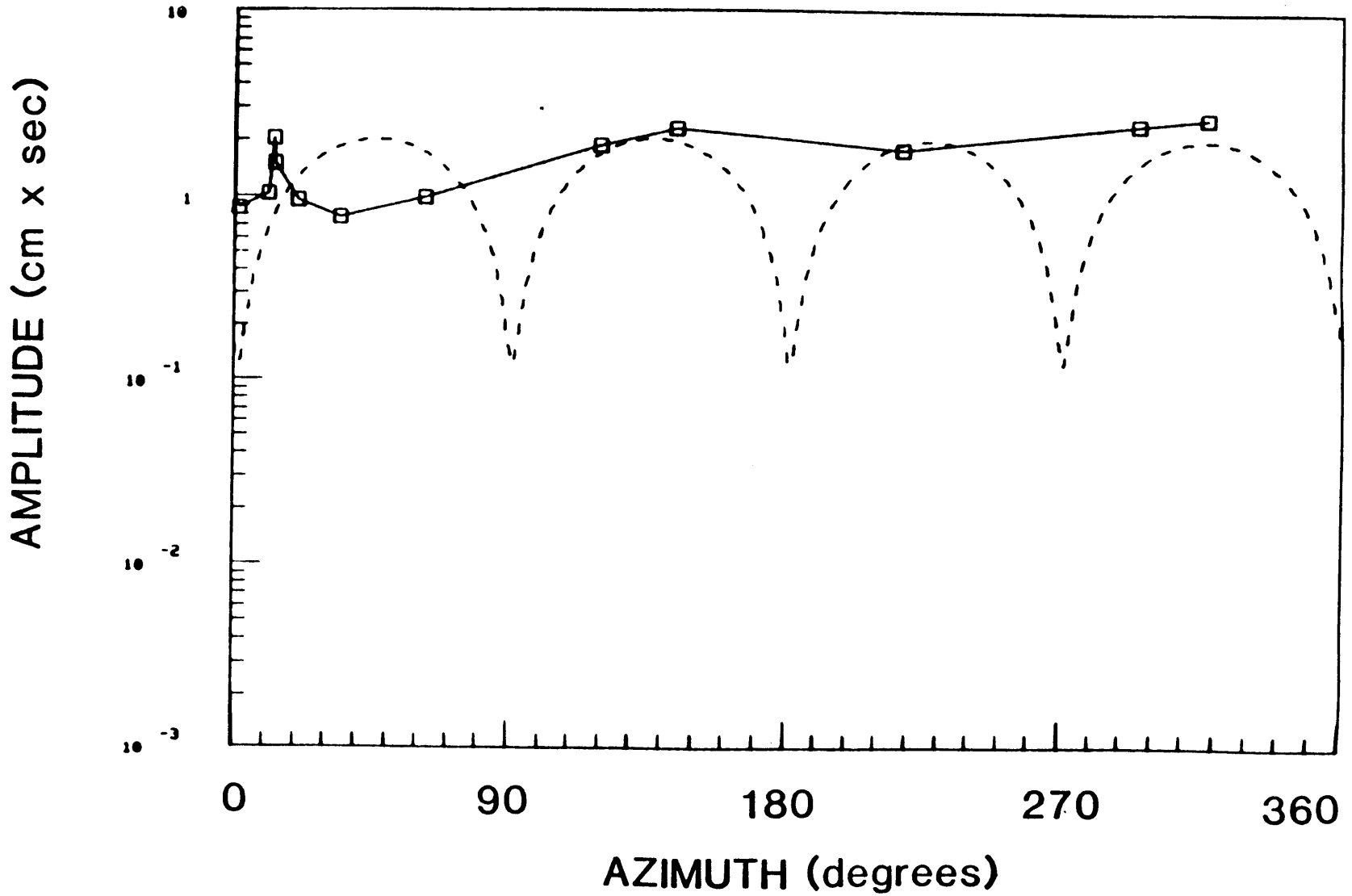

FIGURE B.41e

PERIOD 98 sec

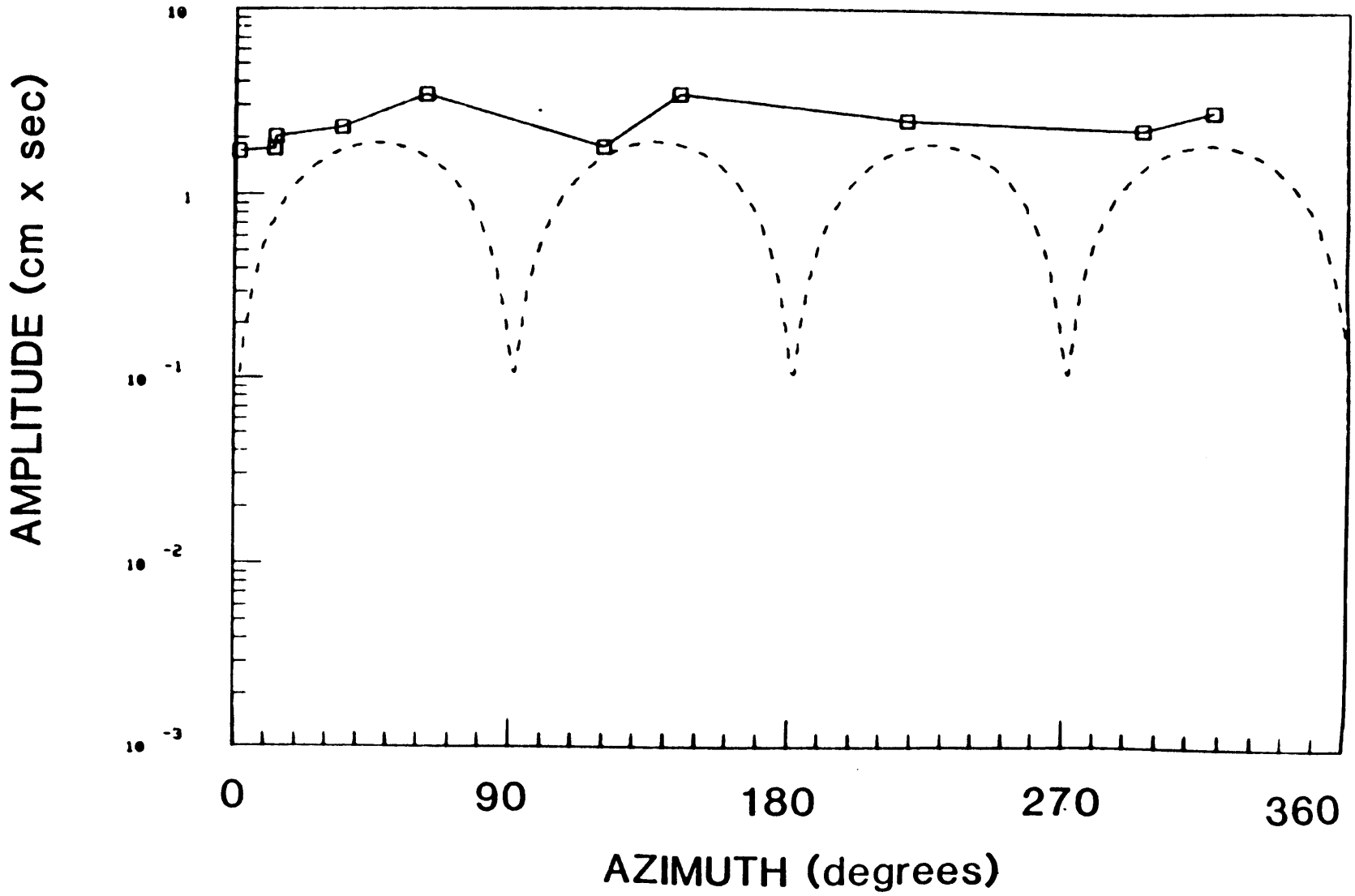

FIGURE B.42a

10/17/77

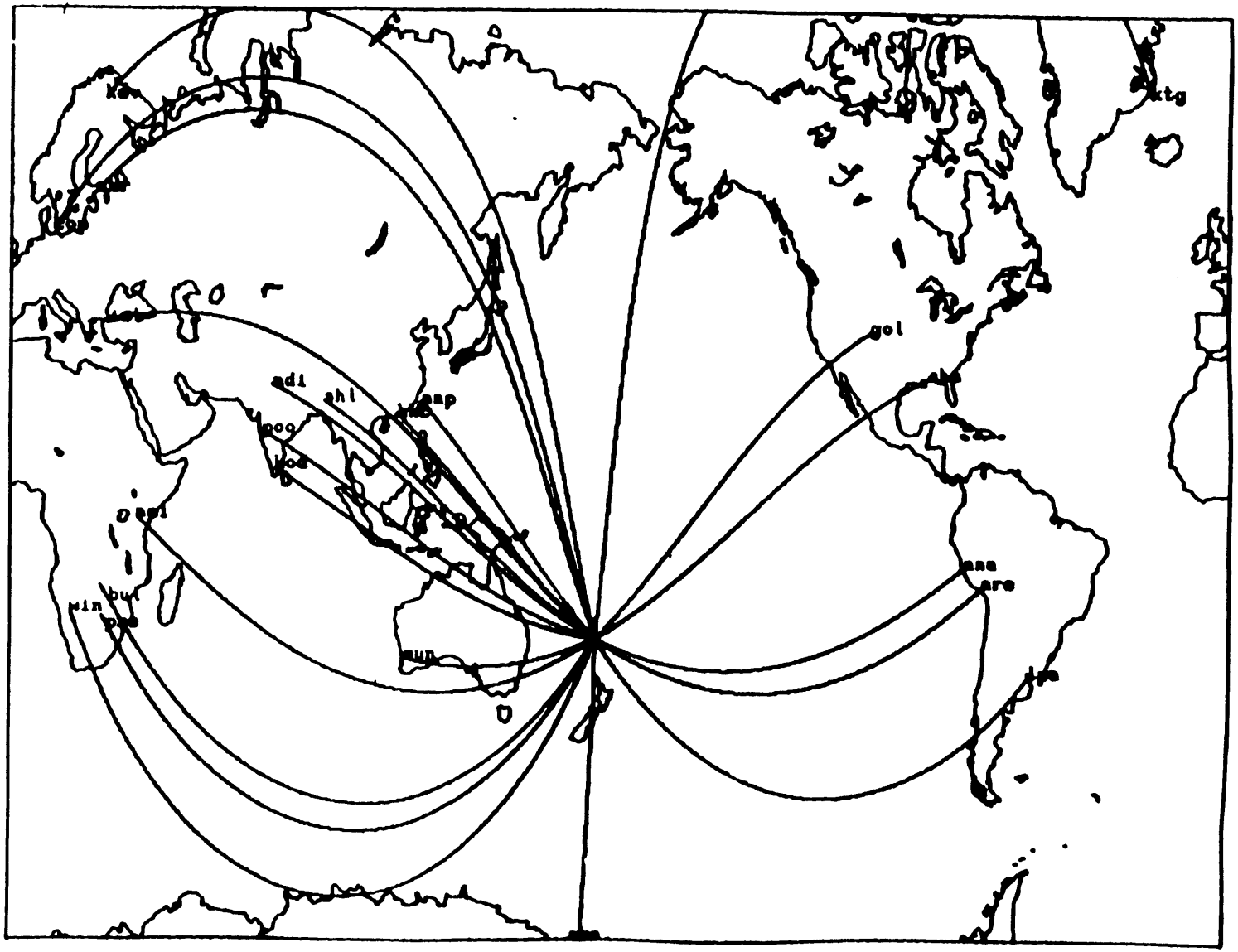

FIGURE B.42b

PERIOD 30 sec

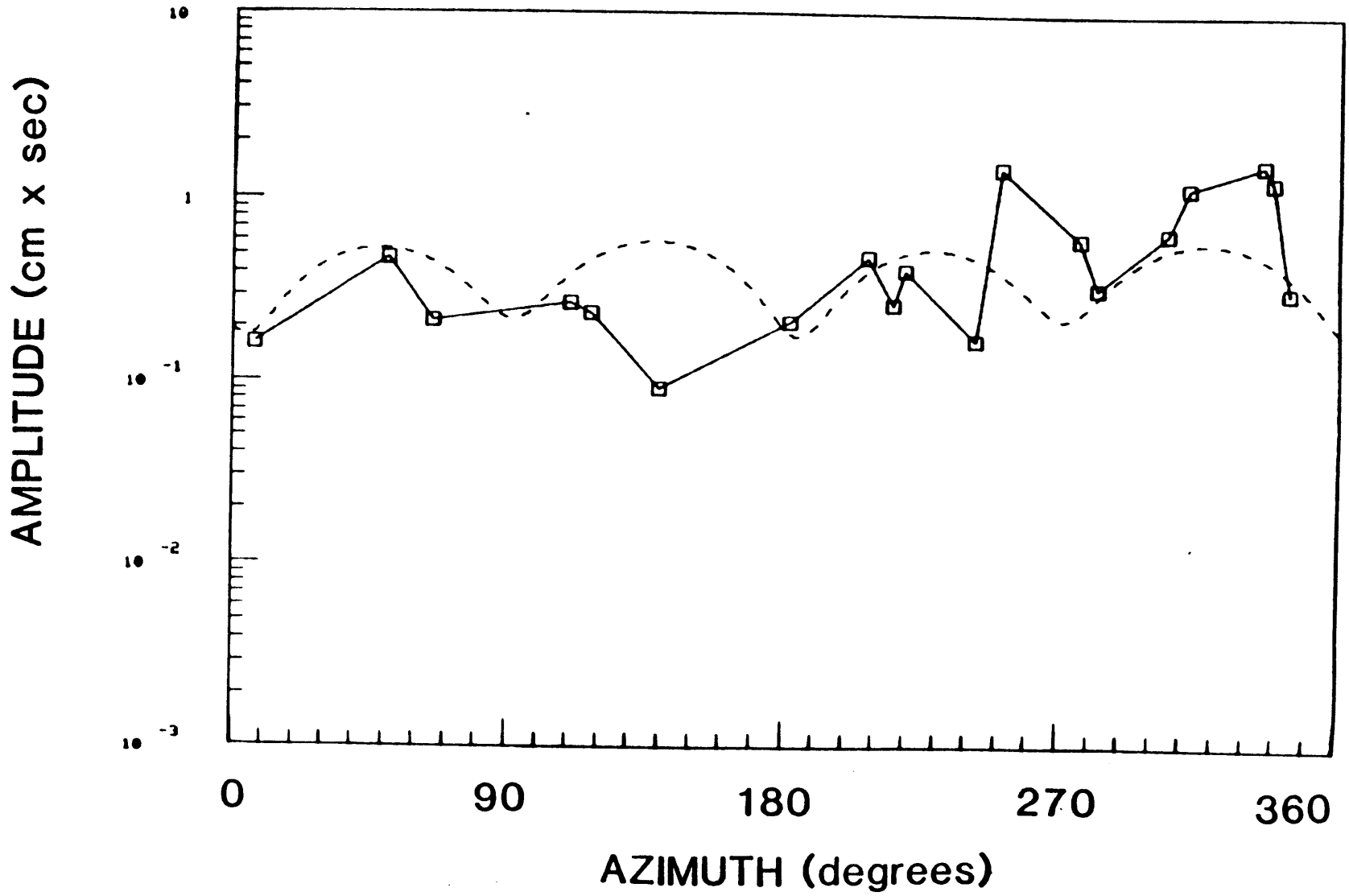

FIGURE B.42c

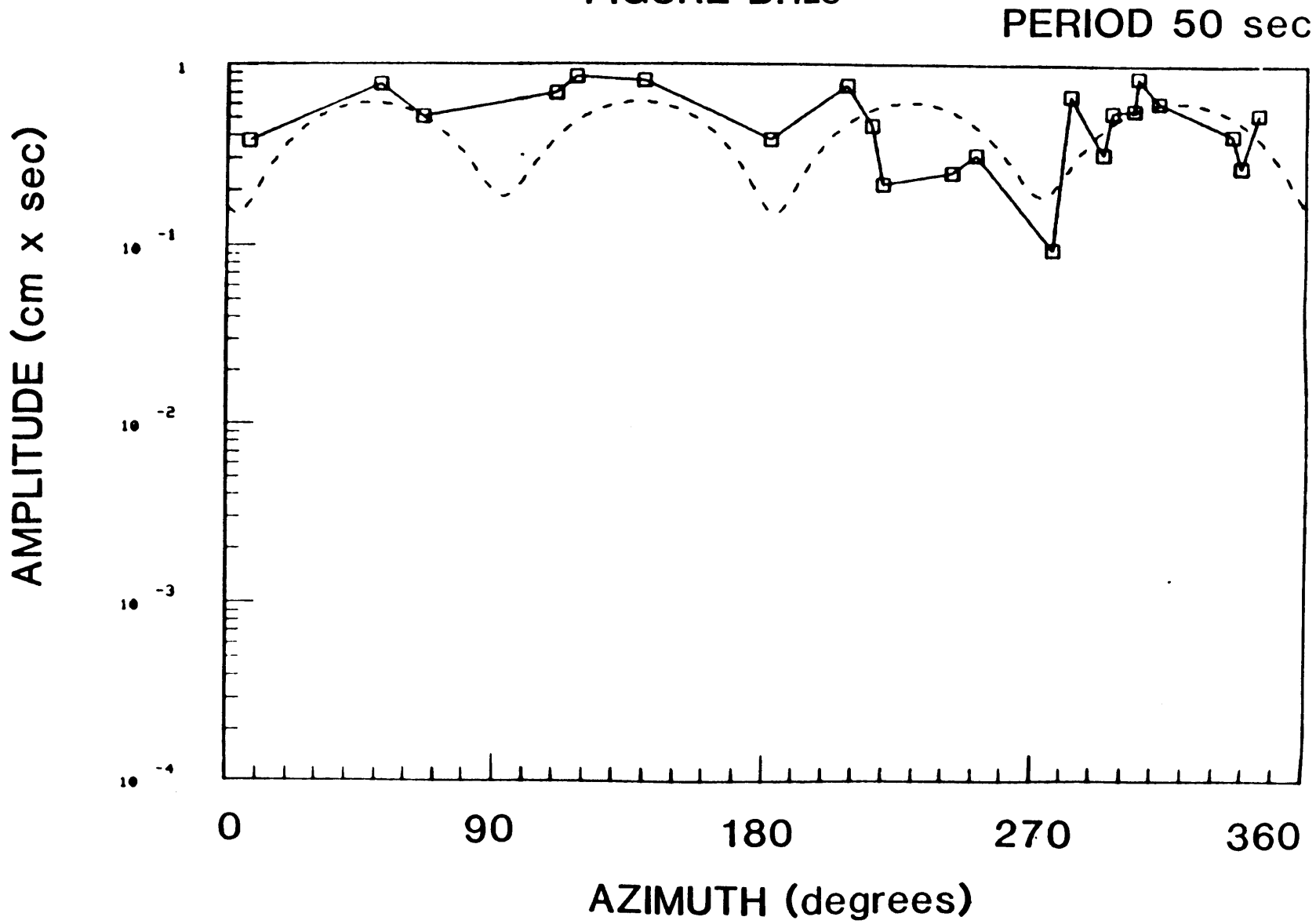
PERIOD 50 sec
AMPLITUDE (cm x sec)
1
10 -1
10 -2
10 -3
10 -4
0
90
180
270
360
AZIMUTH (degrees)

FIGURE B.42d

PERIOD 70 sec

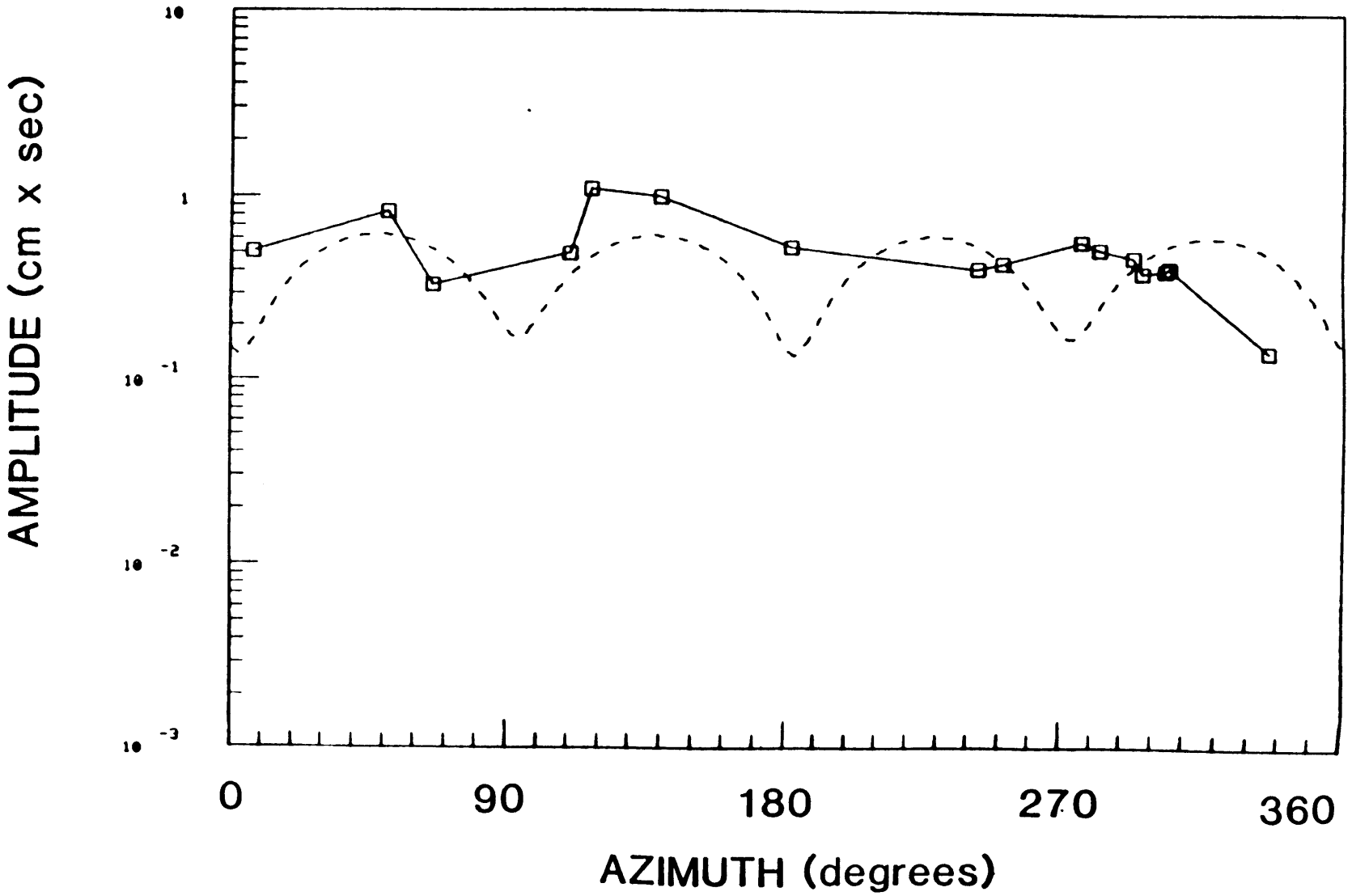

FIGURE B.42e

PERIOD 98 sec

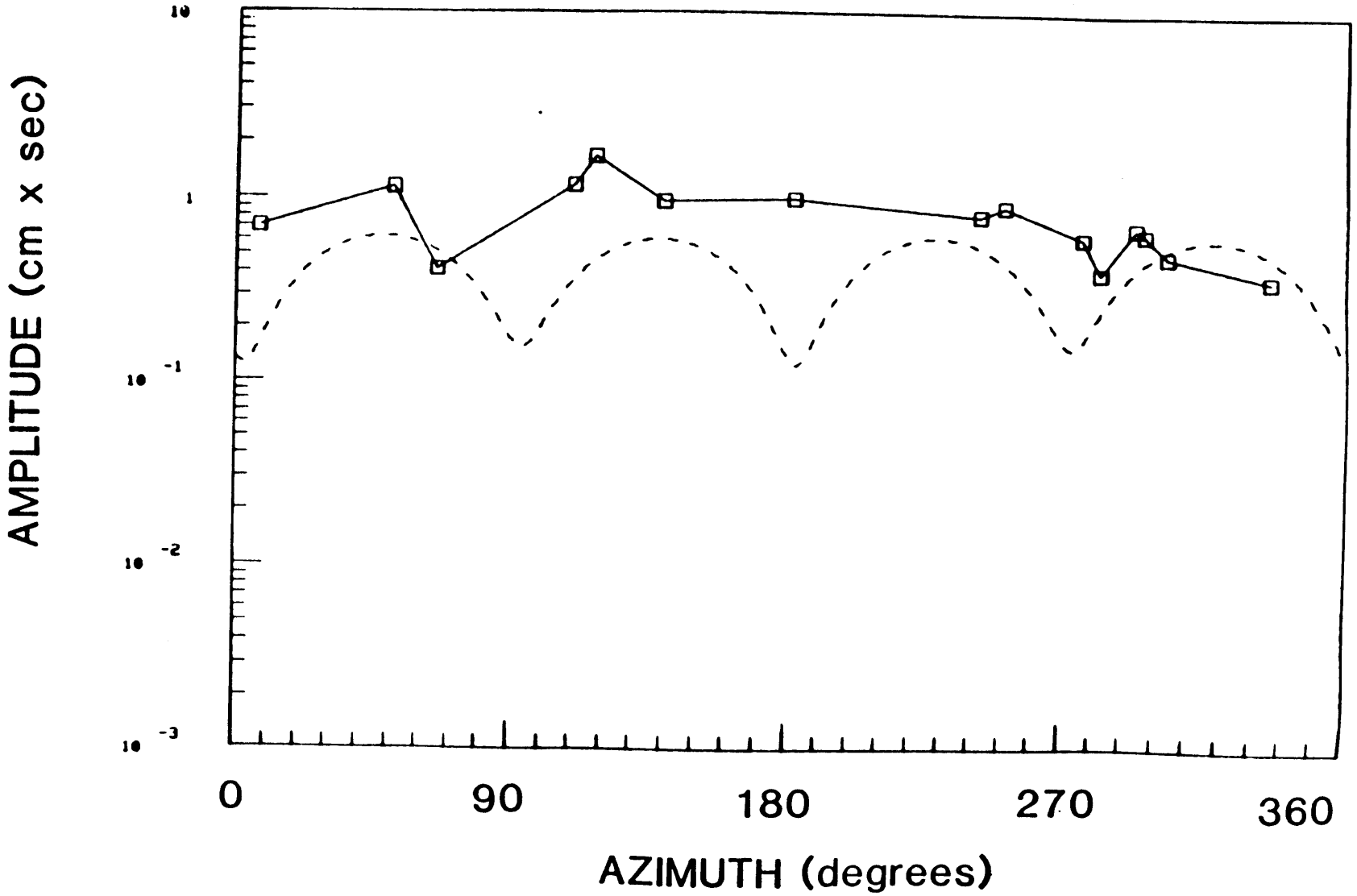

FIGURE B.43a

12/13/77

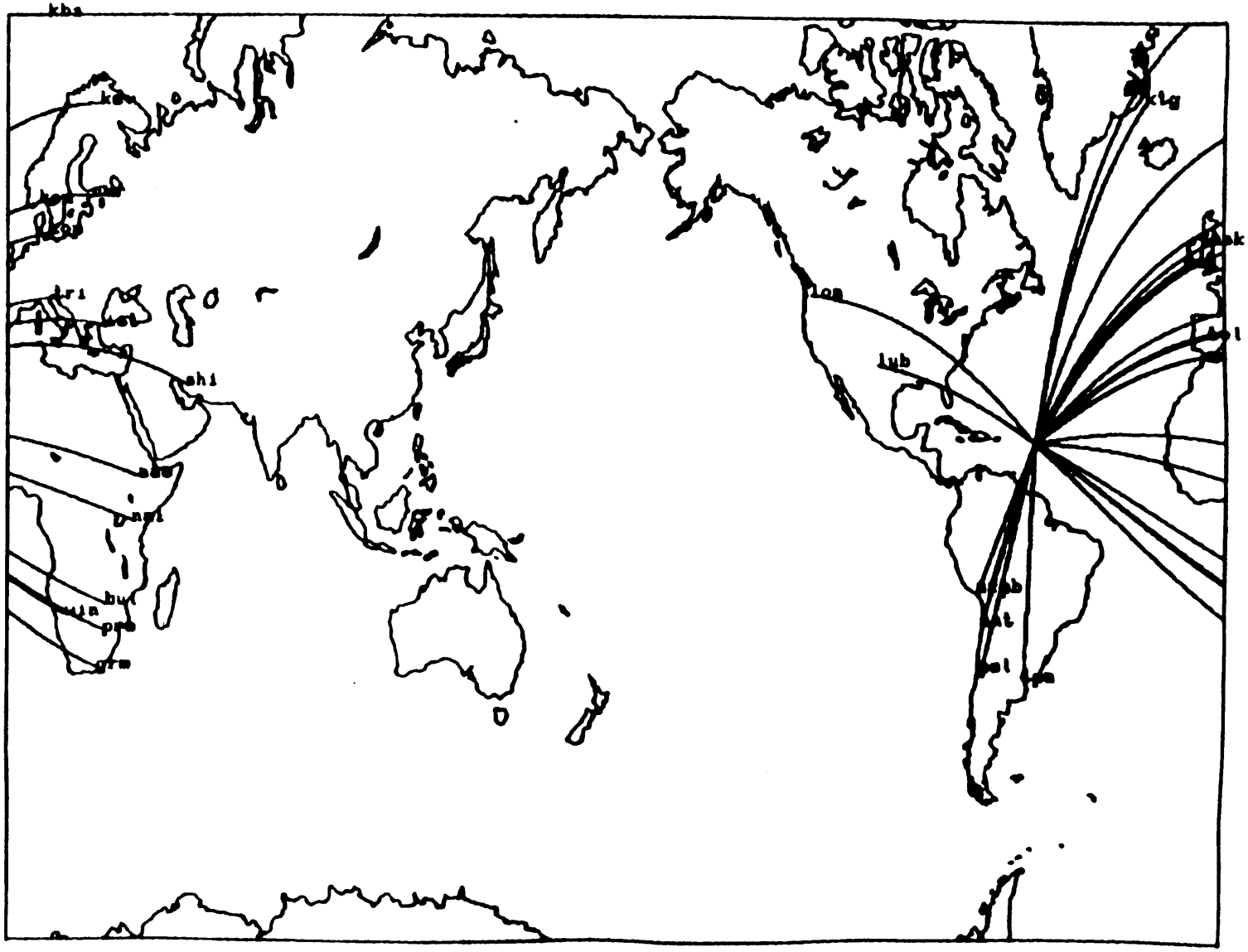

FIGURE B.43b

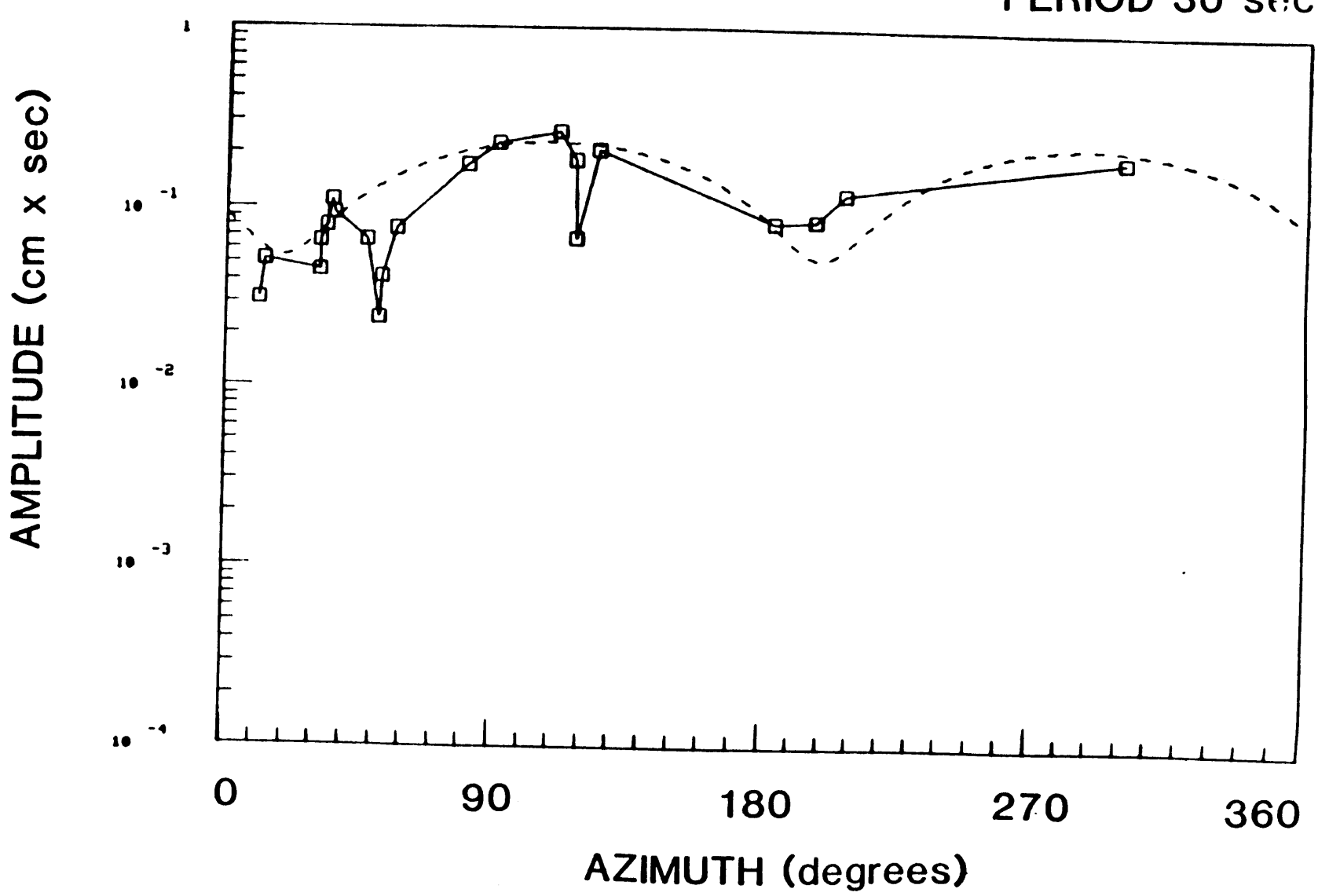
PERIOD 30 sec
AMPLITUDE (cm x sec)
1
10 -1
10 -2
10 -3
10 -4
0
90
180
270
360
AZIMUTH (degrees)

FIGURE B.43c

PERIOD 50 sec

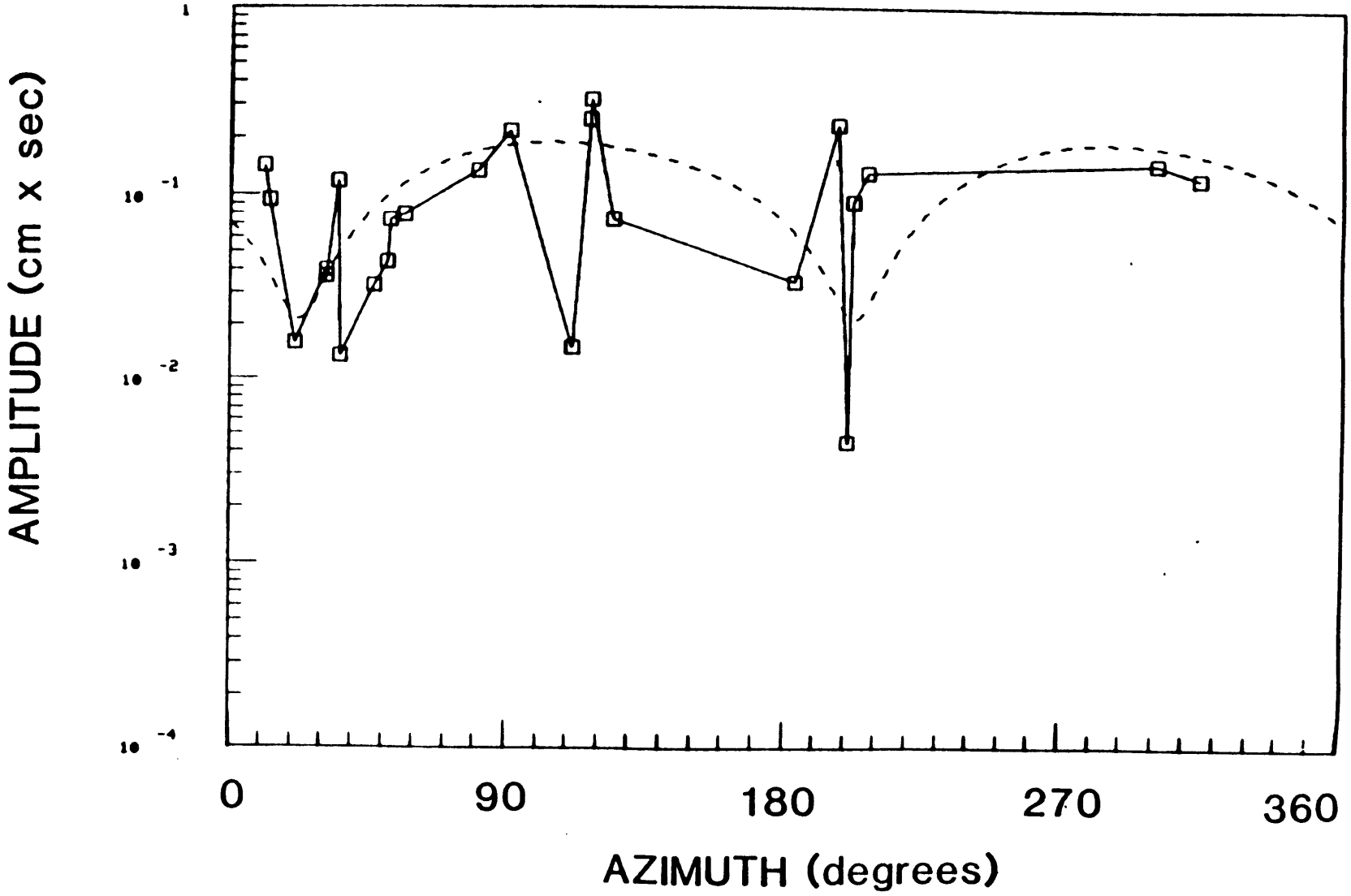

FIGURE B.43d

PERIOD 70 sec

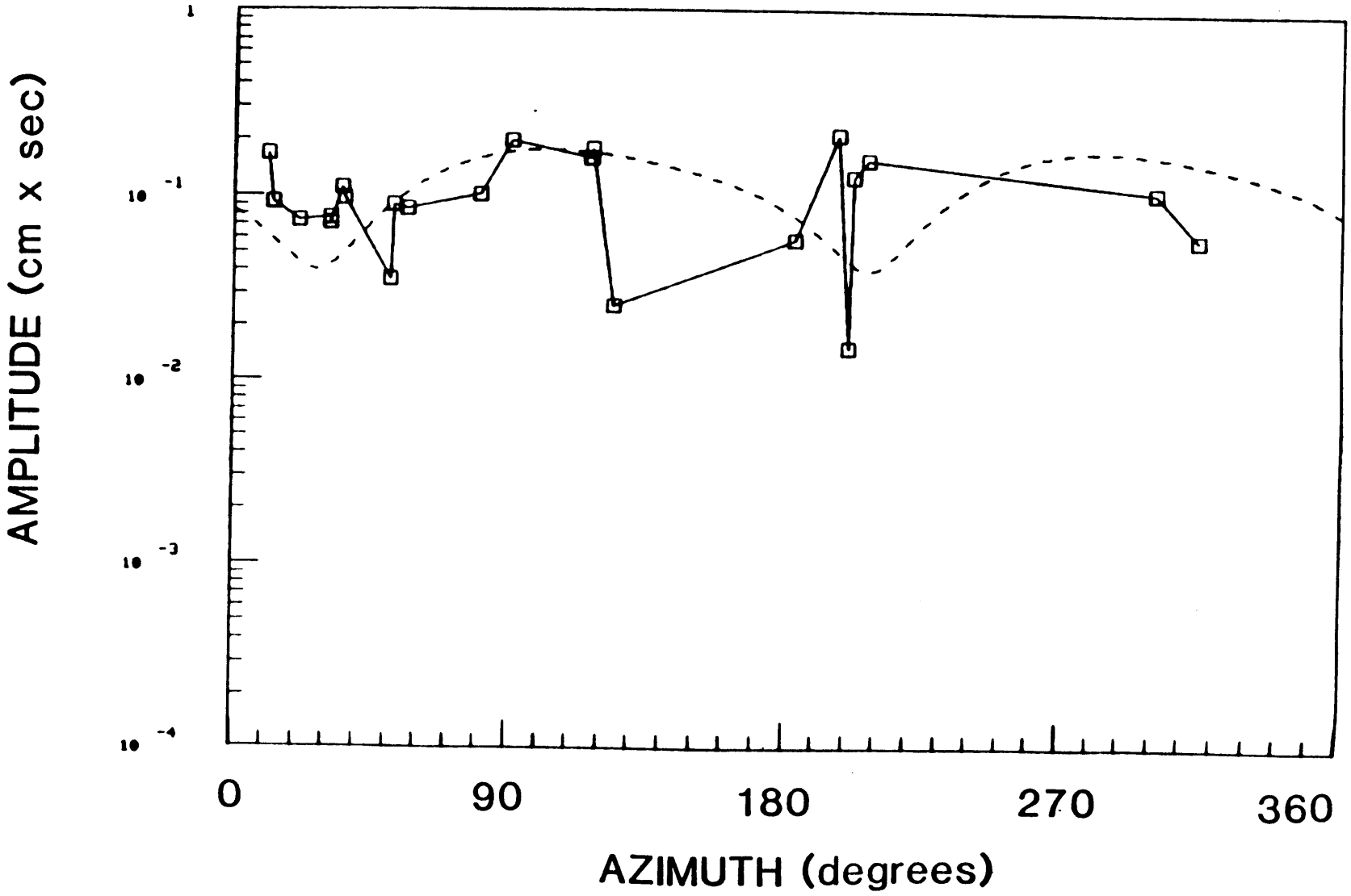

FIGURE B.43e

PERIOD 98 sec

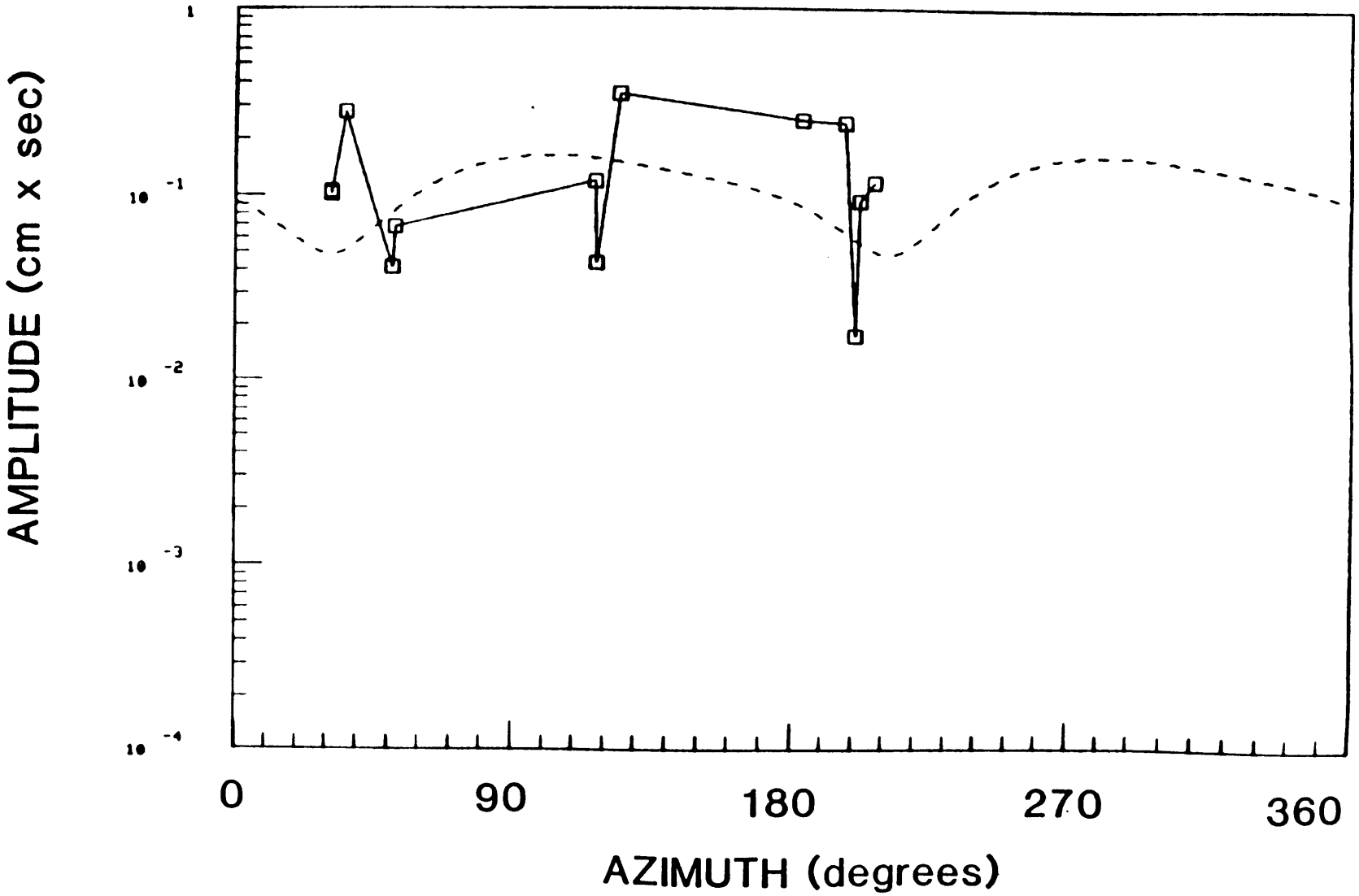

FIGURE B.44a 03/24/78

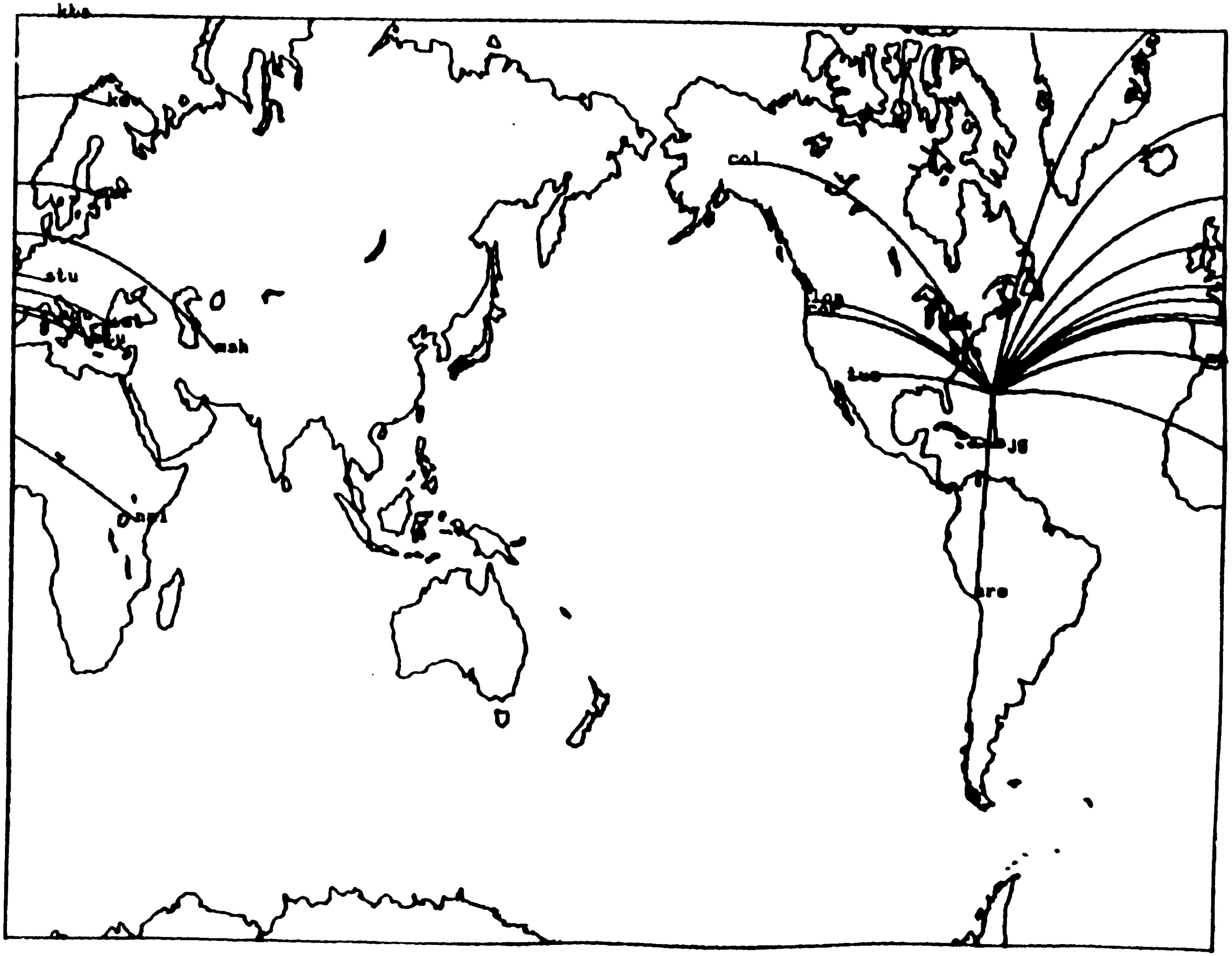

FIGURE B.44b

PERIOD 30 sec

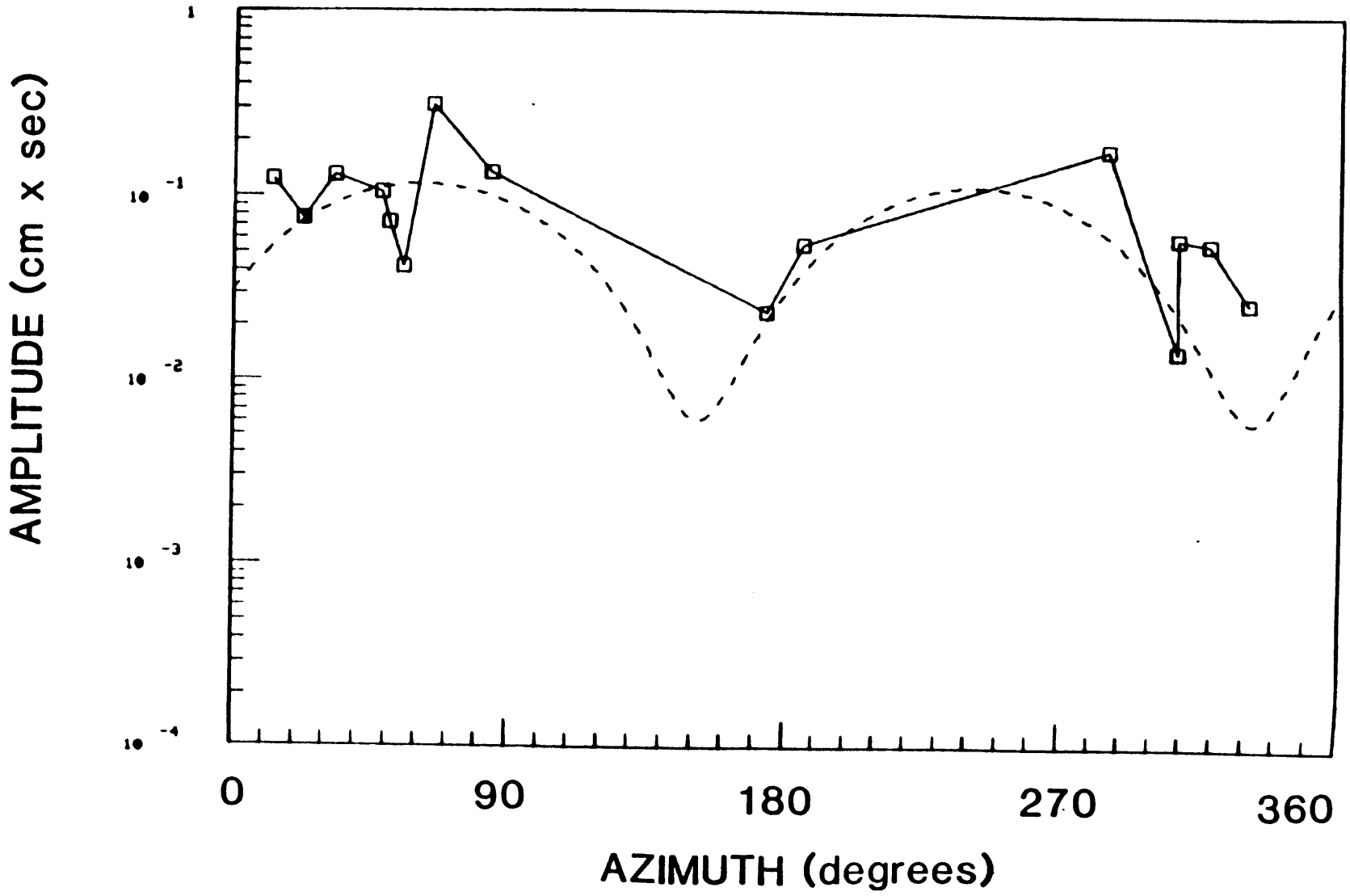

FIGURE B.44c

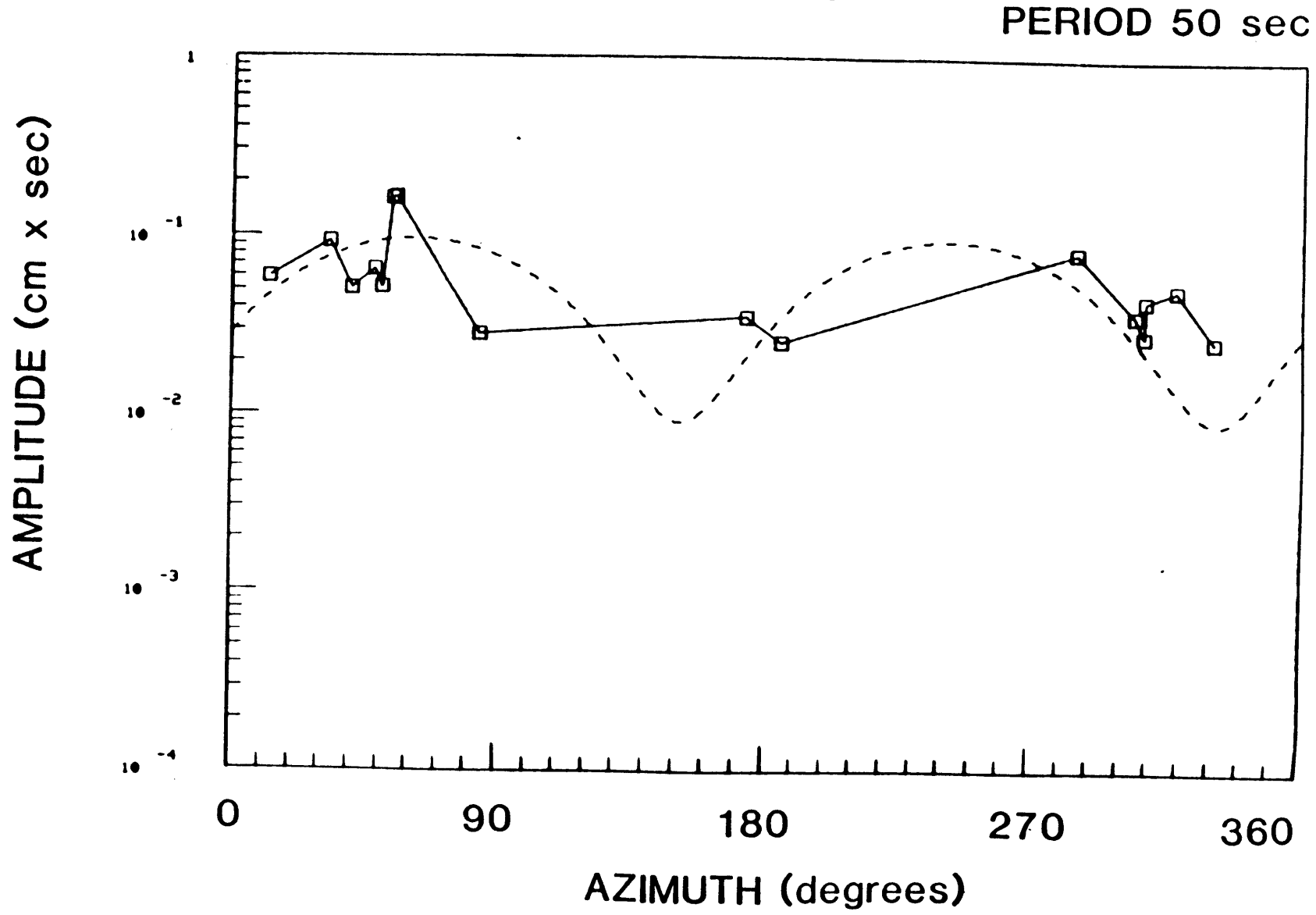
PERIOD 50 sec
AMPLITUDE (cm x sec)
1
10 -1
10 -2
10 -3
10 -4
0
90
180
270
360
AZIMUTH (degrees)

FIGURE B.44d

PERIOD 70 sec

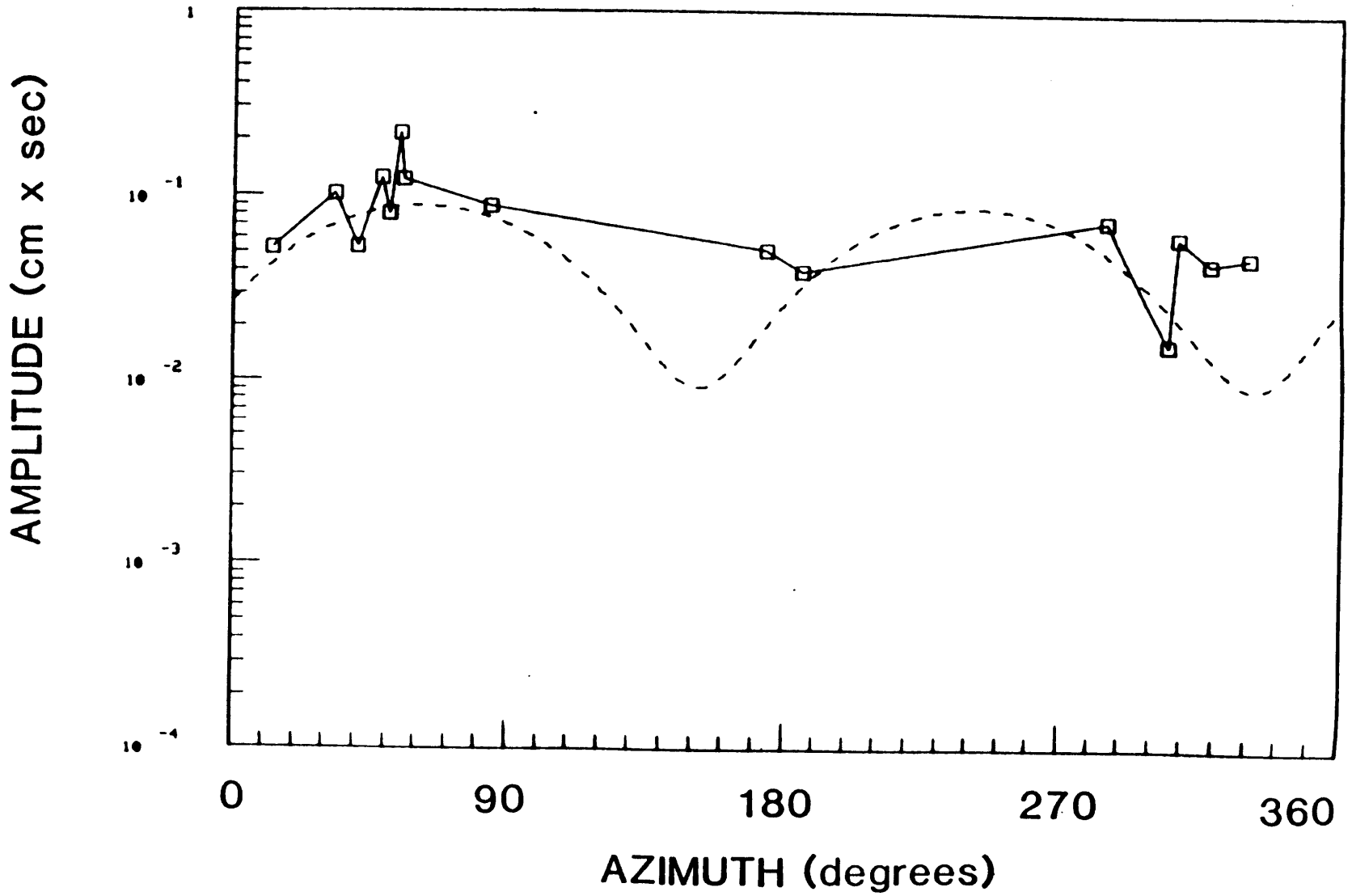

FIGURE B.44e

PERIOD 98 sec

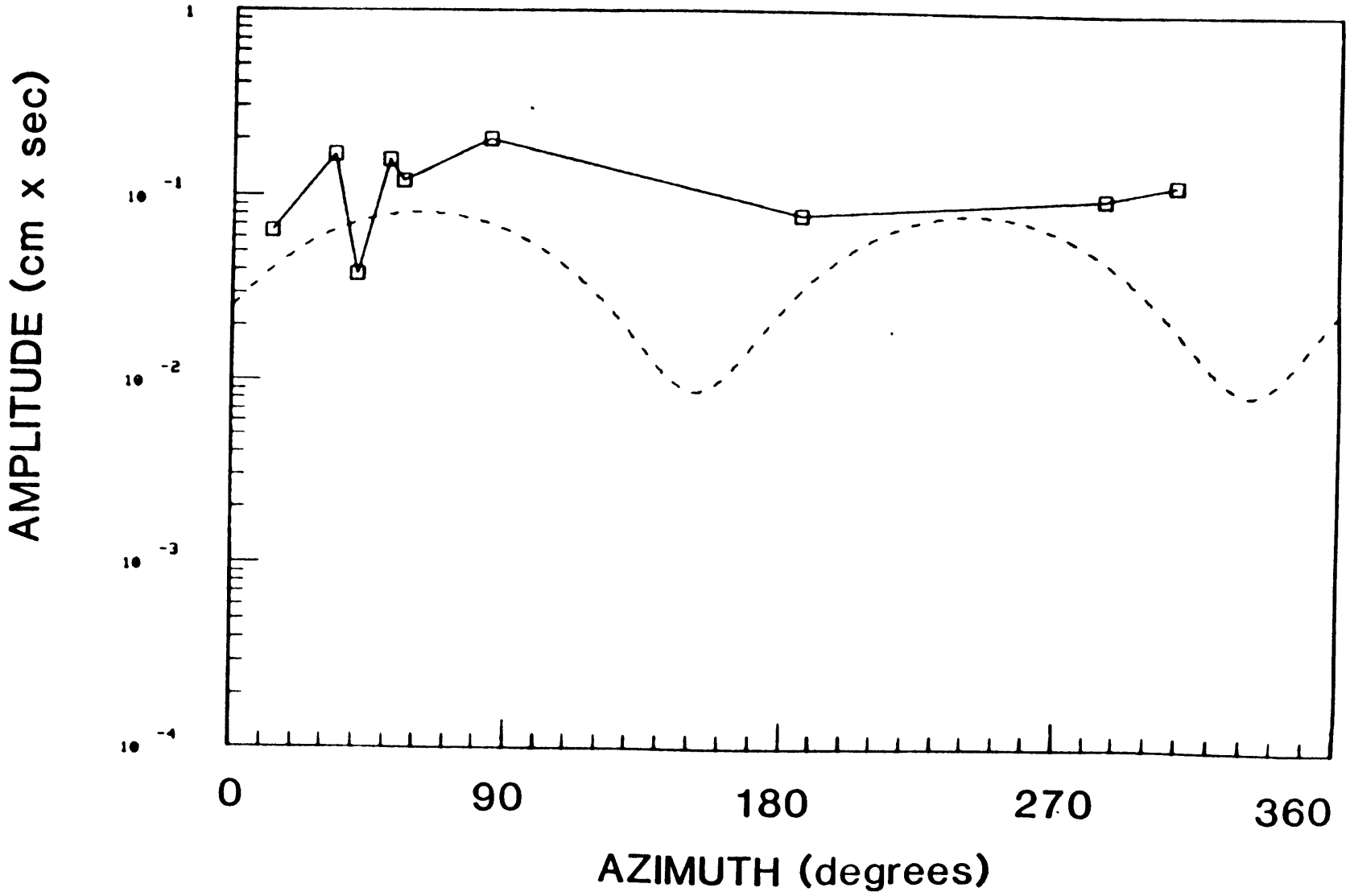

FIGURE B.45a

01/28/79

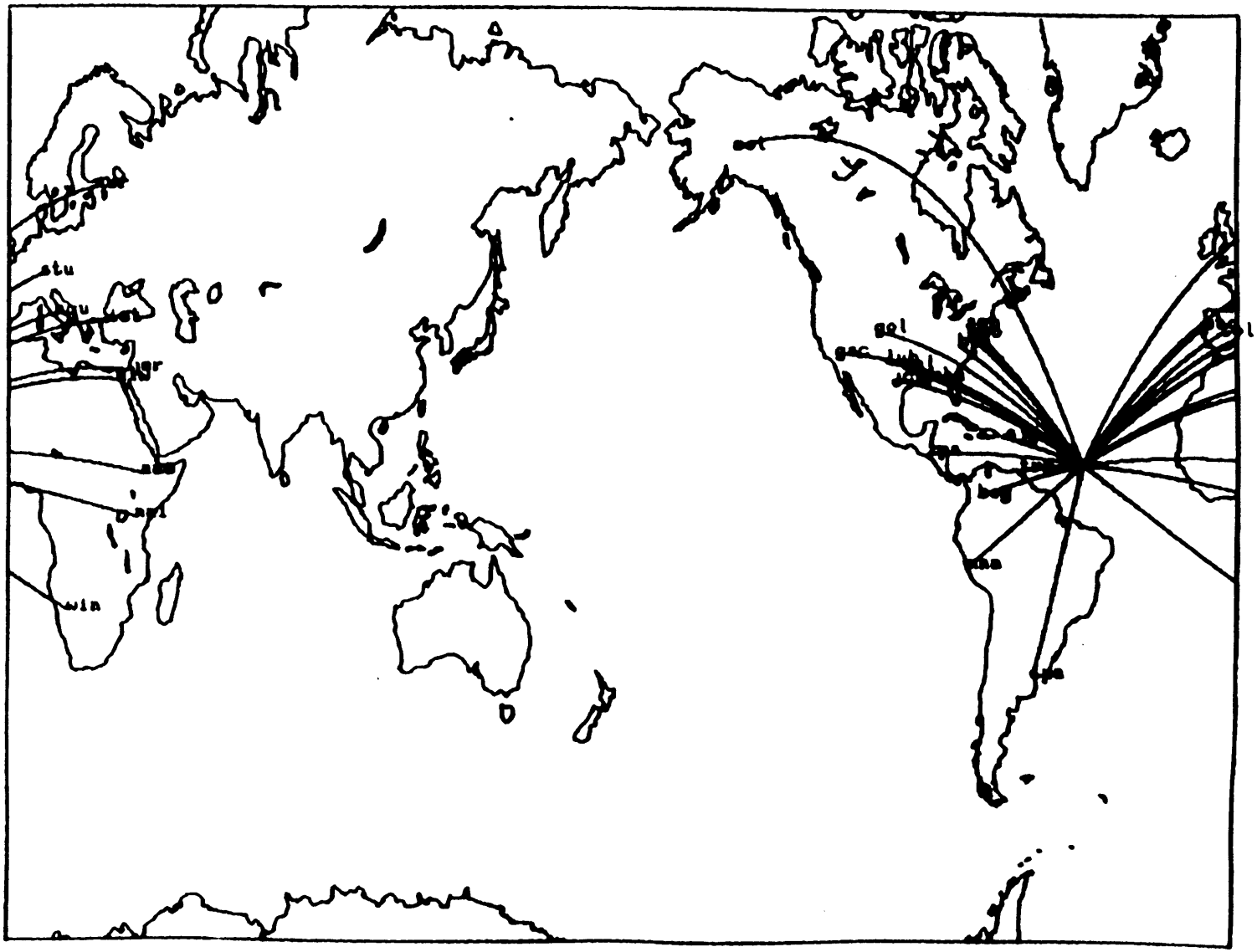

FIGURE B.45b

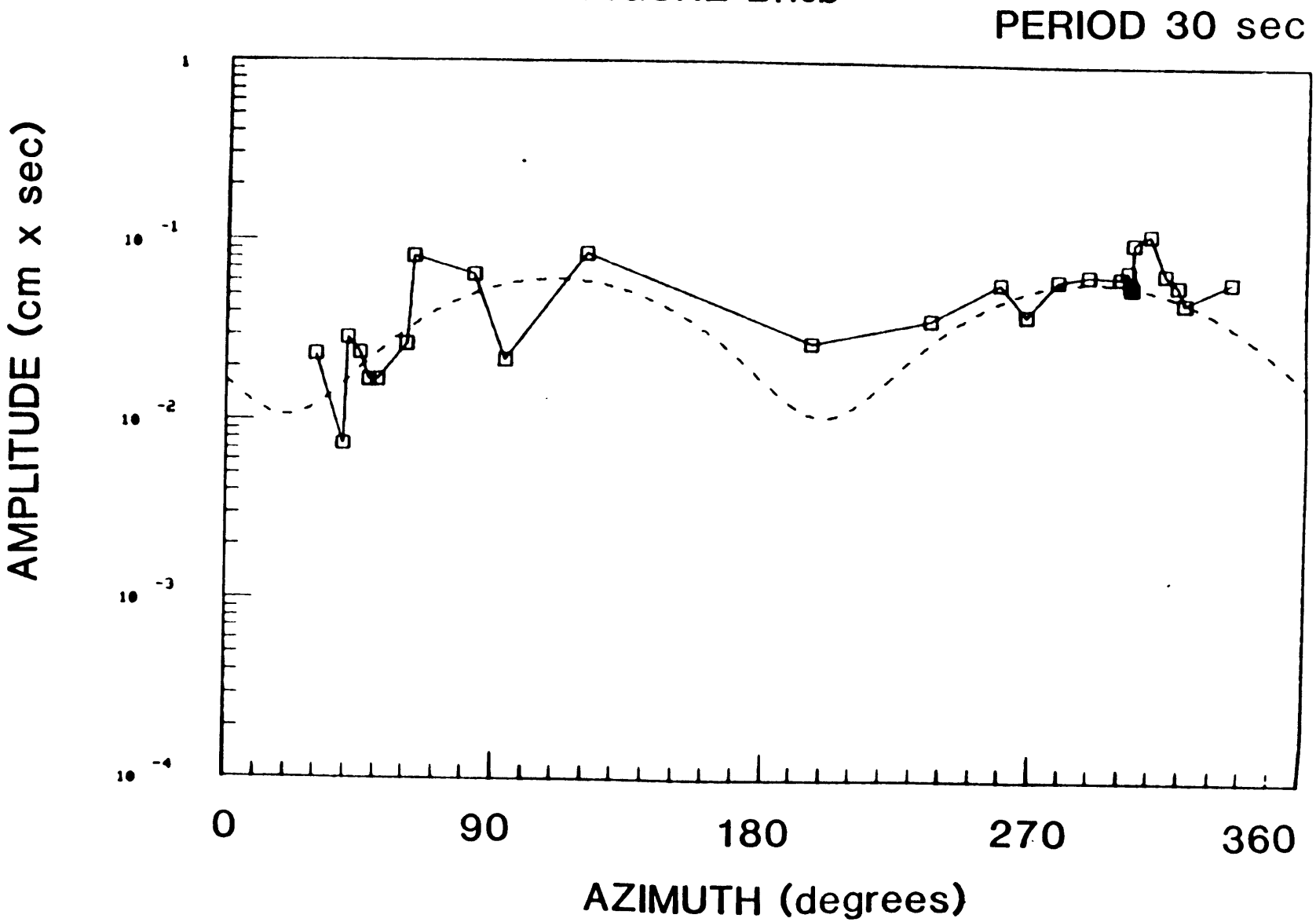
PERIOD 30 sec
AMPLITUDE (cm x sec)
1
10 -1
10 -2
10 -3
10 -4
0
90
180
270
360
AZIMUTH (degrees)

FIGURE B.45C

PERIOD 50 sec

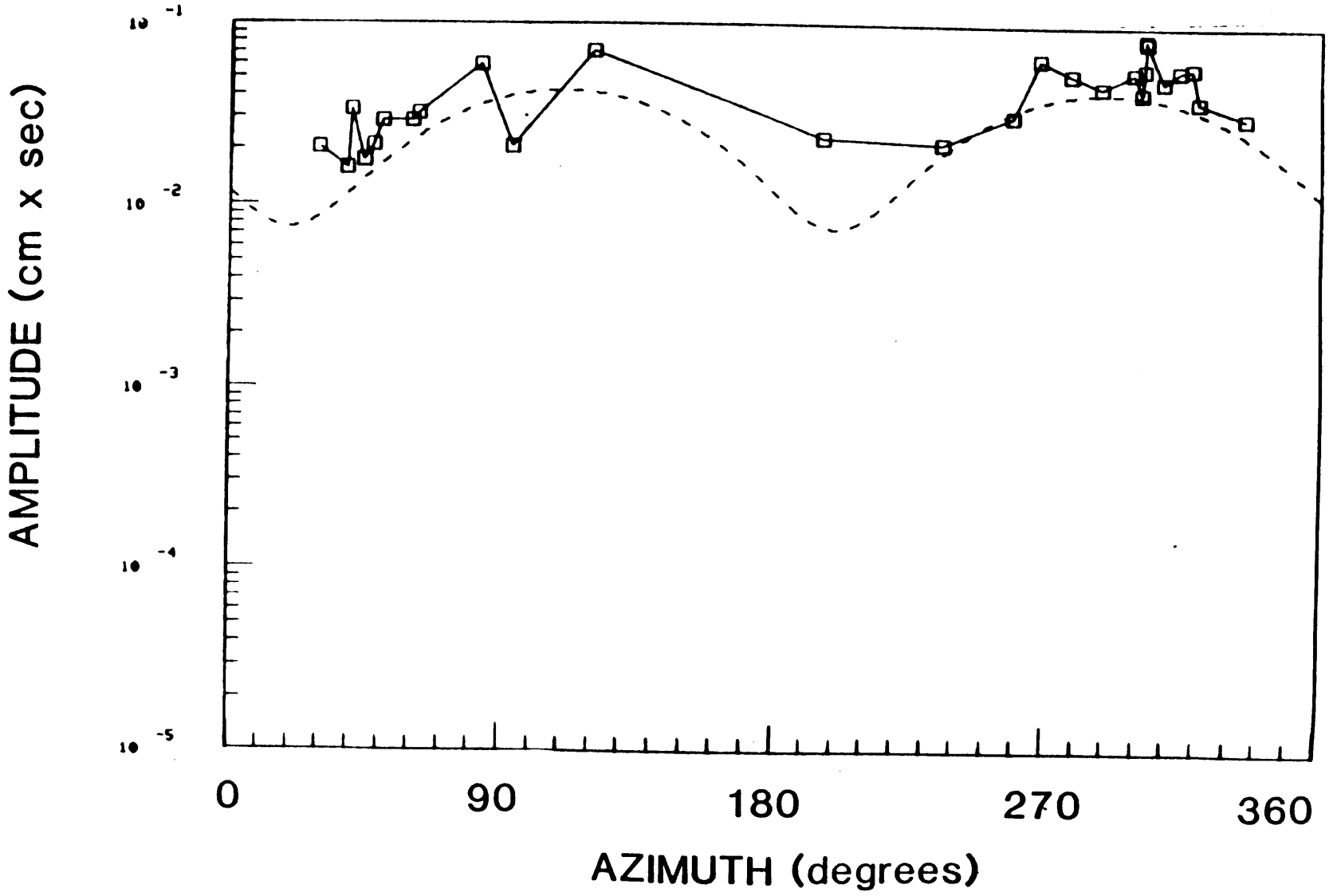

FIGURE B.45d

PERIOD 70 sec

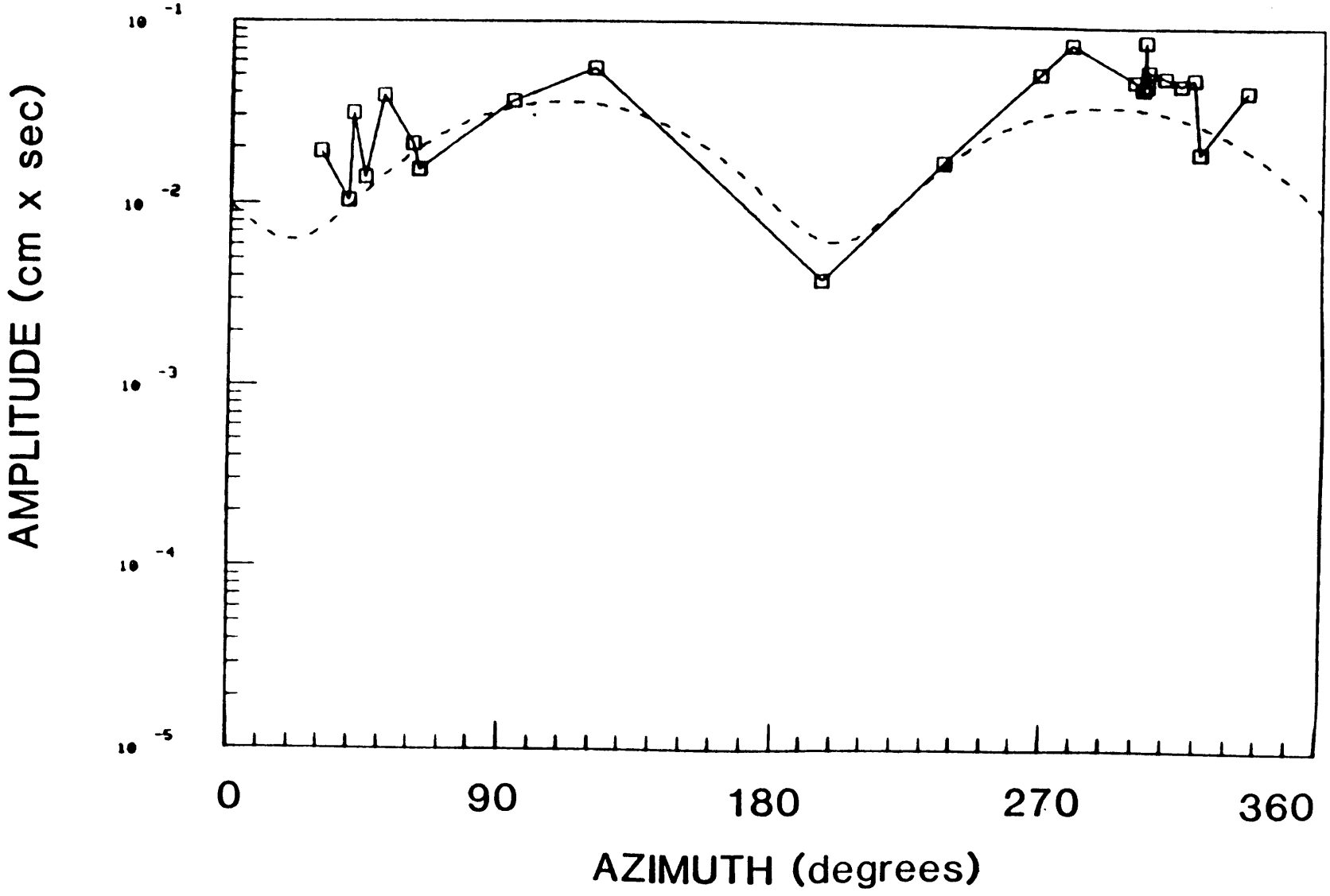

FIGURE B.45e

PERIOD 98 sec

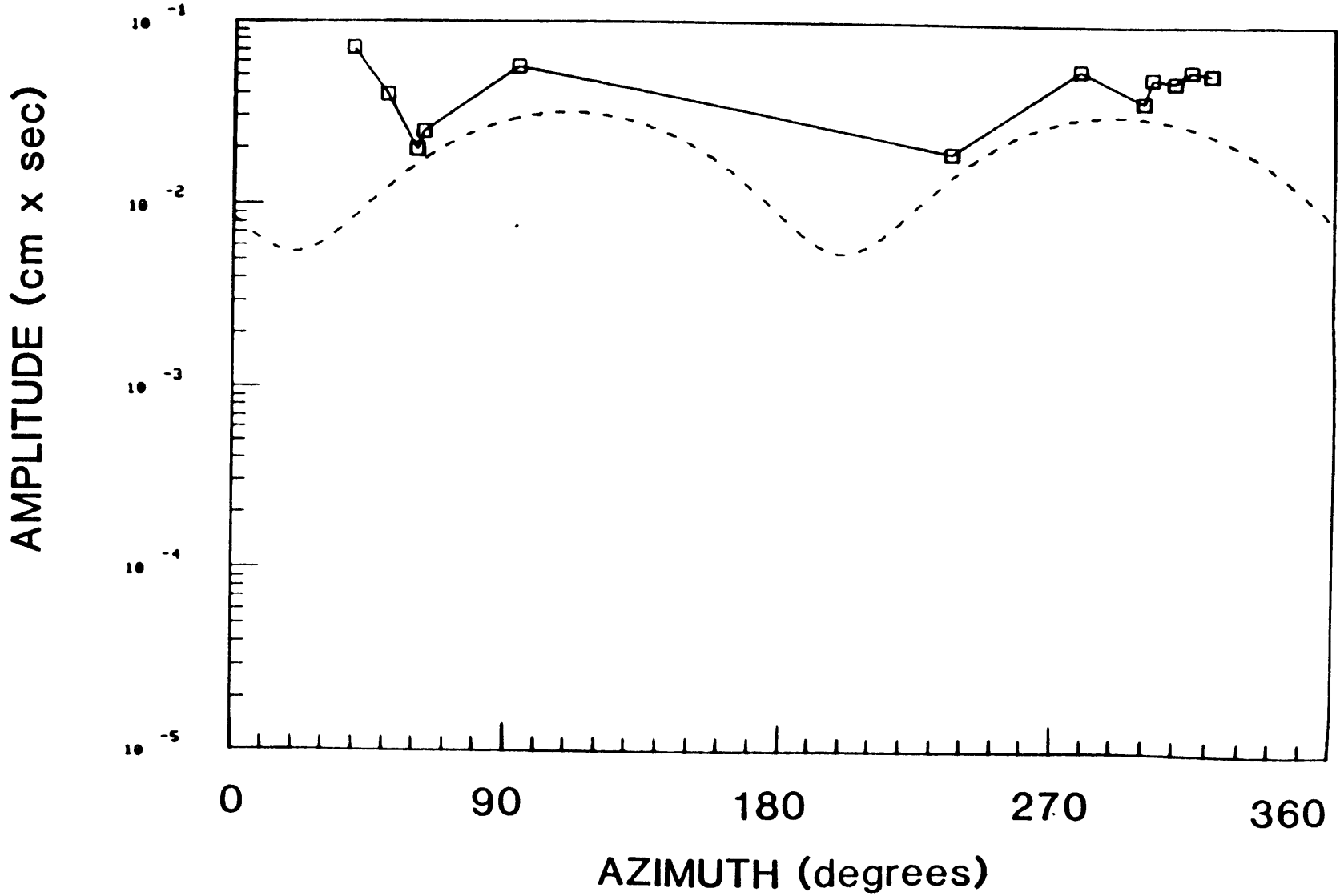

APPENDIX C

Distribution function of measured group velocity values of fundamental mode Rayleigh waves for the period range 20 to 100 sec.

Figures C.1a thru C.9a - Geographical distribution of greatcircle paths corresponding to the reference periods 20 thru 98 sec, for which we measured the group velocity. The latitude ranges from 75°N to 70°S in each map.

Figures C.1b thru C.9b - Histograms of group velocity data for periods 20 thru 98 sec respectively, separated from our data and corresponding to paths that have a portion larger than 40% of their total length inside the region-type 'a' of the model of Jordan (1981). Each plot was made using an increment of 0.01 km/sec in the group velocity value.

Figures C.1 thru C.9 - Indices c thru g - Same as above, for the region-types 'b', 'c', 'p', 'q', and 's', respectively, of the model of Jordan (1981).

Figures C.1 thru C.9 - Indices h thru k - Same as above, for the region-types 'N', '=', '0', and '⌀', respectively, of the model of Lévèque (1980).

Figures C.1 thru C.9 - Indices 1 thru r - Same as above, for the region-types 'N', '#', '=', '-', '0', '.', and '~', respectively, of the model of Okal (1977).

FIGURE C.1a

PERIOD 20 sec

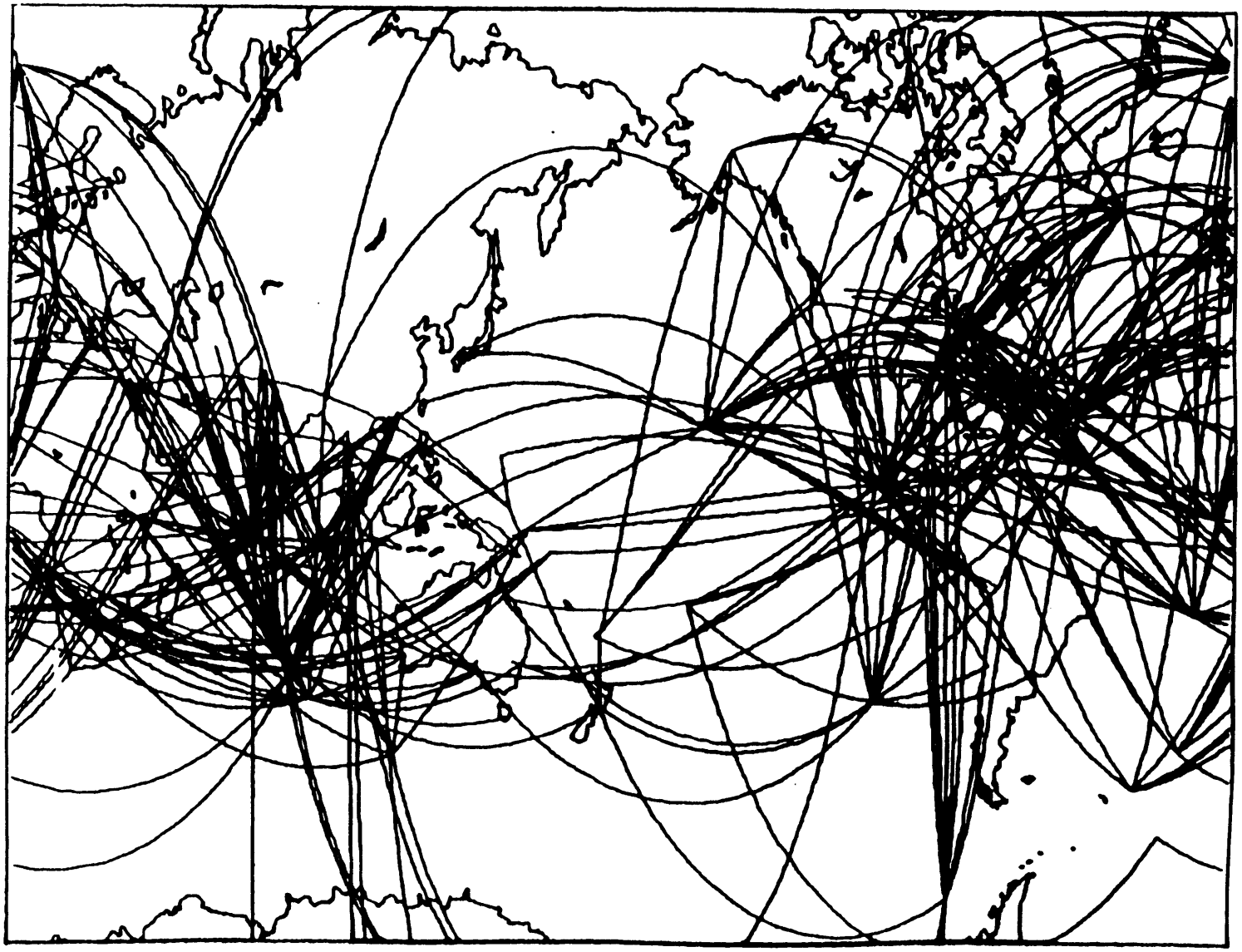

FIGURE C.1b REGION a

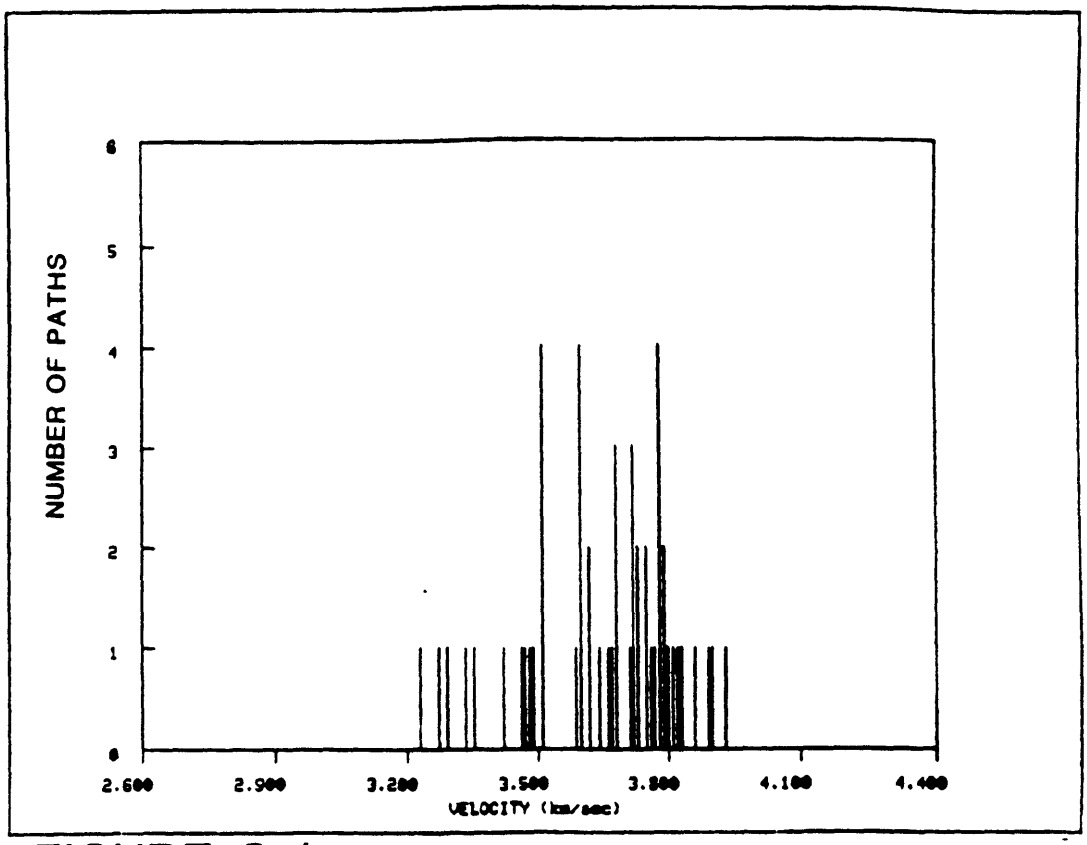

FIGURE C.1c REGION b

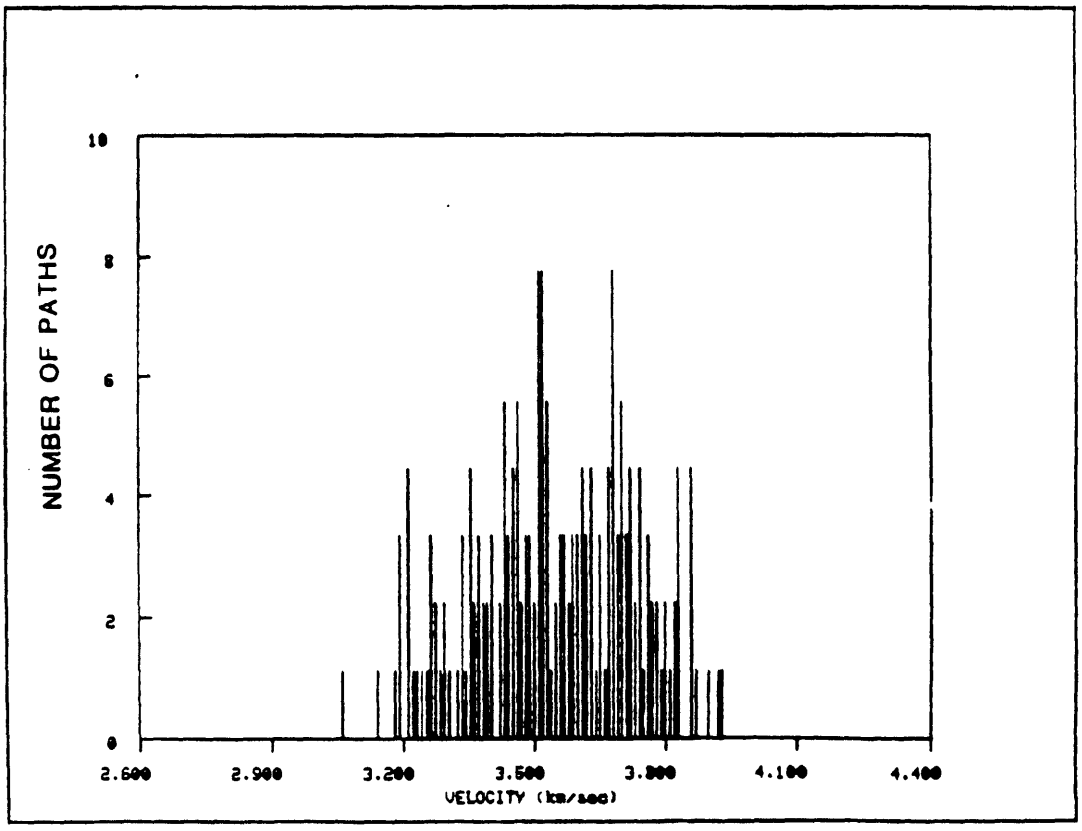

FIGURE C.1d REGION c

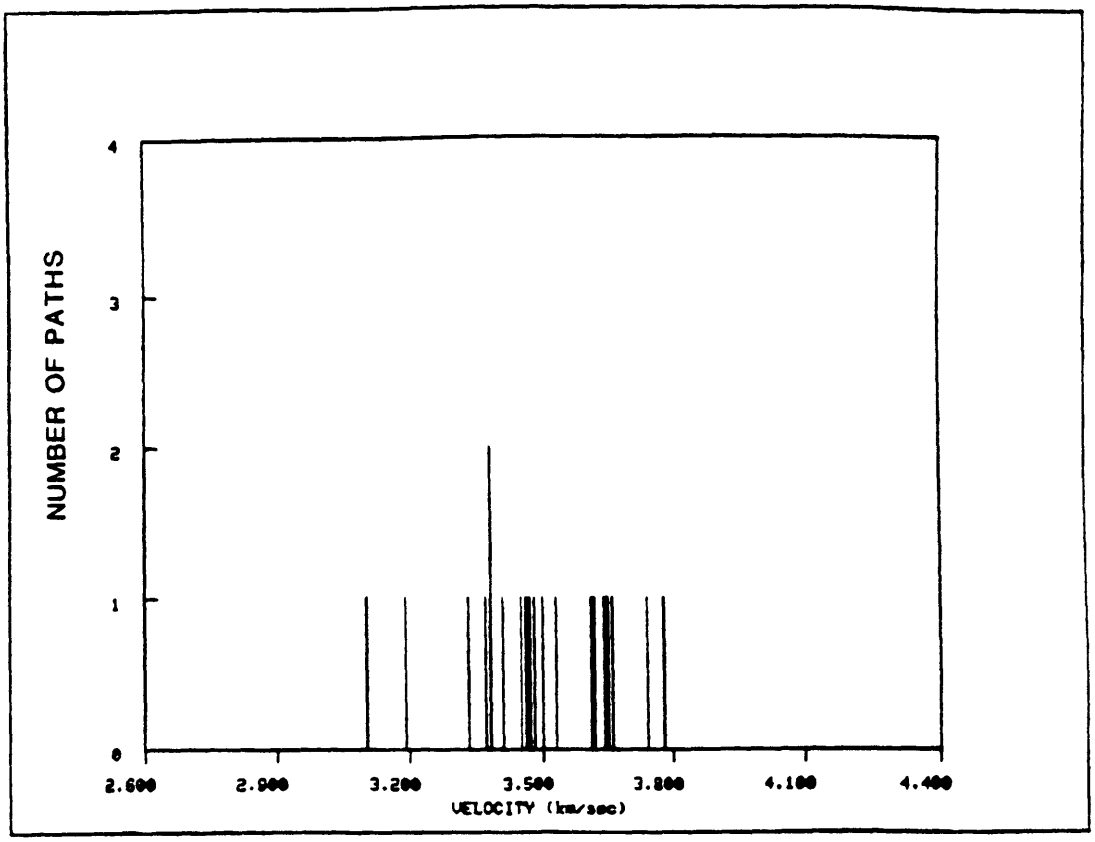

FIGURE C.1e REGION p

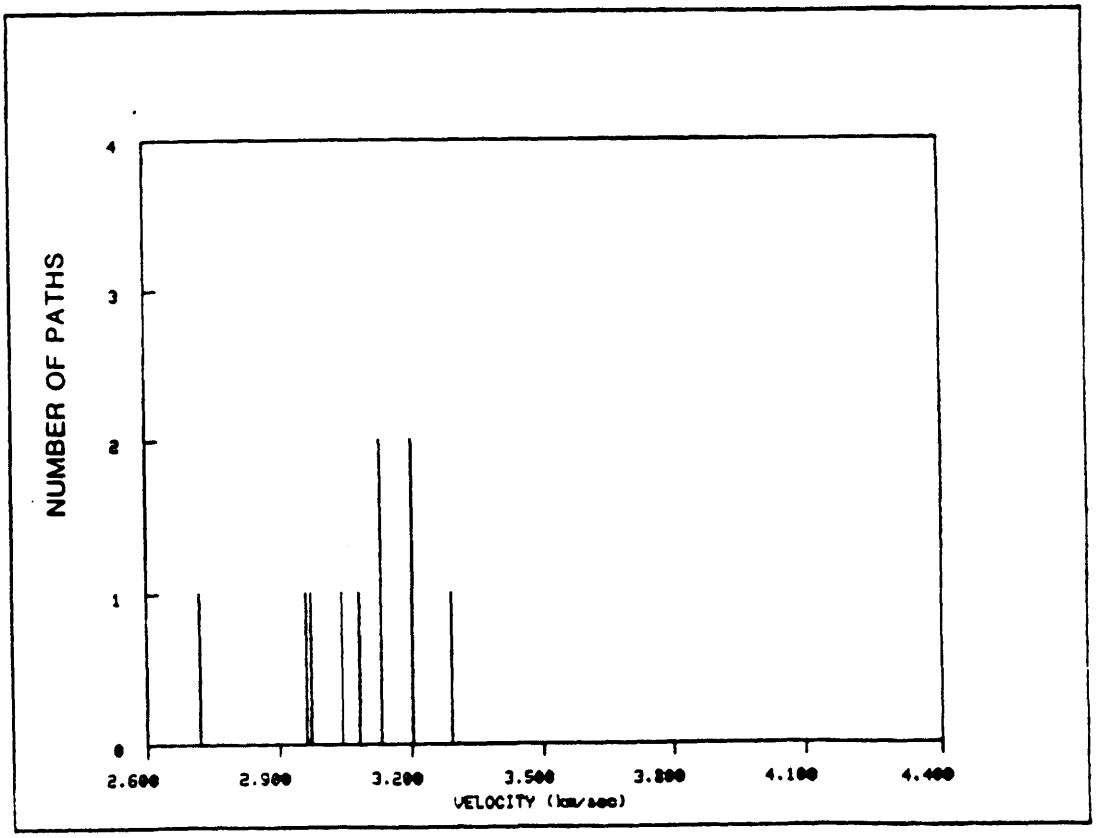

FIGURE C.1f REGION q

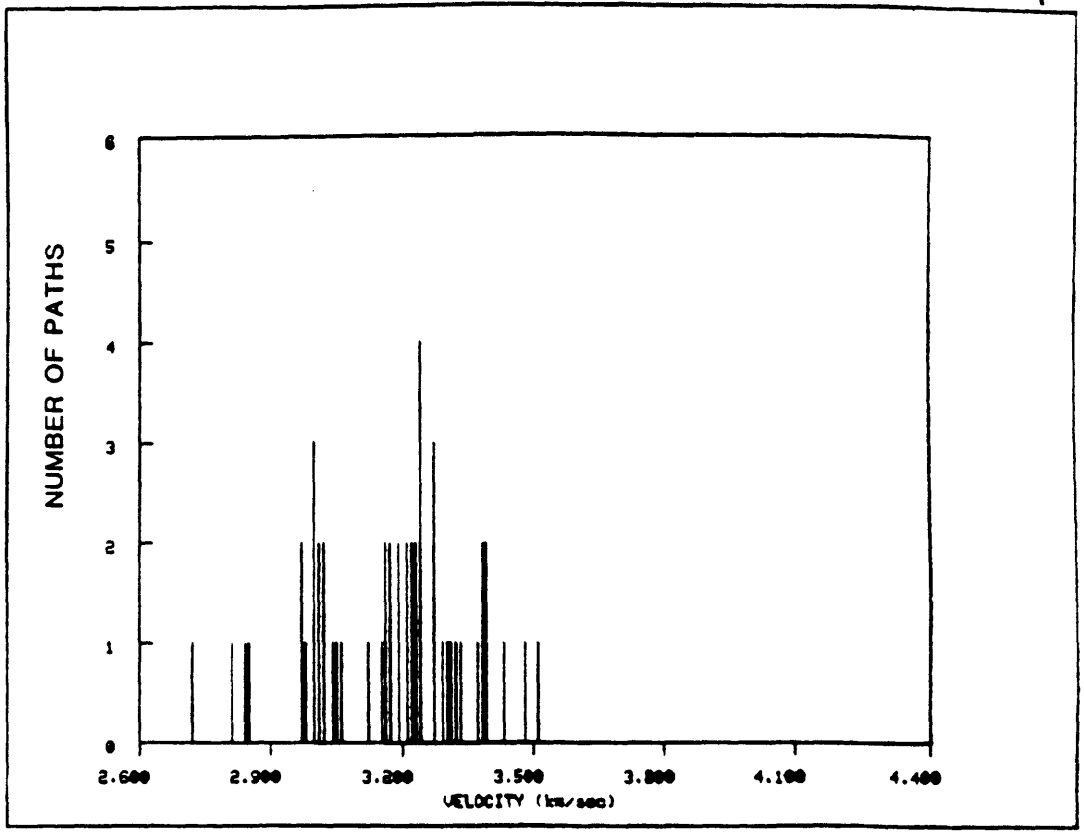

FIGURE C.1g REGION s

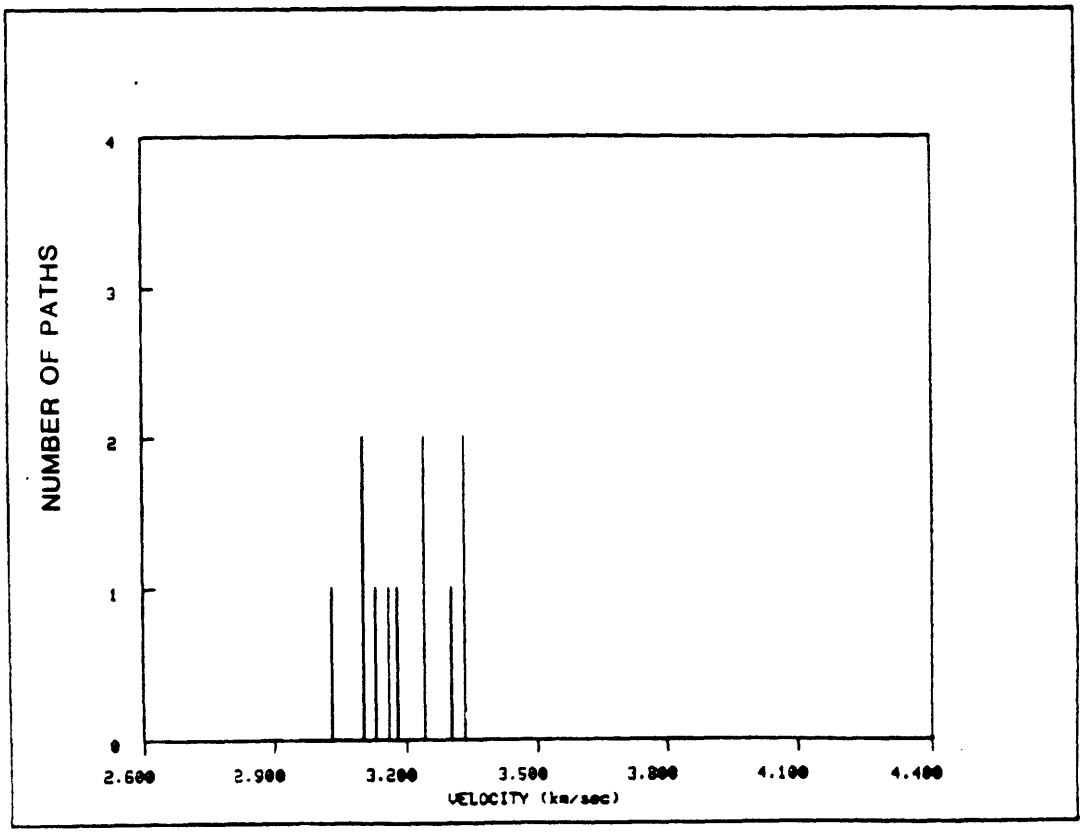

FIGURE C.1h REGION N

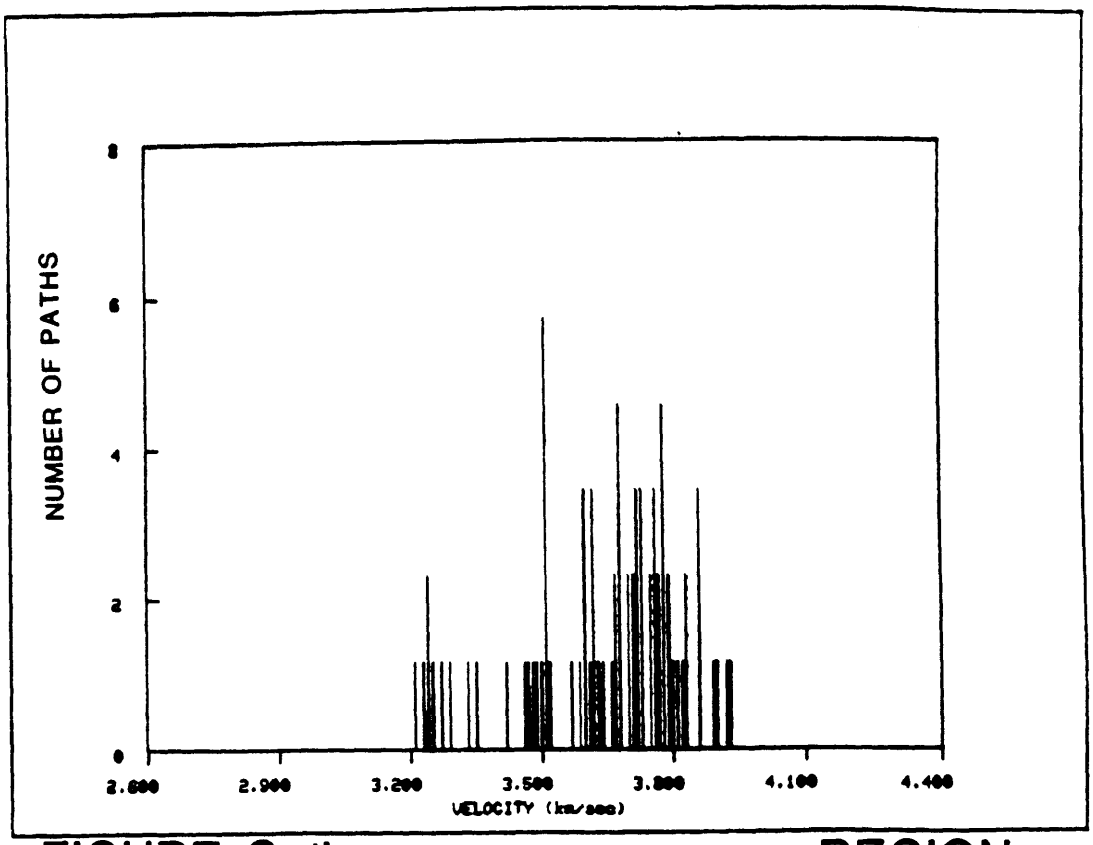

FIGURE C.1i REGION =

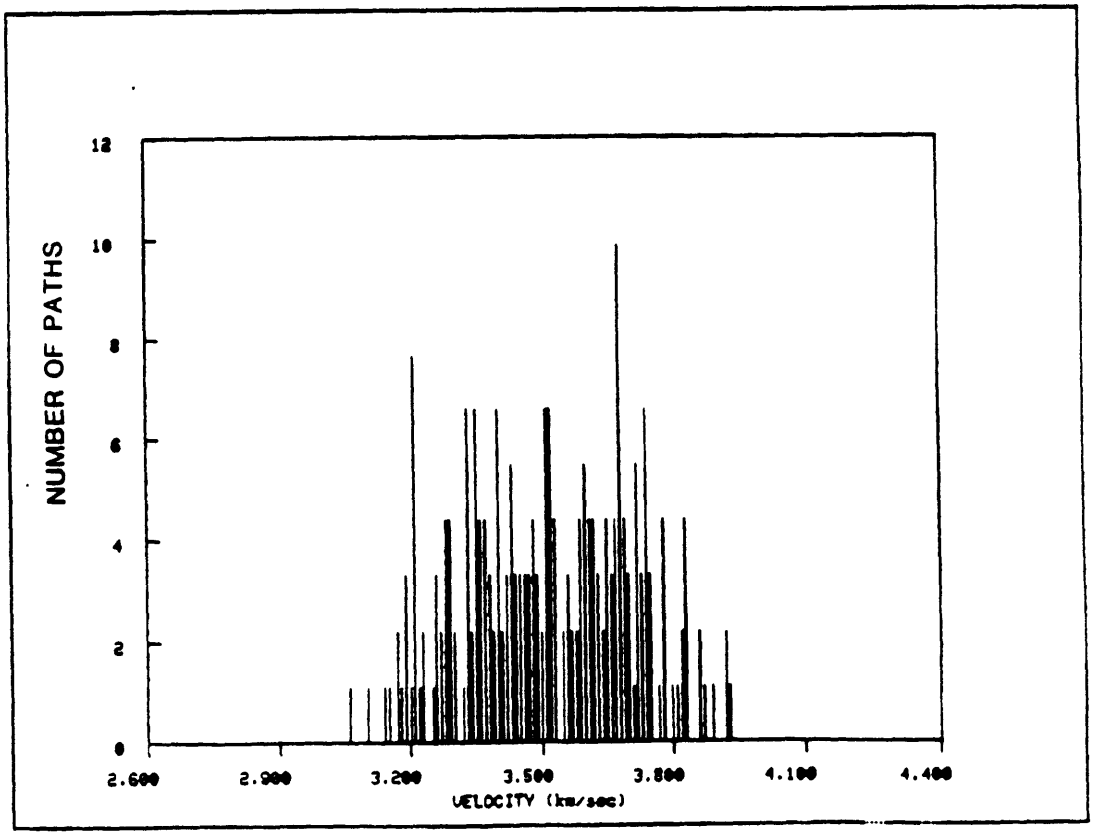

FIGURE C.1j REGION 0

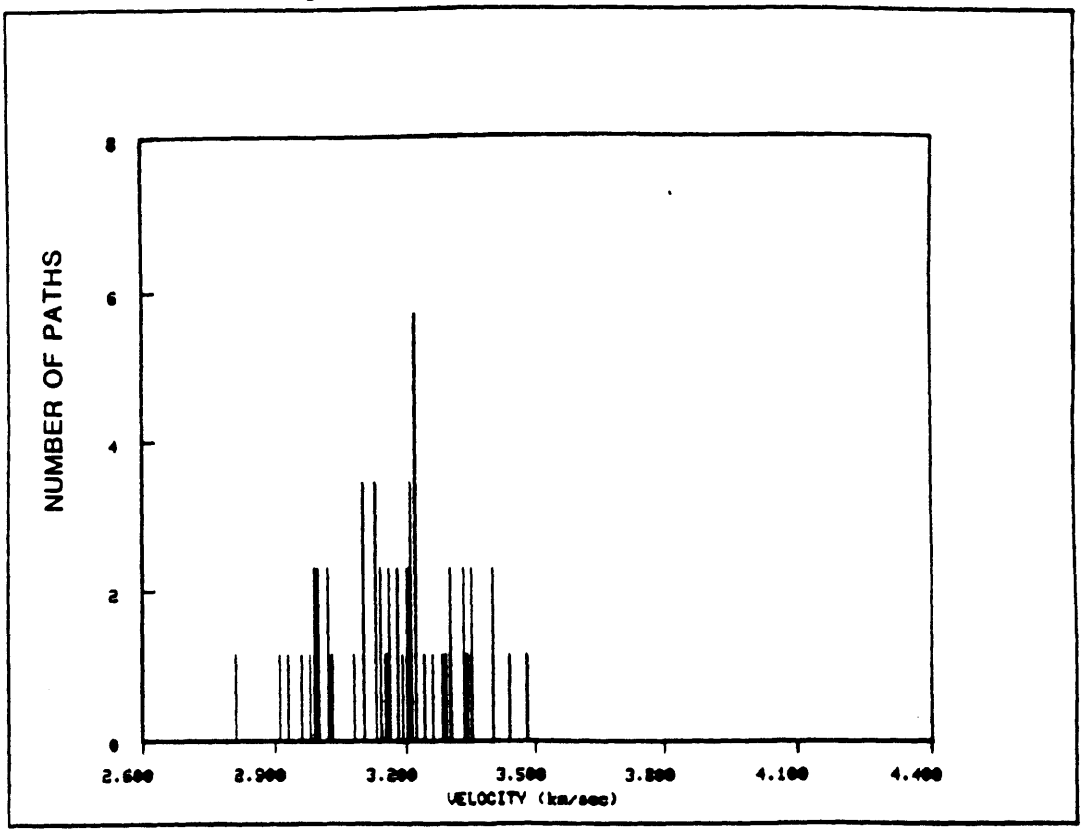

FIGURE C.1k REGION ~~0~~

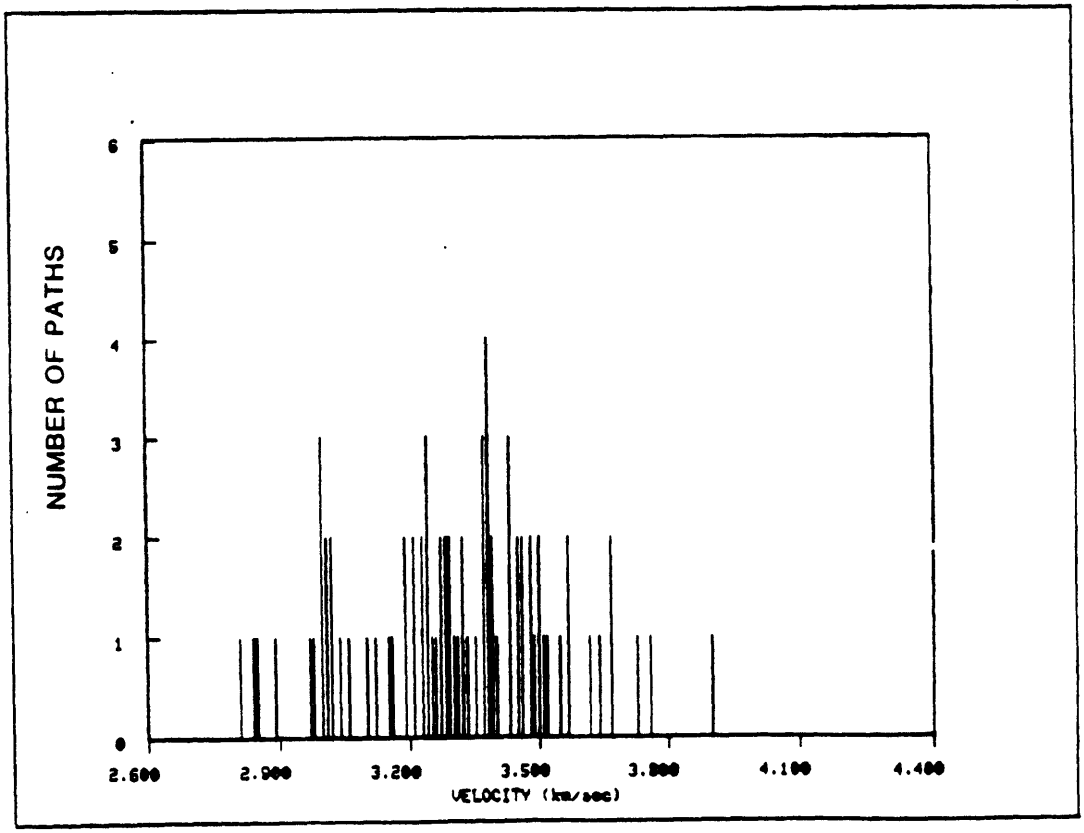

FIGURE C.1l REGION N

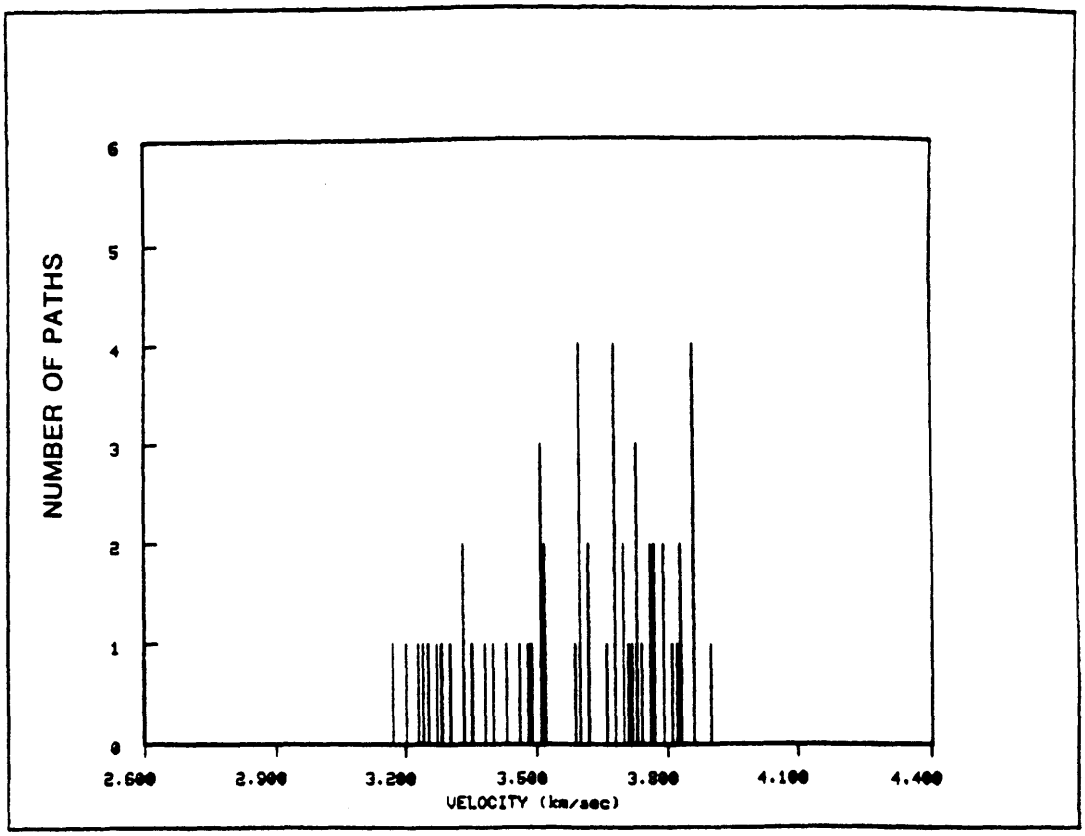

FIGURE C.1m REGION #

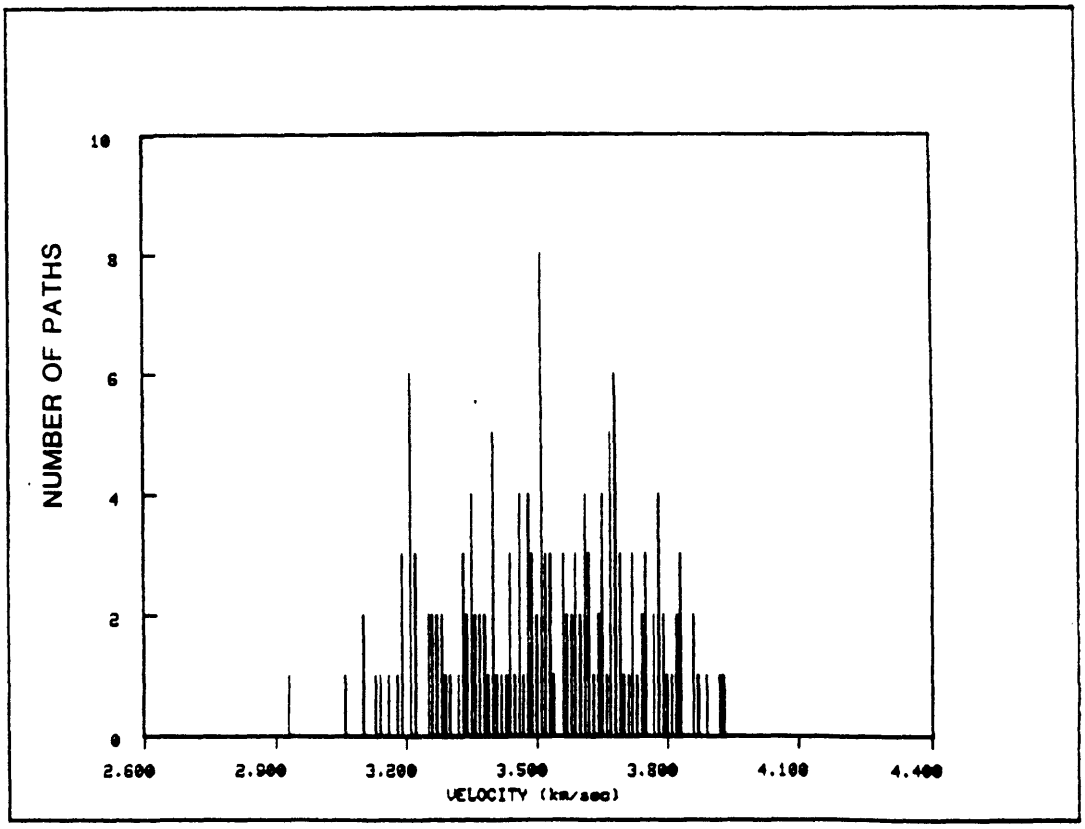

FIGURE C.1n REGION =

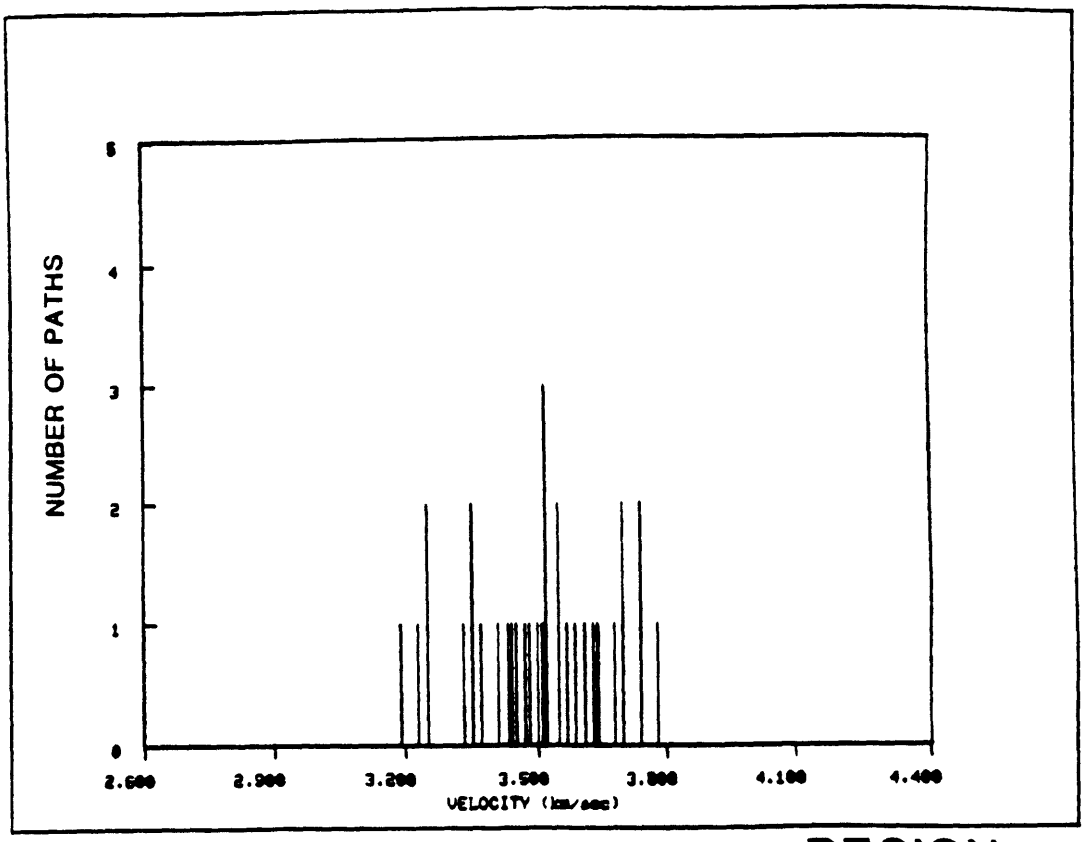

FIGURE C.1o REGION –

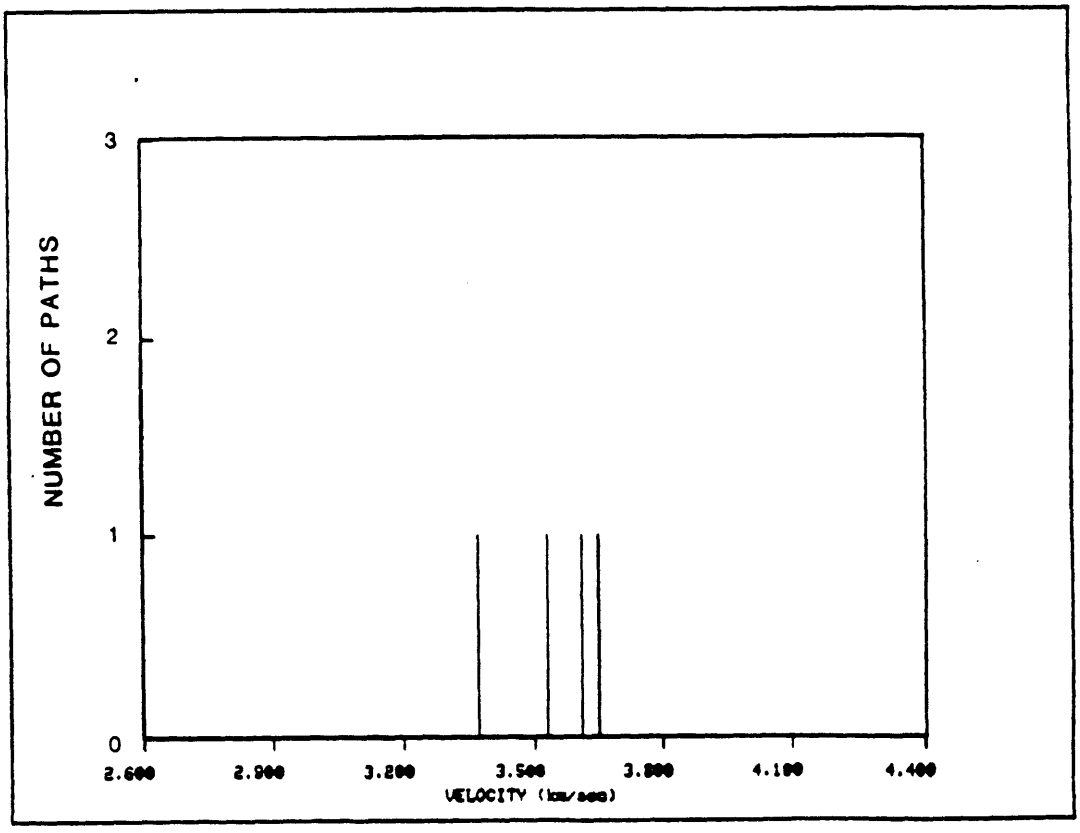

FIGURE C.1p REGION 0

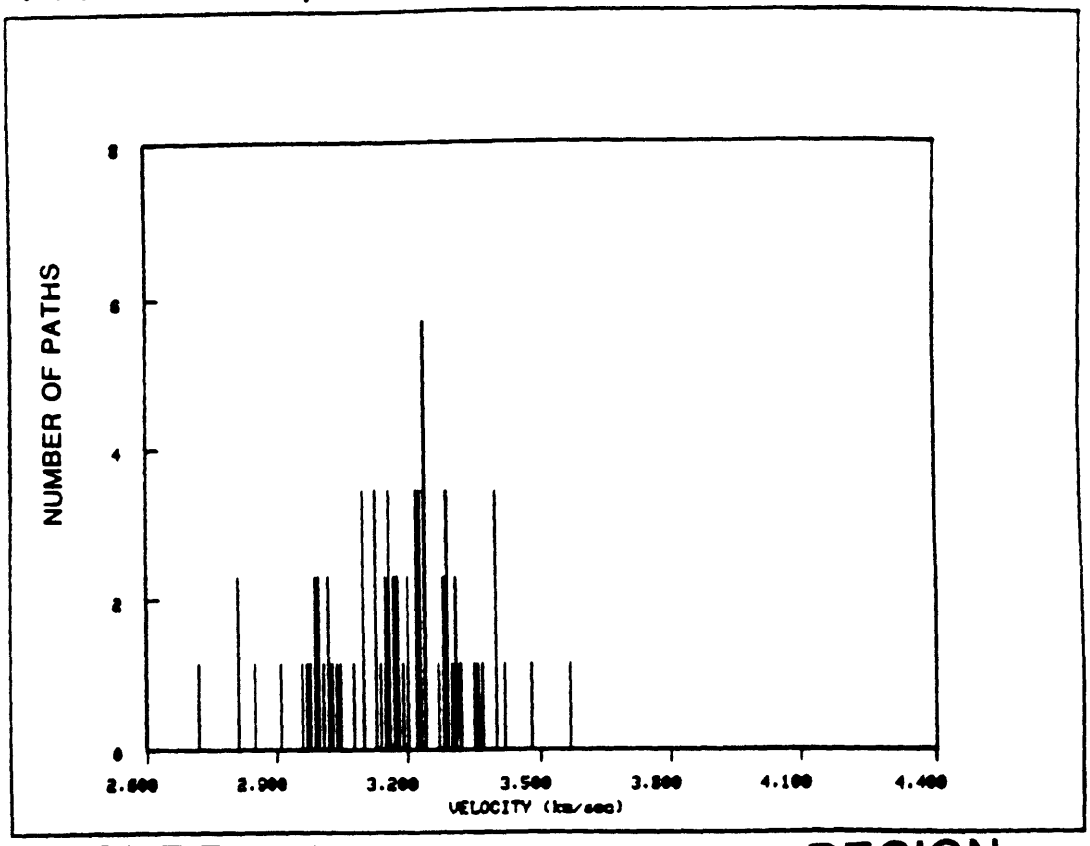

FIGURE C.1q REGION .

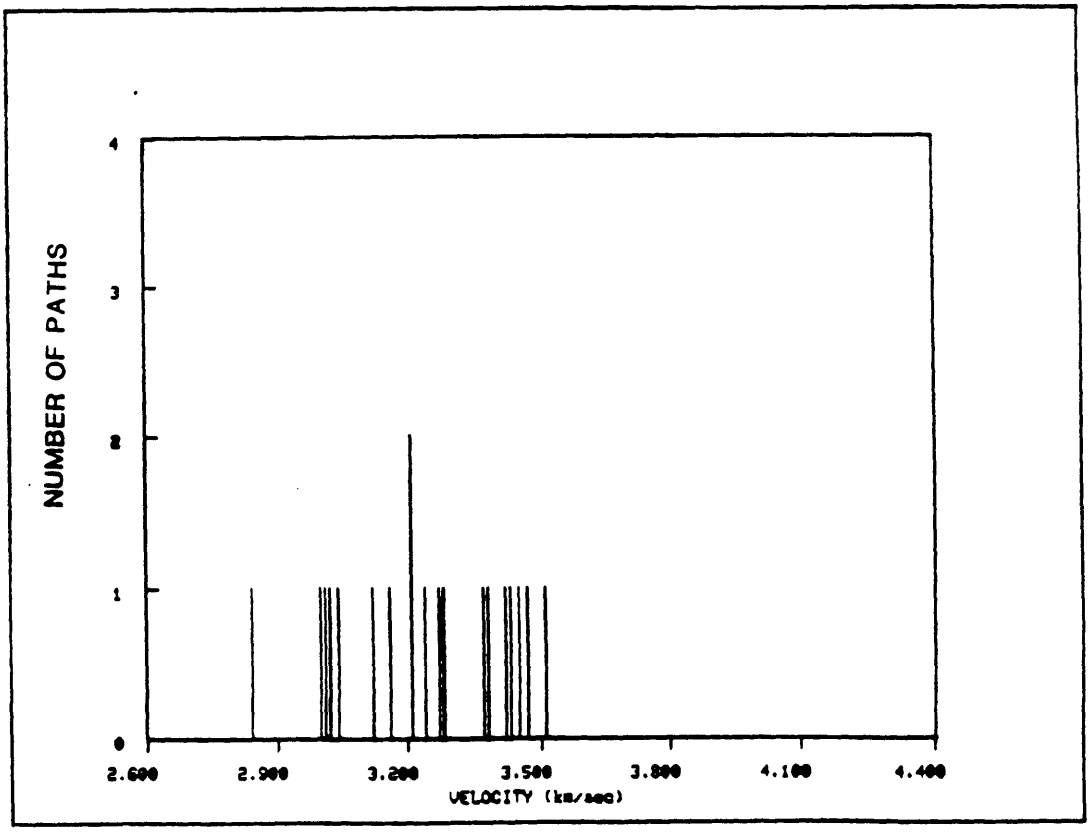

FIGURE C.1r

REGION ø

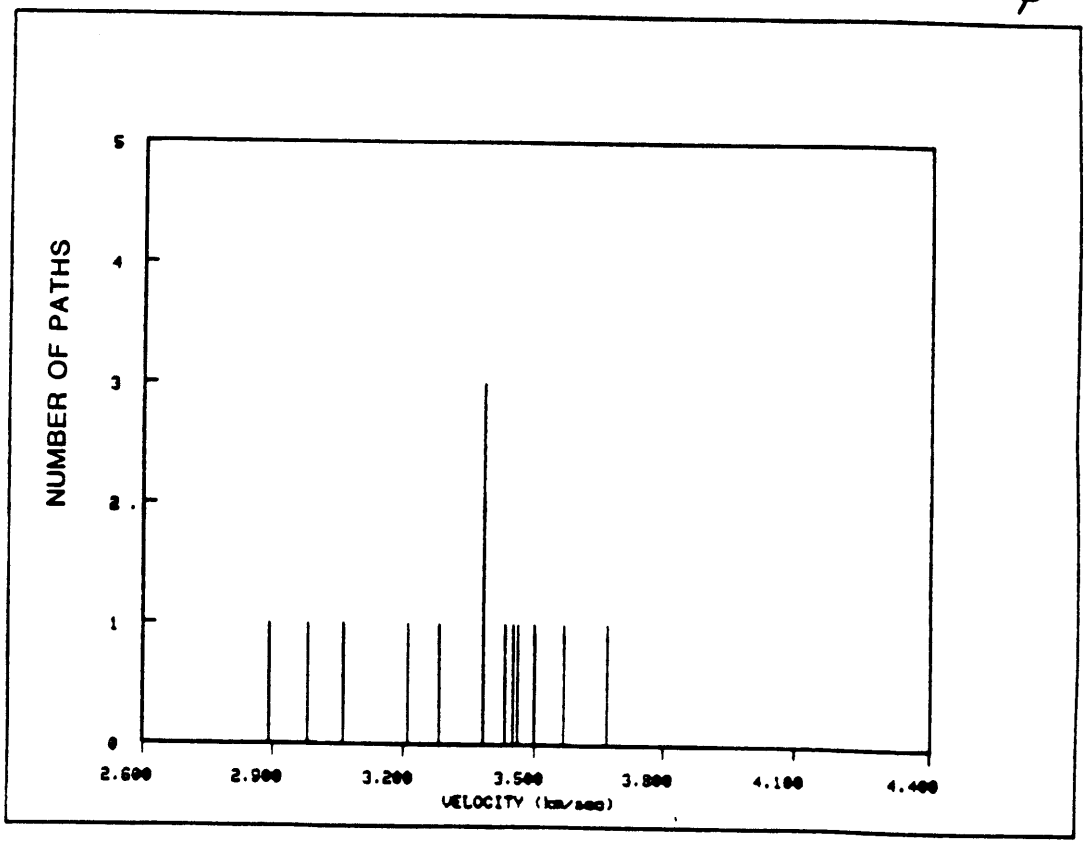

FIGURE C.2a

PERIOD 30 sec

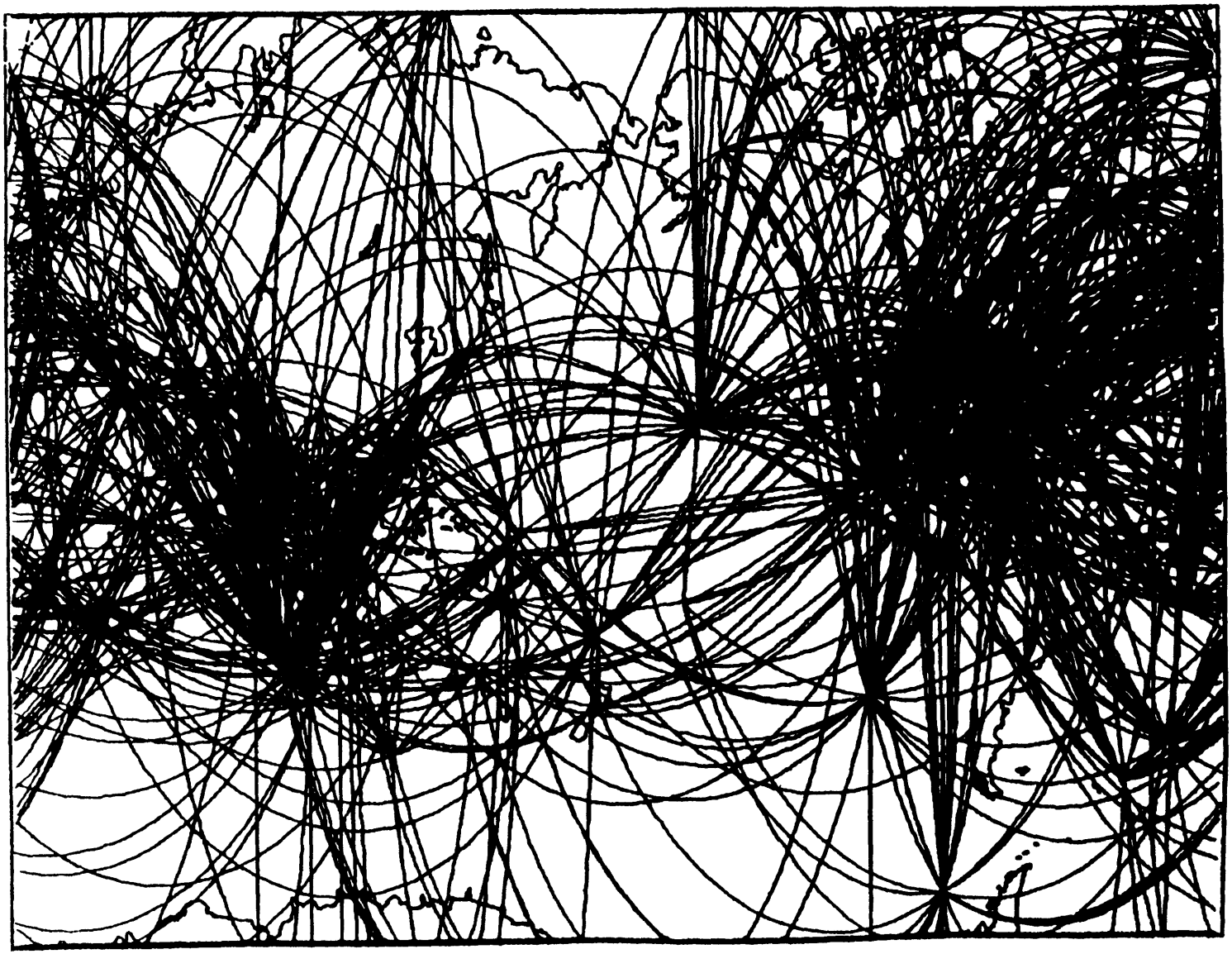

FIGURE C.2b REGION a

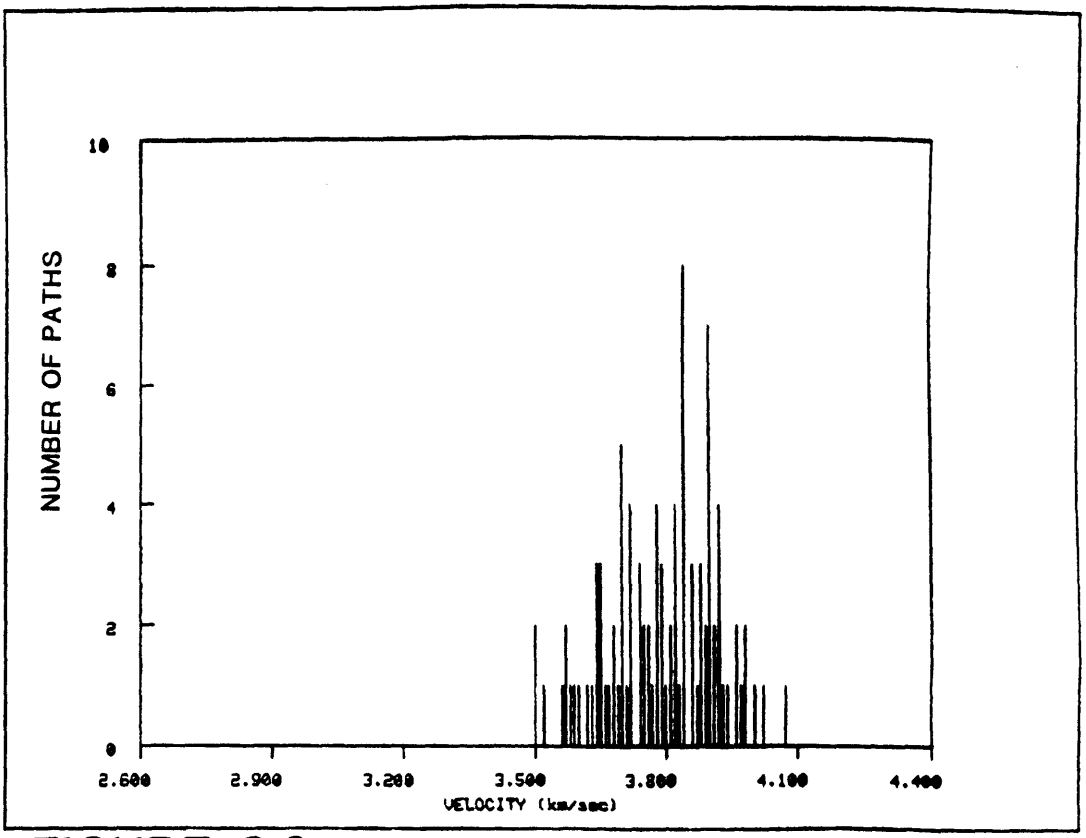

FIGURE C.2c REGION b

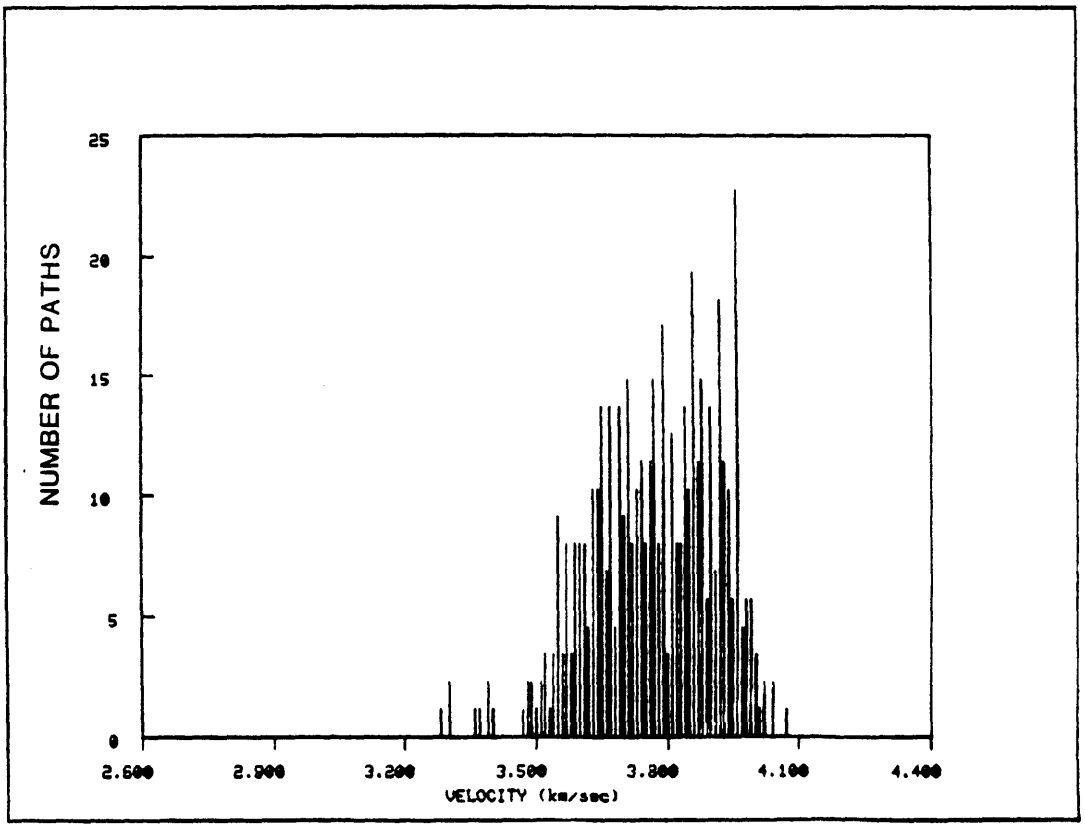

FIGURE C.2d REGION c

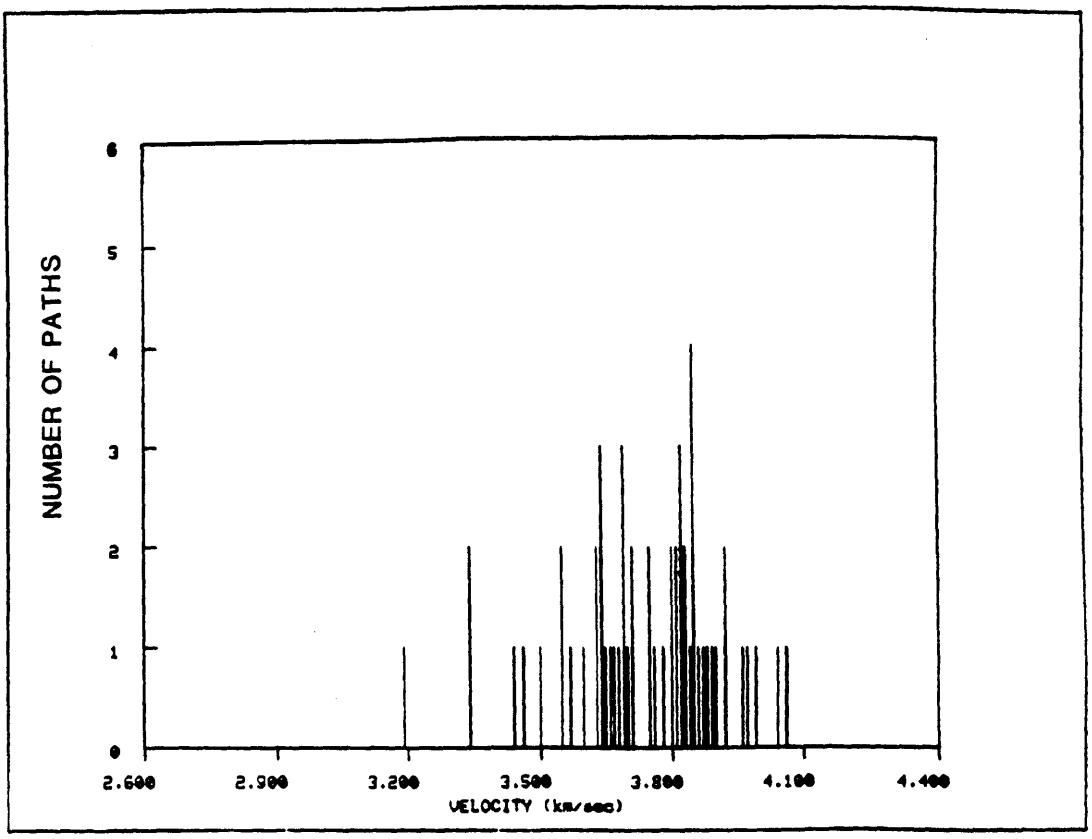

FIGURE C.2e REGION p

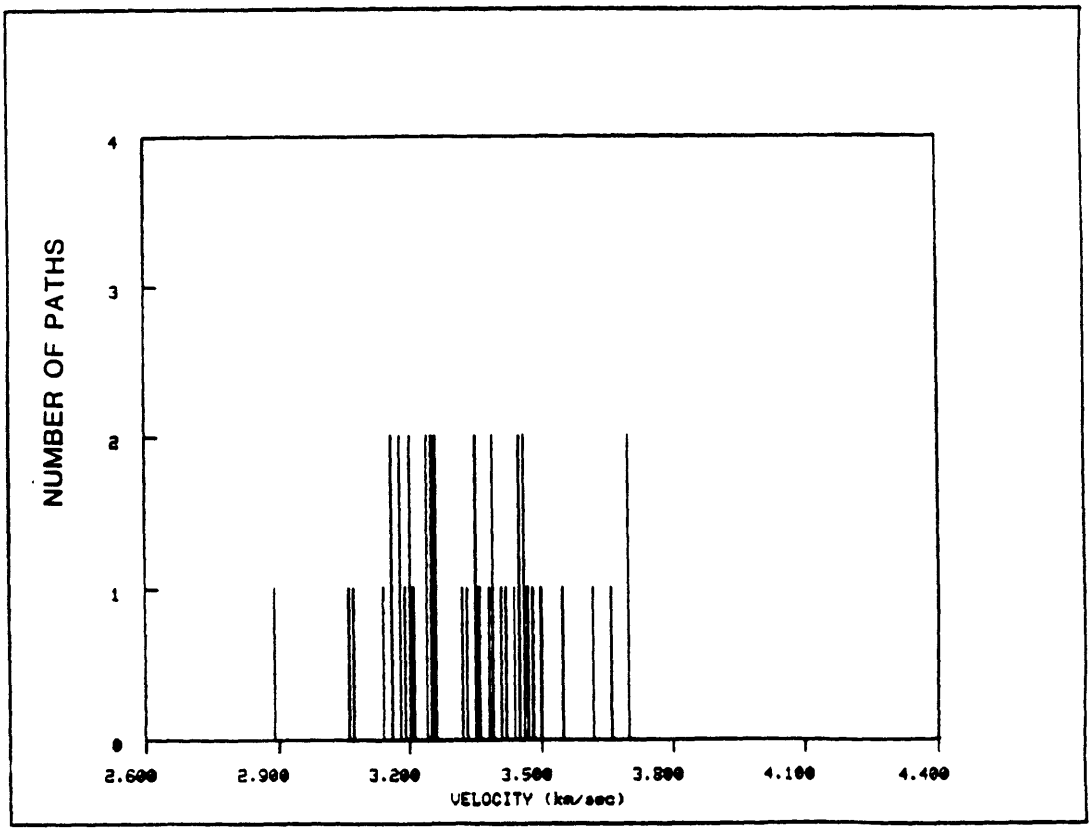

FIGURE C.2f REGION q

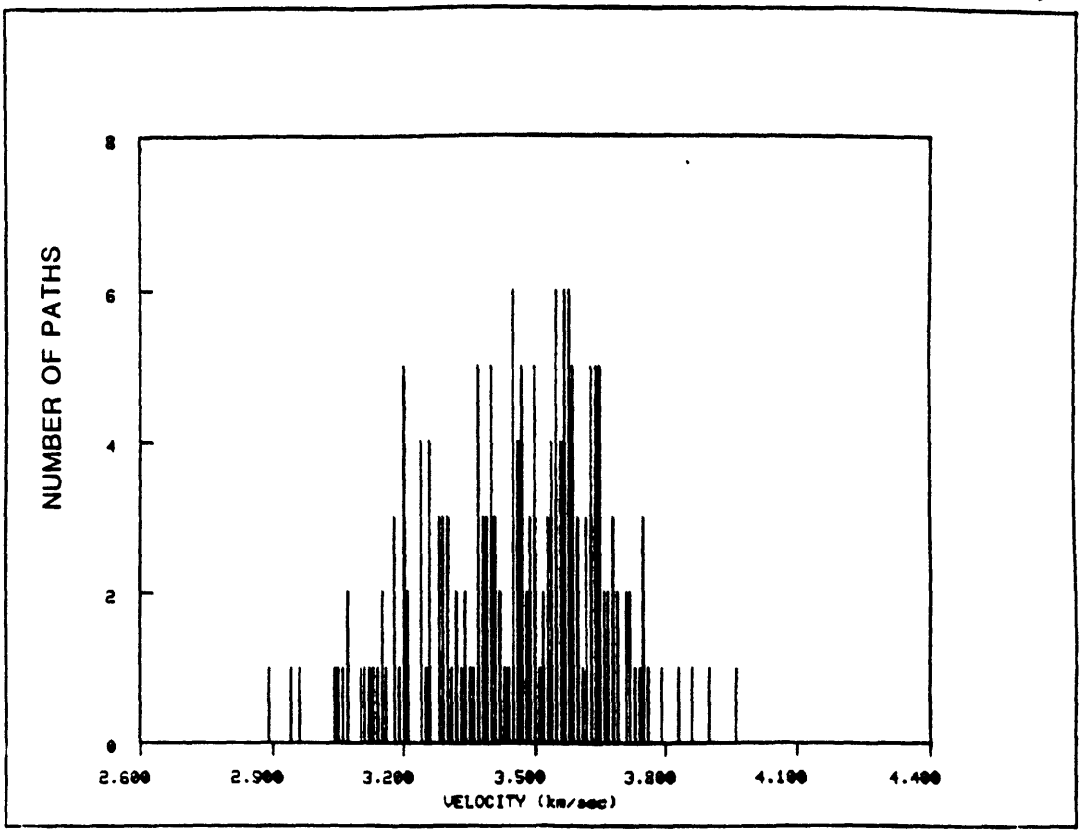

FIGURE C.2g REGION s

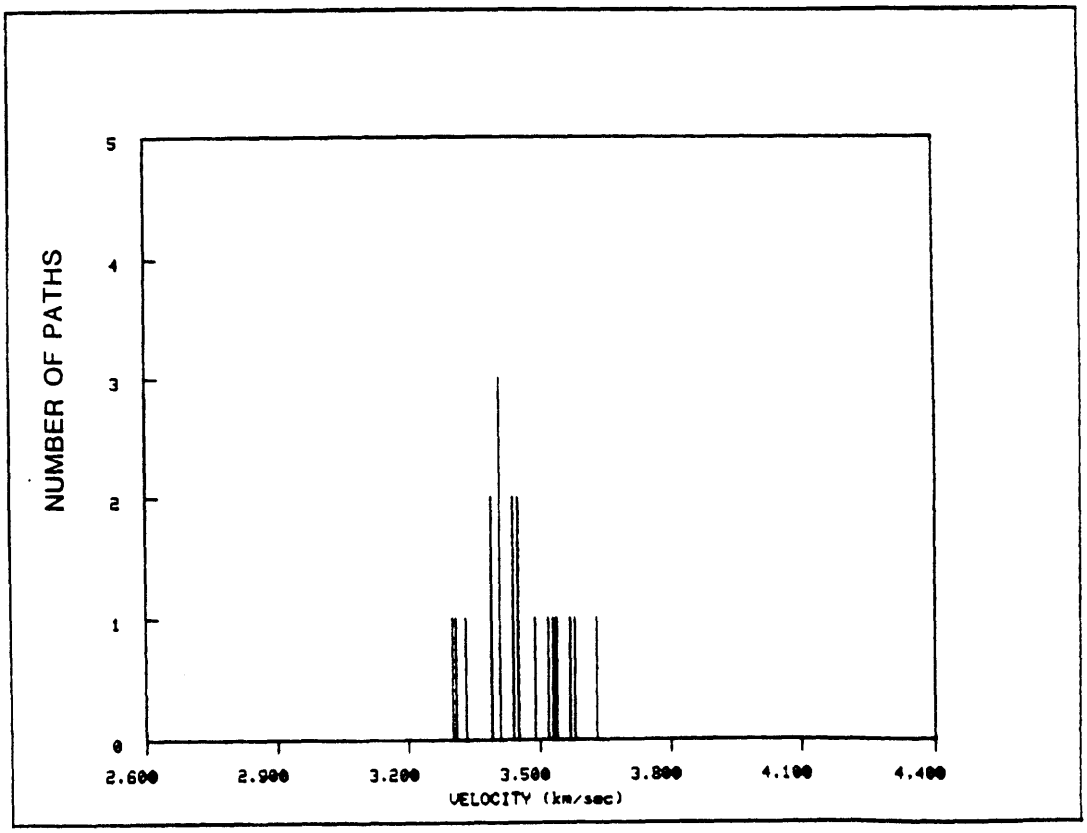

FIGURE C.2h REGION N

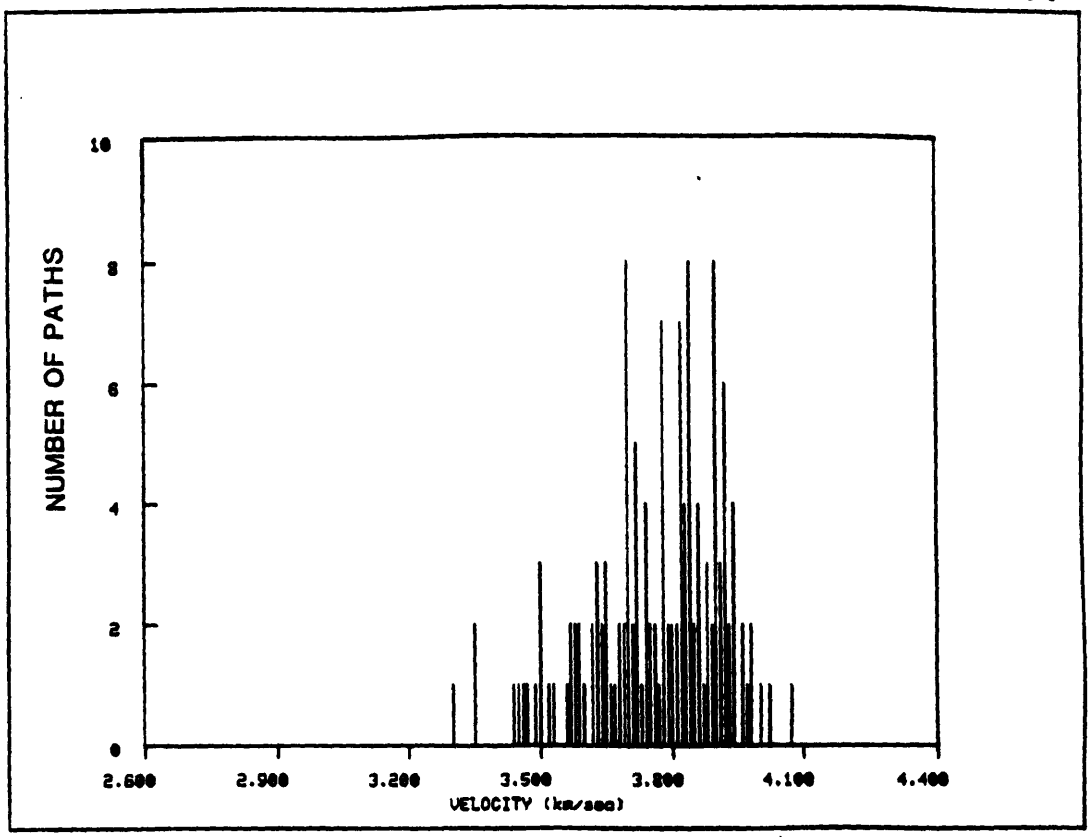

FIGURE C.2i REGION =

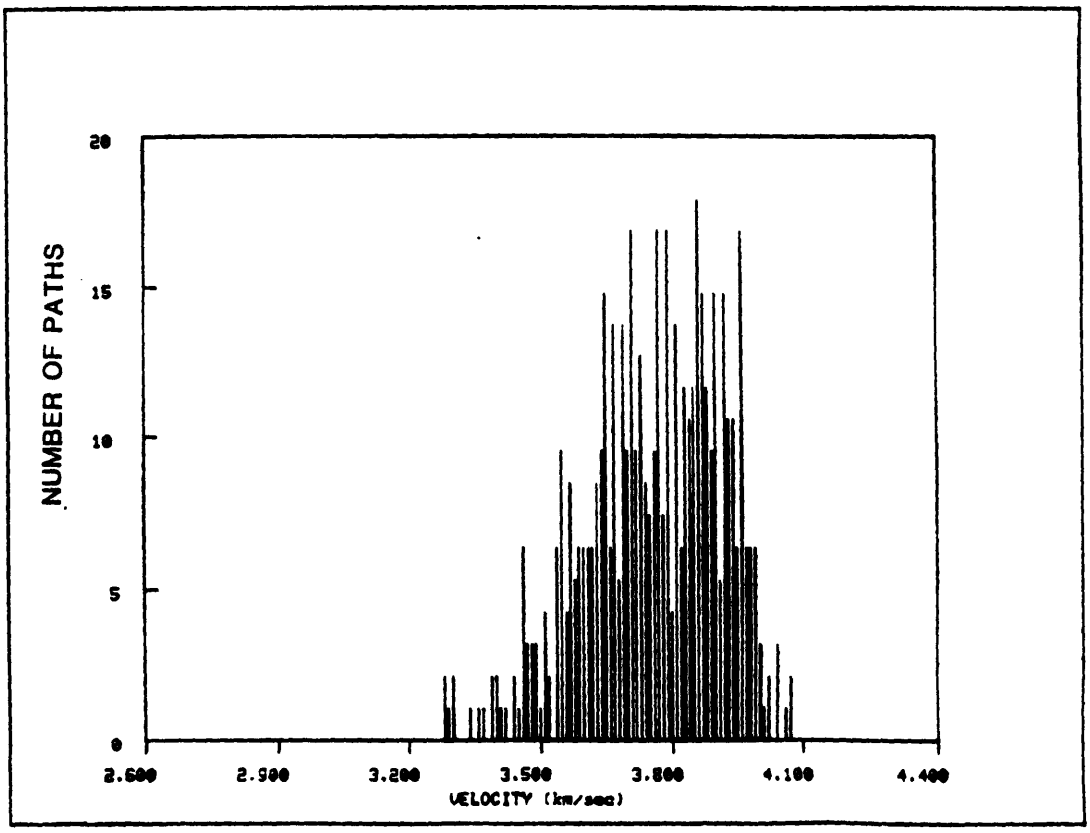

FIGURE C.2j REGION 0

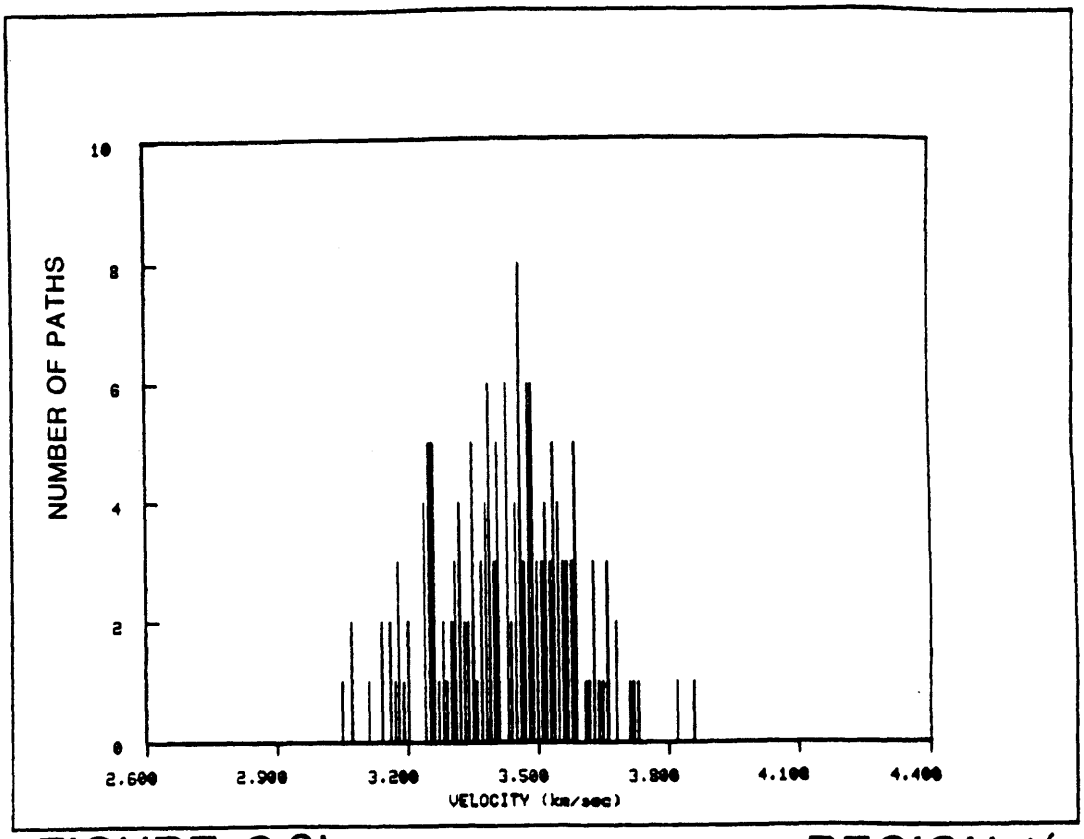

FIGURE C.2k REGION ~~0~~

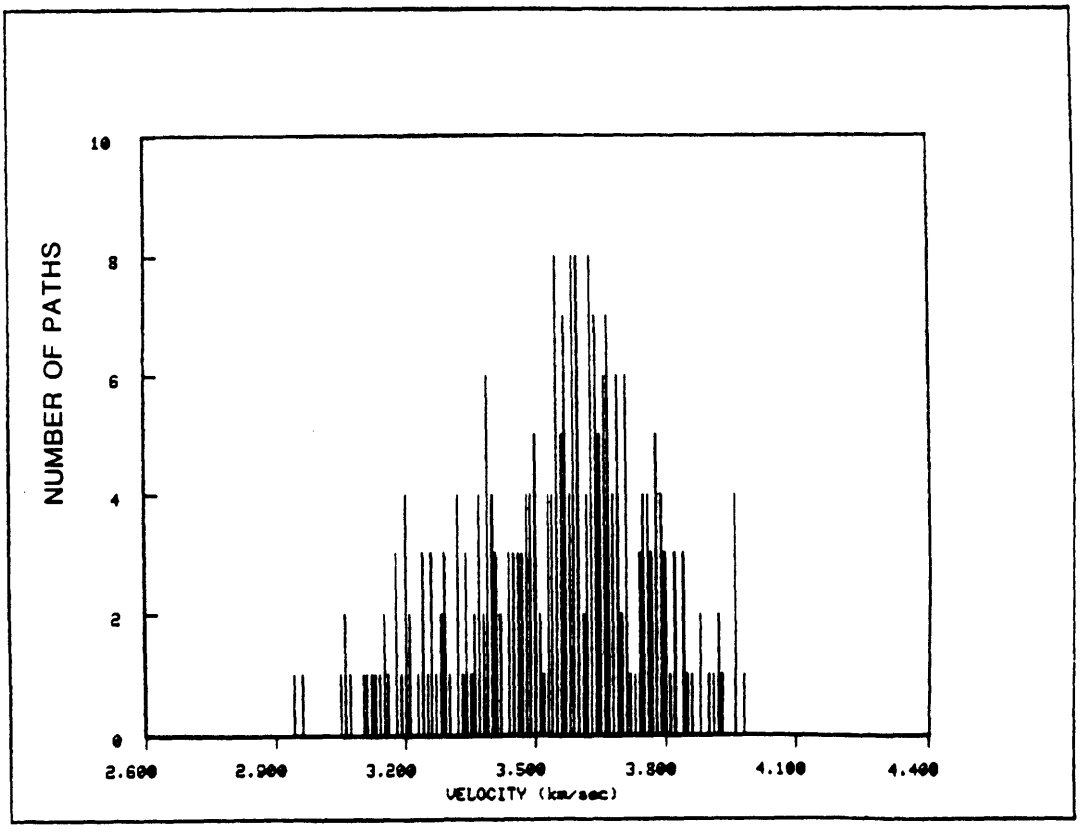

FIGURE C.2l REGION N

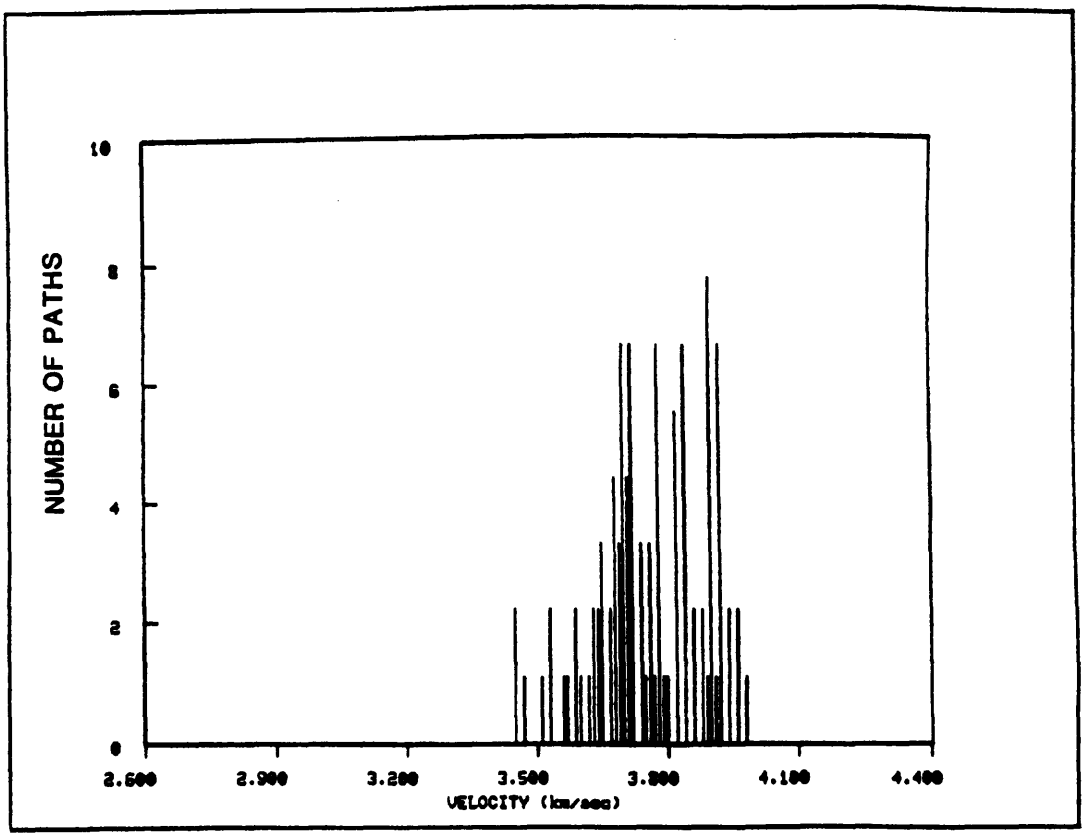

FIGURE C.2m REGION #

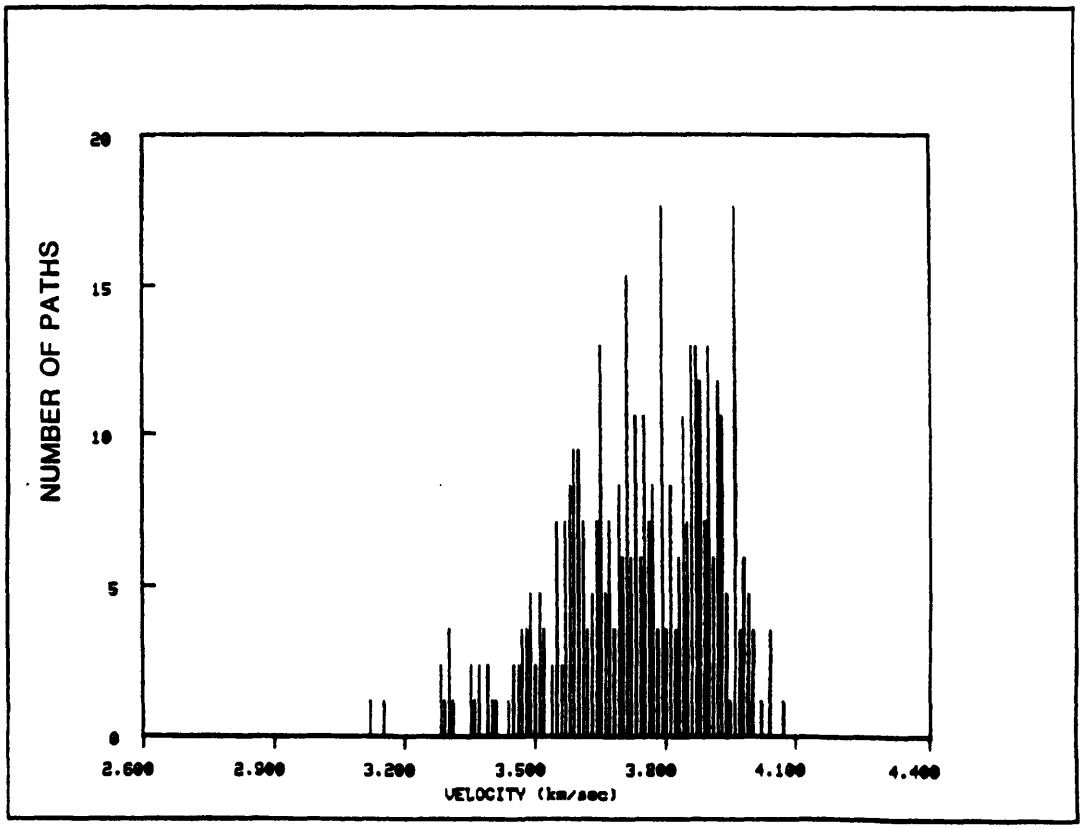

FIGURE C.2n REGION =

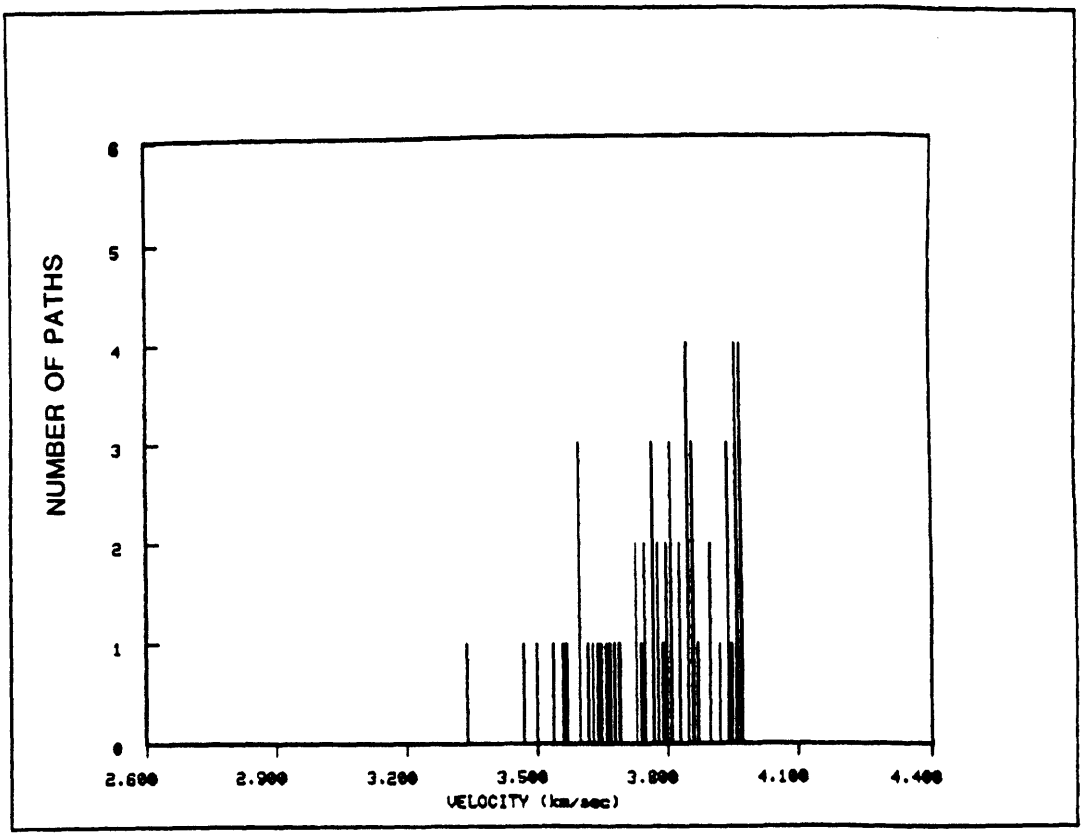

FIGURE C.2o REGION -

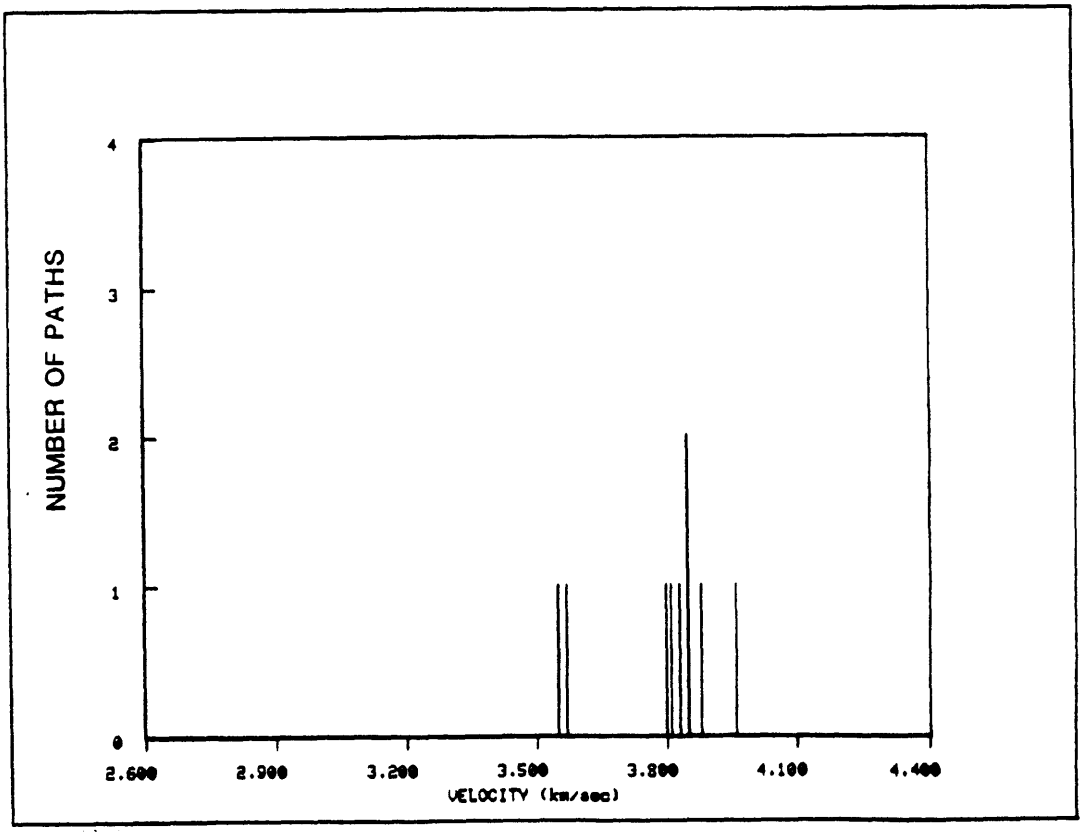

FIGURE C.2p REGION 0

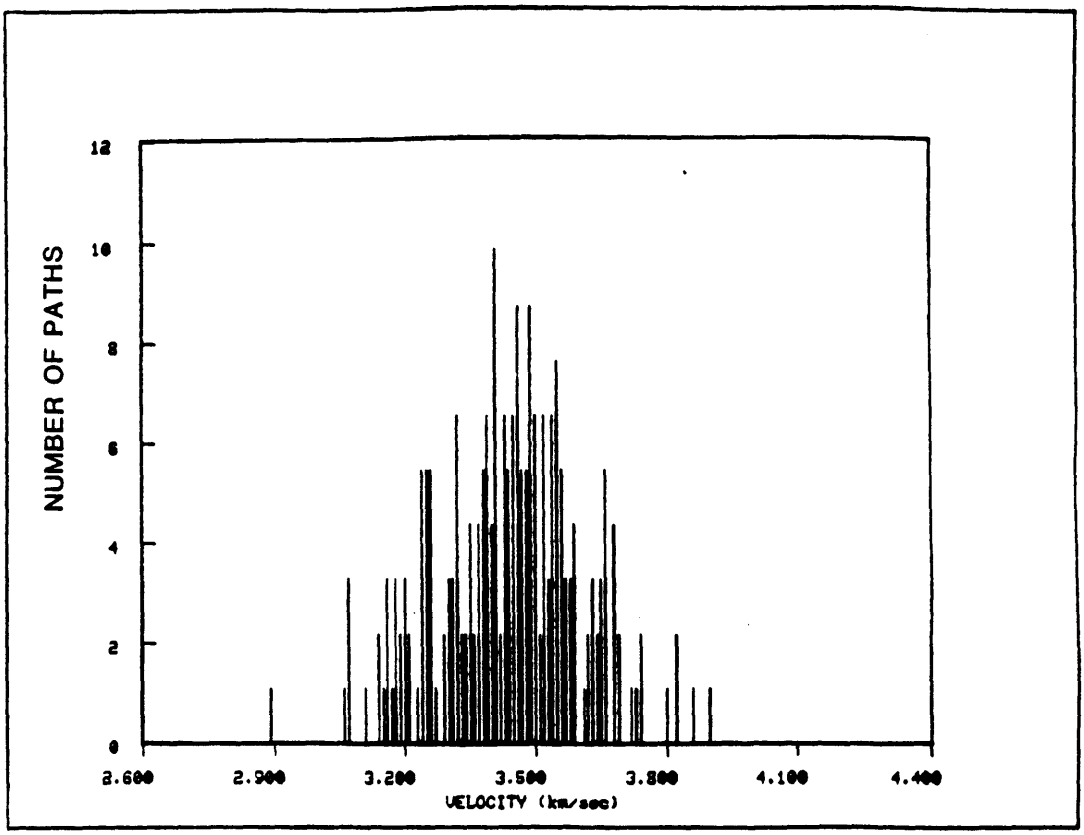

FIGURE C.2q REGION .

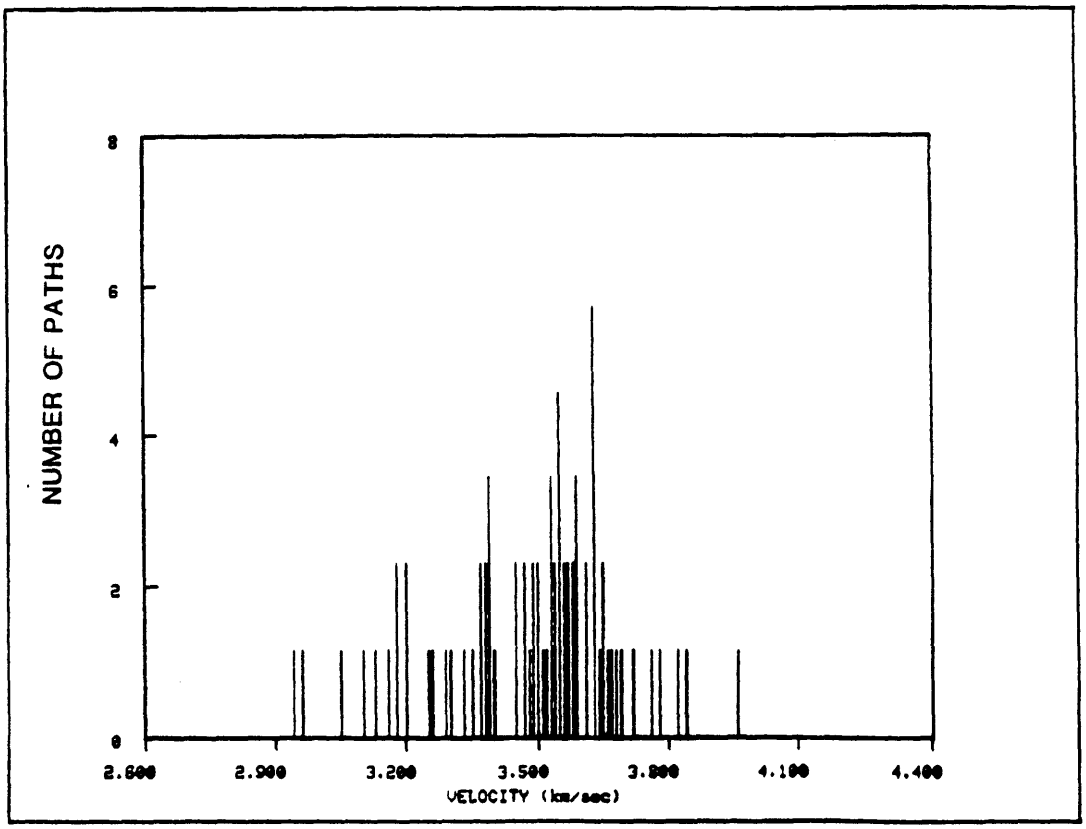

FIGURE C.2r REGION ø

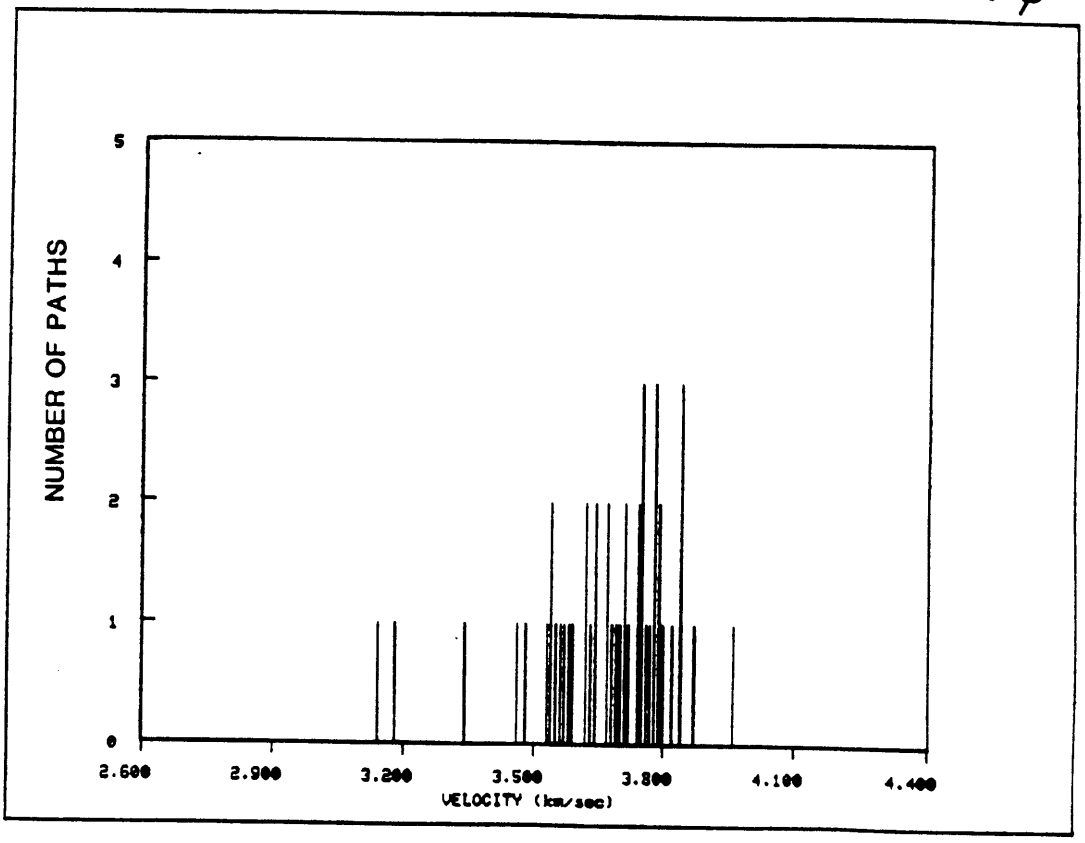

FIGURE C.3a

PERIOD 40 sec

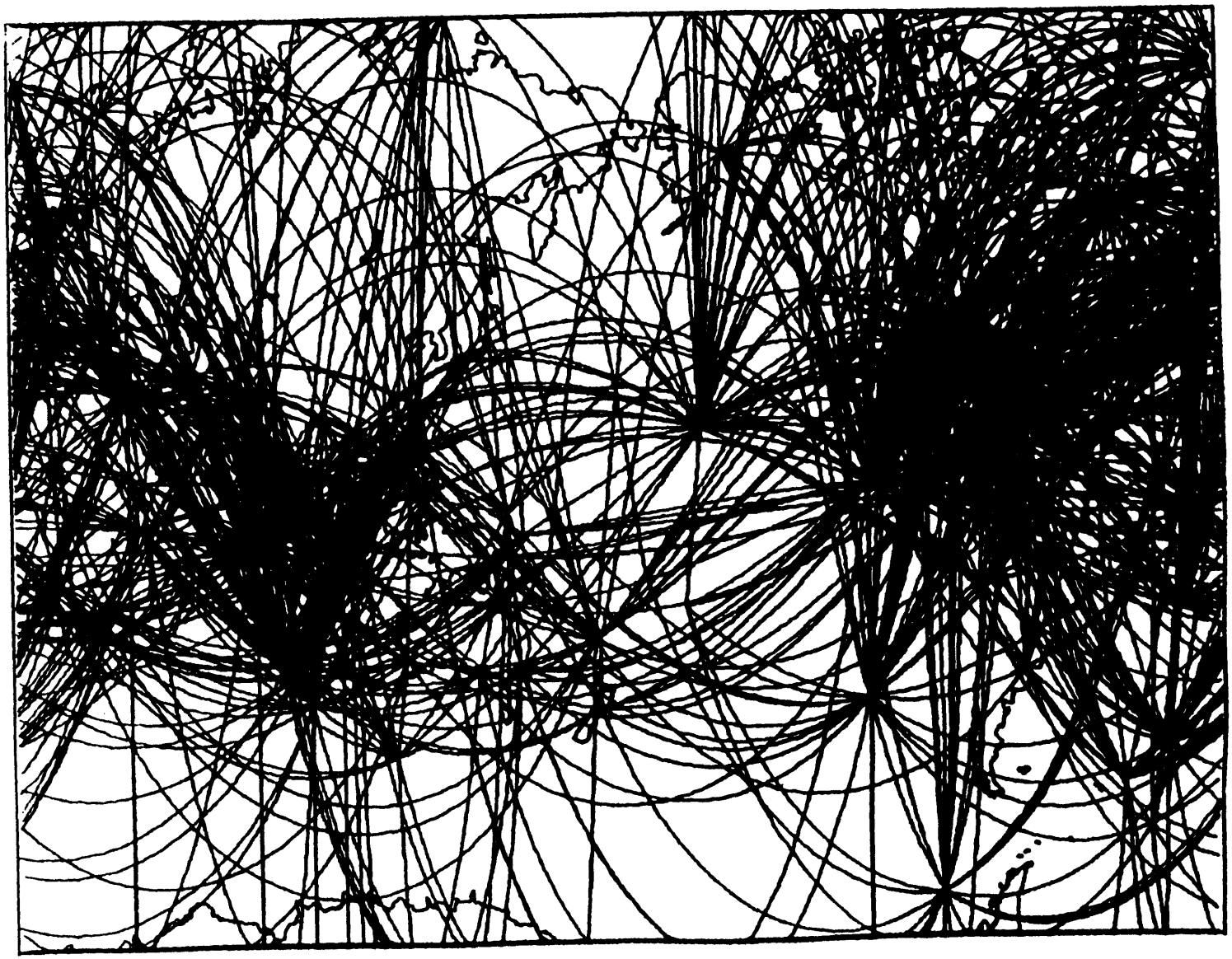

FIGURE C.3b REGION a

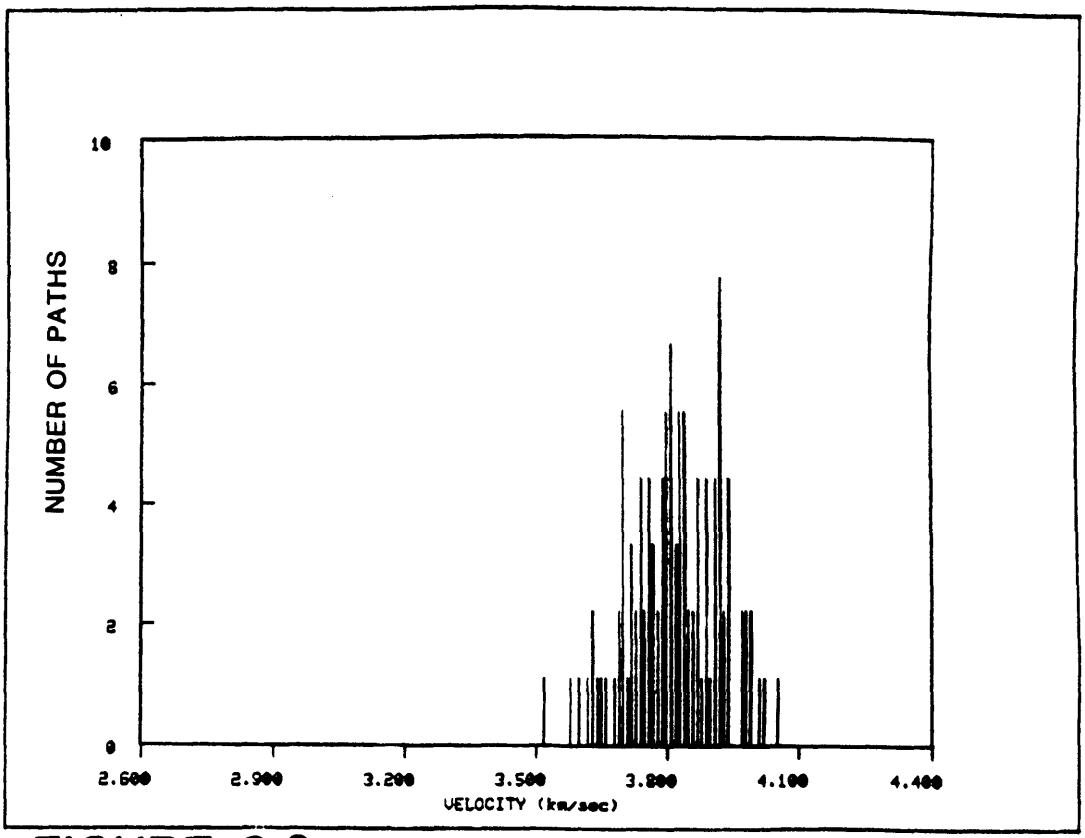

FIGURE C.3c REGION b

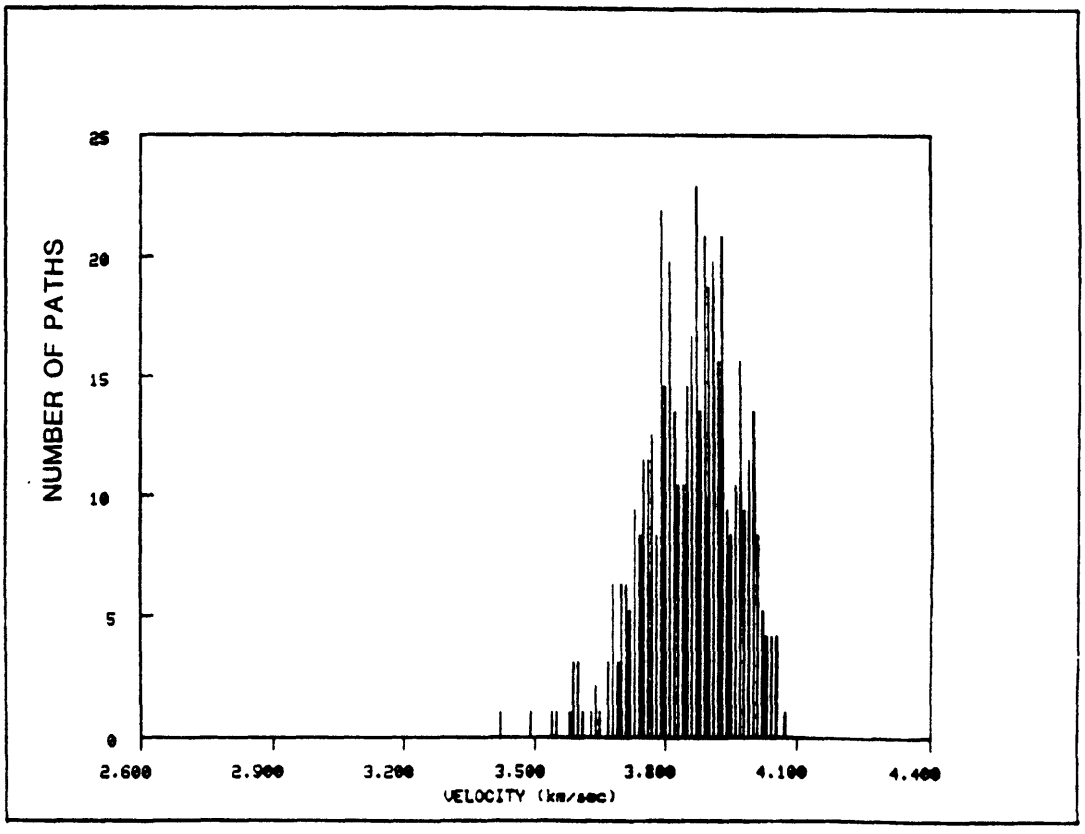

FIGURE C.3d REGION c

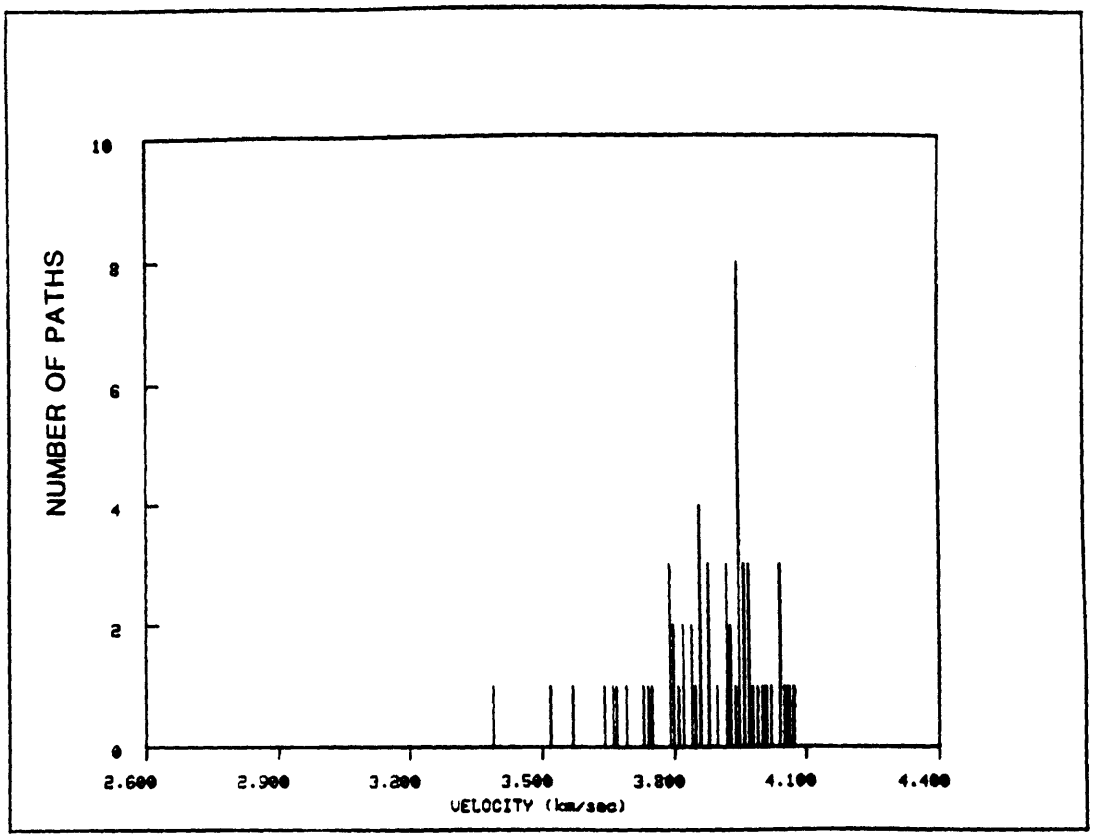

FIGURE C.3e REGION p

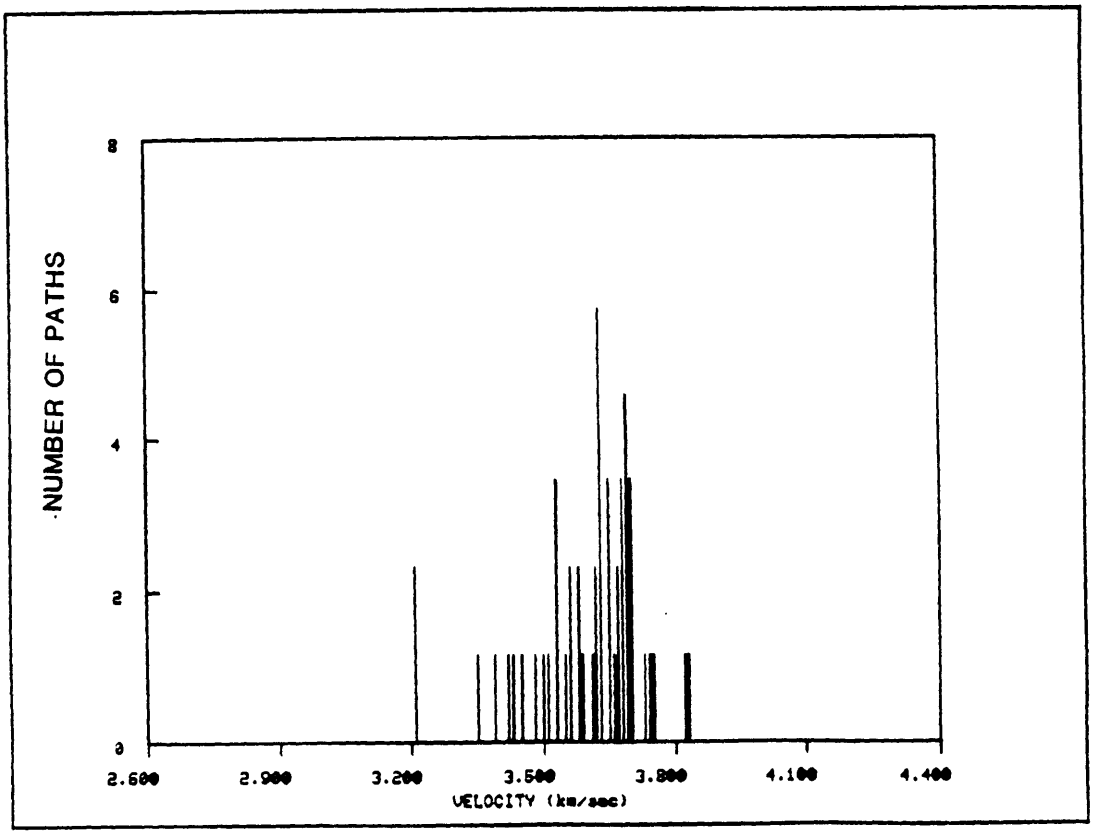

FIGURE C.3f REGION q

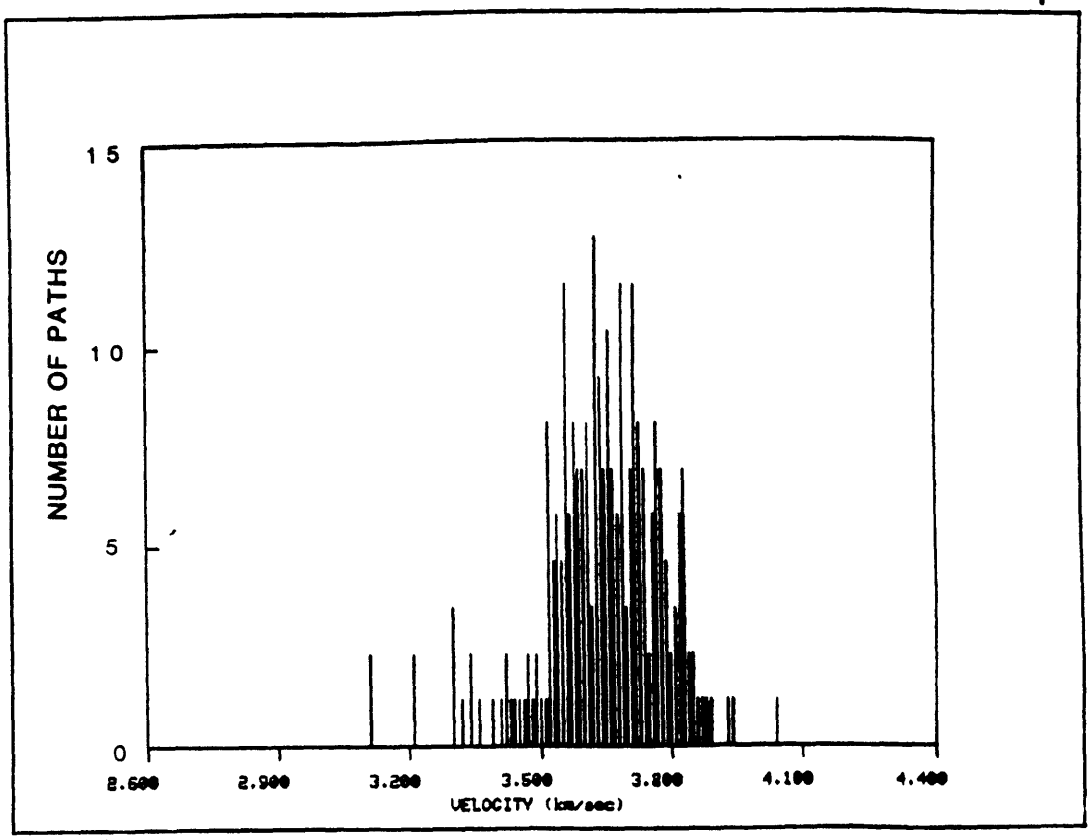

FIGURE C.3g REGION s

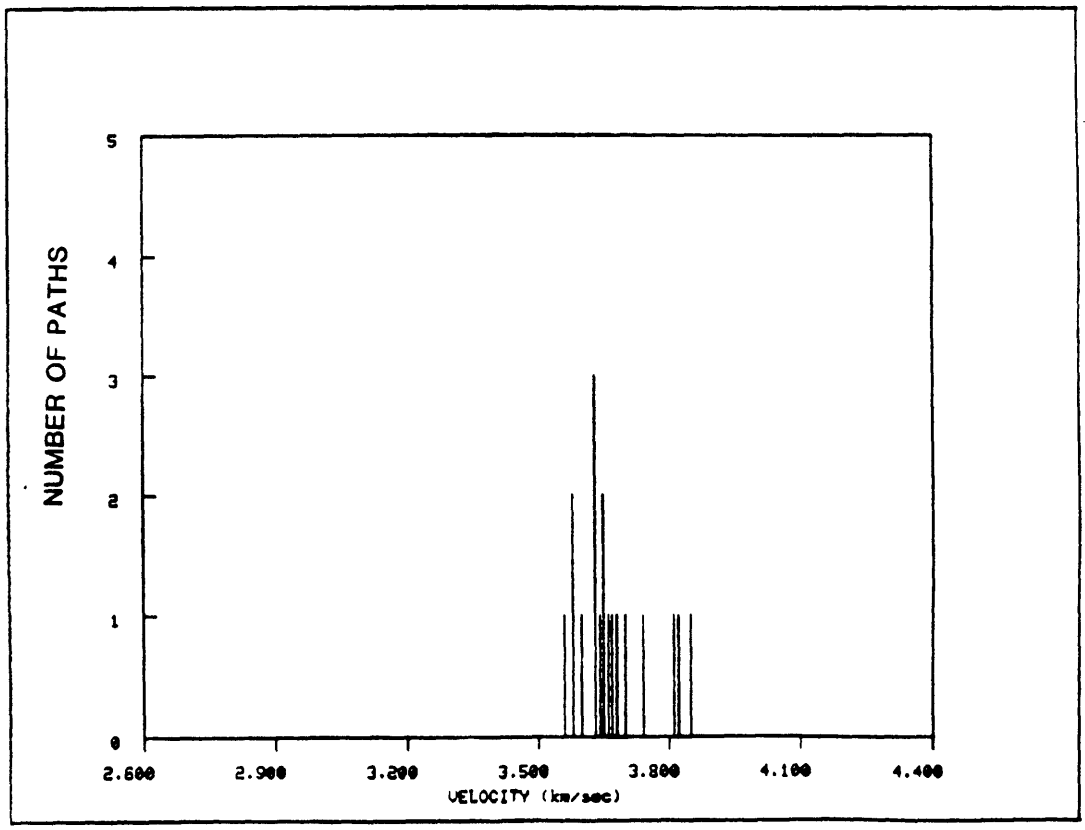

FIGURE C.3h REGION N

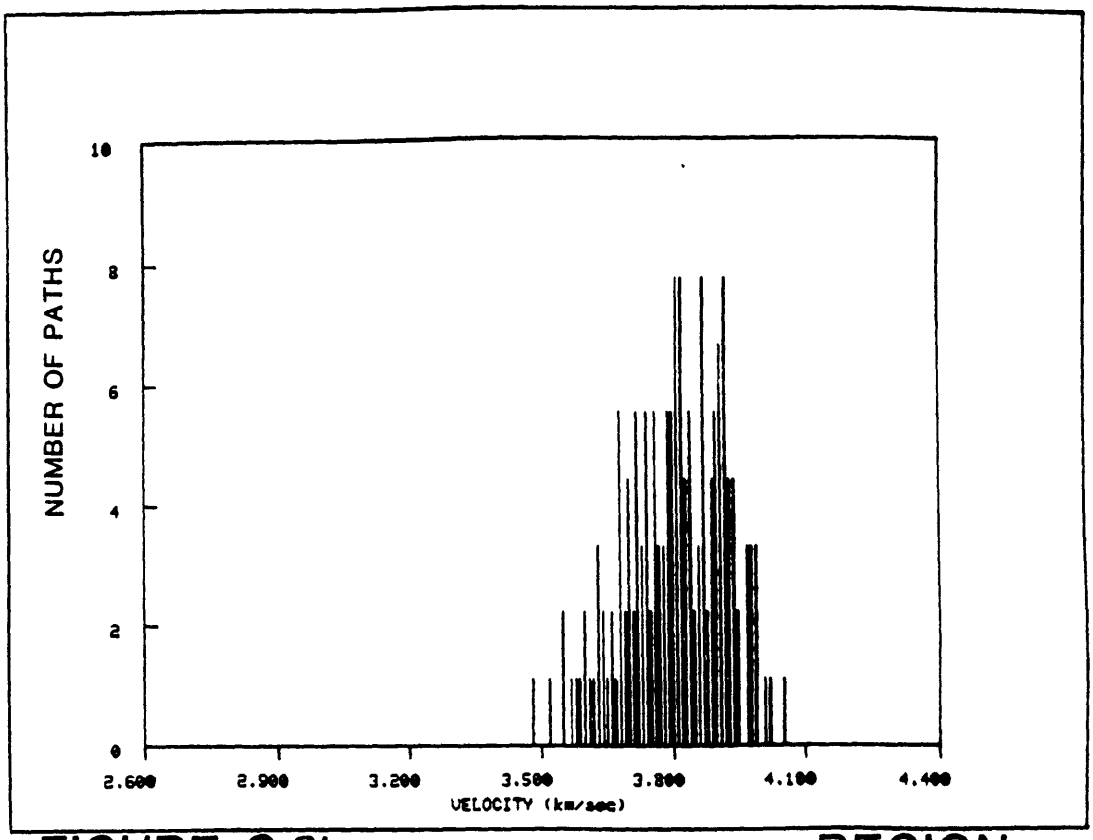

FIGURE C.3i REGION =

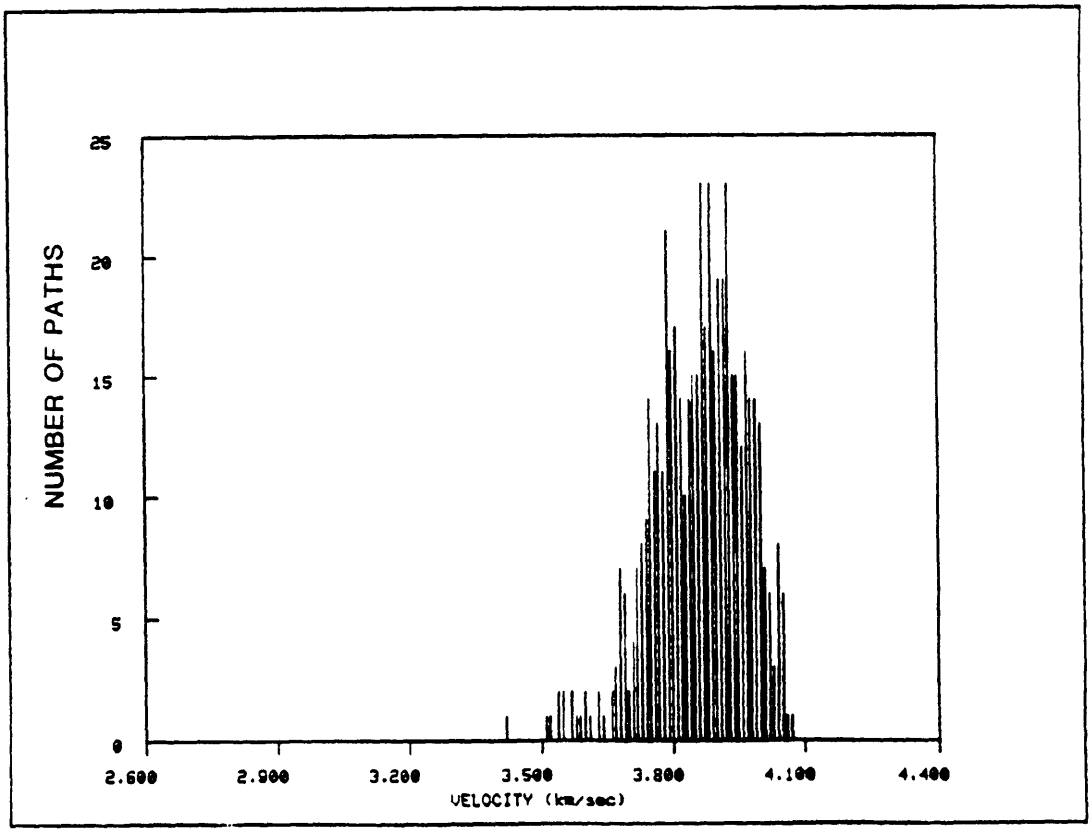

FIGURE C.3j REGION 0

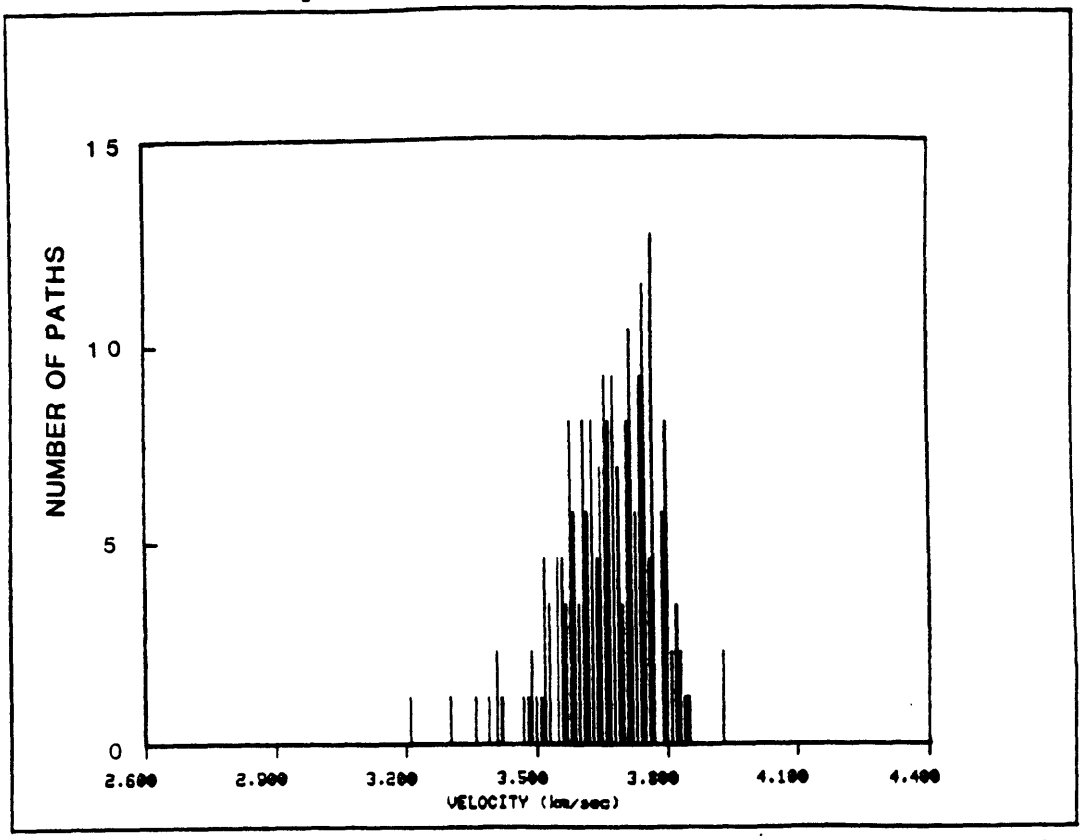

FIGURE C.3k REGION ~~0~~

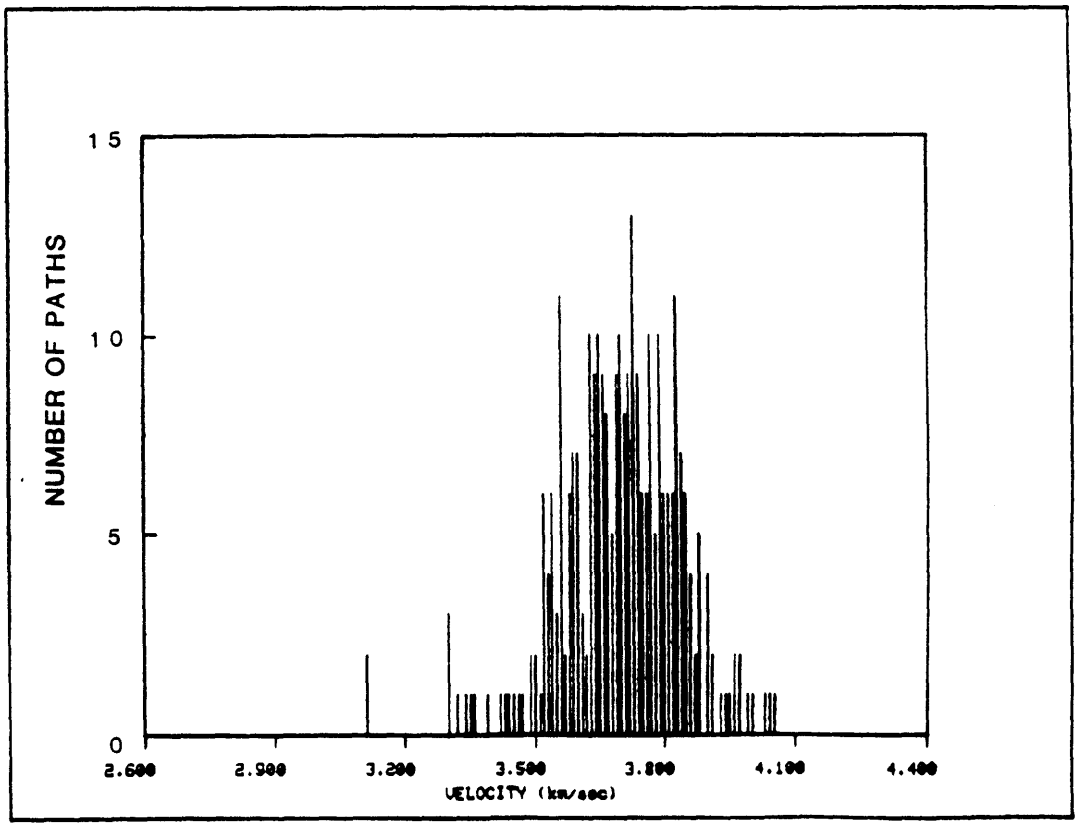

FIGURE C.3l REGION N

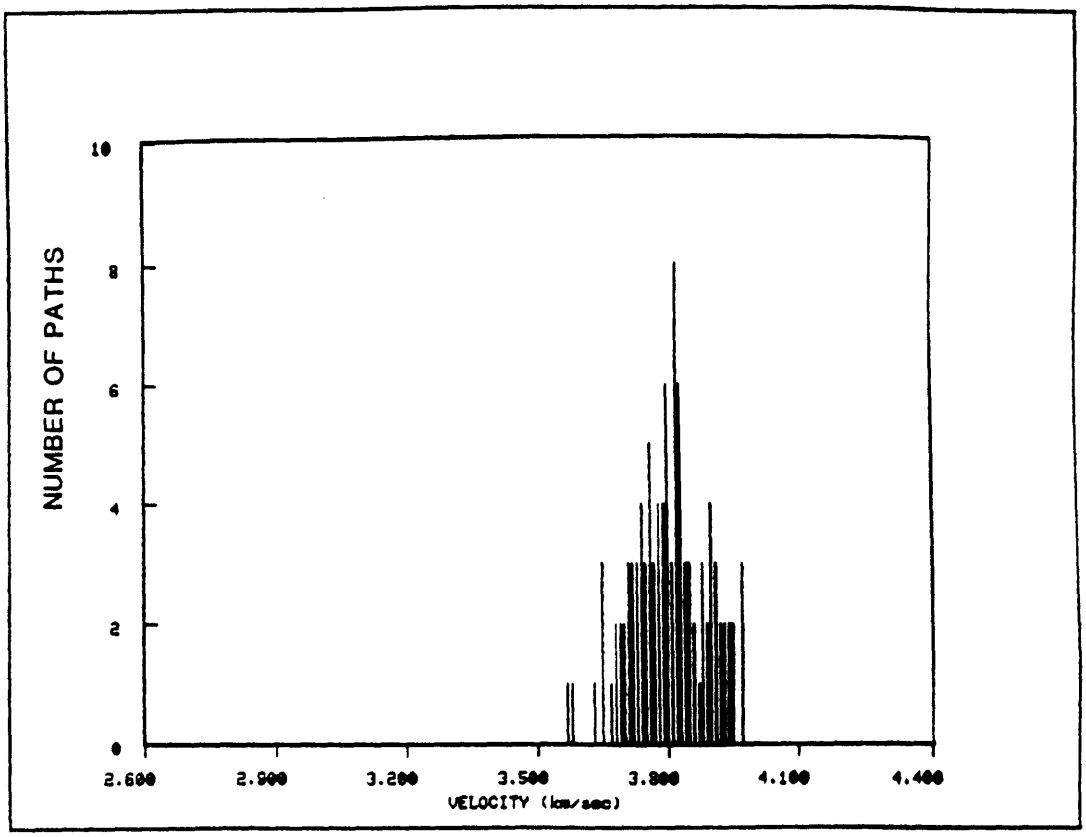

FIGURE C.3m REGION #

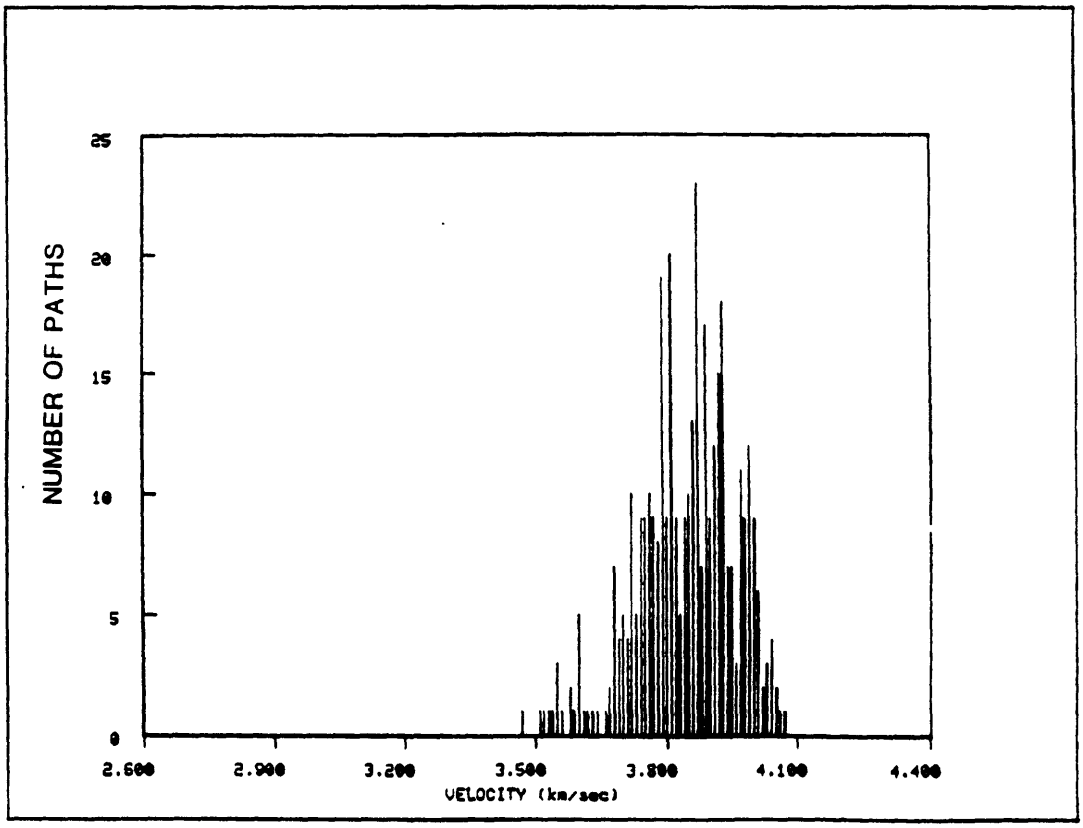

FIGURE C.3n REGION =

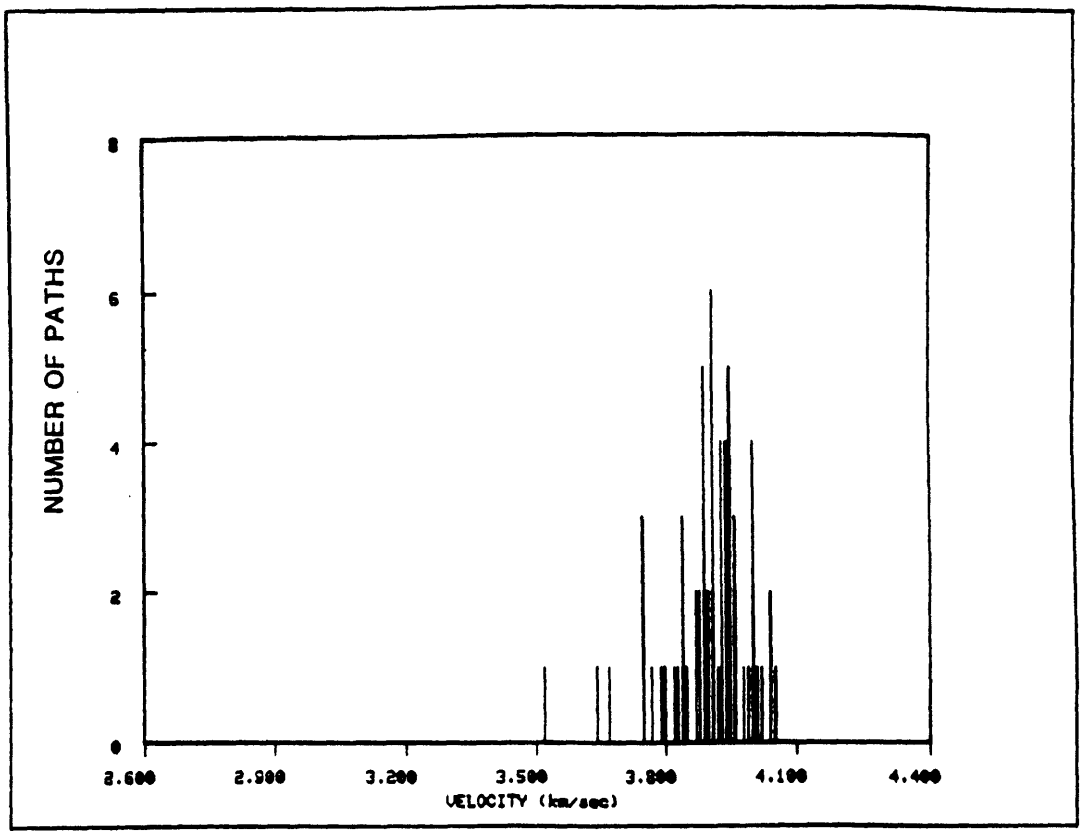

FIGURE C.3o REGION -

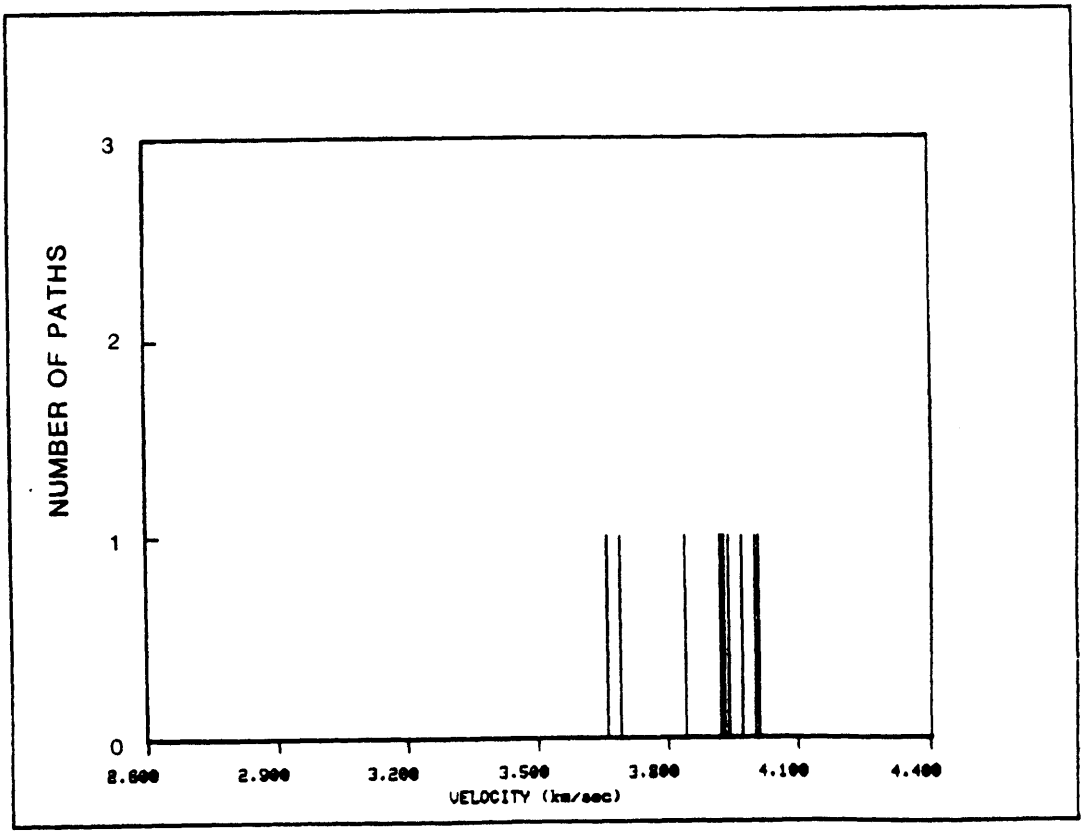

FIGURE C.3p REGION 0

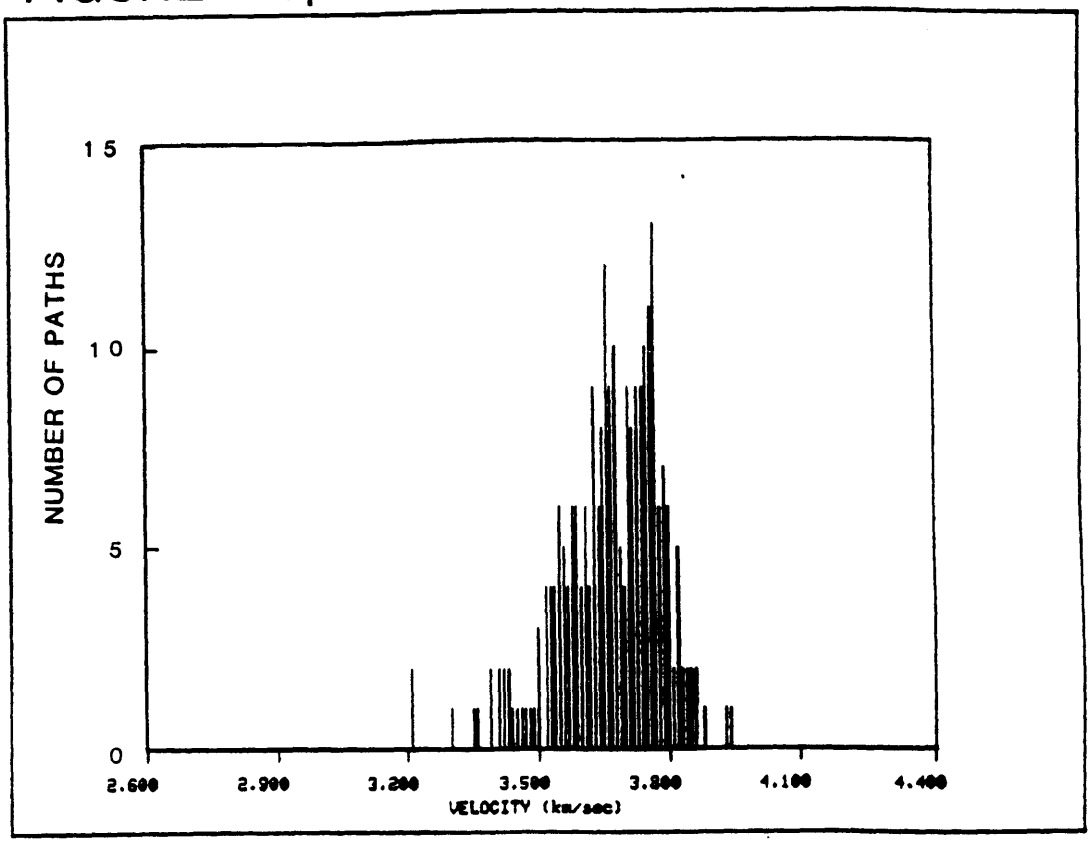

FIGURE C.3q REGION .

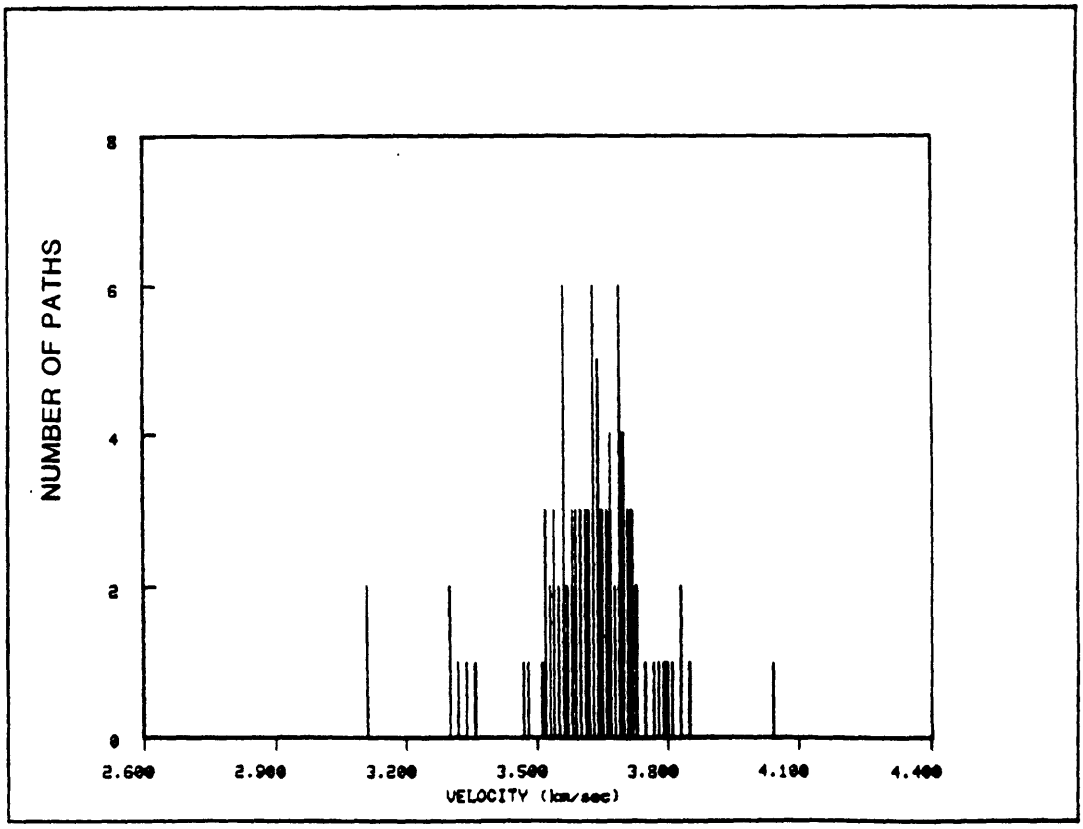

FIGURE C.3r

REGION ø

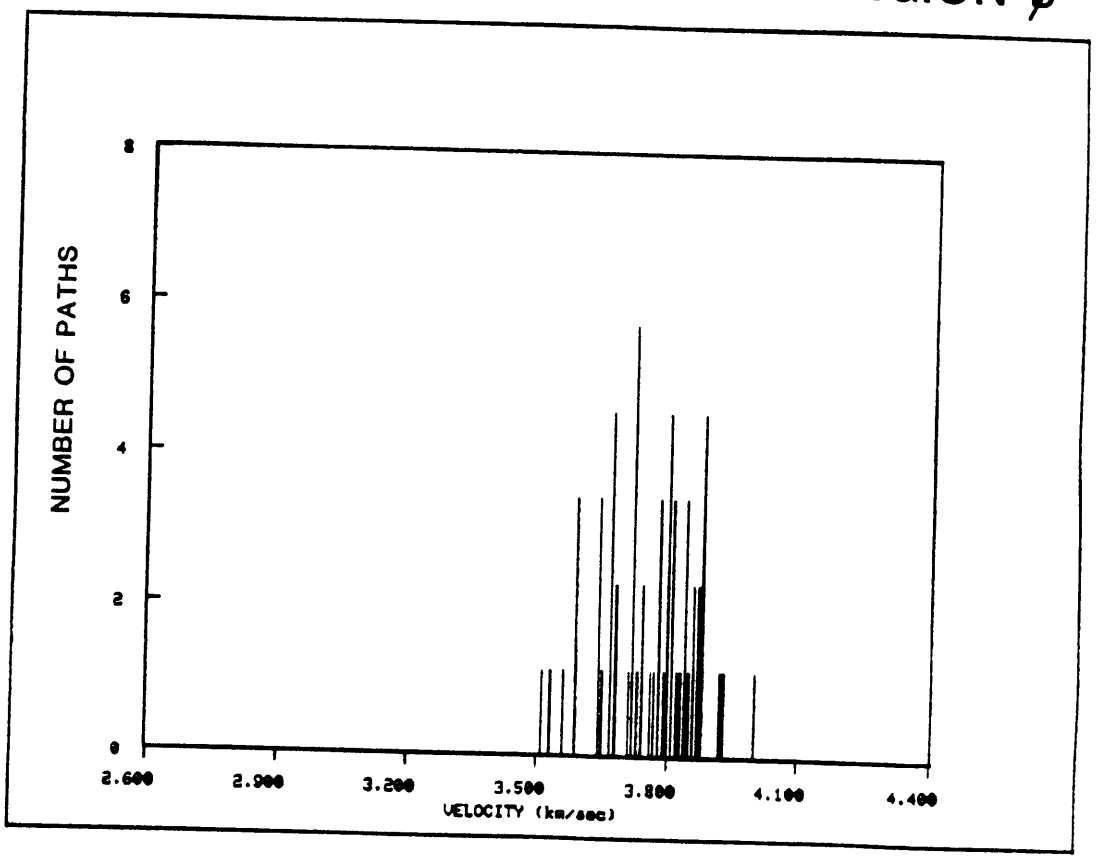

FIGURE C.4a

PERIOD 50 sec

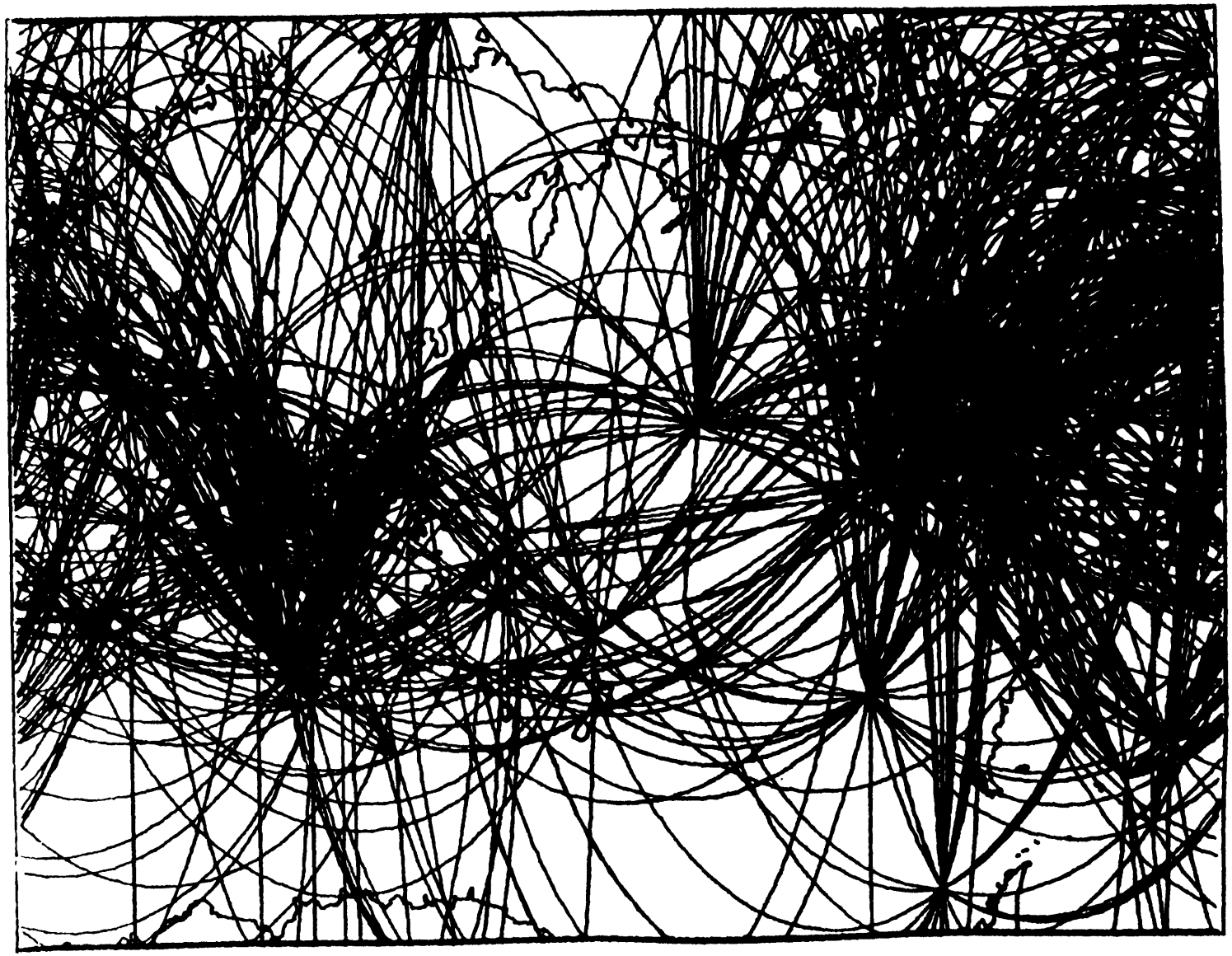

FIGURE C.4b REGION a

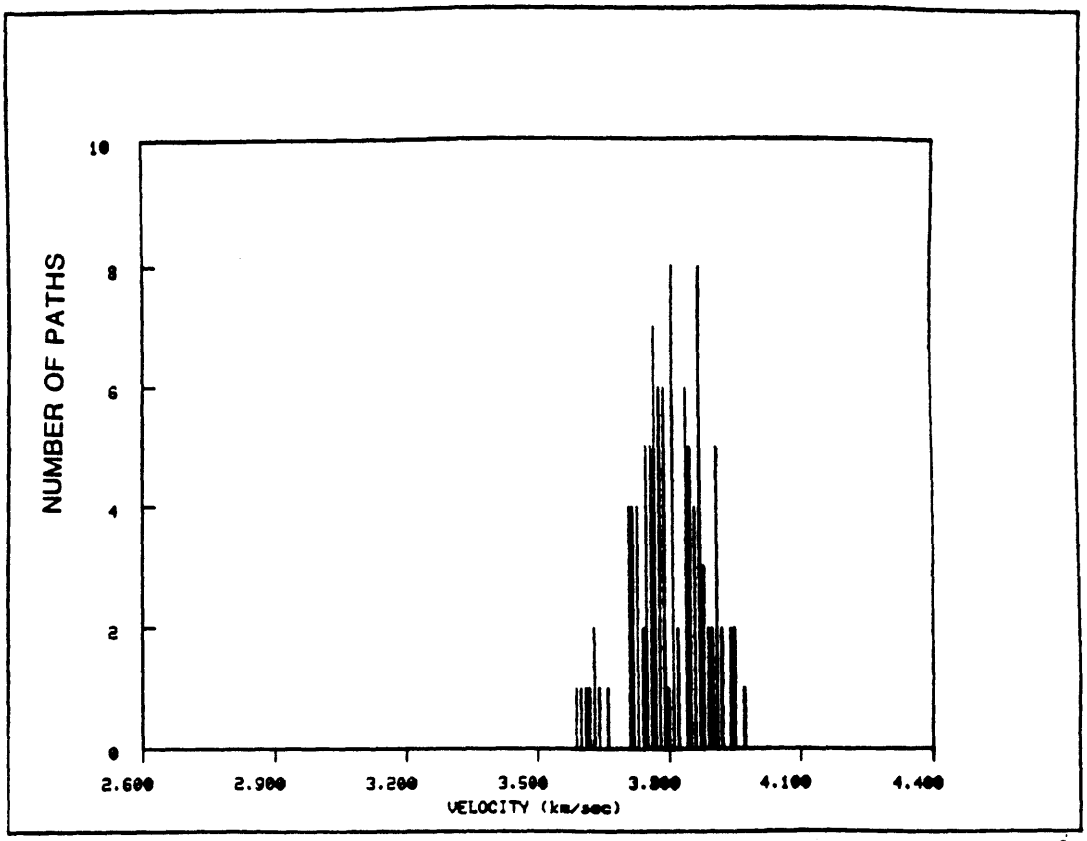

FIGURE C.4c REGION b

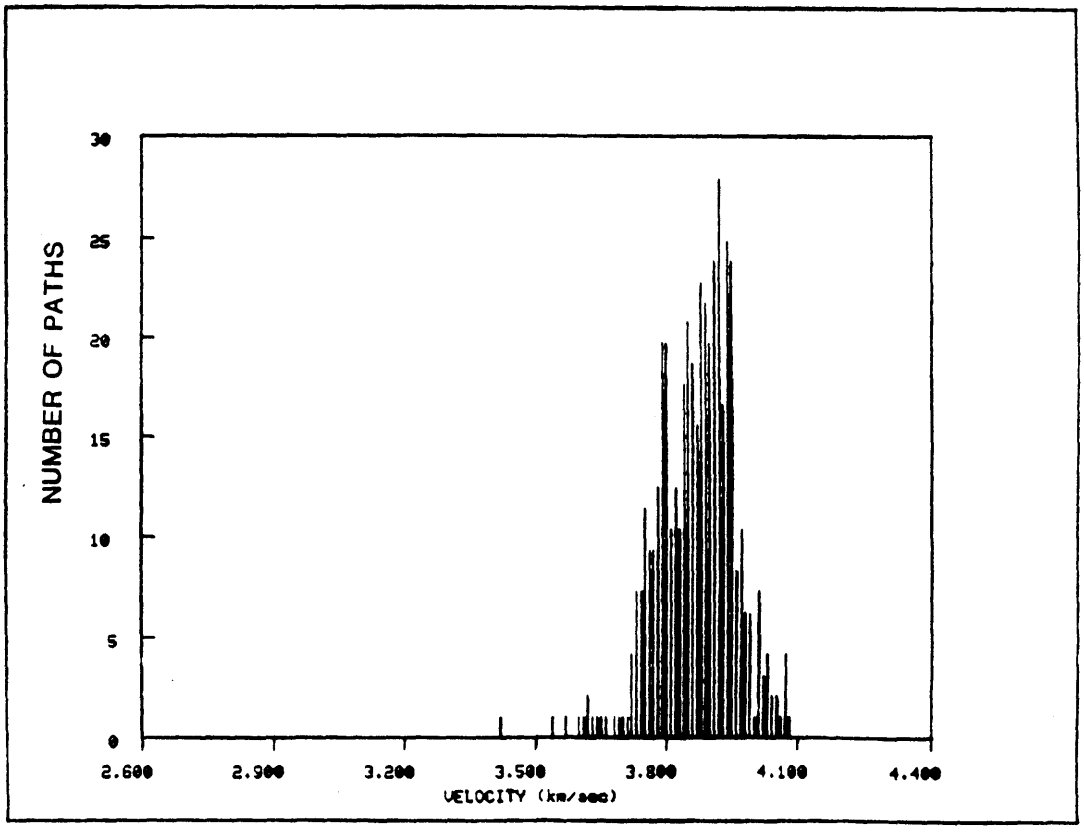

FIGURE C.4d REGION c

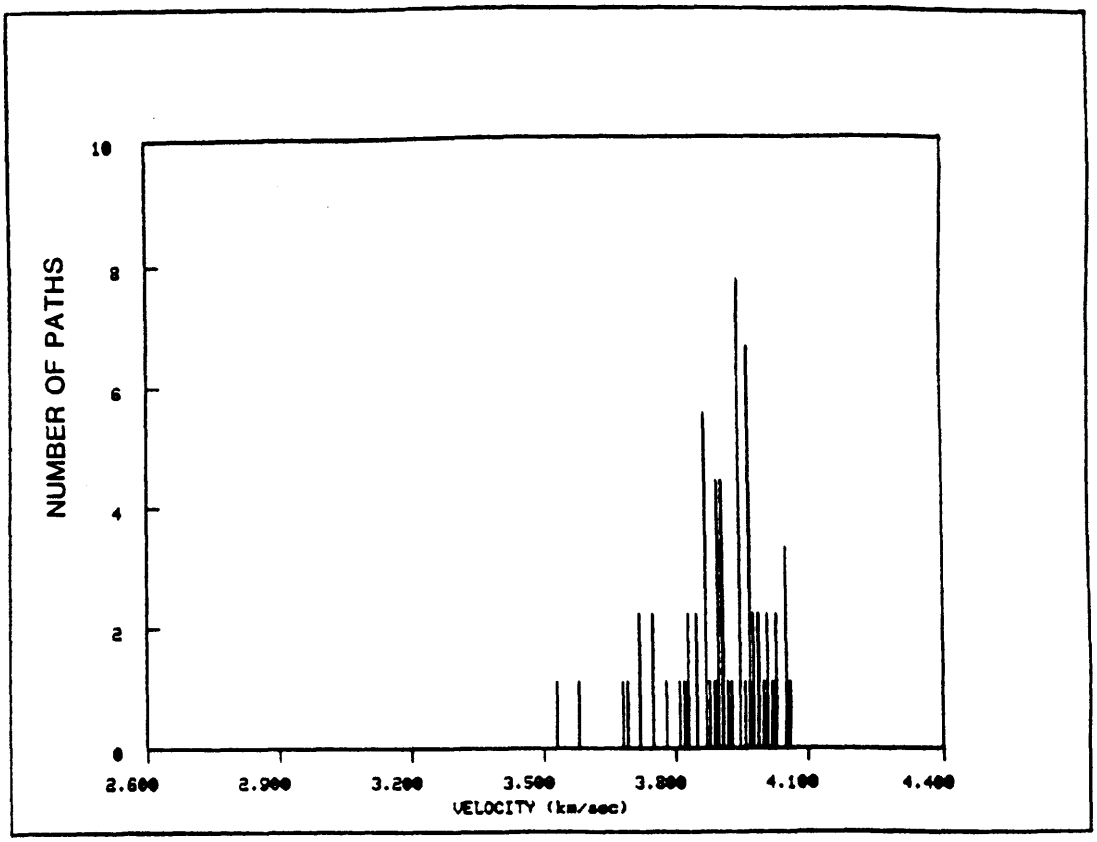

FIGURE C.4e REGION p

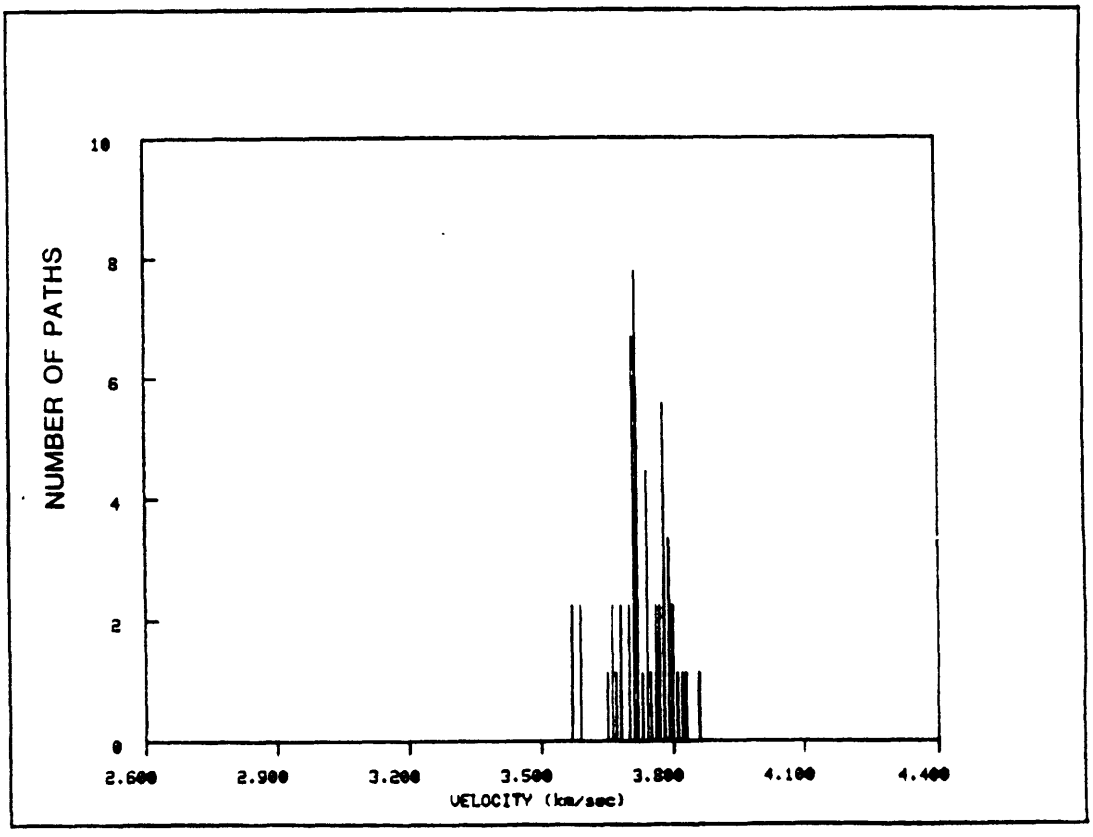

FIGURE C.4f REGION q

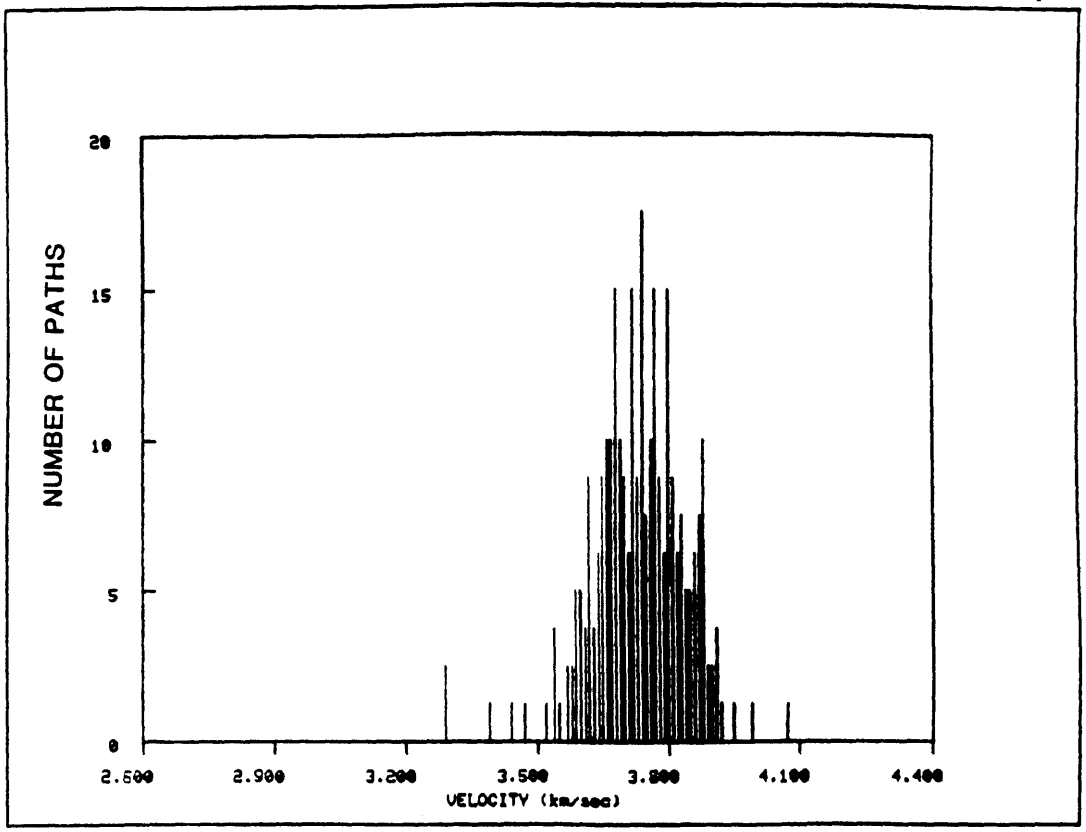

FIGURE C.4g REGION s

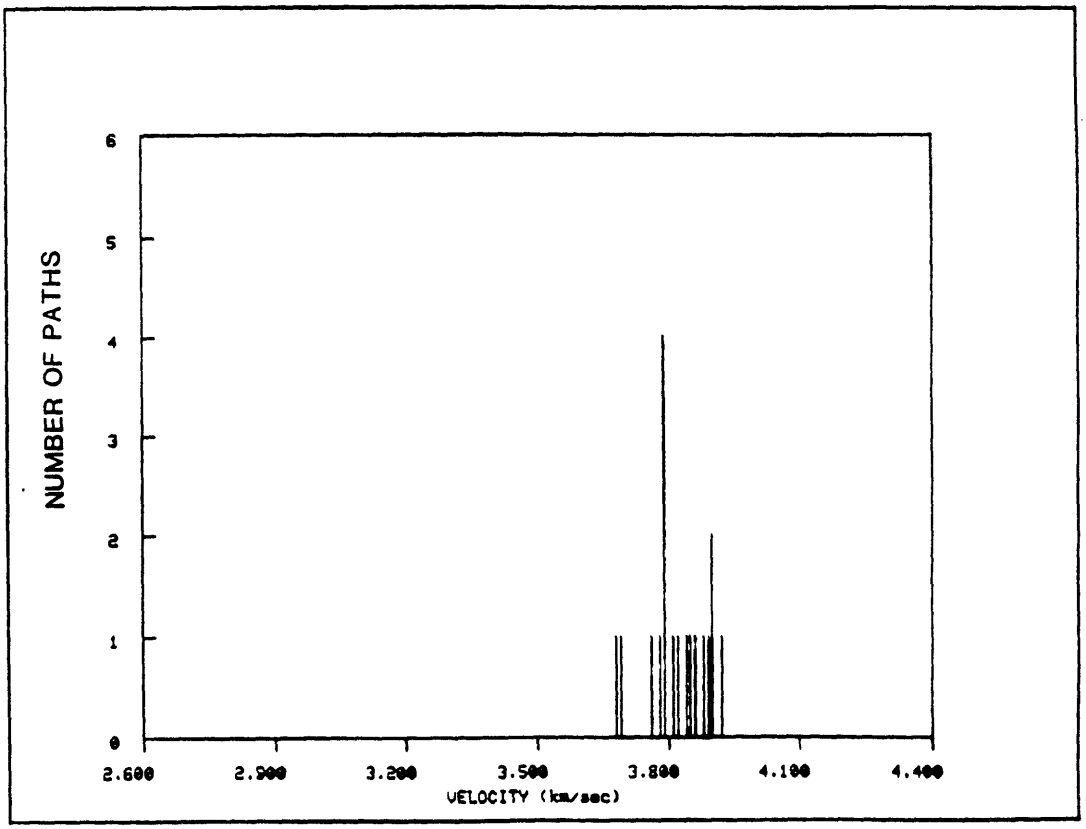

FIGURE C.4h REGION N

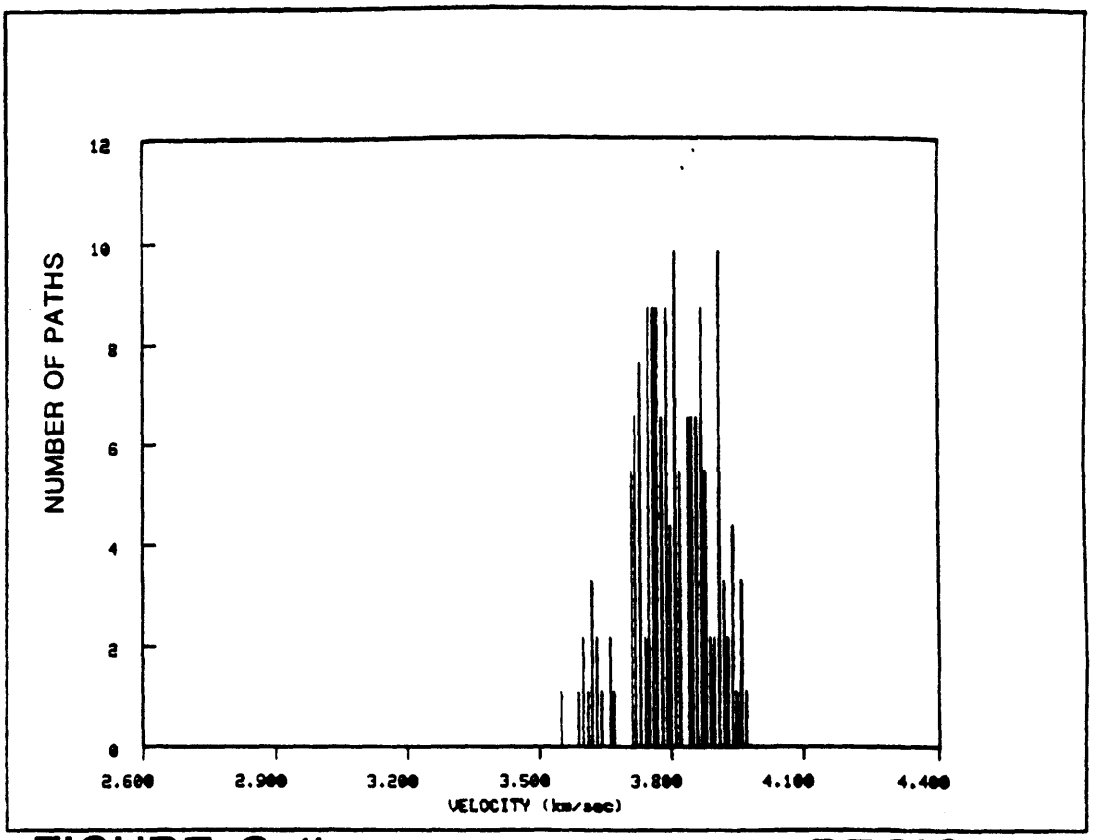

FIGURE C.4i REGION =

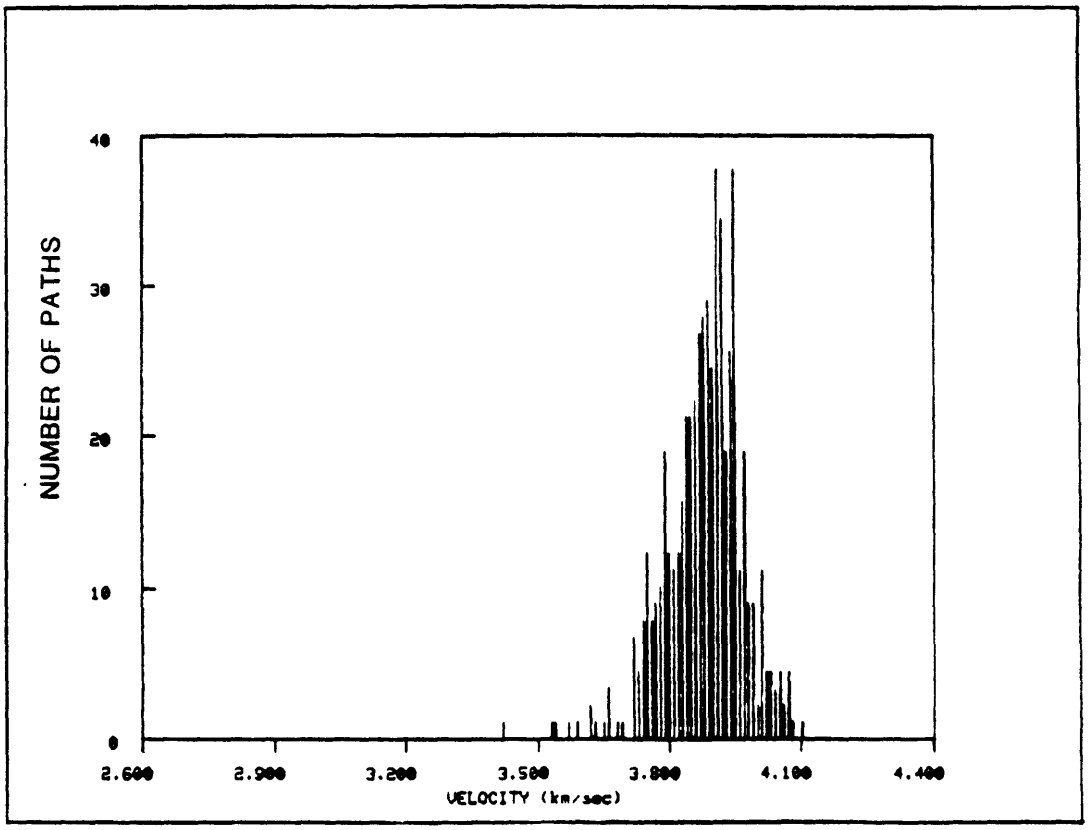

FIGURE C.4j REGION 0

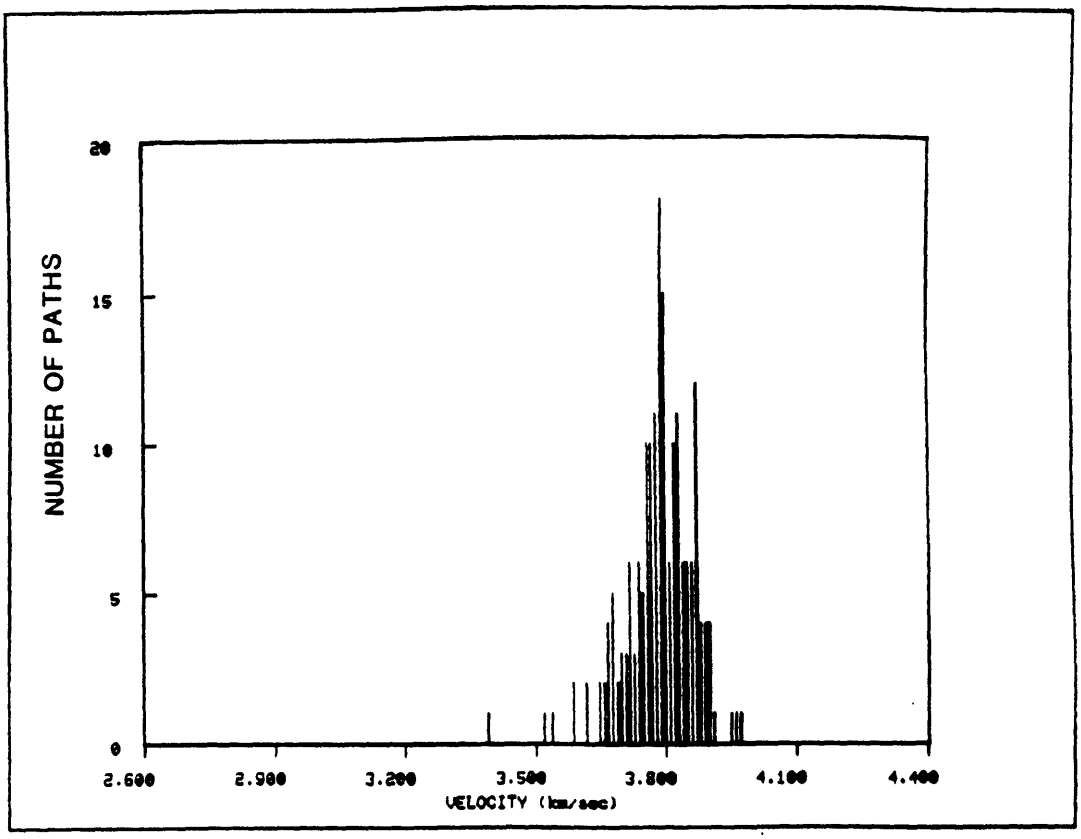

FIGURE C.4k REGION Ø

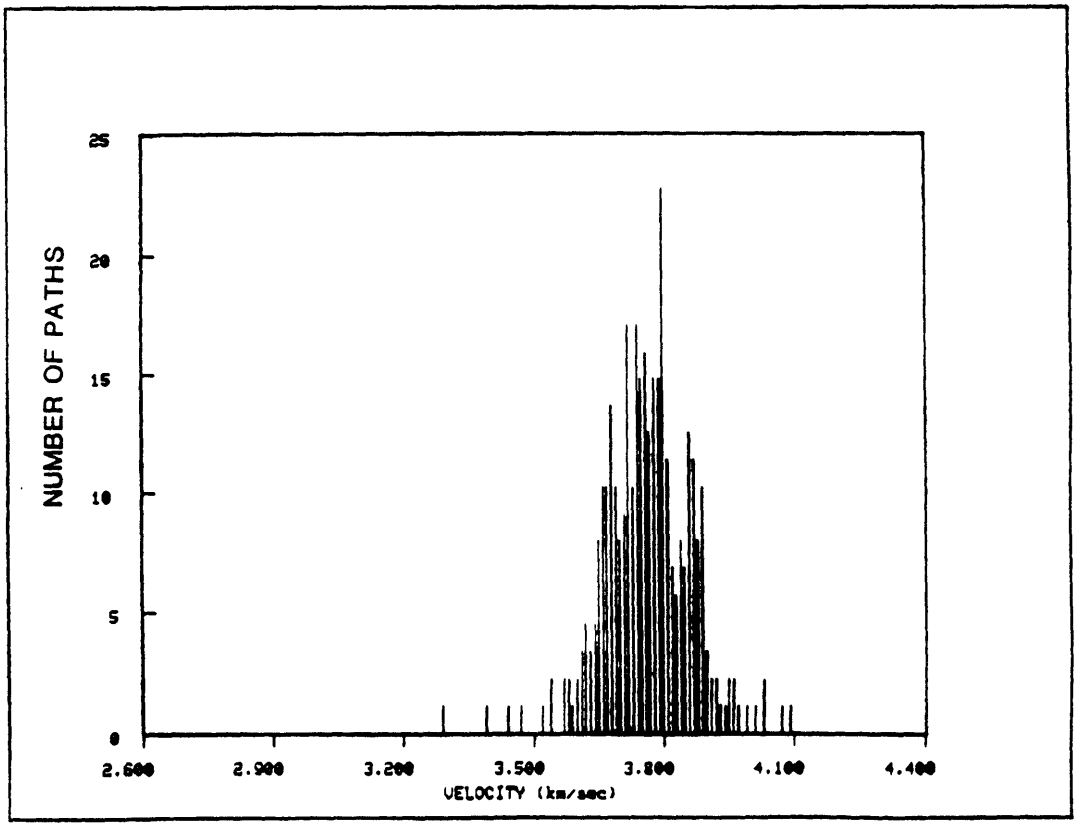

FIGURE C.4l REGION N

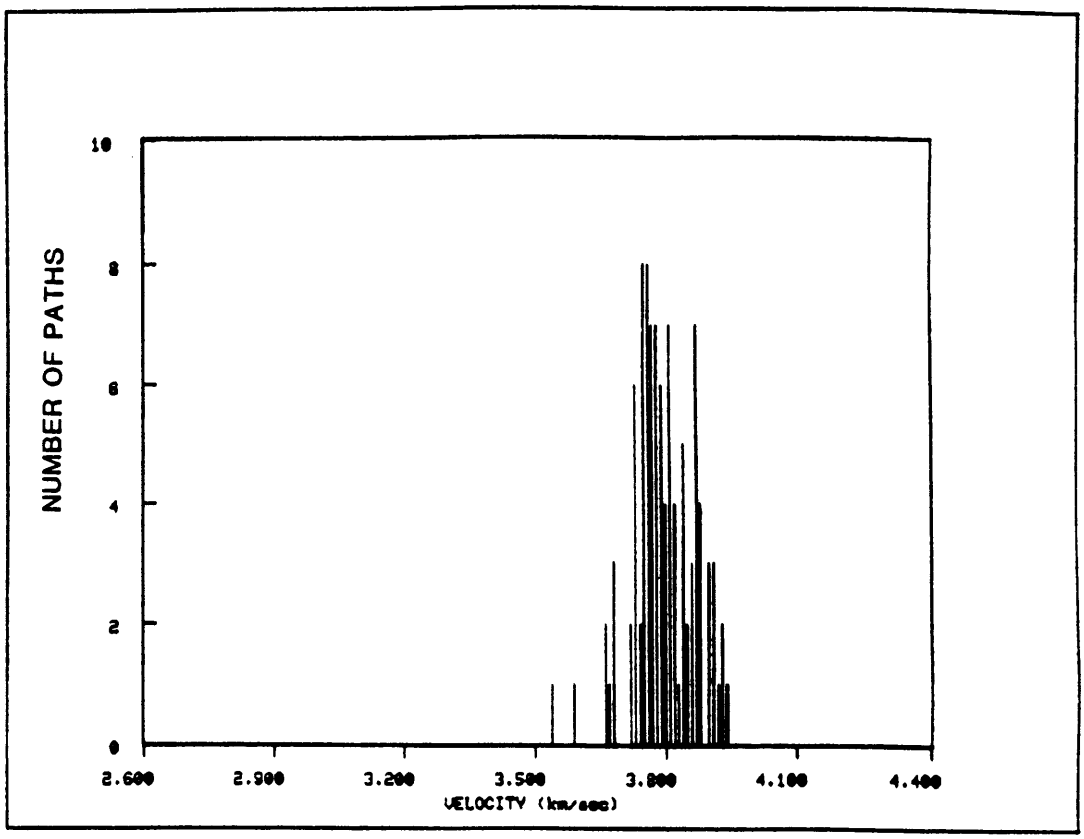

FIGURE C.4m REGION #

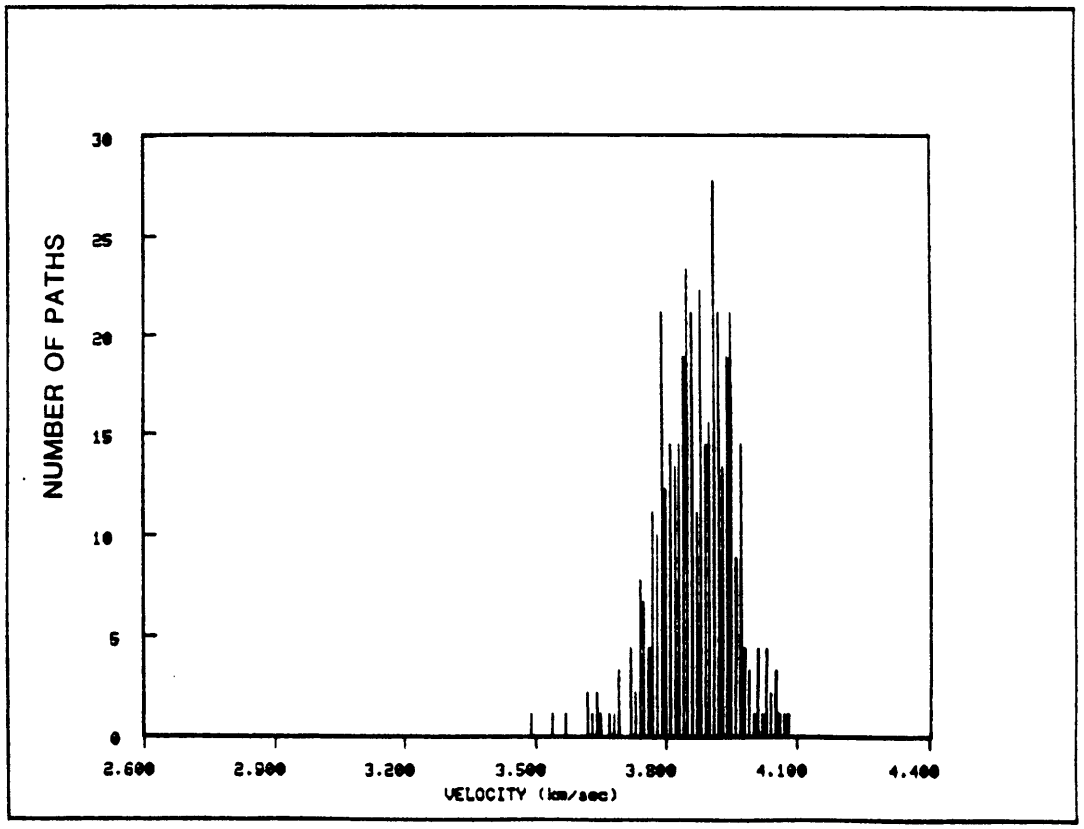

FIGURE C.4n REGION =

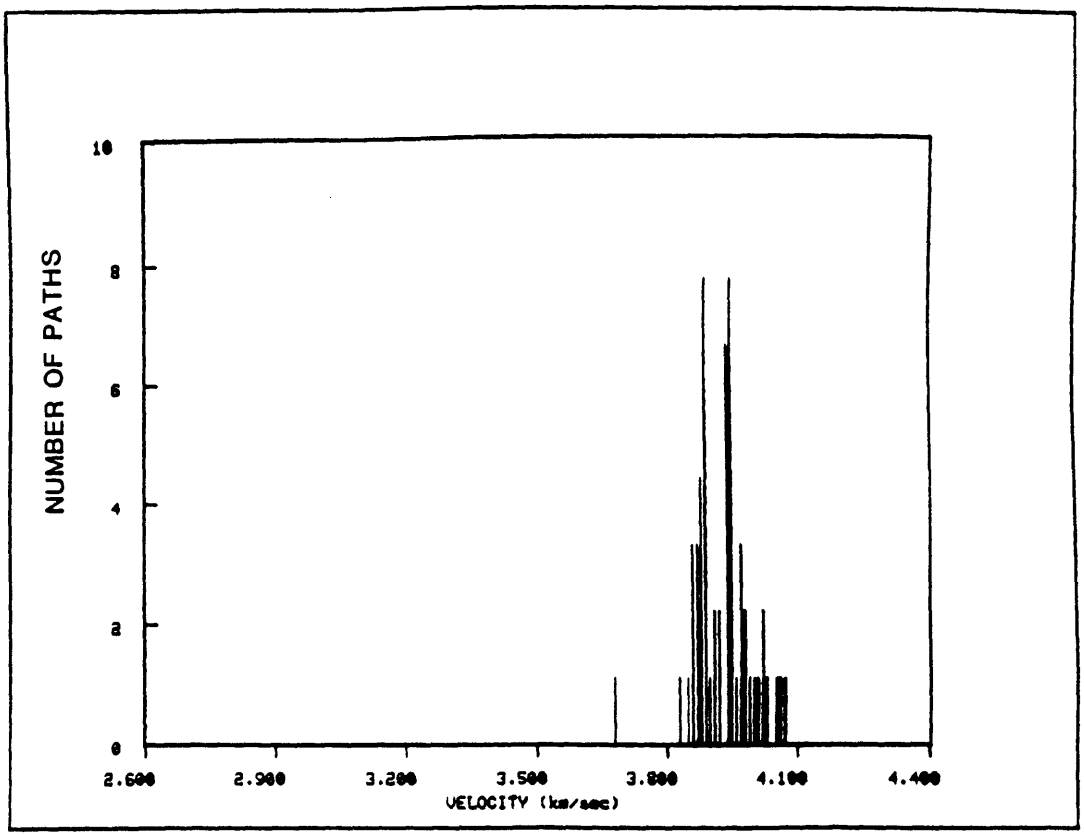

FIGURE C.4o REGION –

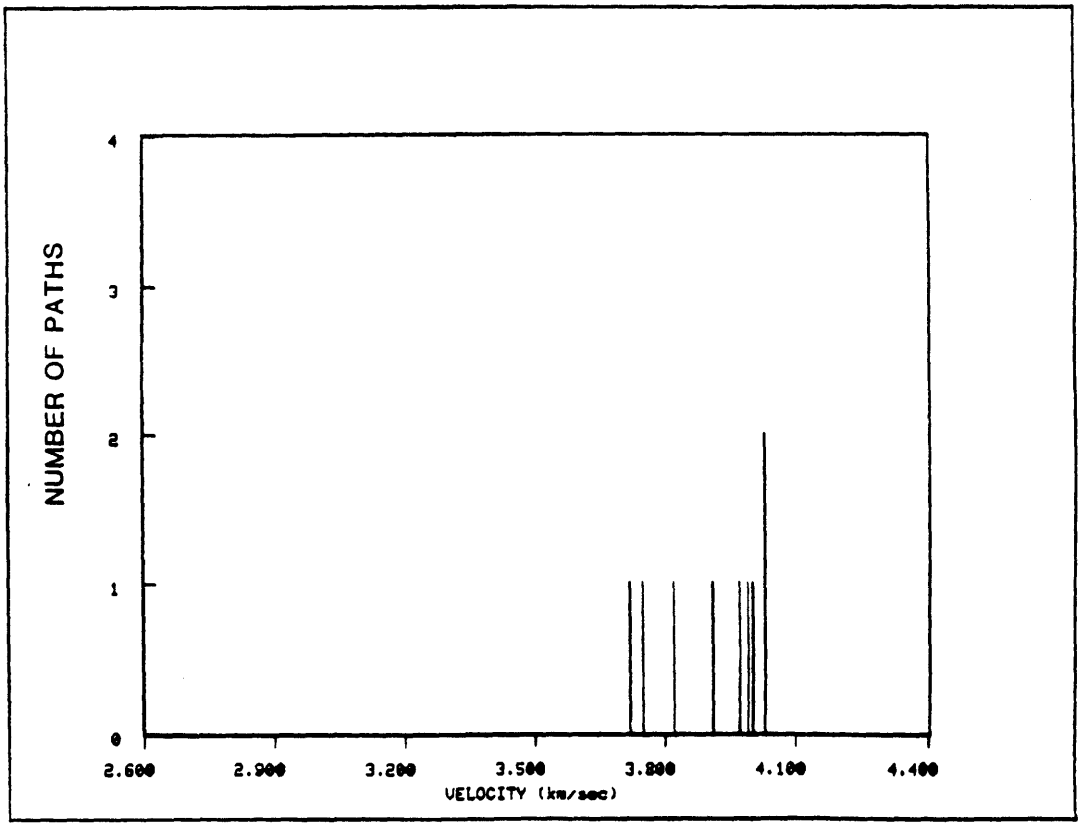

FIGURE C.4p REGION 0

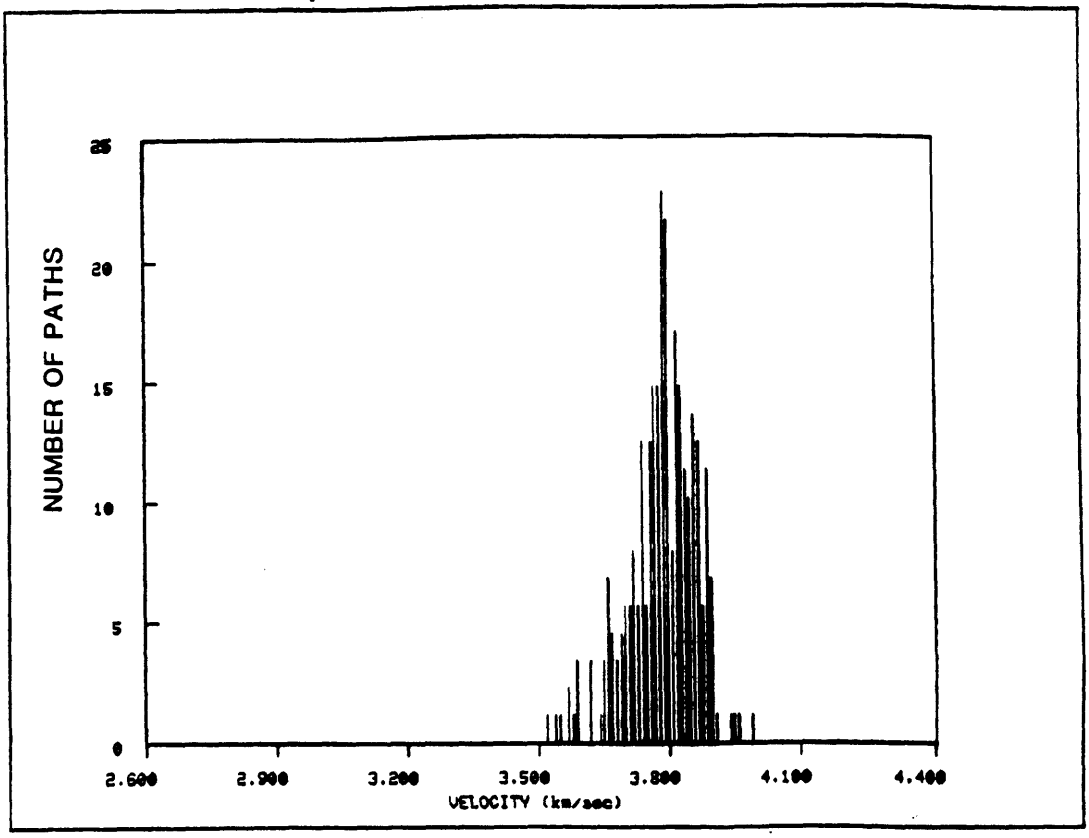

FIGURE C.4q REGION .

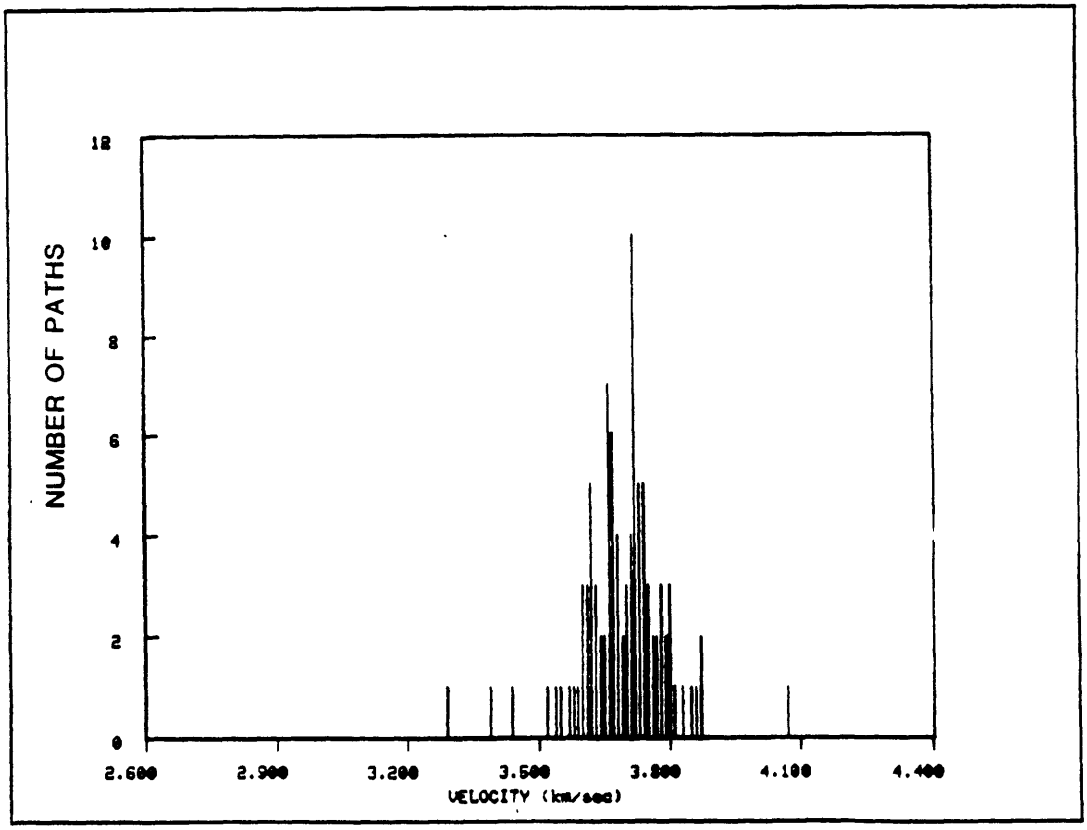

FIGURE C.4r

REGION ø

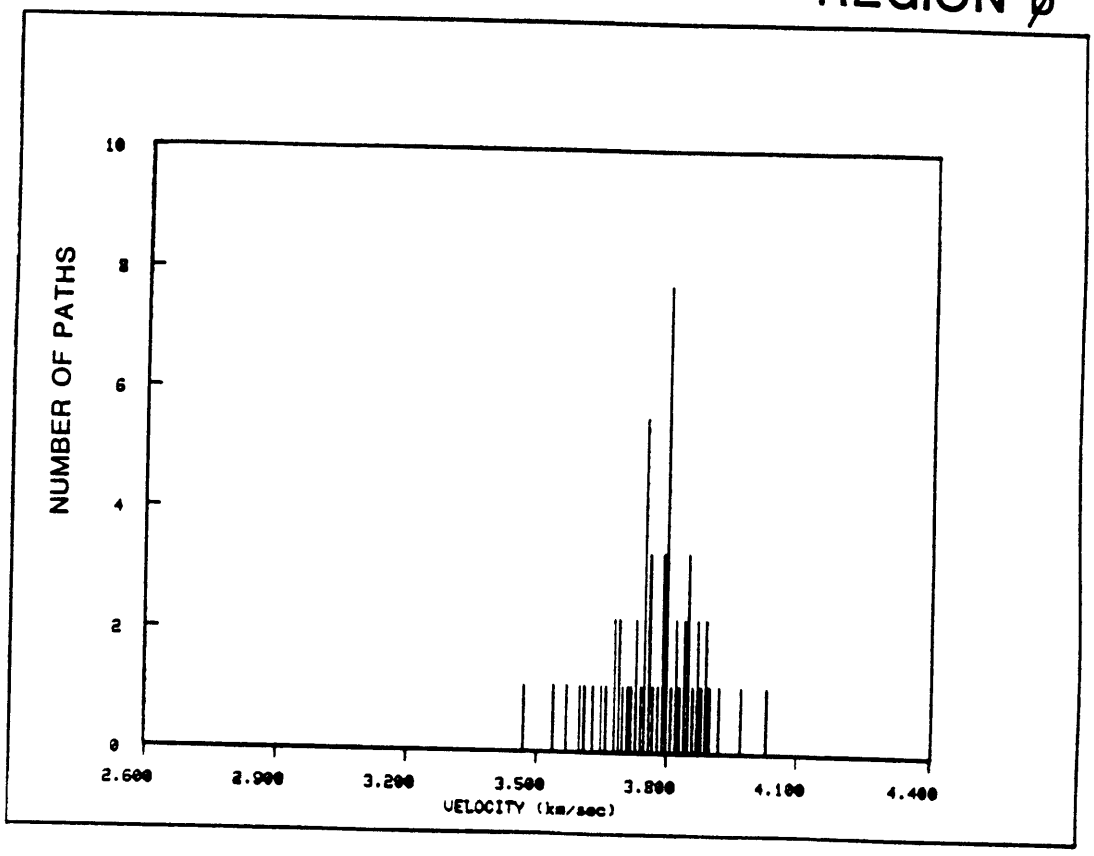

FIGURE C.5a

PERIOD 60 sec

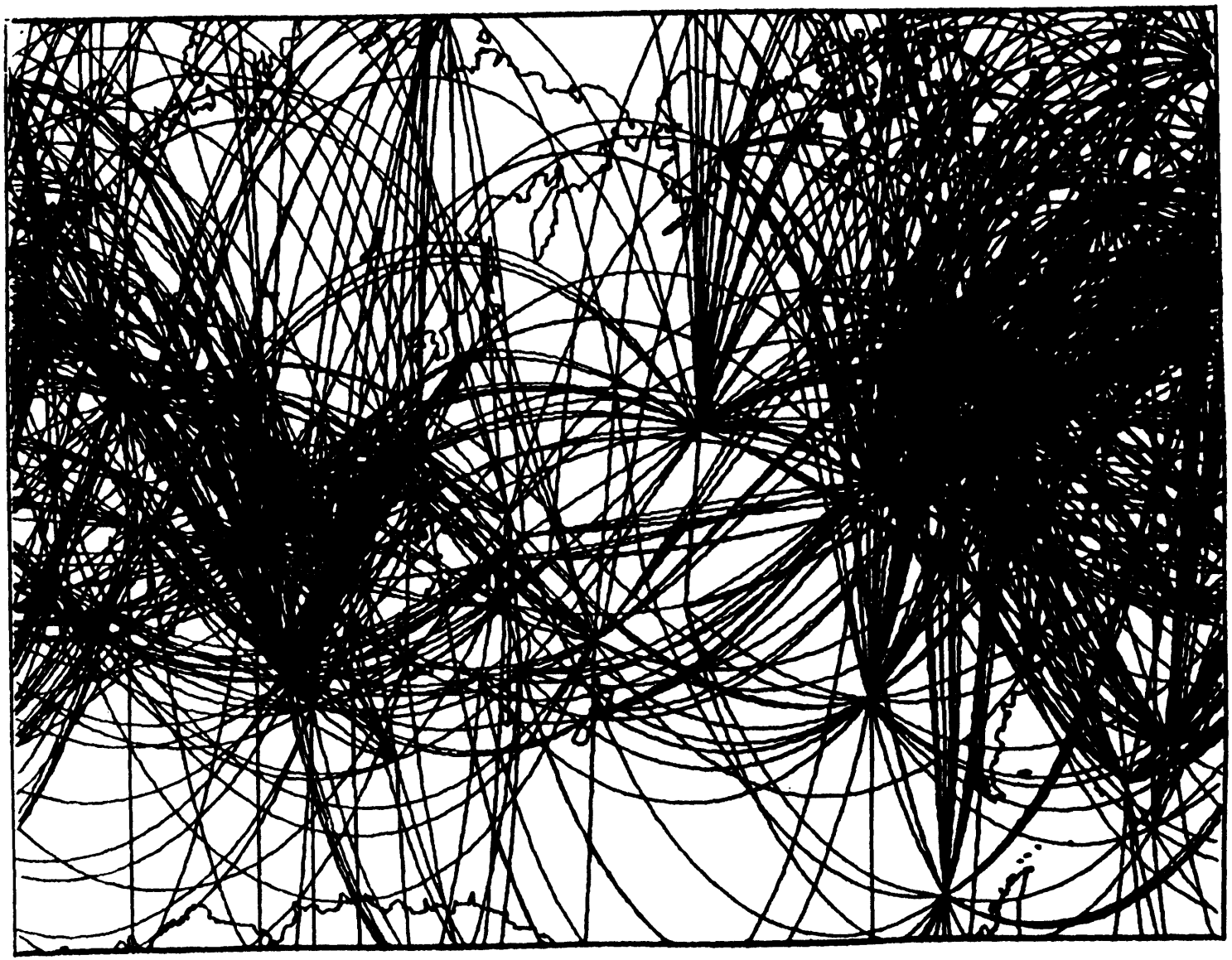

FIGURE C.5b REGION a

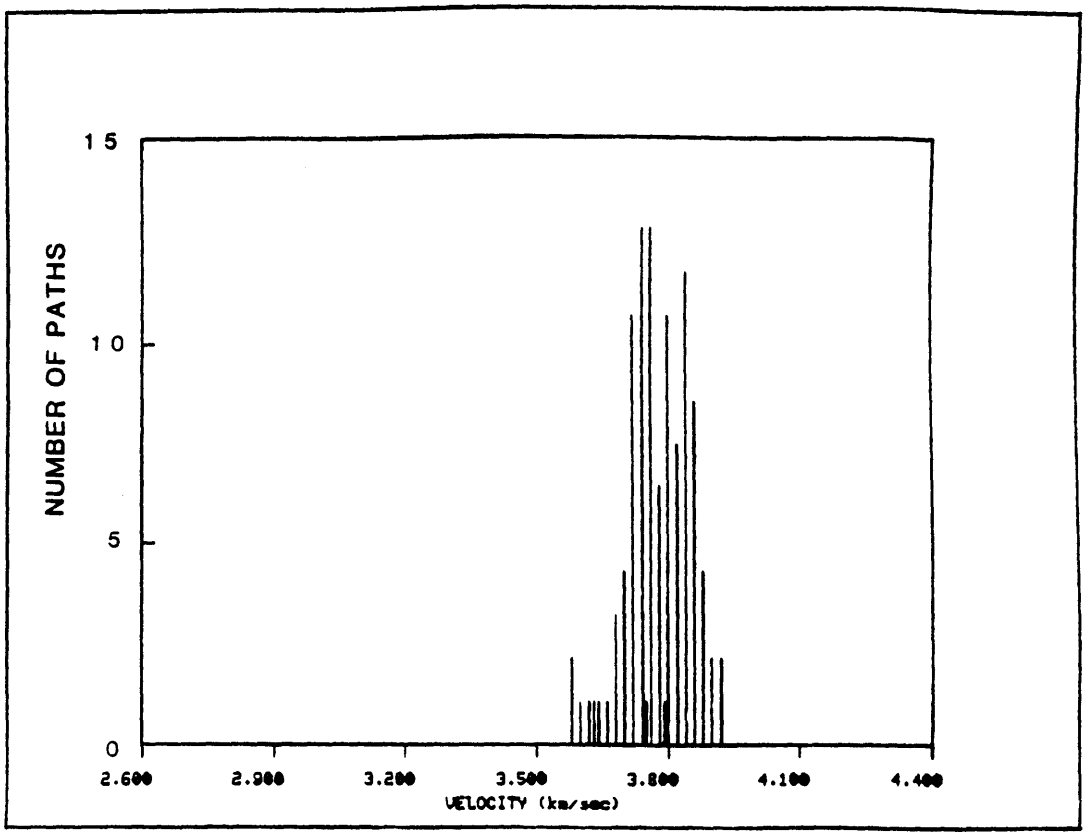

FIGURE C.5c REGION b

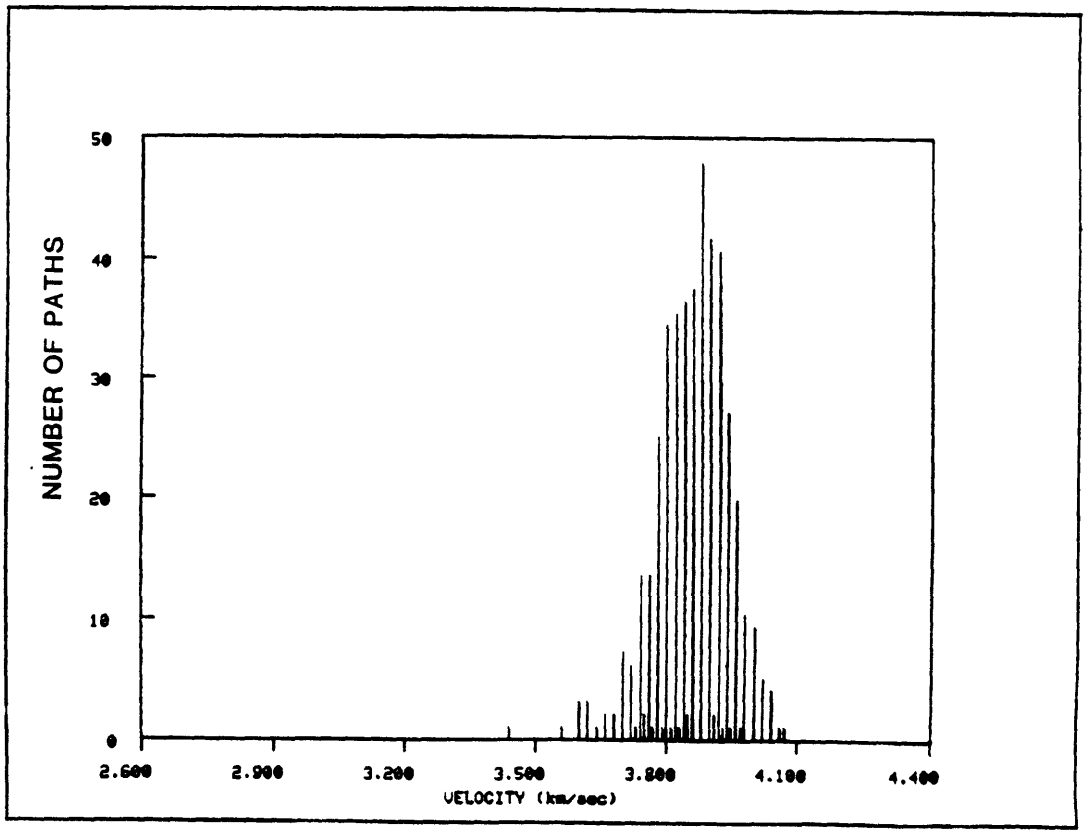

FIGURE C.5d REGION c

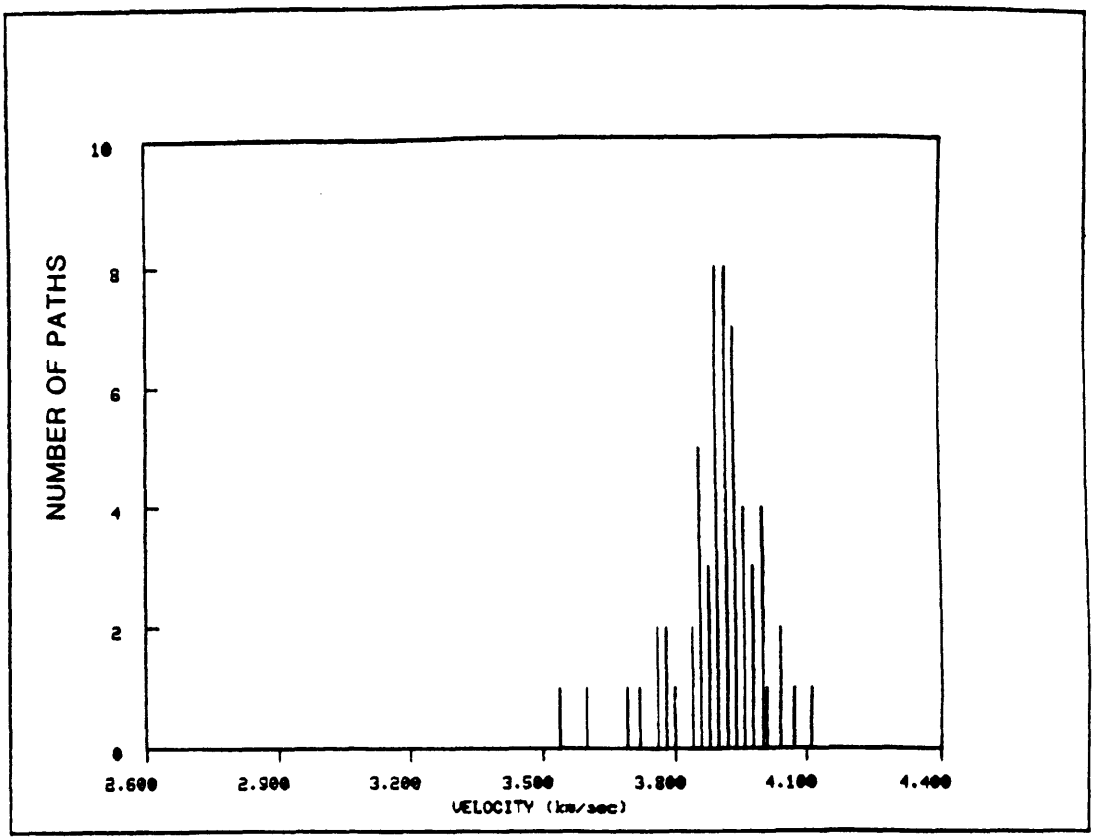

FIGURE C.5e REGION p

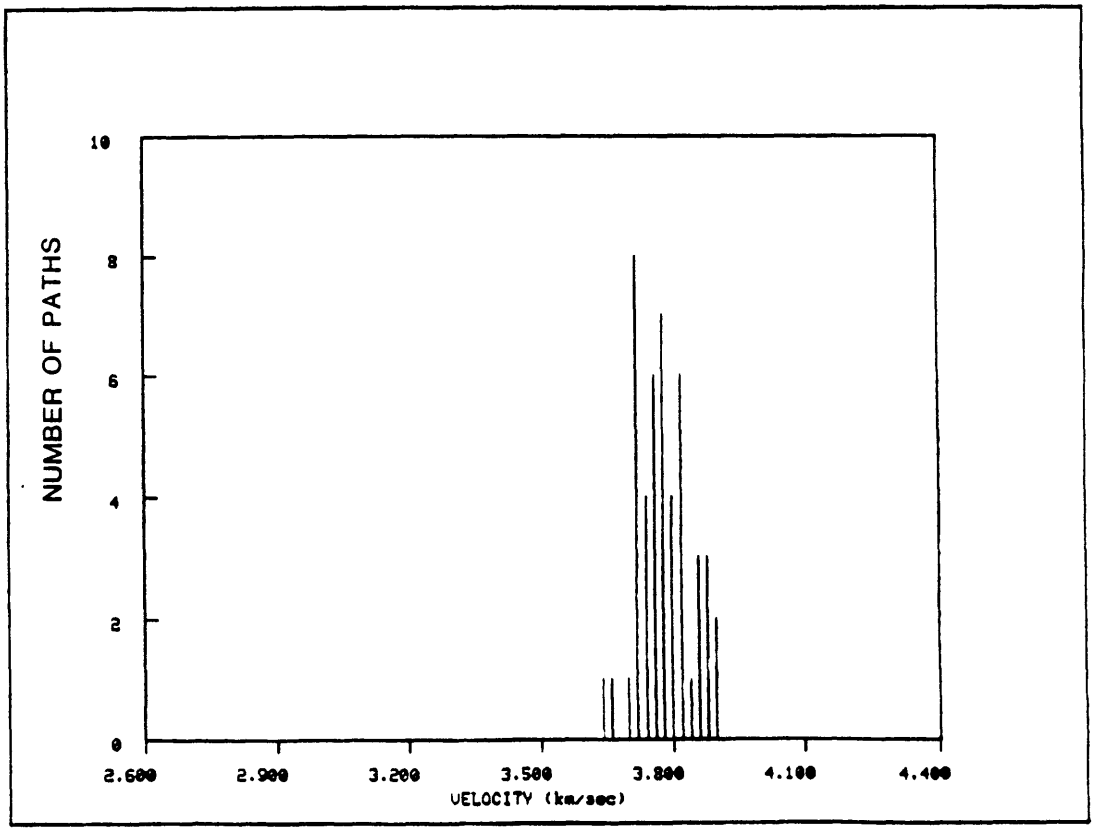

FIGURE C.5f REGION q

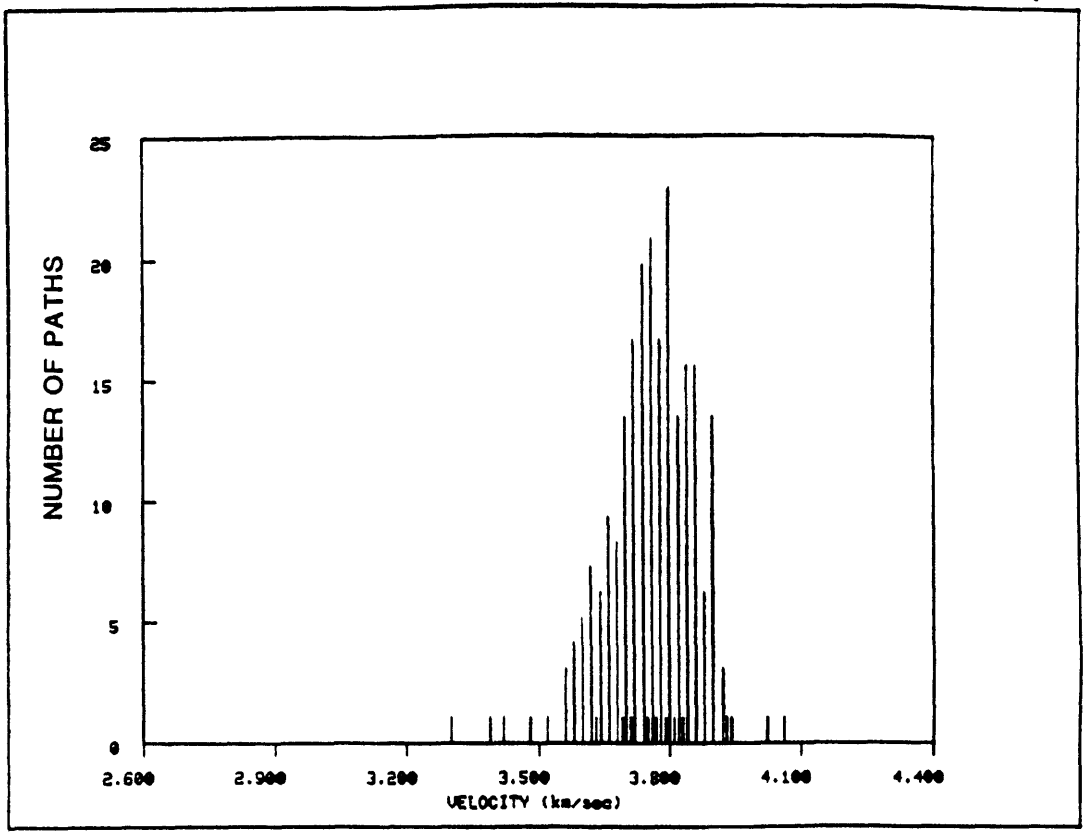

FIGURE C.5g REGION s

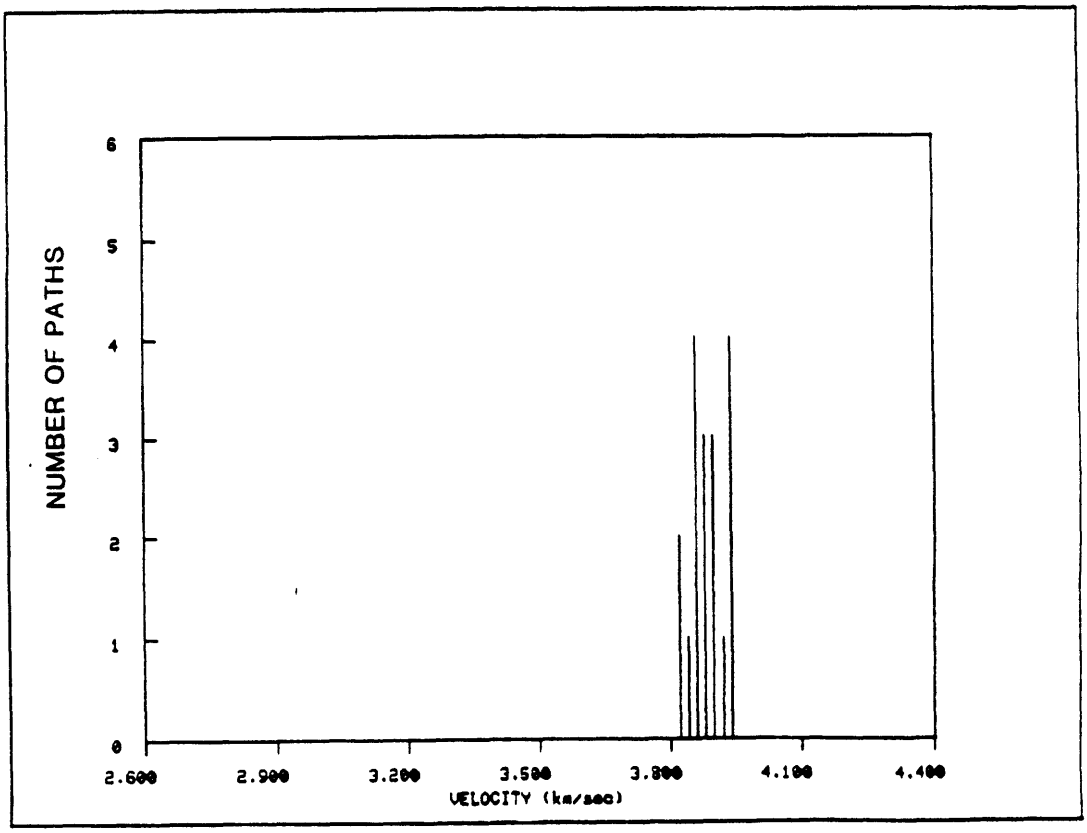

FIGURE C.5h REGION N

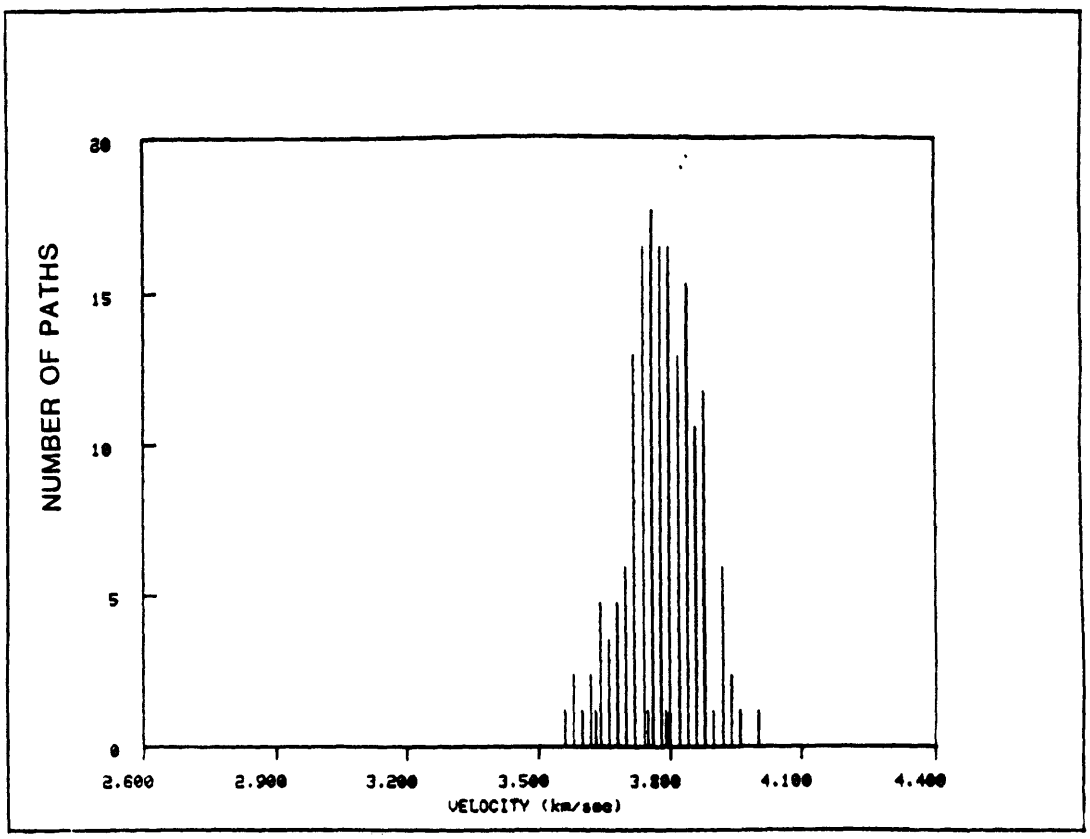

FIGURE C.5i REGION =

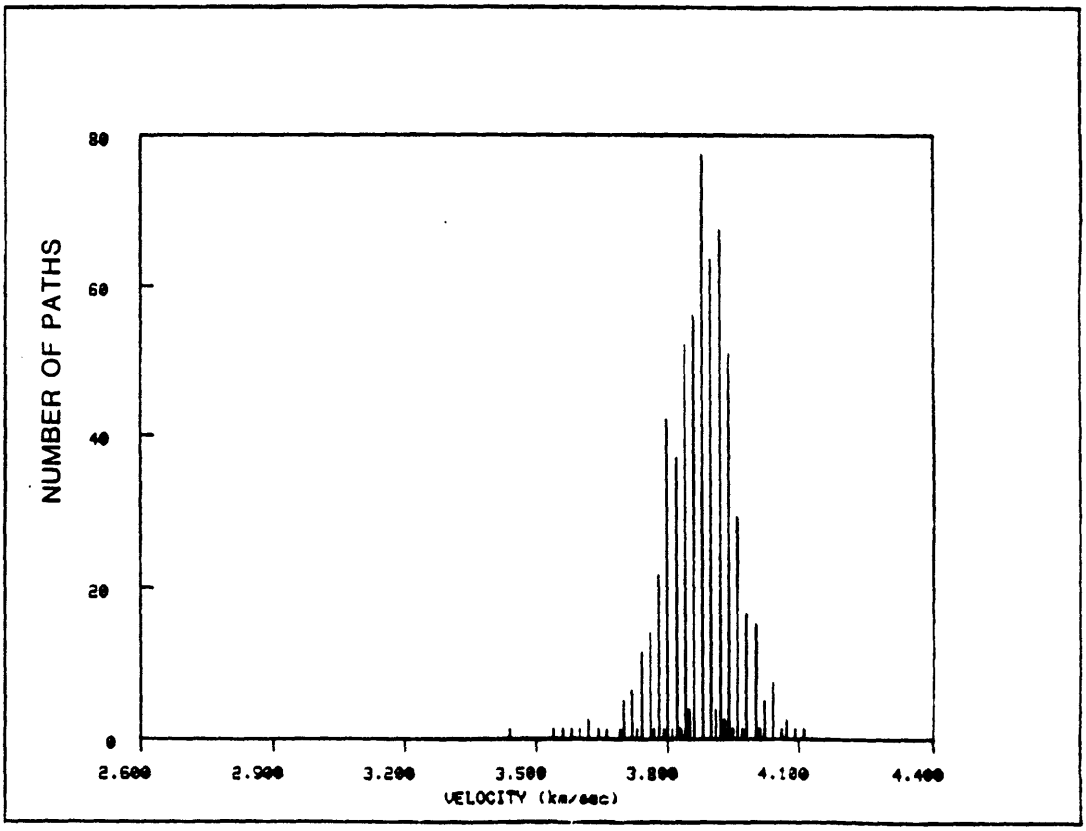

FIGURE C.5j REGION 0

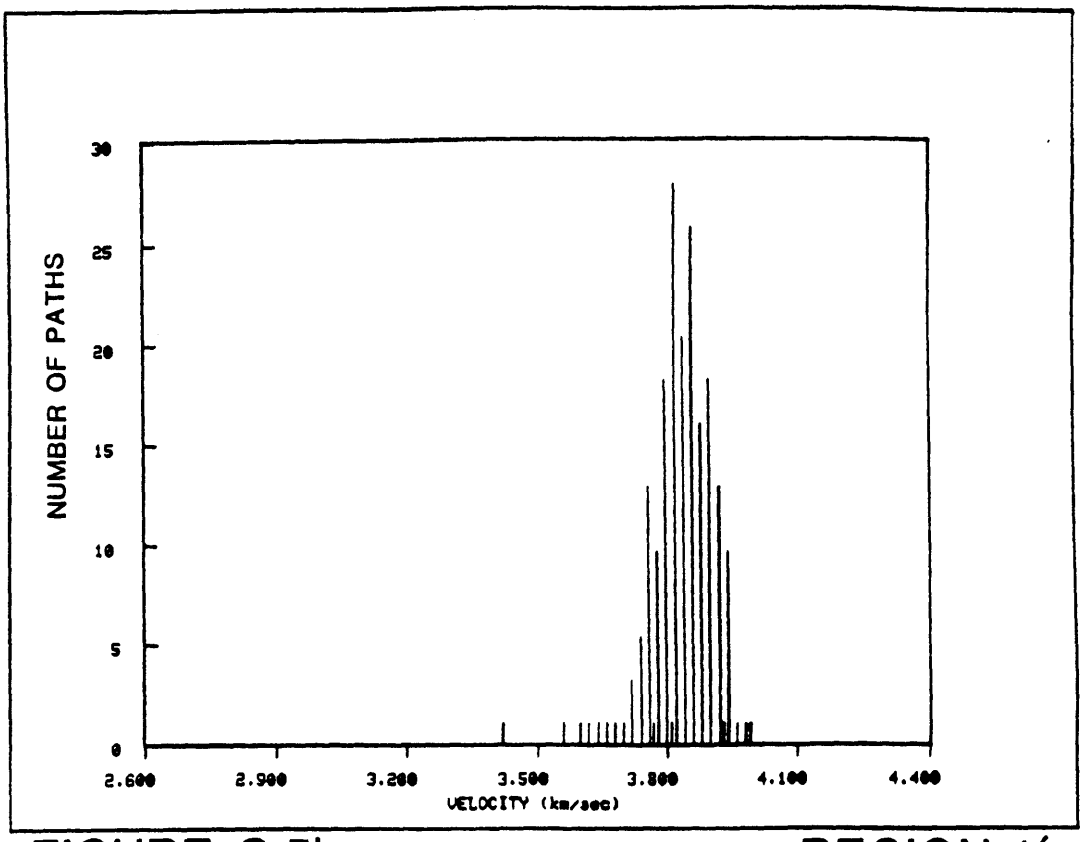

FIGURE C.5k REGION ~~0~~

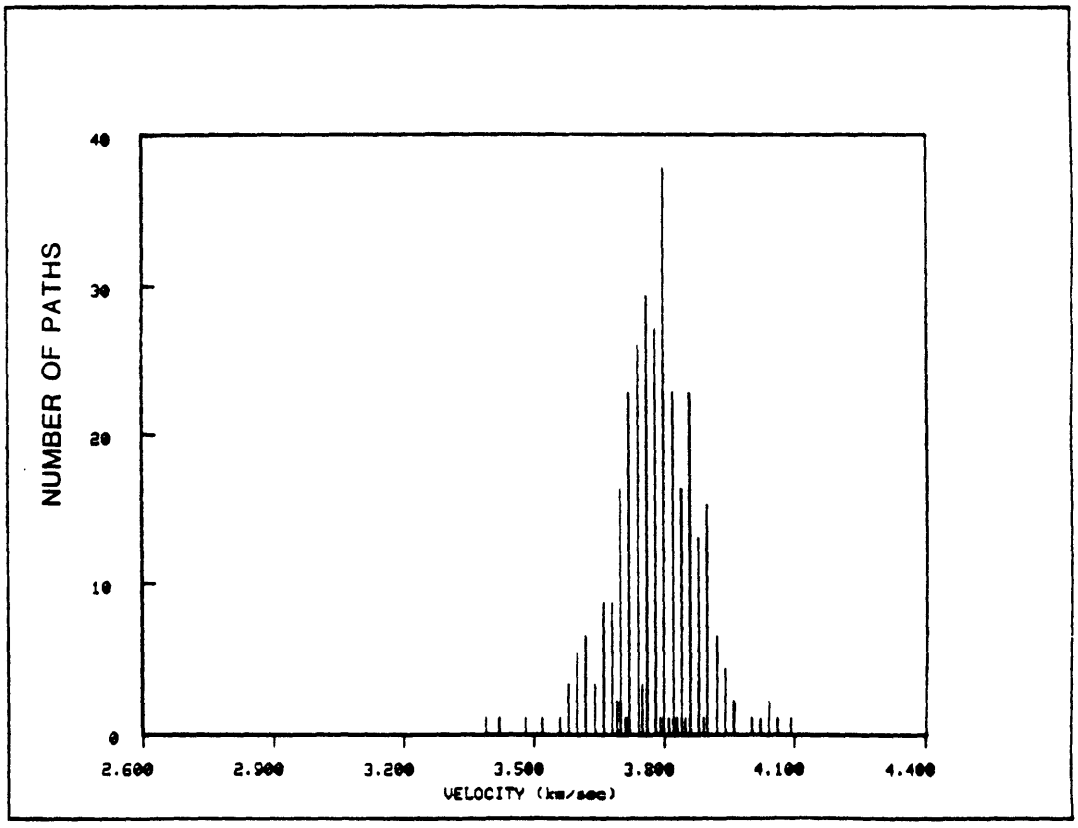

FIGURE C.5l REGION N

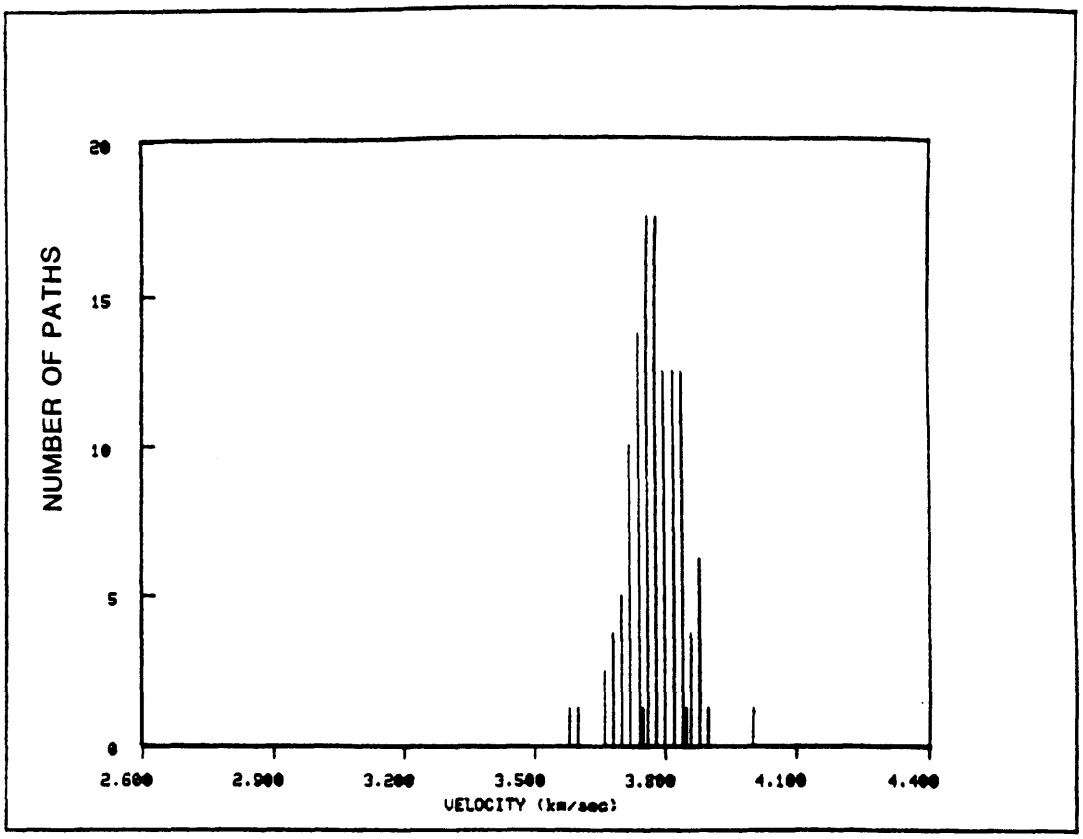

FIGURE C.5m REGION #

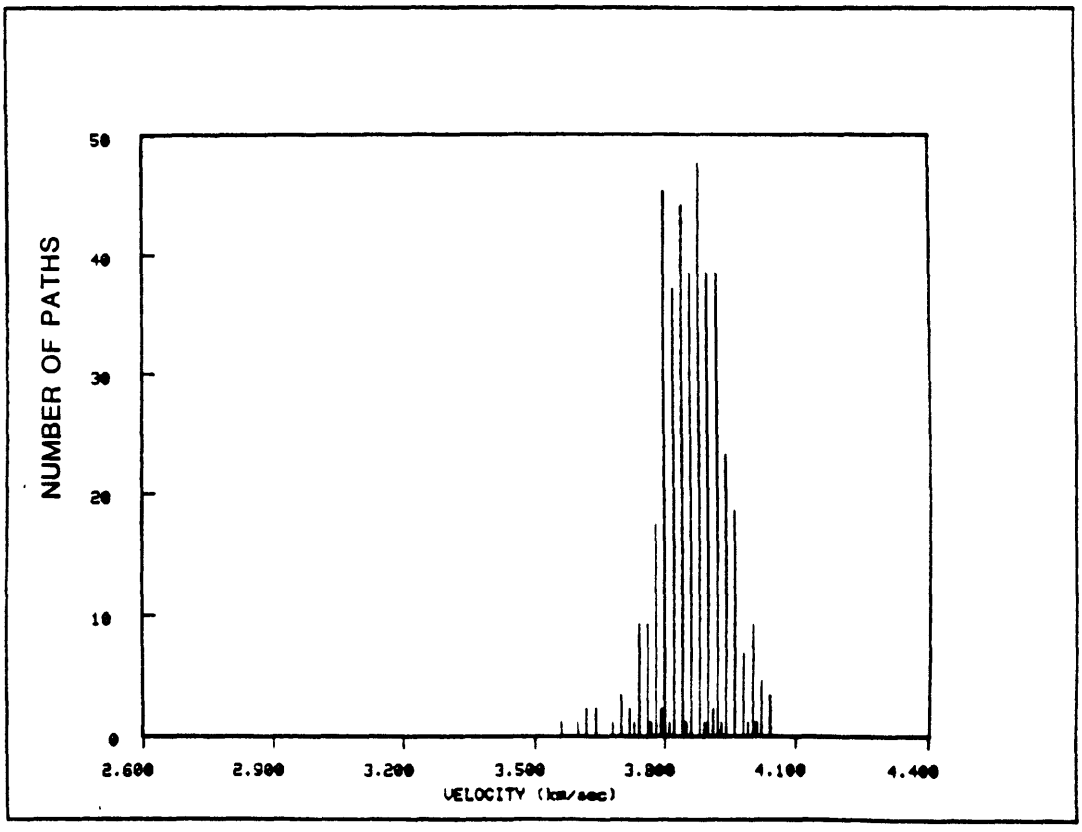

FIGURE C.5n REGION =

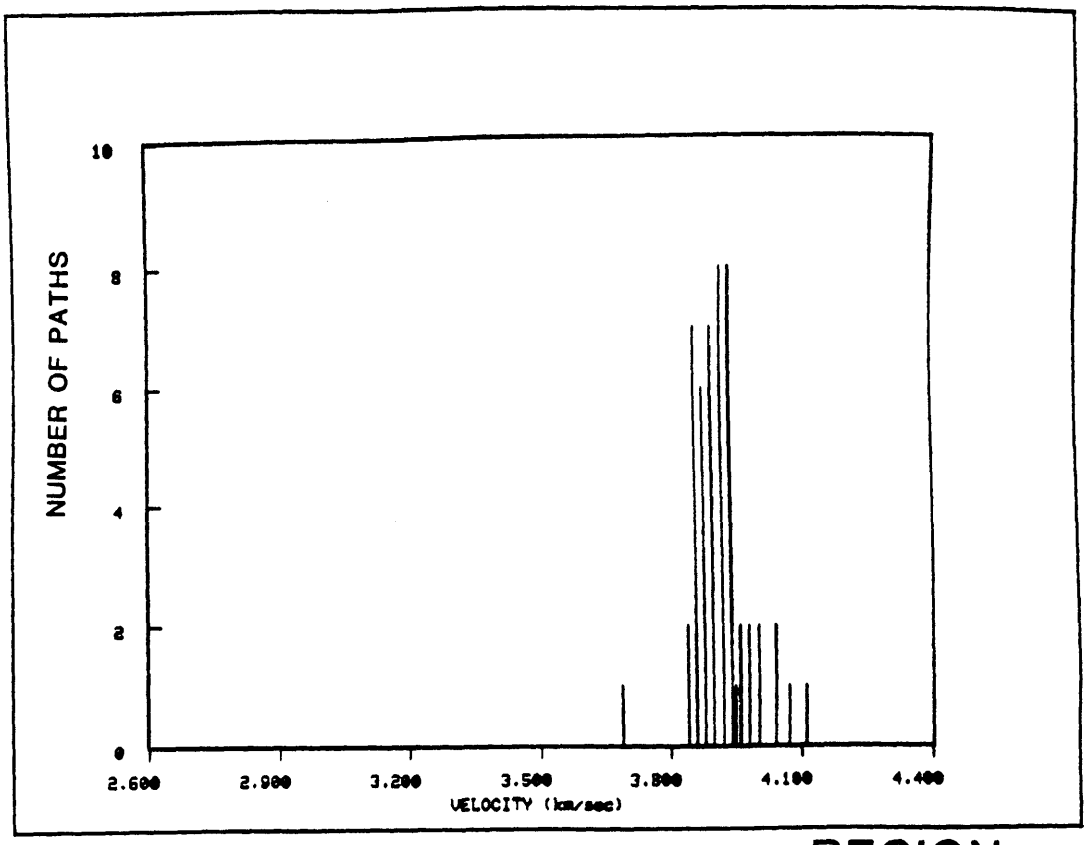

FIGURE C.5o REGION -

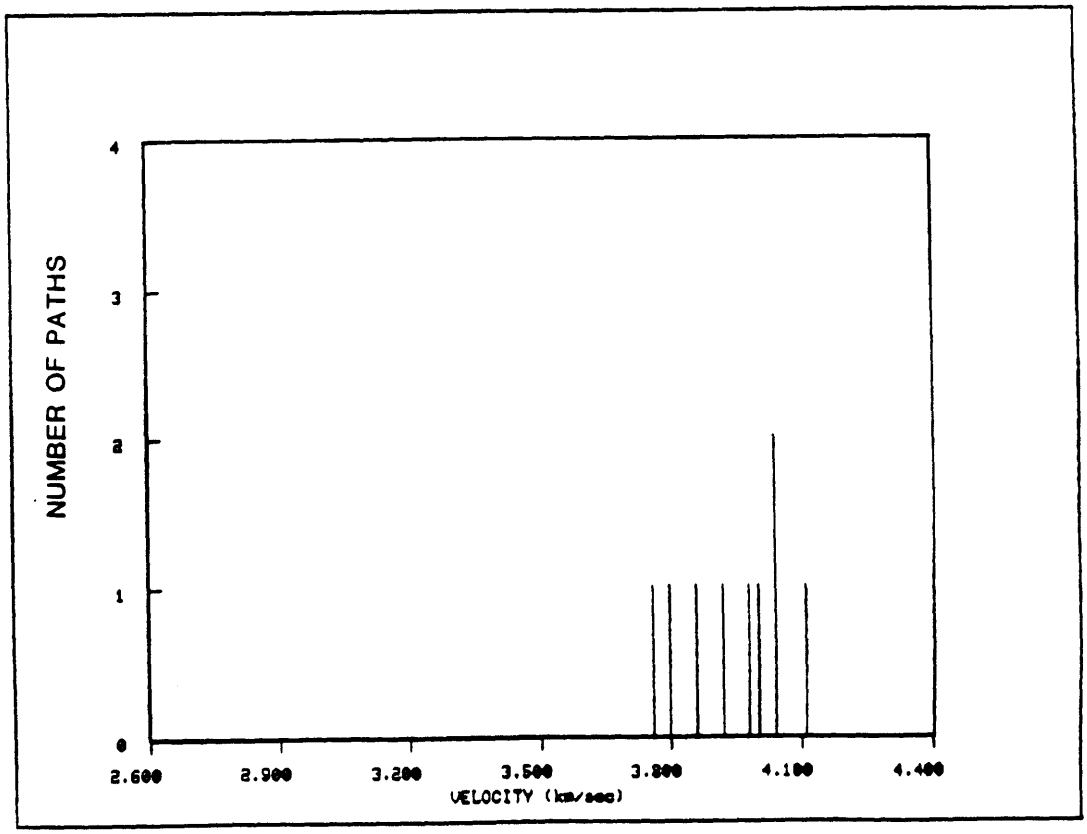

FIGURE C.5p REGION 0

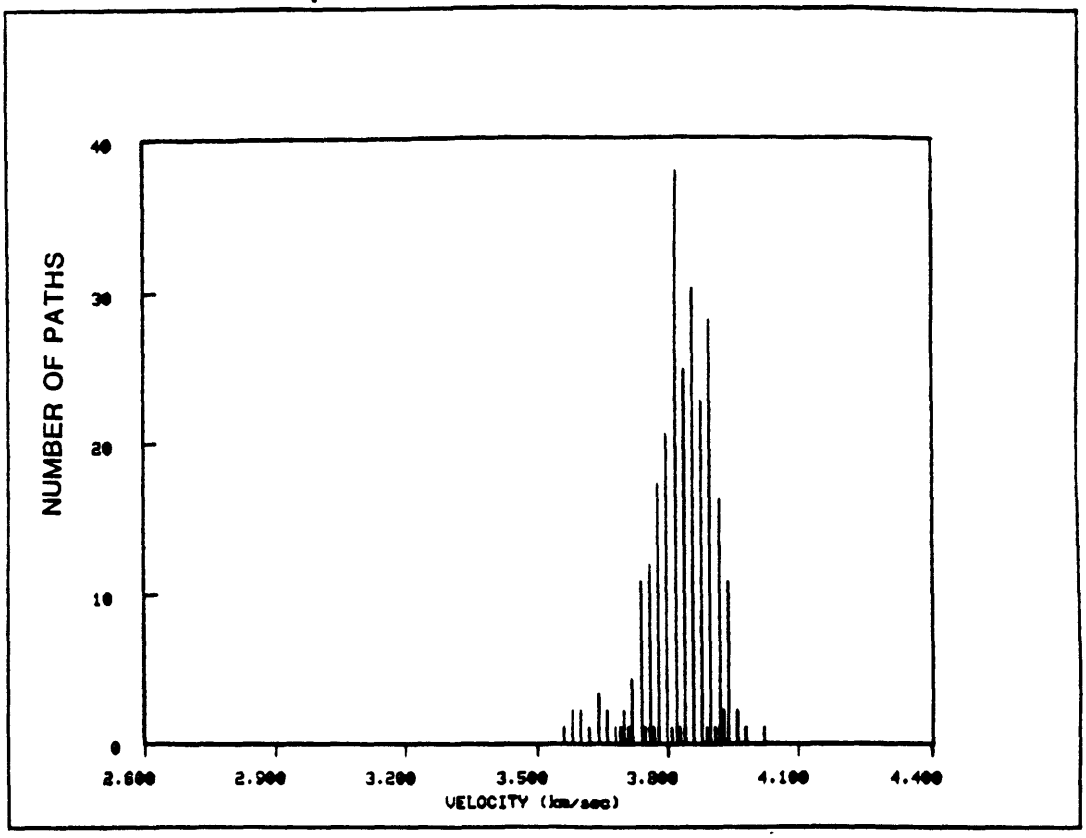

FIGURE C.5q REGION .

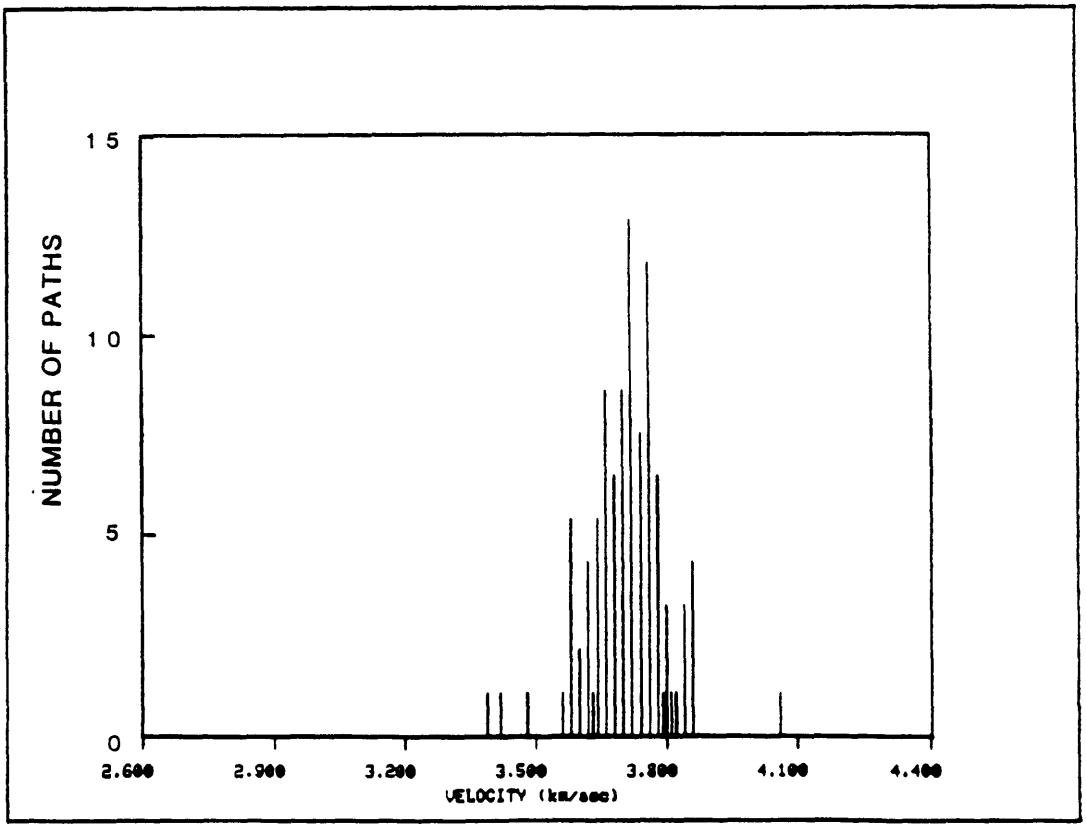

FIGURE C.5r

REGION ø

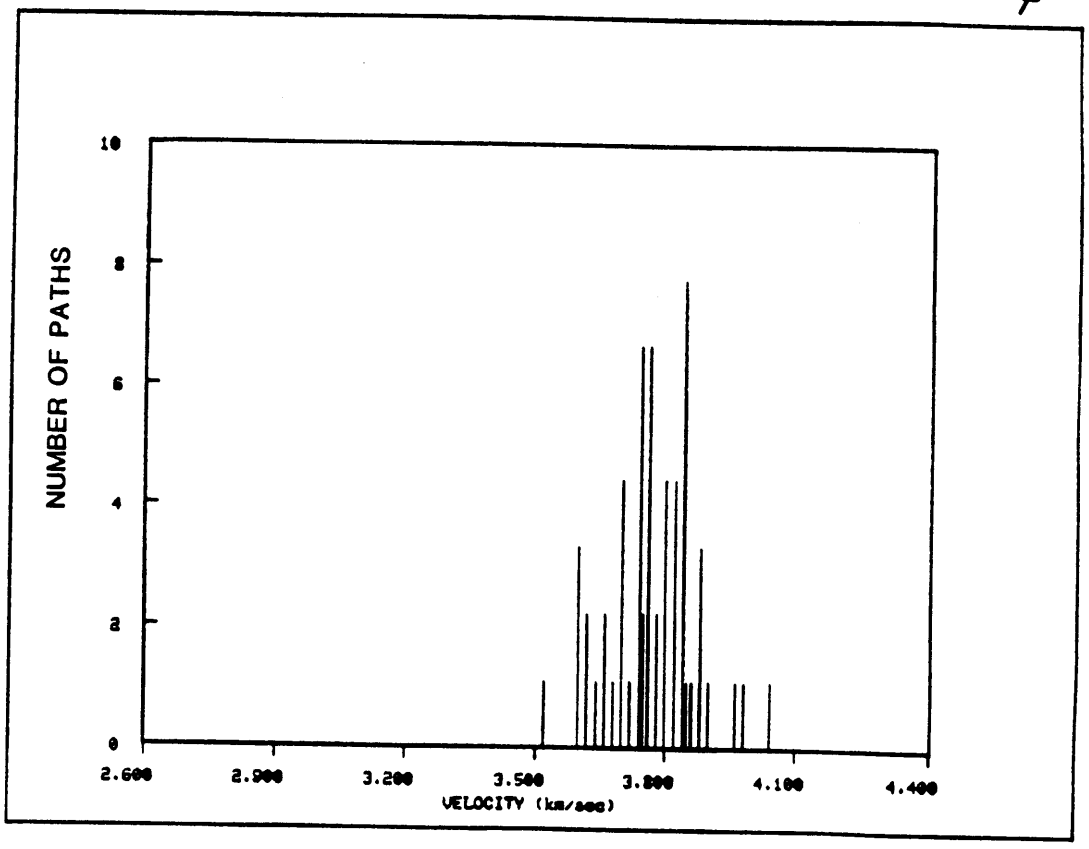

FIGURE C.6a

PERIOD 70 sec

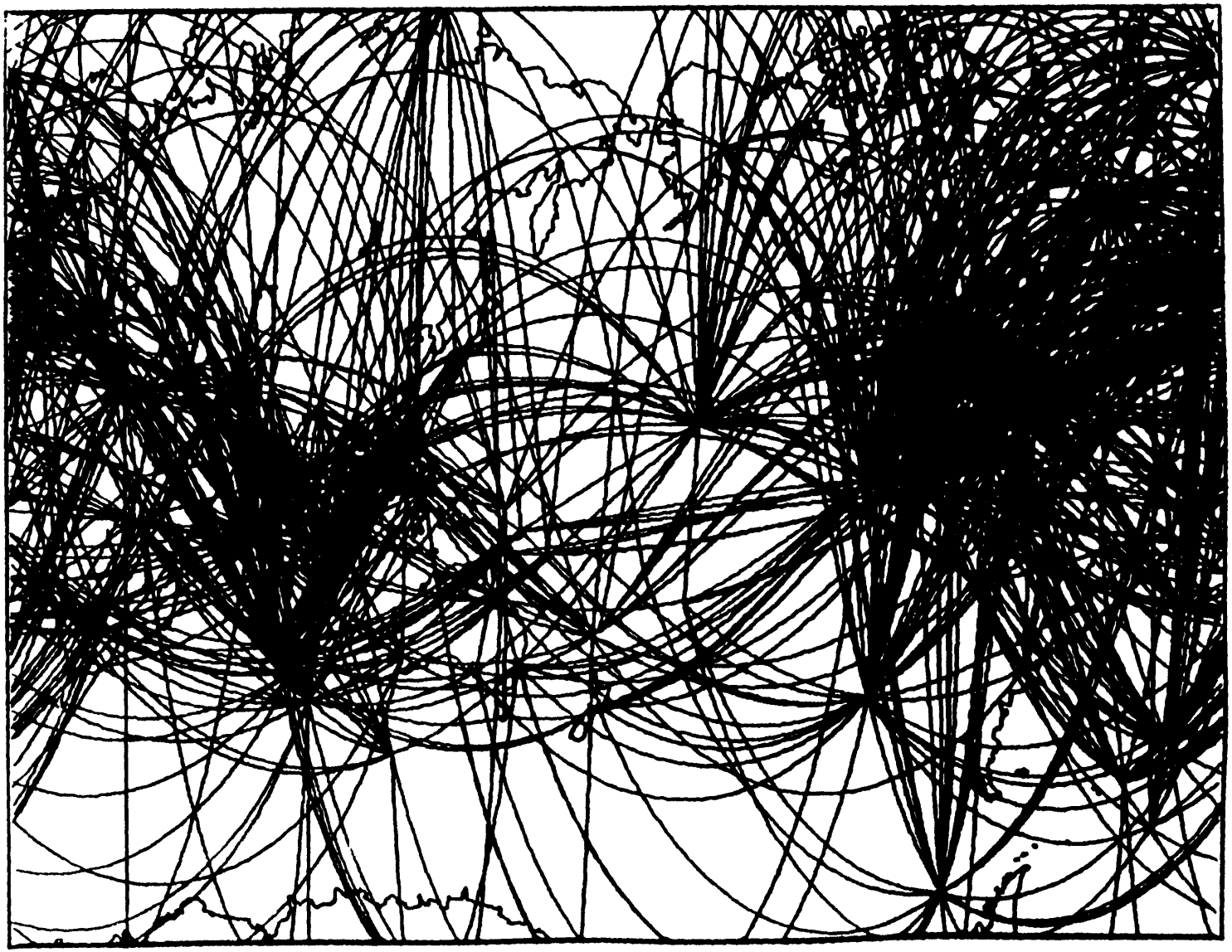

FIGURE C.6b REGION a

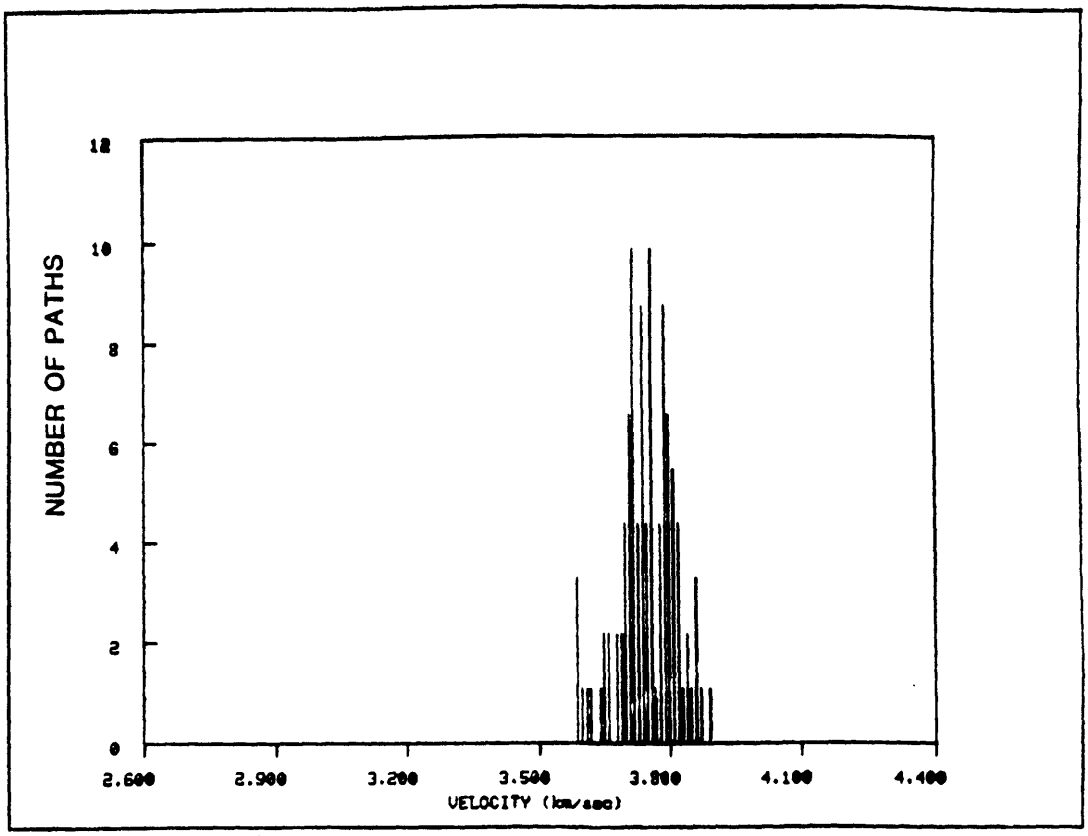

FIGURE C.6c REGION b

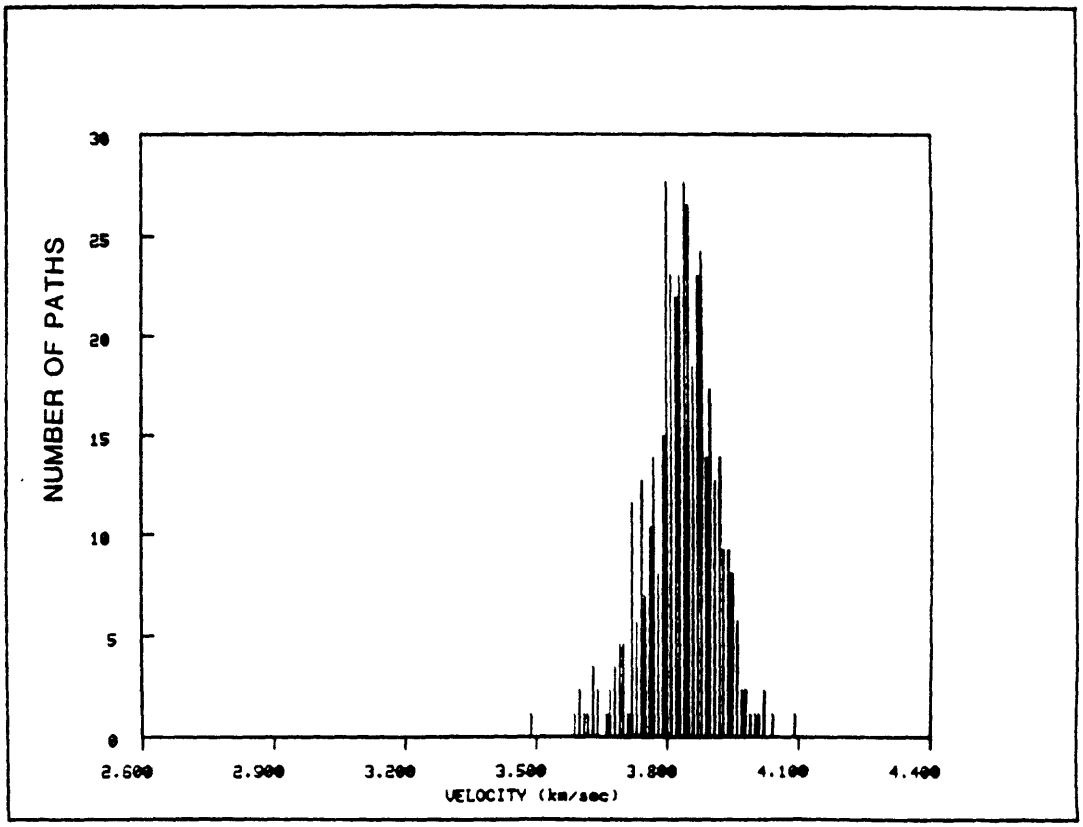

FIGURE C.6d REGION c

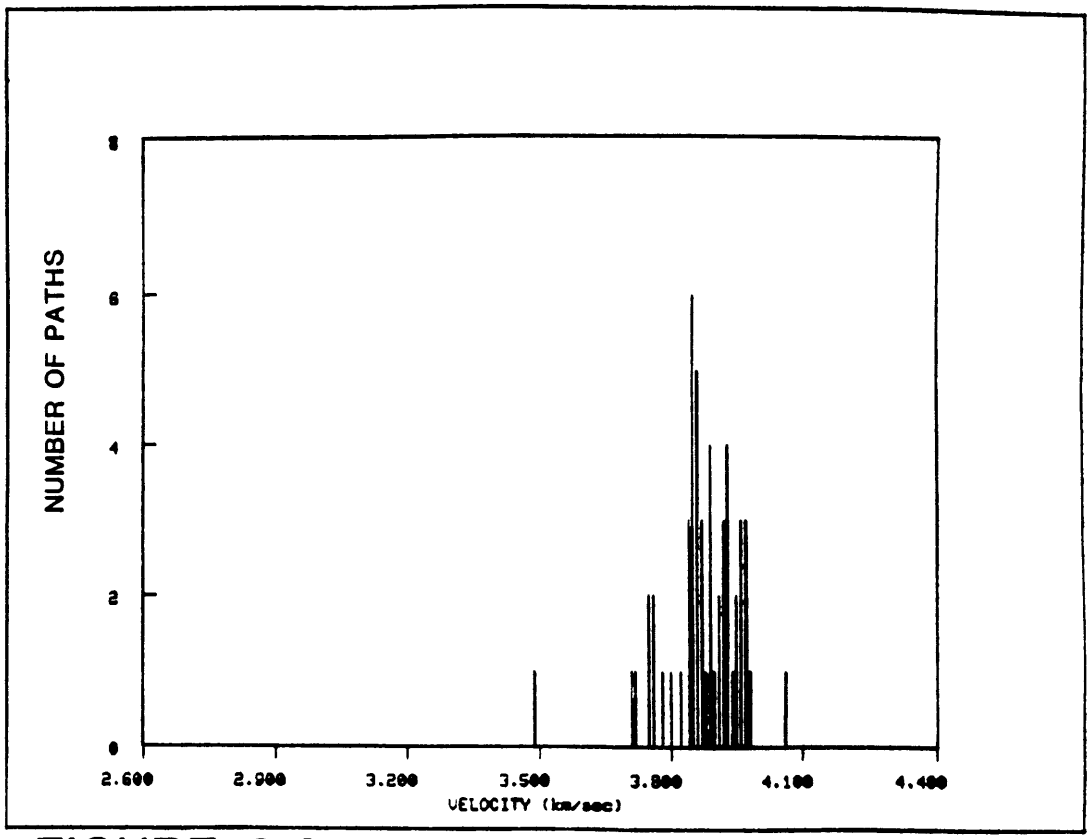

FIGURE C.6e REGION p

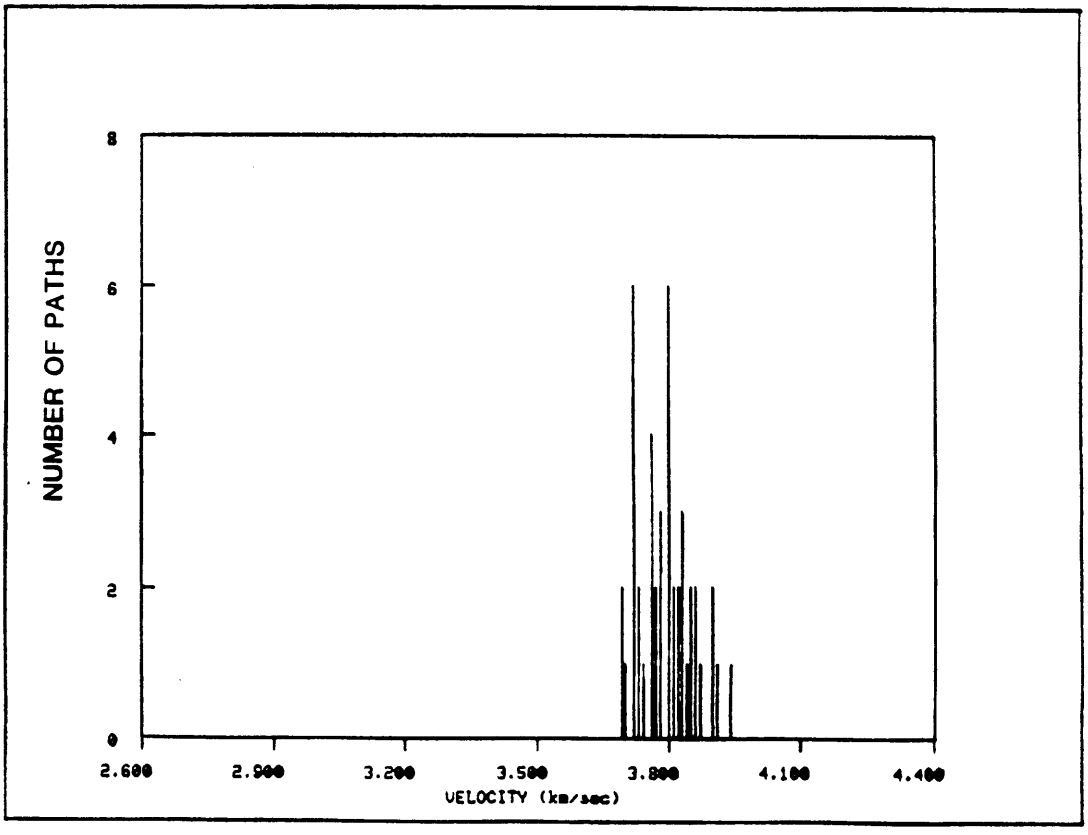

FIGURE C.6f REGION q

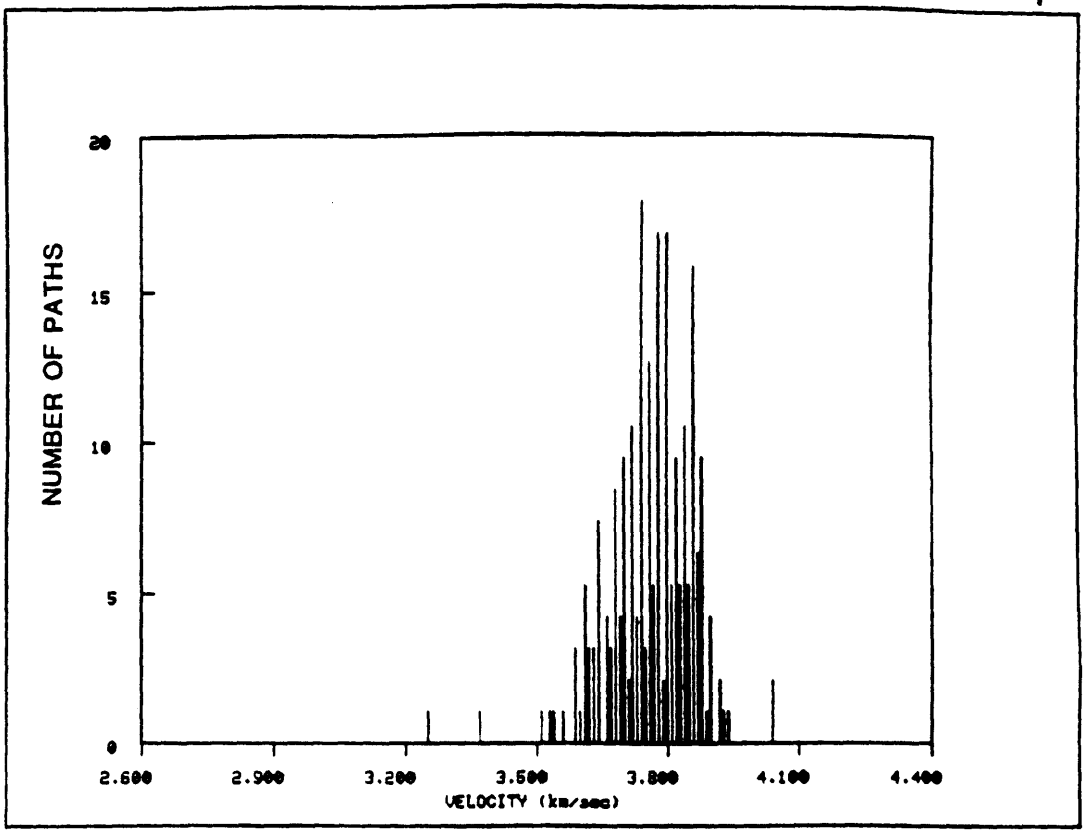

FIGURE C.6g REGION s

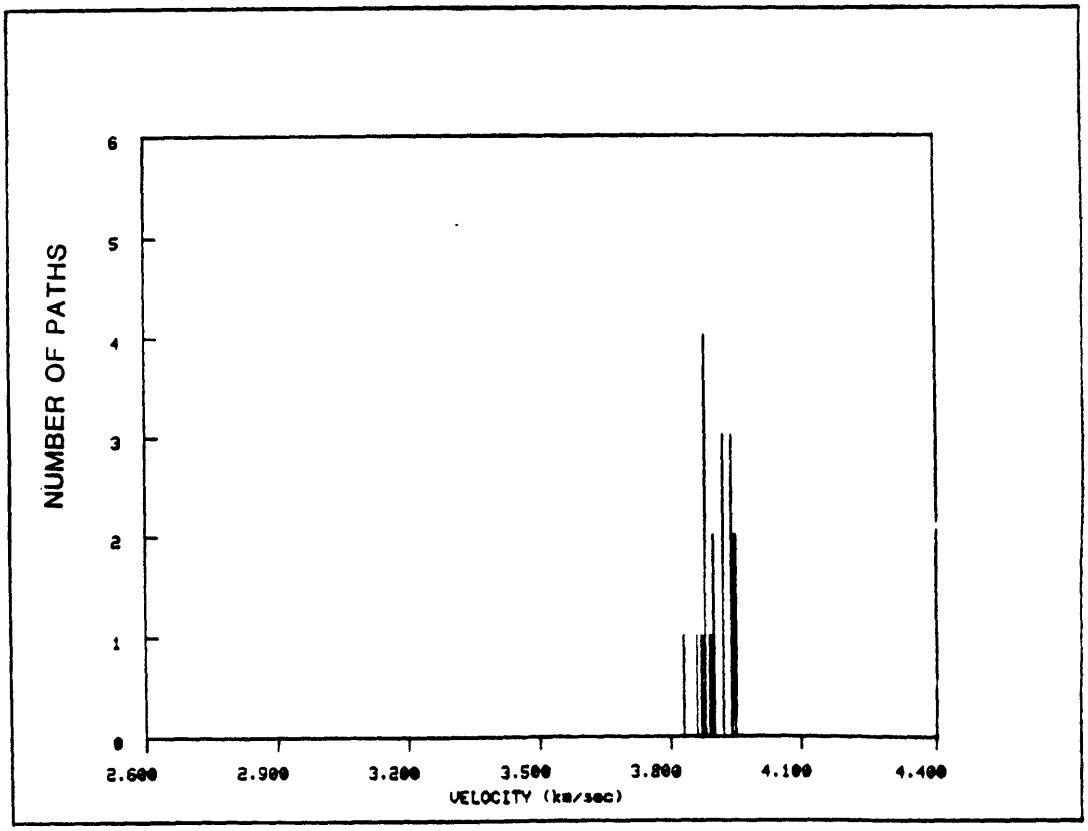

FIGURE C.6h REGION N

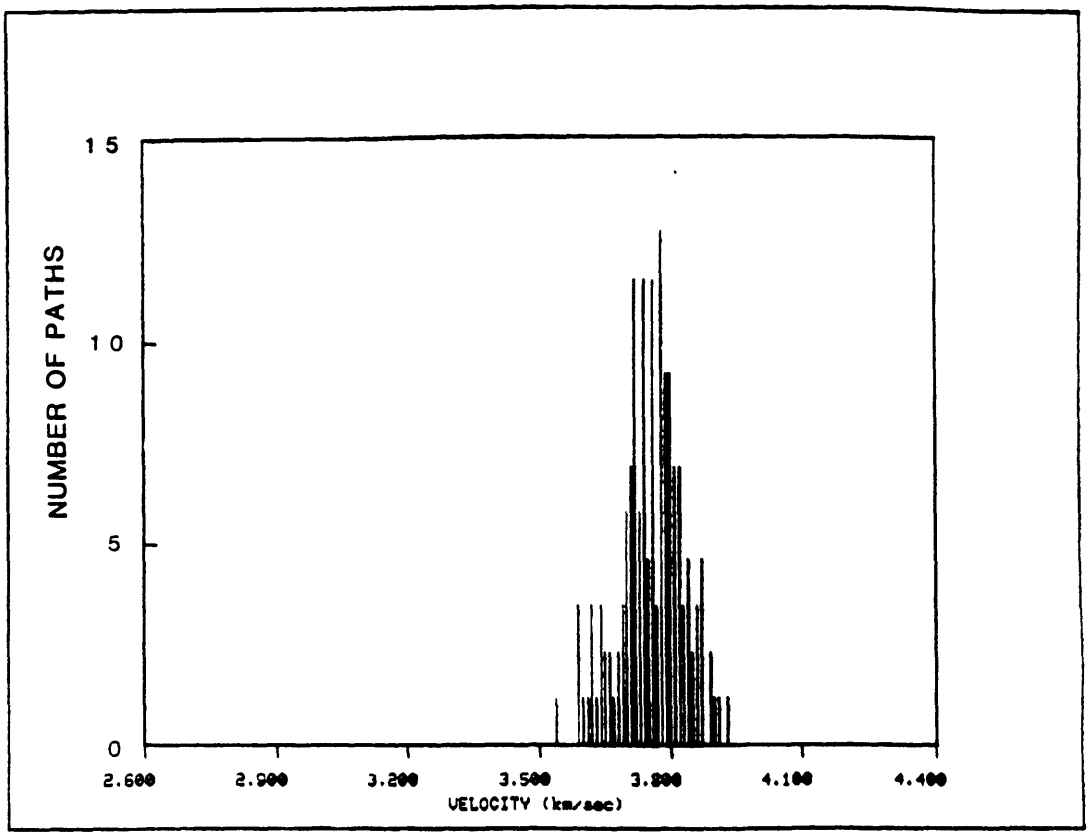

FIGURE C.6i REGION =

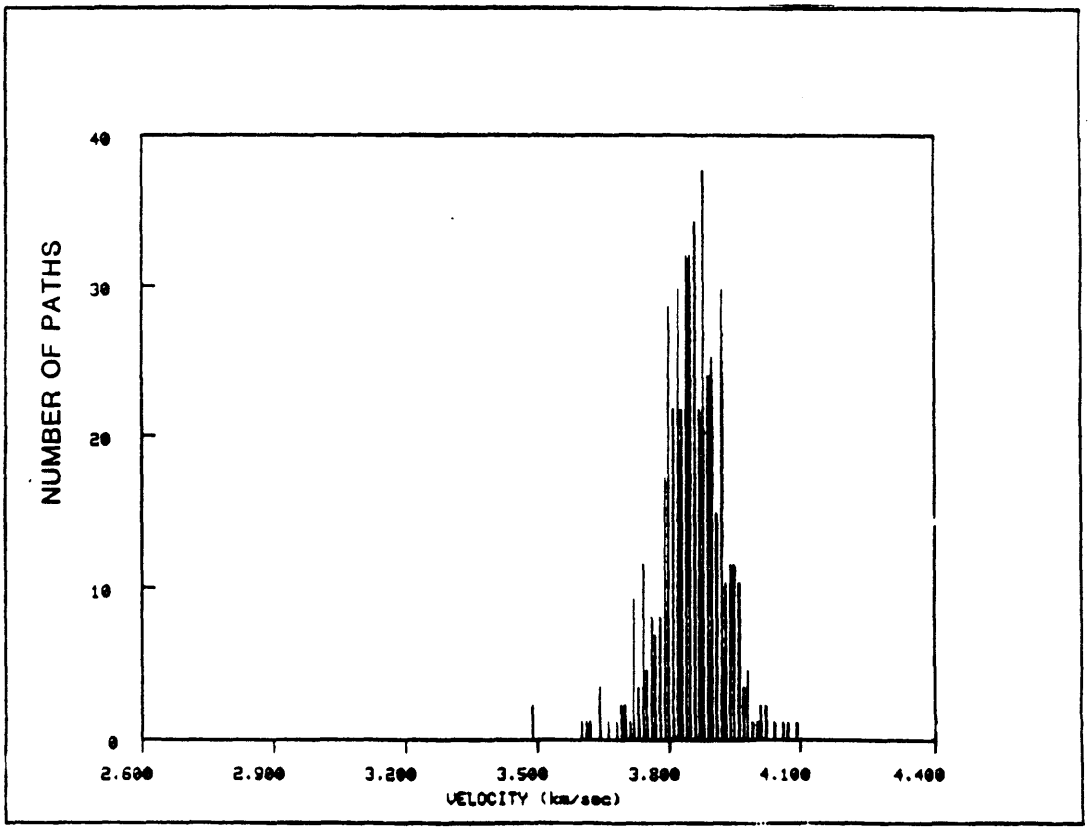

FIGURE C.6j REGION 0

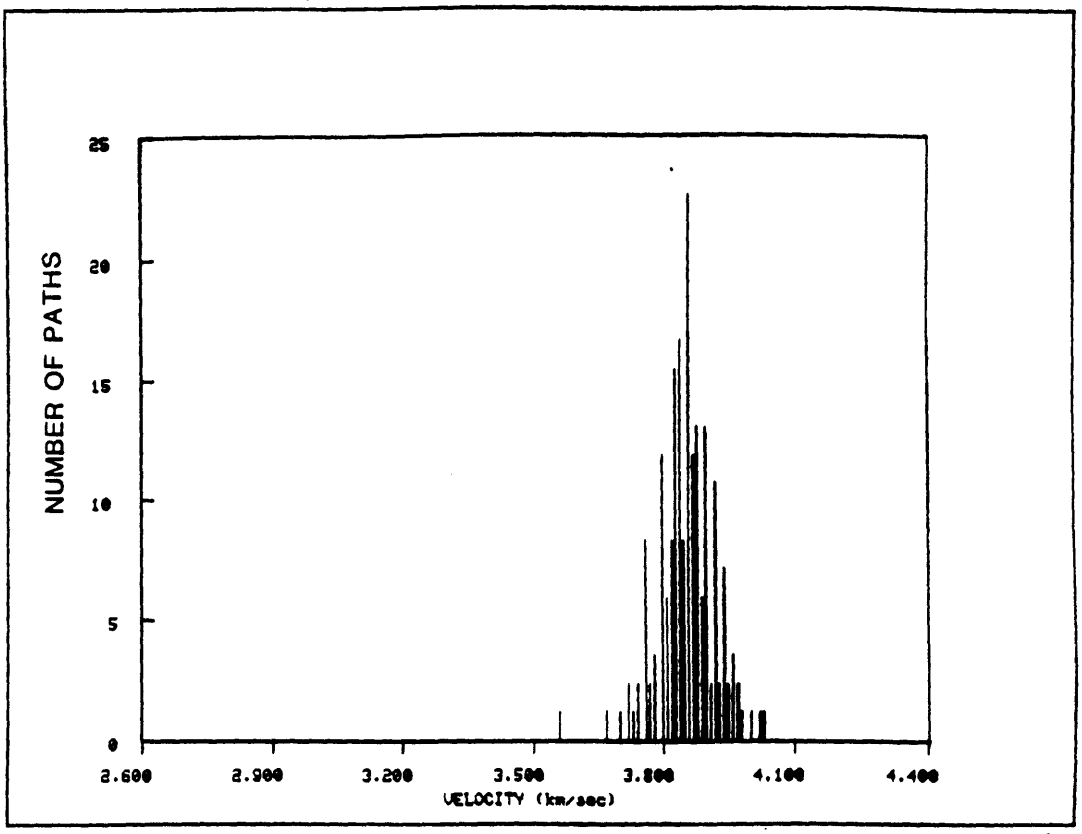

FIGURE C.6k REGION ~~0~~

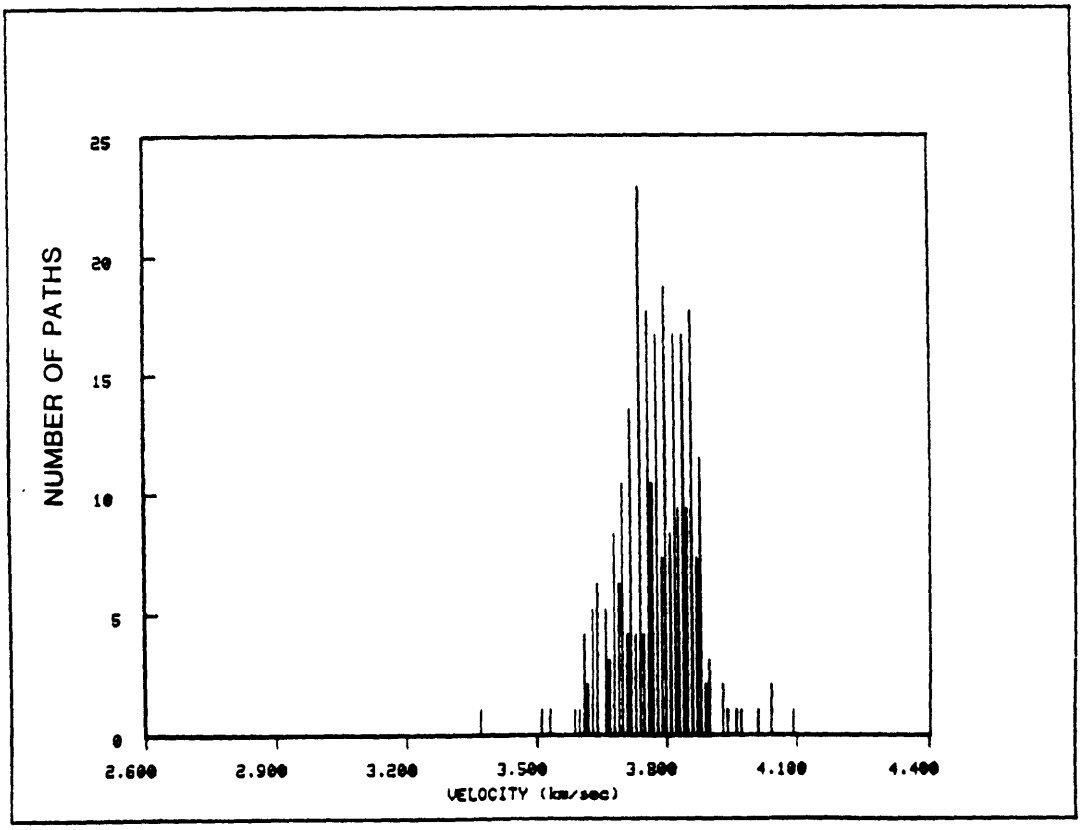

FIGURE C.6l REGION N

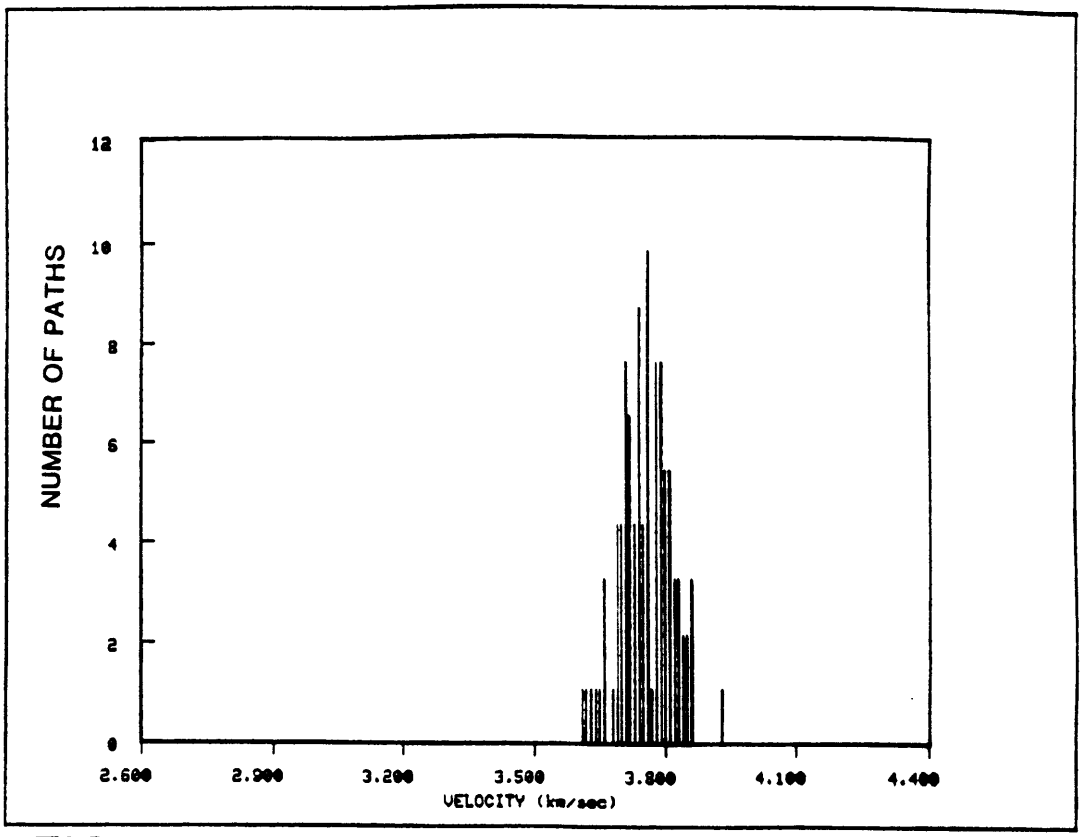

FIGURE C.6m REGION #

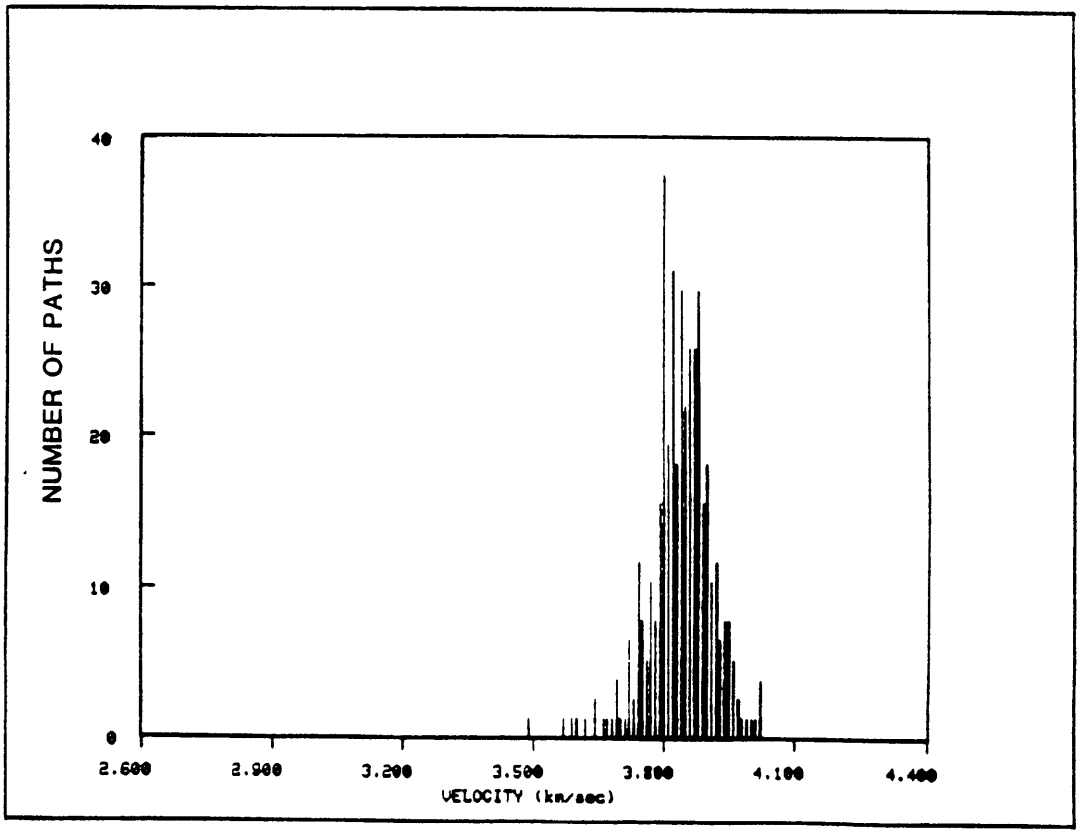

FIGURE C.6n REGION =

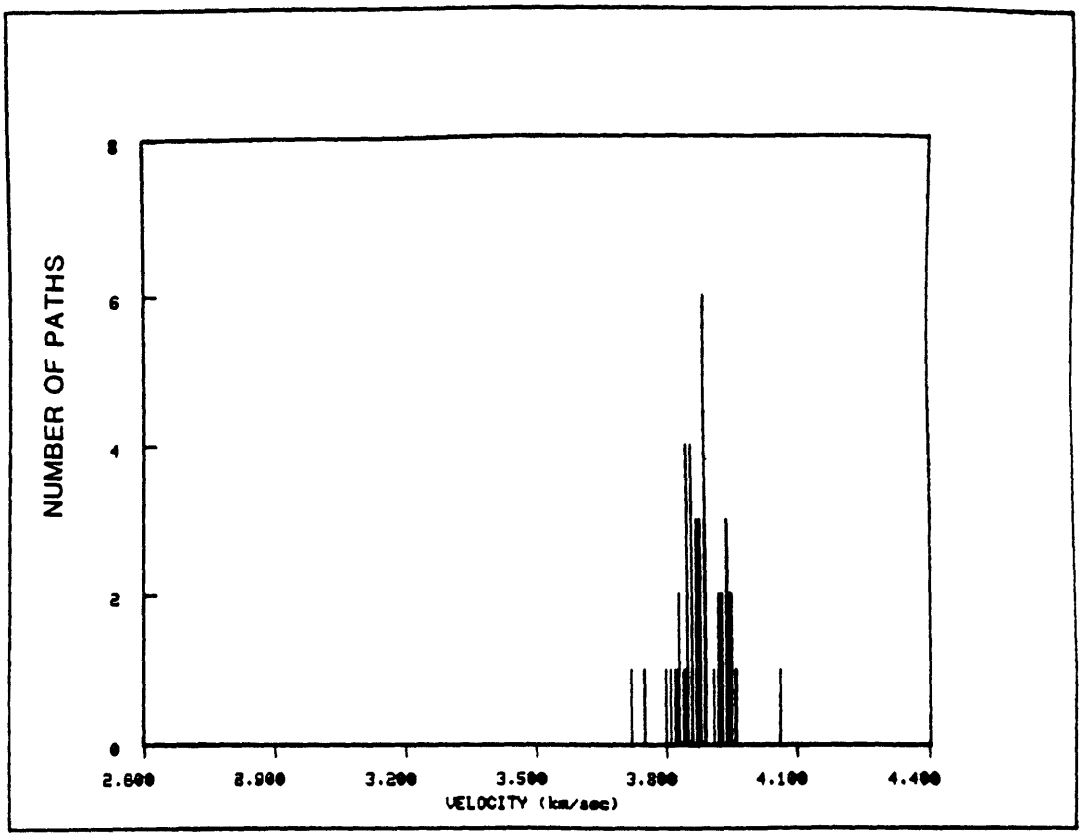

FIGURE C.6o REGION -

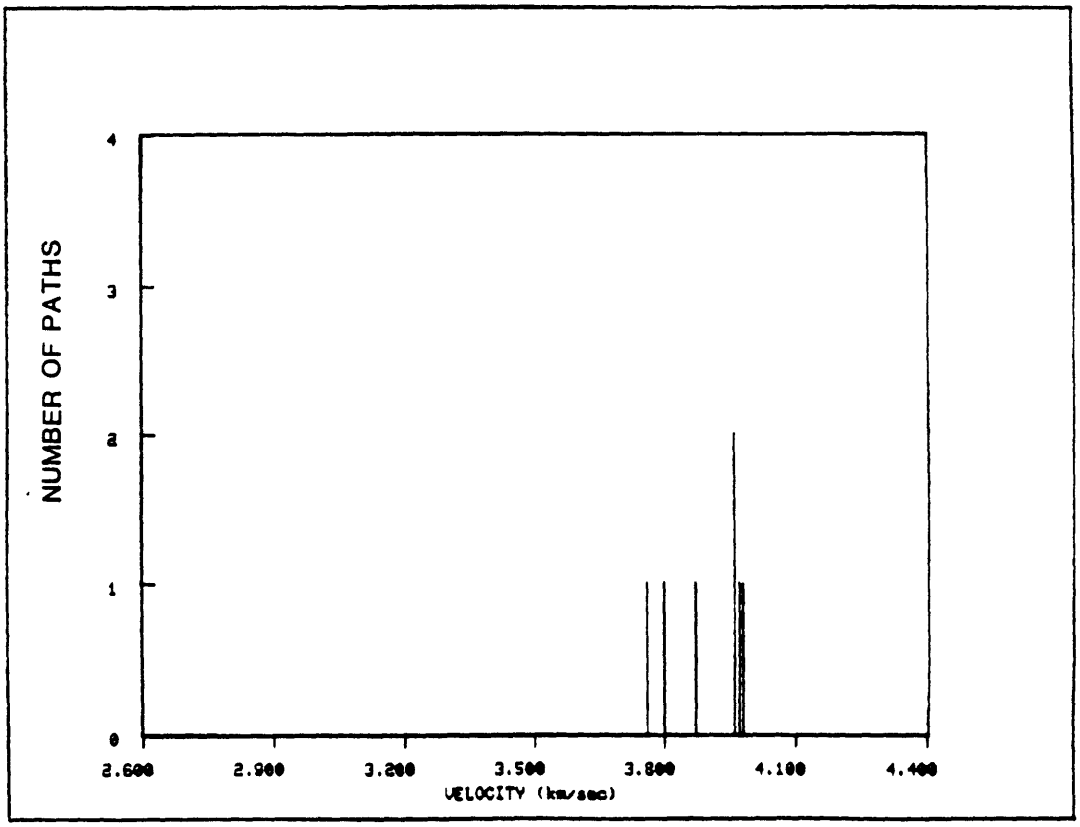

FIGURE C.6p REGION 0

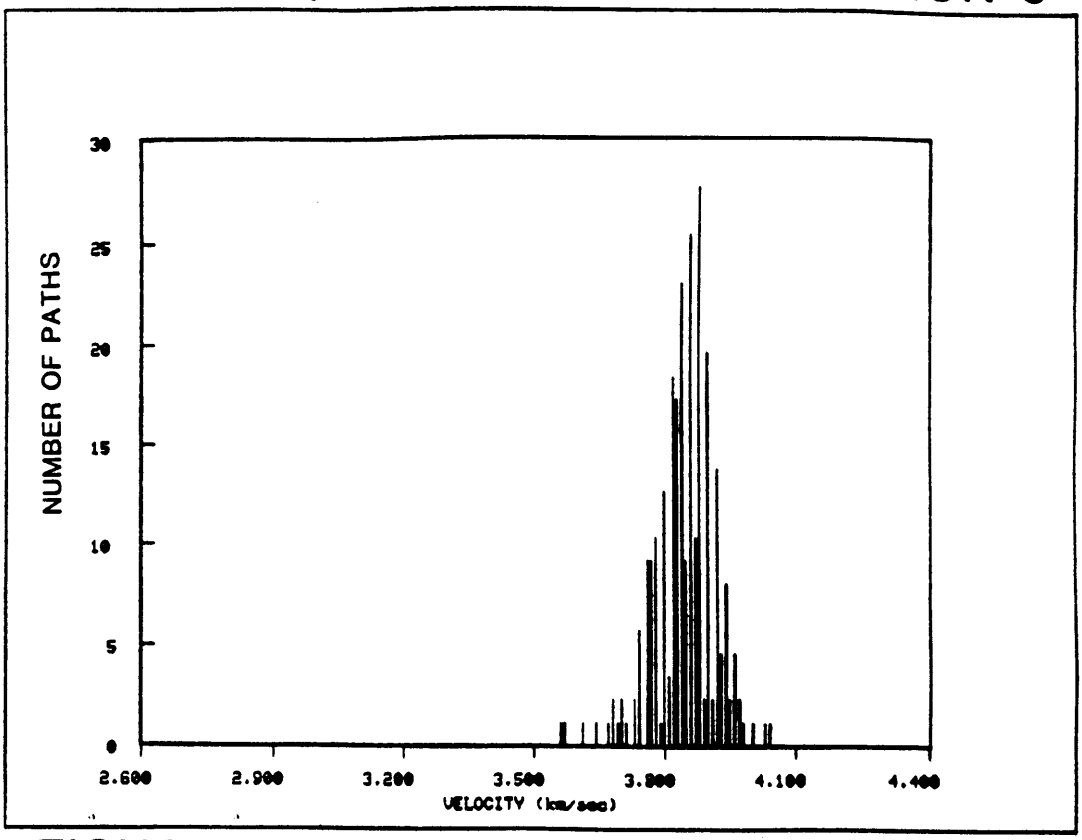

FIGURE C.6q REGION .

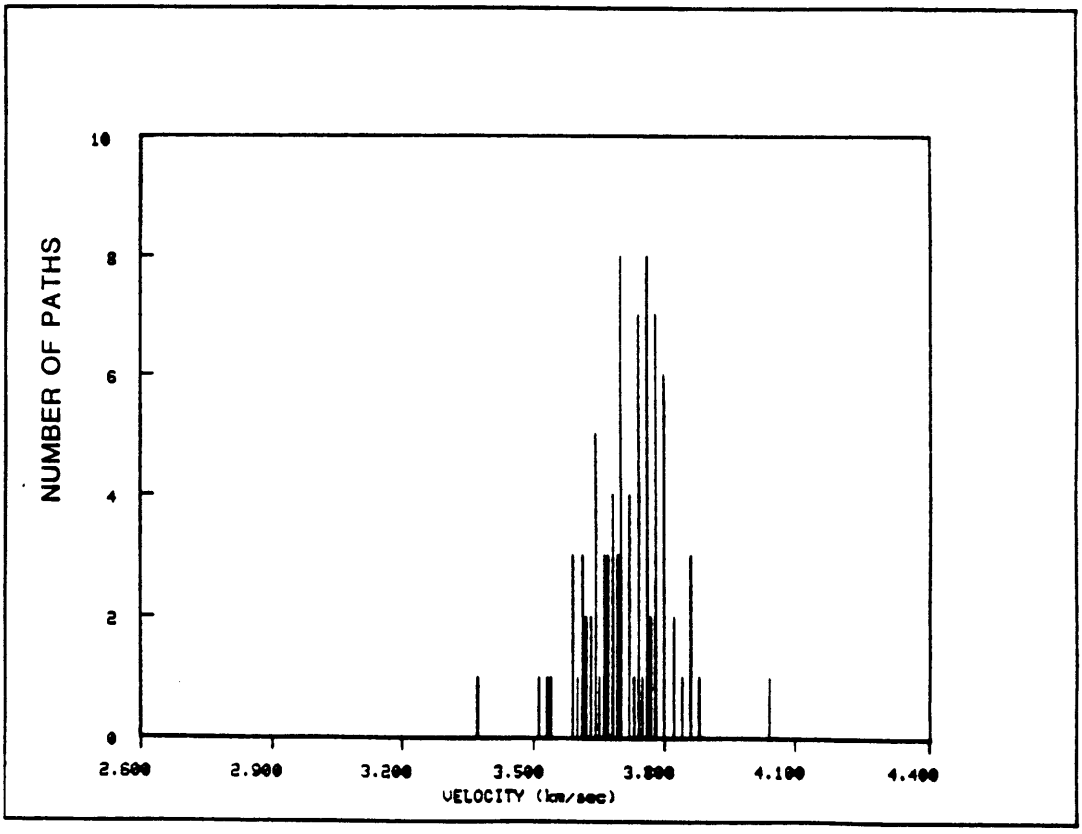

FIGURE C.6r

REGION ø

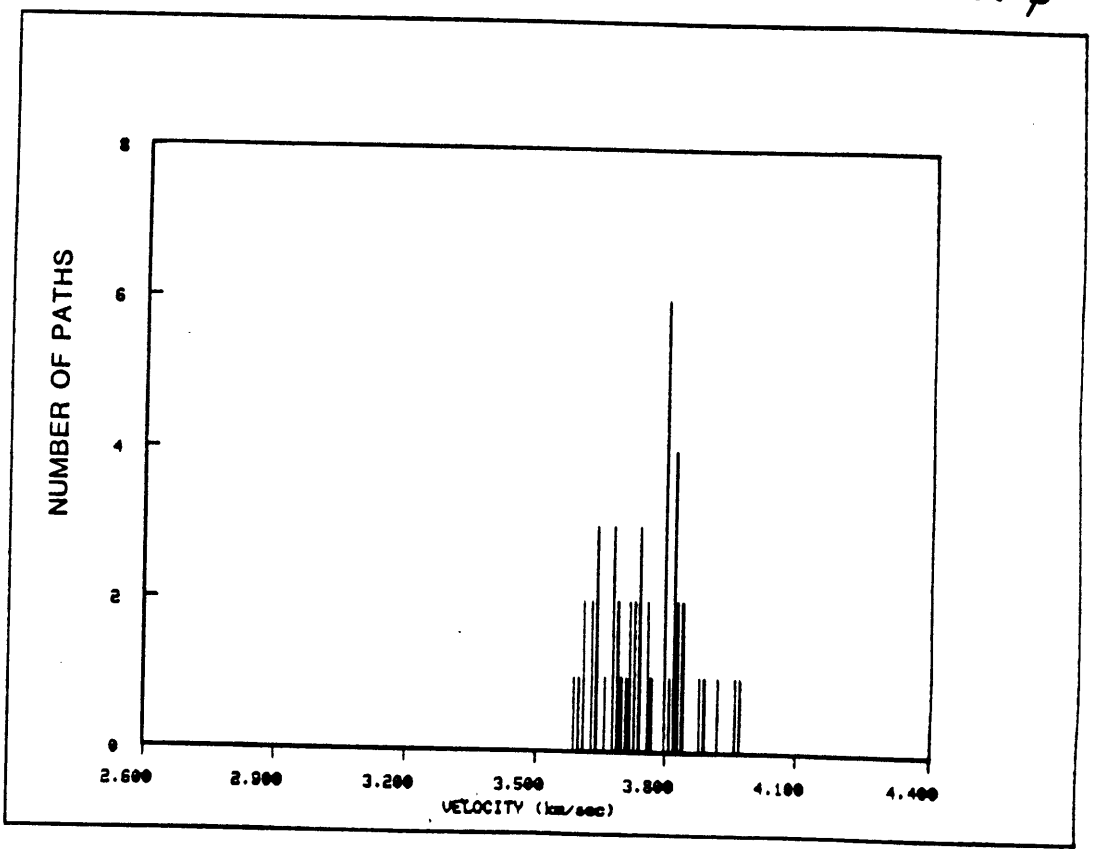

FIGURE C.7a

PERIOD 80 sec

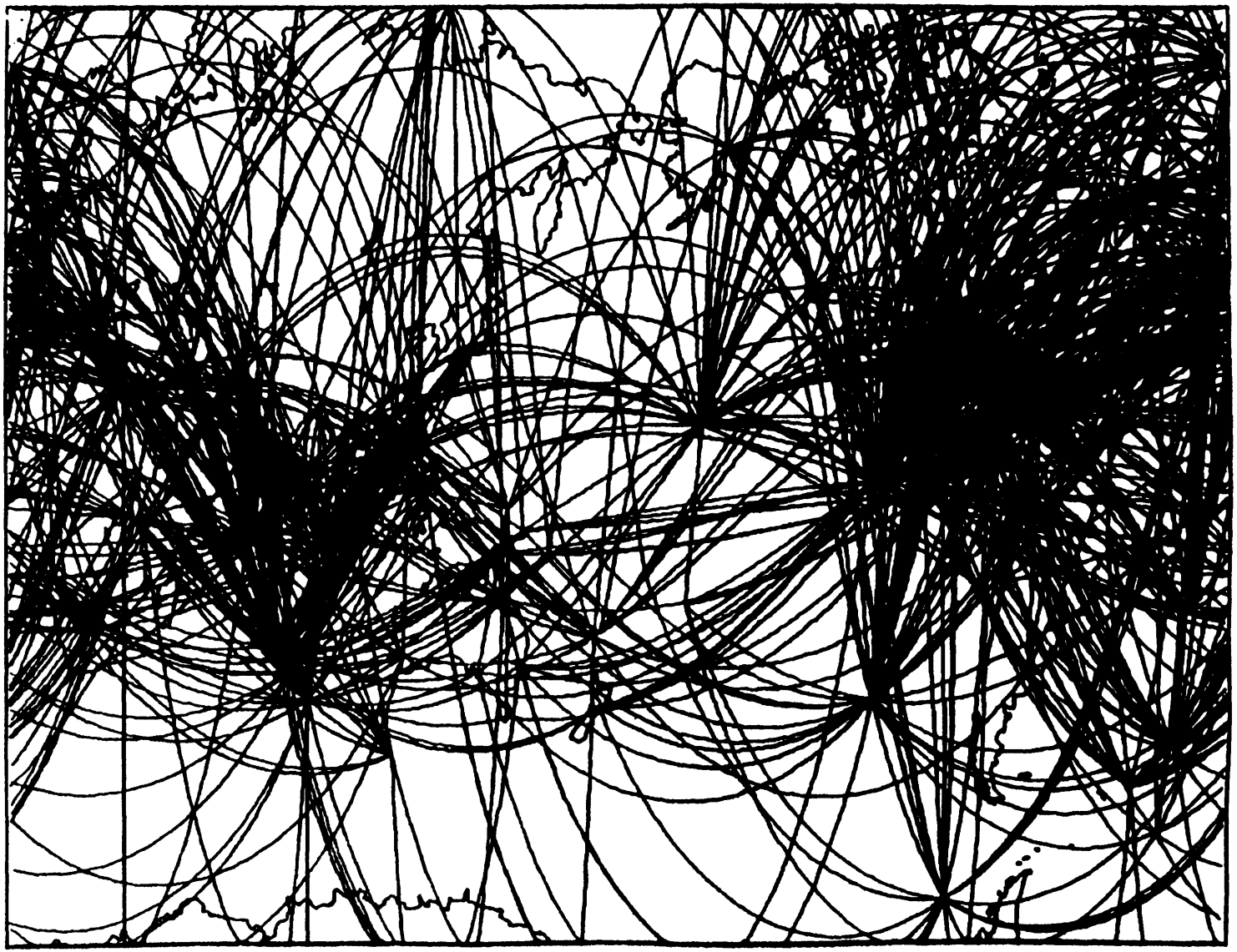

FIGURE C.7b REGION a

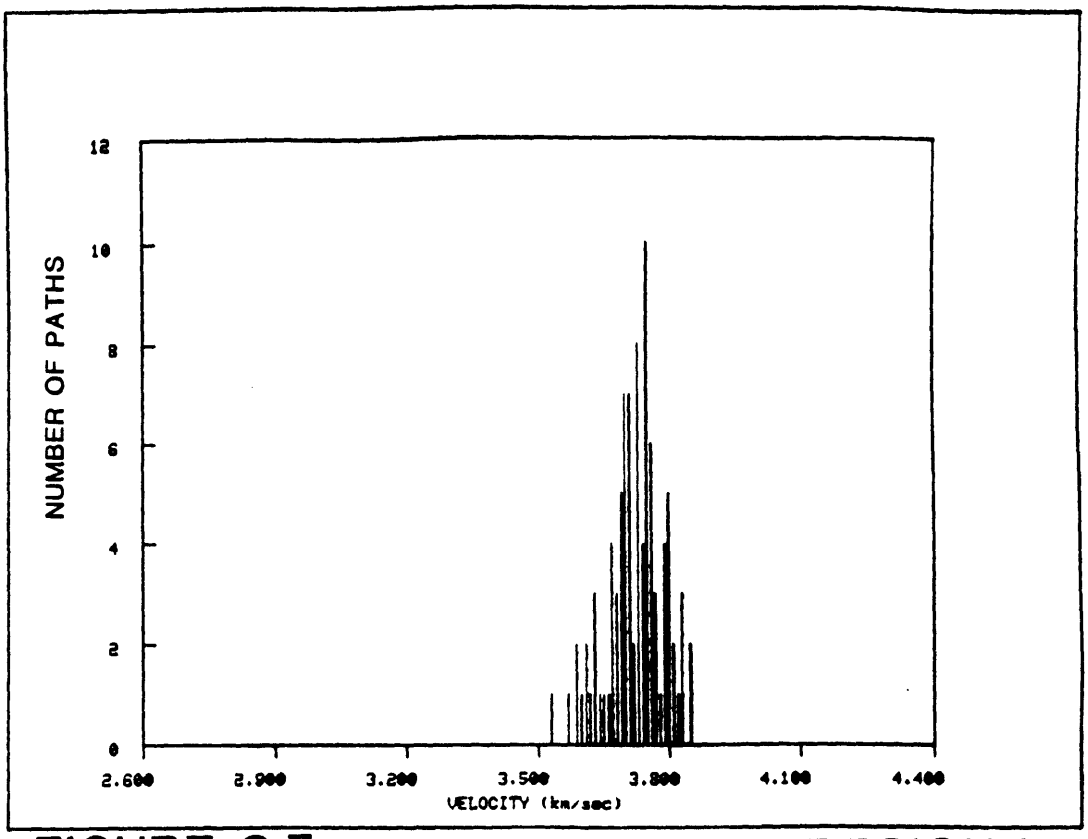

FIGURE C.7c REGION b

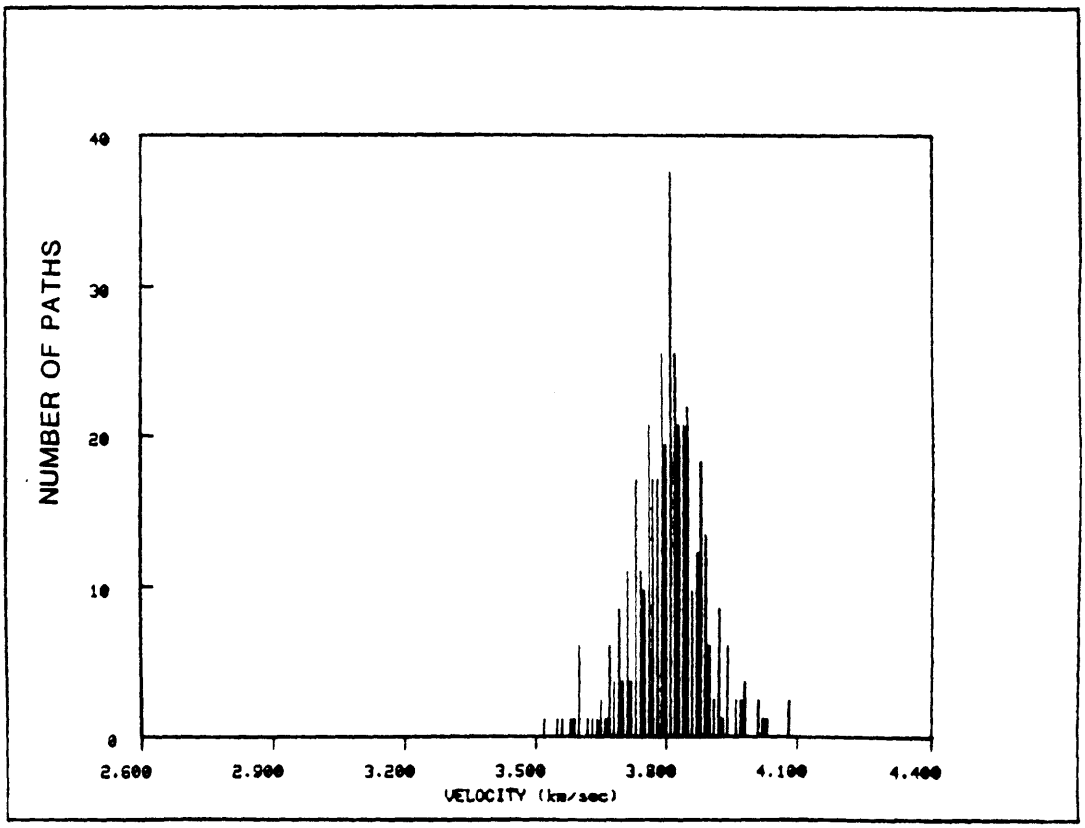

FIGURE C.7d REGION c

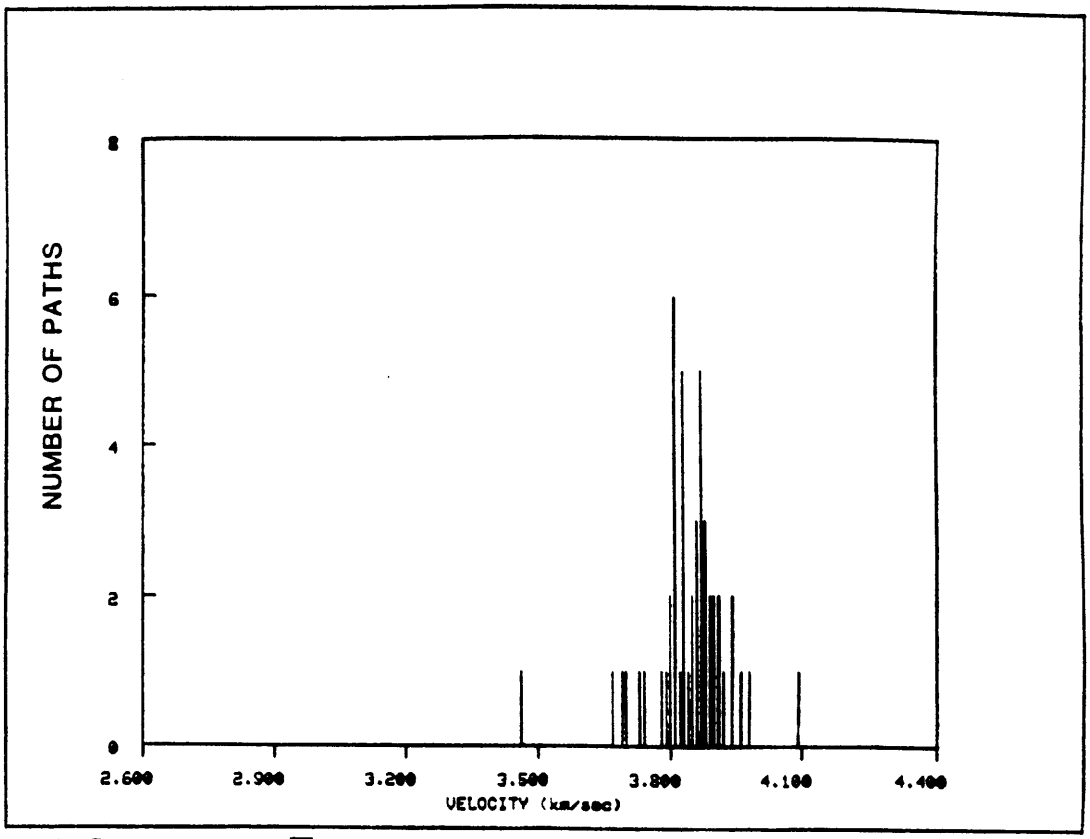

FIGURE C.7e REGION p

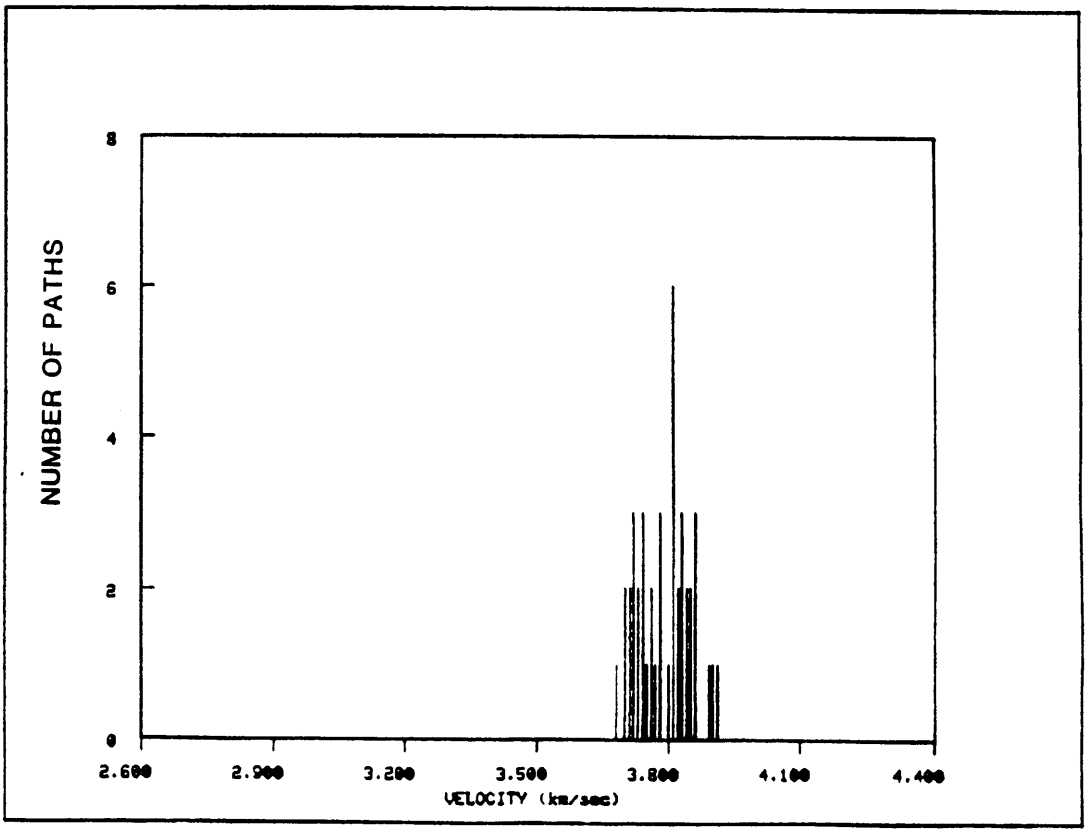

FIGURE C.7f REGION q

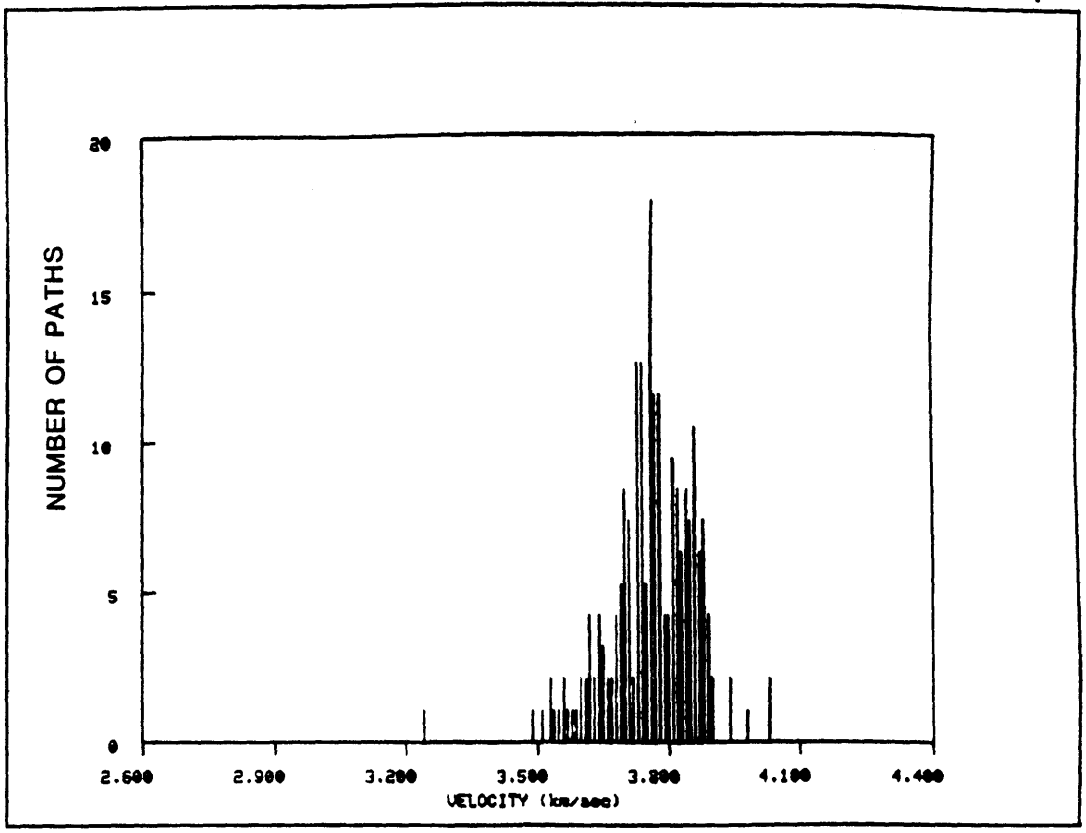

FIGURE C.7g REGION s

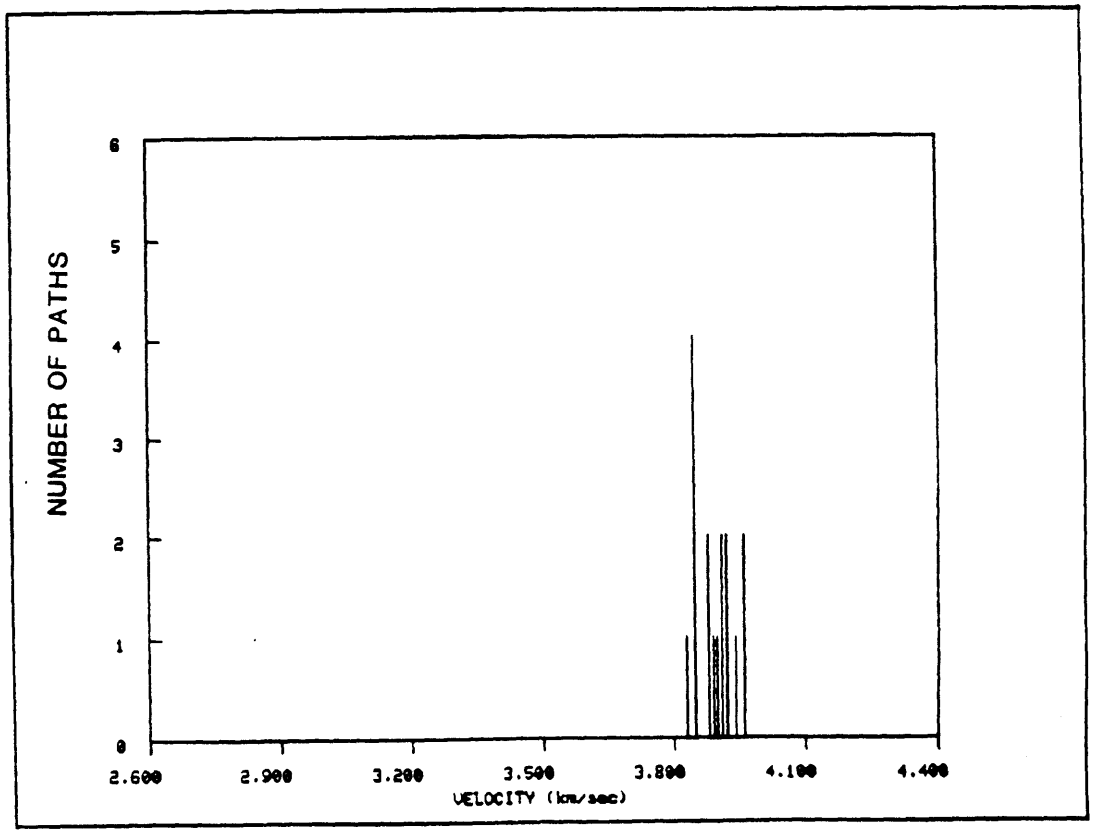

FIGURE C.7h REGION N

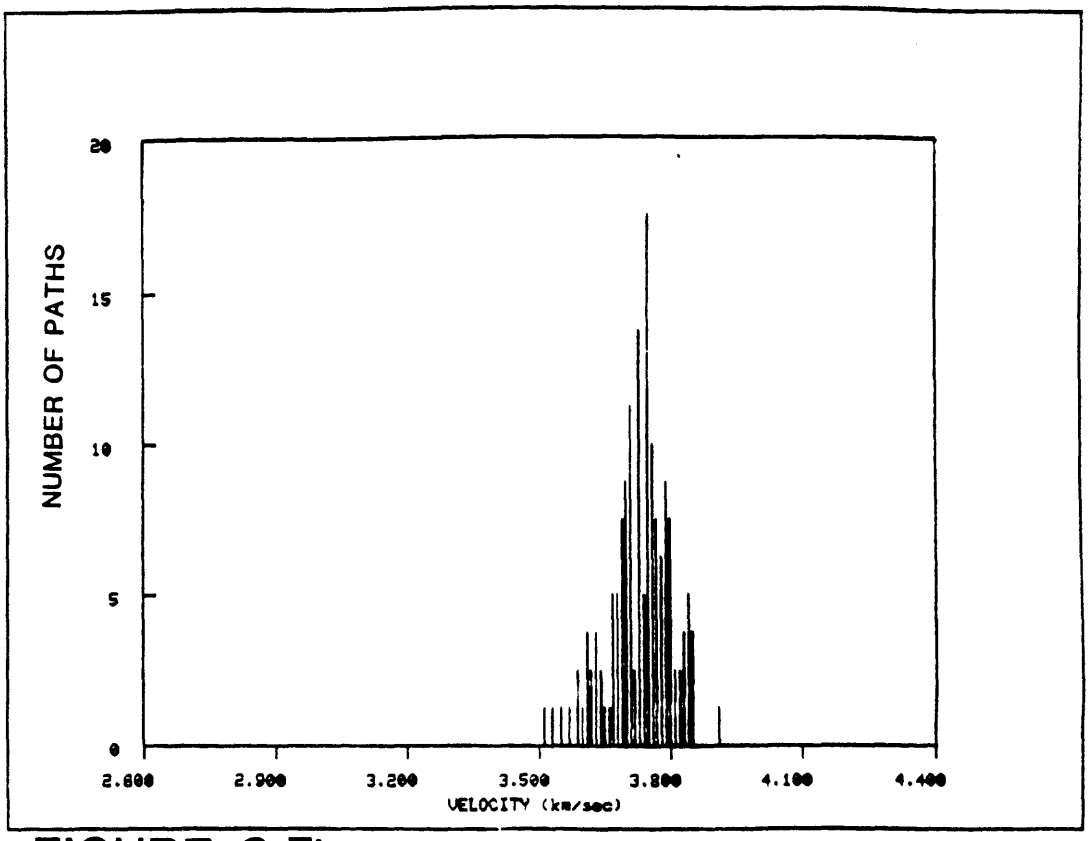

FIGURE C.7i REGION =

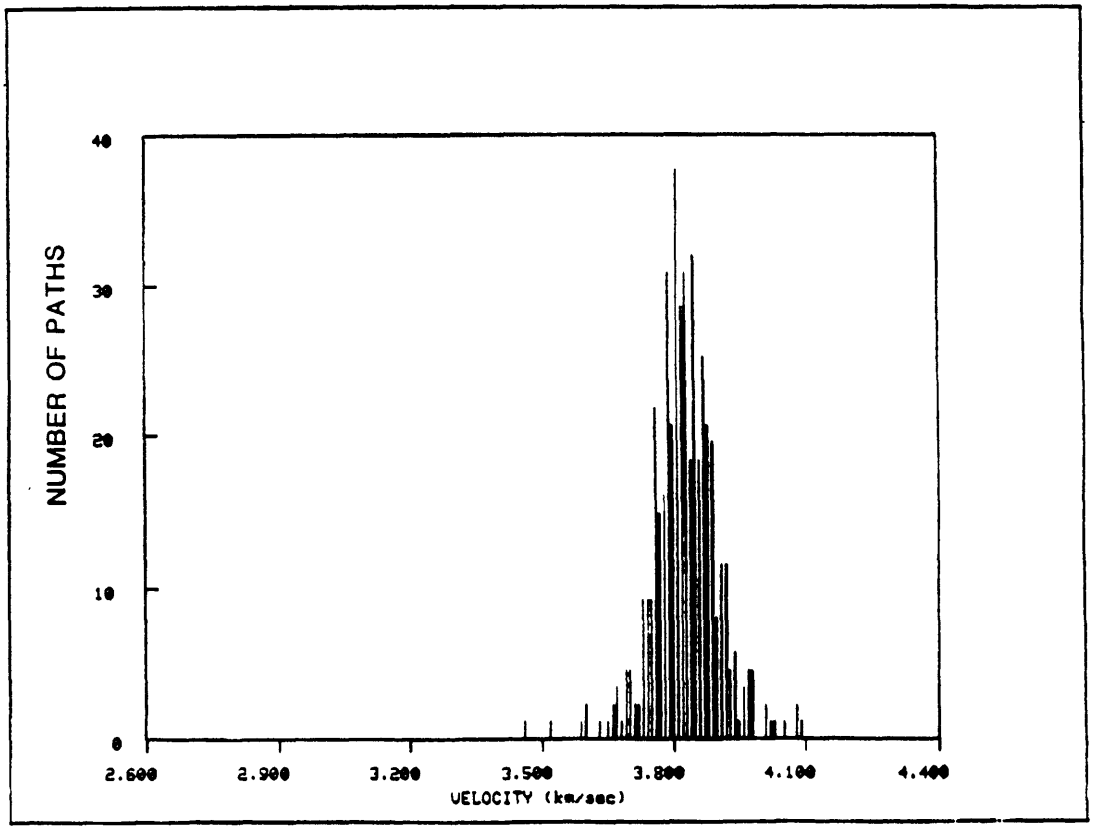

FIGURE C.7j REGION 0

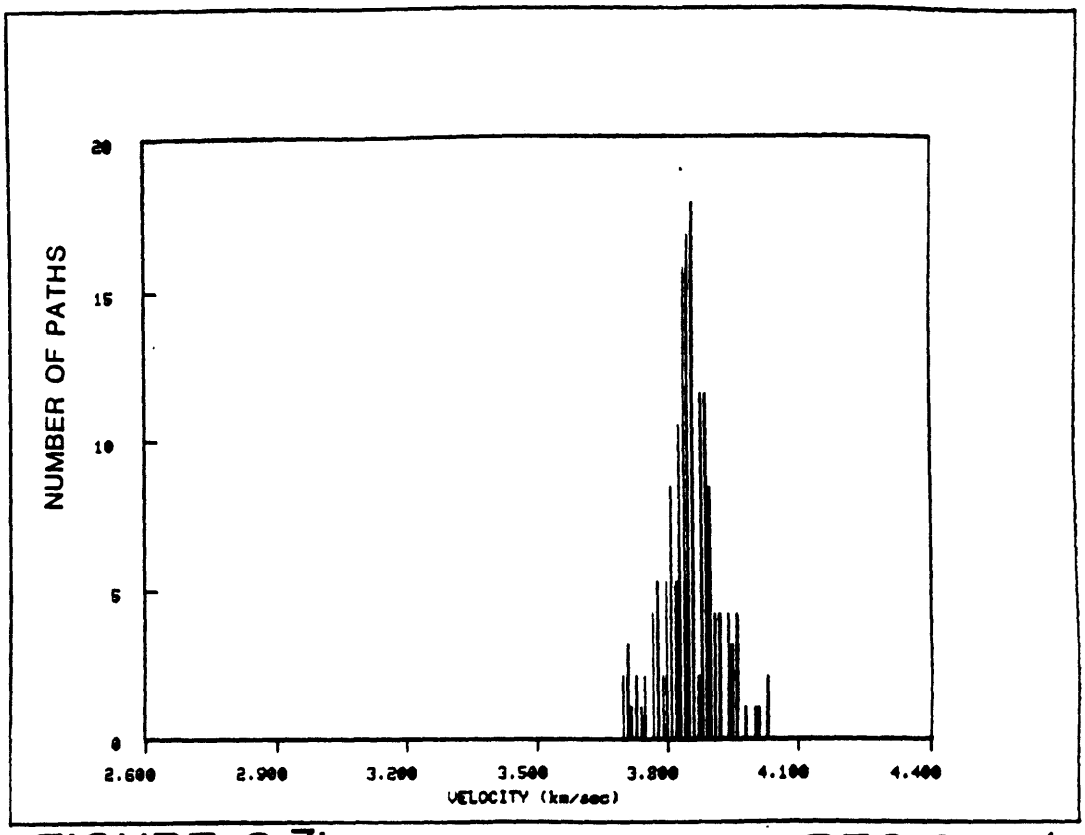

FIGURE C.7k REGION ~~0~~

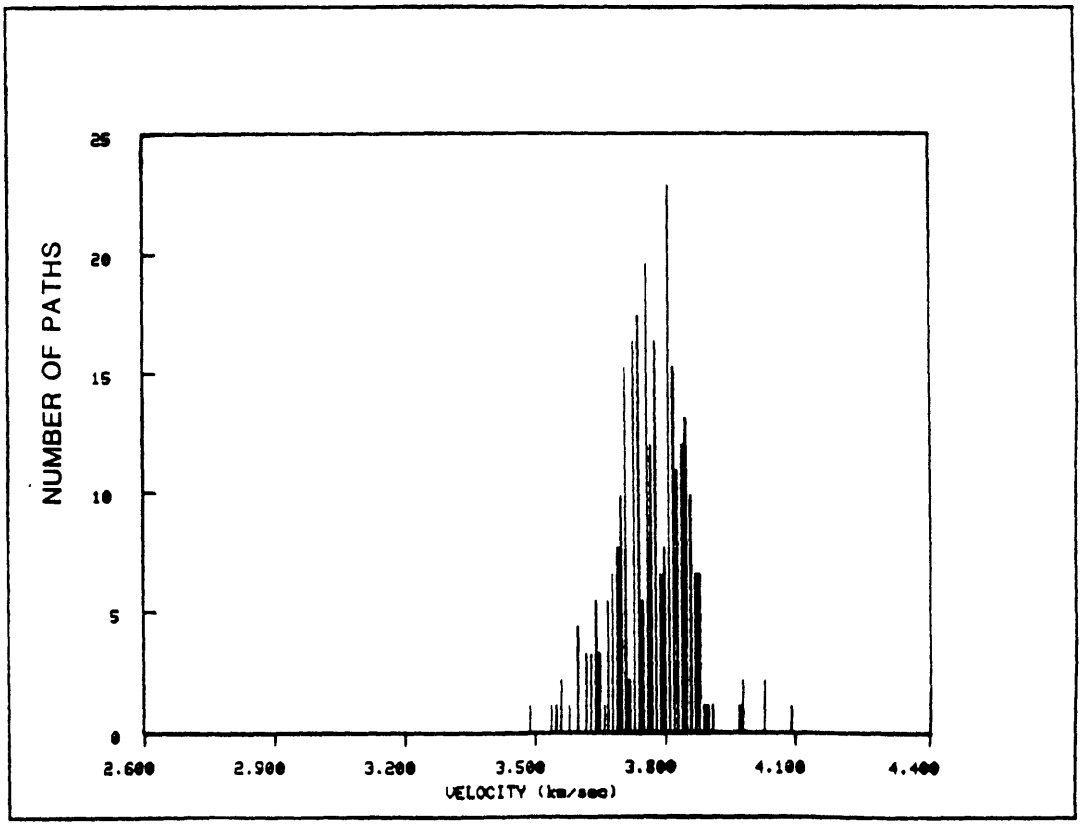

FIGURE C.7l REGION N

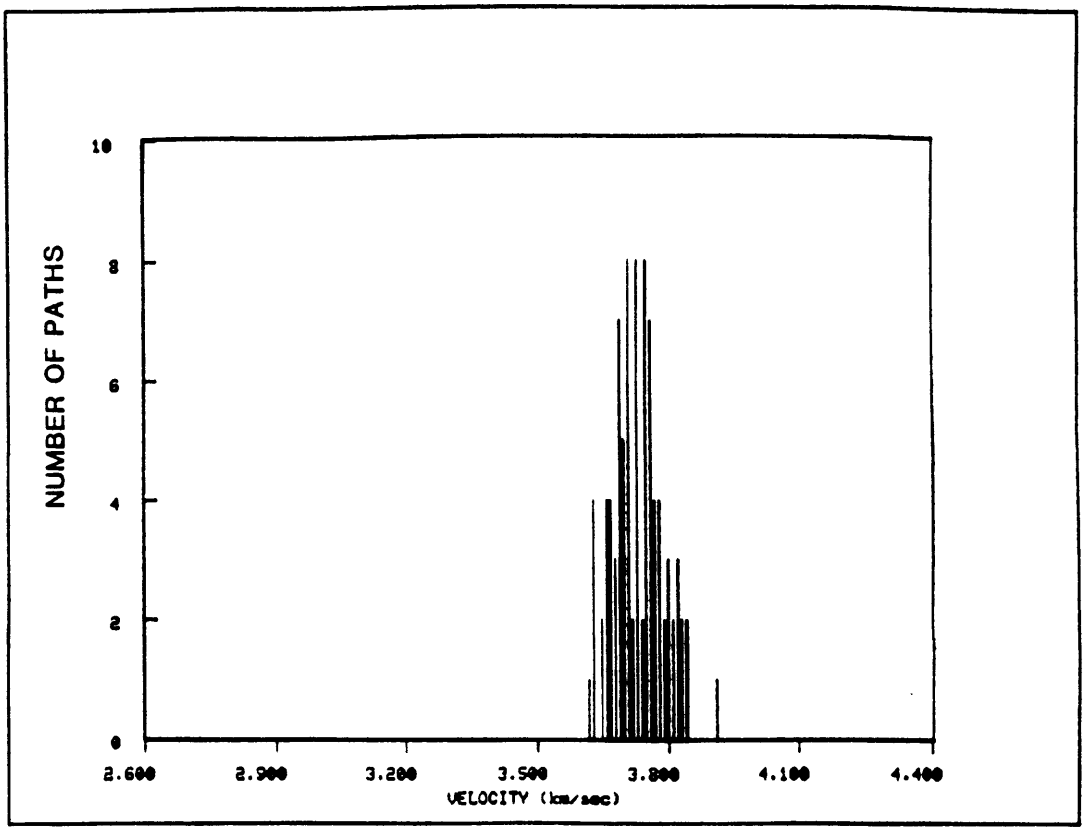

FIGURE C.7m REGION #

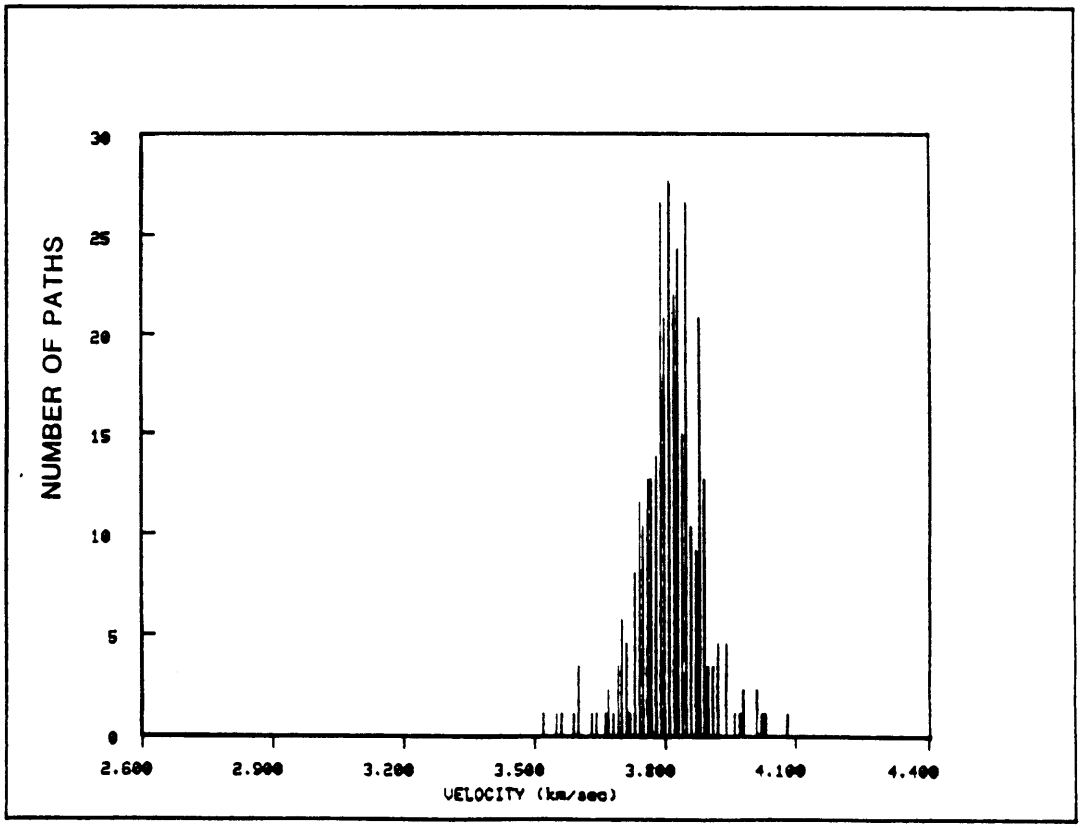

FIGURE C.7n REGION =

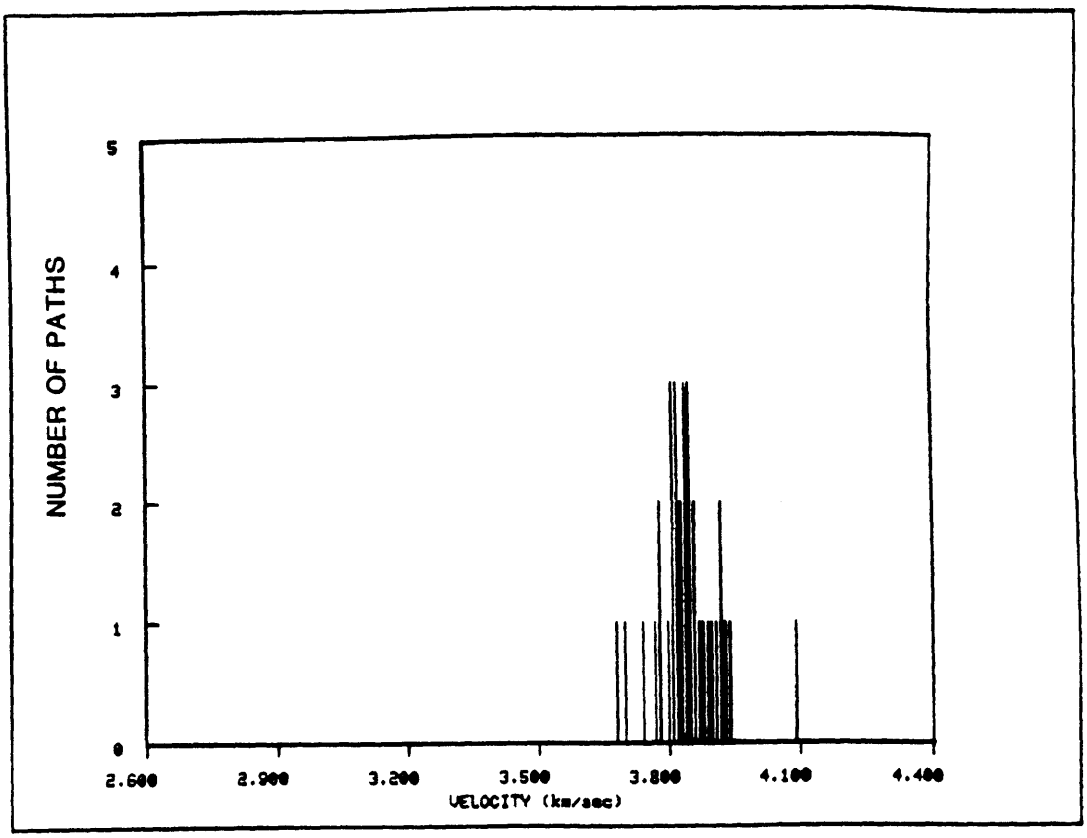

FIGURE C.7o REGION –

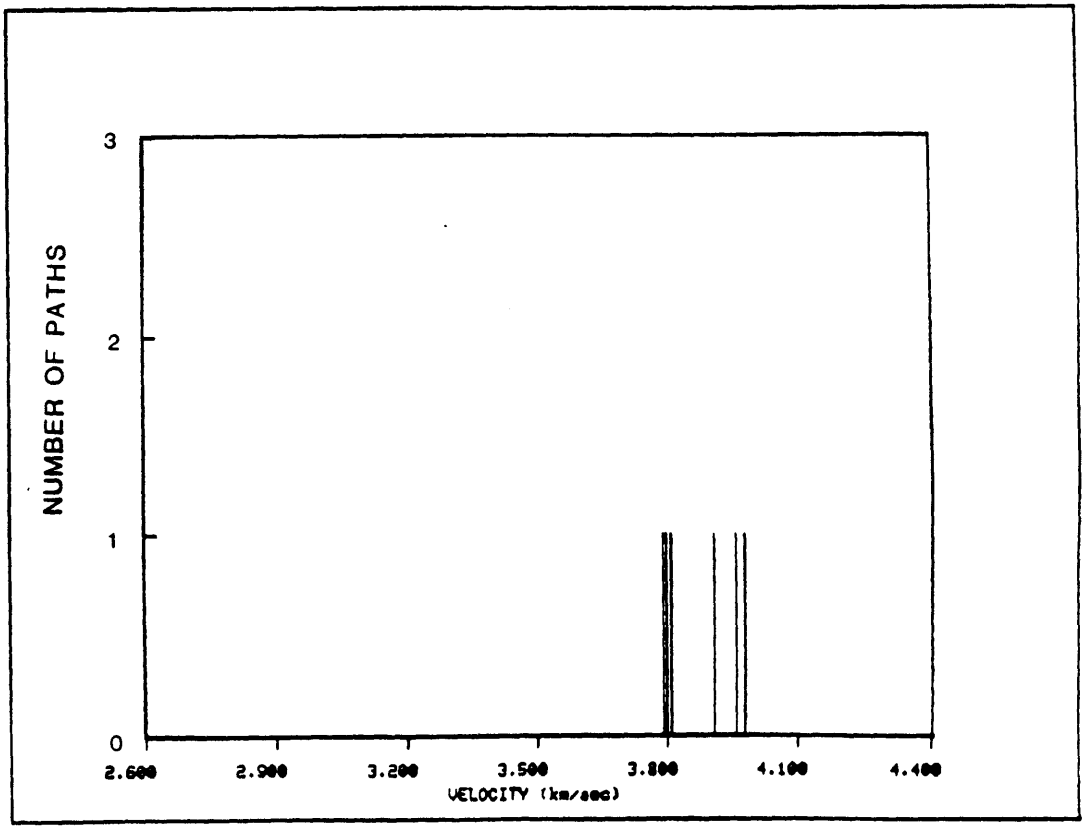

FIGURE C.7p REGION 0

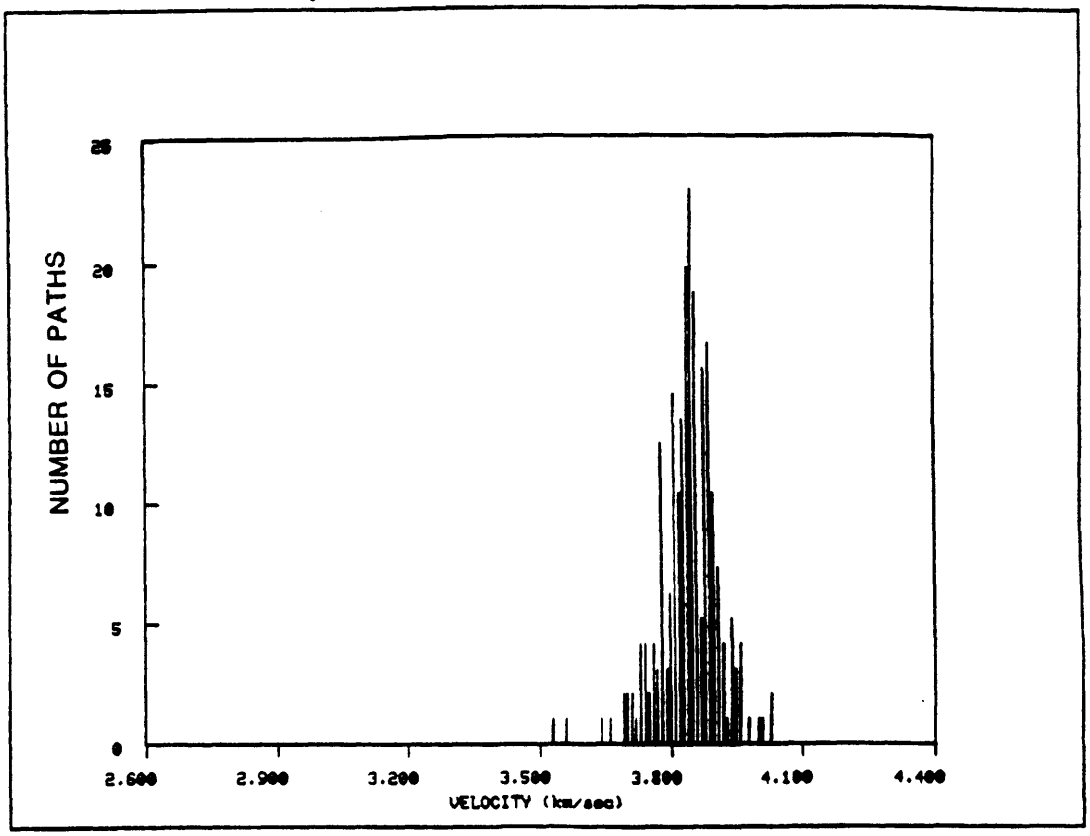

FIGURE C.7q REGION .

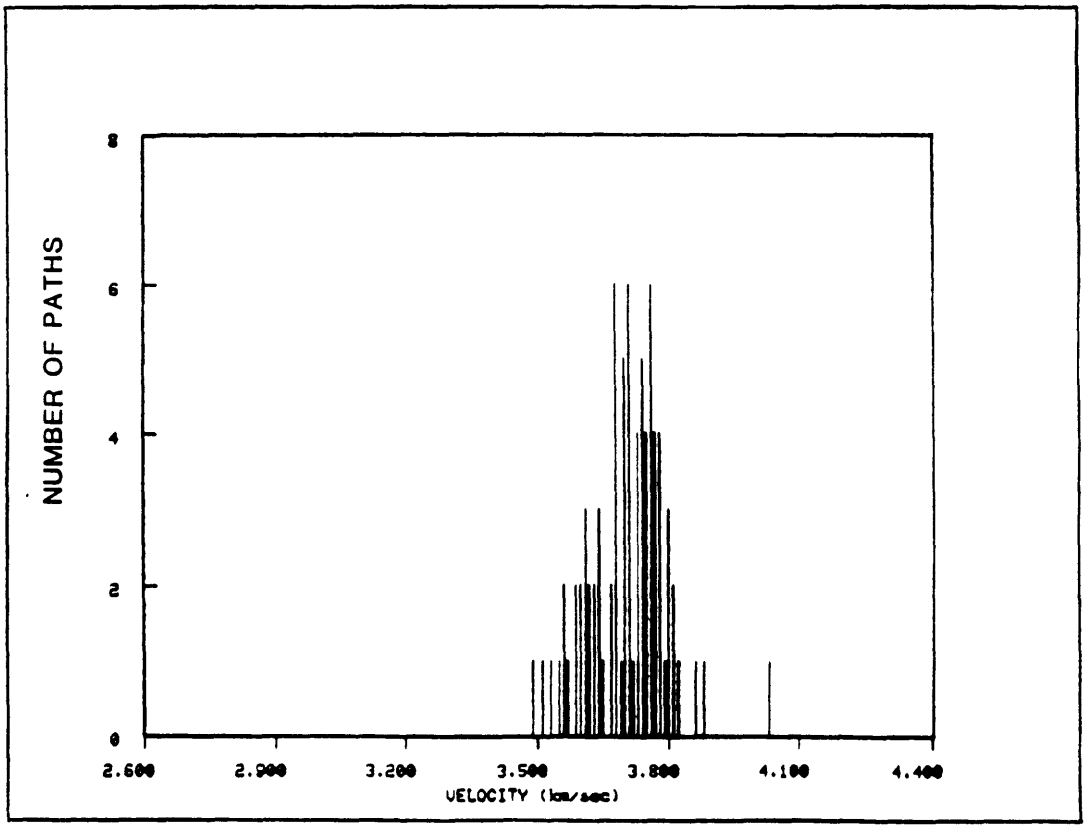

FIGURE C.7r

REGION ø

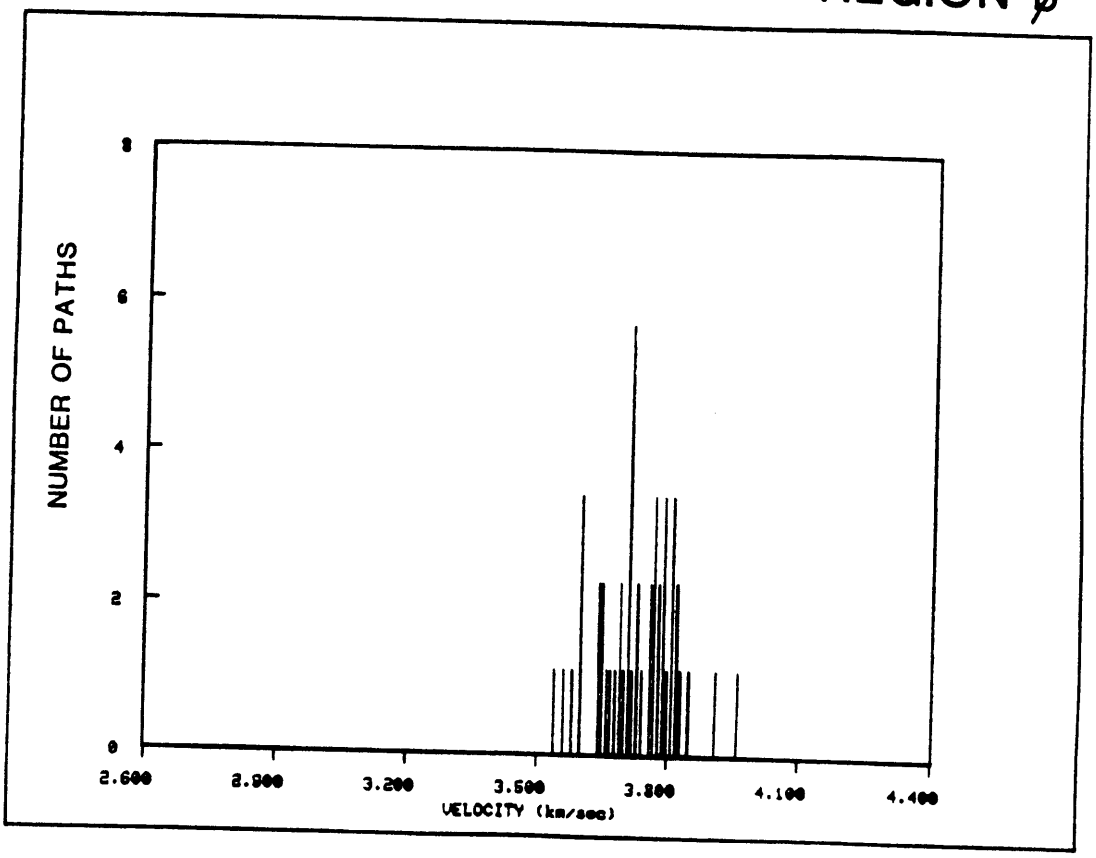

FIGURE C.8a

PERIOD 90 sec

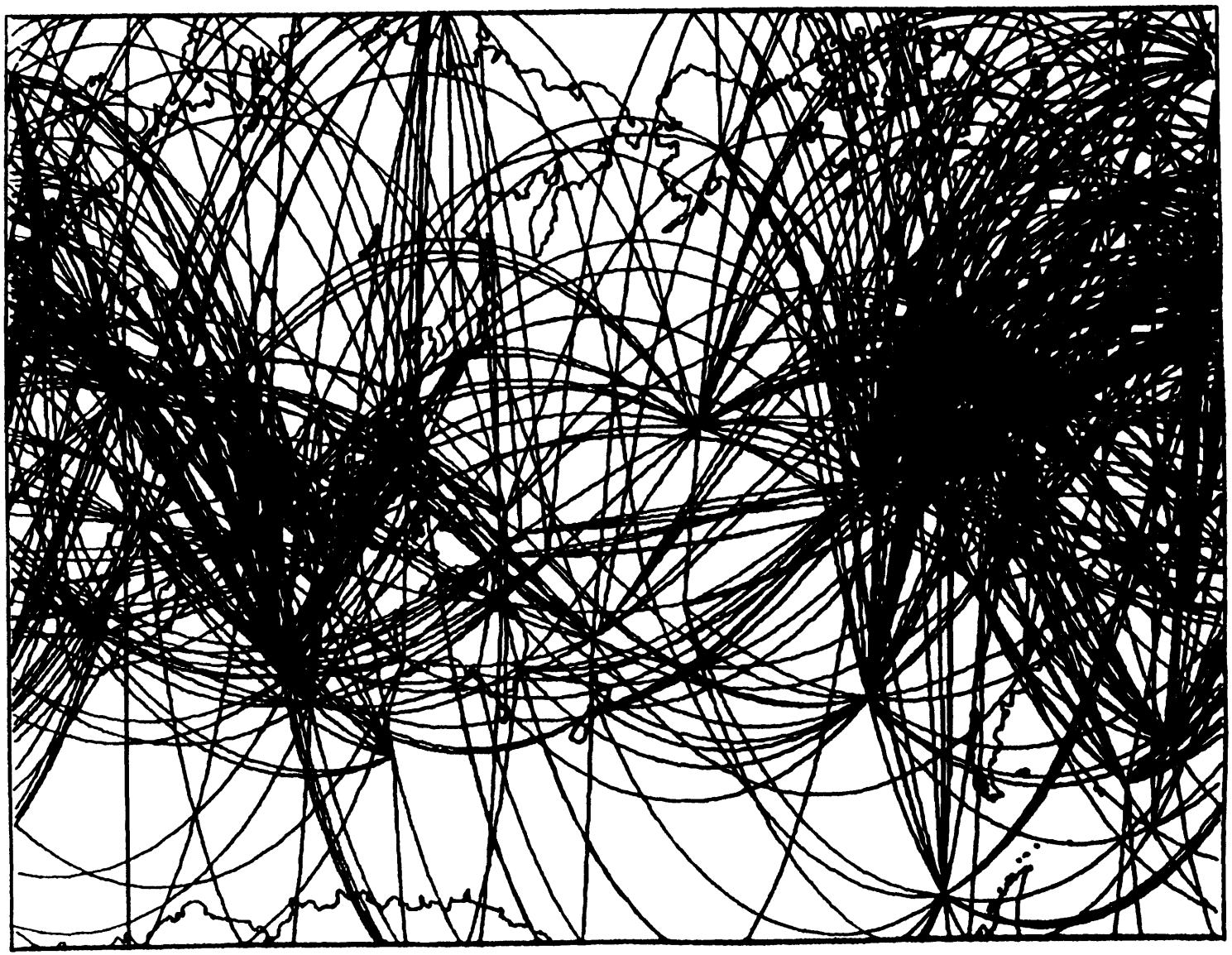

FIGURE C.8b REGION a

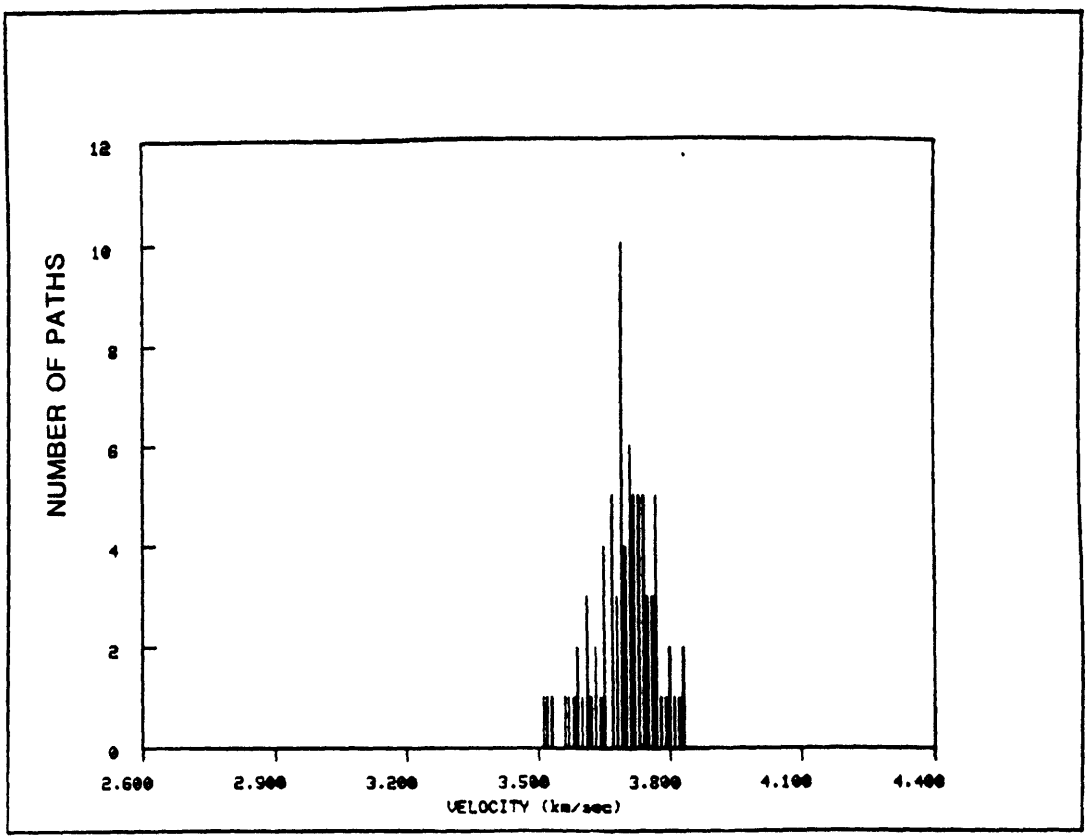

FIGURE C.8c REGION b

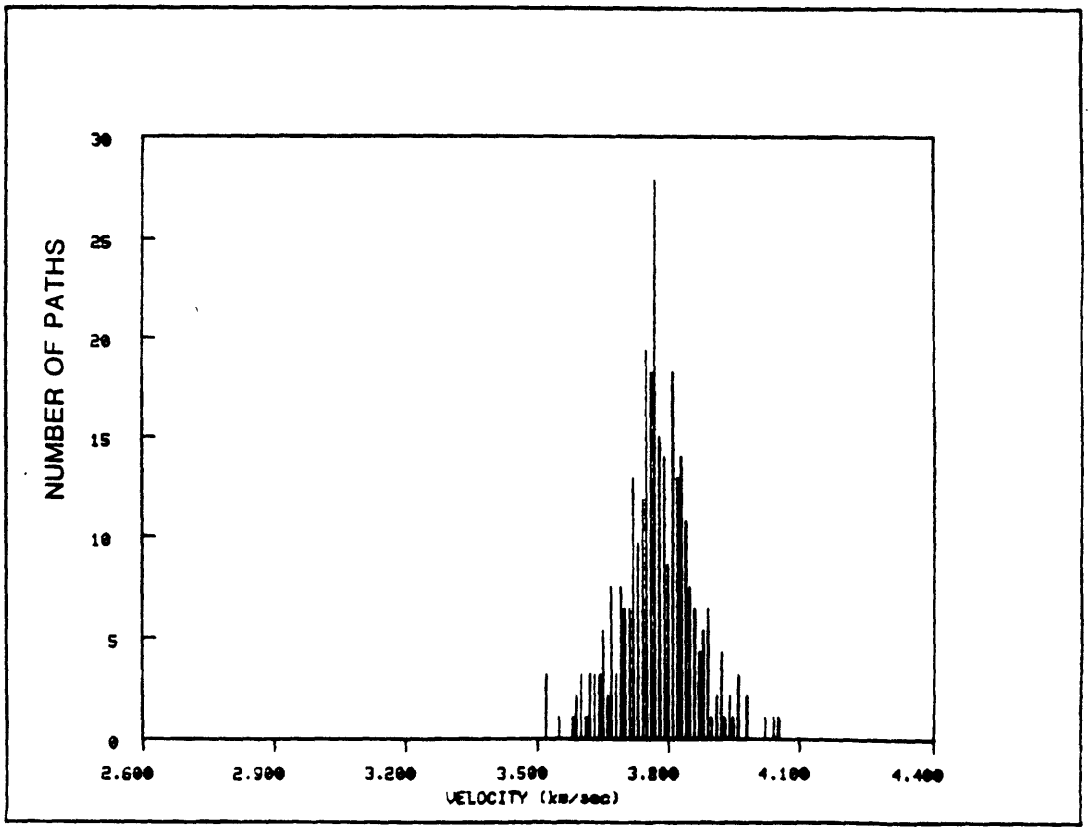

FIGURE C.8d REGION c

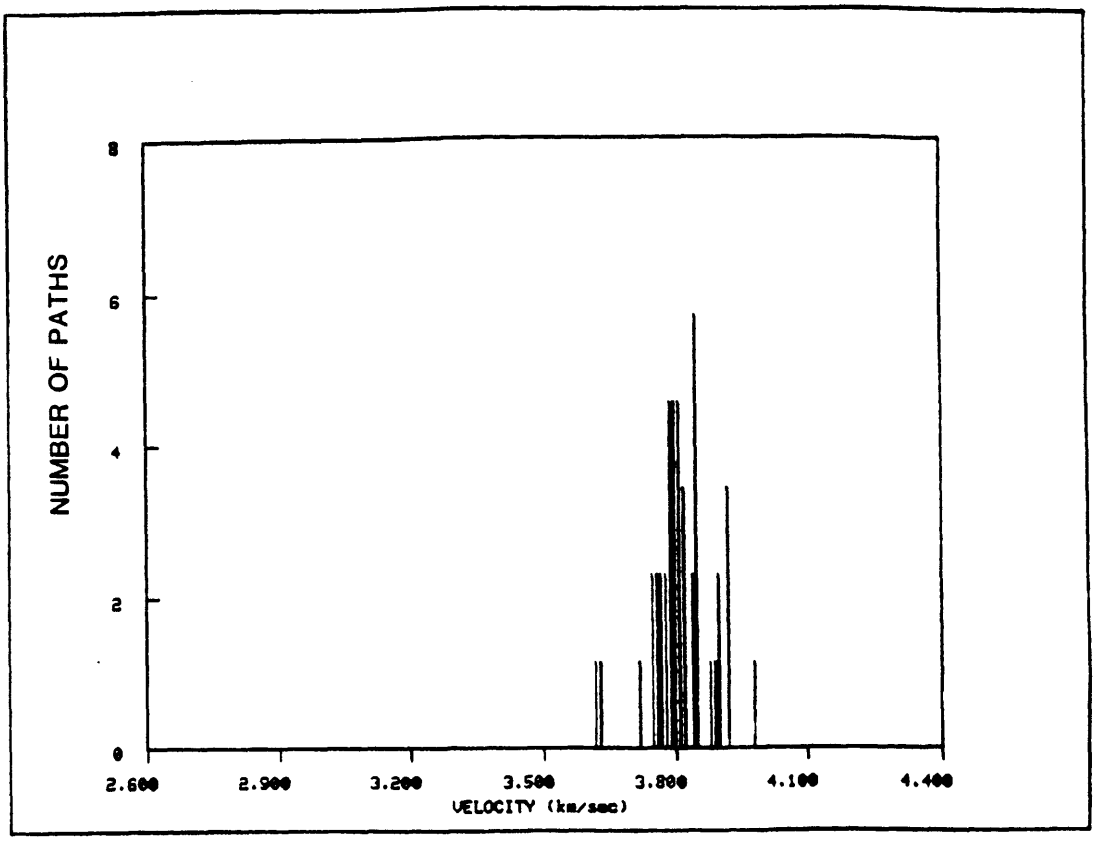

FIGURE C.8e REGION p

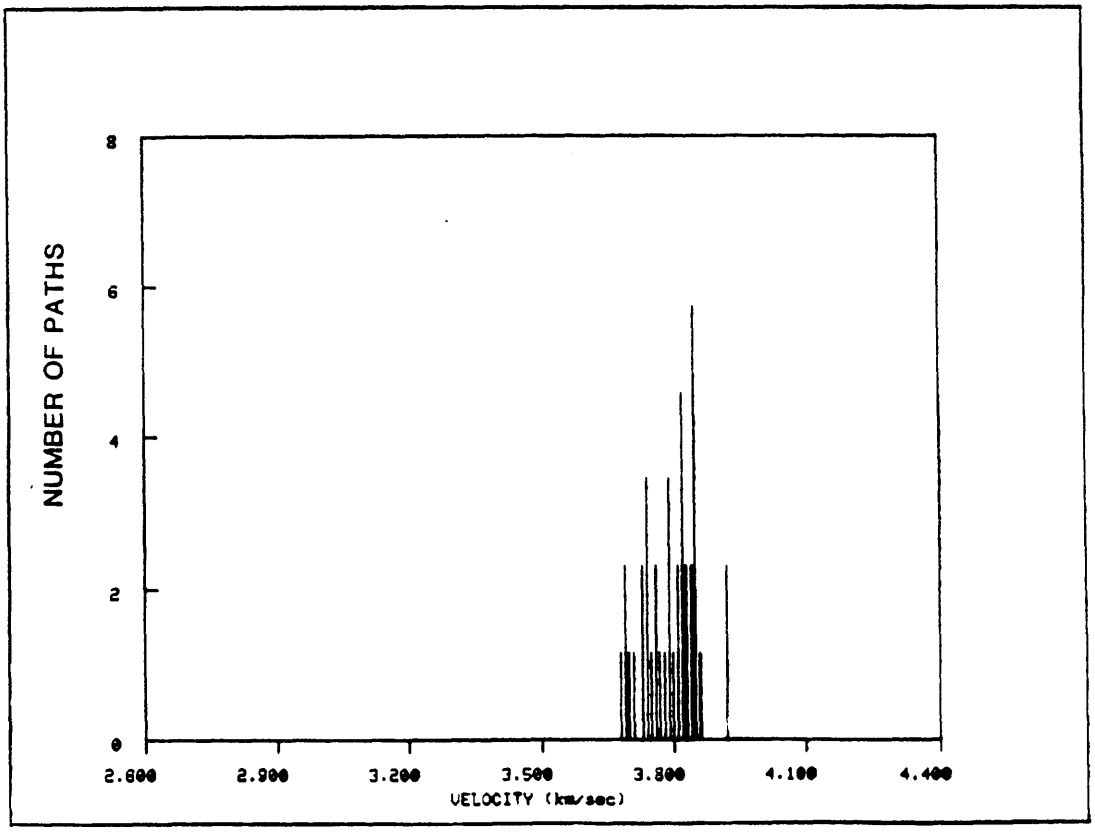

FIGURE C.8f REGION q

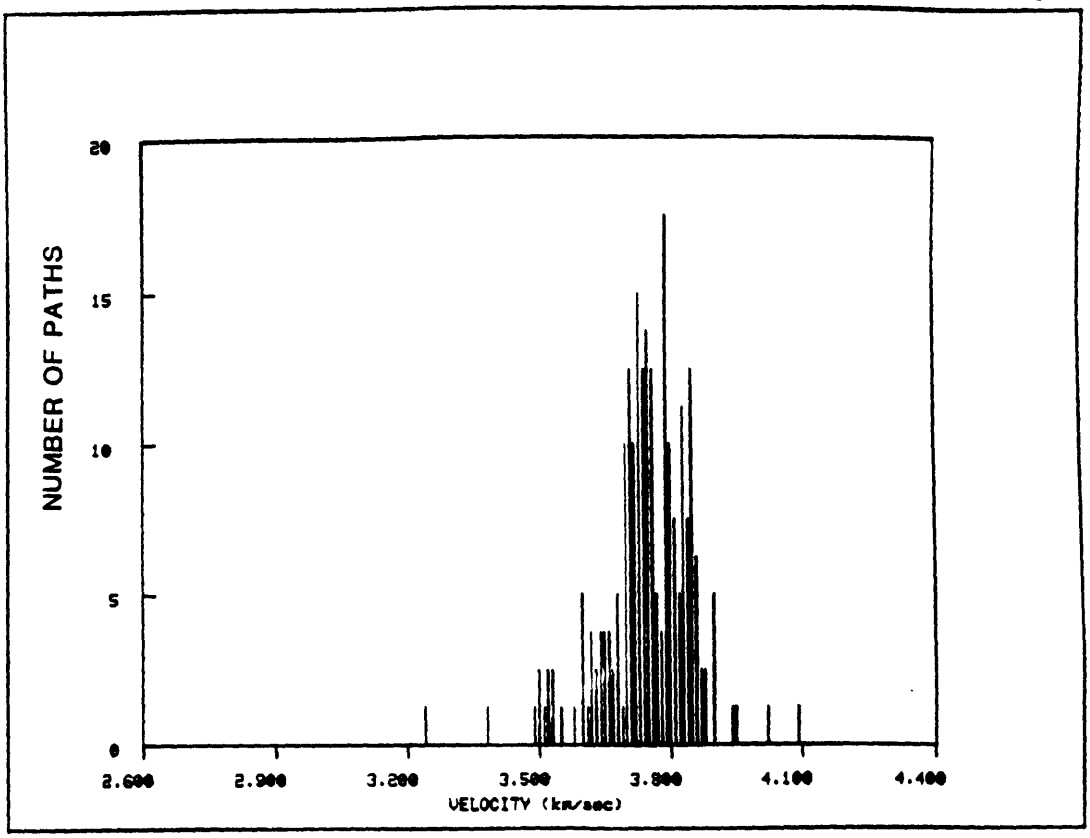

FIGURE C.8g REGION s

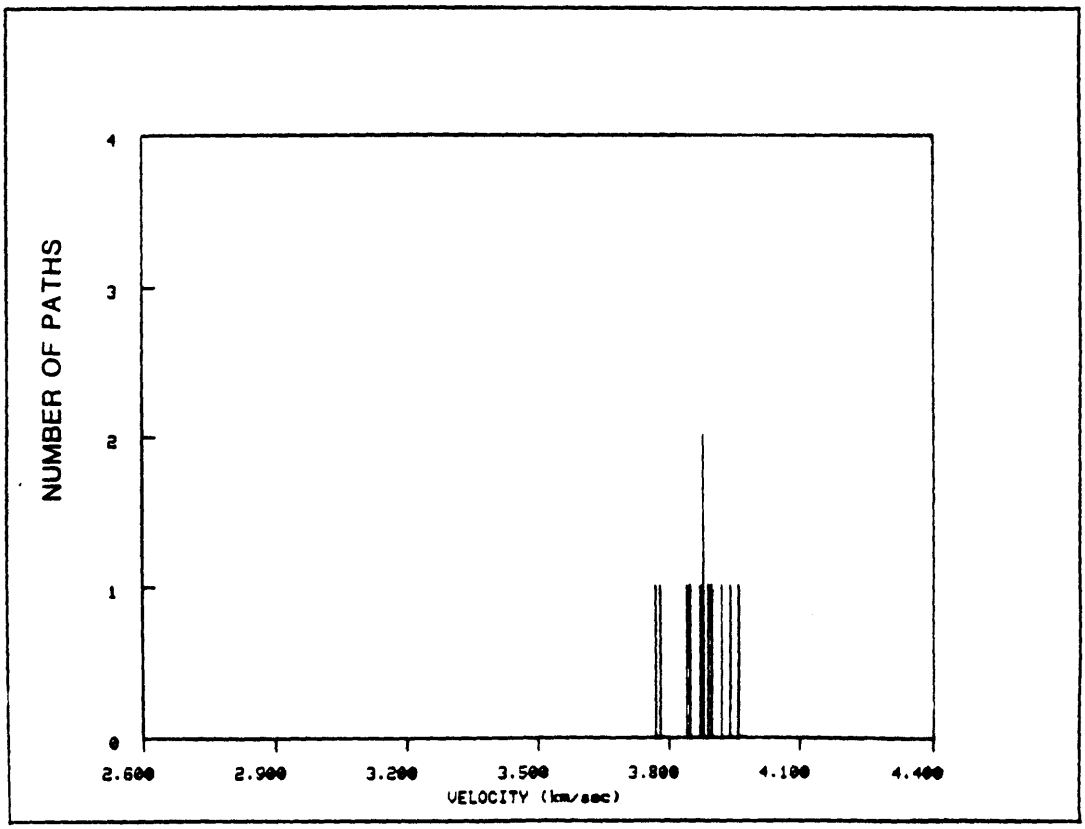

FIGURE C.8h REGION N

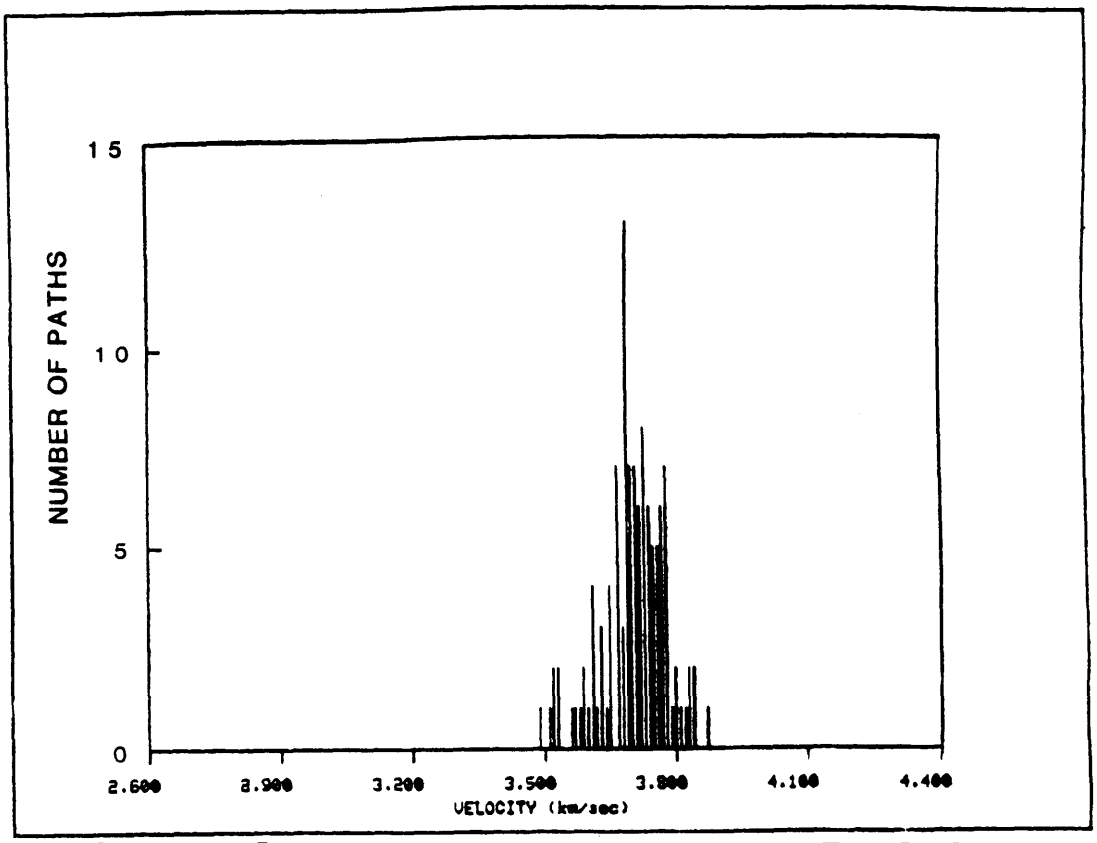

FIGURE C.8i REGION =

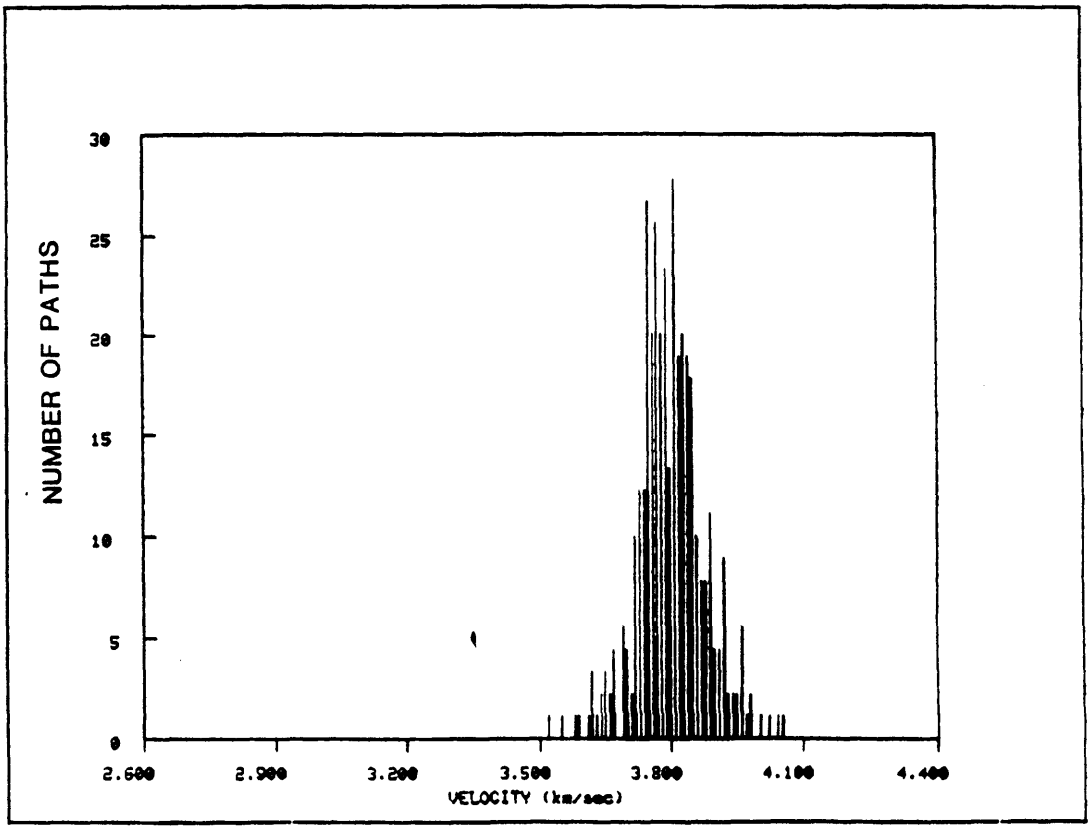

FIGURE C.8j REGION 0

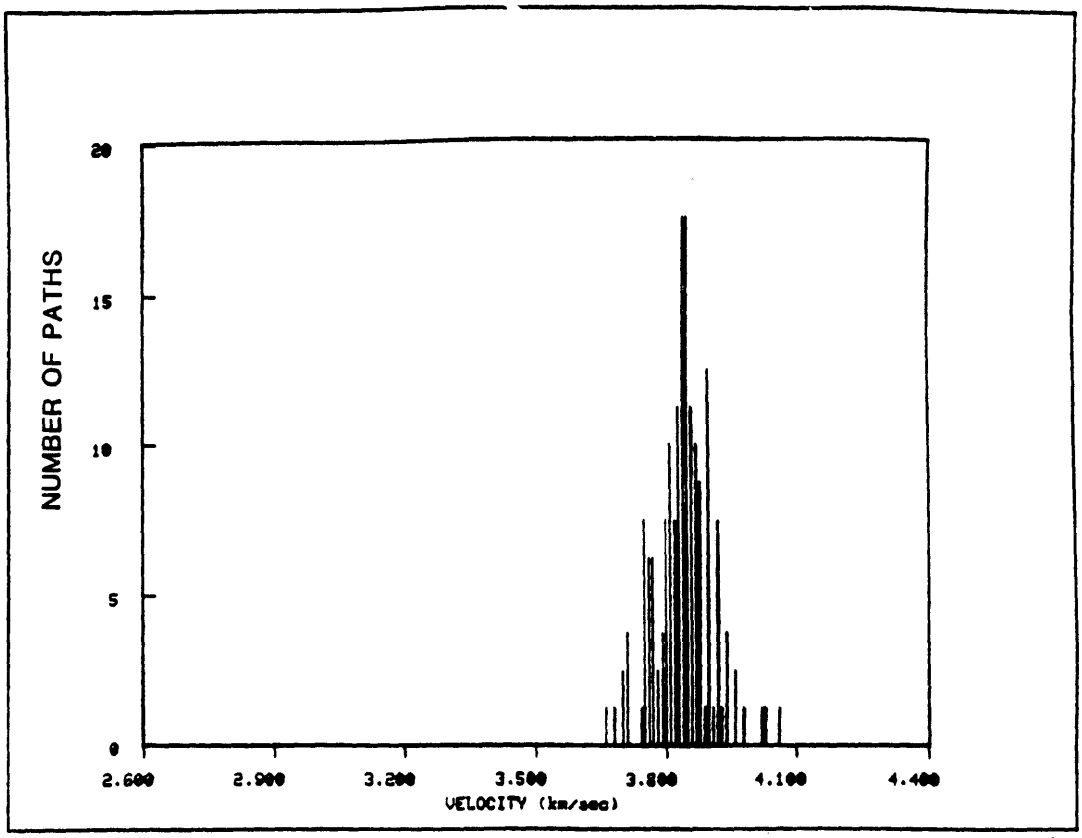

FIGURE C.8k REGION ~~0~~

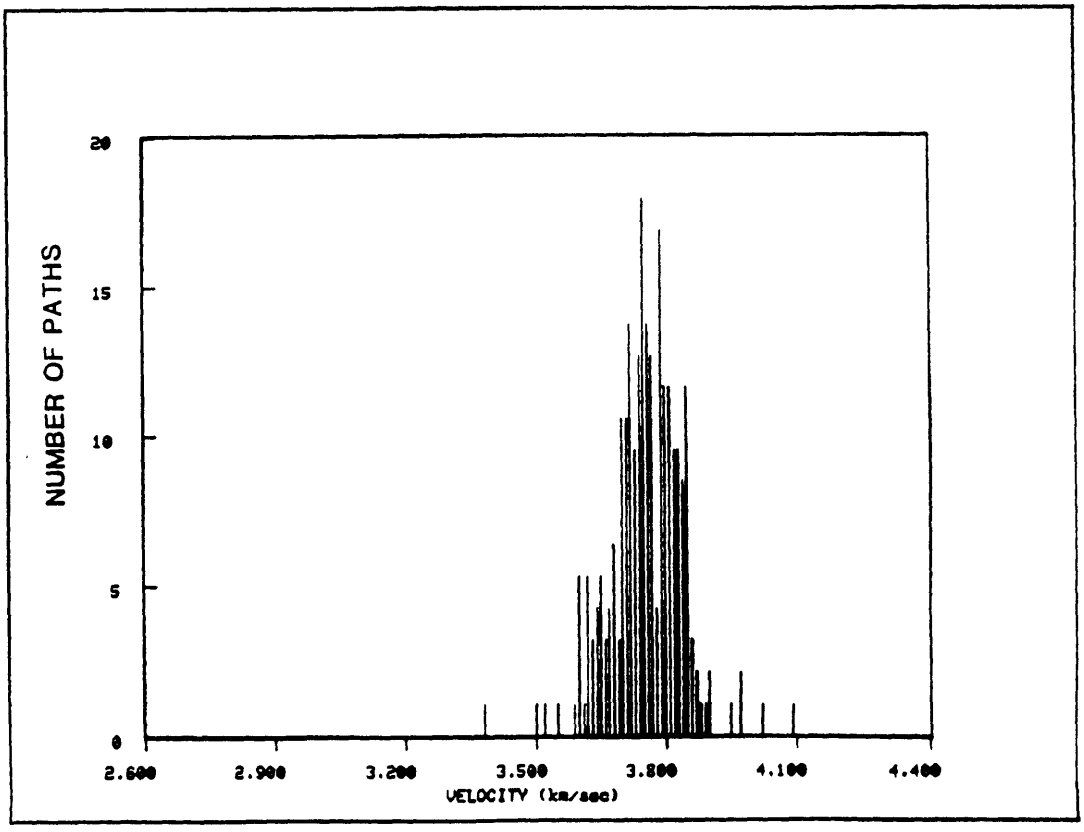

FIGURE C.8l REGION N

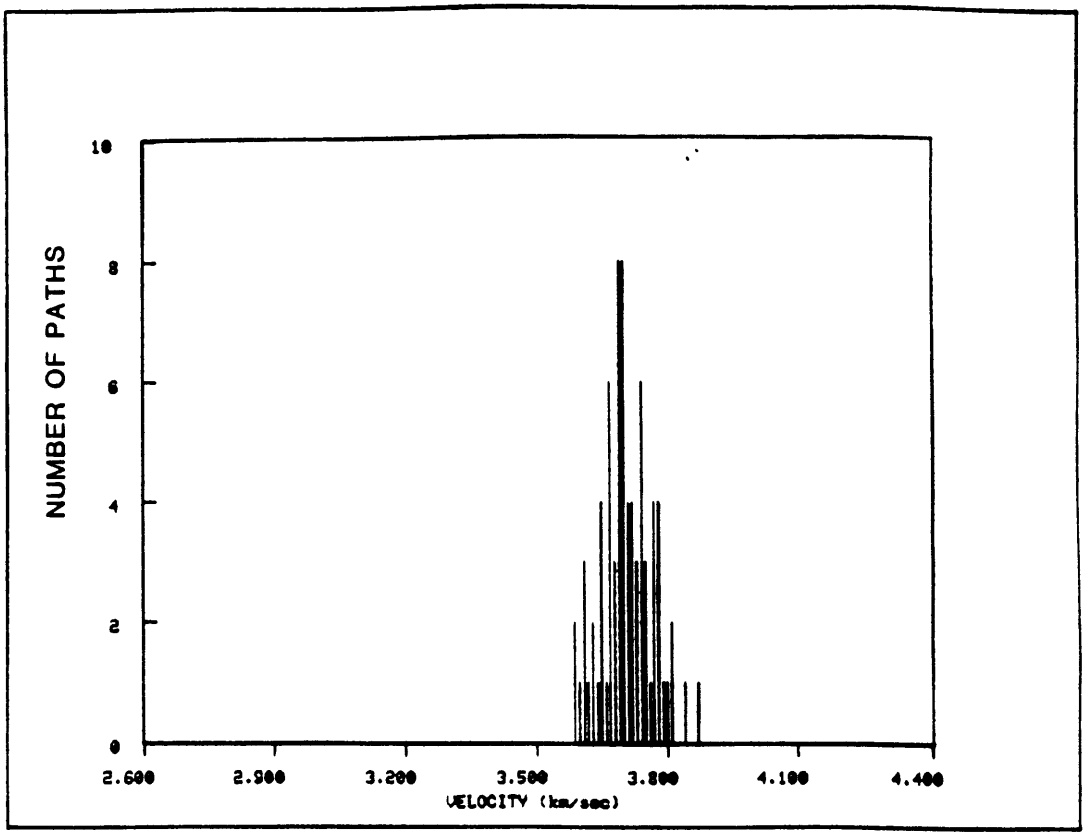

FIGURE C.8m REGION #

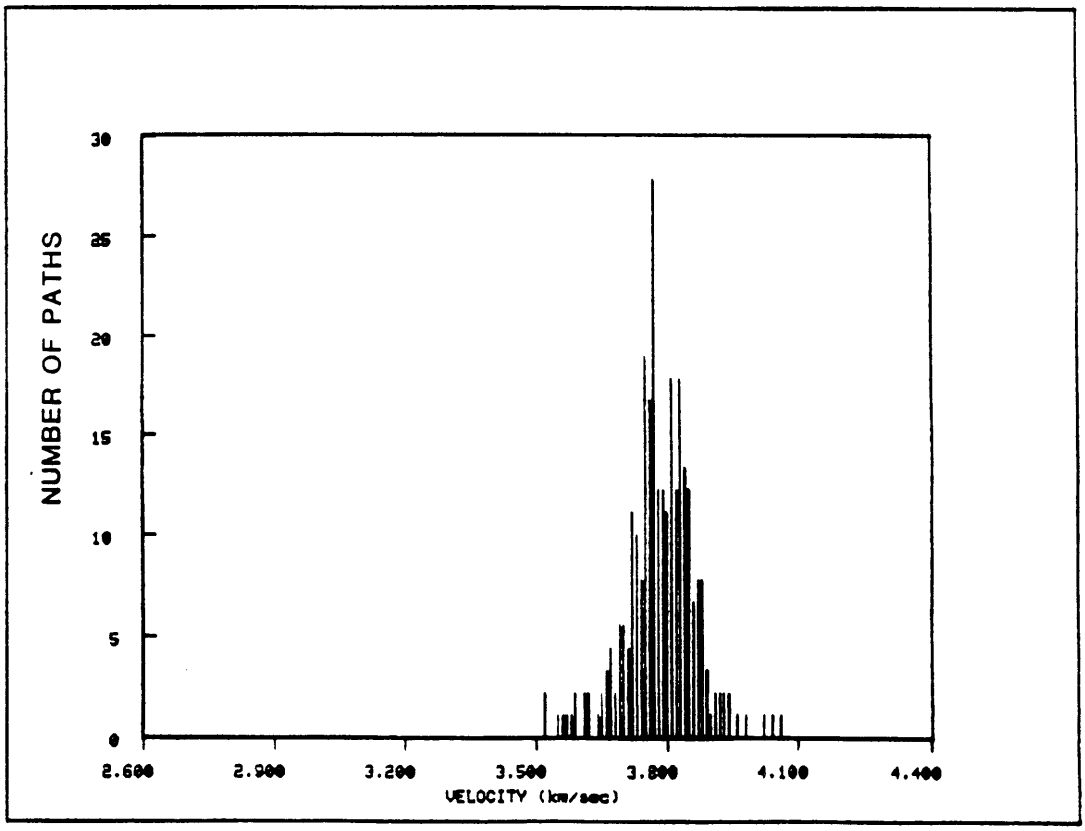

FIGURE C.8n REGION =

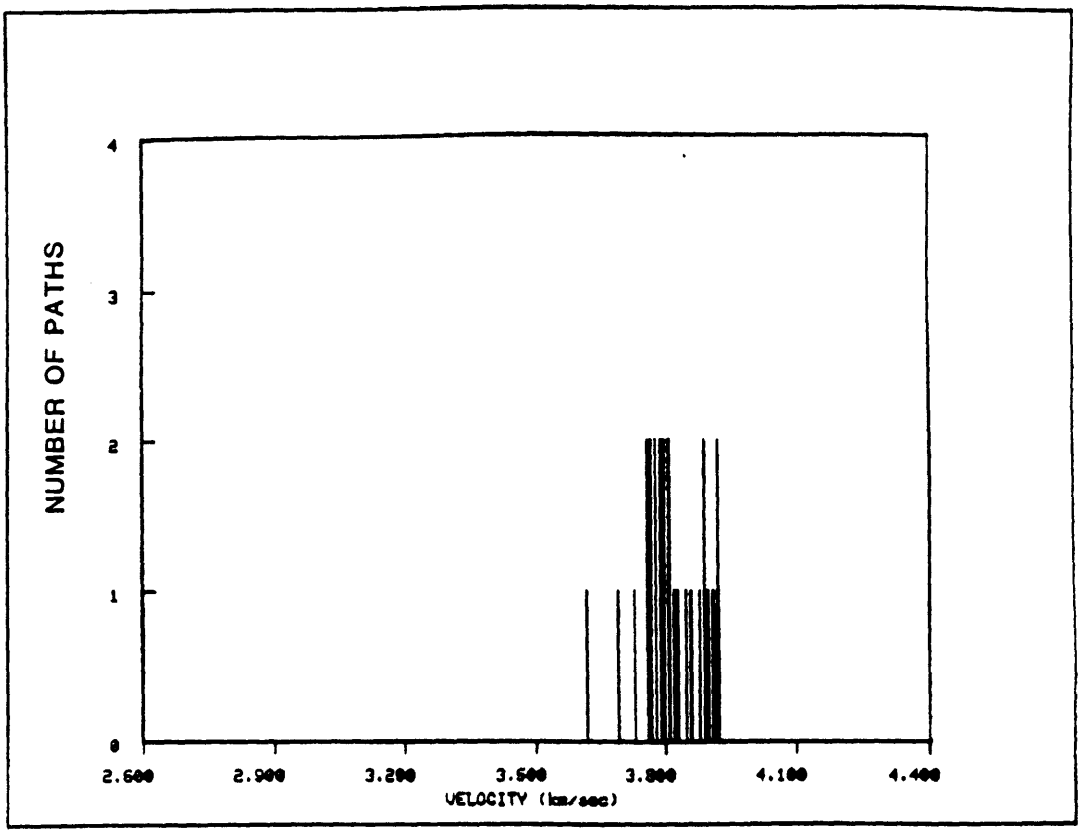

FIGURE C.8o REGION -

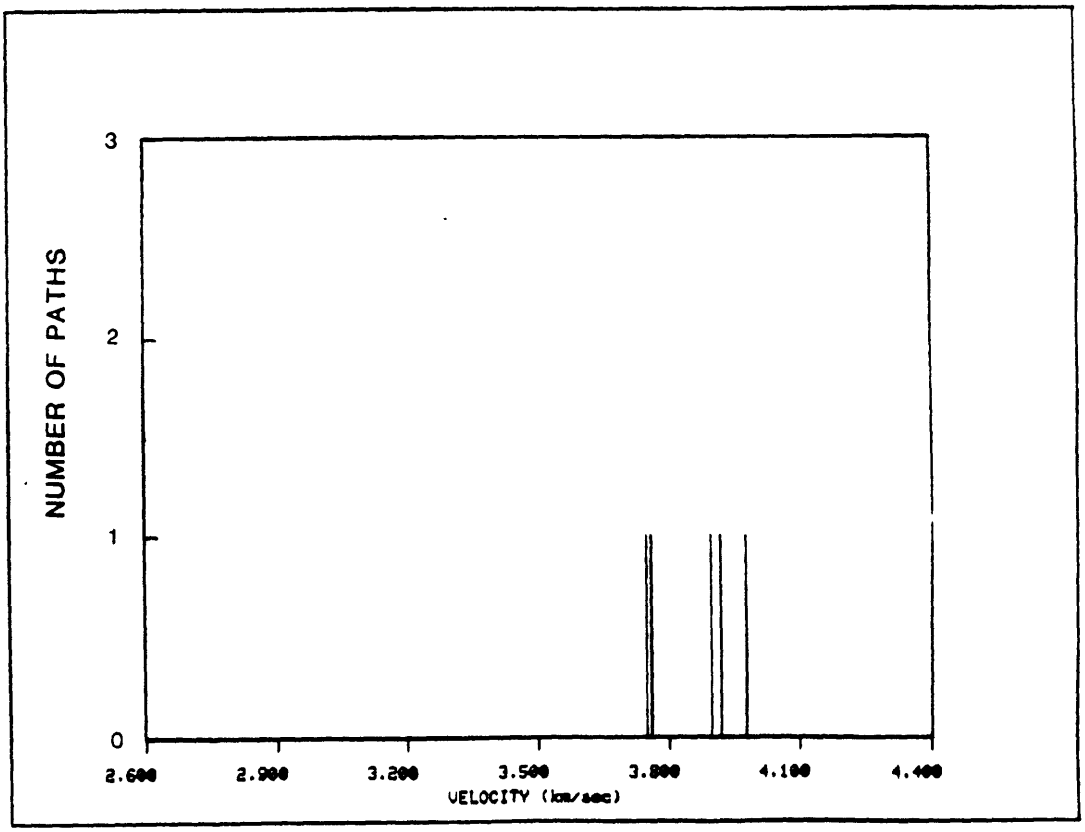

FIGURE C.8p REGION 0

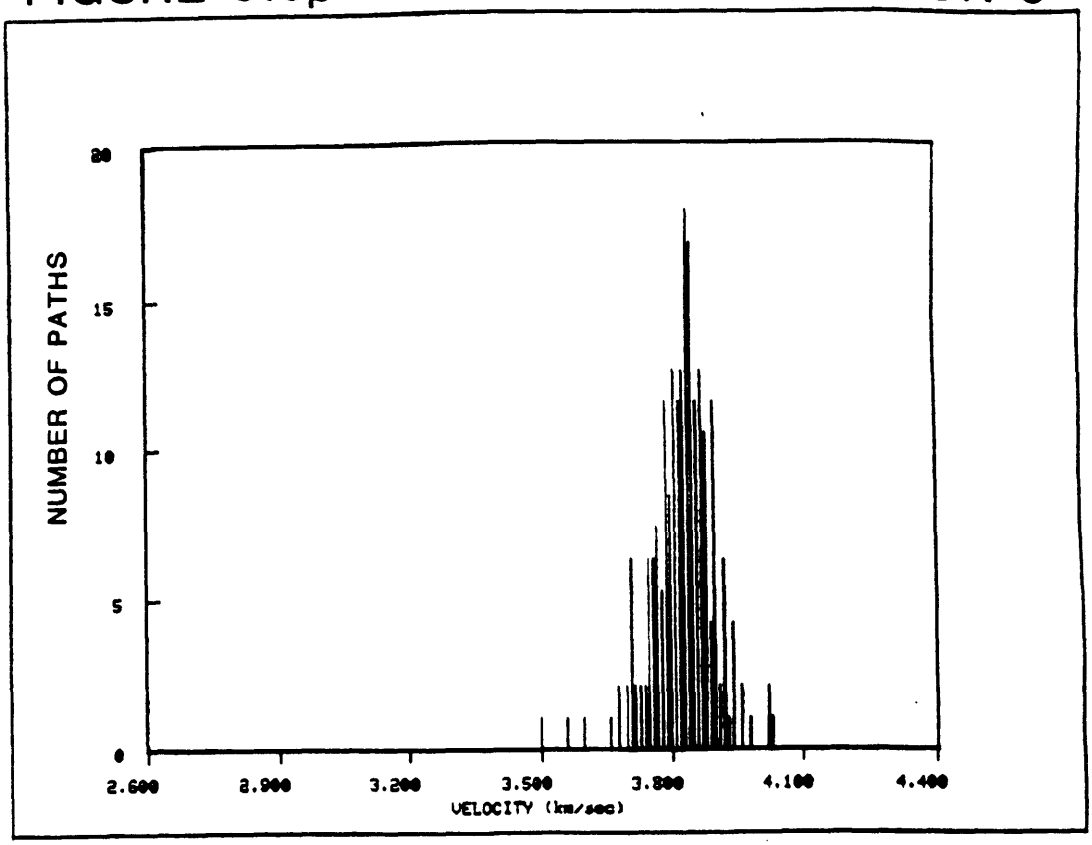

FIGURE C.8q REGION .

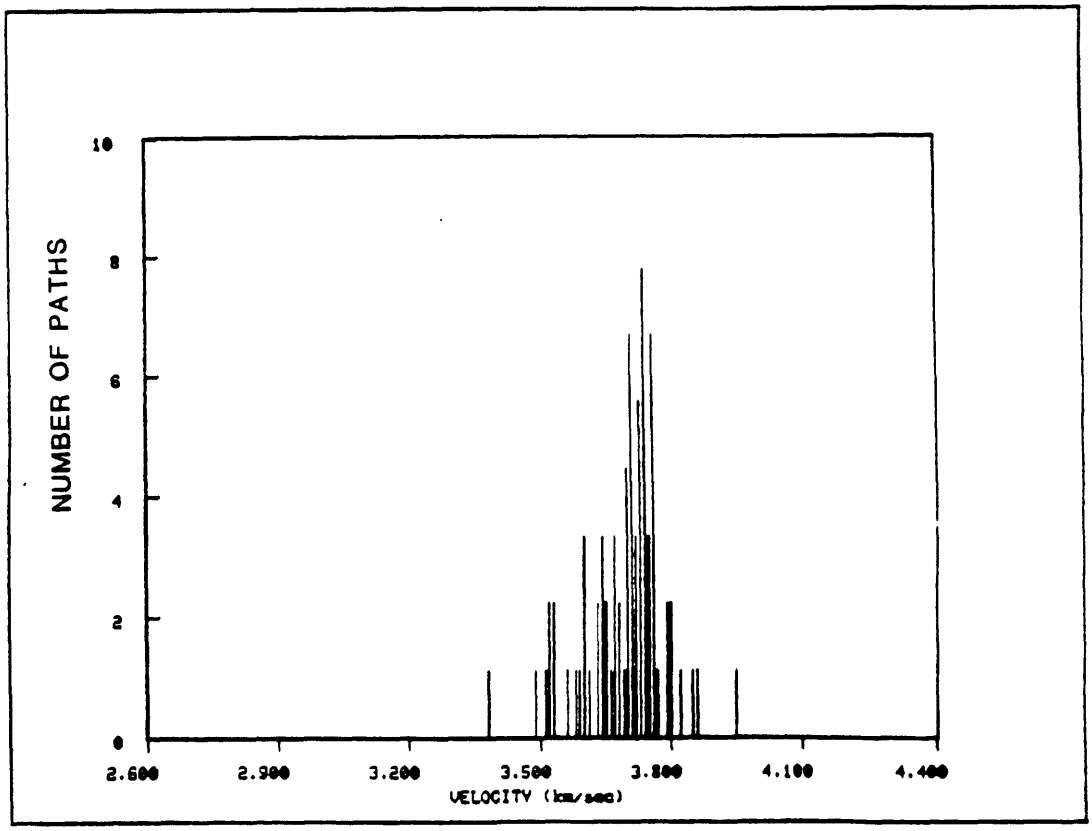

FIGURE C.8r

REGION ø

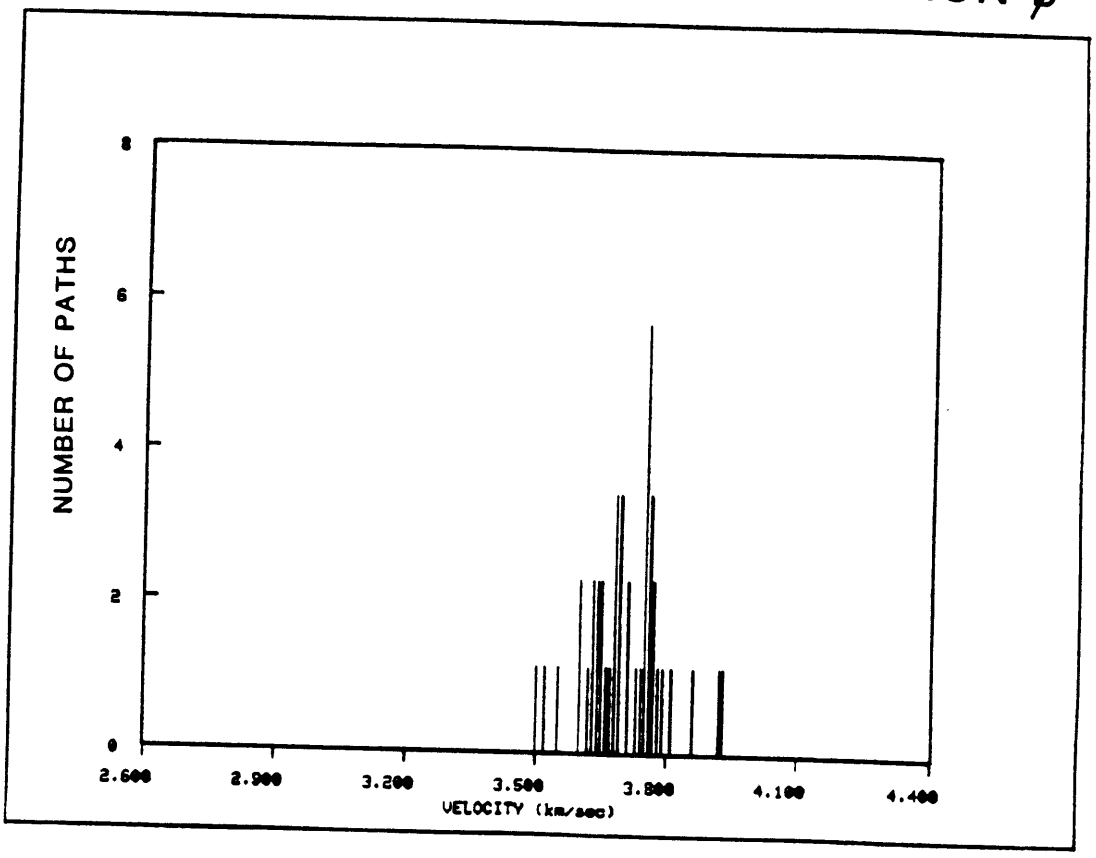

FIGURE C.9a

PERIOD 98 sec

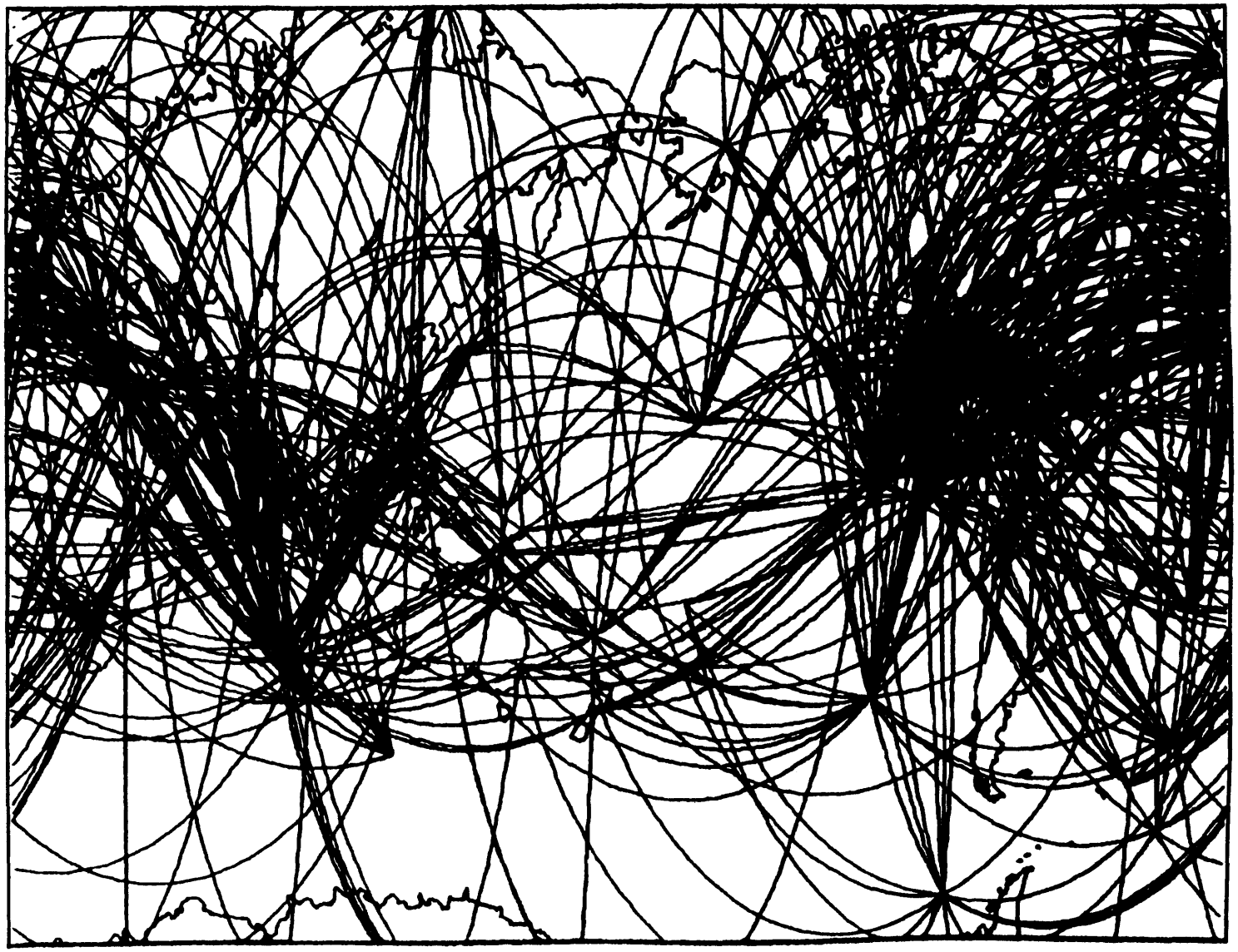

FIGURE C.9b REGION a

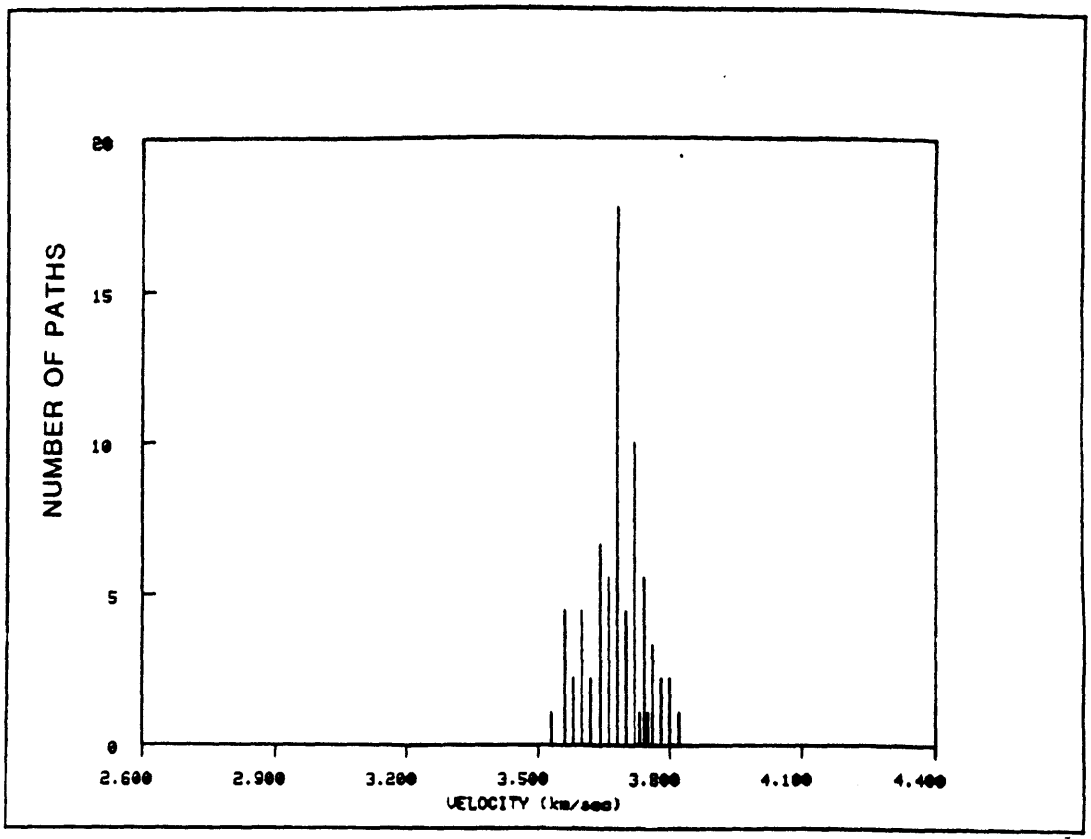

FIGURE C.9c REGION b

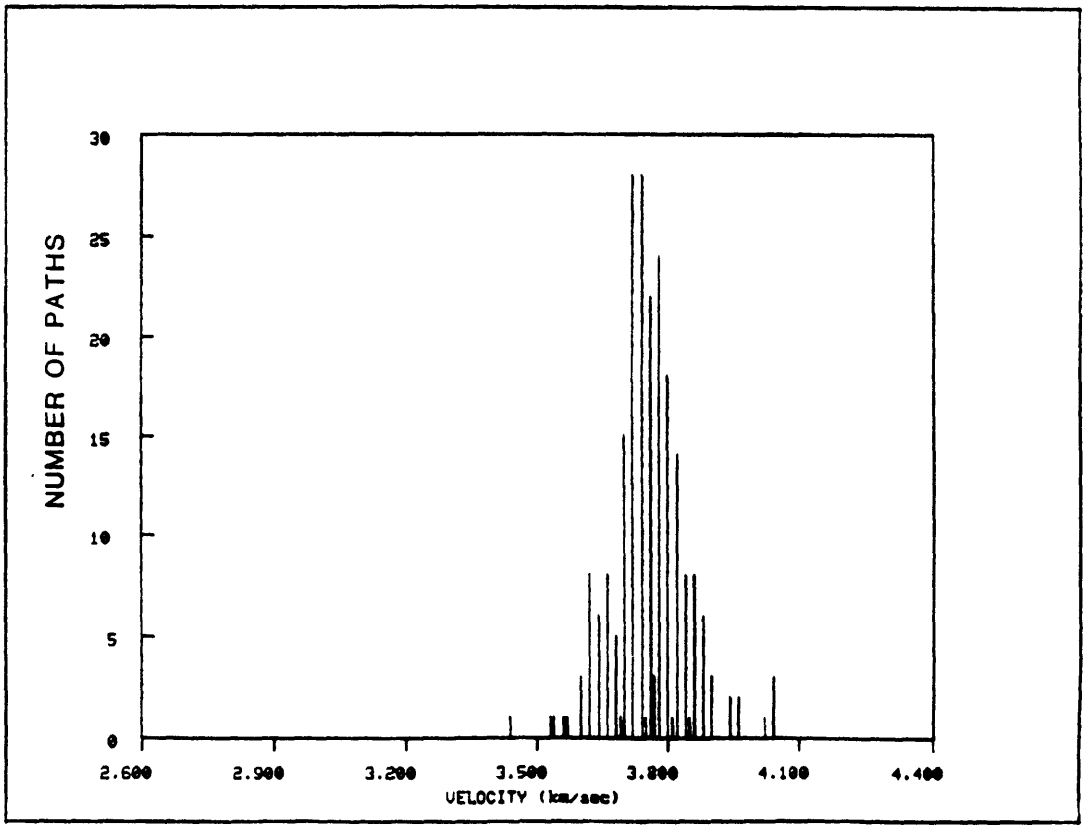

FIGURE C.9d REGION c

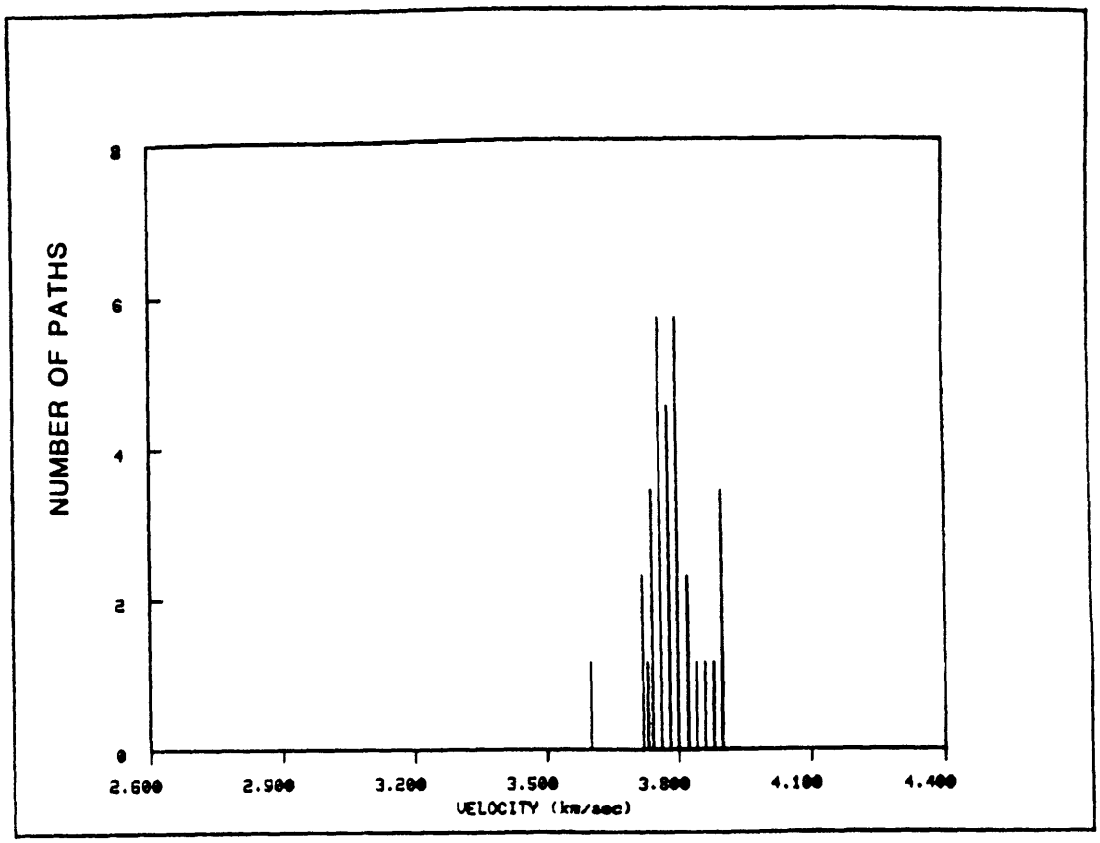

FIGURE C.9e REGION p

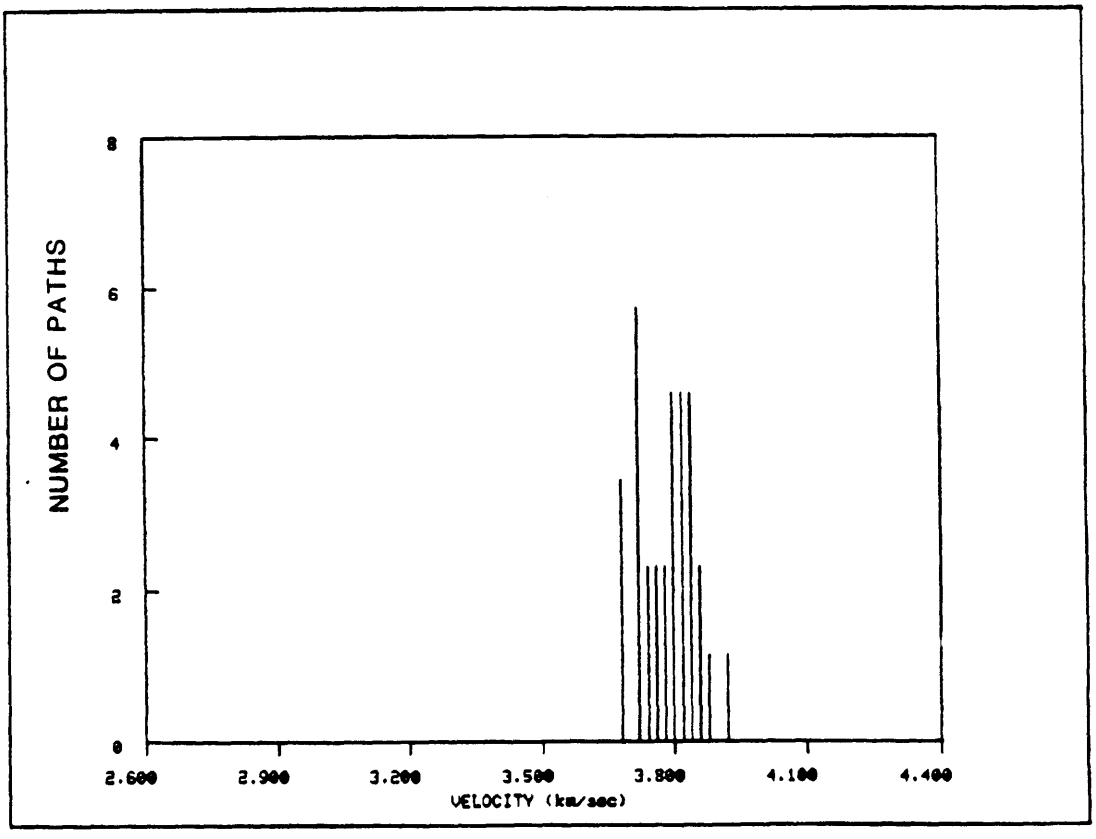

FIGURE C.9f REGION q

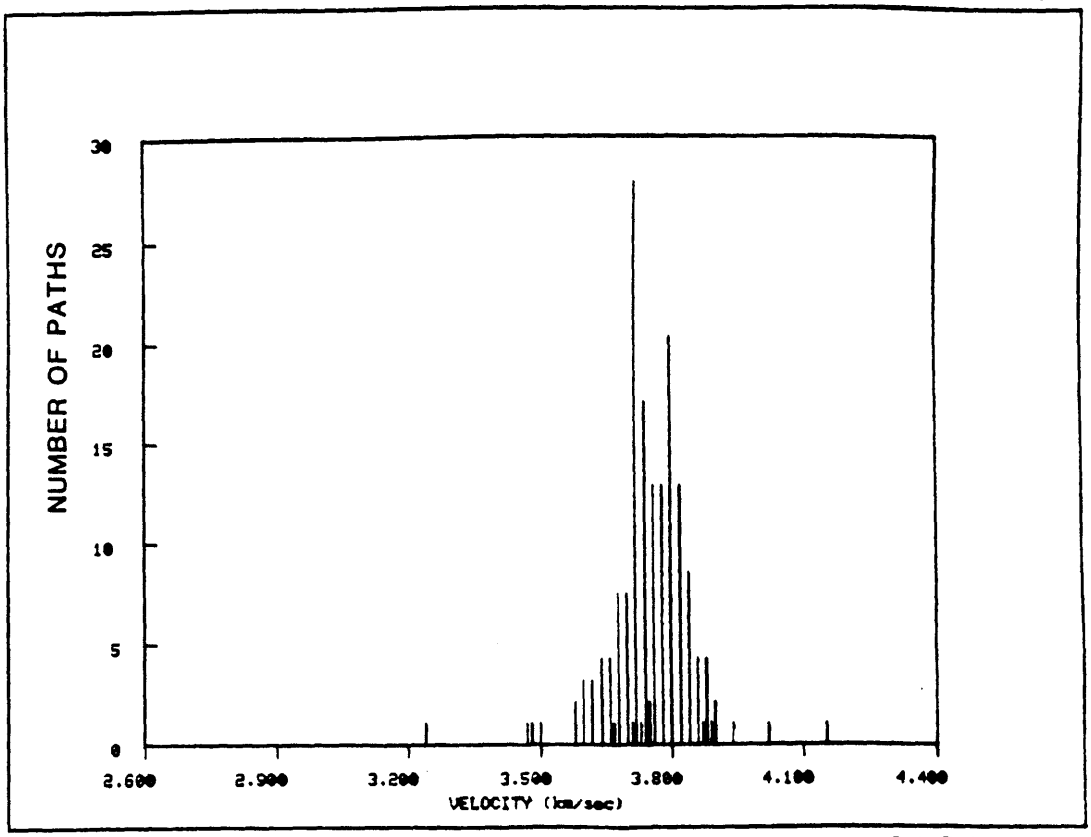

FIGURE C.9g REGION s

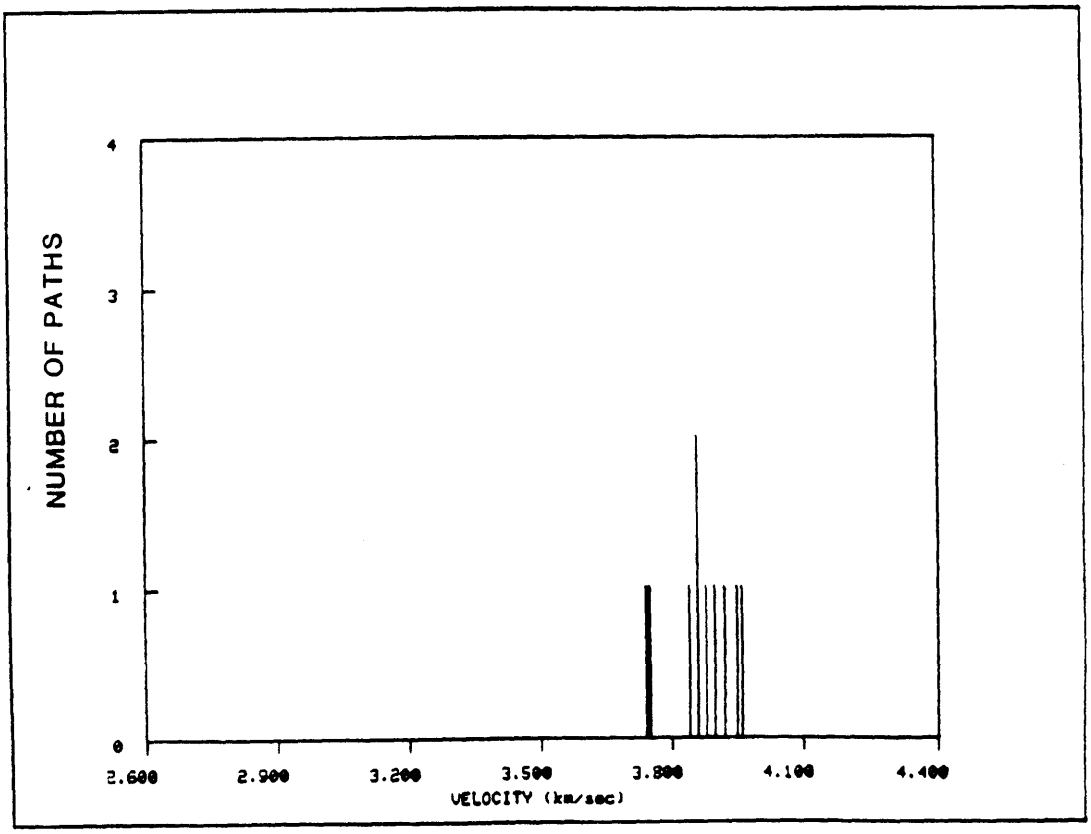

FIGURE C.9h REGION N

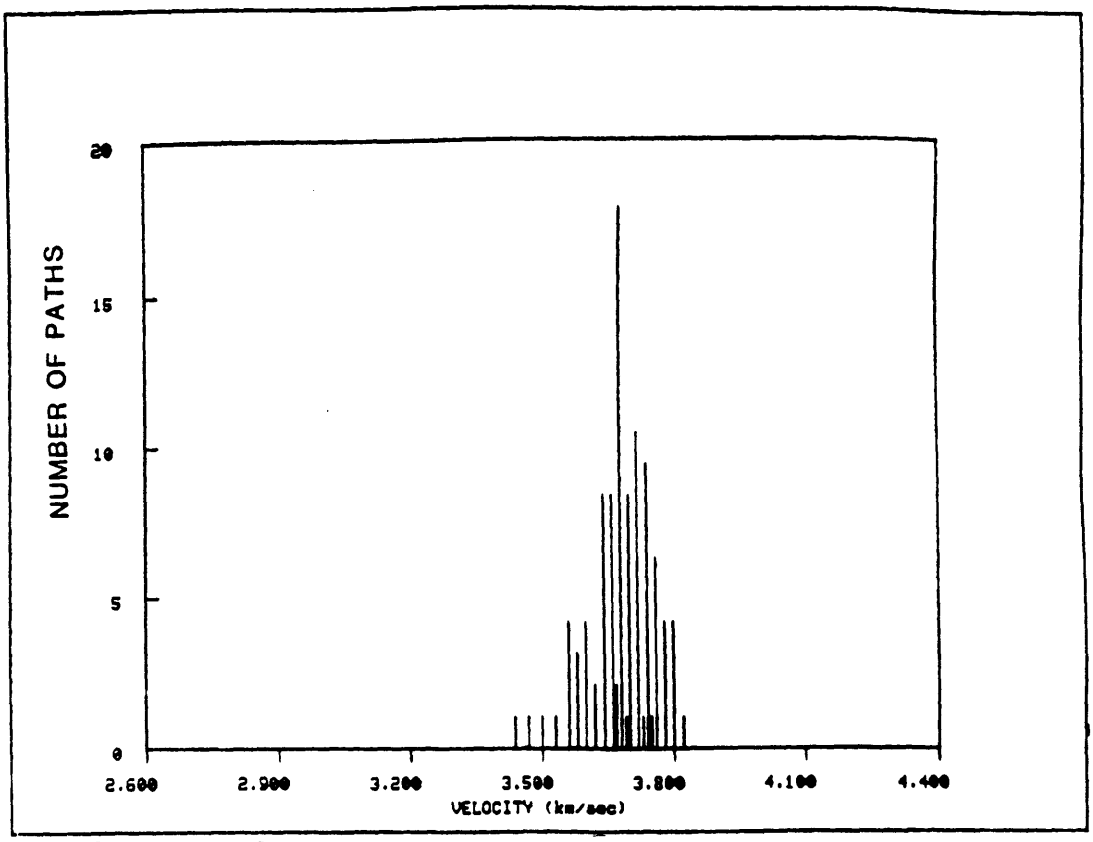

FIGURE C.9i REGION =

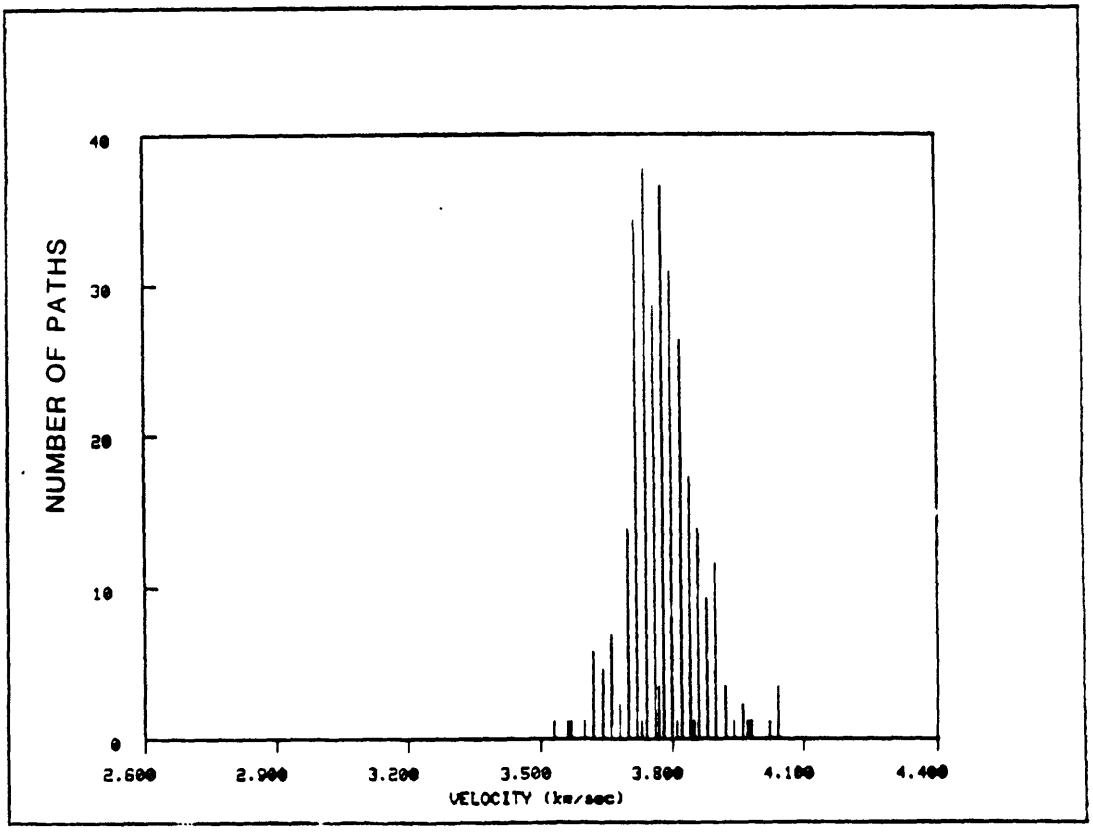

FIGURE C.9j REGION 0

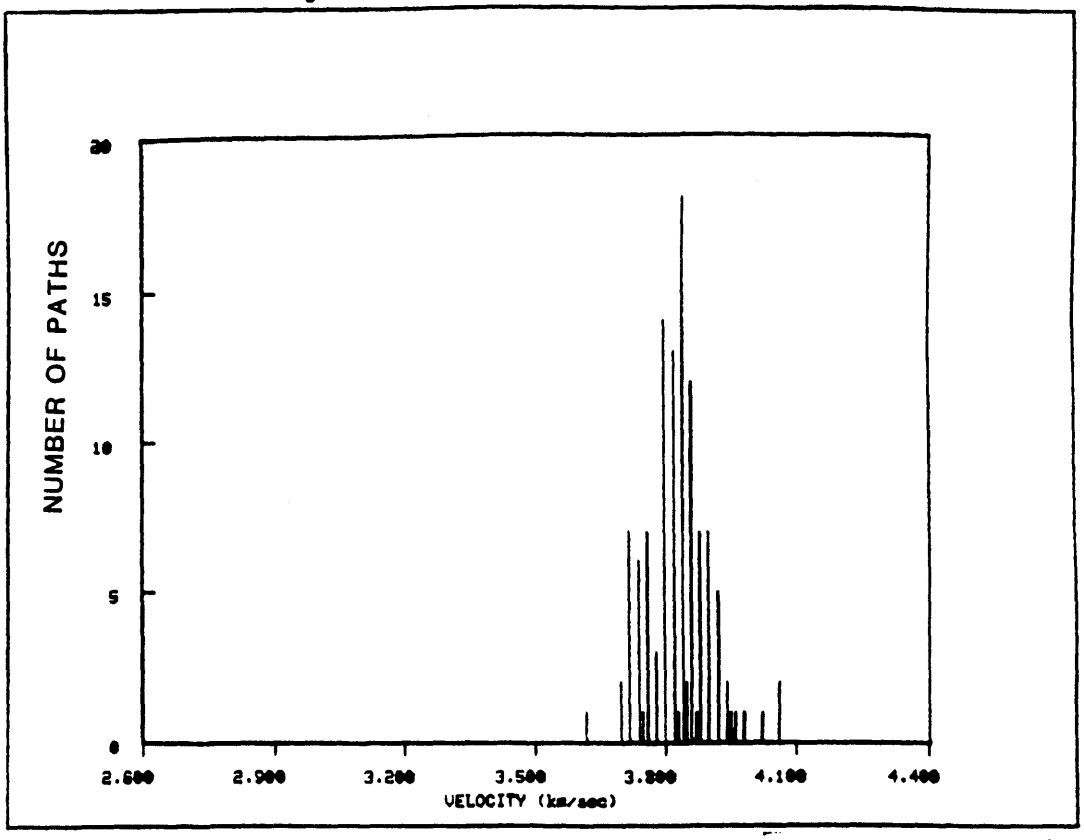

FIGURE C.9k REGION ~~0~~

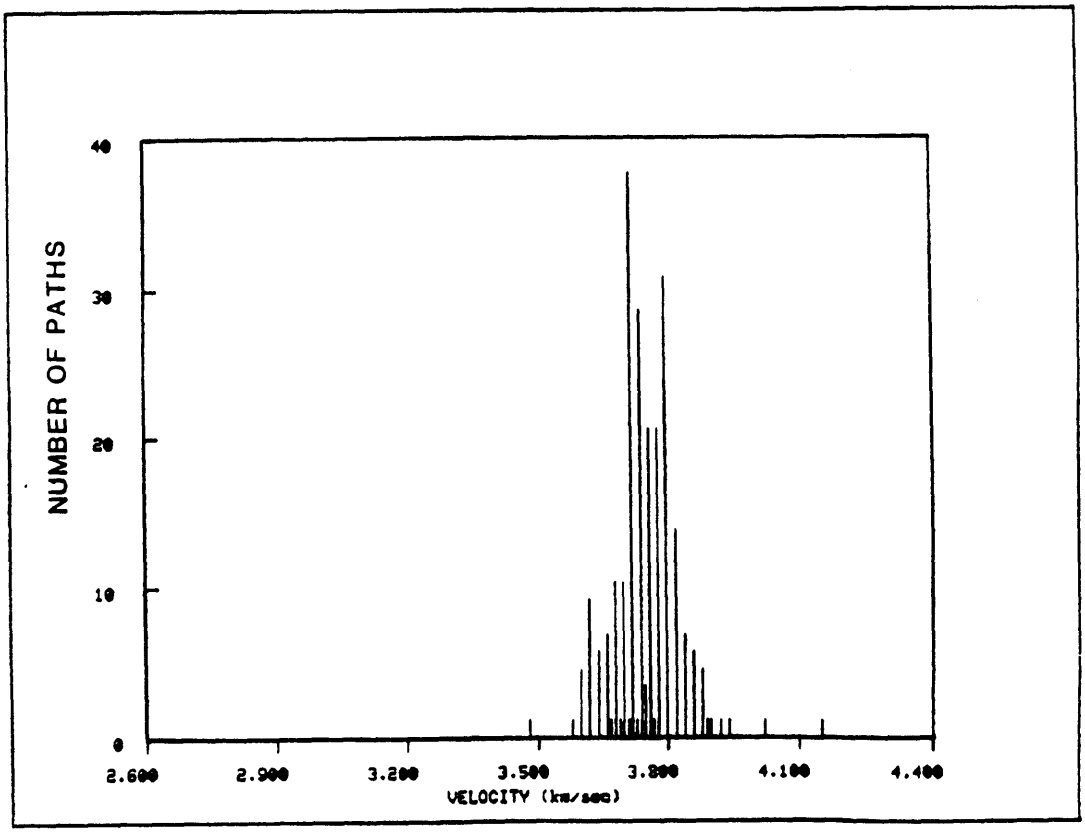

FIGURE C.9l REGION N

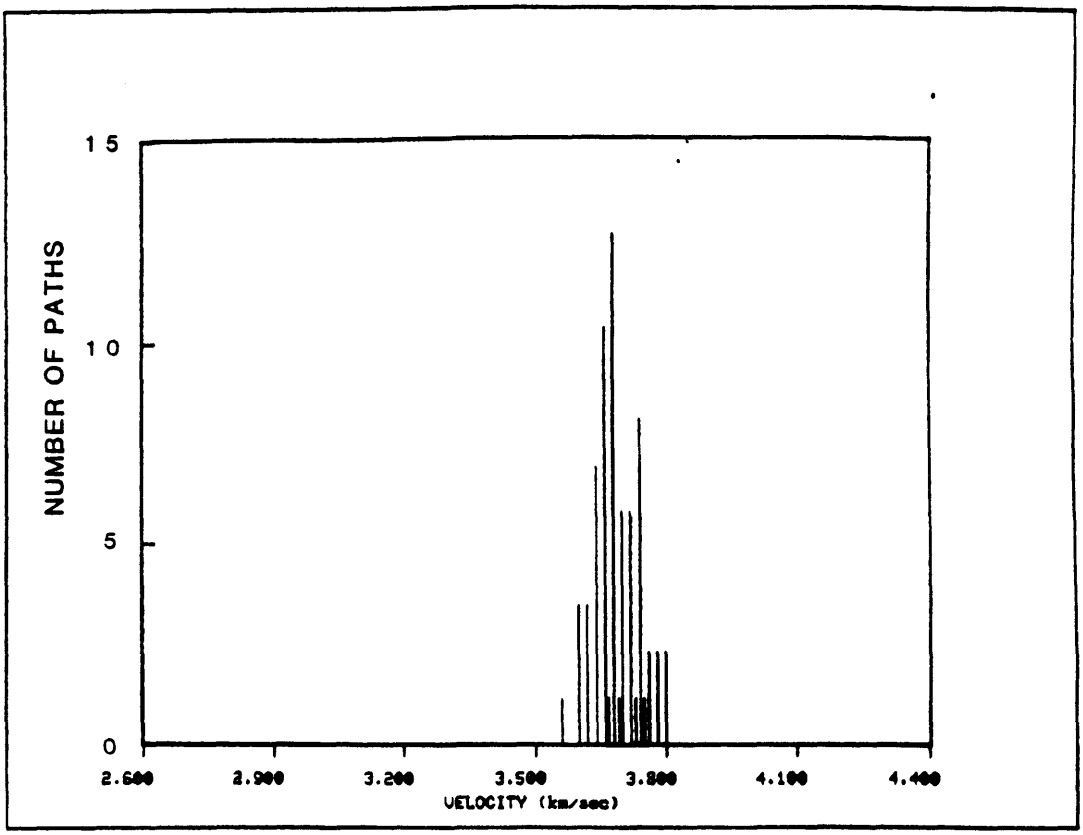

FIGURE C.9m REGION #

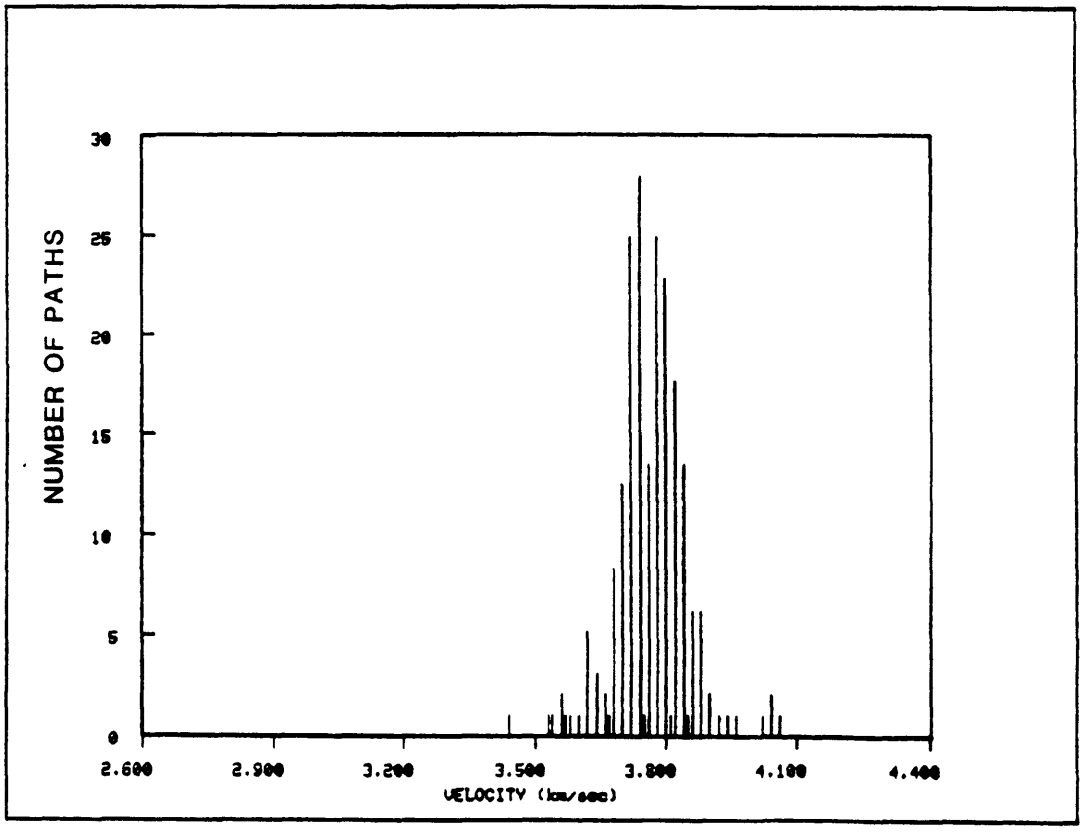

FIGURE C.9n REGION =

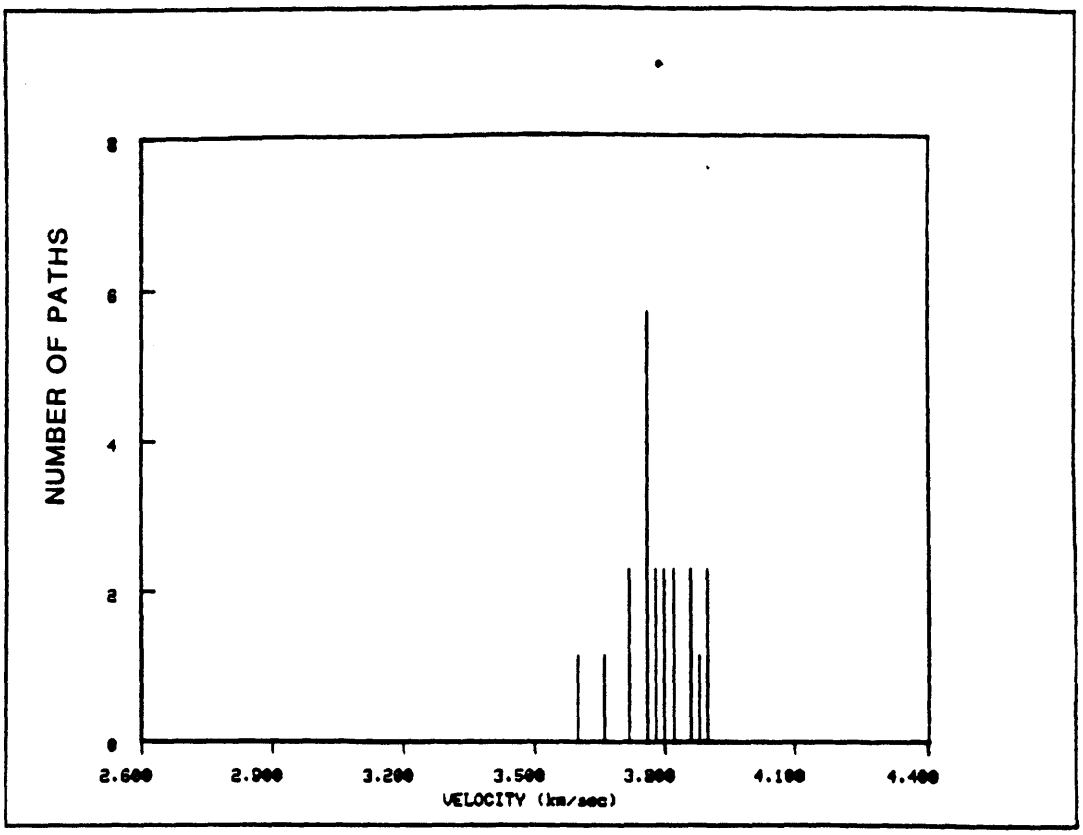

FIGURE C.9o REGION –

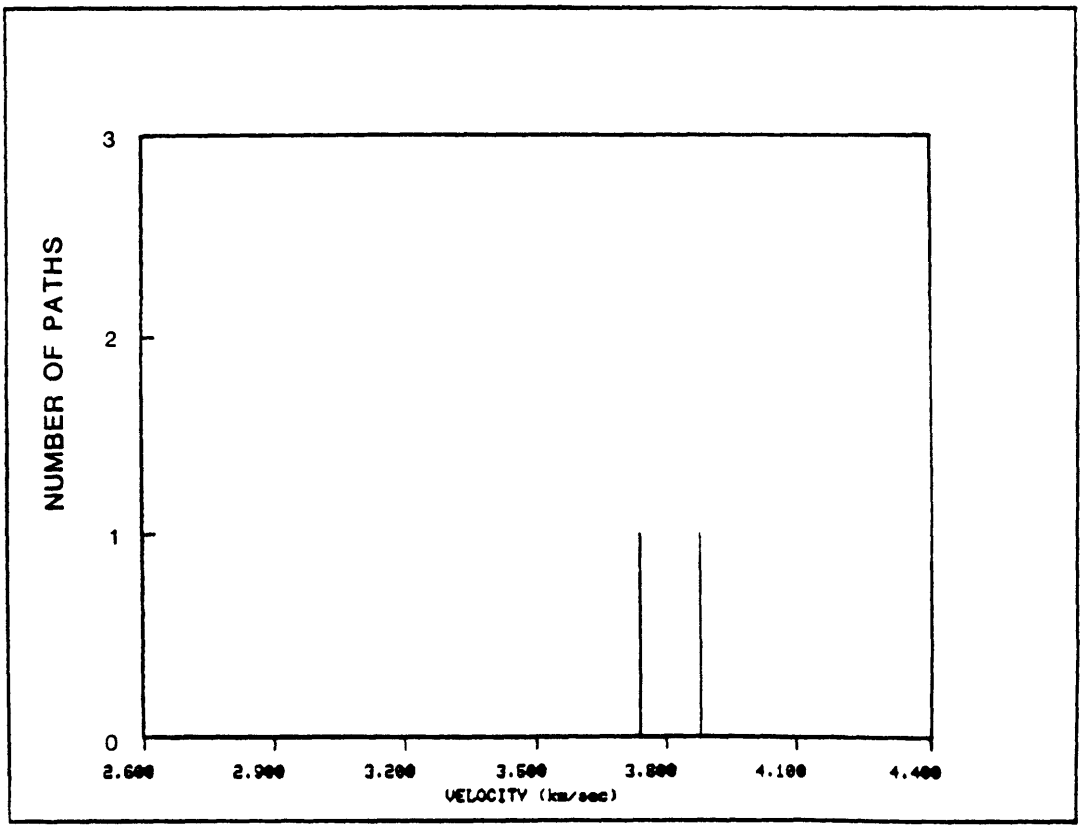

FIGURE C.9p REGION 0

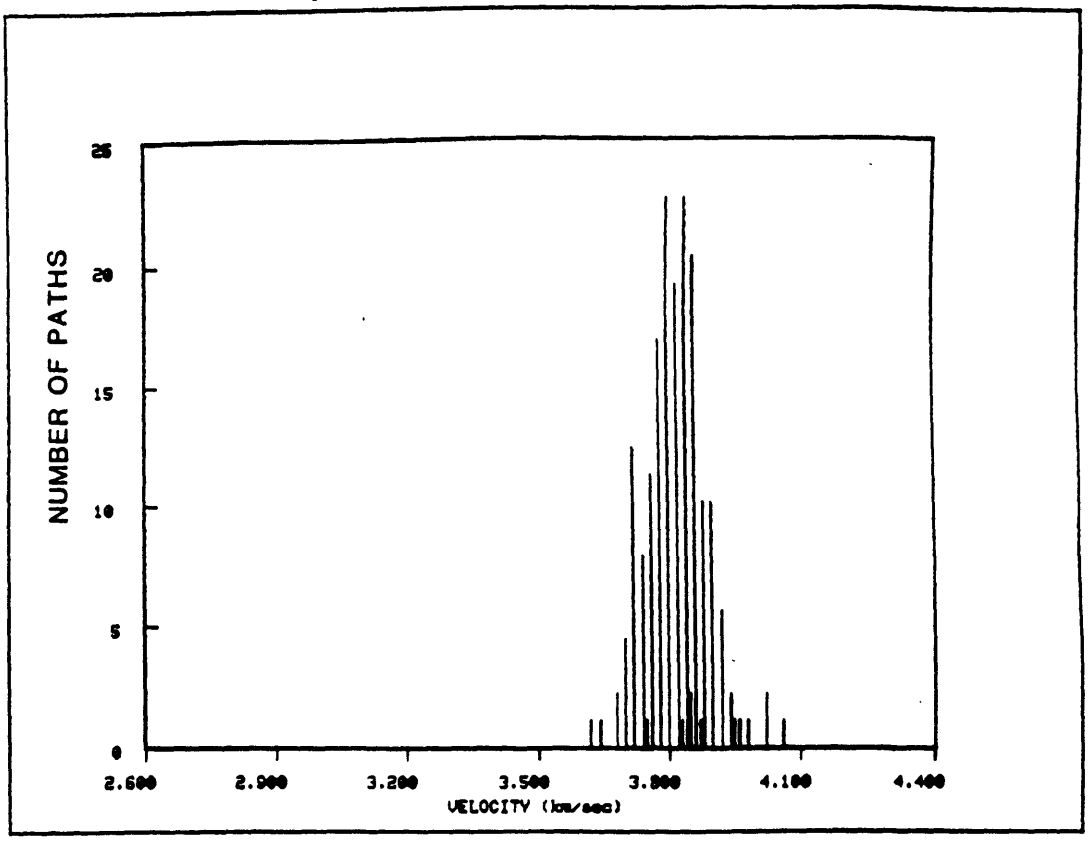

FIGURE C.9q REGION .

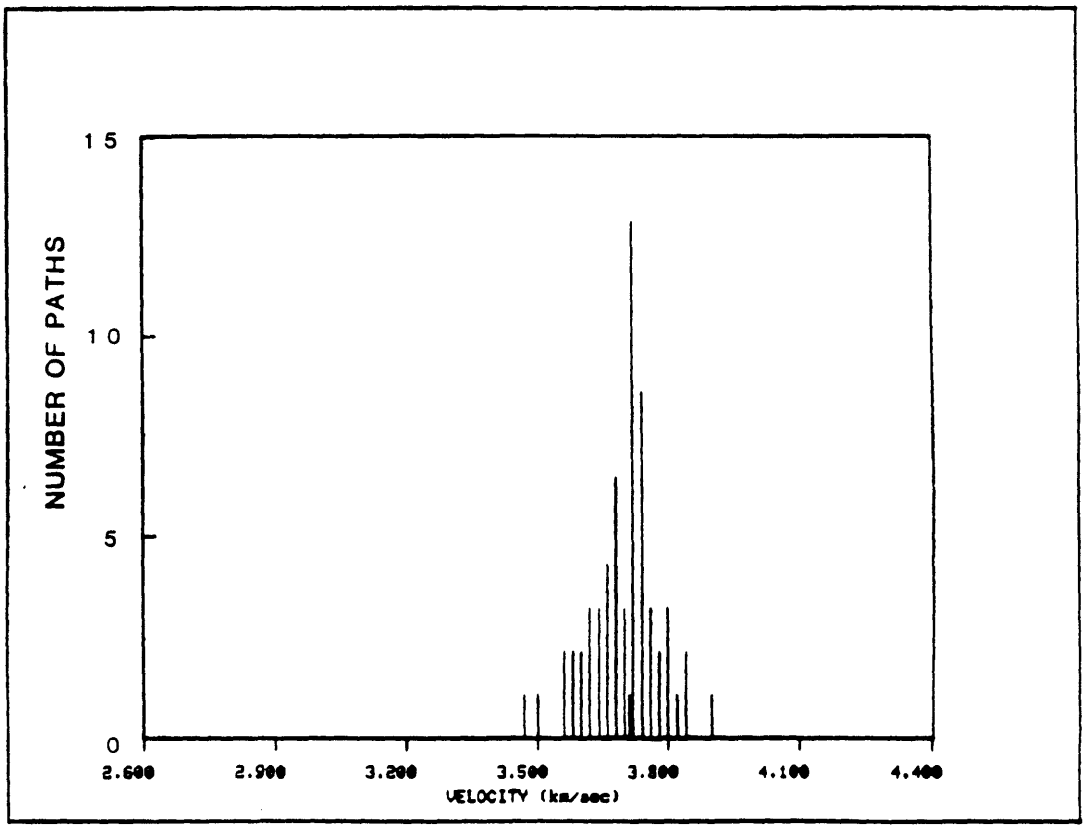

FIGURE C.9r

REGION ø